



UNIVERSITY OF NOVI SAD
FACULTY OF TECHNICAL SCIENCES
DEPARTMENT OF PRODUCTION ENGINEERING
NOVI SAD, SERBIA



11th INTERNATIONAL SCIENTIFIC CONFERENCE
MMA 2012 - ADVANCED PRODUCTION TECHNOLOGIES



PROCEEDINGS

Novi Sad, 20-21 September 2012

PROCEEDINGS OF THE 11th INTERNATIONAL SCIENTIFIC CONFERENCE
MMA 2012 - ADVANCED PRODUCTION TECHNOLOGIES
Novi Sad, 2012

Publisher: **FACULTY OF TECHNICAL SCIENCES
DEPARTMENT OF PRODUCTION ENGINEERING
21000 NOVI SAD, Trg Dositeja Obradovica 6
SERBIA**

Organization of this Conference was approved by Educational-scientific Council of Faculty of Technical Sciences in Novi Sad

Editor: Dr Ilija COSIC, professor, dean

Reviewer's team:
Dr Bogdan SOVILJ, professor
Dr Dragisa VILOTIC, professor
Dr Djordje VUKELIC, assistant professor
Dr Igor BUDAK, assistant professor
Dr Janko HODOLIC, professor
Dr Marin GOSTIMIROVIC, professor
Dr Milan ZELJKOVIC, professor
Dr Miodrag HADZISTEVIC, associate professor
Dr Miroslav PLANCAK, professor
Dr Slobodan TABAKOVIC, assistant professor
Dr Pavel KOVAC, professor
Dr Velimir TODIC, professor

Technical treatment and design:
Dr Mijodrag MILOSEVIC, assistant professor
MSc Igor BESIC, assistant
MSc Ivan MATIN, assistant
MSc Alena ZAJAC
MSc Branislav MILANOVIC
MSc Darko MILANKOVIC

Manuscript submitted for publication: September 10, 2012

Printing: 1st

Circulation: 150 copies

CIP classification:

CIP - Каталогизacija u publikaciji
Biblioteka Matice srpske, Novi Sad

612.7/.9(082)

**INTERNATIONAL Scientific Conference MMA 2012 Advanced
Production Technologies (11 ; 2012 ; Novi Sad)**

Proceedings [Elektronski izvor] / 11th International Scientific Conference
MMA 2012 - Advanced Production Technologies, Novi Sad, 20-21
September, 2012 ; [editor Ilija Cosic]. - Novi Sad : Faculty of Technical
Sciences, Department of Production Engineering, 2012 (Novi Sad : FTN,
Graphics Centre GRID). - 1 elektronski optički disk (CD-ROM)
: tekst, slika ; 12 cm

Printing by: FTN, Graphic Centre
GRID, Novi Sad

Nasl. sa naslovnog ekrana. - Tiraž 150. - Bibliografija uz svako rad.

ISBN 978-86-7892-419-4

a) Производно машинство - Зборници
COBISS.SR-ID 273838087

Financing of the Proceedings was sponsored by the Ministry of Education, Science and Technological Development of the Republic of Serbia and supported by the Provincial Secretariat for Science and Technological Development of AP Vojvodina.



11th INTERNATIONAL SCIENTIFIC CONFERENCE NOVI SAD, SERBIA, SEPTEMBER 20-21, 2012

CONFERENCE ORGANIZER

University of Novi Sad
Faculty of Technical Sciences
Department of Production Engineering
Novi Sad, Serbia

PROGRAMME COMMITTEE

- | | |
|---|--|
| <i>Prof. dr Janko Hodolic, chairman</i> | <i>Prof. dr Marin Gostimirovic, FTN Novi Sad</i> |
| <i>Prof. dr Amaia Igartua, TC Eibar</i> | <i>Prof. dr Milan Majernik, TU Kosice</i> |
| <i>Prof. dr Bogdan Sovilj, FTN Novi Sad</i> | <i>Prof. dr Milan Zeljkovic, FTN Novi Sad</i> |
| <i>Prof. dr Borut Kosec, FS Ljubljana</i> | <i>Prof. dr Miodrag Manic, MF Nis</i> |
| <i>Prof. dr Branko Tadic, MF Kragujevac</i> | <i>Assoc. Prof. dr Miodrag Hadzistevic, FTN Novi Sad</i> |
| <i>Prof. dr Dragan Domazet, UM Belgrade</i> | <i>Prof. dr Mirko Sokovic, FS Ljubljana</i> |
| <i>Prof. dr Dragan Milutinovic, MF Belgrade</i> | <i>Prof. dr Miroslav Babic, MF Kragujevac</i> |
| <i>Prof. dr Dragisa Vilotic, FTN Novi Sad</i> | <i>Prof. dr Miroslav Badida, TU Kosice</i> |
| <i>Prof. dr Drazan Kozak, SF Slavonski Brod</i> | <i>Prof. dr Miroslav Plancak, FTN Novi Sad</i> |
| <i>Prof. dr Dubravka Markovic, MF Novi Sad</i> | <i>Prof. dr Miroslav Trajanovic, MF Nis</i> |
| <i>Prof. dr Dusan Golubovic, MF Sarajevo</i> | <i>Prof. dr Numan M. Durakbasa, TU Vienna</i> |
| <i>Prof. dr Dusan Sormaz, ISE Athens, Ohio</i> | <i>Prof. dr Pavel Kovac, FTN Novi Sad</i> |
| <i>Prof. dr Dzemo Tufekcic, MF Tuzla</i> | <i>Prof. dr Petar Petrovic, MF Belgrade</i> |
| <i>Prof. dr Franci Cus, SF Maribor</i> | <i>Prof. dr Predrag Cosic, FSB Zagreb</i> |
| <i>Prof. dr Goran Simunovic, SF Slavonski Brod</i> | <i>Prof. dr Radivoje Mitrovic, MF Belgrade</i> |
| <i>Prof. dr Gyula Varga, GIK Miskolc</i> | <i>Prof. dr Sergei Alexandrov, RAN Moscow</i> |
| <i>Assist. Prof. dr Heidy Schwarczova, SEVS Skalica</i> | <i>Prof. dr Slavko Arsovski, MF Kragujevac</i> |
| <i>Assoc. Prof. dr Igor Drstvensek, SF Maribor</i> | <i>Prof. dr Sefket Goletic, MF Zenica</i> |
| <i>Prof. dr Ilija Cosic, FTN Novi Sad</i> | <i>Prof. dr Toma Udiljak, FSB Zagreb</i> |
| <i>Prof. dr Ivan Kuric, FME Zilina</i> | <i>Prof. dr Valentina Gecevska, MF Skopje</i> |
| <i>Prof. dr Janez Kopac, FS Ljubljana</i> | <i>Prof. dr Velimir Todic, FTN Novi Sad</i> |
| <i>Prof. dr Jozef Novak-Marcincin, FMT Presov</i> | <i>Prof. dr Vid Jovisevic, MF Banja Luka</i> |
| <i>Prof. dr Jozef Zivcak, TU Kosice</i> | <i>Prof. dr Vidosav Majstorovic, MF Belgrade</i> |
| <i>Prof. dr Joze Balic, SF Maribor</i> | <i>Prof. dr Vlastimir Nikolic, MF Nis</i> |
| <i>Prof. dr Konstantin Bouzakis, AU Thessaloniki</i> | <i>Prof. dr Vojo Visekruna, FSR Mostar</i> |
| <i>Prof. dr Ljubodrag Tanovic, MF Belgrade</i> | <i>Prof. dr Wolfgang Voelkner, FI Dresden</i> |
| <i>Prof. dr Ljubomir Borojev, FTN Novi Sad</i> | <i>Prof. dr Zbigniew Klos, PP Poznan</i> |
| <i>Prof. dr Lubomir Soos, STU Bratislava</i> | <i>Prof. dr Zdravko Krivokapic, MF Podgorica</i> |
| <i>Prof. dr Malik Kulenovic, MF Sarajevo</i> | <i>Prof. dr Zlatan Car, TF Rijeka</i> |



11th INTERNATIONAL SCIENTIFIC CONFERENCE NOVI SAD, SERBIA, SEPTEMBER 20-21, 2012

HONORARY COMMITTEE

Prof. dr Branko Ivkovic, MF Kragujevac
MSc Dragan Banjac, FTN Novi Sad
Prof. dr Dragoje Milikic, FTN Novi Sad
Prof. dr Dragutin Zelenovic, Academician, FTN Novi Sad
Prof. dr Dusan Sebo, SF Kosice
Prof. dr Csaba Gyenge, MBF Cluj-Napoca
Prof. dr Illes Dudas, GIK Miskolc
Prof. dr Jan Madl, FME Prag
Prof. dr Jelena Stankov, FTN Novi Sad
Prof. dr Jerzy Jedrzejewski, UT Wroclaw
Prof. dr Joko Stanic, MF Belgrade

Prof. dr Jozef Rekecki, FTN Novi Sad
Prof. dr Milenko Jovicic, MF Belgrade
Prof. dr Milisav Kalajdzic, MF Belgrade
Prof. dr Miodrag Lazic, MF Kragujevac
Prof. dr Ratko Gatalo, FTN Novi Sad
Prof. dr Ratko Mitrovic, MF Kragujevac
Prof. dr Sava Sekulic, FTN Novi Sad
Prof. dr Slavi Ivanov, TH Sofia
Prof. dr Stanislaw Pytko, PTS Krakow
Prof. dr Vladimir Milacic, MF Belgrade
Prof. dr Vucko Mecanin, MF Kraljevo

ORGANIZING COMMITTEE

Assoc. Prof. dr Miodrag Hadzistevic, chairman
Assist. Prof. dr Aco Antic
MSc Aleksandar Zivkovic, assistant
MSc Alena Zajac, technical secretary
MSc Borislav Savkovic, assistant
MSc Branko Strbac, assistant
MSc Dejan Lukic, assistant

Assist. Prof. dr Djordje Vukelic
Assist. Prof. dr Igor Budak
MSc Igor Besic, assistant, secretary
MSc Ivan Matin, associate
Assist. Prof. dr Mijodrag Milosevic
Assist. Prof. dr Milenko Sekulic
Assist. Prof. dr Slobodan Tabakovic



11th INTERNATIONAL SCIENTIFIC CONFERENCE NOVI SAD, SERBIA, SEPTEMBER 20-21, 2012

ACKNOWLEDGEMENT

Organisation of 11th International Scientific Conference MMA 2012 – ADVANCED PRODUCTION TECHNOLOGIES was made possible with understanding and financial help of following sponsors:

- **MINISTRY OF EDUCATION, SCIENCE AND TECHNOLOGICAL DEVELOPMENT OF THE REPUBLIC OF SERBIA** – Belgrade
- **PROVINCIAL SECRETARIAT FOR SCIENCE AND TECHNOLOGICAL DEVELOPMENT OF AP VOJVODINA** – Novi Sad
- **FACULTY OF TECHNICAL SCIENCES** - Novi Sad
- **DEPARTMENT FOR PRODUCTION ENGINEERING AT THE FACULTY OF TECHNICAL SCIENCES** - Novi Sad
- **MAJEVICA HOLDING** – Backa Palanka
- **OSA RACUNARSKI INZENJERING** - Belgrade
- **HITARD ENGINEERING** – Novi Sad
- **TEHNOEXPORT** - Indjija
- **TPS** – Novi Knezevac
- **MILE DRAGIC PRODUCTION** – Zrenjanin
- **GASTEH** – Indjija
- **TIM CO** – Belgrade
- **FKL** – Temerin
- **ADAMES** - Ada

Being held on a regular basis, like some other conferences with long tradition, the MMA 2012 – ADVANCED PRODUCTION TECHNOLOGIES contributes to continuous application of scientific results and professional know-how in the metalworking industry, regardless of the difficulties this industry has been facing during the last two decades.

By organizing the MMA 2012 Conference, the research potential of our country relies on its traditional enthusiasm and perseverance in order to contribute to advancement of production engineering in this region – not only through application of scientific results and professional know-how in practice, but also in education of engineers in the field of production technologies and techniques.

The eleventh International Scientific Conference MMA 2012 – ADVANCED PRODUCTION TECHNOLOGIES is for the tenth time being held with international participation. Throughout the years, by the number of contributions, their quality and participation of international authors, the Conference has earned a respectable reputation among scientists and industry professionals.

This year MMA – ADVANCED PRODUCTION TECHNOLOGIES focuses on the following topics:

- ◆ METAL CUTTING
- ◆ MACHINE TOOLS AND AUTOMATIC FLEXIBLE TECHNOLOGICAL SYSTEMS, CA_x AND CIM PROCEDURES AND SYSTEMS
- ◆ METROLOGY, QUALITY, FIXTURES, METAL CUTTING TOOLS AND TRIBOLOGY
- ◆ MECHANICAL ENGINEERING AND ENVIRONMENTAL PROTECTION
- ◆ OTHER PRODUCTION ENGINEERING TECHNOLOGIES
- ◆ BIO-MEDICAL ENGINEERING – CA_x

With 129 papers and contributions by international authors from 20 different countries, 11th International Scientific Conference MMA 2012 – ADVANCED PRODUCTION TECHNOLOGIES successfully maintains the high level set by the previous conferences. Participation of a large number of domestic and international authors, as well as the diversity of topics, justifies our efforts to organize this conference and contribute to exchange of knowledge, research results and experience of industry experts, research institutions and faculties which all share a common interest in the field of production engineering.

Novi Sad, September 2012

*PROGRAMME AND ORGANIZING
COMMITTEE*



Contents

Section A: METAL CUTTING

Baralić, J., Nedić, B.: THE EFFECT OF ABRASIVE WATER JET CUTTING PARAMETERS ON KERF GEOMETRY	1
Beniak, J.: OPERATIONAL CHARACTERISTIC OF SHREDDING MACHINES	5
Bilic, B., Trlin, G., Vojkovic, V.: APPLICATION OF SIMULATED ANNEALING METHOD IN THE CUTTING PARAMETERS OPTIMIZATION REGARDING SURFACE ROUGHNESS	9
Gostimirović, M., Pucovsky, V., Kovač, P., Šooš, Lj., Rodić, D., Savković, B.: MODELING OF DISCHARGE ENERGY IN EDM PROCESS BY THE USE OF GENETIC ALGORITHMS	13
Gostimirovic, M., Rodic, D., Kovac, P., Mankova, I., Beno, J., Pucovsky, V., Sekulic, M.: PREDICTION OF SURFACE ROUGHNESS USING NEURAL FUZZY SYSTEMS IN ELECTRICAL DISCHARGE MACHINING	17
Homar, D., Kopač, J., Dolinšek, S.: ADDITIVE MANUFACTURING AND HIGH SPEED CUTTING INCLUDED IN HYBRID MANUFACTURING	21
Janković, P., Radovanović, M.: EFFECT OF PROCESS PARAMETERS ON CUTTING ABILITY IN ABRASIVE WATER JET MACHINING	25
Kopac, J., Cus, F., Stoic, A., Zabkar, B.: SOME IDEAS ABOUT SUSTAINABLE MANUFACTURING CONCEPT	29
Kovač, P., Radonjić, S., Mitrović, A., Sovilj-Nikić, I.: DETERMINING THE PROCESSING PARAMETERS FOR STEEL AISI 6150 IN LASER CUTTING	33
Kramar, D., Sekulić, M., Kovač, P., Gostimirović, M., Kopač, J.: THE IMPLEMENTATION OF TAGUCHI METHOD FOR QUALITY IMPROVEMENT IN HIGH-PRESSURE JET ASSISTED TURNING PROCESS	37
Nagode, A., Klančnik, G., Gojić, M., Kosec, B., Bizjak, M., Zorc, B., Kosec, L.: AN INVESTIGATION OF THE SURFACE DAMAGE OF HOT PLATES AFTER BLACK OXIDE COATING	41
Peterka, J., Kováč, M., Beňo, M., Zvončan, M.: EFFECT OF CUTTING PARAMETERS ON DELAMINATION FACTOR IN ROTARY ULTRASONIC MACHINING OF FIBERGLASS	45

Šogorović, D., Mišković, A., Višekruna, V.: DESIGN OF DEVICE FOR HIGH-PRODUCTIVE CUTTING OF THREADS	49
Tanović, Lj., Puzović, R., Klimenko, S.: THE PHENOMENA OF GRANITE MICRO – CUTTING PROCESS	53

Section B: MACHINE TOOLS

Čiča, Đ., Zeljković, M., Lakić-Globočki, G., Sredanović, B., Borojević, S.: IDENTIFICATION OF CONTACT PARAMETERS OF SPINDLE–HOLDER–TOOL ASSEMBLY USING ARTIFICIAL NEURAL NETWORKS	57
Dučić, N., Čojbašić, Ž., Slavković, R., Radonjić, S.: APPLICATION OF NEURAL NETWORKS FOR PREDICTING CHARACTERISTICS OF ELASTIC SUPPORTS TO PRODUCTION MACHINES	61
Epler, I., Djapic, M., Lukic, Lj.: RISK - BASED MAINTENANCE OF THE FLEXIBLE TECHNOLOGICAL SYSTEM	65
Gyenge, C., Rafa, A., Pacurar, A., Bob, M.: SOME CHARACTERISTICAL ASPECTS REGARDING CNC GRINDING OF SPUR GEARS	69
Milutinovic, M., Slavkovic, N., Milutinovic, D.: KINEMATIC MODELING OF THE TRICEPT BASED 5-AXIS MACHINE TOOL	73
Pecenica, N., Lukic, Lj., Nikolic, N., Djapic, M.: COMPARATIVE ANALYSIS AND FLEXIBLE CONVENTIONAL NC TECHNOLOGY THE EXAMPLE FROM INDUSTRY	79
Popp, I.O.: SOMES ASPECTS REGARDING THE MAINTENANCE OF BEARINGS	83
Šooš, E., Križan, P., Matúš, M.: OPTIMIZATION OF THE SPINDLE-BEARING SYSTEM	87

Section C: METROLOGY, QUALITY, FIXTURES, METAL CUTTING TOOLS AND TRIBOLOGY

Antić, A., Šarić, T., Živković, A.: ANALYSIS ON THE METHOD AND DEVELOPMENT OF THE MODEL FOR THE TOOL WEAR CONDITION MONITORING SYSTEM	93
Assenova, E., Kandeve, M.: TRIBOLOGY and SELF-ORGANIZATION	97
Beju, L.D., Zeljković, M., Navalušić, S.: STRATEGIES FOR IMPROVING THE AGILITY LEVEL IN THE MANUFACTURING BEARING INDUSTRY	101
Benkó, P., Peták, T.: STRAIGHTNESS MEASUREMENT OF LINEAR MOTION GUIDES	105
Borojević, S. , Jovišević, V.: SELECTION AND CONFIGURATION OF MODULAR COMPONENTS FOR MODULAR FIXTURE DESIGN	109

Bouzakis, K.-D., Skordaris, G., Gerardis, S., Bouzakis, E.: ADVANCED ANALYTICAL-EXPERIMENTAL PROCEDURES FACILITATING THE EFFECTIVE APPLICATION OF MICRO-BLASTING ON COATED TOOLS CONSIDERING AMONG OTHERS THE FILM BRITTLINESS	115
Jakovljevic, Z.: POINT CLOUD REDUCTION USING SUPPORT VECTOR MACHINES	121
Koldžin, D., Medić, V.: HOW THE OPEN INNOVATION CONCEPT AFFECT THE INNOVATIVE ENTERPRISE STRATEGIES.....	125
Kravchenko, M.P., Nochvay, V.M., Polonsky, L.G, Melnic, A.L.: STATISTICAL ANALYSIS OF THE QUALITY OF SURFACE COATED PARTS (DEPENDENCE OF ROUGHNESS OF MACHINING ALLOWANCE AND CUTTING MODES).....	129
Krecu, D., Sovilj-Nikić, I., Sovilj, B., Gajić, V., Legutko, S., Varga, Gy.: ANALYSIS OF TOPOGRAPHY OF CYLINDERS MACHINED BY CUTTING TOOLS.....	133
Kukuruzović, D., Berić, J., Kakaš, D., Škorić, B., Kovačević, L., Terek, P., Miletić, A., Vilotić, M.: APPLICATION OF A NEW DEVICE FOR MEASURING HARD COATINGS THICKNESS UNIFORMITY APPLIED ON LARGE SIZE TOOLS	137
Kukuruzović, D., Blagojević, D., Kakaš, D., Škorić, B., Kovačević, L., Terek, P., Miletić, A., Vilotić, M.: THE EFFECTS OF CUTTING PARAMETERS AND TOOL WEAR ON THE ROUGHNESS OF MACHINED SURFACE.....	141
Kuzinovski, M., Tomov, M., Cichosz, P.: INVESTIGATION OF GAUSSIAN AND 2RC FILTRATION IN SURFACE ROUGHNESS MEASUREMENT FROM THE STANDPOINT OF AMBIGUITIES IN STANDARDS. PART I-THEORETICAL ANALYSIS.....	145
Morača, S., Milin, D.: CLUSTERS AND NETWORK VALUE SYSTEM	149
Nemedi, I., Hadzistevic, M., Hodolic, J., Sekulic, M., Todic, V.: BASIS OF MODEL DEVELOPMENT FOR REAL FORM DETERMINATION OF ROUNDNESS MEASURING OBJECTS	153
Penfold, N.: INNOVATIONS IN TOUCH-TRIGGER PROBE SENSOR TECHNOLOGY	157
Peták, T., Benkó, P.: CALIBRATION OF THE LENGTH MEASURING MACHINE.....	163
Radlovački, V., Delić, M., Kamberović, B., Vulcanović, S., Hadžistević, M.: HOW MANAGERS ESTIMATE MANAGEMENT SYSTEMS TODAY IN SERBIA	167
Reibenschuh, M., Zuperl, U., Cus, F., Irgolic, T.: NEW USER INTERFACE FOR DETECTING EDGE WEAR ON CUTTING TOOLS	171
Savic, B., Slavkovic, R., Veg, E., Urosevic, V., Vlajković, H.: USE OF VIRTUAL AND ACTUAL VIBRO-DIAGNOSTICS FOR BETTER CONDITION MONITORING	175
St. Sekulic, S., Nikolic, B.: PROGNOSIS OF RELIABILITY AND MEAN TIME TO FAILURE OF CUTTING TOOL IN FUNCTION OF CUTTING CONDITION OF ELEMENTS IN TURNING.....	179
Šešlija, D., Dudić, S., Milenković, I.: COST EFFECTIVENESS T OF PRESSURE REGULATION ON RETURN STROKE OF PNEUMATIC ACTUATORS	183

Tomov, M., Kuzinovski, M., Cichosz, P.: INVESTIGATION OF GAUSSIAN AND 2RC FILTRATION IN SURFACE ROUGHNESS MEASUREMENT FROM THE STANDPOINT OF AMBIGUITIES IN STANDARDS. PART II - EXPERIMENTAL ANALYSIS	187
Tsiafis, I., Bouzakis, K.-D., Xanthopoulou, M., Tsolis, G., Xenos, Th.: ANALYSIS OF ROLLER BEARINGS' VIBRATION SIGNALS BY HILBERT – HUANG TRANSFORM AS DIAGNOSTIC TOOL.....	193
Vrba, I., Hadžistević, M., Palenčar, R., Lenčič, I.: OVERVIEW OF STANDARDS AND GUIDELINES WHICH DEFINE EVALUATION OF THE MEASUREMENT UNCERTAINTY IN MEASUREMENT OF FREEFORM SHAPED PARTS AT CMM	197
Zuperl, U., Cus, F.: FIXTURE ANALYSIS MODULE, AN ESSENTIAL ELEMENT OF THE INTELLIGENT FIXTURING SYSTEM.....	203
Section D: AUTOMATIC FLEXIBLE TECHNOLOGICAL SYSTEMS, CAX AND CIM PROCEDURES AND SYSTEMS	
Andrejkovič, M., Hajduová, Z., Schwartzová, H.: USE OF OPTIMIZATION TECHNIQUES IN A SELECTED ENTERPRISE	207
Andrejkovič, M., Hajduová, Z., Majerník, M., Bosák, M.: ASSEMBLY OF STRUCTURAL COMPONENTS OF A BUS.....	211
Bojanić, M., Tabaković, S., Milojević, Z., Zeljković, M.: PROCESSING OF DIAGNOSTIC IMAGES OF THE SKELETAL SYSTEM	215
Erić, M., Tadić, B., Stefanović, M., Miljanić D.: MODEL OF REENGINEERING OF TECHNOLOGICAL PROCESSES - ITERATIVE AND VISUAL APPROACH	219
Fuerstner, I., Gogolak, L., Nemedi, I.: DIFFERENT SOLUTIONS FOR A SPECIFIC MECHATRONICS PROJECT	223
Globočki – Lakić, G., Sredanović, B., Čiča, Đ., Milutinović, A.: APPLICATION OF CAD/CAM SYSTEMS FOR MACHINING OF PARTS OF ALUMINIUM PROFILES	227
Jahn, M., Luttmann, A., Schmidt, A.: A FEM SIMULATION FOR SOLID-LIQUID-SOLID PHASE TRANSITIONS DURING THE PRODUCTION OF MICRO-COMPONENTS	231
Jovanovic, V., Wang, H.: MECHATRONICS AND ITS APPLICATIONS IN TRANSPORTATION.....	235
Košarac, A., Zeljković, M.: SIMULATION OF PROCESS CONTROLLED BY PROGRAMMABLE LOGIC CONTROLLER PLC IN THE VIRTUAL REALITY ENVIRONMENT.....	239
Lukić, D., Todić, V., Zeljković, M., Milošević, M., Vukman, J., Jovičić, G.: THE POSSIBILITY AND SIGNIFICANCE OF APPLICATION STEP-NC STANDARD IN THE INTEGRATION OF CAD/CAPP/CAM AND CNC SYSTEM.....	243
Mansour, G., Sagris, D., Tsiafis, Ch., Mitsi, S., Bouzakis, K.-D.: EVOLUTION OF A HYBRID METHOD FOR INDUSTRIAL MANIPULATOR DESIGN OPTIMIZATION.....	247

Miletić, O., Todić, M.: SYNTHESIS OF AUTOMAT FOR GUIDANCE OF THE BAND IN PROCESSING SYSTEM OF MULTIPLE OPERATION PROCESS	251
Milojević, Z., Navalušić, S., Zeljković, M., Vičević, M., Beju, L.: EXTENSION OF THE PROGRAM SYSTEM FOR NC MACHINING PROGRAM VERIFICATION WITH HAPTIC DEVICE.....	255
Milutinovic, D., Slavkovic, N., Kokotovic, B., Milutinovic, M., Zivanovic, S., Dimic, Z.: KINEMATIC MODELING OF RECONFIGURABLE PARALLEL ROBOTS BASED ON DELTA CONCEPT.....	259
Mircheski, I., Kandikjan, T.: DESIGN FOR DISASSEMBLY METHODOLOGY FOR DETERMINATION OF OPTIMAL DISASSEMBLY SEQUENCE BASED ON CONTACT RELATIONS BETWEEN COMPONENTS AND FASTENERS IN THE PRODUCT ASSEMBLY	263
Mladenovic, G., Popovic, M.: MODELLING, CALCULATIONS AND TESTING OF SINGLE GIRDER BRIDGE CRANE AND CRANE RAILS.....	269
Nikolic, N., Lukic, Lj., Vranjevac, I., Djapic, M.: USE OF SIMULATION SOFTWARE IN PRODUCTION TECHNOLOGIES.....	273
Novak-Marcincin, J., Barna, J., Torok, J.: ADVANCED AUGMENTED REALITY APPLICATIONS IN THE PRODUCTION PROCESSES.....	277
Petrović, P.B., Lukić, N., Danilov, I., Miković, V.: CANONISATION OF ACTUATION STIFFNESS MATRIX IN KINEMATICALLY REDUNDANT INDUSTRIAL HUMANOID ROBOTS	281
Petrović, M., Miljković, Z., Babić, B.: OPTIMIZATION OF OPERATION SEQUENCING IN CAPP USING HYBRID GENETIC ALGORITHM AND SIMULATED ANNEALING APPROACH	285
Stevanović, D., Korunović, N., Trajanović, M., Trifunović, M., Milovanović, J., Stojković, M.: FINITE ELEMENT MODEL OF HUMAN TIBIA AND PRELIMINARY ANALYSIS	289
Todić, V., Lukić, D., Milošević, M., Jovičić, G., Vukman, J.: MANUFACTURABILITY OF PRODUCT DESIGN REGARDING SUITABILITY FOR MANUFACTURING AND ASSEMBLY (DfMA)	293
Topčić, A., Cerjaković E., Herić, M.: SIMULATION OF RELOADING SEGMENTS OF INTERNAL TRANSPORTATION SYSTEMS BY ARTIFICIAL NEURAL NETWORKS	297
Vuković, N., Miljković, Z., Mitić, M., Babić, B., Lazarević, I.: AUTONOMOUS NAVIGATION OF AUTOMATED GUIDED VEHICLE USING MONOCULAR CAMERA.....	301
Zadnik, Ž., Karakašić, M., Čok, V., Kljajin, M., Duhovnik, J.: IMPLEMENTATION MATRIX OF FUNCTION AND FUNCTIONALITY IN PRODUCT DEVELOPMENT PROCESS	305
Zeljković, M., Živković, A., Blanuša, V.: THERMAL-ELASTIC BEHAVIOR OF A MAIN SPINDLE ASSEMBLY WITH DOUBLE ROW CYLINDRICAL ROLLER BEARINGS.....	309

Section E: MECHANICAL ENGINEERING AND ENVIRONMENTAL PROTECTION

Arsovski, S., Lazić, M., Krivokapić, Z., Tadić, D., Grubor, S.: AN APPROACH TO DEFINE OPTIMAL TECHNOLOGY PORTFOLIO OF ELV RECYCLING	315
Avdic, N., Goletic, S.: SELECTION CRITERIA FOR CLEAN WATER DECENTERS OF SBR WASTEWATER TREATMENT PLANTS	319
Badida, M., Bartko, L., Králiková, R., Sobotová, L.: RESEARCH OF SELECTED ACOUSTIC DESCRIPTORS OF THREE LAYER SANDWICH ABSORBERS	323
Dzoganova, Z., Badida, M.: IMPACT ASSESSMENT OF MECHANICAL PROPERTIES OF DEGRADED PET BOTTLES IN ENVIRONMENTAL DEGRADATION OF HIGHER TEMPERATURE.....	329
Fedorčáková, M., Šebo, J.: THE RESULTS OF APPLICATION OF WASTEWATER BY NEW DEVELOPING ELECTROLYTIC FLOTATION METHODS	333
Georgiadis, P.: DYNAMIC DECISION SUPPORT SYSTEM FOR PLANNING AND CONTROL IN CLOSED-LOOP RECYCLING NETWORKS	335
Goletić, Š., Imamović, N.: IMPACT OF STEEL PRODUCTION TECHNOLOGY ON ENVIRONMENT	339
Hroncová, E., Ladomerský, J.: MODEL FOR EVALUATION OF CO-COMBUSTION OF COMPOSTED SEWAGE SLUDGE	343
Hronec, O., Vilček, J., Adamišín, P., Andrejovský, P., Huttmanová, E.: USE OF PHRAGMITES AUSTRALIS (CAV.) TRIN AND ITS REPRODUCTION IN THE REVITALIZATION OF CONTAMINATED SOILS	347
Kheifetz, M., Pynkin, A., Pozilova, N., Prement, G., Klimenko, S.: DESIGN DECISIONS DURING MODELLING TRANSFER OF QUALITY PARAMETERS IN LIFE CYCLE OF MACHINE DETAILS	353
Kovács, P.V., R., Beszédes, S., Ludányi, L., Hodúr, C., Szabó, G.: DEVELOPMENT OF A CONTINUOUS FLOW MICROWAVE TOROIDAL CAVITY RESONATOR	357
Križan, P., Matuš, M., Šooš, E.: DESIGN OF PRESSING CHAMBER OF BRIQUETTING MACHINE WITH HORIZONTAL PRESSING AXIS	361
Maňko, M., Košíková, A.: ISO 50001 AS THE BASIS FOR IMPLEMENTING AN ENVIRONMENTAL MANAGEMENT SYSTEM.....	365
Milanković, D., Milanović, B., Agarski, B., Crnobrnja, B., Ilić, M., Kosec, B., Budak, I.: LIFE CYCLE ASSESSMENT OF AN INTERMODAL STEEL BUILDING UNIT IN SERBIA	369
Muránsky, J.: DETERMINATION OF THE OPTIMAL PRODUCTION VOLUME RESPECTING THE ENVIRONMENTAL AND ECONOMIC CRITERIONS	373
Petelj, A., Hadžistević, M., Antić, A., Hodolič, J.: DETERMINATION OF ABSORPTION COEFFICIENT OF SAMPLE UNDER NON-LABORATORY CONDITIONS.....	377

Sabolová, J., Fedorčáková, M.: HYDRODYNAMIC MODELING OF FLOOD EVENTS IN SELECTED AREA	381
Šebo, J., Fedorčáková, M.: ECONOMIC OPTIMIZATION OF RECYCLING ORIENTED DISASSEMBLY OF CONSUMER ELECTRONICS: THE CASE STUDY OF MOBILE PHONE.....	385
Sekulić, M., Hadžistević, M., Kovač, P., Gostimirović, M., Jurković, Z.: CURRENT TRENDS IN SUSTAINABLE PRODUCT DESIGN	391
Simonovic, S.: BOTH LEANER AND CLEANER PRODUCTION BY PRODUCT DESIGN	395
Tichá, M., Budak, I.: LCA APPLICATION IN EPD AND ECO-EFFICIENCY	399
Vasiliev, A., Borodavko, V., Kroutko, V., Kheifetz, M., Gaiko, V.: FORMATION OF QUALITY PARAMETERS IN LIFE CYCLE OF MACHINE DETAILS ON THE BASIS OF TECHNOLOGICAL INHERITANCE	403
Vlčej, J., Milanović, B., Milanković, D., Hodolič, J.: IMPLEMENTATION OPTIONS OF LCA METHOD IN PRACTICE IN SLOVAK REPUBLIC	407
Vojinović Miloradov, M., Šenk, N., Okuka, M., Turk Sekulić, M., Radonić, J.: POLYPARAMETER MODEL FOR DEFINING PARTITIONING PROCESSES OF SEMIVOLATILE ORGANIC COMPOUNDS	411

Section F: OTHER PRODUCTION ENGINEERING TECHNOLOGIES

Alexandrov, S., Lyamina, E., Manabe, K.: A THEORETICAL STUDY ON SURFACE ROUGHING IN PURE BENDING OF VISCOPLASTIC SHEETS.....	415
Božičković, Z., Dobraš, D., Božičković, R.: ELIMINATION OF PERMANENT DEFORMATIONS IN THE LONGITUDINAL WELDING PROCESS OF CONICAL PIPES WITH ONE SEAM	419
Brkljač, N., Simić, R., Kovač, P., Brkljač, B.: FEM IN FUNCTION OF PNS - APPLIED IN DERIVING APPROXIMATE FORMULA FOR CALCULATION OF THEORETICAL SCF IN BUTT WELD JOINTS	423
Brüning, H., Vollertsen, F.: SELF-ALIGNING CAPABILITY OF LASER BASED FREE FORM HEADING PROCESS	427
Deželak, M., Stepišnik, A., Pahole, I., Ficko, M.: METHODS FOR SPRINGBACK PREDICTION AND COMPENSATION	431
Ivanisevic, A., Milutinovic, M., Skakun, P., Movrin, D., Kacmarcik, I., Plancak, M., Vilotic, D., Alexandrov, S.: EXPERIMENTAL DETERMINATION OF FORMING LIMIT DIAGRAM FOR BRASS.....	435
Jovanic, D., Jovanovic, M. ECONOMIC EFFICIENCY OF WELDING SIMULATOR USE FOR WELDING PERONNEL TRAINING	439
Jovanovic, V., Langraudi, N., Tomovic, M. M.: BOND GRAPH THEORY AND ITS USE FOR HYDRAULIC SYSTEM MODELING	443
Karpe, B., Kosec, B., Gojić, M., Anžel, I., Kitak, S., Bizjak, M.: MATHEMATICAL MODELING OF THE MELT COOLING RATE IN THE MELT-SPINNING PROCESS	447

Krašnik, M., Vilotić, D., Šidanin, L., Petrović, Ž.: INITIAL MICROSTRUCTURE STATE IMPACT TO STEEL C45E FORMABILITY	453
Kuzman, K., Kacmarcik, I., Pepelnjak, T., Plancak, M., Vilotic, D.: EXPERIMENTAL CONSOLIDATION OF ALUMINIUM CHIPS BY COLD COMPRESSION.....	459
Nedić, B., Jovanović, D., Marušić, V.: SOME SCRATCH TEST RESEARCH RESULTS Zn COATINGS	463
Neugebauer, R., Voelkner, W., Mauermann, R., Israel, M.: CLINCHING IN STEEL AND RAILWAY CONSTRUCTION, SHIPBUILDING AND COMMERCIAL VEHICLES	467
Novak-Marcincin, J., Novakova-Marcincinova, L.: PRODUCTION OF PARTS REALIZED BY FDM RAPID PROTOTYPING TECHNOLOGY AND THEIR TESTING	473
Plancak, M., Stefanovic, M., Pecelj, Dj., Mihajlovic, G., Vilotic, D., Ivanisevic, A.: INFLUENCE OF PROCESS PARAMETERS ON LOAD REQUIREMENT IN ORBITAL FORGING OPERATIONS	477
Radić, N., Jeremić, D.: INVESTIGATION THE INFLUENCE OF ELASTIC MEDIA ON THE BUCKLING NANOPLATE APPLYING NONLOCAL ELASTICITY THEORY	481
Rajnovic, D., Sidjanin, L.: THE DUCTILE TO BRITTLE TRANSITION TEMPERATURE OF UNALLOYED ADI MATERIAL	485
Skakun, P., Plančak, M., Vilotić, D., Lužanin, O., Milutinović, M., Movrin, D.: MANUFACTURING OF GEAR-LIKE COMPONENTS BY METAL FORMING – POSSIBILITIES AND LIMITATIONS	489
Topčić, A., Lovrić, S., Cerjaković, E.: COMPARATIVE ANALYSIS OF RE/RP VERSUS CONVENTIONAL APPROACHES OF TOOL DESIGNING IN SAND CASTING	493
Vilotić, M., Kakaš, D., Terek, P., Kovačević, L., Kukuruzović, D., Miletić, A.: SEVERE PLASTIC DEFORMATION BY COMPRESSION	497

Section G: BIO-MEDICAL ENGINEERING - CAx

Matin, I., Markovic, D., Puskar, T., Hadzistevic, M., Hodolic, J., Vukelic, Dj., Potran, M.: RECONSTRUCTION OF THE DENTAL CAD MODEL.....	501
Petrović, S., Matić, A., Devedžić, G., Ristić, B., Čuković, S.: DIFFERENCES IN TIBIAL ROTATION AND TRANSLATION IN ACL DEFICIENT AND HEALTHY KNEES	505
Puskar, T., Jevremovic, D., Eggbeer, D., Lapcevic, A., Trifkovic, B., Vukelic, D., Williams, R.J.: DETERMINATION OF CORROSION CHARACTERISTICS OF DENTAL ALLOY BY INDUCTIVELY COUPLED PLASMA MASS SPECTROMETRY	509
Radulović, J., Mijailović, N., Trajanović, M., Filipović, N., Radulović, N.: ESTIMATION OF EXPOSURE DOSE OF HUMAN HEAD DURING CT SCANNING PROCEDURE USING MONTE CARLO SIMULATION	513
Raspudic, V.: KINEMATIC ANALYSIS OF LOWER EXTREMITIES IN CAD ENVIRONMENT.....	517

Tabaković, S., Zeljković, M., Živković, A., Grujić, J.: DEVELOPMENT OF THE ENDOPROSTHESIS OF THE FEMUR ACCORDING TO THE CHARACTERISTICS OF A SPECIFIC PATIENT	521
Trajanović, M., Tufegdžić, M., Arsić, S., Veselinović, M., Vitković, N.: REVERSE ENGINEERING OF THE HUMAN FIBULA	527
Uzelac, M., Vilimonović, M.: BASIC PRINCIPLES OF THE USE OF CONE BEAM CT DEVICE IN RADIOLOGY OF A PATIENT'S CRANIOFACIAL REGION	531
Vilotić, M., Lainović, T., Kakaš, D., Blažić, L., Marković, D., Ivanišević, A.: ROUGHNESS ANALYSIS OF DENTAL RESIN-BASED NANOCOMPOSITES	535
Vitković, N., Veselinović, M., Mišić, D., Manić, M., Trajanović, M., Mitković, M.: GEOMETRICAL MODELS OF HUMAN BONES AND IMPLANTS, AND THEIR USAGE IN APPLICATION FOR PREOPERATIVE PLANNING IN ORTHOPEDICS	539
Williams, R.J., Eggbeer, D., Lapcevic, A., Trifkovic, B., Puskar, T., Budak, I., Jevremovic, D.: RE-CAD/CAM APPROACH IN DESIGN AND MANUFACTURING OF DENTAL CERAMIC CROWNS IN COMBINATION WITH MANUAL INDIVIDUALIZATION.....	543
AUTHOR INDEX	547
INFORMATION ABOUT DONATORS	551

11th INTERNATIONAL SCIENTIFIC CONFERENCE
MMA 2012 - ADVANCED PRODUCTION TECHNOLOGIES

PROCEEDINGS



Section A:
METAL CUTTING

Novi Sad, 20-21 September 2012

Baralić, J., Nedić, B.

THE EFFECT OF ABRASIVE WATER JET CUTTING PARAMETERS ON KERF GEOMETRY

Abstract: Kerf geometry is a characteristic of major interest in abrasive water jet cutting. The irregularities in kerf geometry significantly affect limitation on the application of the abrasive water jet cutting. The effect of abrasive water jet cutting parameters on cutting performance is characterized by kerf width and kerf taper. All of the independent abrasive water jet cutting parameters affects kerf width and kerf taper. Those parameters are operating pressure, abrasive mass flow and traverse speed. The aim of this paper is to investigate the effect of machining parameters on kerf geometry. Č4580 (AISI 304) was machined by abrasive water jet under varying traverse speeds, water jet operating pressures and abrasive mass flow rates. The machined kerfs were examined. The research results show that as traverse speed increases, the kerf is narrower. Also, increase in water jet pressure is associated with an increased kerf width.

Key words: abrasive water jet cutting, kerf width, kerf taper

1. INTRODUCTION

The requirements regarding the accuracy of shape and dimensions of the processing part are becoming more stringent today. Also, in terms of contour cutting of materials, regarding the complexity of the contours, the requirements are more complex. Therefore, unconventional machining methods have been more frequently applied in modern production.

Abrasive water jet processing technology is one of the most recent unconventional methods used for materials processing in industry. Abrasive water jet processing technology offers many advantages compared to traditional and other non-traditional processing technologies; no thermal distortion, high machining versatility, minimum stresses on the work piece, high flexibility and small cutting and clamping forces. [1] Also, abrasive water jet processing has some disadvantages; a disparity in quality of the machined surface and kerf taper. Therefore this paper presents the effect of abrasive water jet cutting parameters such as operating pressure, traverse speed and abrasive mass flow rates.

2. KERF GEOMETRY

The quality of the machined surface is a complex concept which includes changes of characteristics of material, structure, and size of the defect layer, roughness of the machined surface and geometrical characteristics of the cut. The quality of some cutting process can be evaluated through measuring certain characteristics such as roughness of the machined surface, through satisfying demands of tolerance, parallelism of the cut sides and their normality to the base surface. When processing with abrasive water jet, the workpiece accuracy depends on the kerf geometry. Kerf geometry is a characteristic of major interest in abrasive water jet processing.

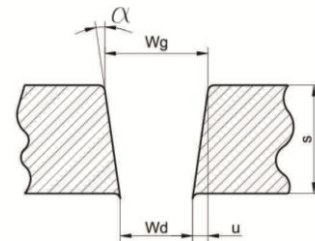


Fig. 1. The kerf geometry

The kerf geometry of a through cut generated by abrasive water jet is characterized by a small rounded corner at the top edge due to the plastic deformation of material caused by jet hitting the surface of the workpiece and small burr at the bottom edge, fig.1. As the kerf is wider at the top than at the bottom, the taper is produced. The kerf taper is usually defined with two parameters; u and α , fig.1.

$$u = \frac{W_g - W_d}{2} \quad (1)$$

$$\alpha = \arctg \frac{u}{s} \quad (2)$$

W_g – width of the kerf on the top
 W_d – width of the kerf on the bottom
 s – thickness of the workpiece

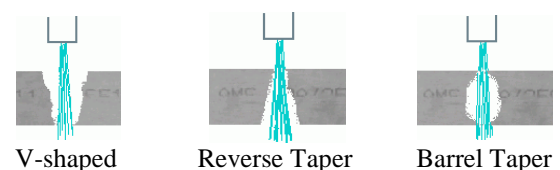


Fig. 2. The different types of kerf taper[2]

Figure 2. shows the appearance of the different types of kerf taper.

V-shaped taper is where the top of the kerf is wider than the bottom. It is the most common type of the kerf taper. This type occurs because cutting energy of the abrasive water jet is larger at the top of the kerf than at the bottom. This kerf taper is more pronounced with increase of the traverse speed, fig. 3.

Reverse taper is where the top of the kerf is narrower than the bottom. This type occurs when traverse speed is very low. Also, it occurs when machined material is very soft.

Barrel taper is where the middle is wider than the top or the bottom. Barrel taper occurs when machined material is very thick.

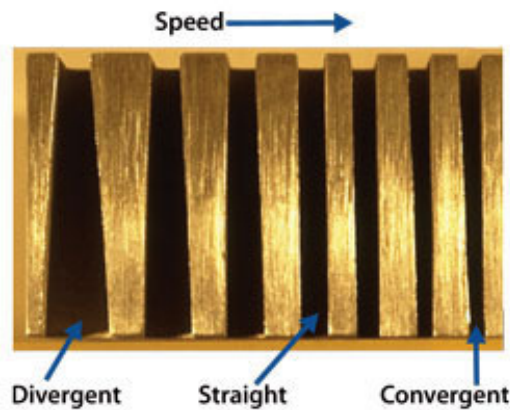


Fig. 3. The kerf geometry for different traverse speed [2]

Figure 3. shows the appearance of the kerf depending on the change of traverse speed. For very low traverse speed bottom of the kerf is wider than the top. It is because abrasive water jet stream expands at the bottom of the kerf and removes more material at the bottom than at the top. With increase of traverse speed, top of the kerf becomes wider, and at the one moment, for specific values of traverse speed, sides of the kerf are parallel. With further increase of traverse speed, top of the kerf becomes wider of the bottom of the kerf.

3. EXPERIMENTAL WORK

All irregularities on the machined surface, obtained either by the standard or unconventional treatment processes (laser, plasma, abrasive water jet), are machined surface characteristics, and they are precisely standardized [3]. The aim of this study is to experimentally investigate the influence of operating pressure, abrasive flow rate and traverse speed on kerf geometry.

The experiment was conducted on a PTV Abrasive Water Jet machine, equipped with a multiplier 60K (pressure up to 4130 bar).

Table 1. shows the values of abrasive water jet cutting parameters for each specimen. The other cutting parameters were kept constant. Abrasive type was garnet, MASH#80, stand off distance was 3mm. The specimens were of 20mm thick stainless steel Č4580 (AISI 304).

Specimen number	Traverse speed V[mm/min]	Operating pressure P[bar]	Abrasive flow rate Qa [g/min]
1.	50	2700	400
2.	50	3200	400
3.	50	3800	400
4.	50	4130	400
5.	50	4130	200
6.	50	4130	250
7.	50	4130	300
8.	50	4130	350
9.	50	4130	400
10.	30	4130	400
11.	50	4130	400
12.	70	4130	400
13.	90	4130	400
14.	110	4130	400

Table 1.

Figure 4. shows the appearance of kerf geometry of 20mm thick Č4580 for different operating pressures, specimens 1 to 4.

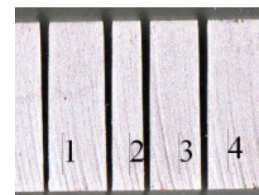


Fig. 4. The kerf geometry for different operating pressures

Figure 5. shows the appearance of kerf geometry of the same 20mm thick Č4580 for different abrasive flow rates, specimens 5 to 9.

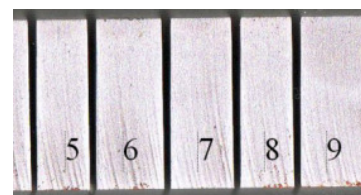


Fig. 5. The kerf geometry for different abrasive flow rates

Figure 6. shows the effect of the traverse speed on the kerf geometry, for 20mm thick Č4580, specimens 10 to 14.



Fig. 6. The kerf geometry for different traverse speed

The kerf geometry (top and bottom kerf widths) was measured from the optical microscope images. The measurements are accurate to 0.01 mm. The results of measurement are given in table 2.

Specimen number	Wd[mm]	Wg[mm]	u[mm]	α [°]
1.	0.642	1.104	0.231	0.662
2.	0.689	1.118	0.2145	0.614
3.	0.754	1.130	0.188	0.538
4.	0.865	1.137	0.136	0.3896
5.	0.732	1.090	0.179	0.513
6.	0.820	1.153	0.1665	0.477
7.	0.811	1.119	0.154	0.441
8.	0.766	1.116	0.175	0.501
9.	0.809	1.153	0.172	0.493
10.	0.995	1.133	0.069	0.198
11.	0.883	1.125	0.121	0.347
12.	0.764	1.060	0.148	0.424
13.	0.651	1.075	0.212	0.607
14.	0.628	1.072	0.222	0.636

Table 2.

The results from Table 2 are shown on the following diagrams.

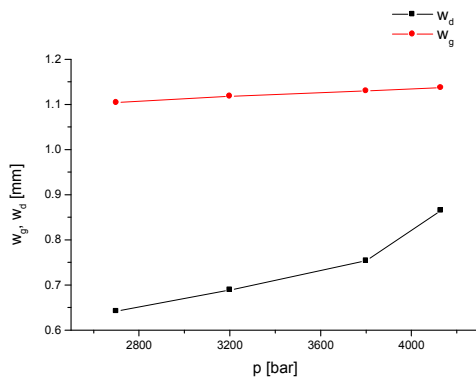


Fig. 7. Operating pressure influence on width of the kerf

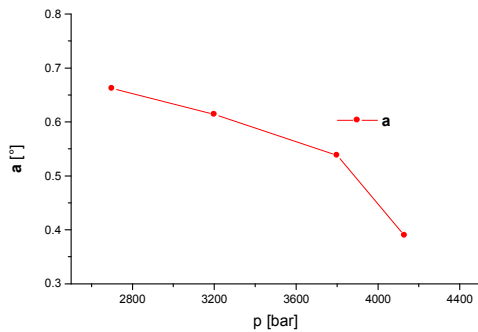


Fig. 8. Operating pressure influence on the kerf taper

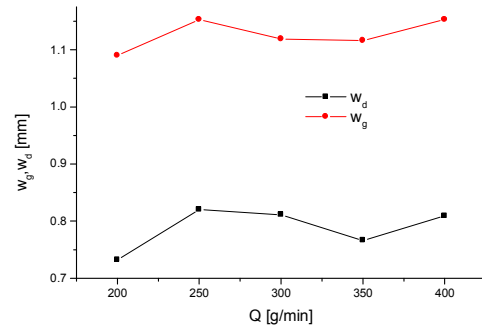


Fig. 9. Abrasive flow rate influence on width of the kerf

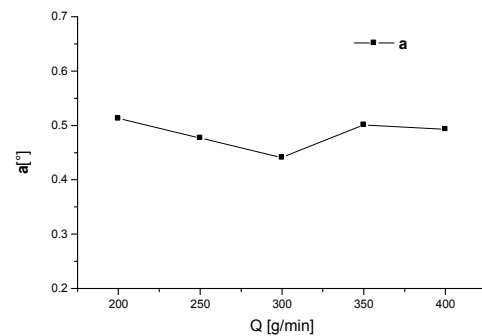


Fig. 10. Abrasive flow rate influence on the kerf taper

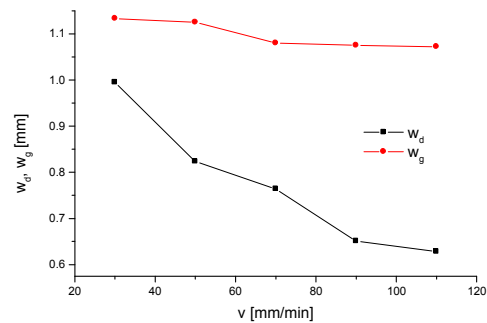


Fig. 11. Traverse speed influence on width of the kerf

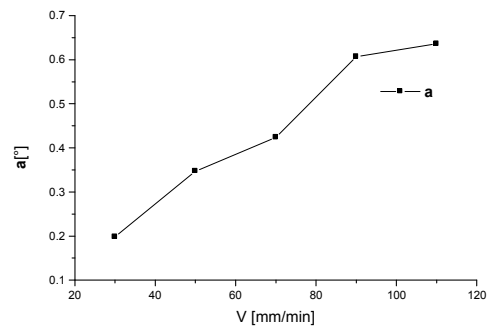


Fig. 12. Traverse speed influence on the kerf taper

Figures 7. and 8. shows influence of operating pressure on the kerf geometry. Increase of operating pressure results in increase of the width of the kerf. Increase of the bottom kerf width is more significant. With increase of the operating pressure, kerf taper

decreases.

Figures 9. and 10. shows influence of the abrasive flow rate on the kerf geometry. There cannot be established a strong correlation between abrasive flow rate and changes in the kerf geometry.

Figures 11. and 12. shows influence of the traverse speed on the kerf geometry. Increase of the traverse speed influences decrease of the width of the kerf. Decrease of the bottom kerf width is more significant than decrease of the top width of the kerf. Increase of traverse speed results in increase of the kerf taper.

4. CONCLUSION

This paper presents the results of the investigation concerning the effect of abrasive water jet cutting parameters on the kerf geometry. The effect of the operating pressure and the traverse speed is evident. The influence of the abrasive mass flow on the kerf geometry cannot be clearly determined.

The increase of operating pressure results in increase of the width of the kerf while increase of the traverse speed influences decrease of the width of the kerf. Changes in the bottom kerf width are more significant than changes of the top width of the kerf.

With increase of the operating pressure, kerf taper decreases. Increase of traverse speed results in increase of the kerf taper.

The basic goal of any processing is more accurate workpiece. When processing with abrasive water jet, the accuracy of workpiece is achieved by reducing the width of the kerf and kerf taper. This can be achieved by proper combination of the abrasive water jet cutting parameters. Special attention should be given to the selection of the operating pressure and traverse speed because they have the most significant influence on the kerf geometry. The best combination is processing with high values of operating pressure and low traverse speed.

ACKNOWLEDGMENTS

The authors would like to thank to the Ministry of Science and Technological Development of the Republic of Serbia. Paper is result of technological project TR35034: "The research of modern non-conventional technologies application in manufacturing companies with the aim of increase efficiency of use, product quality, reduce of costs and save energy and materials" which is supported by Ministry of Education and Science of the Republic of Serbia.

5. REFERENCES

- [1] Wang J.: *A study of abrasive waterjet cutting of metallic coated sheet steels*, International Journal of Machine tools and Manufacture, Vol.No.39, p.p.855-870, 1999.
- [2] <http://www.omax.com/>
- [3] Baralić, J., Nedić, B., Janković, P.: *The traverse speed influence on surface roughness in abrasive waterjet cutting applications*, Proceedings of the 12th International Conference on Tribology, SERBIATRIB, p.p. 349-353 Kragujevac, 11-13.05.2011.
- [4] Herghelegiu E., Radovanović M., Brabie G. , Tampu N.C.: *Influence of abrasive material quantity on surface quality generated by abrasive water jet operation*, International Journal of Modern Manufacturing Technologies, Vol. III, No. 2 ,p.p.43-48, 2011
- [5] Guo N.S., Louis G., Meier G.: *Surface structure and kerf geometry in abrasive waterjet cutting: Formation and optimization*, 7th American Waterjet Conf.,p.p. 1-25, Seattle, Washington, USA, 1993
- [6] Momber A.W., Kovacevic R.: *Principles of Abrasive Waterjet Machining*, Springer, London, 1998.
- [7] Janković P., Radovanović M.: *Identifikacija i klasifikacija faktora koji utiču na proces sečenja abrazivnim vodenim mlazom*, "IMK-14, istraživanje i razvoj, No. 35, Kruševac, Srbija, p.p. 71-76, 2/2010
- [8] Hashish M.: *Characteristics of surfaces machined with abrasive waterjets*, J. Eng. Mater. Technol. Trans. ASME, Vol. 113, No. 3, pp.336-354, 1991.

Authors:

M.Sc. Jelena Baralić, University of Kragujevac, Technical Faculty Čačak, Svetog Save 65, 32000 Čačak, Serbia

Prof. dr Bogdan Nedić, University of Kragujevac, Faculty of Engineering, Sestre Janjic Str. 6, 34000 Kragujevac, Serbia

E-mail: nedic@kg.ac.rs
jbaralic@tfc.kg.ac.rs

Beniak, J.

OPERATIONAL CHARACTERISTIC OF SHREDDING MACHINES

Abstract: *Shredding machines are one of important machines, in the field of biomass processing. These machines are responsible for preparation of different materials before final processing. Are the key point in production lines for briquetting and pelleting, but also in other areas of industry for preparation of materials in primary or secondary material processing. This paper deals with operational characteristics of shredding machines, which are important for correct and efficient machine running.*

Key words: *shredding, disintegration, shredding machines*

1. INTRODUCTION

Nowadays are the shredding machines widely used in primary production and material processing as well as in processing secondary raw material (secondary processing of materials for their further material or energy capitalizing). Shredding devices can be divided by different criteria and form of their utilization. Basic dividing of shredding machines is as follows [1], [2]:

Shredding machines can be divided by functional principle to:

-swing-hammer;	-jaw;	-granulating;
-impact;	-screw;	-cone;
-special;		

By number of rotors:

-single-rotor;	-two-rotor;	-multi-rotor;
----------------	-------------	---------------

By type of tool:

-monolithic;	-segmented;
--------------	-------------

By character of acting force:

-dynamic acting force;	-static acting force;
------------------------	-----------------------

By frequency of rotating:

-low-frequency;	-high frequency;
-----------------	------------------

By mobility:

-mobile;	-static;
----------	----------

By selected technical parameters:

-input power;	-hourly output;	-dimensions;
-feed opening;	-input and output fraction;	

2. MATHEMATICAL FORMULAS DESCRIBING CUTTING PROCESS

By verification of a mathematical model and by implementation of experimental coefficients could be obtained a real tool for practical calculations in the design of disintegration machine. Because there is currently no suitable software for calculation, the engineers are often forced to use only simple approximations and inaccurate calculations; eventually they modify the machines following the results of testing running. In the absence of such an instrument, designed machines are oversized or undersized. Our goal is to find in available literature the mathematical models that would be suitable as a basis to develop a mathematical model for the disintegration process. By analysis, comparison and experimental verification we

could adapt them and use for designing of disintegration machines. Analyzed mathematical models are based on different hypotheses [3]:

- **Matrix model of diminution** [4] – is used to create so-called disintegration schemes in the processing of rocks and simulations of these schemes;
- **Mathematical model for calculation of cutting forces** [5], [6] – based on mathematical models used to calculate the cutting forces in the sawing process of wood by disc tools;

Physical – Technological theory

By Briks [7] the cutting force is as follow:

$$F = K_1 hb + K_2 b = F_{\dot{\epsilon}} + F_{\text{chrb}} \text{ (N)} \quad (1)$$

where:

K_1, K_2	specific cutting resistance (MPa),
$F_{\dot{\epsilon}}$	force on face surface (N),
F_{chrb}	force on back surface (N),
h	chip thickness (mm),
b	width of the chip (mm).

The purpose of this deduction is that the cutting force consists of two components, one of which ($F_{\dot{\epsilon}}$) is directly proportional to the cross-section of the area of chip $b \cdot h$, the second (F_{chrb}) is directly proportional only to the width of the chip b . The Briks deductions are practically expression of space distribution of the forces:

- the forces causing above the level of new creating surface ($F_{\dot{\epsilon}}$),
- the forces causing bellow the level of new surface (F_{chrb}), whereby the level of new surface approximately passing the curvature centroid of edge.

The expression of this methodology is generalizing equation

$$F = K \cdot b \cdot h = F_{\dot{\epsilon}} + F_{\text{chrb}} \text{ (N)} \quad (2)$$

where $K = (K_1 + K_2/h)$ (MPa) is specific cutting resistance (MPa)

Empirical – Statistical theory

In summary can be stated, that physical – technological theory is currently the most sophisticated source of information for dimensioning of drives and also for designers of wood processing tools and machines (by distribution of cutting forces F to the tangential and radial component).

In generally [8], [9] applies to woodworking:

$$F = K \cdot b \cdot h \quad (\text{N}) \quad (3)$$

where: F – cutting force (N),
 K – specific cutting resistance (MPa),
 b – width of the chip (mm),
 h_t – chip thickness (mm).

This mathematics formula expresses the simple dependence, that general cutting force in wood dividing is function of specific cutting resistance and chip size.

By [10], [5] is the shear force in the shear process with parallel shearing tool, calculated by mathematical formula:

$$F = S \cdot \tau \quad (4)$$

where F – shear force (N),
 S – cross-sectional surface area of mat. (mm²),
 τ – strength of the material in shear (MPa).

Necessary shear force for shearing by shears with inclined top shearing tool, can be calculated by mathematical formula [10], [11]:

$$F = \frac{s^2 \cdot \tau}{2 \cdot \tan \varphi} \quad (\text{N}) \quad (5)$$

where: F – shear force (N),
 τ – strength of the material in shear (MPa),
 s – thickness of material (mm),
 φ – interaction angle (°).

For shearing with disc shear is given mathematic formula [10]:

$$F = \sigma_{pt} \cdot s^2 \left(\frac{0,4 \cdot \varepsilon_r}{\tan \varphi} + 0,7 \right) \quad (\text{N}) \quad (6)$$

Where: σ_{pt} – tensile strength of material (MPa),
 s – thickness of sheared material (mm),
 ε_r – (1,2 až 1,6) δ_s ,
 δ_s – relative slit, when shear of material occur (mm),
 φ – interaction angle (°).

3. QUANTITATIVE COMPARISON OF SELECTED MATHEMATICAL MODELS

In the following paragraph are mentioned values of forces, which have been calculated by selected mathematical formulas (tab. 1), mentioned in previous paragraph [12]. From these values should be obvious, how big are the value differences in force calculation for different (selected) way of force calculations (Fig. 1).

We used the same input values and coefficients, which we are able to figure out. In Tab. 1 and on Fig. 1 we can see considerable differences in calculated force values, which are necessary for disintegration of material sample, calculated by different ways by previous mentioned mathematical formulas.

On the Fig. 1 is markedly see, that result value of cutting force by mathematical formula (6) is significant different comparing to other calculated values.

From these significant differences is evident, that will be necessary to make, detail analysis of mentioned mathematical formulas and figure out most reliable mathematical model for calculation of necessary force in disintegrative process.

On the basis of analysis of mathematical models, we decided to use the mathematical formula (4) as a base for creating of new mathematical model, which will be describing the disintegrative process. In this research we will deal exclusively with wood material disintegration, accordingly also the mathematical formula will be created for using in wood processing.

Tab. 1 Values of cutting force

Type of mathematical formula	Equation No.	Force F (N)
General - wood processing	(3)	5 672
Shearing – parallel shear tool	(4)	4 400
Shearing – inclined shear tool	(5)	2 666
Shearing – dick shear tool	(6)	10 533

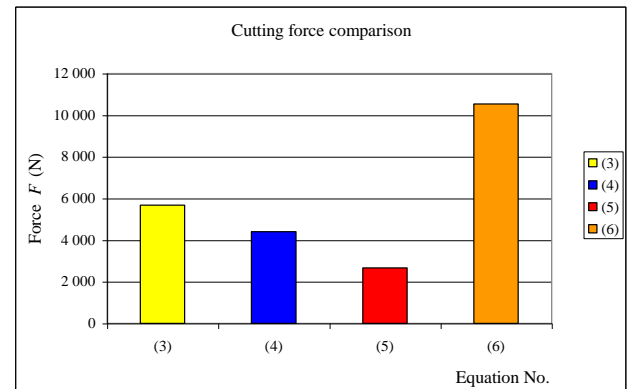


Fig. 1 Comparison of cutting forces

Next result from analysis is that if we want to investigate the influence of individual parameters, which have been mentioned in analysis, is necessary to design and manufacture the measuring stand of disintegrative device, which will allow change of biggest number of defined parameters.

4. PARAMETERS OF THE DISINTEGRATION PROCESS

On Institute of manufacturing systems, environmental technology and quality management we work on development of shredding machines and research of influence of different parameters (factors) on operating characteristics of device. For this purpose we designed and manufactured measurement stand of shredding (disintegrative) machine (Fig. 2).

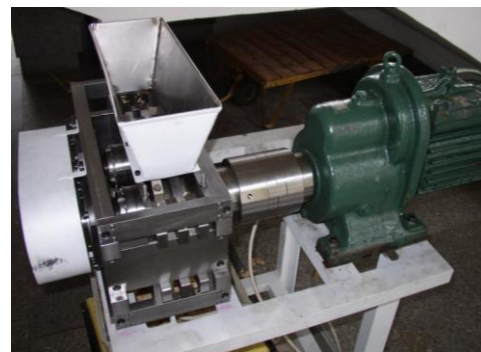


Fig. 2 Measurement stand of disintegrative machine [15]

This device allows setting and variation of several parameters, which relate with machine running. This is mainly concerned to geometrical, dimensional and operational parameters (factors), which can influence the loading of disintegrative machine in the running process.

Eight following factors (A, B, C, D, E, F, G, H) was selected, from which the first have two levels and others seven have three levels:

Factor A: distance between shafts a

Factor B: size of back-off angle α on disinteg. wedge

Factor C: frequency of shaft rotation n

Factor D: cross-sectional surface of disintegrated material S

Factor E: width of disintegrative wedge b

Factor F: size of cutting edge γ on disinteg. wedge

Factor G: moisture content of treated wood w

Factor H: height of disintegrative wedge h

Tab. 2 Description of factors levels for Taguchi experimental scheme L18

Factor	Level 1	Level 2	Level 3
A	165 mm	183 mm	-
B	0 °	10°	20°
C	25 ot/min	47 ot/min	75 ot/min
D	100 mm ²	200 mm ²	300mm ²
E	14mm	18mm	25 mm
F	-10 °	10 °	30 °
G	10%	25%	40%
H	16,5mm	25mm	34,5mm

Following these input parameters (factors) we could prepare experimental scheme.

If we want to make full experimental scheme, which have eight factors and three levels for each factor, we need in case of ten repeated measurements $N_c = 10 \times 3^8 = 65\ 610$ experiments.

For eight factors and two levels for each factor is necessary to perform $N_c = 10 \times 2^8 = 2\ 560$ experiments, in full experimental scheme.

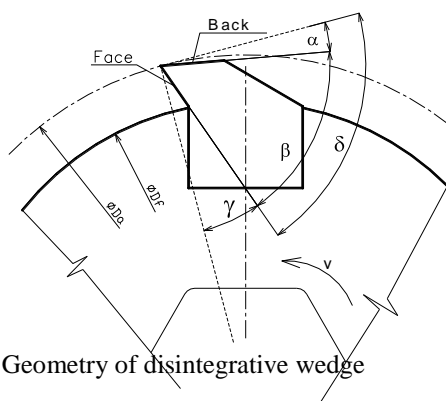


Fig. 3 Geometry of disintegrative wedge

To eliminate this high number of experiments we accede to design of experiment by Taguchi – DOE [13], [14]. For case reported in Tab. 2, when we have eight factors, from which one have two levels and seven have three levels, can be used Taguchi design of experiment L18 ($2^1 \times 3^7$), which dismiss interactions. For ten repeated measurements $q = 10$, so $N_c = 10 \times 18$

= 180 experiments.

The evaluation of such experiment is quite difficult, therefore is desirable to use software for evaluation by standard method ANOVA, or similar methods, for this purpose.

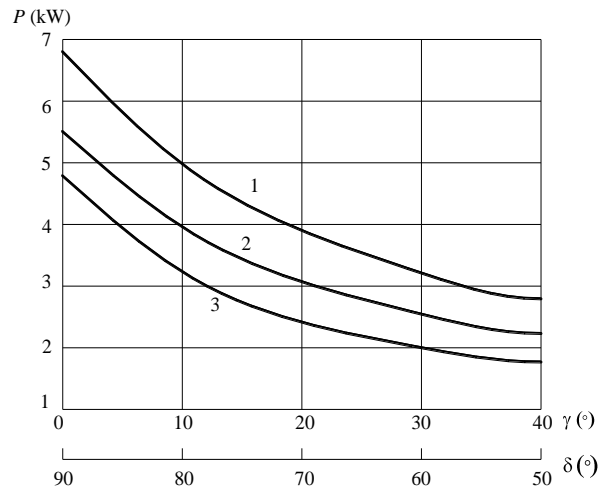


Fig. 4 Geometry impact of disintegrative tool to input power [4]: 1 – hardwood, 2, 3- softwood

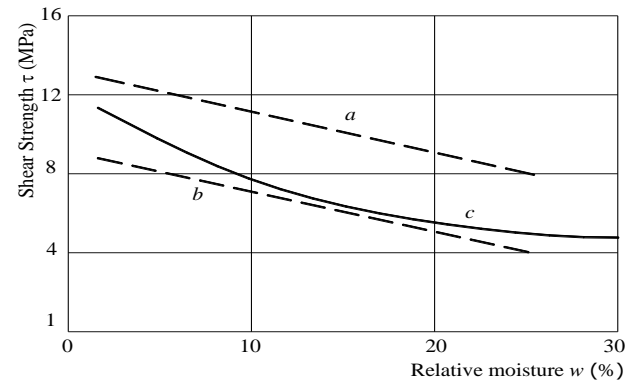


Fig. 5 Moisture and type of wood impact to shear strength of disintegrating material [5]: a,b – Swedish pine (Schlyter), c – spruce (Newlin)

5. EXPERIMENTAL MATHEMATICAL MODEL

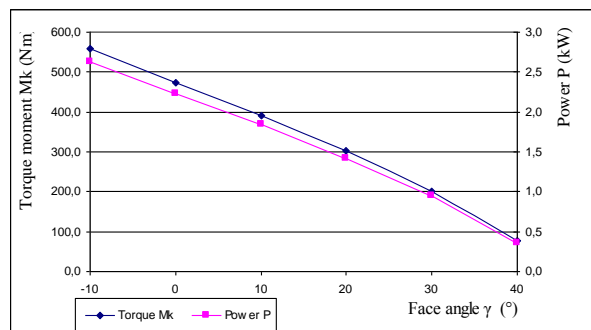


Fig. 6 Torque and input Power in relation to shredding face angle

Following the design of experiment [15] and performed experimental tests we confirm the work hypothesis, that size of disintegrative force is influenced by cutting edge angle, Shear strength of processed material, dimensions of input fraction and also dimensions of

disintegrative machine. The goal of experiment is verify this work hypothesis.

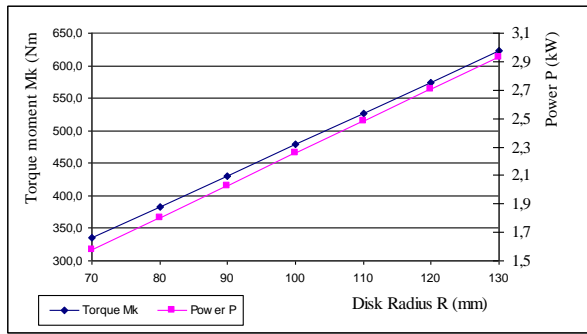


Fig. 7 Torque and input Power in relation to shredding disk radius

Influence of cutting edge angle γ in relation to size of torque moment, which is necessary for material processing, was measured. Following the results of measurement, the basic form of mathematical model describing the disintegrative process has been modified to mathematical formula:

$$M_k = \tau \cdot R \cdot S_m \cdot (1 - \tan \gamma) \quad (7)$$

$$F_{D1} = \tau \cdot S_m \cdot (1 - \tan \gamma) \quad (8)$$

where: M_k – torque moment (Nm), τ - shear strength of material (MPa), R – disintegrative disk radius (mm), S_m – disintegrative surface area (mm²), γ - face angle (°), F_{D1} – disintegrative force for single wedge (N).

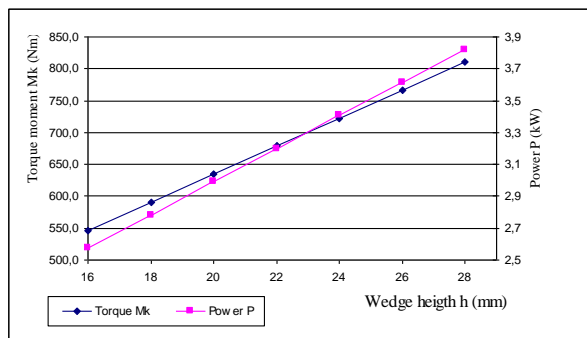


Fig. 8 Torque and input Power in relation to shredding face angle

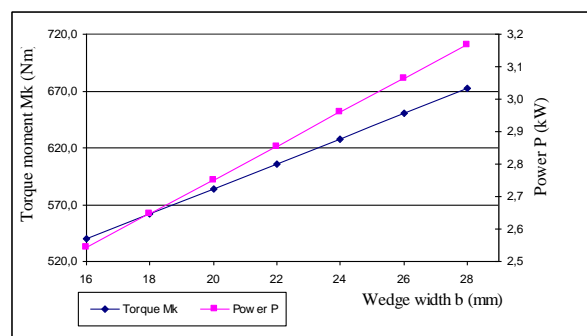


Fig. 9 Torque and input Power in relation to the shredding wedge width

6. CONCLUSION

The presented paper is the sum of the results obtained by experiments conducted by realized experiments on the measurement stand of disintegrative machine.

7. REFERENCES

- [1] Drviče. Názvoslovie., STN 72 9101, SÚTN, Bratislava 1975, s. 45
- [2] Beniák, J. *Efektívnosť dezintegrácie viacrotorových drviacich zariadení*, Recyklace odpadů, 27.10.2000, VŠB-TU Ostrava, s. 191, ISBN 80-7078-822-4
- [3] Letko, M. *Analýza konštrukčných koncepcií dezintegračných strojov*, Písomná práca na dizertačnú skúšku, Katedra výrobnéj techniky, SJF STU Bratislava, 2004
- [4] Leško, M. *Optimalizácia drviacich schém s využitím simulácie*, Zb. "Automatizácia v riadení 90", Vysoké Tatry, 1990, s. 64-68
- [5] Lisičan, J. *Teória a technika spracovania dreva*. Matcentrum, Zvolen 1996
- [6] Beniák, J. *Optimalizácia tvaru a rozmerov rezného nástroja dezintegračného zariadenia s ohľadom na veľkosť reznej sily*, Písomná práca na dizertačnú skúšku, Katedra výrobnéj techniky, SJF STU Bratislava, 2001
- [7] Dítner, O. *Drcení a mletí nerostných surovin*, SNTL, Praha 1984, s. 241
- [8] Emanuel, K. a kol. *Dřevarašská příručka*, 2. část, SNTL Praha, 1989
- [9] Kolektív autorov. *Dřevaraška technická příručka*, SNTL, Praha 1970
- [10] Kováč, A. - RUDOLF, B. *Tvárnice stroje*, SNTL, Alfa, Bratislava 1989
- [11] Janota, B. *Modulová stavba drviaceho stroja*. Diplomová práca SJF STU, Bratislava 1998
- [12] Beniák, J. *Problematika výpočtu reznej sily pri dezintegrácii materiálov*, Medzinárodná konferencia TOP 2001, 27.-28. jún 2001, Častá-Papiernička, s. 427-433, ISBN 80-227-1530-1
- [13] Taguchi. [online]. [citované dňa 15. mája 2007]. Dostupné z: <<http://www.uni-kassel.de/fb15/lbk/Downloads/DOE/Taguchi/>>
- [14] Six Sigma. Taguchiho Orthogonal Arrays, [online] [citované dňa 15. mája 2007]. Dostupné z: <http://www.micquality.com/reference_tables/taguchi.htm#L27>
- [15] Beniák, J.: *Optimalizácia konštrukcie dezintegračného stroja*. Dizertačná práca, Katedra výrobnéj techniky, SJF STU Bratislava, 2007

Author: Ing. Juraj Beniák, PhD, Slovak University of Technology in Bratislava, Faculty of Mechanical Engineering, Institute of Manufacturing Systems, Environmental Technology and Quality Management, Nám. Slobody 17812 31 Bratislava, Phone.: +421 2 572 96 537.

E-mail: juraj.beniak@stuba.sk

Bilic, B., Trlin, G., Vojkovic, V.

APPLICATION OF SIMULATED ANNEALING METHOD IN THE CUTTING PARAMETERS OPTIMIZATION REGARDING SURFACE ROUGHNESS

Abstract: As a basic machining process, turning is one of the most widely used metal removal processes in industry. In modern industry the goal is to manufacture low cost, high quality products in short time. Surface roughness is an important measure of the technological quality of a product and a factor that greatly influences manufacturing cost. This paper deals with the influence analysis of cutting parameters (cutting speed, depth and feed) on the surface roughness for the case of longitudinal turning. Mathematical modeling of surface roughness was carried out by second order central composite experimental design and regression analysis. The cutting parameters in the regression equation are optimized using simulated annealing optimization method.

Key words: longitudinal turning, surface roughness, cutting parameters, simulated annealing

1. INTRODUCTION

In modern industry the goal is to manufacture low cost, high quality products in short time. Automated and flexible manufacturing systems are employed for that purpose along with computerized numerical control (CNC) machines that are capable of achieving high accuracy and very low processing time. Turning is one of the fundamental and most common metal removal operations. It is widely used in a variety of manufacturing industries where quality is an important factor.

In a turning operation, it is important task to select cutting parameters for achieving high cutting performance. Usually, the desired cutting parameters are determined based on experience ("trial and error" approaches) or by use of a handbook. Obviously, the "trial and error" method is not effective and efficient and the achievement of a desirable value is a repetitive and empirical process that can be very time consuming. The dynamic nature and widespread usage of turning operations in practice have raised a need for seeking a systematic approach that can help to set-up turning operations in a timely manner and also to help achieve the desired surface roughness quality, [1].

Cutting parameters are reflected on surface roughness, surface texture and dimensional deviations of the product. Surface roughness is an important measure of the technological quality of a product and a factor that greatly influences manufacturing cost, [2]. The quality of the machined surface plays a very important role since higher surface quality significantly improves fatigue strength, corrosion resistance, creep life, reduction of friction, wearing resistance, light reflection, heat transmission, ability of distributing and holding a lubricant, coating, or resisting fatigue. Therefore it is necessary to develop the techniques to predict surface roughness before machining, in order to select machining parameters that will keep required surface roughness and preserve product quality. The mechanism behind the formation of surface roughness is very dynamic, complicated, and process dependent;

it is very difficult to calculate its value through theoretical analysis. To select the cutting parameters properly, several mathematical models are developed to establish the relationship between the cutting performance and cutting parameters. Most of them are based on statistical regression or neural network techniques. Then, an objective function with constraints is formulated to solve the optimal cutting parameters using optimization techniques. Therefore, considerable knowledge and experience are required for this approach, [3].

There are several surface roughness parameters used in the industry, such as: average roughness (R_a), root-mean-square roughness (R_q), and maximum peak-to-valley roughness (R_y or R_{max}), etc. The most commonly used parameter is R_a . The average roughness (R_a) is the area between the roughness profile and its mean line, or the integral of the absolute value of the roughness profile height over the evaluation length. Parameter R_a is specified by the following equation:

$$R_a = \frac{1}{l} \int_0^l |y(x)| dx \quad (1)$$

where R_a is the arithmetic average deviation from the mean line, l is the sampling length and y is the ordinate of the profile curve.

This paper focuses on optimizing turning parameters based on the design of experiments and simulated annealing method to minimize surface roughness.

2. EXPERIMENTAL DESIGN AND STATISTICAL ANALYSIS

Turning is a widely used machining process in which a single-point cutting tool removes material from the surface of a rotating cylindrical workpiece. A common method of evaluating machining performance in a turning operation is based on the surface roughness. Surface roughness is correlated with insert radius and cutting parameters (cutting speed, depth of cut, and feed rate). This paper deals with the influence analysis of cutting parameters on the surface roughness for the

case of longitudinal turning. Proper selection of the cutting parameters can obtain better surface roughness. The cutting experiments were carried out on CNC lathe machine. Workpiece material which was used in the experiments is alloy steel 34CrNiMo6 (DIN). Diameter of steel bar was 50 mm. This material is heat treatable steel for high strained automotive and motor construction components. Chemical composition and mechanical properties of 34CrNiMo6 steel are shown in Tables 1 and 2, respectively.

C	Cr	Ni	Mo	Mn	Si
0.34	1.5	1.55	0.25	0.5	0.25

Table 1. Chemical composition of 34CrNiMo6 steel (values in %)

Hardness (HB)	Tensile strength (N/mm ²)	Yield strength (N/mm ²)	Fracture elongation (%)
248	1100	800	min. 11

Table 2. Mechanical properties of 34CrNiMo6 steel

The experiments are carried out by the tool for external machining, which consists of:

- toolholder mark PTG NR 2020K 16
- insert mark TNMG 16 04 08 - PF 4015 (insert radius of 0.8 mm; coated carbide - ISO grade P20).

Experiments have been conducted using full factorial central composited design 2³, [4]. Values of cutting parameters used in the experiments are shown in the Table 3.

Cutting parameters	Coded values of cutting parameters				
	$x_{-i\alpha}$	$x_{-i,\min}$	x_{i0}	$x_{i,\max}$	$x_{+i\alpha}$
$x_1 = v_c$ (m/s)	-1.682	-1	0	+1	+1.682
$x_2 = a_p$ (mm)	0.4	0.6	0.9	1.2	1.4
$x_3 = f$ (mm/rev)	0.12	0.16	0.22	0.28	0.32

Table 3. Physic values and coded levels of cutting parameters used in the experiments, [5]

Measured values of average roughness (R_a) obtained by experiments are presented in the Table 4.

Analysis of variance (ANOVA) was carried out to identify the significant factors affecting surface roughness. ANOVA has shown that the feed rate and interaction between feed rate and depth of cut are the most significant cutting parameters for affecting the surface roughness. Surface roughness is not strongly correlated with cutting speed.

By using regression analysis (i.e. second order response surface), the dependence of an average roughness and examined factors can be expressed as

$$\hat{R}_a = 4.66053 - 3.20204v_c + 10.25733f + 11.01266a_p f + 0.70539v_c^2 - 1.5154a_p^2 - 19.41288f^2 \quad (2)$$

since the coefficient of multiple determination $R^2 = 0.9926$.

Experiment number	Cutting parameter level			Measured surface roughness R_a (μm)
	v_c (m/s)	a_p (mm)	f (mm/r)	
1	0.8210	0.6	0.16	4.10
2	2.0525	0.6	0.16	2.70
3	0.8210	1.2	0.16	3.55
4	2.0525	1.2	0.16	2.10
5	0.8210	0.6	0.28	5.10
6	2.0525	0.6	0.28	3.77
7	0.8210	1.2	0.28	5.30
8	2.0525	1.2	0.28	3.92
9	1.4367	0.9	0.22	3.78
10	1.4367	0.9	0.22	3.80
11	1.4367	0.9	0.22	3.81
12	1.4367	0.9	0.22	3.79
13	1.4367	0.9	0.22	3.78
14	1.4367	0.9	0.22	3.79
15	0.4010	0.9	0.22	5.87
16	2.4724	0.9	0.22	3.30
17	1.4367	0.4	0.22	3.55
18	1.4367	1.4	0.22	3.30
19	1.4367	0.9	0.12	2.49
20	1.4367	0.9	0.32	4.78

Table 4. Experimental results for surface roughness, [5]

3. SIMULATED ANNEALING

Simulated annealing represents a class of solution methods for combinatorial optimization problems whose common basis is found on the analogies which can be drawn between those problems and the physical process of annealing. It was introduced in 1982 by Kirkpatrick et al., [6]. Combinatorial minimization is the optimization of functions that may assume several distinct discrete configurations. These problems are characterized by the usefulness in achieving near-optimum solutions in adequate processing time, e.g. it may not be necessary to fully determine the global optimum, since the small incremental gain in the objective function would only be achieved at a great expanse in central processing unit (CPU) time.

Annealing is the physical thermal process of melting a solid by heating it, followed by slow cooling and crystallization into a minimum free energy state, namely a stable state. If the cooling rate is not carefully controlled or the initial temperature is not sufficiently high, the cooling solid does not attain thermal equilibrium at each temperature. In such circumstances, local optimal lattice structures may occur which translate into lattice imperfections, namely metastable state. Thermal equilibrium at a given temperature is characterized by a Boltzmann distribution function of energy states. Under these conditions, even at a low temperature, a transition may occur from a low to a high energy level, albeit with small probability. Such transitions are assumed to be responsible for the system reaching a minimum energy state instead of being trapped in a local metastable state.

The Metropolis algorithm was the first proposed to

simulate this process. Starting from a high energy state E_i , corresponding to a particular system temperature T_i , a series of new energy states E_j are stochastically generated. Each new system configuration is accepted if $E_j \leq E_i$. Otherwise, and by analogy with the Boltzmann distribution for energy states at thermal equilibrium, E_j will be accepted as an improved state with a probability given by $P(\Delta E) = \exp [(E_i - E_j)/k_B T_i]$, where T_i is the current system temperature and k_B is Boltzmann's constant. At high temperature this probability is close to 1. At each temperature it is assumed that thermal equilibrium is reached. As the system temperature decreases, the probability of accepting a higher energy state as being an improved energy states approaches 0, [7].

4. DETERMINATION OF OPTIMAL CUTTING PARAMETERS

Since SA algorithm has been available and used for almost 30 years, nowadays it is included in many computational software packages. Various SA algorithm variations are included in today's leading engineering and mathematical tools, [8,9,10]. This paper uses Matlab/Simulink's SA solver for minimizing the function (2). Simulink's SA solver provides rich set of options enabling fine tuning of SA minimization process.

If we introduce the following labels: $Y = \hat{R}_a$, then the equation (2) can be written in this form:

$$Y = 4.66053 - 3.20204x_1 + 10.25733x_3 + 11.01266x_2x_3 + 0.70539x_1^2 - 1.5154x_2^2 - 19.41288x_3^2 \quad (3)$$

with constraints:

$$0.4010 \leq x_1 \leq 2.4724; \quad 0.4 \leq x_2 \leq 1.4; \quad 0.12 \leq x_3 \leq 0.32.$$

Matlab program used to run simulated annealing metaheuristics:

```
ObjectiveFunction = @fun
X0 = [0.5 0.5 0.5]; % Starting point

lb = [0.4010 0.4 0.12];
ub = [2.4724 1.4 0.32];

[x,fval,exitFlag,output] =
simulannealbnd(ObjectiveFunction,X0,lb,
ub)
```

Function *simulannealbnd()*, representing SA algorithm in Matlab, accepts four parameters: *ObjectiveFunction* – function to be minimized (target function)

X0 – initial state, *n* component vector

lb – lower bounds, *n* component vector

ub – upper bounds, *n* component vector.

Return values of *simulannealbnd* function are:

x – state *s* at function's minimum, *n* component vector

fval – minimum value

exitFlag – reason for SA algorithm stopping

output – additional information about SA algorithm performance, i.e. execution time.

Matlab test program has been written to run SA for $N = 100$ times and gather the information on the SA algorithm performance.

Results:

The following SA characteristics had been measured:

- Number of iterations
- Execution time in seconds
- Function parameters (x_1, x_2, x_3)
- Function minimum value

The obtained results are shown in Table 5.

Measurement	Mean value	Standard deviation	Confidence interval (95%)
Iteration count	2791.5	969.3017	852.9 – 4730.1
Execution time (s)	1.0461	0.3701	0.3058 – 1.7864
x_1	2.2736	0.0391	2.1954 – 2.3517
x_2	1.3999	$1.3036 \cdot 10^{-4}$	–
x_3	0.1200	$2.8961 \cdot 10^{-5}$	–
Function minimum	0.8583	0.0029	0.8536 – 0.8652

Table 5. Results obtained by simulated annealing

Results of the experiment are depicted in Figures 1-5. Red straight lines in these figures indicate CI 95% interval, given by $m \pm 2*s$, where *m* is mean value and *s* is standard deviation of a particular measure.

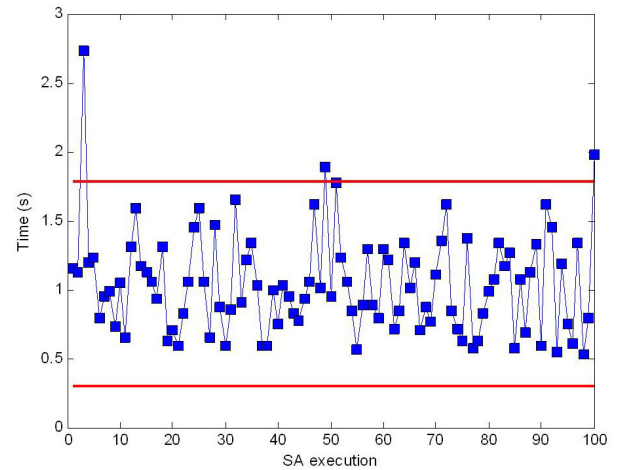


Fig. 1. Execution time in 100 executions

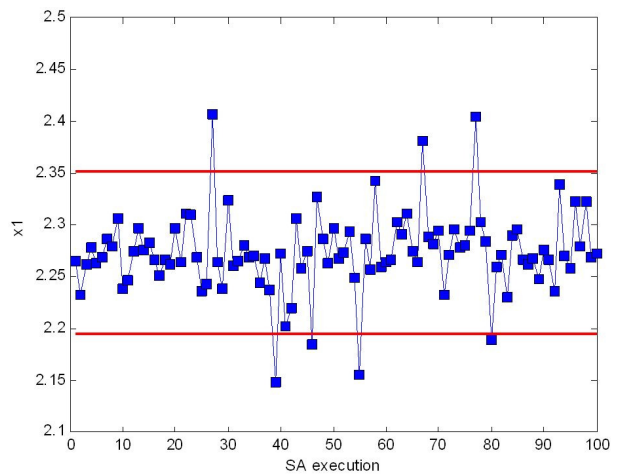


Fig. 2. x_1 parameter value in 100 executions

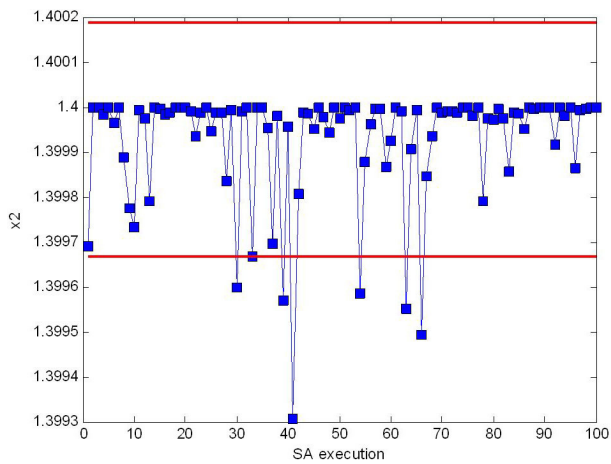


Fig. 3. x_2 parameter value in 100 executions

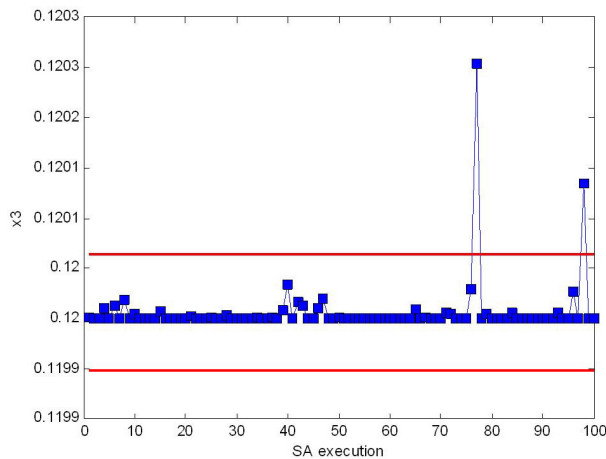


Fig. 4. x_3 parameter value in 100 executions

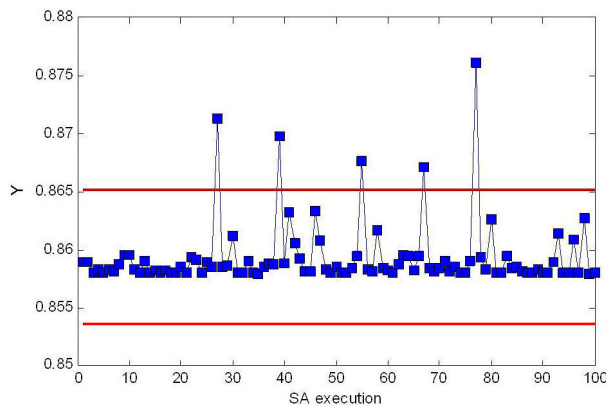


Fig. 5. Minimum function in 100 executions

5. CONCLUSION

This paper has presented an application of the experimental design, regression analysis and simulated annealing method in the optimization of turning operations. The following conclusions can be drawn:

- Full factorial central composited experimental design and regression analysis are suitable to analyze the surface roughness (metal cutting) problem as described in this paper.
- Minimum of objective function (minimal value of the average arithmetic roughness) $R_a = 0.8583$ has been obtained in the case of the following cutting parameters: $v_c = 2.2736$ m/s, $a_p = 1.4$ mm, $f = 0.12$ mm/r.

- The experimental results demonstrate that the feed rate is the main cutting parameter among the three controllable factors that influence the surface roughness in longitudinal turning 34CrNiMo6 steel. Interaction between feed rate and depth of cut has also significant influence on the surface roughness. The increase of the cutting speed in a certain interval effects the improvement of the surface roughness but soon after, due to the layer on the cutting edge and vibrations, it deteriorates.
- Simulated annealing algorithm applied in this paper successfully minimized the objective function, with respect to the provided parameter boundaries. Execution time was 2.15 s per execution which can be considered as acceptable.

6. REFERENCES

- [1] Zhang, J. Z., Chen, J. C., Kirby, E. D.: *Surface roughness optimization in an end-milling operation using the Taguchi design method*, Journal of Materials Processing Technology 184, p.p. 233–239, 2007
- [2] Vojković, V.: *Izbor optimalne varijante tehnološkog procesa*, Graduate thesis, University of Split, Faculty of electrical engineering, mechanical engineering and naval architecture, Split, Croatia, 2004
- [3] Nalbant, M., Gökkaya, H., Sur, G.: *Application of Taguchi method in the optimization of cutting parameters for surface roughness in turning*, Materials and Design, 28, p.p. 1379–1385, 2007
- [4] Montgomery, D. C.: *Design and analysis of experiments*, John Wiley and sons, Inc, 2001.
- [5] Bilić, B., Bajić, D., Veža, I.: *Optimization of cutting parameters regarding surface roughness during longitudinal turning*, Proceedings of the 15th DAAAM International Symposium: Intelligent Manufacturing & Automation, p.p. 039-040, Wien, 2004
- [6] Kirkpatrick, S., Gellat, C. D., Vecchi, M. P.: *Optimization by simulated annealing*, Science, 220(4598), pp. 671-680, 1893
- [7] Cardoso, M. F., Salcedo, R. L.: *Nonequilibrium simulated annealing: A faster approach to combinatorial minimization*, Industrial & Engineering Chemistry Research, 33 (8), p.p. 1908–1918, 1994
- [8] <http://www.mathworks.com/products/global-optimization/description7.html>.
- [9] <http://mathworld.wolfram.com/SimulatedAnnealing.html>
- [10] <http://octave.sourceforge.net/optim/function/samin.html>

Authors: Prof. Ph.D. Boženko Bilić, B.Sc. Trlin Goran, B.Sc. Vojković Vjeran., University of Split, Faculty of Electrical Engineering, Mechanical Engineering and Naval Architecture (FESB), R. Boškovića 32, 21000 Split, Croatia, Phone.: +385 21 305-032, Fax: +385 21 305-776
E-mail: bbilic@fesb.hr
gtrlin@fesb.hr

Gostimirović, M., Pucovsky, V., Kovač, P., Šooš, Lj., Rodić, D., Savković, B.

MODELING OF DISCHARGE ENERGY IN EDM PROCESS BY THE USE OF GENETIC ALGORITHMS

Abstract: *Electro Discharge Machining (EDM) is a complex process which uses electrical energy to erode and form workpiece. Using wrong set of parameters can lead to inefficient exploitation of the process and sometimes can even do more harm than good. Modeling dependence between the process parameters and output results is something that can save considerable amounts of funds. Discharge energy which is directly transformed into thermal energy, is used as a machining process and because of that it presents a primary point of interest in modeling procedure. In this paper, link between discharge energy and output results of machining process is found using genetic algorithms as a type of artificial intelligence. It also presents a comparison between two types of modeling approach with specific conclusion about more accurate one.*

Key words: *EDM, discharge energy, machining parameters, genetic algorithms*

1. INTRODUCTION

Everybody who worked with EDM knows that the only requirement for machining to take place is that both the tool and the workpiece have to be electro conductive. By meeting this requirement, arcing between the tool and the workpiece can take place. This will result in ionization of small volume of dielectric around arcing zone, reaching a temperature up to 40.000 °C, consequentially heating workpiece surface to 10.000 °C. Small area on workpiece surface, under the influence of this high temperature, is melted and when electric arc is cut off a strong pressure wave is generated. Melted material is then washed off from workpiece surface and flushed away with dielectric fluid. Described process is repeated until desirable results are met.

Machining ability of workpiece depends on its thermal properties and not its hardness like in conventional machining processes. Because of this EDM is preferable choice in processes like machining hard materials, mould making, precision machining or individual production. As can be noted from above mentioned, EDM is rarely used in mass production. Machining each part with different demands is very challenging and in order to keep minimum cost it requires a profound knowledge of process parameters and their influence on final result. This would mean that one should spend large amount of funds and time on becoming familiar with process of EDM to exploit it properly. In order to make EDM more accessible, various forms of simulations are created. Many of these simulations are based on artificial intelligence, which is gaining ever more popularity among scientific and technical circles. Following trends, this article presents modeling of EDM process and finding relationships between process parameters and process outputs based on experimentally obtained results. Genetic algorithm, a type of artificial intelligence, is used as a tool for finding those relationships.

Parameters used to describe quality of EDM process are: productivity, which is expressed through material

removal rate, accuracy represented by dimension tolerances and type of shape of workpiece, and finally surface integrity expressed through machined surface roughness. In this article all three of these parameters will be modeled, but what is new is comparison between direct modeling of parameters and through discharge energy. By using this approach a conclusion will be drawn from this analysis and more accurate method determined.

2. EDM PROCESS

In EDM discharge energy is directly transformed into thermal energy and it becomes an instrument for machining. Discharge energy E_e is calculated as the mean value of electrical energy per one impulse which is transformed into heat, and can be expressed by the following equation:

$$E_e = \int_0^{t_e} u_e(t) \cdot i_e(t) \cdot dt \cong U_e \cdot I_e \cdot t_e \quad (1)$$

where U_e is discharge voltage, I_e is discharge current and t_e is discharge duration.

In proper machining conditions, electrical discharge occurs instantaneously and is independent from other electric values [1]. With this fact in mind ignition delay time can be neglected, $t_d \approx 0$, meaning that the discharge duration is equal to pulse duration, $t_e \cong t_i$. By this simplification the final expression for discharge energy has more practical form:

$$E_e = U_e \cdot I_e \cdot t_i \quad (2)$$

As can be seen from Eq. (2), the discharge energy is influenced by the discharge voltage, discharge current, and pulse duration. Their influences are interconnected and depend on the rest of the machining parameters [1].

The discharge voltage depends only on materials of workpiece and electrode. For every combination of workpiece and electrode there is a specific value of discharge voltage. This value can range from 15 to 30 V [2,3] and cannot be influenced under the given machining conditions.

Parameter which directly impacts the discharge energy is discharge current. But this impact is limited by the current density at the electrode. Stability of impulse discharge will be threatened in case when the current density oversteps the limit for the given machining conditions (approximately 10÷25 A/cm²) [4,5]. By exceeding this threshold, the continuous current flow will be established, and arcing or short circuiting will take place. This event will lengthen the time of deionization of the discharge channel, and consequentially reduce the efficiency of EDM.

Direct control of discharge energy can be achieved by varying the pulse duration. However, arbitrarily regulation of process parameters is limited. Experience has taught us that pulse duration must be limited for a particular discharge current. Otherwise, an electric arcing occurs which damages both tool and workpiece [1].

3. EXPERIMENT

Experimental investigation was conducted on EDM machine tool "FUMEC – CNC 21" of South Korea. The work material used in the experiment was manganese-vanadium tool steel, ASTM A681 (0,9% C, 2% Mn, and 0,2% V), hardness 62 HRc. The tool was made of electrolytic copper with 99,9% purity, 20×10 mm cross-section. The dielectric was petroleum and natural flushing was used.

The range of the discharge current was $I_e=1÷50$ A (current density 0,5÷25 A/cm²), while the pulse duration was chosen from the interval $t_i=1÷100$ μs to accommodate the chosen current. The rest of the parameters of electric impulse were held constant, according to manufacturer's recommendations.

During the experiment input parameters were varied and the resulting machining parameters of EDM process were monitored and recorded. Measured parameters were material removal rate V_w , gap distance a , and surface roughness R_a .

Material removal rate (ratio of removed material volume and the effective machining time) was measured indirectly, by monitoring the machining time for the set eroding depth. The depth and time of eroding were monitored using the machine tool CNC control unit. The machining accuracy of EDM was monitored through the change of side gap distance. Gap distance was calculated as the half of difference between the tool and workpiece contour dimensions. Measurements were conducted using electronic callipers. Surface integrity was assessed by measuring surface roughness and research of the surface layer properties. "PERTHOMETER S5P" of Mahr, Germany was used to measure the arithmetic average deviation of the assessed *profile* (ISO 4287) [1]. Experimental data are shown in Table 1.

4. GENETIC ALGORITHMS

Genetic algorithms (GA) have become an indispensable tool for solving tasks related to production processes [6]. They present a method of artificial intelligence belonging to the group of evolutionary based optimization algorithms. Their principle is based on thesis "survival of the fittest", in other words best solutions have the most chances to mate and pass their genetic material onto next generation. Worst solutions are more likely to "die" because they are not fit enough. Whole process of evolution towards best solution can be summarized in three steps. Observing a group of solutions, and dividing them so that every solution is one individual, process of selection is conducted respecting rules on which the selection is based. At the end of this process so called mating pool will be created and individuals within it will be paired to perform crossover, the second step of algorithm. Offspring will be produced and some of them will pass through third step which is called mutation. Some of their features will be randomly changed and thus new genetic material will be introduced. This step is important because it prevents algorithm to get stuck in local optimum.

5. MODELING PROCEDURE

In this paper, as mentioned before, two equations were used to model EDM process parameters. Both are derived from machining energy resp. Eq. (2).

Model-1 for material removal rate, gap distance and surface roughness is given by equations:

$$\begin{aligned} V_w &= C_1 \cdot I_e^{x_1} \cdot t_i^{x_2} \\ a &= C_2 \cdot I_e^{x_3} \cdot t_i^{x_4} \\ R_a &= C_3 \cdot I_e^{x_5} \cdot t_i^{x_6} \end{aligned} \quad (3)$$

where $C_1, x_1, x_2, C_2, x_3, x_4, C_3, x_5$ and x_6 are unknown and to be found by GA.

Model-2 for same parameters, but in direct relationship with discharge energy, is given by equations:

$$\begin{aligned} V_w &= C_4 \cdot E_e^{x_7} \\ a &= C_5 \cdot E_e^{x_8} \\ R_a &= C_6 \cdot E_e^{x_9} \end{aligned} \quad (4)$$

Coefficients C_4, x_7, C_5, x_8, C_6 and x_9 are also unknown.

All of these coefficients will be determined to correspond to Δ , minimum sum of percent errors for every parameter, expressed through formula:

$$\Delta = \sum_{i=1}^n \left| \frac{P(i) - D(i)}{P(i)} \right| \times 100\% \quad (5)$$

where P is experimentally obtained value and D is modeled value for every parameter.

Experiment number	Discharge current I_e (A)	Pulse duration t_i (μ s)	Current density γ (A/cm ²)	Discharge energy E_e (μ J)	Material removal rate V_w (mm ³ /min)	Gap distance a (mm)	Surface roughness R_a (μ m)
1	1	1	0.5	20	0.86	0.055	1.8
2	1	2	0.5	40	1.28	0.055	1.9
3	1	5	0.5	100	2.35	0.06	2.1
4	1	7	0.5	140	1.97	0.06	2.3
5	5	1	2.5	100	3.22	0.09	3.9
6	5	2	2.5	200	4.16	0.095	4.2
7	5	5	2.5	500	6.47	0.10	5.1
8	5	7	2.5	700	4.31	0.105	5.1
9	9	2	4.5	360	7.71	0.13	8.2
10	9	5	4.5	900	14.89	0.14	8.8
11	9	7	4.5	1260	9.49	0.155	9.0
12	9	10	4.5	1800	5.24	0.155	9.8
13	13	2	6.5	520	6.13	0.165	9.2
14	13	5	6.5	1300	18.71	0.18	9.4
15	13	7	6.5	1820	10.71	0.20	9.7
16	13	10	6.5	2600	6.62	0.21	10.3
17	20	5	10	2000	24.49	0.20	10.2
18	20	7	10	2800	31.82	0.22	10.4
19	20	10	10	4000	26.70	0.23	10.8
20	20	20	10	8000	17.11	0.24	11.2
21	30	7	15	4200	39.92	0.23	10.8
22	30	10	15	6000	53.30	0.24	11.3
23	30	20	15	12000	56.82	0.25	11.8
24	30	50	15	30000	40.48	0.26	12.5
25	50	10	25	10000	46.36	0.28	11.8
26	50	20	25	20000	66.83	0.30	12.5
27	50	50	25	50000	72.92	0.31	13.2
28	50	100	25	100000	60.60	0.33	13.4

Table 1. Experimental data used in modeling procedure

σ_{V_w} model-1 (%)	σ_{V_w} model-2 (%)	σ_a model-1 (%)	σ_a model-2 (%)	σ_{R_a} model-1 (%)	σ_{R_a} model-2 (%)
29,9	37,9	5,9	14,8	14,7	24,3

Table 2. Values of average deviation of results for **model-1** and **model-2**

For practical realization of model software Matlab was used.

Number of individuals in every generation was 150 and tournament type of selection was used to fill mating pool. Tournament size was in this case 24 individuals. Elite count was 12, which means that from every generation 12 individuals with best fitness were automatically moved to next generation. 110 individuals will be created by crossover of their predecessors from mating pool and 28 will be created by mutating randomly selected individuals from mating

pool. After 30.000 generations following results, for **model-1**, were obtained:

$$\begin{aligned}
 V_{w(\text{model-1})} &= 0,86 \cdot I_e^{0,901} \cdot t_i^{0,202} \\
 a_{(\text{model-1})} &= 0,054 \cdot I_e^{0,397} \cdot t_i^{0,055} \\
 R_{a(\text{model-1})} &= 1,998 \cdot I_e^{0,461} \cdot t_i^{0,062}
 \end{aligned} \tag{6}$$

Parameters of GA for **model-2** were slightly

different and in this case tournament size was 16, elite number 8 and generation count was 20.000. Difference is explained by simplification of modeled expression. Results for **model-2** are:

$$\begin{aligned} V_{w(\text{model-2})} &= 0,188 \cdot E_e^{0,532} \\ a_{(\text{model-2})} &= 0,026 \cdot E_e^{0,247} \\ R_{a(\text{model-2})} &= 0,905 \cdot E_e^{0,279} \end{aligned} \quad (7)$$

6. RESULTS

Dependence between results obtained by experiment, **model-1** and **model-2**, for material removal rate, gap distance and surface roughness, are shown in Fig 1-3.

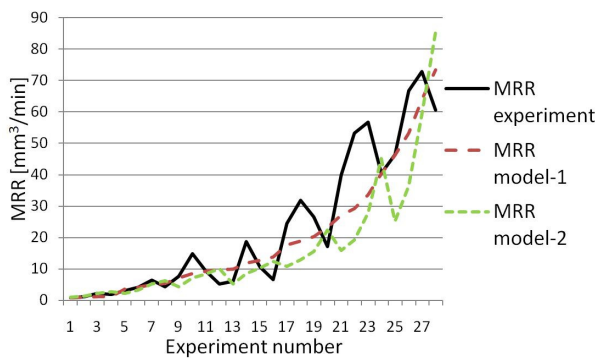


Fig. 1. Dependence between material removal rate (MRR) values

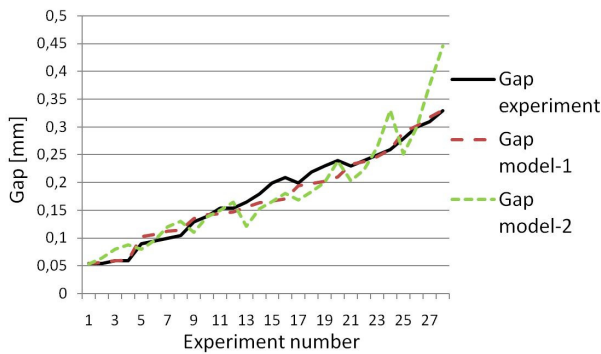


Fig. 2. Dependence between gap distance values

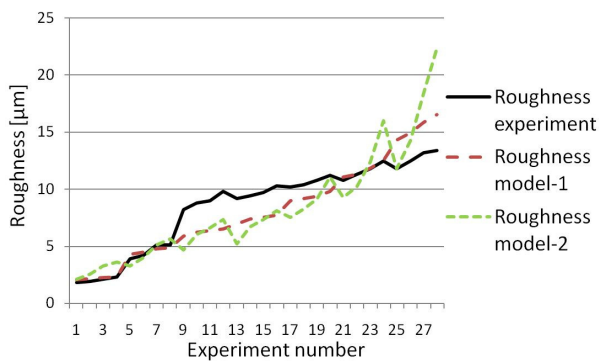


Fig. 3. Dependence between roughness surface values

Numerical values of average percent deviation (σ) for modeled results from experimentally obtained results are shown in Table 2.

7. CONCLUSION

It is clearly visible that **model-1** in all three cases predicted more accurate values for process parameters. Time difference between forming models is measured in seconds and is not worth of obtaining that much of a difference in results accuracy. Simplification by introduction of **model-2**, did not yield any satisfying results. One of the most important advantages of this type of models is that specific coefficients are obtained and models can be used independently. For later research more experiments are suggested. It is speculated that this would enable to yield more accurate results without drastically prolonging computational time. Also more workpiece materials could be investigated to crosscheck model validity.

8. REFERENCES

- [1] Gostimirovic, M., Kovac, P., Sekulic, M., Skoric, B.: *Influence of discharge energy on machining characteristics in EDM machining*, Journal of Mechanical Science and Technology, 26 (1), pp. 173-179, 2012
- [2] Liu, K., Reynaerts, D., Lauwers, B.: *Influence of the pulse shape on the EDM performance of Si3N4-TiN ceramic composite*, CIRP Ann-Manuf Techn, 58, pp. 217-220, 2009.
- [3] Ferreira, J. C.: *A study of die helical thread cavity surface finish made by Cu-W electrodes with planetary EDM*, Int J Adv Manuf Techn, 34, pp. 1120-1132, 2007.
- [4] Tsai, Y. Y., Lu, C. T.: *Influence of current impulse on machining characteristics in EDM*, J Mech Sci Technol, 21(10), pp. 1617-1621, 2007.
- [5] Rebelo, J. C., Dias, A. M., Kremer, D., Lebrun, J. L.: *Influence of EDM pulse energy on the surface integrity of martensitic steels*, J Mater Process Technol, 84, pp. 90-96, 1998.
- [6] Kovac, P., Rodic, D., Pucovski, V., Mankova, I., Savkovic, B., Gostimirovic, M.: *A review of artificial intelligence approaches applied in intelligent processes*, Journal of Production Engineering, 15(1), pp. 1-6, 2012.

Authors: Prof. Dr. Marin Gostimirovic, M.Sc. Vladimir Pucovsky, Prof. Dr. Pavel Kovac, M.Sc. Dragan Rodic, M.Sc. Borislav Savkovic, University of Novi Sad, Faculty of Technical Sciences, Institute for Production Engineering, Trg Dositeja Obradovica 6, 21000 Novi Sad, Serbia.

Prof. Dr. Ljubomir Šooš, Faculty of Mechanical Engineering STU in Bratislava, Námestie Slobody 17, 812 31 Bratislava 1, Slovak Republic.

E-mail: maring@uns.ac.rs
pucovski@uns.ac.rs
pkovac@uns.ac.rs
lubomir.soos@stuba.sk
rodicdr@uns.ac.rs
savkovic@uns.ac.rs

ACKNOWLEDGEMENT

This paper presents a part of researching at the project N° 660-00-140/2012-09/04.

Gostimirovic, M., Rodic, D., Kovac, P., Mankova, I., Beno, J., Pucovsky, V., Sekulic, M.

PREDICTION OF SURFACE ROUGHNESS USING NEURAL FUZZY SYSTEMS IN ELECTRICAL DISCHARGE MACHINING

Abstract: *Electrical Discharge Machining (EDM) is one of the important and cost-effective non-conventional methods of machining complex geometry workpieces and difficult-to-machine materials. Surface roughness is the main indicator of quality of a component for EDM. A new approach in modeling surface roughness which uses artificial intelligence tools is described in this paper. The objective of this study is to design an adaptive neuro-fuzzy inference system (ANFIS) for prediction of surface roughness in EDM. The input parameters of model are discharge current, pulse duration and output parameter is surface roughness. The results indicate that the ANFIS modeling technique can be effectively used for the prediction of surface roughness in machining of manganese-vanadium tool steel.*

Key words: *EDM, Discharge current, Pulse duration, Surface roughness, ANFIS.*

1. INTRODUCTION

In recent years materials with unique metallurgical properties, such as tungsten carbide, titanium, vanadium based alloys and other super-alloys, have been developed to meet the demands of extreme applications. The machining of difficult-to-cut materials is an important issue in the field of manufacturing. Different non-traditional machining techniques are increasingly employed to manufacture different high quality industrial components. Among the non-traditional methods of machining processes, electrical discharge machining (EDM) is used for machining complex geometry workpieces and difficult-to-machine materials, for which conventional methods are not applicable. EDM is the process of machining electrically conductive materials by using precisely controlled sparks that occur between an electrode and a workpiece in the presence of a dielectric fluid [1]. EDM is based on the erosion of electrically conductive materials through the series of spatially discrete high frequency electrical discharges (sparks) between the tool and the workpiece [2].

The main and crucial advantage of this process is that performance is independent from the mechanical qualifications of machined materials and doesn't entail a cutting force. Thus, very hard, brittle materials can be manufactured easily and in desired forms/shapes [3].

Artificial intelligent techniques have been successfully applied to machining processes through recent years. A broad literature survey has been conducted on the application of artificial intelligence systems to predict surface roughness. Kovac et al [4] used fuzzy logic to predict the surface roughness and compare with regression analysis in face milling process. Caydas et al used [5] adaptive neuro-fuzzy inference system (ANFIS) model has been developed for the prediction of the white layer thickness (WLT) and the average surface roughness achieved as a function of the process parameters. Rao et al [6] have been made to develop the mathematical model for

predicting die-sinking electrical discharge machining of aluminum alloy characteristics such as the metal removal rate (MRR), the tool wear rate (TWR), the surface roughness (R_a) and the hardness(HRc) using fuzzy mathematical method.

In the present work, an attempt has been made to develop the intelligent model for predicting surface roughness using ANFIS mathematical method. The process parameters taken in to consideration were the discharge current (I_c) and pulse duration (t_i). The model predicted values and measured values were fairly close to each other. Model validation is the process by which the input vectors from input/output data sets on which the FIS was not trained, are presented to the trained ANFIS model, to see how well the ANFIS model predicts the corresponding data set output values. The data which not used for training the model have been successfully predicted. Their propinquity to each other indicates the developed model can be effectively used to predict the R_a in EDM process.

2. ADAPTIVE NEURO-FUZZY INFERENCE SYSTEM (ANFIS)

The acronym ANFIS derives its name from adaptive neuro-fuzzy inference system. *Fuzzy inference system* (FIS) is a rule based system consisting of three components. These are:

- a *rule-base*, containing fuzzy if-then rules,
- a *data-base*, defining the Membership Functions (MF) and
- an *inference system* that combines the fuzzy rules and produces the system results.

The main problem with fuzzy logic is that there is no systematic procedure to define the membership function parameters. ANFIS eliminates the basic problem in fuzzy system design, defining the membership function parameters and design of fuzzy if-then rules, by effectively using the learning capability of neural network for automatic fuzzy rule generation and parameter optimization [7]. Using a

given input/output data set, the toolbox function ANFIS constructs a fuzzy inference system (FIS) whose membership function parameters are tuned (adjusted) using either a back propagation algorithm alone or in combination with a least squares type of method. This adjustment allows fuzzy systems to learn from the data they are modeling.

A network type structure of ANFIS is similar to a neural network. The entire system architecture consists of five layer, namely, the fuzzy layer and total output layer. Five network layers are used by ANFIS to perform the following fuzzy inference steps:

Input nodes – layer 1:

The general structure of ANFIS with two inputs x and y and one output z is shown in Fig. 1. Example of model with two rules as follows:

Rule1: If x A_1 and y is B_1 then $z_1 = p_1x + q_1y + r_1$

Rule2: If x A_2 and y is B_2 then $z_2 = p_2x + q_2y + r_2$

Where A_1 , A_2 and B_1 and B_2 are fuzzy sets of input premise variables x and y respectively.

Each node in this layer generates membership grades of the crisp inputs and each node's output. An example of a node function is the generalized *Gaussian* membership function:

$$O_i^1 = \mu_{A_i}(x) = e^{-\frac{(x-c)^2}{2\sigma^2}} \quad (1)$$

Where x , c and σ is the parameter set.

Rule nodes - layer 2:

The outputs of this layer called firing strengths are the products of the corresponding degrees obtained from the layer 1.

$$O_i^2 = w_i = \mu_{A_i}(x)\mu_{B_i}(y) \quad i=1, 2 \quad (2)$$

Where μ_A and μ_B are the membership functions for A_i and B_i linguistic labels, respectively. Where w_i is output weight of each neuron.

Average nodes - layer 3:

The i -th node calculates the ratio of the i -th rule's firing strength to the total of all firing strengths. The firing strength in this layer is normalized \bar{w}_i as:

$$O_i^3 = \bar{w}_i = \frac{w_i}{\sum_i w_i} \quad i=1, 2 \quad (3)$$

Consequent nodes - layer 4:

Every node in this layer is with a node function $w_i f_i$ where w_i is the output of layer 3 and $\{p_i, q_i, r_i\}$ is the parameter set. These parameters are referred to as consequent parameters.

$$O_i^4 = \bar{w}_i f_i = \bar{w}_i(p_i x + q_i y + r_i) \quad i=1, 2 \quad (4)$$

Output nodes - layer 5:

This layer is called as the output nodes. The single

node in this layer computes the overall output as the summation of contributions from each rule.

$$O_i^5 = f(x,y) = \sum_i \bar{w}_i \cdot f_i = \bar{w}_1 f_1 + \bar{w}_2 f_2 = \frac{\sum_i w_i f_i}{\sum_i w_i} \quad (5)$$

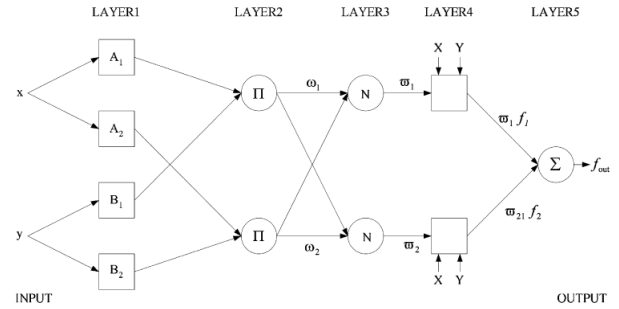


Fig. 1. Basic ANFIS architecture

The details and mathematical background for these algorithms can be found in [8].

Fig. 2. shows the flowchart for predicting the surface roughness via ANFIS. The process followed in this study is illustrated in Fig. 2.

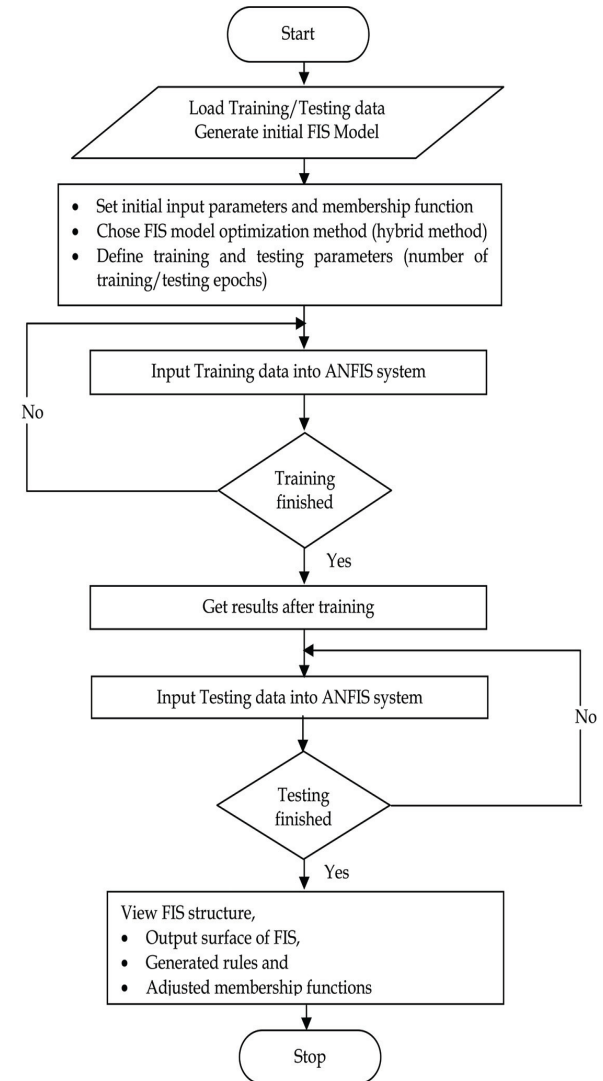


Fig. 2. Flowchart of surface roughness prediction of ANFIS system [9]

3. DESIGN OF EXPERIMENTS

Experimental investigation was conducted on an EDM machine tool "FUMEC – CNC 21" in South Korea. The work material used in the experiment was manganese-vanadium tool steel, ASTM A681 (0,9% C, 2% Mn, and 0,2% V), hardness 62 HRc. The tool was made of electrolytic copper with 99,9% purity and 20×10 mm cross-section. The dielectric was petroleum. Due to small eroding surface and depth, natural flushing was used.

The machining conditions included variable discharge current and pulse duration. The range of the discharge current was $I_e=1\div50$ A (current density $0,5\div25$ A/cm²), while the pulse duration was chosen from the interval $t_i=1\div100$ μs to accommodate the chosen current. The rest of the parameters of electric impulse were held constant, according to the manufacturer's recommendations (open gap voltage $U_o=100$ V, duty factor $\tau=0,8$ and positive tool electrode polarity).

The experiments were conducted according to the specified experiment plan. Input parameters were varied and the resulting machining parameters of EDM process were monitored and recorded.

Measured parameter was surface roughness R_a . Surface integrity was assessed by measuring surface roughness and research of the surface layer properties. "PERTHOMETER S5P" of Mahr, Germany was used to measure the arithmetic average deviation of the assessed profile (ISO 4287) [10].

4. ANFIS RESULTS AND DISCUSSION

Using a given input/output data set, the ANFIS method constructs a fuzzy inference system (FIS) whose membership function parameters are tuned (adjusted) using either a back propagation algorithm alone, or in combination with a least squares type of method.

For this model, main parameters for the experiments are discharge current I_e , pulse duration t_i (input data set) and surface roughness R_a (output data set).

The training dataset and testing dataset are obtained from experiments. The input/output dataset was divided randomly into three categories: training dataset, consisting 18 of the input/output dataset, checking dataset, consisting 5 of the data and validation (unknown to model) data set, which consists 5 of data.

Training process is accomplished by using Mat Lab 6.0. In order to determine the optimal network architecture, various network architectures were designed; different training algorithms were used. The number and type of membership functions, method optimization hybrid or back propagation, and number epoch were changed. Then the best adaptive network architecture was determined. The training epoch for each network is 500, hybrid method optimization, the best results given 3 membership functions Gaussian type. When the network training was successfully finished, the ANFIS was tested with validation data.

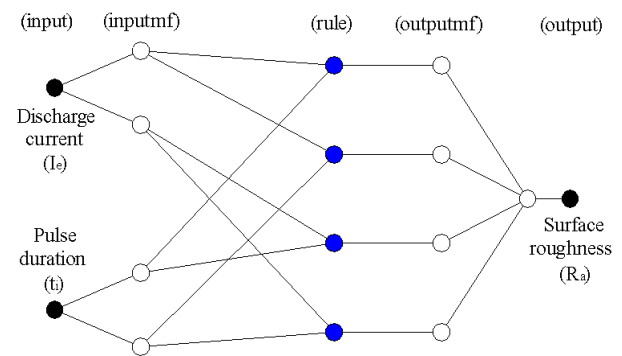


Fig. 3. ANFIS structure for prediction of surface roughness

Fig. 4 describe the comparison of experimental and ANFIS results for the surface roughness, respectively. It proved that the method used in this paper is feasible and could be used to predict the Ra in an acceptable error rate for EDM. The compared lines seem to be close to each other indicating with good agreement.

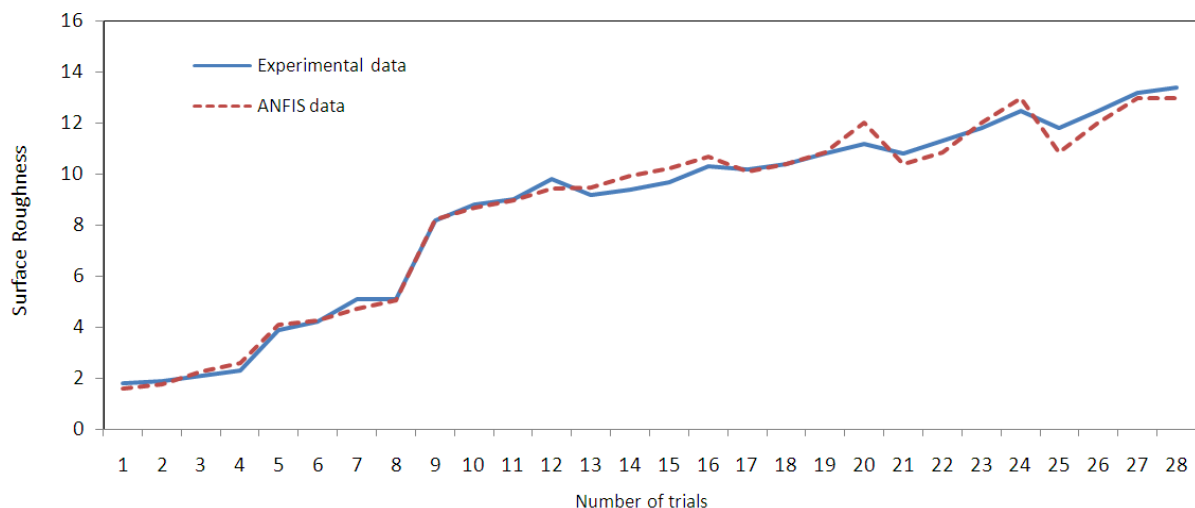


Fig. 4. Correlation between experimental and ANFIS surface roughness value

Table 1. Surface roughness in EDM

Discharge current	Pulse duration	Surface roughness		Error abs. value
		Eksp.	ANFIS	
I_e	t_i	$R_{aeksp.}$	R_{aanfis}	E
(A)	(μ s)	(μ m)	(μ m)	(%)
Training data				
1	1	1,8	1,58	12,22
1	5	2,1	2,26	7,61
5	1	3,9	4,07	4,35
5	7	5,1	5,06	0,78
9	2	8,2	8,21	0,12
9	7	9	8,98	0,22
9	10	9,8	9,44	3,67
13	2	9,2	9,47	2,93
13	5	9,4	9,92	5,53
13	10	10,3	10,66	3,49
20	5	10,2	10,08	1,17
20	10	10,8	10,82	0,18
20	20	11,2	12,02	7,32
30	7	10,8	10,38	3,88
30	50	12,5	12,95	3,6
50	10	11,8	10,82	8,3
50	50	13,2	12,95	1,89
50	100	13,4	12,97	3,2
<i>Training data Average Error = 3,92</i>				
Checking data				
1	2	1,9	1,75	7,89
5	2	4,2	4,23	0,71
9	5	8,8	8,678	1,38
20	7	10,4	10,38	0,19
30	20	11,8	12,02	1,86
<i>Checking data Average Error = 2,41</i>				
Validation data (unknown data)				
1	7	2,3	2,6	13,04
5	5	5,1	4,73	7,25
13	7	9,7	10,21	5,25
30	10	11,3	10,82	4,24
50	20	12,5	12,02	3,84
<i>Test data Average Error = 6,72</i>				

5. CONCLUSION

In this paper an ANFIS is used to estimate surface roughness in EDM. Table 1 shows the compared values obtained by experiment and estimated by ANFIS model. The average deviation of the training data is 3,92 %, average deviation of the checking data is 2,41%, while the average deviation data which unknown to the model is 6,72%. Research showed that ANFIS model gives accurate prediction on surface roughness. The ANFIS predicted surface roughness values show a good comparison with those obtained experimentally. It is evidence that the fuzzy logic technique can be help to better prediction of the experimental data.

6. REFERENCE

[1] Jameson, E.C.: *Description and development of electrical discharge machining (EDM)*. Society of Manufacturing Engineers, pp.12 Dearborn, Michigan, 2001.

- [2] Llanes, L., Idanez, E., Martinez, B., Casas, J.E.: *Influence of electrical discharge machining on the sliding contact response of cemented carbides*. International Journal of Refractory Metals and Hard Materials, 19, pp. 35–40, 2001.
- [3] Tsai, H.C., Yan, B.H., Huang, F.Y.: *EDM performance of Cr/Cu-based composite electrodes*. Int J Machine Tools Manuf, 43, pp. 245-252, 2003.
- [4] Kovac, P., Rodic, D., Pucovsky, V., Savkovic, B.: Gostimirovic, M., *Application of fuzzy logic and regression analysis for modeling surface roughness in face milling*. Journal of Intelligent Manufacturing, doi: 10.1007/s10845-012-0623-z, 2012.
- [5] Caydas, U., Hascalik, A., Ekici, S.: *An adaptive neuro-fuzzy inference system (ANFIS) model for wire-EDM*. Expert Systems with Applications, 36, pp. 6135–6139, 2009.
- [6] Rao, S., Prasad, E., Reddy, B.: *Fuzzy modeling for electrical discharge machining of aluminum alloy*. International Journal of Research and Reviews in Applied Sciences, 9, pp. 1–13, 2011.
- [7] Yurdusev, M.A., Firat, M., Turan, M.E.: *Adaptive neuro fuzzy inference system approach for municipal water consumption modeling*. Turkey. J. Hydrol., 365(3-4), pp. 225–234, 2009.
- [8] Jang, J.S.R. ANFIS: adaptive-network-based fuzzy inference system, *IEEE Transactions on Systems, Man and Cybernetics*, 23(3), pp. 665–685, 1993.
- [9] Ahmad, T.A.: *Fuzzy Systems: 5 Adaptive Neuro-Fuzzy Systems*. ISBN 978-953-7619-92-3, pp. 216, 2010.
- [10] Gostimirovic, M., Kovac, P., Skoric, B., Sekulic, M.: *Effect of Electrical Pulse Parameters on the Machining Performance in EDM*. Indian Journal of Engineering & Materials Sciences, 18, pp. 411–415, 2012.

Authors: Prof. Dr. Marin Gostimirovic, M.Sc. Dragan Rodic, Prof. Dr. Pavel Kovac, M.Sc. Vladimir Pucovsky, Assist. Prof. Dr Milenko Sekulic. University of Novi Sad, Faculty of Technical Sciences, Department for Production Engineering, Trg Dositeja Obradovica 6, 21000 Novi Sad, Serbia, Phone.: +381 21 450-366, Fax: +381 21 454-495.

Prof. Dr. Ildiko Mankova, PhD Jozef Beno, Technical University of Košice, Department of Technology and Materials, Faculty of Mechanical Engineering, Masiarska, 04001 Kosice 74, Slovakia, Phone: +421 55 602-2013.

E-mail: maring@uns.ac.rs
rodicdr@uns.ac.rs
pkovac@uns.ac.rs
ildiko.mankova@tuke.sk
jozef.beno@tuke.sk
pucovski@uns.ac.rs
milenkos@uns.ac.rs

ACKNOWLEDGEMENT

This paper presents a part of researching at the project "Application of artificial intelligence on monitoring of precision machining". Project number 680-00-140/2012-09/09.



11th INTERNATIONAL SCIENTIFIC CONFERENCE NOVI SAD, SERBIA, SEPTEMBER 20-21, 2012

Homar, D., Kopač, J., Dolinšek, S.

ADDITIVE MANUFACTURING AND HIGH SPEED CUTTING INCLUDED IN HYBRID MANUFACTURING

Abstract: *The aim of this paper is to present the benefits if we use two manufacturing processes to make one product. In our case we use subtractive and additive manufacturing technology. Subtractive process is the high speed cutting and additive process is the selective laser melting. We want to combine these two technologies in hybrid manufacturing. Hybrid manufacturing combine benefits of both processes and eliminate limitations. On the end of this paper is presented developed computer software which analyse a geometric design of product and determine which part of product will be done with specific technology.*

Key words: *Hybrid manufacturing, additive manufacturing, high speed cutting, conformal cooling*

1. INTRODUCTION

Because with the CNC milling is impossible to do certain geometric shapes, we decide that we combine this process with additive process in hybrid manufacturing. For additive process is chosen selective laser melting. In last 10 years that process progressed in process which can produce parts with similar mechanical properties as have the parts made by conventional processes. In the past some researches combined this two technic of production parts, but their main purpose were make near-net shape and then milling on the end shape. [1] Other scientists divided CAD model of products into two or more modules, where some modules make with milling and another with additive process, subsequently assembled in end product. [2] In our case milling combines with metal powder bed additive manufacturing or Selective Laser Melting (SLM). SLM is the process where the layer of metallic powder is melted and fused together layer by layer with the high powered laser, direct from CAD data, to create functional metal parts. Our goal is in order to part of product which is possible produce with conventional subtractive process will be manufacture with this milling and another part of product with complex geometry, which is difficult, impossible or very costly to machine, it will be manufactured with SLM. Therefore the product will be split, with straight plane, before the processing into two parts. For this purpose, we developed computer software for automatic splitting CAD model that is described below. The basic part, in most cases the biggest part, will be manufactured with milling and then the operator or robot will move the intermediate product from milling machine in machine for SLM. Subsequently, operator will fill building chamber with metal powder and then a machine will start building the second part of product from the upper surface, where the milling machine finished the its part of product.

2. BENEFITS AND LIMITATIONS OF BOTH TECHNOLOGIES

There are two or more processes at hybrid manufacturing. In our case it is about adding and subtracting materials. Every process of production has its advantages and disadvantages. The main goal of hybrid manufacturing is combining both processes and thus eliminating as much disadvantages as possible. The cutting process enables us to produce very accurate products with a high quality surface in a relatively short amount of time. Problems occur with products which have a complex geometrical structure. That is because the geometrical shape of the tool itself prevents us from producing a complexly structured product. The process of adding steel powder (our particular case is selective laser melting) is the exact opposite of the cutting process. The selective laser melting enables us to create any form because the product is created by adding materials in layers. But this process is not suitable for manufacturing big parts with relatively basic geometry, because is too time-consuming and too expensive for this kind geometry. On the other hand conventional manufacturing achieve high production speed for massive parts. The highest downside of all additive manufacturing processes is bad roughness of surface due building the products layer by layer and this principle leave the stair on surface known as the stair-stepping phenomenon. [3] This stair is eliminated with finishing machining. Therefore our goal is to make most of the product with cutting as it is a much faster and cheaper process. The product of the cutting process would than serve as the base on which we would begin to add materials with the selective laser melting process. This is in order to produce the part which we could not be made by conventional cutting because of the geometrical structure of conventional tools. The subtractive processes have a lot of material consumptions, but the additive processes have minimized material consumption. Because of these reasons, additive manufacturing is good options for production some part of the product where it is necessary to subtract a lot of material if a product is machined from cylindrical or cuboid of raw material. The cost of machining product increases with increasing the amount of subtracted material and with

geometric complexity of products. But the cost of product, which is made with additive technology, increases with increasing the amount added material, while the complexity doesn't affect the cost of product. On the Fig. 1 you can see that the cost depending on amount of subtracted/added material increase faster for additive manufacturing than the machining. [4]

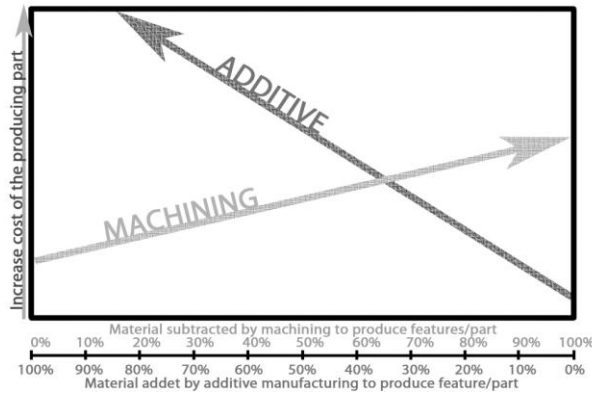


Fig. 1. The graph shows increasing the cost for machined part and additive manufactured part depend on amount of subtracted or added material.

Nowadays the materials, which are available for additive manufacturing, have excellent mechanical properties. Furthermore SLM process can build the part in variable material composition. The biggest problem with additive technology is that it isn't very known by toolmaker or other technologist and because this is very rarely used in manufacturing. Many technologists are very conservative, and with thus they are afraid to use new technology for manufacture products.

3. TOOL INSERT WITH CONFORMAL COOLING

Hybrid manufacturing is primarily intended for manufacturing injection moulding tool inserts with conformal cooling system. The conformal cooling system is a term for cooling channel which conform to the contours of the insert or cavity of injection moulding tool or tool for die casting. Difference between conventional cooling management and conformal cooling management is presented on Fig. 2. [5]

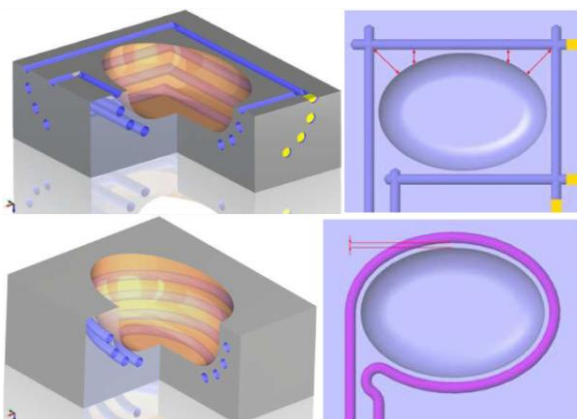


Fig. 2. Above: conventional cooling management; below: conformal cooling management [5]

With conformal cooling system is achieved a better dimensional accuracy of the moulded part, better mechanical properties of the part and reducing cycle time of injection moulding up to 40% [6, 7]. Every toolmaker wants to do the tool, with conformal cooling channel. But for conformal cooling system is decided by toolmaker only in special cases, due is not possible to do this system with conventional processes and additive manufacturing processes are too expensive for making entire tool. With hybrid manufacturing, we want to do moulds for injection moulding with conformal cooling channel cheaper, that it will be accessible for more toolmaker. On Fig. 3 we can see the example of tool insert with conformal cooling channels.

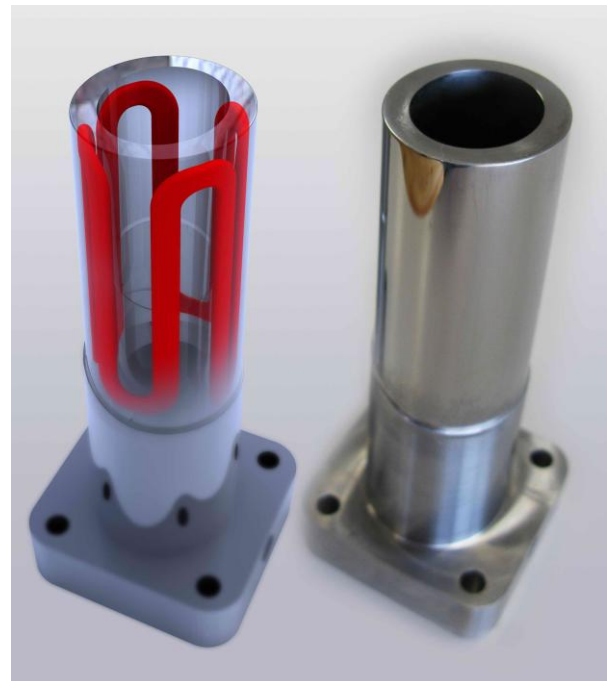


Fig. 3. Tool insert with conformal cooling channels [8]

4. ALGORITHM FOR THE AUTOMATIC SECTION OF THE CAD MODEL

We developed computer software which analyse a geometric design of product and determine which part of product will be done with CNC milling and which part will be done with additive technology. Subsequently it split the CAD model of product on two or more part and save part for CNC milling in format which is used for making CNC code and save part for additive manufacturing in STL format. This means that we developed algorithm for automatic determining the most suitable manufacturing sequences and technologies and also for converting this algorithm in computer software. Algorithm is implemented in Solid-Works CAD software by C# programming language.

Within the research project a hybrid manufacturing whose purpose is the development of tool inserts for the injection of polymers with adjusted cooling channels is developed [9]. Such an insert is shown on Fig. 4. The lower massive part of the insert will be

produced with the cutting process as the cooling channels in this part are only straight. The upper part however has its cooling channels adjusted to the surface of the tool and therefore do not have a straight shape. This is not possible to machine with conventional milling, so this part shall be developed by the technology of adding steel powder.

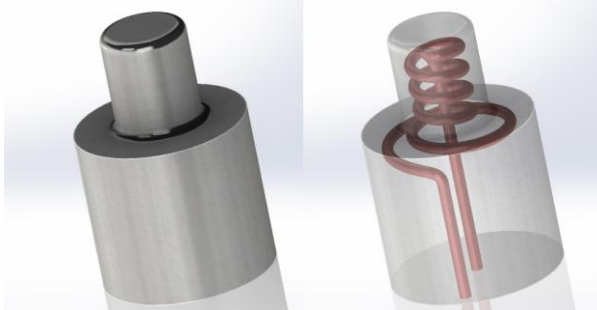


Fig. 4. Tool insert with conformal cooling channel

The goal is to achieve a high level of automation of hybrid manufacturing. That is why we are also developing an algorithm for the section of the CAD model into two parts. We are aiming to insert the whole CAD model into the control system of the hybrid cell, after which the computer will recognize by itself to which altitude can it produce the model by means of cutting. Following this, the program would divide the analysed part into two and it would save the upper part in the STL format, which is the most wide spread format for layer manufacturing technologies. Lower part would be saved in the STEP or any other format

which enables the generation of the CNC code for the milling machine.

4.1 How algorithm works

We have developed a new algorithm model for the automatic section of the CAD model. Figure 6 presents a flowchart of the aforementioned algorithm. It works by first enveloping two points. The first one represents the minimal coordinates of the presented model and the second one represents the maximal coordinates. Further analysis shall be carried out in a rectangular space which is defined by these two points. Then we start to intersect the model with parallel vectors. The starting points of the vectors are beneath the basic plane. The vectors are perpendicular to the basic plane, as shown on Fig. 5.

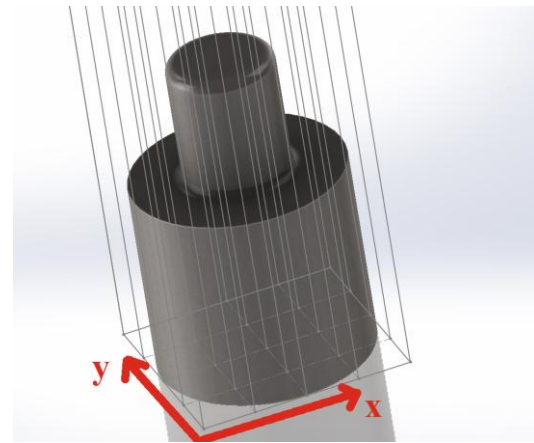


Fig. 5. Presentation of analysed model with vectors

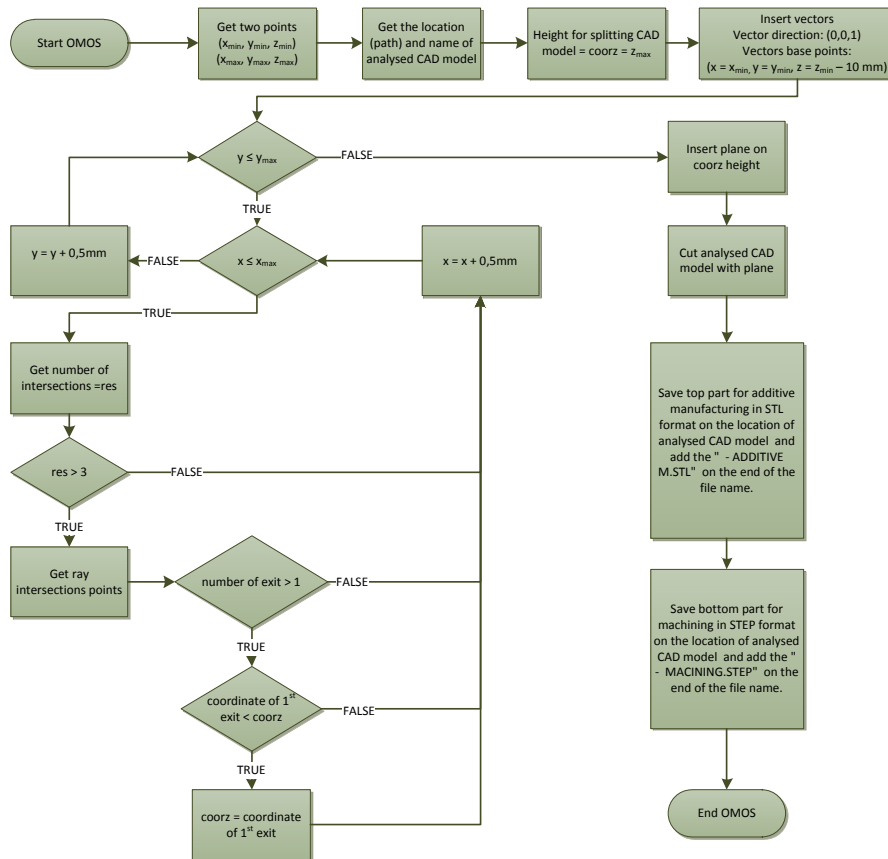


Fig. 6. Flowchart of algorithm for CAD model analysis

The key data for the analysis are the intersections of the vectors and the model (entrances and exits of vectors which are going in out of the model). Only vectors that have more than 3 intersections with the model shall be used. That is because the model also has an inner form at such spots. A minimal value of the Z coordinate of the first vectors exit with more than 3 intersections is a height to which the model can be made. On the basis, that a vector cannot reach the highest point of the model without intersecting, we can conclude that the cutting tool cannot reach the highest point without collision. That is why we can use the cutting process only to the aforementioned height.

4.2 Algorithm implemented in computer software

The algorithm has been implemented into the Solid-Works modeler through the API interface which enables us to automatize function of the programs, those which already exist. Also, new functions with mathematical support and support other operations can be generated. API allows us to write programs in different programming languages. Our algorithm has been implemented with using C#. The main added value is introduction of the vectors and how to search for the intersections with the model.

Developed algorithm defines the height to which it is possible to produce with conventional tools. After which the program on the defined height inserts a reference plane which parallels the main lower plane of the developing tool. At last it divides the CAD model into two pieces. The program saves the lower part in the STEP format in the folder which contains the former CAD model. The STEP format is meant for generating CNC code for milling. The upper part is saved in the STL format, for it is the most wide spread entry datum among technologies for adding materials.

5. FURTHER WORK AND CONCLUSION

The aforementioned algorithm needs to be further developed, for it enables a correct analysis only for models which have the beginnings of the cooling channels at the lower basic plane of the insert. In contrast, many of tools' inserts for injection-moulding of polymers have the cooling channel's beginnings at the side of the insert. Therefore it is appropriate that we apply the aforementioned analysis to more than just the lower side, as it is conducted now. We would then combine the results of different directions and acquire the correct height of the division of the CAD model.

The hybrid production shall enable to produce one work-piece with two different processes. As such we will enable manufacturing of products in any form with minimal production expenses. It is quite visible, that technologists avoid accepting new technologies if they are not easy to use and/or if they produce more expenses. We expect that they will be more warmly open the aforementioned technology when most of operations will be automated. In conclusion, in such a way we would be more effective in introducing layer manufacturing technologies into the tool shops, as selective laser melting of metal powders.

6. REFERENCES

- [1] K.P. Karunakaran, S. Suryakumar, Vishal Pushpa, Sreenathbabu Akula, Low cost integration of additive and subtractive processes for hybrid layered manufacturing, *Robotics and Computer-Integrated Manufacturing*, Volume 26, Issue 5, October 2010, Pages 490-499, ISSN 0736-5845,
- [2] Olivier Kerbrat, Pascal Mognol, Jean-Yves Hascoet, A new DFM approach to combine machining and additive manufacturing, *Computers in Industry*, In Press, Corrected Proof, Available online 6 May 2011, ISSN 0166-3615, DOI: 10.1016/j.compind.2011.04.003.
- [3] S.O. Onuh, K.K.B. Hon, Optimising build parameters for improved surface finish in stereolithography, *International Journal of Machine Tools and Manufacture*, Volume 38, Issue 4, March 1998, Pages 329-342, ISSN 0890-6955, DOI: 10.1016/S0890-6955(97)00068-0.
- [4] Todd Grimm: User's guide for rapid prototyping, United States of America, Society of manufacturing Engineers, 2004, ISBN 0-87263-697-6.
- [5] Boivie K., Dolinšek S., Homar D.: Hybrid Manufacturing: Integration of Additive Technologies for Competitive Production of Complex Tools and Products, *Proceedings of the International Research/Expert Conference: "Trends in the Development of Machinery and Associated Technology" TMT 2011*, Prague, Czech Republic, 12-18 September 2011
- [6] B. Duleba and F. Greškovič, "Conformal cooling for plastic injection moulding," *IT-strojar*, pp. 1-5, 12. 12. 2011.
- [7] Gerd Pötsch, Walter Michaeli: Injection molding: an introduction, Munich, Carl Hansen Verlag, 2008, ISBN 978-1-56990-419-0
- [8] <http://www.texerdesign.it/en/tool/tecnology.html>, 17.7.2012,
- [9] Dolinšek, Slavko, Panjan, Peter, Syvanen, Tatu, Ramovš, Jože. Laser-sintered tools for the die-casting of aluminium. *Stroj. vestn.*, 2006, letn. 52, št. 11, str. 738-751.

Authors: David Homar; prof. dr. Janez Kopač, univ. dipl. inž., Dr. h. c.; izr. prof. dr. Slavko Dolinšek, univ. dipl. inž. MBA; Faculty of Mechanical Engineering, University of Ljubljana, Laboratory for cutting, Aškerčeva 6, 1000 Ljubljana, Phone.: +386 1 477 14 38, Fax: +386 1 477 17 68, E-mail: david.homar@fs.uni-lj.si
janez.kopac@fs.uni-lj.si
slavko.dolinsek@fs.uni-lj.si

Janković, P., Radovanović, M.

EFFECT OF PROCESS PARAMETERS ON CUTTING ABILITY IN ABRASIVE WATER JET MACHINING

Abstract: The process of the abrasive water jet cutting of materials, supported by the theories of fluid mechanics, abrasive wear and damage mechanics, is a high-tech technologies that provides unique capabilities compared to conventional machining processes. It is defined by numerous influencing factors, which determine depth of cut, volume of separate material, as cut quality. Substantial efforts has bin made in understanding effects of individual influencing factors, lake: diameters of water and abrasive orifice (nozzle), water pressure, abrasive flow rate, workpiece thickness, distance of cutting head from material surface, feed rate, etc.

The paper presents results of research on the effect of the most influencing parameters on the linear cutting speed to just barely cut through material as geometry of the cut.

Key words: abrasive water jet cutting, material processing, separation cutting speed, kerf geometry

1. INTRODUCTION

Abrasive water jet (AWJ) cutting is a non-conventional machining process that uses high velocity water with abrasives for cutting a variety of materials. It is most suitable process for very thick, highly reflective or highly thermal-conductive materials, as well as hard materials. Abrasive water jets can cut a wide range of thickness. Typical thickness are 100 mm for stainless steel, 120 mm for aluminium, 140 mm for stone, 100 mm for glass, but not limited [1]. AWJ makes it possible to cut random contours, very fine tabs and filigree structures. Abrasive water jet cutting is capable of produce parts which do not require further processing with tolerances of ± 0.1 mm. Toxic fumes, recast layers, slag and thermal stress are totally eliminated.

Abrasive water jet cutting belongs among complicated dynamical and stochastic processes with incomplete information about mechanism and side effects character. In AWJ cutting, the final cut quality and the dimensional accuracy depends on the process parameters selection [2], [3].

Process optimization, as a background of its successful application, is provided by correct choice of influencing factors. First step toward to this goal is identification and understanding of process influencing factors.

In this paper, an experimental investigation of the process parameters effect on cutting ability of EN AW-6060 aluminium alloy and EN X2CrNi19-11 stainless steel sheets machined by abrasive water jets is presented. Special attention has been paid to the determination of cutting speed limits, as well as the size and geometry of the cut.

2. PARAMETERS OF AWJ CUTTING PROCESS

Accuracy and quality of the cutting process depend on a wide range of parameters and technological effects of these parameters. These parameters can be classified according to the Fig. 1.

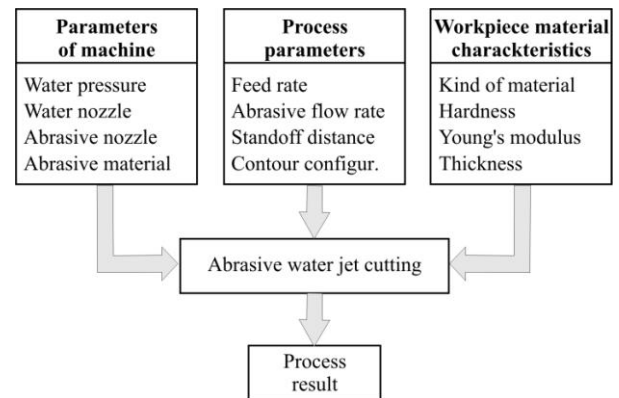


Fig. 1. Parameters of abrasive water jet cutting process

High-pressure pump is the most important element, i.e. "heart" of the machine for abrasive water jet cutting (Fig. 2). It creates the required operating pressure and supplies the machine on the adequate amount of water flow rate [4].

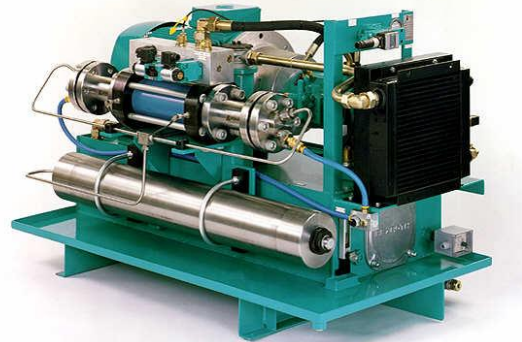


Fig. 2. High pressure pump for AWJ cutting

In industrial processes are used high-pressure piston pumps power from 18 to 75 kW, providing flow rate of 2 to 7.6 l / min. Maximum water pressure is used is up to $p=413$ MPa.

Reputable manufacturers of machinery for abrasive water jet cutting develop their own high pressure pumps (Flow Corporation, Omax, Bystronic), while most manufacturers decided to use specialized equipment manufacturers such as Ingersoll-Rand, KMT Waterjet, RESATO, Jet Edge and other.

In the process of abrasive water jet cutting a high pressure supply line directs the pressurized water from the pump to the cutting head (Fig. 3).

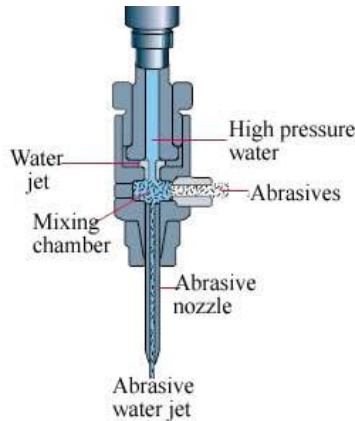


Fig. 3. Abrasive water jet cutting head

When the pressurized water comes out from the orifice, a water jet is created. The result is a very thin, extremely high velocity (approx. 900 m/s) water jet. Then, solid abrasive particles are added and mixed with the water jet. Resulting abrasive water jet is focused to the material through abrasive nozzle.

It is recommended that, as part of the cutting head, use of abrasive nozzle with an openings diameter 3 to 4 times larger than the openings diameter of the water nozzle. Thus, the commonly used "combination" diameter the openings of water and abrasive water nozzle (d_0/d_A) are the following: 0.25/0.76; 0.30/0.89; 0.30/1.02; 0.33/1.02 and 0.36/1.14 mm.

Abrasive in the form of fine particles is a component of the abrasive water jet. Abrasive particles are made of various materials, sizes and shapes, depending on the application. The most widely used abrasive in abrasive water jet process is the mineral garnet. It is tough, hard and inexpensive mineral of pink color. Depending on the application, is produced in a variety of sizes. Finer grain with average grain diameter of 150 μm is used to cut fine-quality, medium sized with average grain diameter of 180 μm is the most widely used, while coarse grain with average grain diameter of 210 μm is used to rough cut quality but with a greater cutting speed. The most famous manufacturers of garnet for industrial use are companies from the United States (Barton Mines), Australia (GMA Garnet), China (Dragon Abrasives) and India (Stain Stones), and these are the countries that export significant amounts of garnet. Russia and Turkey also produces industrial garnet in large quantities, but it does not export significant quantities of this material. For use in abrasive water jet cutting abrasives are mostly supplied in packages of 25 kg. Price varies depending on the manufacturer and size of the abrasive particles, ranging from 70 to over \$ 300 per ton.

Feed rate (cutting speed) is the speed of the relative movement of the cutting head relative to the workpiece. The feed rate is an important parameter of this technology because it affects the quality of the cut and amount of removed material. Also, depends on the type and thickness of material being cut, and the desired cut quality.

The abrasive flow rate is the amount of abrasive material per unit of time, which is added to water jet, for mixing and forming abrasive water jet. In the newer machines abrasive flow can be regulated during operation, specified by the program. Higher flow rates leads to higher productivity and better quality of the cut, but with the increased processing costs. Depending on the desired productivity and quality of cut, in practice, abrasive flow rate takes values between $q = 300$ and $q = 400$ g/min.

3. EXPERIMENTAL WORK

3.1. Experimental set-up

A series of water jet cutting experiments were conducted using a Byjet 4022 abrasive water jet cutting machine (Bystronic AG, Switzerland). As workpiece material, aluminium alloy AA-ASTM 6060 (Al MgSi) and stainless steel AISI 304 (EN X2CrNi19-11) was used. These materials are chosen as a workpiece material because they are very attractive, possess resistance to corrosion and can provide significant value for the end user. Also, these materials are characterized by high reflectivity and thermal conductivity. This makes them relatively difficult to cut with lasers. Abrasive water jet cutting, which does not create an observable heat affected zone, is much more useful for cutting aluminum and stainless steel for modern applications.

Although AWJ cutting involves a large number of variables and virtually all these variables affect the cutting results (kerf width, taper and surface roughness), only few major and easy-to-adjust dynamic variables were considered in the present study. Those are: feed rate (the speed at which the cutting head moves along workpiece during cutting operation), material thickness and abrasive flow rate. The other process parameters were kept constant using the standard machine configuration ($d_0 = 0.3$ mm; $d_A = 1.02$ mm; $p = 400$ MPa).

3.2. Separation speed

Firstly, through a series of experiments was determined linear cutting speed at which still comes to the realization of complete cut, i.e. to just barely cut through material. In this way a boundary line that separates the area in which the cut is complete, the ones where we have only a partial cut (Fig. 4) is defined.

The survey was conducted on prepared specimens with thickness of: $s = 6, 8, 10, 12, 15$ and 20 mm. Other parameter values of the process were:

- workpiece material: stainless steel and aluminium alloy,
- water pressure: $p = 400$ MPa,
- water nozzle diameter: $d_0 = 0,30$ mm,
- abrasive nozzle diameter: $d_A = 1,02$ mm,
- abrasive flow rate $q = 300$ and 400 g/min and
- distance of the cutting head to workpiece $z = 2$ mm.

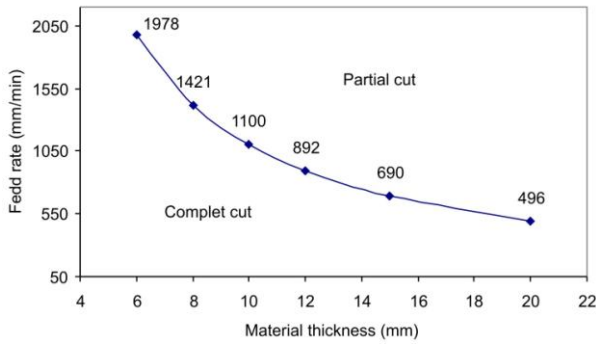


Fig. 4. Cut-through speed boundary line

Feed rate (v) is, for each cut, gradually increased, until there was no cut in which the sample is not completely cut through, as shown in Fig. 5.



Fig. 5. Incomplete cut (view from the bottom side)

3.3. Kerf geometry

Geometry of cut is a characteristic of major interest in abrasive water jet cutting process. Cutting using AWJ can create tapered edges on the kerf, especially when cutting at high feed rates.

The kerf geometry of a through cut generated by abrasive water jets may be described as in Fig. 7. A top and bottom kerf width was measured from the optical microscope images with 40 times magnification, equipped with a CMOS camera and USB connection to a PC (Fig. 6). Camera sensor size is 1/2 inch, a resolution of 1280x1024 dots and wide field of view of 5.4 mm.

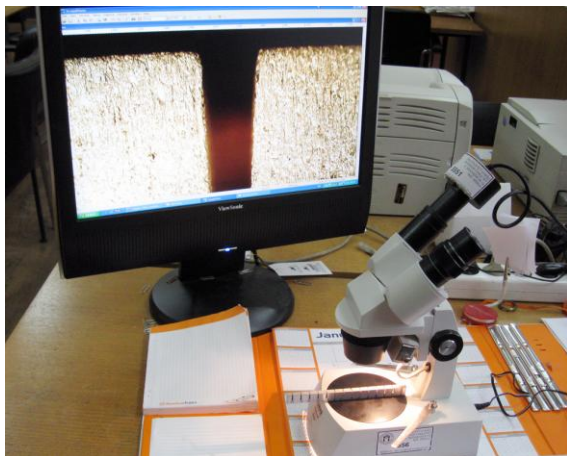


Fig. 6. Optical microscope with CMOS camera

These measurements were taken for each cut away from the ends of the slots to eliminate any effect of the cutting process at the jet entry and exit. The standard establishes a zone of significance for the measurements of widths at the top and bottom edge by a distance, Δs , related to material thickness as specified in the standard.

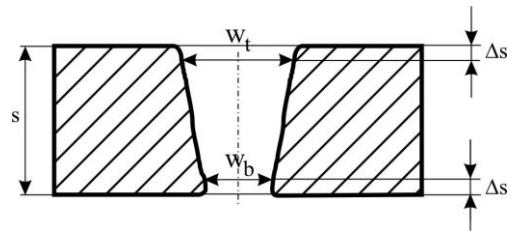


Fig. 7. Cut geometry by AWJ cutting

The top kerf is commonly wider than the bottom due to the decrease in abrasive water jet power as a unique feature of AWJ technology. As a result of this, a taper is produced. The large kerf taper ratio worsens the perpendicularity of the straightness of the cutting cross-section, resulting in an inaccurate dimensional quality.

4. RESULTS AND DISCUSSION

The value of the cutting speed at which there is a complete separation of material through its whole thickness is influenced by many factors, among which the most important are: the type of material, its thickness, abrasive flow rate and water pressure. With consideration that, in practice, for cutting we always use the maximum pressure that the machine can achieve, the influence of water pressure, even though it has a major impact on the ability of AWJ cutting has not varied, but the maximum value of water pressure of $p=400$ MPa was used.

Diagram showing the influence of the type of material, thickness of the workpiece and the abrasive flow rate on cut-through cutting speed (feed rate) is presented in Fig. 8.

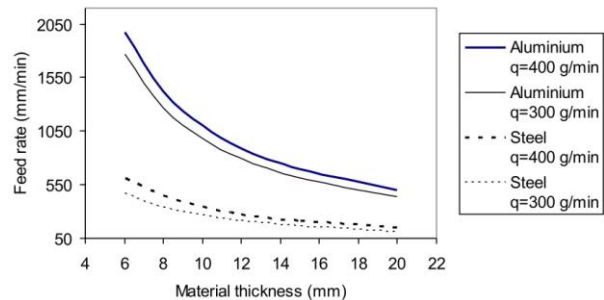


Fig. 8. Effect of process parameters on separation speed

It may be noted that the type of material and its thickness have great influence on the cutting speed limit. For example, the maximum speed at which it is possible to cut stainless steel with thickness of $s=8$ mm is $v=440$ mm/min, while the workpiece made of aluminum alloy, with the same thickness, can be cut at a speed of $v=1421$ mm/min. The results show that, the greater the amount of abrasive grains that participate in the process of cutting material, separation effect is larger, and therefore the depth of cut increases. Kerf is characterized by a small rounded corner at the top edge due to the plastic deformation of material caused by jet bombardment. As the kerf is wider at the top than at the bottom, a taper is produced. As shown in Fig. 9, abrasive water jets will generally open a tapered

slot with the top kerf W_t being wider than the bottom kerf W_b .

Fig. 9 and Fig. 10 show some typical and representative trends and relationships between the kerf geometry (top kerf width W_t and bottom kerf width W_b) and the cutting parameters.

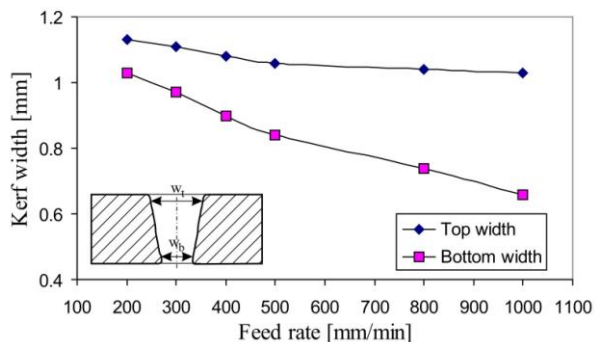


Fig. 9. The effect of feed rate on the kerf geometry

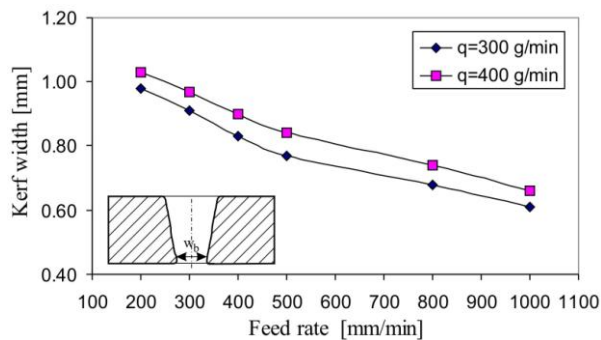


Fig. 10. The effect of abrasive flow rate on bottom kerf width

The effect of feed rate on the top kerf width and bottom kerf width is shown in Fig. 9. It can be seen from the figure that the feed rate has a negative effect on both the top and bottom kerf widths. The negative effect of the feed rate on both the top and bottom kerf widths is because a faster passing of abrasive water jet allows fewer abrasives to strike on the jet target and hence generates a narrower slot.

In contrast to brittle materials, ductile materials are sensitive on number of abrasive particles that hits material surface. By increase of abrasive flow rate the larger number of abrasive particles share in machining process, which has positive effect on kerf geometry. The effect of abrasive flow rate is shown in Fig. 10. It can be seen that higher abrasive flow rate produce greater kerf widths, especially bottom kerf width.

5. CONCLUSION

The flexibility and cool cutting characteristics of the AWJ make it an important tool for cutting applications of new materials such as composites and sandwiched materials that are difficult to machine with traditional machining processes, and is also a cost-effective way of cutting stainless steel and aluminum alloys.

Although there are no restrictions on the types of workpiece material by the use of AWJ, however there

is a limit to the thickness of the workpiece that can be cost-effective machined, compared to other cutting processes. Therefore, the knowledge of material cutting speed limit and influence of process parameters is step towards ensuring optimum cost of production and meeting the demands of customers.

The primary interests in sheet steel processing are the kerf shape (kerf width). The kerf profile changes with feed rate. Cuts at low feed rate generate almost straight cutting cross-section, whereas high feed rates generate a convergent shape.

In this study, the cutting ability and kerf geometries of the machined surfaces in terms of process parameters in AWJ-machined aluminium alloy and stainless steel were investigated experimentally. Summarizing the main features of the results, the following conclusions may be drawn:

- The value of process parameters at which the cut is complete, depend primarily on the type of material and thickness of the workpiece. During the processing of steel, cutting speed is 3 times less a processing aluminum of the same thickness.
- As the feed rate increases, the AWJ cuts narrower kerf. This is because the feed rate of abrasive water jet allows fewer abrasives to strike on the jet target and hence generates a narrower slot.
- Higher abrasive flow rate produce greater kerf width, especially bottom kerf width because the larger number of abrasive particles share in machining process which has positive effect on kerf geometry.

It should be noted that if the kerf width can be predicted, they may be compensated for in the design and process planning stages and by controlling the nozzle in the machine.

6. REFERENCE

- [1] Janković, P., Radovanović, M., Radenković, G: *The ability to process modern materials by abrasive water jet cutting*, Mechanical Engineering in XXI Century, Faculty of Mechanical Engineering, Niš, Serbia, 2010.
- [2] Hloch, S. and Fabian, S: *Qualitative analysis of AWJ factors affecting the surface roughness*, Wissenschaftliche Beiträge, TFH Wildau, Germany, 113-119, 2006.
- [3] Lebar, A. and Junkar, M: *Simulation of abrasive water jet cutting process*, Modeling Simul. Mater. Sci. Eng. 12, 1159-1170, 2004
- [4] Janković, P, Radovanović M, Vičovac N: *Pumpa visokog pritiska – "srce" mašine za konturno sečenje abrazivnim vodenim mlazom*, HIPNEF, str.113-118, 2004

ACKNOWLEDGMENTS

Paper is result of technological project TR35034 which is supported by Ministry of Education, Science and Technological Development of the Republic of Serbia.

Authors: Dr. Predrag Jankovic, Dr. Miroslav Radovanovic., University of Nis, Faculty of Mechanical Engineering.
E-mail:jape@masfak.ni.ac.rs, mirado@masfak.ni.ac.rs

Kopac, J., Cus, F., Stoic, A., Zabkar, B.

SOME IDEAS ABOUT SUSTAINABLE MANUFACTURING CONCEPT

Abstract: Crises are not necessary in productions and in selling market. Reasons are mostly in wrong state policy. Some solutions are brought by engineers with their deep knowledge in prediction technique. Paper presents some ideas how to save energy by prediction and ways of sustainable manufacturing.

Key words: Sustainable manufacturing, reducing costs, MQL, HP jet cooling, cryogenic machining.

1. INTRODUCTION

The crises have been going up and down for the last hundred years after technical revolution. The reasons were mainly gap between production and policy of governments. To spend more as country can produce firstly means inflation, then restriction, the demonstrations of workers and citizen... If government prepares solution on base, how to save money on workers in public administration, they go to strike. More countries all over the world produce less than their citizens consume. Reason is a gap between production sector and group of people employed in public administration so called workers, which are not connected directly or indirectly with productions or service activity. Many of them have jobs and salaries without the beneficial work.

Technical sector, engineers and manufacturers can help partly with solutions in manufacturing areas with their high education of modern production. To produce better, it is necessary to know more than 50 different concepts. From classical machining, CNC machine tools to the adaptive processes as MQL, LN cryo assisting, HP jet cooling, HSC, RP, etc. Big specter of information and knowledge allows engineers that they can find the appropriate procedure from the beginning of the process. Till now, engineers were forced in system of mass production with motto: faster/cheaper with minimal respect to nature/ecology.

To care only about ecology is not enough. It is something partly connected with nature, but not including workers and other population properly. Sustainable concept is something more, including people properly and their social needs. To define what means recession for people, we can show in my old and well known diagram.

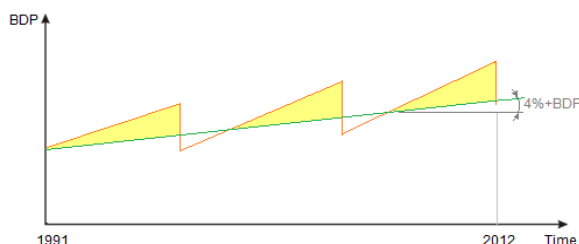


Fig. 1: Fluctuations in production. [1]

2. INFLUENCE OF FLUCTUATIONS ON PRODUCTION

Hatched areas [1] “so called negative work” are also quantity measurement for workers – they are stressed. What are people doing under stress we know! If we know this up and down phenomena, stress by people and short period of satisfaction, we don’t need to hurry too much. After few years we will be on the same quantity level of product with bigger satisfaction, we can say with sustainable approach.

Work represents a big part of employee life time. Why is he working? In order he needs money to make a living for himself and his family. It is only new concept, new way for surviving. For thousands years people have lived in many different ways that they came to food. Today money is food, so he is looking as first on money. Main part of work and production should stay to him. But it isn’t so. The money is shared on too many different things just for case. Today workers are too much taxed. It is one of the reasons how and where money disappears. Next reason is owner of the factory. He can divide money/benefit properly or unfairly. There are many cases when money disappeared from factory account before salaries were given to workers. Okay, we know more or less all this story of dirty management. From this philosophy we continue to our area – production. Where and how can we save money with technology.

3. THEORETICAL BACKGROUNDS TO ELEMENT WHICH ACHIEVE ON SUSTAINABLE EFFECTS

Machinability is always questionable by new pair of material that we cut and cutting tool. Criteria are old and well known. To define machinability, we have to measure tool wear, cutting forces, surface roughness and define chip shapes. Tool wear varies widely due different cooling system, even we have the same pair of workpiece material and cutting tool material because of different friction coefficient (μ).

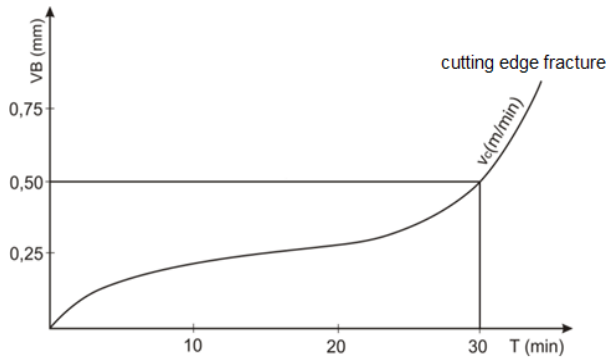


Fig. 2. Tool wear curve [2]

Cutting force is shared on x, y, z components. The main cutting force F_c is mostly affected by depth of cut (a_p) and cutting speed (v_c).

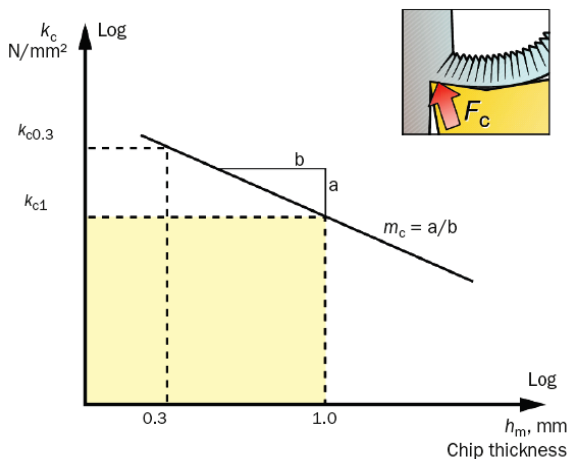
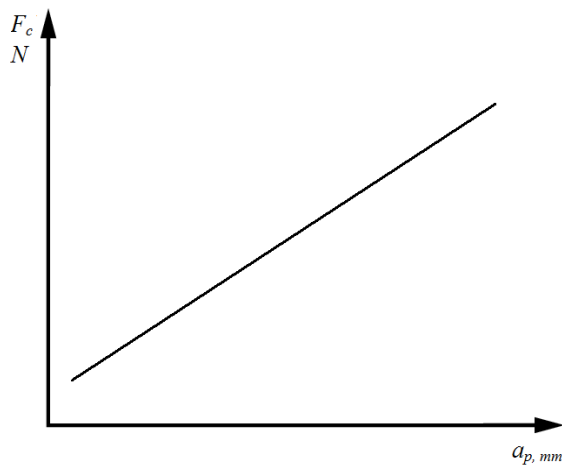


Fig. 3. Main cutting force and specific cutting force [3,4]

$$k_c = \frac{k_{c1} \times l}{h^z} = \frac{F_c}{A} = \frac{F_c}{bh} \quad (1)$$

$$P_r = F_c v_c = k_{c1} b h^{1-z} v_c \quad (2)$$

Specific cutting force k_c is measure for energy consumption of process (2). It is calculated with Kinzle equation (1). First we have to specify the technology of machining. Second step to achieve better efficiency is with adequate sharing depth of cut to rough and fine

cut. Thin chip and small depth of cut cause higher specific force.

We have to find additional sources for minimizing cutting forces. [3] They are connected with friction (μ). Friction and tribology are always present on cutting tool during machining. The influence is on tool wear, so in every cutting fluid we can find additives for reduce sliding coefficient. It reduces length (l) of shear zone chip formation area.

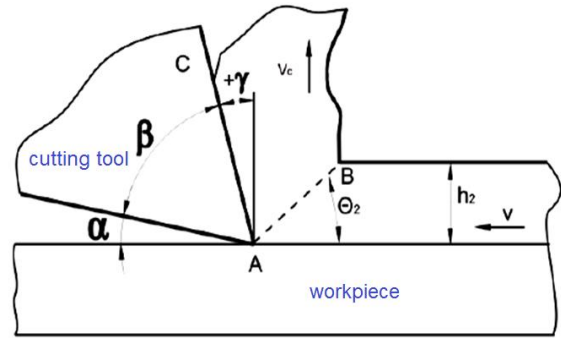


Fig. 4. Cutting zone, chip formation area [3]

$$\tau_s = \frac{F}{A} = \frac{F}{bl} \quad (3)$$

Shearing stress (3) depends on cutting force (F), length (l) of shear zone and chip thickness (b). The sliding of chip over rake face of cutting tool is mostly depend from friction coefficient (μ) between workpiece material and cutting tool material. Therefore we use difference coating layers on cutting tool inserts.

	PVD HARD COATINGS			SOFT COATINGS
	TiN	TiCN	TiAlN	MOVIC
Debelina (μm)	1,5-3	1,5-3	4-8	0,2-0,5
Trdota (HV 0,05)	2200	3000	3300	30
Maks. temp. ($^{\circ}\text{C}$)	<600	<450	<800	<300
Koeficient trenja	0,4	0,3	0,25	0,05-0,1

Fig. 5. MOVIC self-lubricating and anti-adhesive coating [5]

With reducing cutting coefficient (μ) from 0,8 to 0,1 (possibility), we also reduce cutting force. Of course the ratio is not the same, but generally in in range of 10 – 50%. To have right data of cutting force values, we have to measure them. Measured cutting forces are one of important data in technological data bank.

$$P_c = F_c \cdot v_c \quad (4)$$

Electro energy consumption of process (4) depends of cutting force F_c and cutting speed v_c . As case, we can discuss relationship to minimizing power consumption for 30%. More than thousands machine tools which are operating day and night in money factories in many countries. We can reduce electricity production for more than 10%. This is something. We can close on this way some electro power plants that cause environmental pollution with their operating state. This represents important part of sustainable manufacturing.

4. ADAPTED MODERN CUTTING PROCESSES

Engineering challenges of sustainable production are going forward. We have modern adaptive processes for machining as MQL, HP jet cooling, LN Cryogenic machining.



Fig. 6. MQL [6]

Minimum quantity lubricant can save money, improve tool life and improve the part finish. But it may involve changes to both the equipment and the processing strategy. The cost of coolant is approximately 15 percent of the life-cycle operational cost of a machining process. This cost continues to rise. It includes the costs associated with procurement, filtration, separation and disposal. Already the costs for disposal of coolant are higher than the initial cost of the coolant, and they are still rising. Even stricter regulations are under consideration for coolant usage, disposal and worker protection. As a result of all of this, coolant in wet machining operations is a crucial economic issue. An alternative, machining with “minimum quantity lubricant,” or MQL, is gaining acceptance as a cost-saving and environmentally friendly option in place of some wet machining processes.

MQL (Fig. 6) permits dramatic cuts in coolant costs, while protecting workers and the environment. It also delivers improved tool life and surface finish, even though tool life is often the reason why wet machining is applied. MQL can deliver better life for two reasons: the optimum concentration of lubrication can be specified for a given operation, and silicon particle contamination suspended in the cutting fluid is eliminated [7].

Removing coolant from machining presents challenges related to heat, tool life and chip removal, but certain systems and strategies can address these challenges. Heat dissipation without coolant requires a different approach to processing the part. Special tooling using lubricant ducts (as well as high-performance coatings and heat-resistant materials) is also required. Chip evacuation systems must be used as well [7].

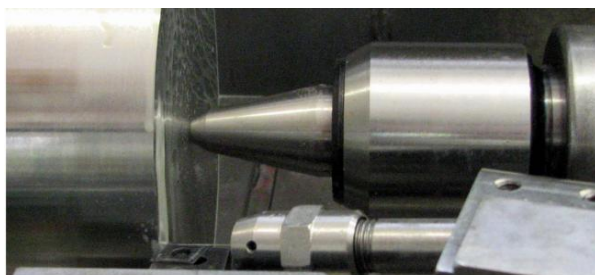


Fig. 7. HP jet cooling [8]

In high – pressure coolant condition (Fig. 7) the average cutting temperature reduced by 16% than dry condition. As the temperature at the chip-tool interface is one of the most important factor influencing the machining process, so high – pressure jet cooling is complimentary for machining process.

High-pressure jet – assisted machining has become a powerful technique for increasing production efficiency. The main advantages of HP jet cooling cutting process are:

- Increasing of cutting speed and federate up to 35 percent for pair of cutting material and workpiece.
- Improved chip control.
- Increased tool life.
- Drastically reduced cutting edge temperature compared to conventional flooded cooling.
- Better surface integrity.
- Reduction of cutting forces.

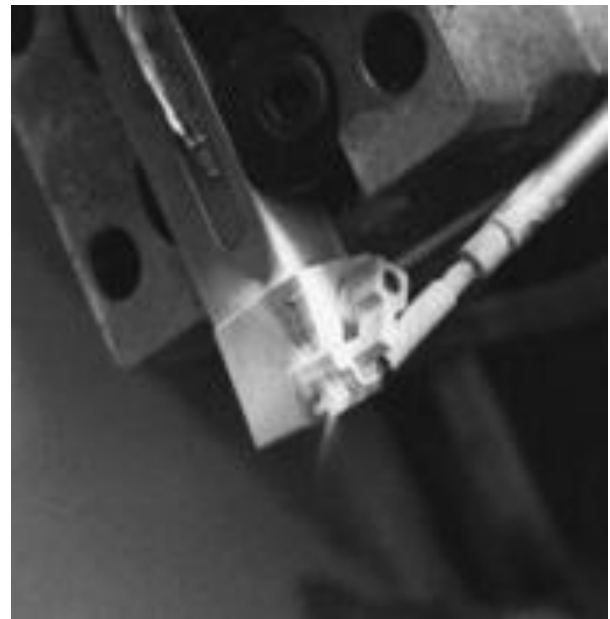


Fig. 8. Cryogenic machining [9]

It is known that oil-based cooling lubricating fluids (CLF) are one of the most unsustainable elements of machining processes. Most CLFs are formulated from mineral oils, which are extracted from crude oil, primarily for economic reasons.

In cryogenic machining a cryogenic CLF (non-oil-based) is delivered to the cutting region of the cutting tool, shown in Fig. 7, which is exposed to the highest temperature during the machining process, or to the part in order to change the material characteristics and improve machining performance. The CLF is nitrogen fluid, which is liquefied by cooling to $-196\text{ }^{\circ}\text{C}$ (liquid nitrogen – LN). Nitrogen is a safe, non – combustible, and noncorrosive gas. The LN in cryogenic machining systems quickly evaporates and returns to the atmosphere, leaving no residue to contaminate the part, chips, machine tool, or operator, thus eliminating disposal costs. Additionally, cryogenic machining could help to machine parts faster, with higher quality, increased machining performance, and a reduced overall cost [10].

Some potential benefits of cryogenic machining are:

- Considerably reduced friction coefficient on the tool – chip interface.
- LN applied locally to the cutting edge is superior to emulsion in lowering the cutting temperature.
- Increased tool-life due to lower abrasion and chemical wear, increased material removal rate with no increase in tool-wear and with reduced cutting tool changeover cost, resulting in higher productivity.
- Improved machined part surface quality with the absence of mechanical and chemical degradation of the machined surface.

In the machining of high-temperature alloys, conventional oil-based CLFs are not always effective enough in terms of decreasing the high cutting temperature, increasing tool life, reducing machining costs and improving environmental/social sustainability. The problem is that conventional CLFs do not access the toolpart and tool-chip interfaces, which are under high contact pressure, as they vaporize at a high temperature generated close to the cutting tool edge. Taking this into account, it becomes clear that technologies employing conventional CLFs are ineffective and unsustainable when machining materials with high shear strength and low thermal conductivity. In this case, the avoidance of conventional CLFs, would yield an enormous gain from the sustainability point of view.

5. CONCLUSION

Study to be engineer and working on average level is not enough. Engineer has to be innovative, full of ideas and always looking for new, better and more ecological manufacturing concept. It must be visible also by cost of production. With adapted modern cutting processes we can achieve higher productivity with lower environmental pollution. Choice of adaptive process depends on the machining application. In general all of mentioned processes have many advantages in view of sustainable machining, and this is a key to increasing productivity.

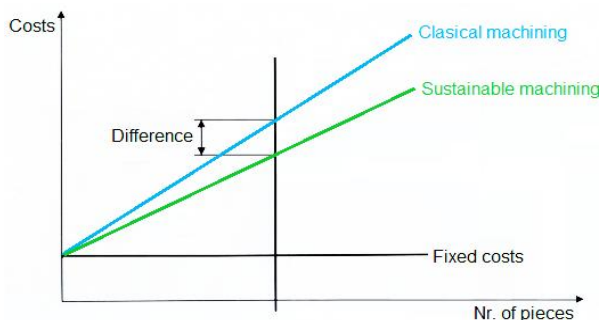


Fig. 9. Costs in production

Difference of costs and better benefit should be shared also to workers in production. This is a guaranty for more intensive work. All advanced ideas should be taken in to consideration and tested, because we will never know everything, and in many cases some solutions reveals beneficial results.

6. REFERENCES

- [1] F. Pušavec, J. Kopač (2011). Sustainable production - a goal or just words? *MIT SLIM conference*.
- [2] J. Kopač, M. Sokovic, S. Dolinsek (2001). Tribology of coated tools in conventional and HSC machining. *Journal of Materials Processing Technology*, vol 118, Issues 1–3, 3 p. 377–384.
- [3] Kopač J. (2008). *Odrezavanje: teoretične osnove in tehnološki napotki*. Ljubljana, Littera picta.
- [4] Online catalogue, <http://www.sandvik.coromant.com>, accessed on 2012.
- [5] Coatings for tools, <http://www.sts-group.it/eng/movic.html>, accessed on 2012.
- [6] F. Čuš, M. Soković, J. Kopač, J., Balič (1998). Model of complex optimization of cutting conditions. *Journal of Materials Processing Technology*, vol. 64, Issues 1–3, p. 41–52.
- [7] Understanding MQL. <http://www.mmsonline.com/articles/understanding-mql>, accessed on 2012.
- [8] D. Kramar, P. Krajnik, J. Kopač (2009). Capability of high pressure cooling in the turning of surface hardened piston rods. *Journal of Materials Processing Technology*, vol 210, Issue 2, p. 212–218.
- [9] F. Pušavec, J. Kopač (2011). SusCryMac kot čista tehnologija obdelave - inovacija, ki prepolovi stroške. *IRT 3000 : inovacije, razvoj, tehnologije - tri smernice, en cilj*, p. 24-27.
- [10] F. Pusavec, D. Kramar, P. Krajnik, J. Kopač (2010). Transitioning to sustainable production – part II: evaluation of sustainable machining technologies. *Journal of Cleaner Production*, vol. 18, Issue 12, p. 1211–1221.
- [11] A. Stoić, J. Kopač, G. Cukor (2005). Testing of machinability of mould steel 40CrMnMo7 using genetic algorithm. *Journal of Materials Processing Technology*, vol. 164–165, p. 1624–1630.
- [12] F. Pušavec, E. Govekar, J. Kopač, I.S. Jawahih (2011). The influence of cryogenic cooling on process stability in turning operations. *CIRP Annals - Manufacturing Technology*, vol. 60, Issue 1, p. 101–104.

Authors:

J. Kopač, B. Zabkar

Faculty of Mechanical Engineering, University of Ljubljana, Askrceva 6, 1000 Ljubljana, Slovenia

F. Cus

University of Maribor, Faculty of Mechanical Engineering, Smetanova 17, 2000 Maribor, Slovenia

A. Stoić

Machine Tools and Technologies Department, ME Faculty, University of Osijek, Trg I. B. Mazuranic 18, HR-35000 Slavonski Brod, Croatia

Kovač, P., Radonjić, S., Mitrović, A., Sovilj-Nikić, I.

DETERMINING THE PROCESSING PARAMETERS FOR STEEL AISI 6150 IN LASER CUTTING

Abstract: Laser processing is very precise and economical method of material processing. The advantages of laser cutting over conventional cutting methods are reflected in the high-speed processing capability, narrow width of the cut, straight cut edges, low roughness of cut surfaces and the possibility of creating complex profiles. The process of laser cutting and cut quality depends on proper selection of cutting parameters. A set of cutting parameters is supplied with each laser and they are optimized for cutting certain materials. The paper presents the process of defining new parameters for cutting parts made of spring steel (AISI 6150) for which the recommended cutting parameters have not been provided by Byspeed 4020 laser manufacturer. Adequate accuracy of the quality and shape of the cut has been reached. Therefore, the obtained parameters are reliable and are further used in the production process.

Keywords: laser cutting, cutting parameters, production process

1. INTRODUCTION

Laser *Byspeed 4020* is a product of Swiss company Bystronic that belongs to latest generation of lasers. Its cutting speed of thin sheet metal exceeds all previous Bystronic models and other competitor's products. For example, some tasks such as cutting steel plates 10 mm thickness which classic laser performed for 330 to 360 minutes, the laser can do for 160 minutes. Therefore, this type of laser shows a drastic difference in the speed of making pieces, which is nowadays very important, regarding the very short deadlines for making appropriate job. Also, it should be noted the high accuracy of this machine which was not the case with lasers. For sheets up to 6 mm thickness, this machine has an accuracy of one tenth of making up, on sheet thickness and 10 mm accuracy varies by three tenth, which are remarkable results.



Fig. 1. Laser Byspeed 4020

Laser is used solely for cutting certain types of metal. It can cut stainless steel and acid resistant steels up to thickness of 10 mm. In the process of cutting it is necessary to add the appropriate gas so that cutting could be done. In above mentioned laser it is used oxygen and nitrogen. When cutting stainless steel, acid resistant, fire-resistant steels, nitrogen is used, and in the case of cutting carbon steel it is used oxygen, regarding that laser can cut carbon steel up to thickness of 25 mm. Laser can cut aluminum, but the quality is

somewhat lower, because aluminum is a good conductor. The maximum thickness of aluminum that can be cut is 15 mm, but the higher speeds produces even lower quality. Also, laser can cut brass and copper to a thickness of 3 mm. Because they are even more conductors the cut could lose in drastically in quality.

2. LASER CUTTING PROCESS

Laser processing of materials is based on the use of highly concentrated light energy received by stimulated radiation for heating, melting or evaporation of material. The laser beams has become a universal tool that can manage all types of materials [1]. Directing laser beam on the workpiece (Fig. 2) can derive a number of manufacturing operations such as drilling, cutting and welding. Thanks to high orientation - focusing the beam (on the surface of 10^{-6} mm²), high density energy beam (up to 10^8 kW/mm²), the ability to easily control a laser beam and processing in different environments, laser processing is gaining more importance and has many advantages [2].

Laser cutting can be classified into three types: laser fusion cutting, laser gas cutting and laser sublimation cutting.

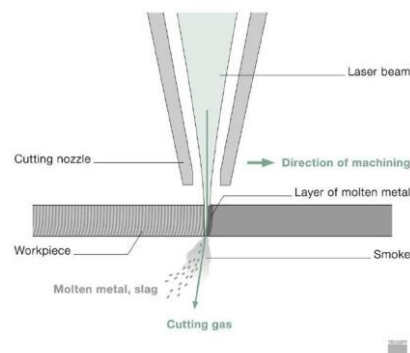


Fig. 2. Basic principle of laser cutting

During *laser fusion cutting*, the workpiece is locally melted and vaporized with the aid of gas (e.g. nitrogen). The material is transported only in liquid or

molten phase, which is why the process is called fusion cutting. An inert cutting gas of extreme purity is inserted into the laser beam, which ejects the molten material from the cut, without participating in the process of cutting. The oxidation of edges does not occur during laser fusion cutting which makes it suitable for cutting ferrite materials. Characteristics of the laser fusion cutting: working gas nitrogen or argon; laser power 80 ... 100% of maximum power; gas pressure 10 ... 20 bars; focal position approximately on the lower face of the sheet (Fig.3).

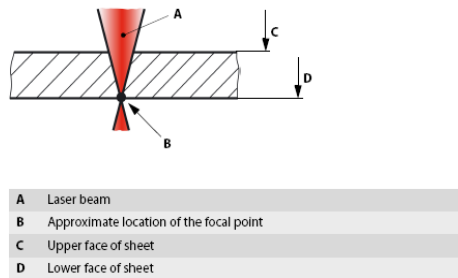


Fig. 3. Location of the focal point for fusion cutting

Laser gas cutting is differentiated from laser fusion cutting by the use of oxygen as the cutting gas. During laser gas cutting, the melting zone is further heated by the flow of oxygen into the cut and reaches temperatures approximating the boiling point of materials. This causes profuse evaporation and removal of the material. The cutting gas jet is also used for driving out the molten material from the lower side of the workpiece. Given that the interaction of oxygen with heated metal causes a reaction which further heats the material, cutting speeds achieved in mild steel cutting are higher than the ones achieved in fusion cutting of sheet of 6 mm and thicker. Laser cutting by oxygen is critical when cutting fine contours and acute shapes because of the risk of burning. Characteristics of the laser gas cutting: working gas oxygen; laser power 25 ... 80% of maximum power; gas pressure 0,5 ... 5 bars; focal position approximately on the upper face of the sheet (Fig.4).

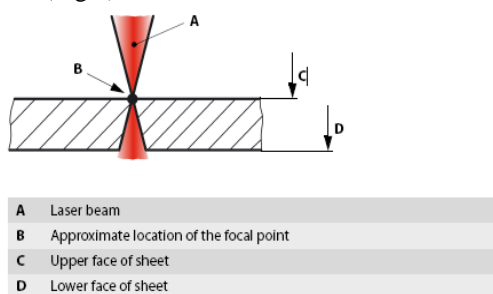


Fig. 4. Location of the focal point for laser gas cutting

In **laser sublimation cutting** the material evaporates directly into the cut, without the occurrence of the liquid phase. This method requires high laser power that is dependent on thermal properties of materials. Typical materials that are cut by this method are plastics, wood, paper and leather.

3. PROCESSING PARAMETERS

In order to execute the operation of laser cutting it is necessary to know the processing parameters [1]. Processing parameters include the characteristics of the

laser cutting process that can be modified to improve the quality of the cutting process and achieve the required results of cutting [3]. The parameters of the laser cutting process can be classified into four major categories: specified parameters of laser cutting, input parameters of laser cutting, operating parameters of laser cutting and output parameters of laser cutting.

The specified parameters of laser cutting are: gas type, gas purity, gas pressure, the diameter and shape of the nozzle. Gas pressure and the shape of the nozzle have an effect on the roughness of the cut. The consumption of cutting gas depends on gas pressure and diameter of the nozzle. Cutting by low pressure gas requires the pressure of up to 5 bars, whereas in cutting by high pressure gas, the pressure can reach 20 bars. Conventional nozzles have a circular, conical opening. The distance between the nozzle opening and the surface of the workpiece must be as small as possible. The smaller the distance, the greater is the amount of gas that enters the cut. The gap width usually ranges from 0,5 to 1,5 mm.

Operating parameters of laser cutting with which the quality of cutting can be optimized are: focus position, laser power, gas pressure, feed rate and the distance between the nozzle and the cutting surface. Original cutting parameters are optimized to ensure maximum reliability of the process. Each laser is supplied with a set of cutting parameters. Cutting parameters are given for the materials of specific type and thickness. For materials for which the laser manufacturer did not provide the recommended values, new cutting parameters could be set. The paper presents the process of defining new parameters for cutting parts made of steel AISI 6150 with the achievement of adequate accuracy of the quality and shape of the cut.

4. CUTTING PARAMETERS OPTIMIZATION

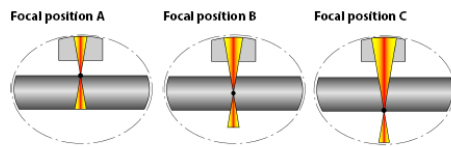
Cutting parameters are scalar values which have a direct effect on the process of cutting. In order to properly modify the cutting parameters it is important to know how the part has been programmed and which cutting technology is used. The cutting of new material must be preceded by experimental cutting. If any problems concerning the quality of cutting should arise in the experimental phase, they can be fixed by adjusting the original cutting parameters. The optimization of cutting parameters can be derived from the existing samples, and their recommended list [4]. Table 1 shows the order in which cutting parameters should be adjusted depending on the type of cutting gas. The reasons for the need of adjusting cutting parameters are: different material composition, variations of tolerances in the thickness of sheet, different nature of the surface and considerable temperature variations in the material used (reference temperature = +20 ° C).

The following conditions must be met in order to obtain high quality of the cut: the laser cutting machine and laser beam source must be in perfect condition, the lenses of the cutting head must be flawless, and the cutting head and the nozzle must be consistent with the cutting parameters.

Step	Cutting with oxygen (O ₂)	Cutting with nitrogen (N ₂)	Cutting with compressed air (Air) Option
1	Focal position	Focal position	Focal position
2	Laser power	Feed rate ± 10% OK	Feed rate ± 10% OK
3	Gas pressure	Laser power	Laser power
4	Feed rate ± 10% OK	Gas pressure	Gas pressure
5	Nozzle distance	Nozzle distance	Nozzle distance

Table 1. Order in which cutting parameters should be adjusted

The **position of the focus** or focal point denotes the smallest diameter of the laser beam. The maximum power density is concentrated in the focus. The lenses of the cutting head focus the laser beam. The focus position basically depends on the type of gas used (Fig. 5). Depending on the material that is cut, the focal point can be located: on the workpiece (focal position A), in the workpiece (focal position B) and under the workpiece (focal position C).



The focus position basically depends on the cutting gas used.

Cutting gas	Laser cutting method ⁽⁴⁾	Focal position
Oxygen O ₂	laser cutting	Focal position in upper region of main sheet. Focal position A
Nitrogen N ₂	Fusion cutting	Focal position in lower region of main sheet.
Compressed air ⁽⁵⁾ Air	Fusion and gas cutting	Focal position C

Fig. 5. The position of the laser beam focus

The central position of the focus varies depending on the condition of the lenses. Dirty or old lenses can shift the focus position upward. This dislocation can be up to several millimeters depending on the age or degree of impurity of the lenses. It is therefore important to regularly clean the lenses. The focus position can be modified (Fig. 6) by the input of a new numerical value in millimeters. The higher numerical value shifts the focus position downward, the lower numerical value shifts the focus position upward, while the numerical value 0 corresponds to the surface of the sheet (A).



Fig. 6. Change of focus position

Laser power is a parameter that defines the power of the laser during continuous operating mode of the laser (cw-continuous wave). It should be noted that there is a difference between continuous wave and pulse wave (pw). In continuous operating mode, the nominal power of the laser beam is continuously available, while in pulse operating mode it is emitted at intervals [5].

Gas pressure depends on the cutting gas and the nozzle used. In oxygen (O₂) assisted cutting, the higher value results in higher cutting temperature and rougher shape of the cut. With the use of nitrogen (N₂) and

compressed air, the material is ejected and cooled more easily. In cutting with O₂ the maximum gas pressure is 10 bars, in cutting with N₂ the maximum gas pressure is 24 bars, whereas in cutting with compressed air the maximum pressure is 12 bars.

Feed rate is a parameter that defines the cutting speed during continuous operating mode of the laser (cw). Feed rate is a variable which is dependent on other factors. If it is not possible to achieve the minimum feed rate during the production, the laser machine must be tested by the manufacturer's service personnel. It should be noted that the reduction of the feed rate by 10 - 20% leads to significant improvement of quality and process reliability in almost all cases.

Nozzle distance is a parameter that defines the distance between the nozzle and the surface of the workpiece during the cutting process. This distance affects the flow of gas, which further has a direct effect on cutting performances and cutting quality. If the nozzle distance is larger than 1 mm, significant variations in pressure will occur. It is recommended that the nozzle distance be smaller than the diameter of the nozzle, because greater distance can result in turbulence and considerable changes in pressure in the gap between the nozzle and the workpiece [3]. The nozzle distance <1 mm leads to increased wear and impurity of the nozzle, whereas the nozzle distance >1mm leads to poor quality of the cut.

5. SETTING THE CUTTING PARAMETERS FOR STEEL AISI 6150

Experimental research was conducted on a *Byspeed 4020* laser, a product of Bystronic from Switzerland [6]. The recommended values of cutting parameters for materials of specific type and thickness were given by the laser manufacturer. The recommended values for cutting materials made of steel AISI 6150 were not provided. Therefore, new cutting parameters were defined with the aim of achieving satisfactory quality of the cut. Nitrogen was used for cutting in continuous operating mode of the laser (cw).

A figure 7, 8, 9, 10 shows the shape of the cut depending on the focus position, gas pressure laser power and feed rate. In order to achieve optimum quality of the cut, the situation and the possible solution have been provided for each parameter. The images are magnified 10 times and this is why the stripes and irregularities can be seen even in the image with the optimal shape of the cut (Fig 11).

Focus position too low

Situation: The focus is in the upper section which is wrong for this kind of material. It would be correct to set focus in the central zone of the cut.

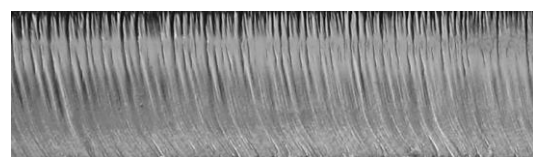


Fig. 7. Focus position too low

Solution: Set a greater numeric value of focus position.

Feed rate too low, focus position too low

Situation: The focus is in the upper section of the cut but material damage also occurs in the central zone of the cut (increased roughness).

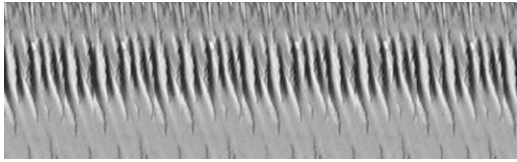


Fig. 8. Feed rate too low, focus position too low

Solution: Set a greater numeric value of focus position. Increase the cutting speed so that the laser beam less damages (melted) material in the central zone of the cut.

Laser power too high, focus position too low, feed rate too high

Situation: The focus is in the upper section, the material damage in the central zone of the cut but this time with an emphasized curvature lines that are generated in the process of cutting.

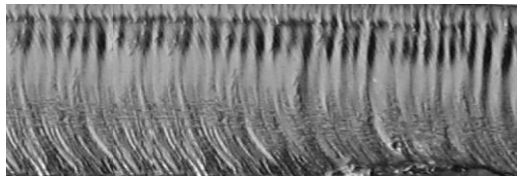


Fig. 9. Laser power too high, focus position too low, feed rate too high

Solution: Set a greater numeric value of focus position. This time the damage in the central zone of the cut cannot be solved by increasing the cutting speed because curved lines formed in the cutting point to the excessive cutting speed. Reducing power of the cut which eliminates damage materials and reduce the cutting speed eliminating the curvature lines generated in the process of cutting.

Gas pressure too low, laser power too high, and focus position too low

Situation: The focus is in the upper section, the material damage in the central zone of the cut and the formation of slag in the lower zone of the cut which clearly indicates that the cutting material is not done until the end.

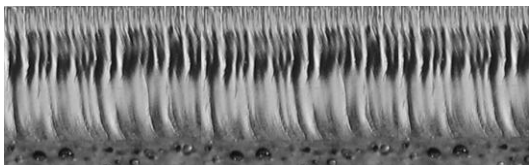


Fig. 10. Gas pressure too low, laser power too high, and focus position too low

Solution: Set a greater numeric value of focus position, the material damage in the central zone may be solved by two ways: by increasing the cutting speed and reducing power. There is always tendency to increase cutting speeds because of the cost-effectiveness and productivity of the machine. Slag in the lower zone of the cut is then easily removed by increasing the gas pressure for only 2-3 bars.

Optimal cut for steel AISI 6150

Fig. 11 shows the optimal cut for steel AISI 6150 thickness of 10 mm. It is important to note that in the process of designing program it is used technology for cutting stainless steel, otherwise all these changes in the cutting do not achieve the desired result (this type of material cannot be cut using the technology for cutting steel). The values of established processing parameters are as follows: cutting speed 900 mm / min, 4400 W laser power, focus position 10,5 mm, 18 bar gas pressure, nozzle distance from the surface of the material 0,5 mm.

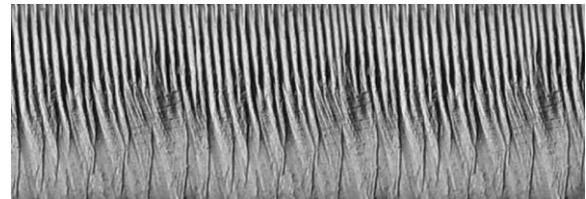


Fig. 11. Optimal cut for steel AISI 6150

6. CONCLUSION

Experimental research in laser processing of materials AISI 6150 led to the optimal cut (Figure 11). Optimal cut for AISI 6150 thickness of 10 mm sheet obtained by the following cutting parameters: cutting speed 900 mm / min, 4400 W laser power, focus position 10,5 mm, 18 bar gas pressure, nozzle distance from the surface of the material 0,5 mm. It should be also noted achievement of the same understanding of laser cutting technology, which enables the formation parameters for other kinds of materials such as AISI 314 or AISI 4140.

7. REFERENCES

- [1] Lazarević D., Radovanović M.: Nekonvencionalne metode, obrada materijala odnošenjem, Mašinski fakultet, Niš, 1994.
- [2] Nedić B., Lazić M., Obrada metala rezanjem, Mašinski fakultet, Kragujevac, 2007.
- [3] Wandera C., Laser cutting of austenitic stainless steel with a high quality laser beam, Lappeenranta University of Technology, 2006.
- [4] Bystronic: Cutting technology, Laser AG, 2007.
- [5] Gostimirović M.: Nekonvencionalni postupci obrade, Fakultet tehničkih nauka, Novi Sad, 2012.
- [6] http://www.bystronic.com/cutting_and_bending/gb/en/products/laser/byspeed/index.php

Authors: Prof. dr Pavel Kovač, MSc Ivan Sovilj-Nikić, University of Novi Sad, Faculty of Technical Sciences, Institute for Production Engineering, Trg Dositeja Obradovica 6, 21000 Novi Sad, Serbia, Phone.: +381 21 450-366, Fax: +381 21 454-495.
E-mail: pkovac@uns.ac.rs;
diomed17@yahoo.com

Prof. dr Snežana Radonjić, Univerzitet u Kragujevcu, Tehnički fakultet, Svetog Save 65, 32000 Čačak, Serbia, Phone: +381 032/302-733, Faks: +381 032/342-101
E-mail: snezar@tfc.kg.ac.rs

Kramar, D., Sekulić, M., Kovač, P., Gostimirović, M., Kopač, J.

THE IMPLEMENTATION OF TAGUCHI METHOD FOR QUALITY IMPROVEMENT IN HIGH-PRESSURE JET ASSISTED TURNING PROCESS

Abstract: In this paper, the cutting of Inconel 718 using high-pressure jet assisted turning process has been reported. The Taguchi method, with orthogonal arrays and signal-to-noise ratio, has been used to analyse impact of various process parameters on surface roughness and to find optimal levels of the process parameters. An attempt was made to minimize the number of experimental runs and increase the reliability of experimental results. The study shows that the Taguchi method is suitable to solve the stated problem with minimum number of trials.

Key words: Taguchi method, High-pressure jet assisted turning

1. INTRODUCTION

Determination of optimal machining parameters is continuous engineering task which goals are to reduce the production costs and to achieve the desired product quality. With the more precise demands of modern engineering products, the control of surface texture with dimensional accuracy has become more important. Surface roughness is the characteristic of surface which describes the surface quality, with regard to machining. This is a widely used index of product quality and in most cases a technical requirement for mechanical products. Achieving the desired surface quality is of great importance for the functional behaviour of a part. Following modern production requests and technologic-economic analysis of processing operations, during the designing process, it is necessary to determine optimal cutting parameters in order to achieve minimal expenses or minimal production time [1].

High pressure jet assisted turning (HPJA) presents an innovative method of lubricating and/or cooling the cutting zone during machining. This machining process is able to cutting of nickel-based alloys. Nickel-based alloys are well known to yield a very poor machining performance. The subject of this study is to analyse dependence of surface roughness on the following five HPJA parameters: the diameter of the nozzle D_n , the pressure of the jet P , the cutting speed V_c , the feed rate and distance between the impact point of the jet and the cutting edge d .

The Taguchi method of experimental design is one of the widely accepted techniques for off line quality assurance of products and processes. This method is a traditional approach for robust experimental design that seeks to obtain a best combination set of factors/levels with lowest cost societal solution to achieve customer requirements. In this research work the roughness parameter R_a is measured experimentally during high pressure jet assisted turning of Inconel 718. Taguchi method and ANOVA analysis are used to analyze the effect of cutting parameters on surface roughness.

2. TAGUCHI METHOD AND EXPERIMENTAL DETAILS

2.1 Taguchi method

Robust Design method, also called the Taguchi method, pioneered by Dr. Genichi Taguchi, greatly improves engineering productivity. Taguchi parameter design is based on the concept of fractional factorial design. The main objective of parameter design is to minimize the process or product variation and to design robust and flexible processes or products that are adaptable to environmental conditions [2]. Taguchi's approach to design of experiments is easy to adopt and apply for users with limited knowledge of statistics; hence it has gained a wide popularity in the engineering and scientific community. Many companies around the world have saved hundreds of millions of dollars by using the method in diverse industries: automobiles, xerography, telecommunications, electronics, software, etc.

Taguchi method uses orthogonal array to execute experiments and for analyzing. Signal to noise ratio and orthogonal array are two major tools used in robust design. The S/N ratio characteristics can be divided into three categories when the characteristic is continuous: nominal is the best, smaller the better and larger is better characteristics. For the minimal roughness, the solution is „smaller is better“, and S/N ratio is determined according to the following equation:

$$S/N = -10 \log \left(\frac{1}{n} \sum_{i=1}^n y_i^2 \right) \quad (1)$$

Where n is the number of replication and y_i is the measured value of output variable. The minimal R_a is achieved using the cutting parameters where S/N ratio is maximal. The influence of each control factor can be more clearly presented with response graphs [3]. Optimal cutting conditions of control factors can be very easily determined from S/N response graphs, too. Parameters design is the key step in Taguchi method to

achieve reliable results without increasing the experimental costs. The experimental layout for the machining parameters using $L_{27}(3^{13})$ orthogonal array was used in this study. The experimental results were analyzed with Analysis of Variance (ANOVA), which is used for identifying the factors significantly affecting the performance measures.

2.2 Experimental details

High pressure jet assisted turning (HPJA) is a process where cooling lubrication fluid (CLF) is delivered into the cutting zone region under extremely high pressure of up to $P=300$ MPa and at a lower volume flow rate than in the conventional case, providing improved lubrication, cooling and chip breaking effects, Fig. 1. This is innovative method of lubricating and/or cooling the cutting zone during machining.

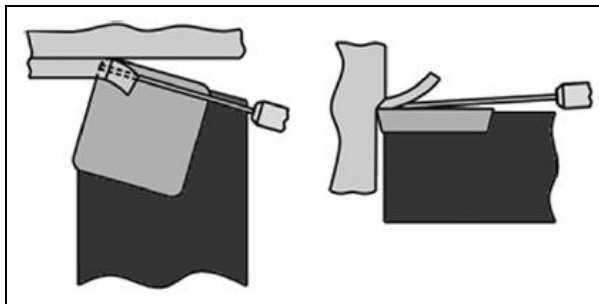


Fig. 1. HPJA CLF delivery jet direction sketch [4]

Some potential benefits of this machining are [4] : more sustainable machining through lower flow rates of CLF in comparison to conventional machining, decreasing the cutting tool-chip contact length, resulting in lower cutting forces and longer tool life, drastic improvement in chip breakability etc.

The experimental work was carried out at the Laboratory for Machining, the Faculty of Mechanical Engineering in Ljubljana. The experiments were conducted in longitudinal turning process on conventional lathe, fitted with a Hammelmann high-pressure plunger pump of 150 MPa pressure and 8 l/min capacity. The fluid used was the Vasco 5000 cooling lubricant from Blaser Swissslube Inc., a 5,5% emulsion without chlorine on the basis of vegetable oil mixed with water (pH 8,5-9,2).

Machining performance was investigated according to the following HPJA parameters: the diameter of the nozzle D_n (0.25, 0.3 and 0.4 mm), the pressure of the jet P (50, 90 and 130 MPa), the cutting speed V_c (46, 57 and 74 m/min), the feed rate f (0.2, 0.224 and 0.25 mm/rev) and the distance between the impact point of the jet and the cutting edge d (0, 1.5 and 3 mm).

All experiments were carried out using the nickel-based alloy Inconel 718 supplied as bars (145 mm diameter x 300 mm long) with hardness between 36 and 38 HRC by orthogonal arrays with three levels (coded by: 1, 2 and 3), Table 1. A PVD TiAlN-coated carbide tool (grade P25) SNMG 12 04 08-23 has been chosen.

Surface roughness was measured with a stylus-type instrument Mitutoyo-Surfteft SJ-301, Fig. 2. The

surface roughness response is the average reading of three consecutive measurements.

Symbol	Parameters	Levels		
		1	2	3
A	Diameter of the nozzle, D_n (mm)	0,25	0,3	0,4
B	Dist. between the impact point of the jet and the cutting edge, d (mm)	0	1,5	3,0
C	Pressure of the jet, P (MPa)	50	90	130
D	Cutting speed, V_c (m/min)	46	57	74
E	Feed, f (mm/rev)	0,2	0,224	0,25

Table 1. Machining parameters and their levels

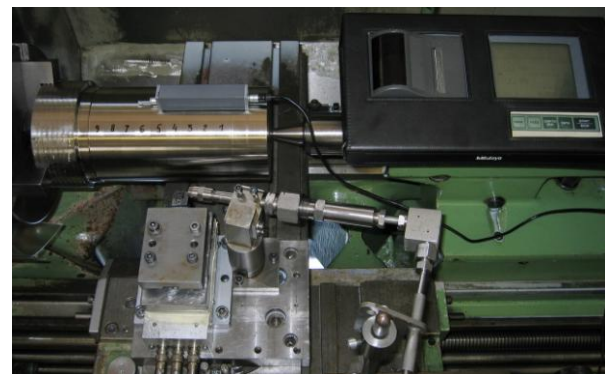


Fig. 2. Measurement of 2D roughness parameters [5]

3. RESULTS AND DISCUSSIONS

Experimental results, together with their transformations into signal-to-noise ratios are given in Table 2. In this study all the analysis based on Taguchi method is done by Minitab14 and Qualitek-4 software to determine the main effects of the cutting parameters, to perform the analysis of variance (ANOVA) and establish the optimum conditions.

From Table 3. it can be determined which control factors have strong influence on roughness parameter R_a in high-pressure jet assistance turning (HPJA). Optimal cutting conditions of these control factors can be very easily determined from the S/N response graphs in Fig. 3. The response graphic of roughness parameter R_a has been shown for all five factors. The best roughness parameter R_a is at the higher S/N values in the response graphs. Parameter influence on output process variable shows angle of inclination of the line which connects different parameter levels.

It can be seen from the presented graphs that feed has the greatest influence on the roughness parameter R_a . The diameter of the nozzle D_n , distance between the impact point of the jet and the cutting edge d and pressure P have small influence. Cutting speed has insignificant influence on the roughness parameter R_a . Optimal cutting conditions are shown in Table 2.

Control parameters	Level	Setting		R _a obtained using Taguchi method	R _a obtained using verification test
D _n (mm)	3	0,4	Require add. exp.	S/N=-7,109 R _a =2,267 μm	R _a =2,45 μm
d (mm)	3	3,0			
P (MPa)	1	50			
V _c (m/min)	3	74			
f (mm/rev)	1	0,20			

Table 2. Optimal settings of control parameters

The optimization of cutting parameters inside offered factors levels, with regard to criterion “smaller is better”, gives the combination of control factors: A=3, B=3, C=1, D=3, E=1. This combination enables the lowest roughness parameter R_a. A verification test has to be performed after optimal settings of control factors have been determined with the goal to approve the calculated value of the quality characteristic. Difference between the calculated and yielded value of roughness parameter R_a is very small.

№	Factors					Parameters					R _a (μm)	S/N
	A	B	C	D	E	D _n (mm)	d (mm)	P (MPa)	V _c (m/min)	f (mm/rev)		
	D _n	d	P	V _c	f							
1	1	1	1	1	1	0,25	0	50	46	0,2	2,54	-8,097
2	1	1	1	1	2	0,25	0	50	46	0,224	2,77	-8,85
3	1	1	1	1	3	0,25	0	50	46	0,25	3,76	-11,504
4	1	2	2	2	1	0,25	1,5	90	57	0,2	2,86	-9,128
5	1	2	2	2	2	0,25	1,5	90	57	0,224	3,09	-9,8
6	1	2	2	2	3	0,25	1,5	90	57	0,25	4,07	-12,192
7	1	3	3	3	1	0,25	3	130	74	0,2	2,63	-8,4
8	1	3	3	3	2	0,25	3	130	74	0,224	2,86	-9,128
9	1	3	3	3	3	0,25	3	130	74	0,25	3,85	-11,71
10	2	1	2	3	1	0,3	0	90	74	0,2	2,63	-8,4
11	2	1	2	3	2	0,3	0	90	74	0,224	2,85	-9,097
12	2	1	2	3	3	0,3	0	90	74	0,25	3,84	-11,687
13	2	2	3	1	1	0,3	1,5	130	46	0,2	3,10	-9,828
14	2	2	3	1	2	0,3	1,5	130	46	0,224	3,33	-10,449
15	2	2	3	1	3	0,3	1,5	130	46	0,25	4,31	-12,69
16	2	3	1	2	1	0,3	3	50	57	0,2	2,54	-8,097
17	2	3	1	2	2	0,3	3	50	57	0,224	2,76	-8,819
18	2	3	1	2	3	0,3	3	50	57	0,25	3,75	-11,481
19	3	1	3	2	1	0,4	0	130	57	0,2	2,52	-8,029
20	3	1	3	2	2	0,4	0	130	57	0,224	2,75	-8,787
21	3	1	3	2	3	0,4	0	130	57	0,25	3,74	-11,458
22	3	2	1	3	1	0,4	1,5	50	74	0,2	2,45	-7,784
23	3	2	1	3	2	0,4	1,5	50	74	0,224	2,68	-43,76
24	3	2	1	3	3	0,4	1,5	50	74	0,25	3,67	-11,294
25	3	3	2	1	1	0,4	3	90	46	0,2	2,41	-7,641
26	3	3	2	1	2	0,4	3	90	46	0,224	2,63	-8,4
27	3	3	2	1	3	0,4	3	90	46	0,25	3,62	-11,175

Table 3. Orthogonal array L₂₇(3¹³) with experimental results and calculated S/N ratio

The experimental results were analyzed with Analysis of Variance (ANOVA), which is used for identifying the factors significantly affecting the performance measures are shown in Table 4.

Percentage contribution of parameter is obtained by dividing the sum of squares for each parameter with total sum squares.

Col # / Factor	DOF (f)	Sum of Sqrs. (S)	Variance (V)	F - Ratio (F)	Pure Sum (S')	Percent P(%)
1 Dn	2	3.345	1.672	126.807	3.318	5.225
2 d	2	3.047	1.523	115.518	3.02	4.756
3 P	2	1.992	.996	75.53	1.965	3.095
4 Vc	2	.381	.19	14.474	.355	.559
5 f	2	54.525	27.262	2067.047	54.499	85.821
Other/Error	16	.21	.013			.544
Total:	26	63.503				100.00%

Table 4. ANOVA table

4. CONCLUSIONS

This paper has discussed dependence of roughness parameter R_a of the five high-pressure jet assistance turning (HPJA) parameters. Taguchi method has been used to determine the main effects, significant factors and optimum machining conditions to the value of the roughness parameter R_a . From analysis using Taguchi's method, results indicate that among the all-significant parameters, feed is the most significant. Results obtained from Taguchi method closely matches with ANOVA.

5. REFERENCES

- [1] Bajić, D., Jozić, S., Podrug S.: *Design of experiment's application in the optimization of milling process*, Metalurgija, Vol 49, pp. 123-126, 2010.
- [2] Roy, R. K.: *Design of experiments using the Taguchi approach: 16 steps to product and process improvement*, John Wiley & Sons, Inc., 2001.
- [3] Sekulić, M., Hadžistević, M., Jurković, Z., Kovač, P., Gostimirović, M.: *Application of Taguchi method in optimization of face milling parameters*, 34th International Conference on Production Engineering, p.p. 57-60., Niš, Serbia, 2011.
- [4] Pušavec, F., Kramar, D., Krajnik, P., Kopač, J.: *Transitioning to sustainable production-part II: evaluation of sustainable machining technologies*, Journal of Cleaner Production, Volume 18(2010), p.p. 174-184, 2010.
- [5] Kramar, D.: *High-pressure cooling assistance in machining of hard-to-machine materials*, PhD Thesis, Faculty of Mechanical Engineering, Ljubljana, 2009.

Authors: Assist. Prof. Dr. Davorin Kramar, Prof. Dr. Janez Kopač, University of Ljubljana, Faculty of Mechanical Engineering, Aškerčeva 6, 1000 Ljubljana, Slovenia, Phone: +386 1 47 71 737

Assist. Prof. Dr. Milenko Sekulić, Prof. Dr. Pavel Kovač, Prof. Dr. Marin Gostimirović, University of Novi Sad, Faculty of Technical Sciences, Department for Production Engineering, Trg Dositeja Obradovića 6, 21000 Novi Sad, Serbia, Phone.: +381 21 450-366, Fax: +381 21 454-495.

E-mail: davorin.kramar@fs.uni-lj.si
janez.kopac@fs.uni-lj.si
milenkos@uns.ac.rs
pkovac@uns.ac.rs
maring@uns.ac.rs

Nagode, A., Klančnik, G., Gojić, M., Kosec, B., Bizjak, M., Zorc, B., Kosec, L.

AN INVESTIGATION OF THE SURFACE DAMAGE OF HOT PLATES AFTER BLACK OXIDE COATING

Abstract: After the black-oxide coating brown stains were observed forming on the surfaces of grey-cast-iron hot plates made for an electric stove. These stains were metallographically examined using a scanning electron microscope (SEM) equipped with an energy-dispersive X-ray spectrometer (EDXS). For the phase identification we also employed X-ray diffraction (XRD) analyses. The results of the analyses indicated that the stained surfaces of the hot plates were covered with whiskers of hematite (Fe_2O_3), while on the surfaces of the non-defective hot plates only magnetite (Fe_3O_4) was present. The thermodynamic calculations confirmed the possibility of the formation of hematite (Fe_2O_3) as a result of the oxidation of magnetite (Fe_3O_4) if the partial pressure of oxygen is increased during the black-oxide-coating process.

Key words: whiskers, grey cast iron, magnetite (Fe_3O_4), hematite (Fe_2O_3)

1. INTRODUCTION

A damaged surface of a hot plate made of grey cast iron used for the electric stove exhibits many brown stains (Fig. 1) after black oxide coating (blackening). The blackening [1] is mainly used to produce a protective dark (grey) oxide layer [2,3] on the surface consisting predominantly of magnetite (Fe_3O_4); however, it also prevents against corrosion and abrasion [4]. Before blackening the grooves on the surface of the hot plate are made by turning [5-7].

The black oxide coating process of hot plate was held in the furnace at 650 °C. For the appropriate atmosphere for producing a thin oxide layer on the surface of grey cast iron the wood was burned [8]. The maximum temperature in the furnace of 650 °C is reached after four hours, while the whole process lasts eight hours.

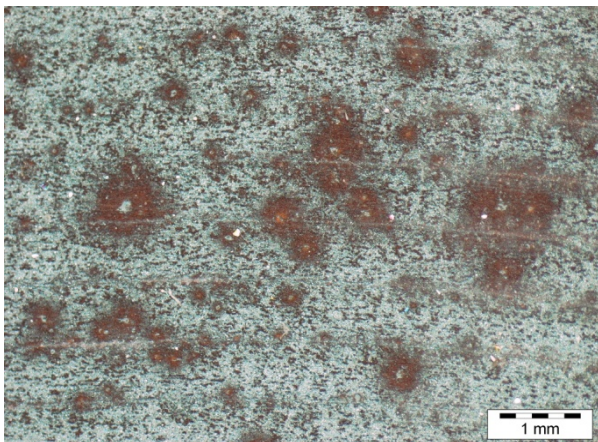


Fig. 1 Brown stains on the surface of grey cast iron after blackening

2. EXPERIMENTAL

For the microstructural characterization of the

brown stains on the surface of grey cast iron which have been observed after blackening a scanning electron microscope Jeol JSM 5610 equipped with energy dispersive X-ray spectrometer (EDXS) was used [9]. The accelerated voltage of electron beam was 20 keV. For phase identification an X-ray diffraction analysis was also performed. For that analysis, an X-ray diffractometer PANalytical X'Pert PRO (radiation wavelength $CuK\alpha_1 = 1,5406 \text{ \AA}$) with Johansson monochromator for flat samples has been used.

3. RESULTS AND DISCUSSION

A detailed observation of the surface of grey cast iron after blackening using scanning electron microscope (SEM) revealed that the surface with brown stains (Fig. 1) is covered with whiskers [10-14] (Fig. 2), while the surface where no brown stains have been observed shows typical oxide pattern (Fig. 3) which reflects grain orientation of the base material.

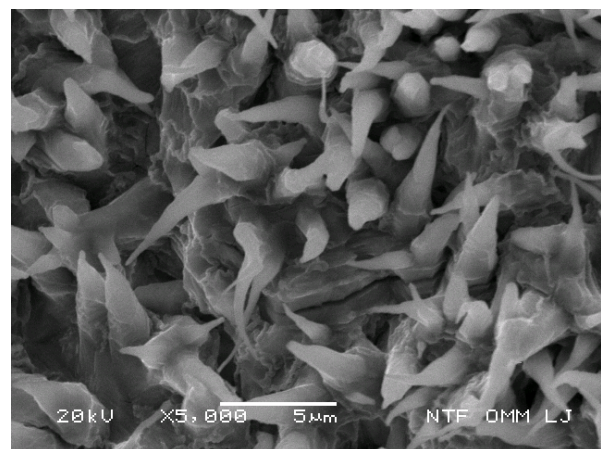


Fig. 2 Surface of grey cast iron covered with whiskers; SEI

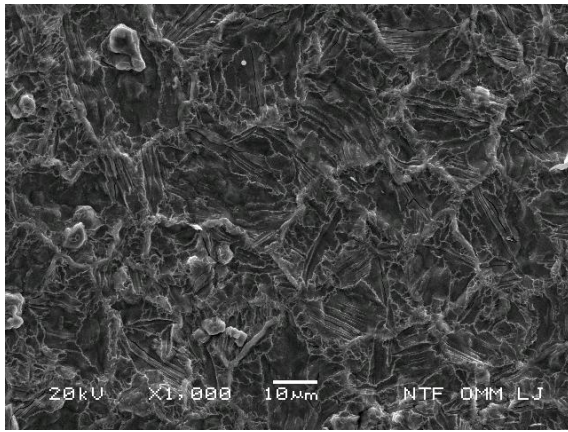


Fig. 3 Typical oxide pattern after black oxide coating; SEI

Backscatter electron image (BEI) of the cross section of the sample covered with whiskers (Fig. 4) shows, chemically, two different oxide layers on the base material (grey cast iron), i.e., the outer (light contrast) and the inner (dark contrast) oxide layers. However, a detailed EDXS analysis (Table 1) shows that whiskers as well as the upper part of the outer oxide layer is composed of pure Fe-oxide, while in the lower oxide layer EDXS analysis indicates FeMn-oxides. The EDXS analysis of the inner oxide layer (dark contrast) confirms the presence of Fe, Mn and Cr; however, the increased content of Si indicates that the inner layer is composed of Si-rich Fe(MnCr) oxide..

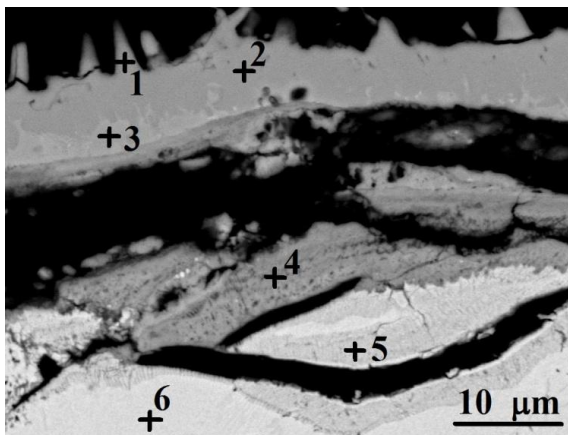


Figure 4. Cross section of the sample covered with whiskers; BEI

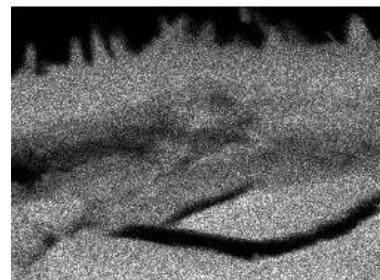
Site of interest	Fe	O	Mn	Si	Cr
1	93,5	6,5	-	-	-
2	95,9	4,1	-	-	-
3	96,0	1,9	1,1	-	-
4	95,9	3,1	0,4	0,3	0,3
5	95,8	0,6	0,7	2,2	0,6
6	97,4	-	0,6	1,3	0,7

Table 1. EDXS analysis of the sample covered with whiskers in cross section /wt. %

In Fig. 4 the internal oxidation of the matrix around the graphite flakes near the surface can also be seen. The internal oxidation actually consists of iron

oxidation ($x\text{Fe} + y\text{O} \rightarrow \text{Fe}_x\text{O}_y$) as well as graphite oxidation ($2\text{C} + \text{O}_2 \rightarrow 2\text{CO}$ or $\text{C} + \text{O}_2 \rightarrow \text{CO}_2$). The formation and growth of the Fe-oxide in the subsurface is promoted by oxygen penetration through the graphite boundaries with the metallic matrix [15, 16].

In order to show the element distribution on the cross section of the sample covered with whiskers an energy dispersive X-ray spectroscopy (EDXS) maps are presented. EDXS maps confirm above mentioned results of EDXS quantitative analysis. Distribution of carbon shows graphite flakes at the bottom of the image, however, at the top of the image the signal of C shows the signal C, $K\alpha$ X-rays which come from the bakelite that the sample for metallographic preparation has been put in.



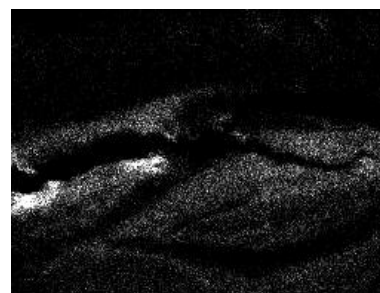
Fe, $K\alpha$



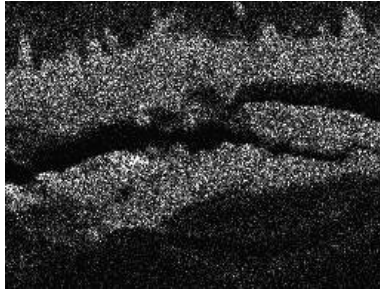
Mn, $K\alpha$



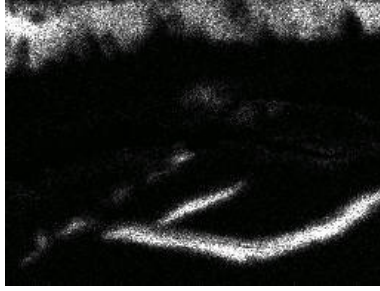
Cr, $K\alpha$



Si, $K\alpha$



O, K α



C, K α

Figure 5. EDXS maps of Fe, Mn, Cr, Si O and C

The X-ray diffraction analysis was used for a phase identification of the surface covered with whiskers as well as for the surface without them. The analysis showed that the only difference between two XRD patterns lies in the ratio of the peak intensities between the hematite (Fe_2O_3) and the magnetite (Fe_3O_4). Namely, a detail from the XRD spectrum (2 theta = 32 ° - 2 theta = 36 °) of the surface covered with whiskers shows a higher peak-intensity ratio between the hematite (Fe_2O_3) and the magnetite (Fe_3O_4) (Fig. 6a) in comparison to the X-ray diffraction pattern of the surface without whiskers (Fig. 6b). Since the surface with brown stains is covered with whiskers this result indicates that the whiskers are composed of hematite (Fe_2O_3).

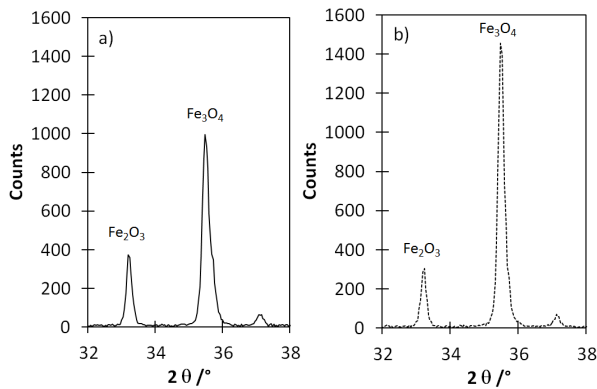


Figure 6 A. detail of XRD spectrum of the surface; a) covered with whisker; b) without whiskers

4. THERMODYNAMIC CALCULATIONS

For the calculation of particular phase diagram, Fig. 7, the data for pure elements were taken from Dinsdale [17], for the substances data from Ansara [18]. Thermodynamic assessments on the Fe-O phase diagram were done by Sundman [19] and Selleby and

Sundman [20]. The calculation of the phase diagram was done using Thermo-Calc software (TCW5).

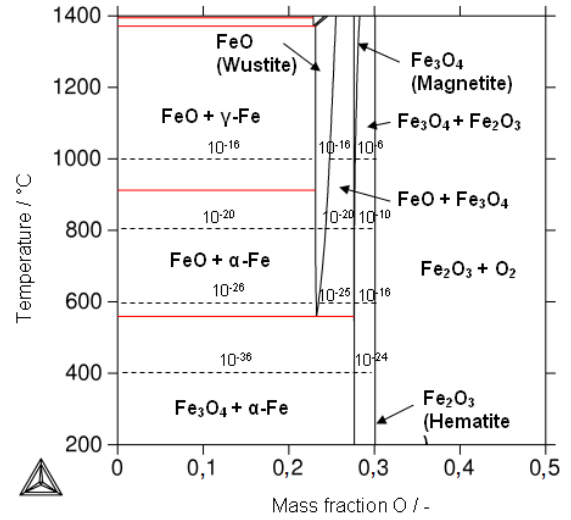
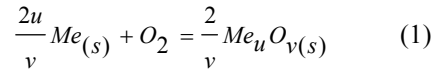
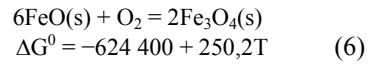
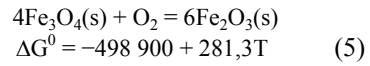
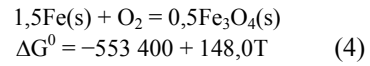
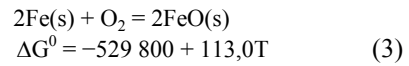


Figure 7. Fe-O phase diagram, and partial pressure of oxygen at 400 °C, 600 °C, 800 °C and 1000 °C

The calculations were performed using equation 1 and equation 2. The activity of oxide was taken to be 1 as in the case of pure metal. The standard state of the gas is 1 atm. The equation for oxidation of pure metal is given with equation 1:



$$\Delta G = \Delta G^0 + RT \ln po_2^{-1} (eq.) = \Delta G^0 - RT \ln po_2 (eq.) \quad (2)$$



where ΔG represents the Gibbs energy change of the reaction when all reactants and products are at their respective arbitrarily states and the standard Gibbs energy of formation (equations 3-6). R is the gas constant ($8,3144 \text{ Jmol}^{-1}\text{K}^{-1}$), T temperature (K) and $po_2 (eq.)$ (atm) is equilibrium (dissociation) pressure of iron oxide. The calculations were done for equilibrium conditions. Constant isobars at specific temperatures revealed large variations of dissociation pressures of iron oxides existing between different oxide regions. So, proper heating and cooling conditions (with controlled partial pressure-oxygen content inside the gas reservoir) are needed for controlled growth of oxides, Fig. 7. If the value po_2 for a given atmosphere under consideration lies under the dissociation pressure of iron oxide $po_2 (eq.)$, this oxide will dissociate into the oxygen and metal (or another oxide). On the contrary, if the value po_2 lies above the dissociation

pressure of iron oxide p_{O_2} (eq.), then the iron oxide is stable. So, increased partial pressure of oxygen relative to dissociation pressure at temperature of interest the formation of the hematite on the pre-existing magnetite is possible. The content of particular oxide (Fe_2O_3 on Fe_3O_4) is a time-dependant function.

5. CONCLUSIONS

After the black-oxide coating the brown stains on the surface of hot plates made of grey cast iron were observed. SEM observations showed that these stains were caused by whiskers growth on the surface and aesthetically damaged it. Detailed investigation showed that whiskers were growing from the top oxide layer on the surface of grey cast iron. An EDXS analysis confirmed that the oxide on the surface of the grey cast iron consists, chemically, of three different types of oxides, i.e., whiskers and the outer oxide layer are pure Fe-oxide, below it is a narrow layer of FeMn-oxide, while the inner layer consists of Si-rich Fe(MnCr) oxide. An X-ray diffraction pattern of the surface covered with whiskers shows a higher Fe_2O_3/Fe_3O_4 peak-intensity ratio according to the X-ray diffraction pattern of the surface without them. This indicates that the whiskers are from hematite (Fe_2O_3). The results of the thermodynamic calculations revealed that at 650 °C only magnetite (Fe_3O_4) will be present if the p_{O_2} is between 10-14 and 10-23 atm. If the p_{O_2} is higher than 10-14 atm hematite (Fe_2O_3) is expected to be formed. For the proper oxidation (uniform growth of Fe_3O_4 oxide) of grey iron a better control of the partial pressure of oxygen at a certain temperature is needed.

6. REFERENCES

- [1] Arab, N., Rahimi, M., Soltani, N.: A study of coating process of cast iron blackening, *Journal of Applied Chemical Research*, 9 (2009), p.p. 13-23, 2009.
- [2] Gojić, M., Črnko, J., Kundak, M., Kosec, L.: Analysis of the scale formed on steel blooms during heating, *Kovové Materiály*, 41 (2003), p.p.158-166, 2003.
- [3] Bizjak, M., Zalar, A., Panjan, P., Zorko, B., Praček, B.: Characterization of iron oxide layers using Auger electron spectroscopy, *Applied Surface Science*, 253 (2007), p.p. 3977-3981, 2007.
- [4] Nagode, A., Klančnik, G., Schwarczova, H., Kosec, B., Gojić, M., Kosec, L.: Analyses of defects on the surface of hot plates for an electric stove, *Engineering Failure Analysis*, 23 (2012) 1, p.p. 82-89, 2012.
- [5] Tušek, J., Klobčar, D.: Current Development Trends For Material Joining In The Automotive Industry, *Journal of Mechanical Engineering*, 50 (2004) 2, p.p. 94-103, 2004.
- [6] Budak, I., Soković, M., Barišić, M., Accuracy improvement of point data reduction with sampling-based methods by Fuzzy logic-based decision-making, *Measurement*, 44 (2011) 6, 1188-1200, 2011.
- [7] Klobčar, D., Kosec, L., Kosec, B., Tušek, J.,

Thermo fatigue cracking of die casting dies, *J., Engineering Failure Analysis*, 20 (2012)1, 43 – 53, 2012.

- [8] Medved, Malenković, M., Dervarič, V., E., *Technics Technologies Education Management*, 6 (2011) 2, 247-255, 2011.
- [9] Kosec, G., Nagode, A., Budak, I., Antić, A., Kosec B., Failure of the pinion from the drive of a cement mill, *Engineering Failure Analysis*, 18 (2011) 1, 450-454, 2011.
- [10] Tholence, F., Norell, M., High Temperature Corrosion of Cast Alloys in Exhaust Environments I-Ductile Cast Irons, *Oxidation of Metals*, 69 (2008), 13-36, 2008.
- [11] Schmid, B., Aas, N., Ødegård, R., High-temperature oxidation of iron and the decay of wüstite studied with in situ ESEM, *Oxidation of Metals*, 57 (2002), 115-130, 2002.
- [12] Higginson, R.L., Green, G., Whiskers growth morphology of high temperature oxides grown on 304 stainless steel, *Corrosion Science*, 53 (2011), 1690-1693, 2011.
- [13] Kim, J.W., Choi, J.W., Lee, D.B., Characterization of oxide scales formed on low carbon steel between 1100 and 1250 °C in air, *Metals and Materials International*, 11 (2005), 131-134, 2005.
- [14] Ivanič, A., Lubej, S., Rudolf, R., Anžel, I., *Science and Engineering of Composite Materials*, 18 (2011) 3, 181-186, 2011.
- [15] Robertson, J., Manning, M.I., Healing Layer Formation in Fe-Cr-Si Ferritic Steels, *Materials Science and Technology*, 5 (1989), 741-753, 1989.
- [16] Lin, M-B., Chaur-Jeng, Volinsky, A.A., temperature Oxidation Behavior of flake and spheroidal graphite cast iron, *Oxidation of Metals*, 76 (2011), 161-168, 2011.
- [17] Dinsdale, A.T., SGTE Data for Pure Elements, *Calphad* 15 (4) (1991), 317-425, 1991.
- [18] Ansara, I., SGTE substance database (2000), 2000.
- [19] Sundman, B., *Journal of Phase Equilibrium*, 12 (1991), 127-140, 1991.
- [20] Selleby, M., Sundman, B., *Calphad* 20 (1996), 381-392, 1996.

Authors: Ass. Prof. Dr. Aleš Nagode, Dr. Grega Klančnik, Ass. Prof. Dr. Milan Bizjak, Prof. Dr. Borut Kosec, Dr. Borut Zorc, Prof. Dr. Ladislav Kosec, University of Ljubljana, Faculty of Natural Sciences and Engineering, Aškerčeva 12, 1000 Ljubljana, Slovenia, Phone: +386 1 20 00 410, Fax: +386 1 47 04 560.

E-mail: ales.nagode@omm.ntf.uni-lj.si
grega.klanclnik@omm.ntf.uni-lj.si
milan.bizjak@omm.ntf.uni-lj.si
borut.kosec@omm.ntf.uni-lj.si
borut.zorc@omm.ntf.uni-lj.si
ladislav.kosec@omm.ntf.uni-lj.si

Prof. Dr. Mirko Gojić, University of Zagreb, Faculty of Metallurgy, Aleja narodnih heroja 3, 44103 Sisak, Croatia, Phone: +385 43 533 379, Fax: +385 43 533 380.

E-mail: gojic@simet.hr

Peterka, J., Kováč, M., Beňo, M., Zvončan, M.

EFFECT OF CUTTING PARAMETERS ON DELAMINATION FACTOR IN ROTARY ULTRASONIC MACHINING OF FIBERGLASS

Abstract: The article deals with influence of cutting parameters on delamination factor of fiberglass in rotary ultrasonic machining. In machining of fiberglass the effect of delamination occurs. Delamination is negligible effect in machining process, where the layers of fibers are damaged at the edge of material after machining process. The aim of the experiment described in the article was to verify, if the rotary ultrasonic machining is suitable for machining fiberglass and how does the technology and its parameters affects the delamination. Input parameters are cutting speed, cutting fluid's pressure and feed. Based on experiments, the delamination depends on feed and cutting fluid's pressure at the most. The values of delamination coefficient were from 1 to 2. The disadvantage of rotary ultrasonic machining is the need of cutting fluid in the machining process. The cutting fluid damaged the fiberglass, because of the saturation of fiberglass which raises the delamination factor.

Key words: ultrasonic machining, fiberglass, delamination

1. INTRODUCTION

Composites are materials created by at least two different materials usually the matrix and fibers. Composite materials can be machined as other standard materials, however due to their structure there are some limits. Because of the fibers are usually very hard in comparison to the matrix, there is high tool wear is conventional machining and also the delamination is negligible effect. These negligible effects may be reduced by optimizing cutting conditions and by using covered carbide tools.

On the other hand there is possibility to use new, nonconventional machining technologies to lower delamination and tool wear. One of the machining technologies, where the tool wear is at very low level is rotary ultrasonic machining. Based on theoretical knowledge, the vibrations of the tool help to reduce burrs [1]. The burr origin is similar to the delamination process; therefore there is a presumption that rotary ultrasonic machining may help to reduce delamination of fiberglass.

2. THEORETICAL BACKGROUND

Delamination is splitting of layers of composite material, such as fiberglass. The delamination is highest in drilling, where the feed of the tool is perpendicular to the layer according to Figure 1. The red lines in the figure are the layers of composite material, the tool feed direction is figured with arrows. As can be observed from the figure the last layers are pulled off when the tool is coming through the material called push down delamination. Beside low tool wear rate, on the advantages of ultrasonic machining presented in literature are lower cutting forces in comparison to the conventional milling or drilling. Therefore the pressure on layers of composite materials

should be lower, which provides lower delamination [3]. Delamination in drilling is the ratio of maximum delamination and tool diameter.

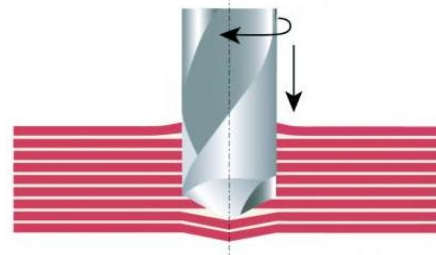


Fig. 1 Delamination in drilling [2]

The schematic model of delamination in drilling is depicted in Figure 2a. The blue circle is the maximum delamination, the red color is real shape of the delamination and the yellow one is the tool diameter.

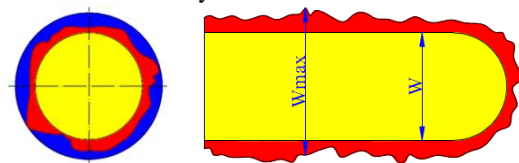


Fig. 2 Schematic model of delamination in a) drilling b) milling

The delamination in milling is depicted in Figure 2b. The color scheme is the same.

There is the difference of tool feed according to the layer between milling and drilling. Therefore the effect on delamination should be different for drilling and for milling.

The critical force of delamination F_A can be calculated as:

$$F_A = \sqrt{\frac{8G_{IC}E(nht)^3}{3(1-\nu^2)}}$$

where: G_{IC} is fracture toughness
 E – Young modulus

n – number of non-machined layers
 h_i – thickness of one layer,
 ν – Poisson's ratio.

The delamination is evaluated by a number which is obtained from following equations. The value of delamination factor for drilling is calculated as:

$$F_d = \frac{D_{\max}}{D_0}$$

Where: F_d is the factor of delamination
 D_{\max} is the maximum delamination
 D_0 is the diameter of the tool

And for milling as :

$$F_d = \frac{W_{\max}}{W}$$

Where: F_d is the factor of delamination
 W_{\max} is the maximum delamination
 W is the diameter of the tool

3. EXPERIMENTAL SETUP

Based on theoretical knowledge written herein before an experiment was designed. The input variables were cutting fluid's pressure and feed. Rotations are constant. The levels of input variable for drilling are in Table 1. Each experiment were performed three times. Cutting conditions for milling are in Table 2.

Table 1 Cutting conditions for drilling.

Feed	Cutting fluid's pressure	Rotations
50, 100, 150 mm/min	5, 10 bars.	2000 min ⁻¹ .

Table 2 Cutting conditions for milling.

Feed	Cutting fluid's pressure	Rotations
500, 1000, 2000 mm/min	5, 10 bars.	4000 min ⁻¹ .

The delamination factor was evaluated in drilling and milling using rotary ultrasonic machine tool DMG Sauer Ultrasonic 20 linear with diamond tools. For drilling the Schott HB-Da.8-0,6-8-35-D107H was used and for milling Schott F-Da.8-1,5-6-20-MES-D107H. Both tools are coated with diamond grains using metal binding with diameter of 8 mm and the grit size 107 μ m.

The material of workpiece is fiberglass, mechanical properties are in Table 3.

Table 3. Mechanical properties of workpiece

Young modulus	Tensile strength	Yield strength	Hardness	Fracture toughness
20 GPa	180 MPa	150 MPa	15 HV	12 MPa.m ^{1/2}

4. EXPERIMENTS EVALUATION

The delamination was evaluated for drilling and milling in the same way, using equations written herein before. The principle of evaluation is in the next for the first cutting conditions in drilling. Results from other experiments are summed in the next without the calculation.

Cutting conditions for the first drilling experiment:

rotations = 2000 ot.min⁻¹,
 feed = 150 m.min⁻¹,
 material 's thickness = 3 mm,
 cutting fluid 's pressure = 10 bar

Measured values of delamination D_{\max} are in Table 4.

Run	$\varnothing D_0$ (mm)	$\varnothing D_{\max}$ (mm)	Delamination factor
1	8	16,897	2,112
2	8	16,963	2,120
3	8	15,693	1,962

Table 4. Max. delamination and delamination factor.

Delamination factor calculation:

$$F_{d1} = \frac{D_{\max}}{D_0} = \frac{16,897 \text{ mm}}{8 \text{ mm}} = 2,112$$

$$F_{d2} = \frac{D_{\max}}{D_0} = \frac{16,963 \text{ mm}}{8 \text{ mm}} = 2,120$$

$$F_{d3} = \frac{D_{\max}}{D_0} = \frac{15,693 \text{ mm}}{8 \text{ mm}} = 1,962$$

Total delamination factor:

$$F_{dv1-1} = (F_{d1} + F_{d2} + F_{d3})/3 = \frac{6,194}{3} = 2,065$$

Values of delamination factor in drilling according to cutting conditions are in the Table 5. The results of delamination for milling are in the Table 6.

Rotations [min ⁻¹]	Feed [mm/min]	Cutting fluid's pressure [MPa]	Delamination factor [-]
2000	150	10	2,065
2000	100	10	1,995
2000	50	10	2,056
2000	150	5	2,159
2000	100	5	1,891
2000	50	5	1,610

Table 5. Delamination factor in drilling

Rotations [min ⁻¹]	Feed [mm/min]	Cutting fluid's pressure [MPa]	Delamination factor [-]
4000	2000	10	1,263
4000	1000	10	1,557
4000	500	10	1,237
4000	2000	5	-
4000	1000	5	1,973
4000	500	5	1,599

Table 6. Delamination factor in milling

From measured values it is clear, that the delamination is higher with higher cutting fluid's pressure and with higher feed for drilling. The graphical interpretation of results from drilling is in Fig 3.

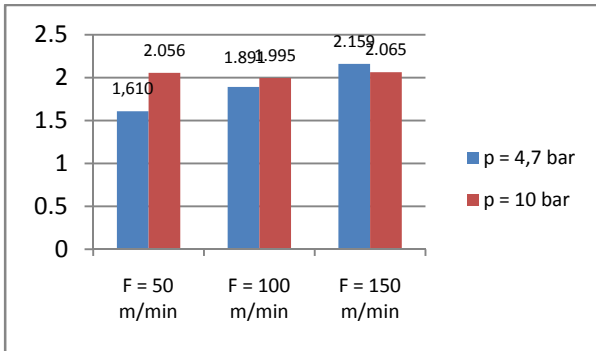


Fig. 3 Delamination in drilling.

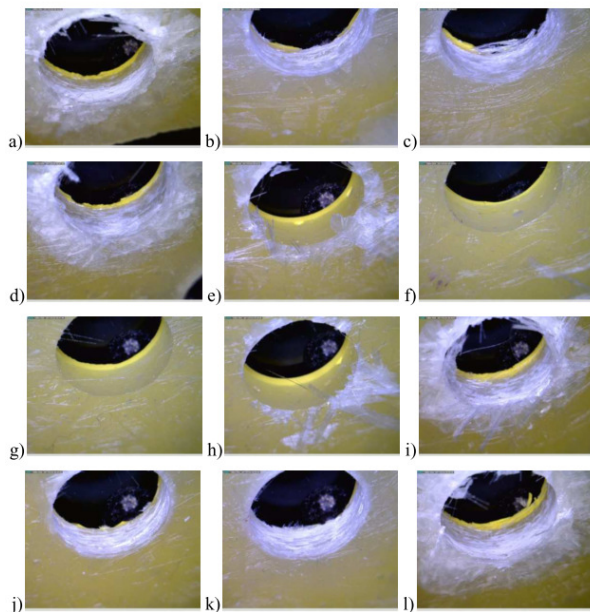


Fig. 4 Delamination in drilling, magnification 25 x

The photograph of delamination is in the figure Fig.4. Cutting conditions for each hole are as following:

- a) F = 150 m/min , P = 4,7 bar,
- b) F = 150 m/min , P = 4,7 bar,
- c) F = 100 m/min , P = 4,7 bar,
- d) F = 100 m/min , P = 4,7 bar,
- e) F = 50 m/min , P = 4,7 bar,
- f) F = 50 m/min , P = 4,7 bar,
- g) F = 50 m/min , P = 10 bar,
- h) F = 50 m/min , P = 10 bar,
- i) F = 100 m/min , P = 10 bar,
- j) F = 100 m/min , P = 10 bar,
- k) F = 150 m/min , P = 10 bar,
- l) F = 150 m/min , P = 10 bar.

The lowest value of delamination is visible in Fig. 4f and 4g which stands for low level of feed, but both high and low level of cutting fluid's pressure.

The same observation was performed for milling experiment, Fig.5. The cutting conditions according to the figure are as following:

- a) F = 2000 m/min, P = 10 bar,

- b) F = 500 m/min, P = 10 bar,
- c) F = 1000 m/min, P = 10 bar,
- d) F = 1000 m/min, P = 4,7 bar,
- e) F = 500 m/min, P = 4,7 bar.

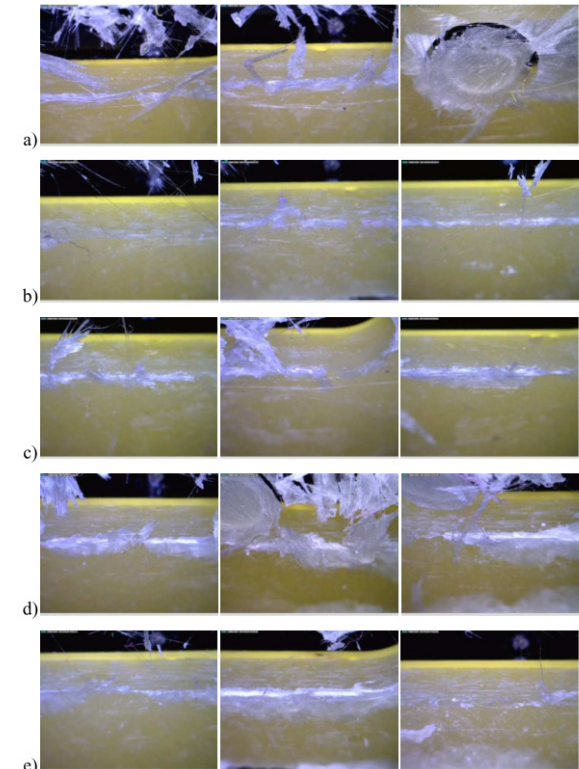


Fig. 4 Delamination in milling, magnification 25 x

It can be concluded that the lowest level of delamination was earned for lowest level of feed, however the difference is not so high as or drilling, which is caused by the different kinematics of processes and the relation between feed direction, ultrasonic vibrations direction and fibers direction in the material.

The tool wear was also observed as can be seen in Fig.6. On the left figure is new tool, on the right the one after experiments. The scratches from fibers in binding are clearly visible, as well as diamond grains. The surface of the tool after the process is full of the matrix material from the fiberglass because the temperature in machining process was higher than the melting point of the material. This is negligible effect which leads also into higher tool wear; the tool has to be cleared respectively.

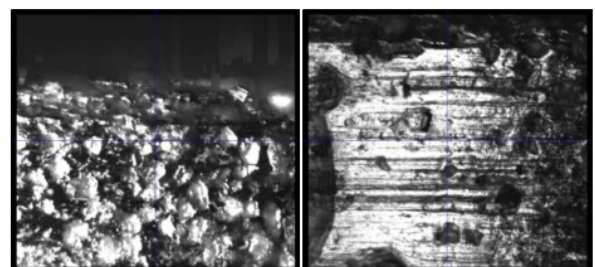


Fig. 6 Tool wear in rotary ultrasonic fiberglass machining, magnification 200x
a. new tool, b. used tool

5. CONCLUSION

In submitted article the delamination in composite materials is explained. Since it is a serious problem, more techniques for its reduction were proposed in literature. The one possibility of delamination lowering is using non-conventional machining technology such as rotary ultrasonic machining. A set of experiments were performed using ultrasonic machine tool in order to verify the presumption that vibrations may reduce the delamination factor both for drilling and milling. The influence of machining variables was evaluated in the next. Based on experiments following conclusion can be stated. The delamination factor is affected both by feed and cutting fluid's pressure. In the first experiment the holes were created by diamond drill with vibrations frequency of 21300 Hz, rotations of 2000 min⁻¹, and three levels of feed and cutting fluid's pressure. The lowest level of delamination was measured for the lowest level of feed 50 mm/min and low level of pressure 5 bar. Very similar value of delamination was also observed for the combination of low feed and high cutting fluid's pressure. According to that can be assumed, that the level of cutting fluid's pressure has no significant effect on delamination in drilling. On the other hand the effect of feed was significant and the relation of delamination factor on feed is quasi linear. That means for lower delamination the lower feed is suitable, which confirms the presumption. In general can be said, the cutting fluid has negligible effect on delamination, because of the destruction of layers. The matrix of fiberglass is absorptive. During the machining process the material absorb cutting fluid and damage the edge of machined hole. However it is not possible to machine without cutting fluid, because the temperature raising in the place of cut is higher than the melting point of the material's matrix which causes melting of the matrix, pulling off of the fibers and filling the tool with the melted matrix material.

The results from milling experiments are as following. The delamination in general was lower than in drilling, however the negligible effect of cutting fluid was not so high, what more the higher cutting fluid's pressure helps to reduce the delamination under cutting condition F 500 mm/min and 2000 mm/min. The higher delamination was observed for pressure 5 bar than for the pressure 10 bar. This effect can be explained by different kinematics of these two processes. In milling the direction of feed in not perpendicular to the direction of fibers in layers and therefore the pressure of the tool is not so high on the last layers. The higher pressure helps to reduce the delamination because its direction is perpendicular and in fact it cuts off the last layer which is better for delamination.

It can be concluded that rotary ultrasonic machining with diamond tool is suitable for fiberglass machining, however the need of cutting fluid decrease the advantage of the machining process. As was already mentioned the cutting fluid damage the material and machining without it causes melting of the material and filing the tool. Therefore the disadvantages exceed the

benefits of the technology. The solution may be ultrasonic machining with standard tool with cutting edge with defined geometry, which is the topic for next research.

6. REFERENCES

- [1] Simon S.F. Chang, Gary M. Bone, McMaster.Burr size reduction in drilling by ultrasonic assistance. Manufacturing Research Institute (MMRI), McMaster University, Hamilton, Ontario, Canada, 2004.
- [2] Sedláček, J.: Problémy přiobrábění kompozitních materiálů, 2007. www.mmspektrum.com <<http://www.mmspektrum.com/clanek/problemy-pri-obrabeni-kompozitnich-materialu>>
- [3] Kubovič, P.: Výskum delamina čnéhofaktora privítaní, Trnava, 2009.
- [4] Li, Z., C., Pei, Z., J.: Experimental study on rotary ultrasonic machining of graphite/epoxy panel, 2003.
- [5] Javitz, A.E. DESIGN. [AUT.] R.A. BAREŠ. *Kompozitní materiály*. Praha : SNTL, 1965.
- [6] Berghezan, A. Nucleus 8. [AUT.] R.A. Bareš. *Kompozitní materiály*. Praha : SNTL, 1966.
- [7] Líška, J.: Obrábaniekompozitnýchmateriálov, Trnava, 2010.

ACKNOWLEDGEMENTS

Authors want to thank to the National Grant Agency and European Fund for Regional Development for financial support.

This article has been realized under the research and development OP for project Centre of Excellence of Five axis Machining ITMS 26220120013 co-financed by European Fund for Regional Development



Supporting research activities in Slovakia/
Project is co-financed by European Community

Authors:

Prof. Dr. Ing. Jozef Peterka, Ing. Matúš Beňo, Ing. Martin Kováč, Ing. Marek Zvončan
Slovak University of Technology in Bratislava
Faculty of Materials Science and Technology with seat in Trnava
Paulínska Street 16, 917 24 Trnava, Slovak Republic
E-mail:

Jozef.peterka@stuba.sk

Matus.beno@stuba.sk

Martin.kovac@stuba.sk

Marek.zvoncan@stuba.sk

Šogorović, D., Mišković, A., Višekruna, V.

DESIGN OF DEVICE FOR HIGH-PRODUCTIVE CUTTING OF THREADS

Abstract: The aim of the paper is developing of technology that enables a high-productive thread cutting (with a high speed and a small chip diameter) at the classic lathe machine using a device – motor unit.

The paper shows the solution of design of device for eccentric cutting of threads on a universal lathe machine, and an experimental study of cutting forces depending on the chip diameter for titanium alloy.

All researches have been done in a laboratory conditions at the Laboratory for Machining with Cutting and Machine Tools at Faculty of Mechanical Engineering and Computing, and the model and design solution have been created in software package SolidWorks®.

Key words: production of threads, eccentric cutting of threads, cutting forces, chip diameter, cutting speed, cutting time.

1. INTRODUCTION

The demands for higher productivity of thread cutting in comparison with productivity realized with lathe tool are given by market conditions. A fulfilment of those demands could be done by using of developed device, which enables an additional movement of tool – head with lathe tools and thread cutting with increased machining speed, improved quality and reduced cutting time. In this paper, a view of method, machining schemes, a kinematics of a process, as well as an experimental study of cutting forces depending on the chip diameter for titanium alloy are presented. Machining with cutting in an area defined with small chip diameter and increased cutting speeds is realized. It is clearly shown that using of this device results in higher technical and technological level of a lathe.

2. ECCENTRIC CUTTING OF THREADS ON THE LATHE MACHINE

The production of the thread with device shown on Fig. 1 represents a new method for production of threads with higher speed of cutting and, in same time, with higher productivity compared with classical methods (production of thread with lathe tool using the leading spindle of lathe machine. Project represents the whole device (aggregate) which is placed in front porter of lathe machine.

The head with lathe tools produces the main rotation with a high speed ($v = 140 - 500$ m/min) moved by electric engine with simultaneous low longitudinal mowing together with porter of lathe, while work piece placed in clamp head of main spindle making slow miscellaneous rotation. The porter of the head with lathe tools is placed like special device on the porter of the lathe machine and in that way produces longitudinal mowing. This longitudinal mowing has to be harmonized with rotation of working part so for one rotation of work piece, head moves longitudinal for one thread feed.

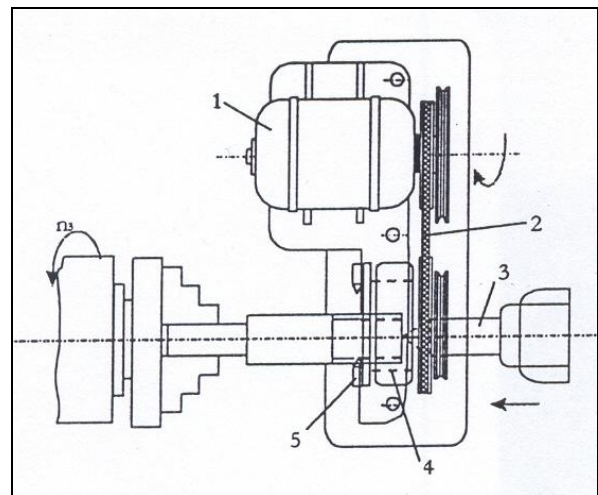


Fig. 1. Scheme of mowing (1 - electric engine, 2 - belt, 3 - dead centres, 4 - bearing, 5 - cutting head) [1]

The principle of thread production with eccentric cutting, (ger: Gewindewirbeln, rus: Vihrevoje) consists of placing of the lathe tool for cutting of thread (Figure 2.) into special head whose axis is inclined toward the axis of the work piece for angle of thread φ .

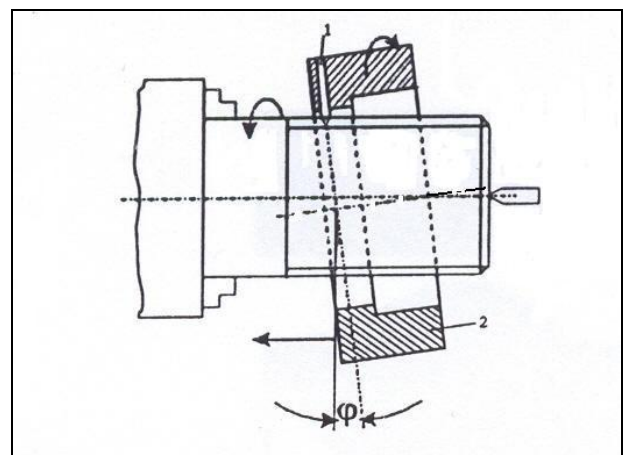


Fig. 2. Principal of eccentric cutting of thread [1]

3. KINEMATICS OF ECCENTRIC CUTTING

Eccentric cutting of threads is basically process of production of threads by milling. During the production, teeth of milling tool are replaced with turning tools. They are placed in device – head for cutting. External cutting of threads is produced with two different ways; depending on placement of work piece and head of cutting: the work piece is into head (more often – Figure 3.) and work piece is out of head.

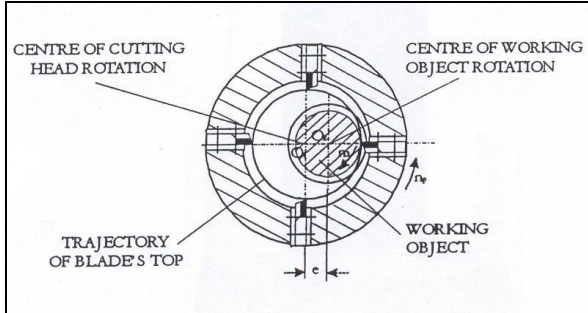


Fig. 3. Kinematics of external eccentric cutting

Next figure represent chip look.

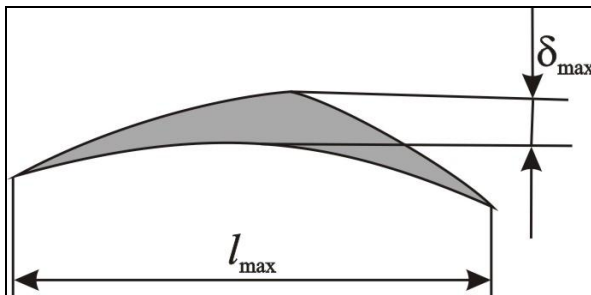


Fig. 4. Chip in eccentric cutting

3.1. Selection of processing parameters

Processing parameters in eccentric cutting of threads are:

- cutting speed (edge speed of head) v_g ,
- edge speed of work part v_p ,
- feed rate (same as thread feed) s .

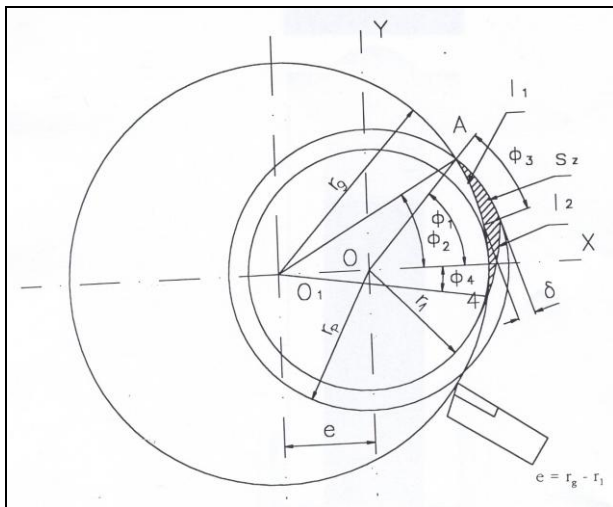


Fig. 5. Geometric relation in eccentric cutting

From Fig. 5., the following parameters are defined as:
 d_p – work piece diameter (main diameter of thread) [mm]

d_1 – internal diameter of thread [mm]

D_g – diameter of head of cutting [mm]

e – eccentricity (distance between axis of work piece and axis of head) [mm]

s_z – length of arc on work piece cut by one lathe tool [mm]

z – number of lathe tools in head

n_p – number of rotation of work piece [min^{-1}]

n_g – number of rotation of head [min^{-1}]

According to [1] the relation is $D_g/d_p = 1,4 - 1,6$.

Speed of head v_g is 140 m/min - 500 m/min which depends on material of work piece, material of lathe tools, dimension and profile of thread and on coolant device.

$$v_g = \frac{D_g \cdot n_g \cdot \pi}{1000} \left[\frac{m}{\text{min}} \right] \quad (1)$$

$$v_g = 140 - 500 \text{ [m/min]}$$

$$n_g = \frac{1000 \cdot v_g}{\pi \cdot D_g} \left[\text{min}^{-1} \right] \quad (2)$$

Length of arc s_z is defined by equation:

$$s_z = \frac{\pi \cdot d_p \cdot n_p}{z \cdot n_g} \text{ [mm]} \quad (3)$$

and it's value is in interval of 0,4 – 1,2 mm which depends on characteristics of material of work piece according to table 1. [1]

Tensile strength of material [N/mm ²]	R _m =550	R _m =650	R _m =750	R _m =850
s_z [mm]	1.0-1.2	0.8-1.0	0.6-0.8	0.4-0.6

Table 1. Length of arc cut by one tool

From equation (3) it is following:

$$n_p = \frac{s_z \cdot n_g}{\pi \cdot d_p} \left[\text{min}^{-1} \right] \quad (4)$$

$$v_p = \frac{\pi \cdot d_p \cdot n_p}{1000} \text{ [m/min]} \quad (5)$$

Feed rate "s" is equal to feed of thread.

The main machining time is calculated according to equation:

$$t_g = \frac{L}{n_p \cdot s} \text{ [min]} \quad (6)$$

where are:

L – the effective length of thread enlarged for empty cut

s – feed of thread

n_p – number of rotations of work piece

4. DESIGN OF DEVICE FOR ECCENTRIC CUTTING OF THREADS ON LATHE

This paper shows (Fig. 6.) model of device which have been created in software package SolidWorks. This device is designed for threads with main diameter up to 65 mm. It has been designed two possible number of rotation of head due to design of belt wheels. The four lathe tools are used in this device.

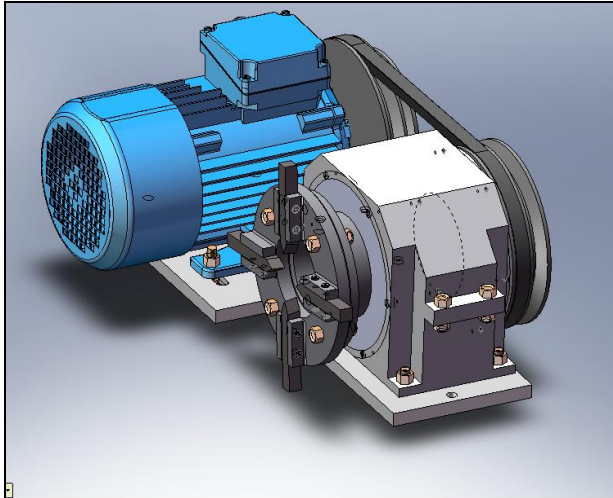


Fig. 6. Model of device [2]

The way of setting a device to lathe machine is shown on Fig. 7.

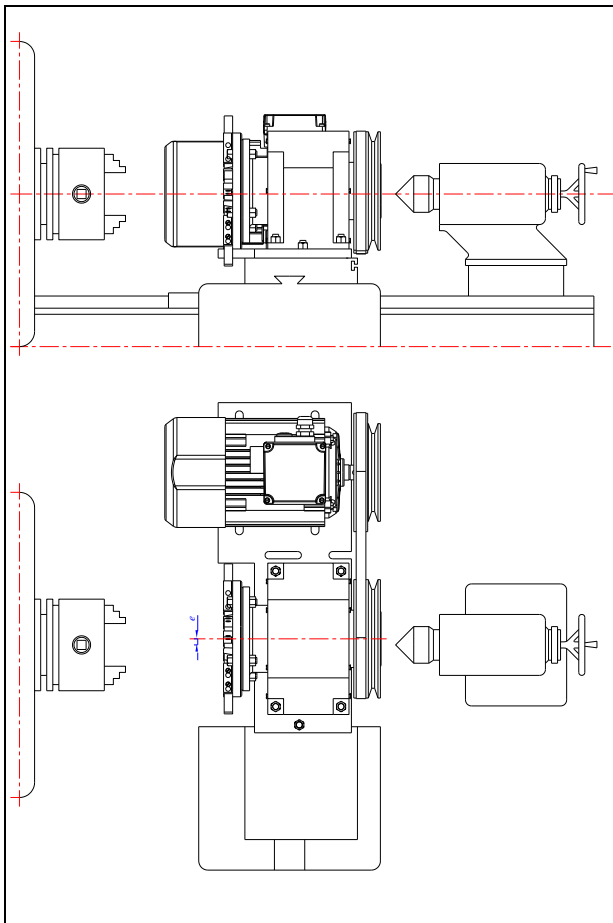


Fig. 7. Scheme of the setting a device to lathe machine

Design of this device is limited to characteristic of a lathe machine i.e. dead centres height. This device is designed for universal lathe machine TNP-200 (Prvomajska Zagreb).

The maintenance of this device is very simple due to its design which is simple, functional and cheap. All connection are separable (thread connection) and therefore it is simple to replace all part of device. The lubrication of the bearings are provided and it is recommended to use lubricants LITMA-1, LITMA-2 or LITMA-3TM.

5. RESEARCH OF CUTTING FORCES IN DEPENDENCE OF CHIP INTERSECTION IN PROCESS OF THREADS CUTTING

The further researches will be focused on making of prototype of device. For that reason it is necessary to perform of research of cutting forces in dependences of chip intersection. This device will be used mainly in thread cutting in titanium alloy UT-A6V.

For this research, the factorial experimental plan 2² has been used. All experiments has been performed on universal lathe machine TNP-200 (Fig. 8.) and with standard lathe tools for threads cutting (Fig. 9.).



Fig. 8. Universal lathe machine TNP-200

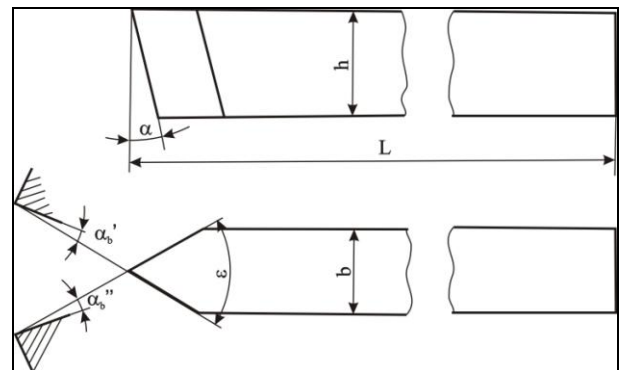


Fig. 9. Standard lathe tool for threads cutting

The dynamometer KIAG Swiss type 9257 (Kistler Instrumente AG – Fig. 10), camera and software package has been used as a measuring equipment.

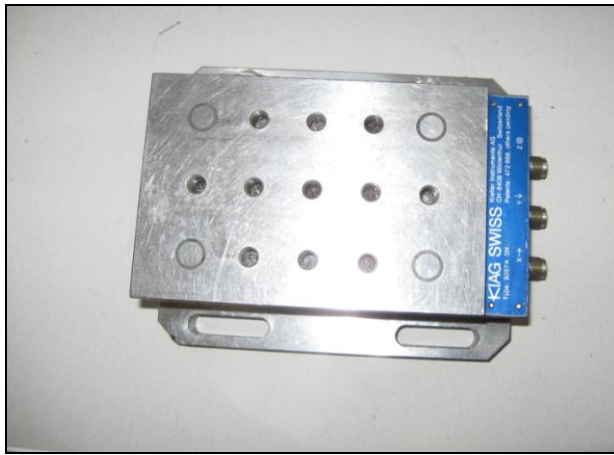


Fig. 9. Dynamometer

Input parameters are length (l) and diameter (a) of chip. Output parameters are three components of cutting force: main force F_1 , force of penetration F_2 and force of auxiliary mowing F_3 . In this paper, only the results for main force are presented.

5.1. Results of testing [2]

No. of experiment		Input parameters		Results
Stand. No.	Performing No.	Lenght l [mm]	Diameter a [mm]	Main force F_1 [N]
1	8	0,400	0,120	187
2	7	1,417	0,120	434
3	5	0,400	0,290	313
4	1	1,417	0,290	783
5	4	0,909	0,205	373
6	3	0,909	0,205	373
7	2	0,909	0,205	373
8	6	0,909	0,205	373

Table 2. Results of testing

According to results of testing, regression analyze has been done by using of software package Design Expert 8.0.1. In that way we got the mathematic model for main force depending on intersection of chip (length and diametre).

ANOVA

Source	Sum of Squares	D f	Mean Square	F-Value	P-Value Prob>F
Model	1,849×10 ⁵	2	92464,25	24,64	0,0026
A- lenght l	1,285×10 ⁵	1	1,285×10 ⁵	34,25	0,0021
B-diamet. a	56406,25	1	56406,25	15,03	0,0117
Residual	18760,38	5	3752,08		
Lack of Fit	18760,38	2	9380,19		
Pure Error	0,00	3	0,00		
Cor Total	2,037×10 ⁵	7			

Regression Statistic			
Std. Dev.	61,25	R-Squared	0,9079
Mean	401,13	Adj. R-Squared	0,8711
C.V. %	15,27	Pred. R-Squared	0,4352
PRESS	1,150×10 ⁵	Adeq. Precision	15,889

Factor	Coefficient Estimate	D f	Standard Error	95%CI Low	95%CI High
Intercept	401,13	1	21,66	345,45	456,80
A-length l	179,25	1	30,63	100,52	257,98
B-diamet. a	118,75	1	30,63	40,02	197,48

Table 3. Regression analyze of results of testing

The model of main force F_1 in coding form is:

$$F_1 = 401,13 + 179,25 \cdot A + 118,75 \cdot B \quad (7)$$

De-coding model of main force F_1 is:

$$F_1 = -205,52501 + 352,50737 \cdot l + 1397,05882 \cdot a \quad [N]$$

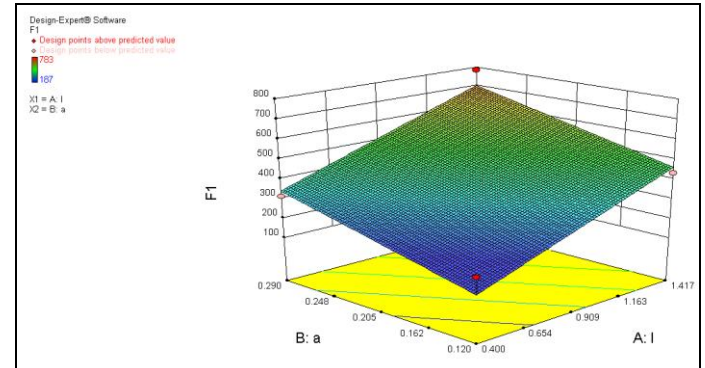


Fig.10. The influence of chip on main cutting force

6. CONCLUSION

In regard to shown in paper, it can be concluded:

- by using of device for eccentric cutting of threads, the threads can be produced with a high quality with increasing of cutting speed and reducing of cutting time,
- the eccentric cutting reduces the cutting time up to 90% in comparison with classic method of producing threads on lathe and it is high-productive methods,
- the cutting force in production of threads mostly depends on dimension of chip so the method of eccentric cutting is favourable because the chip intersection and length are very small.

7. REFERENCES

- [1] Mišković, A., Šogorović, D.: *A Description of High-productive Method for Thread Cutting on Lathe*, Proceedings of 12th International Research/Expert Conference TMT 2008, p.p. 5-9, Istanbul, Turkey, TMT, Zenica, 26-30 August 2008.
- [2] Šogorović, D.: *Prilog studiji o visokoučinskom rezanju navoja na univerzalnom tokarskom stroju*, Master thesis, Faculty of Mechanical Engineering and computing, Mostar, 2011.
- [3] Šogorović, D., Mišković, A.: *Izrada navoja visoke kvalitete ekscentričnim rezanjem*, 7. Naučno-stručni skup s međunarodnim učešćem "KVALITET 2011", p.p. 393-397, Neum, BiH.

Authors: Mr.sc. Danijel Šogorović, Prof.dr.sc. Ante Mišković & Prof.dr.sc. Vojo Višekruna, University of Mostar, Faculty of Mechanical Engineering and Computing, Matice hrvatske bb, 88000 Mostar, BiH, Phone.: +387 36 337-001, Fax: +387 36 337-012.

E-mail: danijel.sogorovic@sve-mo.ba
ante.miskovic@sve-mo.ba
vojo.visekruna@sve-mo.ba

Tanović, Lj., Puzović, R., Klimenko, S.

THE PHENOMENA OF GRANITE MICRO – CUTTING PROCESS

Abstract: The paper shows the results of investigations performed in the brittle materials micro-cutting at the Faculty of Mechanical Engineering, Belgrade University. The interactions between a single diamond grain and the machined granite are analyzed. The change in the normal cutting force as a function of grain penetration speed and depth was experimentally established in micro-cutting of two types of granite originating from Serbia. Based on the grain traces on granite and the generated cracks, the critical grain penetration depth for the formation of brittle fracturing was established. The experiments are intended to assist in the optimization of the grinding and polishing processes as technologies dominant in the granite finishing.

Key words: granite, cracks, diamond grains, chip, cutting force

1. INTRODUCTION

Many technological operations involve two or more contacting bodies sliding relative to one another. A series of damage mechanisms may occur in these situations, for instance, fretting fatigues and wear. Incommensurable economic losses can be ascribed to these phenomena. In a totally different context, scratching and cutting represent fundamental manufacturing processes, as is the case of precious and ornamental stone cutting. Therefore, the mechanics of these processes has been an important object of research for many years.

The specificity of surface finish technology demands a good knowledge of all the granite's characteristics including its structural-textural (continuum, homogeneity, and isotropy), physical-mechanical (specific gravity, porosity, moisture, water-permeability, hardness, toughness, and abrasiveness) and mineralogical-petrography (grain size, type and content of colored components, etc) properties.

2. OVERVIEW OF CHIP FORMATION MECHANISMS

A large number of researchers dealing with the development of model for deformation and fracturing regarded the cutting action of a diamond grain in the grinding wheel as being identical to the indentation effects caused by a diamond indenter during hardness measurements. Considering the investigations on brittle materials, they go into two directions: by how the force acts during the indentation (dynamic and static) and by the shape of the indenter.

Inasaki [1] and Brook [2] tested the penetration of an oval-tip indenter into brittle and ductile materials. Depending on the radius of the oval-tip and the load on the indenter, the stress zone was defined, so that the transition from brittleness to elasticity was observable. As the radius of the tip increases, the stress-deformation state exceeds a certain critical level in the zone and adjoins the circular contact zone. Two principal crack systems emanate from the plastic zone: median/radial and lateral cracks. Median/radial cracks

are usually associated with strength degradation, and lateral cracks with material removal. While this approach was originally developed for static normal loading, it has also been extended to include the effect of a tangential load. The annular crack grows, and its propagation is always cone-shaped, Fig. 1 (upper part).

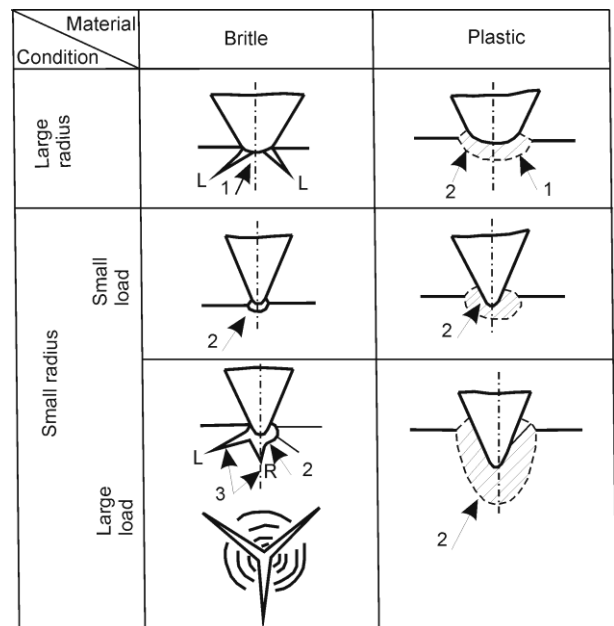


Fig. 1 – Deformation and crack formation model during indentation (1 = elastic deformation, 2 = plastic deformation, and 3 = crack formation; R-median/radial; L-lateral) [1,2]

Lawn and Wilshaw [3] think that fracture patterns in brittle materials, under blunt indenters, usually start as ring surface cracks immediately outside the contact area. By increasing the normal load, these surface cracks evolve into the so-called Hertzian cone cracks (Fig.2).

Anton and Subhash [4], unlike the traditional static indentation models, which cannot capture the strain rate effects, consider that the current dynamic indentation experiments can provide a more realistic representation of the influence of loading rate on the material removal

mechanisms during a dynamic process.

Lawn and Swaine [5] investigated indentation with a sharp indenter (cone and pyramid) and found that an embedded penny-shaped crack is increased, its propagation reaches the surface and the penny cracks evolve into the half-penny configuration.

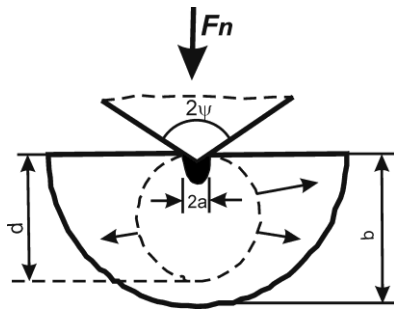


Fig. 2 – Indentation fracture in brittle materials: transition from splitting penny-shaped cracks to median-vent cracks under sharp indenters

Conway and Kirchner [6] analyzed the mechanics of crack initiation and propagation beneath a moving sharp indenter. A fracture mechanics solution for a single embedded penny-shaped crack was used to predict the propagation depth of pre-existing defects.

The second group of researchers, though to a lesser extent, performed the cutting process in a variety of brittle materials by a single diamond grain.

Mishnaevsky [7] performed the real cutting process in brittle materials, observing different physical mechanisms involved in material destruction (deformation, crushing, cracking and spalling). He considers that neither Hertzian cone cracks nor circumferential cracks are formed. Instead, penny-shaped cracks in the cutting force vector direction are formed.

Chiaia [8] provides a system analysis for the current approaches to the issues of micro-cutting processes in brittle and quasi-brittle materials. It was shown that various interaction mechanisms beneath the tools during the penetration process are essentially reduced to plastic deformation and brittle fracturing.

The third group of researchers studied the crack formation and development in brittle materials.

Labuz et al. [9] analyzed crack propagation in rock and inferred that it is characterized by microcracking around the crack tip covering the fracture process zone and together with the fracture free length defines the effective crack length.

Germanovich et al. [10] carried out a series of triaxial compression tests of sandstone loaded to different stress levels, i.e. 100%, 80% and 50% of the corresponding compressive strength and then examined the tested specimens microscopically. On the basis of test results, a mechanism was proposed for the transition from microcrack proliferation to the formation of the main structure.

Abe et al. [11] investigated the formation and proliferation of cracks in the granite and their effects on the fracture process zone.

The fourth group of researchers performed the real cutting processes, such as circular sawing and grinding,

in brittle materials and analyzed the crack propagation and chip brittle fracturing mechanisms. They measured the cutting forces, the cutting strength and tool wear in ceramics and granite machining with the aim to recommend the efficient abrasive machining [11-17].

3. MICRO-CUTTING EXPERIMENTAL SCHEMES

In the current work to establish the micro-cutting characteristics in granite grinding, experiments with single diamond grains were performed. The experiments were aimed at identifying the phenomena associated with the diamond grain-granite interactions to determine the magnitude of the resulting cutting force and chip formation mechanisms along the grain's trajectory. In actual grinding there are multiple grain trajectories and mutual interactions. Micro-cutting was performed according to the scheme shown in Fig. 3.

A diamond indenter grain with a 1200 tip angle and a 0.1 mm tip radius, was placed and rigidly fastened to an aluminum disc 150 mm in diameter that was statically and dynamically balanced. On a cutting-table of a HMC 500 machine, a dynamometer was mounted with a fixture for clamping the marble specimen. The fixture enabled the rotation of the granite specimen under an inclination (1:200) relative to the axial motion of the cutting grain, thereby achieving varying depth cutting through rotation of the grain disk (V_s) and axial shifting of the platform with the granite and dynamometer (V_w).

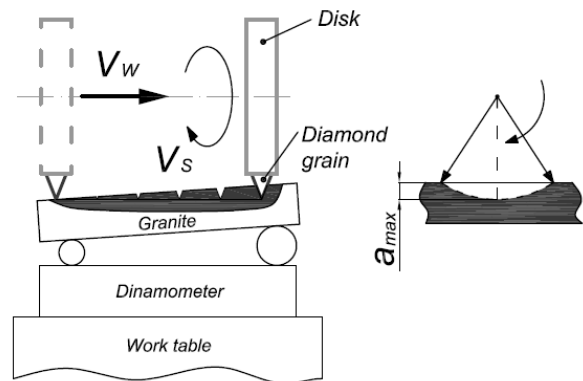


Fig. 3 – Micro-cutting with a diamond grain with a rotary and axial motion

4. RESULTS AND DISCUSSION

The micro-cutting process was performed on two types of granite: fine-grained "Josanica" (GJ) and medium-grained "Bukovik (GB), whose physical-chemical properties were examined and presented in Tab. 1.

The values of the listed properties are mean values obtained from a larger number of measurements, depending on the petrography nature of granite. The micro-hardness measurements indicate that GB had more uniform however lower hardness compared to GJ. Experiments were carried out using the following measuring instruments: a two-component dynamometer (Kistler 5007), a data acquisition card + 10V 105kHz, a computer, a microscope (Leitz wetzlar) with a Sony

video camera.

Properties	Granite	
	Josanica GJ (VB)	Bukovik GB (PT)
Specific gravity, KN/m ³	29.70 ± 0.3	25.6 ± 0.1
Micro-hardness, HK75/HK25	3.1	2.6
Compressive strength, Mpa	185 ± 20	102 ± 8
Ultimate strength, Mpa	16.6 ± 1	15.0 ± 2
Cohesion, MPa	31.8	22.0
Abrasion coefficient, %	21.5- 23.0	23.5-24.5

Table 1. Granite physical – mechanical properties

Fig. 4 shows diagrams of changes in the normal cutting force (resistance) as a function of grain penetration depth at speeds of $V_s = 7.85 - 11.1 - 15.7 - 22$ m/s. The non-linearity in the change of F_n is the consequence of the granite's non-uniformity. Also, as the grain penetration depth increases, the cutting force increases. It can be stated that at places where the force decreases this is the result of a soft phase presence in the granite.

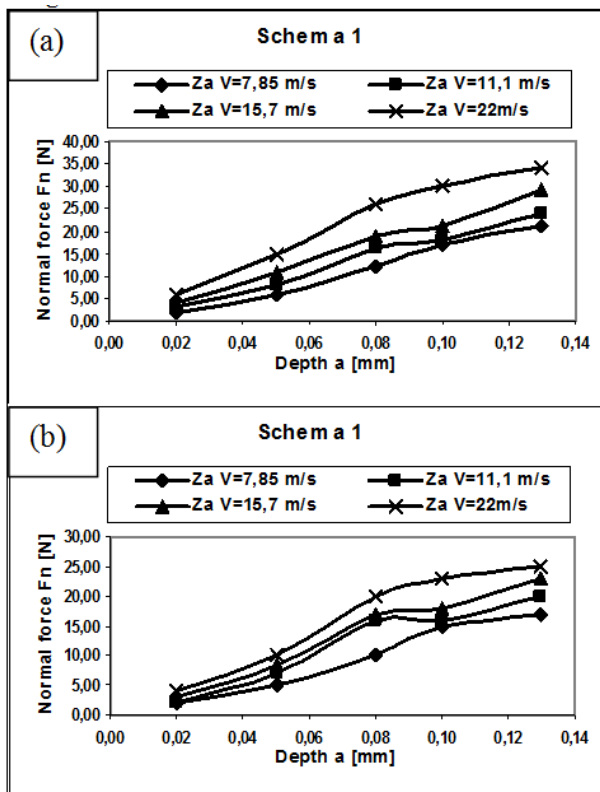


Fig. 4 – Change of the normal force as a function of grain penetration depth in micro-cutting:

(a) GJ granite and (b) GB granite

The analysis of the traces from the micro-cutting experiments on the two granites can provide the description of the chip formation mechanism.

(a) At smaller cutting depths, ahead of the diamond grain, in the fracturing core region, there occur plastic deformations followed by median and lateral cracks.

(b) As cutting depth increases the mentioned

cracks increase, so that lateral cracks reach the surface of the machined work-piece and radial cracks occur. At some instant those cracks become interconnected, which is followed by granite grains chipping, crushing and detachment, causing the non-uniform chipping along the diamond grain's trajectory, Fig.5.

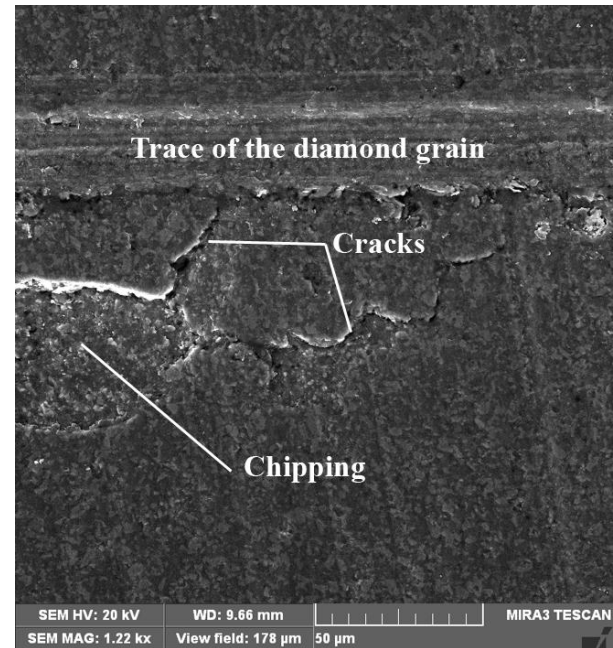


Fig. 5 – Occurrences on the GJ granite micro-cutting, scheme 1 ($a=0.05$ mm, $V_s = 7.85$ m/s, $x125$)

(c) Cracks remain under the machined surfaces that originate not only from the chip formation process but also from the pores that exist in the granite. These cracks can exert a critical influence on the workpiece's strength. Therefore, crack formation due to processing should be minimized, to maintain fracture-induced detachment of the processed material at the lowest volume.

(d) In granite micro-cutting initial ductile flow progressively changes to brittle fracture after the critical depth of cut is reached. Each trace created in the granite by micro-cutting was analyzed. The mechanism of granite machining is manifested through brittle fracture and plastic deformations. Brittle fracture indicates that there are two mechanisms of crack propagation: median cracks are usually associated with strength degradation, and lateral/radial cracks with chip formation.

In granite micro-cutting two regions are evident. They can be defined by the grain penetration depth (critical depth) that restricts the region of plastic deformation followed by crack formation from the region of fracture-induced detachment of the machined material. The critical depth can be used as one of the criteria for the optimization of the grinding process.

The GB granite has smaller hardness compared to the GJ granite, so in micro-cutting, at equal penetration depths, the radial cracks are less pronounced in the GB granite for both micro-cutting schemes. The analysis of the grain traces on the granites shows a more pronounced chipping in the GB granite as the result of

a greater coarse-grained structure and a greater grain detachment.

The measurements established the critical grain penetration depth of 0.020 mm for GJ ($V_s = 7.85$ m/s) and that the critical depth declines to 0.015 mm as the speed increases to 15.7 m/s. The lengths of the radial cracks at the critical depth are 0.35 and 0.30 mm for the range of penetration speeds given above.

Under identical penetration conditions, the critical depth in GB is slightly greater and ranges from 0.022 mm ($V_s = 7.85$ m/s) to 0.018 mm ($V_s = 15.7$ mm), while the lengths of radial cracks are 0.28 and 0.23 mm.

5. CONCLUSION

The development and application of new diamond tools for granite processing necessitates the understanding of physics of the processes that take place at the point of interaction between the diamond grain and work-piece. Cutting experiments provided the establishment of the critical grain penetration depth, thereby granite processing and the change in the normal component of cutting resistance as a function of speed and grain penetration depth.

Beneath the machined surface there remain cracks created not only in the granite formation process but also in the machining process, so their influence on the body strength can be considerable. This is an indication that it should be tended to as small processing-induced cracks as possible because the detached fractures of the processed material will be smaller in volume and the corresponding quality of the machined surface lower respectively. Comparisons of the micro-cutting traces in GJ and GB granites revealed that fine-grained types are more suitable for machining, because the occurrence of grain chipping and detachment is less pronounced than in coarse-grained structures.

The lengths of the radial cracks in GJ granite, range from 0.30 to 0.35 mm, while for GB from 0.23 to 0.28 mm. The critical grain penetration depth in GB is greater compared to GJ, which is explained by a greater presence of the soft phase and smaller hardness.

When the micro-cutting forces are compared, it is inferred that at equal depths and cutting speeds the cutting force is higher by 40% in GJ compared to GB, which is explained by greater hardness.

6. REFERENCES

- [1] Inasaki, I., 1987, Grinding of Hard and Brittle Materials, *Annals of the CIRP*, 36/2: 463-471.
- [2] Brook, B., , 2002, Principles of Diamond Tool Technology for Sawing Rock, *Int. J. Rock Mechanics and Mining Sciences*, 39: 41-58.
- [3] Lawn, B.R., Wilshaw, R, 1975, Indentation Fracture: principles and Applications, *J. Mat. Sci*, 10: 1049-1081.
- [4] Anton, R.J., Subhash, G., 2000, Dynamic Vickers Indentation of Brittle Materials, *Wear*, 239/1:27-35.
- [5] Lawn, B.R., Swain, M.V., 1975, Microfracture beneath point indentations in brittle solids, *J. Mat. Sci*, 10: 113-122.

- [6] J.C. Conway, J.C., Kirchner, H.P.,1980, The mechanics of crack initiation and propagation beneath a moving sharp indenter. *J. Mat. Sci.* 15: 2879–2883.
- [7] Mishnaevsky, L.L.,1994 , Investigation of the cutting of brittle materials. *Int. J. Mach. Tools Manuf.*, 34: 499–505.
- [8] Chiaia, B., Fracture Mechanisms Induced in a Brittle Material by a Hard Cutting Indenter, *International Journal of Solids and Structures*, 38/44-45: 7747-7768.
- [9] Labuz, J.F., Shah, S.P., Dowding, C.H., 1987, The Fracture Process Zone in Granite: Evidence and Effect, *International Journal of Rock Mechanics and Mining Sciences*, 24/4: 235-246.
- [10] Germanovich, L.N., Salganik, R.S., Dyskin, A.V., Lee, K.K., 1994, Mechanisms of Brittle Fracture of Rock with Pre-existing Cracks in Compression, *Journal Pure and Applied Geophysics*, 143 ; 117-149.
- [11] Abe, H., Saka, M., Ohba, S., 1992, Does the Process Zone Control Crack Growth?, *Applied Mechanics Reviews*, 45/8: 367-376.
- [12] Xu, X., Li, Y., Malkin, S., 2001, Forces and Energy in Circular Sawing and Grinding of Granite, *Journal of Manufacturing Science and Engineering*, 123/1: 13-22.
- [13] Huang, H., Li, Y., Shen, J.Y., Zhu, H.M., Xu, X.P., 2002, Micro- Structure Detection of a Glossy Granite Surface Machined by the Grinding Process, *Journal of Materials Processing Technology*, 129/1-3: 403-407.
- [14] Yang, S.Q., Dai, Y.H., Han, L.J., Jin, Z.Q., 2009, Experimental Study on Mechanical Behavior of Brittle Marble Samples Containing Different Flaws Under Uniaxial Compression, *Engineering Fracture Mechanics*, 76: 1833-1845.
- [15] Tanovic, Lj., Bojanic P., Puzovic, R., Klimenko, S., 2009, Experimental Investigation of Micro-cutting Mechanisms in Marble Grinding, *Journal of Manufacturing Science and Engineering, ASME Transactions*, 131/6.
- [16] Tanovic Lj., Bojanic P., Puzovic R., Milutinovic M., 2011, Experimental Investigation of Microcutting Mechanisms in Granite Grinding, *ASME Journal of Manufacturing Science and Engineering*, 133/2.

Authors: Prof. dr Ljubodrag Tanovic, Prof. dr Radovan Puzovic, University of Belgrade, Faculty of Mechanical Engineering, Department for Production Engineering, Kraljice Marije 16, 11120 Beograd 35, Serbia, Phone.: +381 11 3370-045, Fax: +381 11 3370-364.

E-mail: ltanovic@mas.bg.ac.rs
rpuzovic@mas.bg.ac.rs

Prof. Klimenko S, “V. Bakul Institute for Superhard Materials of the National Academy of Sciences of Ukraine”; Avtozavodsky str. 2; 07074 Kiev, Ukraine
E-mail: atmu@ism.kiev.ua

11th INTERNATIONAL SCIENTIFIC CONFERENCE
MMA 2012 - ADVANCED PRODUCTION TECHNOLOGIES

PROCEEDINGS



Section B:
MACHINE TOOLS

Novi Sad, 20-21 September 2012

Čiča, Đ., Zeljković, M., Lakić-Globočki, G., Sredanović, B., Borojević, S.

IDENTIFICATION OF CONTACT PARAMETERS OF SPINDLE-HOLDER-TOOL ASSEMBLY USING ARTIFICIAL NEURAL NETWORKS

Abstract: The most important requirements of spindle assembly exploitation are parameters of dynamic behavior. This paper explores the use of artificial neural networks in predicting the contact parameters of machine tool spindle – holder – tool assembly. Based on error analysis it was concluded that artificial neural networks, if they used in a systematic way, which includes detailed data preparation and application of optimization techniques to train the network, can be successfully applied in predicting different mechanical properties of the mechanical system, such as the contact parameters spindle–holder–tool assembly.

Key words: neural networks, prediction, contact parameters

1. INTRODUCTION

Most of the research of machine tools, are related to spindle-holder-tool assembly, since its characteristics, such as static and dynamic behavior, power, speed, the types of bearings, among many others, have a decisive impact on machine tools performance. Dynamic instability is one of the major disturbance factors, which influences the quality and productivity of machine tools. In order to avoid self-excited vibration of machine tools during the cutting process, Tlustý [1] proposed a stability lobe diagram, obtained on the basis of the tool point frequency response function (FRF) of the assembly. Common way of obtaining tool point FRF is performing experimental modal analysis. However, any change in the spindle–holder–tool assembly, such as tool and/or tool holder changes, requires a new test, since the system dynamic is change. Therefore, the use of experimental modal analysis is not always very practical, since it requires a lot of time, because the measurements must be performed for each combination of the spindle–holder–tool assembly. In order to minimize experimentation, the receptance coupling theory of structural dynamics can be used for modelling the spindle–holder–tool dynamics [2-5]. On the other hand, in order to obtain the tool point FRF of an assembly with analytical methods, contact parameters should be known accurately. Therefore, fast and accurate identification of contact parameters in spindle–holder–tool assembly is crucial. Since neural networks are a burgeoning area of artificial intelligence and are applied in many engineering applications, the aim of the present study is to investigate the possibility of their application in prediction of the contact parameters of spindle–holder–tool assembly.

2. IDENTIFICATION OF CONTACT PARAMETERS

Components of the spindle–holder–tool assembly should be coupled elastically due to flexibility and damping introduced by contacts at spindle–holder and

holder–tool interfaces. Furthermore, we have applied the approach [2, 3], where part of the holder inside the spindle is considered as integrated to the spindle, because this approach provides a more realistic model, because only the dynamics due to the masses of these subsystems will be included into the model or it will be required to include their stiffness effects with distributed springs. Similarly, the part of the tool inside the holder is considered rigidly joined to the holder, so the receptance matrix of the tool can be coupled with the rest of the system, as depicted in Figure 1.

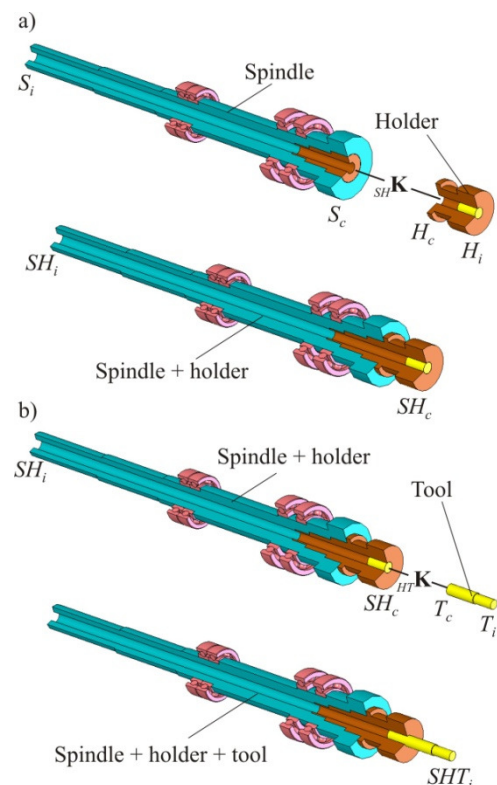


Fig. 1. Elastic coupling of the spindle–holder system (a) and elastic coupling of the spindle–holder–tool system (b)

Assuming that response matrices of the subsystem S

(spindle with bearings) and subsystem H (holder) are known, then it is possible by using a method of receptive coupling, to obtain the global system response matrix SH (spindle–holder) at the holder tip:

$$\mathbf{SH}_{ii} = \mathbf{H}_{ii} - \mathbf{H}_{ic} \cdot (\mathbf{H}_{cc} + \mathbf{S}_{cc} + {}_{SH}\mathbf{K}^{-1})^{-1} \cdot \mathbf{H}_{ci} \quad (1)$$

Complex stiffness matrix, which representing the spindle–holder interface dynamics has the following form:

$${}_{SH}\mathbf{K} = \begin{bmatrix} {}_{SH}k_t + i \cdot \omega \cdot {}_{SH}c_t & 0 \\ 0 & {}_{SH}k_r + i \cdot \omega \cdot {}_{SH}c_r \end{bmatrix} \quad (2)$$

where: ${}_{SH}k_t$ – translational stiffness, ${}_{SH}c_t$ – translational damping, ${}_{SH}k_r$ – rotational stiffness and ${}_{SH}c_r$ – rotational damping at the spindle – holder interface.

Receptance matrix of the global system SHT (spindle–holder–tool) at the tool tip has the following form:

$$\mathbf{SHT}_{ii} = \mathbf{T}_{ii} - \mathbf{T}_{ic} \cdot (\mathbf{T}_{cc} + \mathbf{SH}_{cc} + {}_{HT}\mathbf{K}^{-1})^{-1} \cdot \mathbf{T}_{ci} \quad (3)$$

In the equation above, \mathbf{T} is a subsystem of a tool and ${}_{HT}\mathbf{K}$ is the complex stiffness of holder–tool interface dynamics:

$${}_{HT}\mathbf{K} = \begin{bmatrix} {}_{HT}k_t + i \cdot \omega \cdot {}_{HT}c_t & 0 \\ 0 & {}_{HT}k_r + i \cdot \omega \cdot {}_{HT}c_r \end{bmatrix} \quad (4)$$

where: ${}_{HT}k_t$ – translational stiffness, ${}_{HT}c_t$ – translational damping, ${}_{HT}k_r$ – rotational stiffness and ${}_{HT}c_r$ – rotational damping at the holder – tool interface.

In order to be able to use equation (3) to predict the frequency response function of the tool tip, we need to know translational and rotational dynamic response for each of the components of the spindle - holder - tool assembly. Response matrix of the tool and holder can be obtained by an analytical method, using some of the beam theories or through the FEM analysis. Defining spindle response poses a problem because data regarding dimensions, material, the manner of bearing, the number, and type of bearings are unknown so their modeling is critical and therefore we use experimental method to obtain spindle FRF. The spindle–holder–tool assembly shown in Figure 2 is suspended to obtain free-free end conditions for performing an impact test.

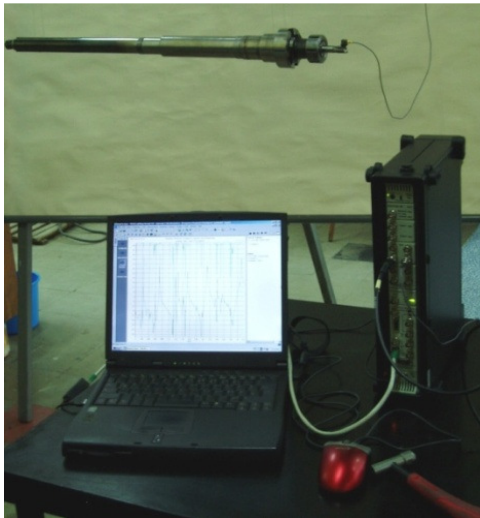


Fig. 2. Measuring chain for the identification of dynamic behavior of the spindle–tool holder–tool system

In order to provide sufficient data for learning neural networks 178 measurements was made with different combinations of spindle–holder–tool assembly. Since contact parameters depend on tool diameter (D) and overhang length of the tool (L), in experimental tests these two parameters are varied ($D = 9 \div 30$ mm and $L = 16 \div 83$ mm). After that, the contact parameters of spindle–holder–tool assembly are identified using the methodology presented in [5]. The results are used to train neural network which can be used for prediction of contact parameters of spindle–holder–tool assembly for different cases.

3. THE DESIGN OF NEURAL NETWORK AND RESULTS

The Matlab's Neural Network Toolbox was used as a tool for the design, implementation, and simulation of neural networks. Backpropagation method of teaching artificial neural networks was used. It is supervised learning technique which is most useful for feed-forward networks. In order to avoid overfitting or for improving generalization, early stopping technique was applied. Levenberg-Marquardt algorithm was used to train the networks faster, where: initial value of the Marquardt's parameter is 0.001, reduction factor of the Marquardt's parameter is 0.1 and increase factor of the Marquardt's parameter is 10. Neural network learning is stopped when the value of the Marquardt's parameter rises above the threshold that is set to 10^{10} . Bipolar sigmoidal function in hidden layer and linear function in output layer are selected as activation functions. Limit level of the learning accuracy is set with normalized root mean square error $NRMSE = 0.05$.

The identified data, relating to the translational and rotational stiffness of spindle–holder–tool assembly for different combinations of tools, are divided into three sets: the learning set, the validation set and the test set. In the present case a feedforward neural network model was used, consisting of three layers: the input layer, the hidden layer and the output layer. In order to test how well neural network adapt to the input-output pairs of data, or how well the network based on the given input values provides output parameters, in all three data sets errors were analyzed using the following parameters: correlation coefficient, normalized root mean square error and mean relative error. Network optimization is performed over the number of neurons in the hidden layer, while the number of neurons in the input and output layers correspond to the number of input and output variable, respectively, and can not be changed. The most favorable number of neurons in the hidden layer was determined by monitoring of errors in the validation set and the test set. The initial values of weights are determined by the Nguyen-Widrow algorithm. Whenever the number of neurons and the slope of activation function in hidden layer are changed, the same initial values of weights are set, whereas before each learning of neural network these values are reloaded.

According to the above described procedure, first is established neural network for prediction of translational stiffness of the spindle–holder–tool

assembly. The input variables for neural network are tool diameters and overhang length of the tools, while the output variable is the translational stiffness at the holder–tool interface. As the best combination, which gives a minimum value of the normalized root mean square error of 0.0585, mean relative error of 3.45%, the highest correlation coefficient value of 0.99828 and determination coefficient value of 0.99656, was chosen network structure with 20 neurons in the hidden layer and with slope of activation function $\sigma = 2$.

Figure 3 shows the correlation between predicted and measured values of translational stiffness at the holder–tool interface in the test set, with its direction of regression, linear correlation coefficient, and drawn towards full correlation ($R = 1$). The correlation coefficient of test set is $R > 0.9$, so it can be concluded that is obtained very good correlation between measured and predicted values.

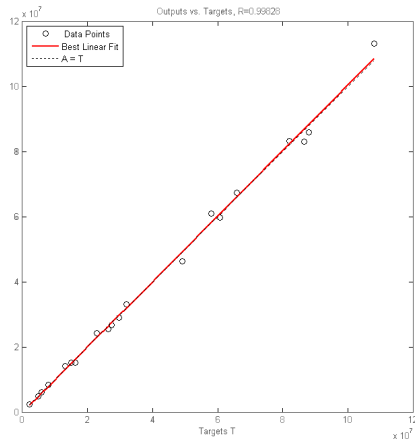


Fig. 3. The correlation between predicted and measured translational stiffness of the test set

By comparison of measured and predicted values of translational stiffness at the holder–tool interface from the test set, it was observed that the maximum relative error of 7.81% is obtained for the tool with a diameter $D = 13$ mm and overhang length $L = 39$ mm. Furthermore, the mean relative error in the test set, which consist twenty different combinations of the spindle–holder–tool assembly, is 3.45%, while the standard deviation is 2.05. Figure 4 simultaneously shows measured and predicted values of translational stiffness at the holder–tool interface from the test set.

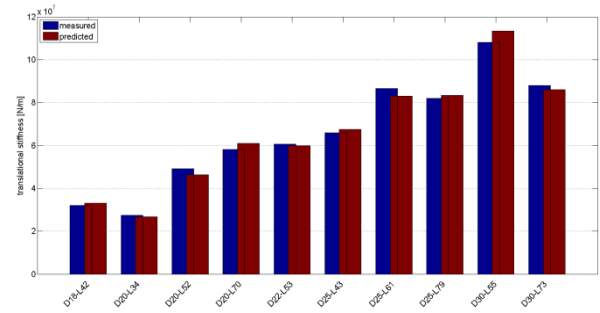
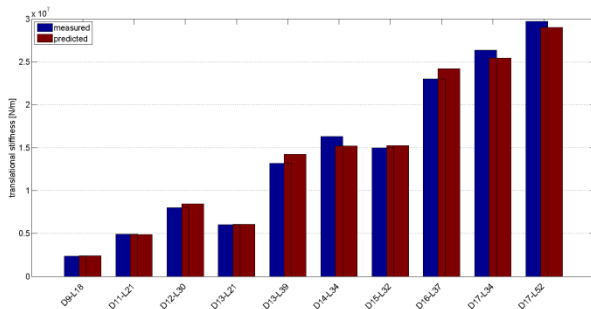


Fig. 4. The measured and predicted values of translational stiffness at the holder–tool interface in the test set

Similarly, there was performed a prediction of rotational stiffness at the holder–tool interface. The results are shown in Figure 5. In this case, the maximum relative error of 2.21% is obtained for the tool with a diameter $D = 25$ mm and overhang length $L = 43$ mm, while the mean relative error in the test set is 0.38% and a standard deviation is 0.47. Significantly fewer errors in the prediction of the rotational stiffness are result of much smaller spread values of input variables.

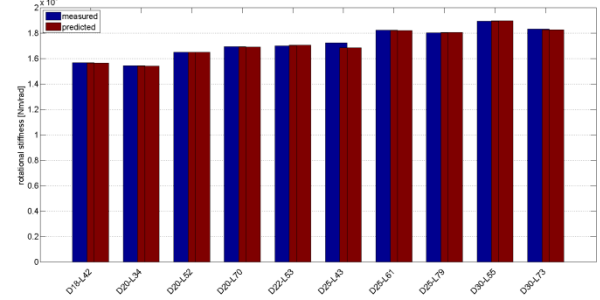
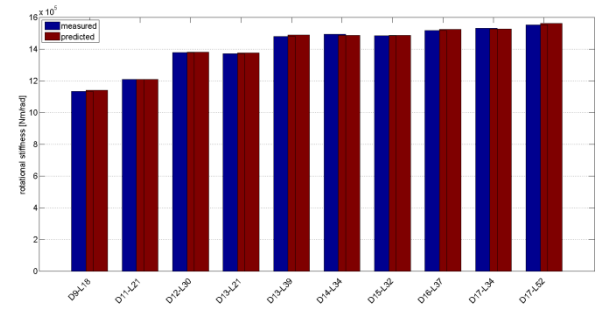


Fig. 5. The measured and predicted values of rotational stiffness at the holder–tool interface in the test set

In order to investigate the accuracy of neural network in prediction of translational and rotational stiffness, combination of the spindle–holder–tool assembly for which network generate the greatest error of 7.81% for the translational and 0.61% for the rotational stiffness is selected. Then, with predicted parameters of translational and rotational stiffness (${}_{HT}k_t = 1,421 \cdot 10^7$ N/m, ${}_{HT}k_r = 1,489 \cdot 10^6$ Nm/rad) at the holder–tool interface, receptance matrix of 13 mm diameter tool with 39 mm overhang length is coupled with rest of system. The tool point frequency response function on the same assembly obtained with contact parameters from experimental results and with contact

parameters identified with neural network are shown in Figure 6. It can be concluded that neural network prediction of contact parameters is quite satisfactory, especially if one considers that instead of the mean error of 3.45%, is taken into account the maximum error of translational stiffness of 7.81%.

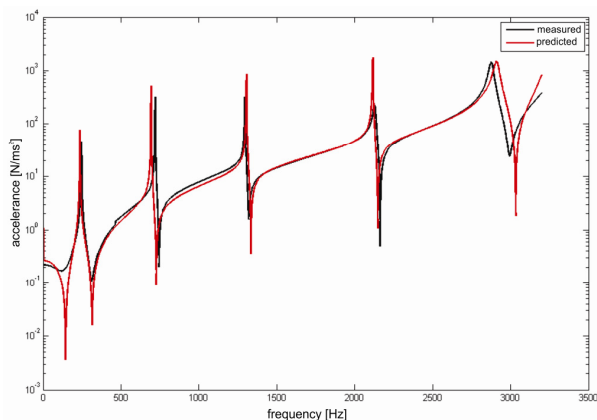


Fig. 6. Tool point obtained with contact parameters from experimental results and with contact parameters identified with neural network

4. FINAL REMARKS

Artificial intelligence is one of the areas of science which is the fastest growing in recent decades. Parallel with these development growth and expectations of the discipline. Artificial intelligence systems are designed to address problems that can not be solved by conventional computer systems. The important type of artificial intelligence are artificial neural networks. The main areas of concentration neural networks that have been used in mechanical engineering problems are control, identification and damage detection. The main advantages of ANN are its adaptivity, fault tolerant, noise resistant and its ability to approximate an arbitrary nonlinear function with a predefined accuracy.

The aim of this study is develop a methodology using artificial neural networks to train and predict the contact parameters of the spindle-holder-tool assembly. The artificial neural network was trained using a feed-forward network with back-propagation that has proven to be successful in many engineering applications. Analysis results show that artificial neural networks, if they are used in a systematic way, which includes detailed data preparation and application of optimization techniques to train the network, has the ability to predict contact parameters of the spindle-holder-tool assembly. Furthermore, artificial neural networks can also effectively deal with uncertain and incomplete information, thereby making them highly promising tool for identifying systems that are typically encountered in structural dynamics.

5. REFERENCES

- [1] Tlustý, J., Poláček, M.: *The stability of machine tools against self-excited vibrations in machining*, Proceedings of the ASME International Research in Production Engineering, p.p. 465 – 474, Pittsburgh, 1963.
- [2] Erturk, A., Ozguven, H.N., Budak, E.: *Analytical modeling of spindle-tool dynamics on machine tools using Timoshenko beam model and receptance coupling for the prediction of tool point FRF*, International Journal of Machine Tools & Manufacture, vol. 46, p.p. 1901-1912, 2006.
- [3] Erturk, A., Ozguven, H.: *Effect analysis of bearing and interface dynamics on tool point FRF for chatter stability in machine tools by using a new analytical model for spindle-tool assemblies*, International Journal of Machine Tools & Manufacture, vol. 47, p.p. 23-32, 2007.
- [4] Schmitz, T.L., Davies, M.A., Kennedy, M.D.: *Tool Point Frequency Response Prediction for High-Speed Machining by RCSA*, Journal of Manufacturing Science and Engineering, vol. 123, 2001.
- [5] Čiča, Đ., Zeljković, M., Lakić-Globočki, G., Sredanović: *Modeling of dynamical behavior of a spindle-holder-tool assembly*, Strojarstvo, in review

Authors: PhD Assistant Professor Đorđe Čiča, PhD Full Professor Milan Zeljković, PhD Associate Professor Gordana Lakić-Globočki, BSc Branislav Sredanović, MSc Stevo Borojević, University of Banja Luka, Faculty of Mechanical Engineering, Vojvode Stepe Stepanovića 75, 78 000 Banja Luka, Republic of Srpska, BiH, Phone.: +387 51 462-400, Fax: +387 51 465-085.

E-mail: djordjecica@gmail.com
 milan.z@uns.ns.ac.rs
 gordana.globocki@gmail.com
 sredanovic@gmail.com
 stevoborojevic@hotmail.com

Dučić, N., Čojbašić, Ž., Slavković, R., Radonjić, S.

APPLICATION OF NEURAL NETWORKS FOR PREDICTING CHARACTERISTICS OF ELASTIC SUPPORTS TO PRODUCTION MACHINES

Abstract: *Vibration and noise are unavoidable in the operation of variety of technological equipment (machines, appliances, transportation and other mobile devices). Effective contribution to solving these problems provides the application of elastic supports. This paper presents the idea of applying neural networks (whose architecture is created based on table 2) in the process of defining the static characteristics of support. As a result of analysis of many different architectures applied on the results obtained by the measurement, the most favourable architecture of predictive model of neural network is presented. Deformation assessment of supports can significantly facilitate the work for people involved in the design of technology foundation.*

Key words: *Neural networks, modeling, supports, vibroisolation*

1. INTRODUCTION

Foundation of machines should damped vibrations and shocks that are transmitted from technological equipment on the environment, or from the environment to technological equipment. In such conditions, machine as technological equipment and the system of elastic supports constitute an oscillatory system, which can be viewed as a dynamic model with one (Fig. 1) or more degrees of freedom (Fig. 2.) of movements which differ in place of the malfunctions. Vibroisolation can be active and passive. Active izloacija - a malfunction occurs in the work process of a machine that is the object of foundation. Passive izloacija - malfunction comes from the surrounding technological equipment and it is transferred to the machine over the place of reliance.

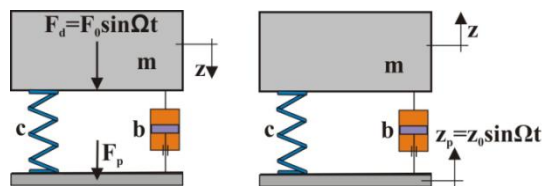


Fig. 1. Dynamic model of founded machine modeled by one degree of freedom

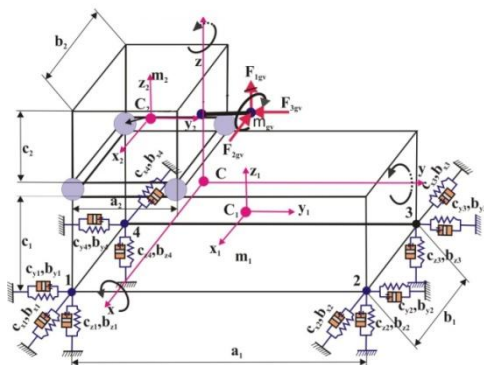


Fig. 2. Dynamic model of founded machine modeled by several degrees of freedom in active isolation of vibrations

Differential equation of oscillations of the system with one degree of freedom in active isolation of vibration is given by equation (1), and in passive vibration isolation by equation (2):

$$m\ddot{z} + b\dot{z} + cz = F_d \quad (1)$$

$$m\ddot{z} + b(z - \dot{z}_p) + c(z - z_p) = F_d \quad (2)$$

For the case of dynamic system with n - degrees of freedom of movements of differential equation of oscillations are given with system equation (3):

$$[M]\{\ddot{\delta}\} + [B]\{\dot{\delta}\} + [K]\{\delta\} = \{F(t)\} \quad (3)$$

where:: $[M]$ - matrix of mass system, $[B]$ - matrix of system damping, $[K]$ - matrix of system stiffness, $\{F(t)\}$ - vector of malfunctions, $\{\ddot{\delta}\}$, $\{\dot{\delta}\}$, $\{\delta\}$ - vector of acceleration, speed and movements.

An important feature of the elastic supports is stiffness that depends both on the type and form of elasto-viscose element and in most cases is a non-linear characteristics. In such cases it is necessary to define the stiffness and muffling of the elastic support as very important quantity in identification of system dynamics by given equations (1), (2) and (3), based on loads and corresponding deformation of elasto-viscose element.

2. MEASUREMENT METHODOLOGY

To make the neural network model that provides reliable estimates of supports deformations, appropriate measurements related to the static tests of elastic supports were carried out. Supports, type A and type B (Fig. 3.), different hardness, are exposed to the effects of force in the vertical direction (Fig. 4.).

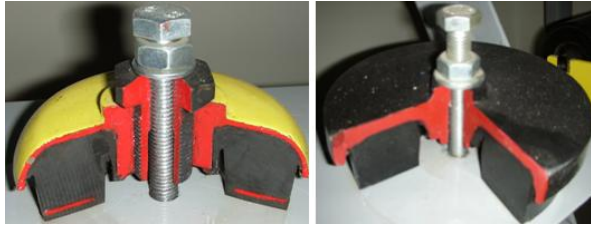


Fig. 3. Supports: type A and type B

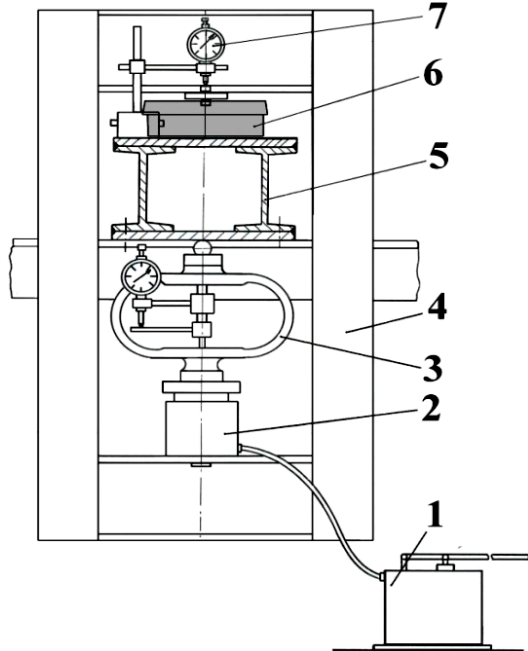


Fig. 4. Device for static examination of supports in vertical direction

Load of supports is performed by using hydraulic pumps (1), with the cylinder (2) through a dynamometer (3) on which the value of static force F is read. Static force is, through the frame (4) transferred to mat examined (6) which is mounted on a stand of the device (5), while the deformation of h mat under load and relief, is read on measurement clock (7).

3. PREDICTION OF SUPPORT DEFORMATION BY USE OF NEURAL NETWORK

Neural networks are complex systems consisting of neurons, interconnected by respective links, where the knowledge of the network is stored. The neural network is characterized by its architecture, the weight vectors, and transfer functions used in hidden and output layers of the network. Neurons in the input layer receive the input data. Each neuron sums inputs and one input per neuron in the input layer, but more inputs per neuron in the hidden layer. Information between neurons in different layers are transmitted using the transfer function. Due to the different weights of connections, neurons receive different signals. The output of each neuron in the output layer is compared to the desired output. In order to minimize the difference between these two outputs, weight adjustment between neurons is performed.

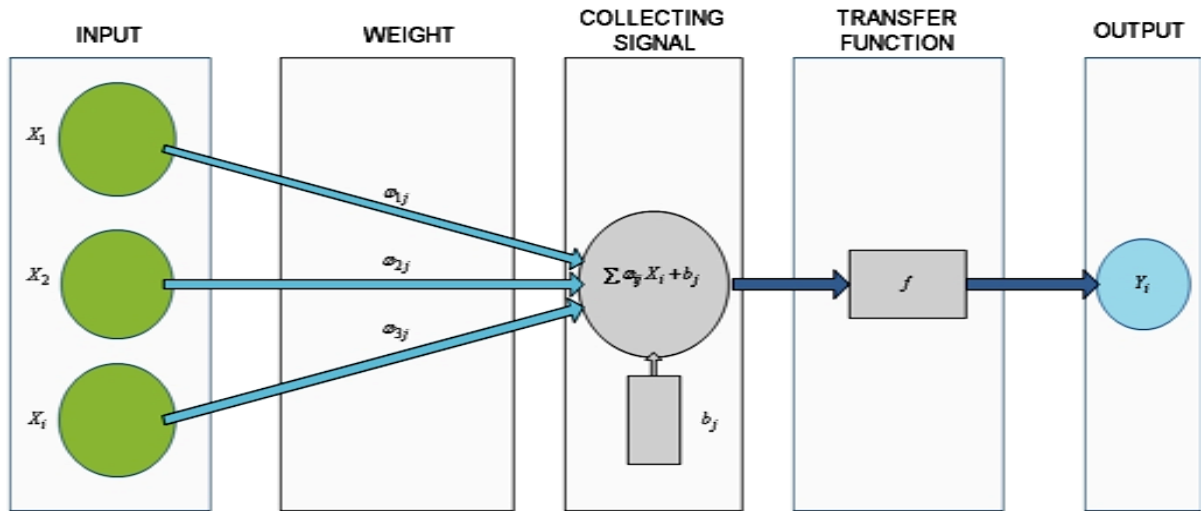


Fig. 5. Structure of artificial neuron

The most commonly used neural networks are multilayer perception networks trained by algorithm with back propagation. Networks of this type are general-purpose models with good generalization ability and are relatively simple for practical use. For training the neural network that uses algorithm with back propagation, learning process implies that data set for training is available. Each element of this set is defined by the input vector $x^{(k)} = [x_1^{(k)}, x_2^{(k)}, \dots, x_i^{(k)}]$ and desired output vector $t^{(k)} = [t_1^{(k)}, t_2^{(k)}, \dots, t_i^{(k)}]$.

Learning objective is to determine the network parameters (connection weight and threshold of activation b_j) such that $t^{(k)} = [t_1^{(k)}, t_2^{(k)}, \dots, t_i^{(k)}]$ is equal to $y^{(k)} = [y_1^{(k)}, y_2^{(k)}, \dots, y_i^{(k)}]$. Criterion function, which describes how the actual output of the network differs from the desired is given by (4):

$$E = \frac{1}{2} \sum_{i=1}^s (t_i - y_i)^2 \quad (4)$$

When k sample of data set for training is led to the input, function has the following form [1]:

$$E^{(k)} = \frac{1}{2} \sum_{i=1}^s (t_i^{(k)} - y_i^{(k)})^2 \quad (5)$$

An error in this type of network spreads backwards through the network to the input layer where according to the desired output values of neural network connection weights in the network are set. Adaptation of the connection weights $\omega_{i,j}$ and threshold of activation of neurons b_j is determined from the condition that the function (5) is minimal. Parameters of the $n+1$ step are determined as follows [1]:

$$\omega_{i,j(l)}(n+1) = \omega_{i,j(l)}(n) - \eta \frac{\partial E^{(k)}}{\partial \omega_{i,j(l)}} \quad (6)$$

$$b_{j(l)}(n+1) = b_{j(l)}(n) - \eta \frac{\partial E^{(k)}}{\partial b_{j(l)}}$$

where: l – mark for neuron layer, η – learning coefficient.

The set of input data includes: $x_1 = \text{load } F[N]$, $x_2 = \text{type of support}$, $x_3 = \text{hardness } [Sh]$, and set of output data consists of: $y_1 = \text{deformation in case of load}$ and $y_2 = \text{deformations in case of relief}$. Set of input and output data defined the architecture of network (Fig. 6.) in the aspect of number of neurons in input layer and output layer.

Number	Input quantity	Bottom value	Top value
1.	Load [N]	250	30000
2.	Hardness [Sh]	45	75
3.	Type of support	1	2

Table 1. Input quantities with values

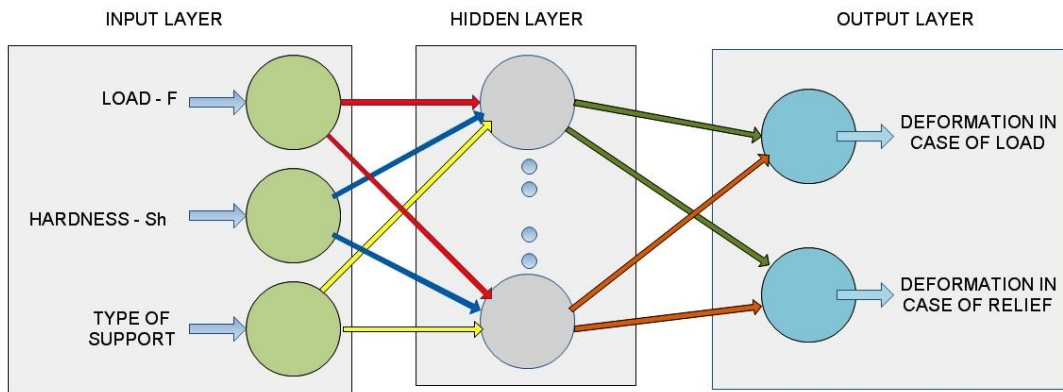


Fig. 6. Architecture of neural network for prediction of the deformations of support

Three-layer neural network has the following architecture: the input layer - three neurons to represent the load, type of supports and hardness, one hidden layer, output layer - two neurons to calculate deformations during loading and unloading. The data are divided into three groups: data for network training, data validation and data for network testing. The training sample (60 data) was presented to the network during training, and the network was adjusted according to its error. The validation sample (20 data) was used to measure network generalisation, and to halt training when generalisation stopped improving. Finally, the testing sample (20 data) had no effect on training and so provided an independent measure of network performance during and after training. Modeling was performed in the MATLAB software system. The parameters of the network architecture are given in Table 2.

No.	Parameter name	Value
1.	Input number of neurons	3
2.	Output number of neurons	2

3.	Nuber of neurons in hidden layer	12
4.	Transfer function in hidden layer	Tansig
5.	Transfer function in output layer	Purelin
6.	Learning function	Trainlm
7.	Number of epochs that is presented	300
8.	Number of epochs	10000
9.	Momentum	0.9
10.	Learning coefficient	0.05
11.	Training error	0.001

Table 2. Parameters of architecture that has provided the best results

MATLAB code created based on the parameters given provides a satisfactory response whose evaluations confirm high accuracy of this model. Correlation coefficient is $R = 0.99758$, and mean absolute percentage error in case of predicting the deformations

occurred by loading is 1.81%, while in case of predictions caused by unloading its value is 2.08%. Fig. 7 presents the overview of mean square error of model created.

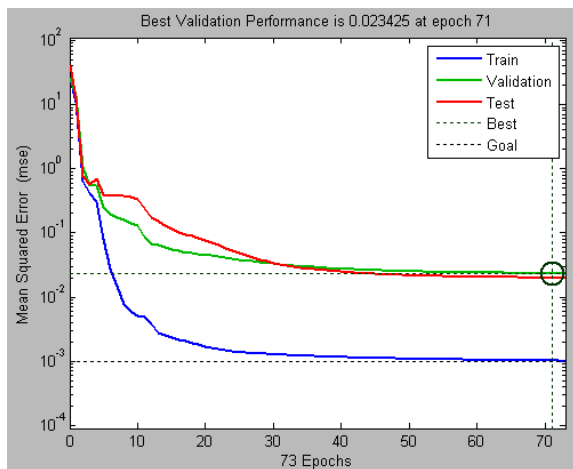


Fig. 7. Mean square error of the model created

Performances of neural network for prediction of deformations of supports occurred by loading and unloading are given in Fig. 8. and Fig. 9.

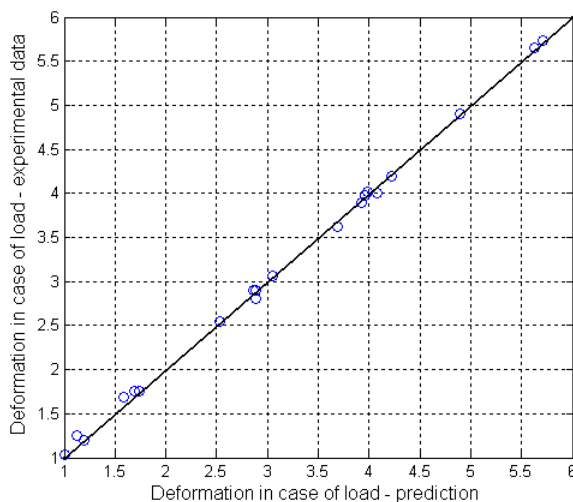


Fig. 8. Performances of neural network for prediction of support deformations occurred by load

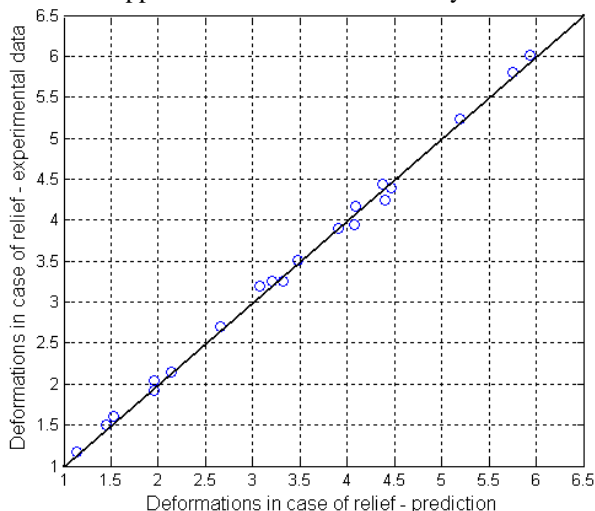


Fig. 9. Performances of neural network for prediction of support deformations occurred by unloading

4. CONCLUSION

Main concept of neural network with back propagation is presented in this paper and the results of its application in estimation of mat deformations made under the effect of load in vertical direction are described. Having in mind that vibrations of elastically relied technological equipment are executed around the position of stable balance and that those are small oscillations, such approach when defining static characteristics of elastic supports gives great contribution to further successful analysis of system's dynamics.

5. ACKNOWLEDGEMENT

Authors are grateful to the company I.K.G. Guca for cooperation during realisation of experiments and writing this paper.

6. REFERENCES

- [1] Rankovic, V.: *Intelligentno upravljanje*, Faculty of Engineering University of Kragujevac, Kragujevac, 2008.
- [2] Simunović, G., Saric, T., Lujić, R.: *Surface quality prediction by artificial neural networks*, Technical Gazette 16, 2(2009), pp. 43-47.
- [3] Mandic, M., Radovanovic, M.: *Methodology of developing optimal BP-ANN model for prediction of cutting force in turning using early stopping method*, FACTA UNIVERSITATIS – Mechanical Engineering Vol 9, No 1, 2011, pp. 21-32..
- [4] <http://www.learnartificialneuralnetworks.com/back-propagation.html>
- [5] <http://www.mathworks.com/products/neural-network/>

Authors:

M.Sc. Nedeljko Dučić University of Kragujevac, Technical faculty Cacak, Sv. Save 65, 32000 Cacak, Serbia, Phone.: +381 32 302-733, Fax: +381 032/342-101. E-mail: nedeljkod@gmail.com

Prof. dr Žarko Čojbašić University of Niš, Mechanical Engineering Faculty Niš, Aleksandra Medvedeva 14, 18000 Niš, Serbia. Phone.: +381 18 500606, Fax: +381 18588244. E-mail: zcojba@ni.ac.rs

Prof. dr Radomir Slavković, University of Kragujevac, Technical faculty Cacak, Sv. Save 65, 32000 Cacak, Serbia, Phone.: +381 32 302-733, Fax: +381 032/342-101. E-mail: slavkovic@tfc.kg.ac.rs

Prof. dr Snežana Radonjić University of Kragujevac, Technical faculty Cacak, Sv. Save 65, 32000 Cacak, Serbia, Phone.: +381 32 302-733, Fax: +381 032/342-101. E-mail: snezar@tfc.kg.ac.rs



11th INTERNATIONAL SCIENTIFIC CONFERENCE NOVI SAD, SERBIA, SEPTEMBER 20-21, 2012

Epler, I., Djapic, M., Lukic, Lj.

RISK - BASED MAINTENANCE OF THE FLEXIBLE TECHNOLOGICAL SYSTEM

Abstract: *The aspect of risk in the maintenance of capital equipment and industrial technological system has become in recent years the most important element in the strategy of effectiveness and economy of production systems in the industry. To ensure minimum downtime and failures, it is necessary to implement a model of maintenance management based on modern scientific and research findings and theory of reliability, which will allow maximum efficiency of production system. This paper presents a model of maintenance management flexible technological systems with aspects of risk management, in order to ensure maximum productivity and efficiency, as well as the degree of utilization of machining centers of the unique integrated production system. The presented model was originally developed for use in technical systems, special purpose, and with some additions and changes it is adapted for use on production systems in the metal processing industry.*

Keywords: *Risk management, maintenance, flexible manufacturing systems*

1. INTRODUCTION

The company engaged in industrial production, and has Flexible manufacturing System (FMS), seeks to ensure maximum utilization rate of machining centers and maximum efficiency throughout the production process. Production in the FMS is based on the plan of processing, plan of preparing work pieces, plan of preparation tools which are precisely defined in the driver cell controllers, so that every failure causes a disturbance in the production process. Therefore, the biggest problem is the risk of failure in the cell controllers and Automatic Guided Vehicle (AGV), which leading to downtimes in the work of whole FMS. Smaller consequences are caused by failures in the work of machining centers, work pieces washing machines, measuring machines and computer control systems in the places of preparatory tools and work pieces. Downtime of individual modules and the reduction of production capacity of whole FMS are caused by those failures. In order to achieve continuous production without failure, for a period of e.g. 6 months (failure-free operation at 3240 hours), it is necessary to ensure high reliability of key components and modules in the FMS. It is very important to carry out risk assessment and define preventive maintenance plan based on these assessment. Modern methods in the application of reliability theory [1], with the methods of risk assessment, provide that a complete maintenance strategy would based on the elements of risk [2], and thus establishing a high efficiency and productivity of FMS.

2. CHARACTERISTICS OF THE PRODUCTION PROCESS IN FMS

The optimal manufacturing process in a classical production system arises as a result of optimal performing of individual technological operations when

machining each work piece according to multifunctional dependencies between the machine tool, work piece material, tools and elements of the machining mode. In FMS technological processes this isn't the case, because procedural dependencies are very important in processing alongside the functional. Optimizing the technological process in FMS is based on a much more complex model, because production in FMS has a series of production specifics in regard to classic production system [3]:

- The work pieces for processing in FMS are geometrically and technologically of similar characteristics,
- Simultaneous – simultaneous processing of multiple same and/or different work pieces in FMS,
- Processing same and/or different work pieces is performed simultaneously on multiple different or same manufacture centers,
- The work pieces are processed usually in different series (whereby each work piece type has its own specific series in which it should be manufactured),
- On one machining center are performed several machining operations with different tools,
- On one palette can be several same or different work pieces,
- Tool change is done automatically in two levels – change from the main spindle and tool magazine on the machining center and change of all tools from the machining center magazine,
- Simultaneous tool change from the machining center magazine conditions for one of the goal functions during optimization to be an even level of blade wear on all tools, and for each tool to have durability approximately equal to its cutting time,
- Changing work piece palettes is done automatically,
- Moving work pieces in a technological process is performed via an automatic transport system,

- Storing work pieces between individual technological phases in the manufacture process is performed on buffers – special palette storages,
- The preparation places for secondary and gripping requisites, tools and work pieces are specially organized and are set on palettes available to automatic transport systems,
- The delivery of preparation pieces is especially regulated (castings, forgings, welded blanks) to the FMS line and delivery of processed parts.

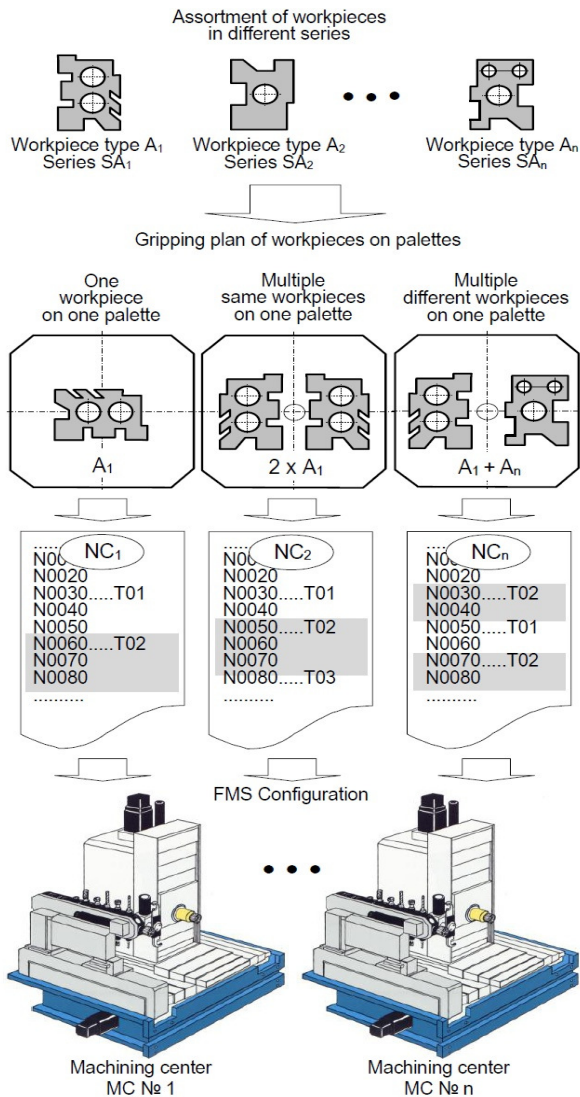


Fig. 1. The production model of the FMS

Flexible manufacturing systems are designed for highly automated flexible manufacturing very complex work pieces in small batches. Work pieces must be manufactured in strictly defined range, where the series is defined for each type of workpieces and the given amount of time in which production has to be realized.

The total effective processing time (TSA) of all work piece types in a given series can be determined by adding the processing time

$$TSA = TA_1 \cdot SA_1 + TA_2 \cdot SA_2 + TA_3 \cdot SA_3 + \dots + TA_n \cdot SA_n$$

$$TSA = \sum_{i=1}^n TA_i \cdot SA_i$$

Since it is impossible for a predetermined FMS configuration to organize the production process so that all manufacture centers are maximally utilized, the total effective time for processing a group of parts (TSA) should be corrected according to the rate of utilization of machining centers (e) and thus get the real required time (TSA_R) for processing a group of parts in a given series. If the rate of utilization is expressed so that it is ($e < 1.00$), we'll get the real time of processing by increasing the effective time (TSA),

$$TSA_R = TSA \cdot 1/e$$

Lost production time due to downtime or failure of FMS, must be compensated by increasing the intensity of the machining tool or higher utilization rate of tools or using the tools of high quality. That situation leading to increase production cost. It is, therefore, very important system for preventive maintenance based on risk which will not allow unplanned downtime in production.

3. RISK-BASED MANAGEMENT MAINTENANCE METHODOLOGY OF FLEXIBLE TECHNOLOGICAL SYSTEM

It is necessary to simultaneously observe the aspect of reliability and availability with parameterized probability of failure and consequences of downtime aspect [4], in order to realistically consider the consequences of downtime of FMS. The risk is defined as the product of failure probabilities and consequences:

$$\text{Risk} = \text{probability of failure} \cdot \text{consequence of the failure.}$$

Designing of concept of preventive maintenance system is based on the clear definite answers on the key questions:

- Which disorders of manufacturing process can cause failure of module of machining center or FMS, like whole system?
- Which phenomenological appearance of the processing can lead to failure?
- How can reaching to disturb of functionality of module and failure?
- What is the probability of failure of module of machining center or a computer control system (cell controller)?
- What are the consequences of failure of the modules or machining centers or FMS, as a whole?

The overall objective of the FMS maintenance process is to increase the profitability of the FMS. Risk assessment integrates reliability with safety and in some cases environmental issues and therefore can be used as a

decision tool for preventive maintenance planning. Maintenance planning based on risk analysis minimizes the probability of system failure and its consequences. It helps management in making correct decisions concerning investment in maintenance or related field.

Risk analysis is a technique for identification, assessment and evaluation of the losses, incurred due to unwanted downtime of work FMS. Maintenance management model, from the point of risk analysis, involves the analysis of probability and consequence of failure

Risk assessment can be quantities or qualitative. The output of a quantitative risk assessment will typically be a number, such as cost impact per unit time. Quantitative risk assessment requires a great deal of data both for the assessment of probabilities and assessment of consequences. Fault tree or decision trees are often used to determine the probability that a certain sequence of events in machining process will result in certain consequences.

Qualitative risk assessment is less rigorous and the results are often shown in the form of a simple risk matrix where one axis of the matrix represents the probability and the other represents the consequences. If a value is given to each of probability and consequence, a relative value for risk can be determined. The proposed risk-based maintenance (RBM) strategy aims at reducing the overall risk of failure of operating facilities. In areas of high and medium risk, a focused maintenance effort is required, whereas in areas of low risk, the effort is minimized to reduce the total scope of work and cost of maintenance program in structured and justifiable way.

The value of risk is used to prioritize inspection and maintenance activities on that way that suggest a set of recommendations on how many preventive tasks are needed.

The RBM methodology is broken down into three main modules [5]:

1. risk determination, which consist of risk identification and estimation,
2. risk evaluation, which consist of risk aversion and risk acceptance analysis, and
3. maintenance planning considering risk factors.

A failure scenario is base for risk study and represents description of a series of events which may lead to a system failure (figure 2). The expectation of scenario does not mean it will need to occur, but that there is reasonable probability that it would occur. It tells us what may happen so that we can prepare means of preventing or minimizing the possibility of its occurrence. The developed failure scenarios are then screened to short list. Systematic procedure-maximum credible accident scenario (MCAS) provides the criteria to form this short list.

Consequence analysis is based on prioritize modules of FMS on the basis of their contribution to a system failure because failure of some machining centers modules do not always lead total loose or downtime of

system. Consequence analysis involves assessment of likely consequences if a failure scenario does materialize. Overall consequence assessment is combination of four major categories which calculate to each accident and failure scenario:

1. System performance loss (factor A),
2. Financial loss (factor B),
3. Human health loss (factor C),
4. Ecological loss (factor D).

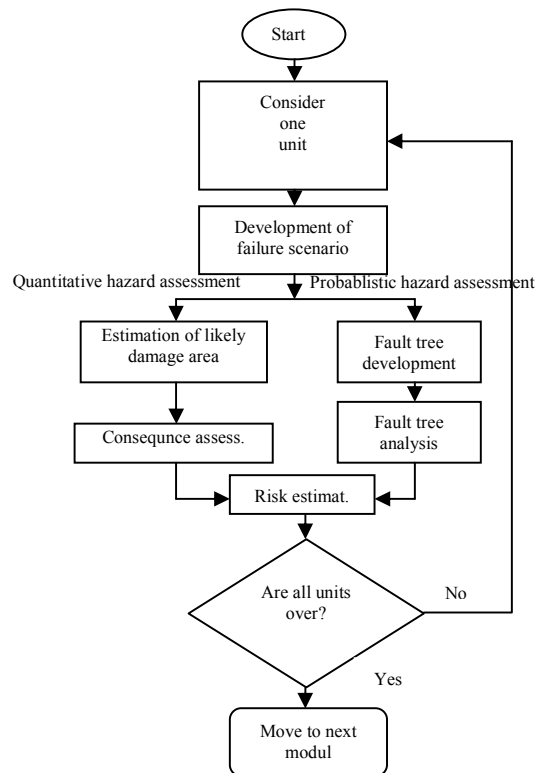


Fig.2. Algorithm of risk estimation model

Probabilistic failure analysis is conducted using fault tree analysis, using a methodology called “analytical simulation” [6]:

- Fault tree development: The top event is identified based on detailed study of the process, control arrangement, and behavior of components of the FMS. A logical dependency between the causes leading to the top event is developed.
- Boolean matrix creation: The fault tree developed is transformed to a Boolean matrix. Used Structural modeling technique the fault tree can be modeled into a number of smaller sub modules with dependency relations among them.
- Finding of minimum cut sets and optimization: Minimum cut sets are determined from Boolean
- Probability analysis: Monte – Carlo simulation method is recommended.
- Improvement index estimation.

Risk evaluation (figure 3) comprised two steps:

- Recognizing specific acceptance criteria like ALARP, Dutch and USEPA [7].
- Risk comparison against acceptance criteria for each module. Modules whose estimated risk exceeds the acceptance criteria are identified and their maintenance plan must be improved.

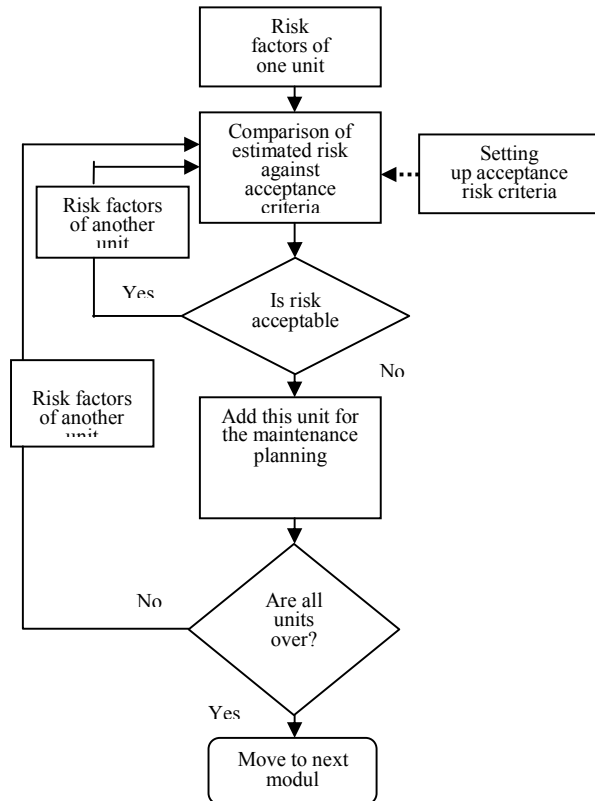


Fig.3. Algorithm of risk evaluation module

Maintenance planning for AGV, cell controller, machining centers and other modules, for which failures risk is estimated, under allowed level, according to defined criteria, study detailed with objective to reduction risk level through improved maintenance plan. Improved maintenance is carried out through evaluation of the optimal system maintenance, with objective to identify the individual causes of failures and their impact on reducing the probability of failure. At the same time, through the inverse analysis of adverse events, in the machining process, it can take influence to decrease the probability of failure of key modules of FMS, in order to define the reliable maintenance plan. Re-evaluation and iterative evaluation of risk must be leaded, until total allowable level of risk of FMS was determined.

4. CONCLUSION

Contemporary business practice show us how important risk analysis and assessment is for running a business successfully and for operations of any

organization, enterprise or individual. On the other hand, we have witnessed a rapid development and implementation of holistic approaches to risks management in enterprises, unified in the modern business practice by the name of **Enterprise Risk Management (ERM)** (ISO 31000:2009).

Modern commercial and industrial practices imposed the need to analyze and assessment risks of each organization's manufacturing processes, especially those that have installed programmable, and highly automated manufacturing systems just like FMS.

Giving the possible failure consequences, development of risk-based preventive maintenance model of FMS represent one of the most important segment of modern, economical and highly productive manufacturing in metal industrial ~~metal~~.

5. REFERENCES

- [1] Epler, I.: Model upravljanja održavanjem tehničkih sistema specijalne namene, Magistarski rad, Univerzitet u Istočnom Sarajevu, Mašinski fakultet, Istočno Sarajevo, 2012.
- [2] Djapic, M., Zeljkovic, V., Lukic, Lj., Veselinovic, M., Dancuo, Z.: Risk Assessment as a Base for Product Safety Improvement, Proc. 6th International Quality Conference, Kragujevac, 8. Jun 2012, (CD ROM izdanje).
- [3] Lukic, Lj.: Flexible Manufacturing Systems – Structure, construction, control and technology, Monographs, University of Kragujevac, Faculty of Mechanical Engineering of Kraljevo, 2008. (In Serbian).
- [3] Djapic, M., Lukić, Lj., Zeljković, Z.: Koncept standardizacije u oblasti menadžmenta rizika, XIII Naučno stručni skup "Sistem kvaliteta uslov za uspešno poslovanje i konkurentnost", Vrnjačka Banja, 24-26. Novembar, 2011.
- [5] Faisal I. K., Mahmoud M. H.: Risk based maintenance: a quantitative approach for maintenance/inspection scheduling and planning, Journal of Loss Prevention in Process Industries 16, 561- 573, 2003.
- [6] Khan F. I. & Abbasi S. A.: Analytical simulation and PROFAT II: A new methodology and computer automated tool for tree analysis in chemical process industries. Journal of Hazardous Materials 75, 1-27, 2000.
- [7] Lees F. P.: Loss prevention in chemical process industries, London, 1996.

Autors: **Igor Epler**, MSc, Mech.Eng., Vojna Akademija Beograd, ep Igor@open.telekom.rs, **Doc. Mirko Djapic**, PhD, assistant professor, Faculty of Mechanical Engineering Kraljevo, University of Kragujevac, djapic.m@mfkv.kg.ac.rs, **Prof. Ljubomir Lukić**, PhD, vice-dean for science, research, & development, Faculty of Mechanical Engineering Kraljevo, University of Kragujevac, lukic.lj@mfkv.kg.ac.rs.

Gyenge, C., Rafa, A., Pacurar, A., Bob, M.

SOME CHARACTERISTICAL ASPECTS REGARDING CNC GRINDING OF SPUR GEARS

Abstract: In this paper we will present some theoretical and practical aspects of CNC grinding of cylindrical gears with different profile modification. Also in this paper, there will be presented some concrete practical results and measurement diagrams.

Key words: gears, CNC grinding, profile modification, involute curves

1. INTRODUCTION

For a lot of new gear industrial application (precision devices, measurement apparatus, wind turbines, vehicles, etc.) is needed high precision and very different gear tooth profile modifications. In order to can manufacture these gears our team in collaboration with EMSIL TEHTRANS from Oradea and UNIO companies from Satu Mare (Romania) developed one special CNC grinding machine equipped with FANUC numerical control equipment. For obtaining the multitude necessary parameters for programming different grinding process phases, it was necessary to develop a series of mathematical algorithms that hold in to about not only the teeth geometrical characteristics, but also the machine movement command possibilities. The experimental testing and industrial application was at UNIO Company, where we had also the possibilities for high precision measurement of realized gears. In this paper we will present the main aspect of our theoretical and practical results.

2. THE DEVELOPED CNC GEAR GRINDING MACHINE

As we mentioned in the introduction the machine was developed by modernizing a NILES type machine. The necessary movements for manufacturing and coordinate axis orientation can be seen in Fig. 1.

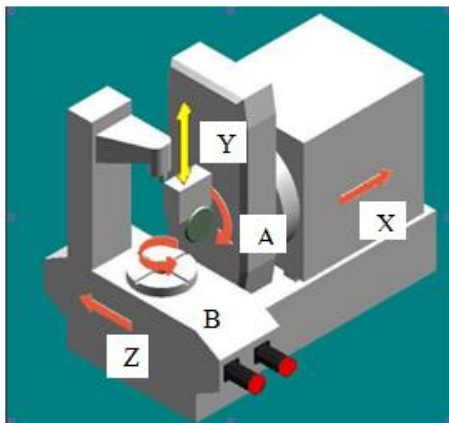


Fig.1. CNC gear grinding machine and axis orientation

For involute spur gear profiles' grinding it is necessary to have a numerical commanded **B** and **Z** axis. For involute helical gear grinding it is necessary to have a numerical commanded for **Z** and **A** axis. In case of modified profile gears, the teeth sections are realized by involute curves with different parameters. At the machine programming we must introduce the effective value of the distance that has to be covered on the **B** and **Z** axis directions.

Taking into account the diversity of gears that had to be grinded it was necessary to elaborate a set of mathematical and kinematical algorithms,

For all algorithms it was applied the version of grinding with different type of angles with the same grinding wheel. From lack of space in this paper we will present only the main parts of the A1 algorithm.

3. THE ALGORITHM

The determination of cnc programming parameters for the CNC spur or helical gear grinding machine, for gears with profile modification regardful of those gears that satisfy the following condition:

$$R_f \leq R_b \cdot \cos \alpha_t,$$

The developed algorithm is part of a series of algorithms :

- A1 algorithm: for spur gears with $R_f \leq R_b \cdot \cos \alpha_t$;
- A2 algorithm: for spur gears with $R_f \geq R_b \cos \alpha_t$;
- A3 algorithm: for gears with tip profile modifications;
- A4 algorithm: for gears with foot profile modifications;
- A5 algorithm: for gears with tip and foot profile modifications;
- B1 algorithm: for with right-hand helical teeth gears;
- B2 algorithm: for gears with left-hand helical teeth right-hand helical teeth;

In Fig. 2 we can see the graphical representation of the relative position between the left flank of the gear teeth space and the double conical grinding wheel, corresponding to the relative position at the beginning and the ending position of the grinding process. Also in the figure it is represented a general case when the profile angle α_{st} of the tool is different from the frontal gearing angle α_t . Thus the algorithm gives the

possibility of grinding gears with different types of gearing angles with the same grinding wheel. As it can be observed from the figure above the grinding starts in the point T_s and ends in the point A_s , for moving into position these two elements it is necessary to make a rotation of the gear with the angle ϕ and a translation along the axis Z with b . According to the figure we can write the following expressions:

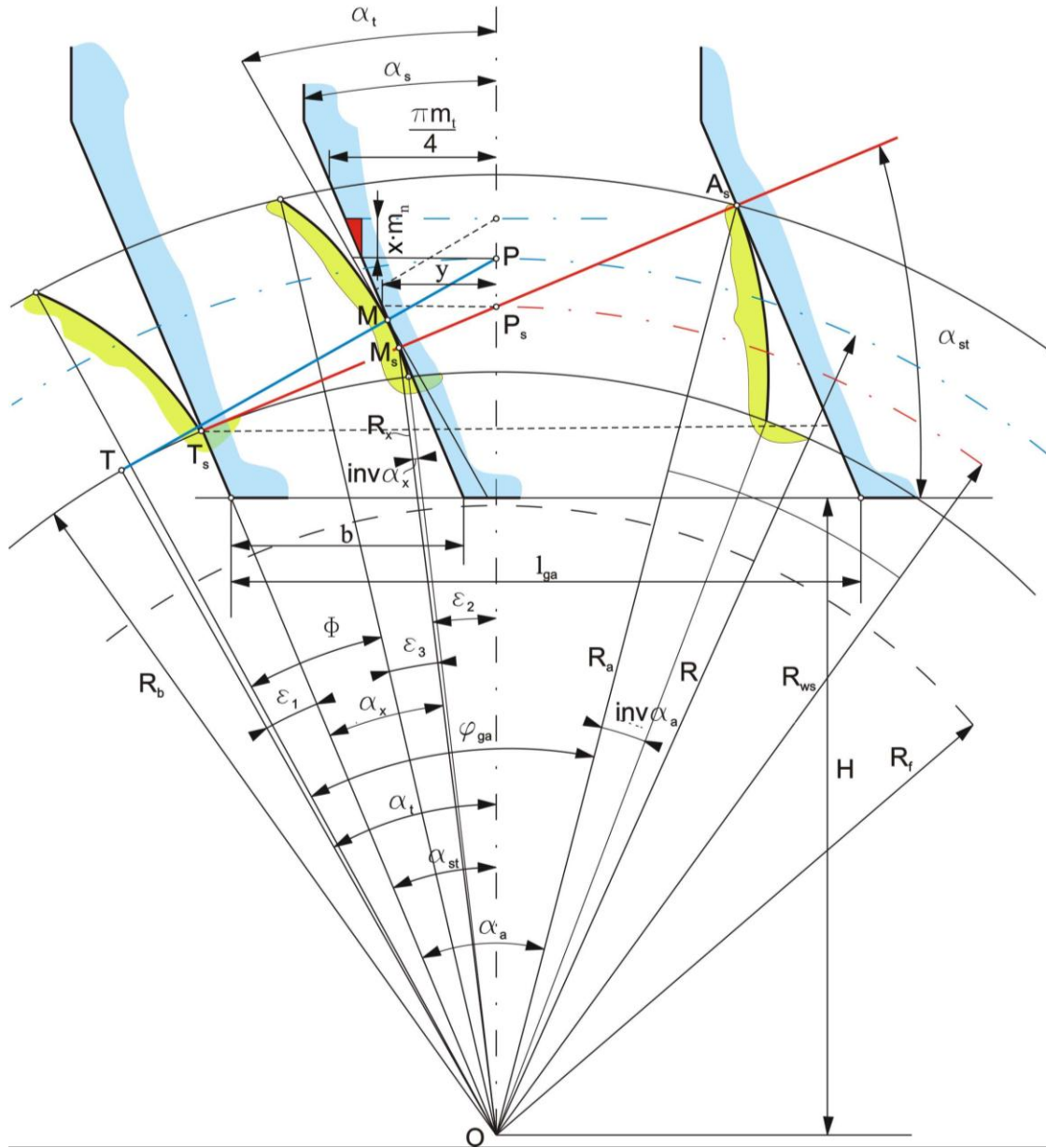


Fig.2. The graphical representation of the relative position between the technologic systems elements at the left tooth gap flank grinding.

$$b = \frac{\sqrt{R_{ws}^2 - R_b^2}}{\cos \alpha_{st}} - y \quad (1)$$

where: R_{ws} – technological gearings rolling radius, R_b – base circle radius. The y parameter is calculated with the following equation:

$$y = \frac{R_b}{\cos \alpha_{st}} \cdot [(tg \alpha_{st} - tg \alpha_t) + \frac{1}{R} \left(\frac{\pi m_t}{4} - x \cdot m_n \cdot tg \alpha_t \right) + (\alpha_t - \alpha_{st})] \quad (2)$$

For the next parameters, after a series of calculations we obtained:

$$\phi = \frac{\sqrt{R_x^2 - R_b^2}}{R} \quad (3)$$

$$b = \frac{\sqrt{R_{ws}^2 - R_b^2}}{\cos \alpha_{st}} - y \quad (4)$$

$$\varphi_{ga} = \frac{\sqrt{R_a^2 - R_b^2}}{R_b} \quad (5)$$

$$l_{ga} = - \left(\frac{\sqrt{R_a^2 - R_b^2}}{\cos \alpha_{st}} \right) \quad (6)$$

$$R_a = m_n \left(\frac{z}{2 \cos \beta} + x + 1 - k \right) \quad (8)$$

$R_a = OA_S$ defines the distance of the final tangent point between the tools flank and the tooth flank and it is given by the expression (8)

$R_b = OT_s$ defines the distance of the starting tangent point between the tools flank and the tooth flank, located on the base circle radius.

The $A_s T_s$ segment represents the trajectory of the contact point tools flank and the tooth flank.

4. GEAR MEASUREMENT AND CONTROL

The measurement and control of the gears manufactured using the deloped technology, was done on the CNC measuring center GHIBLI-TRAX (Fig.3.). The measuring equipement has a special software module for gear measuring and control.

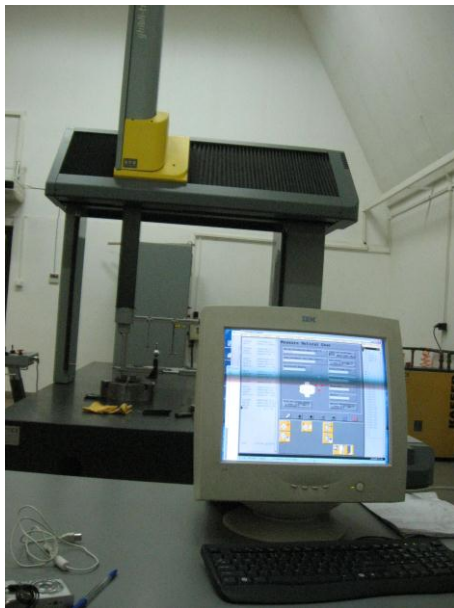


Fig.3. CNC measuring center GHIBLI-TRAX

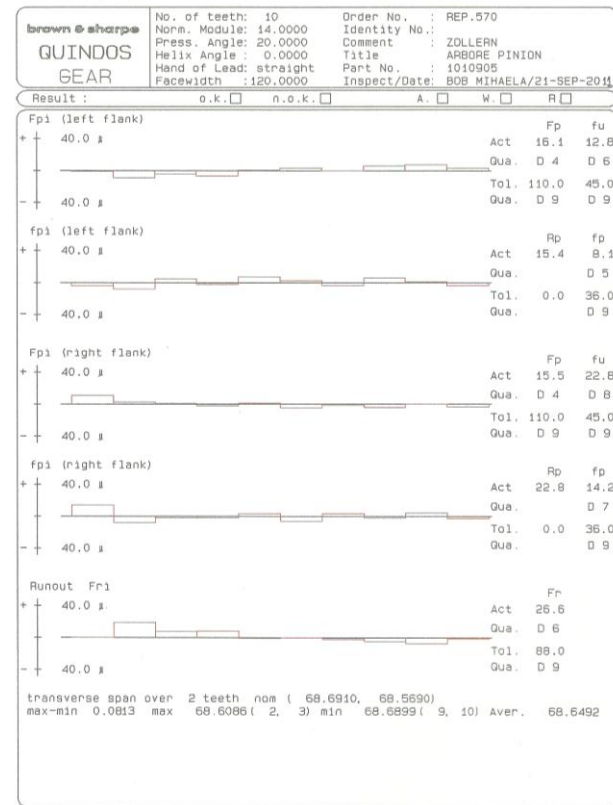
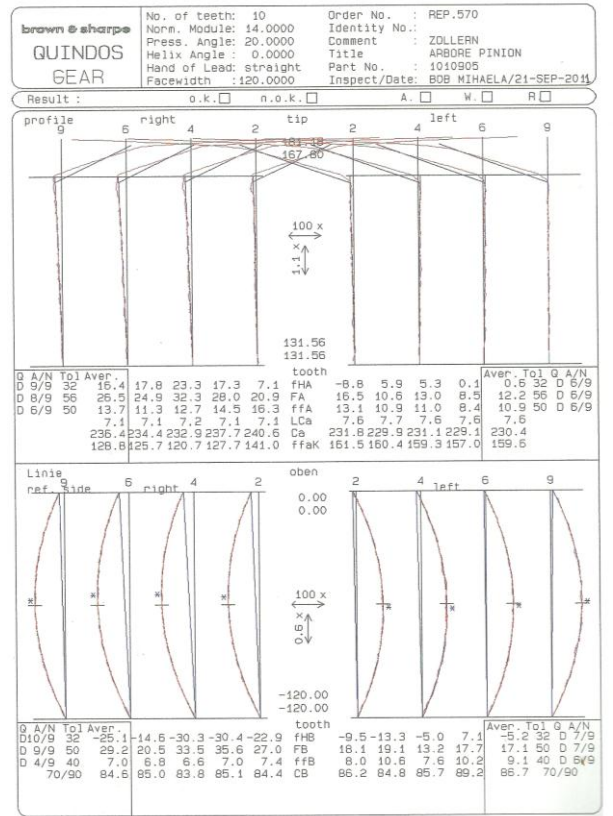


Fig.4. Gear profile measuring diagrams of a machined gear

From the two measuring diagrams (fig. 4.), we can conclude that the gears manufactured on the CNC machine (fig.1.) are situated between 7 – 8 precision classes, for both profile and pitch precision. For achieving higher precision classes it is necessary to

purchase a higher precision grinding machine that can be equipped with the same numerical command equipment and work programs.

5. CONCLUSIONS

With the presented algorithm we can determine very precise the values of the parameters necessary for programming of gear grinding, determined after different standards (STAS, DIN, AGMA, etc.). The large number of experimental results has highlighted the faultlessness of the method. After the measurements was found that the gears which have been manufactured using the elaborated method are included in the range of precision classes 5...7. Also another positive aspect of this research is that old machines can be upgraded at a lower cost instead of disposing them and buying new expensive equipments.

6. REFERENCES

- [1] Karpuschenwsky, B., Knoche, M.. *Gear finishing by abrasive processes* CIRP Annals - Manufacturing Technology Volume 57, Issue 2, p.p.621–640, 2008.
- [2] Bouzakis, K.-D., et. all., *Manufacturing of Cylindrical Gears by generating cutting processes: a Critical synthesis of Analysis*, CIRP Annals - Manufacturing Technology Volume 57, Issue 2, p.p. 676–696, 2008.
- [3] Bradley, B. An International Wind Turbine Gearbox Standard.
- [4] Gyenge, Cs., et al.: *CNC and environment friendly technologies development for cylindrical gears manufacturing in the local industry*. - Research project Sapientia Institute Cluj-Napoca 2004/2005.
- [5] Gyenge, Cs., BOB, M.: *Aspecte caracteristice ale controlului digital complex al roților dințate cilindrice cu modificări de profile*. - 12 International Conference on Tools ICT-2007., Miskolc.
- [6] Gyenge, Cs., Rafa, A., et. al.: *Constructive and technological particularities for wind turbines gear components*. - The 5th PSU-UNS International Conference on Engineering and Technology (ICET-2011), Phuket, May 2-3, 2011.
- [7] Litvin, F. L., Fuente, A.; *Geometria angrenajelor si teorie aplicata*. - Second edition, Cluj-Napoca 2009;
- [8] American Gear Manufacturers Association “*Standard for Design and Specification of Gearboxes for Wind Turbines*” AGMA Standard.
- [9] Rao, J.S., Puri, T., John, J.: *Computer-aided design of gears in transmissions of gears in transmission systems* - International Conference on Gearing, Transmissions and Mechanical Systems, p.p.213-222, 2000;
- [10] Piazza, A., Uberti, M., *Influence of tooth flank deviation classes on vehicle gear performances* - International Conference on Gearing, Transmissions and Mechanical Systems, p.p.315-325, 2000.
- [11] Rafa, A., Gyenge, Cs., Pacurar, A.: *Applied mathematical algorithm at the manufacturing of gears with profile modifications, Transmissions and Mechanical Systems*, Acta tehnica napocensis – Applied mathematics and mechanics, Volume 55, Issue 1, p.p.249-252, 2012;

Authors: Prof.Dr.Dr.h.c Gyenge Csaba, Eng., Ph.D. Student Annamaria Rafa, Dr. Eng. Teaching Assistant, Ancuta Pacurar, Technical University of Cluj-Napoca, Department of Manufacturing Engineering, B-dul Muncii, no.103-105, 400641, Cluj-Napoca, Romania
Phone: 0040-264-401721, Fax: 0040-264-501001
E-mail: gyenge_cs@yahoo.com
annamariarafa@yahoo.com
ancuta.costea@tcm.utcluj.ro

Milutinovic, M., Slavkovic, N., Milutinovic, D.

KINEMATIC MODELING OF THE TRICEPT BASED 5-AXIS MACHINE TOOL

Abstract: This paper is aimed in presenting a study on the kinematic modeling of the Tricept based five-axis vertical machine tool. Since the machine comprises 3-DOF parallel structure and 2-DOF serial wrist kinematic modeling also comprises serial and parallel part. As solution of direct and inverse kinematics of 2-DOF serial wrist is well known the study in this paper will focus on the parallel structure only.

Key words: Hybrid mechanism, kinematic modeling, machine tool

1. INTRODUCTION

Compared with serial structured machine tools and robots, parallel kinematic machine tools and robots have many advantages. Basic knowledge about diverse aspects of parallel kinematic machines has already been published. Many different topologies of parallel mechanisms with 3-6 DOF has been used [1-3]. Considering that some limitations are indeed due to the use of parallel mechanisms, it is appealing to investigate architectures based on hybrid arrangements where serial and parallel concept are combined [3]. The Tricept robot or Tricept machine tool is based on parallel tripod combined with passive chain, and equipped with serial 3- or 2- DOF wrist. The inventor of this structure is K.-E. Neuman [4] while the mechanics has been constructed by Neos [5].

The primary application of commercially available Tricept robots was area of assembly where large insertion forces are required, e.g. as in the automobile industry.

Conceptual model of the Tricept based vertical five-axis machine tool considered in this paper, Fig. 1, is planned for HSC-milling of aluminium, steel as well as large model making, plastic and foam machining.

This paper is aimed in presenting a study on the kinematic modeling of the Tricept based five-axis vertical machine tool. Since the machine comprises 3-DOF parallel structure and 2-DOF serial wrist kinematic modeling also comprises serial and parallel part. As solution of direct and inverse kinematics of 2-DOF serial wrist is well known the study in this paper will focus on the parallel structure only.

2. KINEMATIC MODELING

Figure 2 represents a geometric model of the Tricept based vertical five-axis machine tool, Fig. 1, which comprises 3-DOF parallel structure and 2-DOF serial wrist. Parallel structure consists of four kinematic chains, including three variable length legs with identical topology and one passive leg connecting the fixed base B and the moving platform P. Three variable length legs with actuated prismatic joints $d_i, i=1,2,3$ are connected to the base B by Cardan joints and to movable platform P by spherical joints.

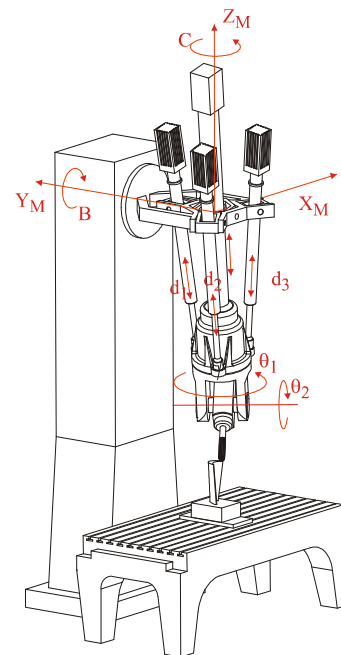


Fig. 1. Conceptual model of the Tricept based five-axis machine tool

The fourth chain (central leg) connecting the centre of the base B to the platform P is passive constraining leg. It consists of Cardan joint, a moving link, a prismatic joint and the second moving link fixed to the platform P. This fourth leg is used to constrain the motion of the platform to only 3-DOF. These 3-DOF are described by spherical coordinates i.e. by the axial translation $p_{Op} = \left| {}^M \mathbf{p}_{Op} \right|$ along the central leg and by two rotations Ψ and θ about two axes orthogonal to the central leg itself. Two-DOF serial wrist executes rotational motions i.e. tool orientation with actuated rotational joints θ_1 and θ_2 .

To adequately control the position and orientation of the tool during machining processes, kinematic model is required to establish mathematical description for the machine tool. Kinematic modeling of parallel structure involves solving of inverse kinematics, Jacobian matrix as the basis for numerical solution of direct kinematics, and direct kinematics. Based on

machine inverse kinematics the workspace has been analyzed in order to select machine prototype design parameters.

2.1 Machine joint and world coordinates

As can be concluded from Fig. 1 i.e. Fig 2, Tricept based five-axis machine tool will be considered below as a specific configuration of the five-axis vertical milling machine (X, Y, Z, B, C) spindle-tilting type [6].

The machine reference frame {M} has been adopted according to the standard for this machine type [7]. Frame {P} is attached to the moving platform in a way that z_P axis coincides with the axis of the central leg and with the axis of joint θ_1 . The tool frame {T} is attached to the milling tool at the tool tip T, so that the axis z_T coincides with tool axis, and the frame {W} is attached to the work piece. Vectors \mathbf{v} referenced in frames {M}, {W}, {P} and {T} are denoted by ${}^M\mathbf{v}$, ${}^W\mathbf{v}$, ${}^P\mathbf{v}$ and ${}^T\mathbf{v}$.

To solve direct and inverse kinematics, joint and world coordinates will be defined first.

Joint coordinates vector for this 5-axis Tricept based machine tool is represented as

$$\mathbf{q} = [d_1 \ d_2 \ d_3 \ \theta_1 \ \theta_2]^T \quad (1)$$

where $d_i, i=1,2,3$ and $\theta_i, i=1,2$ are scalar joint variables controlled by actuators.

The description of world coordinates is based on tool path calculated by CAD/CAM systems defined by the set of successive tool positions and orientations in the work piece frame {W}, Fig. 2. The thus calculated tool path is machine independent and is known as a cutter location file (CLF). A tool pose is defined by the position vector of the tool tip T in the work piece frame {W} as ${}^W\mathbf{p}_T = [x_{TW} \ y_{TW} \ z_{TW}]^T$ and tool orientation is defined by unit vector of the tool axis as ${}^W\mathbf{k}_T = [k_{TWx} \ k_{TWy} \ k_{TWz}]^T$. In the general case, the tool tip position vector and tool axis vector in machine reference frame {M} can be expressed as

$$\begin{aligned} {}^M\mathbf{p}_T &= [X_M \ Y_M \ Z_M]^T = {}^M\mathbf{p}_{Ow} + {}^M\mathbf{R} \cdot {}^W\mathbf{p}_T \\ {}^M\mathbf{k}_T &= [k_{Tx} \ k_{Ty} \ k_{Tz}]^T = {}^M\mathbf{R} \cdot {}^W\mathbf{k}_T \end{aligned} \quad (2)$$

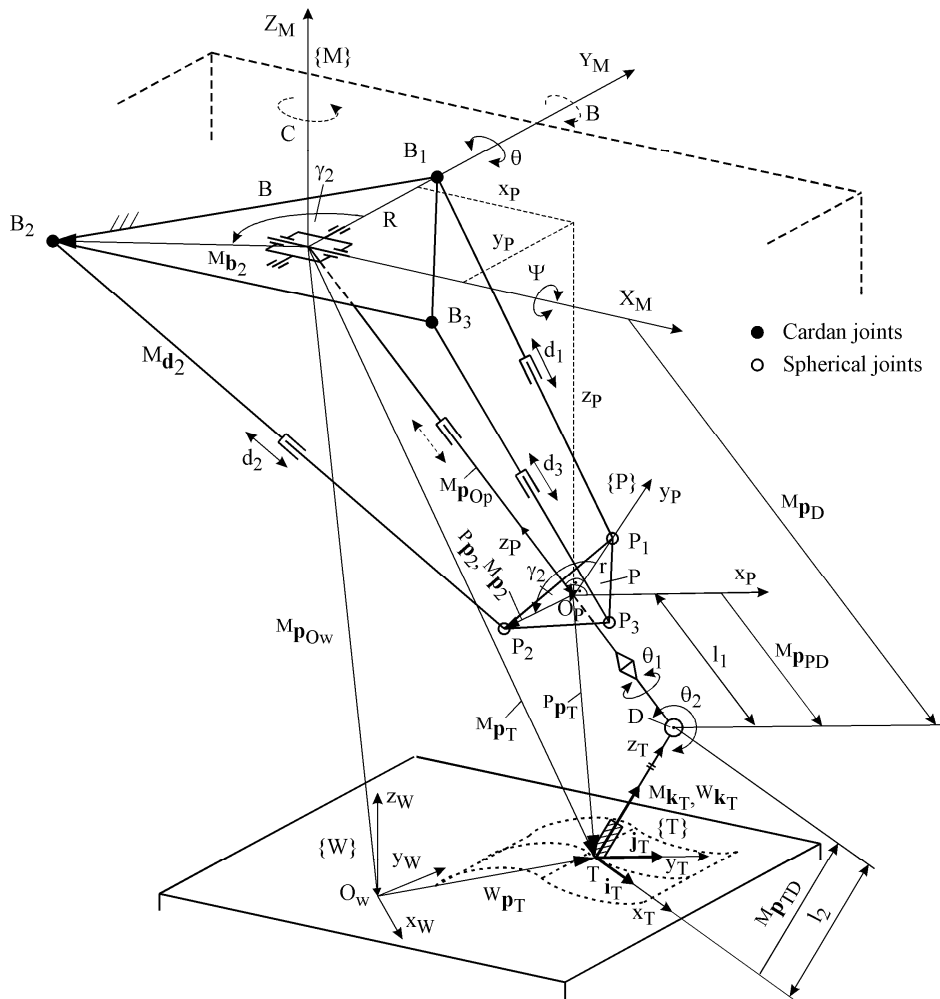


Fig. 2. Geometric model of the Tricept based vertical five-axis machine tool

where ${}^M \mathbf{p}_{Ow} = [x_{Ow} \ y_{Ow} \ z_{Ow}]^T$ is the position vector of the origin of work piece frame {W}. Determining the position vector ${}^M \mathbf{p}_{Ow}$ and the orientation of the work piece frame {W} is conducted according to the standard procedure for 5-axis CNC machine tools. It should be noted that determining the orientation matrix ${}^M_W R$ in equations (2) is determined and executed later in control system without changing G-code. To complete the vector of world coordinates, it is also needed to determine the tool orientation angles B and C which define direction of tool axis z_T that also coincides with axis of the last link, Fig. 2. Given that the machine has 5 DOF, only the direction of tool axis z_T is controllable, while axes x_T and y_T will have uncontrollable rotation about it. The position and orientation of the tool frame {T} relative to robot reference frame {M} can be described by homogenous coordinate transformation matrix 4x4 [8-10] as

$${}^M_T T = \begin{bmatrix} {}^M_T R & {}^M \mathbf{p}_T \\ 0 & 1 \end{bmatrix} = \begin{bmatrix} i_{Tx} & j_{Tx} & k_{Tx} & X_M \\ i_{Ty} & j_{Ty} & k_{Ty} & Y_M \\ i_{Tz} & j_{Tz} & k_{Tz} & Z_M \\ 0 & 0 & 0 & 1 \end{bmatrix} \quad (3)$$

where the rotation matrix ${}^M_T R$ represents the orientation, while vector ${}^M \mathbf{p}_T$ represents the position of the tool frame {T} with respect to the machine reference frame {M}. To bring the tool axis z_T to a desirable orientation with respect to frame {M}, the tool frame {T} must be rotated first about axis Y_M by angle B, and then about axis Z_M by the angle C, as prescribed by the convention for 5-axis vertical milling machine (X, Y, Z, B, C) spindle-tilting type. As it is known, the rotation matrix ${}^M_T R$ specifying the orientation of tool axis z_T can be derived as

$${}^M_T R = R_{ZM,C} \cdot R_{YM,B} \quad (4)$$

where $R_{YM,B}$ and $R_{ZM,C}$ represents basic rotation matrices [10] and where “s” and “c” refer to sine and cosine functions. As it is of interest only orientation of the tool axis z_T specified by unit vector ${}^M \mathbf{k}_T = [k_{Tx} \ k_{Ty} \ k_{Tz}]^T$, by equating corresponding members of matrix ${}^M_T R$ from equation (4) the angles B and C can be determined [11]. This way, the world coordinates vector can be expressed as $\mathbf{x} = [X_M \ Y_M \ Z_M \ B \ C]^T$.

2.2. Kinematic modeling of parallel mechanism

As it was mentioned, the passive central leg is used to constrain the motion of the platform to only 3-DOF. According to Fig. 2 these 3-DOF can be described by spherical coordinates

$$\mathbf{x}_{sp} = [p_{Op} \ \Psi \ \theta]^T \quad (5)$$

where:

- $p_{Op} = |{}^M \mathbf{p}_{Op}|$ is axial translation along central leg, and
- Ψ and θ are the rotation angles of the central leg's Cardan joint about axes X_M and Y_M respectively.

Vector ${}^M \mathbf{p}_{Op} = [x_p \ y_p \ z_p]^T = \mathbf{x}_P$ is the position vector of origin O_p of the frame {P} attached to the moving platform with respect to machine reference frame {M}, and represents Cartesian world coordinates vector.

As noticeable from Fig. 2 joint axes of 2-DOF serial wrist intersect at point D (wrist centre). From this fact it is easy to conclude that the position of wrist centre D is influenced only by joint coordinates d_1, d_2 and d_3 of parallel mechanism.

For specified position vector of the tool tip ${}^M \mathbf{p}_T = [X_M \ Y_M \ Z_M]^T$ and for specified tool orientation angles B and C the rotation matrix ${}^M_T R$ from equation (4) is calculated first. Then by using only vector ${}^M \mathbf{k}_T$ from calculated rotation matrix ${}^M_T R$

$${}^M \mathbf{k}_T = [cC \cdot sB \ sC \cdot sB \ cB]^T \quad (6)$$

the position vector of the wrist centre D ${}^M \mathbf{p}_D$ and its module p_D , according to Fig. 2 can be calculated as

$$\begin{aligned} {}^M \mathbf{p}_D &= \begin{bmatrix} x_D \\ y_D \\ z_D \end{bmatrix} = {}^M \mathbf{p}_T + {}^M \mathbf{p}_{TD} = \\ &= {}^M \mathbf{p}_T + l_2 \cdot {}^M \mathbf{k}_T = \begin{bmatrix} X_M + l_2 \cdot cC \cdot sB \\ Y_M + l_2 \cdot sC \cdot sB \\ Z_M + l_2 \cdot cB \end{bmatrix}^T \end{aligned} \quad (7)$$

and it's module as

$$p_D = |{}^M \mathbf{p}_D| = \sqrt{x_D^2 + y_D^2 + z_D^2} \quad (8)$$

As the position vectors ${}^M \mathbf{p}_{Op}$, ${}^M \mathbf{p}_D$ and ${}^M \mathbf{p}_{PD}$ are collinear and coincide with central leg, and as $|{}^M \mathbf{p}_{PD}| = l_1$ the module $p_{Op} = |{}^M \mathbf{p}_{Op}|$ can be calculated as

$$p_{Op} = p_D - l_1 \quad (9)$$

Now, the description of the position and orientation of the frame {P} attached to the moving platform with respect to machine reference frame {M} can be represented as

$${}^M_P T = \begin{bmatrix} {}^M_P R & {}^M \mathbf{p}_{Op} \\ 0 & 1 \end{bmatrix} \quad (10)$$

where rotation matrix ${}^M_P R$ represents the orientation while vector ${}^M \mathbf{p}_{Op}$ represents the position of frame {P} with respect to the machine frame {M}. Frame

${}^M P T$ can be further derived using homogenous transformation matrices 4x4 as

$${}^M P T = \text{Trot}(X_M, \Psi) \cdot \text{Trot}(Y_M, \theta) \cdot \text{Tran}(Z_M, -p_{Op}) = \begin{bmatrix} c\theta & 0 & s\theta & -p_{Op} \cdot s\theta \\ s\Psi \cdot s\theta & c\Psi & -s\Psi \cdot c\theta & p_{Op} \cdot s\Psi \cdot c\theta \\ -c\Psi \cdot s\theta & s\Psi & c\Psi \cdot c\theta & -p_{Op} \cdot c\Psi \cdot c\theta \\ 0 & 0 & 0 & 1 \end{bmatrix} \quad (11)$$

where

$${}^M \mathbf{p}_{Op} = \begin{bmatrix} -p_{Op} \cdot s\theta \\ p_{Op} \cdot s\Psi \cdot c\theta \\ -p_{Op} \cdot c\Psi \cdot c\theta \end{bmatrix} = \begin{bmatrix} x_p \\ y_p \\ z_p \end{bmatrix} \quad (12)$$

As the vectors ${}^M \mathbf{p}_D$ and ${}^M \mathbf{p}_{Op}$ are collinear, calculated components of vector ${}^M \mathbf{p}_D = [x_D \ y_D \ z_D]^T$ in equation (7) can also be described by spherical coordinates according to equation (12) as

$${}^M \mathbf{p}_D = \begin{bmatrix} -p_D \cdot s\theta \\ p_D \cdot s\Psi \cdot c\theta \\ -p_D \cdot c\Psi \cdot c\theta \end{bmatrix} = \begin{bmatrix} x_D \\ y_D \\ z_D \end{bmatrix} \quad (13)$$

From equations (13), (7) and (8) the platform's orientation angles Ψ and θ can be determined as

$$\theta = A \tan 2(x_D / -p_D, \sqrt{1 - (x_D / -p_D)^2}) \quad (14)$$

$$\Psi = A \tan 2(y_D, -z_D) \quad (15)$$

As can be seen from equation (13), equation (14) is valid when $c\theta \neq 0$ i.e. $\theta \neq \pm 90^\circ$. This condition is always satisfied since angles Ψ and θ usually vary within the limits $\pm\pi/3$ specified by the ranges of passive joints motions.

This way, the spherical world coordinates vector of parallel mechanism \mathbf{x}_{sp} in equation (5) or Cartesian world coordinates vector \mathbf{x}_p in equation (12) are completed.

2.2.1. Inverse kinematics of parallel mechanism

The inverse kinematics of parallel mechanism from Fig. 2 deals with calculating the leg lengths d_i , $i=1,2,3$ when platform pose is given.

Observing geometric relations on the example of leg vector ${}^M \mathbf{d}_2$ shown in Fig. 2 the following equations can be derived

$${}^M \mathbf{d}_i = \begin{bmatrix} d_{ix} \\ d_{iy} \\ d_{iz} \end{bmatrix} = {}^M \mathbf{p}_{Op} + {}^M \mathbf{p}_i - {}^M \mathbf{b}_i \quad (16)$$

where:

- ${}^M \mathbf{d}_i = [d_{ix} \ d_{iy} \ d_{iz}]^T$, $i=1,2,3$ are vectors of the actuated legs defined in the machine frame $\{M\}$,

- ${}^M \mathbf{p}_{Op} = [x_p \ y_p \ z_p]^T$ is the position vector of the origin O_P of the frame $\{P\}$ attached to the moving platform with respect to machine frame $\{M\}$ and is given in equation (12),

- ${}^P \mathbf{p}_i = \begin{bmatrix} p_{ix} \\ p_{iy} \\ 0 \end{bmatrix} = \begin{bmatrix} r \cdot c\gamma_i \\ r \cdot s\gamma_i \\ 0 \end{bmatrix}$, $i=1,2,3$ are position

vectors of the joint centers at the platform located on the circle of radius r with angular position

$$\gamma_i = \frac{2\pi}{3}(i-1), \text{ and are defined in the frame } \{P\},$$

- ${}^M \mathbf{p}_i = {}^M P R(\psi, \theta) \cdot {}^P \mathbf{p}_i$, $i=1,2,3$ are position vectors of the joint centers of the platform expressed in the machine frame $\{M\}$,

- ${}^M \mathbf{b}_i = \begin{bmatrix} b_{ix} \\ b_{iy} \\ 0 \end{bmatrix} = \begin{bmatrix} R \cdot c\gamma_i \\ R \cdot s\gamma_i \\ 0 \end{bmatrix}$, $i=1,2,3$ are position

vectors of the joint centers at the base located on the circle of radius R with angular position

$$\gamma_i = \frac{2\pi}{3}(i-1) \text{ and are defined in the frame } \{M\}.$$

By substituting corresponding vectors in equation (16) vectors ${}^M \mathbf{d}_i = [d_{ix} \ d_{iy} \ d_{iz}]^T$, $i=1,2,3$ can be obtained from which inverse kinematics equations

$$d_i = \sqrt{d_{ix}^2 + d_{iy}^2 + d_{iz}^2}, \quad i=1,2,3 \quad (17)$$

are derived as

$$d_1 = (p_{Op}^2 + r^2 + R^2 - 2 \cdot p_{Op} \cdot R \cdot c\theta \cdot s\Psi - 2 \cdot R \cdot r \cdot c\psi)^{1/2} \quad (18)$$

$$d_2 = [p_{Op}^2 + r^2 + R^2 + p_{Op} \cdot R \cdot (c\theta \cdot s\Psi - \sqrt{3} \cdot s\theta) + \frac{r \cdot R}{2} (-3 \cdot c\theta - \sqrt{3} \cdot s\theta \cdot s\Psi - c\Psi)]^{1/2} \quad (19)$$

$$d_3 = [p_{Op}^2 + r^2 + R^2 + p_{Op} \cdot R \cdot (c\theta \cdot s\Psi + \sqrt{3} \cdot s\theta) + \frac{r \cdot R}{2} (-3 \cdot c\theta + \sqrt{3} \cdot s\theta \cdot s\Psi - c\Psi)]^{1/2} \quad (20)$$

This way, the joint coordinates vector of parallel mechanism can be expressed as

$$\mathbf{d} = [d_1 \ d_2 \ d_3]^T \quad (21)$$

where d_i , $i=1,2,3$ are scalar variables controlled by actuators.

2.2.2. Jacobian matrix and direct kinematics of parallel mechanism

The direct kinematics problem for parallel mechanism consist of finding vector of world coordinates \mathbf{x}_{sp} or \mathbf{x}_p as a function of joint coordinates \mathbf{d} . Generally, such problem does not have

analytical solutions and different numerical algorithms based on Jacobian matrix are used.

Differencing equations. (18) – (20) with respect to the time the Jacobian matrix is obtained as

$$J = \begin{bmatrix} \frac{\partial d_1}{\partial p_{Op}} & \frac{\partial d_1}{\partial \Psi} & \frac{\partial d_1}{\partial \theta} \\ \frac{\partial d_2}{\partial p_{Op}} & \frac{\partial d_2}{\partial \Psi} & \frac{\partial d_2}{\partial \theta} \\ \frac{\partial d_3}{\partial p_{Op}} & \frac{\partial d_3}{\partial \Psi} & \frac{\partial d_3}{\partial \theta} \end{bmatrix} = \begin{bmatrix} J_{11} & J_{12} & J_{13} \\ J_{21} & J_{22} & J_{23} \\ J_{31} & J_{32} & J_{33} \end{bmatrix} \quad (22)$$

where:

$$J_{11} = (p_{Op} - R \cdot c\theta \cdot s\Psi) / d_1$$

$$J_{21} = [2 \cdot p_{Op} + R \cdot (c\theta \cdot s\Psi - \sqrt{3} \cdot s\theta)] / 2 \cdot d_2$$

$$J_{31} = [2 \cdot p_{Op} + R \cdot (c\theta \cdot s\Psi + \sqrt{3} \cdot s\theta)] / 2 \cdot d_3$$

$$J_{12} = (-p_{Op} \cdot R \cdot c\theta \cdot c\Psi + r \cdot R \cdot s\Psi) / d_1$$

$$J_{22} = [p_{Op} \cdot R \cdot c\theta \cdot c\Psi + r \cdot R \cdot (s\Psi - \sqrt{3} \cdot s\theta \cdot c\Psi) / 2] / 2 \cdot d_2$$

$$J_{32} = [p_{Op} \cdot R \cdot c\theta \cdot c\Psi + r \cdot R \cdot (s\Psi + \sqrt{3} \cdot s\theta \cdot c\Psi) / 2] / 2 \cdot d_3$$

$$J_{13} = p_{Op} \cdot R \cdot s\theta \cdot s\Psi / d_1$$

$$J_{23} = [p_{Op} \cdot R \cdot (-s\theta \cdot s\Psi - \sqrt{3} \cdot c\theta) + r \cdot R \cdot (3 \cdot s\theta - \sqrt{3} \cdot c\theta \cdot s\Psi) / 2] / 2 \cdot d_2$$

$$J_{33} = [p_{Op} \cdot R \cdot (-s\theta \cdot s\Psi + \sqrt{3} \cdot c\theta) + r \cdot R \cdot (3 \cdot s\theta + \sqrt{3} \cdot c\theta \cdot s\Psi) / 2] / 2 \cdot d_3$$

This so called analytical Jacobian matrix [12] relates the spherical velocity vector $\dot{\mathbf{x}}_{sp}$ to the joint velocity vector $\dot{\mathbf{d}}$ and is used in this paper as a basis for simple numerical algorithm to solve direct kinematics for the purpose of simulation. The algorithm is based on constant Jacobian matrix calculated for the centre of workspace i.e. for the initial position [13].

At step (n+1), the estimated position of the platform is given by

$$\mathbf{x}_{spn+1} = \mathbf{x}_{spn} + J^{-1}(\mathbf{x}_{sp0}, \mathbf{d}_0) \cdot (\mathbf{d} - \mathbf{d}_n) \quad (23)$$

where:

- $\mathbf{x}_{spn+1} = [p_{Opn+1} \quad \Psi_{n+1} \quad \theta_{n+1}]^T$ is the estimated position of the platform at the step n+1,
- $\mathbf{x}_{spn} = [p_{Opn} \quad \Psi_n \quad \theta_n]^T$ is the estimated position of the platform at the step n,
- $\mathbf{d}_n = [d_{1n} \quad d_{2n} \quad d_{3n}]^T$ joint position (leg lengths) corresponding to the estimated platform position at the step n, result of the inverse kinematics of point \mathbf{x}_{spn} ,
- $J^{-1}(\mathbf{x}_{sp0}, \mathbf{d}_0)$ is the inverse Jacobian matrix for the initial platform position \mathbf{x}_{sp0} and joint position \mathbf{d}_0 as the result of inverse kinematics of point

\mathbf{x}_{sp0} .

For the purpose of simulation, this algorithm converge in 1 to 5 steps depending on the distance between the initial position and actual position. This comes from the large workspace at the parallel mechanism on one hand and the other hand from the high accuracy provided by position sensors. The direct kinematics model takes almost twice as much time as the inverse model.

3. WORKSPACE ANALYSIS

Beside the selection appropriate kinematic topology the most important step in the parallel machine design is to select the right geometric dimensions [12].

Based on inverse kinematics, it is possible to determine the position and orientation workspace of the Tricept based five-axis milling machine. The applied approach proved to be very useful and is based on the definition of position and orientation workspace for parallel kinematic chains [14].

In the case of the Tricept based five axis machine tool considered in this paper, the position and orientation workspace are given by

$$W_S(X_M, Y_M, Z_M, B, C) = \{0,1\} \quad (24)$$

which represents a Boolean function whose value is equal to 1 if the tool pose-defined by the quintet (X_M, Y_M, Z_M, B, C) is reachable without exceeding the limited motion range of the joints. Starting from the selected point in the workspace volume, the estimation is made by specific step-by-step strategy that locates tool in a given pose in the workspace and that determines whether the pose is reachable or not by taking into account a limited motion range of the joints [6]. Based on selected design parameters: $R = 350\text{mm}$, $r = 100\text{mm}$, $l_1 = 300\text{mm}$, $l_2 = 150\text{mm}$, $d_{\min} = 934\text{mm}$, $d_{\max} = 1520\text{mm}$ the determined workspace for three-axis machining ($B = 0^\circ, C = 0^\circ$, i.e., spindle axis is perpendicular to the $X_M Y_M$ plane) is shown in Fig. 3.

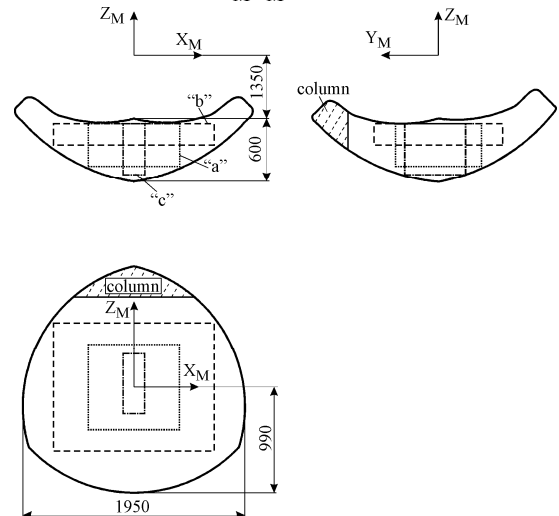


Fig. 3. Workspace in the case of three-axis machining ($B = 0^\circ, C = 0^\circ$)

For programmers and operators familiar with CNC machine tools, the determined workspace can be reduced to the parallelepiped “a” as indicated in Fig. 4. As it is known from practice, adopted portion of workspace in the form of parallelepiped “a” can be changed in form “b” or “c” depending on the workpieces’ shape and dimensions.

4. CONCLUSION

The results of a study on the kinematic modeling of the vertical Tricept based five-axis machine tool have been reported in this paper. For parallel structure inverse kinematics is solved analytically while direct kinematic is solved numerically based on constant Jacobian matrix calculated for the centre of workspace. Based on machine inverse kinematics workspace has been analyzed in order to select machine prototype design parameters. The focus of the current research, one part of the results being presented in this paper, is related to the prototype development of the Tricept based five-axis machine tool.

ACKNOWLEDGEMENT

The authors would like to thank the Ministry of Education and Science of Serbia for providing financial support that made this work possible.

5. REFERENCES

- [1] Weck, M., Staimer, D.: *Parallel Kinematic Machine Tools - Current State and Future Potentials*, Annals of the CIRP, Vol. 51, No. 2, pp. 671–681, 2002.
- [2] Pritschow, G., Wurst, K.H.: *Systematic Design of Hexapods and other Parallel Link Systems*, Annals of the CIRP, Vol. 46, No. 1, pp. 291–295, 1997.
- [3] Pierrot, F.: *Towards non-hexapod mechanisms for high performance parallel machines*, Proceedings of 26th Annual Conference of the IEEE, IECON, Vol. 1, pp. 229 – 234, Nagoya, 2000.
- [4] Neumann, K.-E.: *Robot (US Patent 4,732,525, Neos Product HB, Norrtalje, Sweden, 1988)*.
- [5] Neos Robotics, Home page at <http://www.neorobotics.com/>.
- [6] Milutinovic, M.: *Diploma work* (in Serbian), University of Belgrade, Mechanical Engineering Faculty, 2004.
- [7] ISO 841:2001 *Industrial automation systems and integration—Numerical control of machines—Coordinate system and motion nomenclature*.
- [8] Craig, J.J.: *Introduction to robotics: mechanics and control, 2nd edn.*, Addison-Wesley, New York, 1989.
- [9] Spong, M.W., Vidyasagar, M: *Robot Dynamics and Control*, Wiley, Chichester, 1989.
- [10] Fu, K.S., Gonzalez, R.C., Lee, C.S.G.: *Robotics: control, sensing, vision, and intelligence*, McGraw-Hill, New York, 1987.
- [11] Milutinovic, D., Glavonjic, M., Slavkovic, N., Dimic, Z., Zivanovic, S., Kokotovic, B., Tanovic, Lj.: *Reconfigurable robotic machining system controlled and programmed in a machine tool manner*, The international journal of advanced manufacturing technology, Vol. 53, No. 9-12, pp. 1217-1229, 2011.
- [12] Milutinovic, D., Glavonjic, M., Kvirgic, V., Zivanovic, S.: *A New 3-DOF Spatial Parallel Mechanism for Milling Machines with Long X Travel*, Annals of the CIRP, Vol. 54, No. 1, pp. 345–348, 2005.
- [13] Begon, Ph., Pierrot, F., Dauchez, P.: *High-precision, High-speed, Insertion with a 6 d-o-f parallel robot*, Proceeding of 24th International symposium on Industrial Robots, , pp. 145-152, Tokyo, 1993.
- [14] Innocenti, C., Parenti, C.V.: *Exhaustive enumeration of fully parallel kinematic chains*, Dyn Syst Contr, Vol. 55, pp. 1135–1141, 1994.

Authors: M.Sc. Milan Milutinovic, Tehnikum Taurunum - High Engineering School Vocational Studies, Nade Dimic 4, Zemun,11080 Beograd, Serbia, Nikola Slavkovic, dipl.ing., prof. dr Dragan Milutinovic, University of Belgrade, Faculty of Mechanical Engineering, Department for Production Engineering, Kraljice Marije 16, 11120 Belgrade, Serbia, Phone.: +381 11 3302-415, Fax: +381 11 3370-364.

E-mail: mmilutinovic@tehnikum.edu.rs
nslavkovic@mas.bg.ac.rs
dmilutinovic@mas.bg.ac.rs

Pecenica, N., Lukic, Lj., Nikolic, N., Djapic, M.

COMPARATIVE ANALYSIS AND FLEXIBLE CONVENTIONAL NC TECHNOLOGY THE EXAMPLE FROM INDUSTRY

Abstract: The optimum technological process in the classical production system, resulting from the optimal performance of individual unit operations during the development of each workpiece to multi functional dependencies between the machine tool, workpiece material, tools and elements of the machining. The technological process in the FTS-not, as a very important addition to the functional and procedural dependence.

This paper presents a comparative analysis of NC technologies that are implemented on conventional machine tools with NC control and technologies that are implemented in a flexible manufacturing system, the selected example from industrial practice. At the same time presents the methodology and design of flexible technology, with emphasis on the characteristic elements of production in flexible manufacturing systems.

Keywords: CAD/CAE/CAM, NC technology, FMS

1. INTRODUCTION

Modern production is based on the optimal design of technological processes and the selection of the appropriate production system. Short product life and the desire of designers to adjust the maximum functionality of the product to customer requirements require maximum attention on the analysis of productivity and efficiency of production processes. Increasing the level of automation and programmability of the production system does not ensure greater effectiveness in all technological conditions. Sometimes it is a highly automated production system, despite the high degree of flexibility, less cost than conventional machining with CNC control system.

In small series production work parts for injection molding tools with high spatial processing of complex multiaxial surfaces, it frequently occurs that the dilemma is more efficient development of the autonomous machining centers and flexible manufacturing systems. In the selected example from industrial practice a comparative analysis of methods of design technology was carried out, with indicators of the manufacturing process for the treatment of classic CNC machining centers and flexible manufacturing system. The analysis allows the definition of technological areas in which the economical processing of the flexible manufacturing system.

2. CNC TECHNOLOGIES CONVENTIONAL

In the last few decades have been widely applied in machine tools with NC control, and development of computer systems and CNC software engineering technologies have become the conventional method for

processing spatial complex surfaces on the parts of the metal processing industry. The productions facilities are often used as a machining center machining systems are adequate for making the working parts for plastic injection molds, casting or forging. Machining centers as autonomous machining systems have servers of which supervises the implementation of NC programs, tool changing machining center in a warehouse, is shrinking and the workpiece placed on the desk and finally disposed of workpieces with machining process is completed. Under a series of complex workpieces to be processed effectively autonomous machining centers - CNC using conventional technology, but the question of criteria in order to adequately evaluate the case when there are alternative options for the implementation of FMS and conventional CNC technology (Fig. 1).

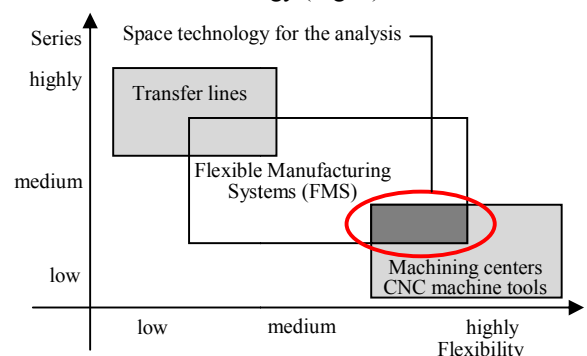


Fig. 1. Application areas of autonomous FMS and CNC machining centers

Greater flexibility in the range of workpieces with small series production determines the priority use of

conventional CNC technology, a large series of similar parts are generally processed the transfer lines, which is characteristic of production in the automotive industry. For the medium series of workpieces with high flexibility to implement flexible technology in FMS systems. Interestingly, the area is in part overlap with FMS machining centers, which should establish criteria for evaluating the effectiveness of the production process in FMS or on autonomous machining centers.

3. FTS

The optimum technological process in the classical production system, resulting from the optimal performance of individual unit operations during the development of each workpiece to multi functional dependencies between the machine tool, workpiece material, tools and elements of the machining. In technological processes in the FTS-not, because in addition funkcionalnih very important, and procedural dependence. Optimization of technological processes in the FTS-in is based on a much more complex model, because production in the FTS in a number of specific features in relation to the production of the classic production system (Fig. 2). Basic characteristics of the FTS-processing in the:

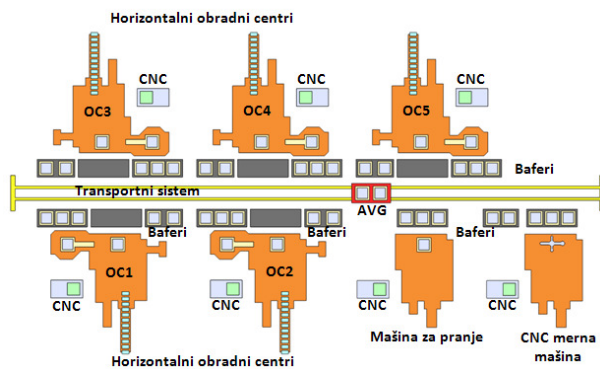


Fig. 2. FTS Configuration for the treatment of prismatic parts

- workpieces are geometrically and technologically similar characteristics,
- at the same time-simultaneous processing is performed more različitih workpieces,
- workpieces are usually processed in different batches (where each type obradakaima his series in which a given must be made),
- The processing is performed simultaneously on the same or more different machining centers,
- On one pallet can be more of the same or different workpieces,
- Editing tools are performed automatically at two levels - changes from the main spindle and the tool storage and processing center changes svih tools from warehouses machining center,

- Change the range of workpieces is done automatically,
- The movement of workpieces in the technological process is carried out with automatic transmission system.

Because of the high degree of automation, management, computer-based control systems, investing in FMS is much larger than inesticije in a production system based on machining centers and conventional CNC machine tools. Therefore, the FMS-kd and a higher depreciation costs, and thus the hourly rate of pay.

4. TECHNOLOGY FOR CONVENTIONAL NC MACHINE TOOLS

In the phase of designing NC technology play a key role sovfverski CAM packages that offer great creative options when generating tool paths and NC-code format. NC technology for designing parts for injection molding tools for plastics, used EdgeCAM is one of the most widely used CAD / CAM software packages for integrated product design and technology. Complete EdgeCAM software system includes support for generating NC code and computer communication - numerically controlled machine tool for processing the following types, namely:

- 2 ½ to 3 axis processing
- 5 axis processing
- 2 to 4 Multi-axis turning
- 2 to 4 axis wire processing elektroeroziona
- Editor
- The module for generating NC code (Code Wizard)

Design of NC processing technology on a conventional machining center includes the most important parts of tools for plastic injection pressure which is necessary to define all of the technological parameters. For example from industrial practice (Fig. 3), it is necessary to design the technology for processing plate 14 nests with tools and two upper plate molding tools.

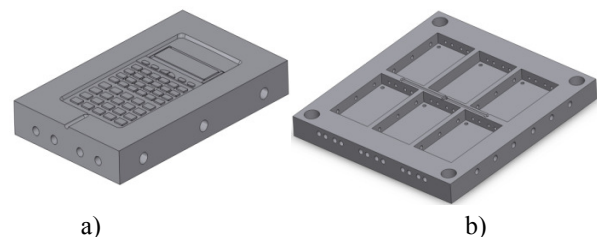


Fig. 3. Workpieces a) plate nests with tools and b) upper mold plate

When designing the EdgeCAM NC technology in the milling process is necessary to first define the plan contract and treatment plan, and then define the type of operation, the tool, cutting conditions, a strategy, a way of approaching and moving away from the workpiece

tools and other technological parameters for each operation . Simulation after the definition of each operation , and the entire flow machining process parameters are analyzed and projected effects of technology (Fig. 4). Depending on the results of simulations can be performed and the changes of the machining tools in the technological operations, and define an entirely new machining conditions (Fig. 5) which will enable greater productivity and efficiency of machining processes.

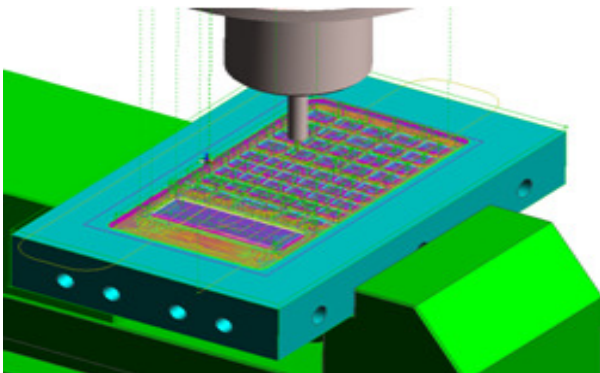


Fig. 4. The trajectories of cutting boards nests processing tools for plastic injection

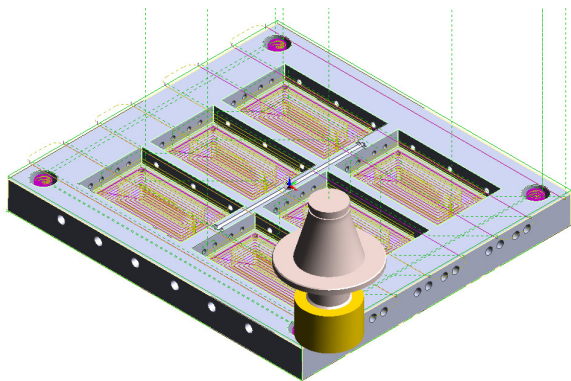


Fig 5. Tool path to process the upper mold plate

Simulation is a realistic overview of processing, thus showing the movement of the tool and the material removal process. The simulation (Fig. 6) allows identifying any errors or collision of tools or tool holders in contact with the workpiece. For example. simulator will detect the error if the cutting geometry is not adequate, so the tool touches the workpiece, not only cutting edge, but the handle. Also, it is often the case that the short handle tools, and tool holder is in contact with the workpiece. CAD / CAM system allows the geometric collision case, make corrections, that in case of unfavorable indicators of a machining process optimization approaches, as well as tool path optimization of the machining parameters.

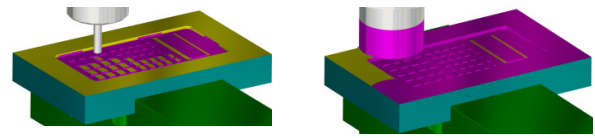
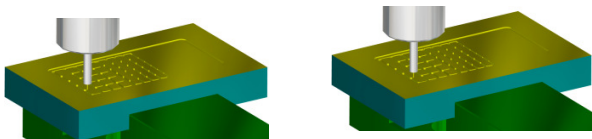


Fig. 6. Simulation of technological operations in the processing of conventional machining system

5. TECHNOLOGY FOR FMS

In the FTS in flexible production simultaneously to deal with several workpieces in a single technological operation, which is not related to a workpiece, but for a group of workpieces which are placed on a pallet. All workpieces to be processed in one production cycle in the FTS in the similar geometrical and technological characteristics and belong to one and the same classification group. Therefore, you can use the same type of rail and ancillary equipment in setting workpieces on pallets (Fig. 7). Schedule workpies on pallets to a large extent depends on the series in which to develop a range. When several identical workpieces placed on a raft, a complete range of content is seen as one entity, so that using the principles of group technology in NC programming and processing of all parts of the range is realized with one NC program (Fig. 8).

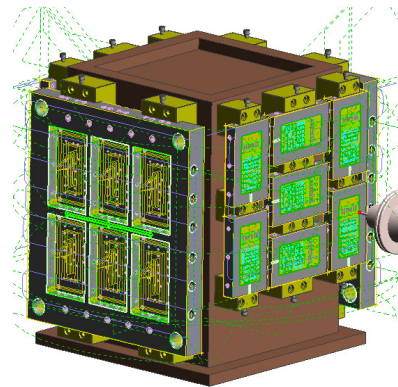


Fig. 7. The trajectories of cutting boards nests processing tools for plastic injection-FMSu

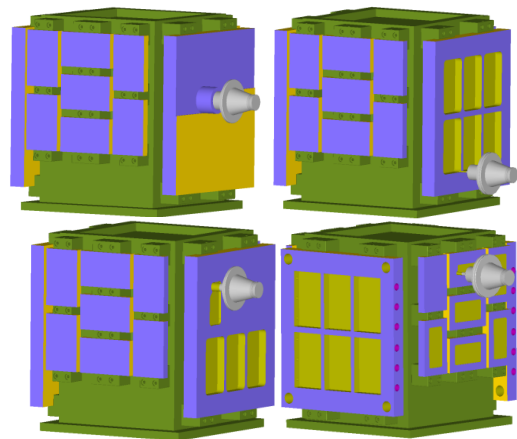


Fig. 8. Simulation of machining processes in the FMS

6. ANALYSIS TECHNOLOGY FOR CNC MACHINE TOOLS AND TECHNOLOGIES

To assess the effects of processing on conventional CNC machine tools and FMS-in, it is necessary to make analysis and comparative look at the basic technological parameters of the process through clamping plan, plan tools, the number of unit operations and processing time. The technological process for conventional CNC machine tools, which takes place using conventional rail equipment requires significantly more contraction than was the case for the treatment of FMS.

The conventional method of processing to machining centers required to process slabs from the nests of tools for plastic shrinkage $S1 = 22$, a treatment of the upper mold plate $S2 = 6$ contractions. Time for clamping plate nests with the $TS1 = 10$ min, and the tightness of the upper mold plate is $Ts2 = 30$ min. Bearing in mind the whole time series, which need to be processed on machining centers or CNC machine tools, the time required for clamping workpieces is 400 min. For processing technology in FMS-in, bearing in mind the possibility of setting up multiple prismatic clamping workpieces to the accessories that are on a rotating table can be processed from multiple sources, processing boards nests tools for plastic injection can be realized in a tightening ($S1 = 1$). Also the processing of the upper mold plate can be realized in a tightening ($S2 = 1$). The FTS-in time needed to be clamped workpieces does not affect the machine processing time, because the workpieces placed on a pallet in independent of cycle time of a machining center. The only time you need to bear in mind the time of the pallet exchanger, which takes the range of workpieces automatically governed Vehicle (AGV) and brings it into the workspace machining center, while at the same time range is from the cutting zone machining center and places it on the AGV. Pallet change time is 23 seconds, which is very short compared to the machine processing time to spend in the range of workspace machining center when cutter engaged with the workpiece material.

When processing is used 13 different types of tools, of which 10 tools for milling and drilling tools 3. You can use the same tools Sandvik Coromant and in the case of processing in FMS in the process of machining centers and CNC machines tools, so that part of the plan there is no advantage of tools FMS. The choice of the cutting blade geometry and material tools can be made based on recommendations from the manufacturer's catalog Coromant.

In the conventional method of processing on CNC machines altka processor board with 14 nests for plastic injection molds, 52 needed technological operations, and processing two upper mold plate 26 is necessary to perform the technological operations. In the case of processing in FMS, the processing of all 14 plates with nests is performed in 22 operations, and processing of the two upper mold plates are held in six operations.

Total processing time on conventional CNC machine tools for all 16 workpieces is $TU = 4220$ min, and the processing of the FMS is $TU = 4190$ min, which is a significant advantage (about 0.72%) on the FMS.

7. CONCLUSION

Given the low range of workpieces, the spatial configuration of land for five-axle operating that do not require treatment, but can be processed in troosnoj processing, machine processing time, during the preparation of workpieces, in this example from industrial practice is preferred for the treatment of autonomous processing center in relation processed in the FMS. We should bear in mind the much higher costs of depreciation and operating costs FMS compared to conventional CNC machine tools and processing of parts of smaller dimensions used in the treatment of troosnoj specialized production facilities with conventional machining centers and CNC machine tools. For simultaneous processing of large workpieces asotimana larger size in the small and medium series in višeosnoj processing, the advantage is on the FMS in comparison to conventional machining centers and CNC machine tools.

8. REFERENCES

- [1] Pecenica, N.: *Projektovanje tehnologija za obradu u FMS-u sa uporednom analizom konvencionalnih i fleksibilnih tehnoloških sistema*, *Master's thesis*, Faculty of Mechanical Engineering Kraljevo, 2012.
- [2] Nikolić, N.: *Design of CNC Technology and automatic generation of NC programs for the treatment of working tools for the production of plastic parts*, *Master's thesis*, Faculty of Mechanical Engineering Kraljevo, 2011.
- [3] Djapić, M., Lukić, Lj., Arsovski, S.: *Integrated Management Systems – Requirement of Contemporary Business Practices*, Proceedings The Sixth Triennial International Conference "Heavy Machinery HM 2008", Kraljevo, 24-29 June 2008, pp.G.1-G.6.
- [4] Lukic, Lj.: *Flexible Manufacturing Systems – Structure, construction, control and technology*, Monographs, University of Kragujevac, Faculty of Mechanical Engineering of Kraljevo, 2008.

Autors: **Novo Pečenica, MSc**, Mech.Eng., University of Kragujevac, Faculty of Mechanical Engineering Kraljevo, pecenica.n@mfkv.kg.ac.rs, **Prof. Ljubomir Lukić, PhD**, vice dean for scientific research affairs, Faculty of Mechanical Engineering Kraljevo, University of Kragujevac, lukic.lj@mfkv.kg.ac.rs, **Nenad Nikolić MSc**, Mech.Eng., Faculty of Mechanical Engineering Kraljevo, University of Kragujevac, nikolic.n@mfkv.kg.ac.rs, **Doc. Mirko Đapić, PhD**, assistant professor, Faculty of Mechanical Engineering Kraljevo, University of Kragujevac, djapic.m@mfkv.kg.ac.rs.

Popp, I.O.

SOMES ASPECTS REGARDING THE MAINTENANCE OF BEARINGS

Abstract: *This paper presents some aspects of diagnosis bearings in preventive maintenance and the importance of bearing repair as an alternative to replacing them.*

Key words: *maintenance, diagnosis bearings, bearings repair.*

1. INTRODUCTION

The growing investment machine tools and production systems requires their maximum availability. The complexity of such systems, which are highly automated and consist of many modules which are linked and have to work together without failure, increases the risk of breakdowns.

Monitoring is the automatic supervision of machine tool functions (or of processes). The monitoring system has to ensure that a machine works correctly without malfunctions. The result of its operation is a corresponding message about the machine state. This test can be performed according to a plan, periodically or continuously. A diagnosis system goes further, identifying the incorrect function and the reason for this malfunction. It gives an indication of the reasons and it is initiated when an incident occurs or upon demand.

Different methods can be applied for M & D (monitoring and diagnosis) [1]:

- signal-based M & D (heuristic);
- model-based M & D with signal prediction;
- model-based M & D on parameters;
- feature recognition or classification;
- knowledge-based M & D.

Considering the trends of manufacturing developments, the following reasons can be pointed out to explain why monitoring technology is becoming more and more important in modern manufacturing systems:

(1) Large-scale manufacturing systems should be operated with high reliability and availability because the downtime due to system failure has a significant influence on the manufacturing activity. To meet such a demand, individual unit processes should be securely operated with the aid of reliable and robust monitoring systems. Monitoring of large-scale systems is already beyond the capability of humans.

(2) Increasing labor costs and shortage of skilled operators necessitate operation of the manufacturing system with minimum human intervention, which requires the introduction of advanced monitoring systems.

(3) Ultra-precision manufacturing can only be achieved with the aid of advanced metrology and the technology of process monitoring.

(4) Use of sophisticated machine tools requires the integration of monitoring systems to prevent machine failure.

(5) Heavy-duty machining with high cutting and grinding speeds should be conducted with minimum human intervention from the safety point of view.

(6) Environmental awareness in today's manufacturing requires the monitoring of emissions from processes.

2. DIAGNOSIS SYSTEMS AND FAILURE DETECTING

In current industrial practice there is an offer of a wide range of products, from portable measurement and control instruments, the continuous monitoring systems and complete software to centralize and evaluate the results.

Monitoring tools cover a wide range of measurements [2]:

- vibration measurements with FFT signal analysis and automatic evaluation of results;
- shock pulse measurements to determine the conditions of lubrication of bearings and early detection of wear;
- measurements of speed;
- temperature measurements;
- measurements of analog signals;
- determining the resonance frequencies of the machine;
- orbit calculation for sliding bearings.

These equipments detect operating faults since their infancy, thus offering the possibility of planning repairs or maintenance work, resulting in minimizing or eliminating downtime of the production process. A continuous monitoring system consists of sensors installed permanent camps dynamic equipment and connecting them to the monitoring unit. These sensors can be, for example:

- vibration transducer;
- shock pulse transducer;
- temperature sensor;
- speed sensor; and more...

Measurement units of measurement signals have specific responsibilities, local assessment of the

measurements and conditional triggering of certain local events (warning, open / close relay power supply, etc.). And, last but not least, the transmission results in different formats to a centralized unit (control room).

3. DIAGNOSING BEARINGS

All equipment for assessing and analyzing the frequency made at this time in the world captures the vibration signal, processes and provides information on the technical state of camp, location and nature of defect.

In modern industrial practice there are equipments and work procedures based on this principle. It is known that if a bearing get to vibrate, already bearing is compromised and does not provide reliability. It is shown a method of measuring and monitoring of the lubricant film thickness rolling elements and taxiways, which allow identification of the moment when, for one reason or another (as lubricant, additional tasks camps etc) film lubricant is thinning and surface roughness of the metal balls / rollers and roller paths, get in contact directly [3].

By this method it can be determined what led to this situation, necessary corrections could be made in time, thus coming back to "wellness" page. Otherwise, the elements bearing wears, wear later will lead to the appearance of vibrations. Only in the due course, equipment to measure and analyze vibrations proves their usefulness, but already too late: the bearing is compromised.

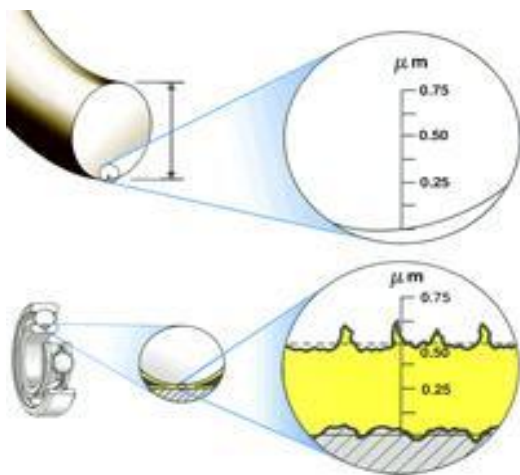


Fig. 1. Location and nature of the bearing defect

This method it called Shock Pulse Method (SPM). The main advantage of the shock pulse method is just finding its expertise in shock. When a ball / roller hits the defective area path produces a shock wave in a metal machine table. These shock waves are starting with a short stroke that pays off quickly. In a recording time displayed on an oscilloscope, these waves are observed superimposed on the overall machine vibration. When their frequency corresponds to the frequency of crossing objects rolling or cage, is a testament to the defect occurred in the capital. SPM transducer shock wave excites the characteristic

frequency ≈ 32 kHz resonance, amplifying the signal. Circuit analysis of electrical and mechanical signal is calibrated to filter out other signals of vibration [4].

Due to the sensitivity shock pulse method can be measured even overall lubrication of the bearing, the parameter dBc. Filtered transducer signal reflects the variation of pressure in the contact area between rolling objects and ways of rolling bearings.

When the lubricant film is thick, the shock pulse is low, no significant peaks (green). Level increases when the lubricant film thickness decreases, but still not present significant amplitude components (yellow area). Wear causes strong pulses at irregular intervals (red zone- Fig. 2).

The shock pulse method can be extended by performing an FFT analysis (Fast Fourier Transformation) of the signal taken, leading to more thorough analysis possibilities [4].

By identifying each bearing their own frequent (symptoms can now be identified these common SPM spectrum, thus diagnosing component even showing wear (running path inside / outside, roller / ball, cage).

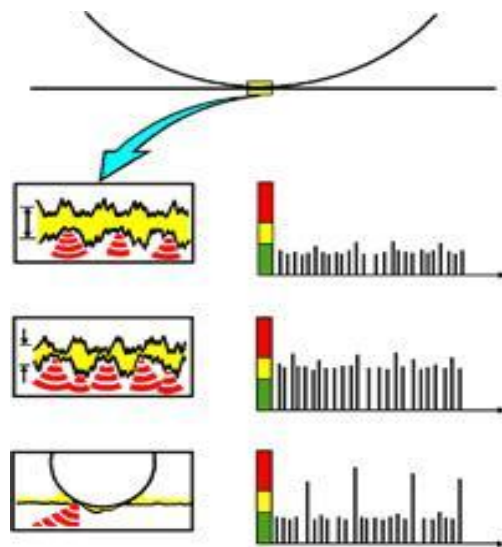


Fig. 2. Lubricant film thickness measurement

The advantages of implementing a maintenance system based on periodic measurements and analysis of shock pulse signal:

- Saving of materials and spare parts;
- Shortening the residence time in repair;
- Increasing the availability of equipment .

Basically, measurements are performed on all equipment camps (Fig. 3). The instrument acquires a sample shock pulse signal, it breaks down, the Fast Fourier Transformation (FFT), resulting in SPM spectrum, and where frequencies are shown in the pulse occurs predominantly from running bearing.

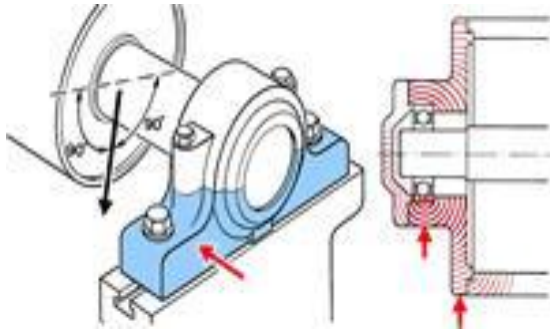


Fig. 3. Measurements of the machine bearings

In terms of defects that can be detected can include:

- lubrication failure / improper camp;
- early wear on the outer raceway;
- early wear on the inner raceway;
- early wear on the roller rolling object / ball;
- wear the cage early.

Specialized software associated test equipment must contain a rich database symptoms being able to automatically diagnose the probable causes of failure of bearing.

At the end of a round of measurements, it releases a report of measurements, including assessment of shock pulse signal level standards in force, diagnosing and locating possible causes of wear of the bearing and the recommendations on what action should be taken when appropriate.

4. BEARINGS REPAIR: AN ALTERNATIVE TO REPLACEMENT

Bearing repair is not a new concept, nor has it changed a great deal over the years — and that's good news. Repairing damaged bearings is a precise science that has been fine-tuned over time through careful and gradual enhancements to provide superior results.

Just as new designs and technologies improve bearings, growing expertise and technology of bearing repair continues to increase the reliability and performance of reconditioned bearings, keeping it an economical alternative to purchasing new bearings. Knowing and understanding the value of bearing repair means knowing what repair can do, when to use it, and where to get it done.

4.1 When to repair

Although it offers many benefits, reconditioning is not always the best option for a damaged bearing. The challenge of properly utilizing bearing repair services is determining if and when a bearing needs repair, and deciding which options is the best economical and long-term decision.

- Visual inspection serves as the first step in deciding if a bearing needs repair. Careful review of additional criteria assists in determining the need for repair, such as:
- Is the bearing nearing or has it exceeded its suggested life expectancy?
- Have operating temperatures exceeded 200 F?

- Has the bearing been exposed to excessive vibration?
- Has the bearing been subjected to sudden changes in lubrication or temperature?

Early detection of a problem through routine checks can spare companies' unnecessary downtime and expense and help to capitalize on the capabilities and benefits of bearing repair.

Regardless of the manufacturer, type of bearing, or application, proper treatment may preserve a bearing and restore it to like-new condition for continued use. Bearings with little or no damage often can be reconditioned and recycled easily and at low cost.

4.2 Remanufacturing process

Once a bearing is damaged, it should undergo a rigorous process to determine if it is a candidate for repair.

Bearings to be repaired should be thoroughly cleaned. Next, and the most critical step, is a detailed inspection on 100% of the bearing. Inspection begins with a careful review for major damages such as fractures, significant spalling, and bluing due to excessive heat. Any evidence of these usually results in scrapping the bearing.

If the bearing passes the first stage of inspection, it should undergo further review. This step serves to reveal a mode of damage, assessment of damage, and the scope of repair. The degree of bearing repair typically fits into three types [5].

Type I reconditioning is used for minor trouble spots and includes polishing, resetting of internal clearances, and spot grinding of any small surface defects to prevent further damage.

Type II repair is for bearings with more extensive damage. This level involves major procedures such as regrinding of races, new spacers, and polishing of the bore and cup OD. The regrinding of raceways will also necessitate the manufacture of oversize rollers to maintain bearing geometry and clearance.

Type III remanufacturing takes Type II repair one step further by replacing one or more of the major components of the bearing that are not repairable. These levels of repair have traditionally been suited for bearings with a minimum bore size of 200 mm. However, reclamation service can be done for bearings as small as 75 mm.

Smaller bearings that were often thrown away can now be repaired if there are large quantities. Cleaning, inspection, and the application of a polished finish can return used bearing to good-as-new condition for a fraction of the cost of replacement.

Turnaround time on reconditioning and repairs can be as short as 2-4 weeks, depending on the needed repairs. Companies utilizing bearing repair should always request a complete quote, including cost and estimated repair time, when requesting any type of repair service.

4.3 Expertise in bearing repair

Technology and material advancements contribute to an increased potential for bearing remanufacturing and reconditioning programs. However, experience in recognizing and treating various types of damage is the only way to guarantee an accurate inspection and proper repair.

It is important to have any bearing repair performed by properly trained and experienced personnel, because unnecessary repairs can lead to additional damage and limited bearing life. Common reconditioning mistakes include [5]:

- Improper roller polishing that creates flat spots
- Excessive deep spot grinding
- Mixing of preset components.

In addition to expertise, proper equipment is required not only to fix the problem, but also to ensure all damage has been reviewed and addressed. Magnifying glasses and proper lighting and measuring equipment are essential to perform thorough inspections and repairs

5. FINAL REMARKS

Repair after damage their equipment is expensive and takes time. Repair equipment based on the number of hours of operation is expensive and it is possible to scrap parts that would have run.

Simple measurement of vibration will indicate if the vibration is normal, still acceptable or unacceptable, but we will provide information on which the defect and where it is located. The problem is more complicated for complex machinery where vibration evaluating a camp, we will not know if they come from working, the clutch, the gear etc.

The advantages of implementing a maintenance system based on periodic measurements and analysis of vibration signal:

- Saving of materials and spare parts;
- Shortening the residence time in repair;
- Increasing the availability of equipment for production.

Bearing design takes into account the use and application of the bearing and establishes an appropriate prediction for service and fatigue life. No matter who the manufacturer is, bearings often deviate

from these expectations due to factors such as contamination, inadequate lubrication, and misalignment.

When a bearing is damaged, the entire machine of which it is a part suffers. Conventional practice suggests that a damaged bearing should be scrapped and replaced. The growing popularity of bearing repair has helped companies understand its value by providing an efficient and cost-effective way to resolve the problem.

Bearings often can be returned to original specification for less time and money than purchasing new ones. A quality repair and reconditioning program can result in significant savings compared to discarding and replacing bearings. Depending on the scope of the work, bearing repair can save as much as 50% to 90% of the cost of purchasing a new bearing. Beyond the cost, repairs often save time compared to ordering replacement bearings, reducing costly downtime.

Another value-added service of bearing repair is using damage analysis as a tool to identify difficult conditions and prevent future problems.

6. REFERENCES

- [1] Popp, Ilie., Barsan, Ioan., *Considerations regarding the monitoring system for preventive maintenance*, Annals of the Oradea University, Vol.8, No.18, ISSN 1583-0691, pp. 1368-1372, (2009).
- [2] Popp I., Barsan, I. *Considerations regarding the monitoring and diagnostic of manufacturing systems for preventive maintenance*, Proceedings of the International Conference on Manufacturing Systems ICMaS, Vol. 4, ISSN 1842-3183, University Politehnica of Bucharest, 2009
- [3] Kennedy, S., *Learn about condition monitoring beyond oil analysis, temperature and vibration* in Sheila Kennedy's monthly Technology Toolbox column, "New tools for PdM" www.plantservices.com.
- [4] -----: A collection of maintenance papers on the Internet.
- [5] -----: www.plantservices.com.

Author: Assoc. Prof. Dr. Eng. Ilie Octavian Popp., "Lucian Blaga" University of Sibiu, Romania, Engineering Faculty, Emil Cioran st. no. 4, 550025 Sibiu, Phone +40-269-217928, Fax +40-269-212716, E-mail: ilie.popp@ulbsibiu.ro

Šooš, E., Križan, P., Matúš, M.

OPTIMIZATION OF THE SPINDLE-BEARING SYSTEM

Abstract: The quality of machine tools is critical in determining their productivity and the accuracy of the finished work piece. The headstock of the machine tool has the greatest impact on these parameters. The tool or work-piece holder must meet specific demands for maximum speed and rigidity. These two parameters are variable, but always in contradiction, and depend mainly on the Spindle-Bearings System (SBS). In this context, SBS are increasingly being produced in combination with roller bearings, and with various combinations of radial ball bearings with angular contact. This is mainly because the radial ball bearings allow groupings of different combinations to achieve the optimal compromise between the required maximum speed and the desired stiffness of the SBS. Stiffness, especially in ball bearings, is not constant but dependent on the magnitude of the load. The SBS is a statically indeterminate system, and an accurate calculation of the bearings and its nodes, as well as the whole system, is only possible using iterative methods. Maximal speed and rigidity depend of maximal temperature and of stiffness SBS. Selection of the optimal configuration is achieved by analyzing a number of potential, alternative SBS solutions. Depend on arrangement radial ball bearings with angular contact in bearings nodes is changing preload in bearings and temperature. It has very big influence to maximal speed and rigidity bearings nodes. The paper presents original procedures for simplified bearing node calculations in relation to temperature.

Keywords: ball bearings with angular contact, bearing nodes, spindle bearing system (SBS) machine tool spindle, stiffness, high speed, temperature optimization of SBS.

1. INTRODUCTION

The number of headstocks supported on ball bearings with angular contact is increasing proportionally with the increasing demands on the quality of the machine tool [2]. This is because these bearings can be arranged in various combinations to create bearing arrangements which can enable the reduction of both radial and axial loads. The possibility of varying the number of bearings, their preload value, dimensions and the contact angle of bearings used in the bearing nodes, creates a broad spectrum of combinations which enable us to achieve the adequate stiffness and high speed capabilities of the **Spindle-Bearings System** (SBS) [2], [3]. Adequate revolving speed and stiffness of the headstock are necessary conditions for meeting the manufacturing precision quality and machine tool productivity required by industry.

1.1 Stiffness

The total static stiffness of machine tools is create as a serial spring arrangement all parts of machine tools and it is evident that the resulting stiffness machine tool is limited by the stiffness of the weakest part - Spindle-Bearings System. Amongst all the elements, the Spindle-Bearings System of the machine tool plays the most important role.

From results of structural analyses, the headstock can be considered as the heart of the whole machine tool. The design and quality of the machine tool must respect the quality of the drives and their features. The headstock (as tool, or work-piece carrier), has a direct influence on the static and dynamic properties of the

cutting process. The Spindle-Bearing System's stiffness also influences the final surface quality, profile, and dimensional accuracy of the work-piece.

The headstock stiffness must be calculated according to the deflection at the front end of the spindle, because the deflection at this point directly affects the precision of the finished product. The deflection at the spindle front end is the accumulation of various other, more or less important, partial distortions. The radial headstock stiffness can be calculated as follows:

$$K_{rc} = \frac{F_r}{y_{rc}} \quad (1)$$

Resulting static distortion of the front-end spindle equals

$$y_{rc} = y_0 + y_1 + y_t + y_a + y_v + y_{sb} + y_h \quad (2)$$

and depend from:

- y_0 - deflection of the spindle from bending moments
- y_1 - bearing compliance
- y_t - spindle deflection by transversal forces
- y_a - axial forces
- y_v - deflection of the headstock box
- y_{sb} - stiffening effect of bearings
- y_h - drive forces

Our experience has shown that whatever mathematical method and software is used, the spindle distortion caused by *bending moments* y_0 and by *bearing compliances* y_1 have the greatest influence on the resulting front end spindle distortion, [6].

Then

$$y_{rc} = y_0 + y_1 \quad (3)$$

where the distortion caused by bending moments is as follows:

$$y_o = \frac{F_r a^2}{3E} \left[\frac{a}{J_a} + \frac{L}{J_L} \right] \quad (4)$$

and the deflection caused by bearing compliance is as follows:

$$y_l = \frac{F_r}{L^2} \left[\frac{a^2}{K_B} + \frac{(L+a)^2}{K_A} \right] \quad (5)$$

The resulting static distortion of the spindle front-end can be explicitly described by a multi-parametrical equation in the form of:

$$y_F = f [E, F_r, a, L, J_a, (D_a, d_a) J_L (D_L, d_L), K_A, K_B, \rho] \quad (6)$$

and depend from:

- spindle material and dimensions (E, D_a, d_a, D_L, d_L)
- loading forces position, orientation and magnitude (F_r, N, r_F, b)
- bearing arrangement configuration and stiffness (K_A, K_B)
- spindle and bearing arrangement space configuration (L, a)
- spindle box construction (k_ξ, ρ)

1.2 Speed

The productivity of a machine tool can be increased in at least two different ways:

- a. Externally - by shortening working time - within a working cycle
- b. Internally - by reducing machining times (increasing the cutting width) - technological issues

The philosophy of intelligent manufacturing systems applied to production processes minimise lost time. Further reducing lost time is expensive and has limited effectiveness at current levels of technological development. It has been shown that increased productivity can be achieved for example by changing the cutting speed. However this has a direct effect on tool life and on the dynamic stability of the cutting process. The cutting speeds in machining processes depend on the technology applied, the cutting tool, and the *work-piece* material. The cutting speed also relates directly to the high-speed capability, and average diameter, of the bearings, the so-called factor

$$N = n_{max} \cdot d_{mid} \quad (7)$$

Thus, from the point of view of the required cutting speed, the most important factor is the revolving frequency capacity of a spindle which is supported on a bearing system. The calculation of the headstock's maximum revolving speed is relatively simple. The highest revolving speed of a bearing node is calculated on the basis of the highest revolving speed of one bearing, multiplied by various coefficients reflecting the influence on the bearings, the bearing arrangement, bearing precision, their preloaded value, and lubrication and cooling conditions.

2. ARRANGEMENTS OF NODAL POINTS

The number of spindle bearing systems supported on ball bearings with angular contact increases

proportionally with increasing demand on the machine tool. Usually, radial ball bearings with angular contact arrangements in their nodal points contain 2, 3 or more bearings. By varying the bearings and their arrangement in the bearing nodes (DB, DF, DT, TBT, TTF, QBC, ..), the value of the contact angle, magnitude of preload, and type of flanges can be optimized to suit the required, resulting stiffness and speed-capability of the spindle-bearing system.

2.1 Criteria for selecting the arrangement of bearings

Spindle mountings using only radial bevelled bearings, (table 1), [10] can be divided into 2 basic types:

- spindles mounted on bearing nodes with "directionally" arranged bearings, with equal orientation of contact angles in each nodal point, "1", "2", "3", and "7" scheme in table 1.
- spindles mounted on nodal points with bearings arranged according to shape "4", "5", "6" scheme in table 1. Bearings are arranged in "O" or (X) shape, in combination with "T".

A typical feature of the nodes of spindle bearings is the application of pre-load, which provides the stiffness of the nodal point and reduces any skidding of the rollers at high revolutions.

Pre-load can be achieved through three flange design principles:

- a) Sprung flange: thermal expansion (dilatation) is eliminated by changing the length of the elastic materials positioned between the flange and the bearings, which ensures minimum change in the pre-stress value.
- b) Stiff (Rigid) flange: provided by a fixing nut or casing. This design provides better stiffness characteristics. The pre-load value is changed due to the influence of thermal dilatation.
- c) Controllable flange: axially adjustable (by means of hydraulics), which ensures the required pre-load for different operational conditions.

The highest values of the coefficient "N" can be achieved by using spindles mounted on nodes with a "directional" arrangement of bearings, "1", "2" and "3". When used in conjunction with the controllable flange, the correct types of lubrication and cooling, speeds which are comparable with the maximum revolutions of the bearings themselves can be achieved. Thus they can be applied in high-speed machining [10]. These mounting types, in combination with the sprung support, are mostly used for grinding. For difficult technological operations requiring considerably higher stiffness in the radial and axial directions, nodal points with bearings arranged according to shape "4" and "6", together with fixed supports are typical.

There is negligible use of hybrids of the basic types of mounting (mounting "5"), as shown in table 1. In such cases one nodal point has bearings arranged according to shape, while the other has directionally arranged bearings. The pre-stressing in the front nodal point is

ensured by a stiff flange and in the rear nodal point by a sprung flange.

3. OPTIMIZATION OF THE SPINDLE-BEARING SYSTEM IN RELATION TO TEMPERATURE

In addition to the bearing arrangements, the temperature properties of the bearing supporting node have an increasingly greater significance on the high-speed capability of the bearing. The main goal of this section is to show the SBS design under real operating conditions, taking into consideration the temperature-related behaviour of the spindle and bearing nodes.

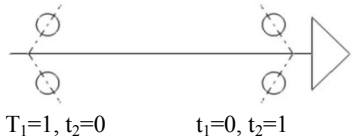
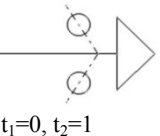
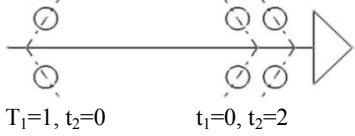
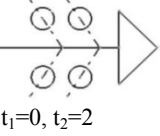
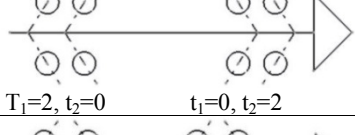
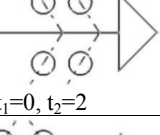
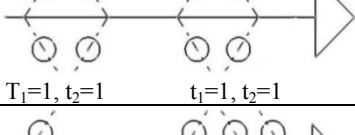
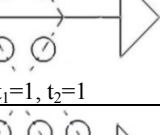
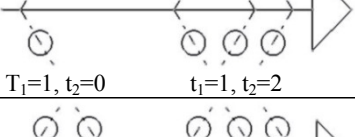
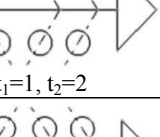
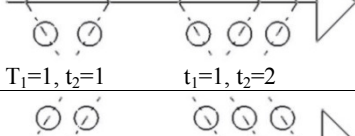
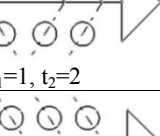
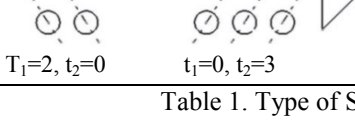
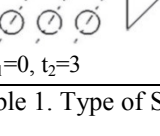
Seq. No.	CONFIGURATION		$N = n_{max} \cdot d_{mid} \cdot 10^6$ [mm.min ⁻¹]	Characteristic	Use
	Rear bearing node	Forward bearing node			
1.	 $T_1=1, t_2=0$	 $t_1=0, t_2=1$	1,2 -2,5	- single direction of rotation - light axial and radial loads	- grinding internal holes
2.	 $T_1=1, t_2=0$	 $t_1=0, t_2=2$	0,8 - 1,6	- suitable for extremely short spindles - medium axial loads	- finishing machines - drilling of deep holes
3.	 $T_1=2, t_2=0$	 $t_1=0, t_2=2$	0,8 -1,4	- medium radial loads - very common method of use	- grinding internal holes - milling - drilling
4.	 $T_1=1, t_2=1$	 $t_1=1, t_2=1$	0,6 - 1	- machining light metals - medium radial loads	- grinding - precision drilling - turning/ lathe
5.	 $T_1=1, t_2=0$	 $t_1=1, t_2=2$	0,5 - 0,9	- medium axial loads	- drilling of deep holes - milling
6.	 $T_1=1, t_2=1$	 $t_1=1, t_2=2$	0,4 - 0,9	- medium axial loads - very common method of use	- turning/ lathe - drilling
7.	 $T_1=2, t_2=0$	 $t_1=0, t_2=3$	0,3 - 0,6	- high axial loads medium radial loads	- milling - boring

Table 1. Type of SBS using radial ball bearings with angular contact [10]

The value of the changes in SBS temperature depends on the temperature gradient, the type of bearing arrangement (DB, DF, DT, ...), the contact angle of the bearing, and the distance between the bearings arranged in the node.

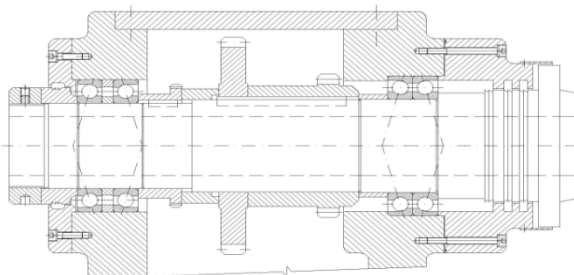


Fig. 1. The Headstock of the precision boring machine DB 24 fy. Ex-Cell-O GmbH., Eislinger, [8]

The analysis identified the optimal stiffness, which was then applied to the headstock of the DB 24 fy. Ex-Cell-O GmbH., Eislinger precision boring machine, Fig. 1, [8]. The stiffness of the given example was analysed using the application software “*Spindle Headstock*” [3], developed in our department.

3.1 The optimisation of shs with regard to temperature

The temperature dilatation of the spindle can be described by the equation:

$$\Delta L = \lambda_t \cdot L \cdot \Delta t \quad (8)$$

If the distance between the bearings in the “DB” arrangement is short (Figure 3a), the dilatations in a

radial direction is greater, [18]. The temperature gradient causes the dilatation of the inner bearing rings to be greater than that of the outer rings. Consequently, the original preload increase in temperature will be higher in the bearing node. The elevated temperature will influence the temperature gradient, and the preload value could cause bearing node failure.

The optimal bearing separation distance from the point of view of temperature can be deduced from:

$$B_{mopt} = D_m \cdot \frac{\cos \alpha}{\sin \alpha} - \frac{l_0 \cdot (t_I + t_A - 2t_0)}{t_I - t_A} \cdot \left(\frac{1}{\sin \alpha} \right) \quad (9)$$

Figure 2 shows the change of optimal bearing distance at various values of the temperature gradient for the analysed SBS, Figure 1.

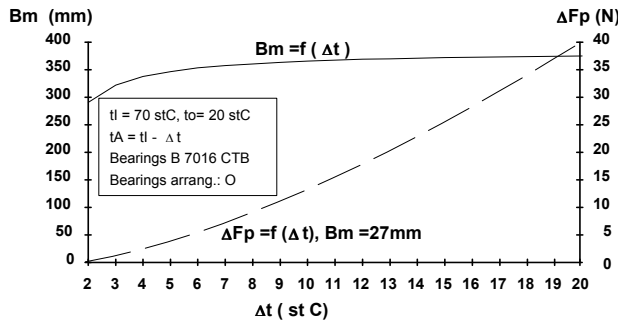


Fig. 2. The inter - dependence of bearing preload change, ideal distance between bearings and change of temperature in the bearings arrangement system.

3.2 Recommendations for improvements in construction

The recommendations from the point of view of temperature optimisation for the DB 24 SHS boring machine are based on the results of the analysis undertaken. From the perspective of temperature, it can be seen that a change in bearing node arrangement to individual spindle supports from "DB" to "DT" would be advantageous, Fig. 3.

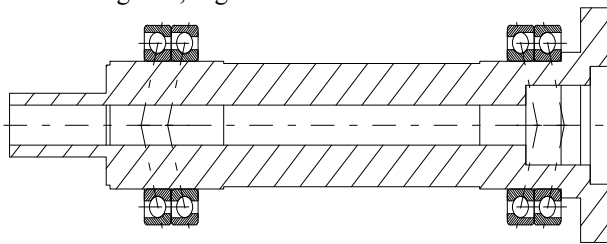


Fig. 3. Model of the spindle

4. OPTIMIZATION SBS

The application software is used for calculating the SBS of machine tools supported on rolling bearings. The programme enables us to determine all elements and calculate the properties of the spindles and shafts which are supported on rolling bearings. The application software enables very fast and user-friendly calculation of the radial spindle stiffness in the bearing arrangement in a bearing unit.

The architecture of the programme contains a number of mathematical formulae which have been

experimentally verified. These models respect the conditions of the spindle working accuracy in terms of the external load cutting forces, driving forces, and also spindle rotation speed.

The basic interactive programme offers:

1. the ability to input user-determined conditions for the calculation and optimisation of the spindle fitting system;
2. the ability to select the most appropriate bearing or bearing node arrangements (Figure 4). Data about selected bearings can be gained from extensive databases according to the users requirements within the bearing inner diameter range;
3. the identification and selection of the standardized spindle nose for turning, milling, grinding and boring;
4. the choice of the design parameters and spindle suitability for different working conditions (working accuracy, preloading, flange type, lubrication system, cooling), Figure 5;
5. the calculation and optimisation of the cutting parameters for the required material to be machined (cutting force, torque, feed, power), Figure 6;
6. Calculation and optimization of the design and fitment with regard to the applied conditions (revolving speed, radial stiffness, axial stiffness, rating life) for the bearing units and the fitting as a whole, for all of the identified bearing types.

Results for spindle with arrangement DT - B - DT

	Rear support	Front support
Bearings		
- type.	2pc. 2pc.[B7016CTB]	[B7016 CTB]
- arrangement:	<<	>>
- grade:	P4	P4
Preload:	Light	Light
Flange:	Fixed flange	Fixed flange
Max. speed (min ⁻¹):	Zn _{max} =5 256	Pn _{max} =5 256
Pre-load (N):	ZF _p = 404	PF _p = 402 N
Reactions (N):	R _A = 205	R _B = 1 205
Radial stiffness (Nmm ⁻¹):	K _{rA} = 530 630	K _{rB} = 483 969
Axial stiffness(Nmm ⁻¹):	K _{aA} = 141 436	K _{aA} = 141 436
Durability (hours):	T _{rvZ} = 2 753 228	T _{rvp} = 829 951
Bearings distance (mm):		L = 297
Total displacement at the end (mm):	y _{r(L+a)} = 0.00436617	
Total stiffness (Nmm ⁻¹):	K _{rc} = 229 033	

Optimal values

Optimal bearings length (mm):

$$L_{opt} = 317.2$$

Optimal displacement at the end LOpt (mm):

$$y_{rmin} = 0.00436088$$

Optimal stiffness(Nmm⁻¹):

$$K_{rcopt} = 229 311$$

Write input data on marked position ?
Desired data confirm by ENTER !

Manufactured bearings					Input data	
Number	Designation	d	Alfa0	D	Alfa0=	grad
1	B 7224 CATB	120	12	215	d=	mm
2	B 7224 CTB	120	15	215	D=	mm
3	B 7224 ATB	120	25	215	B=	mm
4	B 7224 AATB	120	26	215	dA=	mm
5	B 7024 CATB	120	12	180	dU=	mm
6	B 7024 CTB	120	15	180	rA=	mm
7	B 7024 ATB	120	25	180	rU=	mm
8	B 7024 AATB	120	26	180	dW=	mm
					cA=	N
					z=	
					N2=	1/n.

Select bearing num. : 1
F1-New 'd'

F1-Continue
F2-Variants
F3-Data
F4-Cancel
F5-Database

Rear support Variant-17
Front support Variant-7 "OT"

Fig. 4. Changing data of the bearings mounting

Ctrl-F1 Help
F1 - Continue
Enter - Current speed and pre-load

Lubrication
Oil
Plastic grease

Cooling
Additional cooling
Good cooling
Bad cooling

Operating speed N= 32001/min
If not suitable change work.conditions!

Front support

Bearings grade
P2
P4
P5

Pre-load
No
Light
Medium
Heavy

Max.speed PNmax= 31501/min
Pre-load PFp= 491N

Rear support

Bearings grade
P2
P4
P5

Max.speed ZNmax= 37801/min

Fig. 5. Entering preliminary data for the bearings conditions

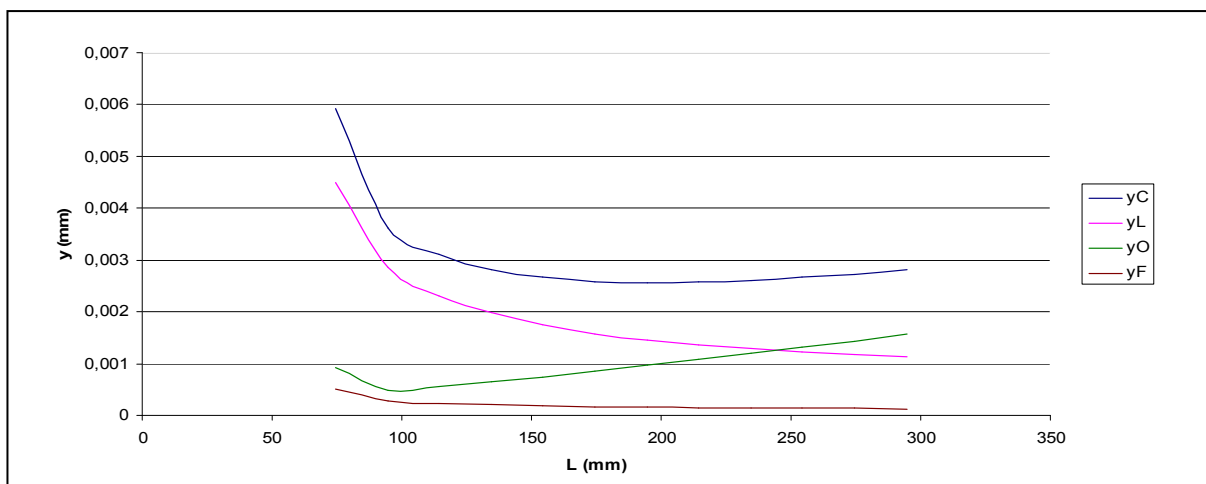


Fig. 6. Graphical output of the dependence of partial deflection on bearing node distance

In comparison with the original bearing node arrangement, the radial stiffness of the rearranged spindle-bearing system will drop slightly, but its axial stiffness will increase. The advantage of the reconfigured SBS is that at real mean values of temperature gradient, the SBS stiffness will be almost fixed.

NOMENCLATURE

N - high-speed ability
 E - modulus of elasticity of the material
 J – quadratic moments of inertia
 i – number of bearings
 α – contact angle
 D, d – diameter
 n – high spindle revolutions
 L- distance between bearings nodes
 a- spindle front-end
 K - stiffness
 R- reactions
 y - deflection

INDEXES

a- axial direction
 r – radial direction

5. REFERENCES

- [1] Weck, M., - Hennes, N. - Krell, M.: *Spindles and Toolsystems with High Damping*. In: *Cirp Annals-manufacturing Technology - CIRP ANN-MANUF. TECHNOL*, vol. 48, no. 1, pp. 297-302, 1999.
- [2] Marek, J a kol.: *Konstrukce CNC obráběcích strojů*. MM Publisching, s.r.o., Praha 2010, ISBN 978-80_254-7980-3, 419 s p.
- [3] Lee, D. - Sin, H. - Sun, N.: *Manufacturing of a Graphite Epoxy Composite Spindle for a Machine Tool*. CIRP, , 34, number 1, pp. 365 - 369.
- [4] Šooš, E.: *Quality of design engineering: Case of machine tools headstock*. In: *Quality Festival 2008 : 2nd International quality conference*. - Kragujevac, May 13-15, 2008. Kragujevac: University in Kragujevac, ISBN 978-86-86663-25-2.
- [5] Šooš, E. : *Contribution to the research of static and dynamic properties of CNC turning machine* In: *Strojnícky časopis = Journal of Mechanical engineering*. ISSN 0039-2472. - Roč. 59, č. 5-6 (2008), pp. 231-239
- [6] Šooš, E. : *Approximate methodology calculations of stiffness nodal points*. In: *World Academy of Science, Engineering and Technology*. - ISSN 2010-376X. - Year 7, Issue 80, pp. 1390-1395.
- [7] Šooš, E.: *Radial stiffness of nodal points of a spindle*. In: *MATAR Praha 2008. Part 2: Testing, technology: Proceedings of*

international congresss. - Prague 16th-17th September, Brno 18th September 2008. - Praha: České vysoké učení technické v Praze - ISBN 978-80-904077-0-1. - pp. 43-47.

- [8] Šooš, E. - Šarkan, P. : *Design of spindle –bearing arrangement of angular ball bearings*. In.: *MMA 94: Fleksibilne tehnologije : 11th International conference on Flexible Technologies*. Novi Sad, 8 – 9.6.2004. - Novi Sad : Institut za proizvodno mašinstvo -pp. 271-275.
- [9] Šooš, E.: *Spindle - housing system SBL 500 CNC*. In: *Eksploatacja i Niezawodność = Maintenance and reliability*. - ISSN 1507-2711. - Č. 2 (2008), pp. 53-56.
- [10] Šooš, E. *New methodology calculations of radial stiffness nodal points spindle machine tool*. In: *International symposium on Advanced Engineering & Applied Management - 40th Anniversary in Higher Education : Romania /Hunedoara/ 4-5 November, 2010*. - Hunedoara: Faculty of Engineering Hunedoara, 2010. - ISBN 978-973-0-09340-7. - III-99 - III-104.
- [11] Balmont, V.B. - Russkich, S.P.: *Rasčet radialnoj žestkosti radialno - upornogo podšipnika*. *Trudy instituta. M., Specinformcentr VNIPPa, 69, 1978, č.1, s..pp. 93 - 107.*

6. ACKNOWLEDGMENT

As shown calculation maximal speed and rigidity bearings depend on arrangement radial ball bearings with angular contact in bearings nodes. Depend arrangement radial bearing in nodes change preload and temperature in bearings. It has very big influence to maximal speed and rigidity for all SBS.

The applied software technology has been used in the industry to improve the working accuracy of the machine tools made by TOS Trenčín-Slovakia, for SN and SPSI type lathes, (2), and to design the boring headstocks for the modular single-purpose machine tools made by TOS Kuřim-Czechoslovakia, (5) TOS Lipník, SKF, GMN and INA Skalica. The programme is very effective and reliable and t comparison of the results between experiments and calculations show good correlation, never exceeding 10 %.

Authors:

Prof. Eubomír Šooš, PhD.

MSc. Peter Križan, PhD.,

MSc. Miloš Matúš,

Slovak University of Technology in Bratislava, Faculty of Mechanical Engineering, ÚSETM, Nám. Slobody 17, 81231 Bratislava, Slovakia,
 Phone.: +421 2 572 96 537, Fax: +421 2 524 97 809.

E-mail: lubomir.sooš@stuba.sk,
peter.krizan@stuba.sk;
milos.matus@stuba.sk;

11th INTERNATIONAL SCIENTIFIC CONFERENCE
MMA 2012 - ADVANCED PRODUCTION TECHNOLOGIES

PROCEEDINGS



Section C:
**METROLOGY, QUALITY, FIXTURES,
METAL CUTTING TOOLS AND TRIBOLOGY**

Novi Sad, 20-21 September 2012

Antić, A., Šarić, T., Živković, A.

ANALYSIS ON THE METHOD AND DEVELOPMENT OF THE MODEL FOR THE TOOL WEAR CONDITION MONITORING SYSTEM

Abstract: *The paper presents the acquisition and signal processing methods for separating significant features which are the topic of contemporary research in order to increase the efficiency of the tool monitoring system. The research and development of such system imposes a demand to find a fast and secure monitoring of the tool wear condition in the turning process. To fulfil the set demands for solving the set problem, a concrete tool monitoring system model is presented, following the requirements specified for the contemporary monitoring systems. The presented solution utilizes the vibration accelerating sensor set in the close range to the cutting zone, on the tool shank, which is then used to separate the features for the tool condition identification.*

Key words: *Tool wear, sensors, signal processing*

1. INTRODUCTION

The realization of the constantly present requirements demands to increase the degree of reliability and flexibility of the processing system all the time insuring the set product quality. In that sense, one of the most significant tasks imposes the development of the system for tool monitoring and processing that will be able to identify the condition of the tool and the processing system in the real time [1]. The fulfilment of the set demands for the product cost rationalization enables the usage of new technologies. Active participation of a larger number of researchers in overcoming the present problems has directed the research focus on topics such as the following: selection of the sensor type [2], sensor fission and the application of a multi-sensor system, signal processing and the choice of the function for selecting the sensor signal / feature separation [3], experiment design and setting [4], and selection of an artificial intelligence technology [5]. Designing a system for tool and process monitoring in machining systems is problem-oriented. Therefore, the selection of a sensor system and sensor properties is closely related to the specific characteristics of the machining operations.

Contemporary intelligent systems for tool wear monitoring in the cutting processes should have good enough properties in order to replace and improve the conventional systems and should allow the possibility for continual, fast and precise determination of tool wear condition, in order to:

- Increase the degree of safety of a processing system, especially important in the situations of high wear degree and tool fracture,
- Enable the optimization of processing parameters considering the demanded tool stability, and considering the technological process limitations,
- Insure the necessary dimensional workpiece stability and the quality of the processed surface,
- Additionally rationalize the production costs.

2. GENERAL DEVELOPMENT PROPERTIES OF THE TOOL MONITORING SYSTEM

Respecting the set demands, one of the possible solutions for the development of an intelligent monitoring system comprises the following key steps, illustration on Fig. 1 [6]:

- **Sensor selection:** The cutting process can be characterized by diverse physical values. The adequate sensors, such as dynamometers, AE sensors, momentum, power/stress sensor, temperature, and the like transform the physical quantifications into appropriate electric signals. It is important to consider the reliability of each sensor, the price and the purpose in order to select the most appropriate sensor system to monitor a certain phenomenon.
- **Signal processing:** Signal processing can be more or less complex. It is related to amplifying and filtering the signal (analogue low-pass frequency, wide band-pass, or high-pass frequency filters). Sampling frequency is limited by the acquisition device properties and it has to be considered in order to avoid disturbances. Furthermore, the application of digital signal processing using digital filters and the signal segmentation operation are considered to be able to remove (withhold) a part of signal being of interest.
- **Feature separation:** Sensor signal has to be transformed with the possibility to describe the signal in an adequate, satisfying manner. Many diverse methods are being used for this purpose, like time domain, frequency domain and wavelet domain.
- **Feature selection / significant feature choice:** In order to develop a robust and reliable monitoring model, it is important to use the properties that best describe the machining process. The function of selecting and separating features presents two methods that enable the definitions of the most useful sensor properties.

- **Process of modelling the available knowledge.**

- (a) Setting the experiment: Performing the processing experiment, as well as modelling, present the economically expensive and long-term processes, so the well designed experiment has to enable the application of the acquired knowledge onto a monitoring system in the industry.
- (b) Artificial intelligent methods: Monitoring systems demand for reliable models capable of being trained for complex non-linear relations between the variable process performances and variable machining processes. The adequate selection of an AI method has a key significance for developing reliable processing models. This selection mostly depends on the number of experimental samplings, stochastic process nature, demanded model accuracy, explicit or implicit model nature, and previous knowledge

on the technical process.

Integration of the sensors for monitoring and for process control is an approach expected to have a great impact on the production in a period to come [2]. In practice, two monitoring methods are generally accepted: direct and indirect. Direct methods include laser, optical and ultrasound sensors that enable direct measuring of the tool wear condition. These methods are still very expensive and have a limited application in production surroundings [3]. On the other hand, indirect methods are more economic for the machining process monitoring since they use sensors that define the machining process condition by measuring the cutting forces, vibrations, temperature, power consumption, etc. In practice, there are four types of sensors that are widely applied in monitoring the machining process condition; these are dynamometers, accelerometers, AE sensors and power sensors.

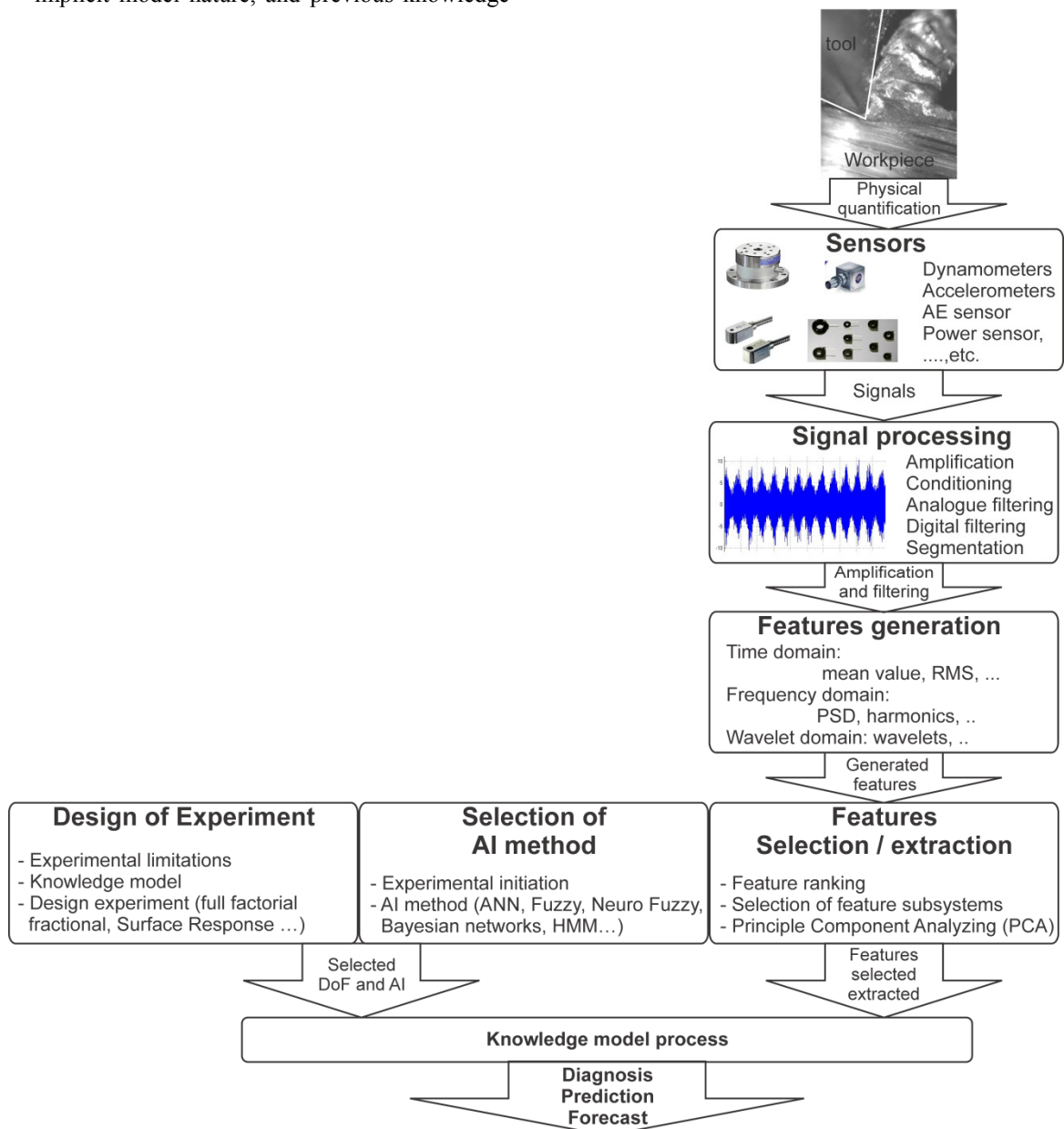


Fig. 1. General model for the development of an intelligent system for tool and machining process monitoring

3. MODEL FOR THE TOOL WEAR MONITORING SYSTEM

The application of prior experiences in the development of diverse system models based on the application of artificial intelligence and presented in the read papers has served as a good starting foundation for the development of a new model. Considering the previously stated facts in the introduction, the following demands have been set for the development of a new laboratory system:

- Usage of a sensor for vibration acceleration measuring in order to properly detect dynamic properties of the cutting process and implement them into the monitoring system.
- Usage of new algorithms in the application of artificial intelligence in the field of tool wear monitoring based on the application of a priori knowledge on the tool wear condition.
- Finding a satisfactory manner to separate the vector of input properties by applying transformations in the time-frequency domain.

On applying and including these demands, the model for the tool wear monitoring system has been developed and it is presented in Fig. 2.

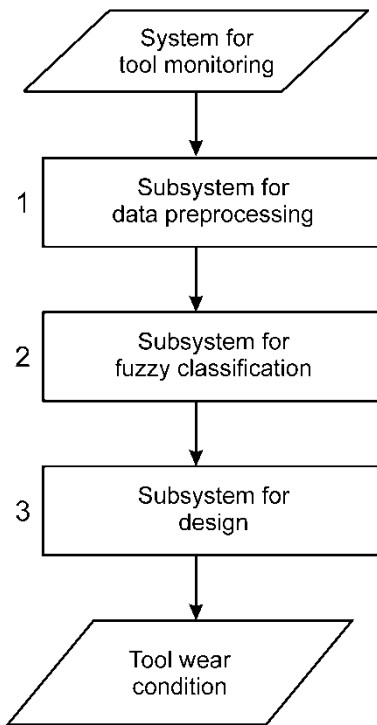


Fig. 2. Algorithm of the developed system

System model can essentially be observed through three segments unified in an entity. The developed segments (subsystems) of the tool wear monitoring system are the following:

- Subsystem for data preprocessing,
- Subsystem for fuzzy classification,
- Subsystem for design.

3.1 Development of the subsystem for preprocessing

The structure of the subsystem for preprocessing can be observed through three phases. In the first phase known as the data fuzzy-acquisition, data acquisition is

performed from the sensors, together with the selection of the filtering band. In the concrete case, the application of the low-frequency Butterworth filter, the filtering of diverse types of noises that deform the measuring signal is performed.

The selection of the filter type primarily depends on the type of the monitored signal, tool properties, machine properties, workpiece properties, processing parameters, as well as other processing conditions.

Within the performed research, the “Leung-Malik” LM set has been used for filtering the vibration signal spectre since it presents a multi-scale and multi-oriented filter bank with 48 filters. Two versions of the LM filter bank have been considered. The filters occur in the basic scale $\sigma = \{1, \sqrt{2}, 2, 2\sqrt{2}\}$. On the application of the first and second derivative, filters occur in first three scales with the elongation factor of 3 (i.e. $\sigma_x = \sigma_y$ and $\sigma_x = 3\sigma_y$). Laplace operator occurs in four main scales, while 8 filters occur in $\sigma = \{1, \sqrt{2}, 2, 2\sqrt{2}\}$. The large LM (LML) filters occur in the basic scale $\sigma = \{\sqrt{2}, 2, 2\sqrt{2}, 4\}$ [7]. The expended filter bank is presented in Fig. 3.

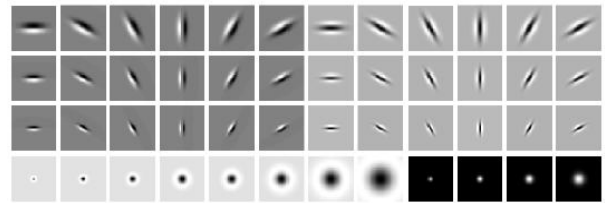


Fig. 3. Leung-Malik (LM) filter bank [7]

3.2 Defining the input property vector

Considering the observed methods for feature separation presented in the existing literature, i.e. considering the applied solutions for input property vector separation and the statement that this is not properly and adequately applied, this paper has selected the following statistic parameters for the input vectors of the system: mean value, mean value deviation, asymmetry coefficients (Skewness) and excess coefficients (Kurtosis), in statistics known as central moments. For continual uni-variation distribution of probability with the probability density function $f(x)$, the mean value moment is μ .

$$\mu(k) = E \left[(X - E(X))^k \right] = \int_{-\infty}^{+\infty} (x - \mu)^k f(x) dx \quad (1)$$

Since the distribution function is unknown, the expectation assessment is performed, where:

$$\hat{E}(x) = \frac{1}{N} \sum_{i=1}^N x_i \quad (2)$$

$$\hat{\mu}(x) = \hat{E} \left[(X - \hat{E}(X))^k \right] = \frac{1}{N} \sum_{i=1}^N \left(x_i - \frac{1}{N} \sum_{i=1}^N x_i \right)^k \quad (3)$$

The moment of generated function of the random variable X can be written as:

$$M(t) = M_X(t) = E \left[e^{tX} \right] \quad (4)$$

where t is a real number, and one should bear in mind that $M(t) = 1 + tX + t^2 X^2/2! + t^3 X^3/3! + \dots$ if $\mu_n = E(X^n)$

is the n -th moment of X ; hence, one can write the expectation:

$$M(t) = 1 + \mu_1 t + \frac{\mu_2 t^2}{2!} + \dots + \frac{\mu_n t^n}{n!} + \dots + \quad (5)$$

Since the coefficient t^n in the Taylor's order $M_n(0)/n!$, where M_n is the n -th derivation from M , and then $\mu_n = M_n(0)$. The characteristic function is approximated via moments, and moments present the input property vectors for the fuzzy classifier. Distribution is obtained on the basis of first four moments for the frequency spectre bands on applying the Discrete Fourier Transform (DFT). On the filtered signal, the Discrete Fourier Transform has been performed and the obtained spectre form is presented in Fig. 4.

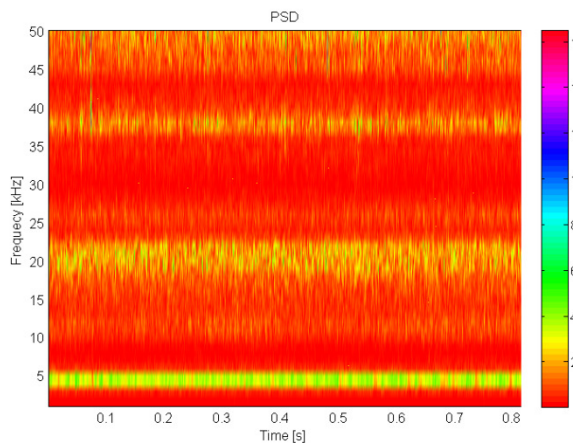


Fig. 4. Spectrogram of the filtered signal

For further analysis from the obtained signal spectrogram, the upper part of the signal spectre, the high-frequency segment marked on the Figure, has been separated due to the set hypothesis that there are discriminative features characterizing the cutting tool wear condition in that spectre segment.

By separating the upper band of the signal spectrum, Fig. 5, the observation is focused only to that spectre segment. By applying this method, the influence of the PSD is decomposed, thus increasing the feature discrimination applied in the fuzzy classifier.

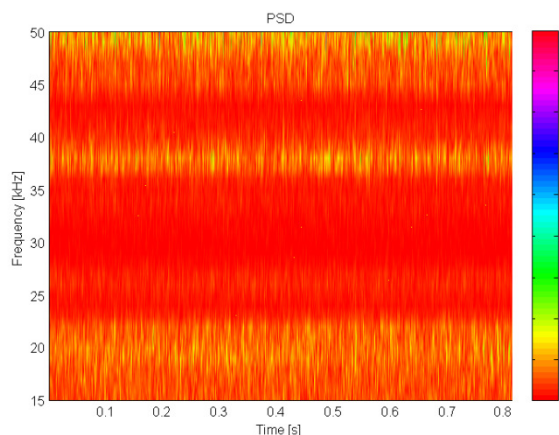


Fig. 5. Separated range of the signal spectre

4. CONCLUSIONS

The presented problems in the paper include the observations on the influence of tool wear onto: (i) the segmentation and formation of the certain chip shape; (ii) the development of vibrations in the close range to the cutting zone which occur due to the chip segmentation shape; as well as (iii) the development of a fuzzy classifier for the continual monitoring of the cutting tool wear during the turning process, based on the application of indirect monitoring methods. The continual tool wear process monitoring is considered to be one of the most complex methods whose applicable industrial solutions are still not on the desired level. The selection of the signal for tool wear monitoring is one of the most significant segments in the development of the tool monitoring system.

ACKNOWLEDGEMENTS

This paper presents a segment of the research on the project number TR 35025, financed by the Ministry of Education and Science of the Republic of Serbia, and research over our of mobility and scholarships in the scope of the network CEEPUS III RO 0202.

5. REFERENCES

- [1] Antić, A., Petrović, B.P., Zeljković, M., Kosec, B., Hodolić, J.: *The influence of tool wear on the chip-forming mechanism and tool vibrations*, *Materiali in tehnologije/Materials and technology* 46 (3), pp.279–285, 2012.
- [2] Zhou, Y, Orban, P, Nikumb, S.: *Sensors for intelligent machining-a research and application survey*. In: *Systems, man and cybernetics IEEE international conference on intelligent systems for the 21st century 2*, pp.1005–1010, 1999.
- [3] Ertekin, Y.M, Kwon, Y, Tseng, T.L.: *Identification of common sensory features for the control of CNC milling operations under varying cutting conditions*. *International Journal of Machine Tools and Manufacturing* 43, pp.897–904, 2003.
- [4] Zhang, J.Z., Chen, J.C.: *The development of an in-process surface roughness adaptive control system in end milling operations*, *International Journal of Advanced Manufacturing Technology* 31, pp.877–887, 2007.
- [5] Abburi, N.R., Dixit, U.S.: *A knowledge-based system for the prediction of surface roughness in turning process*. *Robotic and Computed Integrated Manufacturing* 22, pp.363–372, 2006.
- [6] Jose, V., Abellan-Nebot, F., Romero, S.: *A review of machining monitoring systems based on artificial intelligence process models*, *International Journal of Advanced Manufacturing Technology* 47, pp. 237–257, 2010.
- [7] Leung, T., Malik, J.: *Representing and Recognizing the Visual Appearance of Materials using Three-dimensional Textron*, *International Journal of Computer Vision* 43 (1), pp. 29-44, 2001.

Author: DrSc Aco Antić, Assist. Prof., MSc Aleksandar Živković, Assistant, University of Novi Sad, Faculty of Technical Sciences, Novi Sad, Serbia.

DrSc Tomislav Šarić, Professor, J. J. Strossmayer University of Osijek, Mechanical Engineering Faculty in Slavonki Brod, Croatia.

E-mail: antic@uns.ac.rs, acoz@uns.ac.rs, tsaric@sfsb.hr

Assenova, E., Kandeveva, M.

TRIBOLOGY and SELF-ORGANIZATION

Abstract: As indicated by tribology, friction and wear are monitored by the behavior of the third body, which divides and unifies contacting bodies. Adaptation to the dynamic conditions of contact interaction is often realized by self-organization and synergy mechanisms. One of the phenomena of self-organization - the selective transfer of material between the friction surfaces, leads to reduced wear and friction in the contact zone. The problem is significant seeing that investigations of the selective transfer resulted in development of new lubricants, wear-resistant and self-healing materials and coatings used in exposed operating conditions, as in aircraft, mining industry, space research, etc.

Key words: tribology, contact interaction, self-organization phenomena

1. INTRODUCTION

Being the science and engineering of surfaces in contact, tribology studies the processes in contact systems with emphasis on processes in the contact, i.e. in the interface between solid surfaces or between a surface and a fluid. The interaction of “contact systems” with the environment and the exchanged mass-, energy- and information flows make of them “immersed systems”, so their behavior becomes informative if only they are regarded as imbedded into their milieu. Self-organization is the spontaneous creation of a pattern out of the local contact interactions. The usefulness of tribological investigations in self-organization resides in the comprehension that the contact body could be “trained”. Under specified circumstances, structures of the contact body can be formed spontaneously like surface arrays of clusters with wished micro- and nano-size and spacing [1÷4]. The spontaneity is consequence of an impact given by the researcher of the process, stimulating the release of internal mechanisms for the formation and maintenance of those structures, in accord with the validity of the principle for minimal entropy production, which determines the self-coordination of the flows of energy dissipation, heat, absorbed energy, wear, temperature gradient, structure imperfections, etc. So the system is able to pass from one balance state to another one, more adequate to the external conditions [5]. The problem of the character and extent of the admissible external affect is sought in system ability to rearrange its structures and homogenize its elements in a manner to become most adaptive to the modified external circumstances.

The paper will focus on the phenomenon of self-organization during selective transfer of materials in the contact of friction surfaces and the tribological processes that take place during friction under conditions of selective transfer.

2. TRIBOLOGY and SELF-ORGANIZATION

2.1 Tribology

Overall said, tribology is the science of contact interaction, mostly concerning the processes of friction, wear, lubrication, hermeticity, contact conductance, etc. Tribology is defined as “The science and technology of interacting surfaces in relative motion and of the practices related thereto. Tribology encompasses the science and technology of friction, wear and lubrication, regarding processes related to physics, mechanics, metallurgy and chemistry [6]. The term was introduced in 1966 by Prof. H. Peter Jost, then the chairman of a working group of lubrication engineers, in his published report for the UK Department of Education and Science [7]. It was reported that huge sums of money have been lost in the UK annually owing to the consequences of friction, wear and corrosion. As a result, several centres for tribology were created in many countries. Since then, the term has diffused into the international engineering field. Tribological studies involve the efforts of mechanical engineers, material scientists, chemists and physicists – tribology is an interdisciplinary science [8]. Some of the results are new materials, like composites [9] and coatings [10] with improved tribological properties or new design approach [11]. Many new areas of tribological studies have been developed that are at the interface of various scientific disciplines, and various aspects of interacting surfaces have been the focus of tribology, for example, nanotribology, biotribology, the tribology of magnetic storage devices and microelectromechanical systems (MEMS), green tribology (ecotribology), etc. [8]. The research in these areas is driven mostly by the advent of new technologies and new experimental techniques for surface and interface characterization.

2.2 Self-organization

A basic tribological conception is that friction and wear are most easily monitored and controlled by means of the behavior of the thin material layer – the third body – which divides and unifies sliding, rolling

and impacting bodies. If the original contact pair does not possess a separate intermediate layer, its formation can be evoked by the contact processes themselves. An ambition of tribology is either to find out an optimal material – that third body, which to be put in the contact, or to predict the succession of events and phenomena by means of which the contact shall form its own protective layer.

Adaptation to the variable and complicated conditions of contact interaction of tribo-couples is realized by self-organization and synergy mechanisms. Synergy, may be defined as two or more agents working together to produce a result not obtainable by any of the agents independently. In fact, a system constitutes a set of interrelated components working together with a common objective: fulfilling a designated need [5,12].

Self-organization is related to open systems. Tribosystems are considered as open systems exchanging material, energy and information with the milieu. The ability of a system “to forget” the external perturbations is related to a specific organization of the system – self-organization. Due to the flow of mass, energy and information towards and from the system and far from equilibrium, new structures arise (new patterns like clusters, micro- and nano-clusters). Their formation is characterized by spontaneity. Furthermore, it is intentional, not fully arbitrary. The aim of the system is to survive in spite of the external perturbation [13]. The latest only stimulates (unlocks) internal mechanisms in the system, as a result of which the new structures are formed.

In tribology there are many effects connected to self-organization: the effect of extremely low friction after irradiation of the surfaces with alpha-particles or ultrasound; the effect of selective transfer of material between the contacting surfaces; the effect of surface-active additives in lubricants which cause decrease of surface strength; the effect of autovibrations, etc. In all cases formation of new structures is observed – these are secondary protective surface structures [1÷5,13]. The study of the secondary protective surface structures is a central question in the study of self-organization. The problem of optimizing the tribosystem is related to the possibility of optimizing the conditions, under which the system being introduced in operating regime, forms secondary protective structures. Generally, the affect is on the working surface (material, preliminary structure) and on the conditions of the process, in such way that the internal for the system factors of its self-organization could be switched on.

3. SELECTIVE TRANSFER

D.N. Garkunov and G. Polzer are of the first researchers of the selective transfer of material during friction of Cu-containing contact surfaces with special surface-active substances, the corresponding formation of the “servovite layer” (notion adopted as per analogy with the contact in animal articulation), and the resultant high reduction in friction and wear [2,3,14,15]

Characteristic for the selective transfer in tribology applications is the fact that an inoxidable layer with low shift resistance is formed in the contact. This

protective layer cannot accumulate dislocations and is highly antifrictional. The self-organization phenomena depend on the interface energy and the material exchange with the environment. Generation of that layer requires special combination of materials of the contact surfaces, as well as special lubricant between them. Conditions for the continuous reproducibility of the layer are also needed because of its short life in the contact body. Thus, synergy effect in the forming of new contact structures in the contact between surface materials and lubricant appears to be desirable as optimization of the contact couple.

Many studies on selective transfer [2,3, 14÷17] were conducted with bronze, brass and copper specimens in alcohol-glycerin mixture. Investigations showed that selective transfer exists on the contacting surfaces of almost all constructive steels. Ultra-low friction is also obtained rapidly with the friction-induced films on steel, chemisorbed from MoDTP solution, a layer of MoS₂ being transferred [18].

Reassigning models and methods of the ordered classical sciences to the basics of new interdisciplinary sciences is difficult and suspicious. The main difficulty is in the generalization of the concepts and the formulation of the tasks, which should permit the usage of well-known classical procedures. As a result the real complex system is being replaced by a model assumed to be equivalent, and its macroscopic behavior should on the average correspond to the observed macroscopic relationships.

4. ILLUSTRATION ON SELECTIVE TRANSFER APPLICATIONS

Antifriction and antiwear effects resulting from the selective transfer processes are shown below.

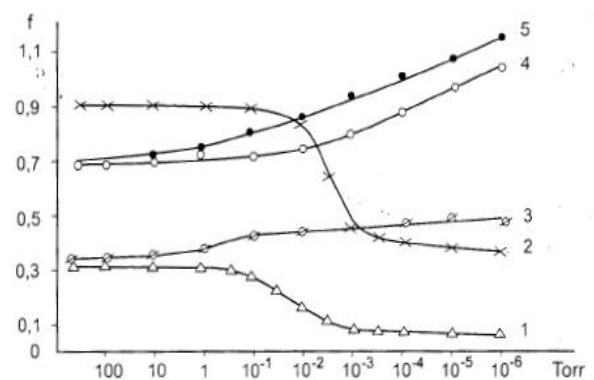


Fig.1 Friction coefficient vs. vacuum degree for various tribocouples; 1- lead bronze/Ti alloy; 2 – Fe/Pb; 3 – graphite bronze/Al; 4 – Cu/Steel; 5 –Be

The first example is extracted from the common work between the Space Research Institute of the Bulgarian Academy of Sciences and the Tribology Centre – Sofia in the study of the properties of new antifriction materials adaptable to friction conditions. One of the most interesting materials (Fig 1) for vacuum (also for UHV) is **lead bronze** [19]. The structure of the material is on copper basis (solid solution of α -copper

and Cu_3P , alloyed with Mn and P), and contains lead configurations in the form of globular clusters. Friction and wear properties were studied by means of the developed by the team vacuum tribometer [19,20]. During friction, lead comes on the surface and forms thin intermediate layer, acting as a lubricant. The X-ray microanalysis of the surface shows that at friction under atmospheric conditions the friction layer contains lead oxide, and under vacuum – it is a friction layer of metallic lead. The antifriction properties result by the quantity, distribution and form of lead components. At vacuum was obtained a significant decrease of friction and wear intensity. The contact pressure has been found, at which the surrounding atmosphere cannot manage with the formation of regenerated secondary structures on the surface after their abrasion, and the system enters the pathological regime.

Next example shows the influence of **electric current** in selective transfer. Diverse processes which take place on contact surfaces as a result of the selective transfer become more complicated under the effect of electric current. Experiments show that electric current in the initial stage makes surfaces covered with an extremely thin copper layer [21]. The copper film formation rate and its thickness are functions of the current density and direction. Overall said electric current intensifies the selective transfer.

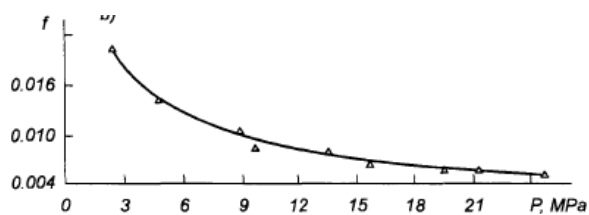


Fig. 2 Coefficient of friction f vs. specific load P at sliding speed $V= 1.6$ m/s; running-in process, steel-bronze couple, and galvano-electromagnetic force in the glycerin as lubricant [21]

The surface passivation in selective transfer accompanied by formation of a plastic copper film on both copper alloy and steel is determined to a greater extent by electrochemical processes of selective dissolution of the copper alloy and transfer of dispersed copper particles to the steel surface. In this case also the synergy effect of both agents – surface material and lubricant – is observed. A favorable combination of materials of contact pairs (bronze-steel) and lubricant (glycerine, oils with surfactant additives) results in spontaneous origination of intermediate layers on the contact surfaces which produce the minimum friction.

Below follows an example of increasing the antiwear properties of lubricants. The quantitative transition from rough- to ultradispersion of copper particles leads to considerable qualitative changes of the maintenance properties of metal-plating lubricants. This is a new generation of multifunctional additives on the basis of copper and its oxide of colloidal dispersion. Interesting results regarding the antiwear characteristics of the lubricant were attained in the tests of the influence of additives on gear oils (Fig.3). While using the

ultradispersed CuO additive in motor oils, redox reactions take place. Copper oxide reduces to free copper. Transfer and adhesion of their particles to the sliding surfaces occurs, particularly to surface defects and irregularities [17].

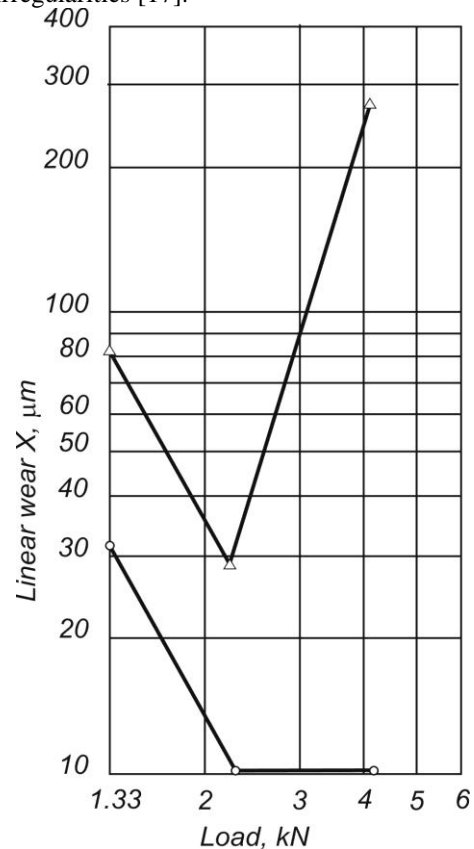


Fig. 3 Wear vs. load for Transsol SP-10 gear oil; Δ) reference oil; \circ) reference oil + 0.006% ultradispersed CuO [17]

5. CONCLUDING REMARKS

The paper aims to emphasize the existence of self-organization and the possibility to optimize contact systems through the observation and investigation of the processes related to self-organization and selective transfer between the contacting surfaces.

In tribology we consider ways of optimization of the behavior of contact systems influencing the contact body. The contact joint is under dynamic, variable, often exposed conditions. So, the contact is in crisis. The system wants to protect itself and to survive in these conditions, i.e. to keep its integrity. Responsible for the survival is the contact. We help the contact through tribology either by finding out the optimal material – that third body, which to be put in the contact, or by predicting the succession of events and phenomena by means of which the contact shall form its own protective layer. In the first case, based on previous experience and knowledge, we find optimal material surfaces with or without coating and/or suitable intermediate layer between them (e.g. lubricant). The second case is related the opportunity to use self-organization processes in the contact body. They are connected to the adaptation of the tribosystem to the variable/dynamic conditions and are realized by self-organization and synergy mechanisms.

The **synergy** corresponds to the mutual work of two or more agents working together to produce a result not obtainable by any of the agents independently. At the **self-organization**, due to the flow of mass, energy and information towards and from the system, arise with **spontaneity** new structures – secondary protective surface structures. Their formation is intentional, not fully arbitrary. The aim of the system is to persist and keep on functioning in spite of the external perturbation. The later only stimulates (unlocks) internal mechanisms for the formation of the new structures.

The investigations of self-organization in the mode of selective transfer of materials have lead to the development of new lubricants, self-lubricating, wear-resistant and self-healing materials used in friction joints in exposed operating conditions, as in aircraft, mining industry, space research, etc.

ACKNOWLEDGEMENT

The paper is related to the activities of the **International Faculty Agreement** between the Faculty of Mechanical Engineering at the University of Belgrade, Serbia and the Faculty of Industrial Technology at the Technical University of Sofia, Bulgaria

6. REFERENCES

- [1] Manolov, N., Assenova, E., Danev, K., Über die Modellierung von selbstorganisierenden Tribo-systemen. Forschungswerke des Seminars “Neue Prinzipien und Prüfmethode in der Tribotechnik”, Zwickau, 1989.
- [2] Garkunov, D.N., *Tribology based on self-organization*. Proc. Int. Conf. BULTRIB’12, Sofia, 2012.
- [3] Meissner, F., Polzer, G., Grundlagen zu Reibung und Verschleiss. VEB Deutscher Verlag für Grundstoffindustrie, Leipzig, 1976.
- [4] Nosonovsky, M.: *Entropy in Tribology: in the Search for Applications*, Entropy, 12, p.p.1345-1390, 2010.
- [5] Assenova, E., Kandeve, M., Self-organization in tribology: the role of synergism and selective transfer, 7th International Conference on Tribology BALKANTRIB, p.p.305-310, Thessaloniki, 2011.
- [6] Kajdas C.K. et al., *Encyclopaedia of Tribology*, Elsevier, 1990.
- [7] *Historical Review. Tribology: How a word was coined 40 years ago*. Tribology & Lubrication Technology, pp. 24-29, March 2006, http://www.kluberfood.com/pdfs/tlt_tribology_just%203-06.pdf
- [8] Assenova, E., Majstorovic, V., Vencl, A., Kandeve, M., *Green tribology and quality of life*, International Convention on Quality 2012, Belgrade (Serbia), 05-07.06.2012, Proceedings, p.p. 32-38, Published in: Advanced Quality, 40, 2, p.p.26-32, 2012.
- [9] Marinković, A., Vencl, A., *Influence of the solid lubricant particles reinforcement on composites tribological properties*, Proceedings of the 11th International Conference on Tribology – SERBIATRIB ‘09, p.p. 78-83, Belgrade (Serbia), 13-15.05.2009.
- [10] Vencl, A., Mrdak, M., Cvijović, I., *Microstructures and tribological properties of ferrous coatings deposited by APS (Atmospheric Plasma Spraying) on Al-alloy substrate*, FME Transactions, 34, 3, p.p. 151-157, 2006.
- [11] Rac, A., Vencl, A.: *Tribological and design parameters of lubricated sliding bearings*, Tribology in Industry, 27, 1-2, p.p. 12-16, 2005.
- [12] Haken, H., *Synergetics, an Introduction: Nonequilibrium Phase Transitions and Self-Organization in Physics, Chemistry, and Biology*, 3rd rev. enl. ed. New York: Springer-Verlag, 1983.
- [13] Heylighen, F., *The Science of Self-organization and Adaptivity*, in: L. D. Kiel, (ed.) Knowledge Management, Organizational Intelligence and Learning, and Complexity, in: The Encyclopedia of Life Support Systems (EOLSS), Eolss Publishers, Oxford, 2001.
- [14] Garkunov, D.N., Kragelskii, I.V., *Selective Atomic Transfer*, Scientific Discovery Diploma No. 41, in: USSR Discoveries for 1957-1967, Moscow, TsNIPI, p.p.52-53, 1968 (in Russian).
- [15] Polzer, G., Tserma, Assenova E., *Frictional coatings under conditions of selective transfer*. Proc. Int. Conf. BULTRIB’12, Sofia, 2012.
- [16] Garkunov, D.N., *Triboengineering (wear and non-deterioration)*. Moscow Agricultural Academy Press, Moscow, 2000.
- [17] Shpenkov G.P. *Friction Surface Phenomena*, Tribology Series, 29, Ed. D. Dowson, Elsevier, 1995.
- [18] Martin, J.M., Le Mogne, Th., Grossiord, C., Palermo, Th., *Adsorption and friction in the UHV tribometer*, Tribology Letters, vol.3 No. 1, p.p. 87-94, 1997.
- [19] Simeonova, Yu., Guizdova, N., *Antifriction parameters of lead bronze at dry friction in vacuum*, J. Balkan Tribological Association, vol.2, No. 3-4, p.p.186-189, 1996.
- [20] Simeonova, Yu., Danev, K., Guidikova, N., Assenova, E., Guizdova, N., *Study of basic parameters of some metals and alloys under dry friction vacuum conditions*, J. Balkan Tribological Association, vol.1, No. 1-2, p.p.156-159, 1995.
- [21] Shpenkov, G.P., Podalov, A.N., and Chelyshev, A.P. Vestn. Akad. Nauk BSSR, Ser. Fiz-Tekh. Nauk, No. 3, p.p.59-62, 1973 (in Russian).
- [22] Garkunov, D.N., Kharkhasov, B.D., Shpenkov, G.P., *An Antifriction Lubricant*, USSR Inventor’s Certificate 690063, MKI C 10 M 5/02. Otkryt. Izobret., No. 37, 1979 (in Russian).
- [23] Garkunov, D.N., *Scientific Discoveries in the Field of Wear-Free Friction and Hydrogen Wearing Process in Solving Problems of Green Tribology and Global Climate Improvement*, Int. Scientific-Practical Conf. “Tribology and Ecology”, Moscow, 2010.
- [24] Kornik, P., *Experience in the application of tribo-technical works to the mining enterprises of Kazakhstan*, Proc. Int. Conf. BULTRIB, Sofia, 2012.

Authors:

Assoc. Prof. Dr. Emilia Assenova, M.Sc., The Society of Bulgarian Tribologists, Technical University of Sofia, Bulgaria, *E-mail:* emiass@abv.bg

Assoc. Prof. Dr. Mara Kandeve, M.Sc., Technical University-Sofia, Faculty of Industrial Engineering, Tribology Center; 8, Blvd Kl. Ohridski, 1156 Sofia, Bulgaria, *E-mail:* kandeve@tu-sofia.bg

Beju, L.D., Zeljković, M., Navalušić, S.

STRATEGIES FOR IMPROVING THE AGILITY LEVEL IN THE MANUFACTURING BEARING INDUSTRY

Abstract: The paper presents the results of a project focused on reducing wastes in the manufacturing bearing industry, which fits into the broader strategy of continuous improvement. The first stage consisted in the analysis of the companies' agility. Waste detection was done through questionnaires and production flow analysis. After determining the waste causes, a future Value Stream Map can be built with pull flow and kanban system. Finally, the analysis of the proposal implementation and the obtained results allows the underlining of the obtained savings.

Key words: lean manufacturing, kanban, value stream mapping

1. INTRODUCTION

The Toyota manufacturing system, developed by Taiichi Ohno, has as main purpose the continuous reduction and ultimately elimination of any form of waste. The companies implementing this system work with low inventories, reduced production times as well as low "lead time". They try to reduce the breakdown, to make the technological flux more fluid, to achieve zero defects, and so on. The JIT concept can be described as always having the supply of right parts in the right quantity in the right place and at the right time and it has revolutionised the management and organisation of businesses. It was applied at first primarily in the automotive industry, but it is nowadays also better spread in other branches of the industry and services.

Lean Manufacturing consists of a set of instruments, a management system or a philosophy, depending on the extent, the strategy and the development level of the organisation and of the organisational culture in which it is applied [2].

"Lean Manufacturing" is currently the most effective management model of the activities of an organisation.

The present paper endeavours to present a methodology for the analysis and improvement of the agility level in the bearing manufacturing industry.

2. ANALYSIS OF THE COMPANIES' AGILITY LEVEL

The initial step is to establish a clear sense of the need to change and improve. This vision must be built together with the top levels of the organisation management, but also had to be shared with all members of said organisation. A group of individuals was chosen to participate in this project.

In order to analyse the general agility of the company, a number of general indicators were firstly computed, such as the net profit, the return on investment (a percentage of the investment) and the cash flow (the amount of cash available for day to day operations), to name a few. Additionally, the

performance coefficients of the production process were computed: the throughput (the actual rate of sales generated by the system), the inventory (all the money invested in things that are intended to be sold) and the operating expense (money spent to convert inventory into throughput) [5]. This includes direct and indirect labour, materials, depreciation, administrative costs etc.

2.1. Questionnaire for evaluation of the company's agility

The next phase consisted in identifying the areas of interest upon which it was necessary to act. For this purpose a questionnaire was devised, evaluating the following fields: inventories, the team, processes, maintenance, layout and handling, suppliers, quality, scheduling and control.

The evaluation questionnaire contains questions for each analysed field. Each question has a set of possible answers. Depending on the answer selected in accordance with the situation, a number of points are granted. Finally, for each field a total is compiled, representing a certain stage on a scale from 0 to 100%. This percentage (the red curve in Fig. 1) is then compared with the target imposed by the company (the blue curve).

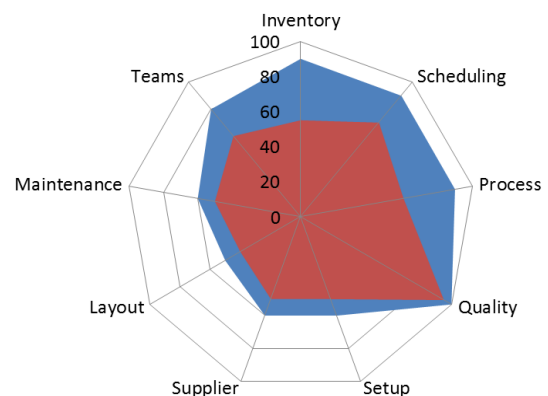


Fig. 1. Evaluation of the agility level of a bearing company based on questionnaires (target- blue; actual -red)

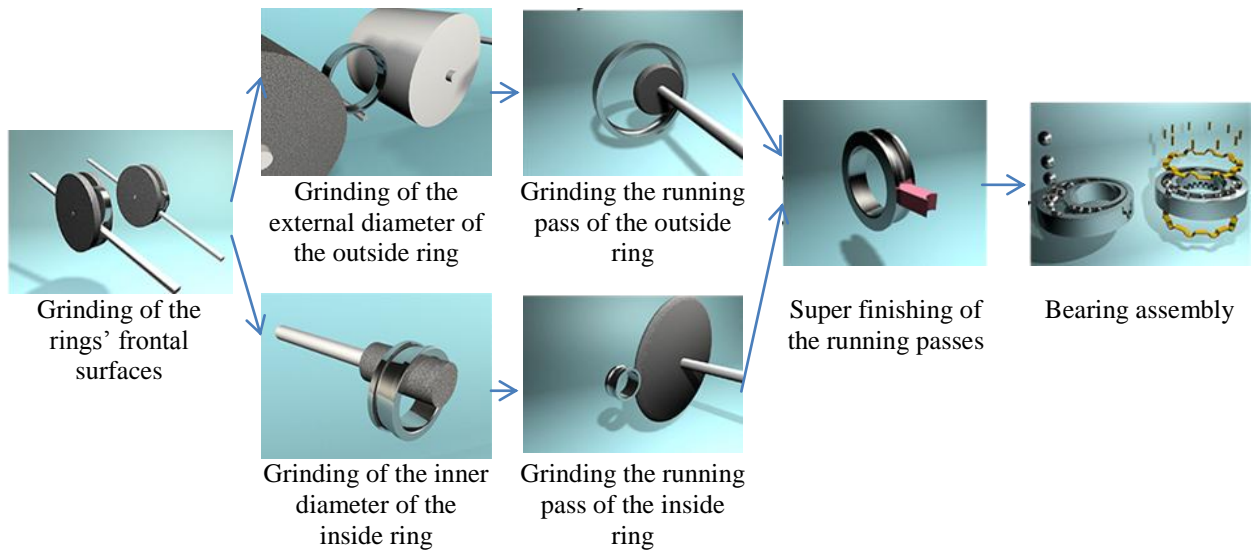


Fig. 2. Technological process for the manufacturing of the radial ball bearings

The field in which the difference between the current situation and the set goal is the highest is also the field in which most urgent action is required. The questionnaire was answered by managers on the top and intermediary level. From the analysis of the result, as shown in Fig. 1, it can be seen that the field requiring the first actions was the organisation of production, stocks and production planning. The improvement of the activity in this field could not be performed without a careful analysis of the existing technological process. The analysed process is the manufacturing of radial ball bearings. The necessary sequence of steps is shown in Fig. 2.

2.2. Actual Value Stream Mapping

The more detailed analysis of the production process implied building the Value Stream Mapping (Fig.3). Value Stream Mapping is an instrument for describing both material and informational streams within a production process, from the point of placing the order, to the shipment of the finite products [6].

The current state value stream mapping presents the push production stream with all the important parameters characterising it, more precisely: the outside sources of material with the order lead times, the mode of materials' shipment, including transportation

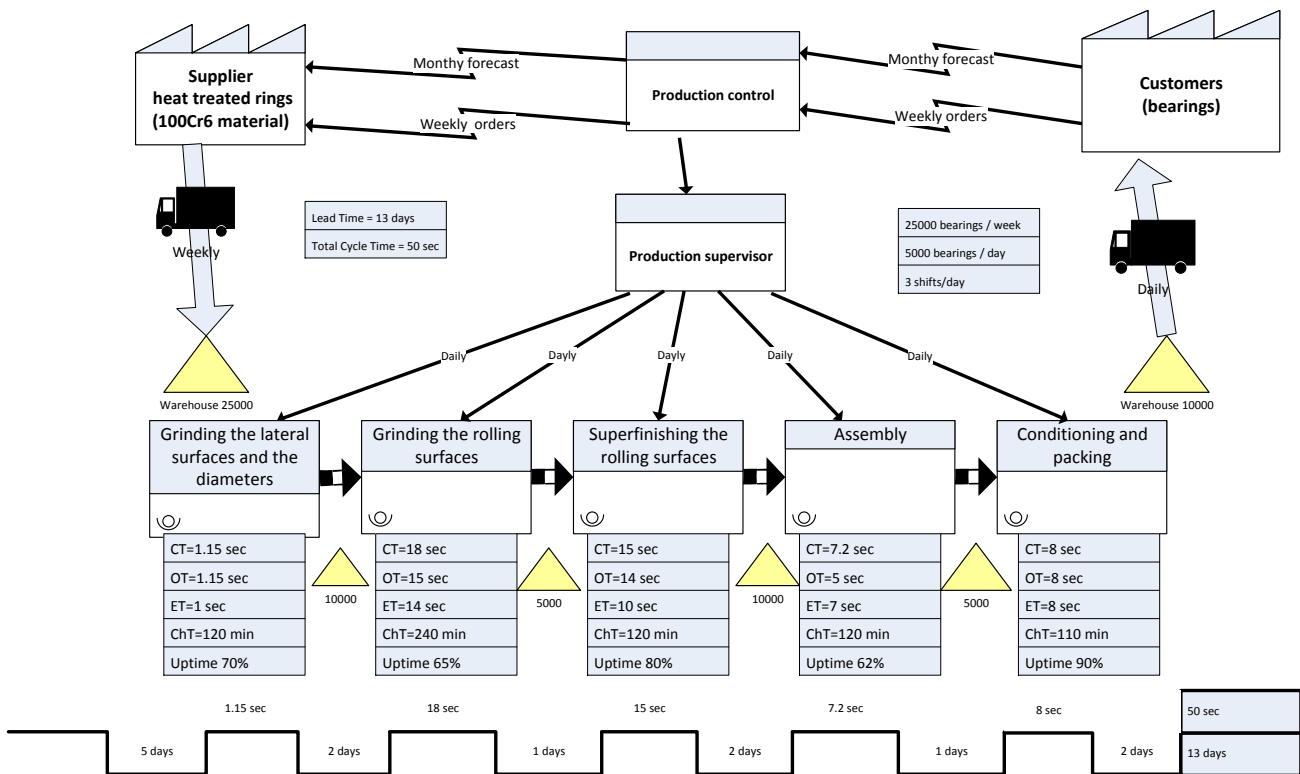


Fig. 3. Actual value stream mapping

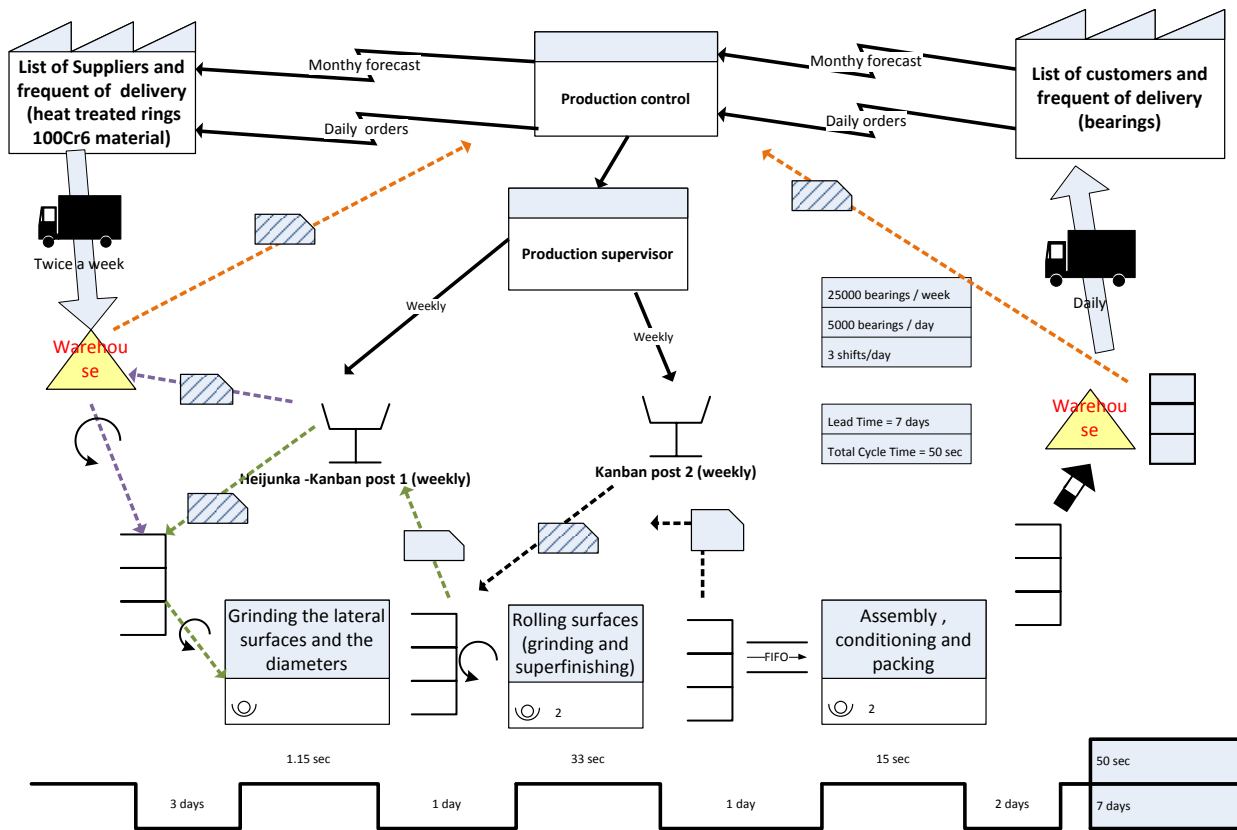


Fig. 4. Future value stream mapping

frequencies and time, receiving and inventory points (including the warehouse for received material, work-in-process, and finished goods inventory), production processes, flow of work-in-process between production processes, mode of shipment of finished product to the customers including transportation frequencies and time,. VMS shows also the current information flows (electronic or manual) which are part of the enterprise resource planning. Illustrations of the VSM current state is shown Fig. 3.

3. BUILDING A NEW VISION OF THE COMPANY

Based on the data on this map, the continuous improvement team set its goal to change the existing “push” type production stream with a “pull” type one, through the implementation of the Kanban production system.

The KANBAN system is an instrument that plays a key role in the JIT production system, and was developed by Taiichi Ohno at the Toyota Company [3]. A “kanban” is basically a card containing all the information required for the production and assembly of a product at each stage, and it details its path of completion [1]. The kanban system allows production and control scheduling, as well as inventory levels. This system facilitates a high production volume and high capacity utilization with reduced inventories, production time and work-in-process.

The analysis of the current VMS showed that bottlenecks are in tight connection with the grinding and super finishing of the rolling surfaces. These

machine tools are complex and they require a considerable amount of setup time for adjustment whenever the manufacturing changes. This made it impossible to create manufacturing cells that are dedicated to product families. Because of this, the production area was divided into three modules: one for grinding lateral surfaces and diameters, one for manufacturing the rolling surfaces, and one for assembly, conditioning and packing.

A Heijunka –Kanban post triggers production [4], as its main role is that of a pace maker of the production system.

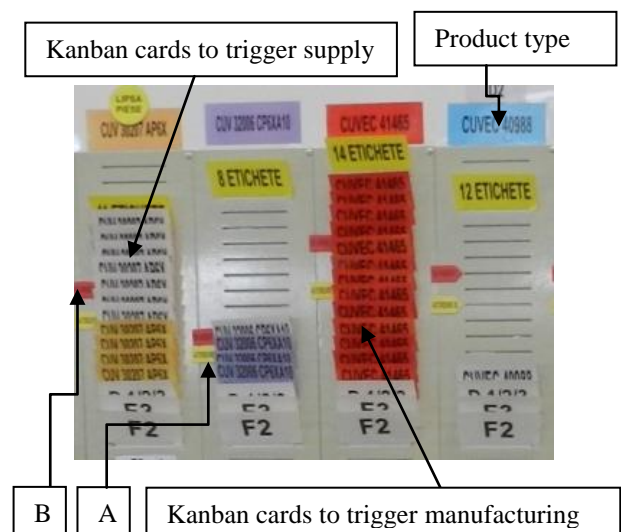


Fig. 5. Heijunka –Kanban post (detail)

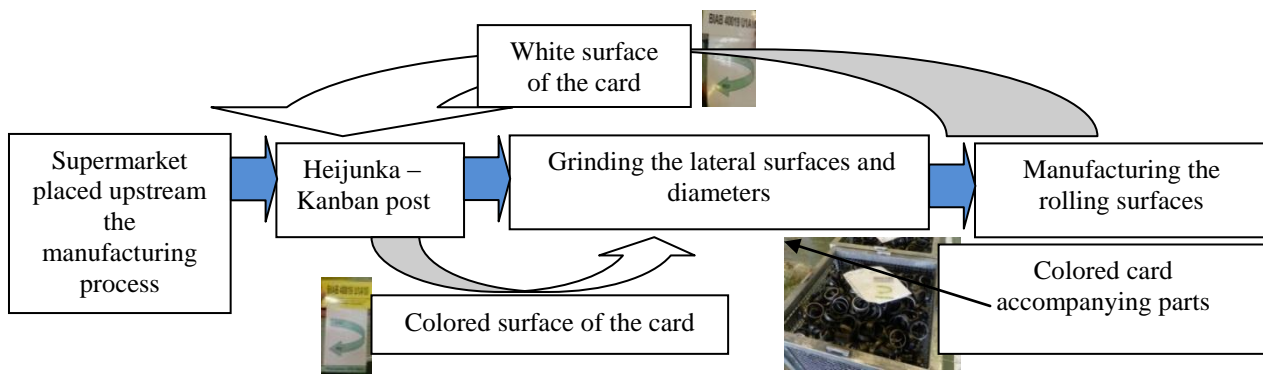


Fig. 6. Pull production system through the cards placed on Heijunka Kanban post

On the other hand, the same post regulates the supply of work pieces in the supermarket inventory that precedes production. This double role is played by the kanban cards, having meaningful symbols on both sides. The coloured side of the card triggers production, while the symbols on the opposite white side of the card indicate that the supermarket stock needs to be supplied. In Fig. 5, a fragment of the Heijunka – Kanban picture is presented. When the number of cards placed on the coloured side exceeds the yellow indicator (A), the type of products can start to be manufactured. When this number reaches the red indicator (B), the products must start working. A supply train that inspects the Kanban post every two hours takes the data from the cards that are placed with the white side facing out and supplies the supermarket stock upstream accordingly.

After applying the solutions found during the KAIZEN activity, the following conclusions were drawn:

- The **Lead time** decreased from 13 to 7 days.
- The visual management implementation using the Heijunka post brings visible improvements in production planning and each operator now has better access to information and can be better aware of the status of the production in a week.
- The use of “production Kanban” helps us to achieve a better accuracy in the time needed to fill the inventories, as well as better production management because of the implementation of “pull” streams using differently coloured Kanban cards.
- OEE (Overall equipment effectiveness) grows from 40% to 70 %.

This paper presents the results of a Kaizen continuous improvement project, which consisted in the fundamentally different reorganising of the technological process in bearing manufacturing industry, as well as specifically applying the Kanban system. The novelty of this system consists in the use of the Heijunka –Kanban post for both production triggering and for resupplying the supermarket type inventory placed upstream of the production process.

This improvement project was an important turning point in the production organisation and will most definitely be followed by other continuous

improvement projects aiming at the optimisation of the production processes and diminishing of losses.

4. ACKNOWLEDGEMENTS

In this paper some results of the project: CONTEMPORARY APPROACHES TO THE DEVELOPMENT OF SPECIAL SOLUTIONS RELATED TO BEARING SUPPORTS IN MECHANICAL ENGINEERING AND MEDICAL PROSTHETICS – TR 35025, carried out by the Faculty of Technical Sciences, University of Novi Sad, Serbia, are presented. The project is supported by Ministry of the science and technological development of the Republic of Serbia.

5. REFERENCES

- [1] Al-Tahat, M., Dalalah, D., Barghash, M., (2012) Dynamic programming model for multi-stage single-product Kanban-controlled serial production line, *J Intell Manuf* 23:37–48.
- [2] Cil, I., & Turkan, I., (2012) An ANP-based assessment model for lean enterprise transformation *Int J Adv Manuf Technol*,
- [3] Kumar, S., Panneerselvam, R., (2007), Literature review of JIT-KANBAN system, *Int J Adv Manuf Technol* 32: 393–408.
- [4] Matzka, J., Di Mascolo, M., Furmans, K., (2012) MODELS OF HEIJUNKA-LEVELLED KANBAN-SYSTEMS, *J Intell Manuf* 23:49–60.
- [5] Peter, K., Lanza, G., (2011) Company-specific quantitative evaluation of lean production. *Methods, Prod. Eng. Res. Devel.* 5:81–87.
- [6] Singh, B., Garg, S., Sharma, S., (2011), Value stream mapping: literature review and implications for Indian industry, *Int J Adv Manuf Technol* 53:799–809.

Authors:

Prof. Dr. Livia Dana Beju, “Lucian Blaga” University of Sibiu, Romania, Sibiu, E. Cioran 4, 550025, livia.beju@ulbsibiu.ro

Prof. Dr. Milan Zeljković, Prof. Dr. Slobodan Navalušić, University of Novi Sad, Faculty of Technical Sciences, Institute for Production Engineering, Trg Dositeja Obradovica 6, 21000 Novi Sad, Serbia, Phone.: +381 21 485-2351, Fax: +381 21 454-495.

E-mail: milanz@uns.ac.rs
naval_sl@uns.ac.rs

Benkó, P., Peták, T.

STRAIGHTNESS MEASUREMENT OF LINEAR MOTION GUIDES

Abstract: Geometrical accuracy of linear motion, which is the part of axis motion devices, for example machine tools or measuring machines and the others is necessary to determine the straightness of the measured axis linear motion as one of the main geometrical characteristics. This article describes methods of straightness measurement based on length and angle measurement. Also carry out measurement experiments and show the results, compare methods and make interpretation of advantages and disadvantages.

Key words: length measuring machine, laser interferometer, calibration, uncertainties of measurement

1. INTRODUCTION

For accuracy of linear positioning is necessary to keep straightness of the linear motion guides. While in the past these measurements were carried out with dial gauge or spirit level gauge, today the situation is absolutely different. Nowadays for measurement of geometrical properties of mechanical parts or assemblies using 3D coordinate measuring machine or laser interferometer. Main utilizing for laser interferometer is for distance measurement, but with another optic kit is possible to use for flatness, straightness or perpendicularity measurement. Excellent metrological characteristics insert this measurement instrument in traceability chain on the top rank. One of the most important constraints for accurate positioning is the straightness of the linear guides. From this reason in this contribution we describe new methods for straightness measurement.

2. WHAT IS THE STRAIGHTNESS?

When we measure straightness we could differentiate between straightness in plane and straightness in space.

Straightness [2] in plane is defined as a line in plane in given distance, while all of their points lie between two line parallel with main direction of the line and their distance equal with tolerance.

The main direction of the line has to representative and must be choosing with regard to minimize deviation of the straightness. It is possible determined by two methods:

- two points suitable chosen near at the end of the linear guide
- by calculating of the measured points i.e. by the methods of least squares

Straightness in the space is the line whose projection on two perpendicular planes is parallel with main direction of the line.

For better understanding error [2] of the straightness is defined by perpendicularity on direction of movement. Consider ideal straight line, any deviation from the straight line give error of the straightness

depend on whether measurement is carried out in horizontal or vertical plane.

3. MEASUREMENT OF THE STRAIGHTNESS

Straightness of the measurement is based on two methods:

- measurement of the distance
- measurement of the angle

For the measurement of the straightness by distance method is important to choose two reference points. Measurement device provides measurement of the deviation from the straightness from the datum. Reading is possible in different distances of the measured line.

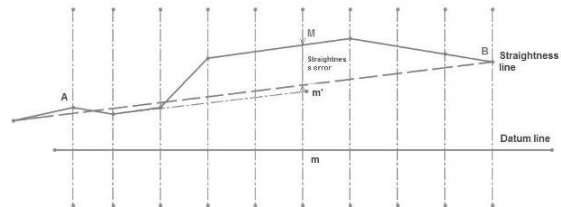


Fig. 1. Straightness line fit through straightness error

In measurement of the straightness by angle method moving part of the measurement device is in contact with measured line in P and Q point, which are spaced in distance d . Moving part is always coincident with neighborhood positions. P_0Q_0 with P_1Q_1 . Measurement device located in plane perpendicular on line is changing angles.



Fig. 2. Straightness measurement by angle measurement

As shown in Fig. 1, let the actual travel path with perpendicular motion in the vertical plane be $Z(x)$, and define the reference as a straight line passing through the initial point and the end point. That is $Z(0) = Z(L) = 0$. The local slope is:

$$\frac{dZ(x)}{dx} = \tan(\theta) \quad (1)$$

Assuming the radius of curvature R is much larger than the measurement increment Δx . $\tan(\theta)$ is approximately equal to θ . Hence:

$$Z(x) = \int_0^x \frac{dZ(x)}{dx} dx = \int_0^x \theta(x) dx \quad (2)$$

The total number of point N is equal to $L/\Delta x$. Let $X_n = n\Delta x$ then,

$$Z(x_n) = \sum_{i=0}^n \theta(x_{i-1}) \Delta x + const. \quad (3)$$

Since $Z(0) = Z(L) = 0$, Eqn (4) becomes

$$Z(x) = \sum_{i=0}^n \theta(x_{i-1}) \Delta x - \sum_{i=0}^n \frac{n}{N} \theta(x_{i-1}) \Delta x + const. \quad (4)$$

where $Z(X_n)$ is the straightness in the vertical plane, $\theta(X_n)$ is the measured pitch angle, Δx is the increment of the measurement, and N is the total number of points.

Method of the straightness measurement [1] by laser interferometer is belonging to method of measurement distance – Wollaston method. Wollaston method is designed for “movement in space” measurements – e.g. the movement of a machine table or working tool can be characterized. Datum is given by the position of the retro-reflector with mirrors twist in center. Wollaston polarizers optics also used here. Wollaston polarizers consist of two birefringent right angle prisms cemented together, such that their optical axes are perpendicular. As laser passes through the polarizer, a symmetric deviation between the ordinary and extraordinary beams is created. The resulting beams are of orthogonal linear polarization states and have equal intensity and a large angular deviation. By this way is possible to find out position of the focus point to axes of symmetry of the retro-reflector. Principle of the measurement by Wollaston optics is based on changes of the length of optical path of two divergent beams which is proportional to the vertical or horizontal displacement.

When the interferometer is moved along the profile to be measured, interference phenomena are generated in the signal coming back to the receiver, because the two beams recombined by the interferometer are subjected to paths of different length, as consequence of the profile geometry. Analyzing the originated fringes pattern, displacements of the interferometer

with respect to a straightness reference (given by the laser beam projected by the head), as moved along the stage, are estimated, and so the straightness deviation Δz can be calculated.

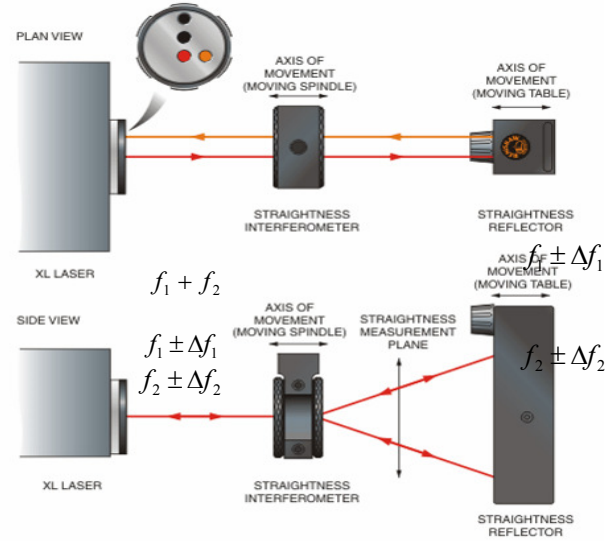


Fig. 3. Principle of the straightness measurement by Wollaston optics

For the straightness measurement Renishaw has in the optic kit two optics for measurement short distance – measurement range from (0,1 to 4) m and for long straightness measurement from (1 to 30) m. For both case is possible to measure straightness to $\pm 2,5$ mm.

Another way of straightness measurement is by angle optics, like optical autocollimator. Angle optics [1] are two beam splitter optics and two retro reflectors. For reference datum is using interferometry optics. If two optical sets interferometry optics and retro-reflectors are parallel, is it 0° . After rotating retro-reflector optics difference between two optical path give angle, which is evaluated by trigonometric expressions.

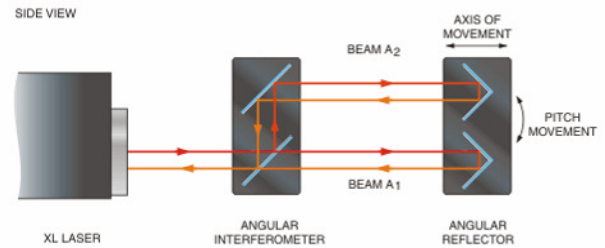


Fig. 4. Principles of the angle measurement by laser interferometer

4. EXPERIMENT OF THE STRAIGHTNESS MEASUREMENT

This section describes [2] experiment whose aim was to compare two methods of straightness measurement by laser interferometer. The measurement was carried out on linear guide used for positioning board for calibration of level gauge. The linear guide way is 16 m long. Because the alignment and setting of laser beam is very difficult and time

consuming operation, we decided to measure to 9 m with 25 cm steps. As reference the retro-reflector was on stable position at the end of measuring range and interferometry optics, the Wollaston prism was on moving part. Every 25 cm the value was recorded by the Renishaw straightness software. A same procedure was carried out by angle optics. In this case, after measurement the unit of measurand was transfer from (mm/m) to (mm) by next expression (5):

$$E_{h+i} = d + \tan(\alpha_{hi}) \quad (5)$$

where:

- E_{h+i} – straightness in (mm),
- d – distance between two points,
- $\tan(\alpha_{hi})$ – angle of the inclination.

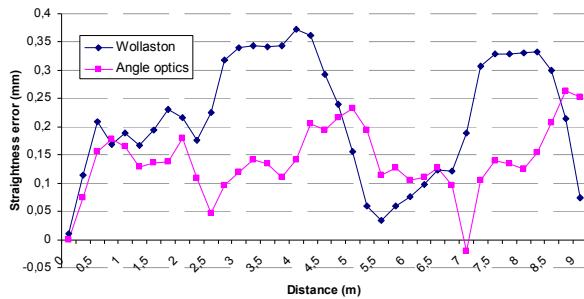


Fig. 5. Graph – Straightness measured by Wollaston and angle optics

5. UNCERTAINTY OF MEASUREMENT

The model of measurement [7] can be defined by the functional relationship reported by Equation

$$Z(x_i) = f(x_1, x_2, \dots, x_n) \quad (6)$$

In Equation 6 each X_i quantity represent the measure (displacement or angle) obtained on the considered profile at the i -th position. The f function resume the procedure needed to calculate the $Z(x_i)$ quantity, once the x_i values are known, including the definition of a representative line and of the two parallel lines of minimum reciprocal distance containing the acquired profile. Each x_i measure is affected by uncertainty; propagating all the n uncertainty contributions through the model given by Equation 6, also the uncertainty affecting $Z(x_i)$ can be estimated.

Due to non-linearity of the measurement model and to the presence of reciprocal correlation for measures x_i (in the specific case of angular measurements), the approach proposed by ISO GUM and adopted by ISO 230-9:2005 cannot be successfully applied for uncertainty propagation, since the method proposed by such documents assume a linear model and the absence of correlation for the input quantities x_i .

The proposed method is based on the Monte Carlo numerical technique, which is used for the uncertainty

propagation, in order to estimate a probabilistic distribution of values for $Z(x_i)$ and so to calculate its uncertainty. According to this method, each input quantity $Z(x_i)$ as well as the output quantity $Z(x_i)$ are treated as random variables and the propagation of the probability distribution functions assigned to all the $Z(x_i)$ is numerically operated through the model f , by means of a sampled approach as follows.

1. A suitable probability distribution function (pdf) $g(X_i)$ is assigned to each X_i . In the case of length measures operated by the laser-interferometer instrumentation this pdf is given by a Gaussian distribution whose standard deviation is defined according to the calibration diagram constructed during the preliminary characterization. The mean value for each distribution is given by the obtained measurement reading concerning the displacement or the angle measured at the i -th position along the considered profile.

2. For each X_i variable M x_{ij} values are generated according to the $g(X_i)$ function. By this way M vectors of possible values for the X_i variables are defined, defining M possible shapes for the measured profile.

3. For each one of the M possible profiles the straightness deviation value $Z(x_i)$ is estimated, and so a sample of M values for the $Z(x_i)$ variable is constructed.

4. A confidence interval is constructed for $Z(x_i)$ starting from the M sampled values and so uncertainty affecting the $Z(x_i)$ measure is estimated.

6. CONCLUSION

While measurement by angle optics is faster and easier to align laser beam the result of measurements are referred to the reference, which is retro-reflector optics. Until Wollaston optics is better for straightness measurement because the laser beam divergent on Wollaston prism, their optical axes always perpendicular to each other and by this way we have reference line to refer deviation of the straightness.

The commonly used Wollstone prism optics is expensive and very difficult to adjust although it gives the most accurate results. Operation of the system with the Wollstone prism optics requires highly skilled personnel. the accuracy of the straightness measurements depends on the precision of the alignment of the measured axis. It is recommended that the position of the crosses during alignment procedure to be set to the center of the screen. Vibrations of the base where the tripod is placed and air density fluctuations are the source of noise that lower accuracy of the measurement. This fact is presented on the Fig. 5.

7. ACKNOWLEDGMENTS

The research work was performed to financial support Ministry of Education of the Slovak Republic, grant No. VEGA 1/0584/12.

8. REFERENCES

- [1] Renishaw – *User manual – Straightness measurement*
- [2] STN ISO 23-1 *Test code for machine tools – Part 1: Geometric accuracy of machines operating under no-load or finishing conditions*
- [3] VDI/VDE 2617: *Accuracy of Coordinate Measuring Machines*, Verein Deutscher Ingenieure, 1986.
- [4] Vysloužil, Z., Zelko, J.: *Meranie v strojárstve*, Alfa, 63-036-73, 1973
- [5] Laser Interferometer LSP 30 -3D, *User manual*
- [6] Wang, P., Ch.: *Straightness measurement by Laser Doppler Displacement Meter Technique*, Optodyne Inc.
- [7] Magalini, A., Vetturi, D.: *Laser Interferometry for Straightness measurement in a weakly controlled enviroment*; XVIII IMEKO WORLD CONGRESS - Metrology for a Sustainable Development; September, 17 – 22, 2006, Rio de Janeiro, Brazil

Authors: Ing. Peter Benkó, PhD., Ing. Tomáš Peták,
ÚAMAI Sjf STU Bratislava, Námestie slobody 17,
Bratislava 1, 812 31, Slovak Republic, Phone.: +421
02/52497193, 02/52494311, Fax: +421 02/52495315.
E-mail: peter.benko@stuba.sk
tomas.petak@stuba.sk

Borojević, S. , Jovišević, V.

SELECTION AND CONFIGURATION OF MODULAR COMPONENTS FOR MODULAR FIXTURE DESIGN

Abstract: This paper presents a module for automation the design phase of modular fixture which is related to the selection and configuration of modular components. Methodology of selection and configuration of the modular components are based on production rules, classification numbers, geometrical and topological information of the workpiece, with contributing of the SolidWorks software system, API and object-oriented programming. Databases and knowledge bases are designed as an integral part of the module for the selection and configuration of modular components. Verification of this module is done by selecting and configuration of modular components in functional modular units, which are necessary for positioning and clamping of the hydraulic cylinder.

Key words: Modular components, modular functional units, automation

1. INTRODUCTION

Automation of modular fixture design is a very important link in the chain of full automation of the process planning design [1], [2]. From many types of fixtures, an increasingly important role in the production process has a modular or aggregate fixture. Because of its modular structure and concept, this type of fixtures is suitable for automation design [3]. The problem of time consumption has a significant impact in the fixture design, because process of fixture design generally can only begin after a complete definition of the process planning. It is estimated that the total time that the designer has available for process planning design, an average of 25% makes the fixture design [4]. Previously exposed facts define evidences that the automation of the modular fixture design increases the level of automation design of process planning. Thus, it is very important to introduce new technologies to the modular fixture design in the phase of selection and configuration of modular components [5].

2. SELECTION AND CONFIGURATION OF MODULAR FIXTURE COMPONENTS

Through preliminary performed analysis of the faces for positioning and clamping, and through the overall analysis of the object, it was generated information for the purpose of selection and configuration of modular fixture components. The above analysis is performed using the program application for determining the functionality of the workpiece faces, the general geometric analysis of the workpiece using the developed algorithms and adopted typical schemas and models for positioning and clamping of the workpiece [6]. The most important information resulting from the above mentioned analysis of the objects are:

- Type and number of faces for positioning and clamping;
- The surface quality of the selected face;

- The size of each selected face (the dimensional values and values in square mm);
 - Accessibility of each face from the point of view of possibility for placing of modular fixture components;
 - The overall dimensions of the workpiece;
 - The existence of through holes in the workpiece;
- Knowing the above mentioned information about the workpiece, and applying the typical schemas and models for positioning and clamping, it is executed a selection and configuration of modular fixture components for positioning and clamping of the workpiece.

2.1 Selection of modular fixture components

Selection of modular fixture components was carried out based on previously developed production rule and logic of reasoning procedure, which is associated with a unique classification number of modular fixture component. Classification number of modular fixture component is the holder of the geometrical and structural information about the component. Classification number consists of 10 elements of which the first seven encoded according to Table 1., while the last three digits are used as a statement of the amount of the active height of component, which is also shown in this table. The system of classification, with appropriate meanings of each of the elements is shown in Fig. 1.

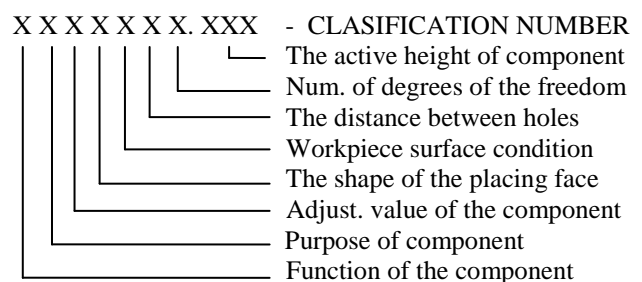


Fig.1. Component classification number [6]

Mark	Values
Function of component	1 - for positioning 2 - for clamping 3 - general component
Purpose of component	1 - basic (contact) 2 - auxiliary (lifting) 3 - additional (screws, etc)
Adjustment of component	1 - non-adjustable 2 - adjustable
Shape of component	1- prismatic 2 - cylindrical 3 - angled
Surface finish of workpiece face	1 - for all surfaces 2 - for un-machined surf. 3 - for rough surfaces 4 - for fine surfaces
Distance between screws	1- point (one screw) 2- serial 3 - diagonal
Degrees of freedom	0-0; 1- 1; 2-2; 3-3;4-4
Max. active height	20; 30; 50; 100; 120

Table 1. Defining the code of the classification number

After analysis of the workpiece, the classification of components and assigning unique classification number to each of the modular fixture components, it is executed a selection of the appropriate components according to block diagram of module for the selection and configuration of the modular fixture components (Fig. 2).

Selection of modular fixture components is divided into three levels. The first level is selection of components for bottom positioning of workpiece; the second-level is selection of components for side positioning and the third level is selection of components for clamping. All three levels are associated with a database of 3D models of modular fixture components. The database, along with algorithmic data flow is associated with a knowledge base which containing production rules as means of the selection process of modular fixtures components. The process of selecting modular fixture components was carried out on the basis of production rules [7] of the following type:

if

TSB = TSB1
PSTR1=1
 $100 \leq PAV1 \leq 110$
 $50 < A_{max}PSTR1 \leq 150mm$
KVALP1 =BO

then

KBP = 1 x 1213130.55
1 x 1111211.20
1 x 3211130.50

Production rules which were developed for selection of modular fixture components, as input information use information obtained from the analysis of the workpiece and defined typical schemes of positioning.

Process of selection of modular components is done using production rules that generate the classification number of modular fixture component.

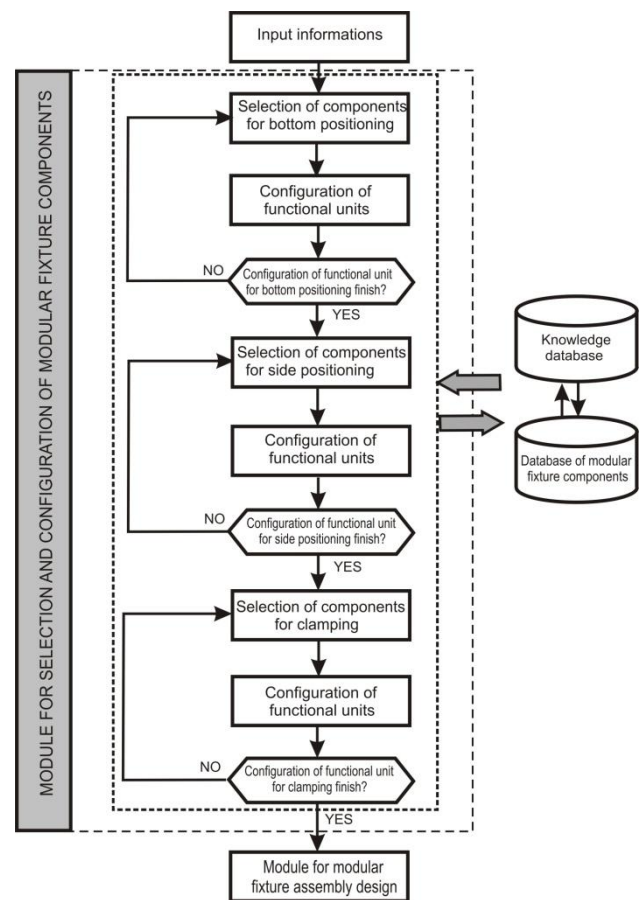


Fig. 2. Block diagram of the module for the selection and configuration modular fixture components [6]

2.2 Configuration of modular fixture components

By selecting the modular fixture components, it is provided the configuration process of modular fixture components in modular configure units. Modular configure units are a set of one or more modular fixture components, that performs a unique function of positioning or clamping of the workpiece. The configuration process of modular fixture components is shown in Fig. 3, in the form of sub-module for the configuration of the modular fixture components, which is the part of the module for the selection of modular fixture components, which together with it make a unit in overall automated system for modular fixture design. Configuration process of modular fixture components starts if in the process of selection of modular fixture components appears at least one auxiliary or raise component, next to the executive (contact) component.

Modular fixture components are previously defined in terms of additional information that is later used in the software configuration process. In addition to the classification number, which is located within the name of the components, in modular fixture components have been added extra information about reference mating cases.

Name of Mate Referenc	Mate Reference
RAVAN1	coincident
RAVAN2	coincident
CILINDAR1	concentric
CILINDAR2	concentric
CILINDAR3	concentric
CILINDAR4a	concentric
CILINDAR4b	concentric

Table 2. Additional information for components

Additional information, as shown in Table 2, were assigned to modular fixture components using the SW tools Mate Reference and stored in such a way as additional information of modular fixture components. This information is a relatively easy identify by programs and processes which were used for the configuration of modular fixture components.

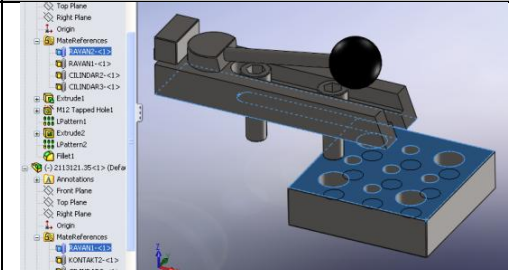
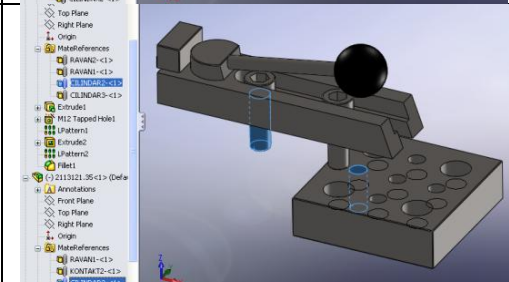
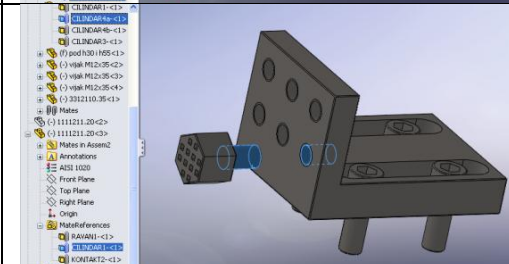
Configuration case	Description	Figure
RAVAN2 with RAVAN1	Configuration process with object RAVAN2 of one component and object RAVAN1 from other component in relationship coincident	
CILINDAR2 with CILINDAR2	Configuration process with object CILINDAR2 of one component and object CILINDAR2 from other component in relationship concentric	
CILINDAR1 with CILINDAR4a	Configuration process with object CILINDAR1 of one component and object CILINDAR4a from other component in relationship concentric	

Table 3. Some of the cases for configuration of modular fixture components

Previously predefined configuration cases of modular fixture components are not the only possible cases of configuration components, because it is possible to expand the configuration cases of modular fixture components.

The process of configuration of modular fixture components is performed for a set of modular fixture components for each of the previously selected faces for positioning and clamping. According to the module for configuration of modular fixture components, as shown in Figure 3, the configuration process begins by searching the general components of modular fixtures from the set of selected components. If the module identifies the general component, it opens in a 3D environment of the program system SolidWorks. Then the search is continuing and if the next general component was find it is also placed in same 3D environment and process of configuration of these two

components is executed. If no general components (or the next general component), the process of configuring of the modular fixtures components continues searching for the lifting/rising components. If lifting component is identify it is placed in 3D environment and configured with the general component. The same process is repeated for the next lifting component, if it exists.

If there is no next lifting component, the contact component is placed in same 3D environment of program system and its configuration is done with one of the pre-configured components. If there is no general, no lifting component in the set of selected components, process of generation of the contact component were executed. Adjustment of the modular configuration unit or just contact component is the final process in the module for configuration of modular fixture components.

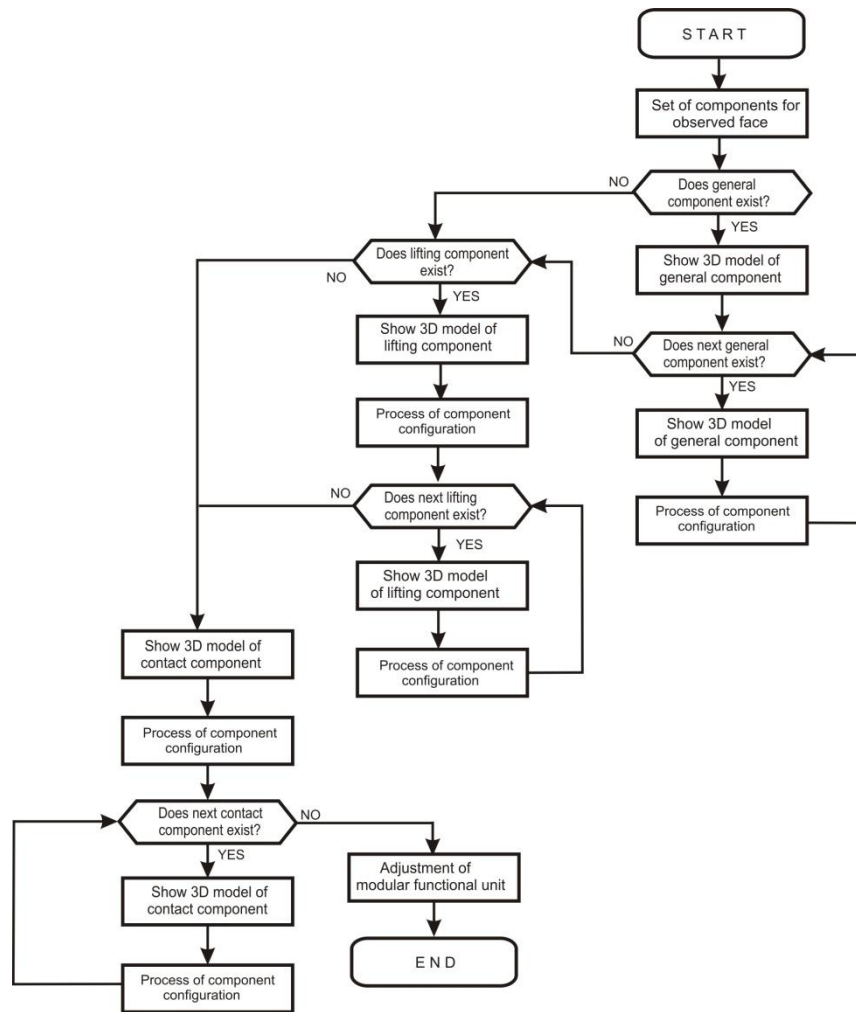


Fig. 3. Algorithmic data flow of sub-module for the configuration of the modular fixture components [6]

Adjustment of the modular fixture components or functional modular units is made regarding the value of active height of component that needs to take in order to perform a proper positioning or clamping of workpiece.

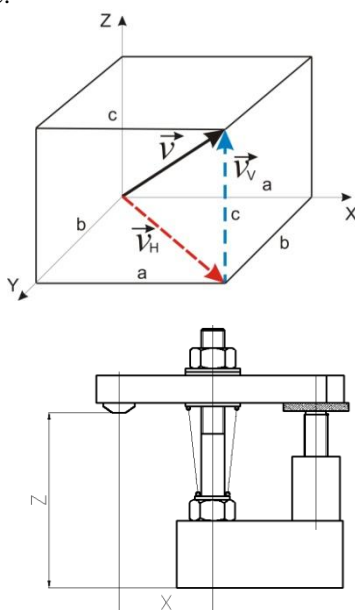


Fig. 4. Generating information over the position vector

Adjustment of modular fixture components and functional modular units is based on previous analysis of the workpiece and the existing information in the form of distribution of holes in the baseplate of the modular fixture. Fig. 4a shows the general case of generating information over the position vector \mathbf{V} . Thus, if we look at modular component shown in Fig. 4b the distance X must be set to the value of V_H and Z value to value V_V . In this way it is generating information that is used during configuring of modular fixture components, while the process of adjustment of the components executed at program manner, by using the SW tools Advanced Mates - Distance.

3. VERIFICATION OF MODULE FOR SELECTION AND CONFIGURATION OF MODULAR FIXTURE COMPONENTS

Verification of module for selection and configuration of modular fixture components is performed on the example of a hydraulic cylinder which solid model is the shown in Fig. 5.

Selection of modular fixture components was carried out in an automated way based on production rules that take into account the previously selected standard scheme for positioning and clamping, classification numbers of modular fixture components, as well as the

geometric parameters obtained by analysis of accessibility of functional faces. For hydraulic cylinder it is executed a selection of modular fixture components for the purpose of positioning and clamping, as shown in Table 4.

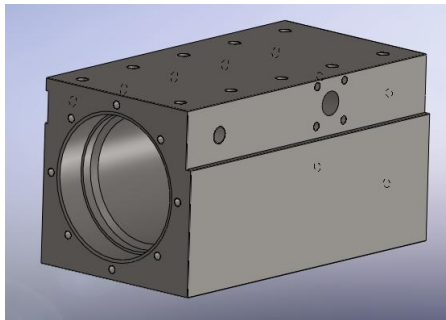


Fig. 5. Solid model of the hydraulic cylinder

After the selection of modular fixture components, the configuration process of modular fixture components for the hydraulic cylinder is executed. The configuration of modular components is performed in a fully automated manner, based on a developed algorithmic data flow and rules as set out in chapter 2 of this paper. The outputs from the process configuration of modular fixture components are functional modular units, which are shown in Figure 6

for the example of hydraulic cylinder. Adjustment the functional modular units were made on the basis of functional analysis of faces and information about position of hydraulic cylinder in relation to the baseplate of the modular fixture.

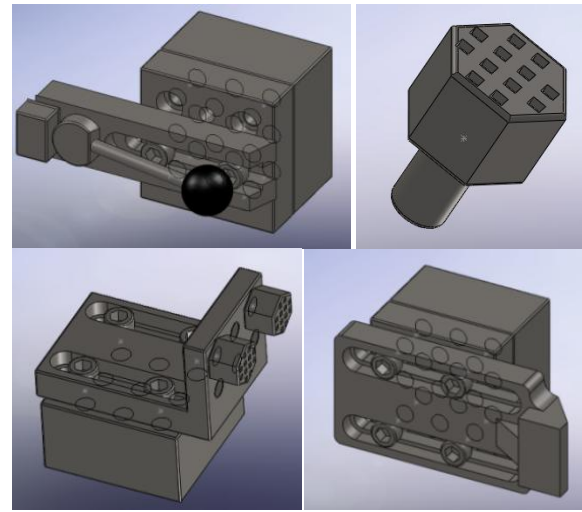


Fig. 6. Functional modular units for positioning and clamping of hydraulic cylinder

Num.	Face ID of hydraulic cylinder	Mark of functional modular unit	Mark of modular fixture component	Normal vector of observed face	Adjustable values	Coordinates of modular unit in assembly
0	10	10_1	1111211.2	(0.00, 0.00, 1.00)	0	(-125, -75)
1	10	10_2	1111211.2	(0.00, 0.00, 1.00)	0	(-125, 25)
2	10	10_3	1111211.2	(0.00, 0.00, 1.00)	0	(75, -75)
3	6	6_1	3211130.5	(1.00, 0.00, 0.00)	104	(-300, -100)
			1113331.3			
			3211130.25			
4	6	6_2	3211130.5	(1.00, 0.00, 0.00)	104	(-300, 50)
			1113331.3			
			3211130.25			
5	11	11_1	3211130.5	(0.00, 1.00, 0.00)	79	(-100, -200)
			1213130.55			
			1111211.2			
6	11	11_2	3211130.5	(0.00, 1.00, 0.00)	79	(50, -200)
			1213130.55			
			1111211.2			
7	9	9_1	2113121.35	(0.00,-1.00, 0.00)	129	(-100, 200)
			3211130.5			
			3211130.25			
8	9	9_2	2113121.35	(0.00,-1.00, 0.00)	129	(100, 200)
			3211130.5			
			3211130.25			
9	1	1_1	2113121.35	(-1.00, 0.00, 0.00)	104	(250, -100)
			3211130.5			
			3211130.25			
10	1	1_2	2113121.35	(-1.00, 0.00, 0.00)	104	(250, 50)
			3211130.5			
			3211130.25			

Table 4. List of the modular fixture components with additional information

List of the modular fixture components with additional information in the form of classification number, the required number of modular fixture components, which are used during the implementation of automation of the modular fixture design for the hydraulic cylinder, markings of selected modular fixture components, and the positions of functional modular units with orientation defined by the normal vector, are given in Table 4, as a output result of verification of the module for the selection and configuration of modular fixture components.

4. CONCLUSION

Based on the developed algorithms, production rules, using the previously generated geometric and topological information about the workpiece, it is possible to automate the process of selection and configuration of the modular fixture components in purpose of overall automation of modular fixture design. Figure 8 shows the assembly of the modular fixture for the hydraulic cylinder which automated modular fixture design is supported with module for selection and configuration of modular fixture components, presented in this paper.

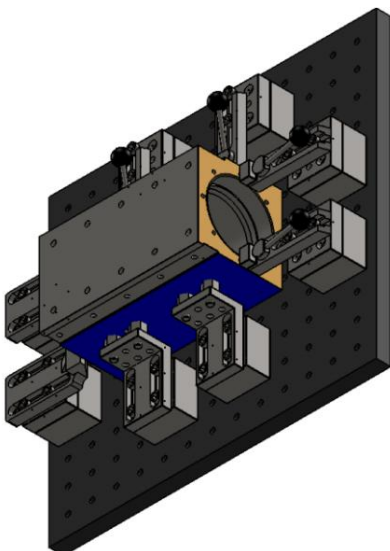
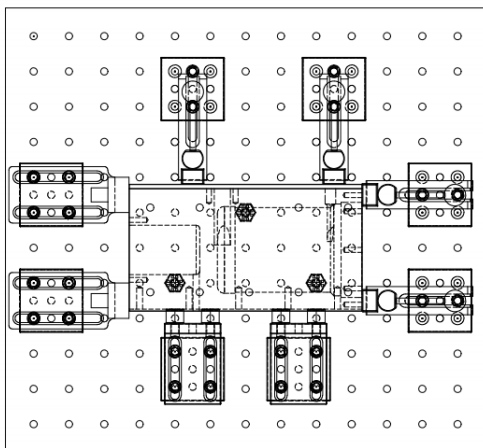


Fig. 7. Final assembly of modular fixture design for hydraulic cylinder

Phase of selection and configuration of modular fixture components, in the process of automated modular fixture design, can be realized with the support of the new CAD technology and object-oriented programming. The automation of this phase of modular fixture design reduces the total time for the modular fixture design, which increases the level of automation of process planning design.

5. REFERENCES

- [1] Jovišević, V.: *Projektovanje tehnoloških procesa*, Mašinski fakultet Banjaluka 2005.
- [2] Todić, V.: *Projektovanje tehnoloških procesa*, FTN Izdavaštvo, Novi Sad 2004.
- [3] Hodolić, J., Vukelić, Đ. *Pribori*, FTN Izdavaštvo, Novi Sad, 2008
- [4] Rodić, M. *Razvoj strukture integralnog sistema za automatizovano projektovanje pribora*, Doktorska disertacija, Novi Sad, 1992.
- [5] Zuperl, U.: *Development of systems for computer-aided design of modular fixtures*, Proceedings of the 11th International DAAAM, Opatija 2000.
- [6] Borojević S.: *Autumatizacija projektovanja modularnih pomoćnih pribora*, magistarski rad, Mašinski fakultet, Univerzitet u Banjoj Luci, Banjaluka 2011.
- [7] Milošević, M.: *Razvoj specijalizovanog CAD/CAPP/CAM rešenja primenom savremenih programskih sistema opšte namene*, magistarska teza, Fakultet tehničkih nauka, Univerzitet u Novom Sadu, Novi Sad 2005.

Authors: M. Sc. Stevo Borojević; Prof. Dr. Vid Jovišević, University of Banjaluka, Faculty of Mechanical Engineering, Stepe Stepanovića 75a, 78000 Banja Luka, Bosnia and Herzegovina, Phone.: +387 51 462-400, Fax: +387 51 465-085.

E-mail: vid.jovisevic@blic.net
stevoborojevic@hotmail.com

Bouzakis, K.-D., Skordaris, G., Gerardis, S., Bouzakis, E.

ADVANCED ANALYTICAL-EXPERIMENTAL PROCEDURES FACILITATING THE EFFECTIVE APPLICATION OF MICRO-BLASTING ON COATED TOOLS CONSIDERING AMONG OTHERS THE FILM BRITTLINESS

Abstract: Micro-blasting on coated surfaces is an efficient method for improving the coated tool life. During micro-blasting residual compressive stresses are induced into the film structure, thus increasing coating hardness. Simultaneously, abrasion phenomena are activated, which may lead to roughness augmentation, film thickness reduction and substrate revelation. Micro-blasting parameters have a pivotal effect on the developed films' mechanical and geometrical data and thus on the coated tools' cutting performance. For investigating such effects advanced experimental procedures have been developed such as of nanoindentations, nano-impacts etc. These tests, supported by FEM models, facilitate the determination of coating properties gradation and brittleness changes.

Keywords: PVD coatings, micro-blasting, hardness, brittleness

1. INTRODUCTION

Micro-blasting on PVD films has been documented as a potentially efficient method for improving the cutting performance of coated tools [1,2,3,4,5]. This process induces residual compressive stresses into the film structure, thus increasing the coating hardness, but its brittleness too [6,7,8]. In this context, micro-blasting parameters such as pressure, time as well as grains' material, size and shape have a pivotal effect on the developed films' mechanical and geometrical data and thus on the coated tools' cutting performance. For investigating such effects advanced experimental procedures have been developed such as of nanoindentations, repetitive nano-impacts, nano-scratches etc. Combinations of these procedures jointly with FEM supported computations contribute to the determination of coating properties gradation and film brittleness changes after micro-blasting. The paper aims at highlighting the capability of the mentioned analytical-experimental procedures to determine potential effects of micro-blasting on coating's data. In this way, optimum micro-blasting conditions can be determined, which eliminate the risk of cost intensive sudden cutting process breaks as a result of coating damage and subsequent abrupt tool catastrophic failure damage.

2. MICRO-BLASTING WORKING PRINCIPLE

Fig. 1. illustrates the working principle of the applied wet micro-blasting procedure. In this operation, water with abrasive grains is guided into the blasting nozzle, where an incoming air flow of adjustable pressure, accelerates the mixture and generates the water jet. Sharp-edged Al_2O_3 abrasive grains and spherical ZrO_2 ones, with smooth surfaces and average diameter of approximately 10 or 100 μm can be employed. The wet micro-blasting treatments were conducted by a NP10 machine of WIWOX GmbH Surface Systems. The tool rake and flank are treated in

separate micro-blasting procedures.

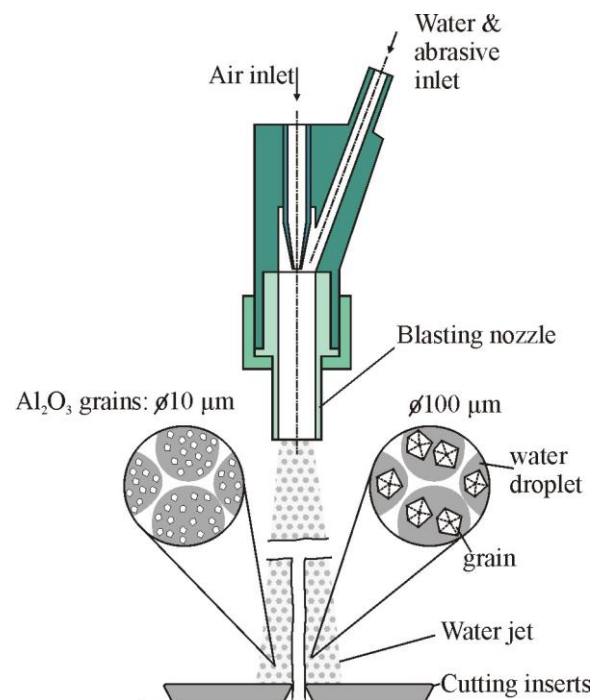


Fig. 1. Working principle of wet micro-blasting

3. COATING THICKNESS DISTRIBUTION ON THE CUTTING EDGE AFTER MICRO-BLASTING AND ITS EFFECT ON THE TOOL'S CUTTING PERFORMANCE

The cutting edge geometry might be changed after micro-blasting at various conditions, caused by abrasion [2,3,4]. These potential effects of micro-blasting are schematically demonstrated in Fig. 2a. For investigating cutting edge roundness changes induced by micro-blasting on coated tools, confocal measurements along the tool edge of variously micro-

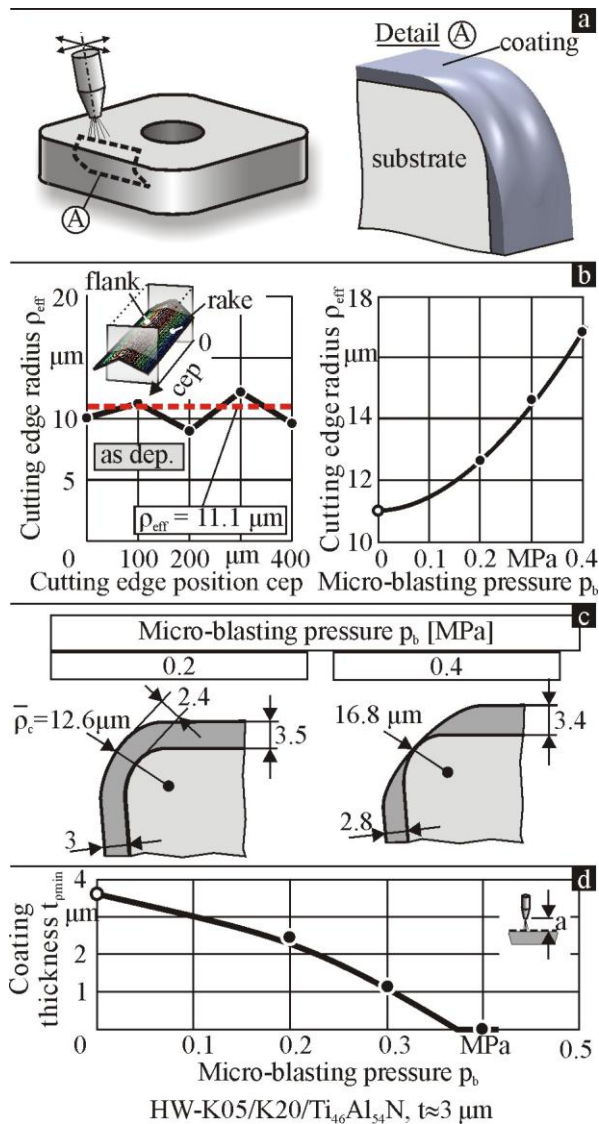


Fig. 2. (a) Micro-blasting effects on cutting edge geometry, (b) Cutting edge radius ρ_{eff} , (c) cutting edge geometries, (d) minimum coating thickness t_{pmin} of wet micro-blasted coated inserts at various conditions

blasted coated cutting inserts can be employed [3]. In this way, successive cross sections of the cutting edges can be monitored and the corresponding tool wedge radii as well as the average value and the fluctuations of the cutting edge roundness, before and after micro-blasting at various pressures can be estimated. A characteristic example, for an as deposited TiAlN coating case is demonstrated in Fig. 2b. The course of cutting edge radius versus the micro-blasting pressure is shown at the right of Fig. 2b. These results reveal that by increasing the micro-blasting pressure, an enlargement of the cutting edge radius develops. This growth is more visible at micro-blasting pressures over 0.2 MPa. Taking into account the previous results, the coating thickness distributions along the cutting edge, after micro-blasting at various pressures, can be analytically determined. The calculated coated cutting edge cross section geometries at pressures of 0.2 and 0.4 MPa are shown in figure 2c. The coating thickness t_{pmin} may diminish to zero at 0.4 MPa. Thus, substrate

revelations may develop, as it is also indicated in the diagram of Fig. 2d. A coating thickness t_{pmin} diminution leads to substrate thermal and mechanical loads growth and thus, the coated tool cutting performance may be deteriorated, although the augmentation of the cutting edge radius in general within a certain range improves the wear behaviour [9, 10].

4. STRENGTH PROPERTIES GRADATION AND BRITTLINESS AFTER MICRO-BLASTING

Residual compressive stresses can be induced into the film structure up to a certain depth from the coating surface via micro-blasting [8]. Depending on the micro-blasting conditions, the deformed film depth varies, thus affecting the coating's performance in different applications. A method has been already introduced for determining mechanical strength properties gradation in coatings after micro-blasting [8]. The residual stresses are measured in the coating before and after micro-blasting and the related stress changes determined at a certain depth from the film surface. These changes are compared to corresponding ones, calculated by a developed algorithm supported by finite elements method calculations. This algorithm describes the continuous penetration of individual blasting grains into the coating material and determines residual stresses after micro-blasting. Considering these results, the grain penetration depth and moreover, the developed distribution of the film yield stress after micro-blasting versus the coating thickness are estimated.

The von Mises stresses, developed after micro-blasting along the grain impression symmetry axis, depend on the distance from the coating surface and can be determined, as shown in Fig. 3a. The shaded areas indicate film material plastic deformation. The applied grain penetration depth h_g at a micro-blasting pressure of 0.2 MPa amounts to 120 nm [8]. The determined residual stress distributions along the impression symmetry axis are developed under every point of the film surface, since after a sufficient micro-blasting time; the grains deform uniformly the entire coating surface. The yield strength of the untreated coating, which has unique strength properties, amounts to 4 GPa. Film regions, not plastically deformed during micro-blasting, possess the pristine yield stress of the as deposited material i.e. of 4 GPa. In turn, a plastically deformed region possesses yield strength equal to the locally developed maximum von Mises stress. The developed stress distribution in the coated cutting edge region at the maximum undeformed chip thickness h_{cu} , when micro-blasted coated inserts at 0.2 MPa are used, was determined considering the real cutting edge geometry and is displayed in Fig. 3b. Moreover, the mechanical properties gradations versus the coating thickness, which are shown in Fig. 3a, were taken into account. The equivalent peak stress develops on the film surface at the cutting edge roundness, close to the flank. This maximum stress is higher than the film yield strength in the "as deposited" untreated film case (see Fig. 3c), thus leading to a comparable more intense wear evolution at this cutting edge position.

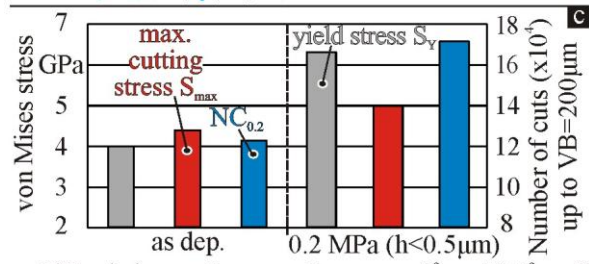
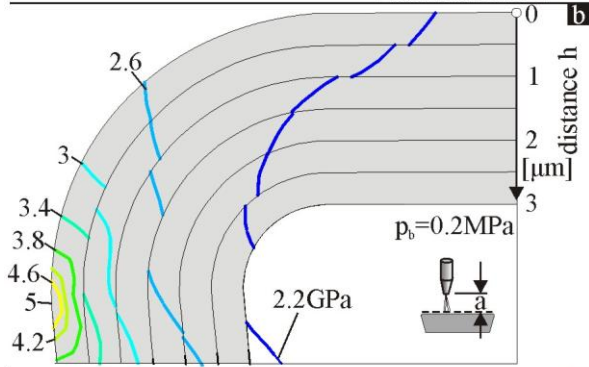
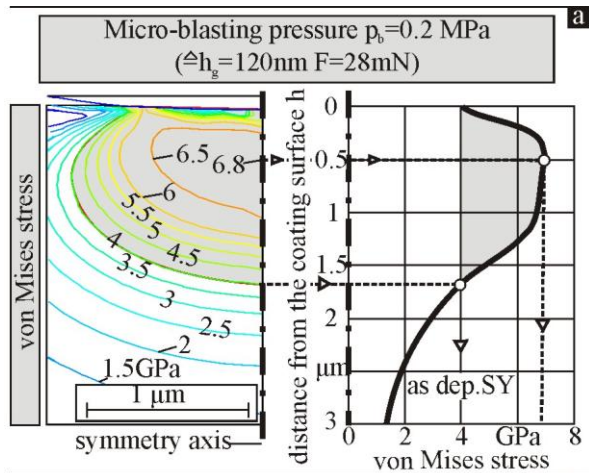


Fig. 3. (a) Calculated von Mises plastic stress distributions in a TiAlN coating after micro-blasting, (b) Stress distributions in the coated cutting edge region after micro-blasting at a pressure of 0.2 MPa, (c) Achieved number of cuts up to a flank wear of ca. 0.2 mm in the as deposited case and after micro-blasting at 0.2 MPa.

The conduct of micro-blasting at 0.2 MPa, provides sufficient strength to the film for withstanding the cutting loads. Thus, it contributes to a significant increase of the achieved number of cuts up to the same width of flank wear land compared to the corresponding ones of the as deposited coated tool.

The induced coating residual stresses after micro-blasting may increase simultaneously the film brittleness. Characteristic cases are presented in Fig. 4. PVD coated tools were subjected to wet micro-blasting by sharp-edged Al_2O_3 abrasive grains and spherical ZrO_2 ones, with smooth surfaces and

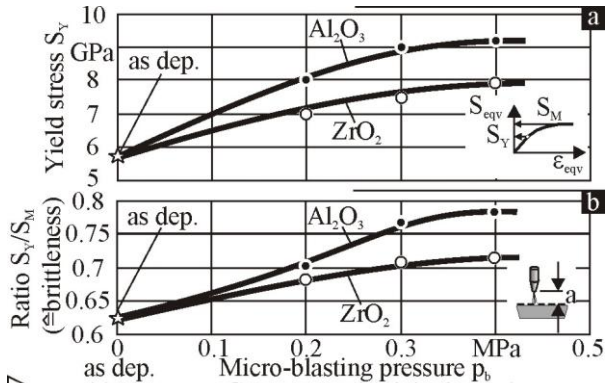


Fig. 4. (a) Yield stresses and (b) SY/SM ratio of post-treated coatings by wet micro-blasting with Al_2O_3 and ZrO_2 grains.

average diameter of approximately 100 μm [4]. In generally, a gradation of the yield stress versus the film thickness develops after micro-blasting [8]. For simplifying the related calculations, it was assumed that an evenly distributed yield stress versus the coating thickness, up to a depth of 1.5 μm from the film surface occurs. Due to the larger coating material deformation, induced by the Al_2O_3 grains, the yield stress increase versus the pressure is higher compared to the corresponding one, when ZrO_2 grains at the same process conditions are applied (see Fig. 4a). The determined yield stresses in both grain material cases remain practically unaffected over a pressure of 0.4 MPa. Moreover, Fig. 4b exhibits the yield to rupture stress ratio (SY/SM) course versus the micro-blasting pressure. An increase of this ratio indicates a simultaneous film brittleness growth i.e. fracture at less plastic deformation.

5. NANO-IMPACT TEST AND ITS FEM SIMULATION FOR ASSESSING FILM BRITTLENESS

The coatings' brittleness and toughness can be assessed by nano-impact tests [2,3,4,11,12]. In this test, a solenoid is used to pull the indenter off the coated specimen surface and to re-accelerate it from a distance against the film. An appropriate automation enables repetitive impacts at the same position on the sample surface at a set frequency. The evolution of the indentation depth, due to the progressing film damage during the repetitive impacts, is continuously monitored. Fig. 5a displays related test results at various impact loads on coating subjected to micro-small blasting by spherical ZrO_2 grains at a pressure of 0.4 MPa. The impact load increase up to 30 mN is associated with a continuous depth growth. At the impact load of 40 mN, a comparable steeper depth augmentation occurs, caused by the coating overloading and brittleness increase at high pressures.

The courses of the maximum attained nano-impact depths at various impact loads versus the micro-blasting pressure, when coarse Al_2O_3 blasting grains are employed, are displayed in Fig. 5b. Although up

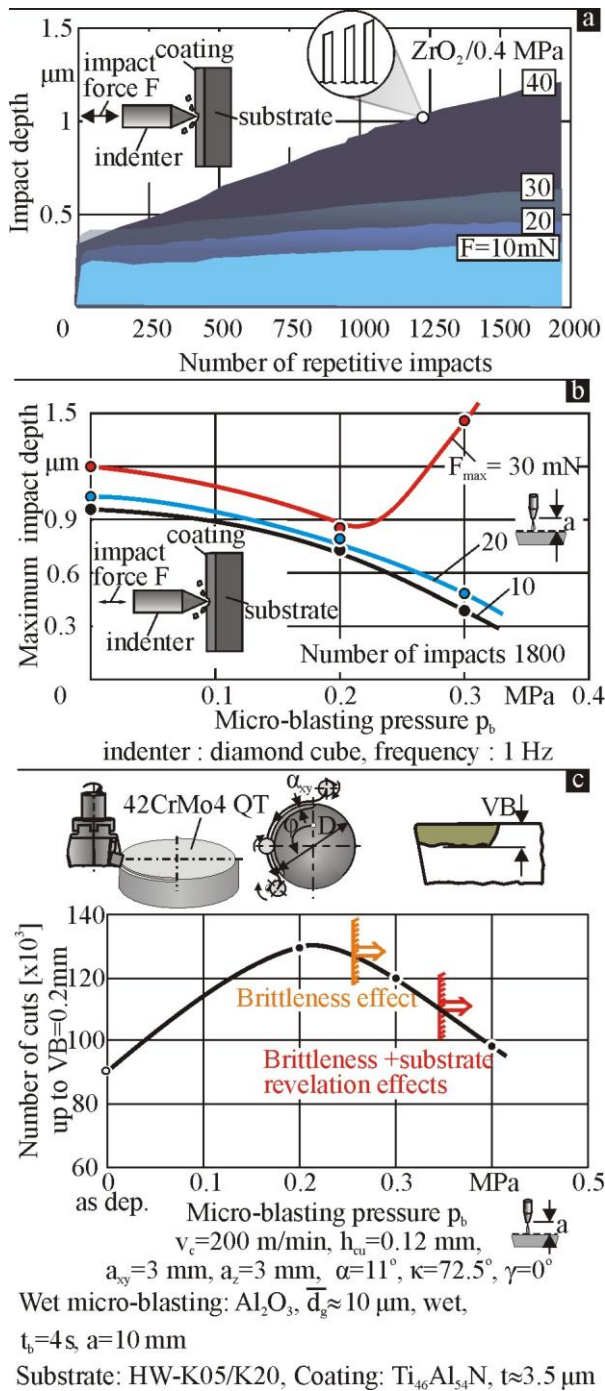


Fig. 5. (a) Nano-impact results on wet micro-blasted coatings by ZrO_2 grains at 0.4 MPa, (b) Impact depths at different impact forces on micro-blasted coatings by Al_2O_3 grains at various pressures, (c) Achieved number of cuts up to a flank wear of ca. 0.2 mm of micro-blasted coated inserts at various pressures.

to a repetitive impact load of 20 mN, the higher micro-blasting pressure of 0.3 MPa seems to improve the film strength, at 30 mN, the increased coating brittleness leads to a larger film failure. This effect has to be considered for explaining the cutting performance of micro-blasted coated tools (see Fig. 5c). The wear resistance of coated tools subjected to wet micro-blasting at various pressures by Al_2O_3 grains of an

average diameter of ca. 100 μm was checked in milling. The applied tool-workpiece system and the main characteristics of the undeformed chip geometry are illustrated in the same figure. Micro-blasted tools at a pressure of 0.2 MPa exhibited the best cutting performance, reaching a tool life of approximately 130,000 cuts. A slight tool life reduction at 120,000 cuts up to the same flank wear of 0.2 mm was encountered at a pressure of 0.3 MPa. Hence, over this critical micro-blasting pressure, which depends on the micro-blasting conditions, the higher micro-blasting pressure increases the film brittleness. In this way, the coated tool wear resistance is also deteriorated. At the higher micro-blasting pressure of 0.4 MPa, the cutting performance is additionally restricted by substrate revelation effects [2,3,4].

A 3D-FEM model was developed for simulating the nano-impact procedure, considering a piecewise linear plasticity material law (see Fig. 6). In a previous published FEM model, the strength properties of the film material were uniformly distributed versus the coating thickness [13]. By micro-blasting at various pressures, the attained maximum yield stress varies depending on the depth from the coating. In order to overcome this problem, a new 3D-FEM model was created, in which, the coating thickness was described by several material layers, with own elasto-plastic properties, developed after micro-blasting. The employed software was the LS-DYNA package. In these calculations, the simulation of the applied cube corner indenter geometry is in accordance to the manufacturer specifications. The boundary conditions and the finite elements discretization network are exhibited in this figure. The material properties and the coating thickness are variable and changeable

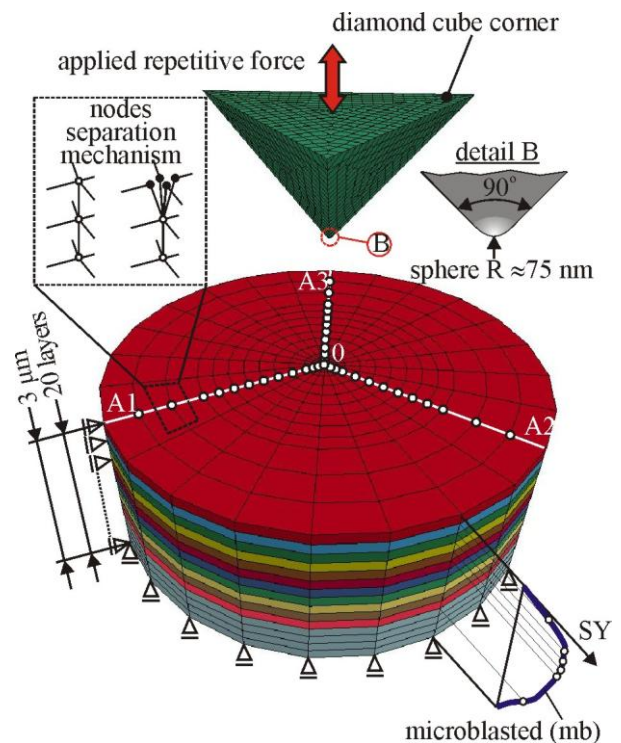
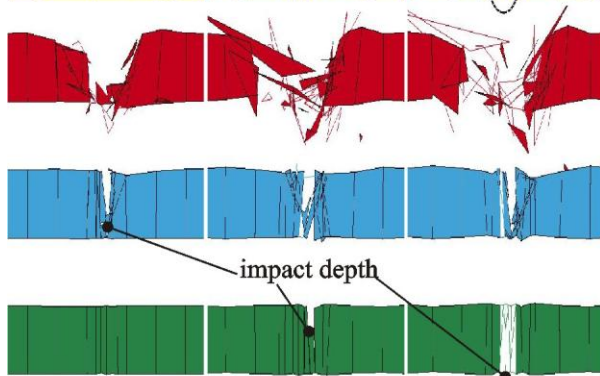
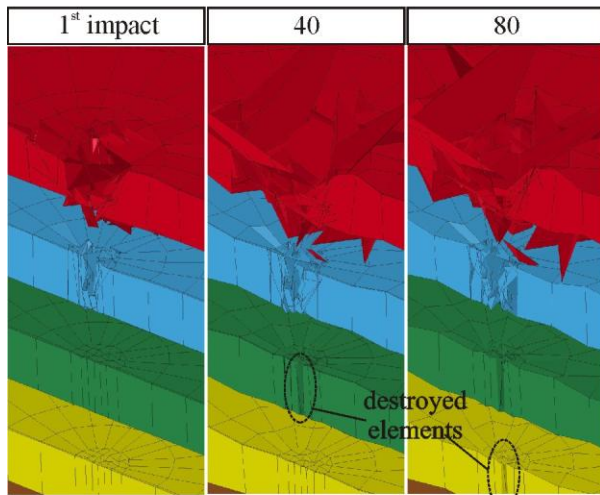
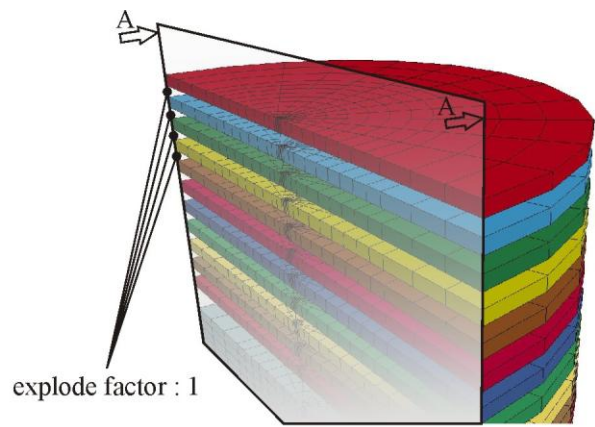


Fig. 6. The developed FEM model for simulating nano-impact test on micro-blasted tools



substrate:HW-K05/K20, coating:Ti₄₆Al₅₄N, t≈3.5 μm
indenter:cube corner,
frequency: 1 Hz, impact load: 30mN

Fig. 7. 3D-depiction of the crack propagation during nano-impact test on micro-blasted coatings

parameters. The coating thickness was described by 20 material layers.

During the indenter penetration into the film, it is assumed that the coating at the FEM model node regions can withstand the applied load up to a maximum value, which corresponds to the coating layer rupture stress and the associated maximum plastic strain limit. Over these limits, the related nodes are disconnected from the neighbouring finite elements. If all nodes of an element are disconnected, the element is released for simulating a crack formation and becomes an inactive separate entity. For minimizing the FEM

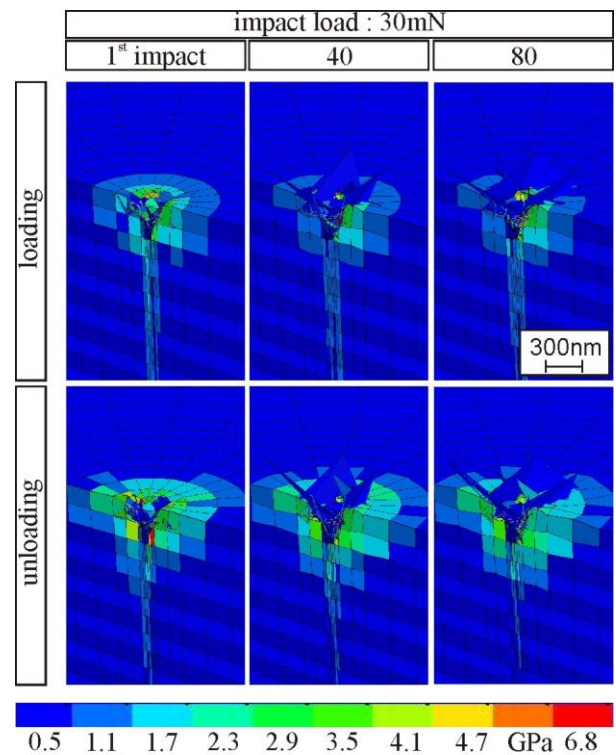


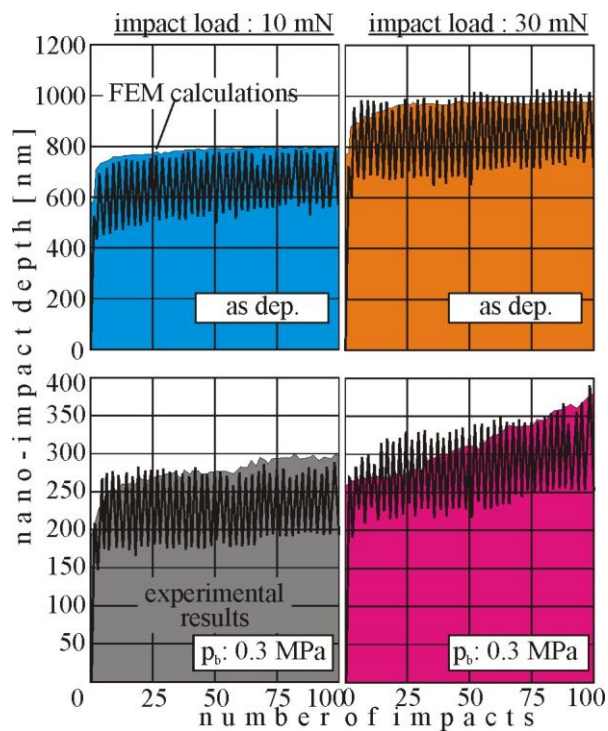
Fig. 8. Von Mises stress distribution and imprint geometry on micro-blasted coatings during loading and after indenter removal at various impact loads.

calculations solving time, the nodes' ability to be disconnected is restricted to those nodes, which are located on the perpendicular to the coating surface section levels OA1, OA2, OA3. The edges of the cube corner indenter lie on these levels during the indenter penetration into the film material. In this way, the stress fields developed in the coating and its fracture evolution in terms of imprint depth versus the repetitive impacts can be analytically described. A characteristic example, indicating the crack propagation and thus the impact depth versus the number of impacts is shown in Fig. 7.

Characteristic results attained by the developed FEM model during loading and after indenter removal are illustrated in figure 8. A comparison between measured and FEM calculated imprint depths on as deposited and micro-blasted coatings at impact load of 10 mN and 30 mN during the first 100 impacts is displayed in Fig. 9. The course of the FEM calculated imprint depths versus the number of impacts converges sufficiently with the measured results at all impact loads. In this way, micro-blasting conditions on films can be analytically optimized, for avoiding an undesired level of film brittleness.

6. CONCLUSIONS

In the paper, innovative experimental- analytical procedures for determining coating strength properties gradation, film brittleness as well as coating thickness



substrate: HW-K05/K20, coating: $\text{Ti}_{46}\text{Al}_{54}\text{N}$, $t \approx 3.5 \mu\text{m}$
 indenter: cube corner, frequency: 1 Hz,
 impact load : 30 mN

Fig. 9. Comparison between experimental and FEM-calculated imprint depths versus the number of impacts

distribution after micro-blasting are presented. These processes render possible a targeted optimization of micro-blasting conditions, leading to improved coated tool life.

7. REFERENCES

- [1] Klocke, F., Schroeder, T., Bouzakis, E., Klein, A., *Manipulation of coating and subsurface properties in reconditioning of WC-Co carbide cutting tools*, Surface and Coatings Technology, 202, p.p. 1194-1198, 2007.
- [2] Bouzakis, K.-D., Klocke, F., Skordaris, G., Bouzakis, E., Gerardis, S., Katirtzoglou, G., Makrimallakis, S., *Influence of dry micro-blasting grain quality on wear behaviour of TiAlN coated tools*, Wear, 271, p.p. 783-791, 2011.
- [3] Bouzakis, K.-D., Bouzakis, E., Skordaris, G., Makrimallakis, S., Tsouknidas, A., Katirtzoglou, G., Gerardis, S., *Effect of PVD films wet micro-blasting by various Al_2O_3 grain sizes on the wear behaviour of coated tools*, Surface and Coatings Technology, 205, p.p. S128-S132, 2011.
- [4] Bouzakis, K.-D., Skordaris, G., Bouzakis, E., Tsouknidas, A., Makrimallakis, S., Gerardis, S., Katirtzoglou, G., *Optimization of wet micro-blasting on PVD films with various grain materials for improving the coated tools' cutting performance*, CIRP Annals - Manufacturing Technology 60 (1), p.p. 587-590, 2011.
- [5] Kennedy, D. M., Vahey, J., Hanney, D., *Micro shot blasting of machine tools for improving surface finish and reducing cutting forces in manufacturing*, Materials and Design, 26, p.p. 203-208, 2005.
- [6] Barbatti, C., Garcia, J., Pitonak, R., Pinto, H., Kostka, A., Di Prinzio, A., Staia, M.H., Pyzalla, A.R., *Influence of micro-blasting on the microstructure and residual stresses of CVD- Al_2O_3 coatings*, Surface and Coatings Technology 203, p.p.3708-3717, 2009.
- [7] Klaus, M., Genzel, Ch., Holzschuh, H., *Residual stress depth profiling in complex hard coating systems by X-ray diffraction*, Thin Solid Films, 517, p.p. 1172-1176, 2008.
- [8] Bouzakis, K.-D., Skordaris, Klocke, F., Bouzakis, E., *A FEM-based analytical-experimental method for determining strength properties gradation in coatings after micro-blasting*, Surface and Coatings Technology, 203, p.p. 2946-2953, 2009.
- [9] Rech, J., *Influence of cutting edge preparation on the wear resistance in high speed dry gear hobbing*, Wear, 261, p.p. 505-512, 2006.
- [10] Bouzakis, K.-D., Michailidis, N., Skordaris, G., Kombogiannis, S., Hadjiyiannis, S., Efstathiou, K., Erkens, G., Rambadt, S., Wirth I., *Effect of the cutting edge radius and its manufacturing procedure, on the milling performance of PVD coated cemented carbide inserts*, CIRP Annals - Manufacturing Technology 51, p.p. 61-64, 2002.
- [11] Beake, B.D., Vishnyakov, V.M., Colligon, J.S., *Nano-impact testing of TiFeN and TiFeMoN films for dynamic toughness evaluation*, Journal of Physics D: Applied Physics, 44/8, art. no. 085301, 2011.
- [12] Beake, B.D., Smith, J.F., *Nano-impact testing - An effective tool for assessing the resistance of advanced wear-resistant coatings to fatigue failure and delamination*, Surface and Coatings Technology, 188-189, p.p. 594-598, 2004.
- [13] Bouzakis, K.-D., Gerardis, S., Skordaris, G., Bouzakis, E., *Nano-impact test on a TiAlN PVD coating and correlation between experimental and FEM results*, Surface and Coatings Technology, 206, p.p. 1936-1940, 2011.

Authors: Prof. Dr.-Ing. habil., Dr.-Ing. E.h., Dr.h.c. Konstantinos-Dionysios Bouzakis, Assist. Prof Dr.-eng. Georgios Skordaris, Dr.-Eng. Stefanos Gerardis, Dr.-Ing. Emmanouil Bouzakis,
 Laboratory for Machine Tools and Manufacturing Engineering, Mechanical Engineering Department, Aristoteles University of Thessaloniki, GR-54124, Greece, and
 Fraunhofer Project Center Coatings in Manufacturing, Centre for Research and Technology Hellas (CERTH) GR-57001 Thessaloniki, Greece, and Fraunhofer Institute for Production Technology (IPT) D-52074 Aachen, Germany
 Phone: +30 2310 996079, 996021, Fax: +30 2310 996059.
 E-mail: bouzakis@eng.auth.gr
gskor@eng.auth.gr
gerardis.stefanos@gmail.com
e.bouzakis@certh.gr

Jakovljevic, Z.

POINT CLOUD REDUCTION USING SUPPORT VECTOR MACHINES

Abstract: This paper explores the possibilities of point cloud reduction using ε insensitive support vector regression (ε -SVR). ε -SVR is a technique that can carry out the regression using different kernel functions (sigmoid, radial basis function, B-spline, spline, etc.) and it is suitable for detection of flat regions and regions with high curvature in scanned data. Using ε -SVR the density of preserved points is adaptive – preserved points are denser at highly curved region and rare at flat regions. Adjusting the error cost in the regression, the number of preserved points can be fine tuned.

Key words: Reverse engineering, point cloud reduction, support vector machines

1. INTRODUCTION

The application of reverse engineering (RE) of the freeform shaped parts is rapidly dispersing over the years. Besides the reproduction of parts when original drawings are not available, RE is applied in the design of new products (e.g., in automotive industry where the sheet metal forming tools for car bodies are created based on wooden or clay models; in consumer products industry where aesthetic design is important; in generation of custom made accessories and prostheses for human) [1].

During the first step of RE, the surface of the physical object is digitalized and 3D point cloud is obtained. Contemporary measurement devices [2] and especially ones based on lasers have high measurement speed and resolution, giving large and dense point clouds at output. Although the sampling rate of measurement device can be adjusted according to the character of digitalized surface, the operator usually acquires as many points as possible because he is not sure about the needed density of points for adequate reconstruction of certain parts of scanned surface. Generally, a significantly larger amount of point cloud data is acquired than one that is sufficient and that can be efficiently handled during surface reconstruction. In order to operate with reconstructed surfaces at reasonable computational cost, the amount of point data should be reduced.

The easiest solution for data reduction is uniform downsampling. Nevertheless, in order to preserve the shape of original surface points, highly curved regions in point cloud should have high density, while for relatively flatter areas lower point density is acceptable. In order to address given issues a number of data point reduction techniques have been proposed.

The simplest way to create a surface model from point cloud is to generate a polygonal mesh over it. Consequently, the first methods for data point reduction were based on simplification of polygonal meshes [3] (the research has origins in image processing), while recent methods are based on direct cloud point data reduction. The most of the methods for direct cloud point data reduction are based on the estimation of the

importance of each point in the cloud. For the importance evaluation different measures are used e.g., deviation of normal vectors in the vicinity of the point [4, 5], Hausdoff distance [6], and maximum deviation distance [7]. In order to improve decision making fuzzy logic has been employed [7].

Support vector machines are an emerging technique for data regression and classification. In this paper a possibility of ε insensitive support vector regression (ε -SVR) application in data point reduction is explored, and a method for point cloud reduction is proposed.

2. SUPPORT VECTOR REGRESSION

Given is the training data set $\{(\mathbf{x}_1, y_1), (\mathbf{x}_2, y_2) \dots (\mathbf{x}_l, y_l)\}$ where \mathbf{x}_i represent independent, and y_i dependant variables. The goal of ε -SVR is to find a function $f(\mathbf{x})$ that is *as flat as possible* and that *has maximum ε deviation* from y_i . The errors lower than ε are insignificant. In other words, all the y_i should lie in the ε -tube around $f(\mathbf{x})$. In the case of linear dependence, the function $f(\mathbf{x})$ is in the form:

$$f(\mathbf{x}) = \langle \mathbf{w}, \mathbf{x}_i \rangle + b \quad (1)$$

$f(\mathbf{x})$ is flat if \mathbf{w} is small. In order to ensure the flatness:

$$\frac{1}{2} \|\mathbf{w}\|^2 \quad (2)$$

should be minimized, subject to:

$$|y_i - \langle \mathbf{w}, \mathbf{x}_i \rangle - b| \leq \varepsilon \quad (3)$$

Nevertheless, in reality the scenarios in which all of the data lie within ε tube are extremely rare and optimization of the problem (2, 3) is infeasible. In order to create $f(\mathbf{x})$, anyway, the violation of the condition that all y_i are within ε tube is allowed. To formalize this approach, slack variables ξ_i, ξ_i^* are introduced and optimization problem (2, 3) is reformulated [8]:

$$\begin{aligned} & \text{minimize} && \frac{1}{2} \|\mathbf{w}\|^2 + C \sum_{i=1}^l (\xi_i + \xi_i^*) \\ & \text{subject to} && \begin{cases} y_i - \langle \mathbf{w}, \mathbf{x}_i \rangle - b \leq \varepsilon + \xi_i \\ \langle \mathbf{w}, \mathbf{x}_i \rangle + b - y_i \leq \varepsilon + \xi_i^* \end{cases} \end{aligned} \quad (4)$$

Constant C introduces the tradeoff between function flatness and number of points out of ε tube.

Optimization problem (4) can be represented in dual form [9]:

$$\begin{aligned} \text{maximize} \quad & \begin{cases} -\frac{1}{2} \sum_{i,j=1}^l (\alpha_i - \alpha_i^*) (\alpha_j - \alpha_j^*) \langle \mathbf{x}_i, \mathbf{x}_j \rangle \\ -\varepsilon \sum_{i=1}^l (\alpha_i - \alpha_i^*) + \sum_{i=1}^l y_i (\alpha_i - \alpha_i^*) \end{cases} \quad (5) \\ \text{subject to} \quad & \sum_{i=1}^l (\alpha_i - \alpha_i^*) = 0 \text{ and } \alpha_i, \alpha_i^* \in [0, C] \end{aligned}$$

where α_i, α_i^* represent Lagrange multipliers. Only for $|f(\mathbf{x}_i) - y_i| \geq \varepsilon$ Lagrange multipliers are nonzero, while for vectors (points) inside ε tube α_i, α_i^* vanish. The vectors with nonzero α_i, α_i^* are called *support vectors*.

The solution of the problem (5) is given by:

$$\mathbf{w} = \sum_{ns} (\alpha_i - \alpha_i^*) \mathbf{x}_i \quad (6)$$

where ns is the number of support vectors, leading to:

$$f(x) = \sum_{ns} (\alpha_i - \alpha_i^*) \langle \mathbf{x}_i, \mathbf{x} \rangle + b \quad (7)$$

The presented methodology can be applied for nonlinear regression by mapping data from the input space into a high-dimensional space where the regression is linear. It is worth noting that for optimization problem (5), it is enough to know only the inner product in the high-dimensional space i.e. it is not necessary to define the high-dimensional space in explicit form. Rather opposite, it can be defined using kernel $K(\mathbf{x}, \mathbf{x}_i)$, which represents inner product in the space of higher dimension. Introducing $K(\mathbf{x}, \mathbf{x}_i)$, problem (5) becomes:

$$\begin{aligned} \text{maximize} \quad & \begin{cases} -\frac{1}{2} \sum_{i,j=1}^l (\alpha_i - \alpha_i^*) (\alpha_j - \alpha_j^*) K(\mathbf{x}_i, \mathbf{x}_j) \\ -\varepsilon \sum_{i=1}^l (\alpha_i - \alpha_i^*) + \sum_{i=1}^l y_i (\alpha_i - \alpha_i^*) \end{cases} \quad (8) \\ \text{subject to} \quad & \sum_{i=1}^l (\alpha_i - \alpha_i^*) = 0 \text{ and } \alpha_i, \alpha_i^* \in [0, C] \end{aligned}$$

while the function $f(x)$ is defined by:

$$f(x) = \sum_{ns} (\alpha_i - \alpha_i^*) K(\mathbf{x}_i, \mathbf{x}) + b \quad (9)$$

and it is a hyperplane in the high-dimensional space.

The kernel can be any function that satisfies the conditions of Mercer's theorem [8]. For example, these are polynomial kernels, Gauss kernel, sigmoid kernel, some wavelets. New kernels can be defined by summing or multiplication of simpler kernels.

For the application at hand, two kernels are of the significance. The first is the B-spline of order $2n + 1$, defined by $2n + 1$ convolution of unit interval:

$$\begin{aligned} K(\mathbf{x}, \mathbf{x}_i) &= B_{2n+1}(\|\mathbf{x} - \mathbf{x}_i\|) \\ \text{with } B_k &= \otimes_{i=1}^k \mathbf{1}_{\left[-\frac{1}{2}, \frac{1}{2}\right]} \end{aligned} \quad (10)$$

where $\mathbf{1}_X$ denotes indicator function on the set X and \otimes is the convolution.

The second is the spline kernel of order k having N

knots located at t_s , which is defined by:

$$K(\mathbf{x}, \mathbf{x}_i) = \sum_{r=0}^k \mathbf{x}^r \mathbf{x}_i^r + \sum_{s=1}^N (\mathbf{x} - t_s)_+^k (\mathbf{x}_i - t_s)_+^k$$

3. APPLICATION OF ε -SVR IN DATA POINT REDUCTION

Point data cloud is usually, due to the nature of scanning process, structured into cross sectional curves. Otherwise, it can be restructured using projections on cross section planes. ε -SVR can be applied to each cross section and the function $f(\mathbf{x})$ can be obtained.

The fact that function $f(\mathbf{x})$ is as flat as possible in high dimensional space, i.e. it conforms as much as possible to selected kernel in initial space, can be used for determination of regions where the scanned line is not highly curved. In these regions the number of support vectors will be very small. In order to preserve the curvature, the points can be uniformly downsampled with predefined step.

On the other hand, in regions with high curvature, ε -SVR will not be able to fit all the points inside the ε tube and the number of support vectors will be higher. In these areas support vectors can be preserved points.

Due to the unknown curvature, the best kernels for ε -SVR of freeform surface scans are B-spline and spline. In this paper B-spline is opted to use. The other two parameters that should be set in order to carry out ε -SVR are error margin ε and error cost C .

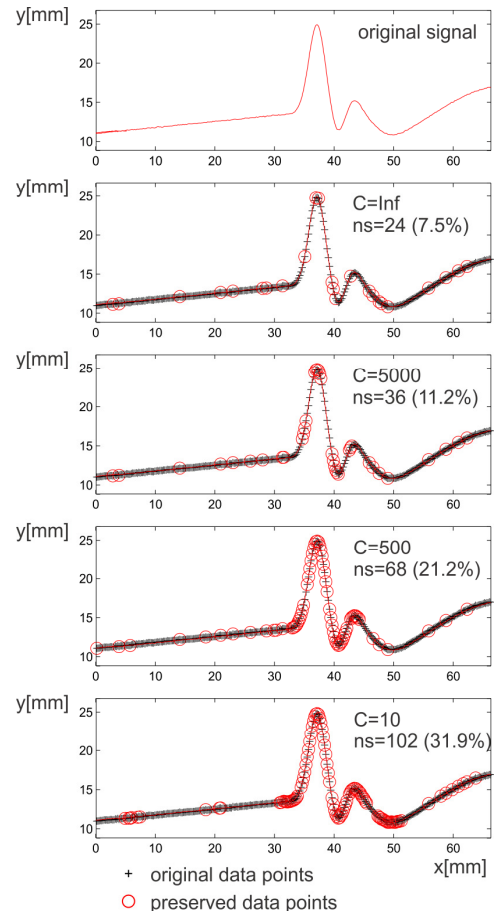


Fig. 1. Identified support vectors on synthesized signals for different values of parameter C ($\varepsilon=0.3$)

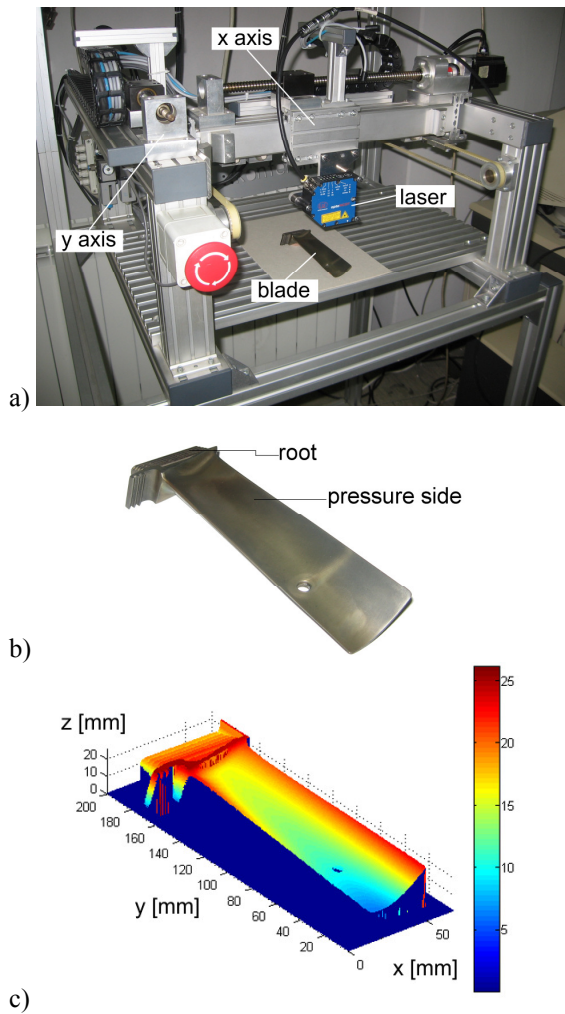


Fig. 2. a) Scanning device; b) A photo of scanned gas turbine blade; c) Obtained point cloud

The value of ϵ is related to the accuracy of scanning device and surface characteristics' tolerance and can be easily defined. The parameter C introduces the tradeoff between flatness and number of support vectors, i.e. preserved points, and it can be used for tuning the number of points that will be preserved in highly curved areas. The lower C will lead to higher number of preserved points, and vice versa.

Fig. 1. shows an example of the ϵ -SVR carried out with different values of C on a curve synthesized in Matlab. In order to get closer to the reality the curve is noised with 20dB of white noise. It can be observed that with the decrease of C the curvature of regression line is lower and the number of preserved points (support vectors) in highly curved regions is higher.

4. TURBINE BLADE EXAMPLE

This Section considers a real world example of the gas turbine blade (Fig. 2b). The pressure side of the blade represents smooth freeform surface, while its root has high curvature. The surface on the pressure side is scanned using set-up shown in Fig. 2a. The scanning device – laser $\mu\epsilon$ OptoNCDT1700-100 is put on the 2d Cartesian manipulator. Laser measuring range is 100mm with 14 bit resolution. Measurement error due to the tilt angles is 0.5% at $\pm 30^\circ$. The accuracy of

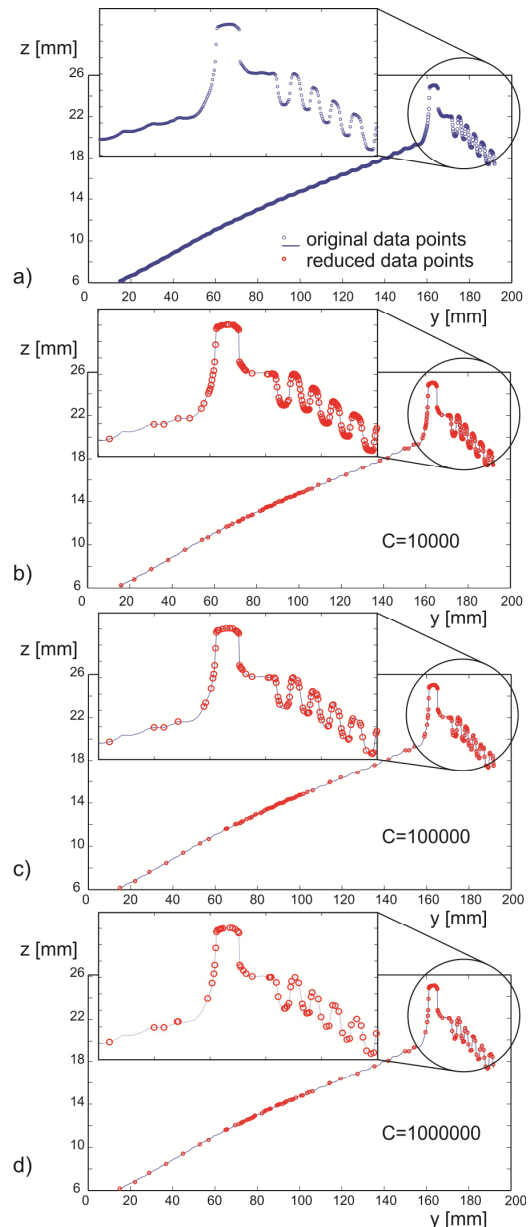


Fig. 3. a) Original points in cross section at $x=28\text{mm}$; b-d) Preserved points in the same cross section

manipulator is significantly lower: $\pm 0.1\text{mm}$. The surface is scanned along y axis in successive cross sections with the step of 0.2mm . Scanning speed was 100mm/s , and sampling rate 625Hz , which gives resolution of 0.16mm . The obtained point cloud has 417,500 points and it is presented in Fig. 2c.

Points are structured into cross sections along which the scanning is performed. Each of the obtained curves is subjected to ϵ -SVR as previously described. Parameter ϵ is set to 0.1mm , in accordance with scanning device accuracy. Parameter C , on the other hand is varied (Table 1).

ϵ -SVR gives support vectors that represent the points that should be preserved. Nevertheless in smooth areas support vectors are infrequent. Thus, in regions where the distance between two subsequent support vectors along abscissa was lower than 8mm the original signal was uniformly downsampled by 8mm (50 samples). In highly curved regions support vectors are dense and only they are preserved.

Point data scanned in one typical cross section at $x=28\text{mm}$ are shown in Fig. 3a. Applying ϵ -SVR together with uniform downsampling where needed, the number of points is adaptively reduced. The points on the pressure side surface are reduced by higher rate, while at highly curved area at blade root the number of preserved points is higher. Reduced point data for $C=10,000$, $C=100,000$ and $C=1,000,000$ are shown in Fig. 3b, 3c and 3d, respectively.

The points in x direction are downsampled uniformly by 10 – the cross sections with the step of 2mm are taken. The number and percentage of preserved points for different values of the cost

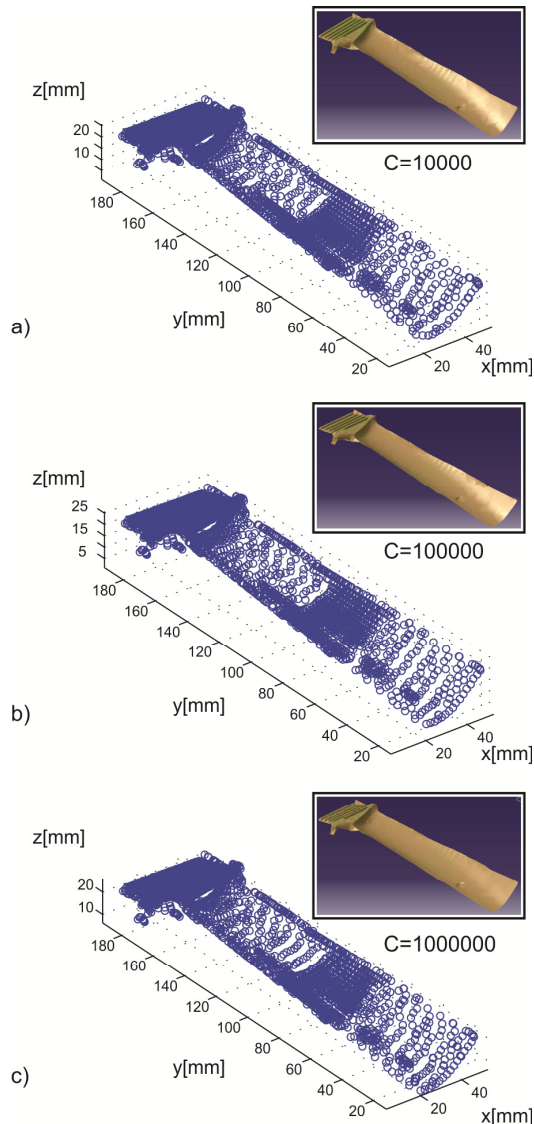


Fig. 4. Reduced point clouds and polygonal meshes

C	# of preserved points	% of preserved points - a^*	% of preserved points - b^{**}
10,000	5185	1.24	23.05
100,000	3351	0.80	14.9
1,000,000	3020	0.72	13.43

Table 1. Number and percentage of preserved points

* Initial number of points in cloud: $a = 417500$

** Number of points after downsampling along x and excluding points with $z=0$: $b=22491$

parameter C are shown in Table 1, while reduced point clouds together with polynomial meshes created in Catia are shown in Fig. 4.

5. CONCLUSION

This paper proposed a method for adaptive data point reduction based on ϵ -SVR. It has been shown that SVR represents a tool that can be effectively used for higher reduction of data points at flat and lower reduction at highly curved areas. Cost parameter C is suitable for fine tuning of the number of preserved points. The B-spline kernel was selected as suitable for regression of freeform curves. Nevertheless, B-spline is prone to oscillation at smooth areas as can be observed in Fig. 3b-3d ($y=70-100\text{mm}$). In order to address this shortcoming the use of combination of spline and B-spline kernel could be explored.

The main shortcoming of the proposed method is the computation cost of SVR optimization problem, which is very high even with the application of sequential minimization algorithm.

6. REFERENCES

- [1] Varady, T., Martin, R., R., Cox, J., *Reverse engineering of geometric models – an introduction*, Computer-Aided Design, 29, p.p. 255-268, 1997
- [2] Savio, E., De Chiffre, L., Schmitt, R., *Metrology of freeform shaped parts*, Annals of the CIRP, 56/2, p.p. 810-834, 2007
- [3] Cignoni, P., Montani, C., Scopigno, R., *A comparison of mesh simplification algorithms*, Computers & Graphics, 22, p.p. 37-54, 1998
- [4] Song, H., Feng, H., Y., *A progressive point cloud simplification algorithm with preserved sharp edge data*, International Journal of Advanced Manufacturing Technology, 45, p.p. 583–592, 2009
- [5] Lee, K. H., Woo, H. Suk, T., *Point Data Reduction Using 3D Grids*, International Journal of Advanced Manufacturing Technology, 18, p.p. 201–210, 2001
- [6] Ma, X., Cripps, R., J., *Shape preserving data reduction for 3D surface points*, Computer-Aided Design, 43, p.p. 902–909, 2011
- [7] Budak, I., Sokovic, M., Barisic, B., *Accuracy improvement of point data reduction with sampling-based methods by Fuzzy logic-based decision-making*, Measurement, 44, p.p. 1188–1200, 2011
- [8] Vapnik VN, *The Nature of Statistical Learning Theory*, Springer-Verlag, New York, 2000
- [9] Smola, A., J., Schoelkopf, B., *A tutorial on support vector regression*, Statistics and Computing, 14, p.p. 199-222, 2004

Author: Doc. Dr. Zivana Jakovljevic, University of Belgrade, Faculty of Mechanical Engineering, Department for Production Engineering, Kraljice Marije 16, 11000 Beograd, Serbia, Phone.: +381 11 3302-264, Fax: +381 11 3370-364.
E-mail: zjakovljevic@mas.bg.ac.rs

Koldžin, D., Medić, V.

HOW THE OPEN INNOVATION CONCEPT AFFECT THE INNOVATIVE ENTERPRISE STRATEGIES

Abstract: *The subject of this paper is to show how the open innovation concept affect the innovative enterprise strategies. The shift from closed to open model of innovation imposed the necessity to readjust the enterprise strategies to these changes. Strategies would, therefore, necessarily need to be upgraded due to changes in the relations between the subjects of innovative activity, need for a stronger connection and cooperation among them, as well as the changes in the intellectual property management.*

Key words: *Innovation, Open Innovation, Strategies, Enterprise*

1. INTRODUCTION

The concept of open innovation, as one of the important trends leads to the transformation of innovation policy in the companies. It significantly affects the change of many known elements of the innovation process, such as intellectual property rights, capital markets, cooperation between the universities and the companies etc. After an introduction, the change of the innovation concept that evaluated from linear to interactive model is explained. In the next part, the main characteristics of closed and open innovation concept are analyzed. In the list of these changes the relationship between the company and its environment is changed too. Basic characteristic of the environment in which companies operate are now networking and cooperation. That also leads to a new way of intellectual property management and the strengthening of the corporate entrepreneurship. Corporate entrepreneurship involves the need that the company looks for new attractive business opportunities, and thus the strategic renewal. Several types of such strategies are described in the continuation of this paper. In the conclusion, the need for these changes and directions for the further harmonization are presented.

2. CHANGES IN CONCEPT OF INNOVATION

The traditional linear model of innovation is based on the idea that research and development is the key to innovations. In this model, [1] the innovation process is described as a chain that links different activities in a certain ordering. The chain starts with formal research and development activities followed by applied research and product development. The step after product development is commercialization. According to the linear model of innovation, more research and development would generate more innovations. Low research and development capacity could explain low innovative activity. The policy implication to be drawn from the linear model is rather straightforward; innovations rely on R&D promotion. Criticism against the linear model showed that the

innovation process did not work in such way [2]. Today it is increasingly recognized that innovation extends beyond formal research and development activities. The ability of firms to innovate depends on their networks with other firms and actors.

There are five main differences between the linear and the interactive model of innovation [1]:

- There is not just one process of innovation from research to commercialization; rather, ideas are generated and developed at all stages of innovation, including production.
- Basic research is not the only initiator stage. This is not to imply that basic research pursued in laboratories is irrelevant to innovation.
- Rather than just being used as the starting point of innovation, research results are used, in one form or another, at all stages of the innovation process.
- The relationship between basic research and commercialization is too complex to be understood as a straight-line relationship. There are feedback loops at all stages.
- The linear model reduces the contribution of the people involved in innovation, to only the first stages, while the interactive model makes it clear that innovation can take place in all stages and by different professions involved.

3. SHIFT FROM CLOSED TO OPEN INNOVATION MODEL

For the most of the twentieth century enterprises [3] were closed enough to their own ideas, to their own manufacturing processes, to their own machines, to their own scientists and workers. They couldn't believe in a network of exchanging information and knowledge among the other companies. There were strategic partners and alliances with severe contracts, protecting the secrets of the company. Secrets were ideas and inventions, closed inside the research labs of the company. The research team should cooperate with the development team for the accomplishing the

company's innovation. Problems were revealed from this communication between the two departments of research and development. Many companies put their ideas coming from the research team on the shelf and after a long time perhaps the development team use these ideas. Many dangerous factors came from this inventory, ideas sitting on the shelf, such as many scientists, watching their ideas to wait, could not afford it and resigned from their current position and went to a better conditions of working and developing their believes.

The view behind the closed innovation model is that successful innovation requires control. It supposes that enterprises must generate their own ideas and then develop them, build them, market them, distribute them, service them, finance them, and support them on their own. This closed paradigm counsels enterprises to be strongly self-reliant, because one cannot be sure of the quality, availability, and capability of others' ideas. [4] The dominant logic behind closed innovation was internally focused: enterprises invested in innovation, which led to many breakthrough discoveries. These discoveries enabled those enterprises to bring new products and services to the market, to realize more sales and higher margins because of these products, and then to reinvest in more internal innovation, which led to further breakthroughs. And because the intellectual property (IP) that arises from this internal innovation was closely guarded, rivals could barely exploit these ideas for their own profit. That concept was closely linked to mass-production and the rise of consumerism, both feeding on strongly integrated enterprises and markets. As mass markets were the dominant type of markets, it was only logical that such innovation structures promised to wipe out competition and enable monopolistic rents.

Open innovation has emerged as a model where firms commercialize both external and internal ideas/technologies and use both external and internal resources. [5] The boundary between a firm and its surrounding environment is more porous, enabling innovation to move easily between the two. In an open innovation process, projects can be launched from internal or external sources and new technology can enter at various stages. Projects can also go to market in many ways, [6] such as out-licensing or a spin-off venture in addition to traditional sales channels.

Open innovation is described as [7] both a set of practices for profiting from innovation and also a cognitive model for creating, interpreting and researching those practices.

Chesbrough defines open innovation as [8] the use of purposive inflows and outflows of knowledge to accelerate internal innovation, and expand the markets for external use of innovation, respectively. Open Innovation is a paradigm that assumes that firms can and should use external ideas as well as internal ideas, and internal and external paths to market, as the firms look to advance their technology. He describes how companies in the 20th century have invested heavily in internal research and development and hired the best people – enabling them to develop the most innovative ideas and protect them with intellectual property

strategies. [5] The generated profit was used to reinvest in research and development – in a virtuous circle of innovation. However, in the end of the 20th century, a number of factors have changed. The mobility of knowledge workers increased and availability of venture capital grow. [5] This has caused the closed innovation process in firms to start breaking up.

Chesbrough identifies a number of factors indicating a shift in how innovation was managed [6]:

- Useful knowledge has become widely diffused
- Companies do not take full advantage of the wealth of information
- Ideas that are not readily used can be lost
- The value of an idea or a technology depend on its business model
- The presence of VC changes the innovation process for everyone
- Companies need to be active sellers and buyers of intellectual property (IP)

4. CHANGES IN THE ENTERPRISE STRATEGIES

In the altered relationship between the enterprise and its environment in the light of open innovation, it is growing the role of connectivity and networking between companies and their environment. Accordingly, the basic characteristics of the environment in which enterprises operate should be networking and cooperation. Cooperative entrepreneurship meant that the company is looking for new attractive business opportunities, and thus strategic renewal. It helps them to build new sources of competitive advantage which will generate above-average income or rebuild their unique advantages by using the results of innovation process. Successful corporate entrepreneurship means that enterprise usually has to go out of current operations and markets in search of new opportunities.

The most important strategies in this regard are:

- The Blue Ocean Strategy and
- Strategy of new ventures

4.1. „Blue Ocean Strategy“

„Blue Ocean Strategy“ is commonly used in industries that record a fall and it is an example of how to open a new market for the company.

„Blue Ocean“ is actually a market where there is a little, or no competition [8]. Using this model of strategy the company can outperform its competitors, who limited their growth to gradually improvement through the introduction and expansion of productive activities in commercial areas where is great competition.

Elements of the „Blue Ocean Strategy“ are [8]:

- *Create uncontested market space*-companies that implement this strategy should not only seek a market without competition, but they alone should make them. This is possible due to rapid development of technologies that open up new opportunities for companies

- *Make the competition irrelevant* – instead of using competition as a benchmark, by using this strategy companies can go outside the borders of certain economic activities so they could offer new, different products. Here technological innovation does not play a decisive role.
- *Create and capture new demand* – means that companies are not fighting in the current market, but looking for good opportunities in unexplored territory
- *Break the value/cost trade off* – companies reject the idea that the balance between value and cost is necessary, but look for opportunities that will bring benefits both in cost structure, and a unique value for customers
- *Align the whole system of a company's activities in pursuit of differentiation and low cost* – companies set up such a system for sustainable business strategies by integrating their capacities, prices and costs.

When companies once create and adopt „Blue Ocean Strategy“ they quickly achieve economies of scale, gain advantages in learning and achieve synergies in all aspects of their organizational system. This strategy opens a way for companies to achieve and maintain competitive advantage, because it is very difficult to imitate them.

4.2. Strategy of new ventures

Companies that use focused approach usually separate corporate enterprise activities of other on going operation in the company. Corporate entrepreneurship by using the capital for new corporate ventures provides the achievement of the entrepreneurial goals independently from other company departments. The advantage is reflected in the fact that members of the entrepreneurial team leaves the freedom to work without restrictions and constraints that impose the organizational routine and norms. This usually leads to innovation and creativity.

Company form groups for new ventures, which aim is to identify and assess the chances of success of the enterprise. These groups typically have greater powers than the departments for research and development and cooperate with the other organizational units within the company, identify potential partners in the ventures, collect resources and launch new products which are the result of an innovative enterprise.

The volume of capital for new corporate ventures is permanently increasing, especially in industries with high growth potential, such as biotechnology and technology. Some companies invest in technologies similar to its basic field enabling potential synergies in future.

5. CONCLUSIONS

If companies want to joint international trends and creating of better competition position they should implement the strategy of innovation and carried out innovation continuously to provide sophisticated markets.

In the world of open innovation, where the basic features of the environment in which companies operate should be networking and cooperation, the new management of intellectual property and corporate entrepreneurship are strongly needed to solve problems and ambiguities that arise between market demands and internal entities. In this regard it is necessary to create a response to these external and internal discontinuities.

Knowledge management should be in function to empower each individual and the company to find answers to unknown changes and to establish a process of continuous improvement in compliance with the strategic management of the company.

6. REFERENCES

- [1] Andersson and Karlsson - Regional Innovation Systems in Small & Medium-Sized Regions, A critical Review & Assessment, CESIS Electronic Working Paper Series, Paper No. 10, August 2004, p.5
<http://www.infra.kth.se/cesis/documents/WP10.pdf>
- [2] Mytelka, L. & Farinelli, F. (2000), *Local Clusters, Innovation Systems and Sustained Competitiveness*, UNU/INTECH Discussion Paper Series, p. 8
- [3] Freund R., Chatzopoulos C., Tsigkas A., Anisic Z, Open Innovation for Entrepreneurs in Central European Region
- [4] Chesborough, H , 2003, Open Innovation: The new imperative for creating and profiting from technology, Harvard Business School Press: Harvard, MA
- [5] Chesborough, H, 2003, The era of open innovation. MIT Sloan Management Review, 44(3): 35-41
- [6] West J., Vanhaverbeke & Chesborough 2006, Open innovation: Researching a new paradigm: 285-307. Oxford: Oxford University Press
- [7] De Jong J.P.J., W. Vanhaverbeke , T. Kalvet & H. Chesborough (2008), Policies for open innovation: Theory, Framework and Cases, Research project funded by VISION Era-Net, Helsinki:Finland
http://www.visioneranet.org/files/408/OIPAF_fin_al_report.pdf
- [8] Kim, WC., Mauborgne, R., *Blue ocean strategy*, 2004.

Authors: Dr Dragica Koldžin, Dr Vera Medić,
Pokrajinski sekretarijat za nauku i tehnološki razvoj,
Bulevar Mihajla Pupina 16, Novi Sad,
Phone: +381 21 487 45 76, Fax: +381 21 456 044.
E-mail: dragica.koldzin@vojvodina.gov.rs

Kravchenko, M.P., Nochvay, V.M., Polonsky, L.G, Melnic, A.L.

STATISTICAL ANALYSIS OF THE QUALITY OF SURFACE COATED PARTS (DEPENDENCE OF ROUGHNESS OF MACHINING ALLOWANCE AND CUTTING MODES)

Abstract: *In this paper the dependence of the quality indicators (for example, the roughness parameter Ra) of machined surfaces of parts with gas-thermal sprayed coating from powder PG-12N-01 system Ni-Cr-B-Si, which had coated flame-spraying of the following melting, the thickness in the range 0.6 ... 2.4 mm from the value of the allowance and accepted of cutting modes are analyzed. The necessity is based of costs probability-statistical method an appointment of allowances for the processing coatings and the specific sequence of technological influences during it.*

Key words: *gas-thermal sprayed coating, flame coating, coating thickness, coating layer, cutting, a layer processing, cutting speed, feed.*

1. INTRODUCTION

The research results of cutting gas-thermal sprayed coatings (GTSC), indicates that the physical and mechanical properties of the latter within them have considerable scatter, and the limits of variations of their values depends on the coating thickness and deposition spraying [1]. Also it is known that within the coating is a interlayer, density and other indicators of quality which is higher in comparison with the upper layers and those that are adjacent to the base. Since the final machining of workpieces with a coating (base + coating) is realized out in the first place to achieve one's object the specified quality surface finish (quality, roughness, microhardness, etc.), it is necessary to appoint such allowance for processing Z, the removal its will form a working (machined) surface in the highest quality interlayer o coatings. Since the cost of parts from GTSC is proportional to the allowances, the rational values of the latter would provide savings in materials and energy during machining. Overstated allowance for the machining of coatings, which are practiced at the present time, usually provides accurate size and shape, but because it is chosen intuitively by far not always guarantees the required quality of the surface (for example, the same roughness). Understated allowance also does not provide the quality of machined surfaces, in addition, gives to obtaining a marriage for the dimensional characteristics. In general, the processing gas-thermal coatings are blurred established notions as: the maximum allowance, the minimum allowance, nominal allowance, the average allowance. As it will show below, the oscillation Z is limited by the thickness (depth) coating area and quality of its location within the coating, as well as the location a certain thickness of the coating based on (the depth of previous treatment basis under the coating).

Unfortunately, the computational-analytical method for the determination allowances, which is based on consideration factors that affects the previous allowances and executing transition process, surface

treatment, and connects Z with limiting size of the drive surface does not allow to receive the specified guaranteed quality of surfaces in the processing of coatings [2]. The reason is that, as a rule, the value of the highest quality interlayer (its slowness to coating thickness) and its location within the coating are unknown. In addition, it is necessary to take into account the ratio of coating thickness h_a and a depth previous treatment basis under the coating, a value waviness of coating surface and to take into account the fact that a range of thicknesses used in practice GTSC (thickness in the range 0,5...3,0 mm) in the presence of tools of polycrystalline super hard materials based on cubic boron nitride (CBN-based PSHM) allows the processing of gas-thermal (including, gas-flame) coating in one pass. And the very definition of an allowance for the first pass (relatively of the processing coatings is often just one) processing workpieces coated has its own specificity - must be considered as a tolerance of the thickness the coating, and the tolerance on size of the basis [2]. In the system the analytical determination of allowances almost no databases and regulatory materials for machining GTSC could be found.

2. EXPERIMENTAL RESULTS AND ANALYSIS

Consider previous in these circumstances it is expedient in the determination of allowances for the processing of coatings to switch to the use of probabilistic-statistical method, which is based on a probabilistic approach, which is theoretically more correct. The mathematical statistical method gives an opportunity to generalize the results of a large number o experiments and provide a high level of accuracy of both the allowance and its components.

To establish the relationship Ra working surfaces of parts with coatings obtained by flame-spraying of the following melting of powder PG-12N-01 system Ni-Cr-B-Si, on the based choice Z and modes of processing (cutting speed V and feed S).

In order to determine the slowness of the thickness and location of the highest quality in the gas-flame coating interlayer with the following melting of the powder PG-12N-01 (TC 48-4206-158-82, PJSC. "Toreztverdosplav") $h_n = 0,6...2,4$ mm have been applied on the basis of the 45 steel, a studded Ra layerwise of machined surfaces 70 of the specimens, simulators cylinder parts, dimensions $\varnothing 44, 8 \dots 45,0$ mm x 100.0 ... 150.0 mm at different depths within the coating h' .

Spraying was realized on specimens installation

KNPA-1,2M, had been designed by the department of mechanical engineering and design of technical systems Zhitomir State Technological University, at the mode and to compliance to the parameters, had been used and recommended for practical application of a measurement, including [3] (Table 1.). Processing of specimens was conducted out at the screw-cutting lathe with continuously variable speeds and feeds 16B05AF1 lathe cutting tool equipped with a circular plate of the PSTM based on the NSC - kiborita (RNMN090300T, $\varnothing 9,52 \times 3.18$ mm).

Working gas	Costs of acetylene	Costs of oxygen	Pressure, MPa	Costs of powder, kg/hour	Distance of spraying, mm	The rate of movement of the burner, m/min
	m ³ /hour					
Oxygen + acetylene	1,00...1,05	6,0	0,4	6,0	150	5,2...5,4

Table 1. Working gases, standards cost of the gases and the powder modes and parameters of the flame spraying of coatings on the specimens

The modes of turning and tool geometrical parameters were chosen based on a number of recommendations, in particular [1]: $V = 1,5$ m /s; $S = 0,1$ mm /rev, rake angle - (-6°); rear corner - 6° .

After conducting experiments at a computer system Mathcad Pro were analyzed the statistics of the were processed surfaces Ra, previously had been obtained in this study, based on regression models. Step by step presentation of data such parameter as the depth location of the machined surface inside the coating and

its determination allows the analysis of Ra, which had a stochastic nature, by reducing the models regression to the trend. The task the statistical analysis for each of the coating thickness was to: 1) statistical evaluation of the true meaning of Ramin, depending on the location of the machined surface, 2) assess the value of finding the depth of the machined surface, corresponding to the true value of Ramin., on the basis of statistical data. Ra values of the treated surfaces located at different h' , are given in Table 2.

№ p/p	$h_n = 0,6$ MM		$h_n = 0,9$ MM		$h_n = 1,2$ MM		$h_n = 1,5$ MM		$h_n = 1,8$ MM		$h_n = 2,1$ MM		$h_n = 2,4$ MM	
	h' , MM	Ra, MKM	h' , MM	Ra, MKM	h' , MM	Ra, MKM	h' , MM	Ra, MKM	h' , MM	Ra, MKM	h' , MM	Ra, MKM	h' , MM	Ra, MKM
1	0,00	1,62	0,00	1,82	0,00	2,32	0,00	2,12	0,00	2,44	0,00	2,15	0,00	2,24
2	0,05	1,23	0,05	1,34	0,05	1,97	0,08	1,56	0,10	2,06	0,10	2,22	0,10	2,16
3	0,08	1,15	0,10	1,09	0,10	2,15	0,16	1,72	0,20	1,74	0,20	1,68	0,20	1,63
4	0,10	0,68	0,14	0,72	0,15	1,86	0,24	1,96	0,30	1,15	0,30	1,32	0,30	1,25
5	0,12	0,65	0,18	0,68	0,20	1,62	0,32	1,34	0,40	0,97	0,40	0,57	0,40	0,91
6	0,15	0,32	0,22	0,41	0,25	1,14	0,40	0,76	0,50	0,62	0,50	0,45	0,50	0,82
7	0,18	0,39	0,28	0,32	0,30	0,87	0,48	0,48	0,60	0,72	0,60	0,34	0,60	0,73
8	0,20	0,62	0,32	0,44	0,35	0,80	0,56	0,52	0,70	0,86	0,70	0,49	0,70	0,58
9	0,23	0,57	0,36	0,64	0,40	0,73	0,64	0,63	0,80	0,68	0,80	0,68	0,80	0,79
10	0,25	0,58	0,40	0,48	0,45	0,99	0,72	0,96	0,90	0,92	0,90	0,57	0,90	0,86
11	0,28	0,51	0,44	0,52	0,50	0,84	0,80	0,85	1,00	1,12	1,00	0,87	1,00	0,99
12	0,30	0,80	0,48	0,80	0,55	0,79	0,88	0,79	1,10	1,07	1,10	0,77	1,10	1,15
13	0,33	0,90	0,52	0,74	0,60	0,87	0,96	1,02	1,20	1,14	1,20	1,23	1,20	1,06
14	0,35	0,82	0,56	1,22	0,65	1,01	1,04	0,92	1,30	1,09	1,30	1,17	1,30	1,21
15	0,38	0,99	0,60	1,08	0,70	1,23	1,12	1,17	1,40	1,43	1,40	1,48	1,40	1,18
16	0,40	1,32	0,64	1,31	0,75	1,16	1,20	1,27	1,50	1,39	1,50	1,73	1,50	1,19
17	0,43	1,35	0,68	1,72	0,80	1,10	1,28	1,15	1,60	1,56	1,60	1,71	1,60	1,23
18	0,45	1,70	0,72	1,56	0,85	1,15	1,36	1,44	1,70	1,83	1,70	1,66	1,70	1,45
19	0,48	1,66	0,76	1,77	0,90	1,21	1,44	1,82	1,80	2,04	1,80	2,01	1,80	1,56
20	0,50	1,65	0,81	1,88	0,95	1,29	1,50	2,07	–	–	1,90	1,97	1,90	1,88
21	0,53	1,65	0,85	1,97	1,00	1,15	–	–	–	–	2,00	2,02	2,00	1,79
22	0,55	1,60	0,90	2,16	1,05	1,55	–	–	–	–	2,10	2,32	2,10	1,91
23	0,52	1,99	–	–	1,10	1,89	–	–	–	–	–	–	2,20	2,14
24	0,60	2,15	–	–	1,20	2,18	–	–	–	–	–	–	2,30	2,38
25	–	–	–	–	–	–	–	–	–	–	–	–	2,40	2,49

Table 2. The Ra surfaces had been treated at different h' inside a coating of PG-12N-01

The first task was solved by building a statistical analysis of the confidence interval for the true meaning of Ramin. For the trend model, Ra, subject to that the equation of the model (trend) was a convex function (as we know, such a function always exists a global minimum), it was found the expected (average minimum) value of Ramin, that is, the center of the confidence interval, and as its boundary.

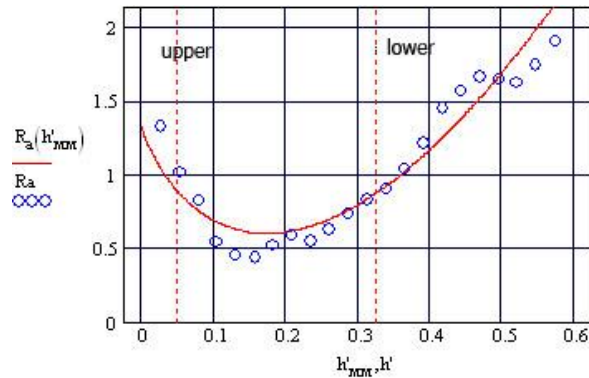


Fig. 1. An approximation of the curve Ra depending on h' (ha = 0.6 mm)

Based on the graph (Fig. 1.), the upper limit of the confidence interval as a line parallel to the axis of the

depth of the machined surface inside the coating, the trend intersects the graph at two points, abscissas of which are the upper and lower limits of the confidence interval of the values of h', which is responsible the true value of Ramin.

The confidence interval covers the true value Ramin with a probability of 0.99, as forecast. Hence, it appears that the confidence interval of the values of h', which corresponds to the true value of Ramin, cover it well with a probability of 0.99.

According to the above have been set forth, for each of the studied ha (0.6, 1.2, 1.8, 2.4 mm) were built by their confidence intervals, with a probability of 0.99 that cover the true values of h', corresponding to the true meaning of Ramin.

Subsequent task of statistical analysis of experimental data processing was to evaluate the dependence of Ramin from ha. For realization this analysis, a sampling of four ha (0.6; 1.2; 1.8; 2.4 mm) was insufficient. Therefore, additional specimens have been treated with ha = 0.9, 1.5 and 2.1 mm. In Table 3. for each with a 7 ha is a list of equations approximation of curves (trends), according to statistics Ra dependence on h', and are based on trends in the upper and lower limits of the confidence intervals of the true values of h', corresponding to the true Ramin.

h_a	The equation of curve approximation	The lower limit of the confidence interval	The upper limit of the confidence interval
0,6	$Ra = 1,32758 - 4,99929h' + 29,55725h'^{1,2}$	0,05075	0,32803
0,9	$Ra = 1,38705 - 19,49908h' + 21,16938h'^{1,2}$	0,10554	0,45970
1,2	$Ra = 2,21190 - 15,59690h' + 14,90000h'^{1,2}$	0,19650	0,87600
1,5	$Ra = 1,86006 - 12,00018h' + 11,26888h'^{1,2}$	0,15450	1,04764
1,8	$Ra = 2,06310 - 11,09320h' + 9,97100h'^{1,2}$	0,32600	1,10420
2,1	$Ra = 1,99210 - 10,62118h' + 9,44807h'^{1,2}$	0,24613	1,30452
2,4	$Ra = 1,65210 - 7,62660h' + 6,61360h'^{1,2}$	0,32520	1,41310

Table 3. Results of statistical data processing

Further statistical analysis was constructed of models approximation of the upper and lower limits of confidence intervals h' (Fig. 2.).

In the graphs (see Fig. 2.) it can determine the location of the coating layer, inside which can be guaranteed to receive the surface with the lowest Ra. For example, to coating ha = 1 mm should be prescribed treatment with Z in the range 0.14 ... 0.64 mm. By these same figures for coatings ha = 1.0 ... 2.4 mm, it can choose Z = 0,32 ... 0,67 mm, coating ha = 1.5 ... 2.4 mm - Z = 0,32 ... 1 00 mm. Finally Z is necessary to determine the value of paying attention to the deterioration of the working surface and the depth of the selected treatment basis under the previous coating. Should try to coating both have a certain thickness on the basis that the beginning of the higher quality of the layer coincides with the working surface detail, and the value does not exceed the allowable depreciation of its length inside the coating.

Given the machined working surface roughness of the parts with coating, was located in the qualitative criterion of Ra layer, can be achieved by varying cutting conditions - in this case, - V and S (do not

forget that the processing of the specimens was being realized out at the recommended (generalized) for this class of coatings modes.)

For this purpose, two-factor experiment was conducted to determine the dependence of Ra = f (V, S). The specimens were being treated with ø45 mm x 100 mm (coating PG-12N-01, ha = 1.5 mm) with an allowance that ensured the formation of a working surface in the high-quality coating layer.

The result of this experiment was a mathematical relationship $Ra = -3,60 - 0,03V0,20 + 12,50V0,08S0,08 - 12,30S0,20$, it allowed to determine V and S to obtain the required surface roughness.

Since GTSC heterogeneous in nature, in order to ensure the required quality of working surfaces is necessary to consider during their mechanical treatment. In this case it is advisable to move to a new technique for designing processing –to take in mind of the properties the material the details (in this case - it is the coating material) and to provide a sequence of technological influences, depending on the operational requirements for it.

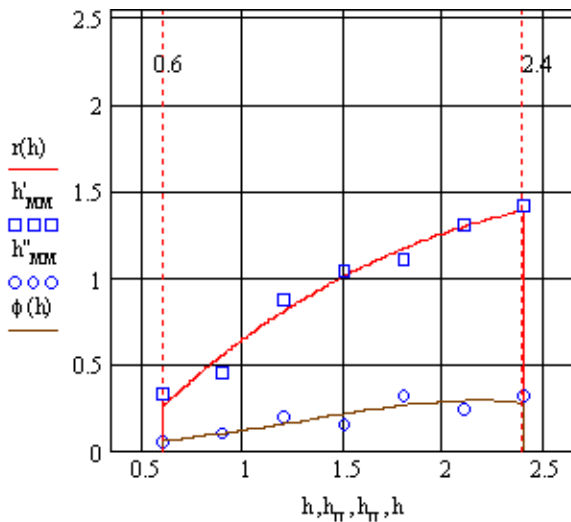


Fig. 2. The curves of the upper approximation (\square) and lower (\circ) outside the confidence intervals h' , which shows the location of the highest quality criterion for the inside coating layer R_a ($h_a = 0.6 \dots 2.4$ mm)

Due to the fact that to removal of various allowances by cutting gives different R_a , and, it is obviously, microhardness, wear resistance and the like of surface finish, it is need to know how the quality depends on Z . Appoint Z should given the structure of the coating and the qualitative and quantitative relationships of physical and mechanical properties within it.

Since the conditions for the formation of the coating thickness of the three zones provides a significant set of factors influence, the optimal Z is expedient to determine the probabilistic-statistical method, which will allow form a working surface of the part in the most appropriate for their performance interlayer. This approach solves the problem of not only the exact size treatment (it can be solved with expensive Z), but also provides the necessary operational parameters of the working surfaces of parts with coatings. In addition, the definition of a single (general) allowance for a certain range of coating thickness is relevant, if to attack attention to the fact that the method of deposition provides a significant dispersion of h_p .

For example, with respect to coating of powder PG-12N-01 $h_a = 1.0 \dots 2.4$ mm, which have the greatest practical use, taking into account the results of the study, it is necessary to assign Z in the range $0.32 \dots 0.67$ mm.

3. CONCLUSION

To determine the optimal location of the Z and coatings based on, that is, providing conditions for the formation of the working surface in the high-quality (for this or that quality criteria) layer, it is advisable to provide the necessary values of R_a the treated surface by varying cutting conditions.

Subsequent studies in this area should be extended to other coating systems Ni-Cr-B-Si, covering not only R_a experiments, but also such quality indicators as

microhardness and wear resistance, and to orient them to the theoretical justification of methods for determining the location of the highest quality within the coating different criteria for the layers. This will provide an opportunity to unify the value of allowances for processing GTSC from different powders and different ranges of thickness.

4. REFERENCES

- [1] Kharlamov, U.A., *Basics of technology reconstruction of machine parts. Tutorial. 2*, Eastern Ukrainian national them, V. Dahl, 2003
- [2] Kosilova, A.G., Meshcheryakova, R.K., *Reference book of technologist-mechanic. In 2 volumes - Mashinostroenie*, Moscow, 1985
- [3] Borisov, U., Kharlamov, U.A., Sidorenko, S., L., Ardatovskaya, E.N., *Gas-thermal sprayed coating of powder materials*, Mashinostroenie, Moscow 1987

Authors: Kravchenko M.P., junior research assistant, Nochvay V.M., associate prof., Polonsky L.G., prof., Melnic A.L., PhD student, Zhitomir State Technological University, stree. Chernyakhovsky, 103, Zhitomir city -5., Ukraine, 10005
E-mail: mans0607@rambler.ru

Krecu, D., Sovilj-Nikić, I., Sovilj, B., Gajić, V., Legutko, S., Varga, Gy.

ANALYSIS OF TOPOGRAPHY OF CYLINDERS MACHINED BY CUTTING TOOLS

Abstract: Surface of real body is complex. On the real surface there are many different errors and irregularities in the macro, micro and nano level. Errors can be both at the mass level and the level of geometric tolerances and substantively influence the processes of friction and wear processes of elements of tribo-mechanical systems. In nature there are no absolutely smooth surfaces. Unevenness, resulting from semi-rough and final operations, can cause major or minor irregularities of triboelements. In this paper the surface topography of cylinder caused by machining by cutting tools and the topography of cylinder surface during the life cycle are analyzed.

Key words: Topography, rollers, tools for machining, wear, tribo-mechanical system.

1. INTRODUCTION

The topography of the contact surfaces has a great influence on the wear and working life of tribo-mechanical systems, but these influences are still not well examined. Contact surface of elements of tribo-mechanical systems after final machining is never absolutely smooth. Technological heritage incurred as a result of semi-rough and final operations is characterized by the parameters of the topography or the topography of contact surfaces [1,2]. The geometric parameters of the contact surfaces under the influence of plastic deformation, formation of other structures and destruction of surfaces during friction are greatly affected. Starting topography, caused by machining technology which becomes exploitation is constantly changing throughout the life cycle [2,3].

2. CONTACT SURFACES TOPOGRAPHY

Real surfaces in engineering, no matter how carefully or expensive they have been prepared, could not have perfect geometry. Taking errors in appearance and form of elements of tribo-mechanical system into consideration surface roughness always exists and it is obvious if analyzed using appropriate devices. Each contact of two surfaces that belong solid has a discrete nature and it is carried out in certain number of points. When two such surfaces burden, the load will first be transferred to their tops of surface roughness or unevenness. The geometry of individual contact points and manner of real contact bulges arrangement along the normal or natural contact surface are obviously interesting to tribologist in an attempt to predict the overall behavior or the history of contact.

Tribological contact is shown in Fig. 1. [4]. The characteristic elements of the tribological model and possible situation can be seen in this figure, where the contact of the two surfaces that is relatively moving can arise tribological problems. Moving of element 1 along element 2 can be achieved with the proper use of energy in breaking the friction connections formed in the contact zone on the top of unevenness of both

bodies in contact. The process of forming friction connections and their breaking is constantly lasting during the forming of contacts and movement of one element along the other.

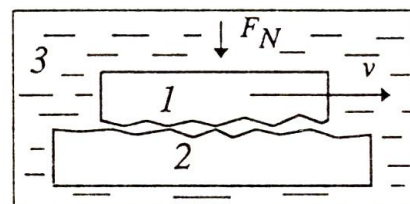


Fig. 1 General tribological contact

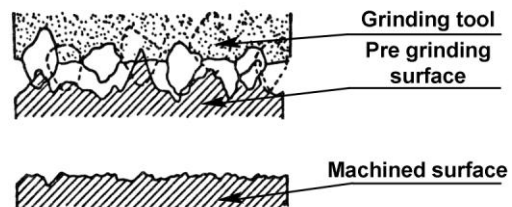


Fig. 2 Schematic design of surface topography obtained by grinding method

Roughness of the surface machined by grinding process is a result of material removal process, because the cutting elements for grinding leave furrows on the ground surface (Fig. 2).

Phenomenon of friction in the contact zones of tribo-mechanical systems of all types is the main cause of energy dissipation in mechanical systems. It is believed that 30 to 50% of the total energy consumed in the industry for relative moving is spent on friction force.

Another process in tribo-mechanical systems is a process of moving masses. In the process of making contact mass transfer occurs between elements and vice versa.

Mass change of elements in contact, change of their shape or dimensions leads eventually to its inability to perform its function or interruption of service of the tribo-mechanical system. After replacing worn element

by new one, tribo-mechanical system is once again able to continue to perform its function.

Interaction between the surfaces during relative motion is a complex phenomenon that involves changes of surfaces of basic materials and any coating created between the two surfaces. These changes are caused by temperature change at the surface, the change in the chemical composition of the surface, changes in metallurgical properties of some layers as well as changes in the physical properties of the lubricant at increased load and temperature created by relative motion. Temperature changes at place of surface interaction appear due to the heat generated as a result of friction. Geometrically complex of surfaces in engineering illustrates how the movement of cutting tools and the nature of the material. The shape of the surface in contact, in principle, is affected by the two types of errors, macro and micro errors. Macro errors are appeared when the form of element deviates from some ideal geometric dimensions and geometric shapes, or in case of geometric errors of position. Micro errors include waviness and roughness (Fig. 3) [1,4,5].

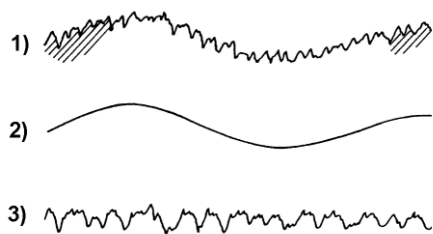


Fig. 3. The components of surface topography: the total profile (1) represents the combined effects of waviness (2) and roughness (3) superimposed on the geometric shape or form of the component surface.

In reality, surface of each body is extremely complex. Its condition is so different from geometric regularity and experts tend to use certain parameters in order to prove how much that surface is distorted.

The study of surfaces is relatively new. Therefore, testing of surfaces raises more questions for technologists and tribologists, such as: What is the optimal surface? Is it possible for an application to find just a special surface that will optimally be suitable for the working conditions? Why are sliding surface inclined to heat loads? Why pieces from wear process between the contact surfaces are plastically deformed despite reasonably low contact loads?

Although it is possible to answer on some of these issues with a current knowledge, many others remain the subject of modern research.

Topography of ground surface has been studied by many authors, but the unambiguous laws have not yet achieved.

3. EXPERIMENTAL RESULTS

Rollers on which the topography parameters were measured are elements of extrusion line. Extrusion line

is a plant for the production of foils and plates. It consists of three extruders. The largest extruder has a worm with diameter of 90mm, medium extruder has a worm with diameter of 60mm and the smallest extruder has worm with 45mm diameter. The total capacity of the extrusion line is 300kg / h. The extrusion line has two tools. One tool is for producing single-layer and three-layer foils and plates, thickness of 1mm to 5 mm and width of 400mm to 1000mm. Another tool is for producing single-, double-layer, three-layer and five-layer foils thickness of 0.5 to 3 mm, a width of 300mm to 700mm. Cooling (crystallization) of the foil is done by rollers (calendaring) that are heated by hot water (Fig. 4). Upper roller diameter is 380mm and the two bottom rollers have a diameter of 500mm. Cutting of foils to the correct width is done by using two circular blade. At the end of the line for the extrusion is device for foil winding or plates cutting to the given dimensions.



Fig. 4. First Rollers

Raw materials (granule, regenerate, master-but) are put into the basket at the entrance of the extruder using the dispensing system. Worms trigger mass which melts at temperatures of 180 Celsius degrees to 250 Celsius degrees and inside the tool thickness and width of the foil are formed.

The concept of swallow tail is about the look of tools where the mass came from the extruder is distributed in width and thickness, and the output from the tool forms a width. A gap between the rolls determines the final foil thickness.

Rollers were machined by grinding tools, nitrated and highly polished (Fig. 4). Additional machining is done in the case of damage by the nitrating and high polish. Parameters of rollers topography were analyzed on three rollers that were in operation and the number of measurement points along the length and circumference of the cylinder is 5 (Fig. 5).

Measurement of topography parameters was performed with Surface Roughness Tester device SJ-301Mitutoyo. In Fig. 5. roughness parameters, profile and percentage distribution curve of profile bearing at the first roller for the measurement point number 3 are given.

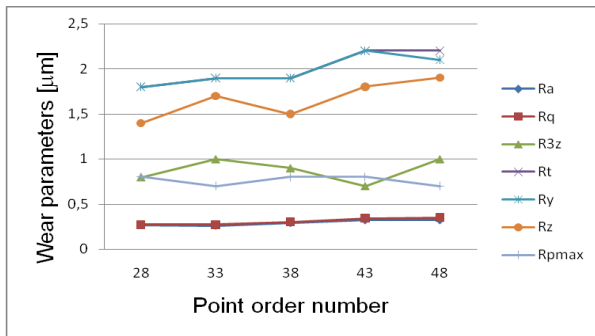


Fig. 11. Roughness parameters in extensive points for the second cylinder in the middle

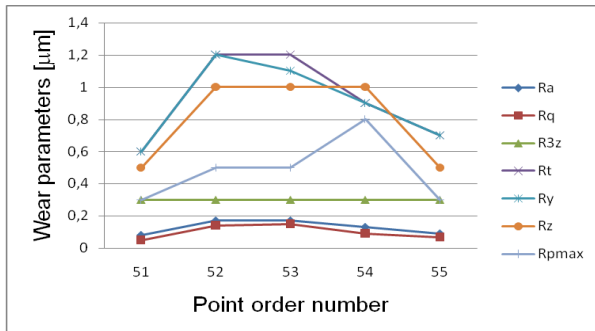


Fig. 12. Roughness parameters in the axial points for the third roller

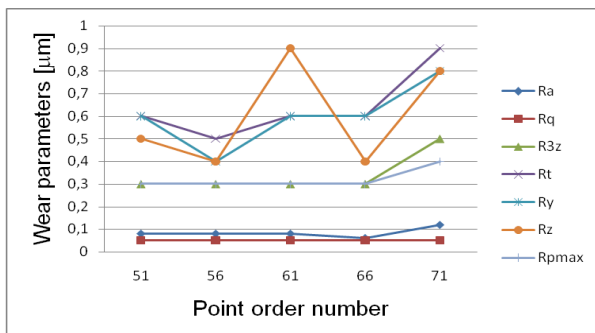


Fig. 13. Roughness parameters in extensive points for the third roller at the right end

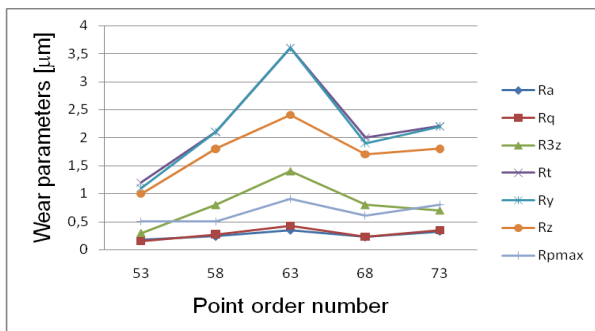


Fig. 14. Roughness parameters in extensive points for the third roller in the middle

The roughness parameters in the axial and extensive points for the first roller are shown in Fig. 6, 7 and 8. Roughness parameters in axial and extensive points for the second roller are shown in Fig. 9, 10 and 11. Roughness parameters in the axial and extensive points for the third roller are given in Fig. 12, 13 and 14. Last measurement points in the axial direction for all three

rollers are located outside the area of the exploitation of these and they are 50mm away from the frontal side of the rollers. In all three rollers inside measuring point are in the exploitation area.

In Fig. 6, 9 and 12 roughness parameters are smaller in area which is not exploitable than in exploitation area. Roughness parameters in the extensive points of exploitation area vary, but are still within the permitted tolerances. Based on the analysis of roughness parameters for all 75 measurement points can be observed that the least variation is for Ra, Rq and R3z, and the greatest variation is for Ry and Rz Rt.

4. CONCLUSION

Quality of machined surface has a significant impact on the performance of tribo-mechanical element. The topography is defined in exploitation area and in the area which is not exploitable for all three rollers. Based on the analysis of experimental measurement results it can be concluded that the roughness parameters are slightly higher in the exploitation area.

ACKNOWLEDGEMENT

This paper presents the research results obtained within the framework of a projects TR - 32035 and TR - 36030, financially supported by the Ministry of Science and Technological Development of the Republic of Serbia.

5. REFERENCES

- [1] Williams, J.A.: *Engineering Tribology*, Oxford university press, New York, 2000
- [2] Tanasijević, S.: *Tribološki isparavno konstruisanje*, Faculty of mechanical Engineering in Kragujevac, Kragujevac, 2004
- [3] Sovilj, B., Sovilj-Nikić, I., Gajić, V., Kovač, P., Pejić, V., Sovilj-Nikić, S., Varga, G.: *The parameters of gear teeth surface topography machined by coated and uncoated model hob milling tools*, Proceedings KOD 2012, pp. 467-472, Balatonfured, FTN, Novi Sad, 2012
- [4] Ivković, B., Rac, A.: *Tribologija*, Yugoslavian tribology society, Kragujevac, 1995
- [5] Myshkin, N.K., Grigoriev, A.Y., Chizhik, S.A., Choi, K.Y., Petrokovets, M.I.: *Surface roughness and texture analysis in microscale*, Wear, Vol. 254, No 10, pp.1001–1009, 2003
- [6] Serban, R. *Tribologie privere de Ansamblu*, Unversitea Tehnica "Gheorge Asachi", Iasi, 1997

Authors: Dojna Krecu¹, Ivan Sovilj-Nikić¹ PhD student., Prof. dr. Bogdan Sovilj¹, Prof. dr. Vladeta Gajić¹, Prof. dr. Stanislaw Legutko³, Assoc. prof. dr. Gyula Varga²
 1., Faculty of Technical Sciences, , Trg Dositeja Obradovica 6, 21000 Novi Sad, Serbia,
 2. University of Miskolc, Faculty of Mechanical Engineering, H3515 Miskolc-Egyetemvaros , Hungary
 3. Politechnika Poznanska, Piotrowo str. 3.,Poznan, Poland
 E-mail: bsovilj@uns.ac.rs, diomed17@gmail.com,
vgajic@uns.ac.rs, gyula.varga@uni-miskolc.hu,
stanislaw.legutko@put.poznan.pl

Kukuruzović, D., Berić, J., Kakaš, D., Škorić, B., Kovačević, L., Terek, P., Miletić, A., Vilotić, M.

APPLICATION OF A NEW DEVICE FOR MEASURING HARD COATINGS THICKNESS UNIFORMITY APPLIED ON LARGE SIZE TOOLS

Abstract: A novel design of equipment for measuring the thickness of thin surface films is presented in this article. In comparison to previous designs the new one brings a possibility to change the test ball position. This allows thickness measurement of coatings applied on large tools. This is of special importance because it is difficult to achieve uniform thickness on large tools and thickness measurement is not possible by using standard equipment. All tests were conducted on steel discs coated with 0.8 μm thick TiN hard coating. Prior to the coating deposition sample surfaces were prepared to a different degree of surface roughness. Obtained results show that the new equipment can be successfully used on large-sized coated tools if a proper measurement method is chosen.

Keywords: ball crater test, thickness, hard coating, large tools

1. INTRODUCTION

There is a great number of different tests used for coating thickness determination, such as profilometry [1], scanning electron microscopy [2] ball cratering method [3] and others. Among them the ball crater test stands up as the mostly used and favorable because it is fast, accurate, inexpensive and can be used of single and multilayered coatings. The test can be used to measure the thickness from 0.1 to 50 μm . Some companies which produce coating research equipment refer to this test as calotest. The test has found widespread use in measuring the thickness of hard and super-hard coatings which are very important for the field of mechanical engineering, particularly in the area of production tools. Casting dies, especially the ones used for pressure casting appear to have significantly large dimensions. Measurement of coating thickness on different areas of such large tools is not possible by using standard ball cratering equipment. When it is not possible to measure the coating thickness, evaluation of the deposition process quality is significantly affected. Lately, the so called industrial calotester [4] was introduced. This device gives a possibility to measure the thickness of surface layers applied on mechanical parts which have larger dimensions. However, this device is characterized by relatively complicated and expensive design. Therefore, we decided to propose a novel design of a ball cratering device which can be easily produced and on low costs. It is proposed that drive shaft have a large overhang, which would enable measurement of coating thickness on different surfaces of large tools.

2. EXPERIMENTAL DETAILS

2.1 Principle of ball crater test

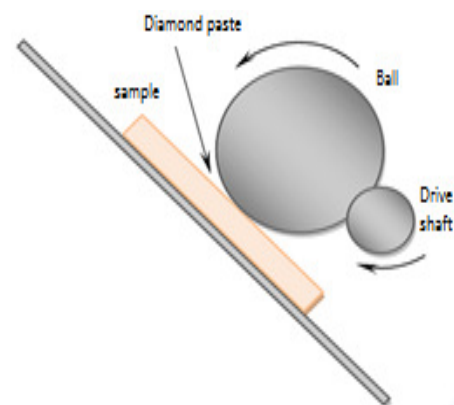


Fig. 1. Schematic of coating thickness measurement

A rotating hardened steel sphere with a known diameter is pressed onto the surface of a coated test sample or an actual coated mechanical component. Diamond abrasive paste is applied to the sphere and as it rotates the crater is abraded through the coating to the substrate [5]. The normal force applied on the sample is determined by the ball weight and angle of the sample holder. The ball is rotated via the via the drive shaft with adjustable rotating speed. A schematic of the ball crater test is presented in Fig. 1.

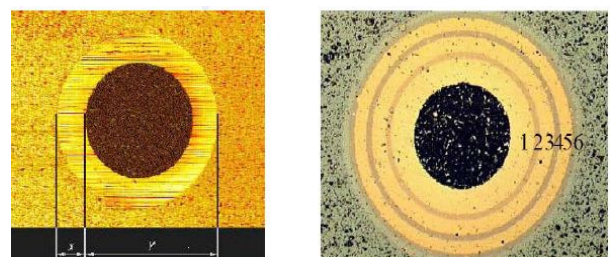


Fig. 2. Typical crater formed after testing a) monolayer, b) multilayer coating [5]

The resulting crater is observed by optical microscope and distances “x” and “y” are measured (Fig. 2). The thickness of the coating is calculated according to sample geometry. Captured images can be stored for future references which is particularly useful when the coating equipment is part of a production department.

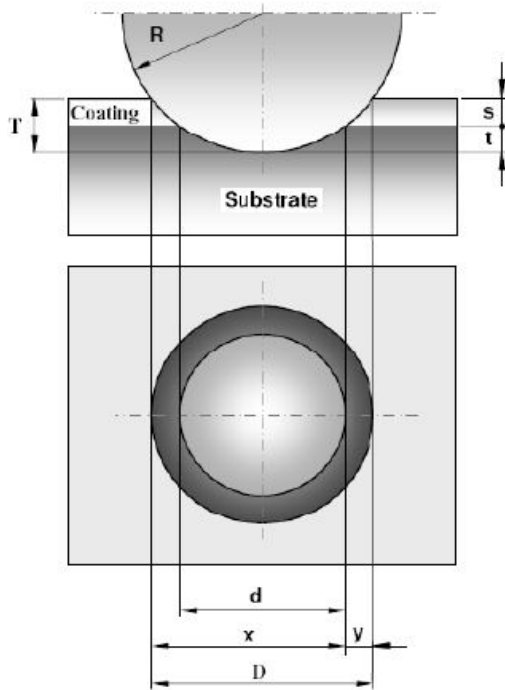


Fig. 3. Determining the coating thickness on a flat sample [5]

Ball crater test can be applied on flat samples, sphere and cylinder samples. Thickness of the coating applied on flat samples can be determined in the following manner (see Fig. 3):

$$s = T - t \quad (1)$$

where T present the depth of penetration:

$$T = R - \left(\frac{1}{2}\sqrt{4R^2 - D^2}\right) \quad (2)$$

t is the depth of penetration in substrate:

$$t = R - \left(\frac{1}{2}\sqrt{4R^2 - d^2}\right) \quad (3)$$

Finally the coating thickness can be determined:

$$s = \frac{1}{2}(\sqrt{4R^2 - d^2} - \sqrt{4R^2 - D^2}) \quad (4)$$

If $d \approx D$ and $D \leftrightarrow R$ it follows that:

$$s = \frac{xy}{2R} \quad (5)$$

2.2 Types of ball crater test devices and their application

Two types of ball crater test devices can be commercially found:

- Compact calotest device
- Industrial calotest device

Compact calotest device (Fig. 4a) is used to measure coating thickness on small samples that can be mounted on a holder [4].

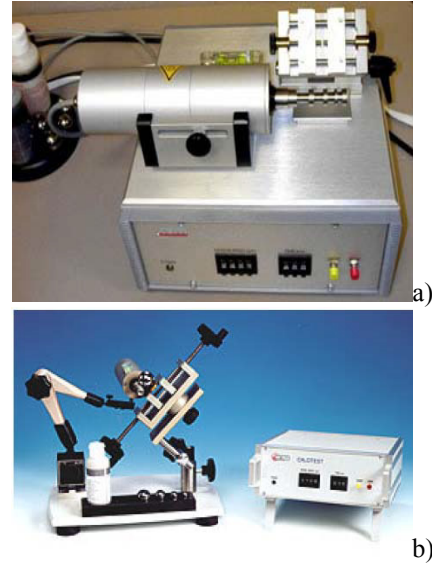


Fig. 4. Types of ball crater test devices : a) compact calotest, b) industrial calotest [4].

Industrial calotest (Fig. 4b) has several advantages: the motorized shaft on which the ball rotates is held by an adjustable arm which allows great flexibility in how the ball is positioned on the sample. For particularly bulky samples which are too big to be mounted in the sample holder provided, the complete arm and motor assembly can be removed and directly clamped to the side of the sample.

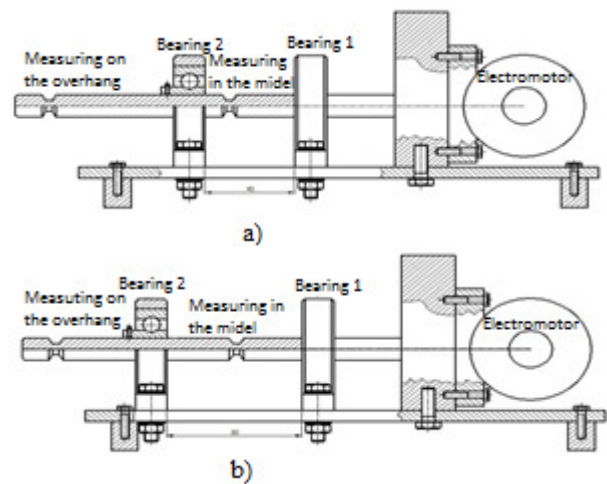


Fig. 5. Position of the bearings in eccentricity measurements: a) Position of gathered bearings, b) Position of widespread bearings

The schematic of new equipment for characterization of large tools is presented in Fig. 5. In order to test the applicability of the device for accurate coating thickness determination the eccentricity of drive shaft for different bearing positions was determined (see Fig. 5). Each measurement was repeated 3 times. After these tests, thickness of TiN coating applied on polished and grounded samples was determined, again with test ball positioned on two different positions. Test balls of two different sizes were used 17.15 mm and 27 mm. Optical microscopy was used for determination of crater dimension.

3. RESULTS

The results of eccentricity measurements are presented in Table 1.

gathered bearings						
angle of measurement	between bearings			on overhang		
	1	2	3	1	2	3
0	0	0	0	0	0	0
90	0	0	0,5	11	11	12
180	0,3	0,5	0,9	26	27	29
270	0,9	0	0,1	11	11	12
widespread bearings						
angle of measurement	between bearings			on overhang		
	1	2	3	1	2	3
0	0	0	0	0	0	0
90	0,5	0,6	0,6	12	13	14
180	0,1	0,7	0,5	25	24	26
270	0,2	0	0	11	9	10

Table 1. Shows the oscillation of the shaft during the measurement influencing the imprint form

Crater dimensions needed for calculation of coating thickness are determined by using the software "ScopePhoto". The method used is shown in Fig. 6.

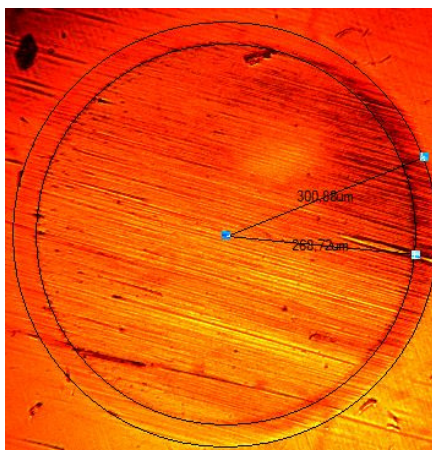
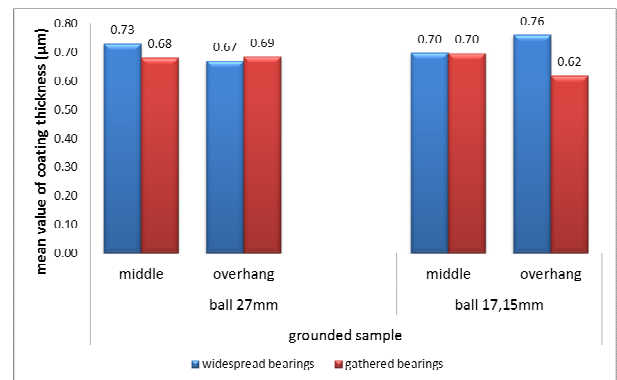
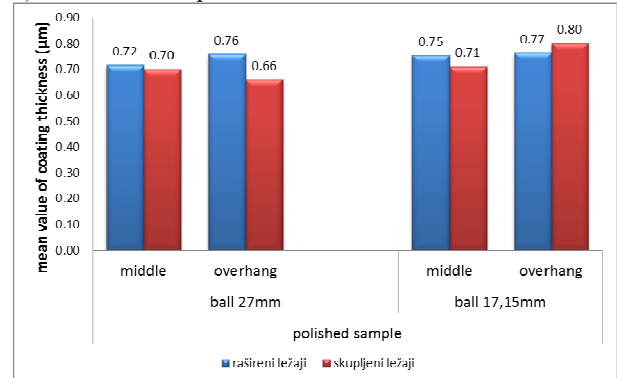


Fig. 6. Example of determination of the crater radius

Mean values of the coating thickness of polished and grounded samples measured with ball of two different diameters at two different ball and bearing positions are presented in Fig. 7.



a) Grounded sample



b) Polished sample

Fig. 7. Mean value of coating thickness

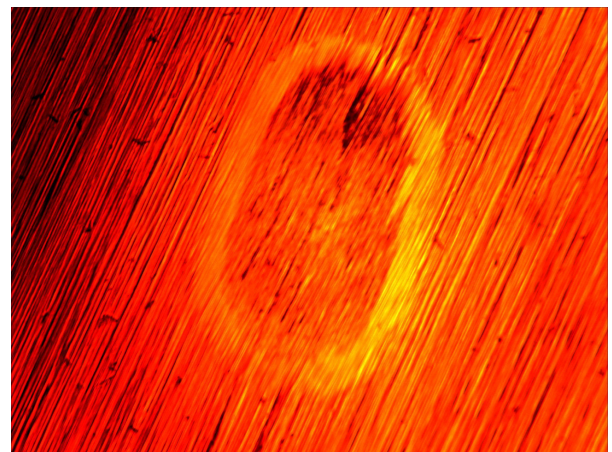


Fig. 8. Image of the crater formed when measuring on the overhang

Fig. 8. shows elliptical print obtained on the overhang. The wear of the coating takes place at an angle when it is conducted on the overhang do too oscillation of the shaft. The angle is measured by line being horizontal, i.e. parallel to the base, and the other line parallel with the trace of wear.

The influence of the angle of wear on dispersions of coating thickness measured on the left and right sides of the imprint can be described by equation 7.

$$S_R = \left(1 - \frac{\cos \alpha}{5}\right) \cdot S_L \quad (7)$$

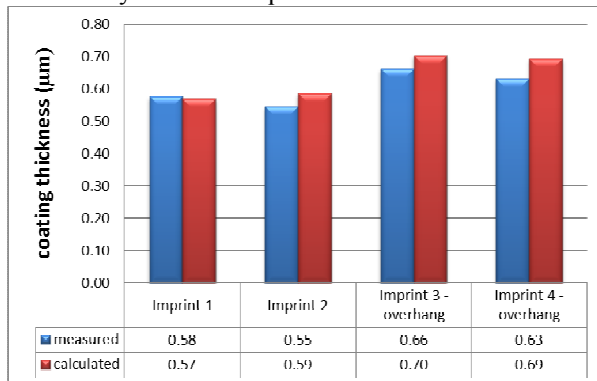
Where:

S_L - medium-measured value of coating thickness on the left mark

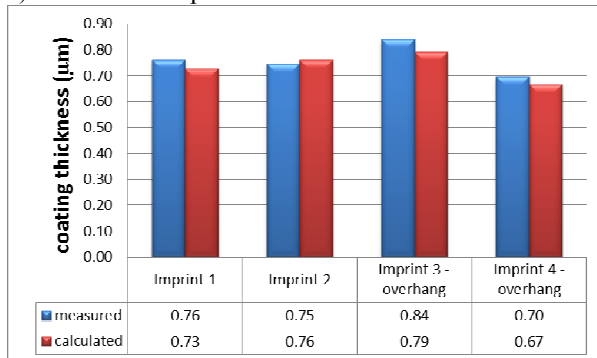
S_R - computed value of the coating thickness on the right track

α - angle tear lines in the horizontal relation

Fig. 9. shows how the measurement direction influences the value of coating thickness which is obtained by the use of equation 7.



a) Grounded sample



b) Polirani uzorak

Fig. 11. Relation of coating thickness values on the right side obtain by measurement and calculation

4. CONCLUSION

The aim of the work was to show the functionality and accuracy of calotest device constructed by the Center for Surface Engineering and Nanotechnology.

Form of wear traces is significantly different if the ball is in the middle (usually a circular footprint), compared to the elliptical shape of the traces if the overhang is used.

By carefully measuring the geometry of the image and averaging the results can be obtained acceptable results in deviations higher than the mean thickness of the coating and the circular and elliptical traces of wear. This means that the device can be used successfully to measure in the middle or on the overhang for coatings with a thickness of one micron or more.

On the basis of previous results, and on the basis of the data we can say that the device constructed in the Center for Surface Engineering and Nanotechnology is suitable for measuring the thickness of coatings on both small and large tools.

5. ACKNOWLEDGMENTS

The research presented in this article was supported by the Serbian Ministry of Education and Science which authors gratefully acknowledge.

6. REFERENCES

- [1] P. Kondaiah, M.C. Sekhar, S.V.J. Chandra, R. Martins, S. Uthanna, E. Elangovan, Influence of substrate bias voltage on the physical, electrical and dielectric properties of RF magnetron sputtered TiO₂ films, Department of Physics, Sri Venkateswara University, Tirupati - 517 502, India, CENIMAT/I3N, Departamento de Ciência Dos Materiais, Universidade Nova de Lisboa, 2829-516 Caparica, Portugal
- [2] P. Panjan, I. Bončina, J. Bevk, M. Čekada, PVD hard coatings applied for the wear protection of drawing dies, Jožef Stefan Institute, Jamova 39, 1000 Ljubljana, Slovenia, Kolektor Pro d. o. o., Vojkova 10, 5280 Idrija, Slovenia, 26 April 2005
- [3] E.H.A. Dekempeneera, L. Poirierb, J.P. Lebrunb, A. Pasgrimaudc, Y. Desalosc, F. Balanckd, Development of an industrialised DLC duplex treatment process, Materials Department, Vlaamse Instelling voor Technologisch Onderzoek, Boeretang 200, 2400 Mol, Belgium, Nitruvid, Rue Jean Poulmarch 9, 95100 Argenteuil, France, Renault Technocentre, Avenue du Golf 1, 78288 Guyancourt, France, Surface Treatment Company, Schurhovenveld 4077, 3800 Sint-Truiden, Belgium
- [4] http://www.csm-instruments.com/en/Coating_thickness
- [5] D. Kakaš, Surface Engineering, Novi Sad, January 2008
- [6] D. Milikić, The technology of machining, Novi Sad 2003
- [7] B. Arsenović, Z. Hedge, B. Ivanović, M. Sarić, J. Pješčić Analysis of mechanical and structural and morphological characteristics of nickel coatings sulfamatnog, , original work
- [8] HOT-GALVANIZED PRODUCTS supply and demand in the domestic market, the Association of Metallurgical Engineers of Serbia Technical paper AMES UDC: 669 581 = 861
- [9] SKF 20 edition, January 2002

Authors: M.Sc. Dragan Kukuruzovic , M.Sc. Jovica Beric, Prof. Dr. Damir Kakas, Prof. Dr. Branko Skoric, M.Sc. Pal Terek, M.Sc. Lazar Kovacevic, M.Sc. Aleksandar Miletic, Marko Vilotic, mag. sci., University of Novi Sad, Faculty of Technical Sciences, Institute for Production Engineering, Trg Dositeja Obradovica 6, 21000 Novi Sad, Serbia, Phone.: +381 69 383-382-2, Fax: +381 21 454-495.

E-mail: ing.kukuruzovic@gmail.com

jovica.beric@gmail.com

kakasdam@uns.ac.rs

skoricb@uns.ac.rs

terekpal@gmail.com

lazarkov@uns.ac.rs

miletic@uns.ac.rs

markovil@uns.ac.rs

Kukuruzović, D., Blagojević, D., Kakaš, D., Škorić, B., Kovačević, L., Terek, P., Miletić, A., Vilotić, M.

THE EFFECTS OF CUTTING PARAMETERS AND TOOL WEAR ON THE ROUGHNESS OF MACHINED SURFACE

Abstract: This paper presents the results of milling experiments performed by the machining center Lola HMC 500. Milling of carburized steel was done by F40M-Seco face mill tool under different machining spindle speeds and cutting speed. Experiment was conducted with new and worn out tools (with blunted edges) coated with same type of TiN coating. After the milling, morphology of machined surfaces was examined by SEM and the parameters of the surface roughness were determined by perthometer. Obtained results clearly demonstrate the correlation between the machined surface roughness and the blunting of the cutting tool. Such correlation allows quick decision on tool replacement or changing milling parameters by monitoring surface roughness.

Key words: Tool wear, face mill, TiN coating.

1. INTRODUCTION

Trends in the metal industry influence development of cutting tools. Given that mechanical engineers are constantly looking for new materials that are lighter, and at the same time have better mechanical properties, cutting tool designers need to develop tools that can process the new materials with the highest possible level of productivity. Tool geometry [1] and protective coatings [2] [3] give tools longer life time. As it is very difficult to achieve a better surface finish with cutting processes, the connection between micro (preparation of cutting edges) [1] and macro (tool rake surface topography) cutting tool geometry is becoming increasingly important. Because of the need for maximum tool utilization, the determination of appropriate time for tool replacement because of tool wear becomes a big problem. [4] This study was therefore conducted by using a completely new tool and a blunt tool, comparing the surface roughness of the processed workpieces.

2. EXPERIMENTAL DETAILS

Experimental testing is based on the sample processed by a blunt and sharp tool, using different processing parameters in order to gain insight into the difference in the quality of machined surface due to wear of tools. Therefore, the aim of this experimental research is the understanding the impact of tool wear on the surface quality of the workpiece and the importance of timely replacement of damaged tools. For this purpose the preparation of samples of low carbon steel were conducted on a horizontal machining center LOLA 500 [5] in HMC Company LLC Indjija techniques. For processing the samples were used two, exactly the same cutting tools (MM08 face mills F40M R05 with TiN protective coatings, manufacturer Seco Tools) with the exception that one of the tools was out of use due to reaching the critical level of wear and failure to achieve desired surface finish, while the other tool was new. In the course of the experiment cutting

parameters (spindle speed, velocity and feed) were varied, using both tools on the same sample. Samples were processed with a blunt and sharp tool with identical parameters. After processing, the roughness of the samples was examined by a perthometer after which the comparisons of mean and maximum height roughness of the samples were defined. Besides roughens tests, samples were subjected to a stereo microscope and SEM to capture the morphology of treated areas and tools cutting edge (new and worn).

2.1 Workpiece

The tested specimens were made of low carbon steel Č.1221, which belongs to the group of hardening steels. The chemical composition of the material of the samples is given in Table 1. Sample dimensions were Ø24 mm x 5 mm and surface preparation was done by grinding.

C	Si	Mn	P	S
0,12÷0,8	≤0,40	0,30÷0,60	≤0,035	≤0,035

Tab. 1. The chemical composition of the material % [6]

2.2 Cutting tool

For the purpose of this experimental study eight millimeters face mills were used, with three cutting edges and protective coating TiN MM08 F40M R05, manufacturer Seco Tools (Fig. 1a). The surface of this tool is coated with a PVD TiN layer (Fig. 1b) for fine processing and medium rough milling. Tools with this coating are designed for milling with small steps and / or low cutting speeds. It is excellent for milling in conditions where there is danger of vibration in terms of application of the coolant and lubricant. It is recommended for treatment of super alloys.



Fig. 1. Face mill MM08 F40M R05 [7]

2.3 Cooling lubricant chemicals (CLC)

CLC used for this investigation is the experimental synthetic liquid BIOSINT 050, FAM manufacturers. BIOSINT 050 is a synthetic biodegradable concentrate for forming a water solution that provides high-quality cooling, lubrication and corrosion protection. High quality surface processing and workable hardened steel, cast iron, non-ferrous metals. It is used for the operation of turning, milling, drilling, reaming and grinding the typical processing conditions, high resistance and high temperature. Performance of cutting fluids is given in Table 2. This concentrate is used for tests mixed with water at a concentration of 3% [8].

Viscosity on 40°C [mm ² /s]	Density on 20°C [g/ml]	pH-value (5% in wather)
4,0	1,040	8,0

Table 2. Cutting fluids properties [8]

2.4 Processing parameters

Processing of samples was performed using two cutting speeds and two spindle speed (n): 2000 and 4000 rpm. There was performed a variation of feed (f): 500, 1000 and 2000 mm/min, in combination with the erlier mentioned spindle speeds. Depending on the combination of spindle speed and feed, there were recorded following values of feed (f): 0.125, 0.25, 0.5 and 1 rpm. Cutting depth of 0.3 mm was maintained constant during the test.

3. RESULTS

Tool wear mechanisms occur during the experimental tests are summarized and discussed in this section. Also, we made a comparison of the surface roughness of the samples processed by sharp and blunt tools with identical cutting parameters.

3.1 Processing parameters

In Fig. 2. is given an overview of the state of cutting edges of worn tools. It is evident that some of the cutting edges wear different during application. The conclusion is reached by analyzing these images, that each edge doesn't wear the same intensity (top cutting edges 1 significantly less damage compared to the cutting edge 2 and 3, while the dorsal area of cutting edge 3 is significantly less damaged compared with the dorsal surfaces of cutting edges 1 and 2). Therefore, when one of the cutting edges reaches a critical level of wear, the tool must be replaced regardless of the degree wear of other cutting edges.

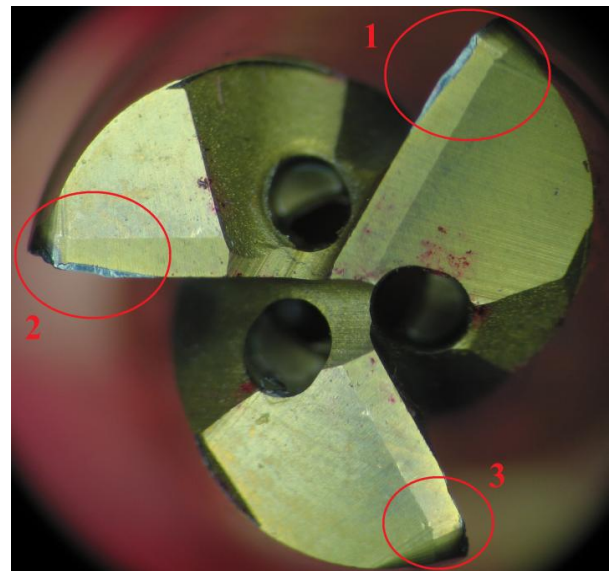


Fig. 2. Overview of the state of cutting edges of blunted tool

The worst damage suffered the second cutting edge. A more detailed insight into wear of the cutting edge of this peak is shown in Fig. 3. The dominant type of wear of the cutting edge is a great damage to the top of the cutting wedge (Fig. 3a). BSE footage of this part of the cutting edge (Fig. 3b) shows the width of the zone on the cutting edge where there has been a removal of protective coating. After removal of the coating, tool wear continued to be carried out by the wear mechanisms of uncoated tools. Therefore, because of the severe processing regime, the process of wear became more and more intense. In this way one can explain the severe damage to the top of the cutting edge.

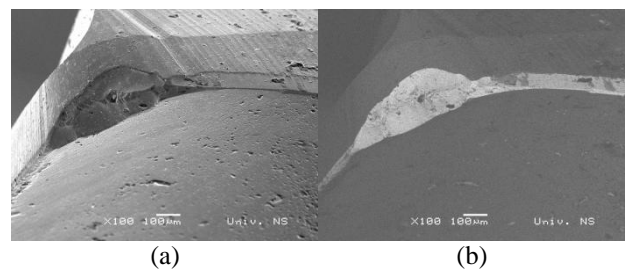


Fig. 3. SEM image. Viwe of cuttin edge 2 wear

3.2 Wear mechanisms of new cutting tool

In order to gain insight into the influence of tool wear on the surface quality of the workpiece, a new tool was used for the processing of samples. Figure 4 provides an overview of the state of the new tools cutting edges. In the picture you can see that the cutting edges of the tool suffered far less damage than the blunt tool. Also, it is possible to note that even with a new tool; different cutting edges do not wear the same intensity.

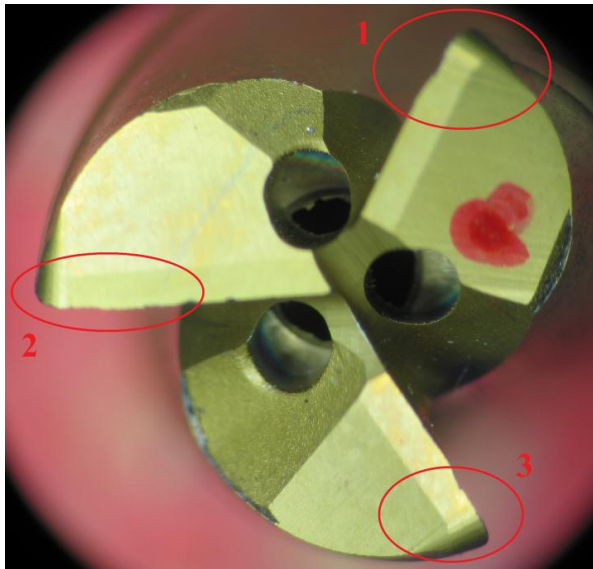


Fig. 4. Overview of the state of cutting edges of new tool

The analysis of images obtained by SEM by observing tool cutting edge surfaces have identified two important defects present on cutting edges 2 and 3. On the cutting edge 2 there was a localized rupture of the coating, while on the rake surface of cutting edge 3 occurred a removal of the protective coating.

The following image shows details of two cutting edges, where there has been considerable damage to the coating. Fig. 5a shows great damage to the cutting edge, and paste formed on the dorsal surface right by the damage. From the picture it can be concluded that the paste was formed by the parts of the broken cutting edge. BSE recording of this zone (Fig. 5b) confirmed the hypothesis and the picture clearly shows that the material from which the paste is formed corresponds to the base metal of the tool. Broken off parts of the cutting edge, immediately after the rupture, welded to the rear surface and thus form a paste. Such damage could result in a stroke that occurred during processing.

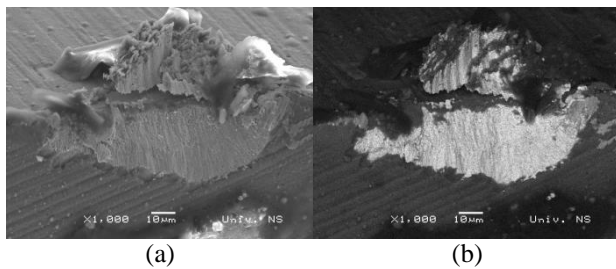


Fig. 5. SEM image. Viwe of damaged cutting edge 2

Detail of damage to the rake area of cutting edge 3 is shown in the following figure. This damage could be a place where there has been a removal of protective coating. The size of this damage was measured in Fig. 6a, where it is clear that its length is about 280 µm and width of 80 µm. BSE footage of damage, as shown in Fig. 6b, shows that at this point, there has really been removal of the coating. Given that this is a new tool, it can be concluded that the adhesion of coating on this part of the rake area was not satisfactory.

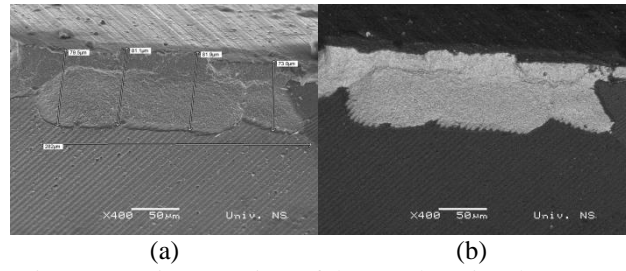


Fig. 6. SEM image. Viwe of damaged cutting edge 3

3.3 Surface quality

Tools, in which the degree of wear was analyzed in the previous section, is based on analyzing samples of low carbon steel. During the experiment, the surfaces were treated with different processing parameters (Table 3). After processing, surfaces were measured using a surface roughness pertometer and surface quality was evaluated by comparing the maximum and average surface roughness.

The following table shows the processing parameters on the surface of some samples, as well as the values of average (R_a) and maximum roughness (R_{max}).

Tool	Sample	Side	n [rpm]	f [mm/min]	R_a [µm]	R_{max} [µm]
Blunt	1	Left	2000	1000	2,394	12,20
		Right	4000	2000	2,486	22,10
	2	Left	4000	1000	3,587	22,30
		Right	2000	2000	2,824	19,20
	3	Left	2000	500	2,732	17,40
		Right	4000	500	3,166	32,70
New	4	Left	4000	500	0,771	5,91
		Right	2000	500	0,720	4,85
	5	Left	2000	1000	0,811	5,05
		Right	4000	1000	0,970	6,84
	6	Right	4000	2000	0,963	5,81

Table 3. Processing parameters of the surface and values of R_a and R_{max}

The analysis of data presented in the above table clearly shows that the surface roughness of the samples processed by the blunt tool is significantly higher than the surface roughness treated with the new tool. It is evident that with increasing of spindle speed, with an unchanged feed, you get a poorer surface quality. Also, the maximum roughness was achieved by processing the samples with 4000 rpm.

Fig. 6. shows the dependence of the average roughness and spindle feed at a constant speed. The treatment of the sample with a blunt tool at 2000 mm/min, there is a notable decrease of average height with increase of spindle speed, while for all other values the average roughness increases with increasing of spindle speed (for new tool slightly).

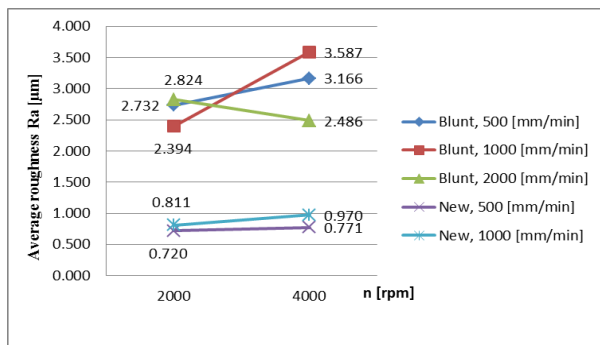


Fig. 6. Dependence of R_a to n at a constant f

Dependence of maximum roughness to spindle speed, with a constant feed, is shown in Fig. 7. During the processing with the new tool, and the feed of 2000 mm/min there were significantly smaller increases in maximum roughness with increasing of spindle speed with respect to feed in relation to the maximum surface roughness obtained with 500 and 1000 mm/min with a blunt tool.

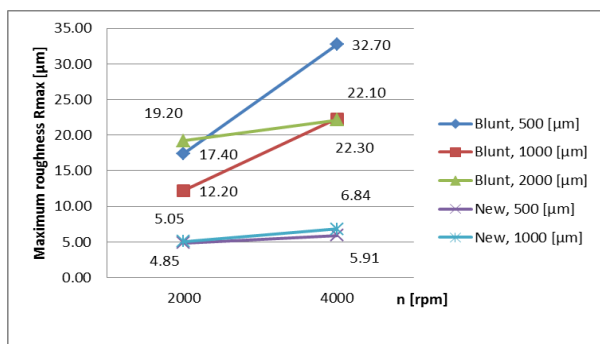


Fig. 7. Dependence of R_{max} to n at a constant f

The following figure shows the surfaces with the highest surface roughness, sample 2 on the left and sample 3 on the right



Fig. 8. Display of surfaces with the highest roughness

4. CONCLUSION

In practice the method for evaluation of surface quality is a suitable criterion for evaluation of tool wear. Therefore, an experiment was made with a brand new and a blunt tool, under various processing modes. The results clearly showed that the worn tool surface quality differs significantly in terms of changes in R_a and R_{max} .

It is noted that the change in the parameter values also affect the surface quality, as well as application of the new and blunt tool. Increasing of spindle speed leads to

the increase in the surface roughness. This phenomenon is more pronounced for worn tools than new unused tools.

One of the important conclusions which occurred as part of this experiment, is the fact that cutting edges of cutting tools do not wear the same manner and with the same intensity in the processing of workpieces. Therefore, the timely replacement of worn tools depends solely on the degree of wear for the most damaged cutting.

5. REFERENCES

- [1] G. Bissacco, H.N. Hansen, L. De Chiffre, Micromilling of hardened tool steel for mould making applications, Department of Manufacturing Engineering and Management, Technical University of Denmark, Building 427 South, Produktionstorvet, DK-2800 Lyngby, Denmark, Received 15 March 2005; received in revised form 27 May 2005; accepted 28 May 2005
- [2] J. Gu, G. Barber, S. Tung, R.J. Gu, Tool life and wear mechanism of uncoated and coated milling inserts, GM Powertrain, USA, Oakland University, Rochester, MI, USA, GM Research and Development Center, USA
- [3] A. Aramcharoen, P.T. Mativenga, S. Yang, K.E. Cooke, D.G. Teer, Evaluation and selection of hard coatings for micro milling of hardened tool steel, Manufacturing and Laser Processing, School of Mechanical, Aerospace and Civil Engineering, The University of Manchester, Manchester M60 1QD, UK, Teer Coatings Ltd., UK
- [4] W. Chang, J. Sun, X. Luo, J.M. Ritchie, C. Mack, Investigation of microstructured milling tool for deferring tool wear, School of Engineering and Physical Sciences, Heriot-Watt University, Edinburgh EH14 4AS, UK
- [5] <http://www.strojopromet.com/crna-metalurgija/>
- [6] http://cent.mas.bg.ac.rs/nastava/statut99/ma/ma_fil/es/pdf/hmc500final.pdf
- [7] http://legacy.secotools.com/upload/north_america/usa/pdf/technical%20info/272-273%20Carbide%20Grades.pdf
- [8] <http://www.fam.co.rs/index.php/products/view/serbian/266>

Authors: M.Sc. Dragan Kukuruzovic, M.Sc. Danijel Blagojevic, Prof. Dr. Damir Kakas, Prof. Dr. Branko Skoric, M.Sc. Pal Terek, M.Sc. Lazar Kovacevic, M.Sc. Aleksandar Miletic, Marko Vilotic, mag. sci., University of Novi Sad, Faculty of Technical Sciences, Institute for Production Engineering, Trg Dositeja Obradovica 6, 21000 Novi Sad, Serbia, Phone.: +381 69 383-382-2, Fax: +381 21 454-495.

E-mail: ing.kukuruzovic@gmail.com

kakasad@uns.ac.rs branko.skoric@uns.ac.rs
terekpal@gmail.com lazarkov@uns.ac.rs
miletic@uns.ac.rs markovil@uns.ac.rs

Kuzinovski, M., Tomov, M., Cichosz, P.

INVESTIGATION OF GAUSSIAN AND 2RC FILTRATION IN SURFACE ROUGHNESS MEASUREMENT FROM THE STANDPOINT OF AMBIGUITIES IN STANDARDS. PART I-THEORETICAL ANALYSIS

Abstract: This investigation provides an elaboration of the significance that the software filtering process has in determining roughness profile from primary profiles. The analysis explored the Gaussian and 2RC filters as the most frequently used filters in practical measurements. Shortcomings and disadvantages of Gaussian filter were examined, along with the possible effects on the determination of roughness profile. En emphasis is placed on the phase distortion of mean line obtained by using 2RC filter and its possible effects on the determination of the roughness profile. Certain ambiguities and differences in terms of the filtering that stem from the International ISO standards and ASME B46.1-2002 standard are illustrated.

Key words: Software filtration, Profile filter, Gaussian filter, 2RC filter

1. INTRODUCTION (GENERAL INFORMATION AND DILEMMAS)

A typical engineering surface consists of a range of spatial frequencies. High frequencies or short wavelength components are referred to as roughness, medium frequencies as waviness and low frequency components as form [1]. Review of geometric structure of the surface as a deviation from form, waviness and roughness is widely accepted and standardized [2,3,4,5,6,7]. Such separation is illustrated in Fig. 1 [2]. The idea for such separation of surfaces originates from the fact that roughness, waviness and form have various effects on the functionality of parts from several standpoints and hence such classification is considered as an important segment of surface texture analysis, according to [8].

A separation of this type may have offered more accurate and wider description of the effects of roughness, waviness and form upon some tribological processes that occur during the exploitation of parts, on one hand, but on the other hand, a rather significant dilemma has emerged: where is the actual boundary that divides roughness, waviness and form?

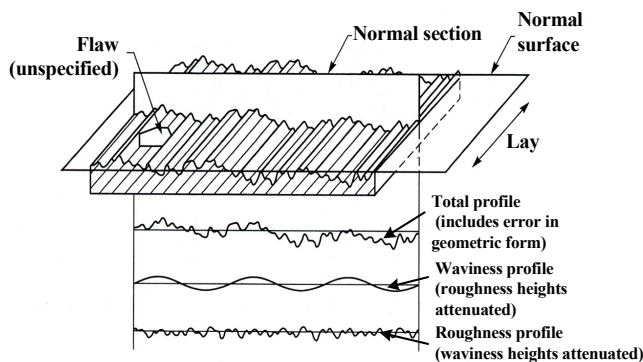


Fig. 1. Schematic diagram of surface characteristics [2]

What to compare the measured roughness profile to, when surface texture (which exists only physically)

consists of roughness, waviness and form.

This dilemma may be the fundamental drive of researchers engaged in surface metrology. The separation of roughness, waviness and form from measured profile can be made through a filtration process. Two filtration methods have prevailed in the measurement technique development, known as E filtration system and M filtration system [8,9]. E filtration system uses the envelope method (rolling a ball with certain diameter against surface) and is a mechanical filtration system characteristic of the oldest measuring instruments. The E system is once again finding new relevance, particularly with the introduction of morphological filtering in the international Standards ISO/TS 16610-40:2006 [10] and ISO/TS 16610-41:2006 [11]. Morphological filtering is essentially a superset of the E system and offers more tools and capabilities [9]. M filtration system involves use of a profile filter. Due to the fact that new instruments can simultaneously measure roughness, waviness and form, the mere term software filtration is nowadays equalized with the M filtration system. The outcomes deriving from the use of profile filters and the procedure for obtaining roughness and waviness profiles is standardized in ISO 4287:1997 [6]. The subjected International standard establishes definition of three profile filters λ_s , λ_c and λ_f . λ_s profile filter removes components with very short wave length (noise, stylus deformation and similar) of total profile. λ_c profile filter separates roughness profile from primary profile, while λ_f profile filter separates waviness from form. The filtration process which involves the use of λ_s , λ_c and λ_f profile filters for contact (stylus) measuring systems is presented in Fig. 2. Also, the literature comes across to profile filters broken down into low-pass with cut-off λ_s and high-pass with cut-off λ_c [9]. It is highly significant to underline that the American national standard ASME

B46.1-2002 [2], does not encompass the λ_f profile filter i.e. it is considered that the length used to determine the roughness profile is too small to additionally determine the form (form deviation) of the surface. Thus, it can be concluded that waviness profile determined pursuant to the international ISO standards can differ from the one determined pursuant to the ASME B46.1-2002 standard. According to ISO 3274:1996 [12], λ_s the profile filter is incorporated in the construction of any stylus instruments, and in most cases the activation for the simpler contact measuring instruments with display is run automatically (regardless of the operator's will).

In the same time with the advent and development of profilometers, an increasing number of experiments were made for replacing the analogue continuous signal with digital signal. The latter is used to present the roughness profile. Simultaneously, probable solutions for replacing E filtration system were also sought. As a result, the analogue (hardware) 2RC filter was developed, constituting an electrical link of two condensers and two resistors. It was used exclusively to distinguish the roughness profile from the measured profile as an analogue signal in real time. Later, Whitehouse and Reason [1,9] performed simulation and replacement of hardware 2RC filter with a software solution. A weighting function was introduced for this purpose, described through a mathematical equation which brought in a term called cut-off (λ). The value of cut-off is currently standardized in ISO 3274:1996 [12] and selected depending on the stylus radius size (for contact measuring systems) and max sampling spacing. Due to the lack of further scientific clarifications, we can say that the recommendations regarding the selection of a cut-off wavelength of the profile filter contained in [12] are the agreed values. The cut-off wavelength of the profile filter is equal to the value of the roughness sampling length. Therefore, the dependencies referred to [12] are directly associated

with the recommendations contained in ISO 4288:1996 [13]. In [13], the roughness sampling length is associated with the roughness evaluation length, the surface type (periodic or non-periodic) and the values of R_a , R_z and R_{sm} for the relevant surface. In addition, there is an overriding need of more thorough researches on the mode of expressing (quantitative) of periodic or non-periodic level of surface, regardless of the parameters used for describing roughness profile.

2. METROLOGY CHARACTERISTICS OF 2RC AND GAUSSIAN FILTERS

2.1 2RC filter

The analogue 2RC (two-resistor-capacitor) filter is the earliest filter used in surface metrology for filtering in compliance with the M system. The digital version of 2RC profile filter has standardized the metrological characteristics contained in ASME B46.1 -2002 [2]. The 2RC profile filter is not presently included in the International ISO standards. The weighting function of 2RC filter is given by [2]:

$$S(x) = \frac{A}{\lambda_c} \left(2 - A \frac{|x|}{\lambda_c} \right) \exp \left(-A \frac{|x|}{\lambda_c} \right) \quad (1)$$

where $A=3,64$ for 75 % transmission of λ_c , x is the position in millimeters from the origin of the weighting function ($-\infty < x < 0$), and λ_c is long wavelength roughness cut-off. The transfer function is given with [2]:

$$\frac{\text{FilterOutput}}{\text{FilterInput}} = \left(1 - ik \frac{\lambda}{\lambda_c} \right)^{-2} \quad (2)$$

where $i = \sqrt{-1}$ and $k = 1/\sqrt{3} = 0.577$. 2RC filter performs 75 % amplitude reduction of sinusoid signal that has a wave length equal to the cut-off, which could be obtained by replacing $\lambda = \lambda_c$ in equation (2).

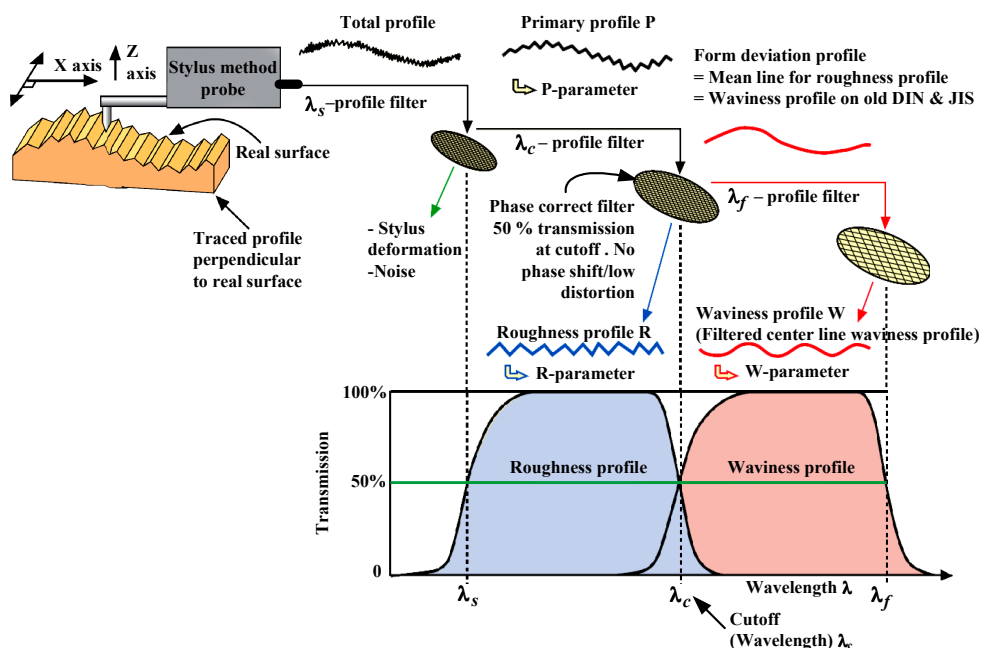


Fig. 2. Filtration process using λ_s , λ_c and λ_f profile filters [7].

According to [2], the transfer function of 2RC filter given by the equation (2) has lower and upper limit.

The mean line is obtained by convolving the primary profile with the weighting function given in the equation (1). In determining the mean line, the weighting function is generated in the interval $-2\lambda_c \leq x \leq 0$, since the filter (its weighting function) is asymmetrical in respect of the origin [1,9]. The mean line determined by using 2RC filter does not represent the waviness profile, considering that this is an unsymmetrical filter [1,9]. Roughness profile can be obtained by subtracting the filter mean line from the primary profile. The major disadvantage of the 2RC filter is its non-linear phase which results in a phase distortion of the mean line in respect of the primary profile, Fig. 3.a. This phase distortion later results into occurrence of deviation and artificial feature of roughness profile, as portrayed in Fig. 3.b. The phase distortion becomes more expressed as the cut-off increases.

Other features that may be seen as disadvantages of the 2RC filter can be the distortion of the mean line on primary profile ends and its sensitivity to deep valleys of the primary profile, which results into pulling down of the filter mean line from the mid part of the profile towards the valley. The distortion of filter mean line on primary profile ends is particularly enunciated in primary profiles comprised of accentuated waviness and deviation of form. To reduce this drawback, the beginning of the primary profile is shortened in length for $2\lambda_c$ [1,8,9]. Due to the subjected shortening of the primary profile length, the 2RC filter cannot be used for measurement of very short profiles.

Another noticeable drawback regarding the 2RC filter with metrological characteristics which is used to obtain the mean line is that it cannot be used for obtaining waviness profile.

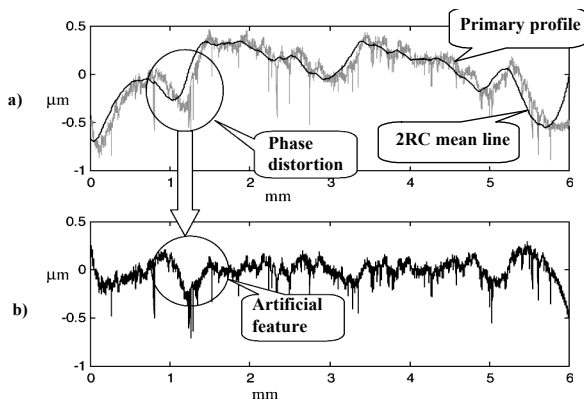


Fig. 3. (a) Primary profile and 2RC mean line (non-waviness profile); (b) roughness profile [1].

2.2. Gaussian filter

The metrological characteristics of the phase correct Gaussian filter for open profiles are standardized in ISO 16610-21:2011 [14] and ASME B46.1-2002 [2]. The weighting function of an open profile filter has the equation of the Gaussian function with the cut-off wavelength λ_c , where c is cut-off. The equation is given by [14,15]:

$$S(x) = \frac{1}{\alpha\lambda_c} \exp\left[-\pi\left(\frac{x}{\alpha\lambda_c}\right)^2\right] \quad (3)$$

where $\alpha = \sqrt{\ln 2 / \pi} = 0.4697$, x is the distance from the centre (maximum) of the weighting function, and λ_c is the cut-off wavelength. The transmission characteristic of the long wave component (mean line) is given by [2, 14,15]:

$$\frac{A_1}{A_0} = \exp\left[-\pi\left(\alpha\frac{\lambda_c}{\lambda}\right)^2\right] \quad (4)$$

where A_0 is the amplitude of a sinusoidal wave profile before filtering, A_1 is the amplitude of this sinusoidal profile in the mean line, and λ is the wavelength of this sinusoidal profile.

It can be seen in equation (4) that the amplitude attenuation of a sinusoid profile is 0.5, when the wavelength is equal to the cut-off ($\lambda = \lambda_c$), which leads to the conclusion that the transmission characteristic of Gaussian filter is 50%. The transmission characteristics of Gaussian filter for value of λ_c of 0.08; 0.25; 0.8; 2.5 and 8 mm are presented in [2].

Gaussian filters can be low-pass or high-pass. The formulas given in equations (3) and (4) refer to the low-pass Gaussian filter [1,9].

Roughness profile of primary profile is obtained as a difference between the primary profile and the mean line determined by a Gaussian filter. According to ASME B46.1 -2002, the mean line determined by a Gaussian low-pass filter represents the waviness profile.

An important property of Gaussian filter is its linear phase, which is a major advantage over 2RC filter.

According to [1,8,9], the Gaussian filter is marked with certain disadvantages. Namely, the mean line determined by Gaussian filter has distortion on the profile ends (end effects) as a result of the openness of the primary profile, Fig. 4. This is not the case when the subjected is applied on closed profiles.

The ISO/TS 16610-28:2010 [16] listed five ways (zero padding, linear extrapolation, line symmetrical reflection, point symmetrical reflection and moment retention criterion) to overcome the distortion at the edges (end effects) of mean line when it is determined by Gaussian filter.

Generally, in the case of zero padding, the distortion of the mean line will always be directed towards the zero-point of the z axis. The distortions will be larger if primary profile ends are more remote from the zero-point of the z axis.

This is the main reason behind the shortening of the roughness profile in respect of the primary profile for one half of λ_c on both profile ends. In order to reduce this negative effect in measuring spherical or cylindrical surfaces, it is recommended to remove the form from the profile in the first place and then to apply the Gaussian filter. As a consequence to the discarding parts of the primary profile in amount of one λ_c , the standardized Gaussian filter is not applicable for

measurement of very short profiles, which can be considered as its second disadvantage.

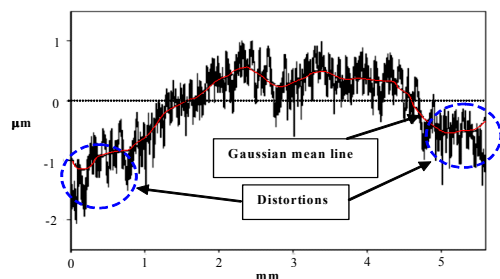


Fig. 4. End effects using standardized Gaussian filter [17].

Third disadvantage is deemed to be its sensitivity to deep valleys on the primary profile, which results in the mean line being pulled down from the mid part of the profile towards the valley, and later in distortion of the roughness profile near the valley, Fig. 5.

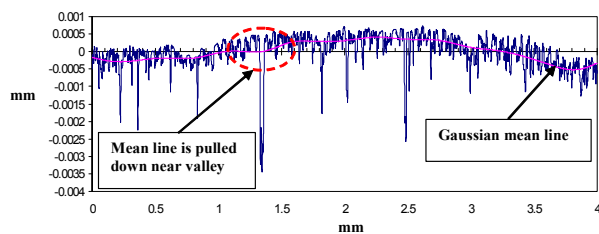


Fig. 5. Pulling down of the mean line from the mid portion of the primary profile towards the valley

To the end of overcoming this disadvantage, ISO 13565-1:1996 [18] foresees special filtration mode of primary profiles with deep valleys, through the use of phase correct filter.

It is significant to mention that the standard ISO 13565-1:1996 [18] provides considerable flexibility in terms of the application of this filtration mode. The only condition for application of this filtration mode is the presence of deep valleys in the primary profile, without precise definition of the number of valleys of certain measuring length or the value that the valleys should have in order to be applicable for this process.

3. CONCLUSION

The disadvantages and limitations of the Gaussian and 2RC filters i.e. their side effects on the roughness profile depend mostly on the primary profile form to which these will be applied.

4. REFERENCES

[1] J. Raja, B. Muralikrishnan, Shengyu Fu. *Recent advances in separation of roughness, waviness and form*. Journal of the International Societies for Precision Engineering and Nanotechnology. 26 (2002), pp. 222–235.

[2] ASME B46.1-2002. *Surface Texture (Surface Roughness, Waviness, and Lay)*. The American Society of Mechanical Engineers.

[3] BS 1134-1. *Assessment of surface texture. Methods and instrumentation*, 1988.

[4] BS 1134-2. *Assessment of surface texture. Guidance and general information*.1990.

[5] DIN 4760. *Gestaltabweichungen. Begriffe. Ordnungssystem*. Juni,1982.

[6] ISO 4287:1997. *Geometrical Product Specifications (GPS)-Surface texture: Profile method-Terms, definitions and surface texture parameters*.

[7] JIS B0601 Standard. *Explanation of Surface Characteristic*, Japan.

[8] D. J. Whitehouse. *Handbook of Surface and Nanometrology* (Second edition). CRC Press, Taylor & Francis Group, 2011.

[9] B. Muralikrishnan, J. Raja. *Computational Surface and Roughness Metrology*. Springer, London 2009.

[10] ISO 16610-40:2006; *Geometrical product specifications (GPS)-Filtration: Morphological profile filters: Basic concepts*.

[11] ISO 16610-41:2006; *Geometrical product specifications (GPS)-Filtration: Morphological profile filters: Disk and horizontal line-segment filters*.

[12] ISO 3274:1996; *Geometrical Product Specifications (GPS) - Surface texture: Profile method-Nominal characteristics of contact stylus instruments*.

[13] ISO 4288:1996; *Geometrical product specifications (GPS)-Surface texture: Profile method-Rules and procedures for the assessment of surface texture*.

[14] ISO 16610-21:2011; *Geometrical product specifications (GPS)-Filtration: Linear profile filters: Gaussian filters*.

[15] ISO 11562:1996; *Geometrical Product Specifications (GPS) - Surface texture: Profile method-Metrological characteristics of phase correct filters*.

[16] ISO/TS 16610-28:2010; *Geometrical product specifications (GPS)-Filtration-Part 28: Profile filters: End effects*.

[17] *Filters in Surface Texture (Explained)-Presentation*. Paul J Scott, the Taylor Hobson Visiting Industrial Professor.

[18] ISO 13565-1:1996; *Geometrical Product Specifications (GPS)-Surface texture: Profile method; Surfaces having stratified functional properties-Part 1: Filtering and general measurement conditions*.

Authors: Prof. Mikolaj Kuzinovski, PhD, Ass. Mite Tomov, MSc, "Ss. Cyril and Methodius" University in Skopje, Faculty of Mechanical Engineering-Skopje, , Karposh II bb, P. Fax 464, 1000 Skopje R.Macedonia., **Prof. Piotr Cichosz, DSc**, Institute of Production Engineering and Automation of the Wroclaw University of Technology, str. Lukasiewicza 3/5, 50-371 Wroclaw, Polska
E-mail: mikolaj@mf.edu.mk
mitetomov@mf.edu.mk
piotrc@itma.pwr.wroc.pl

Morača, S., Milin, D.

CLUSTERS AND NETWORK VALUE SYSTEM

Abstract: *During the last decade, the cluster concept has become central idea of competitiveness and economic development. Industrial clusters have been considered as one of the most important channels towards open innovation and economic excellence. The network value system must be integrated in the core business of the industry cluster. Both of them focus on improving the competitive advantage over their competitors. Importance of clusters and network value creation was discussed in this paper. Basic characteristics of clusters were given, together with ways how knowledge and innovation can be created in cluster networks.*

Key words: *clusters, network value, knowledge creation*

1. INTRODUCTION

During the last decade, the cluster concept has become central idea of competitiveness and economic development. Thanks to the literature and case studies, the reasons for cluster productivity and innovation are better known. Not only that, but encouraging cooperation between companies in clusters is now accepted as an effective instrument for strengthening the company, enabling it to produce goods and services of higher level that will create wealth in domestic and international markets.

Nowadays industrial clusters have been considered as one of the most important channels towards open innovation and economic excellence. There are signs that suggest industrial clusters might improve economic conditions of a region by means of gathering firms together and facilitating business transactions. Also, industrial clusters are often linked with innovation, in developed countries like France, Germany and the USA, where many clusters are about high technology such as information and communication technology (ICT), biotechnology and nanotechnology, or, about the booming knowledge intensive business services (KIBS), such as software systems, business consulting and R&D services. In these particular sector-based clusters, innovation is inherent. Still another importance of the industrial cluster comes from its role of employment in a region. Thus, policy makers have been aware of this phenomenon and are now trying to find out more evidences and formulating corresponding policies and institutions to accommodate the development of clusters [1].

Clusters, which form networks of firms and other institutions, are receiving growing attention in the literature on management [2-7]. Companies are constantly asked to improve performances in order to get the chance to maintain or to improve their own market positions and financial situation.

A network value system is the full range of activities and participants necessary to bring a product or service from the point of being an idea through to delivery to the final consumer while a company can be

found at any of the various steps within the value chain. Various actors can be “clustered”, at any step of the value chain, for training, collective production, bargaining and/or selling to the next step of the value chain. In either case, myriad actors are involved in and influence the development of the value chain or cluster.

The network value system must be integrated in the core business of the industry cluster. Both of them focus on improving the competitive advantage over their competitors. The cluster support the network value system by integrating academic institutes, government agencies, association and supporting industry in order to create the innovation and enhance the knowledge in the value chain.

Knowledge that develops in a network circulates more easily within it. Studies of networks in clusters often consider different types of relations between firms (commercial, directive, subcontracting,...) and assume that these links imply a transference of knowledge, even though the informational content of the links that firms establish within the cluster have not been analyzed. Thus, Bell [2] distinguishes between managerial networks (characterized by the transmission of tacit knowledge) and institutional networks (characterized by the transference of explicit knowledge).

Research about the innovation of a cluster, or of a firm which is geographically embedded into a network, has received much attention recently. When discussing this phenomenon, much emphasis has been placed on environmental issues, such as the infrastructure, the management system, the cultural and social context and so on. One important research theme is about the connotation of the cluster innovation. For those clusters which emphasize on innovation, a major function is to enhance the knowledge creation, storage, flow and application within the clusters [1].

Cluster theory, in effect, builds on the advantages of inter-firm cooperation propounded by value chain theorists. The network value system management integrates processes and builds long-term relationships among firms involved in the flow of products and services from the source through to end-users. All firms

in the network value system can benefit through achieving lower costs, improved customer value and satisfaction, and greater competitive advantage. When members of a network value system all operate in the same general geographic location, they gain the cost efficiencies of supply chain coordination, as well as the boost in competitive drive and innovation that comes from working together in close physical proximity.

A value network is a complex set of social and technical resources. Value networks work together via relationships to create social goods (public goods) or economic value. This value takes the form of knowledge and other intangibles and/or financial value. Value networks exhibit interdependence. They account for the overall worth of products and services. Companies have both internal and external value networks. In a network value system, each participating company operating as an individual enterprise tries to maximize its own corporate goals, thus sub-optimizing the overall performance. An extended enterprise is a part of network, which essentially behave as a single enterprise trying to maximize the corporate goals of the extended enterprise, thus optimizing the performance of each individual enterprise.

Network value system defines the specific roles in an activity and their value creating interactions. Value interactions or deliverables are of two types. Tangible deliverables are the contractual or mandated interactions between participants. Intangible deliverables are the informal, more personal, exchanges of knowledge, favors, and benefits. These are the interactions that help keep things running smoothly and build relationships. Intangible exchanges are actually the practices ignore these important intangible exchanges, but they are made visible with network value system.

2. CREATING KNOWLEDGE IN CLUSTER NETWORKS

The ideas of collective invention are convenient for describing the dynamics of knowledge diffusion through networks and clusters. Collective invention is characterized by high invention rates and fast knowledge accumulation created by disclosure of information between competing agents. It is driven by exchange and circulation of knowledge and information within networks formed by groups of socially connected individuals [8]. When this is the case, the structure of the network over which the transmission of information takes place may be vitally important to the performance of the industry [9].

Networks that interconnect diverse actors promote both knowledge creation and dissemination [10]. Knowledge is created and disseminated within networks consisting of actors and relationships among them. Networks facilitate learning via the transfer of knowledge from one firm to another as a conduit for knowledge transfer. Networks also facilitate mutual learning and become the locus of collective invention [11]. The ability to learn about new opportunities requires participation in networks, thus a wide range of interorganizational linkages is critical to knowledge

diffusion, learning, and technology development [12-14]. Relationships and networks are an important and strategic resource for firms [15]. Firms in a cooperative network can utilize their networks in a variety of ways in addition to the above merits. They not only share the costs and risks of their activities but also obtain access to new markets and technologies and make use of complementary skills [12, 16-18]. The network among actors is the key to understanding the performance of regional clusters [19].

According to Eisingerich et al. [20], a social network helps to develop regional cluster performance. High performing clusters are underpinned by network strength and network openness, but the effects on the performance of a cluster as a whole are moderated by environmental uncertainty. Specifically, the positive effects of network openness on cluster performance tend to increase as environmental uncertainty increases, whereas the positive effects of network strength on cluster performance tend to decrease as environmental uncertainty increases. The networks are instruments that might help firms to voluntarily expand their own competence by means of complementary partners beyond the limitations of their own organisation and of the localities where they are settled. In this context, the process of 'learning' offers a dynamic perspective on the nature of both networking and clustering [20].

Clusters and networks remain fuzzy concepts when we consider their own interrelated relationships and their relationships with the factors and variables of the whole economy, such as institutional arrangements, trading efficiency, level of specialization and agglomeration, as well as their dynamic evolution. The current published literature has addressed many important aspects of clusters and networks, yet there is still a lack of robust frameworks to combine and explore these aspects together within one competitive market.

Clusters have the possibility to develop their own specific mixture of competitive advantages which is created on the basis of locally-developed knowledge as a result of mutual relations, cultural heritage and local characteristics. This is evident in the focus on clusters as an important concept in understanding growth and in thinking about development policy [21].

The idea of localized economies of scale in geographic agglomerations has a long history in economics, going back to Adam Smith's early observations of labour specialization and to explanations of why companies continue to localize in the same areas [22]. Clusters arise in the presence of Marshallian externalities, which signify that companies benefit from the production and innovation activities of neighboring companies in the same and related industries. There is abundant evidence that such externalities exist and lead to industry-level agglomeration [22].

Development of clusters is an effective way to improve quality of the product and the process and bring it to a higher level. Modern business is based on the fast response, quality, flexibility, innovation, connections and building the critical mass of capital and production / service potential. This relatively new

style of doing business requires – network value approach based on cluster concept. Clusters represent the complex organizational systems that are flexible and can be quickly adjusted to oscillatory changes at the sale and purchase markets, generate employment, help the diversification of economic activities and make a significant contribution to exports and trade. Clusters also play an important role in innovation and businesses where there is a need for application of modern technology. Thanks to their innovative flexibility, many of them become more productive and efficient than some large international corporations. In this process, emphasis should be focused on creating a friendly business environment where the transformation of society towards a market economy shall take its place.

Cluster differs from other forms of associations within its geographical boundaries, involvement and utilization of funds, ways of exchange of products and partially finished products, information management - knowledge chains, and the importance of how they are connected. Clusters can be best understood and used as a regional systems and they represent, according to Porter [23] "Geographic concentrations of mutually connected companies, specialized suppliers, service providers, companies from similar industries and institutions tied to them (i.e. universities, standardization agencies, trade unions), who compete, but also cooperate".

3. CHARACTERISTICS OF CLUSTERS

Figures Basic characteristics of clusters are:

- Clusters are based on systemic connections among companies; ties can be built on common or complementary products, production processes, essential technologies, needs for natural resources, demands for certain qualifications and/or distribution channels;
- Clusters are geographically limited, defined mainly by distance and time that people are willing to take because of employment which job makers and company owners consider reasonable for meeting and creating business relationships; geographical range is under strong influence of travel and traffic systems, but also of cultural identity, personal priorities, and family and social conditions;
- Clusters represent natural connection of companies, it must be emphasized that clusters do not operate as an imposed agglomeration, or forced association for any reason; clusters nourish unique attributes of companies and make it possible for them to choose levels and types of cooperation within a cluster, and to define what part of its capacities they will bring into clusters, and what part will remain "freelance", taking into consideration common needs, but also their own benefits as a member of cluster association.
- Associating into a cluster can bring a broad range of benefits to all partners as well as to the economy in general. Some of the benefits are the following:
- Increased level of expertise; associating gives companies better knowledge about supply chain

and makes it possible to companies to learn from each other and to cooperate;

- Capability of companies to join complementary strengths and contract new works of larger scope for which, individually, they would not be able to bid in a public tender procedure;
- Potential for large scale production (economy of scale), which can only be realized via specialized production in each of the companies, through joint purchase of supplies with large discounts or through joint marketing;
- Strengthening of social and other informal connections, which leads towards creation of new ideas and new companies;
- Better information flow within a cluster, e.g. making it possible for investors to identify good entrepreneurs, and for business people to find good service providers;
- Enabling development of services' infrastructure: legal, financial and other specialized business services.

That is why one of more important segments is to determine levels of specialization in companies – participants in a cluster, and what desirable levels of specialization for more effective business are in case we have specialization, in other words, economic diversity. Research that has been done shows that traditional production sectors are inclined to doing better business when densely concentrated in one geographical area. Contrary to this, newer, high-tech and service sectors are more comfortable with economic diversity environment.

General opinion is that specialization means lack of economic diversity and vice versa. If that is the case, then improving industrial clusters bears risk of creation of highly specialized local economies. If local economies are specialized in only one industrial sector or only couple of them, then they are indeed much more sensitive to cyclic falls in those sectors. However, other opinion suggests that specialization and diversification do not necessarily exclude each other. Malizia and Feser [24] define economic diversity as "existence of multiple specializations". It means it is possible for local economies to be highly specialized in certain sectors and, at the same time, to have sound combination of economic activities. So we come to the concept of flexible specialization, which represents possibility of companies to do what they do best, and cluster has the obligation to provide optimal utilization of capacities.

4. CONCLUSION

In summary, despite the movement to global outsourcing, a firm should strategically assess its local area for resources that might provide a lower total cost alternative in better managing its supply chain. Firms considering relocation should analyze geographic regions that currently possess cluster characteristics or that have emerging potential for developing clusters. Network value system helps the organizations acquire process competence and better process control.

Establishment of network value system in complex organizational systems like cluster represents a big challenge because of diversity of clusters and characteristics of member companies. Cluster areas can improve both supply chain and firm performance and allow leveraging of complementarities and external sales. Upstream and downstream partners may exist in these areas that can provide synergistic benefits that do not occur as readily with distant supply chain configurations. The integration of cluster theory and Network value system offers firms a way to build competitive advantage by initially focusing primarily on local resources when selecting supply chain partners, rather than looking only for low cost advantage through distant outsourcing.

5. REFERENCES

- [1] Zhao, Y., Zhou W., Husig S., Vanhaverbeke W., 'Environment, network interactions and innovation performance of industrial clusters Evidences from Germany, The Netherlands and China', 2010, Journal of Science and Technology Policy in China, Vol. 1 No. 3, pp. 210-233
- [2] Bell, G. G. 'Clusters, networks, and firm innovativeness', 2005, Strategic Management Journal, vol. 26, pp. 287.
- [3] Gilbert, B. A., McDougall, P. P., & Audretsch, D. B. 'Clusters, knowledge spillovers and new venture performance: An empirical examination', 2008, Journal of Business Venturing, vol. 23, pp. 405-422.
- [4] Huggins, R., & Johnston, A. 'Knowledge flow and inter-firm networks: The influence of network resources, spatial proximity and firm size', 2010, Entrepreneurship & Regional Development, vol. 22, pp. 457-484.
- [5] Krätke, S. 'Network analysis of production clusters: The Potsdam/Babelsberg film industry as an example', 2002, European Planning Studies, vol. 10, pp. 27-54.
- [6] Rocha, H. O., & Sternberg, R. 'Entrepreneurship: The Role of Clusters Theoretical Perspectives and Empirical Evidence from Germany', 2005, Small Business Economics, vol. 24, pp. 267.
- [7] Tallman, S., Jenkins, M., Henry, N., & Pinch, S. 'Knowledge, clusters, and competitive advantage', 2004, Academy of Management Review, vol. 29, pp. 258.
- [8] Dahl, M.S., Pedersen, C.O.R. 'Knowledge flows through informal contacts in industrial clusters: myth or reality', 2004, Research Policy, vol. 33, pp. 1673-1686
- [9] Cowan, R., Jonard, N., 'The dynamic of collective invention', 2003, Journal of Economic Behaviour and Organisation, vol. 53, pp. 513-532
- [10] Podolny, J.M., Page, K.L., 'Network forms of organization', 1998, Annual Review of Sociology, vol. 24, pp. 57-76.
- [11] Allen, R.C., 'Collective invention', 1983, Journal of Economics Behaviour in Organisations, vol. 4, pp. 1-24.
- [12] Powell, W., 'Neither market nor hierarchy: network forms of organization', 1990, Research in Organizational Behavior, vol. 12, pp. 295-336.
- [13] Powell, W., Koput, W., Smith-Doerr, L., 'Interorganizational collaboration and the locus of innovation: networks of learning in biotechnology', Administrative Science Quarterly, vol. 41, pp. 116-145.
- [14] Powell, W., White, D., Koput, W., Owen-Smith, J., 'Network dynamics and field evolution: the growth of interorganizational collaboration in the life sciences', 2005, American Journal of Sociology, vol. 110, pp. 1132-1205.
- [15] Dyer, J., Singh, H., 'The relational view: cooperative strategy and sources of interorganizational competitive advantage', 1998, Academy of Management Review, vol. 23, pp. 660-679.
- [16] Kogut, B. 'The stability of joint ventures: reciprocity and competitive rivalry', Journal of Industrial Economics, vol. 38, pp. 183-198.
- [17] Eisenhardt, K.M., Schoonhoven, C.B. 'Resource-based view of strategic alliance formation: strategic and social effects in entrepreneurial firms', 1996, Organisational Sciences, vol. 7, pp. 136-150.
- [18] Mowery, D.C., Oxley, J.E., Silverman B.S. 'Technology overlap and interfirm cooperation: implications for the resource-based view of the firm', 1998, Research Policy, vol. 27, pp. 507-523.
- [19] Steinle, C., Schiele, H., 'When do industries cluster? A proposal on how to assess an industry's propensity to concentrate at a single region or nation', 2002, Research policy, vol. 31, pp. 849-858.
- [20] Eisingerich, A. B., Bell S.J., Tracey, P., 'How Can Clusters Sustain Performance? The Role of Network Strength, Network Openness, and Environmental Uncertainty', 2010, Research Policy, vol. 39, pp. 239-53.
- [21] Porter, M., 'The Competitive Advantage of Nations', 1990, Free Press.
- [22] Marshall, A., Principles of economics. (eighth ed.), 1925, Macmillan, London, UK
- [23] Porter, M.E. 'Clusters and the new economics of competition', 1998, Harvard Business Review vol. 76, no. 6, pp. 77-90.
- [24] Malizia, E., Feser, E., 'Understanding Local Economic Development', 1999, New Brunswick, New Jersey: Center for Urban Policy Research.

Authors: Prof. Dr. Slobodan Morača, M.Sc. Dragana Milin, University of Novi Sad, Faculty of Technical Sciences, Department for Industrial Engineering and Management, Trg Dositeja Obradovica 6, 21000 Novi Sad, Serbia, Phone.: +381 21 450-366, Fax: +381 21 454-495.
E-mail: moraca@uns.ac.rs
milin.dragana@gmail.com

Nemedi, I., Hadzistevic, M., Hodolic, J., Sekulic, M., Todic, V.

BASIS OF MODEL DEVELOPMENT FOR REAL FORM DETERMINATION OF ROUNDNESS MEASURING OBJECTS

Abstract: *The set of requests, which are related to the geometry of any working part, are known as geometrical specifications (GPS – Geometrical Product Specifications). It covers the demands of size and dimensions, geometrical tolerance and geometrical surface properties. The aim of GPS standard is the insurance of functionality, safety, reliability and substitutability of analyzed and controlled workpieces. It can be noticed, though, that all GPS modules are concerned only with the satisfaction of the standards of defined geometrical properties, whereas none of the modules deal with the determination of the real form of feature (surface) of controlled measuring workpieces. This paper represents the basis of a developed mathematical model for the case of roundness investigation which can satisfy this request.*

Key words: *roundness, GPS, real form*

1. INTRODUCTION

Each measurement is connected with the determination of numerous values of physical sizes by the aid of which the determined validity features are investigated. Measuring a size, means to determine its numerous relationships with other homogeneous sizes, by which the measuring unit is acquired. When measuring it is necessary to provide the data about different sizes: discrete and continual, constant and variable, dependent and independent. Therefore, measurement is considered as a process of physical equalization of the given size with its physical value which is taken for the measuring unit.

That way, the measurement result is presented as quantity information about the basic features of measuring objects (workpieces), attained as a result of the physical process with a certain level of accuracy.

In this paper a geometrical characteristic, roundness in this case, will be analyzed. Nowadays, this geometrical characteristic is controlled strictly on the basis of internationally appointed, accepted and applied definition [1]. Shunmugam and Venkaiah in their papers represent their results of comparisons of all used methods for measuring data processes concerning roundness. Furthermore, a review of those methods is also provided. [2].

Roundness measurement can be carried out in several ways using different methods. Starting from the straightforward measurement of diameter, continuing with a measuring in a prism (V-block method), [3],[4],[5] and [6], then with computerized coordinate measuring machines (CMM) to the measurements carried out with the aid of special measuring machines for roundness measurements (RDM) (Rotational Datum Method) [7].

The mentioned methods are constantly developing aiming to increase measurement accuracy [5],[7],[8]. An interesting fact should be pointed out that effort is also invested in the improvement of conventional

methods, such as V-block method. V-block method is a widely accepted method for roundness measurement; however, because of its complexity of conventional analysis results by the help of Fourier's transformations, it is extremely difficult to develop software for swift data processes. The solution to this problem is mathematical, with the aid of inverse matrices, which is described in details by Okuyama, Goho and Mitsui [8]. Data process is therefore developing, although the mere measurement principle remains the same, with its disadvantages [9],[10],[11],[12]. Those disadvantages are in the base of the measurement process itself. With V-block method that is in the constant shift of the rotational centre when rotating a measuring object on the reliance surface [3],[4].

The aim of this paper is not the analysis of the used rules concerning roundness, but a representation of principles for the production of models, i.e. software's. It will enable unambiguous determination of the real form of the round object measuring section. The real form, however, is not mentioned at all as relevant information in the definition of roundness, but only the width of its field.

In the production of the mentioned model, the lack of V-block method will be applied – the constant shift of the rotational centre when rotating a measuring object on the reliance surface. In sequel, details follow.

2. ROUNDNESS

2.1 Definition of roundness tolerance

The field of roundness tolerance in the regarded plain is restricted by two concentric circles on the distance t . (Fig. 1)

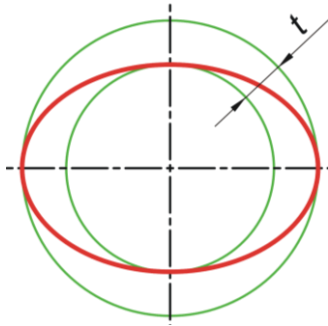


Fig. 1. Definition of roundness tolerance [1],[3],[4]

If the section lines are tolerated, then all section points must lie between two concentric circles on the section plain, on a radial distance of t . This parameter t is the value of roundness tolerance.

2.2 Possible form of roundness deviation

Irregularities on the section of round machining bodies, including both the axis and openings are most often realized in: a) triangular, b) oval, c) multiangle, or d) eccentric forms. These irregularities of forms depend on a number of exterior effects, primarily on rigidity and contact.

Thus, for example, a triangular form of irregularity is mostly achieved with thin-walled pipes, if the contact is done in three points. This means that with roundness control of such a workpiece the appearance of a triangular form can be expected in advance. This is significant, because with classical ways of roundness control not all types of deviance can be measured. The most probable form of irregularity has to be assumed in advance.

Fig. 2 provides a review of the most common roundness errors.

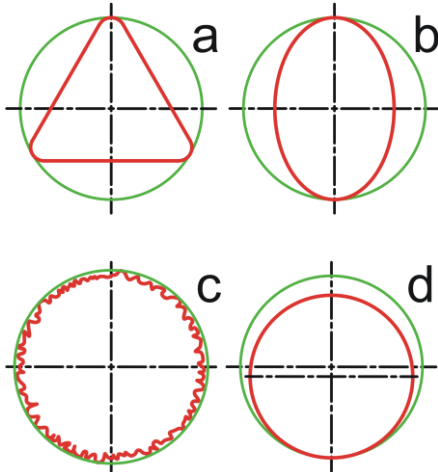


Fig. 2. Possible versions of form irregularity of workpieces in cross section [3],[4],[13]

3. BASES OF METHODS

3.1 Core centre method

The name of this method is given in this form because this way the essence is described with the highest level of accuracy. With classical methods for roundness measurements it is of great importance the prediction of expected real form of circular section. For measuring certain circular sections of annular measuring objects, measures for palpation of measuring

surface in two points are required. Such are the triangular and pentagonal sections. Thus, oval and quadrangular sections are immeasurable with necessary accuracy. There, contact must be carried out in three points. It is necessary to predict which roundness deviations will appear. For that great experience and proficiency are needed.

In technical literature, as the largest problem which arises with these classical methods is the constant centre shift, i.e. the imaginary axis of measurement section.

That problem can be turned into an advantage by the proposed way of measuring results process. It is necessary to follow the shift of those centers and based on their positions a reliable conclusion about the real form of measuring section can be adopted. Thus, the lack of a method turns into the essence of another one.

3.2 Essence of Core centre method

The most straightforward way for representing the essence of this method is graphically. Only ovality will be analyzed because of the lack of available space.

Deviation is of elliptical form. With classical methods this deviation could be analyzed with measuring in two points. Contact in three points would lead to the unwanted shifting of contact circle centers. As it had been mentioned before, in this case, this disadvantage is used for determining the real form, thus the contact should be performed exactly in three points.

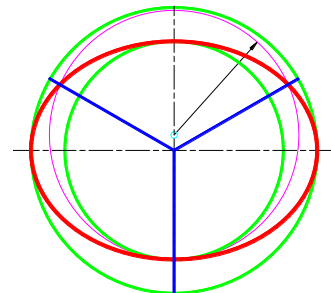


Fig. 3. Circle defined through three contact points with the centre

The contact of real, oval contour in three points is shown in Fig. 3. Across the points of sections of real contour and triaxial systems, an auxiliary circle can be constructed. Its centre is easily determined.

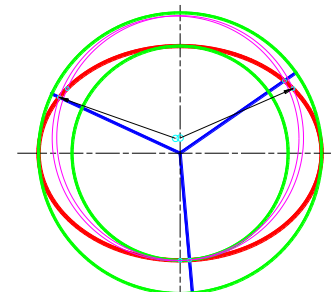


Fig. 4. Representation of two auxiliary circles with their centers

Afterwards, the rotating of the triaxial system for the arbitrary angle follows and the procedure is repeated. That way another auxiliary circle with its centre is obtained. This move is shown in Fig. 4. The described step is repeated n times, until the full round

of contour is reached, and that's how the result shown in Fig. 5 is obtained.

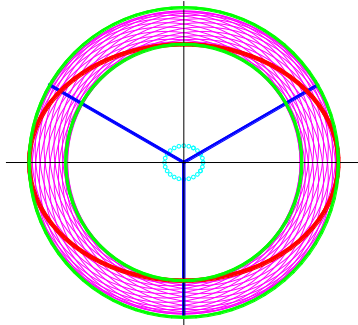


Fig. 5. Result of full contour contact in three points

On Fig. 5 it is clearly visible that the centers of auxiliary circles are arranged according to a certain rule. In fact, the orbit of the section centre shift is shown, i.e. the imagined axis of cylindrical measuring object, when rotating during the time of measurement. At the same time, that orbit reflects the real form of measuring section of round measuring object. In that way, an image is obtained by the aid of auxiliary circles centres in the core section. That is how this method got its name as a core centre method.

4. APPLICATION OF THE METHOD

Based on the represented, a simulation program is produced aiming to analyze the application of methods on various types of anomalies, shown in 2.2. In sequel the functioning of the program will be shown briefly followed by the simulation results.

4.1 Functioning of the POLYGON program

Simulation program, named POLYGON, is designed so that the input parameters can be changed based on which the following conditions can be defined:

- the number of sides of polygon deviation of roundness,
- radius curve rounded at the apex of polygon
- belt width of random deviations of simulated measuring points from the primary curve and real form and
- the number of tangential points (two or three)

The program is designed in MatLab 7 environment and is able to simulate all possible types of anomalies. In sequel the simulation results of ovality will be represented and all elements in connection shown in core centre method.

4.2 Application of POLYGON program for the case of ovality

The drawing of an ellipsis according to the logic of the program is actually a drawing of "diangle". Since ellipsis can be approximated as a unitary circle deformed with two opposite sides. Of course this way an ellipsis cannot be obtained by definition, but this simulation of an ellipsis will also provide a satisfactory result. The curve of the apex has to be taken quite large to obtain an approximate form of the ellipsis. For the beginning it is necessary only the drawing of the

primary curve without random deviations ("roughness"). Finally, contact in three points is done. The result is represented in Fig. 6a.

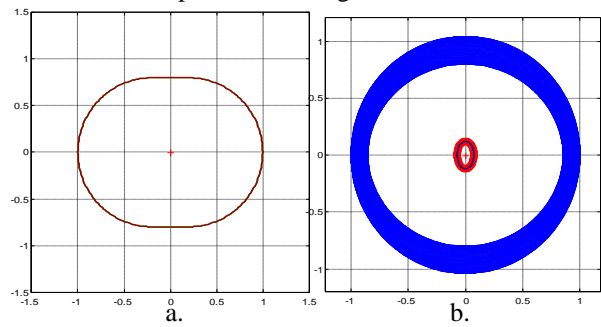


Fig. 6. The result of ovality simulation

In the following step the drawing of the core should be sought. Graphical method analysis has shown that in this case the distribution of auxiliary circle centers must be obtained, so that based on them a conclusion could be derived about ovality of the primary curve. This statement will be verified now. Fig. 6b shows the result of the simulation.

If in the simulation program the same input data are included, with the difference in size of deviation from the primary curve, i.e. if the presence of roughness is also included, the following results are obtained. Fig. 7a shows the primary curve without auxiliary circles and core, whereas in Fig. 7b the auxiliary circles and the whole core are visible.

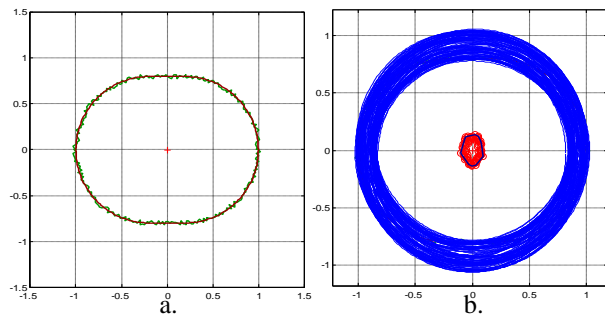


Fig. 7. Ovality simulation results with random deviation representation from the primary curve

For better overview in Fig. 8 enlarged figures of cores are provided.

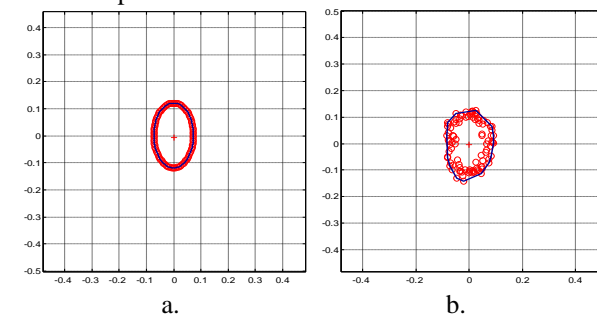


Fig. 8. The overview of enlarged figures of cores without (a) and with random deviations from the primary curve (b)

On the overviews in Fig. 8 the coordinate value systems with abscissa and ordinates are enclosed. The aim of their representation is to enable the comparison of centre point's surface dissipation of auxiliary circles in the cores depending on the size of the field of random deviations from the primary curve.

5. CONCLUSIONS

Based on the results the followings can be concluded:

- For oval deviations from roundness, with three points contact, such a core centre of auxiliary circles is obtained that prediction based on graphical processing is satisfied. The core of the centers assumes a form which clearly reflects the character of deviation from roundness.
- The previous statement is completely valid for the case of analysis of primary curve without random deviations; however, it could also be said for the case with deviations from the primary curve.
- It is of great importance to notice that in the two cases mentioned very similar almost equal surfaces of points dissipation in the core are obtained. Naturally, in ideal case those points are ideally positioned across the elliptical frame, whereas they are dissipated near that frame for the case of real surface simulation.

Previous statements indicate the validity of predictions.

Finally, the primary hypothesis is proved that for this method, the oval deviation analysis from roundness, contact in three points must be used, contrary to classical method measurements, where the controlled objects are measured in two points. This method, however, does not measure the values of cross section of controlled objects (workpieces), but uses the errors of those methods and follows the orbit of axis shift of the controlled object (workpiece) in progress of rotation during the time of measurement.

6. REFERENCES

- [1] ISO/TS 12181-1 and 12181-2, *Geometrical product specifications (GPS) – Roundness*; Part 1: *Terms, definitions and parameters of roundness*; Part 2: *Specification operators*. ISO, Geneva, 2003.
- [2] Shunmugam, M. S., Venkaiah, N.: *Establishing circle and circular-cylinder references using computational geometric techniques*, The International Journal of Advanced Manufacturing Technology, Volume 51, Numbers 1-4, p.p. 261-275, 2010.
- [3] Szilágyi, L.: *Gépipari hosszmerések*, Ipari szakkönyvtár, Műszaki Könyvkiadó, Budapest, 1982.
- [4] Stankov, J.: *Merenje u proizvodnji*, Fakultet tehničkih nauka, Novi Sad, 1984.
- [5] Adamczak, S., Janecki, D., Stepien, K.: *Cylindricity measurement by the V-block method – Theoretical and practical problems*, Measurement, Volume 44, Issue 1, p.p. 164-173, 2011.
- [6] Stepien, K., Janecki, D., Adamczak, S.: *Investigating the influence of selected factors on results of V-block cylindricity measurements*, Measurement, Volume 44, Issue 4, p.p. 767-777. 2011.
- [7] Mills, M.: *The measurement of roundness*, Australian manufacturing Technology, 2007.
- [8] Okuyama, E., Goho, K., Mitsui, K.: *New analytical method for V-block three-point method*, Precision Engineering, Volume 27, Issue 3, p.p. 234-244, 2003.
- [9] Gi-Bum, J., Dong, H. K., Dong, Y.J.: *Real time monitoring and diagnosis system development in turning through measuring a roundness error based on three-point method*, International Journal of Machine Tools and Manufacture, Volume 45, Issues 12-13, p.p. 1494-1503, 2005.
- [10] Wei, G., Satoshi, K., Takamitu, S.: *High-accuracy roundness measurement by a new error separation method*, Precision Engineering, Volume 21, Issues 2-3, p.p. 123-133, 1997.
- [11] Zhang, G.X.: *A Study on the Abbe Principle and Abbe Error*, CIRP Annals - Manufacturing Technology, Volume 38, Issue 1, p.p. 525-528, 1989.
- [12] Ruedi, T.: *Basics of highest accuracy roundness measurement*, Simposio de Metrología, 25 al 27 de Octubre, Chile, 2006.
- [13] Nemedi, I., Hadžistević, M., Hodolič, J.: *Comparative analysis of the results of measuring on the coordinate measuring machines*, 13th International Research/Expert Conference "Trends in the Development of Machinery and Associated Technology", TMT 2009, Hammamet, Tunisia, p.p. 49-52. 16-21 October 2009.

Authors: M.Sc. Imre Nemedi, Subotica Tech – College of Applied Sciences, Department of Mechatronics, Marka Oreskovića 16, 24000 Subotica, Serbia, Phone.: +381 24 655-247, Fax:+381 24 655-255. **Prof. Dr. Miodrag Hadzistevic, Prof. Dr. Janko Hodolic, Prof. Dr. Milenko Sekulic, Prof. Dr. Velimir Todic**, University of Novi Sad, Faculty of Technical Sciences, Institute for Production Engineering, Trg Dositeja Obradovića 6, 21000 Novi Sad, Serbia, Phone.: +381 21 450-366, Fax: +381 21 454-495.
E-mail: nimre@vts.su.ac.rs
miodrags@uns.ac.rs
hodolic@uns.ac.rs
milenkos@uns.ac.rs
todicv@uns.ac.rs

ACKNOWLEDGEMENT

Results of investigation presented in this paper are part of the research realized in the framework of the **project “Research and development of modeling methods and approaches in manufacturing of dental recoveries with the application of modern technologies and computer aided systems”** – TR 035020, financed by the Ministry of Science and **Technological Development of the Republic of Serbia**.

Penfold, N.

INNOVATIONS IN TOUCH-TRIGGER PROBE SENSOR TECHNOLOGY

Abstract: Since the invention of the touch-trigger probe in the 1970s, these devices have formed the main means of sensing for dimensional measurement on co-ordinate measuring machines (CMMs) and machine tools. Scanning sensors are increasingly being used on CMMs to measure complex shapes and to characterise the form of prismatic components. However, touch-trigger sensors still have a major role to play in the inspection of component size and position on CMMs, and in workpiece setup and in-process control on machine tools.

Key words: Kinematic, strain gauge, pre-travel, repeatability

1. KINEMATIC RESISTIVE PROBES

The fundamental requirements for a touch-trigger probe are:

- **compliance** so that the stylus deflects when it meets the surface of the component, applies a low force to the component and allows time for the machine to decelerate before backing off the surface
- **mechanical repeatability** so that the stylus always returns to the same location relative to the machine quill / spindle when it is not in contact with the part
- **electrical repeatability** so that the probe always triggers at the same stylus deflection in any particular direction

The original touch-trigger probe is based on a spring-loaded kinematic arrangement of rods and balls, as shown in Fig. 1. These provide six points of contact, ensuring that the stylus carrier is held in a unique location with excellent repeatability. The mechanism allows the probe's stylus to be deflected as it meets the surface of the part, whilst the spring ensures that the mechanism re-seats when the stylus is in free space.

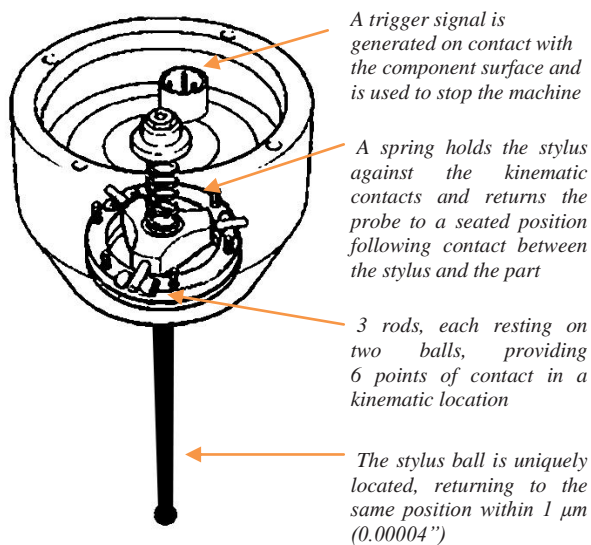


Fig. 1. Schematic of a kinematic resistive probe

The contact elements are made of tungsten carbide, a very hard substance, to ensure that the contact patches (where the material is elastically deformed under the force of the spring) are very small. An electrical circuit runs through the contacts, and it is the resistance through this circuit that is measured by the probe's electronics.

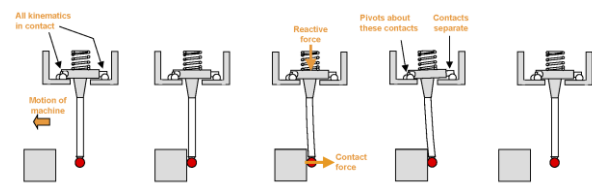


Fig. 2. How a kinematic resistive probe generates a trigger

Fig. 2. illustrates the mechanics of a trigger:

1. As the probe's stylus moves towards the component, the spring is holding all of the kinematic elements in contact, so that the stylus is in a known position relative to the quill / spindle.
2. The stylus meets the surface.
3. As the machine's motion continues to drive the stylus into contact with the component, forces start to build in the probe mechanism. The contact force at the stylus tip creates a moment in the probe mechanism, which is balanced by a reactive moment generated by the spring, pivoting about the same set of contacts. As these forces build, the stylus undergoes bending (greatly exaggerated in the diagram for illustrative purposes).
4. Eventually, the increasing contact moment overcomes the reactive moment and the mechanism starts to pivot about the left-hand set of contacts. The contacts on the right move apart, breaking the electrical circuit in the probe. Before this occurs, a trigger is generated (see the section on electrical switching, below). The trigger signal is used to latch the machine's position at that moment, and to command the machine to slow down and back off the surface.
5. Once the machine backs off the surface, the probe re-seats into its repeatable rest position.

2. ELECTRICAL SWITCHING

An electrical circuit is made through the kinematic contacts. The ball plate is insulated from the tungsten carbide spheres, whilst the cylinders and the stylus carrier are also insulated from one another (see Fig. 3a). Wires in the ball plate carry the current between the contact sets.

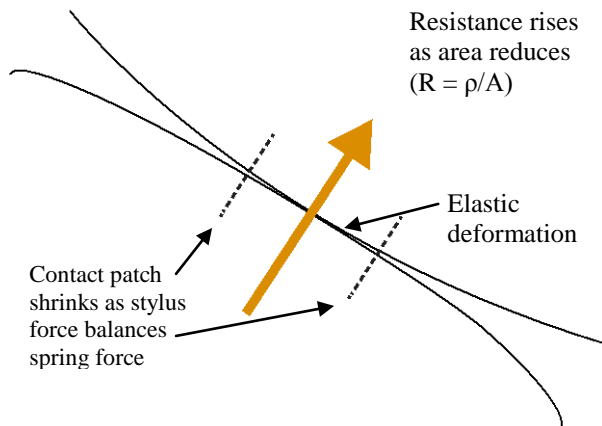
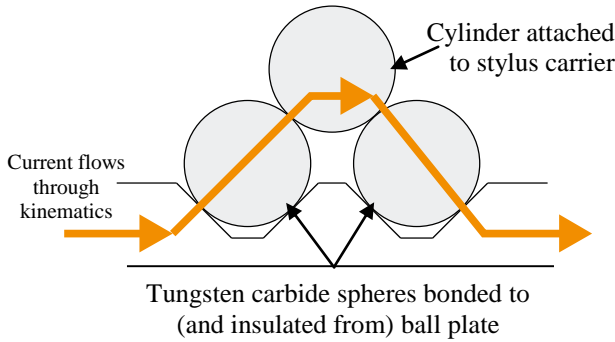


Fig. 3a. and 3b. Electrical circuit through kinematics and close-up of the contact path between elements

Under the load of the spring, the contact elements undergo elastic deformation (see Fig. 3b), creating small contact patches through which the current can flow. The resistance across each contact patch is inversely related to the area of the contact patch ($R = \rho/A$). As the force between the stylus and the component builds, the reactive moment that is generated in the probe mechanism causes the forces between some contact elements to increase, whilst the force between others will decrease. As the force between two contact elements reduces, the contact patch area gets smaller, thus increasing the resistance between those elements. With all six contact patches wired in series, the contacts with the lowest force between them greatly affects the overall resistance in the probe circuit.

When the resistance reaches a threshold, the probe's output is set to 'triggered' (see Fig. 4). Vivaly, the balls and rods are still in contact when the trigger occurs, so that the stylus is in a defined position, providing repeatable measurement.

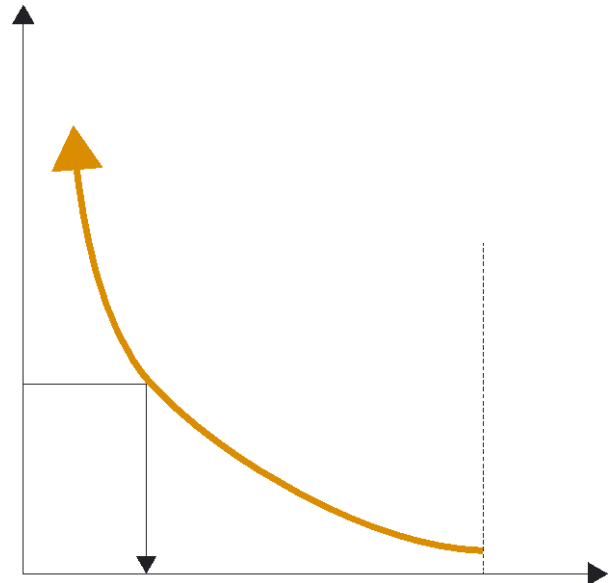


Fig. 4. A trigger is generated when the probe circuit resistance breaches

3. FACTORS IN KINEMATIC RESISTIVE PROBE PERFORMANCE

3.1 Pre-travel

When the stylus is in contact with the surface, a balance of forces is established. Before the trigger threshold is reached, these growing forces cause the stylus to bend. Since the machine is still moving, the amount of bending in the stylus that occurs before the probe triggers affects the latched position of the machine when the trigger is recorded. This stylus bending prior to the trigger is known as **pre-travel**. Referring to figure 5, pre-travel depends on F_c and L , as well as the stiffness of the stylus, according to the formula: **Pre-travel** = $F_c \cdot L^3 / 3EI$ (where E is the Young's modulus of the stylus stem material, and I is the moment of inertia).

Before the contact elements separate, the force balance is as follows:

$$F_c \cdot L = F_s \cdot R \quad (1)$$

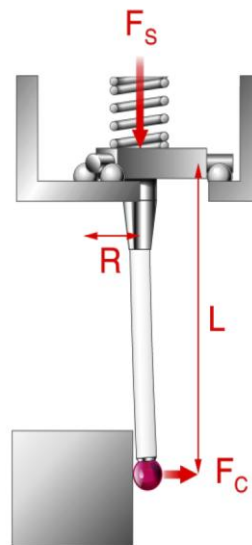


Fig. 5. Force balance in a touch-trigger probe

3.2 Pre-travel variation (lobing)

The contact sets in a kinematic resistive probe form a triangular arrangement. This means that the pivot distance R varies depending on the direction in which the contact force acts in relation to the probe mechanism. For an particular stylus (i.e. L is constant) the contact force F_c is proportional to R .

Figure 6 shows how the contact force for a given stylus varies dependent on the direction of contact.

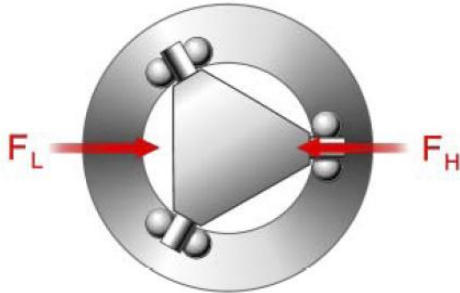


Fig. 6. High and low force directions

In the low force direction (F_L), the pivot distance R is approximately half as long as in the high force direction (F_H). Figures 7a and 7b illustrate this in more detail. Since $R_1 > R_2$ therefore $F_{c1} > F_{c2}$. A larger force is needed to reach the trigger threshold in the high force direction, resulting in more pre-travel in that direction. Trigger force variation results in a phenomenon known as **pre-travel variation (PTV)** or lobing.

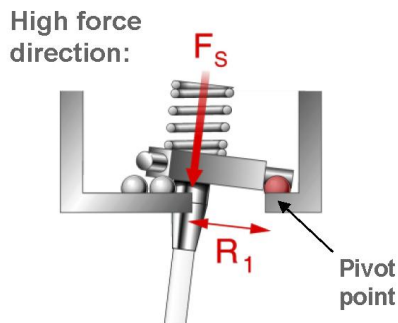


Fig. 7a. Pivot point is further from stylus centre line in high force direction

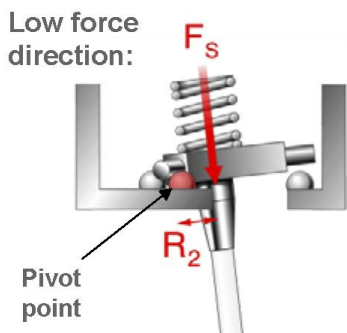


Fig. 7b. Pivot point is closer to stylus centre-line in low force direction

Fig. 8. shows a typical XY pre-travel plot for a TP6 kinematic resistive CMM touch-trigger probe. The three high force directions can be seen as the peak points of this plot. The maximum variation in pre-travel in this case is around $3.3 \mu\text{m}$ (0.00013 in).

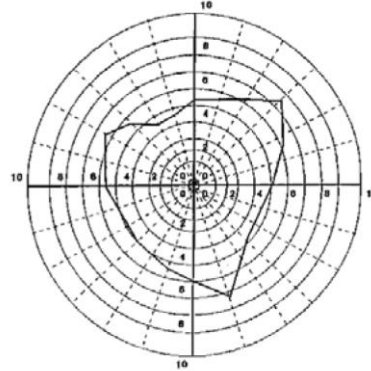


Fig. 8. Pre-travel variation plot for a TP6 CMM probe

3.3 XYZ pre-travel variation

Pre-travel exists not only in the XY plane, but also in the Z direction. In this case, there is no mechanical advantage (lever action) over the probe spring, so the contact force is the same as the spring force (see fig. 9); therefore the trigger force in this direction is much higher than that seen in the XY plane. However, since the stylus is in compression when triggering in this direction, its effective stiffness is much higher and the pre-travel in the Z direction is generally much smaller than in the XY plane.

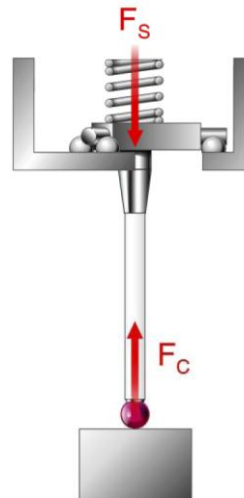


Fig. 9. Force balance in the Z direction

Kinematic resistive probes exhibit 3-dimensional (XYZ) PTV, a combination of the XY and Z pre-travel effects. When measuring complex surfaces, this becomes an important characteristic.

3.4 Probe calibration

Pre-travel itself is not a form of error, since it can easily be compensated by probe calibration. A datum feature, of known size and position, is measured to establish the average pre-travel for the stylus concerned. Once this is complete, the key factor affecting measurement accuracy is the probe's repeatability (see next section). However, there are some limitations. On complex parts,

many probing directions may be needed. If the PTV value for the probe / stylus combination is sufficiently low, then its impact on the measurement accuracy may be acceptable. However, if this potential measurement error is unacceptably large, then it may be necessary to calibrate the probe for each direction in which it is to be used.

3.5 Repeatability

A probe's ability to trigger at the same point each time is known as its repeatability. This is a random error and kinematic resistive probes for machine tool applications typically repeat within 1.0 μm (0.00004 in) (2σ) at the stylus tip. Many CMM kinematic resistive probes can repeat within 0.35 μm (0.000014 in) (2σ). It is important to note that these are test rig values, and do not necessarily represent the system measurement repeatability. Any variability in the time taken to latch the machine position from when the probe issues a trigger signal will manifest itself as an increase in repeatability. Whilst CMM control designs have been optimised around the probe input, for CNC machine tools this is not always the case.

Other factors that can affect the measurement repeatability of machine tool probes include:

- Sample frequency of the probe signal by the machine controller - on CMMs this is normally a real time interrupt, whilst some CNC machine tools are fitted with high speed skip inputs to minimise the uncertainty of position at the point of trigger. However, some CNCs only sample the probe input every few milliseconds.
- Transmission repeatability - the variation in time taken to transmit a probe trigger signal to the controller. Renishaw optical and radio transmissions are designed to have a short and highly repeatable delay.

3.6 Hysteresis

The direction of the preceding probe trigger has a small effect on the point of the trigger - similar to backlash in a ball-screw mechanism. Hysteresis is maximised when a measurement follows a probing move in the opposite direction in the XY plane. This effect increases with stylus length and contact force. However, the kinematic mechanism minimises hysteresis so that it is typically only a small component of the probe's unidirectional repeatability.

3.7 Performance factors ranked in terms of importance

1. Repeatability

This is the key performance requirement of any trigger probe and represents the fundamental limit to system performance. Hysteresis contributes to repeatability.

2. Pre-travel variation

This factor can be removed through calibration, provided all the probing directions are known. Measurement accuracy will be reduced if a probe with a high PTV value is used in an unqualified direction. PTV increases rapidly with stylus length in kinematic resistive probes.

3. Hysteresis

A small factor for probes with kinematic mechanisms.

4. STRAIN GAUGE PROBE TECHNOLOGY

A newer form of sensing technology has addressed the performance limitations of the kinematic resistive probe mechanism: silicon strain gauges. This has been made possible by modern compact electronics and solid state sensing, which Renishaw has engineered for probes as small as 13 mm (0.5 in) in diameter.

Although strain gauge probes still use a kinematic mechanism to retain the stylus, they do not use the resistance through the contact elements as the means to sense a trigger. Instead, a set of strain gauges is positioned on carefully designed webs in the probe structure above the kinematics (see figure 10). These gauges measure the contact force applied to the stylus and generate a trigger once the strain exceeds a threshold value. This provides a low trigger force, and, since the sensing is not dependent on the kinematics, a consistent trigger characteristic in all directions.

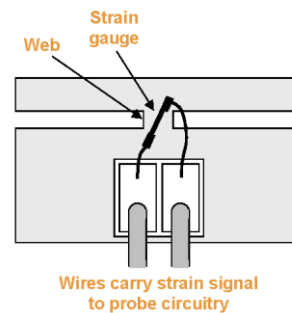


Fig. 10. Strain gauge mounted to web inside probe

4.1 Measuring the contact force

Figure 11 shows a schematic of a strain gauge probe. At low contact forces, the kinematics remain seated and the force is transmitted through them to the probe structure. The strain gauges - three measuring gauges aligned to sense in the X, Y and Z axes - are mounted on thin webs. They detect forces in the structure and their outputs are summed together so that once a force threshold is breached in any direction, a trigger signal is generated. This threshold force is typically a few grams - much lower than the trigger force on an equivalent resistive sensor.

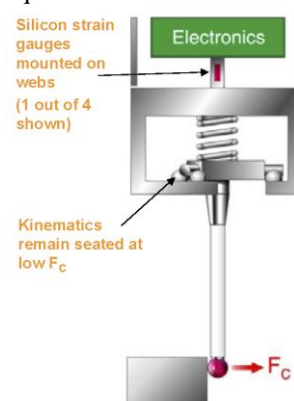


Fig. 11. Schematic of a strain gauge probe measuring the contact force

The strain gauges are highly sensitive to forces on the structure, and will detect vibrations on the machine whilst the stylus is not in contact with the surface of the part. Filtering circuitry inside the probe establishes whether the strains seen at the gauges are the result of a real and persistent deflection of the stylus. To achieve this, a short and highly repeatable delay is inserted into the detection circuit from the moment the force threshold is first breached, after which a persistent and increasing force must be seen before a trigger is issued at the end of the delay period.

4.2 Rejecting false triggers and repeatable measurement

Fig. 12a. illustrates the case where there is significant noise on the strain gauge output value, caused by vibration on the machine. In this case, the threshold is breached by one particular vibration and the fixed delay timer starts. However, the force drops below the threshold and remains at a lower level so that, once the delay period has expired, the electronics can identify that a real trigger has not occurred, so no trigger signal is issued.

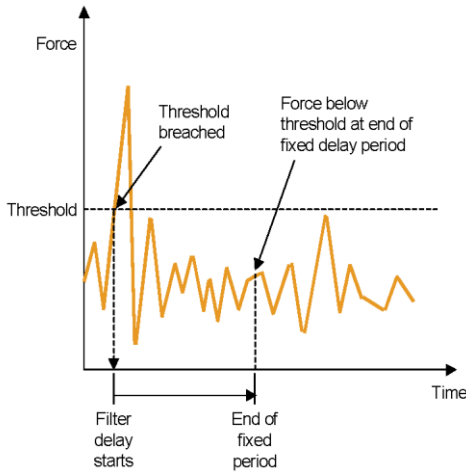


Fig. 12a. A random vibration breaches strain gauge force threshold – no trigger issued

Meanwhile, Fig. 12b. shows the case where the stylus meets the surface. Once the stylus strikes the surface, random vibrations are quickly damped out as the strain gauges measure the contact force. The force seen at the gauges rises persistently, so that once the timer starts, the force never falls below the threshold again. At the end of the repeatable delay period, a trigger signal is issued.

This repeatable delay is easily removed with probe calibration. The net effect is an apparent reduction in the radius of the stylus ball, equal to the distance moved by the machine during the fixed delay period. Provided the machine moves at a constant speed during this period, measurement repeatability is unaffected. This means that the probe must be calibrated at the same programmed feed rate at which measurements will occur, making strain gauge probes suitable only for automated CMMs and CNC machine tools. A further consideration is the programmed target position - the point beyond the expected position of the surface

towards which the machine is programmed to move during the probing cycle. Manufacturing engineers must ensure that as the machine moves towards this target position, it does not start to decelerate before the stylus meets the surface. The over-travel distance must therefore take account of both the likely variation in surface position, as well as the deceleration profile of the machine.

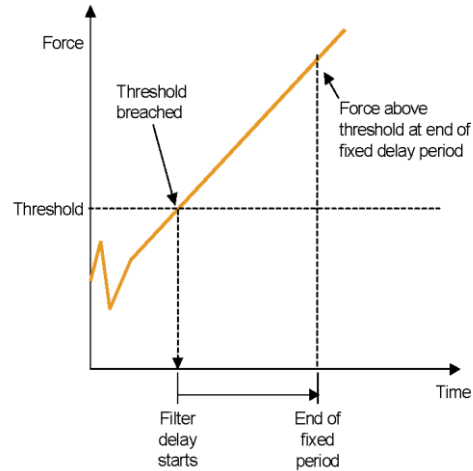


Fig. 12b. A persistent force due to a probe trigger breaches strain gauge force - trigger signal is issued at the end of the delay period

4.3 Performance benefits

Fig. 14. shows a typical pre-travel variation plot for an OMP400 touch-trigger probe where 12 points are taken at 30° increments around a circle. The chart shows a typical PTV plot for an OMP400 touch probe, showing a low and almost uniform pre-travel in all directions. Using a 50 mm stylus, the PTV value in the XY plane is just 0.34 μm (0.000013 in), or roughly 90% less than the PTV value for a similarly sized kinematic touch probe. The OMP400 touch probe typically exhibits XYZ PTV values of less than 1 μm.

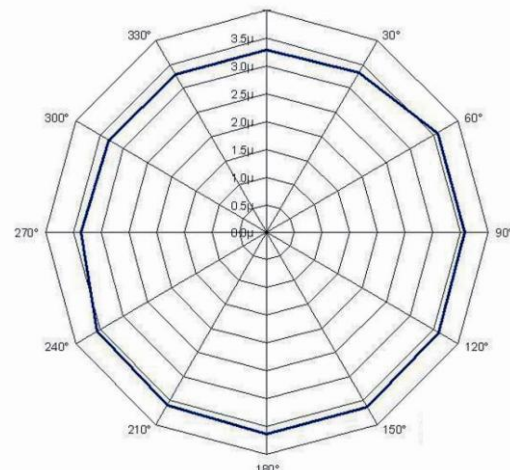


Fig. 14. Pre-travel variation plot for an OMP400 touch-trigger probe

These performance benefits manifest themselves in more accurate measurement, especially on complex parts where many sensing directions are used. The low PTV value means that a simple probe calibration routine can be used.

4.4 Life and reliability benefits

Another benefit of strain gauge technology is the longer operational life that can be achieved - typically more than 10 times longer than resistive probes. Using solid state strain gauges means that there is almost no degradation of the kinematic contacts, which are used solely for their mechanical re-seat properties. In contrast, resistive probes start to exhibit increasing re-seat failures over time. The resistance through the contacts eventually fails to fall below the trigger threshold due to microdegradation of the surfaces. Furthermore, unlike resistive probes, strain gauge sensors do not suffer from vibration-induced false triggers. These characteristics make them suitable for intensive touch-trigger probing applications.

4.5 Flexibility

In kinematic resistive probes, the pre-travel variation increases rapidly with stylus length (PTV is proportional to the cube of the stylus length). This means that measurement performance requirements limit the length of stylus that can be used. Whilst this is overcome in many cases by the use of an extension bar, an indexing head and / or the small size of the probe itself, there are some inspection applications that demand a very long stylus. Strain gauge sensors, with their lower and more consistent trigger forces, can provide superior measurement performance and support much longer styli. In the case of the RMP600 spindle probe for machine tools (see Fig. 15.), styli up to 300 mm long can be used, with only a small decrease in measurement performance.



Fig. 15. RMP600 strain gauge spindle probe

	Stylus length	
	50 mm	100 mm
Repeatability Max. 2σ in any direction of 12	0.25 μm	0.35 μm
2D (XY) lobing Max. deviation from a ring gauge	$\pm 0.25 \mu\text{m}$	$\pm 0.25 \mu\text{m}$
3D (XYZ) lobing Max. deviation from a known sphere	$\pm 1.00 \mu\text{m}$	$\pm 1.75 \mu\text{m}$

Some measurement applications demand very small styli to access the features to be measured. The low probing force of strain gauge sensors means that less rigid styli can still be used.

5. SUMMARY

Touch-trigger probes - kinematic resistive and strain gauge sensors - are the most widely used forms of contact sensor used on CMMs and CNC machine tools. Despite the recent increase in the use of scanning probes on CMMs, touch-trigger probes continue to play an important role in quality assurance and process control in many fields of manufacturing. Their design has evolved to meet the needs of a wide range of measurement tasks, with innovative sensing technology providing improved performance, a longer operating life and increased flexibility.

6. REFERENCES

- [1] RENISHAW PLC, Innovations in touch-trigger probe sensor technology, Document number H-5650-2014-01-A, © 2010 Renishaw plc. All rights reserved.

Author: Nick Penfold, Renishaw, PLC New Mills
Wotton-u-Edge, Gloucestershire GL128JR
T +44 (0) 1453 524125
F +44 (0) 1453 524104
M +44 (0) 7796 335858
E-mail : nick.penfold@renishaw.com

Peták, T., Benkó, P.

CALIBRATION OF THE LENGTH MEASURING MACHINE

Abstract: This contribution describes procedures and interpretation techniques of calibration universal length measuring machine Zeiss ULM 600. As a method for calibration was used direct comparison method. The Aim of this work is to specify a calibration method, design of measurement model, execution of the measurement experiments, statistical evaluation of the measurements, specification of source of uncertainties and interpretation of the results of calibration in terms of the chosen methodology. As a standard was chosen laser interferometer XL 80 from Renishaw. Result of this work is to determine the positioning errors of the length measuring machine with application of corrections of these errors.

Key words: length measuring machine, laser interferometer, calibration, uncertainties of measurement

1. INTRODUCTION

In the calibration of precision measuring systems are increasing requirements for accuracy, evaluation and improvement of new principles and methods of measurement. For this reason is important the implementation of the optical measurement systems for the calibration process.

As a standard for the calibration was chosen laser interferometer Renishaw XL 80 to fulfill requirements for high accuracy and repeatability measurements of the length measuring machine. The laser interferometer is also used in the geometrical quantities measurement.

2. LENGTH MEASURING MACHINE ZEISS ULM 600

Length measuring machine Zeiss ULM 600 is a classic concept with manual control tailstocks. Linear measurement range is 600 mm. Positioning of measuring touch with resolution 0,2 μm is indicated by measuring ruler HEIDENHAIN. This device is used for length measures calibration such as plain plug gages, setting rings, thread gages, thread setting rings, gage blocks, dial indicators, calipers, micrometers and the others.

PERFORMANCE DATA	ZEISS ULM 600
Linear measurement range	0 to 600 mm
Resolution	0,2 μm
Maximum permissible error MPE	$0,3 + L/1500 \mu\text{m}$

Table 1. Basic metrological parameters of Zeiss ULM 600

3. STANDARD – LASER INTERFEROMETER RENISHAW XL 80

Laser interferometer is measuring device that is used in the geometrical quantities measurement such as

length, angle, straightness, flatness or perpendicularity. As a light source is used He-Ne laser (Helium-Neon) methane CH_4 stabilized. Frequency is sufficiently stable to be able measure the frequency and wavelength with high accuracy. Laser interferometer Renishaw XL 80 is based on heterodyne principle; it is therefore dual frequency interferometer.

Device works on the physical principle of the interference comparator. The light source is dual frequency gas laser. The laser emits light radiation at two very close frequencies. Both beams are orthogonal polarized. This allows their separation by polarizing filter. This provides reference and measurement beams. Reference beams f_1 and f_2 fall on a photosensitive element, the measuring beams continue to half mirror. The measuring beams are divided into two parts here. One part of the frequency f_2 is reflected by the corner reflector and after reflection from the semi-permeable mirror returns to the photosensitive element. The second part of the frequency f_1 moves through the half mirror and turns to the corner reflector mounted on the measured object. There is a frequency shift of the beam on value $f_1 + \Delta f$. The beam turns on a photosensitive element. There is an output signal proportional to the frequency change Δf on the output of evaluation unit.

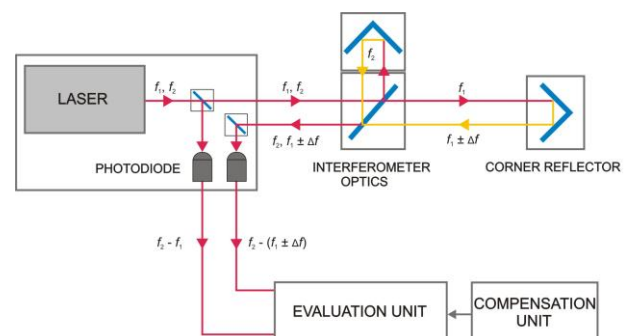


Fig. 1. Schematic sample of the heterodyne laser interferometer

The accuracy of measurement by the laser interferometer affects the refractive index of environment, usually air.

Wavelength of the laser beam varies according the formula:

$$\lambda = \frac{\lambda_0}{n} \quad (1)$$

where:

- λ – wavelength of laser light in air,
- λ_0 – wavelength of laser light in vacuum,
- n – refraction index of air.

The value of the refractive index varies according to changes in temperature, pressure relative humidity and chemical composition of air. Contamination of optical path of laser between interferometer and corner reflector also affects the measurement.

System performance	Renishaw XL 80
Linear measurement range	0 to 40 m
Linear measurement accuracy	$\pm 0,5 \mu\text{m/m}$
Linear frequency accuracy	$\pm 0,05 \mu\text{m/m}$
Resolution	1 nm
Maximum travel velocity	4 m/s
Dynamic capture rate	10 Hz to 50 kHz
Preheat time	< 6 minutes
Specifies accuracy temperature range	(0 to 40) °C

Environmental sensor performance	Renishaw XL 80
Material temperature	(0 to 55) °C Accuracy: $\pm 0,1 \text{ }^\circ\text{C}$
Air temperature	(0 to 40) °C Accuracy: $\pm 0,2 \text{ }^\circ\text{C}$
Air pressure	65 kPa to 115 kPa Accuracy: $\pm 1 \text{ mbar}$
Relative humidity (%)	(0 to 95) % Accuracy: $\pm 6 \text{ } \%$

Table 2. Basic metrological parameters of the laser interferometer Renishaw XL 80

4. CONDITIONS OF THE CALIBRATION EXPERIMENT

As a method for calibration device Zeiss ULM 600 is chosen direct measurement by laser interferometer. The measurement of universal length machine proceeded according to standard VDI/VDE 2617. The calibration must be too complied with a series of basic conditions, such as the measurement is performed in metrological laboratory on the device steady-state temperature, it must be preceded a suitable heating process and positioning part must stop in the measured

position for long enough to allow a capturing of actual position.

Direct to the nature of measurement is chosen as a measuring step the linear bi-directional measuring cycle. It refers to a series of measurement, where setting to the specified position in given axis is performed in both directions of movement.

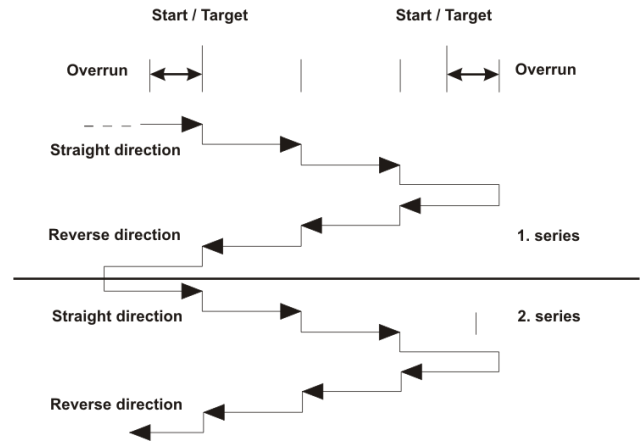


Fig. 2. Sample linear bi-directional measuring cycle

Ambient conditions (air temperature, material temperature, air pressure, relative humidity) are monitored and recorded throughout the measurement to fulfill the requirements VDI standard, but also to correction length value of the laser interferometer in relation to the reference ambient conditions.



Fig. 3. Samples calibration of length measuring machine Zeiss ULM 600

5. MATHEMATICAL MODEL OF THE CALIBRATION

In calibration of the universal length machine there are several sources of errors. Classification and estimation of these potential sources of errors need for evaluation of uncertainty measurement. The most significant sources of errors in length machine measurements is the temperature (or more exactly, the change of the temperature) of the measured machine. For very precise measurements is important to measure the temperature of the controlled part of the machine and to use it in readout corrections.

Uncertainty of the measurement is the qualitative sign of measurement. Absolute knowledge of measurement process requires a lot of information, which could be described by mathematical model (1).

Mathematical model of calibration of NC positioning table is expressed as follows:

$$\Delta L = L_{ULM} - \underbrace{[1 + \alpha(20 - t_m)] \cdot L_{LI}}_{L_c} + \delta L_{\cos} + \delta L_{Abbe} + \delta L_{dp} \quad (2)$$

where:

- ΔL – deviation of position in axis,
- L_{ULM} – measured length value indicated by universal length machine,
- L_c – corrected value of the measured length of the laser interferometer (conventionally true value).

Further corrections in the model are be considered zero and their impact is transferred to the uncertainty of measurement.

Other influencing parameters in the model are:

- α – coefficient of thermal expansion of the mechanical part of the universal length machine,
- t_m – temperature of material,
- L_{LI} – length measured by the laser interferometer expressed as:

$$L_{LI} = \left(\frac{\lambda_0}{64n_{tph}} \right) \cdot N \quad (3)$$

where:

- λ_0 – wavelegh of laser radiation in vacuum,
- 64 – constant of polarization splitter,
- n_{tph} – index of refraction of air at a temperature t , pressure p , relative humidity h ,
- N – number of laser pulses.

The refractive index n_{tph} can be expressed by Edlens equation or using the calculator on the website: <http://emtoolbox.nist.gov/Wavelength/Edlen.asp>.

Expression of Edlens equation shows how the environmental refractive index varies with the temperature, relative humidity and air pressure changes.

The errors caused by the change of the wavelength are less important, but they can not be abandoned. Roughly $1\mu\text{m/m}$ is caused by: the air temperature change of 1°C , the air pressure change of 4hPa and the relative humidity of air change of 30% .

Edlens equation:

$$n_{tph} = n_0 \left[1 + K_t(t - 20) + K_p(p - 20) - K_h(h - 50) \right] \quad (4)$$

Errors that are specified as mechanical sources of uncertainties which are added to overall measurement model are follows:

- δL_{\cos} – cosine error,
- δL_{Abbe} – Abbe error,
- δL_{dp} – dead path error.

A cosine error

If the laser beam is not parallel to a measured axis of a machine (i.e. the optical path is not properly adjusted) than a difference between the real distance and the measured distance occurs. This error of adjustment is known as a cosine error, because its magnitude depends on the angle between the laser beam and the axis of the measured machine.

An Abbe error

An Abbe error occurs when, during measurements, the measured part does not move perfectly straight and there appear angular movements, which cause sloping of the corner reflector.

A dead path error

A dead path error is an error associated with the change in environmental parameters during a measurement. This error occurs when some part of the light path (a dead path) is not included in the temperature (both air and base), pressure and humidity compensation.

6. EVALUATION OF THE CALIBRATION RESULTS

Evaluation of the calibration universal length machine Zeiss ULM 600 is focused to determine positioning errors of machine axis. Metrological verification is made, as well with comparing to manufacturer parameters. As is shown in Figure 3, some measured error points are not in the manufacturer tolerance with the uncertainty of determining the error point. After corrections into the control system of machine Zeiss ULM 600 are all measured error points in accordance with the manufacturers tolerance, as is shown in Figure 4.

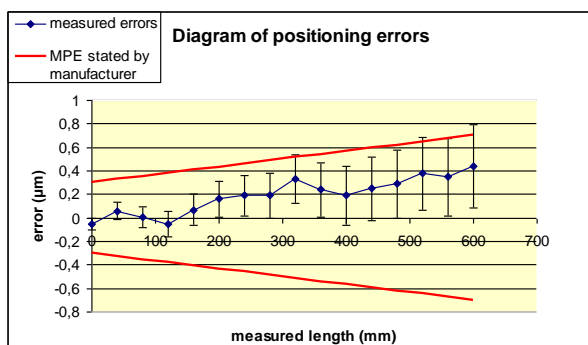


Fig. 4. Diagram of positioning errors of the Zeiss ULM 600

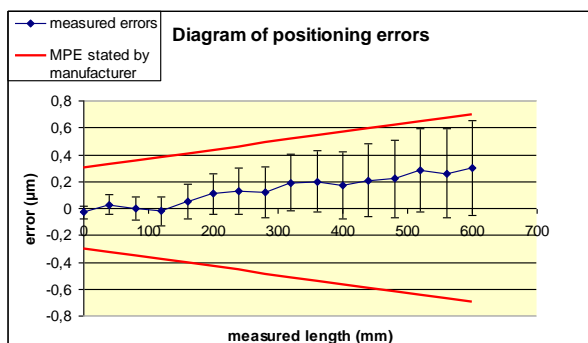


Fig. 5. Diagram of positioning errors of the Zeiss ULM 600 after application of corrections

Uncertainty of measurement in calibration:

$$U = (0,05 + 0,5 \cdot L) \mu\text{m}, L \text{ is length in meters}$$

The reported expanded uncertainty of measurement is stated as the standard uncertainty of measurement multiplied by the coverage factor $k = 2,00$ which for a t-distribution with $\nu_{\text{eff}} = 132,1$ effective degrees of freedom corresponds to a coverage probability of approximately 95%. The standard uncertainty of measurement has been determined in accordance with EAL Publication EAL-R2.

7. CONCLUSION

This contribution describes procedures and interpretation techniques of calibration the universal length measuring machine Zeiss ULM 600 by laser interferometer. Calibration of the universal length machine requires design of calibration model, specification sources of measurement errors and interpretation of the calibration results in accordance to a metrological standard. Contribution also describes the operation process of calibration of universal length machine, conditions of its measurement and shows sample of evaluation the universal length machine before and after corrections.

8. ACKNOWLEDGMENTS

The research work was performed to financial support Ministry of Education of the Slovak Republic, grant No. VEGA 1/0584/12.

9. REFERENCES

- [1] CASTRO, H. F. F. - BURDEKIN, M.: *Dynamic calibration of the positioning accuracy tools and coordinate measuring machines using laser interferometer*. International tools and coordinate measuring journal of machine tools & Manufacture 43, 2003.
- [2] CHUDÝ, V. - PALENČÁR, R. - KUREKOVÁ, E. - HALAJ, M.: *Meranie technických veličín*. Bratislava: STU v Bratislave, 1999, ISBN 80-227-1275-2.
- [3] EA-4/02: *Expression of the Uncertainty of Measurement in Calibration*, European co-operation for Accreditation, 1999.
- [4] *Guide to the Expression of Uncertainty in Measurement*, International Organization for Standardization, 1995.
- [5] JAE, H - LEE, Y. L. - SEUNG-HAN, Y: *Accuracy improvement of miniaturized machine tool*, International journal of machine tools & Manufacture 46, 2006.
- [6] VDI/VDE 2617: *Accuracy of Coordinate Measuring Machines*, Verein Deutscher Ingenieure, 1986.

Authors: Ing. Tomáš Peták, Ing. Peter Benkó, PhD.,
 ÚAMAI SjF STU Bratislava, Námestie slobody 17,
 Bratislava 1, 812 31, Slovak Republic, Phone.: +421
 02/52497193, 02/52494311, Fax: +421 02/52495315.
 E-mail: tomas.petak@stuba.sk
peter.benko@stuba.sk

Radlovački, V., Delić, M., Kamberović, B., Vulanović, S., Hadžistević, M.

HOW MANAGERS ESTIMATE MANAGEMENT SYSTEMS TODAY IN SERBIA

Abstract: *Quality managers in Serbian organisations were asked to estimate the main quality management system dimensions. They are also asked to express their opinion on how they generally estimate their quality management systems. Linear regression is used to find predictors of these general estimates and conclusions are drawn out.*

Key words: *managers' estimates, quality management, transition*

1. INTRODUCTION

Over one million firms worldwide implemented ISO 9001 in last seven years [1].

Nair & Prajogo [2] argue that applying ISO 9001 may result in innovation, and that can generate positive influence on performance of an organisation. Such influence of ISO 9001 is present in developed economies.

As Jimenez & Valle [3] argue, there are technical or administrative innovations. Technical innovation can be a new product/service or modification of an existing process. Administrative innovation can be a new procedure in administration, new policy, new set of rules and/or other set of changes in organising the work. According to some findings, innovations can support organisations dealing with unstable events [4], [3].

This research is carried out in Serbian economy. It is now for a long time in transition [5].

This research is carried out along with some more extensive works in the University of Novi Sad (Faculty of Technical Sciences, Department for Industrial Engineering and Engineering Management), aimed to examine impacts of quality management system (QMS) practices to organisational performance. First results thereof will be published soon.

This research is aimed to find how generally quality managers estimate their quality management systems.

As far as we know, some findings indicate differences between how impacts of quality system dimensions are treated and what their influence is on organisational performance, in developed economies and economies in transition [5], [6]. Many research efforts (and practical as well) have to be made to straighten things out - to find where economies in transition are today and what to do to direct it towards improving their performance.

It is now of a great interest for both researchers and practitioners to examine what quality dimensions are recognised by Serbian managers as predictors of general estimate of QMS (fig. 1, 5 point Likert scale used for estimating).

The assumption as a basis for this study is: all estimates of quality management system dimensions make significant positive relations with the general estimate of a quality management system provided by managers.

Study is carried out using a specially designed questionnaire.

2. METHOD

The questionnaire used in the study was constructed upon results of several studies highly related with this one (e.g. [3], [7], [8], [9], [10]).

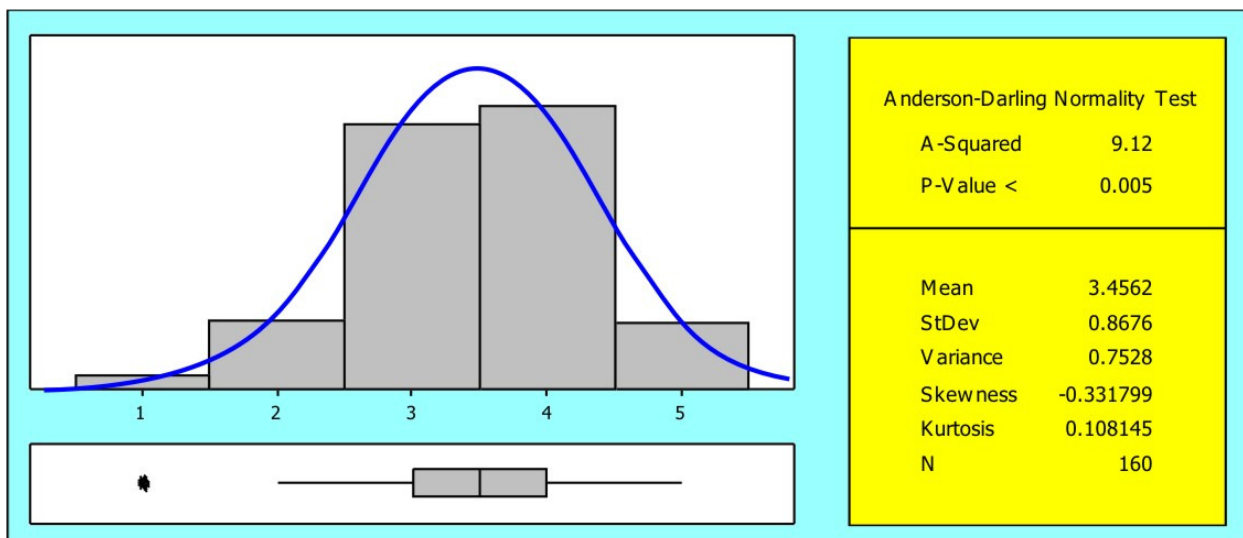


Fig. 1. Descriptive statistics summary for cenral parameter

Pre-final questionnaire was reviewed by experts from the Faculty of Technical Sciences in Novi Sad, IIS - Research and Technology Center Novi Sad and a group of quality managers from industry. Some corrections were made. After them a pre-test was conducted on a sample of 30 cases. Finally, the questionnaire contained 44 items grouped into eight quality management constructs. A five-point Likert scale [11] was used for obtaining estimates.

Data were collected within a time of around three months. An electronic questionnaire was used. After being forwarded to quality managers of manufacturing and service organisations in Serbia, results were collected electronically.

According to Aire [12], unidimensionality analysis is to be conducted by carrying out confirmatory factor analysis (CFA) (here done using LISREL v8.80). After that, the model fit was examined by calculating χ^2 and p values. Finally, for all constructs, the goodness of fit index (GFI) was analysed. Questionnaire reliability test was carried out by calculating Cronbach α [11] coefficients. Bentler-Bonett coefficient was calculated for convergent validity analysis [12]. All of the analysis proved out that questionnaire was reliable and valid for the research.

Discussion and conclusions of this study are based on calculating various parameters of descriptive statistics for observed variables and performing multiple linear regression to find independent predictors of observed estimates.

3. SAMPLE

The survey lasted for three months. An electronic questionnaire was forwarded to quality managers in certified Serbian organisations. Out of over 1000 organisations, 160 valid responses were returned. Descriptives are given in the results section.

4. RESULTS

Organizations from the sample are production, service providers or both (Table 1).

Organisation types	N	%
Production	40	25.0
Service	63	39.4
Production and service	57	35.6
Total	160	100.0

Table 1. Organisation types in the sample

The type of organisation ownership also varies throughout the sample (Table 2).

Property (mainly)	N	%
Government	68	42.5
Private	92	57.5
Total	160	100.0

Table 2. Private and government organizations in the sample

The sample includes micro, small, middle and large organisations (Table 3).

No of employees	N	%
between 1 and 9	26	16.3
between 10 and 49	19	11.9
between 50 and 249	54	33.8
over 250	61	38.1
Total	160	100.0%

Table 3. Size of organisations in the sample

Given the tabular descriptives, sample can be regarded as representative.

Frequencies of QMS dimensions estimates are given in Fig. 2, while Table 4 contains descriptives.

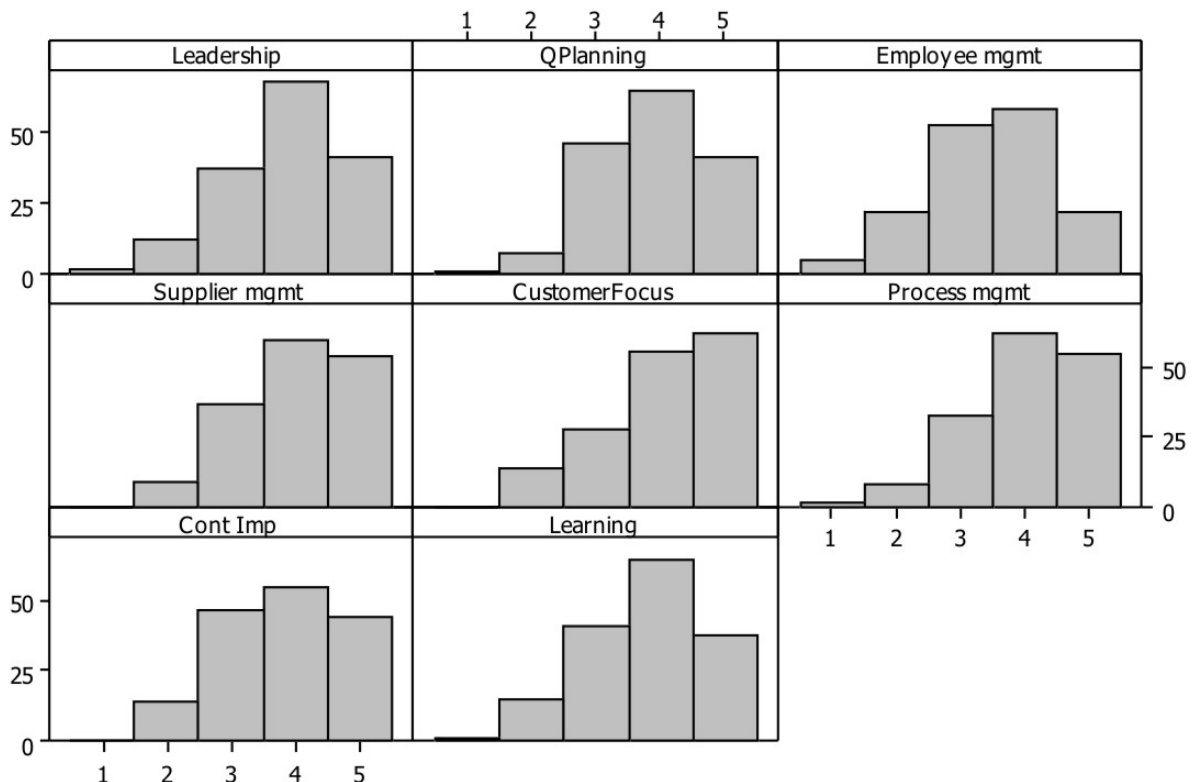


Fig. 2. QMS dimensions: frequency histograms

Variable	Mean*	StDev*	Items
Leadership	3.80	0.869	3
Quality planning	3.75	0.817	4
Employee management	3.43	0.955	5
Supplier management	3.87	0.802	4
Customer focus	3.91	0.909	4
Process management	3.84	0.879	4
Continuous improvement	3.70	0.899	4
Learning	3.69	0.908	4

* Mean and deviation for parameter values scaled to 5 points Likert scale

Table 4. Descriptives: QMS dimensions

General estimates of QMSs provided by quality managers are shown in Fig. 1 and table 5.

QMS estimate	Frequency	Percent
1	3	1.88
2	16	10.00
3	61	38.13
4	65	40.63
5	15	9.38

Table 5. Estimates of QMS provided by Q managers

Fig. 1 uncovers 3 outliers in 160 cases (estimates thereof are 1 at a Likert scale). Other data forms the distribution that can not be considered normal (see Anderson-Darlin test results). Having median right of the mean is caused by outlier values.

Calculation of regression is performed (independent variables are QMS dimensions, and QMS estimate is dependent variable). Model appears to be statistically significant at the confidence level of 99% ($p < 0.01$, table 6).

Source	DF	SS	MS	F	P
Regression	8	83.99	10.49	44.4	0.000
Residual Error	151	35.70	0.236		
Total	159	119.69			

Table 6. Analysis of variance for regression model

Results of linear regression are given in table 7, while graphical interpretation of the model is shown in Fig. 2.

R^2 (determination coefficient) value of 70.2% indicates that around 70% of dependent variable variation can be explained by variations of independent variables.

Regression equation (1) is presented using abbreviations given in table 7. Central parameter (dependent variable) is abbreviated with "QMSEst":

$$QMSEst = -0.080 + \underline{0.0763 LEAD} + 0.0370 QP - 0.0038 EM + 0.0178 SM - 0.0127 CF + 0.0322 PM + \underline{0.0622 CI} + \underline{0.0464 LEARN} \dots\dots\dots (1)$$

Statistically significant parameters are underlined along with their coefficients. At the end, graphical interpretation of a model is given in Fig. 3.

5. DISCUSSION

Values of predictor coefficients are low due to dependent variable domain (1 to 5), while independent variables are scores composed of 3-5 item estimates (with wider domains; see Table 4). P-values can be considered indicators of a predictor statistical significance.

Estimates of leadership appear to be the strongest predictor of QMS estimates. Observed alone, this finding might be a positive indicator. But, one could be justifiably concerned about the situation where, at the same time,

Predictor	Abbreviation***	Coef	SE Coef	T	P
Constant	-	-0.0798	0.2098	-0.38	0.704
Leadership**	LEAD	0.07626	0.02641	2.89	0.004
Quality planning	QP	0.03698	0.02244	1.65	0.101
Employee management	EM	-0.00382	0.01490	-0.26	0.798
Supplier management	SM	0.01784	0.02234	0.80	0.426
Customer focus	CF	-0.01266	0.02160	-0.59	0.559
Process management	PM	0.03220	0.01904	1.69	0.093
Continuous improvement*	CI	0.06224	0.02415	2.58	0.011
Learning*	LEARN	0.04640	0.02028	2.29	0.024

** $p < 0.01$, * $p < 0.05$, ***used in regression equation

Table 7. Linear regression results

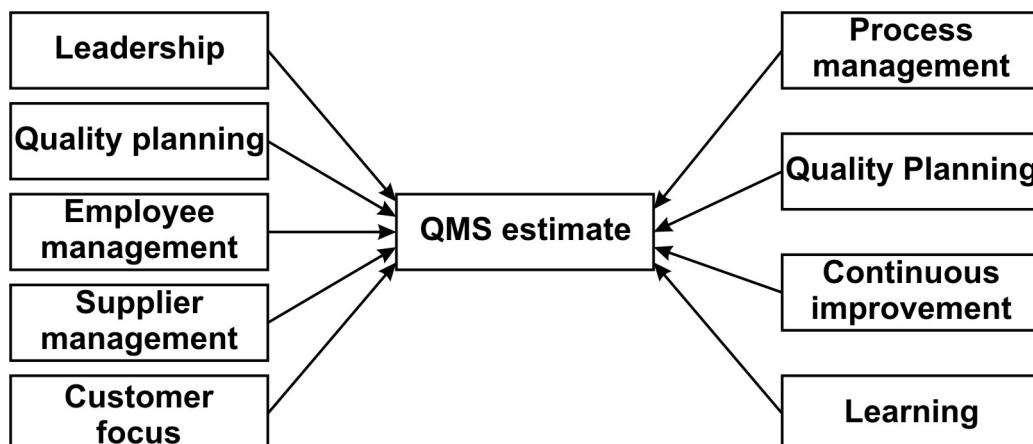


Fig. 3. Model

managers' estimates do not reveal any significant direct relations between process management, customer focus or quality planning from one and central parameter from other side. What does leadership mean without previously listed attributes as predictors? What business behaviour model could any manager offer to employees, and how could he or she make efforts to motivate employees, if not towards efficient process management, higher user satisfaction levels and/or better quality planning?

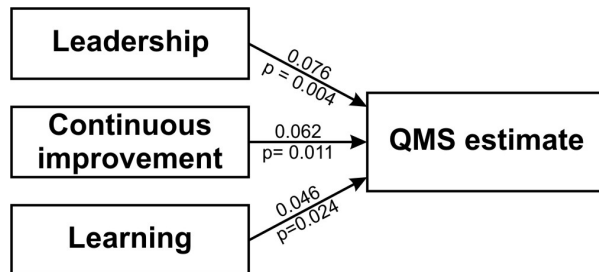


Fig. 4. Significant predictors

Data for the study [5] are acquired little more than a year before this study. Study reveals relations between different dimensions of quality management and the application of quality management principles (QMPA) introduced by ISO 9004 standard. The positive relation between subjective estimates of QMS and QMPA is registered. Among observed dimensions related to QMPA there was process management as well. Now, without this relation, we may assume that generally quality management system is not any more driven to enhance process management any more. This could be the most discouraging conclusion of this study. Human resource management have shown significant positive relation with QMPA. Now, relation between employee management and QMS estimate is not registered. Does it mean that these very important links between employees and QMS simply vanished? The results of this study are more likely to be valid then the previous one, due to three times larger sample.

Customer focus was not found to be related to QMPA. It is now not related to QMS estimate. Assuming that these two findings are both caused by the fact that processes are generally driven by something else (not customer focus), this can be regarded as discouraging as well.

Continuous improvement and learning are found to be predictors of QMS estimate. This is encouraging. It probably means that managers are aware of the importance of all observed elements but are simply not able to straighten things out due to work overload, unfavourable conditions in which organisations operate (transition) and poor workforce motivation.

Findings of this study must be examined in more detail to gain more usable conclusions. "More detail" means larger samples, more sophisticated methodology, access to more relevant data other than "just a few subjective estimates" and support for on-site testing by measuring efficiency of actions designed upon results of valid studies. Such activity needs time, support by authorities and access to a set of relevant resources (such support doesn't exist for a very long time). And, the last, absence of expected relations must not be examined without taking into account conditions in which organisations operate and its impacts to managers' estimates and performance of an organisation.

However, one can never be wrong by making decision to design appropriate actions (for instance trainings, seminars or

improvement projects) to support process management improvement, human resource management improvement, better understanding of customer requirements, implementation of various methods/techniques (statistical, engineering and/or management). Scientific institutions are today not strong enough to carry out such activities on their own.

6. CONCLUSIONS

This study reveals absence of expected relations between quality management systems provided by managers in conditions of transition (in Serbia). The absence thereof is found using the sample of 160 firms, and linear regression.

Authors proposed a framework for design of activities to overcome shortcomings and help firms to direct their businesses towards improvements.

7. REFERENCES

- [1] International Organization for Standardization 2012. <http://www.iso.org/iso/iso-survey2010.pdf>
- [2] Nair, A., & Prajogo, D.: *Internalisation of ISO 9000 standards: The antecedent role of functionalist and institutionalist drivers and performance implications*, International Journal of Production Research, 47(16), p.p. 4545-4568, 2009.
- [3] Jiménez-Jiménez, D., & Sanz-Valle, R.: *Innovation, organizational learning and performance*, Journal of Business Research, 64(4), p.p. 408-417, 2011.
- [4] Pečujlija, M., Nerandžić, B., Perović, V., Jevtić, A., & Simić, N.: *Initiating innovation in Serbian companies' organizational cultures*, African Journal of Business Management, 4(18), p.p. 3957-3967, 2010.
- [5] Radlovački, V., Beker, I., Majstorović, V., Pečujlija, M., Stanivuković, D., & Kamberović, B.: *Quality managers' estimates of quality management principles application in certified organisations in transitional conditions - Is Serbia close to TQM?*, Journal of Mechanical Engineering, 57(11), p.p. 851-861, 2010.
- [6] Radlovački, V., Beker, I., Kamberović, B., Pečujlija, M., & Delić, M.: *Organization performance measurement and quality information system in Serbia-Quality managers' estimates*, International Journal of Industrial Engineering and Management, 2(1), p.p. 13-20, 2011.
- [7] Kaynak, H.: *The relationship between total quality management practices and their effects on firm performance*, Journal of Operations Management, 21(4), p.p. 405-435, 2003.
- [8] Conca, F.J., Llopis, J., & Tari, J.J.: *Development of a measure to assess quality management in certified firms*, European Journal of Operational Research, 156(3), p.p. 683-697, 2004.
- [9] Tari, J.J., Molina, J.F., & Castejon, J.L.: *The relationship between quality management practices and their effects on quality outcomes*, European Journal of Operational Research, 183(2), p.p. 483-501, 2007.
- [10] Alegre, J., & Chiva, R.: *Assessing the impact of organizational learning capability on product innovation performance: An empirical test*, Technovation, 28(6), p.p. 315-326, 2008.
- [11] Nunnally, J., & Bernstein, H.: *Psychometric theory*, McGraw-Hill, 1994.
- [12] Ahire, S.L., Golhar, D.Y., & Waller, M.A.: *Development and validation of TQM implementation constructs*, Decision Sciences, 27(1), p.p. 23-56, 1996.

Authors: Radlovački Vladan, PhD., Delić Milan, M.Sc., Prof. Kamberović Bato, PhD., Vulcanović Srđan, M.Sc., University of Novi Sad, Faculty of Technical Sciences (FTS), Department for Industrial Engineering and Engineering Management, Trg Dositeja Obradovića 6, 21000 Novi Sad, Serbia, phone.: +381 21 485 21 78, Fax: +381 21 6 350 300. and **Miodrag Hadžistević, Ph. D.,** FTS, Department for Production Engineering, phone +381 21 485 23 44
E-mails: rule@uns.ac.rs, delic@uns.ac.rs, bato@uns.ac.rs, srdjanv@uns.ac.rs, miodrags@uns.ac.rs

Reibenschuh, M., Zuperl, U., Cus, F., Irgolic, T.

NEW USER INTERFACE FOR DETECTING EDGE WEAR ON CUTTING TOOLS

Abstract: *Increased demands for condition monitoring and demands to increase productivity need new data acquisition methods and user interfaces. Other possibilities are also researched for implementing the method into production process. Use of high speed data acquisition systems is necessary to fulfill the need for monitoring high speed events. This paper presents preliminary tests and results of developing a software user interface for detecting the wear on cutting tool during machining.*

Key words: *edge wear, machining, high speed camera, data acquisition.*

1. INTRODUCTION

During the last decade there has been a setback in development of acquisition techniques. Researchers and authors use existing techniques which they refine [2, 3, 5, 6, 7, 8, 9]. Solutions and methods used in other scientific fields are implemented [1, 4, 10]. Some of the author use intelligent methods to gather, evaluate, optimize and predict data. Others rely on hardware solutions to do the same job. A decision was made to upgrade the existing system for measurements and gathering data with an additional system. In machining were everything is moving, vibrating, cracking, breaking and heating up, the options for data gathering and applying new techniques seem endless. But there are some limitations that need to be taken care off. These limitations are coupled to the equipment used for measuring and gathering. Usually the equipment used for specific measurements and data acquisition is specific and hard to apply. Different hardware was evaluated; among them are visual sensors, sound, vibration and temperature sensors.

The main representatives in this division were evaluated considering the ability of optional adjusting the parameters and the applicability into other machining applications. The machining processes are time and resource consuming. The cutting procedure itself runs at high speeds, thermal and physical loads are immense therefore the hardware equipment must keep up with the rising demands. Today's cutting speeds depend on the speed of the main spindle. It is common that the spindle rotates at 20.000 rpm's. Temperature sensors give an inside view on how the temperatures are deployed in the material. The main disadvantage of using the thermal sensor is the lack of information about the physical properties of the work piece material or the material of the cutting tool. This information is vital for correct evaluation of gathered data and possible numerical simulations. The manufacturer of the cutting tool or the work piece material usually give very little information about it, therefore the needed data has to be acquired otherwise. Sound – vibration sensor are very sensitive to the surrounding environment. The slightest disturbance can of the cutting tool tip, insert or the chip – in that

cause incorrect measurements and the gathered data can be discarded. In a working environment, there are a lot of disturbances from other machines. With the use of special filters these disturbances can be filtered out and the signal cleared. But the state of the tool or work piece is still unknown. The state of it must be determined with the use of other measurement equipment. The use of a high speed camera reduces some disadvantages of previous mentioned equipment. Its work is similar to the work of an operator behind his machine. The operator listens and visually inspects the errors and if necessary adjusts the settings. Therefore a decision was made to begin testing a colour high speed camera and use it to develop an interface for tool wear detection.

2. HARDWARE EQUIPMENT

The high speed camera enables a maximum speed of 65 frames per second (fps). The resolution of the captured images can range up to 640 x 480 pixels. It also has a built in trigger for using additional light source. A built in 1.6 GHz processor enables fast processing of gathered frames. The camera has also an IP67 protection rating, so that it can be also used in working conditions. To use such a camera a compromise must be done to satisfy the need for speed and the need for accuracy. For example, to determine the length of an insert, the scale can be bigger than 1 mm, but to observe the size of the tool, one must consider the tight tolerances during machining. Therefore the scale must be smaller. For 0.1 mm accuracy, the maximum observed window size at a resolution of 640 x 480 pixels is 21.3 x 16 mm. For an accuracy of 0.01 mm, the maximum area would be 2.13 x 1.6 mm. For practical reasons and use, such values are too small – the inflicted damage results in bigger deformations. Because of that we did not go under the accuracy of 0.1 mm (100 μ m). In our testing, the cutting speeds did not exceed 3900 rpm. At 3900 rpm, the tool rotates at a speed of 65 revolutions per second. If a slower cutting speed is chosen, more images can be gathered during one tool revolutions. The colour lens enables also the spotting of any changes in the colour way the thermal influence can be detected. In

conclusion, this high speed camera enables different options of measurements:

- Detection of parts bigger than 1 mm – detection area of 213 mm x 160 mm,
- Detection of parts bigger than 0.1 mm – detection area of 21.3 mm x 16 mm,
- Detection in colour variations – overheated cutting tool, chip or work piece,
- Detection of every full rotation of the cutting tool at 3.900 rpm,
- Detection of one or more rotations depending on the spindle speed.

Considering all options of detection and classification, a decision must be made which settings to use and which features to monitor during the test.

3. PREPARATIONS FOR TESTING

Before the tests were carried out, the connection between the computer and the camera needed to be established. Because the software is not fully compatible with the new version of Windows, there was a delay in connecting both of them. After the intervention from the manufacturer, a software update solved this problem. Although the computer had to be setup to the same sub net mask (IP address...). The camera is connected via Ethernet port to the computer. One of the cameras feature is also its ability to function without a computer. Because it has a built in chip and a processor, a program can be uploaded. When the program is running it can take frames or overview a process autonomously. In the tests, the camera was connected and ran over the computer. The frames, Fig. 1, were uploaded to the computer and afterwards evaluated.

Set of frames, Fig. 1, shows the conditions during milling. The insert is clearly visible. The used work piece material was a steel alloy with the designation OCR 1.2379. For this set of tests colour frames were used.

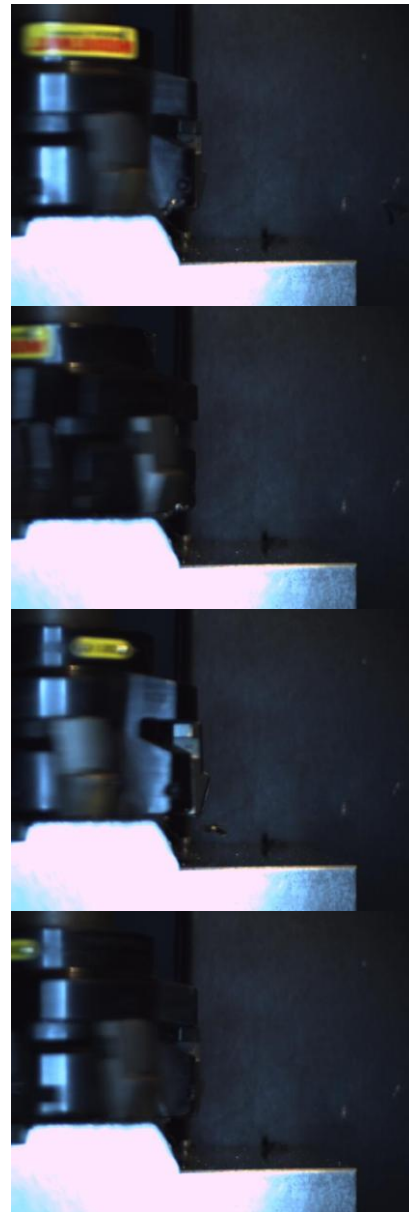
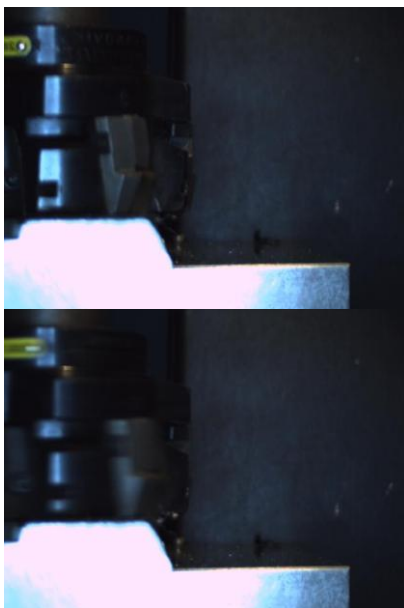


Fig.1. Frames gathered during the testing

4. RESULTS

The first results were used to create a computer program, which recognises specific features, in our case the edge of the insert. The program was developed to recognise the edge of each insert, Fig. 2, and it also compared all gathered frames with inserts with a template frame – the differences are returned (a detection possibility for insert if they are present or not and what size they are). Fig. 2 also shows how the program is set up out of different feature recognition subprograms (steps). Each of these steps offers a variety of settings. With the gathered data (frames) 11 different settings were tested to determine which combination of steps and settings enables the best recognition capability for a certain feature. Use of circular edge detection is a very useful application. This allows recognising a circular edge in a specific region of interest. In the end, an inspection status can be set up to determine if the frame passed the pre-set

requirements. In any case, a rule can be applied that takes actions at specified results and makes changes. These changes can be programmed to do specific tasks. Because the program runs in LabVIEW, additional options are available. For example, if the acquired frame does not match the template, the program can either stop the acquisition or proceed with it.

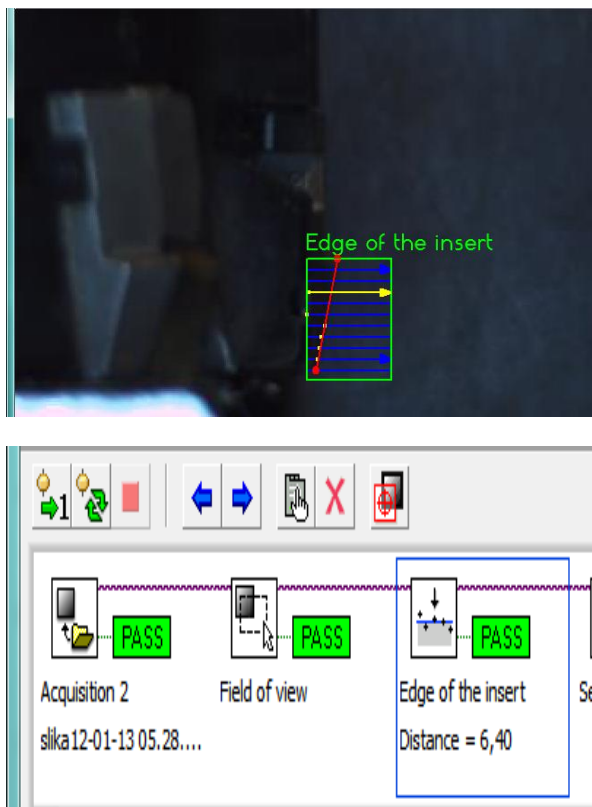


Fig.2. A developed program for insert detection

Other programs similar to the one on Fig. 3 are under development. Different settings and different filters are used. Combinations are tested and comparisons are made between them to determine which one detects more features with greater accuracy and higher speed. More filters and more settings mean longer computational times and use of other resources. Therefore the programs must be as simple, short as possible so that the full capacity of the high speed camera can be used. If the buffer of the camera or the computer is occupied, then the acquisition discontinues and the sequence of the frames is interrupted.

For simpler applications it is also possible to take a frame with another camera and use it as a template. Although it must be mentioned that the base point for taking frames must always be the same so that all settings fit to the observed area, tool position and work piece position. If not, the program can detect other features and recognise them as the desired feature.

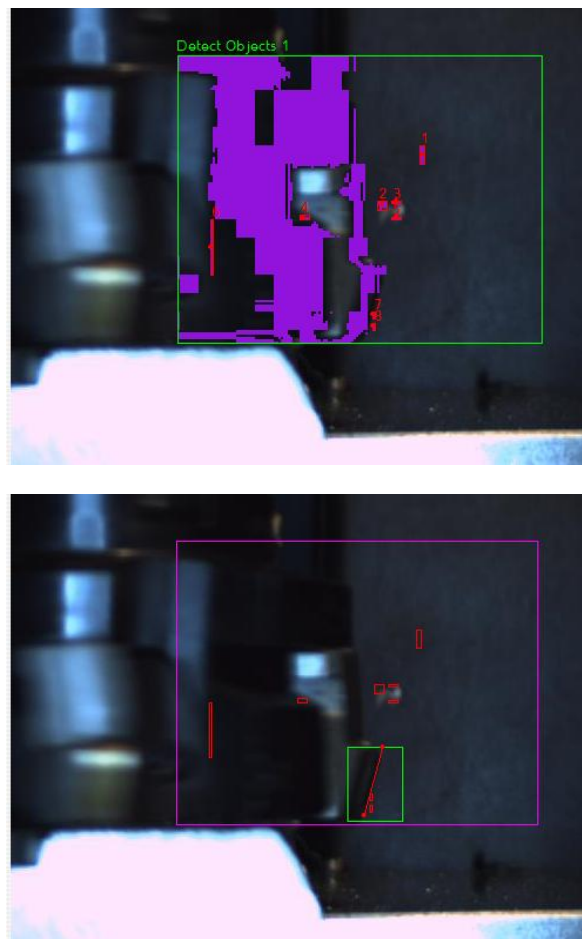
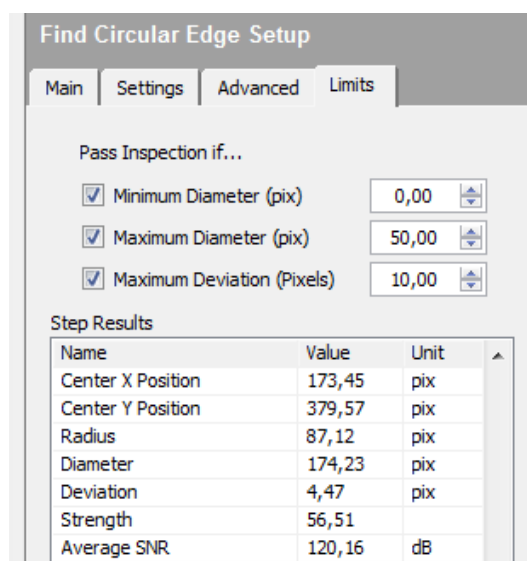


Fig.3. Testing of different settings

On behalf of the gathered frames - results, a limitation is established which prevents the detection of undesired edges or features, Fig. 4. This part of programming is time consuming – it demands the overview of all gathered frames and the measurement of all edges. This is necessary to determine the right values for setting the detection limits. Many other boundary conditions can be set and limited, depending on the inserts physical appearance.



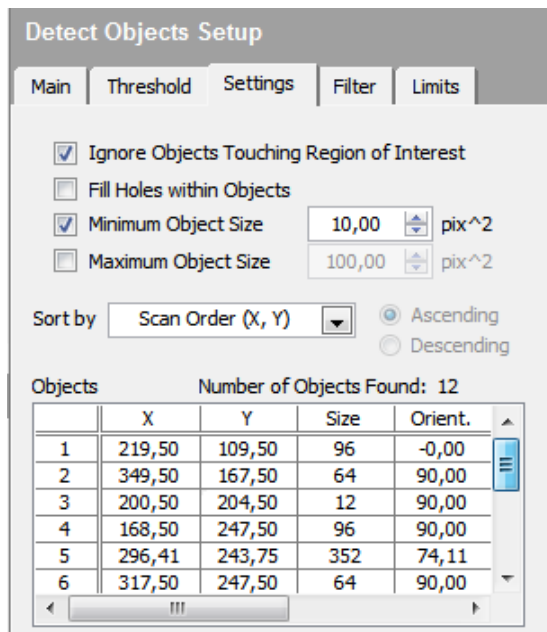


Fig.4. Setting the detection limits

5. CONCLUSION

The results – gathered figures, provide and insight into the insert wear. Clearly visible insert and its size can help determine the correct cutting parameters and prevent the use of damaged inserts. Some suggestions for cutting parameters are in the form of tables and books but because of new advancements in the field of materials, tables for such materials are till now not made. These gathered data are promising in establishing a program for insert wear under different cutting conditions. A chance for chip classification is also possible, which means that the program is able to detect and classify different features as short, broken off chips from long and winding ones, which are hazardous to the cutting tool and work piece. Other programs are in development where the program for insert detection and classification is directly linked to a program for changing the cutting parameters. In doing so, the final program will be able to change cutting parameters during the machining and prevent possible hazardous cutting conditions and tool breakage.

The ability to detect colour deviations is also a useful feature. Data from the camera can also be used for measuring the chip thickness and geometry, depending on the settings of the camera.

6. REFERENCES

- [1] Xiaoli Li, Detection of tool flute breakage in end milling using feed-motor current signatures, 2001, IEEE/ASME Transactions on Mechatronics, Vol. 6, No. 4, December 2001.
- [2] Jantunen E., A summary of methods applied to tool condition monitoring in drilling, 2002. International Journal of Machine Tools & Manufacture, 997-1010.
- [3] Cus, F., Zuperl U. Adaptive self-learning controller design for feedrate maximization of machining process. Adv produc engineer manag, Mar. 2007, vol. 2, no. 1, str. 18-27. http://maja.unimb.si/files/apem/APEM2-1_18-27.pdf.
- [4] Župerl, U., Čuš, F., Reibenschuh, M. Modeling and adaptive force control of milling by using artificial techniques. J. intell. manuf., Published online: 26. oktober 2010, doi:10.1007/s10845-010-0487-z.
- [5] Župerl, U., Čuš, F., Reibenschuh, M. Neural control strategy of constant cutting force system in end milling : review. Robot. comput.-integr. manuf.. [Print ed.], June 2011, vol. 27, iss. 3, str. 485-493, doi: 10.1016/j.rcim.2010.10.001.
- [6] Dixit P. M. (2008) Modeling of metal forming and machining processes: by finite element and soft computing methods, Springer, London.
- [7] Teti R., Jemielniak K., O'Donnell G., Dornfeld D., Advanced monitoring of machining operations, 2010. CIRP Annals – Manufacturing Technology 59, 717-739.
- [8] Sekulic M., Gostimirovic M., Kovac P., Savkovic B., Optimization of cutting parameters based on tool-chip interface temperature in turnin process using Taguchi's method, 2011, 15th international Research/Expert Conference "Trends in the Development of Machinery and Associated Technology" TMT 2011, Prague, Czech Republic, 12-18 September 2011
- [9] Xu C., Chen H., Liu Z., Cheng Z., Condition monitoring of milling tool wear based on fractal dimension of vibration signals, 2009, Strojniški vestnik – Journal of Mechanical Engineering 55 (2009), Vol. 1, pp. 15-25
- [10] Styron J., Infrared cameras improve in-line quality control, 2009, <http://machinedesign.com/article/infrared-cameras-improve-in-line-quality-control-0707>,

Authors: Asistent Marko Reibenschuh, Assistant prof. Uros Zuperl, prof. Dr. Franci Cus, dipl. oec, Asistant Tomaz Irgolic; University of Maribor, Faculty of Mechanical Engineering, Production Engineering Institute, Smetanova 17, 2000 Maribor, Slovenia, Phone.: +386 2 220-7621, Fax: +386 2 220-7996.

E-mail: marko.reibenschuh@uni-mb.si
uros.zuperl@uni-mb.si
franc.cus@uni-mb.si
tomaz.irgolic@uni-mb.si

Savic, B., Slavkovic, R., Veg, E., Urosevic, V., Vlajković, H.

USE OF VIRTUAL AND ACTUAL VIBRO-DIAGNOSTICS FOR BETTER CONDITION MONITORING

Abstract: An intensive development of microprocessors and digital signal processing, made an outstanding impact on vibrodiagnostics and promoted it into the most exploited and reliable method of technical diagnostics. Through an innovative engineering work on development of a new vibro-diagnostics device, based on LabVIEW application, a vast of dynamic measurements were conducted and some of them are deployed in this paper. Data analysis is performed on the records collected with piezoelectric sensor of high sensitivity. The designed instrumentation underwent a true verification in harsh industrial conditions, on actual machinery, in parallel with an appropriate brand name measuring device.

Key words: Vibro-diagnostics, Condition Monitoring, Vibration Measurement.

1. INTRODUCTION

Technical diagnostics is undergoing rapid development and increasing implementation in real time system monitoring. In order to maximize the operational reliability and efficiency, virtual diagnostics is used for system health assessment and machinery failure prediction [1]. Market research showed the lack of powerful yet affordable multifunctional multi channel device for signal analysis. For that purpose a kind of vibro-diagnostic instrument was developed and this paper shows vibration severity measurement results.

Data sets were collected under laboratory conditions, also within industrial environment. The device architecture is based on dedicated signal conditioning module and National Institute data acquisition board. Data measurement and true vibration analysis were carried out with the application software, developed in LabVIEW graphical environment. This multichannel signal analyzer was designed to monitor a cluster of accelerometer signals in order to determine:

- Vibration severity
- Peak tones of spectrum (FFT)
- Time graph of signal trends

The device also provides options to display/store measurement data and input measurement parameters via conventional communication ports and protocols.

2. HARDWARE DESCRIPTION

This concept of multichannel portable device for signal analysis comprises (Fig. 1):

- Set of accelerometer inputs (2-8 channels; 100 mV/g)
- Sophisticated touch screen HMI
- NI cRIO specialized PLC
- Signal conditioning system
- Signal acquisition system (0-6 current inputs 4-20 mA; 1-4 impulse digital inputs 0-5 V) (Fig. 2) [2].



Fig. 1. Measurement device Micro Mon Rotech

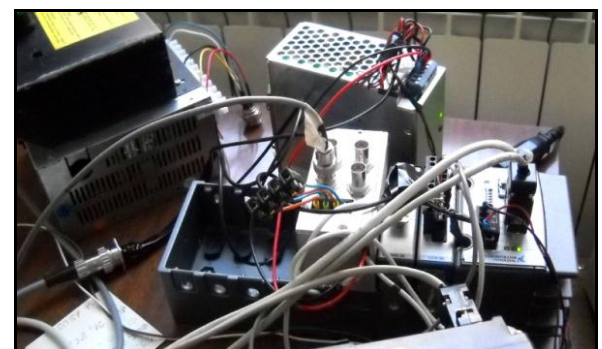


Fig. 2. Signal acquisition system

The role of NI cRIO is to accept analog and digital signals, scan, convert and deliver appropriate data package back to HMI with a strictly defined timing. On the other hand, HMI should receive/display data from PLC and send back input parameters. The measurement performs continually with frequent results refresh rate. The results are arranged in priority descending order. Additional options are accessible through HMI, such as:

- Peak tones of spectrum (FFT)
- Time graph of signal trends

- START UP/COAST DOWN measurements
- Insight balancing [3].

3. SOFTWARE DESCRIPTION

Device software component for vibration monitoring and analysis was developed in LabVIEW graphical environment. The main purpose of the application is data acquisition, data processing and interpretation. Data processing includes digital filtering, order analysis phase tracking, time/frequent domain analysis, ect. The most important achievement in device performance is bidirectional communication between cRIO and touch screen. Full synchronization between Master device (T.S.) and device (cRIO) was crucial for fluent operation, hence data acquisition and data analysis are performed in a strictly determined sequence.*

3.1 Functions and LabVIEW modules

Functions and modules for data management and data analysis can be divided according to the sort of operation:

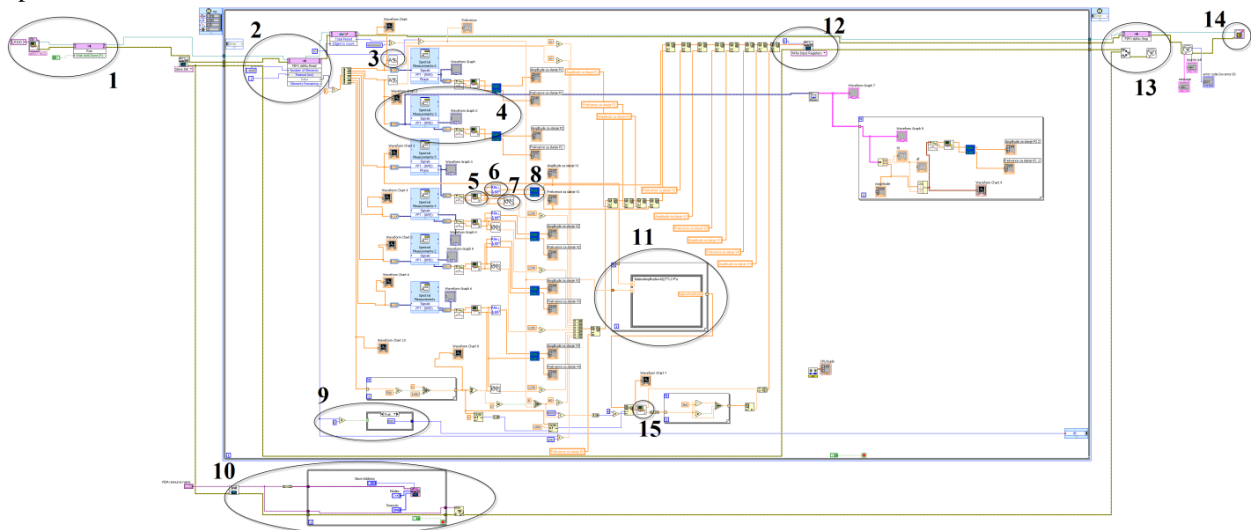


Fig. 3. Block diagram

1. Signal conditioning / process start; 2. Data recall from FPGA level; 3, 4. Signal multi-channeling, data sorting, signal graphical review before/after FFT analysis; 5, 6, 7, 8. Peak tones frequency detection / amplitudes and locations are forwarded to subprograms, for further processing; 9. Code for process quality monitoring; 10. Establishing the connection with touch panel; 11. Calculation of amplitudes; 12. Displaying results on touch panel; 13, 14. Exit FPGA level, errors display, closing the program; 15. Unbalance vector calculus program.

4. VIBRATION MEASUREMENT WITHIN INDUSTRIAL ENVIRONMENT

Experimental testing of the monitoring system was mostly conducted under laboratory conditions on an overhung rotor model. Comparison of the results,

- Numerical/dynamical/string data basic processing
- Program course control
- Hardware/software communication.

The application has hierarchical structure (Fig. 3). User interface is in graphical environment and allows:

- Measurement process control
- Signal parameters defining
- Processed signal display.

NI cRIO controller has built-in real time operating system which is adjusted for the operation under industrial conditions. The controller provides increased durability and reliability at high performance. The device itself combines controller open architecture with industrial I/O modules. Since cRIO controller contains set of FPGA programmable input ports, part of the application is conducted on a hardware level. Due to this feature the wahole system can be used for security purposes.

measured in accordance with ISO 10816 standard, shows high compliance with Micro Mon, or Microlog.

Testing within industrial environment was performed on steam generators turbines (Block 1) at TENT B Obrenovac under following conditions:

Measuring equipment: Micro Mon – Rotech and Microlog CMVA65 – SKF

Measured quantity: vibration acceleration

Derivate quantity: vibration velocity (RMS*)

Principal measuring axis: horizontal H; vertical V; axial A.

Selected measuring points: L₁-L₉ (Fig. 4)

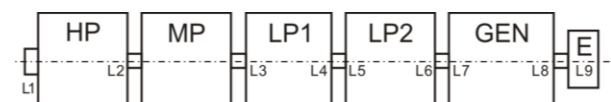


Fig. 4. Measuring points deposition (HP-turbine; MP-turbine; LP_{1,2}-turbine; GEN-generator; E-exciter; L₁-L₉-bearing)

Evaluation of equipment was done according to ISO 10816-2:1996 standard << *Mechanical vibration – Evaluation of machine vibration by measurements on non-rotating parts* » - Large land-based steam turbine generator sets in excess of 50 MW [5], under the “dynamic condition” criteria (Tab. 1)

Quality Zones	Rated speed (RPM)		V _{RMS} (mm/s)
	1500	3000	
A/B	2.8	3.8	3.8
B/C	5.3	7.5	7.5
C/D	8.5	11.8	11.8

Table 1. Operating quality permissible limit according to ISO (A- newly commissioned machines; B- acceptable; C- acceptable for short term operation; D- non acceptable)

Results of vibro severity measurement on block 1 are shown in (Tab. 2,3,4.) (Microlog) and results obtained with Micro Mon (Fig. 7,8.). Outcome of the results comparison apparently shows that developed measuring device Micro Mon meets the appropriate standards.

AXIS	RMS (mm/s)					
	L ₁		L ₂		L ₃	
	V _{RMS}	V _{i/n_i}	V _{RMS}	V _{i/n_i}	V _{RMS}	V _{i/n_i}
H	1,8	1,7(1x)	1,2	0,8(1x)	4,2	4,1(1x)
V	0,7		0,8	0,6(1x)	4,5	4,5(1x)
A	1,0	0,8(1x)	2,7	2,6(1x)	1,6	1,5(1x)

Table 2. Vibration at turbine bearings (Microlog)

AXIS	RMS (mm/s)					
	L ₄		L ₅		L ₆	
	V _{RMS}	V _{i/n_i}	V _{RMS}	V _{i/n_i}	V _{RMS}	V _{i/n_i}
H	3,0	2,9(1x)	3,2	3,1(1x)	5,6	5,6(1x)
V	3,8	3,7(1x)	3,5	3,4(1x)	1,4	1,3(1x)
A	1,4	1,0(1x)	0,5		5,2	5,1(1x)

Table 3. Vibration at turbine bearings (Microlog)

AXIS	RMS (mm/s)					
	L ₇		L ₈		L ₉	
	V _{RMS}	V _{i/n_i}	V _{RMS}	V _{i/n_i}	V _{RMS}	V _{i/n_i}
H	2,7	2,0(1x)	1,0	1,0(1x)	0,6	
V	3,0	2,1(1x)	2,3	1,3(1x)	1,4	0,9(1x)
A	2,0	1,8(1x)	2,7	1,2(1x)	1,1	1,0(2x)

Table 4. Vibration at turbine bearings (Microlog)

Figures 5 and 6 clearly show elevated level of vibration (peak) on L₃, on the basic frequency (50 Hz). Micro Mon results (Fig. 7,8.) confirm that elevated level of vibration exists on H and V axis on a basic frequency (50 Hz). Further construction analysis concluded that the cause of said vibration was a bad alignment of LP turbine axis and MP turbine axis.

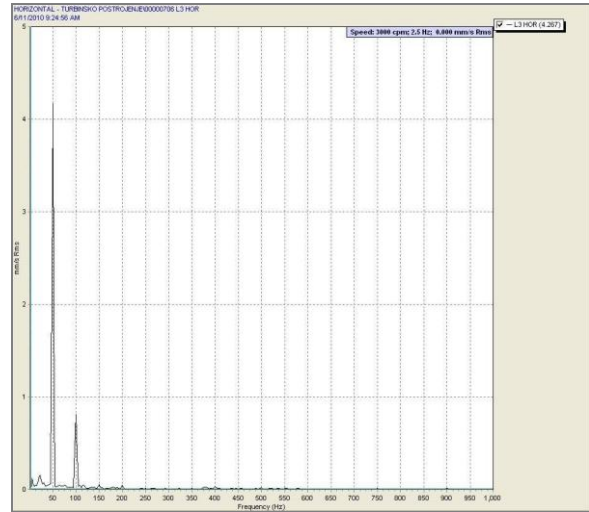


Fig. 5. FFT Spectral analysis (Microlog) (L₃/H)

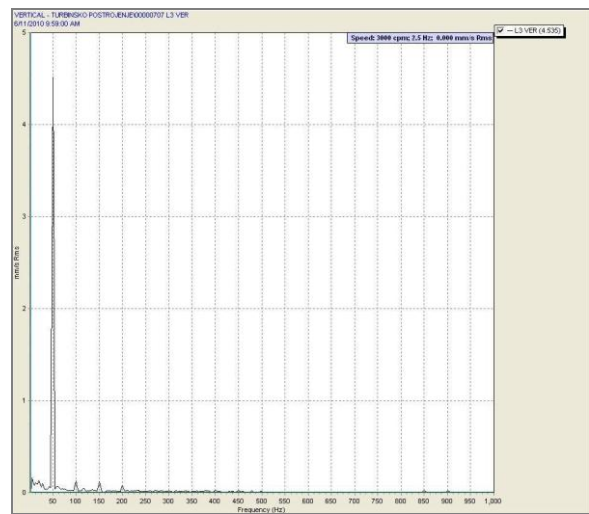


Fig. 6. FFT Spectral analysis (Microlog) (L₃/V)

Report on machine diagnosis Report 1
14.06.2010. 13:15:24

nr.	Tag	Value [mm/s]	FFT data HOR1	
1.	HOR1	3.60	1	f[Hz]
2.	VER1	4.50	1	v[mm/s]
3.			2	50 3.6
4.			3	100 0.8
5.			4	200 0.1
6.			5	373 0.0
7.			6	378 0.0
8.			7	382 0.0
			8	550 0.0

HARD COPY
CLOSE

Fig. 7. Vibration at L₃, H axis

nr.	Tag	Value [mm/s]	FFT data VER1	
1.	HOR1	3.60		
2.	VER1	4.50	1	50 4.5
3.			2	100 0.5
4.			3	167 0.1
5.			4	186 0.1
6.			5	201 0.1
7.			6	251 0.1
8.			7	400 0.0

2	f[Hz]	v[mm/s]
1	50	4.5
2	100	0.5
3	167	0.1
4	186	0.1
5	201	0.1
6	251	0.1
7	400	0.0

HARD COPY

CLOSE

Fig. 8. Vibration at L₃, V axis

Based on the total measurement, the conclusion is that the block 1 vibration level is within the permissible level. On bearings L1, L2, L4, L5, L7, L8, L9 the level of vibration was within the ISO standard recommendation.

On L3 and L6 higher level of vibration was detected. L6 – on H and A axis. Primary cause: bad alignment of LP turbine axis and GEN turbine. Secondary cause: residual vibrations.

5. CONCLUSION

Based on the research exhibited in this paper, laboratory and industrial testing, a “real-time” portable vibro-diagnostic device was developed. Measurement device was verified in the real industrial conditions on turbine block.

Results were in accordance with the results obtained by SKF Microlog CMVA device, and this is an excellent indicator that the developed device is competitive on the market.

6. REFERENCES

- [1] Savić, B.: *Simulation and real vibration measurement and determination of critical system parameters*, Master thesis, Technical Faculty Čačak, 2011.
- [2] Veg, A., Šiniković, G., Miladinović, M., Veg, E., Čolić, K.: *Multichannel processor based data recorder*, Technical innovation No. 197/2, Mechanical Engineering Faculty, University of Belgrade, 2010.
- [3] <http://www.rotech.rs/sr/proizvodi/vibrodiagnostika-i-monitoring/micromon>, mart 2012.
- [4] Vibro-diagnostics report, RoTech, Belgrade, 2010.
- [5] <http://infostore.saiglobal.com/store/Details.aspx?productID=210492>, Mart 2012.

Authors: M.Sc. Biljana Savic, Ph.D. Radomir Slavkovic, M.Sc. Emil Veg, Ph.D. Vlade Urosevic, M.Sc. Hristina Vlajkovic, Higher Education Technical School of Professional Studies, Čačak, Technical Faculty, Čačak, University of Belgrade, Faculty of Mechanical Engineering, Technical Faculty, Čačak, PhD Student, University of Belgrade, Faculty of Mechanical Engineering. Svetog Save 65, 32000 Čačak, Kraljice Marije 16, 11000 Beograd, Serbia, Phone.: +381 32 302-782.

E-mail: biljana.savic@vstss.com
slavkovic@tfc.kg.ac.rs
emilveg@eunet.rs
devlauros@tfc.kg.ac.rs
hristy88@gmail.com

St. Sekulic, S., Nikolic, B.

PROGNOSIS OF RELIABILITY AND MEAN TIME TO FAILURE OF CUTTING TOOL IN FUNCTION OF CUTTING CONDITION OF ELEMENTS IN TURNING

Abstract: *The existing relation between cutting conditions parameters oftenest was based on deterministic approach. As the cutting process is a typical scholastic one, recent literature contains an approach from the probability aspect. In order to establish specific connections and relations, and to analyze cutting tool failures and cutting conditions based on probability approach double-parameter Weibull distribution function was used in this paper.*

Key words: *reliability, distribution function parameters, mean time to failure*

1. INTRODUCTION

In contemporary production circumstances the issue of choosing optimal cutting conditions is a significant task related to the choice of optimal variant of cutting. Developed mathematical models for their calculations require reliable data on cutting abilities. As it is known they can be obtained from the following: 1. Laboratory investigation when strict, controlled conditions referring to the processed item and the tool as well as other conditions are maintained; and 2. Monitoring of tools in production circumstances.

Investigation on the cutting speed – tool life relation in laboratory conditions indicates that for the same conditions during cutting significant tool life dissipation is obtained as a consequence of uneven tribology conditions in cutting. Therefore, preliminary investigations are usually conducted with a larger number of tools during which tools with extreme tool life values are eliminated, while others are systematically tested. From the probability aspect it can be concluded that such a choice of representative tools for the testing of tool life function has no grounds and justification.

By gathering data on tool failures of all kinds in production circumstances, a very massive dissipation can be noticed due to less controlled conditions referring above all to the processed item and the tool but also to other conditions accompanying the process. Besides, in real processing conditions tool failures are not just caused by tribology phenomena in the cutting zone, but by other random disturbances as well.

Accordingly, it is necessary to differ the notion of tool life from operating time without failure in tools, and both notions need more precise definitions, considering that cutting is a typical stochastic process. For instance, for tool life it can be said it is the mean time of effective cutting till blunting defined by a competent wearing criterion occurs, while operating time without failure in production circumstances is the mean time of effective cutting tool failure. Hence, it can be concluded that the mean operating time without failure is shorter than tool life. To make a difference between the two notions is very important, considering the first

refers to tribology characteristics of materials of both the item and the tool, while other conditions are constant, and the second refers to other random disturbances that follow real production circumstances. Depending on the size of series being processed, the number of registered values of tool failures can vary. If the number of registered values is $N > 50$, it is a representative sample, but if $N < 50$, than it is not any more. In both these cases corresponding data processing methodologies should be applied, which enable determining of failure distribution, reliability, frequency and intensity of durability or failure, and mean values of durability or operating time without failure in tools [1, 3, 4, 5].

2. CUTTING TOOL RELIABILITY

The reliability of cutting tool is most commonly defined by means of the following basic characteristics:

- The reliability function (the probability in between time failure),
- The probability distribution function of time failure,
- Frequency of time failure,
- Failure intensity.

According to those given definitions, it is easy to prove, that if one of the four characteristics is known, one can determine the other three characteristics.

If we observe N tools and if we consider $N(t)$ as a number of available tool ready for processing, and $n(t)$ the number of tool in failure after time t , we have all relevant parameters for computing reliability using the following formula

$$R(t) = N(t)/N = (N - n(t))/N \quad (1)$$

The probability of failure is a complement of reliability function

$$F(t) = 1 - p(t) = 1 - N(t)/N = 1 - (N - n(t))/N = n(t)/N \quad (2)$$

The frequency failure is defined as a function as follows

$$f(t) = \Delta n / N \quad (3)$$

where Δn presents the number of tool failures in time interval Δt . We next define failure intensity as

$$\lambda(t) = \Delta n / (N - n(t)) = f(t) / p(t) \quad (4)$$

An additional characteristics is important and the author introduced the term mean time to failure

$$Tm = \frac{\sum_{i=1}^n \Delta n \frac{t_i - t_{i-1}}{2}}{N} = \frac{\sum_{i=1}^n \Delta n t_{im}}{N} \quad (5)$$

where t_{i-1} is a time at beginning, and t_i is a time at the end of i -th interval, and further t_{im} middle time in such time interval.

The most frequent distribution assigned to cutting tool for practical purposes is Weibull distribution in following forms

$$F(t) = 1 - \exp (t/\eta)^\beta \quad (6)$$

determining as follow.

After double logarithming (6) we obtain

$$\ln \ln [1/(1-F(t))] = \beta \ln t - \beta \ln \eta$$

Designing by

$$y = [1/(1-F(t))] \quad (7)$$

and

$$x = \ln t \quad (8)$$

we obtain linear equation

$$y = \beta x - \beta \ln \eta \quad (9)$$

with slope angle β and intercept $b = \beta \ln \eta$

Therefore the determination of Weibull's distribution function parameters can be carried out by the determination of slope angle β and intercept $b = \beta \ln \eta$ in the grid defined by equation (7) (Weibull's probability paper).

Starting from the liner equation

$$y = a x + b \quad (9')$$

and using the least square method gives:

$$(\sum \Delta_i^2)_{min} \quad (10)$$

where Δ_i is the error of the i -th observation. From the condition of minimum, the normal equations are

$$\begin{aligned} \sum(x_i y_i) - a \sum(x_i)^2 - b \sum x_i &= 0 \\ \sum y_i - a \sum x_i - N b &= 0 \end{aligned} \quad (11)$$

and consequently

$$\begin{aligned} A_1 a + B_1 b &= C_1 \\ A_2 a + B_2 b &= C_2 \end{aligned} \quad (11')$$

Where

$$A_1 = \sum(x_i)^2 ; \quad A_2 = \sum x_i = B_1$$

$$B_2 = N ; \quad C_1 = \sum(x_i y_i) ; \quad C_2 = \sum y_i$$

the solutions for the above system are

$$\begin{aligned} a &= \frac{D_a}{D} = \frac{\begin{vmatrix} C_1 & B_1 \\ C_2 & B_2 \end{vmatrix}}{\begin{vmatrix} A_1 & B_1 \\ A_2 & B_2 \end{vmatrix}} = \frac{C_1 B_2 - C_2 B_1}{A_1 B_2 - A_2 B_1} \\ b &= \frac{D_b}{D} = \frac{\begin{vmatrix} A_1 & C_1 \\ A_2 & C_2 \end{vmatrix}}{\begin{vmatrix} A_1 & B_1 \\ A_2 & B_2 \end{vmatrix}} = \frac{A_1 C_2 - A_2 C_1}{A_1 B_2 - A_2 B_1} \end{aligned} \quad (12)$$

The constants A_1, \dots, C_2 can be found in the appropriate tables. The constants a and b are determined by substitution

$$\beta = a$$

and

$$\eta = \exp(b/\beta) \quad (13)$$

The correlation coefficient is

$$r = a(\sigma_x / \sigma_y) \quad (14)$$

where the variance of x-value

$$\sigma_x^2 = (1/N) \sum x_i^2 - \bar{x}^2 = A_1/B_2 - (A_1/B_2)^2 \quad (15)$$

and variance of y-value

$$\sigma_y^2 = (1/N) \sum y_i^2 - \bar{y}^2 = E/B_2 - (C_2/B_2)^2, \quad E = \sum y_i \quad (16)$$

The average of x-values

$$\bar{x} = (1/N) \sum x_i = A_2/B_2 = B_1/B_2 \quad (17)$$

and average of y-values

$$\bar{y} = (1/N) \sum y_i = C_2/B_2 \quad (18)$$

Corresponding substitution for correlation coefficient gives

$$r = \frac{C_1 \cdot B_2 - C_2 \cdot B_1}{A_1 \cdot B_2 - A_2 \cdot B_1} \cdot \left\{ \left[\frac{A_1}{B_2} - \left(\frac{A_2}{B_1} \right)^2 \right] \cdot \left[\frac{E}{B_2} - \left(\frac{C_2}{B_1} \right)^2 \right] \right\}^{\frac{1}{2}} \quad (19)$$

If the correlation coefficient is near one, the correlation between variables is stronger.

The distribution function parameters can be done by pure graphical method. The slope on the line defined coefficient of shape β on scale. The value of the parameter of scale η can be directly determined from the probability paper given in the logarithmic scale, drawing a vertical line in the intersection point of the approximate straight line and median for which is $\ln \ln [1/(1-F(t))] = 0$ which corresponding $F(t) = 0,632$.

When the distribution function of failure is known, the reliability as a complement is

$$R(t) = 1 - F(t) = \exp [-(t/\eta)]^\beta \quad (20)$$

frequency

$$f(t) = dR(t) / dt = \beta \wedge [t/\eta]^{\beta-1} \exp[-(t/\eta)]^\beta \quad (21)$$

density of failures

$$\lambda(t) = f(t) / R(t) = \beta [\eta(t/\eta)]^{\beta-1} \quad (22)$$

The mean time to failures T_m , on the basis of distribution function parameters, via Γ (gamma) functions is

$$T_m = \eta \Gamma(1/\beta + 1) \quad (23)$$

Hypothesis testing can be performed by confidence interval borders using $d\alpha$ - test of Kolmogorov-Smirnov, dependent of size sample N and adopted value of risk α

$$N \leq 50 \Rightarrow d\alpha = 1,388\alpha^{0,120} N^{-0,464} \quad (24)$$

and

$$N > 50 \Rightarrow d\alpha = 1,654\alpha^{0,138} N^{-0,5} \quad (25)$$

In continue, data processing, for all three variants, dependent of sample size, will be presented.

3. EXPERIMENTAL INVESTIGATION

In order to determine changes in failure distribution parameters for cutting tools in turning in real production during different cutting conditions, tools failures were monitored for the following turning operations: exterior, longitudinal, and initial-final, in processing the stubline of "Perkins" engine, while varying 25 different cutting conditions (5 different cutting speeds v and 5 different feeds s , in combination each with each, depth of cut $\delta=0.5\text{mm}$). The material of the item was SL.25 (JUS C J2.020), hardness 98.5-106.5 HRb that is 230-280 HB, centrifugal casting. Over 500 experiments were conducted on the universal lathe made by the Moscow Institute for Tool Machines, type 16K20. As a tool was used the nonstandard cutter with the following cutting geometry: rake angle $\gamma = 5^\circ$, clearance angle $\alpha = 5^\circ$, nous radius $r = 8\text{mm}$, angle of inclination of the cutting edge $\lambda = 4^\circ$.

Table T.1 Estimated values of parameters β and η

		(160)	(200)	(250)	(315)	(400)	
(n, rev/min)		47,226	59,03	73,79	92,98	118,06	
v, m/min		47,226	59,03	73,79	92,98	118,06	
s, mm/rev	0,8	β	3,0	3,1	3,3	2,9	3,65
		η	600	320	158	70	38
	1,0	β	3,28	3,07	2,48	3,2	3,65
		η	290	132	65	31,8	14
	1,2	β	2,72	2,76	2,72	2,75	1,6
		η	170	80	37,5	19	8
	1,4	β	2,91	3,0	3,0	3,02	1,9
		η	118	57	28	12,5	5,5
	1,6	β	3,54	3,2	1,62	2,01	1,4
		η	89	40	17	8	3,5

For every single combination of cutting conditions the repeated failure monitoring was carried out with new tools ($N=20$), which enabled through the graph-analytical data processing to determine parameters of shape β and position η in Weibull double-parameter distribution function [1, 3, 4, 5]:

$$F(t) = 1 - \exp(t/\eta)^\beta \quad (6)$$

Table T.2 Values of mean time to failure T_m for various cutting conditions

		(160)	(200)	(250)	(315)	(400)
(n, rev/min)		47,226	59,03	73,79	92,98	118,06
v, m/min		47,226	59,03	73,79	92,98	118,06
s, mm/rev	0,8	535,8	4,88	141,73	62,44	34,276
	1,0	260,13	3,19	57,655	28,46	12,625
	1,2	151,83	71,21	33,33	16,91	7,168
	1,4	105,26	50,90	25	11,16	4,880
	1,6	80,1	35,8	15,23	7,09	3,190

According which reliability is

$$R(t) = 1 - F(t) = \exp(t/\eta)^\beta \quad (26)$$

And mean operating time without failure

$$T_m = \eta \Gamma(1/\beta + 1) \quad (25)$$

As seen from Tables T.1 and T.2, for each individual cutting condition, values of the shape parameter are

$$2,48 < \beta < 3,65$$

and position parameter values are

$$3,5 < \eta < 600$$

The processing of the experimental data means the determining of the following two pairs of relations:

$$\beta = f_1(v) ; s = const. \quad (27)$$

and

$$\beta = f_2(s) ; v = const. \quad (28)$$

$$\eta = \varphi_1(v) ; s = const. \quad (29)$$

and

$$\eta = \varphi_2(s) ; v = const. \quad (30)$$

The first pair is required in the linear form

$$\beta = a + b v ; s = const. \quad (31)$$

and

$$\beta = c + d s ; v = const. \quad (32)$$

Through data processing the constants are obtained

$$a = 0,3788 + 2,573 s \quad (33)$$

$$b = 0,0463 - 0,0459 s \quad (34)$$

and

$$c = 0,3788 + 0,0465 v \quad (35)$$

$$d = 2,573 - 0,0459 v \quad (36)$$

Through the analogue procedure the values of constants c and d were obtained. By substitutions of constants a and b , in first, and c and d , in second, previously terms, the identical equation for shape parameter as expected.

$$\beta = -0.0459 s v + 0.0465 v + 2.573 s + 0.3788 \quad (37)$$

The second pair of relations was found in the exponential form, too.

And further the relation for the parameter of shape

$$\eta = C v^x ; \quad s = const. \quad (38)$$

and

$$\eta = D s^y ; \quad v = const. \quad (39)$$

Constant C changes in waves so it is not convenient for further processing, and D is looked for in the exponential form, while exponent y is represented by the linear relation:

$$D = 80.866 \cdot 106 v^{-3.2407} \quad (40)$$

$$y = -2.683 - 0.0094 v \quad (41)$$

Hence, the position parameter is

$$\eta = 80.866 \cdot 10^6 v^{-3.2407} s^{-2.683 - 0.0094v} \quad (42)$$

Through analogy it is obtained, when $D = f_1(s)$ for $v = const.$, and $y = f_2(s)$ for $v = const.$

$$\eta = 78.289 \cdot 10^6 s^{-0.565} v^{-0.498 s - 2.7} \quad (43)$$

By comparing the derived expressions, based on probability, we can say that they point to the complexity and delicacy of data usage by solving determining problems, when the introduction of the reliability as the element provides greater safety.

Substituting values of distribution function parameters (37), (42) or (43) in equations (20) and (23) we have

$$R(t) = 1 - F(t) = \exp[-(t/\eta)]^\beta \quad (20)$$

and mean time to failure

$$T_m = \eta \Gamma(1/\beta + 1) \quad (23)$$

numerical values for $R_{(t)}$ and T_m can be determined in function of time

4. CONCLUSION

On the basis of what has been stated earlier, the following can be concluded:

- by studying a set of diagrams for parameters of shape β the second order function can be used,
- for position parameter η , two equal equations in exponential form can be used,
- numerical values for reliability and mean time to failure, for previously adopted cutting conditions, can be prognosed, and
- derived relations can be useful in solving various practical turning operations.

5. REFERENCES

- [1] Sekulic, S., *Statistical Formulation of a Cutting Tool Reliability in a Working Conditions*, Reports of the 21st Conference of the European Organization for Quality Control - EOQC, Varna, 1977.
- [2] Sekulic, S., *Methodologies for Determination of Cutting-tool Reliability*, Drugie miedzynarodowe simpozium NAR@EDZIA 84, Krakow - Janovice – Tarno, Poland, 1984.
- [3] Sekulic, S., *Determination of Cutting-tool Reliability on Flexible Automatic Flow Lines*, Toward the Factory of the Future, Proceedings of the 8th International Conference on Production Research ICPR 85, Stutgard, 1985, Springer-Verlag, Berlin-Heidelberg-NewYork-Tokyo, 1985.
- [4] Sekulić, S., Nikolić, B., *Influence of Cutting Tool Condition Elements on Cutting Reliability Function Parameters in Turning*, Summaries 5, Stream 6+8, 16th International Conference on Production Research ICPR – 16, July 2001, Prague,
- [5] Sekulic, S., Nikolic, B., *Depedence Reliability Function Parameters of Cutting Tools Away Cutting Conditions in Turning*, Proceedings of the International Scientific Conference UNITECH 08, Sept. 2008., Garbovo, 2008., II-239 - II-2

Authors: Prof. Dr Sava St. Sekulić, University of Novi Sad, Faculty of Technical Sciences, Department of Industrial Engineering nad Management, Trg Dositeja Obradovica 6, 21000 Novi Sad, Serbia, Phone: +381 21 485-2153, Fax: +381 21 485-2184.

E-mail: laza@iis.ns.ac.rs

Dr Božo Nikolić, High Technical Professional School in Novi Sad, Skolska 1, 21000 Novi sad, Phone: +381 21 4892 500, Fax: +381 21 4892 515.

E-mail: skola@vtsns.edu.rs

Šešlija, D., Dudić, S., Milenković, I.

COST EFFECTIVENESS T OF PRESSURE REGULATION ON RETURN STROKE OF PNEUMATIC ACTUATORS

Abstract: *Decreasing working pressure leads to overall energy consumption. In this paper, the focus will be on the pressure reduction at the point of use, particularly on the double acting cylinder in retracting stroke without load with pressure reduction. Three cases were examined. For each special case, certain pneumatic equipment was added in the pneumatic circuit.*

Key words: *cost effectiveness, pneumatic, cylinder, pressure regulation*

1. INTRODUCTION

Good quality and reliability of operation of compressed air systems are accomplished with good system management [1], [2]. There are significant issues that influence the overall increase in energy efficiency of the compressed air systems, which are explained in greater detail in [3], [4].

The following technical measures have been identified that can improve the functioning of the entire process chain of a compressed air system [4]:

- improvement of compressed air preparation: reduction of pressure and energy lost in processes of drying and filtering; optimization of filtering and drying as a function of consumer needs [5],
- overall system design, including the systems with multiple pressure levels,
- reduction of pressure losses due to friction in the pipelines and tubes,
- air leakage reduction, [6]
- reduction of operation pressure [3],
- optimization of certain devices that consume compressed air: application of more efficient, better adjusted devices or, in some cases, replacement of compressed air with an electrical drive,
- recycling of used compressed air [7], [8], [9], etc.

Judging by the findings of numerous studies, the measures stated can increase energy efficiency of the pneumatic systems and all of them can be returned (with the most frequent period for ROI of less than 3 years) [3].

In this paper, we will focus on the pressure reduction at the point of use, particularly on the two cylinders, with different diameters and strokes.

1.1 Reduction of operating pressure

It is reasonable to operate compressed air systems at the lowest functional pressure that meets production requirements [3]. Higher pressures increase leakage, and thereby the energy. In many compressed air systems, increase of operating pressure is used to compensate for the lack of capacity due to leakage. However, higher the pressure, higher the leakage, while

the unregulated consumers use more compressed air, and thus more energy. Applications requiring compressed air should be checked for any excessive pressure and any duration longer than necessary. They should be regulated, either by production line sectioning or by pressure regulators on the equipment itself [10]. Tools that do not require operating at system pressure should use a lower pressure delivered by some way of pressure reduction. Case studies show an average payback period for reducing pressure to the minimum required for compressed air applications of about 3 months [3].

Each one *bar* of the pressure increase is followed by an increase in electrical energy consumption required to compress the air in a range between 5% and 8% or, the standard rule of thumb is that reducing pressure settings by 13 kPa will reduce energy consumption by 1% [10, 11].

2. PRESSURE REDUCTION IN RETRACTING STROKE WITHOUT LOAD

Decreasing the supply pressure in retracting stroke enables decreasing of compressed air consumption, but only in cases if retracting stroke is not under load. Pressure reduction in stroke without load is possible to achieve on different ways. In this paper, three possible cases are analysed:

- with pressure regulator and non return valve in by pass line (Fig. 1a),
- with pressure regulator and quick exhaust valve (Fig. 1b) and
- with reversible control valve and pressure regulator (Fig. 1c).

Pressure reduction should not be high because it can cause significant decreasing of force and the speed of piston movement.

In this paper is encompassed measurement of compressed air consumption of double acting cylinder FESTO DSNU-20-50 in retracting stroke without load with pressure reduction. Three cases were examined. For each special case certain pneumatic equipment was added in the pneumatic circuit.

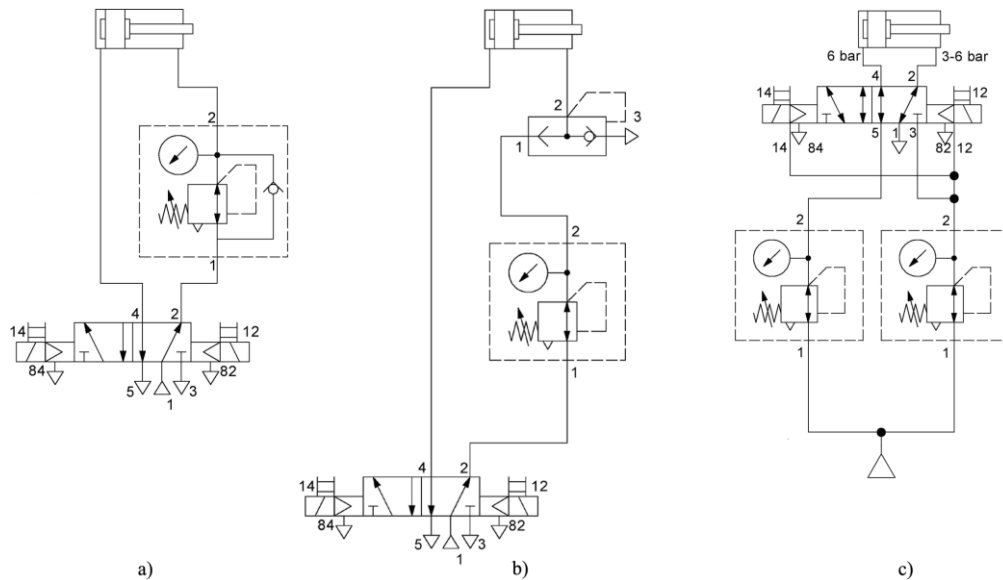


Fig. 1. Pneumatic circuits a) with pressure regulator and non return valve in by pass line, b) with pressure regulator and quick exhaust valve, c) with reversible control valve and pressure regulator

3. EXPERIMENTAL RESULTS

3.1 Case I

First experiment encompassed determination of compressed air consumption in retracting stroke of cylinder, without any load. Pressure regulator FESTO LRMA was used for decreasing the pressure for piston rod chamber of cylinder. Measurement included compressed air consumption for 100 working cycles and different pressure levels. At the beginning pressure levels was 6 bar. Then pressure was reduced by 1 bar, up to the value of 3 bar. Monostable, electrically actuated valve was used for cylinder control. Pneumatic circuit with pressure regulator is shown in Fig. 1a.

Obtained results are presented in Table 1.

DSNU-20-50 LRMA	100 working cycles		
	compressed air consumption Q [l]	savings [%]	
		relative to previous pressure level	cumulative comparing to 6 bar pressure
6 bar	26.93	0	0
5 bar	22.57	4.0	4.0
4 bar	19.17	7.2	10.9
3 bar	16.10	6.8	17.1

Table 1. Compressed air consumption for different pressure levels in retracting stroke without load, with pressure regulator (LRMA)

3.2 Case II

In the second experiment, the pressure in the retracting stroke of the cylinder was decreased using pressure regulator FESTO LR. Quick exhaust valve FESTO SEU is positioned after the pressure regulator. Measurement included compressed air consumption for 100 working cycles and different pressure levels. At the beginning pressure levels was 6 bar. Then pressure was reduced by 1 bar, up to the value of 3 bar. Monostable, electrically actuated valve was used for cylinder control. Pneumatic circuit with pressure regulator and quick exhaust valve is presented in Fig 1b.

Obtained results are presented in Table 2.

DSNU-20-50 LR/SEU	100 working cycles		
	compressed air consumption Q [l]	savings [%]	
		relative to previous pressure level	cumulative comparing to 6 bar pressure
6 bar	26.93	0	0
5 bar	22.57	3.4	3.4
4 bar	19.17	7.5	10.7
3 bar	16.10	4.6	14.9

Table 2. Compressed air consumption for different pressure levels in retracting stroke without load, with pressure regulator and quick exhaust valve (LR+SEU)

3.3 Case III

In the third case, bistable, reversible valve FESTO JMFH-5-1/8-S-B was used for cylinder control and the pressure regulator FESTO LR was used for decreasing the pressure. Measurement included compressed air consumption for 100 working cycles and different pressure levels. At the beginning pressure levels was 6 bar. Then pressure was reduced by 1 bar, up to the value of 3 bar. Pneumatic circuit with reversible control valve and pressure regulator is presented in Fig. 1c.

Obtained results are presented in Table 3.

DSNU-20-50 LR+JMFH	100 working cycles		
	compressed air consumption Q [l]	savings [%]	
		relative to previous pressure level	cumulative comparing to 6 bar pressure
6 bar	26.93	0	0
5 bar	22.57	3.8	3.4
4 bar	19.17	7.2	10.7
3 bar	16.10	11.8	21.4

Table 3. Compressed air consumption for different pressure levels in retracting stroke without load, with pressure regulator and reversible valve (LR+JMFH)

4. COST EFFECTIVENESS OF PRESSURE REDUCTION IN RETRACTING STROKE WITHOUT LOAD

According to the obtained results and compressed air savings as a function of pressure level on the pneumatic cylinder, presented in [12], the following results can be proposed.

Cost effectiveness of previously described pressure reduction in retracting stroke without load for three different cases are presented in Table 4.

On the contrary, installation of devices: 1) pressure regulator LRMA; 2) quick exhaust valve SEU and 3)

pressure regulator LR and reversible valve JMFH-5-1/8-S-B, on the retracting stroke without load, for reduction in compressed air consumption is economical for the cylinders with large diameter and stroke, because the return of investment is very short, Table 5.

Based on the previous analysis we can conclude that installation of devices: 1) pressure regulator LRMA; 2) quick exhaust valve SEU and 3) pressure regulator LR and reversible valve JMFH-5-1/8-S-B, on the retracting stroke without load, for pressure reduction in compressed air consumption is not economical for the cylinders with small diameter and stroke.

	LRMA	LR + SEU	LR + JMFH
price of 1 m ³ of compressed air	0.02 €		
compressed air consumption per cycle for supply pressure of 6 bar	0.29 l/cycle	0.26 l/cycle	0.24 l/cycle
compressed air consumption per cycle for supply pressure of 2 bar	0.22 l/cycle	0.22 l/cycle	0.18 l/cycle
number of working cycles per minute	6 cycle/min		
effective capacity per annum	180,000 min/year		
number of cycles per year	1,080,000 cycle/year		
compressed air consumption per annum for supply pressure of 6 bar	313.20 m ³ /year	280.80 m ³ /year	259.20 m ³ /year
compressed air consumption per annum for supply pressure of 2 bar	237.60 m ³ /year	237.60 m ³ /year	194.40 m ³ /year
difference in compressed air consumption per annum for 2 and 6 bar pressure	75.60 m ³ /year	43.20 m ³ /year	64.8 m ³ /year
the price of saved compressed air per annum	1.51€/year	0.86€/year	1.29 €/year
the price of pressure regulator LR	35€	68€	40€
return on investment	23.17 years	79.06 years	31.00 years

Table 4. Cost effectiveness of pressure reduction in retracting stroke without load with different devices for cylinder DSNU-20-50

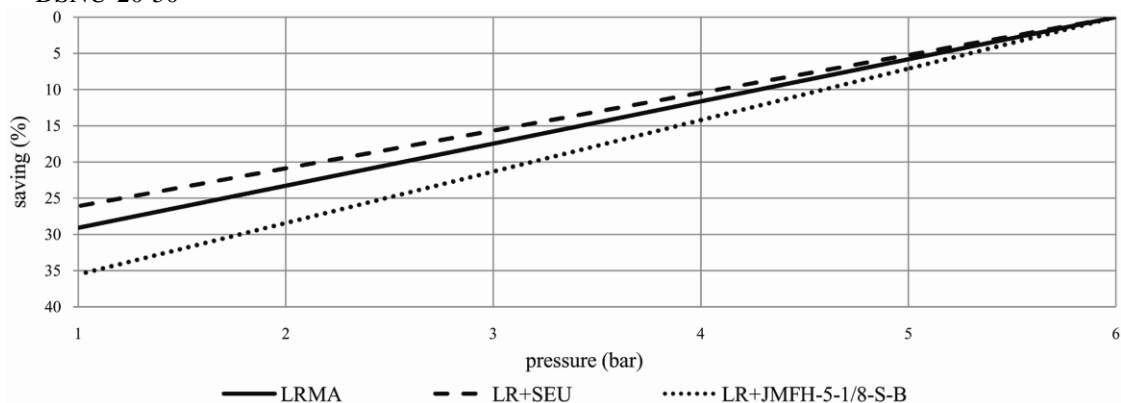


Fig. 2. Savings of compressed air consumption as a function of different pressure level in retracting stroke without load, with different devices

	LRMA	LR + SEU	LR + JMFH
price of 1 m ³ of compressed air	0.02 €		
compressed air consumption for supply pressure of 6 bar per cycle	125 l/cycle	125 l/cycle	125 l/cycle
percents of savings by decreasing pressure in retracting stroke for supply pressure of 2 bar	23 %	21 %	28 %
compressed air consumption per cycle for supply pressure of 2 bar	96,25 l/cycle	98,75 l/cycle	90 l/cycle
number of working cycles per minute	6 cycle/min		
effective capacity per annum	180,000 min/year		
number of cycles per year	1,080,000 cycle/year		
compressed air consumption with retracting stroke per annum for supply pressure of 6 bar	135,000.00 m ³ /year	135,000.00 m ³ /year	135,000.00 m ³ /year
compressed air consumption with retracting stroke per annum for supply pressure of 2 bar	103,950.00 m ³ /year	106,650.00 m ³ /year	97,200.00 m ³ /year
difference in compressed air consumption per annum for 2 and 6 bar pressure	31,050.00 m ³ /year	28,350.00 m ³ /year	37,800.00 m ³ /year
the price of saved compressed air per annum	621 €	567 €	756 €
the price of pressure regulator LR	52.5 €	144 €	63 €
return on investment	30.8 days	92 days	30.4 days

Table 5. Cost effectiveness of pressure reduction in retracting stroke without load with different devices for cylinder DSNU-125-100

5. FINAL REMARKS

Decreasing of working pressure is one of the most effective methods for decreasing compressed air consumption and increasing energy efficiency of entire compressed air systems. However, it should be very careful with decreasing supply pressure, because too low pressure can disable the proper functioning and the aim of the system and process. Decreasing supply pressure on pneumatic cylinder is possible only if the chosen cylinder is bigger than needed.

Based on the measurements of compressed air consumption and cost effectiveness analysis presented in this paper, it could be concluded that decreasing supply pressure in retracting stroke of the cylinder without load is not so profitable for cylinders with small diameter and stroke, but for cylinders with big diameters and/or strokes, the return on investment period is very short.

6. REFERENCES

- [1] Radgen, P., Blaustein, E., *Compressed air systems in the European Union, energy, emissions, saving potentials and policy actions*, Stuttgart, Germany, LOG-X Verlag GmbH, 2001.
- [2] Šešlija, D., Ignjatović, I., Dudić, S., Lagod, B., *Potential energy savings in compressed air systems in Serbia*, African Journal of Business Management, vol. 5, no. 14, pp 5637-5645, July 2011.
- [3] Saidur, R., Rahim, N.A., Hasanuzzaman, M., *A review on compressed air energy use and energy savings*, Renewable and Sustainable Energy Reviews, vol. 14, no. 4, pp. 1135-1153, May 2010.
- [4] Šešlija, D., Stojiljković, M., Golubović, Z., Blagojević, V., Dudić, S., *Identification of possibilities for the increase of energy efficiency in compressed air systems*, Facta universitatis - series Mechanical Engineering, vol. 7, no. 1, pp. 37-60, 2009.
- [5] Ignjatović, I., Šešlija, D., Tarjan, L., Dudić, S., *Wireless sensor system for monitoring of compressed air filters*, Journal of Scientific and Industrial Research, vol. 71, no. 2, pp. 334-340, May 2012.
- [6] Dudić, S., Ignjatović, I., Šešlija, D., Blagojević, V., Stojiljković, M., *Leakage quantification of compressed air using ultrasound and infrared thermography*, Measurement, vol. 45, no. 7, pp. 1689–1694, August 2012.
- [7] Blagojević, V., Šešlija, D., Stojiljković, M., *Cost effectiveness of restoring energy in execution part of pneumatic system*, Journal of Scientific and Industrial Research, vol. 70, no. 2, pp. 170-176, February 2011.
- [8] Blagojević, V., Šešlija, D., Stojiljković, M., Dudić, S., *Efficient control of servo pneumatic actuator system utilizing by-pass valve and digital sliding mode*, SADHANA - Academy Proceedings in Engineering Science (Article in Press).
- [9] Čajetinac, S., Šešlija, D., Aleksandrov, S., Todorović, M., *PWM Control and Identification of Frequency Characteristics of a Pneumatic Actuator using PLC Controller*, Electronics and Electrical Engineering, vol. 7, no. 123, September 2012.
- [10] D'Antonio, M., Epstein, G., Moray, S., Schmidt, C., *Compressed air load reduction approaches and innovations*, Proceedings of Industrial Energy Technology Conference; New Orleans, LA, Energy Systems Laboratory, Texas A&M University, 2005.
- [11] Galitsky, C., Worrell, E., *Energy efficiency improvement and cost saving opportunities for the vehicle assembly industry*, Ernest Orlando Lawrence Berkeley National Laboratory, [LBNL-50939-Revision], 2008.
- [12] Dudić, S., Šešlija, D., Milenković, I., *Impact of pressure regulation of pneumatic actuators on cost effectiveness*, (Submitted to XI International SAUM Conference on Systems, Automatic Control and Measurements Niš, Serbia, November 14th-16th, 2012).

Authors: Prof. Dr Dragan Šešlija, Ass. PhD Slobodan Dudić, Ass. MSc Ivana Milenković, University of Novi Sad, Faculty of Technical Sciences, Mechatronics, robotics and automatization, Trg Dositeja Obradovica 6, 21000 Novi Sad, Serbia, Phone.: +381 21 450-366, Fax: +381 21 454-495.
E-mail: seslija@uns.ac.rs
slobodan_dudic@yahoo.com
ivanai@uns.ac.rs

Tomov, M., Kuzinovski, M., Cichosz, P.

INVESTIGATION OF GAUSSIAN AND 2RC FILTRATION IN SURFACE ROUGHNESS MEASUREMENT FROM THE STANDPOINT OF AMBIGUITIES IN STANDARDS. PART II - EXPERIMENTAL ANALYSIS

Abstract: Disadvantages and limitations of Gaussian filter are analyzed as well as possible effects upon determining roughness profile on periodic and non-periodic etalon surfaces. Mean lines and roughness profiles from real etalon surfaces are determined by applying software Matlab (R2009b). Differences between roughness profile obtained by using Gaussian filter and roughness profile obtained by using 2RC filter are indicated for reviewed real surfaces. New techniques for filtering are noted in the field of surface metrology, developed for overcoming limitations that outcome from usage of Gaussian and 2RC filters.

Key words: Software filtration, Profile filter, Gaussian filter, 2RC filter, Etalon surface

1. INTRODUCTION

In literature [1,2,3], analysis is mostly performed on filtration and effects of disadvantages and limitations of Gaussian and 2RC filter for primary profiles with forms presented in Fig. 3 and 5 from Part I. It is obvious that waviness and form have high participation in the configuration of primary profiles presented on Fig. 3 and 5 (from Part I). It is clear that for such profile forms disadvantages and limitations of Gaussian and 2RC filter will be strongly expressed and changes from them upon roughness profile visually evident.

A need is enforced for determining these effects on primary profiles obtained by measuring real surfaces where waviness and form are not expressed in high extent. The justification for determining these effects comes also from the fact that against ISO 3274:1996 [4] when using contact (stylus) profilometers, which have a pick-up with skid, only roughness profile and partially waviness could be obtained because the skid has already done mechanical filtration with which waviness and form are rejected from measured profile. This means that profiles with forms presented in Fig. 3 and 5 (from Part I) cannot be obtained when applying contact profilometers with skid.

2. DETERMINING FILTER MEAN LINES AND ROUGHNESS PROFILES BY APPLYING MATLAB (R2009B)

For realization of this research real etalon periodic and non-periodic surfaces were measured. Measurements were performed on these surfaces using stylus profilometer Surtronic 3+, while as coordinates of points, with which primary profiles are described, are obtained by means of software TalyProfile, Version 3.1.4. The vertical resolution of stylus profilometer Surtronic 3+ is 10 nm, while as the horizontal resolution is 0,5 or 1 μm depending of evaluation lengths. A pick-up TYPE 112-2672 (DCN 001) with stylus radius of 2 μm and skid radius of 8.7 mm was used.

Software TalyProfile is professional commercial software of closed type where user does not have possibility for detection, correction or reviews of equations against which calculations are done. Recommendations of ISO standards are implemented in it, against which when applying Gaussian and 2RC filter, roughness profile is shorter in length for λ_c i.e. $2\lambda_c$ in terms of primary profile. Therefore it is not possible to use it for determining roughness or waviness profile, which will have length equal to primary profile. Other limitation comes from the point that TalyProfile is not able to provide a view of filter mean lines obtained by applying profile filters but only of waviness profile, which is not the same. Significant disadvantage of TalyProfile could be also considered that when calculating roughness parameters an automatic filtration is performed by means of Gaussian filter without taking into account whether measured profile is obtained with a profilometer with or without a skid.

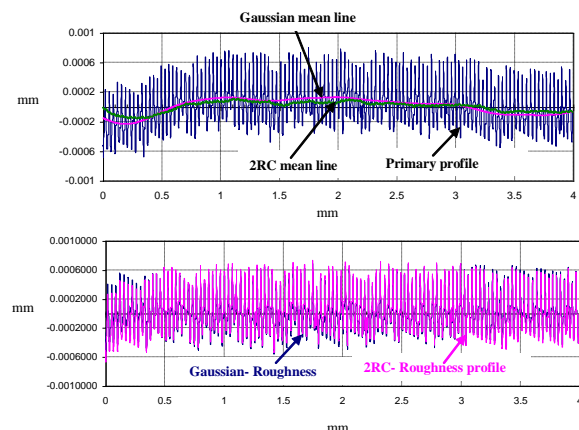


Fig. 1. Primary profile, filter mean lines and roughness profiles obtained from periodic surface - machining with turning, with $R_a=0.2 \mu\text{m}$

Simulation of filtration process by means of Gaussian and 2RC profile filters and obtaining filter mean lines and roughness profile in these researches is done by applying software package Matlab (R2009b). Equations (1) and (3) (from Part I) for weighting functions of Gaussian and 2RC filters are used for obtaining filter mean lines. Primary profiles, filter mean lines and roughness profiles obtained from periodic and non-periodic real etalon surface are presented further below.

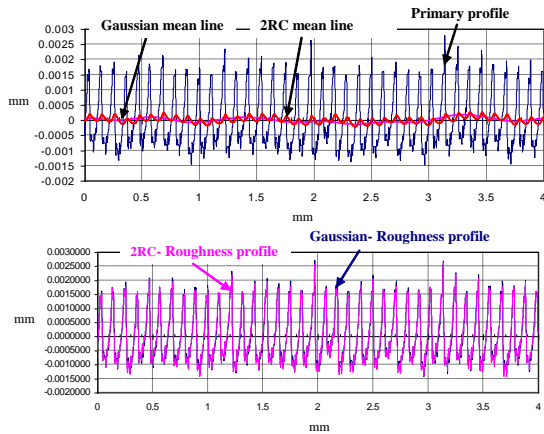


Fig. 2. Primary profile, filter mean lines and roughness profiles obtained from periodic surface - machining with turning, with $Ra=0.8 \mu\text{m}$

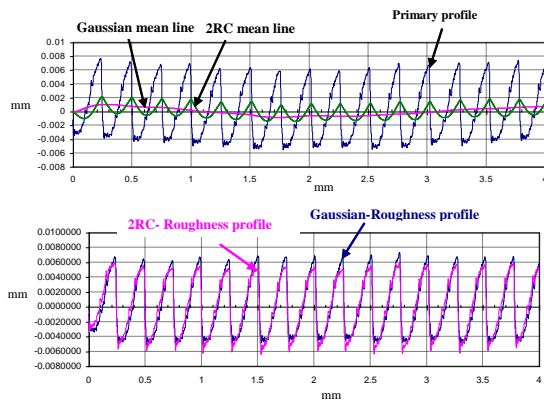


Fig. 3. Primary profile, filter mean lines and roughness profiles obtained from periodic surface - machining with turning, with $Ra=3.2 \mu\text{m}$

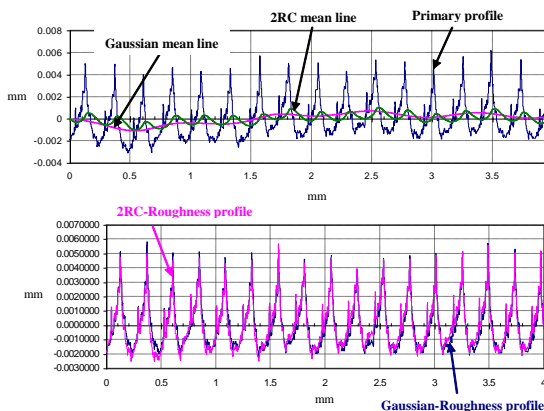


Fig. 4. Primary profile, filter mean lines and roughness profiles obtained from periodic surface - machining with milling, with $Ra=1.6 \mu\text{m}$

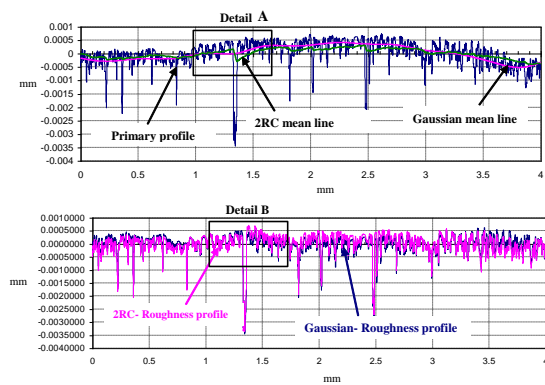


Fig. 5. Primary profile, filter mean lines and roughness profiles obtained from non-periodic surface - machining with grinding, with $Ra=0.2 \mu\text{m}$

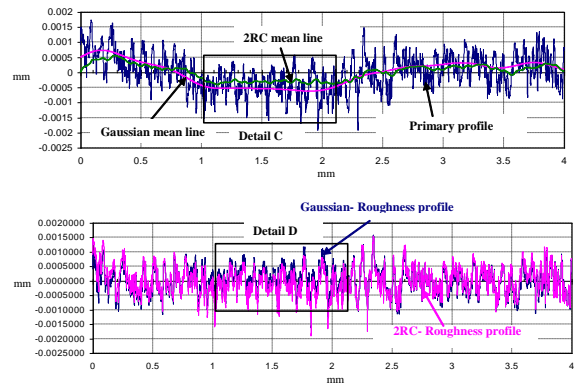


Fig. 6. Primary profile, filter mean lines and roughness profiles obtained from non-periodic surface - machining with grinding, with $Ra=0.4 \mu\text{m}$

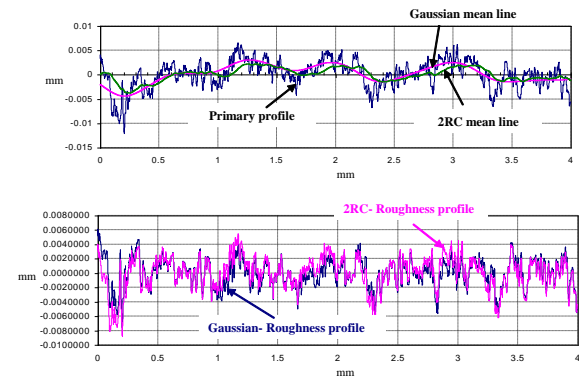


Fig. 7. Primary profile, filter mean lines and roughness profiles obtained from non-periodic surface - machining with grinding, with $Ra=1.6 \mu\text{m}$

3. ANALYSIS OF EFFECTS OF PROFILE FILTERS' CHARACTERISTICS UPON OBTAINED ROUGHNESS PROFILES

For the purpose of obtaining profiles with various forms and characteristics, many etalon surface representatives of one same machining with various Ra are included in the analysis. In Fig. 1, 2 and 3 primary profiles, filter mean lines determined with Gaussian and 2RC profile filter and roughness profiles for periodic surfaces, representatives of machining with turning with various values of Ra are presented.

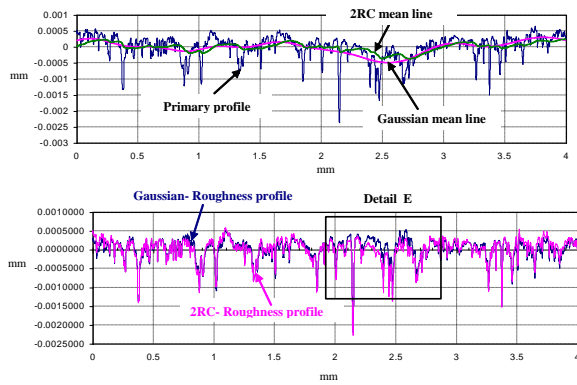


Fig. 8. Primary profile, filter mean lines and roughness profiles obtained from non-periodic surface - machining with lapping, with $R_a=0.2 \mu\text{m}$

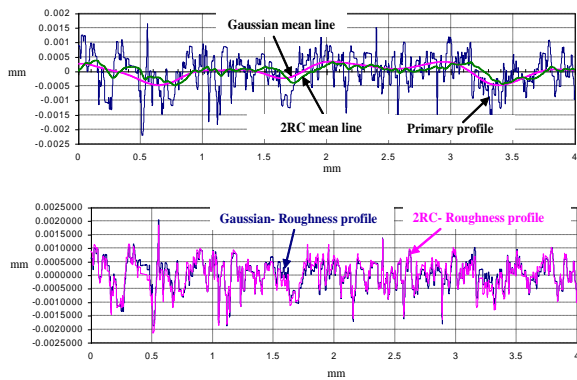


Fig. 9. Primary profile, filter mean lines and roughness profiles obtained from non-periodic surface - machining with lapping, with $R_a=0.4 \mu\text{m}$.

For obtaining filter mean line with lengths equal to the measured profile, the measured profile is extended to a length of λ_c ($2\lambda_c$) in two (one) sides of profile with zero values against z axis, according to one of recommendation in ISO/TS 16610-28:2010 [5].

It could be seen from the form of obtained filter mean lines that filter mean line obtained with 2RC filter is more sensitive on valleys and peaks than the mean line obtained with Gaussian profile filter. This is more expressed by increase of R_a value i.e. by reduction of the number of valleys and peaks within same profile length. Same conclusion could be reached for the phase distortion of filter mean line determined with the 2RC profile filter. It could be clearly seen on Fig. 3 that mean line determined with 2RC profile filter has phase distortion in terms of primary profile. In Part I of this paper was concluded that the mutual disadvantage of filter mean lines obtained by Gaussian and 2RC profile filters is distortion of profile ends. It can be concluded from Fig. 1, 2 and 3 that this occurrence is mostly expressed in cases when waviness participates in primary profile, Fig. 1. On profiles on Fig. 2 and 3 profile ends are not distorted and in such cases profile shortening in terms of primary profile is not necessary. The comparison of roughness profiles obtained by usage of Gaussian and 2RC profile filters clearly indicates that large coinciding of profile forms exists. Largest deviation is noticed on Fig. 3 where the effect of phase distortion of 2RC profile filter starts to

be prominent. This phase distortion is continuous against whole profile length since a periodic profile is in question. A height distortion of one roughness profile in terms of other could be also noticed on the same figure. The reason for such occurrence is higher sensitivity of 2RC profile filter on valleys and peaks in terms of Gaussian profile filter. Such condition of height distortion can mostly affect the position of profile mean line out of which roughness parameters are expressed, while as largest changes on parameters can be expected on R_p , R_v and RS_m .

Profile presented in Fig. 4 is obtained with real etalon surface representative of machining with milling. It has periodic characteristic against whole length with expressed high peaks and rounded valleys. Since waviness is not present in primary profile, effects of distortions on ends of filter mean lines obtained with Gaussian and 2RC profile filters are completely excluded. Phase distortion and high sensitivity of 2RC filter on valleys and peaks has highest effect, which can be seen from the mutual comparison of roughness profiles in Fig. 4.

Non-periodic primary profiles obtained by measuring real etalon surfaces-representatives of machining with grinding with various values of R_a are presented in Fig. 5, 6 and 7. The fact that the form of these profiles is non-periodic against whole profile length permits to see and conclude that the disadvantages of Gaussian and 2RC profile filters will be differently expressed against profile length. Primary profile in Fig. 5 characterizes with small presence of waviness and expressed individual valleys.

Due to waviness absence and the position at start and end of primary profile around zero value per z-axis, distortions of filter mean lines at profile ends will not have much effect therefore shortening of roughness profile in terms of primary profile is not of significant importance. Here, the high sensitivity of 2RC profile filter on individual valleys of primary profile, detail A, Fig. 5, has to be underlined, which results in pulled down of filter mean line from mean part of primary profile towards the valley. This pulled down of mean line later on causes the distortion of roughness profile in valley proximity and creation of artificial features of roughness profile, detail B, Fig. 5. It can be seen on same Fig. that distortion in valley proximity is going to occur also when using Gaussian profile filter, however will be smaller because filter mean line does not have phase dislocation in terms of primary profile i.e. valley. Comparison of roughness profiles obtained by using Gaussian and 2RC profile filters indicates that there are segments of profiles wherein they overlap and segments wherein they significantly differ. Roughness profile obtained by Gaussian profile filter is already "smooth" in terms of zero value per z-axis. Differences of profile forms in some segments contribute to various location of the mean line with which roughness parameters are determined.

Presence of waviness and distortion of primary profile start in terms of zero value per z-axis can be noticed on the profile in Fig. 6. Therefore, distortions of filter mean lines at profile start will be expressed, especially the 2RC filter mean line. In this case,

removing part of roughness profile start is fully justified. Phase distortion of 2RC filter mean line in this case does not have significant effect. Highest discrepancy of roughness profiles is in Detail D as a result of height distortion of 2RC filter mean line in terms of Gaussian one, Detail C. This distortion is a result of the form of the weighting function, symmetrical at Gaussian and non-symmetrical at 2RC profile filter. Expressed waviness per whole length of primary profile is present on profile presented in Fig. 7. In such case the effect of Gaussian and 2RC profile filters' disadvantages is obvious. Distortion on 2RC filter mean line start is extremely expressed. Still, the phase distortion of 2RC filter mean line has crucial role in the discrepancy of roughness profiles against their whole length. Here it can be also noted that roughness profile obtained with Gaussian profile filter is more "smooth" in terms of zero value per z-axis.

Roughness profiles, representatives of machining with lapping, are characterized with deep valleys, Fig. 8 and 9. For such primary profile forms, sensitivity of filter mean lines of Gaussian and 2RC filters on deep valleys and phase distortion of 2RC mean line are main disadvantages that contribute to creation of artificial features of roughness profile, excessively expressed on detail E, Fig. 8.

Disadvantages of Gaussian and 2RC profile filters and their unwanted effects upon roughness profile, analyzed in upper examples, contribute to search for alternative solutions and filtering techniques in surface metrology. So against [1,2] new profile filters are developed: Zero order Gaussian regression filter, Second order Gaussian regression filter, Robust Gaussian regression filter, Spline filter, Robust spline (draft international Standard) filter, Rk (Gaussian) filter, Rk (Spline) filter, Morphological, scale-space filter and Wavelets filter.

Actuality of the software filtration process in surface metrology is confirmed by activities undertaken by the ISO (International Organization for Standardization). So, the members of this technical committee have issued a number of technical specification (ISO/TS) that are directly related to the filtration process. This includes all parts of the series of ISO/TS 16610.

3.1. Filtration according to ISO 13565-1:1996

Presence of deep individual valleys on non-periodic profile, presented in Fig. 5, provides application of filtration process according to ISO 13565-1:1996 [6]. Primary profile with cut valleys below mean filter line is shown in Fig. 10. Fig. 11 clearly indicates that difference exists between filter mean line determined with Gaussian filter and filter mean line determined according to ISO 13565-1:1996.

Therefore, roughness profiles determined with Gaussian filter i.e. against ISO 13565-1:1996 differ significantly, Fig. 12. Largest differences between roughnesses of profiles will occur around deep valleys, details F, Fig. 12. Filtration process according to ISO 13565-1:1996 provides obtaining of "smoothened" roughness profiles in terms of zero value per z-axis.

Since roughness profiles, which do not coincide per

their whole length, are in question, it can be concluded that there are two fully new and various profiles with various mean lines in terms of which roughness parameters are expressed. In such cases a change can be expected almost on all roughness parameters.

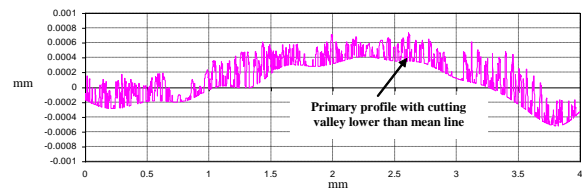


Fig. 10. Primary profile with cut valleys below filter mean line

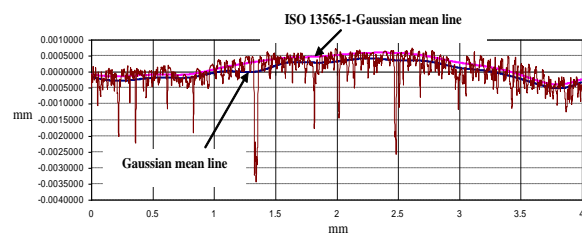


Fig. 11. Primary profile with Gaussian filter mean line and filter mean line determined with filtration process according to ISO 13565-1:1996

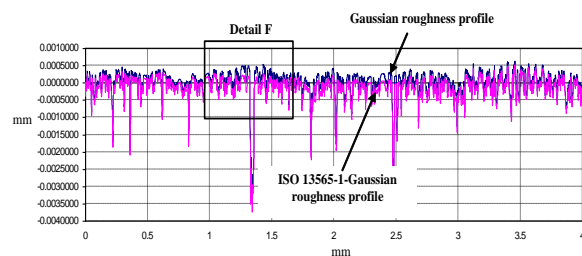


Fig. 12. Roughness profile determined with Gaussian profile filter and roughness profile determined with filtration process according to ISO 13565-1:1996

This indicates that filtration process according to ISO 13565-1:1996 may provide a more realistic roughness profile when waviness is less present, however the large difference in roughness profile forms imposes a dilemma whether the procedure should be applied or not. Maybe the dilemma is larger since on some professional software, as TalyProfile is, a possibility for filtration against ISO 13565-1:1996 is not provided.

Mean line determined against recommendations in ISO 13565-1:1996 is also called Rk (Gaussian) filter mean line [1,2].

4. CONCLUSION

Through analyzed real periodic surfaces the belief that filtration process has main and crucial role in determining roughness profile form was verified. The parallel determining of Gaussian and 2RC filter mean lines for one same primary profile and their mutual comparison provided following conclusions to be reached.

- Cutting start and end or only start of roughness profile for values λ_c i.e. $2\lambda_c$ in terms of primary profile is unjustified if a deterministic surface on which waviness is not present is in question.
- When waviness is not present, phase distortion of filter mean line generated by means of 2RC profile filter can have an affect only when periodic profile characterizes with a smaller number of valleys or peaks or when roughness profile has higher value for RSm.
- Sensitivity of filter mean lines obtained by using Gaussian and 2RC profile filter on deep valleys and peaks does not affect for periodic surfaces. Only by increasing RSm value and using 2RC profile filter can expect certain vertical distortions of roughness profile.
- Analysis of periodic real etalon surfaces demonstrated that there is no significant difference between roughness profiles obtained by application of Gaussian and 2RC profile filter, which justifies the usage of both filters.
- The effect of cut-off size change i.e. filter size is not included in the analysis. It is taken against recommendations provided in International and American standards.
- Analysis of non-periodic profiles showed that classification of surface as “non-periodic” is not sufficient when determining effects of Gaussian and 2RC profile filters.
- It was indicated that if primary profile characterizes with deep valleys then distortion of filter mean line from profile core occurs when using both filters. Additional deviation and obtaining artificial feature of obtained roughness profile will cause phase distortion of 2RC filter mean line.
- It was confirmed that roughness profile obtained by filtration process according to ISO 13565-1:1996 differs per its whole length from roughness profile obtained only by using Gaussian filter.
- Presence of waviness per whole length of primary non-periodic profile provides underlining of all disadvantages of Gaussian and 2RC profile filters. Large deviations and creation of artificial features on roughness profile occur when using 2RC profile filter. Therefore, this analysis provides conclusion that the application of Gaussian filter when obtaining roughness profile from non-periodic surface is justified.

5. REFERENCES

- [1] Raja, J., Muralikrishnan, B., Shengyu Fu: *Recent advances in separation of roughness, waviness and form*. Journal of the International Societies for Precision Engineering and Nanotechnology, 26 (2002), pp. 222–235.
- [2] Muralikrishnan, B., Raja, J.: *Computational Surface and Roughness Metrology*. Springer, London 2009.
- [3]. Paul, J. S., the Taylor Hobson Visiting Industrial Professor. *Filters in Surface Texture (Explained)-Presentation*.
- [4] ISO 3274:1996; Geometrical Product Specifications (GPS) - Surface texture: Profile method-*Nominal characteristics of contact stylus instruments*.
- [5] ISO/TS 16610-28:2010; Geometrical product specifications (GPS)-Filtration-Part 28: *Profile filters: End effects*.
- [6] ISO 13565-1:1996; Geometrical Product Specifications (GPS)-Surface texture: Profile method; Surfaces having stratified functional properties-Part 1: *Filtering and general measurement conditions*.

Authors: Ass. Mite Tomov, MSc, Prof. Mikolaj Kuzinovski, PhD, "Ss. Cyril and Methodius", University in Skopje, Faculty of Mechanical Engineering, Skopje, , Karposh II bb, P. Fax 464, 1000 Skopje R.Macedonia., Prof. Piotr Cichosz, DSc, Institute of Production Engineering and Automation of the Wroclaw University of Technology, str. Lukaszewicza 3/5, 50-371 Wroclaw, Polska
E-mail: mitetomov@mf.edu.mk
mikolaj@mf.edu.mk
piotrc@itma.pwr.wroc.pl

Tsiafis, I., Bouzakis, K.-D., Xanthopoulou, M., Tsohis, G., Xenos, Th.

ANALYSIS OF ROLLER BEARINGS' VIBRATION SIGNALS BY HILBERT – HUANG TRANSFORM AS DIAGNOSTIC TOOL

Abstract: Roller bearings are important elements of high performance mechanical systems, as they support the rotating parts and they reduce the contact friction. Therefore, it is necessary to continuously monitor their performance using non-destructive diagnostic methods. These methods interrogate data signals acquired during the machines operation. In this paper, the method of Hilbert – Huang transform was applied on non-stationary and non-linear vibration signals obtained via accelerometers from a mechanical system which contains a shaft rotating on Roller bearings. Two series of signals were used. The first series obtained from healthy bearings. The second series, obtained from bearings with seeded defects. The experimental study and its results are presented, as well as the conclusions drawn from the results.

Key words: Roller bearings, Hilbert Huang transform, vibration signal

1. INTRODUCTION

Non-destructive testing computational techniques are widely used nowadays, since they are accurate, cost and time efficient and usually easy to apply. Roller bearings are important elements of high performance mechanical systems, as they support the rotating parts and they reduce the contact friction. Therefore, it is necessary to continuously monitoring their performance using non-destructive diagnostic methods. It is obvious, that the method employed for time-frequency analysis must be computationally efficient and accurate in both time and frequency domains. The Wavelet transform, a method widely used for time-frequency analysis, is not suitable for the detection of failures of Roller bearings, since the computational time required for long data series is large, together with the inherent restrictions of the method in non-periodic, non-stationary signals [1]-[2]. Therefore, a modern method, the Hilbert-Huang transform, was introduced in this kind of problems with very promising performance, providing computational versatility and efficiency [18]-[19]. Consequently, it seems that the HHT can prove a perfect tool for Roller bearing failure detection.

The present paper, presents the application of the HHT as a diagnostic tool method in the analysis of Roller bearings' vibration signals from sound and defective samples [3]-[4]. The results prove the suitability of HHT for the detection of the changes occurring in dynamic systems such the evolution of structural defects in a Roller bearing [15]-[16].

By implementing the EMD method and the Hilbert transform to the envelope of the signal, the Hilbert spectrum can be obtained. Thus, the defects on a Roller bearing can be identified and failure patterns can be detected [11]. Using the proposed method in real time test bench analysis of vibration signals, together with a library of standards of sound and defect Roller bearings, can prove a versatile, economic and efficient

non-destructive technique. The results to be presented show the superiority of the proposed method over the traditional methods.

2. HILBERT HUANG TRANSFORM

During the operation of a Roller bearing with local failures, a high-frequency impulse oscillation is produced the range of which is evaluated by the strength of the sampled pulses. The method of the envelope analysis provides an important and effective approach to failure analysis of high frequency impulse signals. Therefore, it has been successfully applied to fault diagnosis regarding Roller bearings [6]-[8]. In order to achieve better implementation of the Hilbert Transform, a combination of the envelope analysis method with the Empirical Mode Decomposition (EMD) into Intrinsic Mode Functions (IMF) and Hilbert spectrum was created. The EMD method is based on local characteristic time scales of a signal and could decompose the complicated signal function in a number of intrinsic mode functions (IMF) [7]. The frequency components of each IMF depend both on sampling frequency and on the signal itself. Moreover, the corresponding Hilbert spectrum does not lead to dissipation and leakage of energy. Therefore, the EMD is a self-adaptive signal processing method that can be seamlessly applied to non-linear and non-stationary processes [12].

To extract the failure characteristics of the vibration signal of defect Roller bearings, the proposed method uses the following procedure: i) the failure vibration signal of a bearing is decomposed through wavelet packet transform in order to reduce the influence of low frequency noise; ii) a signal envelope is obtained by analyzing the wavelet coefficients of the high frequency band using the Hilbert Transform; iii) the IMFs are obtained applying the EMD in the signal

envelope; iv) some special IMF are chosen to obtain the Hilbert spectrum from which the faults in a Roller bearing are diagnosed and failure patterns are identified. The results from the analysis of vibration signals obtained from a Roller bearing with a defect on the inner or outer raceway show that the proposed method is an excellent tool to define the failure characteristics of Roller bearings.

2.1 Empirical Mode Decomposition

The EMD method is developed from the simple assumption that any signal consists of different simple intrinsic oscillation conditions [7]. Each linear or nonlinear condition will have the same number of extremes and zeros. There is only one extreme between two successive zeros. Each situation should be independent of the others. In this way, each signal could be decomposed to a number of IMFs and each of them must satisfy the following requirements:

- (1) In the entire data set, the number of extremes and zeros must be equal or differ at most by one
- (2) At each point, the mean value of the envelope defined by local maxima and the mean value of the envelope defined by local minima is zero.
- (3) If the signal does not have extremes but it has points of inflection, then it can be integrated one or more times in order to show the extremes.

So, one can achieve the decomposition of the signal into n empirical statements and a residue r_n , which is the average trend of $x(t)$. The IMFs c_1, c_2, \dots, c_n contain different frequency bands ranging from high to low. The frequency components contained in each frequency band are different and change with the variation of the signal $x(t)$; while r_n represents the central tendency of signal $x(t)$.

2.2 Hilbert Spectral Analysis

The HHT represents the analysed signal on a time – frequency plane by combining Empirical Mode Decomposition (EMD) with Hilbert transform [11]-[17]. In contrast, the Fourier spectral analysis in which a series of sine and cosine functions of constant amplitude are used to represent each elementary frequency component of the signal, the technique of HHT is based on calculating the instantaneous frequency derived from the Hilbert transform of the signal. In general, the Hilbert Huang transform $HHT[x(t)]$ for each signal $x(t)$ is defined as

$$HHT(t, \omega) = \sum_{i=1}^n HHT_i(t, \omega) \equiv \sum_{i=1}^n a_i(t, \omega_i) \quad (13)$$

where, $HHT_i(t, \omega)$ represents the time - frequency distribution obtained from the i -th IMF signal. The symbol \equiv denotes the "default", and $a_i(t, \omega_i)$ compares the values of range $a_i(t)$ and the values of the instantaneous frequency $\omega_i(t)$ along the signal simultaneously.

3. EXPERIMENTAL SETUP

The test-rig shown in figures 1a and 1b consisted of a shaft rotating on two Roller bearings (NU 202) driven by an electric motor controlled by an inverter for rotational speeds adjustment. An accelerometer,

mounted close to the bearings, was measuring the developed accelerations. The data acquisition and the subsequent signal processing were performed using software developed on Matlab.



Fig. 1a. Experimental setup

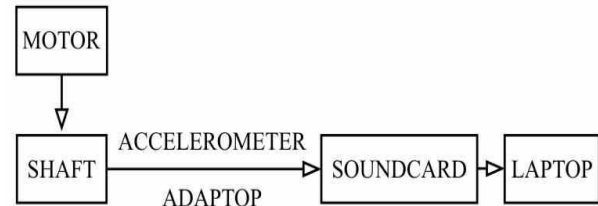


Fig. 1b. Diagram of the experimental setup

4. RESULTS

Each measurement made for each of the 17 Roller bearings, lasted 180 sec. The sampling frequency was chosen very high, 65536 Hz, so that very high frequencies corresponding to transient phenomena, as those investigated, could be identified; this sampling rate gave a data set of 11796480 samples for each measurement.

Due to the large amount of samples obtained in each case and in order to achieve continuity, each initial data series was split into 120, 50% overlapping parts, each of 200000 samples, where the HHT was implemented.

Figures 2a and 2b illustrate the time series of measurements obtained from a sound and a defective Roller bearing respectively.

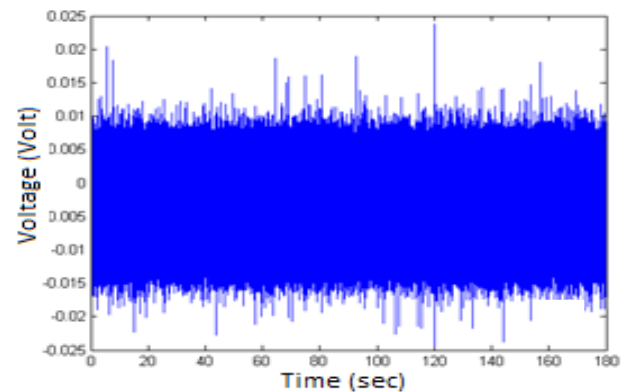


Fig. 2a. Time series of the healthy bearing

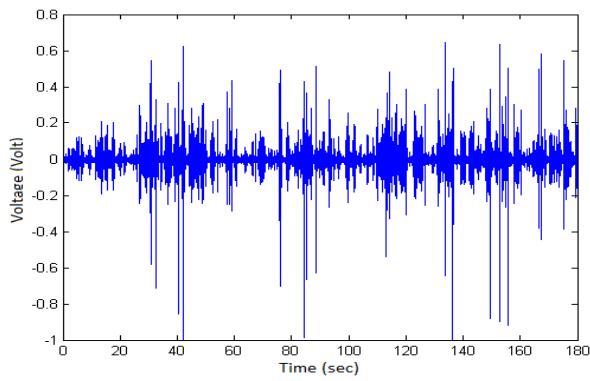


Fig. 2b. Time series of the defective bearing

The time series analysis by means of the HHT revealed strong differences between sound and defective Roller bearings, both in the IMFs (figs 3a, 4a and figs 3b, 4b, respectively) and in the corresponding Hilbert spectra (figs 5a and 5b) [14]. In fact, a comparative study between the relevant IMFs 1 to 5 of the sound and defective bearings (these IMFs correspond to the higher frequencies) reveals very strong differences; these differences tend to fade as the order of the IMF is getting higher i.e. as the frequency is decreasing, something to be expected, since defective Roller bearings tend to produce higher frequency signals compared to sound ones.

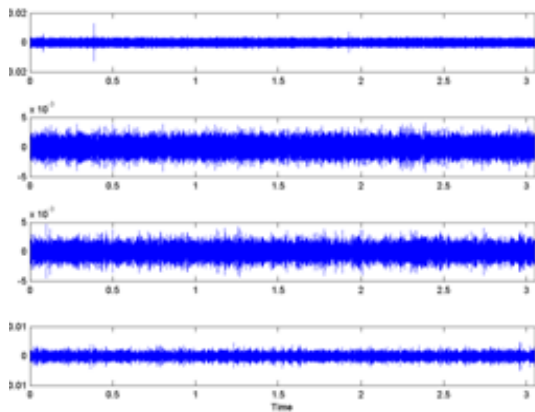


Fig. 3a. IMF 1-4 of sound bearing

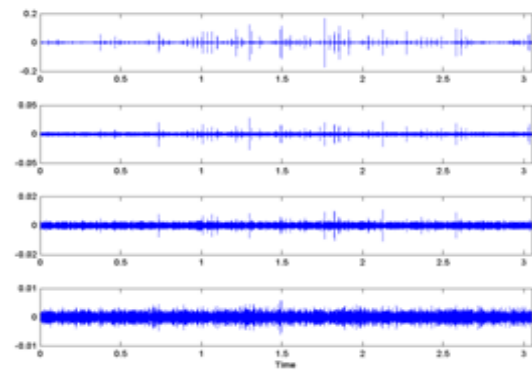


Fig. 3b. IMF 1-4 of the defective bearing

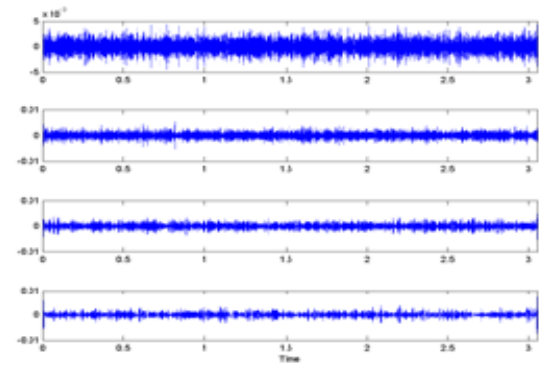


Fig. 4a. IMF 5-8 of the sound bearing

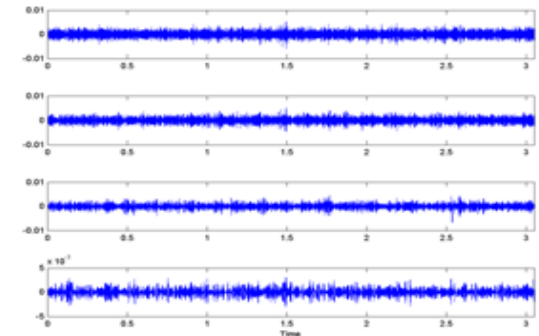


Fig. 4b. IMF 5-8 of the defective bearing

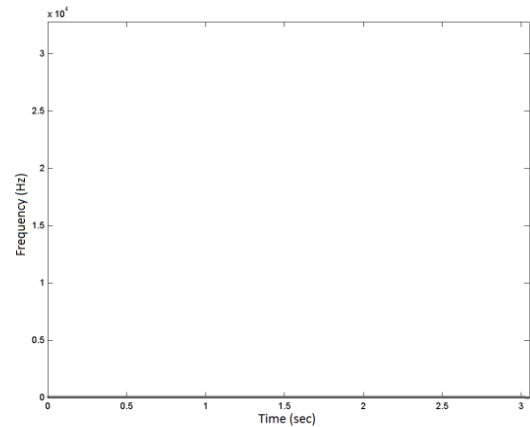


Fig. 5a. Spectrum Hilbert of the soundbearing

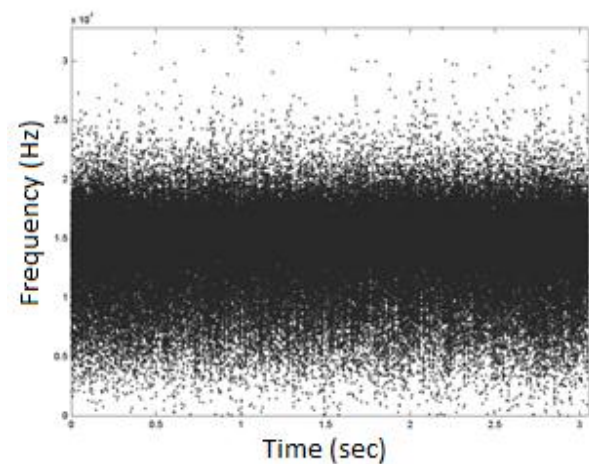


Fig. 5b. Spectrum Hilbert of the defective bearing

5. CONCLUSION

As a time-frequency signal decomposition technique, the HHT provides an effective tool for the analysis of transient vibration signals. Experimental studies on a custom test bench have shown that the deterioration of a test Roller bearing can be effectively detected through time-dependent amplitudes and instantaneous frequencies resulting from the HHT.

6. REFERENCES

- [1] G.A. Radcliff, Condition monitoring of roller element bearings using the enveloping technique. Machine Condition Monitoring. Mechanical Engineering Publication Ltd., London, 1990, pp. 55–67.
- [2] R.B. Randall, Hilbert transform techniques in machine diagnostics. IFToMM International Conference on Rotordynamics, Tokyo, 1986.
- [3] E. Bedrosian, A product theorem for Hilbert transforms, Proceedings of IEEE 51 (1963) 868–869.
- [4] D.E. Vakman, L.A. Vainshtein, Amplitude, phase, frequency — fundamental concepts of oscillation theory, Soviet Physics-Uspokhi 20(12)(1977) 1002–1016
- [5] C. Therrien, The Lee–Wiener Legacy. A history of the statistical theory of communication, November 2002, pp. 33–44.
- [6] S.L. Hahn, Hilbert Transforms in Signal Processing, Artech House, s.l., 1996, p. 305.
- [7] N.E. Huang, et al., The empirical mode decomposition and the Hilbert spectrum for nonlinear and non-stationary time series analysis, Proceedings of the Royal Society Series A: Mathematical, Physical and Engineering Sciences 454 (1971) (1998) 903–995.
- [8] K. Shin, J. Hammond., Fundamentals of Signal Processing for Sound and Vibration Engineers, John Wiley & Sons, Ltd, s.l., 2008.
- [9] Jaideva C. Goswami, Albert E. Hoefel, Algorithms for estimating instantaneous frequency, Signal Processing 84 (2004) 1423–1427.
- [10] Richard G. Lyons, Understanding Digital Signal Processing, Prentice Hall, s.l., 2004, p. 688.
- [11] Daji Huang, Practical implementation of the Hilbert–Huang transform algorithm, Acta Oceanologia Sinica 25 (1) (2003) 1–11.
- [12] Dennis Goge, et al., Detection and description of non-linear phenomena in experimental modal analysis via linearity plots, International Journal of Non-Linear Mechanics 40 (2005) 27–48.
- [13] Gabor D.: “Theory of communications”, Proc IEE, v. 93(III), pp. 429-457, 1946
- [14] M.Feldman, Non-linear system vibration analysis using Hilbert transform - Free vibration analysis method “FREEVIB”, Mechanical Systems and Signal Processing 8 (2) (1994) 119–127.
- [15] D.J. Pines, L.W. Salvino, Structural damage detection using empirical mode decomposition and HHT, Journal of Sound and Vibration 294 (2006) 97–124.
- [16] Anders Brandt, Noise and Vibration Analysis: Signal Analysis and Experimental Procedures © 2010 John Wiley & Sons.
- [17] N.E. Huang, M. C.Wu, S. R. Shen, W. Qu, P. Gloersen, and K. L. Fan, “A confidence limit for the Empirical Mode Decomposition and the Hilbert Spectral Analysis”, in *Proc. Royal. Soc. London. A*, 2003, vol. 459, pp. 2317–2345.
- [18] Ioannis Tsiafis, K.-D. Bouzakis, Antonios Kaplanis, Athanasios Karamanidis, Thomas Xenos , “Fault Diagnosis of Roller Bearings Using the Wavelet Transform”, Romanian Review Precision Mechanics, Optics & Mechatronics, 2011, No. 39 pp. 21-24.
- [19] Ioannis Tsiafis, K.-D. Bouzakis, Georgios Tsolis, Thomas Xenos, “Pectral Methods Assessment in Journal Bearing Fault Detection Applications”, The 3rd International Conference on Diagnosis and Prediction in Mechanical Engineering Systems, May 31 – June 1, 2012, Galati, Romania.

Authors: Assoc. Prof. Dr. I.Tsiafis¹, Prof. Dr.-Ing. habil. K.-D. Bouzakis¹, Dipl. Eng. M. Xanthopoulou¹, Dr. G. Tsolis², Prof. Dr. Th. Xenos²

1 Laboratory for Machine Tools and Manufacturing Engineering, Department of Mechanical Engineering, Aristotle University of Thessaloniki, Greece. Phone: +302310996034, +302310996079, Fax: +302310996059

2 Department of Electrical & Computer Engineering, Aristotle University of Thessaloniki, Thessaloniki, Greece.

E-mail: tsiafis@eng.auth.gr,
bouzakis@eng.auth.gr,
tdxenos@auth.gr,
maxantho84@gmail.com.

Vrba, I., Hadžistević, M., Palenčar, R., Lenčes, I.

OVERVIEW OF STANDARDS AND GUIDELINES WHICH DEFINE EVALUATION OF THE MEASUREMENT UNCERTAINTY IN MEASUREMENT OF FREEFORM SHAPED PARTS AT CMM

Abstract: Industrial manufacturing makes extensive use of simple shapes for the production of goods, with many products having a geometry that is a combination of planes, cylinders, spheres and other simple shapes. These parts are fundamental for the functionality of most mechanical products and, in general, they are easier and less expensive to manufacture than complex parts. However, in some applications they are not adequate, for instance when the functionality of the part is given by an interaction with a fluid or a wave, as is the case of aerodynamics and optics, for example.

Key words: Freeform, CMM, measurement uncertainty

1. INTRODUCTION

Freeform surfaces, sometimes called sculptured or curved surfaces, may be classified as complex geometrical features. According to ISO 17450-1 [3], complex geometrical features have no invariance degree. The invariance degree of a geometrical feature is the displacement of the ideal feature for which the feature is kept identical. Example of freeform shaped part is shown in Fig. 1.

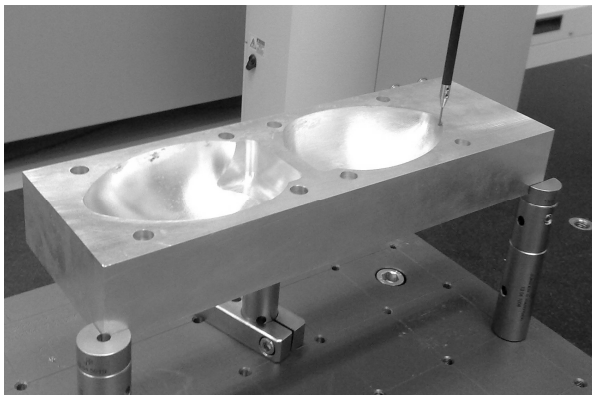


Fig. 1. Example of freeform shaped part

Freeform shaped parts are of great interest in many applications, either for functional or aesthetical reasons. Their relevance for industry is well-known in the design and manufacturing of products having complex functional surfaces. Functional surfaces may have a great influence on the performances of a product. Design, engineering and testing of parts having functional surfaces are key activities for the development of products with better performances [2].

Freeform shapes can be realized by many different manufacturing processes, whose capabilities have been improved for freeform geometry. For some demanding applications, it is advantageous to measure the workpiece during the production process; inprocess metrology allows improvement of accuracy and a reduction of machining time through the elimination of

repositioning and alignment operations. But for more accurate measurement, measurement which is done separated from production process has advantage.

2. SPECIFICATION OF FREEFORM SURFACES

As mentioned before, according to ISO 17450 [3] freeform shaped parts have no invariance degree, which means that geometrical feature cannot be displaced by geometrical primitive such as plane, circle, sphere, etc.

2.1 Definition of nominal shape

Curves and surface geometry is the underlying theory for the description of complex shapes. Traditionally, curves and surfaces have been represented by multiple orthographic projections. Today, the nominal geometry of a freeform shape is typically defined by a CAD model [2].

Freeform shapes are typically mathematically described using parametric surface representations [4]. Commonly used parametric surfaces are Bézier, B-spline and Non Uniform Rational B-spline (NURBS) surfaces. Parametric equations have many advantages over non-parametric forms, such as:

- they are much more convenient to define and control the shape of a curve or a surface,
- their mathematical description is easy to express in term of matrices and this allows the use of standard computation subroutines,
- curves and surfaces descriptions are independent of any coordinate system, therefore the choice of a coordinate system does not affect the shape of surfaces,
- they are convenient for computer graphics software and hardware in terms of speed, since the computation of offset curves and surfaces can be simplified.

Modern CAD systems describe complex geometry using NURBS that represent the industry standard for geometry description in CAD and Computer Graphics applications. NURBS surfaces are a generalization of

Bézier and B-spline surfaces. They are widely used for the representation of freeform surfaces due to their interesting properties such as the ability to handle large surface patches, local controllability and the ability to represent also simple analytical shapes such as planes, spheres, cylinders, cones, tori, etc. A NURBS surface is shown in Figure 2 and it is defined as shown in equation (1) [4]:

$$p(u, v) = \frac{\sum_{i=1}^{n_u} \sum_{j=1}^{n_v} B_{ui}(u) \cdot B_{vj}(v) \cdot w_{ij} \cdot c_{ij}}{\sum_{i=1}^{n_u} \sum_{j=1}^{n_v} B_{ui}(u) \cdot B_{vj}(v) \cdot w_{ij}} \quad (1)$$

where:

- p is a point on the surface and u and v its location parameters identifying the location of a point p within the surface,
- n_u and n_v are the number of control points in the u and v direction,
- $B_{ui}(u)$ and $B_{vj}(v)$ are the normalized B-spline functions in the u and v direction. $B_{ui}(u)$ is uniquely defined by the order k_u and knot sequence t_u with $k_u + t_u$ u -knots. Similarly, $B_{vj}(v)$ is uniquely defined by the order k_v and knot sequence t_v with $k_v + t_v$ v -knots,
- c_{ij} are the control points controlling the shape of the surface and w_{ij} their respective weights. When all the weights are set to 1, a NURBS surface becomes a B-spline surface.

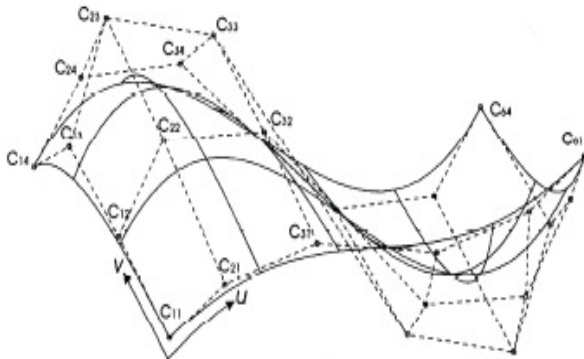


Fig. 2. Example of NURBS representation [4]

2.2 Tolerancing

The specification of tolerances on a freeform shape may be given on the basis of the profile tolerances defined for surfaces, with or without reference to a datum, available from ISO 1101 [5]. Form tolerances restrict the deviations of the real surface from the nominal shape only and have no datum; the definition is as follows (see also Fig. 2.): “The tolerance zone is limited by two surfaces enveloping spheres of diameter t , the centres of which are situated on a surface having the theoretically exact geometrical form.”

Other international standards of relevance are ISO 1660 (drawing indications) [6] and ISO/TR 5460 [7] (verification principles and traditional inspection methods). However, modern specification and verification concepts are not yet supported for freeform surfaces by a well defined normative basis nor a

universally accepted common praxis [8].

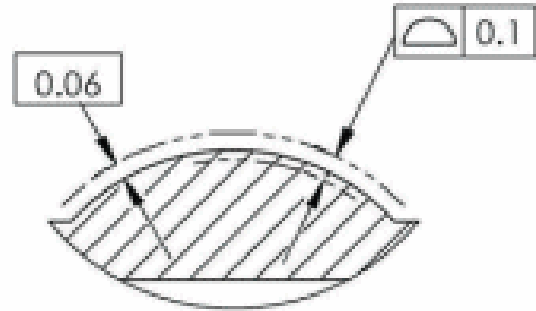


Fig. 2. Definition of profile tolerance not related to a datum

3. MEASUREMENT UNCERTAINTY

A correct statement of the uncertainty is becoming increasingly important as more and more companies strive to maintain traceability in accordance with ISO 9000. In particular, ISO 14253-1 [9] states that a proper uncertainty statement is necessary in order to conclude that products are within or outside of specification.

3.1 Definition of uncertainty in measurements

In general, every measurement process has imperfections that give rise to an error in the measurement result. So the result of measurement process is not a true value of measurand. It is only estimation. Because of that numerous imperfections, every result of measuring process has a parameter that describe a lack of exact knowledge of the value of the measurand called measurement uncertainty.

According to International Vocabulary of Metrology (VIM) [11] measurement uncertainty is “non-negative parameter characterizing the dispersion of the quantity values being attributed to a measurand, based on the information used”. The basic document that establishes general rules for evaluating and expressing uncertainty in measurement that is ISO Guide to the Expression of Uncertainty (GUM) [12]. GUM provides general rules for evaluating and expressing uncertainty in measurement rather than detailed, technology-specific instructions.

In practice, there are many possible sources of uncertainty in a measurement, including: incomplete definition of the measurand, imperfect realization of the definition of the measurand, nonrepresentative sampling – the sample measured may not represent the defined measurand, nonrepresentative sampling – the sample measured may not represent the defined measurand, etc

All of These sources are not necessarily independent, and some of sources may by correlate.

The uncertainty of the result of a measurement generally consists of several components, which may be grouped into two categories according to the method used to estimate their numerical values [12]:

- Type A components: those which are evaluated by statistical analysis of series of observations,
- Type B components: those which are evaluated by other means.

3.2 Evaluation of uncertainty in measurements

In most cases, a measurand Y is not measured directly, but is determined from N other quantities X_1, X_2, \dots, X_N through a functional relationship f :

$$Y = f(X_1, X_2, \dots, X_N) \quad (2)$$

An estimate of the measurand Y , denoted by y , is obtained from Equation (1) using input estimates x_1, x_2, \dots, x_N for the values of the N quantities X_1, X_2, \dots, X_N . Thus the output estimate y , which is the result of the measurement, is given by equation (3):

$$y = f(x_1, x_2, \dots, x_N) \quad (3)$$

As an example of a Type A evaluation, consider an input quantity X_i whose value is estimated from n independent observations $X_{i,k}$ of X_i obtained under the same conditions of measurement. In this case, the input estimate x_i is usually the sample mean [12]

$$x_i = \bar{X}_i = \frac{1}{n} \sum_{k=1}^n X_{i,k} \quad (4)$$

The individual observations X_i differ in value because of random variations in the influence quantities, or random effects and the standard uncertainty $u(x_i)$ to be associated with x_i is the estimated standard deviation of the mean [12]:

$$u(x_i) = s(\bar{X}_i) = \sqrt{\frac{1}{n \cdot (n-1)} \sum_{k=1}^n (X_{i,k} - \bar{X}_i)^2} \quad (5)$$

For an estimate x_i of an input quantity X_i that has not been obtained from repeated observations, the standard uncertainty $u(x_i)$ is evaluated by scientific judgment based on all of the available information on the possible variability of X_i . The pool of information may include [12]:

- previous measurement data;
- experience with or general knowledge of the behavior and properties of relevant materials and instruments;
- manufacturer's specifications;
- data provided in calibration and other certificates;
- uncertainties assigned to reference data taken from handbooks
- inadequate knowledge of the effects of environmental conditions on the measurement or imperfect measurement of environmental conditions
- personal bias in reading analogue instruments;
- finite instrument resolution or discrimination threshold;
- inexact values of measurement standards and reference materials;
- inexact values of constants and other parameters obtained from external sources and used in the data-reduction algorithm;
- approximations and assumptions incorporated in the measurement method and procedure;
- variations in repeated observations of the measurand under apparently identical conditions.

The combined standard uncertainty of the measurement result y , designated by $u_c(y)$ and taken to represent the estimated standard deviation of the result, is the positive square root of the estimated variance

$u_c^2(y)$ obtained from equation (6) [12].

$$u_c^2(y) = \sum_{i=1}^N \left(\frac{\partial f}{\partial x_i} \right)^2 u^2(x_i) + 2 \sum_{i=1}^{N-1} \sum_{j=i+1}^N \frac{\partial f}{\partial x_i} \frac{\partial f}{\partial x_j} u(x_i \cdot x_j) \quad (6)$$

Equation (6) is based on a first-order Taylor series approximation of the measurement equation given in equation (2) and is conveniently referred to as the law of propagation of uncertainty. The partial derivatives of f with respect to the X_i (often referred to as sensitivity coefficients) are evaluated at $X_i = x_i$; $u(x_i)$ is the standard uncertainty associated with the input estimate x_i ; and $u(x_i, x_j)$ is the estimated covariance associated with x_i and x_j [12].

Equation (6) is used when input values x_i are correlated, but when input values are independent and uncorrelated, equation (6) gets its simpler form [12]:

$$u_c^2(y) = \sum_{i=1}^N \left(\frac{\partial f}{\partial x_i} \right)^2 u^2(x_i) \quad (6)$$

In case When some sources of uncertainty are evaluated as Type A, and others are evaluated as Type B, the combined standard uncertainty of the result y is given by equation (7)

$$u_c(y) = \sqrt{u_A^2(y) + u_B^2(y)} \quad (7)$$

The additional measure of uncertainty that meets the requirement of providing an interval is termed expanded uncertainty and is denoted by U . The expanded uncertainty U is obtained by multiplying the combined standard uncertainty $u_c(y)$ by a coverage factor k [12]:

$$U = k \cdot u_c(y) \quad (8).$$

The result of a measurement is then conveniently expressed as

$$Y = y \pm U \quad (9).$$

In general, the value of the coverage factor k is chosen on the basis of the desired level of confidence to be associated with the interval defined by U . Typically, k is in the range 2 to 3. When the normal distribution applies and u_c is a reliable estimate of the standard deviation of y , $U = 2u_c$ (i.e., $k = 2$) defines an interval having a level of confidence of approximately 95 %, and $U = 3u_c$ (i.e., $k = 3$) defines an interval having a level of confidence of approximately 99.7 %.

A detailed procedure for determination of coverage factor k , can be found in European co-operation for Accreditation directive EA 4/02 [13].

4. UNCERTAINTY AND TRACEABILITY IN CMM MEASUREMENTS

As explained in the previous paragraph, uncertainty is expressed as a range of values within which, at a specified level of confidence, the true value of the quantity measured is believed to lie. In CMM-based measurements, a task-specific uncertainty for each Geometric Dimensioning and Tolerancing (GD&T) parameter is necessary.

The ISO defines traceability as "*the property of the result of a measurement or the value of a standard whereby it can be related to stated references, usually*

national or international standards, through an unbroken chain of comparisons all having stated uncertainty." [9]. The prominent role of uncertainty in completing the traceability chain is evident. Simply having a CMM calibrated does not make its measurement results traceable. If CMM-derived GD&T measurements are traceable, defensible task-specific uncertainty evaluations should be included in a report

4.1 Performance verification of CMM

Performance verification is an important documentation of the measurement capability of any measuring device; standards and guidelines are available for the practical implementation of performance verification tests on some measuring instruments. ISO standard that describes the procedures to verify the performance of CMM are series of standards ISO 10360 (Acceptance and re-verification Tests for Coordinate Measuring Machines). Procedure in this series defines the Maximum Permissible Error (MPE) for each type of measurement task. ISO 10360-2 [16] specifies volumetric Length Measuring Error (MPE_L) and Volumetric Probing Error (MPE_P). This standard applies to all measurements of distances, diameters, position tolerance, freeform tolerances, straightness, flatness, roundness and cylindricity. ISO 10360-3 [17] specifies errors caused by rotary table. ISO 10360-4 [18] is applied for every measurement when the CMM is used in scanning mode. ISO 10360-5 [19] specifies multiple stylus errors of location, size and form.

As any other measurement, measurements performed in these tests for ISO 10630 also have uncertainty. Procedure for determining this uncertainty is described in ISO 23165 (still in draft).

Besides series ISO 10630, there is directives published by European co-operation for Accreditation directive that can be applied for performance verification of CMM. These are: EA 4/02 [13], EA-4/16 [14] EAL-G17 [15].

4.2 Techniques for evaluation of the uncertainty on CMM-based measurements

The ISO 15530 series of International Standards is intended to provide terminology, techniques, and guidelines for estimating the uncertainty of CMM measurements. Although the technical committee ISO TC 213 has been working on it since more than a decade it is still largely incomplete. CMMs are considered to be complex GPS measuring equipment, and the estimation of the uncertainty of CMM measurements often involves more advanced techniques than those described in ISO 14253-2 [10]. The techniques presented in the ISO 15530 series are compliant with both and the GUM.

The following paragraphs show a synthesis of ISO 15530 standards. (Geometric Product Specification (GPS) – Coordinate Measuring Machines (CMM): techniques for determining the uncertainty of measurement):

- Part 1: Overview and metrological characteristics.
- Part 2: Use of multiple strategies in calibration of

artefacts.

- Part 3: Use of calibrated work pieces or standards.
- Part 4: Use of computer simulation.
- Part 5: Use of expert judgement, sensitivity analysis and error budgeting

From all of these parts, the only published for now is ISO 15530-3. ISO 15530-2 and ISO 15530-4 are published only in draft version [1,2]. Other ones are still under the attention of ISO Technical Committee TC213. A short description of these parts is given as follows.

ISO 15530-1 aims to introduce the techniques for determining the uncertainty of measurement for a CMM, providing the proper terminology and a reference list of metrological characteristics, i.e. a list of factors that can potentially affect the measurements produced by a CMM. The document is still in a draft version [1,2].

ISO 15530-2 (the document is still in a draft version) aims to introduce the technique of multiple measurement strategies, for determining the uncertainty of measurement related to a work piece measured by a CMM. The multiple measurement strategy aims to combine several orientations of the work piece and point distributions on its surface in order to get a better estimation for the conventional true value of the measurand. In this standard, the uncertainty of measurement is obtained by a non-calibrated objects method [1,2].

ISO 15530-3 aims to provide a technique for a simple uncertainty evaluation of measurements performed by a CMM. This technique applies to specific measuring tasks and to CMM results obtained from both uncorrected and corrected measurements. It is based on three key concepts: non substitution measurement, substitution measurement, similarity condition. Non substitution measurements are results in which the CMM indication is not corrected by systematic errors. On the opposite, in substitution measurement, the CMM indication is corrected by systematic errors. Similarity conditions define the constraints binding the work piece and the material standard of size in the uncertainty assessment [1,2,20].

According to this standard, expanded uncertainty is calculated by equation (10) [20]:

$$U = k \cdot \sqrt{u_{cal}^2 + u_p^2 + u_w^2} + |b| \quad (10)$$

where:

- u_{cal} is standard uncertainty resulting from the uncertainty of calibration of the calibrate workpiece stated in the calibration certificate,
- u_p is standard uncertainty resulting from measurement procedure,
- u_w is standard uncertainty resulting from material and manufacturing variations
- b is systematic error.

ISO 15530-4 aims to define criteria for simulation techniques applied to task-specific uncertainty evaluations. The target of these techniques is to provide measurement results combined with the related measuring uncertainty [1,2].

ISO 15530-5 aims to define the criteria of the

technique for uncertainty evaluation based on expert judgement. The use of expert judgement can be particularly important when type B standard uncertainty is considered in the uncertainty budget. Personnel aiming to provide expert judgements must be properly qualified. ISO 15530-5 is still in draft status. Key concept is concept of qualified personnel [1,2].

4.3 Critical observations

ISO 15530-2 and ISO 15530-3 are two different methods of evaluation measurement uncertainty. In the first standard, the uncertainty of measurement is obtained by a non-calibrated objects method. The uncertainty is the result of three contributions: repeatability of measurements; geometric errors of the piece; error of scale. In the second instead, uncertainty is obtained by a calibrated object method. It's the result of systematic error, repeatability of measurements and uncertainty of calibration and reference object. These methods define uncertainty measurement by an aggregate way, while ISO 15530-4 analytically characterize each uncertainty contribution in the measurement volume of the machine. This is the way promoted by PTB (German metrological Institute), which firstly introduced the concept of "virtual machine" [1]. Even if ISO 15530-2 and ISO 15530-4 are still in draft, there are a numerous publications, where authors were used procedure described in this standards for evaluation of uncertainty.

4.4 Application to freeform

In general, performance verification is based on the use of calibrated artefacts, for which geometry is usually very simple and restricted to simple shapes, i.e. planes or spheres in different configurations. Such procedures are therefore quite different from the typical use on the measuring device when dealing with freeform shaped parts.

To simplify the procedure of evaluation a uncertainty of measurement of freeform shaped parts, the recommendation given by NIST in [21] is to apply the technique of substitute-geometry decomposition, which means that the complex geometry of a part is represented as being composed of the sum of simpler geometric elements. According to this recommendation of NIST, many authors in their papers, for evaluation of uncertainty, uses modular freeform gauges (MFG) (Figure 3). But with this approach, we can only *simulate* the shape of real freeform shape and, in most cases, the real object is not fully *covered* by calibrated shapes. Opposite to this approach is use of non-calibrated object. In this approach, measurement results are compared to nominal geometry from CAD model. Advantage of this approach is that the freeform shape is fully covered, but measurement is much longer and values of evaluated measurement uncertainty are generally larger [22]

5. CONCLUSIONS

Freeform shaped parts represent challenging measurement tasks for a number of instruments such as coordinate measuring machines. Tolerance

specification and verification in connection with freeform geometries rely on the use of a CAD model, with a number of difficulties related to measurement strategy, registration of multiple views, filtering, alignment and evaluation. Metrological issues related to performance verification and traceability rely on the existence of calibrated workpieces. There is a clear need for new methods and standards to ensure traceability of measurements on freeform shaped parts.



Fig. 3. MFG configuration (left) for the uncertainty assessment related to the turbine blade geometry (right) [2]

6. ACKNOWLEDGMENT

The authors wish to thank the Slovak University of Technology in Bratislava and the VEGA grant agency, grant No. 1/0120/12 and the APPV-grant No. 0096-10 and the KEGA grant agency, grant No.005STU-4/2012 for their support.

7. REFERENCES

- [1] Concas, F.: *Design of optimal measurement strategies for geometric tolerances control on coordinate measuring machines*, Dottorato di Ricerca in Progettazione Meccanica, Università degli Studi di Cagliari
- [2] Savio, E., De Chiffre, L., Schmitt, R.: *Metrology of freeform shaped parts*, Annals of the CIRP Vol. 56/2/2007, p.p. 810-835, 2007.
- [3] ISO/TS 17450-1:2005, Geometrical product specifications (GPS) - General concepts - Part 1: Model for geometrical specification and verification.
- [4] Farin G., 2002, Curves and Surfaces for computer aided geometric design, 5th edition, Morgan-Kaufmann.
- [5] ISO 1101:2004, Geometrical Product Specifications (GPS) - Geometrical tolerancing - Tolerance of form, orientation, location and run-out.

- [6] ISO 1660:1987, Technical drawings – Dimensioning and tolerancing of profiles.
- [7] ISO/TR 5460:1998, Technical drawings - Geometrical tolerancing - Tolerancing of form, orientation, location and run-out – Verification principles and methods – Guidelines.
- [8] Meneghello, R., Savio E., Concheri G., 2003, CADbased Measurements in Profile Tolerances Verification, euspen Int. Top. Conf., Aachen, Germany, 2:483-486.
- [9] ISO 14253-1:1998, Geometrical Product Specifications (GPS) – Inspection by measurement of workpieces and measuring instruments – Part 1: Decision rules for proving conformance or non conformance with specification
- [10] ISO 14253- 2:1999 Geometrical Product Specifications (GPS) -- Inspection by measurement of workpieces and measuring equipment -- Part 2: Guide to the estimation of uncertainty in GPS measurement, in calibration of measuring equipment and in product verification
- [11] BIPM JCGM 200:2008: International vocabulary of metrology — Basic and general concepts and associated terms (VIM)
- [12] ISO Guide 1995: Guide to the expression of uncertainty in measurement
- [13] European co-operation for Accreditation EA 4/02 Expression of the Uncertainty of Measurement in Calibration, 1999
- [14] European co-operation for Accreditation EA 4/16 EA guidelines on the expression of uncertainty in quantitative testing, 2003
- [15] European co-operation for Accreditation EAL-G17 Coordinate Measuring Machine Calibration, 1995
- [16] ISO 10360-2 Geometrical Product Specification (GPS). Acceptance and re-verification Tests for Coordinate Measuring Machines (CMM). Part 2 CMMs used for measuring size
- [17] ISO 10360-3 Geometrical Product Specification (GPS). Acceptance and re-verification Tests for Coordinate Measuring Machines (CMM). Part 3 CMMs with the axis of a rotary table as the fourth axis
- [18] ISO 10360-4 Geometrical Product Specification (GPS). Acceptance and re-verification Tests for Coordinate Measuring Machines (CMM). Part 4 CMMs used in scanning measuring mode
- [19] ISO 10360-5 Geometrical Product Specification (GPS). Acceptance and re-verification Tests for Coordinate Measuring Machines (CMM). Part 5 CMMs using multiple-stylus probing system
- [20] ISO/DTS 15530-2, 2005, GPS - CMMs: Techniques for evaluation of the uncertainty of measurement - Part 2: Use of multiple measurement strategies.
- [21] Swyt, D.: *Length and Dimensional Measurements at NIST*, Journal of Research of the National Institute of Standards and Technology, Volume 106, Number 1, p.p. 1-23, January–February 2001
- [22] Savio, E., Hansen, H.N., De Chiffre, L.: *Approaches to the Calibration of Freeform Artefacts on Coordinate Measuring Machines*, CIRP Annals - Manufacturing Technology, Volume 51, Issue 1, p.p. 433–436, 2002.

Authors: Ing. Igor Vrba, prof. Ing. Rudolf Palnčar, CSc., Ing. Ivan Lenčes, Slovak Technical University in Bratislava, Faculty of Mechanical Engineering, Institute of Automation, Measurement and Applied Informatics, Namestie Slobody 17, 81231 Bratislava 1, Slovakia, Phone: +421252497193, Fax: +4212524 5315
 E-mail: igor.vrba@stuba.sk
rudolf.palencar@stuba.sk
ivan.lences@stuba.sk

Prof. dr Miodrag Hadžistević, University of Novi Sad, Faculty of Technical Sciences, Institute for Production Engineering, Trg Dositeja Obradovica 6, 21000 Novi Sad, Serbia, Phone.: +381 21 485-2344, Fax: +381 21 454-495.
 E-mail: midrags@uns.ac.rs

Zuperl, U., Cus, F.

FIXTURE ANALYSIS MODULE, AN ESSENTIAL ELEMENT OF THE INTELLIGENT FIXTURING SYSTEM

Abstract: This paper presents the concept of Intelligent Fixturing System (IFS) which is being developed to hold a family of thin-walled workpieces for machining operations. This is a cost-effective concept which incorporates a fixturing system, fixture analysis module, fixture stability module, clamp optimization module and clamping control system. This paper presents the development of fixture analysis module that can determine the optimal clamping force values considering the cutter location and the three cutting force components.

Key words: intelligent fixturing, fixture analysis.

1. INTRODUCTION

In pace with automation of the work process the development and rationalization stage of fixtures becomes increasingly important and strongly influences the price of the final product. The fixing equipment is a bottleneck in production, therefore in the past decade the efforts in searching for new Intelligent Fixturing System (IFS) were increased. This paper describes the proposed IFS system, which on the basis of given workpiece geometry analyses and optimizes the magnitude/position of clamping forces. The paper is also concerned about the fixture module for the analysis and rationalization of fixtures, suitable for clamping of thin-wall products likely to undergo deformation due to clamping and cutting forces during machining. Software has been made for the evaluation of fixturing scheme, for calculation of the optimum magnitude and positioning of clamping forces, required to enable the workpiece to be safely clamped during machining. The calculation is based on the force analysis method provided with the optimization routine. Especially in cases of machining of thin-walled components, deformation can be minimised by optimizing the location and magnitude of clamping forces. Therefore, in intelligent fixturing system the clamp position and magnitude of clamping forces have to be controlled in real time [1]. More realistic and cost-effective approach is to use off-line optimisation of the clamps location and on-line adjustment of clamping force.

2. INTELLIGENT FIXTURING SYSTEM

An attempt was made to include fixture analysis module into the Intelligent Fixturing System (IFS). Proposed system is able to perform the following operations: off line optimization of clamping forces, monitor the clamping forces and adjust the clamping forces according to the change in geometry of the workpiece. The framework of the system is shown in Figure 1. It consists of the modular fixturing system, off line fixture analysis module, fixturing stability

module, clamping optimization algorithm and clamping control system. At the beginning, the optimal clamping forces are determined by analysis module then the reaction forces are measured through the sensors embedded in locators. The data are sent via force monitoring module to the fixture stability model. The fixture stability module is used to monitor the fixturing stability during the entire machining operation. Once instability appears, the module sends a command to the hydraulic system to increase the corresponding clamping force. This process is repeated until the completion of the machining process. Positive reaction forces at the locators ensure that the workpiece maintains contact with all the locators from the beginning of the cut to the end. The three components of cutting forces in end-milling are predicted using the neural cutting force model developed by [2]. The clamping force optimisation algorithm determines the optimal clamping force values considering the cutter location, the three cutting force components and results of the fixture stability model. The optimal clamping forces are then applied in real-time using an electro-hydraulic clamping system. Soft PLC controls a hydraulic system to apply the required clamping forces as the cutter moves to different locations on the workpiece. The clamping forces are proportional to pressure in hydraulic cylinder.

3. FIXTURE ANALYSIS MODULE

The developed module is useful for technologist since it can routinely determine within a short time the optimum sizes, direction and application points of clamping and locating forces for different cases of clamping. The module is aimed at verifying (analysing) the obtained solution (configuration of the fixture), confirming or rejecting it, if all the set condition are not fulfilled. The worked out programme works on the PC and is programmed in the mathematical programme language MatLab. The clamping principle 3-2-1, requiring three points on the primary locating plane, two points on the second locating plane and one point on the third locating plane, was used for making the

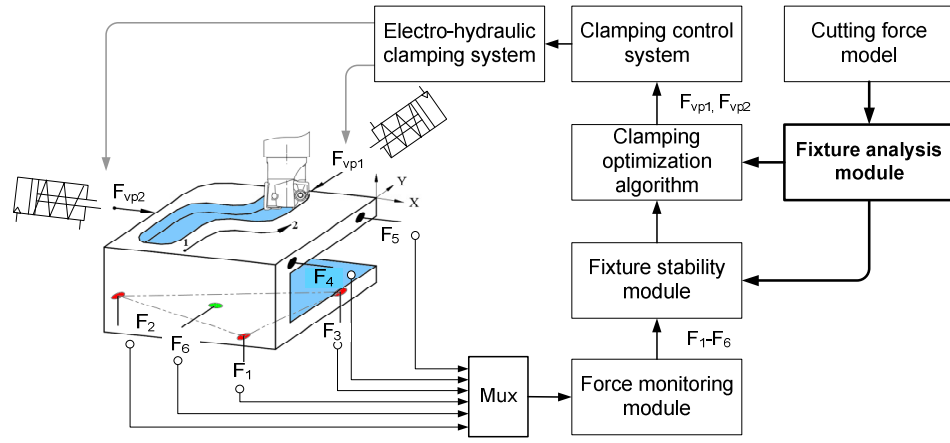


Fig. 1. Framework of the IFS system

module. The clamping force must be great enough and suitable oriented so that the workpiece position during machining does not change due to cutting forces. The clamping forces on the workpiece must not create internal stresses and must not damage or deform the workpiece surface. The objective is to minimize all the controllable and reaction forces. This is expressed as the minimization of the sum of the squares of the clamping and reaction forces.

3.1 Theoretic concept of the fixture analysis module

The workpiece is located on the six- points P_1-P_6 and is held by three clamping forces $F_{vp1}, F_{vp2}, F_{vp3}$ at points P_7, P_8, P_9 (figure 2).

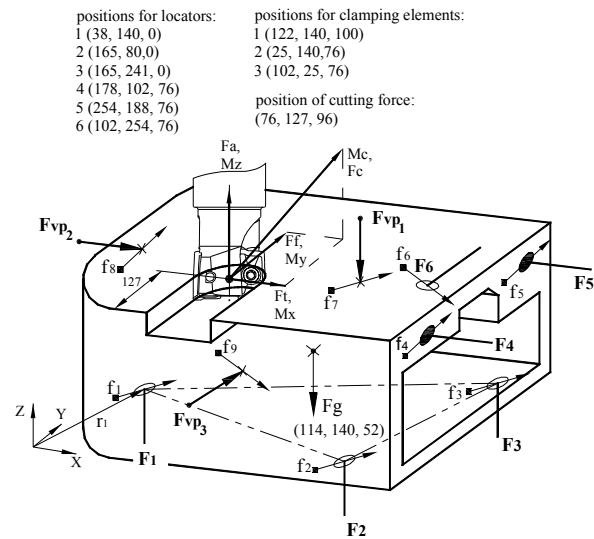


Fig. 2. Forces on a prismatic workpiece during machining of a slot

Where:

- $F_1 - F_6$ - reactions acting on locating elements (N),
- $F_{vp1}, F_{vp2}, F_{vp3}$ - clamping forces acting in the direction of the normal onto positioning planes (N),
- F_t, F_a, F_f - components of cutting force F_c (N),
- M_x, M_y, M_z - components of cutting moment M_c (Nm),
- f_i ($i = 1...9$) - friction forces in contact points (N),
- F_g - force of workpiece weight (N),
- μ - friction coefficient.

The resulting force of friction f_i between the locator and workpiece is $\mu \cdot F_i$ and between the fixing element and the workpiece it is $\mu \cdot F_{vpj}$ ($j=1...3$).

The reactions on the locating elements must be positive, because otherwise the contact between the workpiece and the fixture is lost.

To achieve static equilibrium the resultant force and moment on the workpiece must be zero.

Because of the numerical solving of the problem the equilibrium equations are written in matrix form:

$$[A]_{lok} \cdot [F]_{lok} + [w_e] = 0 \quad (1)$$

$[A]_{lok}$ - normalized geometrical matrix.

$[F]_{lok}^T$ - vector of supporting forces

$[w_e]$ - vector of external forces

After entering the geometrical matrix and the vector of external forces into the equation (1) the equation (5) is obtained.

When the coefficient of the friction between the workpiece and the clamping elements is equal to zero, the equation (5) is simplified and assumed the form (6).

$$[A]_{lok} = \begin{bmatrix} f_{1x} & f_{2x} & f_{3x} & -1 & -1 & f_{6x} \\ f_{1y} & f_{2y} & f_{3y} & f_{4y} & f_{5y} & -1 \\ 1 & 1 & 1 & -f_{4z} & -f_{5z} & -f_{6z} \\ \hline r_{1y} & r_{2y} & r_{3y} & (-f_{4y} \cdot r_{4z} -) & (-f_{5y} \cdot r_{5z} -) & (-f_{6z} \cdot r_{6y} +) \\ -r_{1x} & -r_{2x} & -r_{3x} & (-f_{4y} \cdot r_{4y}) & (-f_{5z} \cdot r_{5y}) & (+r_{6z}) \\ & & & (-r_{4z} +) & (-r_{5z} +) & (f_{6x} \cdot r_{6z} +) \\ & & & (+f_{4z} \cdot r_{4x}) & (+f_{5z} \cdot r_{5x}) & (+f_{6z} \cdot r_{6x}) \\ (-f_{1x} \cdot r_{1y} +) & (-f_{2x} \cdot r_{2y} +) & (-f_{3x} \cdot r_{3y} +) & (r_{4y} +) & (r_{5y} +) & (-r_{6x} -) \\ (+f_{1y} \cdot r_{1x}) & (+f_{2y} \cdot r_{2x}) & (+f_{3y} \cdot r_{3x}) & (+f_{4y} \cdot r_{4x}) & (+f_{5y} \cdot r_{5x}) & (-f_{6x} \cdot r_{6y}) \end{bmatrix} \quad (2)$$

$$[F]_{lok}^T = [F_1 \ F_2 \ F_3 \ F_4 \ F_5 \ F_6] \quad (3)$$

$$[w_e] = \begin{bmatrix} f_{7x} + f_{9x} + F_{vp2} + R_x \\ f_{7y} + f_{8y} + F_{vp3} + R_y \\ -f_{8z} - f_{9z} - F_g + R_z \\ -f_{7y} \cdot r_{7z} - f_{8y} \cdot r_{8z} - f_{8z} \cdot r_{8y} - f_{9z} \cdot r_{9y} - F_{vp1} \cdot r_{7y} - F_{vp3} \cdot r_{9z} - F_g \cdot r_{gy} + M_x \\ f_{7x} \cdot r_{7z} + f_{8z} \cdot r_{8x} + f_{9x} \cdot r_{9z} + f_{9z} \cdot r_{9x} + F_{vp1} \cdot r_{7x} + F_{vp2} \cdot r_{8z} + F_g \cdot r_{gx} + M_y \\ -f_{7x} \cdot r_{7y} + f_{7y} \cdot r_{7x} + f_{8y} \cdot r_{8x} - f_{9x} \cdot r_{9y} - F_{vp2} \cdot r_{8y} + F_{vp3} \cdot r_{9x} + M_z \end{bmatrix} \quad (4)$$

$$[F]_{lok} = \begin{bmatrix} f_{1x} & f_{2x} & f_{3x} & -1 & -1 & f_{6x} \\ f_{1y} & f_{2y} & f_{3y} & f_{4y} & f_{5y} & -1 \\ 1 & 1 & 1 & -f_{4z} & -f_{5z} & -f_{6z} \\ \hline r_{1y} & r_{2y} & r_{3y} & \begin{pmatrix} -f_{4y} \cdot r_{4z} \\ -f_{4y} \cdot r_{4y} \end{pmatrix} & \begin{pmatrix} -f_{5y} \cdot r_{5z} \\ -f_{5y} \cdot r_{5y} \end{pmatrix} & \begin{pmatrix} -f_{6z} \cdot r_{6y} \\ +r_{6z} \end{pmatrix} \\ -r_{1x} & -r_{2x} & -r_{3x} & \begin{pmatrix} -r_{4z} \\ +f_{4z} \cdot r_{4x} \end{pmatrix} & \begin{pmatrix} -r_{5z} \\ +f_{5z} \cdot r_{5x} \end{pmatrix} & \begin{pmatrix} f_{6x} \cdot r_{6z} \\ +f_{6z} \cdot r_{6x} \end{pmatrix} \\ \begin{pmatrix} -f_{1x} \cdot r_{1y} \\ +f_{1y} \cdot r_{1x} \end{pmatrix} & \begin{pmatrix} -f_{2x} \cdot r_{2y} \\ +f_{2y} \cdot r_{2x} \end{pmatrix} & \begin{pmatrix} -f_{3x} \cdot r_{3y} \\ +f_{3y} \cdot r_{3x} \end{pmatrix} & \begin{pmatrix} r_{4y} \\ +f_{4y} \cdot r_{4x} \end{pmatrix} & \begin{pmatrix} r_{5y} \\ +f_{5y} \cdot r_{5x} \end{pmatrix} & \begin{pmatrix} -r_{6x} \\ -f_{6x} \cdot r_{6y} \end{pmatrix} \end{bmatrix} \cdot \quad (5)$$

$$\begin{bmatrix} f_{7x} + f_{9x} + F_{vp2} + R_x \\ f_{7y} + f_{8y} + F_{vp3} + R_y \\ -f_{8z} - f_{9z} - F_g + R_z \\ -f_{7y} \cdot r_{7z} - f_{8y} \cdot r_{8z} - f_{8z} \cdot r_{8y} - f_{9z} \cdot r_{9y} - F_{vp1} \cdot r_{7y} - F_{vp3} \cdot r_{9z} - F_g \cdot r_{gy} + M_x \\ f_{7x} \cdot r_{7z} + f_{8z} \cdot r_{8x} + f_{9x} \cdot r_{9z} + f_{9z} \cdot r_{9x} + F_{vp1} \cdot r_{7x} + F_{vp2} \cdot r_{8z} + F_g \cdot r_{gx} + M_y \\ -f_{7x} \cdot r_{7y} + f_{7y} \cdot r_{7x} + f_{8y} \cdot r_{8x} - f_{9x} \cdot r_{9y} - F_{vp2} \cdot r_{8y} + F_{vp3} \cdot r_{9x} + M_z \end{bmatrix}$$

$$[F]_{lok} = \begin{bmatrix} F_1 \\ F_2 \\ F_3 \\ F_4 \\ F_5 \\ F_6 \end{bmatrix} = \begin{bmatrix} 0 & 0 & 0 & -1 & -1 & 0 \\ 0 & 0 & 0 & 0 & 0 & -1 \\ 1 & 1 & 1 & 0 & 0 & 0 \\ \hline r_{1y} & r_{2y} & r_{3y} & 0 & 0 & +r_{6y} \\ -r_{1x} & -r_{2x} & -r_{3x} & -r_{4z} & -r_{5z} & 0 \\ 0 & 0 & 0 & r_{4y} & r_{5y} & -r_{6x} \end{bmatrix}^{-1} \begin{bmatrix} F_{vp2} + R_x \\ F_{vp3} + R_y \\ F_g + R_z \\ -F_{vp1} \cdot r_{7y} - F_{vp3} \cdot r_{9z} - F_g \cdot r_{gy} + M_x \\ F_{vp1} \cdot r_{7x} + F_{vp2} \cdot r_{8z} + F_g \cdot r_{gx} + M_y \\ F_{vp2} \cdot r_{8y} + F_{vp3} \cdot r_{9x} + M_z \end{bmatrix} \quad (6)$$

r_i - the vectors defining the locating points, (R_x, R_y, R_z) - components of the resultant cutting force F_c

4. EXAMPLE OF FIXTURE ANALYSIS AND OPTIMIZATION

On a milling machine it is necessary to make the slot shown in figure 1. To this end we use the milling cutter of 16 mm diameter with two cutting inserts (R-216-16 03 M-M) with the following cutting conditions: cutting speed ($v=25\text{m/min}$), feedrate ($fz=0,01\text{mm/tooth}$), cutting depth ($a=4\text{mm}$). The values of components of cutting forces ($F_a=450\text{N}$, $F_f=315\text{N}$, $F_t=810\text{N}$), the tool position, the starting positions of clamping/locating elements, the friction coefficient ($\mu=0.4$) and the workpiece weight ($F_g=47\text{N}$) are entered into the window for entering the input data.

Clamping is effected by the three clamping elements. With the upper clamping element the workpiece is clamped in module. the direction of the Z axis and with

the two side elements it is pressed along the vertical locating plane. The equation (1) assumes the form (7). The possible solutions for F_{vp_i} s are those that result in positive values of F_i s; in other words, the workpiece will remain in contact with locators during the entire cutting process.

To solve these six linear simultaneous equilibrium equations with nine unknowns, we assume that F_{vp1} , F_{vp2} and F_{vp3} have the same magnitude. Their values start from zero and are incremented by a constant value in each iteration until positive values of all F_i s are achieved.

The obtained values of F_{vp1} , F_{vp2} and F_{vp3} , which are equal to 440N will be the first set of possible solutions, which are listed as case (1) in Table 1.

Table 1 lists the reaction forces F_i ($i=1\dots6$) on the six locators and the possible solutions for F_{vp_i} s

$$\begin{bmatrix} 0,373 & 0,373 & 0,373 & -1 & -1 & 0,194 \\ 0,145 & 0,145 & 0,145 & 0,229 & 0,229 & -1 \\ 1 & 1 & 1 & -0,328 & -0,328 & -0,35 \\ 5,512 & 1,496 & 9,488 & -2,002 & -3,112 & -0,505 \\ -1496 & -6,496 & -0,696 & -0,696 & 0,385 & 1,985 \\ -1,838 & 0,384 & -2,595 & 5,623 & 9,695 & -5,958 \end{bmatrix} \begin{bmatrix} F_1 \\ F_2 \\ F_3 \\ F_4 \\ F_5 \\ F_6 \end{bmatrix} = \begin{bmatrix} 0,373 \cdot F_{vp1} + F_{vp2} + 0,194 \cdot F_{vp3} + 810 \\ 0,145 \cdot F_{vp1} + 0,328 \cdot F_{vp2} + F_{vp3} + 315 \\ -0,459 \cdot F_{vp2} - F_{vp1} - 450 + 80 \\ -6,38 \cdot F_{vp1} - 2,245 \cdot F_{vp2} - 3,336 \cdot F_{vp3} - 440,95 + 4501,57 \\ 7,034 \cdot F_{vp1} + 3,218 \cdot F_{vp2} + 1,985 \cdot F_{vp3} + 6361,4 + 359,05 \\ -1,359 \cdot F_{vp1} - 5,321 \cdot F_{vp2} + 3,825 \cdot F_{vp3} - 2910,63 \end{bmatrix} \quad (7)$$

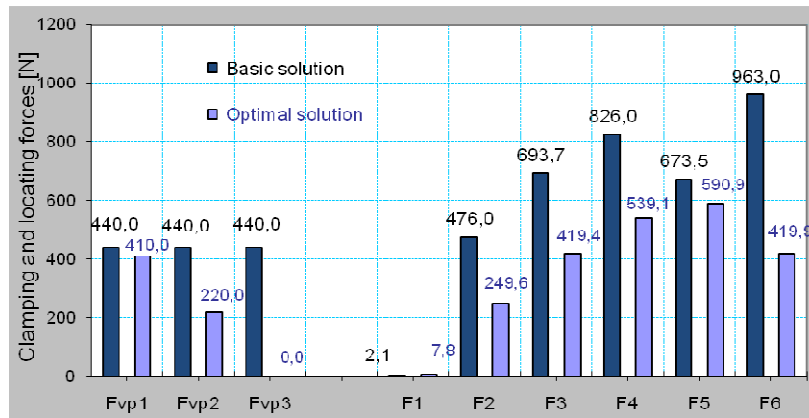


Fig. 3. Comparison of clamping cases

under different clamping conditions.

Forces [N]	(1) case	(2)	(3)	(4)	(5)
Fvp ₁	440	430	440	410	0
Fvp ₂	440	440	440	220	320
Fvp ₃	440	440	0	0	0
F ₁	2,14	0,967	125,57	7,808	0,44
F ₂	475,9	472,12	432,77	249,644	396,842
F ₃	693,7	688,765	613,25	419,354	643,647
F ₄	826,0	823,769	652,30	539,109	618,558
F ₅	673,5	672,009	761,73	590,891	564,291
F ₆	962,9	961,526	522,97	419,862	446,534

Table 1. Reaction on the locating elements for 5 cases.

The case (1) shows the first acceptable solution where all clamping forces are equal (440N). For the other cases (case 2-3) two of the clamping forces are set to value 440N, while the value of the third clamping force is gradually increased until all F_is are positive. By such procedure the value of required clamping forces is reduced. In case (3) the clamping element 3 is not necessary, since the force acting on that element is equal to 0 (Fvp₃=0). The software proposes the optimum solutions of the clamping configuration (case 4 and 5) between the user can choose. The critical point of the fixture is on the locating element 1. During machining the workpiece will first lose the contact with the clamping device just at that point (P₁). The fixture configuration can be improved by: placing on additional clamping element above the critical locating element 1, increasing the value of the clamping force Fvp₁ or changing position of the clamping element 7. With clamping force Fvp=0N up to Fvp=440N the clamping fixture configuration is not suitable for clamping of the workpiece in the given conditions of machining. The maximum loading of the clamping fixture occurs at the point of the locating element 6,

which, during machining in the locating plane XZ, takes all loadings acting in the direction of Y axis. The proposed and analyzed clamping cases (1 and 4) are shown in figure 3.

5. CONCLUSION

A force analysis module, which is a part of the developed IFS is presented that considers the effect of frictional forces for verification, rationalization and improvement of a clamping design. A new iteration method is introduced for determining the optimal clamping and locating force. By the developed module we have significantly reduced the magnitude of clamping forces. It is possible to anticipate and prevent the defects on the workpiece during the clamping and machining process. In the research it has been found out that by taking the friction into account the value of the required clamping force as well as the number of the required clamping elements are strongly decreased.

6. REFERENCES

- [1] Raghu, A., Melkote, S.N.: *Analysis of the effects of fixture clamping sequence on part location errors*, International Journal of Machine Tools and Manufacture, 44, p.p. 373-382, 2004.
- [2] Zuperl, U., Cus, F.: *Tool cutting force modeling in ball-end milling using multilevel perceptron*, International Journal of Materials Processing Technology, 153, p.p 268-275, 2004.

Authors: Assistant prof. Uros Zuperl, prof. Dr. Franci Cus, dipl. oec, University of Maribor, Faculty of Mechanical Engineering, Production Engineering Institute, Smetanova, 17, 200 Maribor, Slovenia, Phone.: +386 2 220-7621, Fax: +386 2 220-7996. E-mail: uros.zuperl@uni-mb.si franc.cus@uni-mb.si

11th INTERNATIONAL SCIENTIFIC CONFERENCE
MMA 2012 - ADVANCED PRODUCTION TECHNOLOGIES

PROCEEDINGS



Section D:
**AUTOMATIC FLEXIBLE
TECHNOLOGICAL SYSTEMS,
CA_x AND CIM PROCEDURES AND SYSTEMS**

Novi Sad, 20-21 September 2012

Andrejkovič, M., Hajduová, Z., Schwartzová, H.

USE OF OPTIMIZATION TECHNIQUES IN A SELECTED ENTERPRISE

Abstract: This contribution is aimed at the use of optimization techniques and statistical methods in a selected enterprise during the assessment of enterprise performance. The enterprise specializes in providing services, namely machinery repairs. The organization represents a small enterprise. This contribution also applies basic tools of process improvement such as Pareto analysis, Ishikawa diagram etc. We shall identify optimal solutions by means of a probability analysis.

Key words: Process, process improvement, improvement, repairs

1. INTRODUCTION

The issue of service quality improvement is currently a broadly discussed area. Today's world of growing and continuous competition among individual service providers proves that the non-existence of sufficient competition is only a desired phenomenon, in fact, almost an unreal one. This only increases the need to improve the quality of services provided and eliminate defects that may create the image of poor quality or insufficient services.

2. PROCESS IMPROVEMENT

Process improvement is hereby implemented via optimization techniques. This contribution considers the use of basic improvement tools as defined in [2] and [4]. Furthermore, the use of improvement tools is governed by the methodology of Six Sigma the aim of which is to reach the highest quality possible. Six Sigma used during this project is applied in accordance with the knowledge within the [1] and [3].

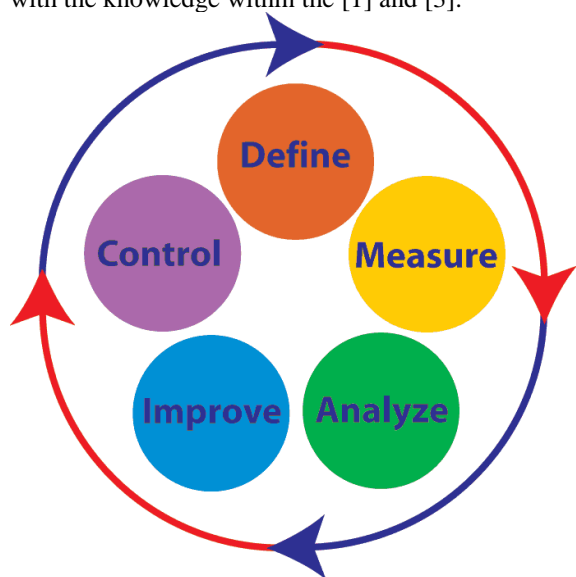


Fig. 1. Six Sigma project steps

We use the Six sigma project as is written in [1], which has five steps, which are shown in previous figure (Fig. 1).

3. IMPROVEMENT PROJECT

The analysis of processes has been aimed at the analysis of occurrence of faults and/or deficiencies. These have been understood in this case as both external faults, i.e. complaints and/or customer claims, but also as internal faults reported by the employees themselves. The above project was performed in the active collaboration with employees who made the effort to improve service quality. Thanks to this, we were able to use the information on internal faults. The process of repairs includes five steps. These stages are divided in other steps. We show only the main stream of process flow – main five steps, without the included sub-steps.

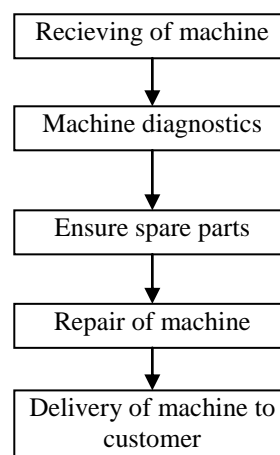


Fig. 2. Process of repairment

We can see that the highest fault ratio is when the employees have been given a time limit, i.e. they fail to repair the machinery in due time. A relatively high number of faults have also been caused by a faulty diagnostics. This reason is mutually interconnected with the previous one - due to the lack of time (time

stress) the technicians perform diagnostics very quickly and thus tend to overlook some faults that subsequently display themselves during the repair of the machinery and the repair is slowed down.

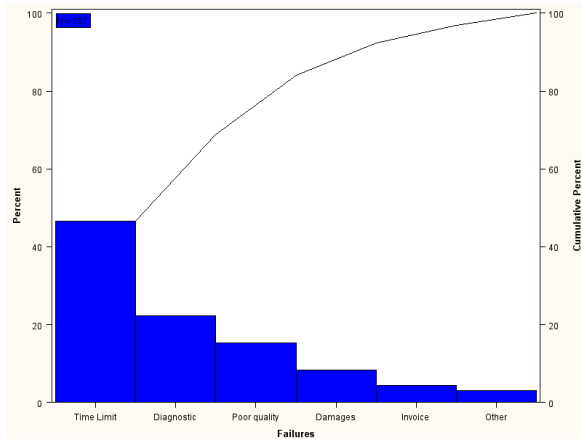


Fig. 3. Pareto diagram of faults and deficiencies

Upon the above facts we shall deal with the issue of time limit. We found out that there is the following average number of individual types of machinery per year:

	Average number of machines per year	Average time of repair
Large milling machines and grinders [LM]	285	3.486
Large lawn mowers, kärcher machinery [LL]	182	2.932
Impact drills [ID]	187	3.014
Manual drills [MD]	495	1.6
Small tools [ST]	398	1.034
Other [Ot]	283	0.97

Table 2. Structure of repairs during one year

For next analysis we need also the calculation of standard deviation. In next figure we also show the minimum and maximum time of repair.

Analysis Variable : Time			
Type	Std Dev	Minimum	Maximum
ID	1.3743444	0.4321929	5.5392149
LL	2.0716228	0.1588609	7.6882244
LM	1.4161739	1.0938968	6.5773801
MD	1.0990824	0.1282904	4.6073895
Ot	0.6900674	0.0106828	2.1288067
ST	1.0522040	0.2794638	4.2545120

Table 3. Analysis of repairs - statistical results

We also calculate the differences between type of machines and its repair time. If the average time of repairs is not statistically different, we can join these

types. But we can see that the differences are statistically significant.

Source	DF	Sum of Squares	Mean Square	F Value	Pr > F
Model	5	193.563	38.712	21.16	<.0001
Error	150	274.433	1.829		
Corrected Total	155	467.996			

R-Square	Coeff Var	Root MSE	Time Mean
0.413601	57.15102	1.352609	2.366727

Source	D F	Anova SS	Mean Square	F Value	Pr > F
Type	5	193.5635481	38.7127096	21.16	<.0001

Table 4. Anova results

Upon this information we may calculate the number of working hours the technicians need for the repair of the above machinery.

	Total number of hours per year
Big milling machines and grinders	993,51
Big lawn mowers, kärcher machinery	533,624
Impact drills	563,618
Manual drills	792
Small tools	411,532
Other	274,51

Table 5. Volume of annual working hours needed

If the changes will not be done, the company will have many claims, because they guarantee the time of repair. This time of repair is done and in case, when it is not respected, the customer pay only the amount of spare parts and the work is free. This is the reason, why the company need to solve this problem.

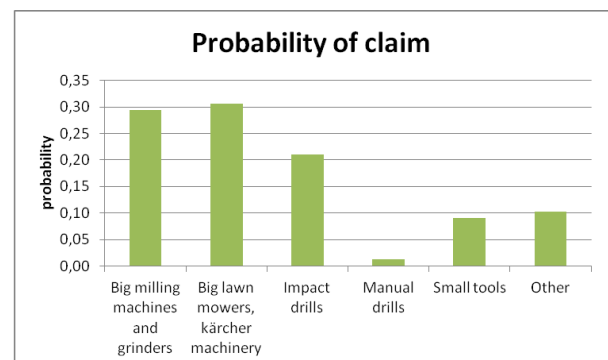


Fig. 4. Probability of claims for each type of machines

The calculation of probability of claim means the basis for next economic analysis of process results. The number of repaired pieces of machines, this probability and the average price of work create the inputs of economic model, which we should use to calculate the

estimated sum of loss from claims in case of exceed the time of repair.

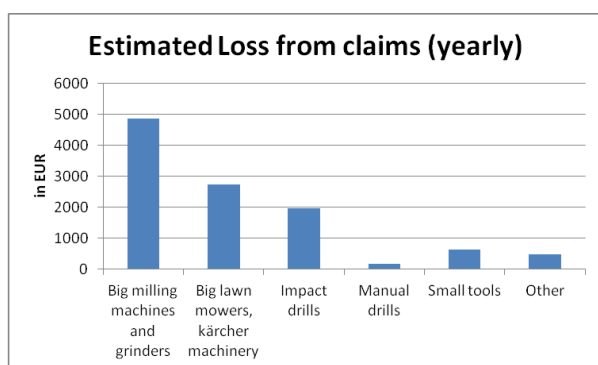


Fig. 5. Estimated loss from claims by year

The listed number of hours represents the total number of app. 3568 h/year and needs to be divided by two as there are two technicians working in the company. We need to emphasize that these times represent real time of machinery repairs including diagnostics and added times of related operations, such as receiving the broken machinery and submitting the repaired machinery to the client.

As follows from the abovementioned, on average there are approximately 1750 working hours a year for one technician, which is on the verge of the real annual working time of an employee. Therefore, there is a strong necessity to re-organize the work of technicians.

Service activities	Number of pieces per hour
Big milling machines and grinders	0,6
Big lawn mowers, kärcher machinery	0,57
Impact drills	0,42
Manual drills	0,24
Small tools	0,2
Other	0,23

Table 7. Secondary activities of workers on type of item

Service activities	Total number of hours
Big milling machines and grinders	171
Big lawn mowers, kärcher machinery	103,74
Impact drills	78,54
Manual drills	118,8
Small tools	79,6
Other	65,09
	616,77

Table 8. Calculation of working hours saved

To sum up, through the work reorganization in the sense of transfer of administrative part of repairs to the staff dealing with direct sale in the office (issuing invoice, returning machinery to the client) we managed to save the time and achieved the level of app. 616 h/year. In such case we need to employ a new technician for a half-time employment. Without reorganization we would have to employ a full-time technician. Thus, we are able to save half of wage expense.

4. CONCLUSION

This contribution describes a solution of a problem we identified in a selected enterprise in Košice dealing with providing services. With the help of improvement tools listed in the Six Sigma methodology we hereby suggest the possibility of remedying an existing defect in the above enterprise.

5. REFERENCES

- [1] El-Haik, B., Yang, K.: *Design for Six Sigma: A Roadmap For Product Development*. New York: McGraw – Hill, 2003. ISBN 0071412085
- [2] Gitlow, H. et al.: *Tools and Methods for the Improvement of Quality*, Boston: Irwin, ISBN 0-256-05680-3. 1989.
- [3] Harry, M.: *The Vision of Six Sigma*. 5. vyd. New York: Sigma Pub Co., ISBN 0-96-435557-4. 1997.
- [4] Tkáč, M.: *Štatistické riadenie kvality*, Bratislava: Ekonóm. ISBN 80-225-0145-X, 2001
- [5] Montgomery, D. C.: *Statistical Quality Control: A Modern Introduction*. New Jersey: John Wiley & Sons. 2009. ISBN 978-0-470-23397-9.
- [6] Stamatis, D. H.: *Six Sigma Fundamentals: A Complete Guide to the System, Methods, and Tools*. New York : Productivity Press. 2004. ISBN 978-1-56327-292-9.

Authors:

Ing. Marek Andrejkovič, PhD.

RNDr. Zuzana Hajduová, PhD.

University of Economy in Bratislava, Faculty of Business Economy in Košice, Department of Business Informatics and Mathematics, Tajovského 13, 041 30 Košice

Tel.: +421557223229/ +421557223227

E-mail: marek.andrejkovic@gmail.com,

zuzana.hajduova1@gmail.com

Ing. Heidi Schwarczová, PhD.

University of Central Europe in Skalica
Kráľovská 386/11, 909 01 Skalica

Tel.: +421346647061-3

E-mail: riaditel@sevs.sk

Andrejkovič, M., Hajduová, Z., Majerník, M., Bosák, M.

ASSEMBLY OF STRUCTURAL COMPONENTS OF A BUS

Abstract: This contribution deals with the optimum assembly of major structural components of a bus manufactured in Slovakia. The above structural components are presented graphically. The whole assembly of structural components is, however, subject to an approved project documentation that we are not allowed to quote in this contribution due to the protection of industrial property rights. This contribution therefore specializes only in the structural components themselves and not in the complete assembly of the bus as such.

Key words: Improvement, structural components, engineering

1. INTRODUCTION

The issue of optimization of structural components is always a current one. Lowering of costs represents the main possibility of improving the economic effectiveness of an enterprise. However, lowering of costs must not have an impact on production quality of individual products. There is a need to optimize placement of structural components that should ensure the safety of bus passengers. Apart from technical solution, it is also desirable to optimize the process of assembly, not only the product itself. From this reason, we shall describe various possibilities of construction.

2. CONSTRUCTION PROCESS

The construction process of a vehicle represents both the engineering and management issue, in which one must define the processes in the most suitable way and optimize individual steps in the production area in order to minimize costs.

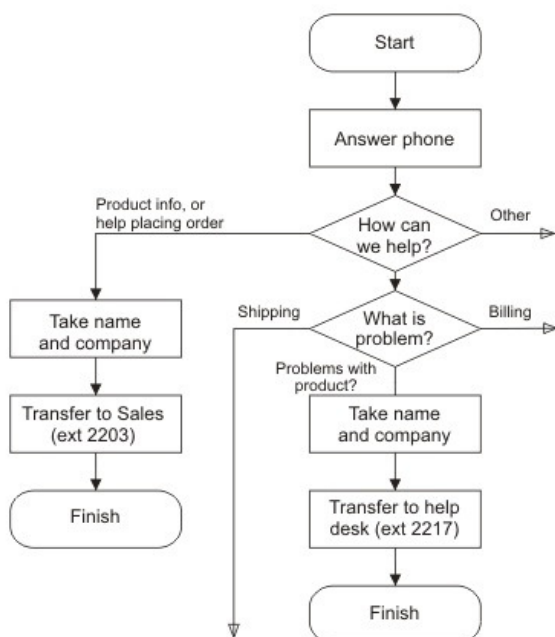


Fig. 1. Process flow diagram

The aim of the above process is to improve the method of assembly while taking into account spatial dimensions of the enterprise. The assembly takes place in a rectangle-shaped hall, where unnecessary transfers of semi-finished products occurred in the past. Results of individual production processes were manually transferred between individual places. Some of these transfers were not necessary at all [1]. Our suggestion defines two simultaneous production lines. The first one completes the body of the bus and the other one enables the chassis completion. These two components are subsequently combined in the final stage of the assembly.

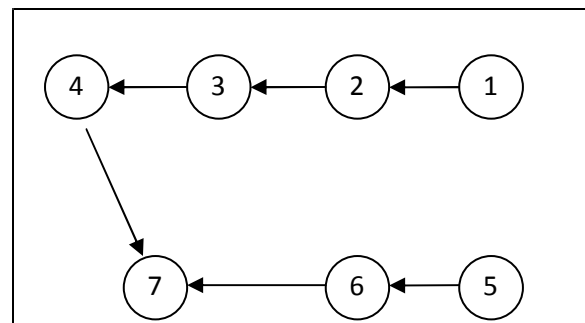


Fig. 2. Process of bus assembly

The first stage provides the selection of basic construction materials in the form of beams. Major beams are combined into larger wholes [2]. The so-called prefabricates are then utilized in the second stage of the production. In this stage, the construction of the bus is formed as we can see in Fig. 3 and Fig. 4 below.



Fig. 3. Structure of bus



Fig. 6. Complete of bus



Fig. 4. Structure of bus

Stages No.3 and No.4 enable the final arrangement of the above body that is later placed upon the individually constructed chassis. Stage No.5 is the completion of chassis, purchased from an external supplier [3]. The chassis itself must be adjusted to meet the requirements of the company and therefore needs to be fully constructed before its attachment to the body [4].



Fig. 5. The chassis of bus

The body structure is subsequently combined with the chassis in Stage No.7. This is the semi-finished product described in Fig.6.

The above alterations of production stages caused that the assembly of the bus required 10% less time. This has naturally reflected in a 7,913 % increase in profit of the enterprise when compared with the profit before the alteration of placement of production steps [5],[6].

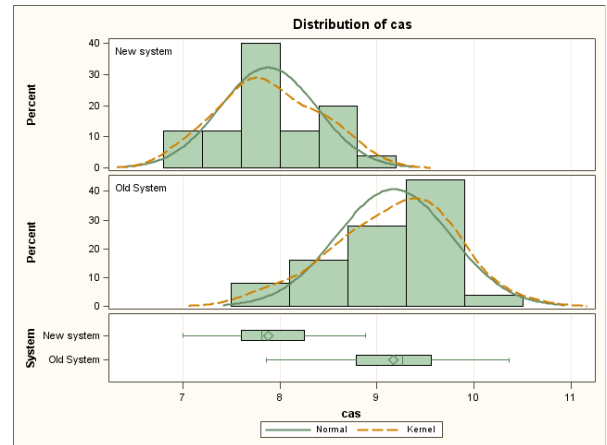


Fig. 7. Statistical analysis of assembly time

The improvement we can prove also by measured results. We use the time of assembly of bus. The time includes all steps during first works on bus till the end changes on the assembled bus. We can see the improvement about 1 day of assembly per bus.

Method	Variances	DF	t Value	Pr > t
Pooled	Equal	48	-8.41	<.0001
Satterthwaite	Unequal	46.691	-8.41	<.0001

Equality of Variances				
Method	Num DF	Den DF	F Value	Pr > F
Folded F	24	24	1.40	0.4136

Fig. 8 Statistical analysis of assembly time

The t-test shows that the difference between the time before change in assembly process and after it is statistically significant. It shows that the improvement get some positive effect on production of company.

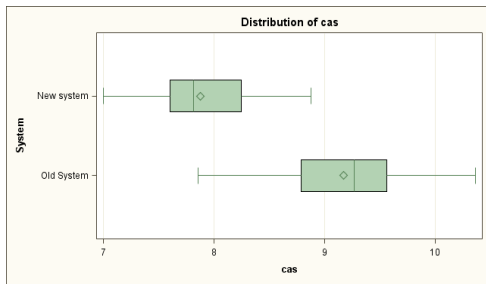


Fig. 9. Box plots of assembly time

The previous result is shown also through box plots. We can see the shift of average time of assembly process. The time is measured in days.



Fig. 10. Semi-product in assembly process

The assembly process continues after the assembly of the skeleton of bus. In next step the bodywork will be picked up on the skeleton.



Fig. 11. Semi-product in assembly process



Fig. 12. Semi-product in assembly process

After the all steps of assembly process the bus is prepared for testing. The bus look like is shown in next figure.



Fig. 13. Semi-product in assembly process

3. CONCLUSION

In conclusion, we may say that the evaluation of quality represents the borderline that enables the limitation of costs. The aim of the enterprise is to minimize production costs, while retaining the defined quality level. The optimization is possible with regard to the length of assembly time and amount of material needed for individual semi-finished products.

4. REFERENCES

- [1] El-haik, B. Yang., K.: *Design for Six Sigma: A Roadmap For Product Development*. New York: McGraw – Hill, 2003. ISBN 0071412085. Internal documentation of company, 2012
- [2] Stamatis, D. H.: *Six Sigma Fundamentals: A Complete Guide to the System, Methods, and Tools*. New York : Productivity Press. ISBN 978-1-56327-292-9, 2004.
- [3] Altair. *HyperWorks Optistruct tutorial*. <http://www.altairhyperworks.com/onlinelearning/interactivetutorials.aspx?AspxAutoDetectCookiSupport=1>
- [4] Sloboda, A.: *Konštrukcia automobilov 1* 1. vyd. Košice : Sjf TU - 402 s. - ISBN 80-8073-718-5, 2009.
- [5] Piša J., Roob J.: *Konštruovanie dopravných prostriedkov - využitím metód optimalizačných metód*, In: Transfer. Roč. 2, č. 1 (2010), s. 22-23. - ISSN 1337-9747, 2010.

Authors:

RNDr. Zuzana Hajduová, PhD.

Ing. Marek Andrejkovič, PhD.

University of Economics in Bratislava

The Faculty of Business Economics with seat in Košice

Tajovského 13, 041 30 Košice, Slovak Republic

E-mail: marek.andrejkovic@gmail.com

zuzana.hajduova1@gmail.com

Prof.h.c. Ing. Martin Bosák, PhD.

Prof.h.c. prof. Ing. Milan Majerník, PhD.

Technical University in Košice

Faculty of Mechanical Engineering

Letná 9, 042 00 Košice, Slovak Republic

E-mail: Martin.Bosak@tuke.sk

milan.majernik@tuke.sk

Bojanić, M., Tabaković, S., Milojević, Z., Zeljković, M.

PROCESSING OF DIAGNOSTIC IMAGES OF THE SKELETAL SYSTEM

Abstract: *Methods of imagining that are now widespread in the medical diagnosis include different methods of scanning are made in order to obtain images of inner structures of the human body. As a result, it usually gets a series of monochrome digital images. Different mathematical operations by which the desired components are extracted for processing of them are used. This paper presents a global procedure for processing of tomography images as well as generally accepted algorithms that allow for easier and better segmentation and spatial reconstruction of bone. That is presented using a scans of the upper half of the femur in order to develop the body of the hip endoprosthesis made to measure.*

Key words: *Medical Imaging, Segmentation, Femur, Endoprosthesis*

1. INTRODUCTION

Images obtained by computerized methods of scanning are a series of digital images that are displayed in parallel planes cross-section the scanning object [8]. Among other things, these images can be used for the spatial reconstruction of the scanning object, which in this work is shown on the example of the femur.

All data from a digital image is collected in a certain format. These formats must be recognizable in communication between different computers, which have been developed in different image formats in medicine, commonly used DICOM (Digital Imaging and Communication in Medicine).

This paper describes the spatial reconstruction of skeleton based on a series of images in DICOM format, the image reconstruction of the upper half of the femur to the hip joint prosthesis design to measure. The process consists of several stages, the most important stages is the identification of different tissues and organs. To identify the different tissues, it is necessary to process image segmentation.

The process of reconstruction of the shape and geometry of the femur on the basis of diagnostic images is one of the most important phases in the design process arthroplasty of the hip joint, which is treated with a range of defects that occur in it [9]. The most common complications of the hip joint are caused by injury, degenerative changes or malignant diseases.

2. TOMOGRAPHIC METHODS OF SCANNING

Diagnostic scanning techniques include radiological diagnostics that shows cross-sections of the body in layers of specified thickness. Imaging methods that are used in this field are divided into digital and analog. Nowadays, of analog methods used X-ray imaging technique (Rtg) and ultrasound scanning with the possibility of digitization. From digital methods are commonly used tomography methods in which the diagnosis of diseases in addition to images can be used for the spatial reconstruction of the scanning object [8].

Tomography is a method of generating 2D cross-sectional image of the body [9]. The best-known tomography methods are:

- ❖ computed tomography (CT), where the image gets X-rays, and
- ❖ magnetic resonance imaging (MRI), in which the images obtained under the influence of a magnetic field oriented.

CT (Computed Tomography) systems make images on a morphological level (anatomical). In these images, are different organs and tissues which have an unequal absorption coefficient of X-rays and on these images can see the value of the absorption coefficient, X-rays, tissue. In CT images can be seen to change the structure or anatomy, which occurred due to the disease. The functional state of these organs cannot be concluded. For example, a CT scan of the brain of the living and the dead man (just after he died) is exactly the same. In Fig. 1, see the first CT scanner, CT scanner the new generation and CT image.



Fig. 1. The first CT scanner, CT scanner the new generation and CT image

The advantages of CT scanners have a clear picture, easy to diagnose (especially bones), as well as its price, and is available in many medical centers. It is possible to scan and built-in patients with any type of implant. The main disadvantage is exposure to harmful X-rays absorbed by the patient during the scanning.

MRI systems (Magnetic Resonance Imaging) provide medical generate certain physical characteristics of the tissue. MRI can visualize different properties of tissue, blood flow and multiple physiological and metabolic functions. MRI imaging may be made in the presence of contrasting agents. Gadolinium based substances (which also gives a strong signal MRI) provides better discrimination of

healthy from diseased tissue. It should be noted that the MRI is based on the effect of nuclear magnetic resonance, and that the principles of image generation tomography image different than that of CT. In Fig. 2, there is an MRI device, and series of images.

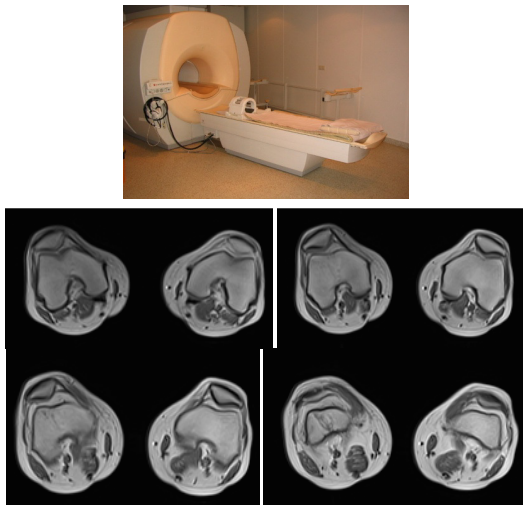


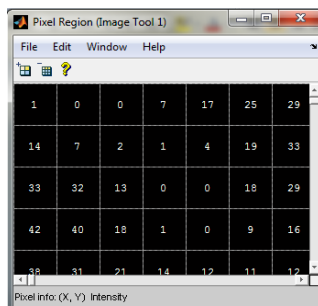
Fig. 2. MRI device and a series of images obtained on it

The main advantage of MRI is the absence of harmful radiation, they use magnetic fields and radio waves, as opposed to the CT scanner. The benefits include more detailed view of the soft tissue in the patient's body. One disadvantages of allocated cost of equipment, scan length and inability to scan some patients with ferromagnetic implants, because the magnetic field can cause the implant movement.

3. PROCESSING DIAGNOSTIC IMAGES

Processing of diagnostic images of the skeletal system in order to obtain a computer model consists of several stages which show the Fig. 3.

Images generated on CT/MRI devices can be saved in different resolutions. Most often used resolution is 512x512 pixels. Each pixel of the image obtained in this way can have a shade of gray, the 12-bit palette (4096 colors).



a)

	1	2	3	4	5
1	1	0	0	7	17
2	14	7	2	1	4
3	33	32	13	0	0
4	42	40	18	1	0
5	38	31	21	14	12
6	31	26	34	40	32
7	25	29	46	50	38
8	25	25	32	33	32
9	27	15	11	14	31
10	31	19	8	12	35

b)

Fig. 4. Matrix display image

Segmentation, for example, in a typical task of identifying objects (organs), the basic step, and sharing

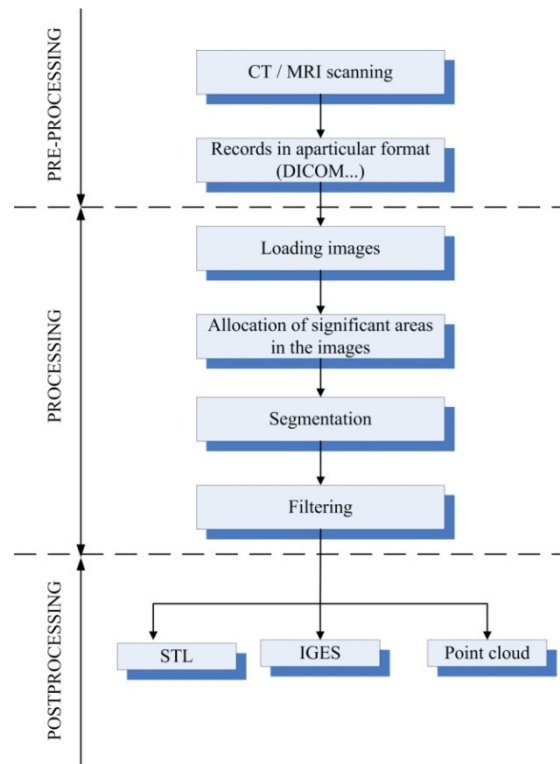


Fig. 3. Stages of obtaining a computerized model

Images obtained on the basis of tomography methods are a series of images that are displayed in parallel planes of intersection of the scanned object. To successfully separate an area that is of interest for the reconstruction of geometry is necessary to make the segmentation of different tissues in the images and translate them into a spatial model. Segmentation involves identifying areas that belong to the corresponding length bodies [7].

In digital image processing using different mathematical operations which are used to receive appropriate modifications initial image. The program for digital image processing, images saved as a matrix. Each pixel on it corresponds to a member of the matrix, as can be seen in Fig. 4. In Fig. 4a is a part enlarged image (see the pixels), and in Fig. 4b of the matrix. Comparing pixel values contrasts with the values of the matrix, it can be concluded that these are the same numbers, the same images.

images on the edges that correspond to different objects. Edge of the image is the boundary or contour which leads to significant changes in some of the physical aspects of the image, such as surface

reflection, illumination and distance of the visible surface of the beholder. Changes in the physical aspect of the image are manifested in the form of changes in the intensity, color and structure of the image.

Image processing can be used a number of software systems both general and specialized applications. The research activities of the most commonly used program system MATLAB. In it, there are several methods for detecting edges:

- ❖ Sobel method
- ❖ Prewitt method
- ❖ Roberts method
- ❖ Laplacian of Gaussian method
- ❖ Zero-cross method
- ❖ Canny method

All of these methods are used to detect edges and intensity images as input. In places where are edges, the matrix element is assigned a value of 1, and in places where are no 0.

The Sobel method finds edges using the Sobel approximation to the derivative. It returns edges at those points where the gradient of image is maximum.

The Prewitt method finds edges using the Prewitt approximation to the derivative. She also returns edges at those points where the gradient of image is maximum.

Similarly to the previous two the Roberts method finds edges using the Roberts approximation to the derivative. It returns edges at those points where the gradient of image is maximum.

The Laplacian of Gaussian method finds edges by looking for zero crossings after filtering image with a Laplacian of Gaussian filter.

The zero-cross method finds edges by looking for zero crossings after filtering with a filter you specify.

The Canny method finds edges by looking for local maxima of the gradient image. The gradient is calculated using the derivative of a Gaussian filter. The method uses two thresholds, to detect strong and weak edges, and includes the weak edges in the output only if they are connected to strong edges. This method is therefore less likely than the others to be fooled by noise, and more likely to detect true weak edges.

In Fig. 5 is presented edge detection methods listed in the example CT scan of the femur.

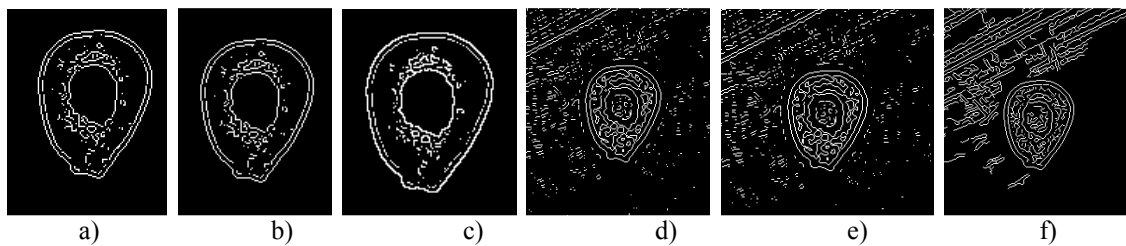


Fig. 5. Edge detection on CT scans of the femur: a) Sobel b) Prewitt c) Roberts d) Laplacian of Gaussian method e) Zero-cross and f) Canny method

Depending on the needs of digital image processing (tomography images) depends on the method to be used.

The need for segmentation of the femur, it is clear from Fig. 5, that the best of the first three methods, because they do not noise, as well as the surrounding organs and tissues.

In commercial applications, such as Mimics, Scan IP, Amira, 3D Doctor, etc. segmentation is not done in detail, edge detection, but uses upper and lower limits of contrast pixels (Tresholding) in the images.

In the example shown below (Fig.6) is a generally accepted method used to define the boundaries of the segmentation (Tresholding). Contrast values for the pixels in the image corresponding tissues are known, and this method can be used for automatic segmentation of a series of images. The main disadvantage of this method is the disconnect between the selected pixels, so it happens that other organs are affected. In such cases it can be done manually remove unwanted pixels, image by image, which is time-

consuming.

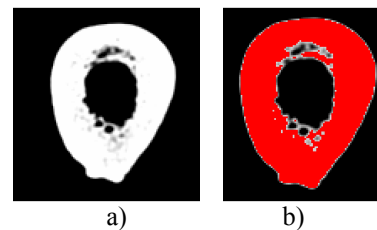


Fig. 6. Segmentation of the femur

After segmentation and removing unwanted pixels, the model contains surface irregularities with cavities and sharp edges, so it is necessary to correct them to filter. Fig. 7 shows the generation of a computer model of the femur, which includes segmentation (Fig. 7a), the translation of surface elements-pixels, voxel-volume elements (Fig. 7b) and filtering, which includes closing surface (Fig. 7c), rounded surfaces taking into account topology and volume model (Fig. 7d) and rounding using Gaussian filter (Fig. 7e) [8].

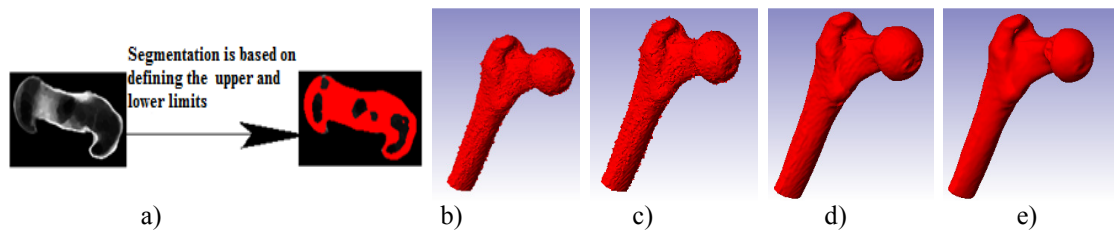


Fig. 7. The process of generating a computer model of the femur

After defining the computer model, the conversion is done in a variety of file formats geometric data of which the most common are: IGES, STEP, STL, and point cloud.

Femur model in Fig. 7e, formed reconstruction CT image for the design total hip to measures of patient. In Fig. 8 is shown the circuit reconstructed femoral prosthesis embedded tumor developed in her.



Fig. 8. Model incorporating femur tumor endoprosthesis [9]

4. CONCLUSION

This paper describes the most commonly applied methods of scanning tomography (CT and MRI) that produce a series of digital images of the internal structure of the human body. Modern tomography scanning provides high reliability in addition to the diagnosis of disease and the formation of spatial computing model.

In the spatial reconstruction of the skeletal elements of the system, one of the most important phases of a procedure for processing images. Depending on the obtained computational models, the shape of orthopedic implants requires greater accuracy, due to the production of better implants that fit the patient's anatomy. This is expressed in the design and production of typical implants and custom made implants. For typical implants, among other things, are important ethnic and age groups.

Contemporary research in medical imaging processing flow in several directions including: training tomography imaging method to get as clear a picture, digital image processing and reconstruction of surfaces in order to increase the accuracy of computer models.

5. REFERENCES

- [1] Baka, N., Kaptein, B. L., de Bruijne, M., van Walsum, T., Giphart, J. E., Niessen, W. J., Lelieveldt, B. P. F.: 2D–3D shape reconstruction of the distal femur from stereo X-ray imaging using statistical shape models, *Medical Image Analysis*, ISSN 1361-8415, Volume 15, Issue 6, Pages 840-850, 2011.
- [2] Biedert, R., Sigg, A., Gal, I., Gerber, H.: 3D representation of the surface topography of normal and dysplastic trochleausing MRI, *The Knee*, ISSN 0968-0160, Vol. 18, Issue 5, Pages 340-346, 2011.

- [3] Cahir, J., Toms, A., Marshall, T., Wimhurst, J., Nolan, J.: CT and MRI of hip arthroplasty, *Clinical Radiology*, ISSN: 0009-9260, Volume 62, Issue 12, Pages 1163-1171, 2007.
- [4] Fritscher, K.D., Grünerbl, A., Schubert, S.: 3D image segmentation using combined shape-intensity prior models, *International Journal of Computer Assisted Radiology and Surgery*, Volume 1, Number 6, ISSN 11548-007-0070-z, Pages 341–350, 2007
- [5] <http://www.mathworks.com/help/toolbox/images/ref/edge.html>, 10.08.2012.
- [6] Miller, T.: Imaging of hip arthroplasty, *European Journal of Radiology*, accepted for publication, 2011.
- [7] Milojević, Z., Tabaković, S., Navalusić, S., Zeljković, M., Vičević, M.: New methods of analysis and processing diagnostic images obtained by MRI and CT recording methods of bone tissue (in Serbian), A study of the project TR 35025, Faculty of Technical Sciences, Novi Sad, 2011, 19 pages
- [8] Tabaković, S., Bojanić, M., Milojević, Z., Živković, A.: Modeling of elements of skeleton systems based on medical images (in Serbian), *Proceedings, 38. JUPITER Conference, 25. Symposium CAD/CAM, Faculty of Mechanical Engineering, Belgrade*, ISBN 978-86-7083-757-7, Pages 2.39-2.44, 2012.
- [9] Tabaković, S., Grujić, J., Bojanić, M., Zeljković, M., Sekulić, J.: Modeling medullar canal of the femur based on a digital signal from CT or MRI in order to dimensioning stem tumor endoprosthesis of the hip joint (in Serbian), *Proceedings, Scientific Symposium on Information Technology-Infoteh, Jahorina*, ISBN 99938-624-2-8, Pages 2.39-2.44, 2012.

Authors: MSc. Mirjana Bojanić, Doc. Dr. Slobodan Tabaković, Doc. Dr. Zoran Milojević, Prof. Dr. Milan Zeljković, University of Novi Sad, Faculty of Technical Sciences, Department of Production Engineering, Trg Dositeja Obradovica 6, 21000 Novi Sad, Serbia, Phone.: +381 21 485-2345.
E-mail: bojanicm@uns.ac.rs; tabak@uns.ac.rs; zormil@uns.ac.rs; milanz@uns.ac.rs

NOTE:

The work is part of a research project on "Modern approaches to the development of special bearings in mechanical engineering and medical prosthetics," TR 35025, supported by the Ministry of Education and Science, Republic of Serbia.

Erić, M., Tadić, B., Stefanović, M., Miljanić D.

MODEL OF REENGINEERING OF TECHNOLOGICAL PROCESSES - ITERATIVE AND VISUAL APPROACH

Abstract: Shortening of the life-cycle for products and technologies as well as the growing competition at the market are characteristics of modern industrial development with which production companies are dealing with today. We are witnesses that nowadays market games start and finish with the "three". That "three" is quick, quality and cheap. The answer to the question "How to make this three?" beside other, can be found in reengineering of technological processes. Characteristics of the technological process as logical, iterative, variant and multidimensional process represented basis for making methodology and information model of reengineering of technological processes. This paper deals with architecture of methodology that is with model of reengineering of technological processes, main approaches at the model as well as its outputs.

Key words: Model, methodology, reengineering, technological processes, information technology

1. INTRODUCTION

Technological environment is the constant technological changes which points are the new engineering and technological knowledge of producing more with the available amount of resources or production data achieved with fewer resources used. This is expressed through shortening of development time, lower costs, more efficient use of funds, materials and optimization of the flow of information and so on.

In order to achieve the above mentioned requirements, among the other things, required is the development of new technologies (and this is primarily an IT supported technology). Regarding it is necessary to shorten the time that lapses from idea to realization of a new product, considered the possibilities of so-called "savings in time" through technological processes and through the process of their design. The concept of the model includes the process of re-engineering (referring to the process of modeling technological processes), notation and tools for modeling. It is clear that all three components are complex. But today, there are more information tools that can help us in every aspect of the development process. In addition, the standards in the methods and computer tools are widely accepted, which makes it possible to put emphasis on the development and implementation.

In order to successfully implement the concept of reengineering and developed an appropriate model must be carried out analysis of the technological process, in terms of flexibility, level of automation, product quality, type of production, the flow of technological processes, relationship with the environment, structure, relationship (connection) elements of the technological process. Reengineering of technological processes are re-thinking on focusing of the process, thereby eliminating the processes and sub processes that are not necessary, and thereby finding more efficient ways of performing the remaining process. Reengineering is focused on

improving the existing system (process) with a high return on investment than it would have been the case for investing in a completely new development.

Reengineering of technological processes, directly or indirectly, should make possible: the reduction of delivery time, price cutback products, improving product quality, easier maintenance and cheaper products, and environmental protection. Also, process reengineering technology should ensure the possibility of increasing production volume.

The model should enable reengineering of redesign of the existing technological processes with all the above mentioned aspects and to give a solution for the improvement of technological processes. The model allows the reengineering and development of new technological processes based on re-engineering of existing (piggybacking), Fig. 1.

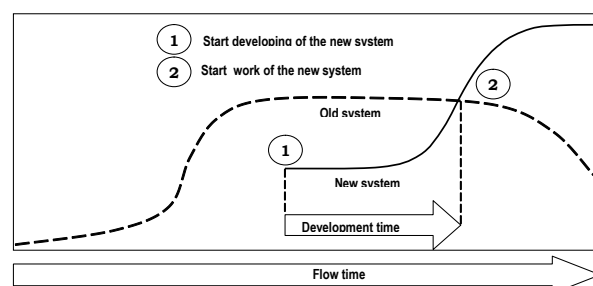


Fig. 1. Piggybacking systems [3]

Piggybacking is not a professional, sophisticated expression, nor is it the unique in the field of the system. And yet, it is a very exact picture of a system that uses the previous system to step into a more advanced status. The concept of piggybacking forced designers, developers and technologists to regularly and continuously reflect on the success of existing, and developing new systems based on the existing one. As such, it requires the application of certain conceptual estimate, such as: (1) when the existing system deteriorates, therefore, it is estimation of life of the

system, (2) how long it will take to develop a new system, and (3) when you should start with the development of the new system.

For the analysis of technological systems (processes) is used a systematic approach. As in nature and society there is a general correlation of objects and phenomena, it is necessary during the observation of any system to perform its elimination of the outside. The technological process of making the product is part of the production process in which the change is in shape, size, aesthetic appearance, the internal properties of materials, and controls, which set the conditions for giving the best technical and economic effects [9]. Before the technological process are set three kinds of requirements must be satisfied. Technical requirements, as a starting point, are arising from the construction documents and functions of individual pieces. These are primarily the shape, tolerance of dimensions, machined surface quality, composition and etc. Another type of request, are economic requirements. It is necessary to achieve the technical requirements and achieve the lowest cost. For optimal design of technological processes and the optimal variant, it is often necessary to compare more economic options, as is generally possible to produce several alternatives of the same product. This way of looking at the technological process and making it, is a variable.

A new, almost daily, knowledge related to engineering and technology has helped to set up a technological process is a subject of changes. This requires engineers to constantly monitor and extend their knowledge of new technological knowledge of the design, so they could be applied on technological processes. One of the engineers task is to constantly improve the technological process. It can be argued that technological process has never been so well designed that it cannot be designed better. This constant review and improvement of technological processes, both in the design phase and development phase of implementation as well as making it iterative.

2. PROPOSED METHODOLOGY REENGINEERING OF TECHNOLOGICAL PROCESSES

Theoretical analysis of the technological process and reengineering, discussed through the "magnifying glass" of principles, approaches and methods of modeling processes and systems are induced reengineering methodology for technological processes, Fig. 2.

The structure of shown methodology is in two parts, CAD and CAPP's. The base of on the CAD parts models and CAD is following: 3D model of part/products, 2D geometric model of parametric, parameter technological model, meta model. CAD models are defined in CAD software (Pro/Engineer, CATIA, AutoCAD, Mechanical Desktop, Solid Works, etc.). 3D model, as a result of a process design and modeling, and the target model as a result of the technological transformation of the model, is the model inputs and technological reengineering process. Target content model carries the same information that is

necessary to define the technological operations and procedures as well as the technological model.

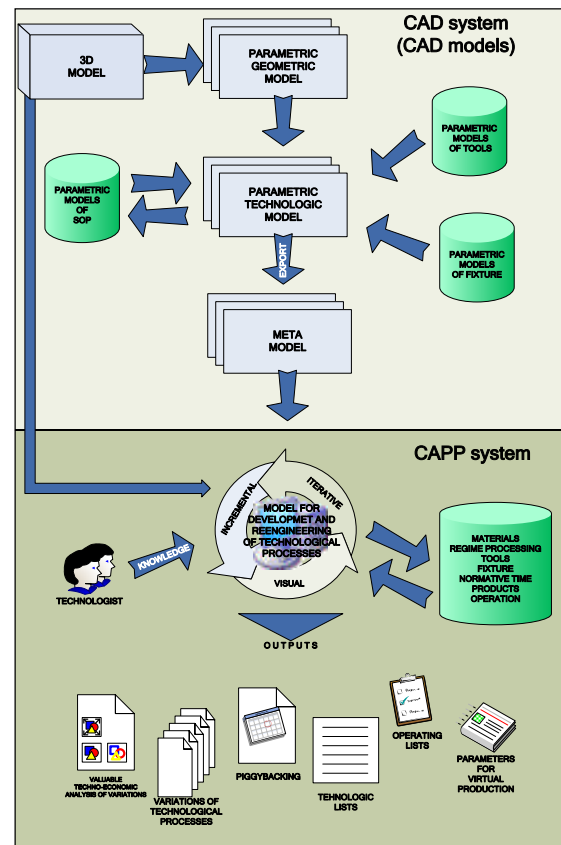


Fig. 2. Architecture Methodology (re)engineering of technological processes [2]

The difference is "only" in the way the information was presented, meta model is in the field of disperse and technology model in the field of vectors. The advantage of vector in the domain changes (modify mode), and the advantage of the raster domain is taking dramatically less storage space (file compression). The advantage of the target model is utilized for visual modeling and composition of technological processes.

The technological model is defined on the basis of geometric models, by adding parametric models tools and if necessary and parametric models of support equipment. The mentioned models are 2D models. At the level of technology CAD model can correspond with the base model by type parametric procedures. In this case, the model of type covers and declares the model and defines the technological model stored in the database as a standardized (standard or group).

All mentioned models in the CAD system have shown the methodology prefix parameter. And in any case should take advantage afforded by parametric modeling, that is, the dimensions defined by the parameters and their values for some of the variations of the model, are stored in appropriate databases. Target model as input into the model for the reengineering and technological processes, must be defined with specific values from the database. Target allocation model also gives an overview or topology elements of the technological process/system.

Entry for the model reengineering and

technological processes that can be used for development/engineering and technological processes is the technology and database-related materials, modes of processing, cutting tools, measuring tools, ancillary supplies, regulations, time, products, operations, etc. Reengineering model for technological processes belongs to CAPP shown methodology. The model enables technology, based on the knowledge and experience gained visual, iterative and incremental approach to implement process reengineering and technological processes.

3. ITERATIVE, INCREMENTAL AND VISUAL APPROACH IN THE REENGINEERING MODEL OF TECHNOLOGICAL PROCESS

Basically, reengineering, in its essence, is the development. The development, which in the iterative and incremental life cycle (Fig. 3), runs in a series of successive iterations, that evolves into the final system, a variant/scenario/alternative or solution. Each of these iterations is composed of changes in one or more components that are declared as "entering" of the technological process.

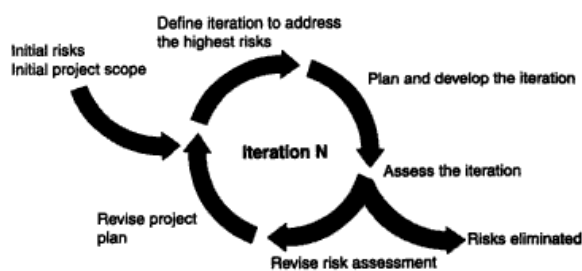


Fig. 3. Iterative and incremental development [5]

Variations in parameter values that are found in some limits (e.g., treatment regimes), the changes in relations between elements of technological processes (e.g. changes in operations or concentration Ordering/differentiation operations), the use of specially designed accessories, or group and aggregated, implementation of special and standard cutting tools provide a designer-technologist opportunity for many assumptions and dilemmas. Assumptions and dilemmas carry the risk in the sense that this variant is not the one that is the most optimal.

All the dilemmas and challenges encountered by designer-technologist in the election of certain options are being resolved so that we must rely on a metric, on which the valuation is the same. The most commonly adopted metric or the system of evaluation is a particular monetary unit.

Iteration planning process should enable the controlled and reasonable number of iterations. By the end of each iteration risks should be re-assessed, and the impact of changing parameters. After that iteration, a variant of the technological process will occur, and their number depends on the evaluation and the knowledge and experience of the designer-engineers.

Output parameters of the model (ordered time, productivity and cost of processing), designer-technologist should be provided by valuable analysis of

the alternatives on the basis of their decision on the final version, version in which the largest number of requests are satisfied.

This type of life cycle is the process of reducing risk. In the early stages of life cycle is assessed the technical risks and gives them priority, and after finishing it during each iteration. Risks are considered in each of this iteration, so that successful completion of iteration minimizes the risks discussed. Variations are also planning to process initially the greatest risks. This method exposes a system and reduces the risks in the system early in the life cycle. The result of this approach, in the life cycle, is decreased risk with minimal investment.

Development of life cycle has an opportunity to give creativity and innovativeness of architects-engineers. At the same time the development process must be measured and controlled in order to ensure successful completion of design. Well-managed iterative and incremental life cycle provides the necessary control and no violation of creativity.

Visual modeling is the process of taking information from the models and their graphical display using a series of standard graphic elements. Standards are necessary in order to benefit from significant drew Modeling communication. Communication between all users of the model and all those involved in designing, modeling and design, is the main purpose of visual modeling.

Three important components for successful implementation of visual modeling are notation, process and tool.

Notation can be learnt, but if you do not know how to use (process), success is likely to be absent. One can have a great process, but if you do not know how to express it (notation), also will not succeed. And finally, if you cannot document the results of their work (tool), you probably will not succeed.

In the model of technological process re-engineering notation is defined meta-model technology. This model represents the topology elements technological processes, tools and case processing at the level of operations/procedures and the building is in the graphic notation of visual modeling of technological processes. Process or function "drag and drop" it is possible to change the place of the object, and thus change the order of operations/procedures in the technological process. The same function can compose a new technological process based on the current, "piggybacking." The function and mechanism of "drag and drop" is a complete system to move through made moves, keeping certain phases of the possibility of changing the future using the past to the present. Results of visual modeling are documented through the technological and operational lists.

4. OUTPUTS MODEL OF TECHNOLOGICAL PROCESSES REENGINEERING

Published models of re-engineering and technological processes are variations of the technological process, piggybacking, technological exchange (treatment plan), operating the list, the

parameters for the valuable techno-economic analysis of the variations, the parameters for virtual manufacturing.

Variations of technological processes (TP) arise as a result of a large number of possible combinations of input parameters, and their relations (order), which differently affect the output characteristics of the technological process. For a TP, in theory can be defined a number of variants.

The concept of "piggybacking" is shown with the basic idea of the development of new technological process based on the current (Fig. 4). It can be applied in the case of products which have a technological resemblance. To the already established structures - target models, the function "drag and drop" used to compose a new technological process. It can be applied in case of rough estimates of development time or cost of treatment, when there is no time to make detailed models of the new technology of similar products. Created a new technological process can be subjected to change and reengineering, which in most cases it is.

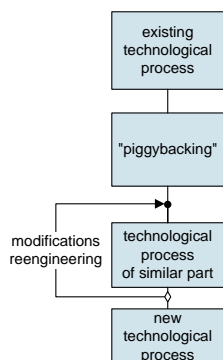


Fig. 4. "Piggybacking" technological processes [3]

Technological exchange and operating lists, as integral technological documents, are the output reports the technological model of technological reengineering process. They are defined based on the structure and content of coating. Technological exchange is a treatment plan and sequence, and one of the basic operating document preparation technologies of production, operating list is the basic document technological workplace.

Parameters for the valuable techno-economic analysis of alternatives were chosen so that it can be calculated based on the input parameters (parameters of the regime of processing the order and concentration of operations, standards of time, parameters related to cutting tools, equipment and machine tools) that directly affect the technological process. Fee, time and productivity are drafting the output parameters that need to complete a picture of the technological process variations. Based on this assessment, personal experience and evaluation, the designer-technologist decides on a final version that will be implemented.

Parameters for virtual production are possible outputs from the model re-engineering and technological processes. The final defined version of the technological process before implementing in production can be simulated in software (DELMIA), which supports the concept of virtual manufacturing.

For the simulation of production, among others, are required also parameters which define the technological process and are in the base model of technological re-engineering process. Thus, the concept of virtual manufacturing is another level that makes it possible to detect an error, try variations, improve processes, and verify the optimality of the adopted parameter values before technological implementation process.

5. CONCLUSION

We present the methodology and software solution, to support the design and engineering and technological re-engineering processes, and they have four main objectives: (1) reduction of manual work during the preparation of technological process, which is a burden for the manufacturing engineers and experienced designers of technological processes, (2) improving / optimization of existing technological processes through the use of available information on machinery, tools, accessories, workability, and so on., (3) systematization of the best observed technological processes for families of components within the enterprise, providing the knowledge and experience of experienced designers, (4) systematization of production time and costs as a presumption for techno-economic analysis.

Advantages of the system, which allows the design of new and reengineering of existing technological processes, are: reduction of time planning, design and lower costs of production, enabled the creation of technological processes of the same validity and quality; rationally production of technological processes, increased productivity etc.

6. REFERENCES

- [1] Burke G., Peppard J.: *Examining Process Reengineering*, Kogan Page, 1995.
- [2] Erić M.: *Model reinženjeringa tehnoloških procesa malih preduzeća*, doktorska disertacija, Mašinski fakultet Kragujevac, 2007.
- [3] Luhman N.: *Teorija sistema*, ΠΛΑΤΩ, Beograd, 1998.
- [4] Stein R.: *Re-engineering the manufacturing system – Applying the theory of constraints*, Marcel Dekker, Inc., New York, 1996.
- [5] Quatrani T.: *Visual Modeling with Rational Rose 2002 and UML*, Addison-Wesley, Boston, 2003.
- [6] Todić V.: *Projektovanje tehnoloških procesa*, Fakultet tehničkih nauka, Novi Sad, 2004.

Authors: Ph.D. Milan Erić, Ph.D. Branko Tadić, Ph.D. Miladin Stefanović, University of Kragujevac, Faculty of Engineering, Sestre Janjić 6, 34000 Kragujevac, Serbia, Phone: +381 34 335-990.

MSc Dragomir Miljanić, Metalik DOO, Trebjeska 6/26, 81400 Niksic, Montenegro, Phone: +382 68 026-025.

E-mail: ericm@kg.ac.rs,
btadic@kg.ac.rs,
miladin@kg.ac.rs
metalik@t-com.me

Fuerstner, I., Gogolak, L., Nemedi, I.

DIFFERENT SOLUTIONS FOR A SPECIFIC MECHATRONICS PROJECT

Abstract: Many projects in mechatronics can be solved in several different ways. The nearly infinite number of solutions is usually limited by constraints as defined by both the purchaser and the supplier of the final product. The paper presents the results of a project that was prepared by third-year students of mechatronics at Subotica Tech. The paper includes the detailed description of the project task. Different solution concepts will be explored with special focus on the various final solutions. A brief comparison of the different solutions will also be given.

Key words: Mechatronics, Product Development, Product Solutions

1. INTRODUCTION

Mechatronics is one of the most popular technical disciplines in the 21st century. It is a multidiscipline science which consists of three main disciplines: electrical engineering, mechanical engineering and information technology [1]. The basic idea of creating this discipline was to satisfy the industrial requirements, since the industry is in need of engineers who have competence in all of these three disciplines.

In mechatronics all of the important and fundamental contents from the above mentioned disciplines are summarized (Fig. 1.). The aim is to achieve practical knowledge which is used in engineering. The combined knowledge in mechatronics allows engineers to think from another perspective. Engineers of mechatronics have different technical intelligence than other colleagues. They can use and combine knowledge from the field of mechanics, electronics, robotics, programming, control systems, CAD/CAM systems, manufacturing and so on. This competence is mainly applied in the field of manufacturing system design and system integration, from small and simple systems to complex manufacturing-assembly systems [2].

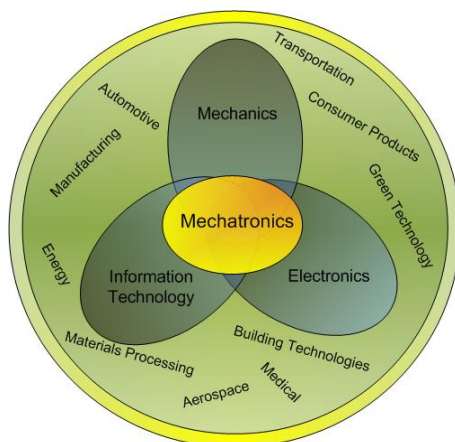


Fig. 1. Mechatronics

The first level and basic task in mechatronics is designing and modeling systems. According to the actual trend, modeling should be done in 3D drawing

software. Standard mechanical elements must be known to design the model of the systems. Accordingly, this level involves knowledge from the field of mechanical engineering. Furthermore, all systems, from the smallest to the biggest ones, contain sensors and actuators as their components. Knowledge from the field of mechanical and electrical engineering is necessary in this next level of mechatronics engineering, for choosing and using these components. Finally, the highest level of mechatronics is applying control systems, which involves programming and competence in information technology. Mechatronics engineers have an insight on each and every element of the system. They are capable of imaging, designing, integrating and implementing the system from the beginning to the end.

At Subotica Tech – College of Applied Sciences, Engineers of mechatronics are educated, to fulfill the need of the industry for this profile of engineers. Third-year students have to present their competences by preparing a project, which demonstrates that they mastered the knowledge and skills needed to develop one product in the field of mechatronics to the level of complete technical documentation.

This paper presents the results of a project that was prepared by the students. The paper is structured as follows. First, the detailed description of the project task is given. Following that, the different developed solutions with a brief comparison are presented. Finally, a discussion of the results and conclusions is presented.

2. PROJECT TASK

A mechatronics device that is able to sort four different cylindrical items (Table 1) should be developed and designed.

The device has the following constraints:

- The sorting is performed on an existing conveyer, which is shown in Fig. 4. It occupies a predefined area (Fig. 2). It is forbidden to make any changes on the conveyer. The conveyer is equipped with an electric motor with speed reducer (Nord, Type: SK 1S40AF-71 L/4, $i=9.25$, $n=151\text{min}^{-1}$) that is to be used for moving the belt;

- The “A” area is reserved for the placement of the cylinder (one cylinder is to be placed at a time by hand, without checking if more than one cylinder is placed at the conveyer). The solution has to secure that during the sorting period no other cylinder could be placed in the “A” area. After the placement of the cylinder, the sorting cycle has to be started with two “Start” push buttons. After the sorting cycle, i.e., when the sorted cylinder leaves the conveyer, the device has to be set to the initial position and stopped;
- The sorting has to be performed in the “B” area. The “C” area is reserved for the fast moving of the sorted cylinder;
- The sorting of the cylinders has to be designed using mechanical and electro-pneumatic solutions;
- The control of the device is performed by PLC (OMRON CJ1G). The choice of sensors is free. For the control of the electric motor a DANFOSS inverter drive has to be used;
- All moving parts have to be guided by bearings;
- Regular safety measures have to be taken into consideration;
- A “Stop” button and a “Reset” button have to be provided;
- The device has to be designed as an independent module;
- A user manual should be provided.

Cylinder type	Diameter (mm)	Height (mm)	Material	Density (kg/m ³)
1	50	30	Steel	7850
2	50	50	Steel	7850
3	50	30	Polypropylene	900
4	50	50	Polypropylene	900

Table 1. Cylindrical items, properties

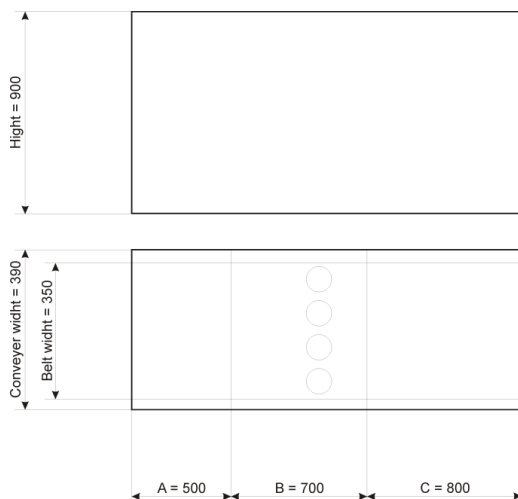


Fig. 2. Existing conveyer's predefined area

3. SOLUTIONS

Based on the project task, third-year students of mechatronics at Subotica Tech prepared their projects. In this paper, six different project solutions are presented, with data regarding the number of used

cylinders, the number of used sensors (optical, inductive and “Reed”), the number of linear motions and the number of rotational motions.

3.1 First project solution

The first project solution (Fig. 3), includes 2 cylinders, 1 inductive sensor, 3 optical sensors, 6 “Reed” sensors. The solution uses 2 linear motions plus the motion of the conveyer, and no rotational motions [3].

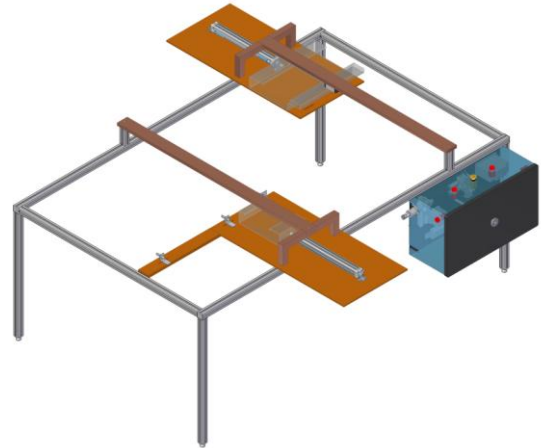


Fig. 3. First project solution [3]

3.2 Second project solution

The second project solution (Fig. 4), includes 2 cylinders, 1 inductive sensor, 2 optical sensors, 4 “Reed” sensors. The solution uses 2 linear motions plus the motion of the conveyer, and no rotations [4].

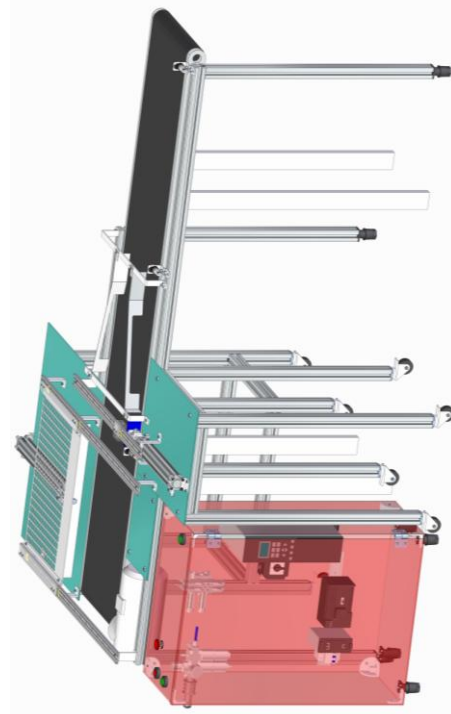


Fig. 4. Second project solution [4]

3.3 Third project solution

The third project solution (Fig. 5), includes 3 cylinders, 1 inductive sensor, 2 optical sensors, 6

“Reed” sensors. The solution uses 3 linear motions plus the motion of the conveyor, and no rotational motions [5].

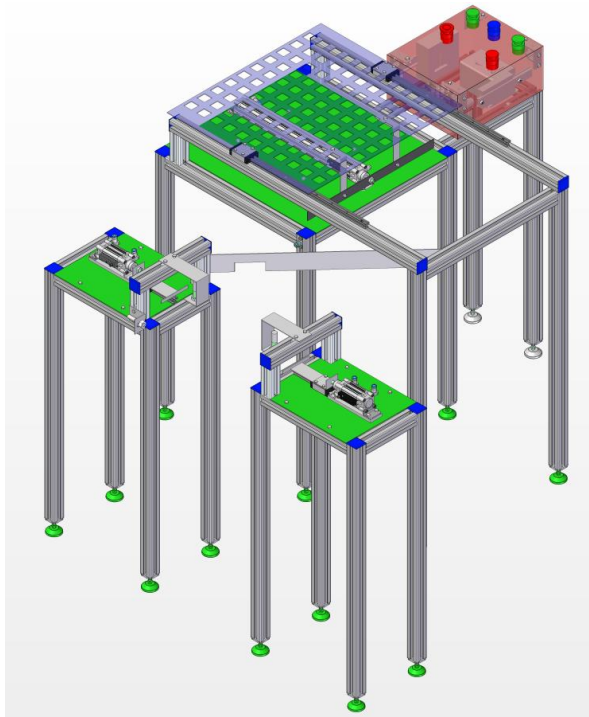


Fig. 5. Third project solution [5]

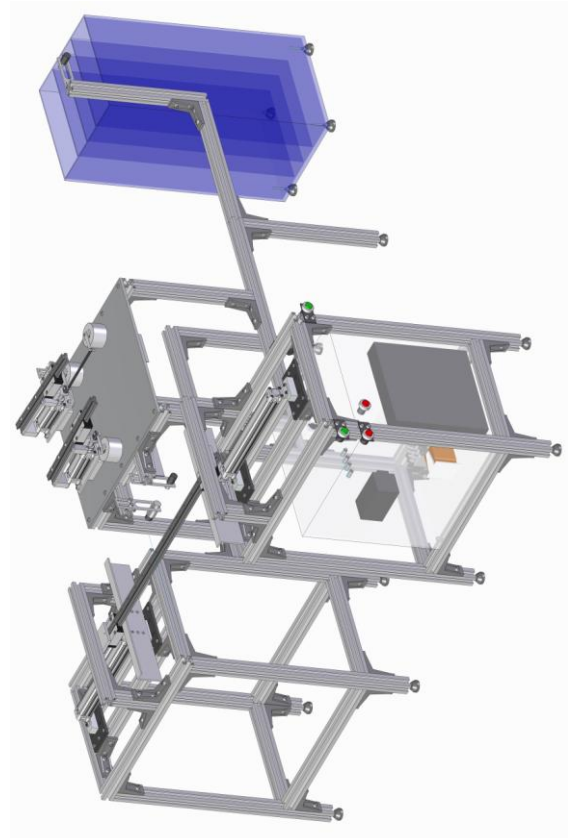


Fig. 6. Fourth project solution [6]

3.4 Fourth project solution

The fourth project solution (Fig. 6), includes 4 cylinders, 1 inductive sensor, 3 optical sensors, 8 “Reed” sensors. The solution uses 4 linear motions, 2 rotational motions and the motion of the conveyor [6].

3.5 Fifth project solution

The fifth project solution (Fig. 7), includes 4 cylinders, 1 inductive sensor, 3 optical sensors, 8 “Reed” sensors. The solution uses 4 linear motions, the motion of the conveyor, and no rotational motions [7].

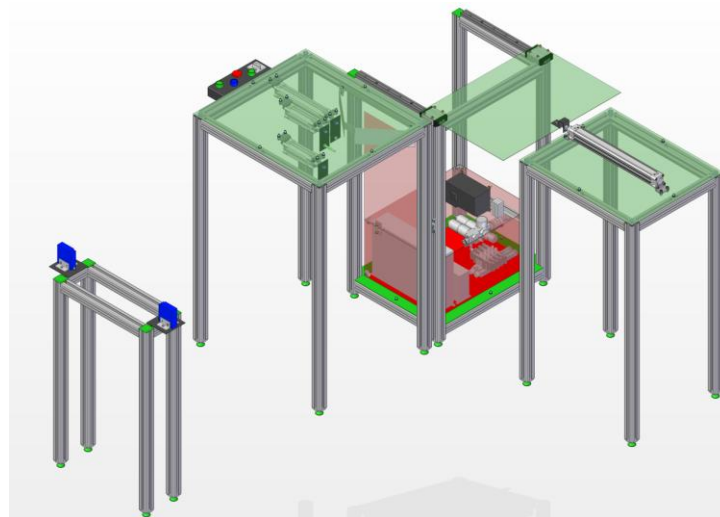


Fig. 7. Fifth project solution [7]

3.6 Sixth project solution

The sixth project solution (Fig. 8.), includes 3 cylinders, 1 inductive sensor, 3 optical sensors, 6

“Reed” sensors. The solution uses 3 linear motions, the motion of the conveyor, and no rotational motions [8].

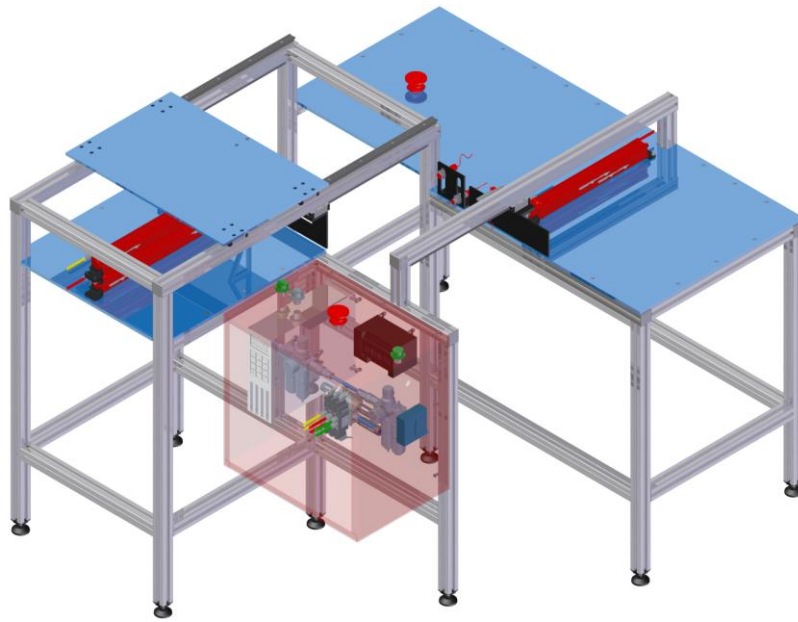


Fig. 8. Sixth project solution [8]

4. DISCUSSION OF RESULTS AND CONCLUSIONS

The project task to develop a mechatronics device that is able to sort four different cylindrical items, yielded six not so different conceptual solutions (Table 2), but completely different solutions (Fig. 3 - Fig. 8). The solutions were compared regarding the number of used cylinders, the number of used sensors, the number of linear motions and the number of rotational motions (Table 2). The only intention for doing this kind of comparison between the solutions was, to show that the same project task can be solved in different ways.

Solution number	Number of cylinders	Total number of sensors	Number of linear motions	Number of rotational motions
1	2	10	2	0
2	2	7	2	0
3	3	9	3	0
4	4	12	4	2
5	4	12	4	0
6	3	10	3	0

Table 2. Comparison between different solutions

The presented solutions have similarities because the project task introduced many constraints and limitations, but it can be concluded that in the field of mechatronics, engineers may indeed show a high level of creativity in solving problems, i.e., in designing products.

5. REFERENCES

[1] Alciatore, D.G., Hstand, M.B.: *Introduction to Measurement and Measurement Systems*, McGraw-Hill, New York, 2012.
 [2] Bolton, W.: *Mechatronics*, Pearson Education Limited, Harlow, 2003.

[3] Olajos, K., et al.: *Seminar task "Designing of mechatronic device for selection of cylindrical products"*, Subotica Tech, Subotica, 2012.
 [4] Bata, Z., et al.: *Seminar task "Designing of mechatronic device for selection of cylindrical products"*, Subotica Tech, Subotica, 2012.
 [5] Lacko, L., et al.: *Seminar task "Designing of mechatronic device for selection of cylindrical products"*, Subotica Tech, Subotica, 2012.
 [6] Sarandi, H., et al *Seminar task "Designing of mechatronic device for selection of cylindrical products"*, Subotica Tech, Subotica, 2012.
 [7] Engi, A., et al.: *Seminar task "Designing of mechatronic device for selection of cylindrical products"*, Subotica Tech, Subotica, 2012.
 [8] Tumbas, L.S., et al.: *Seminar task "Designing of mechatronic device for selection of cylindrical products"*, Subotica Tech, Subotica, 2012.

Authors: M.Sc. Igor Fuerstner, Subotica Tech – College of Applied Sciences, Department of Mechatronics, Marka Oreskovic 16, 24000 Subotica, Serbia, Phone.: +381 24 655-235, Fax:+381 24 655-255.

E-mail: ifurst@vts.su.ac.rs
gogolak@vts.su.ac.rs
nimre@vts.su.ac.rs

Globočki – Lakić, G., Sredanović, B., Čiča, Đ., Milutinović, A.

APPLICATION OF CAD/CAM SYSTEMS FOR MACHINING OF PARTS OF ALUMINIUM PROFILES

Abstract: *This paper presents the procedure for the introduction and implementation of CAD/CAM systems in the machining of parts for the supporting structure of the facade of aluminum profiles. This system was implemented in the manufacturing company from Banja Luka. Automation of design and machining was performed using the CAD program SolidWorks 2011 with a completely integrated module for parametric modeling DriveWorksXpress 2011 and module SolidCAM. The goal of this paper is to show how the use of existing resources, using a flexible designing method for the product and technology - CAD/CAM systems, in the real production environment, can improve the manufacturing process and reduce costs and processing time.*

Key words: *automation, design, parametric model, CAD/CAM systems*

1. INTRODUCTION

The process of developing a new product is a complex task that involves many stages and individual activities. However, increasing competition, the market sets high demands on the producers who are expected to quickly adapt to new product, high quality, low price products and all this in terms of low-volume production. These conditions, designing to the final products, only can be achieved by using the automation of all activities in the production systems: the product design using CAD software packages, the design of process planning and achieving the connection with machining system using CAM software. Product development using CAD/CAM/CAPP system speeds up the overall process, particularly the analysis, redesign of the model, making decisions about the developed solutions, and the choice of an optimal solution with minimum cost and maximum quality. Product design is a critical activity of the manufacturing process because it is estimated that 70-80% of its share in total cost of development and production.

The analysis of production and design methods used in the reporting enterprise that belongs to the category of small and medium enterprises, it was concluded that the need to integrate CAD/CAM system to create new products. It is necessary to apply a more flexible way of designing of the product and technology development, and with application of existing resources at low cost to go to business success.

2. PROBLEM AND THE PROPOSED SOLUTION

The production program of analyzed company is based on the development of supporting structures, facades of different shapes and sizes composed of different materials (glass, plastic, aluminum, MDF, etc.). The analysis of designing and production time and frequency of custom requirements, it was concluded that it is necessary to access the development and integration of a completely new

CAD/CAM systems in relation to, tentatively, the existing level of integration. The currently used system has no possibility of achieving connection between the design (geometry, technology) and development, so the programmer is forced to manually enter the CNC program at the machine control unit, step by step. This type of product design and the introduction of the program require great amount of time and leave space for potential errors. Based on the analysis of the current operation and functioning of information flows in the manufacturing, there are identified certain deficiencies in the exchange of information from design to product manufacturing. The main requirements, which are managed in developing new systems integration, with goal to eliminate of defects, are: minimize the design time of geometry and technology, enable the connection between design and production, minimize the potential errors, facilitate the work of the designer geometry and technology, facilitate the work of the machine operator, allow for flexibility in design and rapid redesign of product model as also reduce the costs and increase productivity.

Implementation of the proposed approach in the integration of CAD/CAM system was carried out in three phases:

1. Designing of parametric model with the basic characteristics based on 3D software package (selected *SolidWorks 2011*).
2. Design of technology in CAM system. It is performed using the integrated CAD/CAM systems, such as the design technology and tool path in CAM model. By changing the dimension and parameters of CAD model automatically changes the tool path, but machining parameters and cutting tools are the same.
3. Making the connection with CNC machine tool controller. Connection is established by CAD/CAM system which generates G-code that is transmitted to the control unit of the machine.



Fig. 1. Machining center MC 304 Ariel – 3

To implement the first phase requires minimal computer equipment, in terms of the software, includes the installation of licensed software SolidWorks 2011, and it is necessary to have adequate CAD/CAM software. In this paper was used the software package SolidWorks 2011 and fully integrated module SolidCAM. Basic model of analyzed product is designed and parameterized. The entire process of modeling, parameterization and technology design of production is performed in the above mentioned software package without leaving the program during the execution of these phases, which is especially important. Technology design is conducted in integrated software SolidCAM, which is module of the SolidWorks software. Both programs share the same model database, created in the design model, which significantly facilitates the work of the designer and the handling of all necessary information.



Fig. 2. Tool charger of MC 304 Ariel – 3

For machining of aluminum profile for the supporting structure of the facade, in the mentioned company, it is available machining center MC 304 Ariel-3 (Fig 1.) which is designed for machining a large part made of light materials. Machining center has four CNC axes and option for circular interpolation. Spindle has the ability to rotate about the x-axis in the range of 180° (± 90°). Workpiece is clamped with pneumatic jigs, which can achieve any position in the direction of the coordinate y-axis. Workspace of the machining center is 7210x1420x500 mm. Machining center has the automatically tool changer (Fig 2.) with ISO 30 toolholder.

3. DESIGN OF PARAMETRIC MODEL BASED ON THE ESSENTIAL CHARACTERISTICS OF PRODUCTS

To access a parameterization model it is necessary first to design each part that makes the whole assembly model. *DriveWorksXpress* is a fully integrated module in the *SolidWorks 2011*. It was developed with goal to facilitate the development parametric model based on fundamental characteristics of real part by the designer. Phases of the parametric model in this module are:

1. **Creating a database.** A condition for its formation is completely defined product assembly, as well as drawings of all its components. Model of the product assembly must contain all the components with which be managed by parameters. Module *DriveWorksXpress* offers the option for forming a database (Fig. 3), with opportunities to enter parts of the assembly, geometry and topology connection, execution conditions, the names and other required information.
2. **Entry model into the database.** This phase is performed through several steps: upload product model (enter all parts of the assembly), defining variables, linking variables with the characteristics of parts, connecting with the changing characteristics of assembly of products, input and connecting 2D drawings (drawings of components, bill of components) and enter information about designer and enterprise.

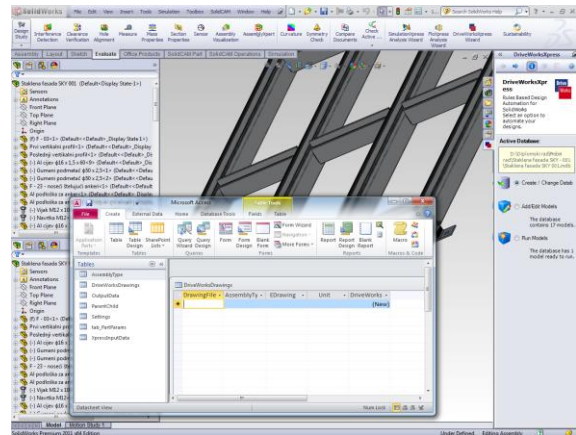


Fig. 3. Creating of database in DriveWorksXpress

3. **Creating the interface form for data entry.** Usually a certain number of textbox windows that are connected to the database, so the developer does not have any time to enter the base and change data. Number textbox window depends on the number of input parameters.
4. **Creating rules.** Essentially, the rules are the formulas (lines of program code) that establish a link between the input parameters and variables. In writing rules can be used all the commands that are used when programming in *Visual Basic* (Fig. 4).

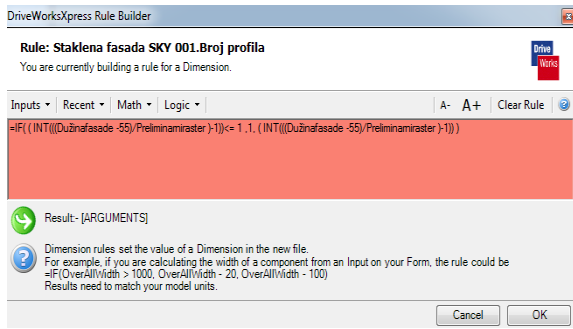


Fig. 4. Creating the rules in DriveWorksXpress

4. DESIGN OF TECHNOLOGY IN CAM SYSTEM

SolidCAM is fully integrated in *SolidWorks*, so the level of communication between CAD and CAM systems is at the highest level. *SolidCAM* supports connection to *DriveWorksXpress* and leaves the possibility of automation. Designing of the technology goes through several stages:

1. **Starting a new document in *SolidCAM*.** This program can be started from a *SolidWorks*, and CAD part automatically can be moved to CAM module. In this module is executed the selection of processing technology (milling, grinding, plasma cutting, etc.) and input data about CAM model, store information about that model and the relationship with the CAD model (Fig. 5).

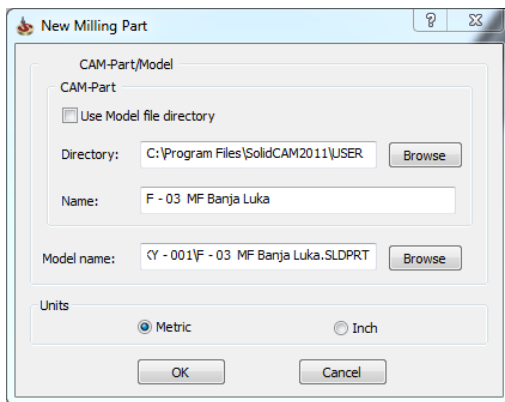


Fig. 5. Creating a new CAM model

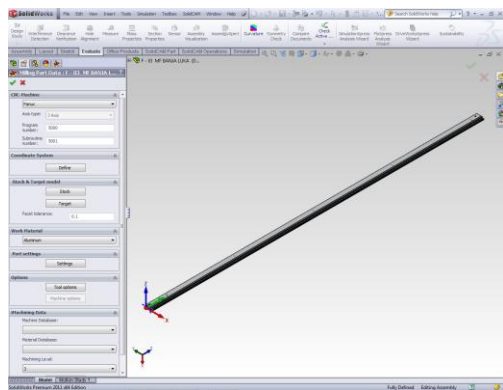


Fig 6. CAD/CAM model in SolidCAM

2. **Transfer of CAD models in CAM model.** This phase is realized through several steps: selection of machines for processing (which automatically select postprocessor), defining the origin of workpiece, stock definition, definition of the parameters of finished part, definition of material processing and definition of tolerance. When setting of the basic technology is finished, CAD model exceeds to the CAM model (Fig. 6).
3. **Design of technology.** Over "technology tree" can be defined the technological connection settings and parameters related to: tools, geometry of machining (it can be inserted automatically in the design of operations), clamping, machining operations (Fig. 7). For the selected machining operation (Fig. 8) is necessary to define the technological parameters and geometry of cutting tools, the cutting depth and tolerance, processing technology and the constrains. When the required parameters are defined, after the simulation, G-code is generated and memorized. The procedure is repeated for all the machining operations and for each part of assembly.

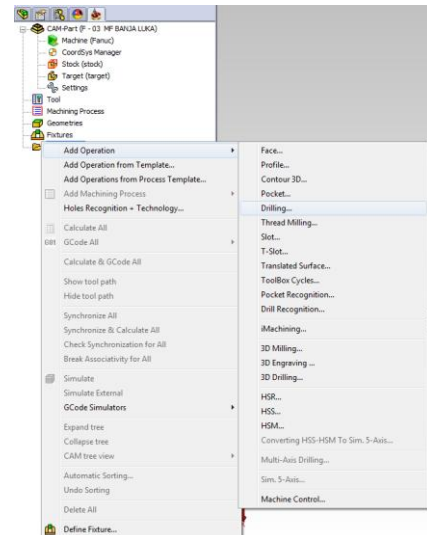


Fig. 7. Design of technology in SolidCAM

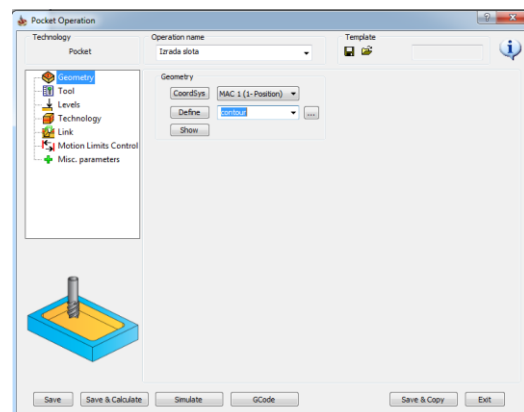
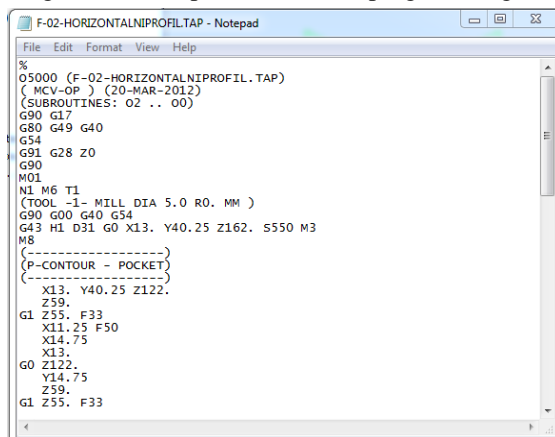


Fig. 8. Defining of machining parameters

4. ESTABLISHING LINKS BETWEEN SOLIDCAM AND DRIVEWORKSXPPRESS.

After the completion of design technology of all parts of assembly, the next step is establishment of connect between SolidCAM and DriveWorksXpress. The reason for linking of mentioned two modules is a fully automated process of designing technology for CAD models incurred by redesign. Redesigned CAD models must be defined at the same way as the basic model, because changing of dimension changes the tool path. Linking process is simple. Each CAM model has its original CAD model and is connected to it. By changing the original CAD model, CAM model is changed. In this process is retained all the manufacturing features. Change of dimensions of the model changing the tool path in automatic recalculation of CAM model. Link between these two models can be adjusted via the technological tree by selecting the option *Change Reference Model*. When the connection is established, it is necessary to recalculate CAM models and generate G-code. The duration of the procedure is about 5 minutes. It is clear what is the saving of time compared to manual programming.



```
File Edit Format View Help
%
O5000 (F-02-HORIZONTALNIPROFIL.TAP)
(MCV-OP ) (20-MAR-2012)
(SUBROUTINES: 02 .. 00)
G90 G17
G80 G49 G40
G54
G91 G28 Z0
G90
M01
M1 M6 T1
(TOOL -1- MILL DIA 5.0 R0. MM )
G90 G00 G40 G54
G43 H1 D31 G0 X13. Y40.25 Z162. S550 M3
M8
(-----)
(P-CONTOUR - POCKET)
(-----)
X13. Y40.25 Z122.
Z59.
G1 Z55. F33
X11.25 F50
X14.75
X13.
G0 Z122.
Y14.75
Z59.
G1 Z55. F33
```

Fig. 9. Generated G code in SolidCAM

5. ESTABLISHMENT OF THE CONNECTION WITH CONTROL UNIT OF MACHINING CENTER

Machining center *MECAL MC 304* has a control unit developed by the company *MECAL*. The hardware interface that connects a manage computer and PLC is *KVARA 6*, software solution is *MESOFT* that supports the 3D CAD programming for standard aluminum parts and ISO programming (G-code). Establishing links between *SolidCAM* and machining center controller is realized by sending the file with G instructions generated in *SolidCAM* on the manage computer on machine that is connected to machine center control unit. Instructions are sent in the format (*.TAP) and can be easily loaded into the *MESOFT* editor for ISO programming (Fig. 9). Problem that can occur when generating of G instruction is that these instruction cannot be accepted by the machine center control unit. The appearance of an unknown instruction is the result of inappropriate use postprocessor for *MECAL* control unit (Fig. 10). To solve this problem it is necessary to

create a new preprocessor and postprocessor or modify the existing.

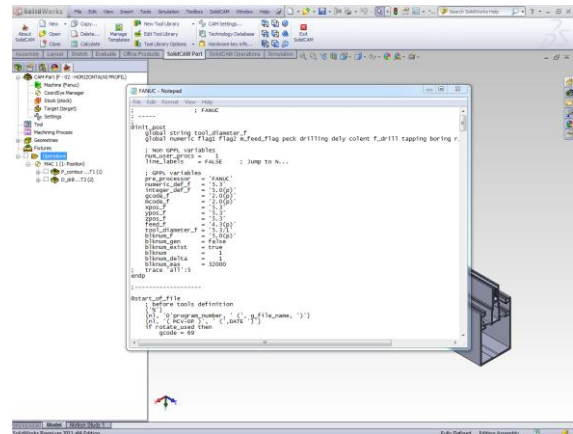


Fig. 10. Postprocessor created in GPPTool

6. CONCLUSION

Based on the analysis of the current producing operations and functioning of information flows in analyzed enterprise, identified certain deficiencies in the information exchange in phase of the design to phase of products manufacturing. The shown procedure of integrated CAD/CAM system allows shortening time of the design geometry and technology, to provide flexibility in the design and rapid redesign of the product model, to reduce costs and increase productivity. Time of design geometry and production technology has been reduced 20 times. Manual entry of program for parts machining lasted a few days with the inevitable mistakes when entering information. Integration of CAD/CAM systems and the development of parametric models for manufacturing of construction of the facade that time are reduced to a few hours only.

7. REFERENCES

- [1] Ognjanović M., „Konstruisanje mašina“, Mašinski fakultet Beograd, 2003.
- [2] Jokanović S., „Geometrijsko modeliranje“, Mašinski fakultet Banja Luka 2006.
- [3] Jovišević V., „Projektovanje tehnoloških procesa“, Mašinski fakultet Banja Luka 2005.
- [4] Globočki-Lakić G., „Obrada metala rezanjem-teorija, modeliranje i simulacija“, Mašinski fakultet Banja Luka, 2010.
- [5] www.alpro-vl.com
- [6] www.mecal.com
- [7] www.solidworks.com
- [8] www.solidcam.com

Authors: Prof. Dr. Gordana Globočki Lakić; M. Sc. Branislav Sredanović; Doc. Dr. Đorđe Čiča; Aleksandar Milutinović, University of Banjaluka, Faculty of Mechanical Engineering, Stepe Stepanovića 75a, 78000 Banja Luka, Bosnia and Herzegovina, Phone.: +387 51 462-400, Fax: +387 51 465-085.
E-mail: gordana.globocki@gmail.com
sredanovic@gmail.com

Jahn, M., Luttmann, A., Schmidt, A.

A FEM SIMULATION FOR SOLID-LIQUID-SOLID PHASE TRANSITIONS DURING THE PRODUCTION OF MICRO-COMPONENTS

Abstract: In advanced engineering, the importance of micro-components has increased significantly during the last decade. During production, a forming process is often included. The Collaborative Research Center 747 developed a two-level cold-forming process based on laser melting that benefit from size effects.

The material accumulation step of this process can be modeled mathematically by coupling the Navier- Stokes equations with a capillary surface and a Stefan problem. This paper presents a FEM simulation of this model combining two different approaches for handling the solid-liquid-solid phase transitions.

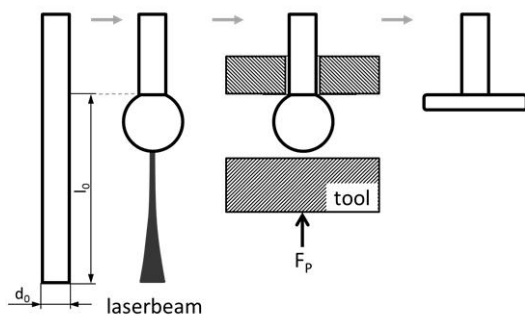
Key words: FEM, Stefan problem, Navier-Stokes

1. INTRODUCTION

Up to now, the production of micro-components is a challenging task. With increasing miniaturization, conventional methods like forming processes are no longer applicable to (semi-finished) work pieces. In macro-scale, usually multilevel cold-forming processes are chosen to change the geometry of a part into a requested shape. Unfortunately, the upset ratio defined by $s = l_0/d_0$, where d_0 is the characteristic length of the work piece (e.g. diameter for a wire) and l_0 is the upsetting length, is strictly limited ($s \leq 2.3$). In micro-scale, this limit decreases even more ($s \leq 1.1$) so that new approaches are needed [1, 2].

The Collaborative Research Center 747 developed a new forming process based on laser heating. A metallic semi-finished product, e.g. a thin wire or sheet, is clamped and a laser beam heats the lower surface. The material melts and a drop or a “collar” is formed. Due to the small scale, this process benefits from size effects. In particular, the ratio of volume to surface area leads to a predominating effect of surface tension regarding gravity allowing an upset ratio up to 80.

After the requested mass is accumulated, the laser is switched off and the solidification process begins. A further forming process can be applied to the solid material accumulation to obtain a requested form. A visualization of the process is shown in Fig. 1.



BIAS

Fig. 1. Sketch of the forming process developed within the Collaborative Research Center 747

In this paper, a FE method for the process of material accumulation is presented. As semi-finished work piece, a small wire ($d_0 \leq 1\text{mm}$) is considered. The process can be modeled mathematically by coupling a Stefan problem with the incompressible Navier-Stokes equations. Due to the interdependences of the geometry, in particular the capillary surface, and the solid-liquid interface, additional challenges are included in the model. A lot of research in the field of numeric for Navier-Stokes equations has been done already, c.f. [3]. We therefore focus here on methods for handling the solid-liquid interface and its coupling with the geometry.

This paper is structured in the following manner: In section 2, the mathematical model is stated and two different approaches for handling the solid-liquid interface are presented, namely an enthalpy method and a sharp interface model. Section 3 discusses the numerical aspects of the FE method and the approaches for handling the interface. In particular, the combination of both approaches is examined. A comparison between the simulation results and the experimental data is presented in section 4.

2. MATHEMATICAL MODEL

For $t \in [t_0, t_f]$, let $\Omega(t) := \Omega_s(t) \cup \Gamma_s(t) \cup \Omega_l(t)$ be the time-dependent domain, where $\Omega_s(t)$ denotes the solid subdomain, $\Gamma_s(t)$ names the solid-liquid interface and $\Omega_l(t)$ stands for the liquid subdomain, c.f. Figure 2. Initially, the domains are $\Omega_s(0) = \Omega_0$, $\Omega_l(0) = \emptyset$ and $\Gamma_s(0) = \emptyset$. In non-dimensional units, the process can be described by the PDE system

$$\partial_t u + u \cdot \nabla u - \nabla \cdot \sigma = f_u(T) \quad \text{in } \Omega_l(t), \quad (1)$$

$$\nabla \cdot u = 0 \quad \text{in } \Omega_l(t), \quad (2)$$

$$\partial_t T + u \cdot \nabla T - \frac{1}{\text{RePr}} \Delta T = 0 \quad \text{in } \Omega_l(t), \quad (3)$$

$$\partial_t T + -\frac{1}{\text{RePr}} q_{ls} \Delta T = 0 \quad \text{in } \Omega_s(t), \quad (4)$$

where u is the fluid flow, p is the pressure, Re is the Reynolds number and Pr is the Prandtl number. The function $f_u(T)$ includes buoyancy forces and the relation of surface tension to gravity. The factor q_{ls} and the stress tensor σ are

$$q_{ls} = \frac{\kappa_s \rho_l c_{p,l}}{\kappa_l \rho_s c_{p,s}} \quad \text{and} \quad \sigma := \frac{1}{\text{Re}} D(u) - p I_d,$$

with density ρ , specific heat capacity c_p and heat conductivity κ . Additional scaling ensures $T_{\text{melt}} = 0$.

On the boundaries, the conditions

$$u \cdot \nu = V_{\Gamma_C} \cdot \nu \quad \text{on } \Gamma_C(t),$$

$$\sigma \cdot \nu = \frac{1}{\text{We}} \mathbf{K} \cdot \nu \quad \text{on } \Gamma_C(t),$$

$$\frac{1}{\text{RePr}} \nabla T \cdot \nu = g_l(T) \quad \text{on } \Gamma_C(t),$$

$$\frac{1}{\text{RePr}} \frac{\kappa_s}{\kappa_l} \nabla T \cdot \nu = g_s(T) \quad \text{on } \Gamma_R(t),$$

$$\frac{1}{\text{RePr}} \nabla T \cdot \nu = 0 \quad \text{on } \Gamma_N(t),$$

are prescribed. Thereby, V_{Γ_C} is the velocity of the capillary surface, We denotes the Weber number, \mathbf{K} stands for the sum of principle curvatures and ν is the outer normal. The right-hand sides $g_{l,s}(T)$ of the conditions depend on the subdomain and include laser heating and heat losses due to forced convection introduced by shield gas, and radiation described by the Stefan-Boltzmann law.

For handling the solid-liquid-solid phase transitions,

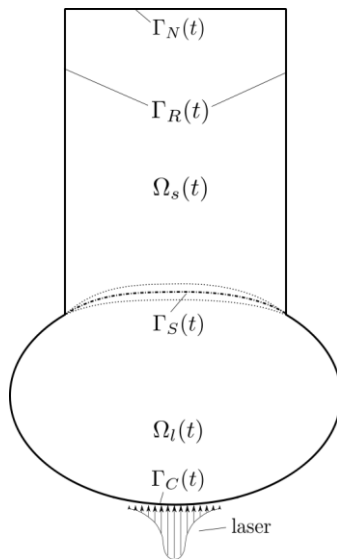


Fig. 2. Sketch of the geometry, including notations of subdomains and boundaries

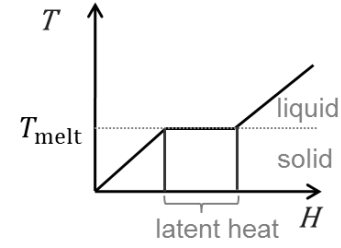


Fig. 3. Temperature-enthalpy relation

two different approaches are presented which pros and cons are discussed in section 3.2.

2.1 Approach I: Energy conservation

The first approach is based on the formulation of the energy balance in the whole domain $\Omega(t)$. A temperature-enthalpy relation is defined by

$$T = \beta(H) := \begin{cases} \frac{1}{c_s} H, & H < 0 \\ 0, & H \in [0, \frac{1}{\text{Ste}}] \\ H - \frac{1}{\text{Ste}}, & H \geq 0 \end{cases} \quad (5)$$

c.f. Figure 3. By applying this relation, the Stefan problem [4]

$$\partial_t H + u \cdot \nabla H - \frac{1}{\text{RePr}} \Delta T = 0 \quad (6)$$

is formulated for the whole domain $\Omega(t)$, with $u \equiv 0$ in $\Omega_s(t)$, c_s is a scaling factor and Ste is the Stefan number. Due to the implicit treatment of the solid-liquid interface $\Gamma_S(t) := \{x \in \Omega(t) | T(x) = T_m\}$, this approach allows for a mushy region in which the material is neither pure solid nor pure liquid.

2.2 Approach II: Sharp interface

The second approach uses a sharp solid-liquid interface $\Gamma_S(t)$ which is formulated explicitly and separates the domain in a liquid and a solid subdomain. Thereby, $\Gamma_S(t)$ acts as an internal boundary on which the conditions

$$u \cdot \nu = \left(1 - \frac{\rho_s}{\rho_l}\right) \cdot V_{\Gamma_C} \cdot \nu,$$

$$u - u \cdot \nu \nu = 0, \\ T = 0,$$

$$\frac{1}{\text{RePr}} [(\nabla T)_l - q_{ls} (\nabla T)_s] = \frac{1}{\text{Ste}} \frac{\rho_s}{\rho_l} V_{\Gamma_S},$$

are prescribed. The last equation is referred to as Stefan condition which describes the movement of the interface depending on the jumps of the temperature gradients. With the use of these conditions, the heat equation can be solved separately for each domain.

3. NUMERICAL ASPECTS

The overall coupled problem is solved by extending the FEM software NAVIER [3], which is a FORTRAN implementation.

3.1 Navier-Stokes equation

Originally, NAVIER was developed to solve the incompressible Navier-Stokes equations with a capillary surface on a time-dependent domain. For this purpose, an unstructured grid is employed on which the equations are discretized by the Taylor-Hood element in space. For the discretization in time, the fractional theta-scheme in an operator splitting variant is applied. For our application (here: a small wire), a rotational symmetric 2D version is used.

3.2 Handling the phase transitions

Both methods for handling phase transitions are based on energy conservation. The enthalpy method considers the whole domain in one equation and derives the solid-liquid interface independent from the element edges implicitly, whereas the sharp interface separates the solid subdomain and the liquid subdomain on element edges explicitly [5].

From a numerical point of view, both approaches show pros and cons in different aspects. On the one hand, a FE method based on the enthalpy model is very straight forward and easy to implement because there is no need for tracking temperature isolines explicitly. Furthermore, a mushy region of material is naturally included in this model. On the other hand, this mushy region is hard to handle. In order to avoid a complex modeling of this region, the following major simplification is assumed: An element is considered to be solid as long as the temperature at one of its nodes is below melting temperature. As a consequence, the element status can either be solid or liquid implying that only phase changes of whole elements are possible. Due to the coupling of the mushy region with the capillary surface (respectively the geometry) a phase change of a whole element from solid to liquid can lead to oscillations and non-physical behavior in the fluid flow.

By the use of the sharp interface approach with a moving mesh, the introduction and modeling of a mushy region is avoided as well as the related problems. In return, the model and implementation complexity increases a lot, especially if a solidification process comes into play. Another disadvantage of this method is that the solid-liquid interface and, accordingly solid and liquid subdomains, have to exist from the very beginning.

To sum it all up, both approaches show advantages and disadvantages. But by taking a closer look, it can be recognized that the pros and cons of the methods are related to different aspects of the simulation. To improve the accuracy of the simulation, NAVIER has therefore been extended extensively to combine both methods. In more detail, the combination works as the following:

Firstly, the nucleation of the liquid phase is simulated by the enthalpy method. After some time-steps, the approach is switched applying now the moving mesh method with a sharp interface to the problem. Therefore, a new mesh is generated by TRIANGLE [6] arranging the elements so that the interface matches the element edges. This method is used to simulate the rest of the melting process. Due to the moving mesh,

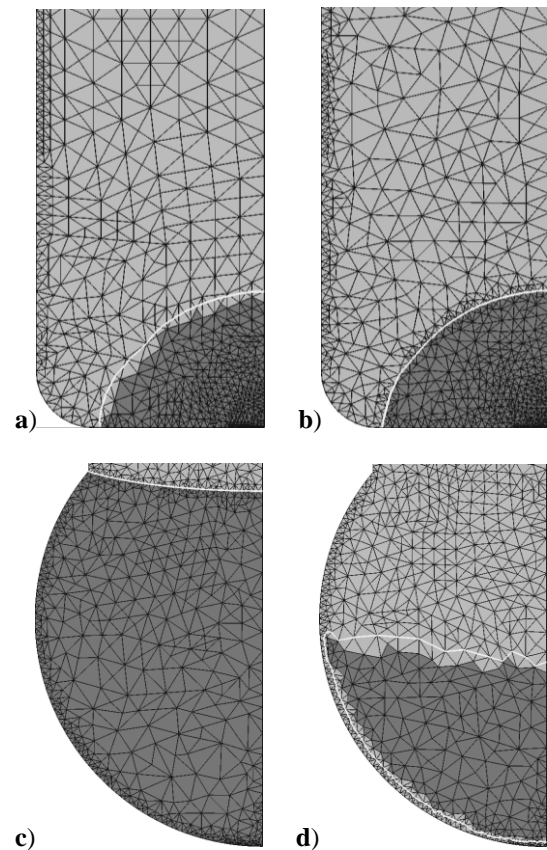


Fig. 4. Different methods during simulation: The liquid subdomain is colored in dark grey and the solid subdomain is colored in light grey. In between both subdomains, the solid-liquid interface is shown. In **a** and **b**, the first change of methods is shown. In **c** and **d**, snapshots of the moving mesh approach during melting process resp. the enthalpy approach during solidification process are shown.

occasional remeshing is performed using TRIANGLE again. When the laser is switched off and the solidification process begins, the approach is switched back to enthalpy method which is used for simulating the rest of the process. Some important steps in the simulation are shown in Figure 4. In Fig. 4a, the simplified mushy region with an isoline across the elements can be noticed. Fig. 4b shows the same time-step after the method is switched to the moving mesh approach. In Fig. 4c, a typical time-step by applying the moving mesh method is shown and in Fig. 4d the solidification process using the enthalpy method again is visualized. The idea of coupling both approaches was first presented in [7].

4. NUMERICAL RESULTS

The FEM simulation results are compared to experimental data. For that purpose, two very important properties of material accumulations are considered. The first property examined is the shape. Material accumulations with different sizes and wire diameters resulting from experiments performed by our industrial partner BIAS are measured by a confocal laser microscope (CLM). For material accumulations with a

diameter $d_{MA} \leq 2\text{mm}$, the simulation results match the data very well. An example for a wire with

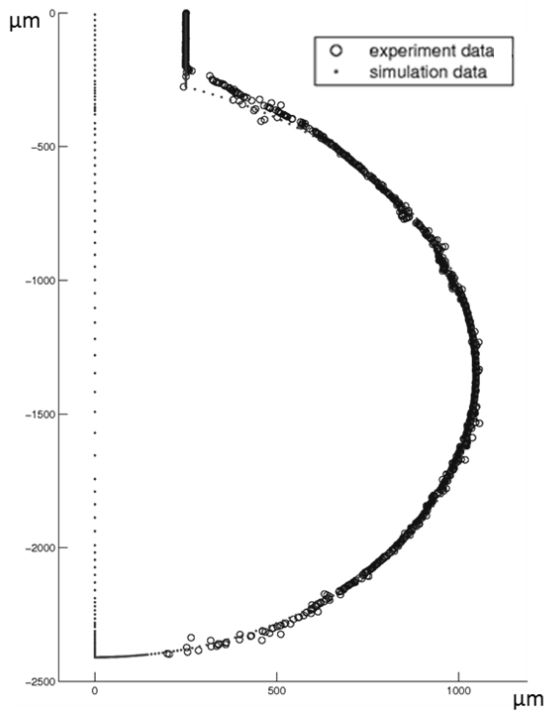
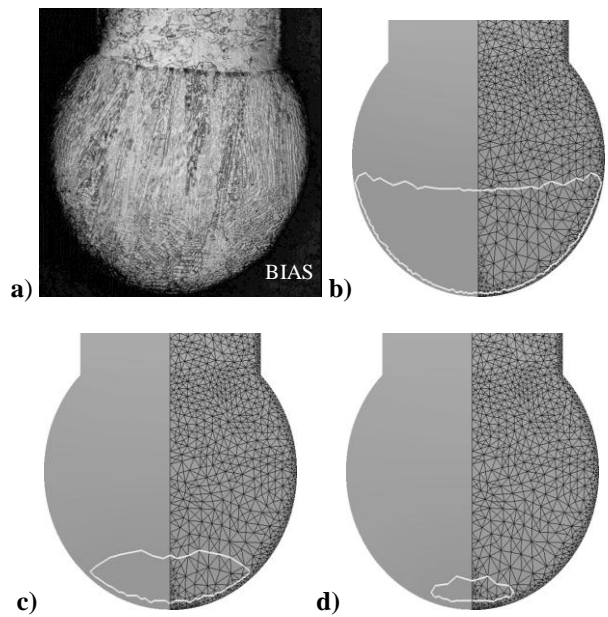


Fig. 5. Comparison of the shape for a wire with $d_0 = 0.5\text{mm}$ and $d_{MA} \approx 2\text{mm}$



Laser type	Trumpf TruFiber 300		
Power	80W	Shield gas	Nitrogen
Pulse duration	50ms	Shield gas flow	20 l/min
Wire diameter	0.5mm		

Fig. 6. In **a**, a cross-section polish of a material accumulation is given. In **b-d**, different time steps during solidification process are shown visualizing the course of the solidification isoline

diameter $d_0 = 0.5\text{mm}$ and $d_{MA} \approx 2\text{mm}$ is shown in Figure 5.

Another important property of a material accumulation is its micro-structure that influences the formability in further processes. Therefore, the BIAS produced cross-section polishes in which the course of the solidification can be examined. Due to the fact that the simulation of microstructure itself is not included in our approach, these cross-section polishes are compared to the course of the solidification isoline. An example is given in Figure 6.

5. ACKNOWLEDGEMENTS

The authors gratefully acknowledge the financial support by the DFG (German Research Foundation) for the subproject A3 within the Collaborative Research Center 747 “Mikrokaltumformen – Prozesse, Charakterisierung, Optimierung”. Furthermore, we thank the Bremer Institute für angewandte Strahltechnik (BIAS) and the AG Prof. Dr. E. Bänsch, University of Nürnberg-Erlangen for cooperation.

6. REFERENCES

- [1] Stephen, A., Vollertsen, F.: *Influence of the rod diameter on the upset ratio in laser-based free form heading*, Steel Research Int., Special Edition: 10th Int. Conf. on Technology of Plasticity (ICTP), p.p. 220-223, (2011)
- [2] Vollertsen, F.: *Categories of size effects*, Prod. Eng.-Res. Dev. 2, p.p. 377-383, (2008)
- [3] Bänsch, E.: *Finite element discretization of the Navier-Stokes equations with a free capillary surface*, Num. Math. Vol. 88 (2001), p.p. 203-235
- [4] Elliot, C. M.: *On the finite element approximation of an of the Stefan problem* IMA Journal of Numerical Analysis, Vol. 1, p.p. 115-125, (1981)
- [5] Bänsch, E., Paul, J. and Schmidt, A.: *An ALE finite element method for a coupled Stefan problem and Navier-Stokes equations with free capillary surface*, Int. J. Numer. Meth. Fluids (accepted)
- [6] Shewchuk, J.R.: *Triangle: Engineering a 2D Quality Mesh Generator and Delaunay Triangulator*, Applied Computational Geometry: Towards Geometric Engineering p.p. 203-222, (1996)
- [7] Jahn, M., Luttmann, A. Schmidt, A., Paul, J.: *Finite element methods for problems with solid-liquid-solid phase transitions and free melt surface*, Proc. Appl. Math. Mech. (submitted)

Authors: Dipl.-math Mischa Jahn, Dipl.-math. techn. Andreas Luttmann, Prof. Dr. Alfred Schmidt, University of Bremen, Faculty of Mathematics, Center for Industrial Mathematics (ZeTeM), Bibliothekstr. 1, 28359 Bremen, Germany, Phone.: +49 421 218-63855.

E-mail: mischa@math.uni-bremen.de
andreasl@math.uni-bremen.de
schmidt@math.uni-bremen.de

Jovanovic, V., Wang, H.

MECHATRONICS AND ITS APPLICATIONS IN TRANSPORTATION

Abstract: Recent developments related to mechatronics systems and computer engineering has led to many advanced applications in the transportation arena. Ranging from the use of modern mobile and regular communication networks, security informatics, artificial intelligence and simulation, advanced sensing techniques, to various navigation techniques, mechatronics systems can be found in many modern vehicles and transportation devices. In addition, they are also serving as a support for more environmentally friendly transportation systems. In this paper, the focus will be given on the review of current trends and research direction in this area.

Key words: Mechatronics, Transportation, Intelligent transportation systems

1. INTRODUCTION

The traditional definition for mechatronics that has originated in the early 1970's, made by Yaskawa Electric Co. has evolved recently into a completely different area of applications. With the developments of information technology and intelligent decision making strategies, this definition has been expanded to a broad area of application beyond traditional electro mechanical systems with purely mechanical motion [1]. Mechatronic systems are also defined as integration of mechanics, electronics, measurement and actuator technology, and information technology [2].

Development of a digital signal processing and availability of low cost microprocessors with their speed and functionality, mechatronics systems have been upgraded to more complex algorithms, use of artificial intelligence, and real time control [3].

Nowadays, mechatronics spans to vehicle control (automotive and aerospace, consumer electronics and industrial equipment [4]. In vehicles, mechatronic systems can be used for various applications such as adaptive control of electro-magnetic and pneumatic actuators, adaptive shock absorbers for vehicle suspension, and electronic drive-chain damping [2]. Today's high speed trains do include mechatronics systems that are related to vehicle dynamics and energy efficiency of its multi-domain energy systems [5].

2. MECHATRONIC DESIGN

The mechatronic design cycle, given in the Figure 1 is explained at the Mechatronics Laboratory Paderborn (MLaP) treats the mechatronic system in a holistic and systematic manner from the initial task to analysis and synthesis to realization [6, 7].

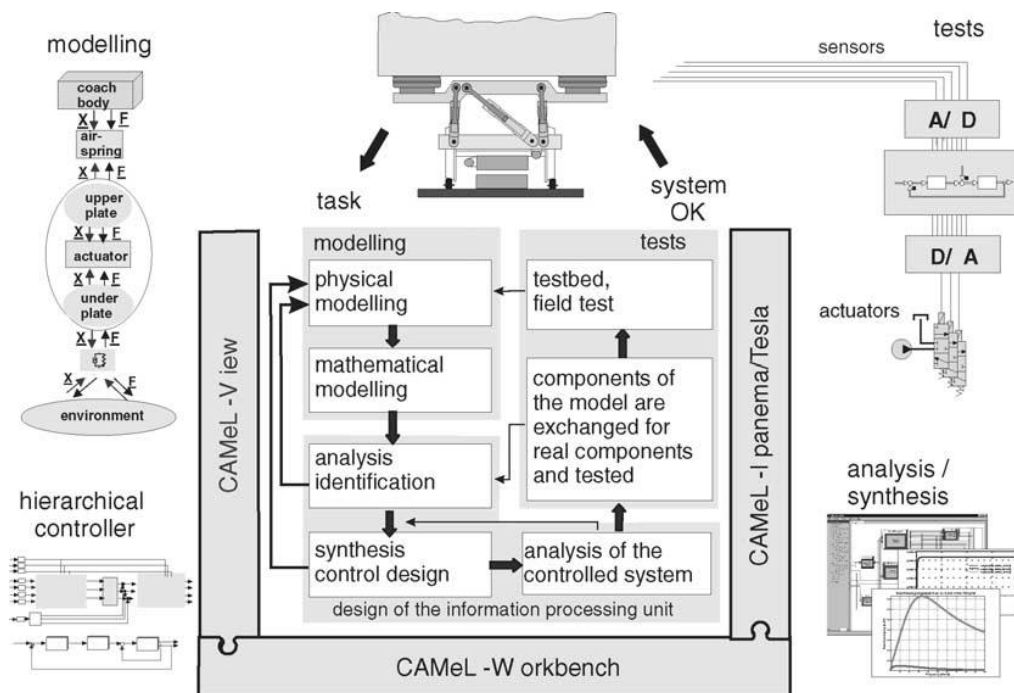


Fig. 1. Mechatronic design cycle [6, 7].

The first phase of mechatronics systems design is modeling. All functional principles and requirements have to be carefully captured and mathematical model that has to be developed has to capture all properties of a physical system [6]. Since mechatronics systems are always complex, this modeling and mathematical model development may include modeling related to different disciplines such as mechanics, electronics, hydraulics, and pneumatics. Control of these systems may be simple such as one controller or it might go up to more complex, multivariable control structures. Once developed, control system is then optimized and tested. These stages might be repeated until the acceptable system is tested.

3. INTELLIGENT TRANSPORTATION VEHICLES

Mechatronics systems in aerospace include full integration of controls and computation and the mechanical and aerodynamic structure through fly-by-wire. Mechatronics also finds applications in military purposes. Some of these are: remotely flown Unmanned Aerial Vehicle (UAV), vehicle stability control system with driver intent recognition, vehicle status measurement and estimation etc.

The application of mechatronics systems is prevalent in automotive modeling including some components such as tilt and pressure sensors, motors, onboard power source, and personal transportation device (Segway). In addition, there were substantial changes in the automotive arena with electronic engine controls and anti-lock braking systems, brake-by-wire, active suspension systems that can to adapt to various driving condition, and steer-by-wire [8-10].

Modern vehicles with mechatronic engine controls are providing better energy efficiency by enabling environmental compliance with environmental

standards that are getting stringer and stringer each year. Being compliant with a current standard related to emissions is related to various parameters in a vehicle. Measuring how different systems are working under various road and environment conditions along a whole lifespan of a vehicle is very challenging task. Different standards are related to emissions, fuel economy and drivability specifications go much further than using the traditional engine controller, the carburetor [1].

Modern vehicles that include On Board Diagnostics (OBD) have much better performance tracking and measurements. These systems are incorporated into the computers on-board modern vehicles to monitor vehicle components and systems [11]. OBD systems are becoming more and more important part [12] of every vehicle due to constant changes in environmental regulations and fuel consumption. Hence, the user can be notified when something in the system is not working according to specifications provided and that some maintenance is necessary for the vehicle to stay inside the specified, regulated guidelines.

The application of mechatronics systems to driving behavior modeling has been explored for various contemporary problems such as adaptive control cruise, collision avoidance, driving performance monitoring and abnormality investigation in the general framework of intelligent transportation system. The integration of mechatronics devices and driving simulation laboratory for real-time hardware-in-the-loop and in-vehicle testing has triggered various human-vehicle interface studies to enhance operator performance [13].

In industry, simulation-based evaluation system and data collection units (DriveSync) is being developed such as Intelligent Mechatronic Systems (IMS) for interactive driving data which monitor carbon footprint and fuel efficiency. The application of mechatronics to fleet monitoring systems helps monitor the time, location, operating speed a fleet vehicle is driven.

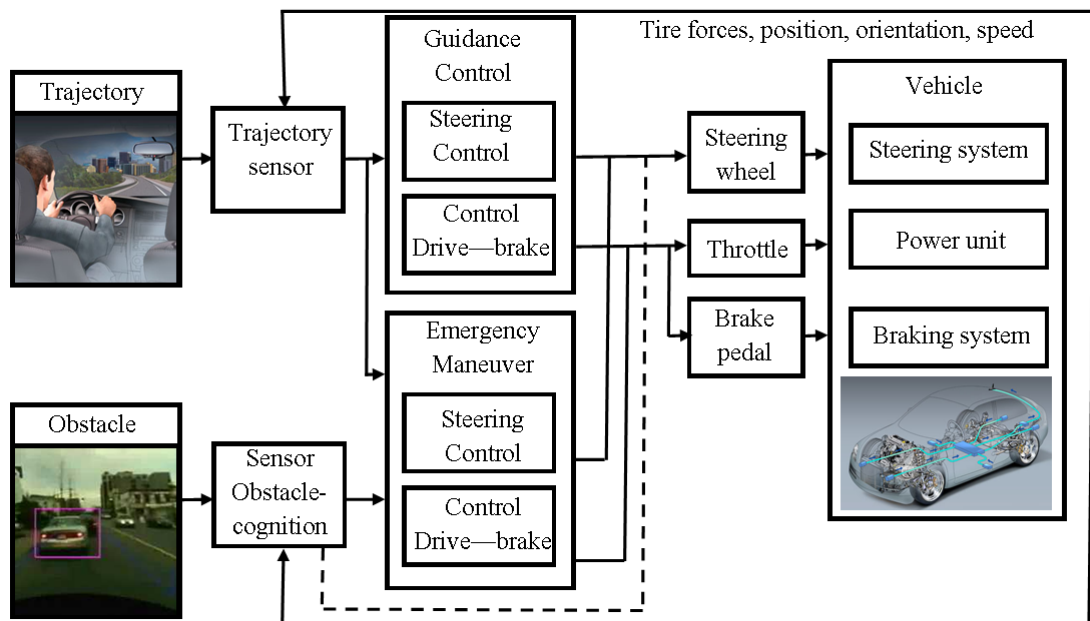


Fig. 2. Driver controller structure [13]

As a critical component of modeling and simulation of a driver-vehicle system dynamics, a 3-level driver controller model is developed by Institute of Robotics and Mechatronics at which essentially considers the environment, driver controller, and the vehicle chassis control system. The application of mechatronics devices is mainly structured in the vehicle system dynamics through mechatronic sensors and actuators. A more specific structure of the driver controller can be found in Figure 2 in which the trajectory of vehicle and the road obstacles can be detected through sensors.

4. RAILROAD SYSTEMS AND APPLICATIONS

Today's design of high speed trains relies on dynamic simulation methodologies that support better wheel rail interface, better acoustics and stability [5]. Next generation trains will include high speed low floor running gears that have real time controls of relative motions of wheels and the rail. These controls are necessary because the contact between the train and the rail are influenced by deformations and they are not always the same. Another application are active

systems in running gears such as driven independently rotating wheels (DIRW) which collect sensory information needed for feedback control all for a purpose of better acoustics and longer components' lifespan.

Other mechatronics applications are related to development of friction-free "drive" function that is based on linear motor. The main purpose of this solution is to relieve the wheels of the "drive" and "brake" functions [6]. One example of such system, developed by suspension/tilt module is to be implemented in a fully active railway carriage developed by the Neue Bahntechnik Paderborn (NBP, Novel Railway System Paderborn) research team is given in Figure 3 [6]. This system has three modules: drive/brake module, suspension/tilt module, and support/guidance module, powered by three hydraulic actuators, each supported by its own mechanical supporting structure, actuator/sensor groups, and controller components. In essence, this system is comprised of three mechatronic sub-systems. It is a cross-linked mechatronic system that corresponds to the highest hierarchical level which includes coupling and decoupling of variables related to all three levels.

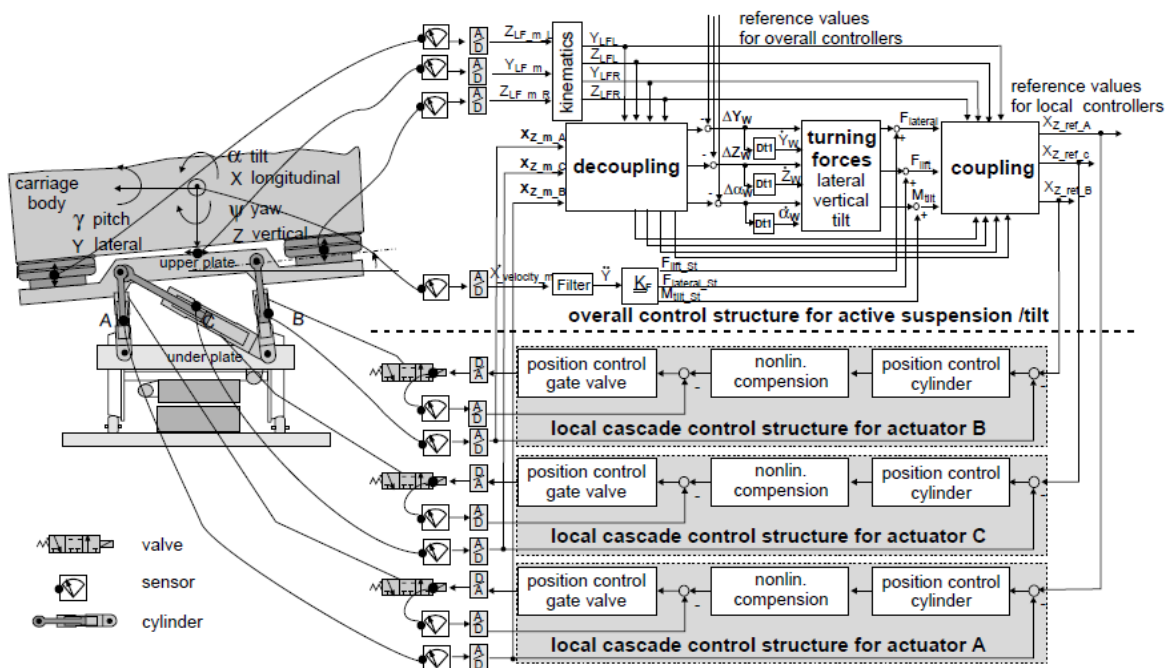


Fig. 3. Sensors and hierarchical control structure of active suspension/tilt module [6].

Nowadays, the majority of railroad systems applications might be considered as "the first generation" systems which rely on limited control laws forced only to actuators. In addition, future developments might be focus at development of "second generation" systems that would include more functionality such as integrated measurement systems for higher reliability and fault tolerance. In this way, a train would be considered as a higher level system from a control perspective. Also, "the third generation" would focus on a higher integration with other vehicle dynamic systems, e.g. traction and braking, satellite positioning system etc. [8].

5. MOBILE COMMUNICATION NETWORKS

In addition, mechatronics systems might also be used for data gathering for oceanographic models, such as in an Autonomous Oceanographic Sampling Network[14] to replace the sampling done from ships, satellites, floats, and moorings. In this kind of system, Autonomous Underwater Vehicles (AUVs) would be used to measure temperature, currents, salinity, and other distributed oceanographic signals. They communicate through a local area network through sound signals and control actuators in response to data gather locally together with an evolving global data. A

model of this kind of network, deployed in a coastal ocean frontal regime and network nodes that consists of a base buoy and a selectable number of small Autonomous Underwater Vehicles (AUVs) is given in Figure 4.

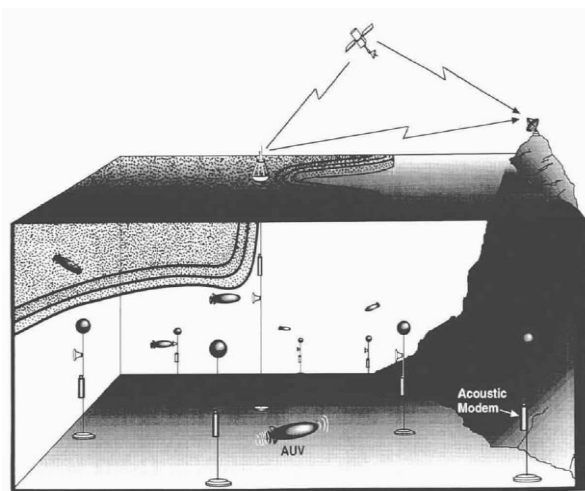


Fig. 4. Autonomous oceanographic sampling network model [14]

In not so distant future, groups of autonomous vehicles (robots) would be possible to use at the same time because of the recent advances in networking area and trends related to decreasing size of electromechanical systems [15] through ad-hoc communication networks. Some possible applications of these technologies are deployments of robots for search and recovery operations, working in environments that might be hazardous to humans, exploration, surveillance, and environmental monitoring for pollution detection and estimation.

According to the Cortes et al. (2004), these vehicles can have various sensors and collect different information from the environment such as vibrations, sound, electro-magnetic field, and infrared (IR) signals as well as carry video cameras to record what is happening in the robot's surroundings [3].

6. CONCLUSION

Future developments in processing power, software, battery life, more reliable communication network systems will lead to additional development related to applications of autonomous mechatronic systems in transportation. In addition, mechatronic systems will be used more and more in vehicles to provide better energy efficiency. Some of these systems currently need better integration and therefore higher reliability and better fault tolerance. Another area of future developments include better vehicle stability that would be also lead to better energy efficiency. Another reason for use of mechatronic systems might also be related to increased safety and better human machine interaction. In addition, using mechatronic systems for data gathering would also be in much wider use with the development of better battery lifecycle and more reliable networking.

7. REFERENCES

- [1] D. M. Auslander, "What is mechatronics?," *Mechatronics, IEEE/ASME Transactions on*, vol. 1, pp. 5-9, 1996.
- [2] R. Isermann, "Modeling and design methodology for mechatronic systems," *Mechatronics, IEEE/ASME Transactions on*, vol. 1, pp. 16-28, 1996.
- [3] H. Hashimoto, "Intelligent mechatronics," in *Industrial Electronics, Control, and Instrumentation, 1993. Proceedings of the IECON '93., International Conference on*, 1993, pp. 445-450 vol.1.
- [4] K. Fuentes, R. Jiménez, and E. Raygoza, "PLM Applied to Didactic Flexible Manufacturing Cells Development," in *XXI Congreso Chileno de Educación en Ingeniería*, Santiago, Chile, 2007.
- [5] A. O. Albu-Schäffer. (2012, August 1). *Railway Systems*. Available: <http://www.dlr.de/rm/en/desktopdefault.aspx/tabid-5307/>
- [6] X. Liu-Henke, J. Lückel, and K.-P. Jäker, "An active suspension/tilt system for a mechatronic railway carriage," *Control Engineering Practice*, vol. 10, pp. 991-998, 2002.
- [7] J. Lückel, "User guide for CAMEl toolsMLaP," University of Paderborn, Germany 1992.
- [8] R. M. Goodall and W. Kortüm, "Mechatronic developments for railway vehicles of the future," *Control Engineering Practice*, vol. 10, pp. 887-898, 2002.
- [9] Y. He and J. McPhee, "Multidisciplinary design optimization of mechatronic vehicles with active suspensions," *Journal of Sound and Vibration*, vol. 283, pp. 217-241, 2005.
- [10] D. Fischer and R. Isermann, "Mechatronic semi-active and active vehicle suspensions," *Control Engineering Practice*, vol. 12, pp. 1353-1367, 2004.
- [11] S. Godavarty, S. Broyles, and M. Parten, "Interfacing to the on-board diagnostic system," in *Vehicular Technology Conference, 2000. IEEE VTS-Fall VTC 2000. 52nd*, 2000, pp. 2000-2004 vol.4.
- [12] C. Fulvio, C. Luca, G. Marcella, O. Massimo, P. Andrea, S. Sara, and D. Daniele Theseider, "Generating on-board diagnostics of dynamic automotive systems based on qualitative models[1]This work was partially supported by the European Commission, DG XII (project BE 95/2128, 'VMBD'). VMBD (Vehicle Model-Based Diagnosis) is a Brite-Euram proje," *AI Communications*, vol. 12, pp. 33-43, 1999.
- [13] J. Bals. (2012, August, 4). *Modeling and Simulation of a Driver in Vehicle System Dynamics*. Available: http://www.dlr.de/rm/en/desktopdefault.aspx/tabid-3861/6311_read-9076/
- [14] T. B. Curtin, J. G. Bellingham, J. Catipovic, and D. Webb, "Autonomous oceanographic sampling networks" *Oceanography*, vol. 6, pp. 86-94, 1993.
- [15] J. Cortes, S. Martinez, T. Karatas, and F. Bullo, "Coverage control for mobile sensing networks," *Robotics and Automation, IEEE Transactions on*, vol. 20, pp. 243-255, 2004.

Authors: **Dr. Vukica Jovanovic**, Mechanical Engineering Technology, Old Dominion University, 1 Old Dominion University, Norfolk, VA 23529, U.S.A., Phone: +1 757 683-3769; **Dr. Haizhong Wang**, School of Civil & Construction Engineering, Oregon State University, Corvallis, OR, 97331, U.S.A. Phone: +1 541-737-8538.

E-mail: v2jovano@odu.edu
Haizhong.Wang@oregonstate.edu

Košarac, A., Zeljković, M.

SIMULATION OF PROCESS CONTROLLED BY PROGRAMMABLE LOGIC CONTROLLER PLC IN THE VIRTUAL REALITY ENVIRONMENT

Abstract: Virtual product design represents one of modern approaches in product development. Apart from visualization itself, this process comprises of the whole range of tests in the virtual reality environment. This paper shows simulation of process controlled by PLC within mentioned environment as an illustration of one of the possibilities in the virtual reality environment. Virtual scenery is created in VRML language for modeling virtual reality, i.e. V-Realm Builder Editor. Process is being controlled by PLC controller and in MATLAB/SIMULINK environment. In the purpose of achieving communication between virtual reality and programmable logic controller OPC standard is used.

Key words: Virtual Product Design, Virtual Reality, Programmable Logic Controllers PLC, OPC standard, MATLAB/SIMULINK.

1. INTRODUCTION

Modern approaches in product development are being developed in accordance with development of information technologies all aiming to shorten the process of product development and to minimize the number of physical prototypes. One of such approaches is the development of virtual products, which, apart from visualization, enables the whole range of product testing in the virtual reality environment [2]. This paper shows simulation, i.e. testing of control algorithm of the process controlled by programmable logic controller PLC in the environment of the virtual reality as an illustration of some of the possibilities during product development process in the mentioned environment. Control algorithm is being controlled by the PLC. MATLAB/SIMULINK that has the possibility to communicate with VR environment and to support OLE for Process Control is used for the implementation. Virtual sensors are modeled in VR scenery or in MATLAB/SIMULINK environment and information from sensors is being forwarded towards PLC controller input. After scanning the input and executing the program, PLC scans output status and changes it if needed. MATLAB/SIMULINK receives information from the output of the PLC controller and controls the movement of 3D objects in VR scenery through VR Sink block. The exchange of data between MATLAB and PLC is implemented in client-server architecture by applying OPC standard, whereby OPC server communicates with PLC, while the client is in the MATLAB/SIMULINK, Fig. 1.

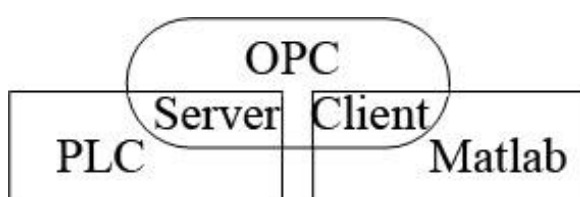


Fig. 1. The connection between MATLAB and PLC using OPC [6]

2. DESCRIPTION OF THE WORKING PROCESS CONTROLLED BY PLC

Considering the purpose of the paper, which is to present the possibilities of connecting PLC and virtual environment and taking into account the size of this paper, the segment of semi-automatic drill operation will be shown, whereby the replacement of part is done manually [8]. The system is combinational circuit with three inputs and four outputs whose description of the working process is shown in the table 1. In the case of physical model the scheme of input and output module wiring for drill would be as shown in the Fig. 2. while controlling system is presented on the Fig. 3. as ladder diagram.

Input	Address	Comment
Limit switch 1	CIO 0.0	Drill head starts in the upper most position with the upper limit switch 1 turned on.
Limit switch 2	CIO 0.1	When the lower limit switch 2 is reached (and thus turns on) the downward drill head motor should turn off.
Start switch	CIO 0.2	When the start cycle button is pressed, the magnetic table should activate, the drill should start moving down and the spindle motor should turn on.

Output	Address	Comment
P	CIO 1.0	Activates magnetic table
M_1	CIO 1.1	Activates spindle motor
M_2^+	CIO 1.2	Activates head motor (downward)
M_2^-	CIO 1.3	Activates head motor (upward)

Table 1. Description of working process

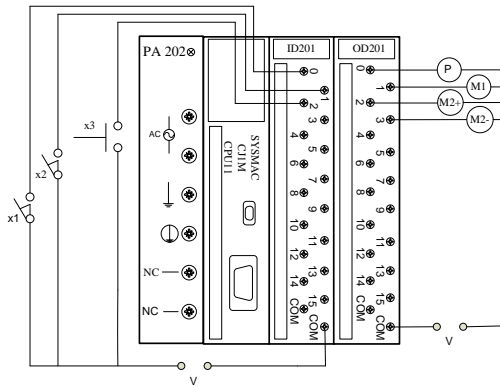


Fig. 2. Input and Output Module Wiring

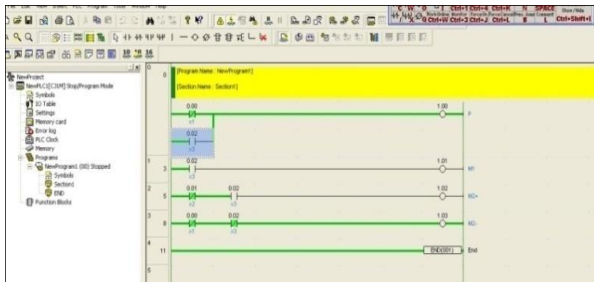


Fig. 3. Ladder diagram

3. PLC OMRON

Programmable logic controller of OMRON manufacturer is being used for the purpose of this paper (CJ series, belongs to microcontroller class). This type of PLC controller is used in many industrial fields, such as CNC machine tools for controlling certain modules, different type machine tools, for packaging, handling of different materials, etc. The group of products that belongs to CJ series is intended to be used for simple sequential circuits up to systems with large number of I/O units.

Full modularity in composing this device provides opportunity for wide range usage of central processor units (CPU) that are fully compatible and can simply be combined with any other PLC module.

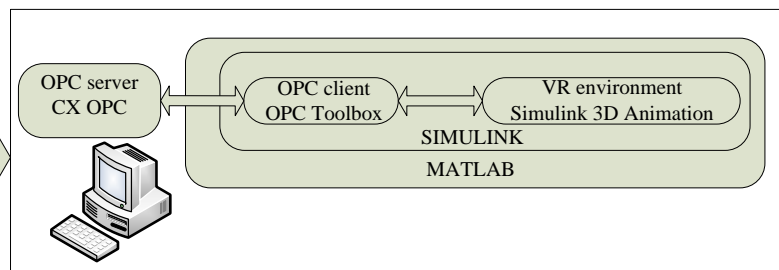
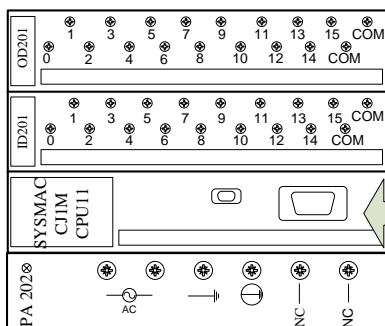


Fig. 4. Data exchange between PLC and MATLAB

Central processor unit CPU11, which is being used in this device, is intended for smaller systems, such as automatic machines, control devices, etc.

The controller has digital input unit with 16 input terminals and digital relay output unit with 16 output terminals.

Standard interface RS 232 is used to connect PLC controller to the computer.

Graphical programming language ladder diagram (LD, Ladder Diagram) CX Programmer is used to program PLC, Fig. 3., as joint programming platform for CS/CJ/C/CV series of OMRON's controllers.

4. THE APPLICATION OF OPC STANDARD FOR DATA EXCHANGE BETWEEN MATLAB AND PROGRAMMABLE LOGIC CONTROLLERS

Aiming to exchange the data between programmable logic controller and virtual reality environment appropriate interface is needed. It is possible to apply OLE for Process Control (OPC), which stands for Object Linking and Embedding (OLE) for Process Control. The standard specifies the communication of real-time plant data between control devices from different manufacturers.

CX OPC server used in this case provides possibility to connect and exchange data between OMRON's PLC controllers series CS/CJ/C/CV and CP and applications running in Microsoft environment that has OPC standard support. CX-Server OPC supports all OMRON's communication protocols.

It should surely be mentioned that other software solution are possible to be used, such as Matrikon OPC that supports communication to PLC controllers of OMRON manufacturer.

On the other hand MATLAB/SIMULINK has a library OPC Toolbox that enables access to OPC server in real time. In other words using this library enables reading data in real time that OPC server overtakes from the PLC controller or sending data from MATLAB to PLC controller. Fig. 4. shows data exchange between PLC and MATLAB.

5. VR MODEL AND VR SIMULATION

For modeling interactive 3D scenery (virtual worlds) language for modeling virtual reality VRML is used. VRML is defined as ISO standard open coded and text based, with the possibility of showing models in web browsers. In order to enable the work in virtual reality environment without full knowledge of this language, some of the editors could be used.

This paper shows usage of V-Realm Builder editor that could be used to model virtual world as well as to import 3D object in virtual scenery, Fig. 5. In order to model objects used in virtual scenery CATIA program is used, having in mind that this editor (V-Realm Builder editor) was not intended to be used for modeling complex scenery.

Objects modeled in CATIA program are saved as .wrl file and then imported to V-Realm Builder editor. It is essential to mention that objects modeled in CATIA program after being imported in virtual reality keep all properties, including the tree structures.

VRML uses the world coordinate system in which the y-axis points upward and the z-axis places objects nearer or farther from the front of the screen. That needs to be considering when objects are being modeled.

After virtual world is created it is possible to manipulate with objects in virtual scenery for MATLAB, i.e. SIMULINK environment, in such way that through MATLAB, i.e. SIMULINK change properties of the field within Transform group (translation, rotation, scale...). Only those transform groups whose initial name has been changed within VRML, i.e. V-Realm Builder can be controlled in MATLAB.

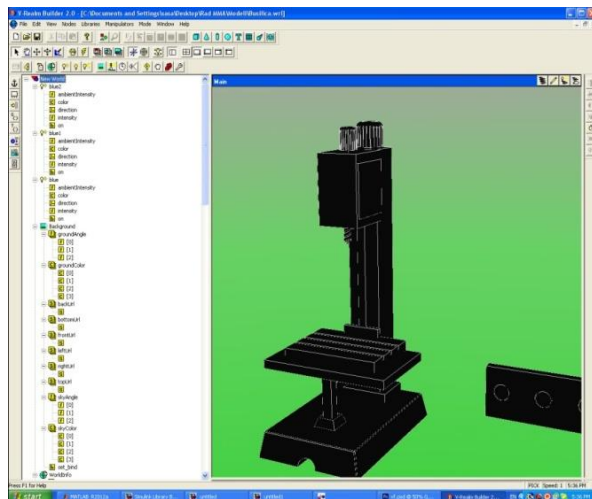


Fig. 5. Virtual scenery in V-Realm Builder

Virtual scenery is shown by application SIMULINK 3D Animation viewer, Fig. 6, being part of VR Toolbox. After .wrl file is imported in to SIMULINK 3D Animation viewer, it is necessary to select fields that the one wants to control by SIMULINK signals in its structure tree. These become inputs into VR Sink, i.e. VR Source blocks that belongs to the library Virtual Reality Toolbox. SIMULINK

signals are being brought to input lines of these blocks, Fig. 7.

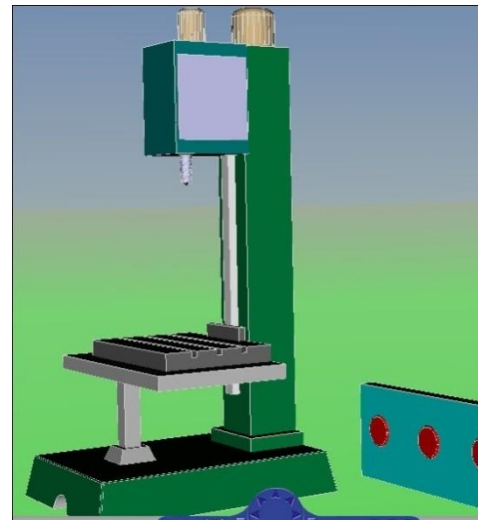


Fig. 6. Virtual scenery in SIMULINK 3D Animation viewer

6. SIMULINK MODEL

Sub-systems to control movement of kinematic modules are built out of blocks of SIMULINK library, Fig. 7. Input signals in SIMULINK model are from virtual sensors, whereby virtual sensor x_3 is created in virtual reality environment and virtual sensors x_1 and x_2 in MATLAB/SIMULINK.

Should head starts in the upper most position, limit switch x_1 is reached and should the head be in lower position limit switch x_2 is reached whereby the position of head is determined by the value of integrator. Virtual limit switches x_1 and x_2 provide signals (Boolean variable), that MATLAB send to OPC server through OPC Write block. Fig. 8. shows addresses defined at OPC server, representing I/O PLC addresses.

OPC send these signals to PLC forcing bits on PLC controller input. PCL controller then executes program, bits value from the output (representing correspondent output) comes to OPC server and then is being sent from OPC server to MATLAB, i.e. SIMULINK by OPC Read block. When user touches the virtual sensor x_3 , the signal for virtual reality environment is being sent to MATLAB/SIMULINK as described below. The user clicks on the left mouse button in virtual reality environment and causes action (click on the x_3 push button). Node Touch Sensor as well as corresponding ROUTE defined in VRML is used and added to sensor x_3 . After user click on x_3 , Boolean variable is forwarded to VR Source block of SIMULINK 3D Animation library. The signal is further sent to PLC controller through OPC server as described previously. It is important to mention that simulation requires for PLC to run in Monitor mode, Fig. 9.

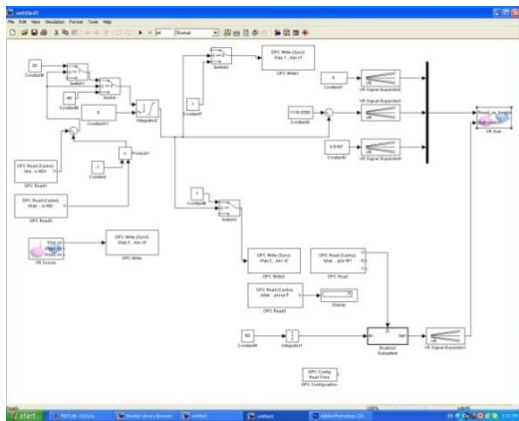


Fig. 7. SIMULINK model

Name	Type	Address
* Ulaz 1 magnetsna ploca P	Point	OMRON plc/I.0/I1/B
* Ulaz 2 Obrtanje bunjele M1	Point	OMRON plc/I.1/I1/B
* Ulaz 3 Nosac alata dole M2+	Point	OMRON plc/I.2/I1/B
* Ulaz 4 Nosac alata gore M2-	Point	OMRON plc/I.3/I1/B
* Ulaz 1 prekidac x1	Point	OMRON plc/F.0/I1/B
* Ulaz 2 prekidac x2	Point	OMRON plc/F.0.1/I1/B
* Ulaz 3 prekidac x3	Point	OMRON plc/F.0.2/I1/B

Fig. 8. Setting I/O addresses at OPC server

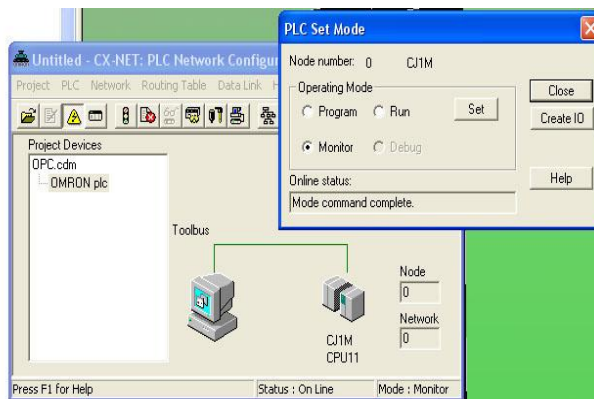


Fig. 9. Adjusting of working mode of PLC controller

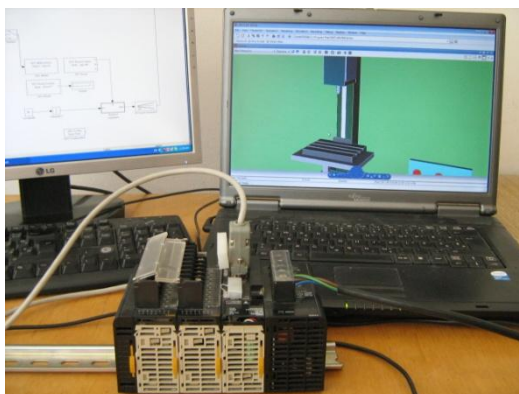


Fig. 10. Adjusting of working mode of PLC controller

7. THE CONCLUSION

This paper shows simulation of process controlled by PLC and MATLAB/SIMULINK. Objects that are being controlled are in virtual world with no physical components of controlled system replaced by MATLAB/SIMULINK environment, i.e. virtual world.

Simulation can be used for testing controlling algorithm in the virtual reality environment. Should there be a physical model, the virtual model could perform certain functions of supervision and control in real time.

8. REFERENCES

- [1] Guzina, M., Stupar, M., Naumović, M.: Mogućnosti komunikacije između MATLAB/Simulink okruženja i procesa upravljanih pomoću programabilnih logičkih kontrolera primjenom OPC koncepta, Infotech-Jahorina Vol. 8, Ref. A-15, p. 66-70, March 2009.
- [2] Košarac, A.: Automatizacija projektovanja i vizuelizacija rada fleksibilnih tehnoloških struktura, Magistarski rad, Fakultet tehničkih nauka, Novi Sad, 2010.
- [3] Matic N.: Uvod u industrijske PLC kontrolere, mikroElektronika, Beograd, 2001.
- [4] OMRON, Technical Library, Multilanguage edition, 2005.
- [5] Pașc, I., Țarcă, R., Popențiu-Vlădicescu, Florin.: The VRML model and VR simulation for a SCARA robot, Annals of the Oradea University, Fascicle of Management and Technological Engineering, Volume VI (XVI), 2007.
- [6] Persin, S., Tovornik, B., Muskinja, N.: OPC-driven Data Exchange between MATLAB and PLC-controlled System, Int. J. Engng Ed. Vol. 19, No. 4, pp. 586-592, 2003 TEMPUS Publications.
- [7] Webb, W. J., Reis, A. R.: Programmable Logic Controllers, Principles and Applications, Fifth Edition, Pearson Education, Inc., Upper Saddle River, New Jersey 07458, 2003.
- [8] Zarić, S.: Automatizacija proizvodnje, Mašinski fakultet Univerziteta u Beogradu, 1984.

Authors:

Aleksandar Košarac, University of East Sarajevo, Faculty of Mechanical Engineering East Sarajevo, Vuka Karadžića 30, 71123 East Sarajevo

Prof. Dr. Milan Zeljković, University of Novi Sad, Faculty of Technical Sciences, Department for Production Engineering, Trg Dositeja Obradovica 6, 21000 Novi Sad, Serbia

E-mail: akosarac@gmail.com

milanz@uns.ac.rs

Lukić, D., Todić, V., Zeljković, M., Milošević, M., Vukman, J., Jovičić, G.

**THE POSSIBILITY AND SIGNIFICANCE OF APPLICATION STEP-NC STANDARD
IN THE INTEGRATION OF CAD/CAPP/CAM AND CNC SYSTEM**

Abstract: Modern approaches to design product and their manufacturing process planning are based on the use of numerous methods and techniques, among which significant is the application of methods based on the features and STEP standard. This paper shows the possibility of integration of CAD/CAPP/CAM and CNC systems using the STEP-NC standard.

Keywords: Features, Manufacturing features, STEP, STEP-NC, CAD/CAPP/CAM/CNC

1. INTRODUCTION

At the beginning of the 20th century, the manufacturing systems have been considerable changes that were caused by the demands of the modern market economy, by increasing flexibility, productivity, economy, etc. [1].

Two basic phases of product development related to design product and process planning of their production. The automatization of design products is successfully solved by the implementation CAD/CAE systems, and automatization of process planning solved by CAPP and CAM systems. By using modern CNC machining systems for various purposes in the manufacturing, significantly increasing its productivity and flexibility. In order to meet the goals of modern market-oriented production is necessary to integrate these activities, which has an important a significant role for techniques and methods based on the features and the application of STEP.

In terms of machining systems, a major revolution was the emergence of computer numerical control (CNC), with whose appearance opened the way to more efficient production and lower costs of production. The initial NC machines and today's modern CNC machines use the same standard for the programming, namely G&M codes formalized as ISO 6983. This programming language is low band-width information transferring ability, because it just describes the machine switch functions and the cutting tool movement. The manufacturing information from specific CAX (CAD/CAPP/CAM) systems is forwarded to CNC machines, so that they can be translated into the appropriate format using post-processors. This information has one way direction flow, and any information from the shop floor level cannot be relayed back to the planning department [2]. Because of disparate data between CAD, CAPP, CAM, CAX and CNC systems approached the development of new standards. The first is developed ISO 10303 standard, which is known as the standard for the exchange of product data (STEP), and then expand to other design and manufacturing activities, and including the STEP-NC standard. STEP standards describe technical information about products so that CAD, CAPP, CAM,

CAE, CMM and CNC systems can exchange and share data [3].

This paper shows the possibility of integration CAD/CAPP/CAM and CNC systems, which is based on the use feature and STEP-NC standard.

2. STEP-NC DATA MODEL

ISO 14649 standard, also known as STEP-NC, provides new possibilities to support high level and standardized information from design to CNC machining systems. Also, this standard allows bi-directional data flow between CAD/CAPP/CAM and CNC systems, without any information loss, (Fig.1). STEP-NC does not describe tool movements for specific CNC machine tool, as it is the case with the G-code, but provides a feature based data model [1].

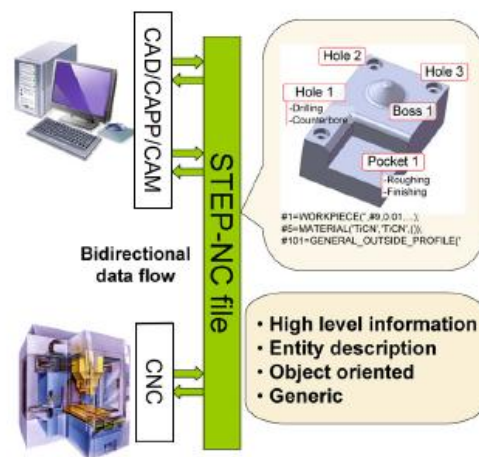


Fig.1. Integration of CAD/CAPP/CAM and CNC systems using the STEP-NC standard

STEP-NC data model includes STEP product feature definitions, which allows easier process planning of their making. Data models include information that defines machining process plan, machining operations, machining strategy, machine function, and all off them are combined to form an object-oriented data structure [4]. In this data structure,

machining workingsteps are essential entities in a STEP-NC data model. Workingsteps represent the basis for the execution of manufacturing tasks [5]. Each workingstep describes usually a single manufacturing operation using one tool and one strategy.

3. FEATURES AND STEP-NC STANDARD

3.1 Representing features in STEP-NC

Features are divided into design features and machining features. Design features have specific functions and can be generated by using different approaches to modeling (B-rep, CSG), while machining features related to the defined volume of material that is removed from the workpiece using different operating sequence.

The basic principles of STEP-NC standard based on use of machining features. Machining features tells CNC systems „what to do“ and „how to do“ manufactured, instead of the direct tool movement [6]. The machining features are recognized by a CAPP system, while they contain geometrical and technological information.

As an example the machining features that are defined in the STEP-NC standard for milling operations: round holes, closed and open pockets, slots, outside profiles, bosses, transition features, etc. [3]. Most of these machining features are defined as a profile along tool path during its processing.

Some examples of machining feature for machining sequence within the turning operations, which is obtained by revolved surfaces area shown in Fig.2 [7].

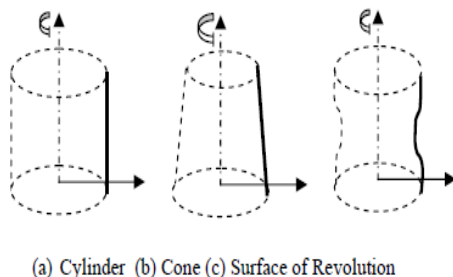


Fig. 2. Machining features that are obtained by revolved surfaces

3.2 Defining features on the product and their interaction

Feature interaction between features is determining factor in micro process planning, and this especially applies to defining the order of machining operations. Feature interaction can be grouping into two different categories: technological interaction and geometrical interaction [8]. Technological interactions related to technological constrains in machining parts, such as fixture interaction, tolerance interaction and tool interaction, while geometrical interaction obtained when two or more machining features have common geometric entities, i.e. surface or volume.

For non-interactive features, the sequence of machining is not so important as when it exists. The order of defining the features on the product can be presented in different forms such as graph, network,

tree and matrix.

For recognizing features, there are several ways:

- Human feature recognition,
- Design by feature,
- Automatic feature recognition and
- The Hybrid Approach: Design-by and Feature Recognition.

The hybrid method for feature recognition use review product CSG and B-rep, namely first perform volume subtraction using Boolean algebra and second perform face adjacency graph. For example product on Fig. 3(a), features volumes (Fig.3(c)) are obtained by subtracting the 3D (Fig. 3(a)) from the raw stock (Fig. 3(b)) and the feature volume faces (Fig. 3(d)) that are coplanar with the raw stock faces alone are used for representing the feature. Six surfaces that define the preform are marked with f'_1 do f'_6 (Fig. 3(b)), and feature volume faces that lie on corresponding raw stock faces are designated from f_1 do f_6 (Fig. 3d) [9].

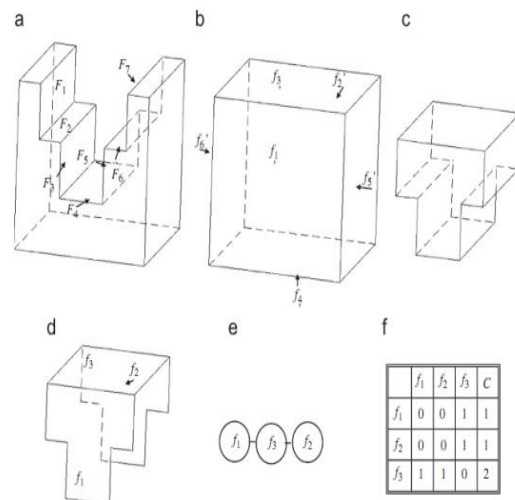


Fig. 3. An example of a hybrid system for recognition features: (a) data model (b) raw stock (c) feature volume (d) feature (e) adjacency graph for feature and (f) adjacency matrix for feature.

For recognizing the feature in rotating parts developed an integrated methodology, which consists of the following algorithms, Fig. 4 [7]:

- Development of geometric data extraction algorithm to extract geometry and topology information from STEP file,
- Development algorithm for recognition turning, which identifies primary turning features, like as cylindrical surface, conical surface, toroidal surface, etc.,
- Development algorithm for recognize radial holes and axial holes on rotational parts and
- Development algorithm for recognize special turning features, like as threading, etc.

Applying the developed methodology to recognition the features according to Fig. 4, is much easier and with less effort made to identify them.

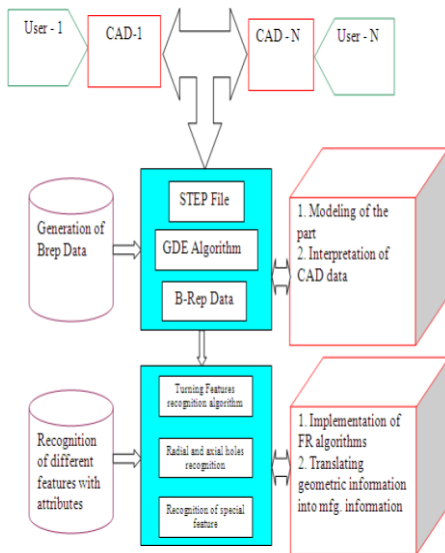


Fig. 4. The methodology for recognize different feature of rotational parts

Feature graph interaction has been simplified, reducing the number of surfaces in the feature volume, so that the complexity of features representation significantly reduced. The methodology that is proposed for the recognition feature of rotating parts is a practical approach to the integration of CAD and CAPP system for rotating parts, which are obtained from STEP files. STEP file provides a good generic representation of the data about parts where are features, geometry, topology, and manufacturing data interrelated. Algorithm to obtain geometric data from STEP files, provides complete information about geometry and algorithm for recognition features is completely possible to identify different types of features.

Figure 5 shows an example of specific feature of part, which they are bridge faces, common volumes and machining faces, while Fig. 6 shows the graph obtained for the interaction of feature part shown in Fig. 5.

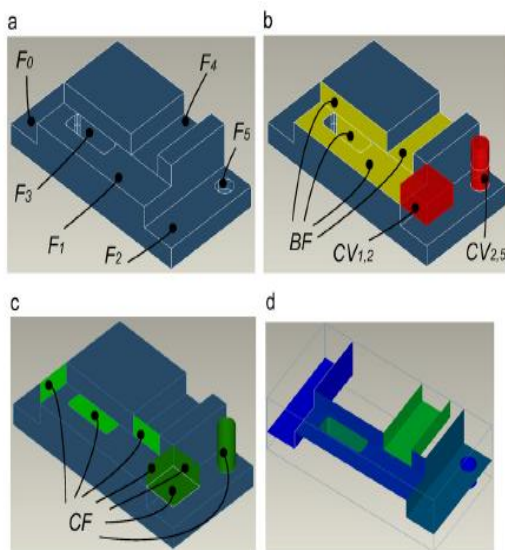


Fig. 5. Example of defining features with (a) features (Fi), (b) bridge faces (BF) and common volumes (CV), (c) connection faces (CF) and (d) machined faces (MF) [4]

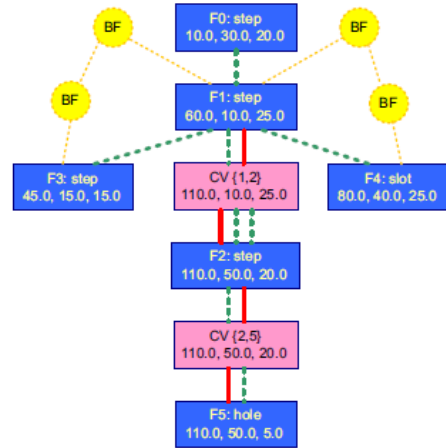


Fig. 6. Obtained graph of feature interaction [4]

4. REVIEW OF THE POSSIBILITY SOME RESULTS OF RESEARCH APPLICATION STEP-NC STANDARD

Computer aided process planning (CAPP) is based on the use of the variant and generative approaches, which in modern terms are based on the standardization of data. CAPP systems represent a link between CAD and CAM systems, by solving the tasks of recognition feature, defining elements of the process planning, defining possibilities and structure of the machining system and its components, etc. Standardization of data can be done by standard for the exchange and sharing of data (STEP), which allows transmission and sharing of data between CAD, CAPP, CAM and other CAX in different computer systems and environments [10].

Rauch et al. [1], proposed the STEP-NC platform for Advanced and Intelligent Manufacturing (SPAIM). This platform is based on an Indirect STEP-NC programming approach, and it can be implemented on most of the current industrial CNC systems and enables them to read STEP-NC files. SPAIM platform is composed of a human/machine interface and several modules for translating STEP-NC data.

Yusof et al. [11] proposed STEP compliant system for turning operations (SCSTO). SCSTO system is based on STEP feature-based design and it defines part data in terms of machining features and their technical attributes based on STEP-AP224. When modeling is done the basic design work-workpiece on which the design machining feature, which define the material that is removed during processing. Also, the authors of Zhang et al. [2] have proposed a architecture system for the design of process planning (PPS) using the STEP-NC. The system PPS consists of five modules namely: program reader, process planer, STEP-NC CAD viewer, STEP-NC CAM viewer and program writer.

Gizaw et al. [12] developed STEP-compliant system for turn-mill operations using XML. Main characteristic of this system is to EXPRESS defined classes of application protocol translation in object-oriented class, and then the data is stored in the format of Part-28. As a result, we have a generic STEP-NC data model based on the technology of standard forms that are defined in the form of AP224.

The authors Habeeb i Xu [13] proposed a generic infrastructure for application of STEP-NC model data. The infrastructure illustrates consists of three different data forms: STEP-NC data, specific CNC machine language and data in the form of ISO 6983. Alvares et al. [14] have proposed a system called WebMachining, that refers to a collaborative approach to the design and manufacturing of cylindrical parts based on the feature. Authors in paper [5] have proposed architecture G2STEP system, which consists of 9 function which realizes G-code translation of the STEP-NC data model for turning operations. In the papers [7, 8, 9] are shown the study focused on defining, recognition and presenting the feature in STEP-NC standard, as well as their interaction.

5. CONCLUSIONS

STEP-NC is based on bi-directional high level information flow between CAD/CAPP/CAM and CNC systems, without use of post-processor, which raises the level of integration of product design and process planning to the manufacturing. It is expected that the application of STEP-NC standard will bring great changes in the field of integration of CAD/CAPP/CAM and CNC systems, by allowing more intensive development of the CAPP system as a bridge between CAD and CAM systems, CNC system to be multi-functional, autonomous, intelligent, user-friendly with open architecture. It also will enable collaborative production supported by the Internet with a tendency of establishing a global e-Manufacturing.

6. LITERATURE

- [1] Rauch, M., Laguionie, R., Hascoet, Jean-Yves, Suh, Suk-Hwan: *An advanced STEP-NC controller for intelligent machining process*, Robotics and Computer –Integrated Manufacturing; Vol. 28(3), p.p. 375-384, 2012.
- [2] Zhang, X., Liu, R., Nassehi, A., Newman, S.T: *A STEP-compliant process planning system for CNC turning operations*, Robotics and Computer-Integrated Manufacturing; Vol. 27, p.p. 349-356, 2011.
- [3] Hardwick, M.: *Third-generation STEP systems that aggregate data for machining and other applications*, International Journal of Computer Integrated Manufacturing, Vol. 23(10), p.p. 893-904, 2010.
- [4] Dipper, T., Xu, X., Klemm, P.: *Defining, recognizing and representing feature interactions in a feature-based data model*, Robotics and Computer-Integrated Manufacturing, Vol. 27, p.p. 101-114, 2011.
- [5] Shin, S.J., Suh, S.H., Stroud, I.: *Reincarnation of G-code based part programs into STEP-NC for turning applications*, Computer-Aided Design, Vol. 39, p.p. 1-16, 2007.
- [6] Ouyang, H.B., Shen, B.: *Research on the Conversion from Design Features to Machining Features Faced on STEP-NC*, Third International Conference on Measuring Technology and Mechatronics Automation, p.p. 103-106, 2011.
- [7] Sreeramulu, D., Rao, C.S.P.: *A new methodology for recognizing features in rotational parts using STEP data exchange standard*, International Journal of Engineering, Science and Technology, Vol. 3(6), p.p. 102-115, 2011.
- [8] Mokhtar, A., Xu, X., Lazcanotegui, I.: *Dealing with feature interactions for prismatic parts in STEP-NC*, J Intell Manuf, Vol. 20, p.p. 431-445, 2009.
- [9] Rameshbabu, V., Shunmugam, M.S.: *Hybrid feature recognition method for setup planning from STEP AP203*, Robotics and Computer-Integrated Manufacturing, Vol.25, p.p. 393-408, 2009.
- [10] Abdul-Rani, A.M.B., Gizaw, M., Yusof, Y.: *STEP Implementation on Turn-mill Manufacturing Enviroment*, World Academy of Science, Engineering and Technology, Vol. 60, p.p. 47-52, 2011.
- [11] Yusof, Y., Case, K.: *Design of a STEP compliant system for turning operations*, Robotics and Computer-Integrated Manufacturing, Vol. 26, p.p. 753-758, 2010.
- [12] Habeeb, S., Xu, X.: *A novel CNC system for turning operations based on a high-level data model*. Int. J. Adv. Manuf Technol, Vol.43, p.p. 323-336, 2009.
- [13] Gizaw, M. Abdul-Rani, A.M.B., Yusof, Y.: *Design of STEP-compliant System for Turn-mill Operations using XML*, Journal of Applied Science, Vol. 11(7), p.p. 1171-1177, 2011.
- [14] Alvares, A.J., Ferreira, J.C.E.: *An integrated web-based CAD/CAPP/CAM system for the remote design and manufacturing of feature-based cylindrical parts*, J Intell Manuf, Vol. 19, p.p. 643-659, 2008.

Authors: Mr. Dejan Lukic , Prof. Dr. Velimir Todic, Prof. Dr. Milan Zeljkovic, Dr. Mijodrag Milosevic, MSc Jovan Vukman, MSc Goran Jovicic, University of Novi Sad, Faculty of Technical Sciences, Institute for Production Engineering, Trg Dositeja Obradovica 6, 21000 Novi Sad, Serbia, Phone.: +381 21 485-2331, Fax: +381 21 454-495.
E-mail: lukicd@uns.ac.rs
todvel@uns.ac.rs
milanz@uns.ac.rs
mido@uns.ac.rs
vukman@uns.ac.rs
goran.jovicic@uns.ac.rs

ACKNOWLEDGEMENT: This paper is part of a research on project "Modern approaches to the development of special bearings in mechanical engineering and medical prosthetics," TR 35025, supported by the Ministry of Education and Science, Republic of Serbia.

Mansour, G., Sagris, D., Tsiafis, Ch., Mitsi, S., Bouzakis, K.-D.

EVOLUTION OF A HYBRID METHOD FOR INDUSTRIAL MANIPULATOR DESIGN OPTIMIZATION

Abstract: In the present paper an evolution of a hybrid optimization method is described to find the geometric design parameters and the joint angles when some end-effector poses are prescribed. The problem is solved by minimizing the sum of the deviation squares between the prescribed poses and the real poses of the considered end-effector. The evolution of the proposed algorithm is developed in MatLab software. The developed method is applied in two degrees of freedom spatial serial RR manipulator, in three numerical examples, where one, two or three end-effector poses are prescribed. Furthermore, a comparison of the results between the evolution of the method on MatLab and the initial one based on Fortran demonstrates a higher efficiency of the Matlab approach, regarding the minimum value of the fitness function as well as the computational time.

Key words: Optimization, Genetic Algorithm, Geometric design, Robot, Industrial manipulator

1. INTRODUCTION

The performance of a robot can be considerably improved by optimal evaluation of the robot geometric design parameters, taking into account different criteria, especially in industrial applications. During the last decades several design methodologies have been developed for spatial task oriented robotic systems. These methodologies may be classified into two categories: exact synthesis and approximate synthesis. The exact synthesis methods [1] have the advantage to find all the possible solutions, but only in few spatial manipulators the geometric design problem has been solved. So, the polynomial elimination technique is used in [2, 3] to determine the dimensions of the geometric parameters of RR and 3R manipulators are prescribed. The approximate synthesis methods, involving an optimization algorithm, are used in geometric design problems, where the precision points are less or more than the exact synthesis required points. A combination of the exact synthesis techniques with optimization methods is used in [4] to design a spatial RR chain for an arbitrary end-effector trajectory. A methodology of dimensional approximate synthesis where the problem is expressed in terms of multiobjective optimization by taking account simultaneously several criteria of performance, regarding a Delta mechanism is presented in [5].

The presented evolution of the optimization methodology, is classified in the approximate synthesis methods. This optimization method is already tested in several problems, such as optimum robot base location [6, 7], as well as geometric design optimization of 3R serial robot with geometric restrictions [8], obtaining remarkable results.

2. MATHEMATICAL FORMULATION

In this paper the manipulator is considered as an open space chain with two revolute joints (Fig. 1). A reference frame P_i attached at each link i ($i=0,1,2$) The

relative position between two successive frames is described using the 4x4 homogeneous transformation matrices and the Denavit-Hartenberg parameters [9]. Using the homogeneous transformation matrices, the pose of the end-effector P_3 with respect to the fixed frame P_0 is given by:

$$A_S^3 = A_S^0 \cdot A_0^1 \cdot A_1^2 \cdot A_2^3 \quad (1)$$

where the matrix A_{i-1}^i describes the pose of frame i with respect to frame $i-1$, through the corresponding D-H parameters. The elements of the matrix A_S^3 are known since they define the position and orientation of the end-effector frame 3 at each prescribed pose, with respect to fixed frame P_0 . The right side of equation (1) contains all the unknown Denavit-Hartenberg parameters that are θ_i , α_i , a_i and d_i ($i=0,1,2$).

In order to determine these unknown parameters the objective function is developed. This function consists of the sum of the deviations squares between the prescribed values of the elements of the matrix and the real values. The objective function can be described by:

$$F = \sum_{k=1}^n \sum_{i=1}^3 \sum_{j=1}^4 A_{S_r}^3(i,j) - A_{S_{pr}}^3(i,j)^2 \quad (2)$$

where n is the number of prescribed poses, $A_{S_r}^3(i,j)$ is

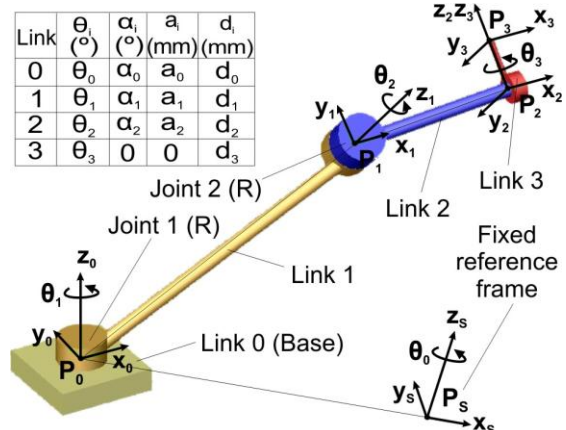


Fig. 1. 2-DOF robot and Denavit-Hartenberg params

the real value of the element (i,j) of the A_S^3 matrix and $A_S^3_{pr\ i,j}$ is the prescribed value of the element (i,j). From the minimization of the objective function, the values of the unknown parameters occur. During the optimization procedure the imposed constraints regarding the unknown variables are described by:

$$x_{\ell \min} < x_{\ell} < x_{\ell \max} \quad \ell=1,2,\dots,m \quad (3)$$

where m is the number of the variables and $x_{\ell \min}$ and $x_{\ell \max}$ are the lower and upper limits of the variable i.

3. PROPOSED ALGORITHM

The described mathematical model is solved with the evolution of a hybrid method [6, 7, 8] that combines a simple genetic algorithm (GA) [10], a quasi-Newton algorithm (QNA) [11] and a constraints handling method (CHM). The basic steps of the proposed algorithm are illustrated in Fig.2.

In the first loop (L1), starting populations are randomly generated to set variables values, which are used to calculate the fitness function value. Genetic algorithm [10] considering these starting populations uses selection, crossover and mutation procedures to create new generations. The optimum variables values of first loop (L1) are inserted in the QNA [11] as an initial variables vector guess. The QNA modifies the values of this vector using a finite-difference gradient method in a way that the fitness function is minimized. Afterwards these output variables values are used in the third loop (L3) to reduce the bounds of each variable, about this optimum selected one.

The minimum calculated value of the fitness function defines the optimum obtained variables values, which represent the location of robot base, the robot links geometry, as well as the robot configurations for all the prescribed end-effector poses.

4. NUMERICAL APPLICATION

The introduced methodology is applied in a spatial manipulator with two degrees of freedom and two revolute joints. The input data used for the algorithm are the variables bounds, the algorithm parameters and the end-effector poses. The initial applied variables limits are presented in Table 1.

Variables i	θ_i (o)	α_i (o)	a_i (mm)	d_i (mm)
0	0-360	0-360	0-1000	0-1000
1	0-360	0-360	0-100	0-100
2	0-360	0-360	0-100	0-100
3	0-360	-	-	0-100

Table 1. Initial variables limits.

Three numerical applications corresponding to one, two and three target points are presented. The three poses of the tool frame (T1, T2, T3) with respect to the fixed Cartesian coordinate system Ps are prescribed. Using these poses the matrices $A_{s_prk}^3$ (k=1,2,3), of the prescribed end-effector poses are evaluated.

For each additional point, two more joints variables are used, which grow up the problem and the solution becomes slower and more difficult.

In order to make obvious the accuracy advantage of the proposed method, four different algorithms were tested in each numerical example. The first one uses only GA, the second combines the GA with the CHM, the third one uses a combination of GA with the QNA and the fourth is the proposed one. The parameters involved in all tests, mainly in GA procedure, are the same and selected as optimum through many applied tests: population of individuals=50, cross probability=70% and mutation probability=8%. All the other algorithm parameters involved in the problem are different in each case and are presented in Table 2. The loops number of GA, QNA and CHM are selected in a way that the total generations number in four tests are equal, in order to be comparable.

Fig. 3., Fig. 4. and Fig. 5. illustrate the value of the fitness function versus the generations number of the four compared methods for the first, second and third numerical example using one, two and three prescribed end-effector poses.

As shown in these figures, the performance of the proposed algorithm is substantially better than that of the three other methods during the whole procedure both in accuracy and computational time. The obtained value of the fitness function in the three examples illustrates clearly the advantage of the proposed algorithm.

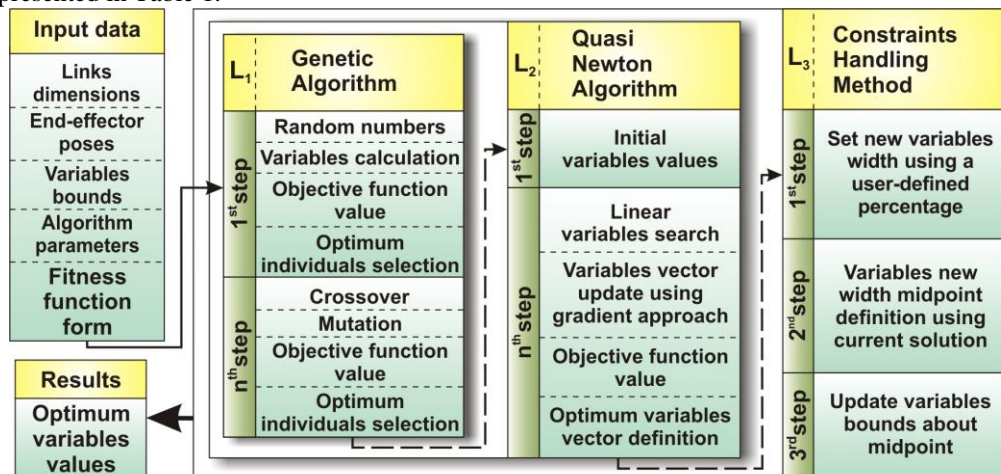


Fig. 2. Flowchart diagram of the developed algorithm.

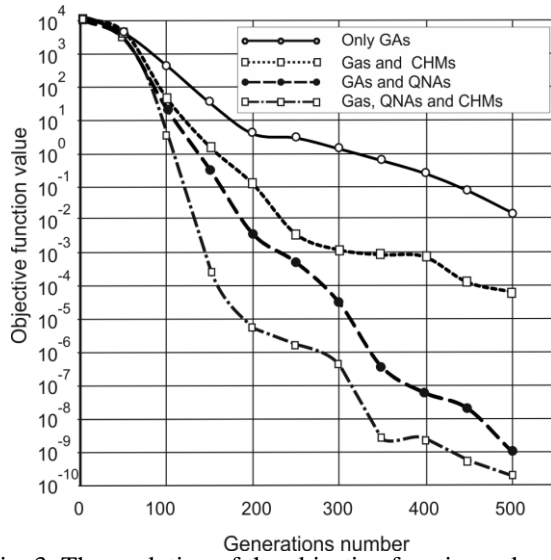


Fig. 3. The evolution of the objective function value for one prescribed end-effector pose.

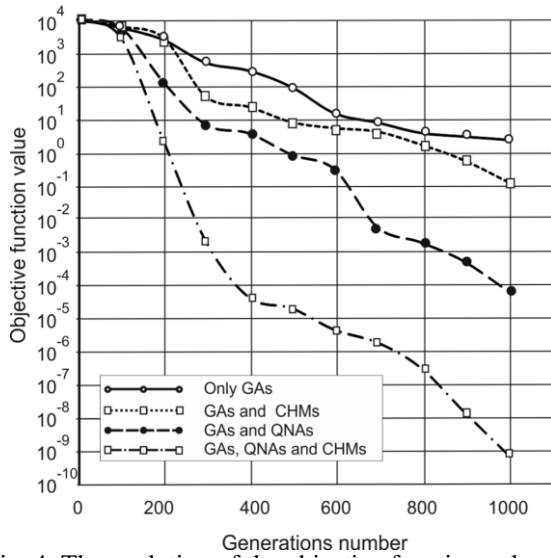


Fig. 4. The evolution of the objective function value for two prescribed end-effector poses.

Regarding the application of the method on the Fortran environment, the comparison between the calculated elements of the matrices and the corresponding elements of the prescribed ones shows

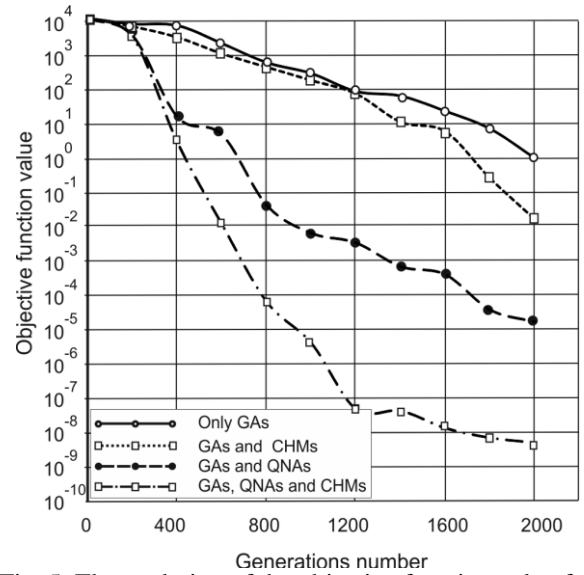


Fig. 5. The evolution of the objective function value for three prescribed end-effector poses.

that the maximum positional deviation is lower than 0.0008 mm. The maximum deviation of orientations is lower than 0.0009 rad (0.052 degrees) in first and second example, which is insignificant value, and lower than 0.0318 rad (1.822 degrees), which is acceptable value.

On the other hand the application of the method on the Matlab environment, obtains better results than FORTRAN regarding the Fitness Function value in a lower computational time as presented in Table 2. The comparison between the calculated elements of the matrices and the corresponding elements of the prescribed ones shows that the maximum positional deviation is lower than 0.0007 mm in the three numerical examples. The maximum deviation of orientations is lower than 0.0006 rad (0.037 degrees), which is insignificant value and even lower than the Fortran approach.

In order to have a clear comparison between the solutions on FORTRAN and MATLAB environments, using the same methodology, an additional test is applied where these two approaches are compared both in accuracy and speed. The testing examples are the same with the presented in Table 2, but two variations

Tool poses	Algorithm	Computational time	Number of loops			Range reduction	Fitness function value
			GA	QNA	CHM		
One	GA	00:35	500	-	-	-	2.10e-02
	GA+CHM	00:32	250	-	2	55%	9.24e-05
	GA+QNA	00:18	10	50	-	-	2.08e-09
	Proposed	00:08	10	10	5	85%	3.64e-10
Two	GA	00:57	1000	-	-	-	3.84e+00
	GA+CHM	01:05	250	-	4	85%	2.24e-01
	GA+QNA	00:38	10	100	-	-	1.26e-04
	Proposed	00:25	10	50	2	35%	1.66e-09
Three	GA	01:43	2000	-	-	-	1.34e+00
	GA+CHM	01:37	500	-	4	15%	2.24e-02
	GA+QNA	01:21	40	50	-	-	2.29e-05
	Proposed	01:08	10	50	4	55%	7.03e-09

Table 2. Algorithms' parameters and obtained fitness function value

Example	Poses	Parameters			Variables range reduction	FORTRAN Results		MATLAB Results	
		Number of loops				Compu-tational time	Fitness value	Compu-tational time	Fitness value
		GA	QNA	CHM					
1 st	1	100	500	4	85%	0:13:04	1.20e-09	0:07:05	3.47e-10
	1	10	10	1	85%	0:00:03	4.73E-06	0:00:03	8.65e-05
2 nd	2	100	500	9	65%	0:36:13	4.33E-06	0:12:53	2.54e-09
	2	100	100	4	65%	0:02:48	2.66E-02	0:01:18	4.57e-05
3 rd	3	100	500	19	30%	2:44:29	4.22E-03	0:53:25	3.39e-10
	3	100	200	9	55%	0:22:06	1.20E-01	0:13:18	7.77e-07

Table 3. Fortran and MatLab approaches comparison.

regarding the repetitions are applied. The first test is applied using a great amount of repetitions in order to examine the efficiency of the Fortran and Matlab approaches regarding the fitness function value, without any computational time restrictions. The second test is applied using a small amount of repetitions in order to examine the efficiency of the compared approaches regarding the computational time, without any fitness function value restrictions.

The parameters of the applied tests, as well as the obtained computational time and fitness function value, are presented in Table 3. The comparison of the proposed method applied on Fortran and MatLab environment, demonstrates an advantage of MatLab approach both on computational time and fitness function value.

5. CONCLUSIONS

In the present paper a comparison between an optimization algorithm based in Fortran and an evolution approach of the same algorithm based in MatLab, to find an optimum solution in a combined problem is presented. The problem involves simultaneously the robot geometry, the robot base position and the joint angles of a 2-DOF spatial RR manipulator. The optimization is obtained through a fitness function that consists of the sum of the deviations squares between the prescribed poses and the real poses of the end-effector, taking into account the workspace restricts and variables limits.

The compared algorithms are written in MatLab and Fortran and the solid graphics are developed in Solid Works environment. Both algorithms and graphics can be modified to agree with any manipulator or problem conditions.

6. REFERENCES

- [1] Pamanes, J.A., Montes, J.P, Cuan, E., Rodriguez, F.C.: Optimal Placement and Synthesis of a 3R Manipulator, International Symposium on Robotics and Automation (ISRA 2000), Monterrey, Mexico, 2000.
- [2] Mavroidis, C., Lee, E., Alam, M.: A New Polynomial Solution to the Geometric Design Problem of the Spatial R-R Robot Manipulators Using the Denavit-Hartenberg Parameters - Transactions of the ASME, Journal of Mechanical Design, Vol. 123, pp.58-67, 2001.

- [3] Lee, E., Mavroidis, C., Solving the Geometric Design Problem of Spatial 3R Robot Manipulators Using Polynomial Homotopy Continuation, Trans. of the ASME, Journal of Mechanical Design, Vol. 124, pp.652-661, 2002.
- [4] Perez, A., McCarthy, M. J.: Dimensional Synthesis of Spatial RR Robots, in: Advances in Robot Kinematics, Kluwer Academic Publ., Netherlands, pp.93-102, 2000.
- [5] Kelaiaia, R. , Company, O., Zaatri, A., Multiobjective optimization of a linear Delta parallel robot, Mechanism and Machine Theory, Vol. 50, pp. 159-178, 2012.
- [6] D. Sagris, S. Mitsi, K.-D.Bouzakis, G.Mansour, 5-DOF robot base location optimization using a hybrid algorithm, Mecatronica, Vol.1, pp.76-81, 2004.
- [7] S. Mitsi, K.-D. Bouzakis, D. Sagris, G. Mansour, Determination of optimum robot base location considering discrete end-effector positions by means of hybrid genetic algorithm, Robotics and Computer-Integrated Manufacturing, Vol.24, pp.50-59, 2008.
- [8] D. Sagris, S. Mitsi, K.-D. Bouzakis, G. Mansour, Spatial RRR robot manipulator optimum geometric design by means of a hybrid algorithm, The Romanian review precision mechanics, Optics & Mechatronics, No. 39, pp. 141-144, 2011.
- [9] Denavit, J., Hartenberg, R.S.: Transactions of the ASME - Journal of Applied Mechanics, E22, 1955, pp.215-22.
- [10] Coley, D.: An Introduction to Genetic Algorithms for Scientists and Engineers - World Scientific Press, 1999.
- [11] IMSL: Fortran Subroutines for Mathematical Applications - Visual Numerics, 1997.

Authors: Ass. Prof. MANSOUR Gabriel, Dr.ing. SAGRIS Dimitrios, TSIAFIS Christos dipl.ing., Prof. MITSI Sevasti, Prof. BOUZAKIS Konstantin, Laboratory for Machine Tools and Manufacturing Engineering, Mechanical Engineering Department Aristoteles University of Thessaloniki, Greece.
E-mail: mansour@eng.auth.gr, dsagris@eng.auth.gr, tsiafis@gmail.com, mitsi@eng.auth.gr, bouzakis@eng.auth.gr

Miletić, O., Todić, M.

SYNTHESIS OF AUTOMAT FOR GUIDANCE OF THE BAND IN PROCESSING SYSTEM OF MULTIPLE OPERATION PROCESS

Abstract: The execution of the optimal automatization of processing system for required technological process should be reimbursed by later synthesis of automat which will achieve the proper conduct of the work area of bar-press tools. Since it takes multiple operation processing, where the work pieces with tools moves from one operation to another together with the band, it is necessary to move with a given accuracy and the possibility of regulating the step size strips.

Key words: automation, band, processing system

1. INTRODUCTION

At layer processing, especially with bands of mechanization and automatization provides more effects, as: increase of productivity, better use of technological equipment, improvement of quality and reduction of production costs, provides conditions for higher security at work etc.

Degree of utilization of possible number of paces at presses is very small (25-30%), at manual conduction of work peace in work area. In case of mechanical, apropos automatically conduction of work peace degree of utilization of number of paces of press is increased for more times. At these devices there is possibility of regulation for different widths and steps of band that is conducted in work area.

Defining of regime of machine work of periodical effect with guaranteed and non-guaranteed pace of executive part is made on principle of work of kinematic part of its operating system which dictates installation of device for conduction of band of basic material in work area. To achieve nominal number of work paces (n_{pn}), apropos possible number of cycles which machine can achieve in unit of time, when between work cycles (t_c) is no pause it is necessary in period of reverse pace of executive part of machine to take out work peace from work area and get in the new work peace.

Relation of achieved and nominal number of work cycles in unit of time should be equal to zero, where comes to burst regime of machine work (no pause between repeated work cycles of machine). To achieve this it is necessary to material-band continuously brings in tune to tact of work press. Shift of band for each tact of machine is done feeder- device for conduction of band trough work area.

2. DESCRIPTION OF DEVICE WORK

On Fig. 1 is shown principle of device work for conduction band through work area of press.

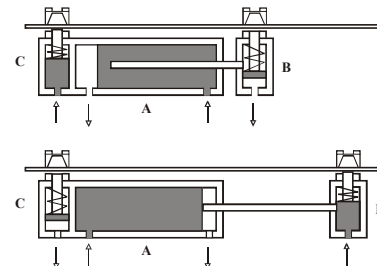


Fig. 1. Device for conduction of band

For executive organs-effectors are used fluidic cylinders: A (for shift of the band), B (for shift of pliers), and C (safety pliers). Lined band in device first is constricted in pliers, and then makes shifts for one step in position for processing. Having in mind that usual marking of plunger movement in cylinder („+“extracted plunger, „-“, drawn in plunger in cylinder), it is necessary that automat in order of device work for conduction of band to order of effectors work, providing next movement: getting back plunger of band for one step in start position (A-) with released transfer pliers (B-); constricted pliers for fixation of band (C+), releasing constricted pliers (C-) constriction of transporting pliers (B+) and suppression of band for one step (A+).

Appointed task of this device, to decrypted technological process, defines order of effectors activation.

(A-B-C+C-B+A+)

3. MOLDING OF FLUIDIC AUTOMAT DEVICE FOR BAND CONDUCTING

Molding is done in three phase:

- coding of entrance and exit,
- determination of block-diagrams of automat and
- Specification of combination board.

For determination /coding of entrance and exit at automat which effectors are fluidic cylinders, it is necessary to know controlling relations with ambience. On Fig. 2 are shown relations with ambience of fluidic effectors.

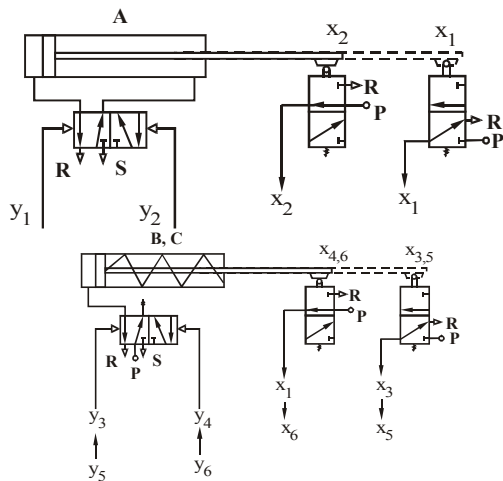


Fig. 2. Controlling relations with ambience

Controlling relations of automat with effectors are provided through memory 5/2 sliding valve on which is made motion of effectors in plus or minus position. Sought order of motion of effectors is provided in information in the form of entrance variables which automat is getting from effectors over positional 3/2 sliding valves. Effectors in certain positions of device

for band conducting activate sliding valves, where on their exits are gained binary variables.

For coding variables and functions is used their binary shape, where for three effectors of this device are necessary six variables ($x_1, x_2, x_3, x_4, x_5, x_6$) and six functions ($y_1, y_2, y_3, y_4, y_5, y_6$). Based on defined variables and functions are gained block-diagrams of automat, Fig. 3.



Fig. 3. Block-diagram of automat

Next step in automat modeling is formation of combinational table, where is absolutely described the work of automat with the state of variables and functions for various positions of effectors. On entrance of automat complexion variables are gained through appropriate position of effectors from positional 3/2 salving valves that make on exit of automat appropriate function $Y_i=1$. Thus formatted complexion variables and their correspondent complexion functions give table of combinations, table 1.

Order number	Q	x_1	x_2	x_3	x_4	x_5	x_6	y_1	y_2	y_3	y_4	y_5	y_6	s	r	Order of activating
41	0	1	0	1	0	0	1	1	0	0	n	n	0	0	n	A-
9	0	0	0	1	0	0	1	n	0	0	n	n	0	0	n	A→-
25	0	0	1	1	0	0	1	n	0	1	0	n	0	0	n	B-
17	0	0	1	0	0	0	1	n	0	n	0	n	0	0	n	B→-
21	0	0	1	0	1	0	1	n	0	n	0	0	1	0	n	C+
20	0	0	1	0	1	0	0	n	0	n	0	0	n	0	n	C→+
22	0	0	1	0	1	1	0	n	0	n	0	0	n	1	0	change of state
86	1	0	1	0	1	1	0	n	0	n	0	1	0	n	0	C-
84	1	0	1	0	1	0	0	n	0	n	0	n	0	n	0	C→-
85	1	0	1	0	1	0	1	n	0	0	1	n	0	n	0	B+
81	1	0	1	0	0	0	1	n	0	0	n	n	0	n	0	B→+
89	1	0	1	1	0	0	1	0	1	0	n	n	0	n	0	A+
73	1	0	0	1	0	0	1	0	n	0	n	n	0	n	0	A→+
105	1	1	0	1	0	0	1	0	n	0	n	n	0	0	1	change of state
41	0	1	0	1	0	0	1	1	0	0	n	n	0	0	n	repetition of process

Table 1. Table of combinations

Because in table of combinations, after,, order number 22” comes to repetition of complexion on entrance (22 and 86) for which on exit of automat-device are gained two different actions of automat, that is two different more complex functions ($n0n00n$ and $n0n010$), which means that there is automat-device with memory, where in the table of combinations are introduced transitional functions r, s and internal variable Q (variables of memory element r, s and exit memory Q). Letter mark,, n” in table of combinations can have value of any bit of $n \in (0,1)$.

4. SYNTHESIS OF MEMORY

Memory that consists from assemblage of memory elements which number depends from number of states

of automat. Memory with „m” memory elements can have from 2^{m-1} to 2^m state. Because automat-device has two states ($2^m=2, m=1$) its memory consists just from one memory element, which is shown in block-diagram, Fig. 4.

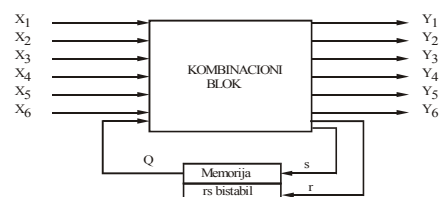


Fig. 4. Block-diagram of automat device

For memory element is taken „r, s” bitable, which action in fluidic performance mach’s 5/2 fluidic

activated salving valve. Exit memory (Q) represents internal variable of automat-device and uses for discrimination from one to the same entrance of more complex of others variables of automat, which eliminates in definition of automat.

5. OPTIMATIZATION OF SYNTHESIS

Synthesis of automat-device is taken based on table of combination and theory of Bulls algebra. Optimal synthesis comes from minimization of logic functions of exit which gives following effects:

- minimal number of logical elements,
- minimal number of relations in automat,
- the biggest reliability in work of automat,
- the lowest price etc.

Because automat of device for conduction of band through work area of press-tool is defined with seven variables, minimization is taken through Veitch-Karnough diagrams, Fig. 5. and 6 (8 diagrams)

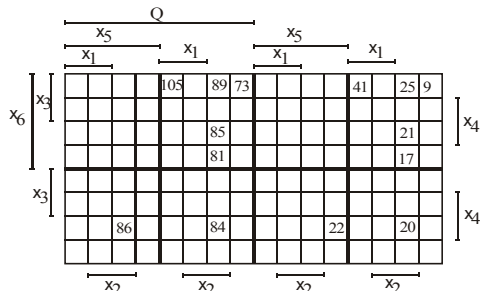
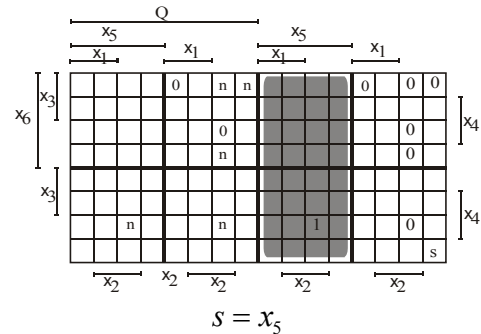
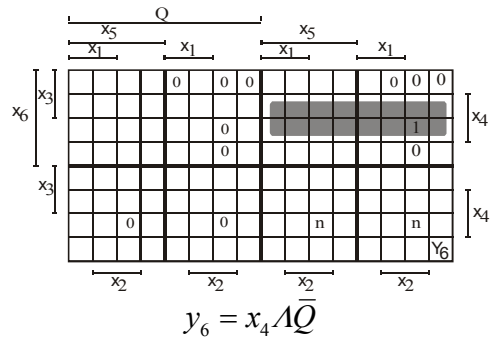
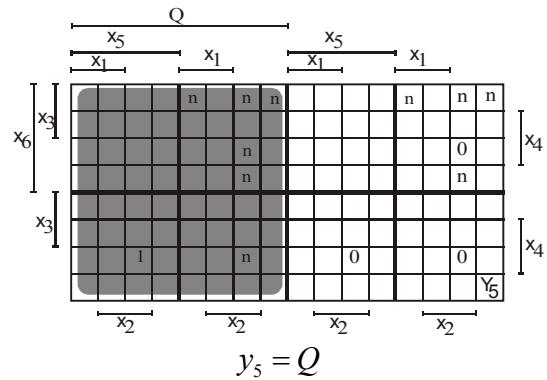
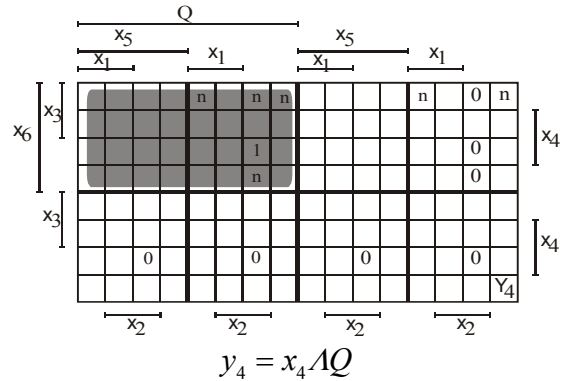
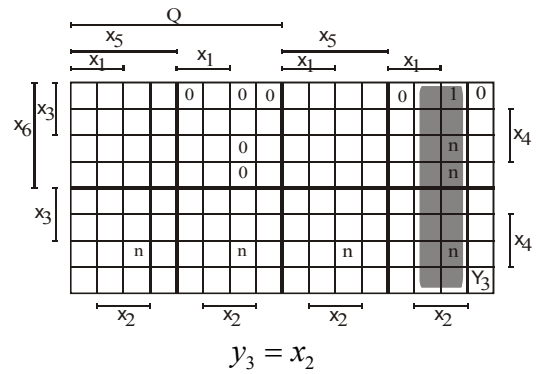
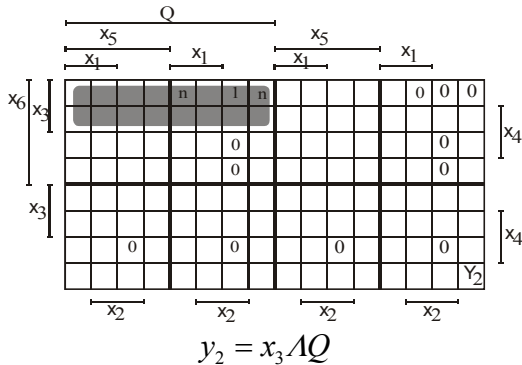
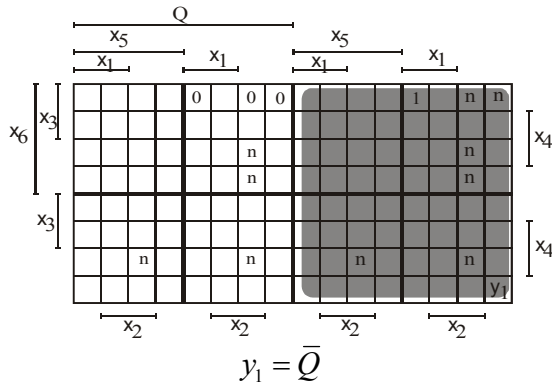


Fig. 5. Veite-Karnough diagram with decimal equivalents of binary more complexes



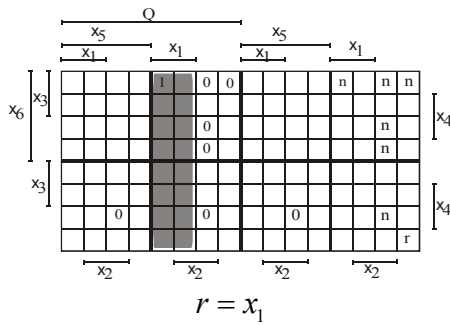


Fig. 6. Veite-Karnough diagram for minimization of functions of automat

In appropriate fields of diagram (Fig. 5) are shown decimal equivalent of binary more complex, which facilitates pursuit for more complex variables and so-called more output minimization.

6. LOGICAL REALIZATION

When operations in logical functions, gained with minimization replace with logical elements is gained logical block-diagram, Fig. 7.

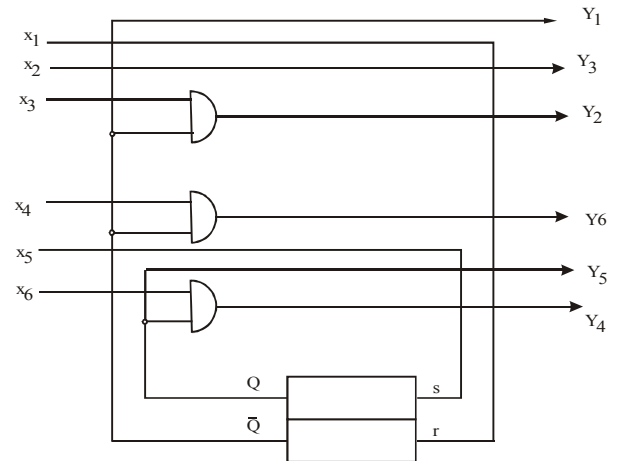


Fig. 7. Logical block-diagram

7. FLUIDIC REALIZATION

Replacement of logical elements, from logical block-diagram, with fluidic logical elements is gained fluidic realization of automat-device for conduction of band through work area of press-tool, Fig. 8.

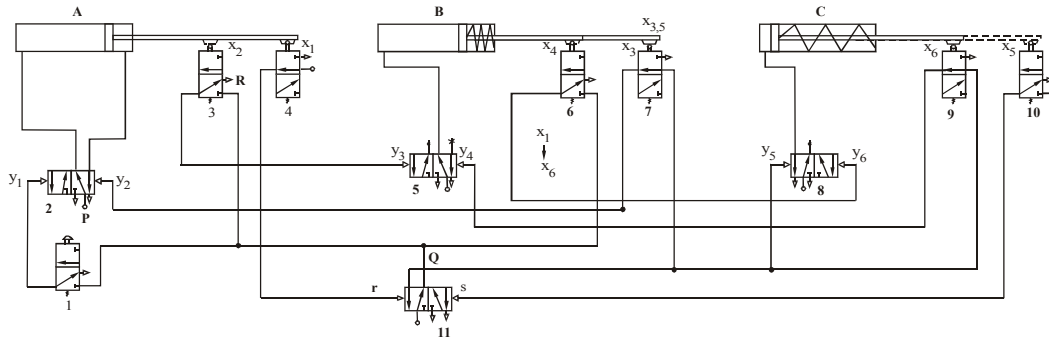


Fig. 8. Fluidic realization of automat-device for conducting band through work area of press

8. CONCLUSION

Executed synthesis of automat using fluidic logical elements, which for realization of logical function use phenomenon mechanic of fluid and energy of fluid for transformation of information. For realization of logical operations of conjunction is used trait of 3/2 salving valve.

Because memory makes only one memory element of type „r, s” bistable, is taken 5/2 fluidic activated salving valve. This provides shifting of band with determinate accuracy with possibility of regulation of step size.

9. REFERENCES

- [1] Miletic, O.: Project of automatically conduction process of scoring of thread in matrix, Engineering Vol. 24. p.p. 245-249, Zagreb, 1982.
- [2] Miletic, O.: Synthesis of fluidic digital automat for mechanical hand at hot rolling, Vol. 33, p.p. 31-36, Zagreb, 1991.
- [3] Miletic, O., Todic, M.: Stability of elastic-plastic system, University book, Banjaluka, 2012.

- [4] Melvin, A.B.: Digital system design automatism: languages simulation & data base, California, 1985.
- [5] Gerc, E.V.: Pnevmaticheskie ustroistva i sistemi v masinostroenim, Moskva, Masinostroenie, 1991.

Authors:

Prof. Dr Ostoja Miletić, University of Banja Luka, Faculty of Mechanical Engineering, Banja Luka
E-mail: ostoja.miletic@unibl.rs
Tel.: ++387 65 673-356
Fax: ++387 51-465-085

Dr. Mladen Todić, University of Banja Luka, Faculty of Mechanical Engineering, Banja Luka.
E-mail: mladentodic@unibl.rs
Fax: ++387 51-465-085
Tel.: ++387 65 176-664

Milojević, Z., Navalusić, S., Zeljković, M., VICEVIĆ, M., Beju, L.

EXTENSION OF THE PROGRAM SYSTEM FOR NC MACHINING PROGRAM VERIFICATION WITH HAPTIC DEVICE

Abstract: In the paper benefits of the haptic interaction in virtual environments and architecture of haptic application are presented. For results, presented in this paper, Sensable PHANTOM Omni device is used, because of that, we presented OpenHaptic developing library for Sensable devices. Earlier developed program system for NC machining program verification is now extended with haptic device support. Because of fact that program system operates in real time and OpenGL graphic library is used for display, OpenHaptics HLAPI is used for haptic device programming which allows significant reuse of OpenGL code User can stop NC verification in any time, and by haptic device can inspect workpiece coordinates.

Key words: haptic interaction, virtual reality, 3-axis milling, virtual manufacturing

1. INTRODUCTION

Virtual reality (VR) technology is often defined as the use of real-time digital computers and other special hardware and software to generate a simulation of an alternate world or environment, which is believable as real or true by the users. In other words, it creates an environment in which the human brain and sensory functions are coupled so tightly with the computer that the user seems to be moving around inside the computer-created virtual world in the same way people move around the natural environment [1].

Haptic interaction with computers implies the ability to use our natural sense of touch to feel and manipulate computed quantities [2]. This ability can make VR space „more real“.

The term “haptics” arises from the Greek root *haptikos*, meaning “able to grasp or perceive”. There are many fields where haptic devices have their application such as medicine, industry, education, arts and entertainment.

In Medicine haptic devices are used for: surgical simulators for training, manipulating robots for minimally invasive surgery, telemedicine, remote diagnosis, etc. In education, for feel phenomena at a variety of spatial and temporal scales, studying complex data sets, etc. In industry in CAD systems, virtual prototyping where assembly and disassembly can guide to the final design, shape sculpting, free-form shape generation and modification.

Avatar is virtual representation of haptic interface in virtual world and user physically interacts with virtually environment by it. If there is a contact between avatar and virtually environment, action and reaction forces are computed and user can feel it by haptic device. Architecture of haptic application is shown on Fig. 1.

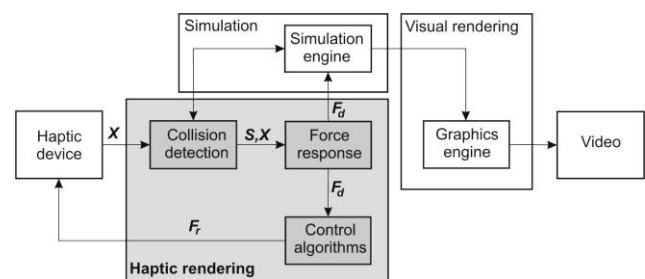


Fig 1. Architecture of haptic application [3]

On Fig. 1, is shown that haptic application is splitted into tree blocks: simulation, visual rendering and haptic rendering. Visual rendering block is responsible for displaying our virtual world. Commonly it is realized by standard graphic libraries like OpenGL. Simulation block consists of simulation engine, which is responsible to compute our virtual word reactions if there are contact between avatar and it. For example contact occurred - move objects, or if we simulate material removing, contact occurred – remove material from virtual object, etc. Haptic rendering block consists of tree modules: collision detection, force response and control algorithms modules. Collision detection module detects collision (contact S) between objects and avatar with its position X in the virtual environment. It can be very simple and check 3DOF point contact of avatar with virtual environments or computationally expensive to check 6DOF contact if avatar presents real 3D object (e.g. virtual tool can be treated as volumetric object). Force response module computes interaction force F_d , between avatar and virtual objects when a collision S is detected. It is based on avatar position X , positions of objects in virtual environment and collision state S . Because haptic device has a limitations to apply an exact force F_d , computed by force response module, control algorithms module calculate F_r force which is applicable to haptic device. Haptic rendering module in common repeats at kHz frequency for more realistic feel of virtual environment.

There are few companies on the market that offer haptic devices some of them are: SensAble Technologies, Force Dimension, Novint, Haption, etc. In this paper SensAble PHANToM Omni haptic device is used .

2. PHANTOM HAPTIC DEVICE

The first PHANToM (Personal Haptic iNTERface Mechanism), which allows one in the human world to interact with objects in virtual reality through touch, was developed by Thomas Massie, while a student of Ken Salisbury at M.I.T. It is relatively low cost force feedback device like a robot arm that is attached to a computer and used as a pointer in three dimensions, like a mouse is used as a pointer in two dimensions. The PHANToM interface's novelty lies in its small size, relatively low cost and its simplification of tactile information. Rather than displaying information from many different points, this haptic device provides high-fidelity feedback to simulate touching at a single point.

Device is introduced in 1995, and was the breakthrough to the growth of haptics. Different PHANToM devices meet varying needs. The Premium models are high-precision instruments and, within the PHANToM product line, provide the largest workspaces and highest forces, and some offer 6DOF (6 degrees of freedom) output capabilities. The PHANToM Desktop and PHANToM Omni devices offer affordable desktop solutions. Of the two devices, the PHANToM Desktop delivers higher fidelity, stronger forces, and lower friction, while the PHANToM Omni is most affordable haptic device at the market [4]. At the Fig. 2 below, PHANToM devices are shown.

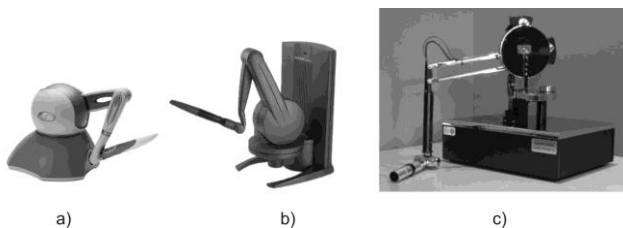


Fig. 2. PHANToM devices, a) Omni, b) Desktop and c) Premium 1.5/6DOF

3. OPENHAPTICS LIBRARY

For haptic application development purpose, there are few libraries on the market, mostly written in C++ programming language some of them are: CHAI3D, H3DAPI and OpenHaptics Toolkit. CHAI 3D is an open source set of C++ libraries for computer haptics, visualization and interactive real-time simulation. CHAI 3D supports several commercially-available haptic devices, and makes it simple to support new custom force feedback devices[chai]. H3DAPI is an open source haptics software development platform that uses the open standards OpenGL and X3D with haptics in one unified scene graph to handle both graphics and haptics. H3DAPI is cross platform and

haptic device independent. In this paper a OpenHaptics Toolkit is used so, it is presented with more details below.

OpenHaptics Toolkit [5] is a commercial software development toolkit specially designed for SensAble devices written in the C++ programming language. Academic Edition for eligible educational institutions can be downloaded for no charge. The OpenHaptics toolkit is divided into these layers: QuickHaptics micro API, Haptic Library API (HLAPI), Haptic Device API (HDAPI), PHANToM Device Driver (PDD) (Fig. 3).

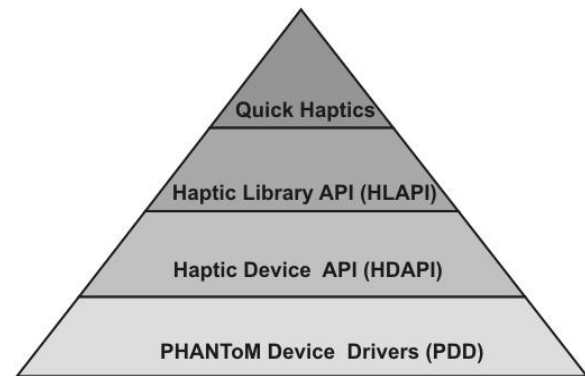


Fig. 3. Open Haptic Toolkit library layers

QuickHaptics micro API, enables any professional with even passing familiarity with C++ to quickly and easily add the kinesthetic feel of what users see and/or hear on a computer screen.

HDAPI (haptic device API) is a low-level foundational layer for haptics rendering and enabling to send force and position manually. HDAPI is a low-level API that handles supported SensAble devices. As every low-level API, it manages the initialization of the device, servo loop, position, rotation and force update

The HLAPI (Haptic Library API) provides high-level haptic rendering and is designed to be familiar to OpenGL API programmers. It allows **significant reuse** of existing OpenGL code and greatly simplifies synchronization of the haptics and graphics threads. HLAPI is a high-level API with the main aim of easier integration of haptics into existing graphics application. It provides mapping of haptic workspace, shape rendering or surface and force effects. A feedback buffer or depth buffer of OpenGL can be used to capture graphics primitives.

4. RESULTS

In this paper we will present developed program system where haptic interaction is included. It is earlier developed program system for NC machining program verification based on approximate dexel approach [6]. NC verification software graphically simulates the material removal process by continuously updating the solid stock shape as the cutter moves along the tool path to produce the final part. NC verification enables following benefits [7]:

- Detect NC program errors and bad or rapid cuts

- Machine parts correctly the first time
- Eliminate expensive and time consuming dry runs and proofing
- Reduce material scrap and overall cost

Developed system enables the real-time simulation for the 3-axis milling and this simulation is not view-dependent. Workpiece and tool are approximated by dexels, which are connected by triangular mesh. Depends on the computer hardware, workpiece and tool resolution may vary. This approach enables that tool and workpiece could be arbitrary shape. System is developed in C++ program language by use of 3D graphics library OpenGL.

The main idea of including haptic interaction in this system is that the user can stop simulation in any time, and touch workpiece in virtual environment. By touch, user can inspect coordinates of workpiece and can detect errors in NC machining program. Also system is extended with stereo display which simulation process makes „more real“. Model of the developed software solution extended with haptic interaction and stereo display is shown on the Fig. 4.

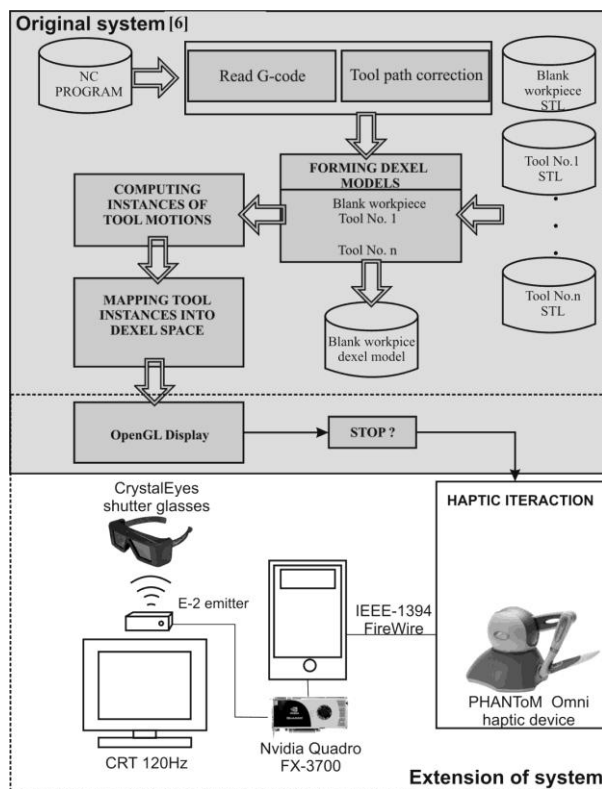


Fig. 4. Model of the developed software solution for NC machining program verification extended with haptic interaction and stereo display

As shown on Fig. 4, the core of original system responsible for NC program reading, dixel models forming, computing instances of tool motion, etc is not changed. System is extended in display module with active stereo support by use of Nvidia Quadro FX-3700 graphic board and CrystalEyes shutter glasses. Also system checks if user selects “stop simulation” option than it includes haptic device interaction and allow user

to inspect workpiece dimensions. Haptic interaction module is shown on Fig. 5 [5].

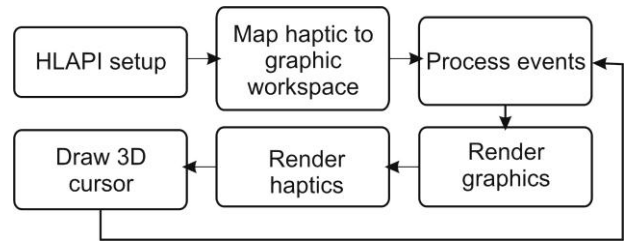


Fig. 5. Haptic interaction module

We use an OpenHaptics HLAPI, because our system is developed by use of OpenGL library and as mentioned earlier in this paper, HLAPI allows significant reuse of OpenGL code.

First, it initializes the HLAPI by creating a haptics rendering context and tying it to a haptic device. Then the program specifies how the physical coordinates of the haptic device should be mapped into the coordinate space used by the graphics. This mapping is used by the HLAPI to map geometry specified in the graphics space to the physical workspace of the haptic device.

Next, the application renders the scene graphics using OpenGL. Then the program processes any events generated by the haptics rendering engine such as contact with a shape or a click of the stylus button. If contact with workpiece exists obtained coordinates are displayed in dialog. Then the haptics are rendered by executing the same code as for rendering the graphics, but capturing the geometry as feedback buffer shape.

We used feedback buffer shape, because second option is a back buffer shape which gives less accurate results than feedback buffer. In addition to rendering scene geometry, a 3D cursor is rendered at the proxy position reported by the HLAPI. Finally, the rendering loop continues by rendering the graphics again. On the Fig. 6, display of our program system is shown.

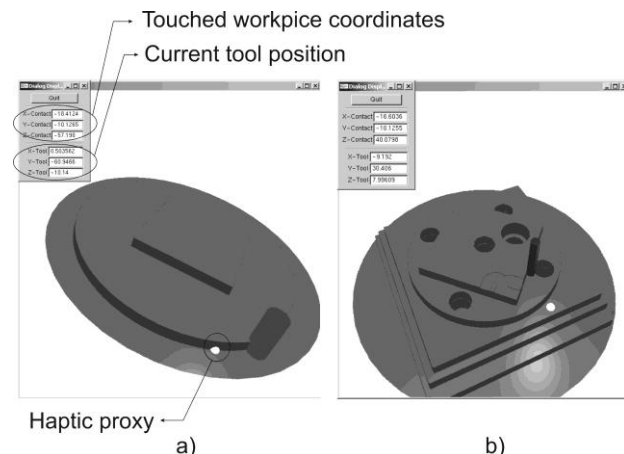


Fig. 6. NC machining program verification display a) cutting process, b) final machined workpiece

5. CONCLUDING REMARKS

In the introductory part of paper, we present importance of the haptic interaction in virtual reality environment.

In addition a benefits of haptic interaction in virtual environments and architecture of haptic application are presented. For results presented in this paper Sensable PHANToM Omni device is used, because of that, we presented OpenHaptic developing library for Sensable devices.

As a results, developed program system where haptic interaction is included is presented. It is earlier developed program system for NC machining program verification based on approximate dixel approach. Now we extended this system with haptic interaction and stereo display support. User can stop machining simulation and by haptic device check a workpieces coordinates.

6. REFERENCES:

- [1] Rheingold, H.: "The Virtual Community - Homesteading on the Electronic Frontier", Addison-Wesley, 1993.
- [2] Bainbridge, W.: "Berkshire Encyclopedia of Human-Computer Interaction" Ed., Berkshire Publishing Group, 2004., pp. 311-316.
- [3] Salisbury, K., Conti, F., Barbagli, F. (2004) : "Haptic Rendering: Introductory Concepts". IEEE Computer Graphics and Applications, vol. 24, 2004., pp. 24-32,
- [4] <http://www.sensable.com/>, Accessed 10.08.2012.
- [5] SensAble Technologies, Inc. (2008): OpenHaptics Toolkit version 3.0 Programmer's Guide, 2008.
- [6] Milojević, Z., Navalusić, S., Zeljković, M. (2007) : "NC Verification as Component of Virtual Manufacturing", Academic Journal of Manufacturing Engineering (AJME), Vol.5, No.2, 2007., pp:48-54
- [7] Mujber, T. S., Szecsi, T., Hashmi, M.S.J.: " Virtual reality applications in manufacturing process simulation", Journal of Materials Processing Technology 155-156, 2004., pp: 1834-1838

ACKNOWLEDGEMENT

In this paper some results of the project: CONTEMPORARY APPROACHES TO THE DEVELOPMENT OF SPECIAL SOLUTIONS RELATED TO BEARING SUPPORTS IN MECHANICAL ENGINEERING AND MEDICAL PROSTHETICS – TR 35025, carried out by the Faculty of Technical Sciences, University of Novi Sad, Serbia, are presented. The project is supported by Ministry of the science and technological development of the Republic of Serbia.

Authors: Dr. Zoran Milojević Assistant Professor, Dr. Slobodan Navalusić Full Professor, Dr. Milan Zeljković Full Professor, Dr. Marija Vičević Assistant Professor, University of Novi Sad, Faculty of Technical Sciences, Trg Dositeja Obradovica 6, 21000 Novi Sad, Serbia, Phone.: +381 21 450-366, Fax: +381 21 454-495.
E-mail: zormil@uns.ac.rs
naval_sl@uns.ac.rs
milanz@uns.ac.rs
marija_vicevic@uns.ac.rs

Dr. Livia Beju Full Professor, "Lucian Blaga" University of Sibiu, "Herman Oberth" Engineering Faculty, Emil Cioran 4, 550025 Sibiu, Romania.
livia.beju@ulbsibiu.ro

Milutinovic, D., Slavkovic, N., Kokotovic, B., Milutinovic, M., Zivanovic, S., Dimic, Z.

KINEMATIC MODELING OF RECONFIGURABLE PARALLEL ROBOTS BASED ON DELTA CONCEPT

Abstract: In order to develop reconfigurable DELTA robot with rotary and translatory actuated joints the generalized modeling approach is discussed. The results of a study on generalization of modeling approach without any use of non-actuated variables has been reported in this paper.

Key words: Delta robot, reconfigurability, kinematic modeling

1. INTRODUCTION

The 3-DOF DELTA structure [1,2] is one of the most famous parallel mechanisms, Fig. 1a. The 4-DOF DELTA robots based on this structure, Figs. 1b and 1c, have been the first real commercial success for parallel robots. The 4-DOF DELTA robot comprise 3-DOF DELTA parallel mechanism and 1-DOF serial wrist for end-effector orientation. Parallel mechanism consist of three kinematic chains with identical topology so that the platform in its motion through the space retains constant orientation. The motors of parallel part of DELTA robot are mounted on fixed base while motor for end-effector orientation may also be on fixed base, Fig. 1b or on the movable platform, Fig. 1c.

The technological structure and capacities of DELTA robot (velocity up to 10 m/s, acceleration over 10g) make it ideal for handling tasks in multitude of sectors such as in food and agriculture, the hygiene sector, beauty care, health care or electronic components. It is also important to mention that DELTA “linear” version is now the base of the fastest machine tools ever produced by industry (acceleration 3.5 - 5g) [4].

The concept of reconfigurable DELTA robots and small machine tools with rotary or translatory actuated joints, Fig. 2, is planned [5,6] with the idea to enable static and dynamic reconfiguration [7]. Several

different approaches in kinematic modeling of DELTA robot with rotary actuated joints have already been published [8-10].

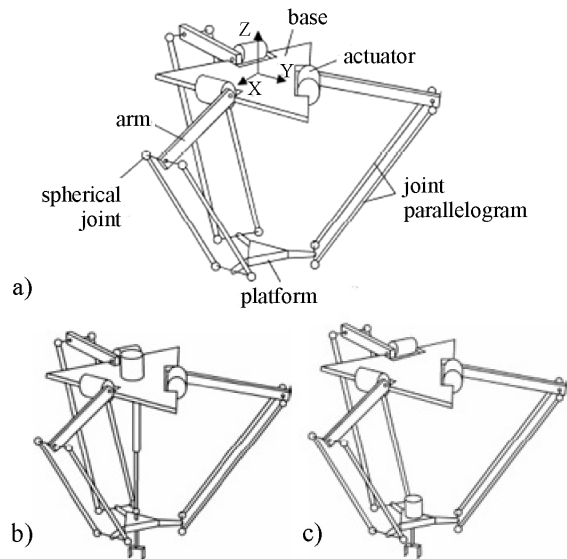


Fig. 1. DELTA robot with rotary actuated joints [3]

Approach presented in [8] uses non-actuated variables while approaches presented in [9,10] does not use any non-actuated variables but lacks generality. One of the most important prerequisites for such widely adopt

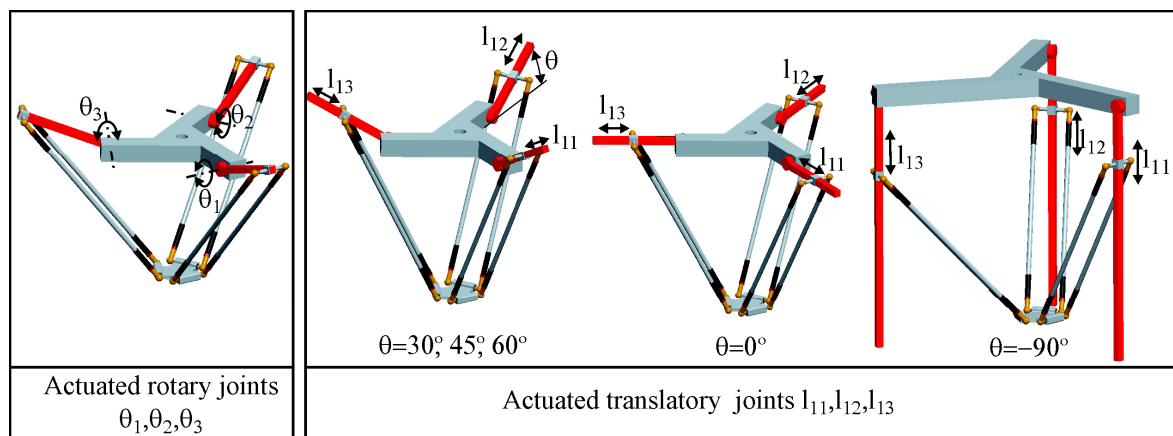


Fig. 2. Concept of reconfigurable DELTA robots and small machine tools with rotary or translatory actuated joints

approach of reconfigurability is generalized modeling approach without any use of non-actuated variables which is reported in this paper.

2. GENERALIZATION OF MODELING APPROACH OF RECONFIGURABLE DELTA ROBOT

Figures 3a and 3b represent geometric models of DELTA robots with rotary and translatory actuated joints from Fig.2, where each parallelogram is represented as a unique rod.

As can be seen from Fig. 3, DELTA robots comprise 3-DOF DELTA spatial parallel mechanisms with rotary or translatory actuated joints and 1-DOF serial wrist for end-effector orientation.

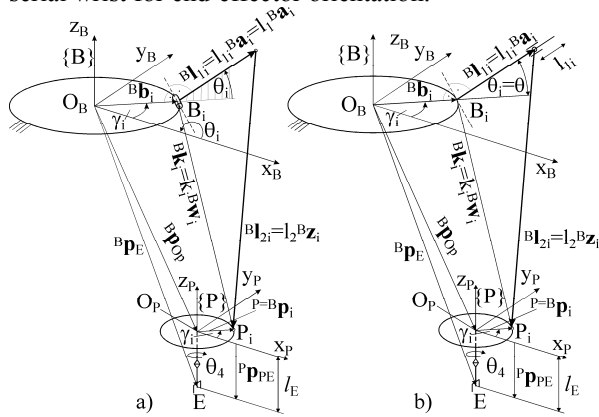


Fig. 3. Geometric models of DELTA robots with rotary and translatory actuated joints

These efficient geometric descriptions of DELTA kinematic structures provide generalized modeling approach without any use of non-actuated variables and implementation of control algorithms on low-cost hardware. Coordinate frames {B} and {P} attached to the base and movable platform are always mutually parallel due to the mechanism's nature. Vectors \mathbf{v} referenced in frames {B} and {P} are denoted by ${}^B\mathbf{v}$ and ${}^P\mathbf{v}$.

Vectors defined by the robot parameters:

$$\bullet {}^P\mathbf{p}_i = [r \cdot c\gamma_i \quad r \cdot s\gamma_i \quad 0]^T, i=1,2,3 \quad (1)$$

are the position vectors of the midpoints P_i between joint centers at the platform located on the circle of radius r with angular position $\gamma_i = 2\pi \cdot (i-1)/3$ and are defined in frame {P}. "c" and "s" refer to cosine and sine functions;

$$\bullet {}^P\mathbf{p}_{PE} = [0 \quad 0 \quad l_E]^T \quad (2)$$

is the position vector of the end-effector tip defined in frame {P} where l_E is length of end-effector;

$$\bullet {}^B\mathbf{b}_i = [R \cdot c\gamma_i \quad R \cdot s\gamma_i \quad 0]^T \quad (3)$$

are position vectors of the points B_i at the base located on the circle of radius R with angular position $\gamma_i = 2\pi \cdot (i-1)/3$ defined in the base frame {B}.

For DELTA robot with rotary actuators points B_i , $i=1,2,3$ represent centers of rotary joints while for

DELTA robot with translatory actuators points B_i represent references points of driving axes;

World coordinates vectors:

$$\bullet \mathbf{x}_E = \begin{bmatrix} {}^B\mathbf{p}_E \\ \phi \end{bmatrix} \text{ represents the position and}$$

orientation of end-effector for all cases of 4-DOF DELTA robots from Fig. 3,

where ${}^B\mathbf{p}_E = [x_E \quad y_E \quad z_E]^T$ is the position vector of end-effector tip E in the base frames {B} while rotational angle ϕ around axis z_B defines end-effector orientations;

$\bullet {}^B\mathbf{p}_{OP} = [x_P \quad y_P \quad z_P]^T = \mathbf{x}_P$ represents location of the platform i.e. origin O_P of the coordinate frame {P} attached to it. The relationship between vectors ${}^B\mathbf{p}_{OP}$ and ${}^B\mathbf{p}_E$ is obvious since coordinate frames {B} and {P} are always mutually parallel i.e.

$${}^B\mathbf{p}_{OP} = \begin{bmatrix} x_P \\ y_P \\ z_P \end{bmatrix} = {}^B\mathbf{p}_E - {}^{P=B}\mathbf{p}_{PE} = \begin{bmatrix} x_E \\ y_E \\ z_E - l_E \end{bmatrix} \quad (4)$$

Vector ${}^B\mathbf{p}_{OP}$ is further considered as world coordinates vector for all cases of 3-DOF DELTA mechanisms.

Joint coordinates vectors:

$\bullet \boldsymbol{\theta}_E = [\theta_1 \quad \theta_2 \quad \theta_3 \quad \theta_4]^T$ is joint coordinates vector for 4-DOF DELTA robot with rotary actuated joints;

$\bullet \mathbf{L}_E = [l_{11} \quad l_{12} \quad l_{13} \quad \theta_4]^T$ is joint coordinates vector for all cases of 4-DOF DELTA with translatory actuated joints.

The relationship between joint angle θ_4 and end-effector orientation angle ϕ , in all cases of 4-DOF DELTA robots, is obvious since frames {B} and {P} are always mutually parallel, i.e. $\theta_4 = \phi$.

Considering this fact, the above joint coordinates vectors $\boldsymbol{\theta}_E$ and \mathbf{L}_E for further considerations are reduced as:

$$\boldsymbol{\theta} = [\theta_1 \quad \theta_2 \quad \theta_3]^T \quad (5)$$

$$\mathbf{L}_E = [l_{11} \quad l_{12} \quad l_{13}]^T \quad (6)$$

where θ_i and l_{1i} , $i=1,2,3$ are scalar variables controlled by actuators.

Unit vectors:

$$\bullet {}^B\mathbf{a}_i = [c\gamma_i \cdot c\theta_i \quad s\gamma_i \cdot c\theta_i \quad s\theta_i]^T, i=1,2,3 \quad (7)$$

unit vectors ${}^B\mathbf{a}_i$ define vectors ${}^B\mathbf{l}_{1i}$ as ${}^B\mathbf{l}_{1i} = l_{1i} \cdot {}^B\mathbf{a}_i$.

For rotary joints, unit vectors ${}^B\mathbf{a}_i$ contain joint coordinates θ_i while $l_{1i} = l_1$, $i=1,2,3$ where l_1 is

fixed arm length.

For translatory joints, unit vectors ${}^B \mathbf{a}_i$ define directions of translatory joints l_{ii} while $\theta_i = \theta$, $i=1,2,3$ is fixed inclination angle of translatory joints. In these cases ${}^B \mathbf{a}_i$ is expressed as

$${}^B \mathbf{a}_i = [c\gamma_i \cdot c\theta \quad s\gamma_i \cdot c\theta \quad s\theta]^T, \quad i = 1, 2, 3 \quad (8)$$

Other vectors and parameters are defined as shown in Fig. 3, where ${}^B \mathbf{w}_i$ and ${}^B \mathbf{z}_i$ are unit vectors while l_2 is fixed length of joint parallelograms.

Based on geometric relations shown in Figs. 3a and 3b the following generalized equations for both geometric models are derived:

$$k_i \cdot {}^B \mathbf{w}_i = {}^B \mathbf{p}_{Op} + {}^{P=B} \mathbf{p}_i - {}^B \mathbf{b}_i \quad (9)$$

$$k_i \cdot {}^B \mathbf{w}_i = l_{ii} \cdot {}^B \mathbf{a}_i + l_2 \cdot {}^B \mathbf{z}_i \quad (10)$$

Vectors $k_i \cdot {}^B \mathbf{w}_i$ in eq. (9) are common for all cases of DELTA robots and using eqs. (1), (3) and (4) can be obtained as

$$k_i \cdot {}^B \mathbf{w}_i = \begin{bmatrix} k_{wxi} \\ k_{wyi} \\ k_{wzi} \end{bmatrix} = \begin{bmatrix} x_p + (r - R) \cdot c\gamma_i \\ x_p + (r - R) \cdot s\gamma_i \\ z_p \end{bmatrix} \quad (11)$$

By taking square of both sides in eq. (10) the following relation is derived

$$l_2^2 = k_i^2 - 2 \cdot l_{ii} \cdot ({}^B \mathbf{a}_i \cdot k_i \cdot {}^B \mathbf{w}_i) + l_{ii}^2 \quad (12)$$

where $k_i^2 = kw_{xi}^2 + kw_{yi}^2 + kw_{zi}^2$.

From this equation inverse and direct kinematics for all cases of DELTA robots can be solved.

2.1 Inverse and direct kinematics for DELTA robot with rotary actuators

Taking into the account that for this case $l_{ii} = l_i$ and substituting eqs. (7) and (11), eq. (12) can be reduced to the well known type of trigonometric equation as

$$\begin{aligned} c\theta_i \cdot (c\gamma_i \cdot kw_{xi} + s\gamma_i \cdot kw_{yi}) + s\theta_i \cdot kw_{zi} &= \\ = \frac{l_1^2 - l_2^2 + k_i^2}{2 \cdot l_i} \end{aligned} \quad (13)$$

from which joint coordinates θ_i , $i=1,2,3$ can be solved.

Equation (13) gives 2 solutions of inverse kinematics, Fig. 4a.

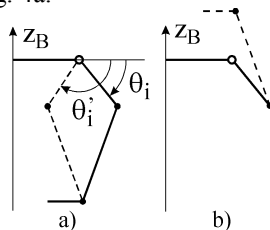


Fig. 4. Two solutions for inverse and direct kinematics

In order to avoid one of the DELTA structure singularities solution θ_i from Fig. 4a has to be chosen. It is important to mention that calculations of each chain in eq. (13) are independent and the algorithm may be implemented on a parallel architecture.

According to eq. (11), eq. (13) in case of direct kinematics represents the system of three equations from which world coordinates x_p , y_p and z_p can be obtained. Among two solutions of direct kinematics only one is physically possible, Fig. 4b.

2.2 Inverse and direct kinematics for DELTA robot with translatory actuators

In case of inverse kinematics, equation (12) is a second order polynomial in terms of l_{ii} and joint coordinates for all cases of DELTA robots with translatory actuated joints are obtained as

$$l_{ii} = ({}^B \mathbf{a}_i \cdot k_i \cdot {}^B \mathbf{w}_i) + \sqrt{({}^B \mathbf{a}_i \cdot k_i \cdot {}^B \mathbf{w}_i)^2 + k_i^2 - l_2^2} \quad (14)$$

Equation (14) gives two solutions of inverse kinematics but only solution with positive square root can be chosen. It is also important to mention that calculations of each chain in eq. (14) are independent and the algorithm may be implemented in parallel architecture.

According to eq. (11), eq. (14) in case of direct kinematics, represents the system of three equations from which world coordinates x_p , y_p and z_p can be obtained. Among two solutions of direct kinematics only solution when $z_p < 0$, is physically possible.

3. DELTA ROBOT FIRST PROTOTYPE

On the basis of adopted concept and design parameters the first DELTA robot prototype with rotary actuators completely has been designed, built and tested in our laboratory, Fig. 5.

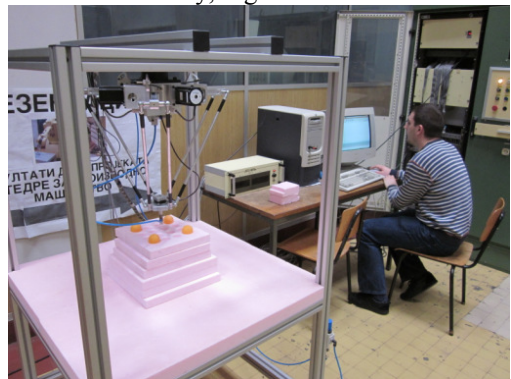


Fig. 5. DELTA robot first prototype

Parallel mechanism provides three degrees of freedom of end-effector positioning. At this stage, actuators are composed of step motors and timing bolts are located on the stationary base. The fourth degree of freedom provides orientation of end-effector and is also actuated by step motor located of the moving plate. End-effector is equipped with standard vacuum cup with pneumatically powered vacuum generator (venturi tube).

Figure 6 represents a simplified structure of control and programming system.

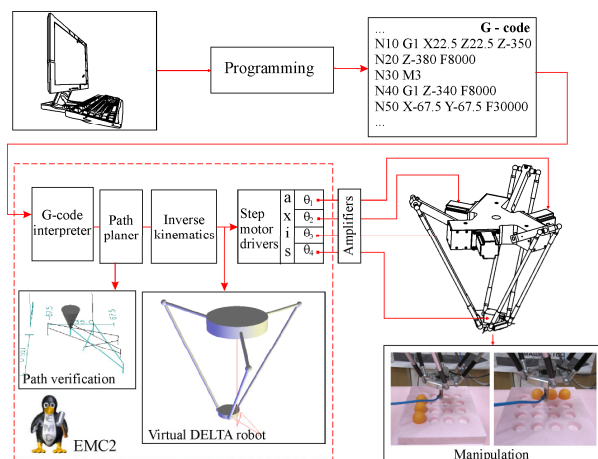


Fig. 6. The structure of control and programming system

Among several proposed OAC (Open Architecture Control), solution the first low-cost control system is based on PC real-time Linux platform with EMC2 software for computer control of machine tools, robots, parallel kinematics machine. EMC2 was initially created by the NIST and is free software released under the terms of the General Public License (<http://linuxcnc.org>). Based on equation (13) kinematics modul is programmed in C language and integrate in EMC2 software system.

In this stage, the programming system is very conventional with the use of G code. During G-code loading, EMC2 software performs path verification. When the program starts running, G-code instructions are executed in real time and generated control signals are directed to real and/or virtual DELTA robot. The virtual DELTA robot makes possible simulation of the real DELTA robot for the user, i.e., verification of the program in robot workspace.

4. CONCLUSION

In order to develop reconfigurable DELTA robot with rotary or translatory actuated joints, the generalized modelling approach is discussed. The results of study on generalization of modelling approach without any use of non-actuated variables have been detailed reported in this paper. Based on analytically solved inverse and direct kinematics, control algorithms are implemented on low-cost hardware with EMC2 computer control software. The developed and investigated prototype indicates that proposed reconfigurable concept with generalized modelling approach will be superior to comparable approaches, which justify further research in this direction.

Acknowledgements. The authors would like to thank the Ministry of Education and Science of the Republic of Serbia for providing financial support that made this work possible.

5. REFERENCES

- [1] Clavel, R.: *Device for the Movement and Positioning of an Element in Space*, United States Patent #4,976,582, Dec. 11 1990.
- [2] Demaurex, M.O.: *The Delta Robot within the Industry*, in: Boer, C.R., Molinari-Tosatti, L., Smith, K.S. (Ed): *Parallel Kinematic Machines*, Springer Verlag, London, pp. 395-400, 1999.
- [3] Rey, L., Clavel, R.,: *The Delta Parallel Robot*, in: Boer, C.R., Molinari-Tosatti, L., Smith, K.S. (Ed): *Parallel Kinematic Machines*, Springer Verlag, London, pp. 401-417, 1999.
- [4] Pierrot, F.: *Towards non-hexapod mechanisms for high performance parallel machines*, Proceedings of 26th Annual Conference of the IEEE IECON, Vol. 1, pp. 229 – 234, Nagoya, 2000.
- [5] Milutinovic, D., Slavkovic, N., Kokotovic, B., Dimic, Z., Glavonjic, M., Zivanovic, S.: *Development of the Domestic Delta Robot Based on a New Kinematic Modeling Approach (in Serbian)*, pp. 3.104-3.111, Proceedings of 38th JUPITER Conference, University of Belgrade, Mechanical Engineering Faculty, Belgrade, 2012.
- [6] Tanovic, Lj., Bojanic, P., Glavonjic, M., Milutinovic, D., Majstorovic, V., et al.: *The development of a new generation of domestic machining systems (in Serbian)*, Annual report (TR-35022), University of Belgrade, Mechanical Engineering Faculty, Belgrade, 2011.
- [7] Schmitt, J., Inkermann, D., Stechert, C., Raatz, A., Vietor, T.: *Requirement Oriented Reconfiguration of Parallel Robotic System*, in: Dutta, A. (Ed): *Robotic Systems – Applications, Control and Programming*, InTech, Rijeka, pp. 387-410, 2012.
- [8] Strenheim, F.: *Computation of the direct and inverse geometric models of the Delta 4 parallel robot*, Robotersystem, Vol. 3, pp. 199-203, 1987.
- [9] Pierrot, F., Reynaud, C., Fournier, A.: *DELTA: a simple and efficient parallel robot*, Robotica, Vol. 8, pp. 105-109, 1990.
- [10] Pierrot, F., Dauchez, P., Fournier, A.: *Fast Parallel Robots*, Journal of Robotic Systems, Vol. 8, No. 6, pp. 829-840, 1991.

Authors: Prof. Dr. Dragan Milutinovic, Nikola Slavkovic, dipl.ing., M.Sc. Branko Kokotovic, Doc. dr Sasa Zivanovic, University of Belgrade, Faculty of Mechanical Engineering, Production Engineering Department, Kraljice Marije 16, 11120 Belgrade, Serbia, Phone.: +381 11 3302-415, Fax: +381 11 3370-364., M.Sc. Milan Milutinovic, Tehnikum Taurunum High Engineering School Vocational Studies, Nade Dimic 4, Zemun, 11080 Beograd, Serbia, Dimic Zoran, dipl.ing., Research and Development Institute LOLA, L.T.D., Kneza Viseslava 70A, 11030, Belgrade, Serbia

E-mail: dmilutinovic@mas.bg.ac.rs
nslavkovic@mas.bg.ac.rs
bkokotovic@mas.bg.ac.rs
mmilutinovic@tehnikum.edu.rs
szivanovic@mas.bg.ac.rs
zoran.dimic@li.rs

Mircheski, I., Kandikjan, T.

DESIGN FOR DISASSEMBLY METHODOLOGY FOR DETERMINATION OF OPTIMAL DISASSEMBLY SEQUENCE BASED ON CONTACT RELATIONS BETWEEN COMPONENTS AND FASTENERS IN THE PRODUCT ASSEMBLY

Abstract: *Design for disassembly (DfD) for product end-of-life is a methodological approach that includes assembly analysis in order to increase the recovery of recyclable materials, and reusable parts and subassemblies. In this paper, a methodology for determination of the optimal disassembly sequence is presented, which is applied in the product design process, and based on the contacts between components and fasteners in the product assembly. The developed procedure for planning of disassembly sequences is based on a component-fastener connection graph and AND/OR logic operations. Disassembly sequence evaluation and obtaining of optimal disassembly sequence is a function of disassembly costs and revenues. In order to present the applicability of the methodology for determination of the optimal disassembly sequence in the early stages of product development, an example is analyzed. The methodology developed in this research is implemented in the programming software Visual Basic for Application (VBA) which runs in a CAD system platform directly on virtual 3D assembly models.*

Key words: *design for disassembly, product recovery, optimal disassembly sequence.*

1. INTRODUCTION

At the end of their useful life, products become waste. The waste from end-of-life products can be defined as unnecessary goods or residues that do not have value for the owner. During the last few decades, the rapid development of automobiles, electric and electronic equipment, resulted in creation of billions tones of waste. Current legal regulations such as Directive 2000/53/EC for end-of-life vehicles and 2002/96/EC for waste electrical and electronic equipment (WEEE), clearly indicate that the technical products should be designed considering the recovery of the product at the end-of-life stage.

Design for Disassembly – DfD is a design tool with a goal to optimize the product structure and other design parameters in order to simplify and improve the disassembly of components for service, replacement or reuse; improve the disassembly of components by separation of proper fastener; group the materials for recycling; limit the disassembly costs; and etc. Also, the goal of design for disassembly is to optimize the product architecture and characteristics of the components in the product assembly. The benefits of the design for disassembly are in increasing of the percentage of reuse for the components; larger percentage of material recycling; limitation of adverse impact on environment; easier servicing and maintenance of products; and greater total return from the end-of-life products.

2. RELATED WORK

Many authors have developed different methods for determining of the optimal disassembly sequence and for planning of the disassembly process. A disassembly hypergraph, called AND/OR graph, which can represent compactly all disassembly sequences, is

proposed by Homem de Mello et al. They developed an algorithm for generation of the AND/OR graph based on a relational assembly model. The input data include answers to queries about the movability of the components in order to determine the feasible disassembly sequences [7]. A.J.D. Lambert et al. in series of papers [1, 3, 5] represents a research of method for linear programming and determination of disassembly sequences for end-of-life products. The method with linear programming gives a contribution in optimization of disassembly process, which is presented in the papers [3, 5].

3. DESIGN FOR DISASSEMBLY METHODOLOGY FOR OBTAINING OF DISASSEMBLY SEQUENCES

The product disassembly is required both during the product life cycle and after the end of the product life. The disassembly process can be destructive and non-destructive. Destructive disassembly represents a process where the stream of end-of-life products is shredded in small fragments which are later separated according to their material composition using special separation techniques. Destructive disassembly process is applied mostly at the product end-of-life, for products that don't have hazard materials inside. Non-destructive disassembly process is applied during the exploitation of the product and at product end-of-life. During the product exploitation, maintenance, service or replacement of some nonfunctional components is needed. While for end-of-life products, non-destructive disassembly process is needed for: recovery of some functional components [2]; removing of hazardous materials from the product, which can have negative influence on the recycling process, and can pollute the environment; extracting of the precious materials from the product; remanufacturing, etc.

The goal of this paper is definition of the methodology for determination of optimal disassembly sequence based on contact relations between components and fasteners in the product assembly.

As shown in Figure 1, the design for disassembly methodology is carried out in three main phases. In the first phase, an algorithm identifies all fasteners, components, contacts between fasteners (F) and components (C) in the product assembly, materials and weight of fasteners and components. The identification is carried out directly from an assembly CAD model. In the second phase, the optimal disassembly sequence is determined in several steps, such as, determination of contact matrix (FC) between fasteners and components, all subassemblies (SA) in product assembly (A), lists for SA, F, C, the disassembly operations, all possible disassembly sequences and the optimal disassembly sequence. Determination of optimal disassembly sequence for virtual assembly model depends on disassembly times, costs and revenues. The third phase is creative phase, which includes product redesign by selection of new fasteners, improvement of product structure and the choice of other types of materials, in order to increase the overall return of the product without change in the product functionality. The changes made in the redesign process, by feedback go to the CAD model of the product assembly, and again pass through the first and second phase.

In the third phase, also, the optimal disassembly sequences for the original and the redesigned product are compared and a choice of best optimal solution for product structure from the aspect of disassembly is made. The overall design for disassembly methodology is an iterative process which gives optimal solution for product structure.

4. PRODUCT REPRESENTATION

The disassembly process is started with the CAD model of the product assembly. The product consists of a number of discrete components, such as, parts, fasteners, etc. Components can be grouped in subassemblies. A subassembly is a connected set of components. If components are physically linked, such link is called a connection. If the components are nearly in touch with each other, this can be considered a virtual connection in some cases [4].

Connections restrict the freedom of motion of the components involved. This can be established in different ways, the most uncomplicated way is mating [3]. In many cases, specialized components, or parts of components, called fasteners, are used for connections. Fasteners can be discrete components such as screws, or non-discrete material objects such as snap fits, press fits, etc [3]. The set of components can be given by the following expression:

$$C = \{C_1, C_2, \dots, C_n\} \quad (1)$$

The set of fasteners can be given by the following expression:

$$F = \{F_1, F_2, \dots, F_m\} \quad (2)$$

where n is number of components in the product and m is number of fasteners in the product. The assembly of product is composed from all components and fasteners and mathematically can be explained with the following mathematical expression

$$A = C_1 C_2 \dots C_n F_1 F_2 \dots F_m.$$

In order to demonstrate proposed design for disassembly methodology, the product hair-dryer is used as example. The main goal of the methodology is the determination of the optimal disassembly sequence. Constituent components of the hair-dryer are: housing which is consisted of two components (called C_1 =Body part and C_2 =Back part), C_3 =Propeller, C_4 =Electric motor, C_5 =Heating element. A discrete fasteners in the hair dryer are: F_1 =F-Bolt M2x8-1, F_2 =F-Bolt M2x8-2, F_3 =F-Bolt M2x28-1, F_4 =F-Bolt M2x8-3, and non-discrete fasteners are: F_5 =F-Holder, F_6 =F-Exit part and F_7 =F-Button. In the Figure 2 is shown CAD model of product assembly for hair-dryer and its constituent elements with exploded view. For simplicity of calculations the abbreviation names for components and fasteners (C_1, C_2, \dots and F_1, F_2, \dots) are applied.

Non-discrete fasteners are material objects and represent the whole with component. For this reason the component which have non-discrete fastener in this paper will be defined as fastener. The set of components in the product for example is $C = \{C_1, C_2, C_3, C_4, C_5\}$ where number of the component is $n=5$ and the set of fasteners is $F = \{F_1, F_2, F_3, F_4, F_5, F_6, F_7\}$, where number of fasteners is $m=7$.

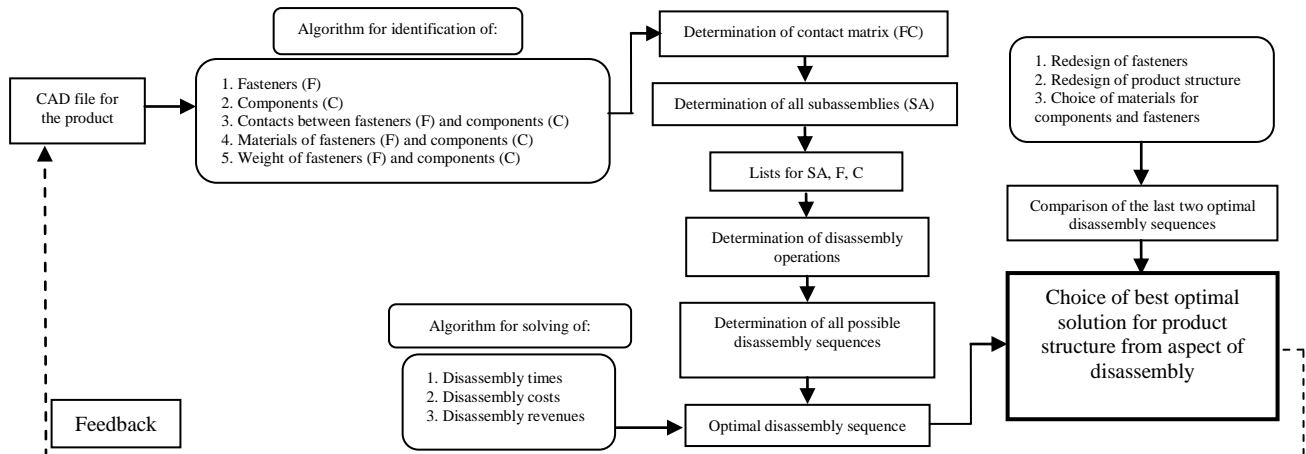


Fig. 1. A methodology for product design for disassembly for determination of optimal disassembly sequence

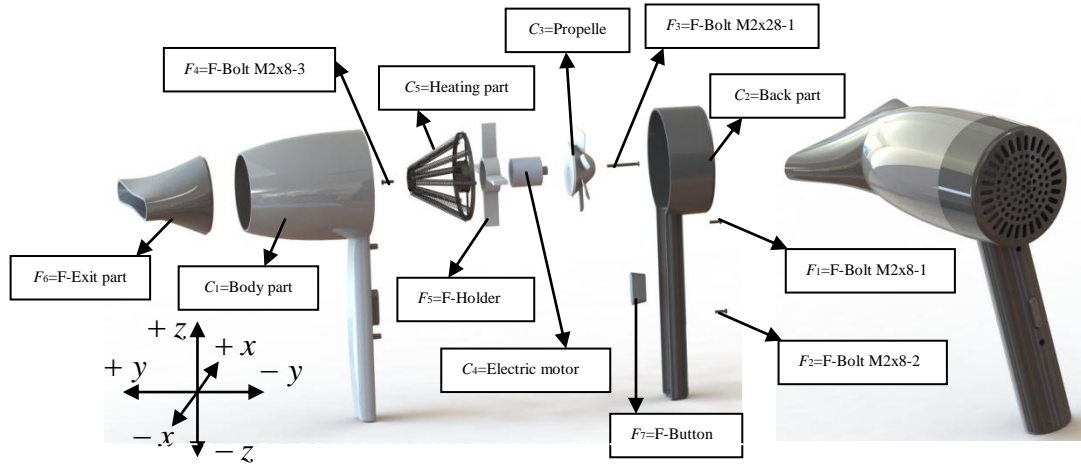


Fig. 2. Exploded view and assembly of hair-dryer

All assembly is represented with the following expression $C_1C_2C_3C_4C_5F_1F_2F_3F_4F_5F_6F_7$.

5. DEFINITION OF CONTACT MATRIX AND DIAGRAM BETWEEN COMPONENTS AND FASTENERS

The relationship between components and fasteners in an assembly is required in order to determine all subassemblies in assembly. For this goal will be defined contact matrix and contact diagram between components and fasteners. The contact diagram represent visualization tool for analyzing of subassemblies in the product assembly. If the component is in contact with some fastener in the assembly the element F_jC_i in contact matrix will be equal of 1, in otherwise 0. The contact matrix can be representing with follow equation:

$$FC = [F_jC_j]_{\substack{j=1,2,\dots,m \\ i=1,2,\dots,n}} \quad (3)$$

In the Figure 3 is given contact matrix and diagram for example hair dryer shown in the Figure 2.

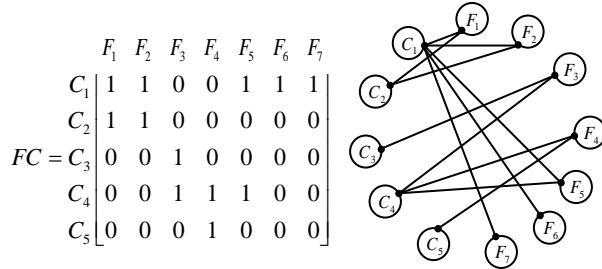


Fig. 3. Contact matrix and diagram between components and fasteners in assembly

6. GENERATION OF ALL FEASIBLE SUBASSEMBLIES IN ASSEMBLY

Subassemblies from the first level are generated on the base of the matrix represented in the Figure 3. Subassemblies from the first level are composed from a components and one fastener.

In the case of the hair-dryer, the set of subassemblies at the first level is: $SA_1 = \{C_1C_2F_1, C_1C_2F_2, C_3C_4F_3, C_4C_5F_4, C_1C_4F_5, C_1F_6, C_1F_7\}$. From the matrix shown in Figure 3, components and fasteners which cross-section of rows and column is 1 are combined.

The set SA_1 obtain from contact matrix in general can be represented with the follow expression:

$$SA_1 = \{C_{i_1} \dots C_{i_k} F_j \mid \quad (4)$$

$$(i_1, j) = (i_2, j) = \dots = (i_k, j) = 1\}$$

where i_k ($k=1, \dots, n$) represents k -th row in the matrix FC and $j=1, \dots, m$ represents column in the matrix FC .

The subassemblies from higher the order in general can be represented with the following expression:

$$SA_{n+1} = \{C_{i_1} \dots C_{i_h} C_{e_1} \dots C_{e_t} F_{j_1} \dots F_{j_{m+1}} \mid \quad (5)$$

$$C_{i_1} \dots C_{i_h} F_{j_1} \dots F_{j_t} \in SA_n \wedge C_{e_1} \dots C_{e_t} F_{j_{t+1}} \dots F_{j_{m+1}} \in SA_n$$

$$\wedge \exists s \in \{1, \dots, h\} \wedge \exists f \in \{1, \dots, t\}$$

$$\text{such that } C_{i_s} = C_{e_f}\}$$

where SA_n is the set from n -th level and SA_{n+1} is the set from $n+1$ level. Members from the set SA_{n+1} are

$C_{i_1} \dots C_{i_h} C_{e_1} \dots C_{e_t} F_{j_1} \dots F_{j_{m+1}}$ which are obtained with combination of the two members $C_{i_1} \dots C_{i_h} F_{j_1} \dots F_{j_t} \in SA_n$ and

$C_{e_1} \dots C_{e_t} F_{j_{t+1}} \dots F_{j_{m+1}} \in SA_n$ and both members are

from the set SA_n where is needed to exist one component which is contained in both members $C_{i_s} = C_{e_f}$. Note: with agreements the same component which exists in both members from the set

SA_n can be written once in the following way $C_1C_1C_2F_1F_2=C_1C_2F_1F_2$. In the framework of the

example the set from the second level is obtained from the members of the set from the first level. The set from the

second level is $SA_2 = \{C_1C_2F_1F_2, C_1C_2C_4F_1F_5, C_1C_2F_1F_6, C_1C_2F_1F_7, C_1C_2C_4F_2F_5, C_1C_2F_2F_6,$

$C_1C_2F_2F_7, C_3C_4C_5F_3F_4, C_1C_3C_4F_3F_5, C_1C_4C_5F_4F_5, C_1C_4F_5F_6, C_1C_4F_5F_7, C_1F_6F_7\}$. The set SA of all possible subassemblies which are obtained from the

product can be obtained with equation:

$$SA = SA_1 \cup SA_2 \cup \dots \cup SA_n \quad (6)$$

In the framework of the example with hair-dryer the set $SA = \{C_1C_2F_1, C_1C_2F_2, C_3C_4F_3, C_4C_5F_4, C_1C_4F_5, C_1F_6, C_1F_7,$

$C_1C_2F_1F_2, C_1C_2C_4F_1F_5, C_1C_2F_1F_6, C_1C_2F_1F_7, \dots\}$. The total number of subassemblies in the example is 57 subassemblies. All possible subassemblies are obtained

with software which is made for analyzing of the disassembly sequences and for obtaining of optimal disassembly sequence.

7. DEFINITION OF DISASSEMBLY OPERATIONS

A component or fastener is material entity that can be separated from a product via nondestructive and destructive disassembly operations [3]. In this paper will be considered nondestructive disassembly process. The input data in definition of disassembly operations are all feasible subassemblies. The disassembly operations are needed for the definition of disassembly sequences, among which the optimal one can be searched for certain parameters are set. The set of disassembly operations can be defined with the following equation:

$$DO = \{DO_{num}, \{XF_{j_1} \dots F_{j_n}, YF_{j_1} \dots F_{j_n}\} \mid$$

$$XF_{j_1} \dots F_{j_n} \in SA \wedge YF_{j_1} \dots F_{j_n} \in SA \wedge \quad (7)$$

$$\{XF_{j_1} \dots F_{j_n}\} \cup \{YF_{j_1} \dots F_{j_n}\} = ZF_{g_1} \dots F_{g_v} \wedge$$

$$ZF_{g_1} \dots F_{g_v} \in SA \wedge \{F_{j_1} \dots F_{j_n}\} \cap \{F_{j_1} \dots F_{j_n}\} = \emptyset\}$$

Note: That component (C) in $Y = C_{e_1} \dots C_{e_w}$ which is repeated in $X = C_{i_1} \dots C_{i_k}$, will be deleted in Y. The set Z is function from union of the components from the product assembly which is obtained from the sets X and Y. $DO_{num} = 1, \dots, D_{on}$, where D_{on} represents total number of disassembly operations.

The example with the hair-dryer is calculated in the special software made for analyzing of the disassembly where are obtained all possible disassembly operations. The total number of disassembly operations is 161. Because there are a lots of numbers of disassembly operations there will be shown only part of them (fig 4).

0	C1C2C3C4C5F1F2F3F4F5F6F7	
1	C1C2C3C4C5F1F2F3F4F5F7	F6
2	C1C2C3C4C5F2F3F4F5F6F7	F1
3	C1C2C3C4C5F1F3F4F5F6F7	F2
4	C1C2C4C5F1F2F4F5F6F7	C3F3
5	C1C2C3C4F1F2F3F5F6F7	C5F4
6	C1C2C3C4C5F1F2F3F4F5F7	F6
7	C1C2C3C4C5F1F2F3F4F5F6	F7

Fig. 4. List of disassembly operations

8. GENERATION OF DISASSEMBLY SEQUENCES

The transition matrix TM and AND/OR graph have the same meaning, and TM can be obtained if all feasible subassemblies and disassembly operations are known. In the previous sections, all feasible subassemblies and disassembly operations are defined. TM can be formulated in the following way: the generic element TM_{ij} is -1 if the j action disassembles parent subassembly i , and is +1 if the j actions create the son subassembly, component or fastener i . All other elements are 0 [6].

Referring to the product assembly shown in Figure 2, the segment from TM is presented in Table 1. The first row in TM represents the product assembly, the second group of rows represents all feasible subassemblies, and the third and fourth groups of rows represent the fasteners and the components in the product, respectively. The columns represent the

feasible disassembly operations. In the matrix, a disassembly operation of a certain subassembly is represented by -1 in the row corresponding to that subassembly. For some subassemblies, there are several feasible disassembly operations, which are shown in the matrix with -1 in the corresponding colons. The columns that show a parent subassembly have -1, and the two or more components and fasteners which are children of that subassembly, have 1 in the same column as the parent subassembly.

For example, the product assembly $C_1C_2C_3C_4C_5F_1F_2F_3F_4F_5F_6F_7$ can be divided with disassembly operation 2 of subassembly $C_1C_2C_3C_4C_5F_2F_3F_4F_5F_6F_7$ and fastener F1. In the row where there is complete assembly will be put -1 and in the rows where complete assembly is divided will be put 1 in the case of subassembly $C_1C_2C_3C_4C_5F_2F_3F_4F_5F_6F_7$ will be put 1 and for fastener F1 will be put 1. After the subassembly $C_1C_2C_3C_4C_5F_2F_3F_4F_5F_6F_7$ can be divided with 19-th disassembly operation of subassemblies $C_1C_3C_4C_5F_3F_4F_5F_7$ and $C_2F_2F_6$. In 19-th column in the row of the subassembly $C_1C_2C_3C_4C_5F_2F_3F_4F_5F_6F_7$ which is divided will be put -1, and in the row of subassemblies $C_1C_3C_4C_5F_3F_4F_5F_7$ and $C_2F_2F_3$ which are obtained will be put 1. Non-destructive disassembly process continues until all components and fasteners in the product are disassembled.

The order of the disassembly operations in a specific disassembly process is called the disassembly sequence [3]. On the base of TM shown in the Table 1, all disassembly sequences for the example shown in the Figure 2 are obtained. With directed arrows lines in the table is shown the way of generating one disassembly sequence. The green directed line shows which subassembly becomes a parent subassembly in the i -th operation, and the black directed lines point to the two or more child subassemblies, components or fasteners, resulting from this operation. In Table 1, with directed line arrows, is shown an example of obtaining of one disassembly sequence: [0, 2, 19, 96, 143, 147, 149, 155, 156, 158]. Part of the generated disassembly sequences is shown in Figure 5.

Many disassembly operations are not possible from the aspect of the priority for removing of the components and fasteners, what limits the number of generated disassembly sequences. The priorities for removing of the components and fasteners are determined from the CAD model of the product assembly by assembly analysis. The analysis gives the possible disassembly directions, represented in a disassembly interference matrix, for removing of components and fasteners.

9. DISASSEMBLY INTERFERENCE MATRIX

Disassembly interference matrix is obtained based on the directions of $\pm x$, $\pm y$ and $\pm z$ axis, respectively [8]. The matrix is with dimension $n+m \times n+m$ which depends on the number of components n and fasteners m in the product. The elements in the matrix are binary pairs of numbers $X_i Y_i Z_i$ where $i = 1, \dots, n+m$.

Disassembly operations		0	1	2	3	4	19	96	143	147	148	149	155	156	157	158
Assembly	C1C2C3C4C5F1F2F3F4F5F6F7	1	1	1	1	1										
	C1C2C3C4C5F1F2F3F4F5F7															
	C1C2C3C4C5F2F3F4F5F6F7															
	C1C2C3C4C5F1F3F4F5F6F7															
	C1C2C4C5F1F2F4F5F6F7															
Subassemblies	C1C3C4C5F3F4F5F7															
	C1C4F5F7															
	C3C4C5F3F4															
	C2F2F6															
	C1F7															
	C1F6															
	C4C5F4															
Fasteners	F7															
	F6															
	F5															
	F4															
	F3															
	F2															
	F1															
Components	C5															
	C4															
	C3															
	C2															
	C1															

Table 1. Segment from the transition matrix for example hair-dryer

0	1	12	61	98	145	148	155	157	
0	1	12	62	106	145	151	155	157	
0	1	12	63	119	131	148	155		
0	1	12	63	119	132	151	155		
...									
0	2	19	96	143	147	149	155	156	158
...									

Fig. 5. Segment of the list from all possible disassembly sequences

If interference exists between components or fasteners C_i or F_i and C_j or F_j , where $j = 1, \dots, n+m$ and $i < j$, in direction of the $+x$ -axis, then the element $x_{i,j}$ in the matrix (8) is equal to 1. In the opposite, the element $x_{i,j}$ in the matrix (8) is 0. If $i=j$ the element $x_{i,j}$ is equal to 0, because no component or fastener can have interference with itself. With the disassembly interference matrix, the priority for detachment of components and fasteners in directions of $\pm x$, $\pm y$ and $\pm z$ axis is defined. The disassembly priority is required in the process of the generation of disassembly sequences, presented in the section 8, with a goal to keep only the feasible disassembly operations.

The general form of the disassembly interference matrix is given with the equation (8). For example, for the hair-dryer shown in the Figure 2, the disassembly interference matrix is given with the equation (9). If all elements in a column of the disassembly interference matrix are zeros, than that component or fastener can be removed in that direction. For example, in the matrix (9) the fastener F_1 can be detached in direction $-y$. Consequently, the column and row of the fastener F_1 can be deleted from the matrix, and the reduced disassembly interference matrix without fastener F_1 is obtained. The process continues until all the components and fasteners from the product are removed. In that way, a list which represents possible orders of removing of components and fasteners is obtained. For one order of removing the components and fasteners from the example shown in the Figure 2

with defined order of removing directions. The order is: $F_1(-y)$, $F_2(-y)$, $C_2(-y)$, $F_3(-y)$, $C_3(-y)$, $C_4(-y)$, $F_4(+y)$, $F_5(-y)$, $C_5(-y)$, $F_6(+xyz)$, $C_1(+xyz)$, $F_7(\pm xyz)$. After determining the priority of detaching for components and fasteners in the product and after definition of lists for all disassembly direction, all disassembly sequences are checked for possibility. Impossible disassembly sequences are deleted and remain only possible disassembly sequences from which after that is obtained the optimal disassembly sequence by some criteria.

10. OPTIMAL DISASSEMBLY SEQUENCE

The optimal disassembly sequence is obtained based on disassembly times, revenues and costs in the disassembly process. The disassembly time of i -th component or fastener in the product is calculated with equation (10).

$$T_{DISi} = T_W + T_F + T_E \quad (10)$$

where: T_W represents the time spent for tool change, tool placement, product placement for disassembling, tool return and removal of a detached component or fastener; T_F represents the time spent for separation of a specific fastener; and T_E represents the time spent depending on the difficulty for detaching of the component or fastener (for example corroded threaded connection). For different fastener types, time T_F is calculated by different function.

The total disassembly time for the product is:

$$T_{DIS} = \sum_i^{n+m} T_{DISi} \quad (11)$$

Costs for i -th operation $C_{costs-i}$ are:

$$C_{costs-i} = T_{DISi} \cdot P_L \quad (12)$$

where P_L is cost of manual labor in euro/hour.

The cost of complete disassembly is given with the following equation (13):

Mladenovic, G., Popovic, M.

MODELLING, CALCULATIONS AND TESTING OF SINGLE GIRDER BRIDGE CRANE AND CRANE RAILS

Abstract: Bridge cranes are used for handling various types of cargo in the production halls, workshops, storage facilities, energy facilities, mills as well as in performing technological processes, assembly or disassembly of equipment. The main characteristic for these cranes are that a major girder (which in most cases is standard I profile) also represents a path on which moving movable hoist. This paper describes the procedures of using the command Frame Generator of the Software Package Autodesk Inventor 2011[®], which use reduces the total time of modeling the structure which consists of standard profiles, as well as the module Frame Analysis which allows to predict the behavior of constructions under the influence of load. The end of the paper gives the experimental results for displacement and stress condition for given crane for the case of static load.

Key words: Single Girder Bridge Crane, Autodesk Inventor[®], Frame Analysis

1. INTRODUCTION

The uses of structures which are composed of standard profiles are common in mechanical engineering. An example of these structures is Single Girder Bridge Crane, Fig. 1.



Fig. 1. Single Girder Bridge Crane

For the cross section is most commonly used hot rolled "I" profile that serves as rails, Fig. 2a. Sometimes it is necessary to achieve stability against side buckling, which can be achieved by placing additional elements on the upper belt Fig. 2b,c.

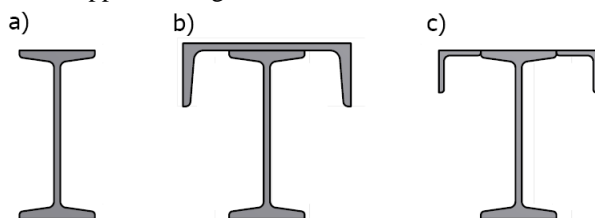


Fig. 2. Examples of cross-section of the main girder and the reinforcement of the upper belt

Therefore it is necessary to find as simply as possible way of modeling and calculations for given constructions. Depending of used software there is different speed of modeling, where most of the software requires drawing a sketch of the cross section, and then the sketch extrude through a trajectory. But, Software Package Autodesk Inventor 2011[®] has the

possibility to select standard profiles from database. First it is necessary to draw skeleton of the structure, and then just set up some of the standard profiles on the corresponding segment of the skeleton. Besides the quick making 3D models, the advantage of this type of modeling is that the Frame Generator assembly is automatically converted into simplified model of beams and nodes with the starting of the Frame Analysis environment and starting a new analysis.

2. MODELING CRANE

As it is said in the introduction, for obtaining a 3D model of constructions which are composed of standard profiles it is first necessary to sketch skeleton of structure. It is enough to draw a sketch in the one "sketch"-a. The look of the skeleton crane is shown on Figure 3.

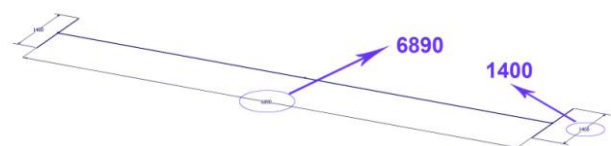


Fig. 3. The skeleton structure with defined dimensions

The command Frame Generator can be used only in environment for working with assemblies. Activation of command (Insert Frame) requires the definition of the standard profile, the choice of materials and segments (lines) on which will be set given profile or defining the start and the end points of segment. It is also defines the position and orientation of the profile in cross section. It can be selected one of the 9 cases, to position the center of gravity of the profile on the selected line or to one of 4 sides profiles match with the projection of line in that plane or the profile that can be moved along the diagonal. For all these cases it is possible to rotate the cross section for the desired angle and to move it by a some direction.

Length of the selected profiles match the length of lines in the sketch and it is necessary to subsequent repair

ends of the profiles using the commands Trim, Extend, Notch, and Miter. Using commands Change it is easy and quick to change a profile on construction which is of great importance for optimization process. For the main girder the standard profile DIN1026 **I260** is used, and for reinforcement for the upper bend the standard profile DIN1026 **U100** is used. For the side girder standard profiles DIN1026 **U120** mutually spaced 110mm are used.

3. CALCULATIONS OF CRANE AND CRANE RAILS

When the skeleton of the construction were formed this way it is possible to calculate the construction by activation of Frame Analysis Environment. Frame Analysis is used to understand the structural integrity of a given frame with respect to deformations and stresses, when subjected to various loading and constraints. Once when the criteria are defined, it is possible to run the simulation and view the behavior relative to the conditions which are defined. Simulations help to identify performance issues and find better design alternatives. Beam elements are linear. Frame analysis does not support curved beams. When the Frame Analysis environment is opened and a new analysis starts, the Frame Generator assembly is automatically converted into simplified model of beams and nodes. In the software it is very easy to define a new node (command Custom Node). There is only a need to define on which beam node is and how away it is from the end of the beam. This very simplifies the calculations of structures and reduces the total time of preprocessing. There are two approaches which give identical results, first to define a new node and then set the load on that place. Another way is to define, on which beam load is acting, and how away from the end of beam is the point on which concentrated force is acting. Besides the request for dimensions of construction another request was capacity of a construction which is designed to be 1t. Also, it was given the constraint that the carts can get close to maximum 500mm from the end of the main girder. As the given modeled crane should be installed into the building described in [4] it is analyzed the four loading cases shown on Fig. 4 and these are:

- (a) The axis of the main girder intersects poles axis, the load on the middle of the main girder
- (b) The axis of the main girder intersects poles axis, load on the 500mm from the end of main girder
- (c) The axis of of the main girder on the middle between the two poles, the load on the middle of

the main girder

- (d) The axis of of the main girder on the middle between the two poles, load on the 500mm from the end of main girder

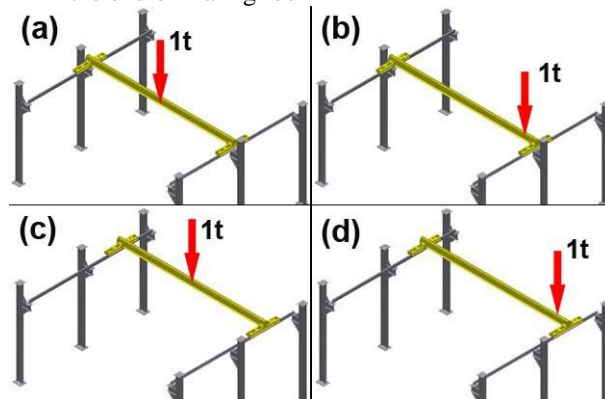


Fig. 4. Four cases of construction loads

Addition to the above the software allows to define rigid links (command Rigid Link) between nodes, which is necessary to do by analyzing the four loading cases. The connection between the crane and crane rails going across wheels, but the Frame Analysis environment works with beams so it is necessary to define a new node on place where wheels are (which is on 150mm from the end of side girder). By analog procedure it is necessary to define a new node on the crane rail at the same vertically relative to the previously formed on the side girder and then mentioned two rigidly connected in order to transferred the crane load to the crane rails as shown on Fig. 5.

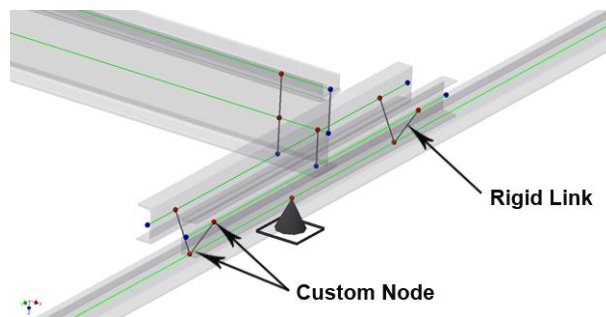


Fig. 5. Defining connection crane with crane rails

Calculation results are given in Table 1. mark δ represents the value of deformation. Beside to considering the stress state of the main and side girders, it was also discussed the stress state for the crane rails for that have been selected standard profiles DIN1026 **U120**, and the length of the crane rails is 3m.

Element	Serial number	δ [mm]	S_{MAX} [MPa]	S_{MIN} [MPa]	$S_{MAX}(M_x)$ [MPa]	$S_{MAX}(M_y)$ [MPa]	$S_{MIN}(M_x)$ [MPa]	$S_{MIN}(M_y)$ [MPa]	Saxial [MPa]
Main girder	a i c	5.05	31.4	-41.49	35.76	8.68	-35.76	-3.9	22.72
	b i d	1.82	12.6	-12.28	10.49	4.04	-10.49	-3.28	8.56
Side girder	a i c	0.13	15.77	-15.77	15.77	0	-15.77	0	0
	b i d	0.20	25.45	-25.45	25.45	0	-25.45	0	0
Crane rails	a	0.38	26.59	-26.59	26.59	0	-26.59	0	0
	b	0.57	40.94	-40.94	40.94	0	-40.94	0	0
	c	4.53	58.68	-58.68	58.68	0	-58.68	0	0
	d	7.12	92.12	-92.12	92.12	0	-92.12	0	0

Table 1. The calculations results for particular construction elements

Based on the table 1, which shows that the according to the stress and deformation, state dimensions of the crane are satisfying. Checking the lateral buckling of the main girder (in case that the cross section is only **I260** profile) was calculated analytically using the forms from [2] according to **JUS U. E7 101/1986**. Limit value for the lateral buckling stresses for this case is

$$\sigma_b = \frac{\sigma_D}{\nu} = \frac{18.86}{1.5} = 12.57 \text{ kN / cm}^2$$

and is greater than maximum normal stresses given in Table 1.

Based on this it can be concluded that there is no side buckling of the main girder. After verifying the previous conditions the creation of complete 3D model of the crane was undertaken. The ribs for reinforcement, bearing wheels with relevant bearings, wheels with relevant shafts were designed. It is foreseen that the drive motor being on the one side, and the motion transfer to the other side with PTO shaft. In accordance to this, the central bearing was projected. Of course, rails on which cables will move, were developed. Crane is designed that it is possible to separate the side girder from the main girder for easier transport or a later redesign of crane. In addition, it is possible to unmount middle bearing PTO. Image of complete 3D model is shown on Fig. 6.



Fig. 6. The complete 3D model of calculated crane

In contrast to crane that satisfies all three criteria, crane rails do not satisfy maximum allowed deformation ($\leq l/1000=3\text{mm}$) so it is necessary to reinforcement the same or change dimensions of the standard profiles which were made.

Based on the fact that the hall has been already made, it was approached to the design of the reinforcement of existing crane rails composed of the standard **DIN1026 U120** profile. The idea was to underside of the crane rails form a truss structure composed of the standard pipes with square cross-section **40x40mm**, with wall thickness of the **2.9mm**. The position of the lower profile is the **500mm** and parallel to the rail. Other profiles consists the grid and placed each other at angle of **45°**, Fig. 7.

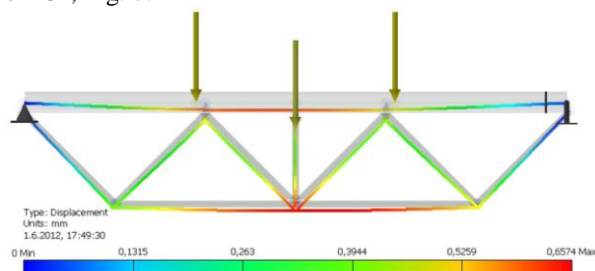


Fig. 7. Image of reinforced rails with corresponding deformation

For this purpose the complete project has not been changed but only the 3D model of reinforced crane rails was made. The effect of the crane was replaced by concentric force that represents the weight of the whole crane that was obtained from the previous analysis, of course with a predefined load capacity of the construction of **1t**. It was considered only the worst case of load (case (d) from fig. 4) and the results for the displacement are shown on Fig. 7 (maximum displacement is **0.6574mm**). The value of maximum normal stress for a given case of load is **32.26 MPa**.

4. MAKING CRANE

Based on the model from item 3 of this paper the creation of technical documentation and making the crane was undertaken. For welding electrodes **Jasenice EVB50 Ø4mm** were used (software has the possibility to define the welded joints, but it is not considered for this time). The wheels are made of cast iron to minimize wear of crane rails. For the drive wheels double row ball bearings **4208** are used which are placed in housings. For a driven wheel single row ball bearing **6208** was used which is placed in the wheels, and the corresponding shaft was fixed, i.e. realized tight fitting in the side girders.

At this stage it was not performed reconstruction of crane rails and the crane was placed on the existing rails.

5. INVESTIGATION OF DEFORMATION CRANE AND CRANE RAILS

Fig. 8 shows the experimental scheme. Crane was loaded with known weights of **Q=360kg** exactly on the middle of the range of main girder. Position of the crane in relation to the crane rails was that the axis of the main girder intersects poles axis. With comparator were measured vertical displacements for two places, the place 1 for measurement deformation of the crane rails, and the place 2 for measurement deformation of the main girder.

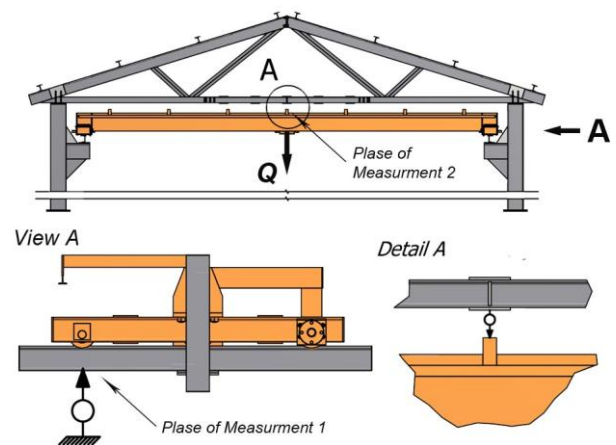


Fig. 8. Experimental scheme

In order to compare calculation results with the actual deformation it is necessary to do the following:

- Calculate the displacement of the 3D model for the case (a) from Fig. 4 only under the influence of self-weight of construction
- After this set a known concentrated load $Q=360\text{kg}$ and calculate the displacement
- The difference of these two displacement should correspond to the comparator measurement because the deformation under own crane weight were included with setting comparator.

Bearing all this in mind another analysis in Frame Analysis environment was done and the results are shown in Table 2. Fig. 9 shows the simulation results (deformation of crane) obtained in Inventor.

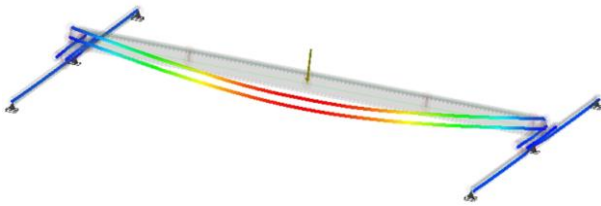


Fig. 9. Simulation from Inventor

	The deformation of the main girder [mm]	The deformation of the crane rails [mm]
The simulation results	1.35	0.09
The measured values	1.48	0.11

Table 2. Simulation results and experimental results

Differences in the data can be explained through the following:

- The dimensions of the profile, because of tolerance for free measures, differ with respect to the tabular values, and consequently are different to the characteristics of the cross section that directly affect on the value of deformation
- The software does not provide the possibility for reading specific deformation on specific place, but the deformation is read based on shades of color from color bar and even then it makes error in reading displacement as in the case of measuring deformation at the contact of the wheels and crane rails.



Fig. 10. Doing the experiment

Figure 10 shows the experimental determination for the deformation for the main girder and the crane rails.

6. CONCLUSION

This paper describes the procedures of construction, calculations and optimization at the example of Single Girder Bridge Crane and corresponding crane rails using a method that provides choice of standard profiles from database. Calculation results are compared with the experimentally determined displacement for made crane according to modeled and calculated 3D model of construction.

Using Frame Analysis environment of software package Autodesk Inventor allows the designer to perform with minimal knowledge of FEM analysis, because the software takes care of the required CP and FE, so it is possible to set a load on any part of the KE (beam) in one step, as a result of very advanced preprocessor that recognize and automatically form a network of FE. Analyzing the results from the software and the measured displacement was seen that there was deviation up to 10%, whose reasons described under item 5 of this paper.

7. REFERENCES

- [1] Kalajdžić M.: *Metod konačnih elemenata, osnovi statike, statika nosećih struktura, dinamika nosećih struktura, primene*, IAMA, Beograd, 1978
- [2] Ostrić D.: *Dizalice*, Mašinski fakultet, Beograd, 1992.
- [3] Mladenović, G., Popović, M.: *DESIGN AND OPTIMIZATION FOR TRUSS CONSTRUCTIONS USING THE SOFTWARE PACKAGE AUTODESK INVENTOR 2011®*, The 7th International Conference HEAVY MACHINERY HM 2011, Proceedings, p.p. 29-32 Vrnjačka Banja, Mašinski fakultet Kraljevo, Vrnjačka Banja, 2011
- [4] Mladenović, G., Popović, M., Tanović Lj.: *DESIGN, CALCULATIONS AND INVESTIGATION OF TRUSS ROOF CONSTRUCTION*, International Conference Maintenance and Production Engineering "KODIP - 2012", Proceedings, p.p. 307-313 Budva, Faculty of Mechanical Engineering – Podgorica, Budva, 2012
- [5] Autodesk Inventor 2011® Profesional – Help
- [6] <http://usa.autodesk.com/>

Authors: Goran Mladenovic, dipl.ing., mr Mihajlo Popovic, University of Belgrade, Faculty of Mechanical Engineering, Department for Production Engineering, Kraljice Marije 16, 11120 Beograd 35, Serbia, Phone.: +381 11 3302-438, Fax: +381 11 3370-364.

E-mail: gmladenovic@mas.bg.ac.rs
mpopovic@mas.bg.ac.rs

Nikolic, N., Lukic, Lj., Vranjevac, I., Djapic, M.

USE OF SIMULATION SOFTWARE IN PRODUCTION TECHNOLOGIES

Abstract: Modern design methods of production technologies are based on the use of simulation software, which enable engineering analysis of the phenomenological events that occur in production processes. The application of simulation software is especially important in tool design for plastic molding, especially injection molding tools for large parts of great complexity. Simulation of the design procedure, which solved the dilemma in engineering product design and optimization technology, defines the characteristic size of the machining process control and quality assurance. At the same time reducing the number of physical prototypes, thereby reducing development costs and shortens the time required for a product to market. This paper presents a practical example of the software package Moldflow Plastic Adviser that provides a realistic simulation of pressure casting and the introduction of modern methods of design tools and technological processes in the plastics industry. Also, presents a new approach to determining pouring points, design of distribution channels and holes, determining the wall thickness, positioning pouring points, and the impact of material and geometric characteristics on productivity.

Keywords: CAD/CAE/CAM, injection molding, integrated manufacturing technology

1. INTRODUCTION

The complex geometric shapes are present in a wide range of parts and products used in all aspects of human activity - that they meet the needs of everyday life, and complex technical systems. Produces complex geometric forms are the achievements of modern technology and adapted to the needs of the user or functional requirements of complex mechanical structures with high demands in terms of quality characteristics. The spatial shape of the workpieces directly connected with production technologies for their processing. Therefore, the modern design technology for the processing of complex spatial area is impossible without the use of computers and modern methods of using CAD / CAM systems, and especially without the software for the simulation of technological processes in production technologies. Phenomenological processes occur in metal cutting, forming and casting is very well can be analyzed using simulation methods. In industrial practice is most widespread application of simulation software in the field of processing technology of plastic parts.

2. INJECTION MOLDING

Injection molding is the most important cyclical process of processing of polymers and achieved by the most sophisticated technological level. This procedure is one of the primary processing of polymers, because the shape of the molded part gets the starting material with no particular form (granules, pieces, etc.). Injection moldings are all polymers form: thermosets, elastomers,

thermoplastic, and is particularly prevalent plastomenih processing of materials, better known under its old name of injection molding. According to the quantities processed by injection molding of polymers is immediately behind extrusion technology. It can be concluded that the injection molding of polymers like casting metal under pressure.

Injection molding is carried out in special machines (Figure 1) comprising an injection unit, the drive system, units for closing the mold, the mold tempering devices and control units.

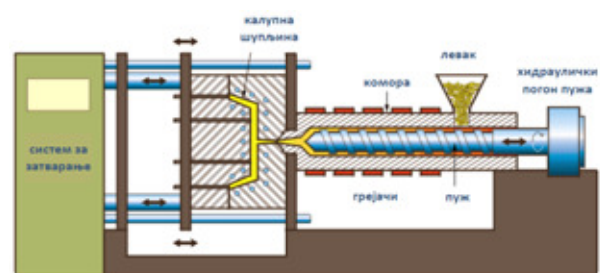


Fig. 1. A production system for injection

Injection molding can be defined as a procedure for processing thermoplastics rapid melt thermoplastic injection mold cavity in the tempered and also harden into the desired product form, pressings. The biggest advantage of this procedure is the possibility that the dimensions of the pallet can be determined in advance by applying certain principles that are valid for a finished molded injection molding.

3. MODELING

Today there are several CAD packages that can successfully be used for geometric modeling of workpieces with spatially complex areas, where the model parameters are generated automatically and directly used in the later stages of design and simulation technologies and technological processes. For the introduction and presentation of contemporary design production technologies based on simulation software, was selected characteristic of the processed plastics for modeling, molded part, and used the program SolidWorks. After modeling the cross-sectional profile of workpiece with the required dimensions, using the command Revolde is done spinning about a fixed axis profile (Figure 2) and form a solid model of the workpiece.

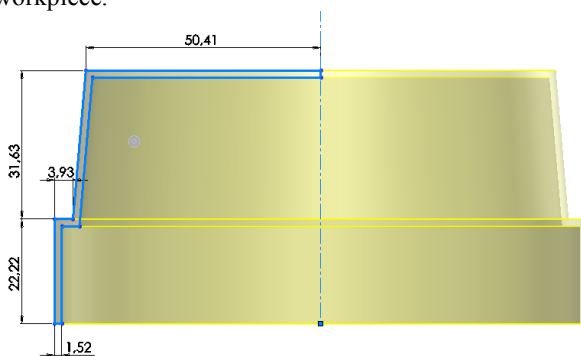


Figure 2. Profile of the workpiece

Using SolidWorks other program features, a very easy to model complete product (in this case the plastic part of kitchen appliances for fruit and vegetables) and really look at and optimize its design, functional characteristics and define the method and the technological process of its development (Fig. 3).



Fig 3. The appearance of the finished model

Modern CAD / CAM systems are fully integrated with other software packages that allow the designer to

efficiently design tools for casting, pressing the space of complex surfaces, operating parts, automatically generates the tool path processing multi-axis working parts of tools, generate NC code and execute a budget cost indicators machining process. It is especially important to determine the characteristic size of the working process and achieve higher quality products.

4. SIMULATION PROCESS INJECTION PLASTIC

In the design phase for the plastic molding tools, especially tools for injection molding of parts of great complexity, great help designers in solving critical technological determinations are specialized software packages for process simulation. In analyzing the process of injection molding software package was used Moldflow Plastic Adviser, which are necessary for the following inputs:

- 3D CAD model of the pallet,
- types of materials and
- injection molding process parameters (temperature of molten polymer, the mold temperature and injection pressure).

As a result of the simulation gets an overview of the process flow and mold filling, cooling time, pressure and temperature distribution on the element and the prediction quality workpiece. Linking CAD and CAE systems, in this case SolidWorks and Moldflow Plastic Adviser, it can be very complex process, because we need to give execute the transfer of geometric and non-geometric information between the two systems. Manufacturers CAD systems in addition to recording data format used in the offer and use of standard formats for data transfer, most notably IGES and STEP. In recent years, the producers of packages software show the tendency of direct downloading of data from other software packages. Moldflow and offers full integration with the following software packages: SolidWorks, Solid Edge, Pro / ENGINEER, Autodesk Inventor, CATIA. In relation to a given material, the program presents value of its own technological base molding process parameters. If for example adopt the temperature of molten polymers 243 ° S, a mold temperature of 36 ° S and the maximum pressure machines from 180.00 MPa, obtained during the opening and closing the mold for 5 seconds, a time of molding plastic is in automatic mode (Figure 4).

Improvement in the design of manufacturing technology, reflected in the selection of the best places for casting plastic tools in space, in terms of phenomenological and temperaturskih appearance in the technological process, which enables software simulation and analysis of the effects of different positions gating system. (Figure 5). The advantage of applying this command is reflected in the fact that for a short period of time we can simulate multiple places to enter the plastic on the ground that you choose the best solution.

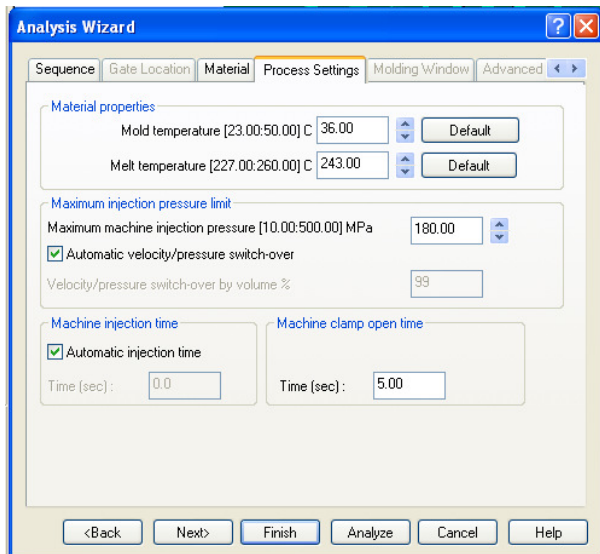


Fig 4. The elements of the technological process

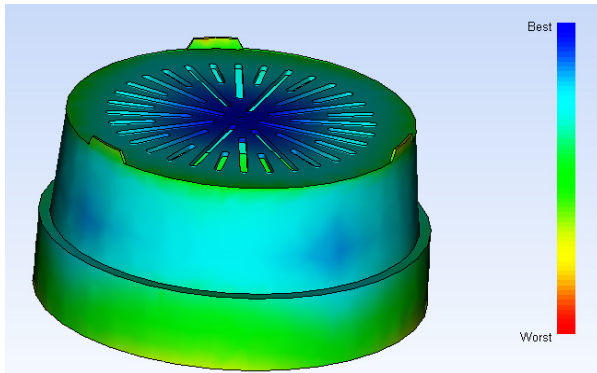


Fig 5. Optimization of injection

Upon completion of the analysis, automatically generate values that are necessary for the design of injection mold tooling, gating system, cooling system and the complete assembly of tools to be placed on the injection molding machine (Figure 6). However, when completing the gating area molten plastics can occur irregularities in the distribution of plastic, the air exiting from the cavities in the mold, casting method, premature hardening plastics, refrigeration, difficulty removing the workpiece from the tool, ... all of which can affect the overall quality of the workpiece. Simulation software allows the detection of adverse effects of the technological process and also allows the optimization of the process by changing the input parameters of the process, the change in geometry by increasing or reducing the wall thickness of the workpiece. Simulation software has a very good GUI (Graphic User Interface), which leads through the visualization process designer through all phases of technology characteristic (Figure 7).

Simulation software allows the presentation and the time required for pouring plastic into the mold and the injection time visualization of the process (Figure 8),

which allows control of managing the process of casting is under design.

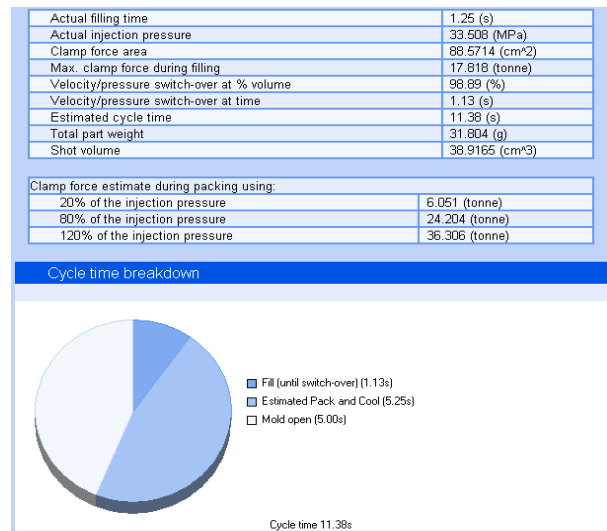


Fig 6. The characteristic size of the injection molding process

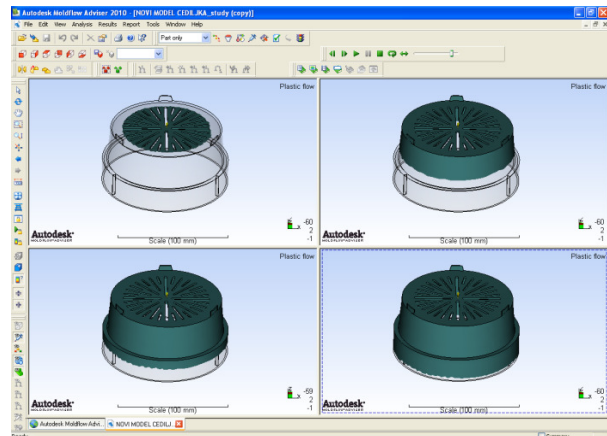


Fig 7. Simulation of the injection process

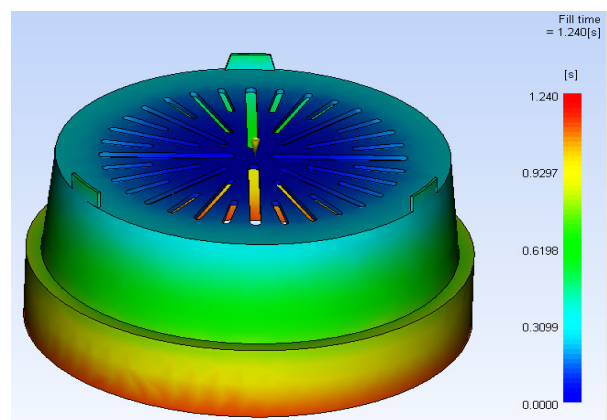


Fig 8. Simulation of injection molding in the timeline

Pressure caused by a temperatur operations in the technological process, are also simulated through the analysis of the intensity of the workpiece. It can be notice that the selected example (Figure 9) the intensity of color-coded pressure, indicating that the greatest pressure in the pouring system in two parts which are nearest to the center of pouring system or in the middle, and lowest on the very edge of the mold parts.

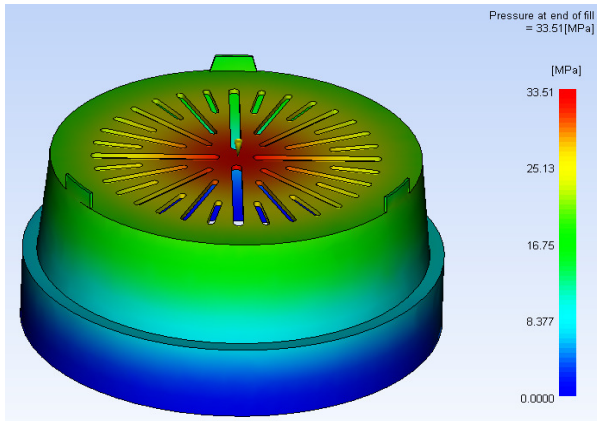


Fig 9. Pressure distribution in the mold during the molding process

In addition to pressure simulation can be analyzed and tepmeratur field in the mold, where the levels directly by temperature in the cooling system correlation tools (Figure 10).

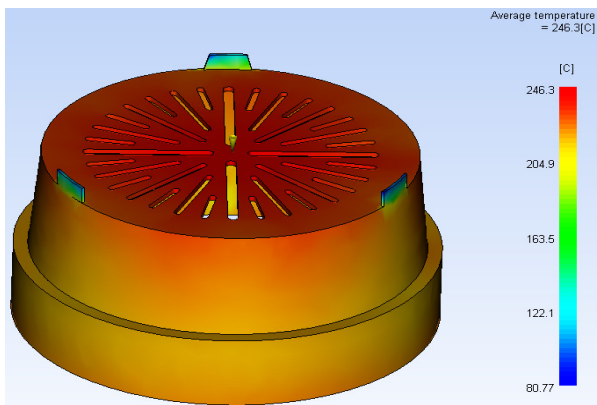


Fig 10. Temperature field in the injection molding process

All the technological parameters and characteristic values can be varied for different conditions of injection and thus investigated the effects of favorable development in structurally complex and geometrically complex parts made of plastic. The complexity of the workpieces can be solved in the design phase, and geometric modeling, so it does not affect the increase in

complexity of design technology, which is the main effect of simulation software in designing the process of plastic injection molding.

5. CONCLUSION

Simulation software enables the development of a new approach to the design of production technologies, the engineering analysis that allows simultaneous integrated design of products, technologies and tools, which provides a new opportunity to develop high quality products technologicality high level of production in advanced manufacturing technologies and agile.

The illustrated example of the workpiece in this paper, only confirms the fact that they can achieve very high technical and technological effects of using software to simulate the machining process in industrial practice.

6. REFERENCES

- [1] Nikolić,N.: Design of CNC Technology and automatic generation of NC programs for the treatment of working tools for the production of plastic parts, *Master's thesis*, Faculty of Mechanical Engineering Kraljevo (2011).
- [2] Polajnar,D., Polajnar,J., Lukić,Lj., Djapić,M.: Complexity Challenges in CAPP Systems and Promises of Multi-Agent Technology, Proceedings The Sixth Triennial International Conference "Heavy Machinery HM 2008", Kraljevo, 24-29 June 2008, pp.F.19-P.24.
- [3] Djapić,M., Lukić,Lj., Arsovski, S.: Integrated Management Systems – Requirement of Contemporary Business Practices, Proceedings The Sixth Triennial International Conference "Heavy Machinery HM 2008", Kraljevo, 24-29 June 2008, pp.G.1-G.6.
- [4] Ivanović,S., Lukić,Lj.: Database Design from Technological and Kinematic Parameters of NC Program for Production in Flexible Manufacturing Systems, Proceedings The Sixth Triennial International Conference "Heavy Machinery HM 2008", Kraljevo, 24-29 June 2008, pp. G.7-G.12.

Autors: **Nenad Nikolić, MSc**, Mech.Eng., Faculty of mechanical Engineering Kraljevo, University of Kragujevac, nikolic.n@mfkv.kg.ac.rs, **Prof. Ljubomir Lukić, PhD**, vice-dean for science, research, & development, Faculty of Mechanical Engineering - Kraljevo, University of Kragujevac, lukic.lj@mfkv.kg.ac.rs, **Ivan Vranjevac MSc**, Mech.Eng., Faculty of mechanical Engineering Kraljevo, University of Kragujevac, vranjevac.i@mfkv.kg.ac.rs, **Doc. Mirko Djapic, PhD**, assistant professor, Faculty of Mechanical Engineering - Kraljevo, University of Kragujevac, djapic.m@mfkv.kg.ac.rs

Novak-Marcincin, J., Barna, J., Torok, J.

ADVANCED AUGMENTED REALITY APPLICATIONS IN THE PRODUCTION PROCESSES

Abstract: *The basic aim of this paper is to introduce possibilities of production process by using special virtual tools from scientific field named Augmented Reality (AR) and their implementation on the real examples. After the introduction which sketch basic information about augmented reality, the first point quickly provides view on the current situation in AR of production processes. The following step is oriented on explanation of main philosophy of AR in order to apply their in the particular applications. The last part of paper observes real examples of possibilities to create AR, not only by commercial software but also by virtual environment which is offered by open source platform. All these mentioned possibilities and examples are implemented in the special virtual environment of the AR, where engineers can see necessary information about material, mass, special conditions etc.*

Key words: *virtual tools, virtual reality, augmented reality, production processes*

1. INTRODUCTION

Presented paper explains main problems and structural logical concept of the production section for two kinds of the Augmented Reality (AR) applications. The AR is scientific field which interprets processes where real environment is connected together by virtual elements and this new conjunction provides the augmented tool in form of a virtual working space for user. As is mentioned in abstract, the beginning of the paper is oriented on the interpretation of basic thought of augmented reality and general logical steps which are explained by algorithm.

The second part of the paper is focused on the current situation in AR of assembling processes and gives visual imagine by enclose figures. However, it can describe advantages and disadvantages of these mentioned processes. The following step is oriented on explanation of main philosophy of AR in order to apply their in the particular applications. By means of the previous information, the last part of paper observes real examples of possibilities to create AR not only by commercial software but also by virtual environment which is offered by open source platform.

The conclusion gives a quickly recapitulation of paper steps and it is focused on the special programming packet which improves elements for the increasing entire quality of the visual area of the AR.

2. THEORY OF AUGMENTED REALITY

Augmented reality systems generate complex view where the virtual areas are covered by real environment and offer the basic working place for the engineer. Production process of AR has new special tool for the engineering area which provides strong elements and hardware components for creation of construction ideas. Final production process proposal include all functional 3D items of assembly without montage mistakes. The production application of AR was developed to determine the exact position and

orientation for production process. Thanks to its possibilities if finds the utilization in many industrial spheres [1].

The problem that must be solved during this visualization step is comprised of two underling causes. The first one has explanation in transformation processes of three-dimensional environment into two-dimensional image on the display. The main task of second one is necessary to knows exact position values of real basic coordinate system of general working table. Many companies use variable devices for observing an exact position of working area. These techniques can be divided into these main groups [2]:

- Motion capture by tracking sensors.
- Motion capture by camera (markers, colour).
- Laser tracking.
- Tracking devices.

2.1 AR based on observing of marker position

VTT's Augmented Reality group started developing virtual application for AR games and entertainment applications. This mentioned engineering group provides the powerfully tool which is used for displaying assembling process of the AR [3].

The software element was designed to gives important information about assembling processes where the engineer needs to know exact position and numerical order for the single parts of the entire assembly structure. Camera provides a real video from working space and exact data about the position and orientation of the working place are obtained from markers which are on the plane of the working place.

Observing marker has its own mathematical matrix which comprise important data packet about its appearance and all variants of its rotation. Marker is made by two different colours, ordinary black and white for better comparing during the tracking process. Comparing loop takes a signal from camera in order to compare signal with marker matrix. On the Fig. 1 is basic example of marker which general structure is made by black and white colour.

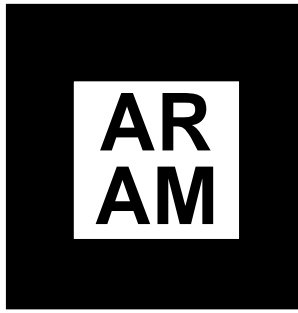


Fig. 1. The example of augmented reality marker

Software of AR has to include an augmented core and library for comparing information packet which are harvested during the observing processes of markers position. On the base of this information the application know the exact position for working area in the real time during the assembling process. VTT's Augmented Reality application for assembling process allows engineer to managed assembling process on the working table only around its own an axis of rotation. The Fig. 2 offers a view on particular example of AR where the marker situated on the desk provide position information for motion capture.

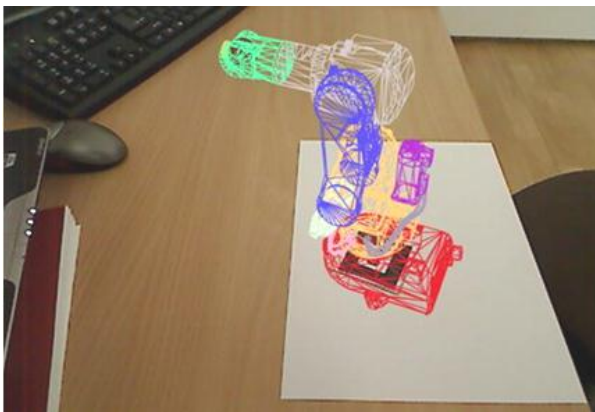


Fig. 2. Example of AR production process where virtual robot is covered by real view in the working place by marker

2.2 Laser projection technologies

Next example from industrial praxis can be found in 3D laser projection. It is accomplished by steering a single laser beam accurately through a series of specific points in space. The laser beam is directed at a pair of mirrors that are powered by a set of galvanometers called computer controlled servo motors which are capable of extremely rapid movement. The produced effect is a highly visible, glowing three dimensional template that is used as a location guide during a manufacturing process. The company Laser Projection Technologies Inc. use rapid characteristic of laser beam. Their systems replace conventional assembly methods and hard manufacturing templates in a wide variety of applications. 3D laser projectors use 3D component or part placement, paint masking and templates creating, vehicle and 3D items of assembly structure and core placement. The entire steps of this technology are described on the Fig. 3 and shows concept of method of laser projection.

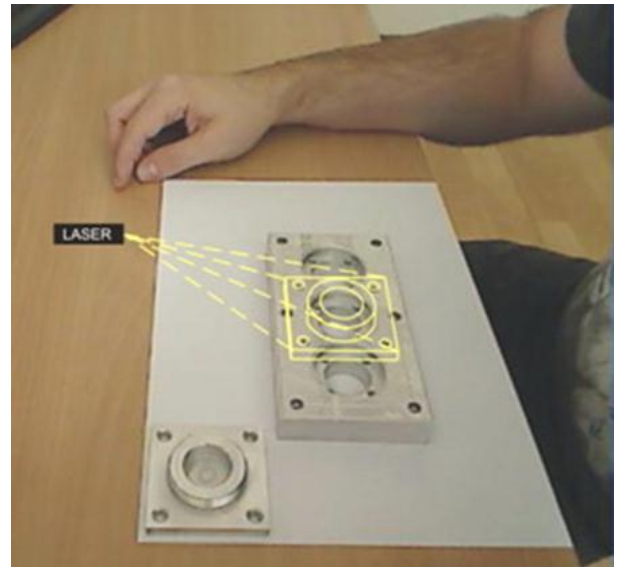


Fig. 3. The example of 3D laser projection method

3. APPLICATION OF AUGMENTED REALITY IN PRODUCTION PROCESSES

The Department of Manufacturing Technologies team created AR application intended to be used as a supporting tool in production processes but can be used also in many other application areas. Following parts of this paper describe the functional principles of this application. It is built on the mechanism that uses logical loops for realization of observation, collecting, evaluating and comparing activities and processing of all these obtained data in order to exploit them in final visualization output. Virtual environment called Virtools was used to create simply example of AR application. Working environment and its elements are based on principles of object programming, where initial conditions, actions and relations are prescribed for particular objects that according to their function change to the so called building blocks of the application (BBs). Rules and actions running between individual blocks or their sections can be graphically expressed in form of behaviour graph which at the same time serves as programming tool itself. Functionality of entire application can be then described through tasks that they are realized thanks different behaviour graphs [4].

BBs present the tool with simple graphical interface that can be used for creation of necessary logical connections defined in form of information packages. Each BBs included in virtual library has an input/output pin that can be tracked and its properties defined with respect to user orders. The environment of application that operates with special software tools offers the possibility for collection and monitoring of information about the data flow between single BBs.

Task of first behaviour graph is to fill the data array with correct values of assembly parts like information about assembly name and their initial conditions (position, geometric data and shape value). Filling process is activated by confirming message which is sent from the BG for the starting button. The first point in this process is an operation where the names of all

3D items from working environment are loaded into the exact position of the data array. This array is filled by means of adjustments of the behaviour conditions of the BBs called Iterator. By using the logical BBs called Get Position and Set Row the name of a 3D part from working environment assigns initial condition and behaviour about its position in the data array. Simple example of logical script of data array is presented on Fig. 4. This method, where the program or composition is realized by logical connection between BBs is called visual scripting.

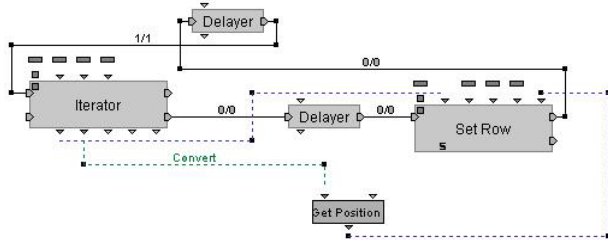


Fig. 4. The basic example of Behaviour Graph

Next part of paper investigates the establishing process of virtual tool that in its logical core utilizes an approach based on the Open Source philosophy exploited for the work with the environment of augmented reality. The goal of this part is to clarify application process for creation and development of virtual software and hardware elements that are necessary for work in the augmented reality environment. The traditional possibilities of how the engineer can use tools of augmented reality in form of normal commercial devices to collect the information about position of observed object in the working environment concern special de-vices with general structure formed by elements of motion tracking systems or technology of visual markers.

The first step in developing process was creation special device for adjusting of exact position of the operating desk in the working space. This element is described as device which gives possibilities to manage the process during the realization of whatever manufacturing situation.

This new device for augmented reality that is outlined as special positioning table which is able to adjust to an exact position of the working desk not only by using the computer interface and its own logical commands but optionally also by manual changes. Exact information about a position of the operating desk are obtained in real time during the process from special sensors that utilize the essential idea of possibility to accumulate the changes of orientation values in the real environment.

First sensor allows the collection and comparing in logical core of software in order to manage the data packets which comprise values about the spatial change of the desk position (X, Y, Z). Second one provides information about rotary motion around the main axis of rotation which is in the centre of operating desk. To simplify, base on this information about the special device and sensors elements the engineer is able to collect and explore the exact data about general movement from the real observed environment.

A process called visual scripting was used for developing procedures and programming orders for the work with logical behaviour loops in open source virtual environment. By using these tools, the application allows engineer to manage an entire data flow between different logical cores of the application (Fig. 5).

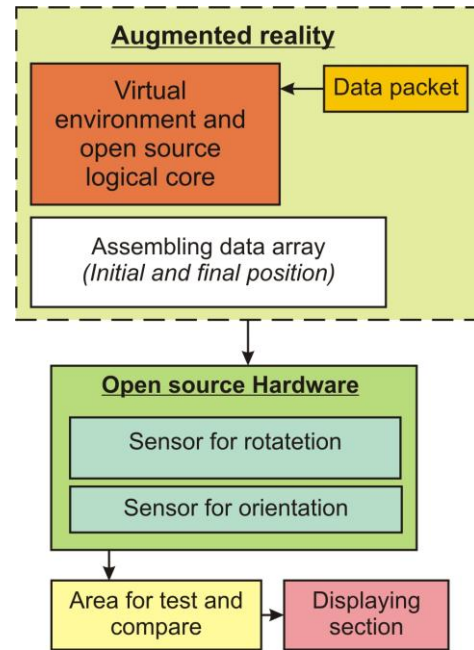


Fig. 5. Basic logical algorithm of AR application built on Open Source idea

In the following phase the general processes and logical steps of new application are described in the theoretical level. The application consists of the 4 main logical levels where the data packets come not only from inner computer elements but also from outer devices such as sensors and measuring devices [5].

First of these loops observes the button section which gives information about the confirming processes. By means of these buttons the logical loop called displaying section tarts viewing process (initial and final position).

Next loop consists of two basic areas (area for testing and comparing, area for position setting). Data packet from these mentioned areas include information about the names of all virtual items and their relevant values of initial vectors together with information about final parameters of position. Then the collected data from outer sensors are sent to the area for testing and comparing with each other and also to area for setting of position (initial, final one).

On the basis of these processes, all new information of position and orientation are sent again into the logical core of the application where the newly received parameters are tested, compared and evaluated between each other. After that, the displaying section is able to see the motion process of virtual item according to its trajectory. The entire process of AR assembling is presented on the Fig. 6 and Fig. 7 where the 3D part is moved on the virtual trajectory and offers exact value about final position for each part (real and virtual part in the same environment). For better understanding the

Fig. 8 gives view on improvement elements of application where each part has different colour and it allows to create assembly more clearly without mistakes [5].



Fig. 6. AR process where the 3D part is moved on the virtual trajectory

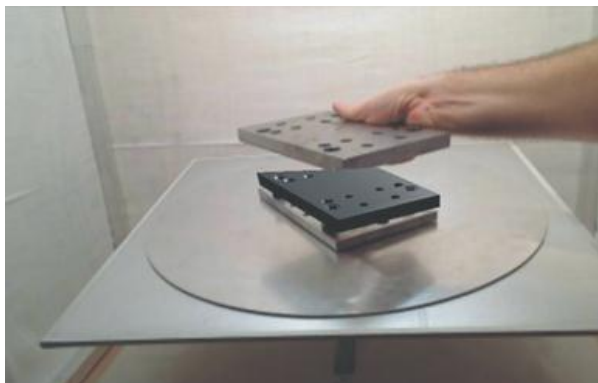


Fig. 7. AR assembling process

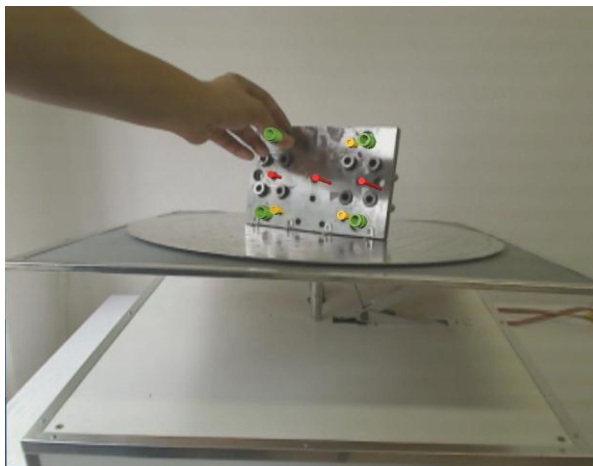


Fig. 8. Assembly process based on parts colours differences

4. CONCLUSION

This paper inform about implementation possibilities of AR for the purposes connected to the sphere of assembling structures creation. The first section presents current situation in an area of AR process. From middle to end part of article, text is focused on the real application not only from commercial side but also from Open Source platform.

It concerns software issues reflecting the model geometry (single 3D items) as well as displaying of final boundaries for all geometry shape of models of the whole structure. Created application was focused on the particular part of the problem where engineer needs to know exact positions of single 3D component of assembly structure in the real environment eventually with respect to auxiliary object. Main feature of prepared software application is utilization of motion tracking system based on the working principles of capture markers. Implementation of augmented reality elements in this manufacturing area shows that these problems are free to be developed and their solutions realized in many industrial spheres.

5. ACKNOWLEDGMENTS

The Ministry of Education, Science, Research and Sport of SR supported this work, contract VEGA No. 1/0032/12, KEGA No. 002TUKE-4/2012 and ITMS project 26220220125.



6. REFERENCES

- [1] Ong, S. K., Nee, A. Y. C.: *Virtual and Augmented Reality Applications in Manufacturing*. Springer-Verlag, London, 2004, ISBN 1-85233-796-6.
- [2] Vallino, J., Kutulakos, K. N.: Augmenting reality using affine object representations. *Fundamentals of Wearable Computers and Augmented Reality*. Barfield W. and Caudell T. (Ed.), Lawrence Erlbaum Assoc. Publ., Mahwah, 2001, p. 157-182.
- [3] *Mixed Reality and Visualization* (<http://www.vtt.fi/>)
- [4] Marcincin, J. N., Barna J., Janak, M., Marcincinova, L. N., Fecova, V.: Utilization of Open Source Tools in Assembling Process with Application of Elements of Augmented Reality. In: *Proceedings of VRCAI 2011: ACM SIGGRAPH Conference on Virtual Reality Continuum and its Applications to Industry*, Hong Kong, 2011, pp. 427-430.
- [5] Marcincin, J. N., Barna, J., Janak, M., Fecova, V., Marcincinova, L. N.: Composite lay-up process with application of elements of augmented reality. *The Engineering Reality of Virtual Reality*, Vol. 8289, 2012, p. 1-6.

Authors: Prof. Ing. Jozef Novak-Marcincin, PhD., Ing. Jozef Barna, Ing. Jozef Torok, Technical University of Kosice, Faculty of Manufacturing Technologies, Department of Manufacturing Technologies, Bayerova 1, 08001 Presov, Slovakia, Phone.: +421 51 7723012, Fax: +421 51 7733453.
E-mail: jozef.marcincin@tuke.sk
jozef.barna@tuke.sk
jozef.torok@tuke.sk

Petrović, P.B., Lukić, N., Danilov, I., Miković, V.

CANONISATION OF ACTUATION STIFFNESS MATRIX IN KINEMATICALLY REDUNDANT INDUSTRIAL HUMANOID ROBOTS

Abstract: This paper presents the novel theoretical and practical approach of generalized stiffness control in industrial humanoid robots. Compliance of robot mechanism and ability of robot control system to precisely adapt the parameters of its generalized stiffness matrix is increasingly gaining in importance concerning specific requirements imposed by new production paradigm of mass customization. Precise control of generalized stiffness requires very complex actuation system, much more complex than it is present in conventional industrial robots.. This paper demonstrates practical applicability of this approach using kinematically redundant planar robot arm. Detailed analysis of its Jacobian null space which is analytically derived using analogy with four bar mechanism shows that is always possible to achieve with arbitrary precision required generalized stiffness, regardless of robot posture freely chosen within configuration space.

Key words: stiffness control, industrial humanoid robots, kinematically redundant planar robot arm

1. INTRODUCTION

Safety is the starting point of human and robot team and collaborative work. Relevant documents which regulate this field are: ISO10218-1: 2006, [1], ANSI/RIA R15.06-1986, [4], and European machinery directive 2006/42/EC. These documents recognize robots as dangerous machines, and explicitly suggest that shearing of common workspace between human workers and robots in collaborative manner of executing work tasks is not desirable and even feasible. According to [2] collaborative work of human and robot in industrial environment is allowed only if robot fulfilled at least one of three conditions: 1) TCP/terminal plate speed ≤ 0.25 m/s, 2) Maximal dynamic power ≤ 80 W and 3) Maximal static force ≤ 150 N. These conditions are general and do not depend on the size or payload of the robot. Restrictivity of these requirements drastically reduces overall performances of the conventional industrial robot and therefore requires a new conceptual basis for robot design in order to solve this contradiction [3].

The essence of the problem lies in the fact that conventional industrial robots are designed based on concept that is used in machine tool design. They are designed to be accurate and fast as much as possible. This implies high stiffness of mechanical and actuation structure, which further on leads to a large mass of the robot. Conventional industrial robots are too rigid and massive to be harmless to humans even by extensive adaptation. Therefore, a fundamentally new approach to robot design was developed as response to the limitations of this type. This approach is based on the following framework:

1. Light weight and high specific load caring capacity;
2. High compliance and pliability of mechanical structure;
3. Ability to work within non-well structured environment, and capability to acquire of

human behavior as well as learning through generalization.

The result is industrial humanoid robot.

Industrial humanoids are developing very fast with exponential growth in accumulation of research activities. EU FP6 projects: PHRINEDS and SMERobot, EU FP7 project: ROSETTA, and pre-commercial project of humanoid DLR/KUKA LWR IV, are typical representatives of research conducted in this area, [4]. Example of industrial humanoid FRIDA developed within FP7 project ROSETTA is given in Fig. 1. It is redundant dual-arm robot with 2 x 7 serial degrees of freedom, having proportions similar to the medium height adult male.



Fig. 1. Industrial dual-arm humanoid FRIDA (*Friendly Robot Industrial Dual Arm*) developed within EU FP7 project ROSETTA for safe cooperative work with humans on the lightweight products assembly lines. In addition to the requirement of small mass and high specific payload, industrial humanoid robot must have the inherently controllable compliance. This

means that industrial humanoid must have lightweight variable compliance actuation system, such as to provide two functions: 1) compliant response to the collisions of TCP or any part of robot kinematic mechanism and 2) to generate arbitrary generalized stiffness matrix, including isotropy.

This paper¹ presents some results of research conducted in the field of synthesis of alternative solutions for the industrial humanoids generalized stiffness control. In particular, it shows the original approach of actuation system stiffness control using kinematic redundancy for achieving canonical form of actuation stiffness matrix.

2. GENERALIZED STIFFNESS

Generalized stiffness of manipulating robot in the task space coordinate system Q_R is defined as:

$$F = K_X(X - X_0) = K_X \delta X \quad (1)$$

where: $F \in R^m$ – the external force acting on the robot tip TCP, $K_X = K_H \in R^{m \times m}$ – the symmetric matrix function of manipulating robot generalized stiffness, $X_0 \in R^m$ – the nominal positions vector of the robot tip, $X \in R^m$ – the actual positions vector of the robot tip, and $\delta X \in R^m$ – the vector of the robot tip displacement (response on the force F excitation).

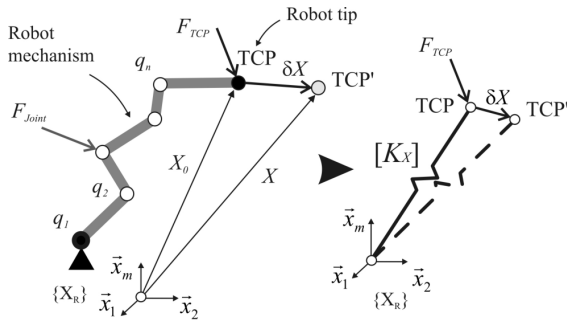


Fig. 2. Generalized stiffness model of industrial humanoid of anthropomorphic configuration.

The dominant influence to the robot generalized stiffness has compliance joint actuation system. Applying the approach given in [4] the congruent transformation of relation (1) leads to:

$$K_X \rightarrow K_q = J^T(q)K_X J(q), K_q \in R^{n \times n} \quad (2)$$

where: K_q is the actuation stiffness matrix, $q \in R^n$ is the vector of generalized robot coordinates, $J(q)$ is the Jacobian matrix operator. Actuation stiffness matrix is always symmetric (congruent transformation preserves symmetry), positive definite and generally non-diagonal [5]. A key task in industrial humanoid generalized stiffness control is design of joint actuation system that always can generate stiffness matrix defined by relation (2). Relation (2) is in general feasible only through the actuation and/or kinematic redundancy [4]. Actuation redundancy can generate of non-diagonal members in the matrix K_q . Actuation

redundancy implies the new actuators in addition to existing non-redundant actuators. This practically means driving of two robot joints simultaneously. Redundancy of this type is shown in Fig. 3 using a simple planar robot with two degrees of freedom as an example. The third actuator, which simultaneously drives the first and second joint, is represented by non-diagonal member in actuation stiffness matrix:

$$K_q = \begin{bmatrix} k_{q1} + k_X & k_X \\ k_X & k_{q2} + k_X \end{bmatrix} \quad (3)$$

In the way redundant actuator provides practical solution for congruent transformation (2).

Actuation redundancy of this type is widespread in biomechanical systems, and also in human's body. For example, the antagonistic muscle groups: *coracobrachialis*, *biceps caput longum*, *biceps caput breve* i *triceps brachii caput longum*, simultaneously actuate complex shoulder and elbow joints of a human arm. Application of redundant actuation in technical systems is a very delicate engineering task. Therefore this approach has very limited practical value.

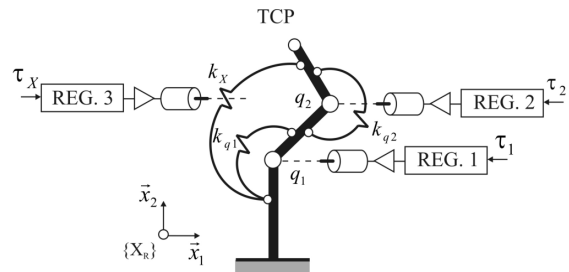


Fig. 3. An example of actuation redundancy which always satisfies relation (2).

Kinematic redundancy can be easily achieved in practice. Application of kinematic redundancy to satisfy relation (2) is based on the following hypothesis: Within the null space of kinematically redundant robot with k degrees of freedom can be simultaneously satisfied: 1) the condition of following nominal trajectory of robot's tip in the relevant task space domain, 2) the condition of nominal generalized stiffness of the robot tip K_{X0} and 3) the condition of canonical form of the actuation stiffness matrix. This hypothesis is based on the assumption that the increased mobility of robot can be used effectively for generation of required generalized stiffness on technically acceptable way.

The null space $\mathcal{N}(J(q))$, defined as:

$$N(J(q)) = \{q : J(q) = 0\} \quad (4)$$

provides internal motions of the redundant robot mechanism that does not cause any movement of the robot tip (TCP) in the task space, [6] (Fig. 4.). Internal mobility allows finding at least one vector:

$$q^* \in N(J(q)) \quad (5)$$

that satisfies the system of following algebraic equations:

$$x_0 = f(q^*) \quad (6)$$

$$k_{q-ij}(q^*) = 0, \quad \forall i \neq j, k_{q-ij} \in K_q(q) \quad (7a)$$

$$q^* \rightarrow \min(k_{q-ij}(q)), \quad \forall i \neq j, k_{q-ij} \in K_q(q) \quad (7b)$$

¹ This work is carried out within the project: **Smart Robotics for Customized Manufacturing**, supported by the Government of the Republic of Serbia, Ministry of Education and Science, Grant No. TR35007.

derived from the starting hypothesis. The relation (7a) reduces K_q matrix to its canonical form whenever the number of redundant degrees of freedom is $k^* = n(n-1)/2$. Relation (7b) is less restrictive and matrix K_q is reduced to its quasi-canonical form when $k < k^*$. Less restrictive relation (7b) is the engineering solution that has greater practical value.

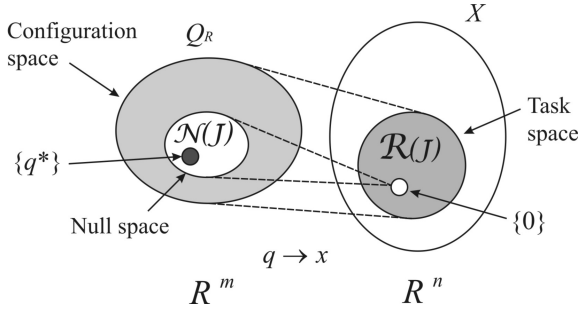


Fig. 4. The mapping of the robot configuration space into corresponding task space, and null space of kinematically redundant robot.

3. CASE STUDY

As an example of the kinematically redundant robot which is the functional equivalent of actuation redundant robot shown on Fig. 3., the planar anthropomorphic robot configuration with 3 degrees of freedom (Fig. 5) is used for the case study. In this case $k = 1 < k^* = 3$.

The redundant joint is driven by soft actuator, and together with two non-redundant joints, which is also soft driven, has the task to generate the null space where it is possible to find such a vector q^* , which simultaneously satisfies the condition (6) and (7b) and in the special case, condition (7a).

Jacobian matrix of this robot is defined by the relations 8a through 8c:

$$x_{TCP} = \begin{bmatrix} x_1 \\ x_2 \end{bmatrix} = \begin{bmatrix} l_1 c_1 & l_2 c_{12} & l_3 c_{123} \\ l_1 s_1 & l_2 s_{12} & l_3 s_{123} \end{bmatrix} \quad (8a)$$

$$J(q) = \frac{\partial x_{TCP}}{\partial q} = \begin{bmatrix} J_{11} & J_{12} & J_{13} \\ J_{21} & J_{22} & J_{23} \end{bmatrix} \quad (8b)$$

$$\begin{aligned} J_{11} &= -l_1 s_1 - l_{12} s_{12} - l_3 s_{123} \\ J_{12} &= -l_{12} s_{12} - l_3 s_{123} \\ J_{13} &= -l_3 s_{123} \\ J_{21} &= -l_1 c_1 - l_{12} c_{12} - l_3 c_{123} \\ J_{22} &= -l_{12} c_{12} - l_3 c_{123} \\ J_{23} &= -l_3 c_{123} \end{aligned} \quad (8c)$$

where for the sake of simplicity the following abbreviations are used for trigonometric functions: $s(\bullet) \equiv \sin(\bullet)$, $c(\bullet) \equiv \cos(\bullet)$ and $(\bullet) \equiv \Sigma(q_i)$. All geometric variables and parameters are defined in Fig. 5.

Analysis of compliance actuation system is further performed in case of isotropic generalized stiffness matrix, thus the relation (2) becomes:

$$K_X = I \rightarrow K_q = J^T(q)J(q), \quad (9)$$

Using relation (8b), the elements of actuation stiffness matrix defined by (9) have the following analytical form:

$$\begin{aligned} K_{q1,1} &= J_{11}^2 + J_{21}^2 \\ K_{q2,2} &= J_{12}^2 + J_{22}^2 \\ K_{q3,3} &= J_{13}^2 + J_{23}^2 \\ K_{q1,2} &= J_{11}J_{12} + J_{21}J_{22} \\ K_{q1,3} &= J_{11}J_{13} + J_{21}J_{23} \\ K_{q2,3} &= J_{12}J_{13} + J_{22}J_{23} \end{aligned} \quad (10)$$

The system of nonlinear functions (10) is visualized in Fig. 6. The robot geometry is normalized, lengths of robot links have anthropomorphic proportions: $l_1 = 1 = (7/5)l_2 = (7/5)^2 l_3$ and configuration space is defined as follows $q_1 = 0$, $q_2 = q_3 = (-\pi, \pi)$.

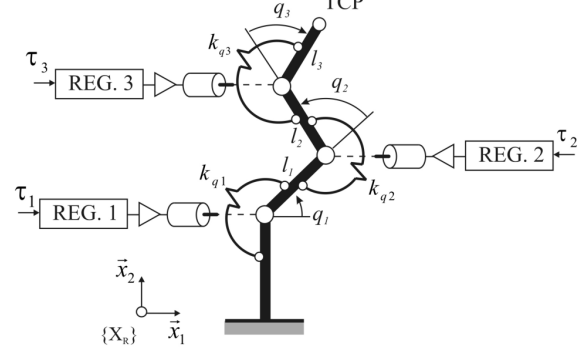


Fig. 5. Model of redundant planar robot with 3 degrees of freedom - SCARA robot with redundant soft actuation system.

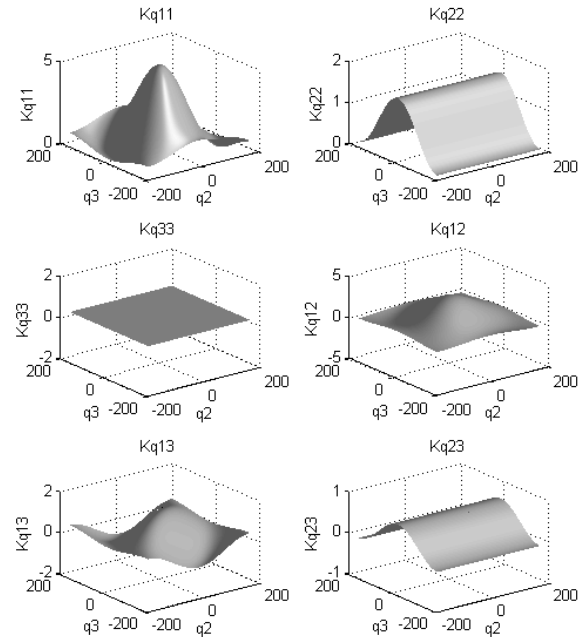


Fig. 6. Graphic representation of the elements of the stiffness actuation K_q .

The internal motion of redundant SCARA robots, or its null space, can be modeled using equivalent four-bar linkage mechanism, so that the robot tip (TCP) is represented as a virtual support that slides along the nominal trajectory. This means that the robot is reduced to an abstract closed kinematic chain with one degree of freedom. The frame of such abstract four-bar linkage is variable and can take a value in the interval which is defined as: $r_1 = (r_{1min}, r_2 + r_3 + r_4)$. Angular coordinates

linkage parameters of the corresponding Freudenstein's model of four-bar linkage mechanism are shown in Fig. 7., while its dimensionless analytical model [7] is defined by following relations:

$$k_1 - k_2 \cos(\varphi_2) + k_3 \cos(\varphi_4) = \cos(\varphi_4 - \varphi_2)$$

$$k_1 = \frac{r_1^2 + r_2^2 - r_3^2 + r_4^2}{2r_2r_4}, k_2 = \frac{r_1}{r_4}, k_3 = \frac{r_1}{r_2} \quad (11)$$

Mapping between the robot generalized coordinates q and angular coordinates used in the Freudenstein's model (11) are: $q_1 = \varphi_2$, $q_2 = \varphi_2 + \varphi_3$ and $q_3 = \varphi_3 - \varphi_4$. In case that $X_U = 0$, relation between the robot coordinate system $\{U\}$ and the coordinate system in the task space $\{X_R\}$ is defined by the rotation matrix:

$${}^U_R R = \begin{bmatrix} \cos(\psi) & -\sin(\psi) \\ \sin(\psi) & \cos(\psi) \end{bmatrix} \quad (12)$$

Using the transformation matrix (12) the analytical model of robot null space given by (11) can be expressed in the robot taskspace.

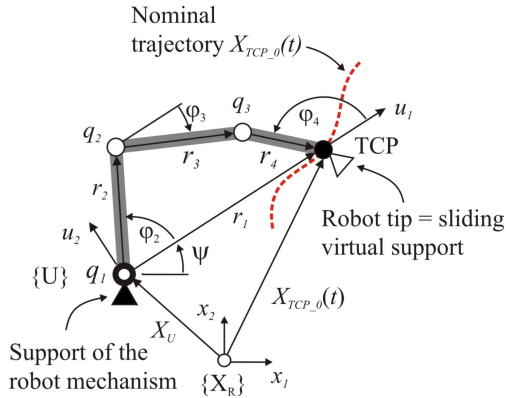


Fig. 7. Equivalent four-bar linkage that is equivalent to the null space of redundant SCARA robot.

The condition (7b) can be further relaxed by introducing Q^* region or configuration subspace robot, which quasi-canonize actuation stiffness matrix (2) for arbitrary given number ε which represents deviation of non-diagonal members from zero:

$$Q^* \rightarrow \bigcap_{\substack{i=1,n \\ j=i+1,n}} k_{q_{ij}}^{bound}(q), k_{q_{ij}} \in K_q(q) \quad (13)$$

where:

$$k_{q_{ij}}^{bound}(q) = \{k_{q_{ij}}(q) \in K_q, \forall i \neq j: |k_{q_{ij}}| < \varepsilon\} \quad (14)$$

Using relations (13), (14) and (10) two pairs of centrally symmetric region Q^*_1 and Q^*_2 are obtained, where analyzed redundant SCARA robot achieves sufficiently good mechanical isotropy (Fig. 8).

4. CONCLUSION

Industrial humanoids are a fundamentally new concept of industrial robots created as an engineering response to the radical demands of collaborative / teamwork and the capability of the acquisition of human behavior. Kinematic redundancy is physically feasible framework for generation of arbitrary generalized stiffness and mechanical impedance. The null space of kinematically redundant robot with $n=m+k$ degrees of freedom is sufficient to generate quasi-diagonal actuation stiffness

matrix. Analytical experiments with redundant SCARA robot confirmed the stated hypothesis.

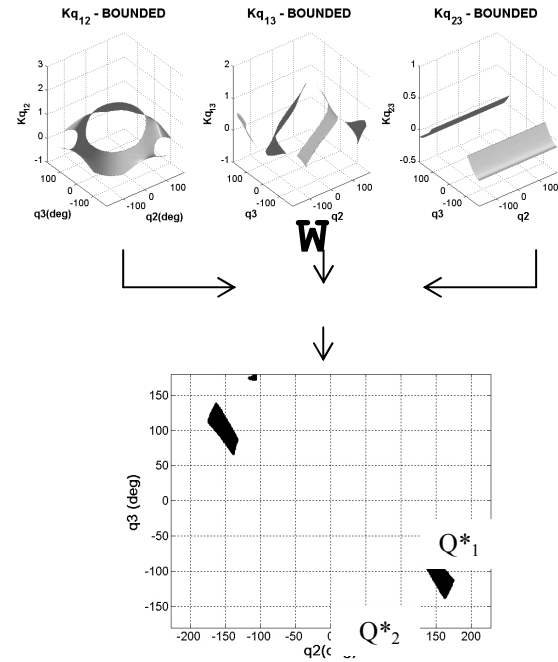


Fig. 8. The configuration subspaces Q^*_i of redundant SCARA robot which satisfy mechanical isotropy condition (7b) and (9).

5. REFERENCES

- [1] ISO10218: Robots for industrial environments - Safety requirements - Part 1: Robot. 2006.
- [2] American National Standards Institute: American National Standard for Industrial Robots and Robot Systems - Safety Requirements, ANSI/RIA R15.06-1986, 1986.
- [3] A. Albu-Schaffer, S. Haddadin, Ch. Ott, A. Stemmer, T. Wimblock and G. Hirzinger, "The DLR lightweight robot: Design and control concepts for robots in human environments", Industrial Robot: An International Journal 34/5, pp: 376-385, 2007.
- [4] Petrović, P., Lukić, N., Danilov, I., "Industrijski humanoidi - novi koncept robota za kolaborativni rad čovek-mašina u sistemima za robotsku montažu", Zbornik radova 38. JUPITER konferencija, 34. simpozijum NU-ROBOTI-FTS, Beograd 2012, str. 3.126-3.139, ISBN: 978-86-7083-757-7
- [5] P.B. Petrović, "Model aktivnog adaptivnog upravljanja procesom spajanja delova u montaži primenom redundantnih robota", Doktorska disertacija, Mašinski fakultet Univerziteta u Beogradu, Beograd, Oktobar 1996.
- [6] A.M. Zanchettin, L. Bascetta, P. Rocco - "Human-like redundancy resolution for anthropomorphic industrial manipulators", IEEE Robotics & Automation Magazine, 2012.
- [7] S. Bai, J. Angeles - "A unified input-output analysis of four-bar linkages", Mechanism and Machine Theory 43 pp. 240-251, 2008.

Authors: Prof. Dr Petar B. Petrović, Nikola Lukić, Ivan Danilov, Vladimir, Dj. Miković, University of Belgrade, Faculty of Mechanical Engineering, Kraljice Marije 16, 11000 Belgrade, Serbia, Tel.: +381 11 3302-435. E-mail: pbpetrovic@mas.bg.ac.rs;

Petrović, M., Miljković, Z., Babić, B.

OPTIMIZATION OF OPERATION SEQUENCING IN CAPP USING HYBRID GENETIC ALGORITHM AND SIMULATED ANNEALING APPROACH

Abstract: In any CAPP system, one of the most important process planning functions is selection of the operations and corresponding machines in order to generate the optimal operation sequence. In this paper, the hybrid GA-SA algorithm is used to solve this combinatorial optimization NP (Non-deterministic Polynomial) problem. The network representation is adopted to describe operation and sequencing flexibility in process planning and the mathematical model for process planning is described with the objective of minimizing the production time. Experimental results show effectiveness of the hybrid algorithm that, in comparison with the GA and SA standalone algorithms, gives optimal operation sequence with lesser computational time and lesser number of iterations.

Key words: genetic algorithms, simulated annealing, operation sequencing, computer-aided process planning, optimization

1. INTRODUCTION

Computer-aided process planning (CAPP) is an important interface between computer-aided design (CAD) and computer-aided manufacturing (CAM). The purpose of CAPP is to determine automatically and optimize the process plans for a design part so that the part can be manufactured economically and competitively to achieve the desired functional specification [1]. The main process planning activities are: manufacturing feature recognition, operation selection and operation sequencing optimization.

The operation sequencing optimization is one of the most important tasks and to solve it in reasonable computational time many approaches have been proposed. Krishna and Rao [2] formulized process planning problem as a traveling salesman problem (TSP) and applied developed metaheuristic, called the ant colony algorithm. Computational time has considerably been reduced by using this ant algorithm as a global search technique for quick identification of the optimal operations sequence by considering various feasibility constraints. Guo et al. [3] modeled operation sequencing as a combinatorial optimization problem, and a modern evolutionary algorithm called the particle swarm optimization (PSO) has been employed and modified to solve it effectively. Li et al. [4] modeled the process planning problem as a constraint-based optimization problem and investigated the application of tabu search approach to solve it effectively. Li et al. [5] developed genetic algorithm (GA) and applied it on CAPP system in distributed manufacturing environment to obtain an optimal process planning considering different resource constraints. Bhaskara et al. [6] also applied GA to generate the optimal sequence of manufacturing operations. The feasible sequences are generated from the feature precedence relationship based on the precedence and geometrical tolerance constraints. An algorithm based on simulated annealing (SA) has been developed to search for optimal or near optimal process plan by simultaneously

considering operation sequences and selection of machines, tools and TADs [7]. In [8], an efficient SA technique is used to obtain feasible optimal sequence with a minimal computational time based on the precedence cost matrix and reward-penalty matrix.

In this paper, the hybrid GA-SA algorithm used to obtain optimal operation sequence. This paper is organized as follows. Section 2 gives process plans representation for operation sequencing in CAPP and Section 3 mathematical model for optimization of operation sequencing. In Section 4 both phases of hybrid algorithm are described and in Section 5 experimental results are presented. Finally, a conclusion, acknowledgements and references are stated in Section 6, Section 7 and Section 8, respectively.

2. PROCESS PLANS REPRESENTATION FOR OPERATION SEQUENCING

In process planning, many types of flexibilities are considered: operation, sequencing, and processing flexibility [9]. Petri-net, AND/OR graphs and networks are some of the numerous methods used to describe these types of flexibilities. In this paper, a network representation method is adopted. Generally, there are three node types in the network representation: the starting node, the intermediate node and the ending node. The starting and the ending node indicate the beginning and the end of the manufacturing process of a job and an intermediate node represents an operation. The intermediate node contains a set of alternative machines that are used to perform the operation and the processing time for the operation according to the machines. All nodes are connected with arrows that represent the precedence between them. For each job, every alternative path in the network starts with an OR-connector and ends with a join-connector. OR-links are used for making decisions as to which of the alternative manufacturing process procedures will be selected. All links that are not connected by OR-connectors must be

visited. Fig. 1 shows process plan networks for operation sequencing for the selected job.

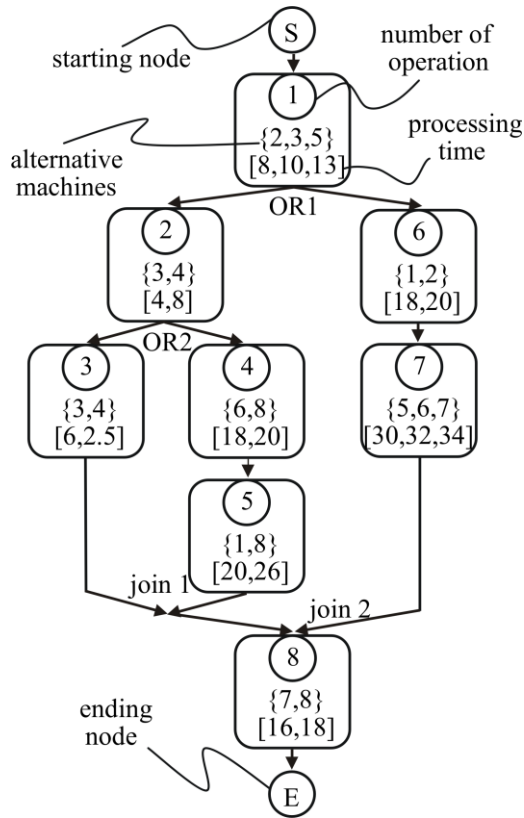


Fig. 1. Process plan network for operation sequencing of selected job

3. MATHEMATICAL MODEL FOR OPTIMIZATION OF OPERATION SEQUENCING

In this paper, the optimization objective of the operation sequencing problem in process planning is to minimize the production time which consists of processing time and transportation time. The notations used to explain mathematical model of operation sequencing problem is described as follows [9]:

- n – total number of jobs;
- G_i – total number of process plans of the i -th job;
- t – 1, 2, 3, ..., M generations;
- o_{ijl} – j -th operation in the l -th process plan of the i -th job;
- P_{il} – number of operations in the l -th process plan of the i -th job;
- k – alternative machine corresponding to o_{ijl} ;
- $TW(i,j,l,k)$ – processing time of operation o_{ijl} on the k -th alternative machine;
- $TP(i,t)$ – production time of i -th job in the t -th generation;
- $TT(i,l,(j,k_1),(j+1,k_2))$ – the transportation time between the k_1 -th and the k_2 -th alternative machine

The production time TP is calculated as shown in Eq. (1).

$$TP(i,t) = \sum_{j=1}^{P_{it}} TW(i,j,k,l) + \sum_{j=1}^{P_{it}-1} TT(i,l,(j,k_1),(j+1,k_2)),$$

$$i \in [1,n], j \in [1,P_{it}], l \in [1,G_i]. \quad (1)$$

The first constraint used here is that each machine can handle only one job at the time and the second is that the operations of one job cannot be processed simultaneously. The objective function is given as follows:

$$\max f(i,t) = \frac{1}{TP(i,t)}, \quad (2)$$

and it defines the alternative process plan with the minimum production time TP .

4. HYBRID GA-SA ALGORITHM

GAs is the most widely used numerical optimization method for solving many engineering problems that are very difficult to solve by conventional techniques. They are based on natural evolution, where GA operators such as selection, crossover and mutation are used to modificate the individuals in a population over generations in order to improve its fitness function value and converge to the best solution of the problem.

SA algorithm is known as one of the useful stochastic search and optimisation algorithm. The main idea of algorithm is to simulate the natural phenomena of annealing of solids implying the process of heating a material to the melting point and then slowly cooling until a thermal equilibrium is reached, so that equilibrium is maintained.

GA algorithm is slow in finding good solution but it is robust for exploring a large and complex space in an intelligent way to find values close to the global optimum. On the other hand, one of the major advantages of SA based approach is effective in finding optimal or near optimal solution in a complex search space with capability of jumping out of local minima and proceeds towards global minima [8]. Hybrid GA-SA algorithm combines the strength of both GA and SA algorithms. This algorithm contains two phases and the steps of each phase are described in following paragraphs.

4.1 Phase#1: GA

The major steps of the GA approach in the first phase of hybrid algorithm are described as follows:

Step 1.1: Generate the individuals for an initial population. Each individual in population consists of two parts with different lengths (Head substring and OR substring), as shown in Fig. 2. It is made up of Genes and each Gene is a structure made up of two numbers. The first position in Gene defines number of an operation and the second number in the Gene is the alternative machine on which the given operations are processed. Further chromosome encoding and decoding is conducted as described in [10].

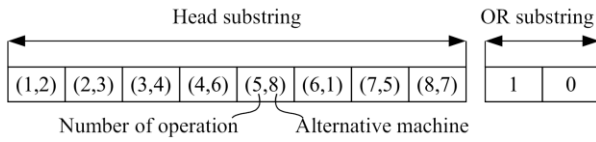


Fig. 2. Individual of initial population

Step 1.2: Evaluate the fitness of the individuals and initialize the parameters of the GA. The fitness function for each individual is calculated as described by Eq. (1) and Eq. (2).

Step 1.3: Selection. After deciding on an encoding phase and generating an initial population, we need to decide on how to choose individuals in the population that will create offspring for the next generation. This phase is called selection and it is a process of selecting two parents from the population for crossing. We adopted the fitness-proportional, roulette wheel selection, where the probability of selection is proportional to an individual's fitness.

Step 1.4: Crossover. According to the defined crossover probability p_c , some individuals are picked out for crossover. For each pair of selected parent chromosomes, a single crossover point is randomly generated and applied for the recombination of process planning individuals. The first part of parent1 (see p1 in Fig. 3) is the same as the first part of offspring1 (see o1 in Fig. 3). The second part of parent2 (see p2 in Fig. 3) is passed to the same position on offspring1 (see o1 in Fig. 3). Analogously, the first part of p2 is passed to the same position on o2 and the second part of p1 is the same as the second part of o2. Fig. 3 shows how two offspring are produced from a parent's pair applying traditional single point crossover to the Head and OR substring of selected chromosomes.

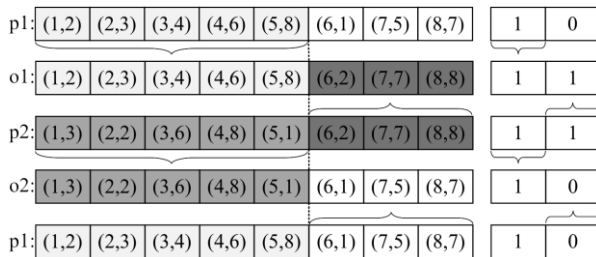


Fig. 3. Crossover for process plan

Step 1.5: Mutation. After the crossover the strings are subjected to mutation. According to the defined mutation probability p_m , some individuals are randomly selected to be mutated. For each selected chromosome a mutation point is randomly chosen and an appropriate operation-machine Gene is obtained. An offspring (o) is generated when a selected machine in parent (p) string Gene is replaced with one from all alternative machines for the selected operation. Mutation is illustrated with an example shown in Fig. 4.

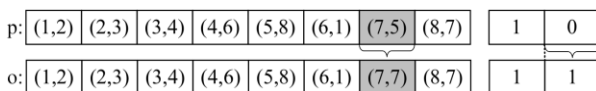


Fig. 4. Mutation for process plan

Step 1.6: Repeat steps 1.2-1.5 for desired number of generations. The number of generation is set in the step 1.2 when we initialize parameters of GA.

Step 1.7: Choose good chromosomes for second phase of hybrid algorithm. After the GA has run for m generations, good chromosomes are chosen randomly and passed to the second phase of hybrid algorithm.

4.2 Phase#2: SA algorithm

The SA algorithm is applied in the second phase of the hybrid GA-SA algorithm and its major steps are described as follows:

Step 2.1: Take a good chromosomes that represents feasible operation sequence and call it current sequence.

Step 2.2: Determine the initial temperature T_0 , the cooling factor T_c and the final temperature T_{lowest} . Set the current temperature T as $T=T_0$.

Step 2.3: Make a change in the current sequence. Changes in current sequence are made using modified method change from [1]. For randomly selected operations in the current sequence we replace current machines with the alternative machines and set current sequence to be temporary sequence.

Step 2.4: Check the validity of the temporary sequence. Check to make sure that temporary sequence is valid and feasible one. If that is not the case, repeat step 2.3.

Step 2.5: Evaluate the fitness's of current and temporary sequence. Calculate the fitness of current sequence $f(\text{current sequence})$ and fitness of temporary sequence $f(\text{temporary sequence})$.

set $\Delta = f(\text{temporary sequence}) - f(\text{current sequence})$
 if $\Delta < 0$
 set temporary sequence to be current sequence
 else
 randomly generate number r from $[0,1]$
 if $r < e^{-\Delta/T}$
 set temporary sequence be current sequence
 else
 set temporary sequence be unchanged
 end if
 end if

Step 2.6: Repeat steps 2.3-2.5 until a criterion is satisfied.

Step 2.7: Lower the temperature T as $T=T-T_c$ and return to step 2.3.

5. EXPERIMENTAL RESULTS

In order to evaluate the performance and illustrate the effectiveness of the proposed hybrid GA-SA approach, the algorithm procedure is coded in Matlab software and implemented on a personal computer with a 3.10 GHz processor. In this experiment, selected job (Fig. 1) with 8 operations and 9 machines is considered and the transportation time between the machines is adopted from [10]. The parameters of the GA in the

first phase of the hybrid algorithm are set as follows: the size of population is 60, the probability of crossover is 0.6, the probability of mutation is 0.1 and number of generations is 30. The parameters of the SA in the second phase of the hybrid algorithm are set as follows: the initial temperature T_0 is set at 0.1660 ($T_0=10*\max(f(i,t))$), the final temperature T_{lowest} is set at 0.00058 ($T_{lowest}=0.25*\min(f(i,t))$) and the cooling factor T_c is set at 0.0058. The parameters for the GA and SA standalone algorithms are set in the same manner as they are in hybrid algorithm.

The objective considered for the operation sequencing problem is to get an optimal operation sequence that results in minimum production time. The fitness function $f(i,t)$ (Eq. (2)) that represent minimal production time is obtained in each iteration of the proposed algorithms and plotted against the iteration number. Fig. 5 illustrates the convergence curves for the GA, SA and GA-SA hybrid algorithm. The obtained optimal sequence is (1,3)-(2,3)-(3,3)-(8,8) with a fitness function value of 0,0116 and it is obtained after 4 iterations by using hybrid algorithm.

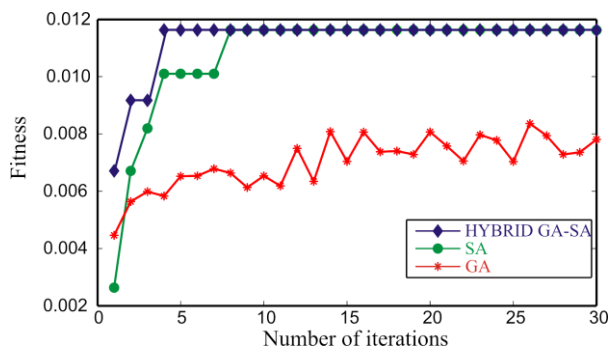


Fig. 5. Comparison of the hybrid GA-SA, single SA and single GA algorithm

6. CONCLUSION

In this paper, the hybrid GA-SA algorithm is proposed to solve optimization problem of operation sequencing in a job-shop environment. The network representation method is adopted to describe operation flexibility and represent job with 8 operations and 9 machines. Optimal operation sequence is found in accordance with minimal production time as criteria. The performance of the presented hybrid algorithm is evaluated in comparison with the results obtained with both GA and SA standalone algorithms. These results indicate that hybrid GA-SA algorithm gives optimal sequence with a lesser computational time and lesser number of iterations. Also, results show that the hybrid algorithm is effective in solving the NP-hard job-shop operation sequencing problems.

7. ACKNOWLEDGMENTS

This paper is part of the project: *An innovative, ecologically based approach to the implementation of intelligent manufacturing systems for the production of sheet metal parts*, financed by the Ministry of Education and Science of the Serbian Government, Grant TR-35004.

8. REFERENCES

- [1] Li, W. D., Ong, S. K., Nee, A.Y.C.: *Hybrid genetic algorithm and simulated annealing approach for the optimisation of process plans for prismatic parts*, International Journal of Production Research, Vol. 40, No. 8, pp. 1899–1922, 2002.
- [2] Krishna, A. G., Rao, K. M.: *Optimisation of operations sequence in CAPP using an ant colony algorithm*, International Journal of Advanced Manufacturing Technology, Vol. 29, No. 1-2, pp. 159–164, 2006.
- [3] Guo, Y.W., Mileham, A.R., Owen, G.W., Li, W. D.: *Operation sequencing optimization using a particle swarm optimisation approach*, Proceedings of the Institution of Mechanical Engineers, Part B: Journal of Engineering Manufacture, Vol. 220, No. B12, pp. 1945–1958, 2006.
- [4] Li, W. D., Ong, S. K., Nee, A.Y.C.: *Optimization of process plans using a constraint-based tabu search approach*, International Journal of Production Research, Vol. 42, No. 10, pp. 1955–1985, 2004.
- [5] Li, L., Fuh, J.Y.H., Zhang, Y. F., Nee, A.Y.C.: *Application of genetic algorithm to computer-aided process planning in distributed manufacturing environments*, Robotics and Computer-Integrated Manufacturing, Vol. 21, No. 6, pp. 568–578, 2005.
- [6] Bhashara, R.S.V., Shunmugam, M.S., Narendran, T.T.: *Operation sequencing in CAPP using genetic algorithms*, International Journal of Production Research, Vol. 37, No. 5, pp. 1063–1074, 1999.
- [7] Ma, G. H., Zhang, Y. F., Nee, A. Y. C.: *A simulated annealing-based optimization algorithm for process planning*, International Journal of Production Research, Vol. 38, No. 12, pp. 2671–2687, 2000.
- [8] Nallakumarasamy, G., Srinivasan, P.S.S., Venkatesh, R. K., Malayalamurthi, R.: *Optimization of operation sequencing in CAPP using simulated annealing technique (SAT)*, International Journal of Advanced Manufacturing Technology, Vol. 54, No. 5-8, pp. 721–728, 2011.
- [9] Li, X.Y., Shao, X.Y., Gao, L.: *Optimization of flexible process planning by genetic programming*, International Journal of Advanced Manufacturing Technology, Vol. 38, No. 1-2, pp. 143–153, 2008.
- [10] Petrović, M., Miljković, Z., Babić, B., Vuković, N., Čović, N.: *Towards a Conceptual Design of Intelligent Material Transport Using Artificial Intelligence*, Strojarstvo, Article in press, 2012.

Authors: M.Sc. Milica Petrović, Prof. Dr. Zoran Miljković, Prof. Dr. Bojan Babić, University of Belgrade – Faculty of Mechanical Engineering, Production Engineering Department, Kraljice Marije 16, 11120 Belgrade 35, Republic of Serbia, Phone: +381 11 3302-264, Fax: +381 11 3370-364.

E-mail: mmpetrovic@mas.bg.ac.rs
zmiljkovic@mas.bg.ac.rs
bbabic@mas.bg.ac.rs

Stevanović, D., Korunović, N., Trajanović, M., Trifunović, M., Milovanović, J., Stojković, M.

FINITE ELEMENT MODEL OF HUMAN TIBIA AND PRELIMINARY ANALYSIS

Abstract: *A procedure for creation of subject specific finite element (FE) models of human tibia is described in the paper. Model geometry and material properties are based on medical images, obtained by computed tomography (CT) scanning. The most important steps of the procedure are: extraction of polygonal model from medical images, creation of surface model based on polygonal model and creation of FE model. An important step in subject specific FE model creation is assignment of material properties, which should also be subject specific. To achieve this goal, material properties were assigned to FE model by means of automatic mapping of CT numbers onto FE models, based on correlation between bone density and elastic properties of bone material. Optimal mesh density was established through convergence checks, performed on a series of FE tibia models of growing mesh density. The paper also describes a preliminary analysis of a created FE model, which was performed in order to check model integrity and validity.*

Key words: *Finite element method, reverse engineering tibia, computed tomography (CT)*

1. INTRODUCTION

Injuries or pathological processes (tumors and others) of human osteoarticular system are very common reasons for large number of surgical interventions. These interventions often require planning the process of surgery, as well as application of different implants or fixators. Nowadays, it is possible to use such medical aids due to increasing application of modern technologies in medicine, which enable computer-assisted planning of surgery [1]. Application of computer technologies results in accurate and precise geometry of bones and fixators [2]. The technique of Reverse Engineering (RE) is usually used for defining the precise geometry of bones [3], while the modeling of implants and fixators is performed by application of computer technologies such as Rapid Prototyping (RP) [4]. These techniques have been applied in planning of complex surgical interventions, modeling and constructing implants, medical devices, surgical tools, as well as in tissue engineering [5]. Mentioned technologies for precise defining of geometry may also be used for simulation of behavior of human osteoarticular system and nested implants or fixators, which would help achieve high efficiency in performing of certain orthopedic surgery.

Common bones fractures are those of long bones, and one of the most often is the fracture of tibia. Tibia fractures can be classified according to place, type and local mechanism of the fracture [6]. These fractures can be divided into two groups, that is, into fractures which appear at proximal and distal ends of tibia [7]. In order to enable easier treatment of the patient and optimize the shape of the implant or fixator which is to be used in the operation, it is necessary to apply the methods of simulation. Method of simulation based on finite element method was developed by Brekelmans in 1972, for the purpose of understanding mechanical behavior of the skeleton under mechanical loads in orthopedic

surgery [8]. Brekelmans described the application of finite element method (FEM) in stress analysis of two-dimensional femur model. FEM based simulation of bone behavior and its application in orthopedics have been expanding ever since. Apart from the fact that this approach can provide answer to many scientific questions, there is still the need to improve this method for its easier and faster application in orthopedic surgery.

Large number of recent studies was based on general bio-mechanical behavior of the entire bone. The study described in this paper relies on bone material properties that are based on values of radiological tissue density, which were obtained from CT. Its aim was to create FEM model of tibia for stress analysis of tibia-implant or tibia-fixator assembly. It also included the creation of CAD model, necessary for FEM model construction. It is very important to note that accuracy of numeric solution of FEM model is influenced by following factors: boundary conditions, accuracy of the shape of finite element mesh created in CAD model based on CT scan data, and regularity of the finite elements shape.

2. PROCESS OF CREATING FEM MODEL OF TIBIA

Process of creating subject specific model of human tibia for testing the state of strain by application of FEM, is performed in following stages:

- Extracting and generating polygonal model based on CT scan.
- Creation of CAD model based on polygonal model.
- Creation of FEM model.

2.1 Extracting and generating polygonal model based on CT scan

First phase of extracting and generating polygonal model of tibia starts with collecting data obtained from

computer tomography, that is, CT scan of lower extremities of the patient. In this case, resolution of CT image was 0.5 mm Fig. 1. [2, 3, 9].

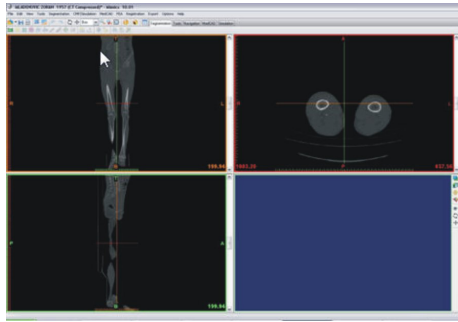


Fig. 1. Image of lower extremities obtained by computer tomography. Views in orthogonal coordinate system are presented in the figure

CT scan provides data necessary for creating “point cloud”, which is later used in selected CAD software for the purpose of creating the geometrical image of the bone by reverse engineering. Using the applications for editing medical images obtained by computer tomography, interest zones for creation of FEM model are being selected. In this case, based on the selected zone, “point cloud” which corresponds to external surface of tibia and the surface which divides internal bone structure into area of bone tissue and area of bone marrow was created. During “point cloud” creation, a large number of points in internal bone structure that do not belong to the surfaces defining its internal zones are often selected Fig. 2. This problem is prominent in older patients, due to common appearance of osteoporosis. Selected points represent “noise” which poses problems in further generating of geometrical model [9].



Fig. 2. Polygonal model of tibia and surrounding bones parts, created based on “point cloud”

2.2 Creation of CAD model based on polygonal model

The following phase, after extracting and generating polygonal model, is removing parts and segments which do not belong to tibia. This primarily refers to removing parts of surrounding bones: femur, fibula and talus, as well as residual parts of soft tissue and veins Fig. 3., which leads to clean polygonal model for further creation of geometrical model.

After cleaning polygonal model, it is necessary to remove triangles on external bone surface which interfere in internal layer of the bone Fig. 4. Due to

residual cracks in polygonal model it is also necessary to perform “healing”.



Fig. 3. Polygonal model of tibia, with removed segments of surrounding bones and soft tissue

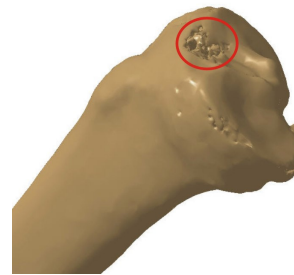


Fig. 4. Polygonal model with chaotic distribution of triangles, grouped according to internal structure of tibia. These cases are most often the consequence of osteoporotic bone scan

The following step is increasing the level of “smoothness”, if necessary. Application of relevant approximation functions helps creation of NURBS surface which represents the external envelope of model of tibia Fig. 5. Final step, after forming the surface model, is creation of solid model of tibia, by filling the volume of external surface.

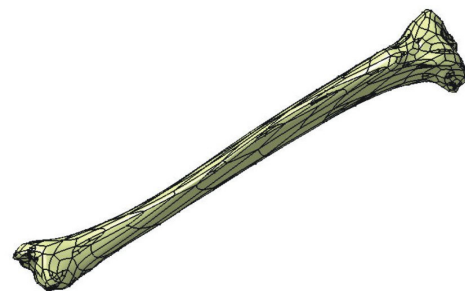


Fig. 5. NURBS surface which represents the external envelope of tibia

2.3 Creating FEM model of tibia

In this phase, the most important steps are creation of finite element mesh of optimal density and assigning appropriate material properties to the model. Process of material properties assignment can be performed in two manners. One of them is mapping the material that is, assigning characteristics of material to each finite element of the model, based on data obtained by CT scan of the patient. The other method is dividing internal bone structure into zones and assigning equivalent module of elasticity of bone tissue to corresponding bone zones.

2.3.1 Creating FEM model for analysis of tibia

Finite element mesh on tibia model consists of tetrahedral finite elements of second order, the size of which grows towards the inside of the model.

The choice of optimal mesh density was based on results convergence test, where several consecutive meshes of growing density were used [10, 11]. Number of elements was increased according to the geometrical progression, whereas every side of the element formed in the previous step was divided by a half of its length.

The convergence was tested by comparison of changes in stress values between two consecutive solutions in selected areas Fig. 6., which are located in the zones with critical values of stress. The difference of stress values in selected nodes, compared to the previous step, was in the range from 0.057 % to 0.666 %. Since the difference was small, it was concluded that optimal mesh may be built using the average value of element edge equal to 2 mm and total number of elements is 145492. It is considered that the discretization error is reduced to minimum in this manner and that potential errors in analysis can be ascribed to other factors, such as material modeling or boundary conditions.

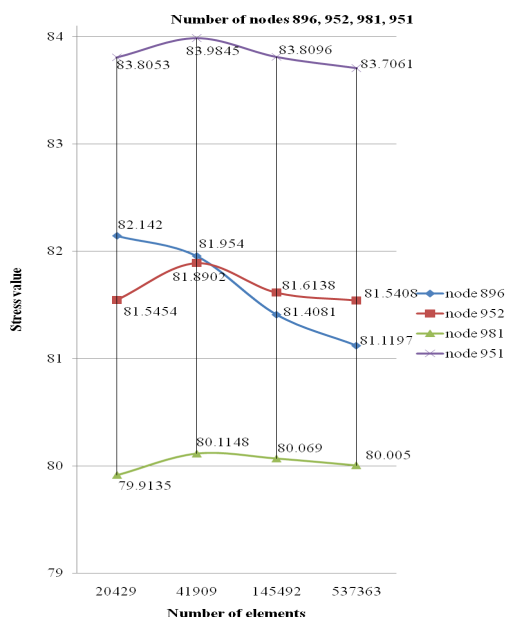


Fig. 6. Test of convergence of necessary mesh density based on monitoring changes of stress values in selected nodes

2.3.2 Mapping of material on finite elements mesh

Material mapping, based on mechanical material properties obtained by correlation with CT image, represents the approach to material modeling which enables the fastest creation of the subject specific model of human bones. It is based on the fact that certain gray values on the CT scan, which are expressed in HU units (according to the Hounsfield's scale), for known parameters of X-ray tube, correspond to certain values of radiological tissue density. On the other hand, these values can be correlated with apparent bone density. Different authors also analyzed the relation between density of different types of bones

and their mechanical characteristics [12]. If it is assumed that the bone is non-homogenous and isotropic, the most common relation is the one between the module of elasticity and apparent bone density.

Morgan's relation [12] defined in 2003, was used in this study and it states:

$$E = 6950 \cdot \rho_{app}^{1.49} \cdot [MPa] \cdot \left(z a \rho_{app} u \left[\frac{g}{cm^3} \right] \right) \quad (1)$$

where E represents the module of elasticity, and ρ_{app} is the apparent bone density. Obtained values of elasticity module are reduced to a hundred constant values; and based on these values, a hundred different materials were defined and assigned to finite elements of FEM model.

2.3.3 Description of preliminary analysis of created FEM model

Preliminary FEA of tibia model was performed, for the purpose of testing the integrity of the model and efficiency of practical application of described principles.

In the process of material mapping, it was necessary to take into consideration the thickness of compact bone. Since the bone is very thin on proximal and distal end, testing the convergence determines the density of mesh which best describes the structure of tibia in these areas, and the final result of the analysis contains the satisfactory level of accuracy.

Surfaces were created on the model envelope, which approximately correspond to the zones of joints and muscles activities. Loads taken from literature [7] were applied at proximal end of tibia, as equally distributed pressure acting on created surfaces of joints and muscles [13, 14]. Distal end of model was encastred.

Distribution of equivalent strain on the surface of FEM model of tibia, obtained by preliminary analysis, is presented on Fig. 7. Maximal values of the strain appear approximately at 1/3 of distance between distal and proximal ends.

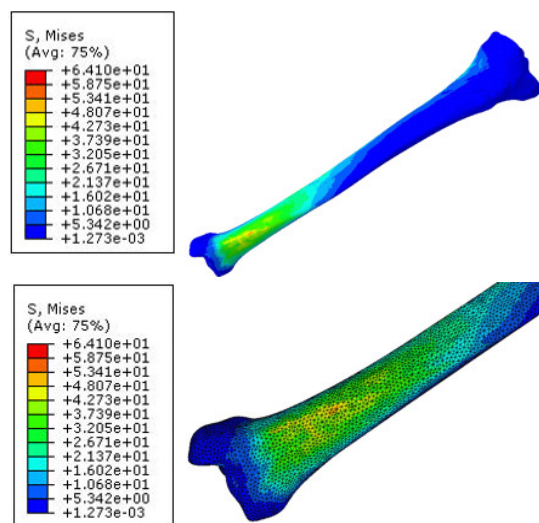


Fig. 7. Results of state of strain obtained by preliminary analysis as spotting critical points around distal end of tibia where the highest values of strain appear

3. CONCLUSION

Computer aided technologies have wide range of application in orthopedic surgery. This study presents their application in analysis of tibia, using FEM. Models obtained in this manner can significantly improve understanding of mechanical behavior of tibia exposed to different loading scenaria. Described procedure for creating FEM model of human tibia can also be used for creating models of other human bones.

Defined procedure for creation of FEM model enables subsequent solving of the following tasks:

- Creating model of bone-implant assembly and stress analysis of its components, for the purpose of choosing the material, optimal shape, dimensions and position of the implant.
- Detailed analysis of typical load cases on tibia, during everyday activities of the patient.

ACKNOWLEDGMENT

This paper is part of project III41017 Virtual human osteoarticular system and its application in preclinical and clinical practice, funded by the Ministry of Education and Science of Republic of Serbia, for the period of 2011-2014.

4. REFERENCES

- [1] Trajanović, M., Mitković, M., Vitković, N., Milovanović, J.: *Definisanje zahteva aplikacije za planiranje operacija u hirurgiji koštano zglobnog sistema*, IMK-14 - Istraživanje i razvoj, Vol. 15(1-2), p.p. 5-11, 2009.
- [2] Veselinovic, M., Vitkovic, N., Stevanovic, D., Trajanovic, M., Arsic, S., Milovanovic, J., Stojkovic, M.: *Study on creating human tibia geometrical models*, Proceedings of the 3rd International Conference on E-Health and Bioengineering - EHB, p.p. 195-198, Iași, Romania, Gr. T. Popa University of Medicine and Pharmacy Publishing House, Iași, Romania, 2011.
- [3] Stojkovic M., Trajanovic M., Vitkovic N., Milovanovic J., Arsic, S., Mitkovic M.: *Referential geometrical entities for reverse modeling of geometry of femur*, Proceedings of the II ECCOMAS Thematic Conference on Computational Vision and Medical Image Processing: VipIMAGE 2009, p.p. 189-194, Porto, Portugal, Taylor & Francis Group, Porto, Portugal, 2009.
- [4] Milovanović, J., Trajanović, M., Vitković, N., Stojković, M.: *Rapid prototyping tehnologije i materijali za izradu implantata*, IMK-14 - Istraživanje i razvoj, Vol. 15(1-2), p.p. 23-30, 2009.
- [5] Simchia, A., Petzoldt, F., Pohl, H.: *On the development of direct metal laser sintering for rapid tooling*, Journal of Materials Processing Technology, Vol. 141 (3), p.p. 319-328, 2003.
- [6] Christian, W., Peter, M., Leif, B. H., Tron, D. P. G.: *Finite element analysis of tibial fractures*, Danish Medical Journal, No. 5, 2010.
- [7] Norio, S., Etsuo, C., Koji, T., Naoya, T.: *Biomechanical analysis for stress fractures of the anterior middle third of the tibia in athletes: nonlinear analysis using a three dimensional finite element method*, Journal of Orthop Science, Vol. 8 (4), p.p. 505-513, 2003.
- [8] Brekelms, W. A. M., Poort, H. W., Slooff, T. J. J. H.: *A new method to analyse the mechanical behaviour of skeletal parts*, Acta Orthopaedica Scandinavica, Vol. 43 (5), p.p. 301-317, 1972.
- [9] Korunović, N., Trajanović, M., Mitković, M., Vulović, S.: *Od CT snimka do modela za analizu naponskog stanja u femuru primenom metoda konačnih elemenata*, IMK-14 - Istraživanje i razvoj, Vol. 16(2), p.p. 45-48, 2010.
- [10] Ingrassia, T., Mancuso, A., Ricotta, V.: *Design of a new tibial intramedullary nail*, Proceedings of IMProVe 2011 International conference on Innovative Methods in Product Design, p.p. 678-684, Venice, Italy, Università degli Studi di Padova Facoltà di Ingegneria Dipartimento di Architettura, Urbanistica e Rilevamento (DAUR), Venice, Italy, 2011.
- [11] Viceconti, M., Davinelli, M., Taddei, F., Cappello, A.: *Automatic generation of accurate subject-specific bone finite element models to be used in clinical studies*, Journal of Biomechanics, Vol. 37, p.p. 1597-1605, 2004.
- [12] Elise, F. M., Harun, H. B., Tony, M. K.: *Trabecular bone modulus-density relationships depend on anatomic site*, Journal of Biomechanical, Vol. 36, p.p. 897-904, 2003.
- [13] Little, R. B., Wevers, H. W., Siu, D., Cooke, T. D. V.: *A three-dimensional finite element analysis of the upper tibia*, Journal of Biomechanical Engineering, Vol. 108, p.p. 111-119, 1986.
- [14] Tarniță, D., Popa, D., Tarniță, D. N., Grecu, D.: *CAD method for three-dimensional model of the tibia bone and study of stresses using the finite element method*, Romanian Journal of Morphology and Embryology, Vol. 47 (2), p.p. 181-186, 2006.

Authors: M.Sc. Dalibor Stevanović, Dr. Nikola Korunović, Prof. Dr. Miroslav Trajanović, M.Sc. Milan Trifunović, M.Sc. Jelena Milovanović, Dr. Miloš Stojković, University of Nis, Faculty of Mechanical Engineering, Laboratory for Intelligent Production Systems, Aleksandra Medvedeva 14, 18000 Nis, Serbia, Phone.: +381 18 500-669.

E-mail: dalibor.stevanovic85@gmail.com
nikola.korunovic@masfak.ni.ac.rs
miroslav.trajanovic@masfak.ni.ac.rs
milant@masfak.ni.ac.rs
jeki@masfak.ni.ac.rs
miloss@masfak.ni.ac.rs

Todić, V., Lukić, D., Milošević, M., Jovičić, G., Vukman, J.

MANUFACTURABILITY OF PRODUCT DESIGN REGARDING SUITABILITY FOR MANUFACTURING AND ASSEMBLY (DfMA)

Abstract: Manufacturability of product design significantly affect on overall quality, both in terms of functionality and utilization, so in terms of manufacturing and assembly. This paper presents systematization and analysis manufacturability of product design with a focus on DFMA methods.

Keywords: Manufacturability of product design, DfX, DfMA methods.

1. INTRODUCTION

Manufacturability of product design, primarily as a measure suitability for manufacturing is a very broad term and is difficult to uniquely define, because it depends on many influential elements, including the conditions in which the manufacturing process to implement.

Design of complex product is evaluated from standpoint of functionality, manufacturing, assembly, utilization and maintenance [11].

In this paper will be presented systematization of methods for analysis manufacturability of product design, with accent on manufacturability of product design regarding suitability for manufacturing and assembly (*DfMA - Design for Manufacturing and Assembly*). At the end of paper will show „DFMA“ software on one specific example.

2. SYSTEMATIZATION METHOD'S FOR ANALYSIS MANUFACTURABILITY OF PRODUCT DESIGN - DfX TOOLS

Design for eXcellence (DfX) requires taking into account of all relevant design objectives and constraints in the early stages of design. DfX is general term, where „X“ may represent manufacturing, assembly, quality, etc. [3].

There are various splitting DfX methods, and here will be displayed DfX methods for scope Design for Efficiency and Green Design, Fig. 1. DfX methods using three ranges of perception: 1) product scope, 2) system scope, 3) eco-system scope [6].

Product scope includes DfM (*Design for manufacturing*), DfA (*Design for Assembly*), DfQ (*Design for Quality*), DfR (*Design for Reliability*), DfD (*Design for Disassembly*), DfMa (*Design for Maintainability*) and DfO (*Design for Obsolescence*), and system scope includes DfSC (*Design for Supply Chain*), DfL (*Design for Logistics*) and DfN (*Design for Networks*).

Green Design includes DfRe (*Design for Recycle*), DfS (*Design for Sustainability*), DfE (*Design for Environment*) and DfLC (*Design for Life Cycle*). Eco-system scope includes DfS, DfE and DfLC, and together with product scope DfRe [6].

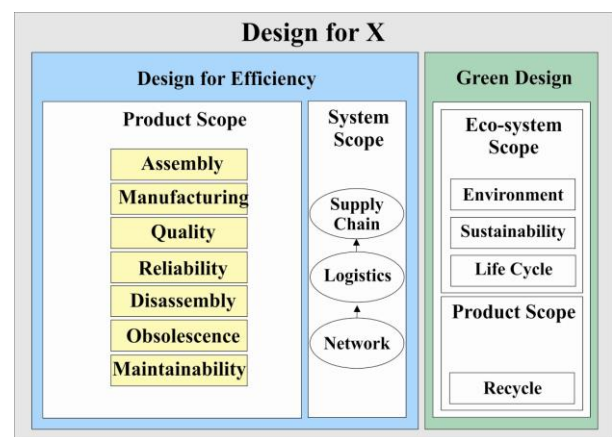


Fig. 1. Structure of DfX tools

The main purpose of design for efficiency is expressed as reducing costs and lead time of a product while sustaining or improving its quality. Product scope focuses on the product aspects which enable efficiencies at the shop floor, while system scope concentrates on the integration and coordination of the value chain, starting with the design stage and ending with the delivery and maintenance system.

DfX concepts and methods have role in reducing the cost items. However, the actual percentage of each DfX concept can not be precisely measured because of the variety of the product type and required production system. Fig. 2 shows the possibilities of reducing price of product considering different sources of costs.

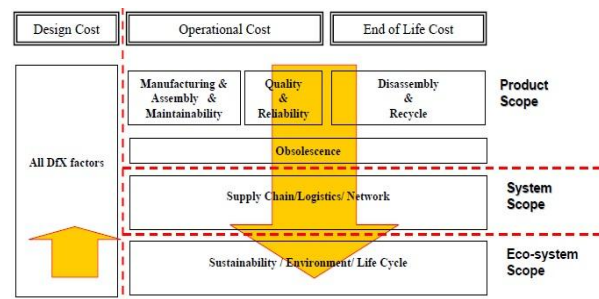


Fig. 2. The benefit of DfX factors in product costs [6]

3. DESIGN FOR MANUFACTURING AND ASSEMBLY (DfMA)

In the concept design for efficiency, design for manufacturing (DfM) and design for assembly (DfA) are methods that take into consideration first.

DfM is actually a systematic approach that allows designers to predict the costs of manufacturing in the early stages of the design process, even when it is known only approximate geometry of the product that is being developed [8].

According [4] design for manufacturing was defined as an approach for designing a product so that the design quickly transitioned into production, the product is manufactured at a minimum cost, the product is manufactured with minimum effort in terms of processing and handling requirements, and the manufactured product attains designed level of quality. Fabricius [5] proposed a procedure of seven steps for design for manufacturing to enhance linkage between design and manufacturing using a three-dimension model. Stoll [10] is described 13 DfM guidelines that are strategy-based and practice oriented. These guidelines focus on three strategies relating to modular design, multi-use parts with standardization, and easy of assembly to increase to manufacturability.

In design for assembly (DfA) estimated design of product based on quantitative characteristics of the product. The most important indicator of efficiency of design is assembly time. Assembly time of product reflects the difficulty of assembly process such as consolidation, adjustment, and alignment. So, DfA aims consolidate the components and functions in a smaller number of components, which affects on reducing assembly time and assembly costs.

DFMA is used for three main activities [2]:

- As the basis for concurrent engineering studies to provide guidance to the design team in simplifying the product structure, to reduce manufacturing,
- As a benchmarking tool to study competitors products and quantify manufacturing and assembly difficulties and
- As a should-cost tool to help negotiate suppliers contracts.

Three of most common DfMA methods by which they are developed appropriate software are [7]:

- DFMA, Boothroyd Dewhurst Inc., USA, software developed according to the methodology developed by Boothroyd i Dewhurst,
- TeamSET, CSC Computer Sciences Ltd, UK, software developed according to the methodology Lucas-Hull and
- AEM Assembly Evaluation Method, Hitachi Corp., Japan, software developed according to the methodology Miyakawa and Ohashi.

3.1 Boothroyd-Dewhurst method

Boothroyd-Dewhurst DfMA method evaluates the product based on design efficiency. The higher design efficiency-better product. Number of parts of the product has significant effect to the design efficiency

value. If the product has many parts, the assembly time will be higher. Higher assembly time means lower design of efficiency. Also, higher assembly time directly means that the assembly cost is higher. Therefore, Boothroyd-Dewhurst DfMA recommends elimination of unnecessary part and combination of many parts into fewer components to reduce the number of parts in a product [7].

DfMA is a method for evaluating the manufacturability of part design and assembly design. It is a way to identify unnecessary parts in assembly, and determine the time of manufacture and assembly costs. The steps applying DfMA methods and corresponding software are shown in Fig. 3.

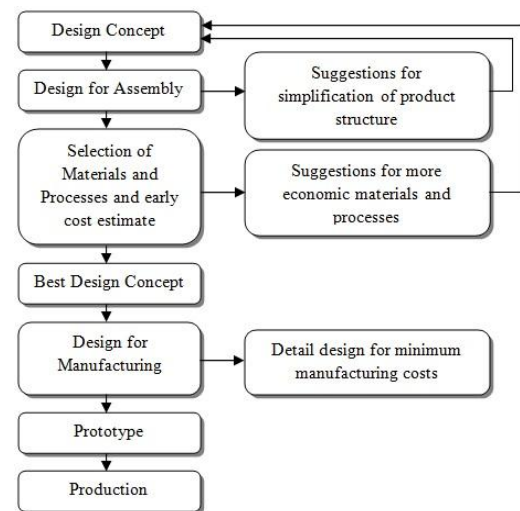


Fig. 3. The steps applying DfMA methods [6]

According Boothroyd claimed that product design for manufacture and assembly can be the key to high productivity an all manufacturing industries comparing to the automation. In his method, the concept of design for assembly was first indicated in the conceptual design phase to ensure the best design concept for materials and processes. Then, the concept was evaluated to minimize the manufacturing costs, which results in a slight increase the time in conceptual design phase. Considerable time savings would be achieved during preliminary design and detail design phases.

This method, namely software can be divided into three main stages [9]:

1) Selection of workpiece

Selection the best type of raw material or workpiece as the first step in applying DfMA depends of many factors that affect their choice, such as:

- Mechanical and chemical properties of the workpiece material,
- Selection standard workpiece and
- Application of near net production technology.

2) Selection machining processes and systems

At determining the most appropriate machining processes and systems should be taken into consideration:

- Type of production,
- Type and shape of workpiece,
- Economically tolerance of product,
- Opportunities machining systems,
- Appropriate tools and supplies, etc.

3) Assembly of the product

During assembly of product, provides the greatest possibility of applying DfMA methods. Proper use of DfMA principles allows produce a high quality products. This principles are based on:

- Reducing the number of parts in the assembly,
- Implementation of symmetric parts when product design allows it,
- Easy design of products,
- Ensure self fixturing,
- Avoid parts that can tangle, etc.

3.2 Lucas-Hull method

Lucas Organization and University of Hull United Kingdom are the two groups behind the development of the Lucas design for assembly (DfMA) method. Lucas DfMA evaluation method takes into consideration the crucial aspects of assemblability and component manufacture [7].

Algorithmic structure of this method is given in Fig. 4.

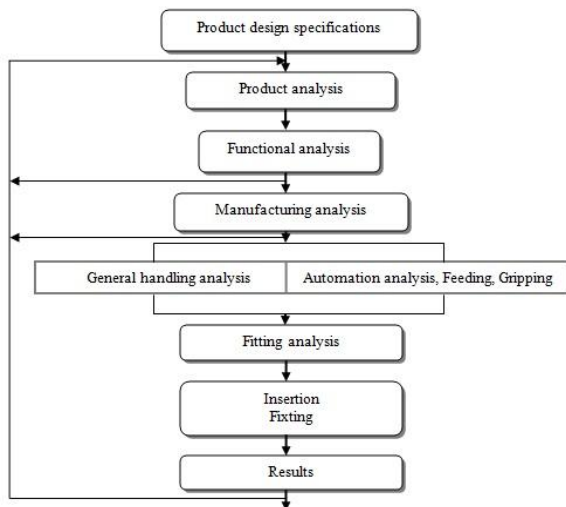


Fig. 4. Lukas-Hull DfMA method [7]

3.3 Hitachi metod (AEM)

Assemblability Evaluation Method (AEM) was developed by Hitachi in 1976 for better assemblability of product by improving design of product. AEM identifies the weakness of the design at the early stage of the design process. The design quality is being evaluated based on two indicators that are [7]:

- ‘E’ refers to an assemblability evaluation score ratio. It determines the difficulty of the operations and
- ‘K’ refers to an assembly cost ratio. It is used to project elements of assembly cost.

Description of algorithmic structure for assessing suitability for assembly by Hitachi is given in Fig. 5.

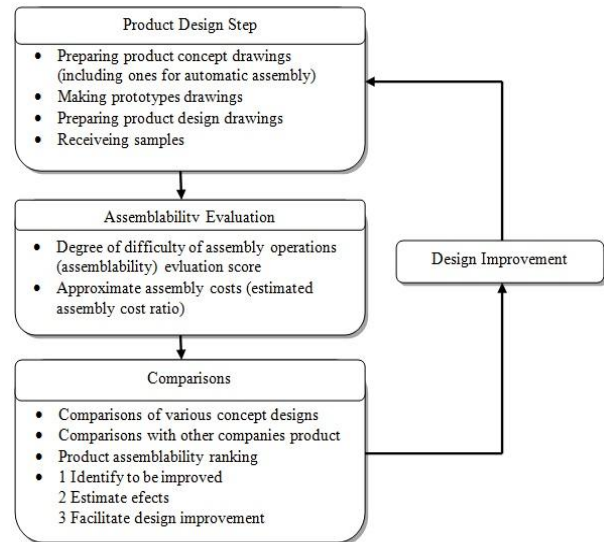


Fig. 5. Assessment of suitability for assembly and redesign [7]

4. REVIEW OF SOFTWARE SOLUTIONS

In the previous section presents the most common software for DfMA, while in this paper provides a brief overview of software *DfM Cost 2.2 i DfMA 9.4* by *Boothroyd Dewhurst Inc.*, in one example. It is also important to note that this is a trial DfMA software was obtained in order to explore it’s possibilities.

It is recommended that first determine the manufacturing costs for various components using DfM application, and then apply DfA application to determine assembly costs. In Fig. 6 shown estimation of the manufacturing costs of the example of cylinder, and Fig. 7 shown estimation assembly costs for example piston assembly [1].

User interface Concurrent Cost 2.2 and Design for Assembly 9.4 consists of three areas:

1. Tree model,
2. Fields to define certain data and
3. Fields for display estimates costs.

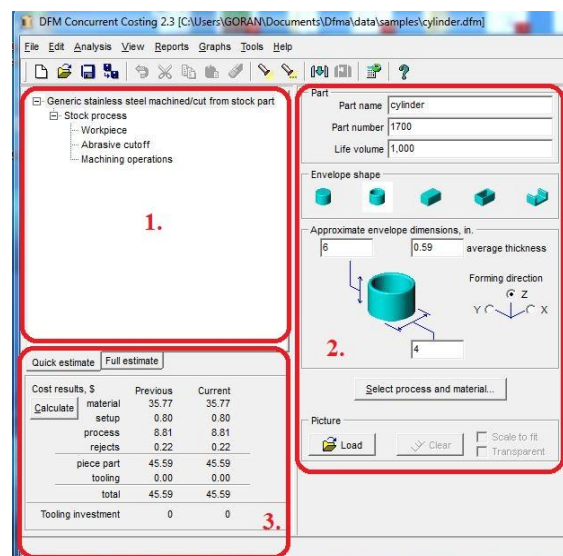


Fig. 6. Cost estimate in the example of cylinder (DfM)

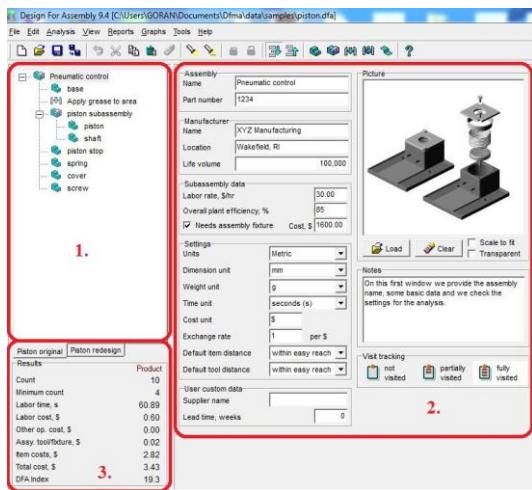


Fig. 7. Cost estimate in the example of piston assembly (DfA) [1]

In DfM applications Concurrent Cost 2.2, under tree model are shown corresponding machining processes some parts of the product, while in the field to define the data, enter data, such as part name, part number, life volume, selection workpiece and it's dimension, selection processes and materials, etc. Selection processes and materials (material-process or process-material) is essential. If you select material first software will show the possible processes for the selected material, and if you select process first, software will show the possible materials for the process. Fields for display estimates costs shows individual costs element, such as cost of material, cost adjustment, tooling cost, etc., and finally total cost.

In DfA applications Design for Assembly 9.4, presents overall structure of the product or assembly, and can serve as an alternative selection for selection technical elements in the implementation of the correction on the product or assembly. In field to define certain data next to the assembly name, part number, manufacturer and life volume performed and data entry such as subassembly data and various settings that include units, dimension unit, weight unit, time unit, cost unit, etc. Field with results shows certain elements for the calculation of cost, DfA index and total cost.

After evaluation of the machining and assembly costs there is the possibility of generating reports in the form of tables or graphs with output results.

5. CONCLUSION

Costs of product design and their manufacturing process planning, participate in a small part of the total price of the product, but decisions made during this process significantly affect the overall cost of developing a new product and is essential for the market success of the product. Therefore, necessary to consider the problem of production as early as possible, even at the stage of the product design, namely, development of it's concept, because the costs of modifications of the product higher if you make changes in the later stages of product development.

In order satisfy these requirements has been developed appropriate DfX methods, whereas in the present study shown the most common methods of DfMA.

6. REFERENCES

- [1] Boothroyd Dewhurst, Inc.: <http://www.dfma.com/>
- [2] Boothroyd, G., Dewhurst, P., Knight, W.: *Product Design for Manufacture and Assembly, Second Edition*, Taylor & Francis, United States, 2001.
- [3] Ching-Chow Yang, Shun-Hsing Chen, Jiun-Yan Shian: *A DfX and concurrent engineering model for the establishment of a new department in university*, International Journal Production Economic, Vol. 107, p.p. 179-189, 2007.
- [4] Das, S.K., Datla, V., Samir, G.: *DFQM – An approach for improving the quality of assembled products*, International Journal of product Research, Vol. 38(2), p.p. 457-477, 2000.
- [5] Fabricius, F.: *Seven step procedure for design for manufacture*, World class design for manufacture, Vol. 1(2), p.p. 23-30, 1994.
- [6] Ming-Chuan Chio, Chun-Yu Lin, Gul Okudan: *An Investigation of the Applicability of DfX Tools during Design Concept Evolution*, Department of Industrial and Manufacturing Engineering, Pennsylvania, http://www.personal.psu.edu/mzc148/APIEMS07_849.pdf
- [7] Nik Mohd Farid Bin Che Zainal Abidin: *Incorporation design for manufacture and assembly methodologies into the design of a modified spark plug*, Faculty of Mechanical Engineering, Universiti Teknologi Malaysia, 2007.
- [8] Ristic, M.: *Product design in terms manufacturability, master's thesis, Mechanical Engineering Faculty, Nis, 2011. (in Serbian)*
- [9] Sharifah Zainaf Binti Wan Abu Seman: *Integration of Design for manufacturing and assembly (DfMA) and theory of inventive problem solving (TRIZ) for design improvement*, Faculty of Mechanical Engineering, Universiti Teknologi Malaysia, 2010.
- [10] Stoll, H. W.: *Design for Manufacture*, Manufacturing Engineering, Vol. 100(1), p.p. 67-73, 1988.
- [11] Todic, V., Penezic, N., Lukic, D., Milosevic, M.: *Technology logistics and entrepreneurship*, Faculty of Technical Sciences, Novi Sad, 2011. (in Serbian)

Authors: Prof. dr Velimir Todić, Mr. Dejan Lukić, Dr. Mijodrag Milošević, MSc Goran Jovičić, MSc Jovan Vukman, University of Novi Sad, Faculty of Technical Sciences, Department of Production Engineering, Trg Dositeja Obradovica 6, 21000 Novi Sad, Serbia, Phone.: +381 21 485-2346, Fax: +381 21 454-495.

E-mail: todvel@uns.ac.rs, lukicd@uns.ac.rs, mido@uns.ac.rs, goran.jovicic@uns.ac.rs, vukman@uns.ac.rs

ACKNOWLEDGEMENT: This paper is part of a research on project "Modern approaches to the development of special bearings in mechanical engineering and medical prosthetics," TR 35025, supported by the Ministry of Education and Science, Republic of Serbia.

Topčić, A., Cerjaković E., Herić, M.

SIMULATION OF RELOADING SEGMENTS OF INTERNAL TRANSPORTATION SYSTEMS BY ARTIFICIAL NEURAL NETWORKS

Abstract: Today on the market there are a number of software solutions which more or lesser fulfil the general requirements related to simulation and modelling of internal transport system, with certain restrictions regarding the implementation of some specific issues that arise within the production systems in daily practice. Therefore, in some cases, it is necessary to find other solutions and approaches for the simulation of the internal transport systems. Thanks to its characteristics Artificial Neural Networks (ANN), supported by other numerical statistical tools, enable the successful simulations of internal transport system and its individual segments, adjusted and implemented for concrete real conditions. In this paper an example of application of Artificial Neural Networks in simulation of three specific reloading segments of internal transport systems installed in various production systems – companies has presented.

Key words: Internal Transportation, Reloading Segments, Stochastic Processes, Simulation, Artificial Neural Networks (ANN)

1. INTRODUCTION

The movement of materials within the production system is the integrating factor in every manufacturing company which by adequate sizing and selection of appropriate transportation/handling devices and equipments provides opportunities for reducing of overall manufacturing costs. Internal transportation system within the company is in essence a network of transportation lines and reloading segments (points for direct linking of different transportation/production processes or phases) whose modelling and simulation is not easy due to high stochastic degree of its internal processes. In principle, if the processes that occur at nodal points perceive in the long term, then the amount of material that can lead to a nodal point (Q_d) must be equal to the amount of material to be brought out of it (Q_o), Fig. 1. Otherwise, depending on the intensity of internal and external factors leads to deviations from the optimal regime of movement of material that slows/stops temporarily (creating queues) or there is a decreasing of utilization of installed transportation and production equipment.

Nodal points of the internal transportation system which, besides connecting of the individual transportation means carry out manipulative tasks of taking on and/or delivery of transportation units, with mandatory subordination to the terms of the transportation, called the reloading segment of the internal transportation systems. The entire process of arriving of transportation units to the reloading place, their acceptance and disposal to the provided space represents a handling process, that depending on its performance can be characterized with various indicators: the number of handling devices, the number of workers who carry out handling processes, speed of handling, queue length, waiting time on handling, duration of handling, number of failures in the handling, etc.

The objective of designing and developing of any kind of internal transportation system is to create a system that meets the desired functions with achieving the highest performance at lowest cost. For design and study of internal transportation systems there are and are developed numerous approaches. It is generally known the fact that modelling and simulation is one of mostly used approaches, which significantly supports decisions making process, based on the results of carried out simulation experiments. The complexity of dynamic internal transportation systems and their segments, as well as, the stochastic nature of the processes inside them, makes the behavioral modeling of these systems by analytical methods impractical and often impossible. This is particularly obvious during analysis of segments of internal transportation system which are consisting from several parallel or serial connected handling devices. Therefore, simulation of internal transportation systems and their segments based on the theory of probability and statistical methods, as well as, artificial neural networks (ANN) is a good alternative for achieving satisfactory results.

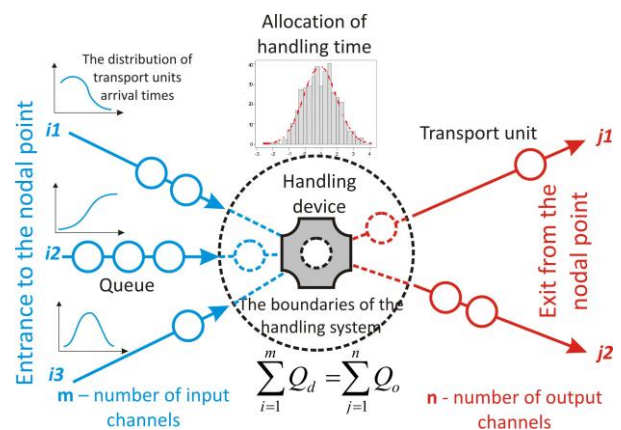


Fig. 1. Processes within nodal point of internal transportation system

2. EKSPERIMENTAL RESEARCH

As a polygon for the simulation study of reloading segments of the internal transportation system the output warehouses in three production systems are adopted: Brewery Tuzla, Salt Factory Tuzla and Detergent Factory Dita Tuzla (Fig. 2) which in essence represents the connection between internal and external transportation. Reloading segments that has studied are characterized by: significant intensity of the flow of materials, transfer of unit loads (pallets), periodic appearance of "impulse loads" on reloading segments, limiting of the available storage space, various external transportation devices for loading, the possibility of involvement of additional reloading equipment (forklifts) once the need arises, and the fact that all three production systems have batch production with a wide assortment of transportation units for manipulation.



Fig. 2. Studied reloading segments of internal transportation systems

For the purposes of the simulation study in all three reloading segments, monitoring of the flow of transportation units - pallets, as well as, determining the real reloading capacity of engaged forklifts for a period of three years has made (Fig. 3). The collected data were statistically processed and prepared for training of artificial neural networks. Data preparation means the execution of a series of simulation experiments based on Monte Carlo algorithm for three possible scenarios (a constant number of reloading units; a constant number of reloading units with subsequent continuous engagement of additional reloading units when a certain critical number of unloaded pallets is reached; a constant number of reloading units with subsequent engagement of additional temporary reloading units when a certain critical number of unloaded pallets is reached), Fig. 4. From all available simulation scenarios for each studied object, scenarios that provide the higher degree of efficiency of reloading units and the ability to arrange shipment of pallets in just-in-time

principles has chosen. By variation of parameters of determinate statistical distribution the following data set was generated: number of intervals and the average length of the interval for primary engaged forklifts, as well as the average number of interval and average interval length of engagement for additional forklifts (Table 1).

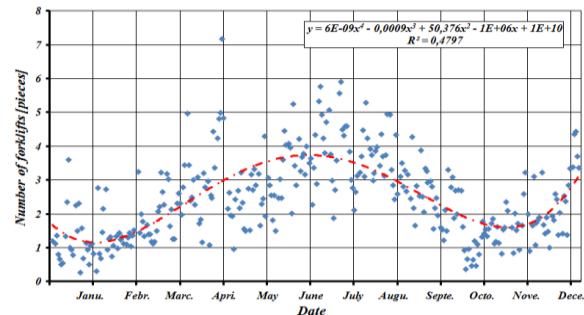


Fig. 3. Annual review of the required number of forklifts on the warehouse of Brewery Tuzla

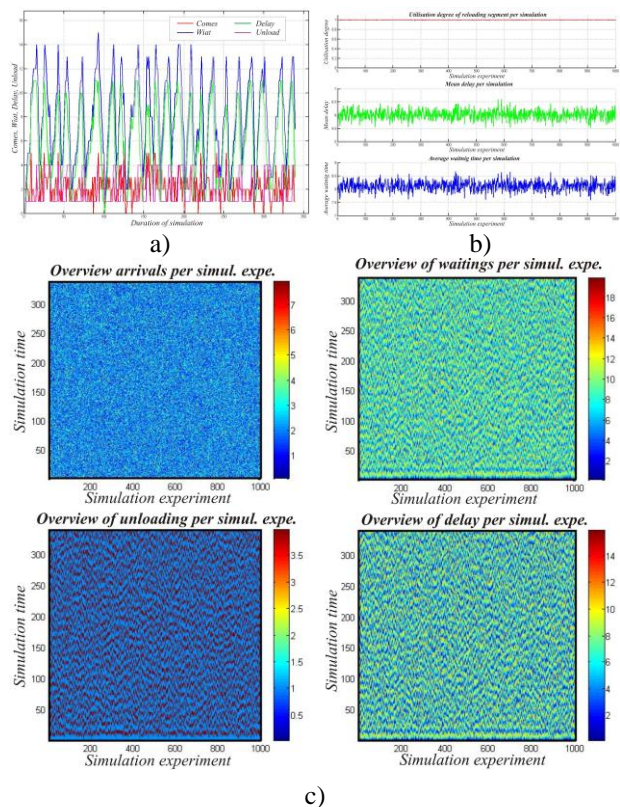


Fig. 4. Review of results for one of Monte Carlo simulation scenarios with one primary engaged and three additional engaged forklifts, and limitations on 1500 pallets in the queue in Salt Factory Tuzla: a) review of number of transportation units (pallets) on reloading segment in phase: comes, waiting, delay, unloading; b) utilisation degree of working place, mean delay, the average waiting time per simulation; c) review of results for 1000 simulation experiments

The obtained results are stored in a database which is essentially a sequence of input-output data sets for training, validation and testing of ANN, classified by

usage of generator for uniformly distributed pseudo-random numbers where 1/2 set was used for training, 1/8 for validation 1/8 for testing– verification of designs for developed artificial neural networks.

	Brewery Tuzla	Salt Factory Tuzla	Dita Tuzla
The interval of the simulation [days]	303	338	258
No. of simulation per experiment	1000	1000	1000
The parameters of the statistical distributions	Gama $\alpha=4,00\div 2,90$ $\beta=0,60\div 1,00$	Weibull $\alpha=1,30\div 1,80$ $\beta=1,60\div 2,40$	Weibull $\alpha=1,55\div 1,30$ $\beta=1,70\div 1,85$
No. constantly engaged forklifts [piece]	1 ÷ 3	1 ÷ 3	1 ÷ 2
No. temporarily engaged forklifts [piece]	1 ÷ 5	1 ÷ 4	1 ÷ 3
Limited number of pallets in queue [piece]	500 ÷ 1300	500 ÷ 2125	210 ÷ 789
Initial data set for training of ANN	Training: 2625 Validation: 657 Test: 657	Training: 2310 Validation: 578 Test: 578	Training: 1250 Validation: 280 Test: 280

Table 1. Plan of parameters variation for identified statistical distribution of the observed reloading segments

According to Alexander and Morton ANN can be defined as massively parallel distributed processors that are good for the memory of experiential knowledge, and they are similar to the human brain in two aspects: knowledge is acquired through the learning process and the connections between neurons are used to store knowledge. These features allow the simulation of any system without an exact knowledge of its mathematical model, as was applied on this case.

By generating a set of series input-output data a sequence of ANN training with variable structure (different number of layers - single and dual layer, and different number of neurons per layers), based on Backpropagation (stands for Back Error Propagation, Figure 5) and Elman's training algorithm, usage of different training functions (Newton training algorithm, Powell-Beale conjugate gradient training algorithm, Levenberg-Marquardt training algorithm, gradient decreasing training algorithm, gradient decreasing adaptive training algorithm, etc.) was carried out.

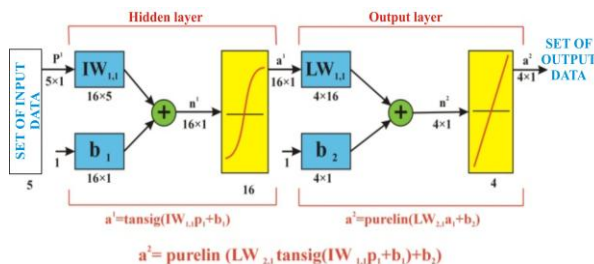


Fig. 5. Schematic review of Backpropagation -BP ANN with two hidden layers of 16 and 8 neurons, and 4 neurons in output layer

In order to improve the generalization of ANN i.e. to prevent overfitting phenomenon by application of early stopping technique - stopping of training process of developed artificial neural network, preprocessing of initial data set was carried out, as follows: scaling of input and output data values, normalisation of averages values and standard deviations of training data sets and reduction of dimension of large input data vectors with redundant components.

After accomplished preparation and preprocessing of input-output data sets, forming of ANN (structures, training algorithms, etc.), and training procedures of ANN were performed. The results of one of the selected scenarios of simulation of work of reloading segments of the internal transportation systems by concrete ANN is presented at Fig. 6.

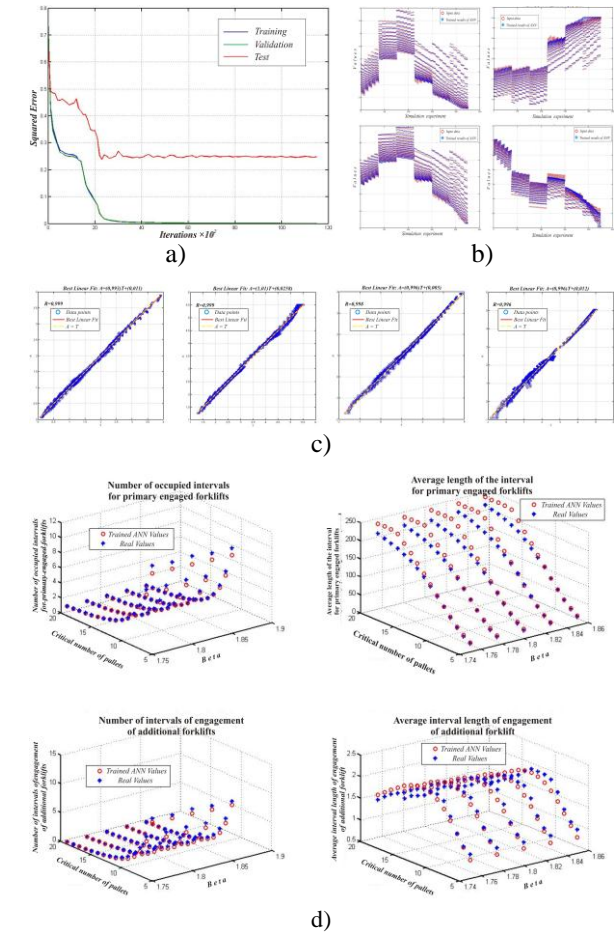


Fig. 6. a) review of accomplished training by BPANN (Powell-Beale conjugate gradient training algorithm with one hidden layer); b) comparison of training results BPANN with targeted values for: the number of occupied intervals for primary engaged forklifts, the average length of the interval for primary engaged forklifts, the number of intervals of engagement of additional forklifts, the average interval length of engagement of additional forklift; c) regression analysis of carried out BPANN training and targeted outcome values; d) results comparison of newly presented vs. test data presented to trained BPANN and targeted output values (for scenario 258-1000-1,35/1,80-2/3-210/798) on reloading segment in Detergent Factory Tuzla

It is important to notice that during training of developed artificial neural networks correlation between the structure and the results achieved in the case of structurally similar ANN with different number of neurons per layers with identical training functions has noted, Fig. 7.

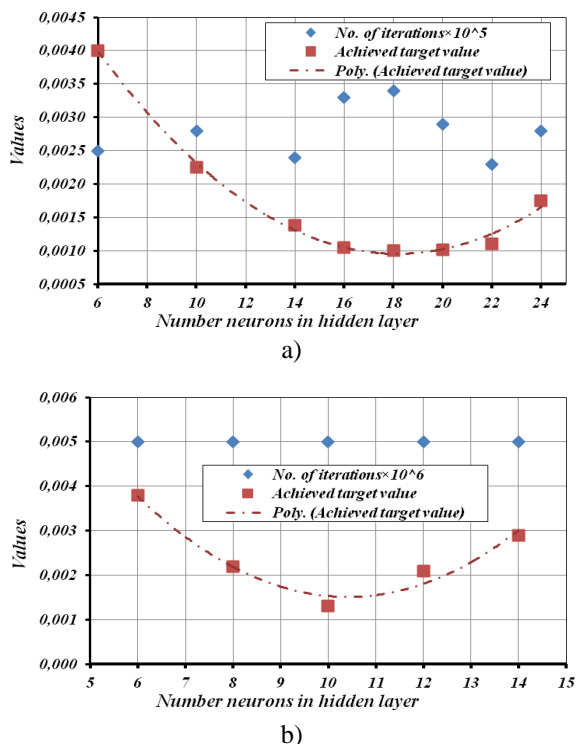


Fig. 7. Review of BPANN structure influence on the results achieved by the learning process in the case of reloading segment of internal transportation system: a) in Salt Factory dd Tuzla accomplished by quasi-Newton's training algorithm with one hidden layer; b) in Detergent Factory Dita Tuzla accomplished by group decreasing gradient training algorithm with one hidden layer

3. CONCLUSION

Application of ANN in simulation of reloading segments of the internal transportation systems allows obtaining results with satisfactory degree of accuracy for all considered scenarios in accordance with established criteria and without generating an exact mathematical model of the studied objects. This approach enabled realization of numerous simulation experiments that provide insights into the required number of forklift trucks at specific time intervals, thus enabling fast loading of transportation units- pallets on hold, with highest possible degree of efficiency of involved forklifts. Of course, faster loading and less waiting time is possible to achieve by involvement of larger number of additionally engaged forklifts, however, the total number of forklifts in any interval is limited by available space at the reloading site.

By analysis of results obtained by the simulation based on usage of ANN, i.e. by comparison of the values of gained targets values with the results

achieved by presentation of new data to trained ANN, certain degree of deviation on the accuracy of the observed parameters was noted (Fig. 6d). The observed degree of deviation is a result of significant scatter of data input/output data sets, as well as, ways of learning of ANN based on the principles of reverse propagation of the mean squared error in the structure of ANN. In this way unequal influence of the mean square error on the input values, corresponding weights and biases has occurred.

In the development of artificial neural networks for purpose of the simulation, the analysis of the structure, architecture and various training techniques impact on the results of training achieved in terms of accuracy, generalization and speed of training was performed. Carried out analysis indicated the existence of dependence between number of neurons in the hidden layer and the architecture of ANN on the achieved results, where is for achievement of satisfactory results in cases with a high degree of dispersion of input/output data a structurally complex artificial neural networks needed to be formed. During the training of considered ANN there are clearly noted the influence of chosen training algorithm on the length of training and on the required amount of memory space, which was absolutely confirmed literature states that treat this issues.

4. REFERENCES

- [1] Šelo, R., Tufekčić, Dž.: *Proizvodni sistemi*, University of Tuzla, Tuzla, 2007.
- [2] Jurković, M., Tufekčić, Dž., Buljan, S., Topčić, A.: *Reengineering of Manufacturing – Improve of achievement competitive capability*, 12th International research/expert conference "Trends in the development of machinery and associated technology - TMT 2008, p.p. 425-428, Istanbul (Turkey), Faculty of Mechanical Engineering Zenica, Mechanica Universitat Politecnica de Catalunya and other., Istanbul, August 2008.
- [3] Topčić, A., Šelo, R., Cerjaković, E.: *Optimisation of reloading segments of internal transportation systems*, Scientific journal Technics, Technologies, Education, Management – TTEM, vol. 5, No. 2 2010, p.p. 259-270, Jun 2010.
- [4] Cerjaković, E., Tufekčić, Dž., Topčić, A., Šelo, R., Čelović Š.: *Stabilisation of production lines by using of simulation study methodology*, International Virtual Journal for science, technics and innovations for industry „Machines Technologies Materials – MTM”, Year IV, Issue 1-2/2010, p.p. 142-145, May 2010.

Authors: Prof. Dr. Alan Topčić, M.Sc. Edin Cerjaković, Muhamed Herić, dipl.ing., University of Tuzla, Faculty of Mechanical Engineering Tuzla, Univerzitetska 4, 75000 Tuzla, Bosnia and Herzegovina, Phone: +387 35 320 944, Fax: +387 35 320 921.

E-mail: alan.topcic@untz.ba
edin.cerjakovic@untz.ba
m.heric@fclukavac.ba

Vuković, N., Miljković, Z., Mitić, M., Babić, B., Lazarević, I.

AUTONOMOUS NAVIGATION OF AUTOMATED GUIDED VEHICLE USING MONOCULAR CAMERA

Abstract: This paper presents a hybrid control algorithm for Automated Guided Vehicle (AGV) consisting of two independent control loops: Position Based Control (PBC) for global navigation within manufacturing environment and Image Based Visual Servoing (IBVS) for fine motions needed for accurate steering towards loading/unloading point. The proposed hybrid control separates the initial transportation task into global navigation towards the goal point, and fine motion from the goal point to the loading/unloading point. In this manner, the need for artificial landmarks or accurate map of the environment is bypassed. Initial experimental results show the usefulness of the proposed approach.

Key words: Automated Guided Vehicle, Image based visual servoing, Epipolar geometry, Monocular SLAM, neural extended Kalman Filter

1. INTRODUCTION

Material Handling System (MHS) represents an automated transport of materials, goods and parts between different locations within manufacturing or industrial facility. Solutions for MHS are based on conveyer belts, powered and non-powered industrial trucks and Automated Guided Vehicles (AGVs). AGV based internal transport relies on infrastructure of the working environment because conventional AGVs need a special kind of guidance system to operate. The guidance system uses wires in the floor for receiving the information from the central control unit. However, recent developments in technology impose a new generation of AGVs that are able to autonomously operate in the working environment. The modern AGV based transport solutions rarely use cameras for acquisition of relevant information from the working environment. Recent advances in computer vision provide a good starting point for integration of camera within modern AGVs. Cameras are cheap, reliable and able to provide a huge amount of spatial information. Furthermore, information extracted from the camera can be used for visual servoing, state estimation, obstacle avoidance and path planning. Therefore, we believe that the next generation of industrial transport solutions based on AGVs should include the camera as one of the sensors for autonomous operation in manufacturing and industrial environments [1].

The motivation for this research are the recent advances in visual SLAM [2] and visual servoing [3], as well as the present state in the field of AGV based industrial transport [4,5,6,7,8]. In this paper we propose a new hybrid control approach that switches between two control loops. The first loop is used when the robot (AGV) is far away from the desired pose (Position Based Control - PBC). By selecting optimal control vector robot decreases the norm between the desired pose and the current pose and moves towards the goal. The second control loop uses Image Based Visual

Servoing (IBVS) in terms of epipolar geometry for generating the controls that should steer the robot towards loading/unloading point. Furthermore, the state estimation of the robot pose is determined in terms of monocular SLAM, via Neural Extended Kalman Filter (NEKF) [9] - Extended Kalman Filter (EKF) coupled with feedforward neural network [10]. NEKF is used to estimate the position and orientation of the vehicle and model unknown disturbances during motion. Compared to standard EKF, NEKF is known to be a better state estimator in terms of accuracy due to its ability to model unknown disturbances.

In this paper the camera is used as the main exteroceptive sensor in twofold ways. Firstly, it acquires information needed for the update step of the visual SLAM within NEKF estimation framework and secondly, it is used for visual servoing when the robot reaches the target pose in the vicinity of the loading/unloading point.

2. THE HYBRID CONTROL APPROACH

Schematic representation of proposed approach is shown in Fig. 1. The PBC loop enables the robot to approach to the desired goal pose when the robot is located far away from the loading/unloading point. It requires only two parameters to store (desired position and desired orientation). The robot moves to a predefined desired pose by decreasing the error between current pose and desired pose using rotation and translation motion sequences; PBC gives the robot accurate information on how much to rotate and/or move translatory. When the robot reaches the desired pose the control is switched to the other control module, which drives a nonholonomic vehicle using image data. Image based scheme used in this paper is the one based on epipolar geometry and it is known as teach-by-showing visual servoing.

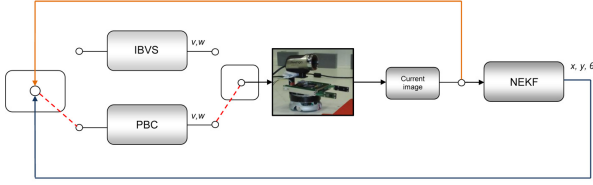


Fig. 1. A block diagram of the hybrid control. Diagram shows two loops: Position Based Control and Image Based Visual Servoing loop.

Teach-by-showing visual servoing relates to the robot control where desired motion is achieved by zeroing the error control vector between the image features from current view and the features in an image taken previously at the desired pose. When the robot finishes incremental motion, it takes the snapshot in the current pose. If the IBVS module is active, that image is used for matching detected features with the one calculated from pre-recorded target image. The same image is used for update of joint state vector of the robot by using NEKF. In the case of PBC, the image is used only for the NEKF for update step. As shown in the Fig. 1, feedback of the NEKF estimation is sent to PBC but the NEKF constantly estimates the robot pose, regardless of which control loop is active.

2.1 Epipole-based visual servoing

Epipolar control law used in this paper is the one presented in [3]. The navigation of the vehicle can be performed by using a feedback control law with the control inputs defined as coordinates of the epipoles. The visual servoing is next transformed into a tracking problem in a nonlinear system, where the reference trajectories of the epipoles are defined. After derivation of the current and target epipoles, we have:

$$\dot{\mathcal{E}}_{cx} = -\frac{t d_x \sin(m-y)}{d \cos^2(m-y)} v + \frac{t d_x}{\cos^2(m-y)} w \quad (1)$$

$$\dot{\mathcal{E}}_{tx} = -\frac{t d_x \sin(m-y)}{d \cos^2(y)} v \quad (2)$$

where t represents focal length of camera, d_x and d_y are the number of pixels per unit distance, and d is the distance between the current and target camera. These equations give the relationship between the input system vector, v and w , and the differentiated output of the system, $\dot{\mathcal{E}}_{cx}$ and $\dot{\mathcal{E}}_{tx}$. To obtain the control input to the robot, a tracking error vector of the current and target epipoles is first introduced. This vector primarily must be multiplied by control gain matrix and then deducted from differentiated desired epipoles. The new epipolar-based control input is defined as

$$\mathbf{v}_e = \begin{bmatrix} \dot{\mathcal{E}}_{e1} \\ \dot{\mathcal{E}}_{e2} \end{bmatrix} = \begin{bmatrix} \dot{\mathcal{E}}_{cx} \\ \dot{\mathcal{E}}_{tx} \end{bmatrix} - \mathbf{K}_f \begin{bmatrix} \dot{\mathcal{E}}_{cx} - e_{cx}^d \\ \dot{\mathcal{E}}_{tx} - e_{tx}^d \end{bmatrix} \quad (3)$$

where $\mathbf{K}_f = \begin{bmatrix} k_c & 0 \\ 0 & k_t \end{bmatrix}$ is the gain matrix, and

$k_c > 0$ and $k_t > 0$. Finally, the control input to the vehicle system $[v, w]$ is calculated as a product of the inverse control matrix and the epipolar-based control input \mathbf{v}_e . For further details refer to [1,3].

2.2 Neural Extended Kalman Filter for monocular SLAM

NEKF is a recursive state estimator that combines two steps in estimation: prediction and update. In the prediction step of NEKF the state vector and the state covariance are propagated using standard state propagation equations.

$$\hat{\mathbf{x}}_{k|k-1} = \begin{bmatrix} \hat{\mathbf{x}}_{v(k|k-1)} \\ \hat{\mathbf{x}}_{w(k|k-1)} \\ \hat{\mathbf{x}}_{m(k|k-1)} \end{bmatrix} = \begin{bmatrix} \hat{\mathbf{x}}_{v(k-1|k-1)} \\ \hat{\mathbf{x}}_{w(k-1|k-1)} \\ \hat{\mathbf{x}}_{m(k-1|k-1)} \end{bmatrix} + \begin{bmatrix} \mathbf{f}_M(\mathbf{x}) \\ \mathbf{x}_{vNET} \\ \mathbf{0} \end{bmatrix} \quad (4)$$

$\mathbf{f}_M(\mathbf{x})$ stands for theoretical motion model, $\mathbf{x}_{vNET} = \mathbf{g}(\hat{\mathbf{x}}_{v(k-1|k-1)}, \hat{\mathbf{x}}_{w(k-1|k-1)}, \mathbf{u}_{k|k-1})$ is network output, $\hat{\mathbf{x}}_{v(k-1|k-1)}$ is an estimate of the robot state at $k-1$, and $\mathbf{u}_{k|k-1}$ is the control vector that initiates motion of the robot from state $k-1$ to state k . The main difference between NEKF and EKF SLAM in the first step can be seen in the state prediction where the output of neural network $\mathbf{g}(\mathbf{x})$ is introduced. As in standard EKF, update step is then performed in the same manner:

$$\begin{aligned} \mathbf{S}_k &= \mathbf{H}_k \Sigma_{k|k-1} \mathbf{H}_k^T + \mathbf{R}_k \\ \mathbf{K}_k &= \Sigma_{k|k-1} \mathbf{H}_k^T \mathbf{S}_k^{-1} \end{aligned} \quad (5)$$

$$\hat{\mathbf{x}}_{k|k} = \hat{\mathbf{x}}_{k|k-1} + \mathbf{K}_k (\mathbf{z}_k - \hat{\mathbf{z}}_k)$$

$$\Sigma_{k|k} = (\mathbf{I} - \mathbf{K}_k \mathbf{H}_k) \Sigma_{k|k-1}$$

$\hat{\mathbf{x}}_{k|k-1}$ and $\Sigma_{k|k-1}$ are predicted joint state vector and its covariance; \mathbf{H}_k is the Jacobian of the measurement model; \mathbf{S}_k is the innovation covariance, \mathbf{R}_k is the measurement covariance matrix and \mathbf{K}_k is the filter gain. $\hat{\mathbf{x}}_{k|k}$ and $\Sigma_{k|k}$ represent the updated values of the joint state vector and its covariance.

3. EXPERIMENTAL RESULTS

Experiments were conducted in a laboratory model of a manufacturing environment with Khepera II mobile robot and the simple web camera on top of it. Proposed hybrid control algorithm is implemented in Matlab environment which is used to control the robot as well (Fig. 2). A desktop computer (AMD Athlon on 2.20 GHz; 1 MB of RAM) was used as a central control unit achieving communication via standard RS232 cable with the robot and via USB cable with the camera. We adopted 0.003 [m] to be increment of translation motion and $3[^\circ]$ to be increment for rotation

for position based control. Incremental motions for translation and rotation are different in IBVS loop and depend on calculated translation and rotation velocities. After robot finishes with incremental motion, it takes a snapshot of the environment (320x240 resolution).

For the NEKF setup we followed Civera et al. [2]. At each step there are ~50 features on the image. At each pass, the filter searches and adds three features. Due to change in lighting intensity number of successfully matched features varies over time. Features are frequently deleted, so the dimension of the NEKF joint state vector tends to be ~300 (neural network weights are counted as well). Experiments were conducted with one processing unit in the hidden layer.

To reduce the effects of lighting the experiments were performed in the controlled environment with artificial light. On average, it takes 250-270 steps/frames for the entire path but the actual number depends on various factors such as intensity of lighting (heavily influences the performance of image feature detectors), errors in the robot control subsystem, etc. We tried to eliminate these influences as much as possible.

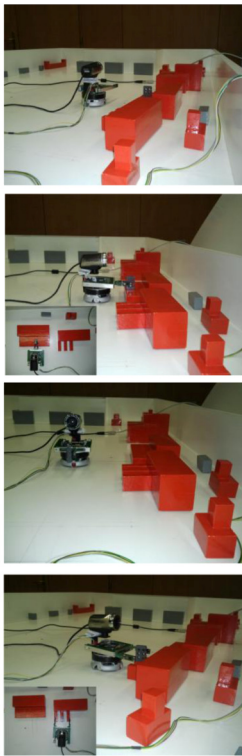


Fig. 2. Robot motion during the experiment

For the IBVS setup, approach presented in [3] is followed. The feature matches on current and target images are obtained using salient robust image interest point detector and descriptor. In our setup, the matches between two images include mismatches so an iterative mathematical method is employed in order to estimate parameters of a mathematical model from a set of observed data which contains outliers. One iteration of the IBVS robot motion (i.e. IBVS control loop) runs at

approximately 0.125 [Hz] which is slow, but even in this case the satisfactory results are obtained.

At the very beginning of the test run, the robot is not able to see the first target image because it is not in camera's field of view. Therefore, the first robot motion is conducted according to position based control, in order to put the first target image in the field of view. When robot achieves desired orientation, the second motion sequence based on IBVS is triggered and performed according to the previously recorded target image. Therefore, the robot is supposed to perform position based control two times and two times visual servoing based on epipolar geometry. The initial position and orientation of the robot define the world frame.

In Fig. 3a the entire robot path as estimated using NEKF is presented. Fig. 3b gives the robot orientation during the experimental run. Fig. 3c shows the forward robot motion from the starting pose towards the loading point and backward robot motion after the object the picked. Experimental results show that the vehicle is able to approach loading/unloading point, pick up the object, and transport it to another location (Fig. 2).

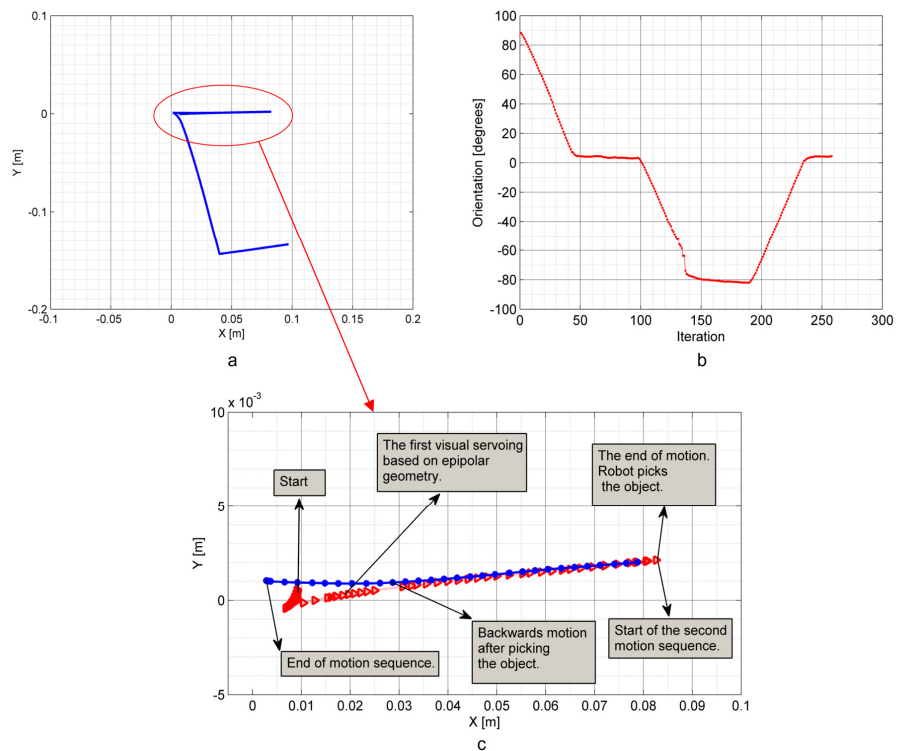


Fig. 3. a) Entire path as estimated by NEKF, b) Evolution of the robot orientation in each experimental control iteration c) Description of the first robot motion step

4. FUTURE WORK AND CONCLUSION

In this paper we have proposed the usage of onboard camera as sensor for autonomous operation of AGVs on the shop floor. The camera is used for visual servoing based on epipolar geometry and for monocular SLAM for localization of the robot in the environment. The new hybrid control approach for intelligent operation of AGVs uses two distinct control loops: the position based control and image based

visual servoing. To operate in the working environment the mobile robot needs to know the target pose and the target image. The target pose is used for global navigation of the robot; when the target pose is reached, the target image is used within second control loop to define controls for fine motions that steer the robot towards loading/unloading point according to calculated velocities. This approach provides the mobile robot with the ability to separate initial control problem into two decoupled blocks. The target pose and the target image are the only parameters needed for autonomous navigation within industrial facility. The important advantage of this approach is that it does not need the accurate map of the environment, but rather the set of target poses (in front of the loading/unloading points) and the set of the target images (to be used for servoing toward loading/unloading points). By applying this approach the mobile robot does not need additional modules for solving the field of view problem. Simultaneously to hybrid control, the mobile robot estimates its pose with neural extended Kalman filter - NEKF. The implementation of NEKF is achieved in terms of the monocular SLAM problem. Multi-layer perceptron neural network is coupled with EKF to improve the state transition model. The main advantage of NEKF is the ability of the neural network to learn a model of the system on-line.

The future work could be extended in several directions. Firstly, the hybrid control can be improved with Reinforcement Learning (RL) as an attempt to exploit previous knowledge gathered in experimental processes to learn the optimal paths. Also, approaches other than epipolar visual servoing should be tested (i.e. traditional IBVS schemes). Secondly, the NEKF's structure allows usage of Gaussian filters (Unscented Kalman Filter or Extended Information Filter) and different types of feedforward neural networks (RBF for instance). Thirdly, our implementation runs on Matlab and desktop PC. To achieve real time performance of 30 [Hz] additional hardware is necessary. Finally, through experiments with the mobile robot and simple camera, we have showed that this approach can be applied but we are eager to assess the final outcome of its implementation in the real manufacturing environment.

5. ACKNOWLEDGMENT

This work is supported by the Serbian Government - the Ministry of Education and Science-Project title: *An innovative, ecologically based approach to the implementation of intelligent manufacturing systems for the production of sheet metal parts (2011-2014)* under grant TR35004.

6. REFERENCES

- [1] Miljković, Z., Vuković, N., Mitić, M., Babić, B.: *New Hybrid Vision-Based Control Approach for Automated Guided Vehicles*, International Journal of Advanced Manufacturing Technology, Article in press DOI: 10.1007/s00170-012-4321-y (Online First Articles - July 2012).
- [2] Civera, J., Grasa. O., Davison, A., Montiel, J.: *I-point RANSAC for EKF filtering. Application to real-time structure from motion and visual odometry*, Journal of Field Robotics, Vol. 27 (5), p.p. 609–631, 2010.
- [3] López-Nicolás, G., Guerrero, J., Sagüés, C.: *Visual control of vehicles using two-view geometry*, Mechatronics, Vol. 20(2), p.p. 315-325, 2010.
- [4] Kelly, A., Nagy, B., Stager, D., Unnikrishnan, R.: *An infrastructure-free automated guided vehicle based on computer vision*, IEEE Transactions on Robotic and Automation, Vol. 14(3), p.p. 24–34, 2007.
- [5] Martínez-Barbera, H., Herrero-Perez, D.: *Autonomous navigation of an automated guided vehicle in industrial environments*, Robotic and Computer Integrated Manufacturing, Vol. 26(4), p.p. 296–311, 2010.
- [6] Pradalier, C., Tews, A., Roberts, J.: *Vision-based operations of a large industrial vehicle - autonomous hot metal carrier*, Journal of Field Robotics, Vol. 25(4-5), p.p. 243–267, 2008.
- [7] Ronzoni, D., Olmi, R., Secchi, C., Fantuzzi, C.: *AGV global localization using indistinguishable artificial landmarks*, Proceedings of IEEE International Conference on Robotics and Automation, China, IEEE, p.p.287-292 Shanghai, 9-13 May 2011.
- [8] Seelinger, M., Yoder, J.: *Automatic visual guidance of a forklift engaging a pallet*, Robotics and Autonomous Systems, Vol. 54, p.p. 1026–1038, 2006.
- [9] Kramer, K., Stubberud, S.: *Tracking of multiple target types with a single neural extended Kalman filter*, International Journal of Intelligent Systems, Vol. 25, p.p. 440-459, 2010.
- [10] Miljković, Z., Aleksendrić, D.: *Artificial neural networks—solved examples with theoretical background* (In Serbian). University of Belgrade-Faculty of Mechanical Engineering, Belgrade, 2009.

Authors: M.Sc. Najdan Vuković, University of Belgrade - Faculty of Mechanical Engineering Innovation Center, Kraljice Marije 16, 11120 Belgrade 35, Phone.: +381 11 3302 468, Fax: +381 11 3302 274.
Prof. Dr. Zoran Miljković, M.Sc. Marko Mitić, Prof. Dr. Bojan Babić University of Belgrade - Faculty of Mechanical Engineering, Production Engineering Department, Kraljice Marije 16, 11120 Belgrade 35, Phone.: +381 11 3302 468, Fax: +381 11 3302 274,
M.Sc. Ivan Lazarević, “Ecolab Hygiene”, Milana Tankosića 8, 11000 Belgrade, Serbia
 E-mail: nvukovic@mas.bg.ac.rs
zmljkovic@mas.bg.ac.rs
mmitic@mas.bg.ac.rs
bbabic@mas.bg.ac.rs
ivan.lazarevic@ecolab.com

Zadnik, Ž., Karakašić, M., Čok, V., Kljajin, M., Duhovnik, J.

IMPLEMENTATION MATRIX OF FUNCTION AND FUNCTIONALITY IN PRODUCT DEVELOPMENT PROCESS

Abstract: This paper presents a short overview of Matrix of Function and Functionality (MFF), which helps designer in early phases of product development. Matrix is presented as a tool inside conceptual phase, where details of a product are not known or are sporadically presented. Matrix is based on mathematical rules and brings into relation functions and functionalities. By means of sub-matrix structures, MFF solves the defined product requirements. MFF also stores design knowledge that provides better understanding of the design process. In addition, the design of modular systems by the developed model of modularity with regard to function and shape is presented.

Key words: Product Development, Conceptual Design, Matrix of Function and Functionality, Function, Functionality, Modularity

1. INTRODUCTION

Market requirements are the basis for defining basic functional requirements, which in turn represent the initial information on a new potential product [1]. At the beginning of the design process, functional requirements are usually unarranged, incomplete and sporadically presented, which makes them necessary to be arranged, complemented and expanded. By means of structural enlargement of functions, product structure can be presented as a functional structure, which is at the same time the basis for defining the shape (physical structure) of the product [2].

With the purpose of solving technical problems different methods were developed [3]. Among these methods is the morphological technique by Zwicky [4], which is concerned with the intrinsic structural characteristics of the formation and content of the thought process. In [5, 6] matrix models were presented, which enable the generation of a functional structure of the product, described in matrices. The background of most matrix models is represented by morphological box [4], which forms the basis for further development.

To generate the product's shape structures, important philosophies of engineering of technical functions must be considered. In [7], the authors describe the functions by defining the terminology that is related to the names of the functions, while others describe the functions of technical systems by means of physical laws [8]. With a view to unique identification, rules were defined [5], by means of which the functions, functionalities and products are described.

Today's market requires ever shorter development times for new products, which triggers the need for a modular architecture of products. Such a modular architecture makes it possible to combine one or several functions in the functional structure with one element that solves them [9]. Such an approach has several advantages, the main one being an increased number of product variants [10]. Erixon [11] developed

the Modular Function Deployment method, using the Module Indication Matrix. The established rules [12] also include modularity rules in terms of the function and modularity with regard to the shape.

2. MATRIX OF FUNCTION AND FUNCTIONALITY

2.1 The MFF concept

MFF matrix is a descriptive matrix developed on the basis of morphological matrix [4] and the matrix model described in [13]. It is built and defined on the basis of a mathematical model and pre-set rules [5], not just on the basis of design intuition. It can be devised if key elements are known, such as initial functional requirements and functionalities. Functional requests are derived from market requirements and represent the most important attributes of the requested system – functions, while functionalities are represented by technical systems [14] or shape models that in part or in whole fulfill the required functions.

Within the MFF, functional requirements are introduced into relation on one side, and functionalities on the other, as shown in Figure 1. The functional requirements represent the basic functions, while the functionalities are represented via technical systems. The functions and functional requirement are generally marked with F_i and are located in the first column, while individual technical systems (functionalities) are marked with TS_j and are located in the subsequent columns.

The MFF vision is that solving the matrix should gradually lead to defining more and more information for a particular functional requirement or function, and that it is solved at the end of the process with a suitable functionality. With a view to fulfilling the function, the differences between particular variants are arranged and the modularity is built.

The links between the functions and the functionalities are created by means of the so-called sub-matrices. These sub-matrices are colored and

highlighted in grey (Figure 1). As a rule, sub-matrices are not logically distributed at the beginning as their internal distribution is determined by how the design process develops and by the presupposed number of functions and functionalities. Parts of the matrix significantly deviating from the main diagonal are usually evidence that the determined function does not have an accurate basis, that it is specifically oriented and cannot be directly applied in a particular variant. The key feature of the MFF is its arranging ability and the modularity of the sub-matrices, which makes it possible to arrange and sort the whole matrix during the design process.

Sub-matrices involving at least one possible solution on at least one function within the presupposed building block or functionality are full and display a partial and complete result for this sub-matrix, while the unsolved sub-matrices are not displayed. The result is displayed in the form of percentage values – numbers in a sub-matrix cell [15].

The MFF model also includes an automatic suggestion for the end solution – the suggested solution in Figure 1 in each row of the first column. It is presupposed that a possible solution is the one that most closely corresponds to the given functional requirement. The end solution is selected on the basis of individual percentage values, solutions' values, making the end solution the one with the highest calculated percentage value.

FUNCTIONAL REQUIREMENTS	FUNCTIONALITIES/SOLUTIONS						
	TS ₁	TS ₂	TS ₃	...	TS _j	...	TS _m
Functional requirement – F ₁ ↓ [Suggested solution R ₁]	X% ↓ + X% ↓				X% ↓ + X% ↓		
Functional requirement – F ₂ ↑↓ [Suggested solution R ₂]		X% ↓ + X% ↓ + X% ↓					X% ↓ + X% ↓
Functional requirement – F ₃ ↑↓ [Suggested solution R ₃]							
⋮ ↑↓							
Functional requirement – F _i ↑↓ [Suggested solution R _i]					X% ↓ + X% ↓ + X% ↓		
⋮ ↑↓							
Functional requirement – F _n ↑ [Suggested solution R _n]		X% ↓ + X% ↓ + X% ↓					X%

Fig. 1. Modularity model of the matrix of functions and functionality.

2.2 Modularity with regard to function and shape

Modularity with regard to shape is referred to as the appearance of a product in one or more variants (versions). According to the shape-modularity principle [15], products can be pooled into modular assemblies. They are checked in terms of the number of their functions that fulfill individual product variants. In the case that a product variant includes all the functions of another variant, as well as the functions that other variants do not possess, that variant can replace the other one (Table 1).

FUNCTION	FUNCTIONALITY			
	Variant 1	Variant 2	Variant 3	Variant 4
Function 1	X	X	X	X
Function 2	X	X	X	X
Function 3	X	X	X	
Function 4	X	X		
Function 5		X		
Function 6				

Table 1. Modularity with regard to shape.

Within the functional structure, more than one product can have identical or similar functions for performing the same or similar process. For such cases it is necessary to check the technical system overload by introducing modularity with regard to function. The modularity function consequently pools the functions for the larger number of variants (Table 2).

FUNCTION	FUNCTIONALITY			
	Variant 1	Variant 2	Variant 3	Variant 4
Function 1		X	X	X
Function 2	X	X	X	X
Function 3	X	X	X	
Function 4	X		X	X
Function 5		X	X	
Function 6				

Table 2. Modularity with regard to function.

2.3 Functional and matrix structure

Matrix structure is composed of the MFF matrices. The matrices are organized by levels and interconnected by binding links for linking towards matrices at the same level and towards matrices at other levels [6]. For matrix structure generation it is necessary to establish rough functional structure. This is input in MFF [16].

Based on rough functional structure and by means of MFF, designers search solutions and determine exactly certain functionalities. In this way the rough functional structure is completed and stored as a detail functional structure [16].

Matrix structure for a listed product is generated from the product detailed functional structure [16]. The detailed functional structure is a starting point for the generation of the product matrix structure. The total number of matrix structure levels corresponds by analogy to the total number of levels of the product's detailed functional structure. In the matrix and functional structure is stored the design knowledge for the listed product.

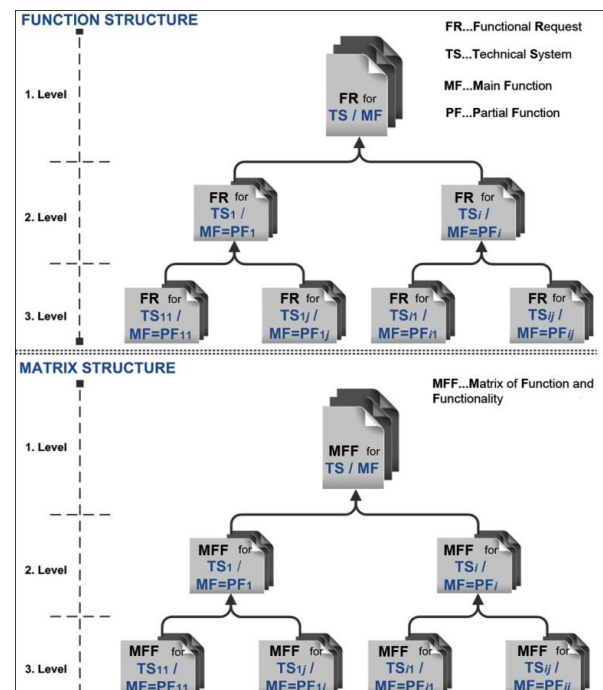


Fig. 2. Functional and matrix structure of product [16]

3. FIGURES

The modularity concept has been included and implemented into the developed Web database management system / application. The MFF model is currently presented and implemented on more than twenty completely different, solved and described products from diverse design areas.

In this paper implementation of modularity is presented on a developed product named *Active Lounge Chair 1 – ALC 1* (Figure 3). The goal of the presented implementation is not to demonstrate the complete *ALC 1*, but to show important aspects of modularity on different assembly parts of the chair.



Fig. 3. Active Lounge Chair 1 – ALC 1.

Generate Update Refresh Truncate Close									
MATRIX FOR [LEVEL 1]: ACTIVE LOUNGE CHAIR 1 SITTING AND RESTING									
Function/ality	Stool	Fixed armchair	3D gel	Variable armchair	Active Lounge Chair 1	Back	Exercise mechanism	Rotating pedestal	
sitting and resting [12 solutions Suggested: holding force]	M 100	M 100 ↓ ↑ S 33	A 100	M 83 ↓ ↑ S 33	M 83 ↓ ↑ S 33	M 100	A 33 ↓ ↑ M 33	S 33	
hand rest [9 solutions Suggested: hand rest]	M 50	S 100 ↓ ↑ M 50	A 50	S 100 ↓ ↑ M 50	S 100 ↓ ↑ M 50	M 50			
possibility of vertical arm movement [11 solutions Suggested: possibility of vertica...]		A 100	M 20	A 100 ↓ ↑ A 60	A 100 ↓ ↑ A 100 ↓ ↑ S 40	S 20	M 60	B 20 ↓ ↑ M 20	
possibility of vertical arm movement independently of lower chair part [11 solutions Suggested: possibility of vertica...]		A 60	M 10	A 100 ↓ ↑ A 30	A 100 ↓ ↑ A 60 ↓ ↑ S 30	S 10	M 35	B 10 ↓ ↑ M 10	
bending [2 solutions Suggested: alleviation possibil...]			M 100			S 100			
possibility of exercising [9 solutions Suggested: possibility of exercis...]		A 67	M 33	A 67	S 100 ↓ ↑ A 67 ↓ ↑ A 67	S 67	M 67 ↓ ↑ S 33		
incline [1 solution Suggested: bending]						S 100			
height adjustment [1 solution Suggested: height adjustment]						A 50			
space movement [8 solutions Suggested: space movement]		A 50		A 50 ↓ ↑ A 50	A 50 ↓ ↑ A 50		M 50	M 100 ↓ ↑ B 50	

Fig. 4. MFF modularity implementation view on the example of ALC 1.

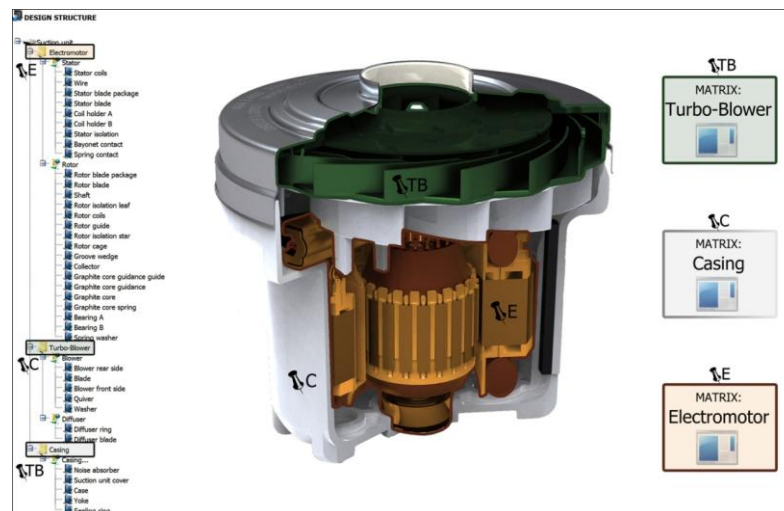


Fig. 5. Suction unit design structure.

The basic functions of *ALC 1* are *sitting, resting and exercising*. The key components of the *ALC 1* are: *the sitting part, the leg/foot rest, the arm/hand rest, the upper body rest, and the hand and leg exercise mechanism*, where each one of the components allows and fulfills a precisely defined function.

The MFF in figure 4 represents the real MFF modularity design view of *ALC 1* design. The matrix involves several possible solutions, cross-corresponding to several functions.

The *ALC 1* modularity development resulted also in assembly optimization, where we managed to reduce

the number of required parts. This reduction was achieved through MFF sub-matrices and function structures, where we discovered some superfluous overlapping functions and parameters. Those functions and parameters were combined, removed, merged and modularly modified. Detail representation of *ALC I* modularity is described in [15].

Figure 5 illustrates the physical structure of the suction unit. The structure is generated from the previously designed matrix structure of the suction unit. The suction unit consists of three levels of matrix structure [6]. Detail representation of Suction unit functional and matrix structure is described in [6].

4. CONCLUSION

The mission of the developed models is to contribute to, and find within the initial design processes, the appropriate fundamentals for better and faster design development. Modularity within the MFF is based on the mutual relation between the function and functionality, which represents the data definition.

The MFF upgrades and updates the deficiencies of the morphological matrix through the application of a mathematically, not intuitionally, based model for creating links between the function and functionality. The MFF and MFF modularity model allow concurrent solving of several open functional requirements, which recognizes requirements for productivity, clear recognition of generators, binders and information users, and reduction of design and development times. Modular solving of functional requirements is widespread also in the areas of self-assessment, auto-solving or automated suggesting of solutions and the possibility of using modularity of individual sub-matrices.

The possibility of functional structure generation, stored in matrix structure, enables full review of data to designer. These data describe the product and present the design knowledge stored in MFF. By the MFF it is possible to use these data for a new product design.

5. REFERENCES

[1] Kušar, J., Duhovnik, J., Tomažević, R., Starbek, M.: *Finding and Evaluating Customers Needs in the Product-Development Process*, Strojniški vestnik, 53, 2, p.p. 78-104, 2007.

[2] Kurtoglu, T.: *A Computational Approach to Innovative Conceptual Design*, PhD Thesis, The University of Texas at Austin, Austin, 2007.

[3] Hales, C., Wallace, K.: *Design research reflections – 30 years on*, International Conference on Engineering Design, ICED 11, København, 2011.

[4] Zwicky, F.: *The morphological method of analysis and construction*, Courant, New York: Intersciences, 1948.

[5] Zadnik, Ž., Karakašić, M., Kljajin, M., Duhovnik, J.: *Functional and Functionality in the Conceptual Design process*, Strojniški vestnik, 55, 7-8, p.p. 455-471, 2009.

[6] Karakašić, M., Zadnik, Ž., Kljajin, M., Duhovnik, J.: *Functional structure generation within multi-*

structured matrix forms, Tehničkivjesnik / Technical Gazette, 17, 4, p.p.465-473, 2010.

[7] Hirtz, J., Stone, R.B., McAdams, D.A., Szykman, S., Wood, K.L.: *A Functional Basis for Engineering Design: Reconciling and Evolving Previous Efforts*, NIST Technical Note 1447, Department of Commerce United States of America, National Institute of Standards and Technology, 2002.

[8] Žavbi, R., Duhovnik, J.: *Conceptual design chains with basic schematics based on an algorithm of conceptual design*, Journal of Engineering Design. 12, 2, p.p. 131-145, 2001.

[9] Pavlič, D.: *Sustav za konfiguriranje proizvoda modularne arhitekture*, magistarski rad, Fakultet strojarstva i brodogradnje u Zagrebu, Zagreb, 2003.

[10] O'Grady, P., Liang, W.Y., Tseng, T.L., Huang, C.C., Kusiak, A.: *Remote Collaborative Design With Modules*, Technical Report 97-0, University of Iowa, Iowa, 1997.

[11] Erixon, G.: *Modular Function Deployment-A Method for Product Modularisation*, PhD Thesis, Department of Manufacturing Systems, The Royal Institute of Technology, Stockholm, 1998.

[12] Pahl, G., Beitz, W.: *Engineering Design – A Systematic Approach*, Second Edition, Springer-Verlag, London, 1996.

[13] Duhovnik, J., Tavčar, J.: *Product Design Test using the Matrix of Functions and Functionality*, In Proceedings of AEDS 2005 Workshop, Pilsen, 2005.

[14] Hubka, V., Eder, W.E.: *Theory of Technical Systems*, Springer-Verlag Berlin, Heidelberg, 1988.

[15] Zadnik, Ž., Čok, V., Karakašić, M., Kljajin, M., Duhovnik, J.: *Modularity within a Matrix of Function and Functionality (MFF)*, Proceedings of the 18th International Conference on Engineering Design (ICED 11), Copenhagen: The Design Society and Technical University of Denmark (DTU), 2011.

[16] Zadnik, Ž.: *Matrika funkcij in funkcionalnosti izdelka v razvojno konstrukcijskem procesu*, Doktorsko delo, Fakulteta za strojništvo, Ljubljana, 2012.

Authors: Žiga Zadnik¹, PhD ME; Mirko Karakašić², assistant professor; Vanja Čok¹, BSc; Milan Kljajin², full time professor; Jože Duhovnik¹, full time professor

¹ University of Ljubljana, Faculty of Mechanical Engineering, Aškerčeva 6, 1000 Ljubljana, Slovenia, Phone: +386 1 4771 740, Fax: +386 1 4771 156.

² J. J. Strossmayer University of Osijek, Mechanical Engineering Faculty in Slavonski Brod, Trg I. B. Mažuranić 2, 35000 Slavonski Brod, Croatia, Phone: +385 35 446 188, Fax: +385 35 446 446.

E-mail: ziga.zadnik@lecad.uni-lj.si
mirko.karakasic@sfsb.hr
vanja.cok@lecad.uni-lj.si
milan.kljajin@sfsb.hr
joze.duhovnik@lecad.uni-lj.si

Zeljковиć, M., Živković, A., Blanuša, V.

**THERMAL-ELASTIC BEHAVIOR OF A MAIN SPINDLE ASSEMBLY
WITH DOUBLE ROW CYLINDRICAL ROLLER BEARINGS**

Abstract: In this paper presents the results of computer modeling thermal-elastic behavior of spindle assembly bearing double row cylindrical roller and ball bearings with angular contact in front support. For computer modeling thermal behavior and defining the displacement and deformation under the effect of heat load was applied finite element method. Analyzed the arrangement temperature field and thermal deformation in the characteristic points for different spindle speed ($n_1=2800$ [rev/min], $n_2=3550$, $n_3=5600$ i $n_4=6300$).

Key words: main spindle assembly, thermal-elastic behavior, double row cylindrical bearings

1. INTRODUCTION

One of the goals of the design process within the main spindle is prediction of its behavior in exploitation under different types of load. In addition to static and dynamic loading spindle assembly is subjected to the heat input. In modern conditions, prediction of behavior of these assembly are usually performed by the finite element method. To define the specific behavior of mechanical structures using finite element method it is necessary to define the same computer model that takes into account as many parameters influencing its behavior. For example, it is necessary to define the parameters: contact elements, constrain movement, thermal conductivity, temperature values in the area heat sources and etc..

The analysis of thermal-elastic behavior of a main spindle assembly for different ways bearings to deal with and has been a relatively large number of authors. Below are listed the results in this field.

Bossmanns and Tu in their paper [4] presented a model of energy flow is the first step in the overall thermal-mechanical model of high-speed bearings. This model includes the basic flow of energy sources of energy bearings such as beds are: developed in the heat of the angular contact bearings under the influence of speed, due to the lubrication, of electric motor heat is developed in the rotor and the stator as a function of torque and speed and heat developed due to viscous shear in the air reversing elements bearing. Prestressing bearing is neglected in the mathematical model. In this paper, based on the research are: the transfer of heat from the source, the variety of transfer mechanisms such as heat conduction to the interior of the spindle housing, conduction through the bearings, the convection from the stator and rotor to the spindle.

Haitao, Jianguo and Jinhua explore thermal effects on the spindle turning center [5]. Examined the effect of thermal deformation, as a result of the thermal load on the main spindle accuracy machining centers. They defined first relations to determine the heat transfer coefficient with the main spindle assembly and after that the deformation the spindle nose of the thermal

load by finite element method. The developed mathematical model was verified by experimental tests and it was found that the deformation obtained numerically approximately the same as those experimentally measured.

Jedrzejewski, J. analyze the effect of the influence of thermal contact resistance on temperature rise and power loss by friction in the bearings with angular contact [6]. The author has put relations for the determination of contact resistance, depending on the clearance between the outer ring and the housing and the spindle and the inner ring, the shape and size of the contact surfaces between the ring and spindle and housing, while proposing placement additional material between the inner ring and mainn spindle and outer ring and housing.

Analysis of thermal-elastic behavior of the main spindle assembly bearing ball bearings with angular contact (X, O and a tandem arrangement) finite element method and experimentally shown in [8, 9, 12]. As an illustration of the results, below (Table 1) shows the temperature rise on the outer rings of ball bearings with angular contact in the X and O on distance, in arrangement for conventional and hybrid bearings for one number spindle speed.

Types of bearings	Variant bearings	Spindle speed [rev/min]	Temperature increase [°C]	
			ΔT_1	ΔT_2
Conventional bearings	„X on distance“	5600	59,3	55,5
	„O on distance“	5600	52,6	47,1
Hybrid bearings	„X on distance“	5600	44,9	44,9
	„O on distance“	5600	47,7	43,7

Table 1. Temperature increase on the outer rings of bearings

Experimentally determined elastic deformation of the spindle nose in radial directions (horizontal and vertical), because of the thermal load, for considered types bearings shown in Fig. 1.

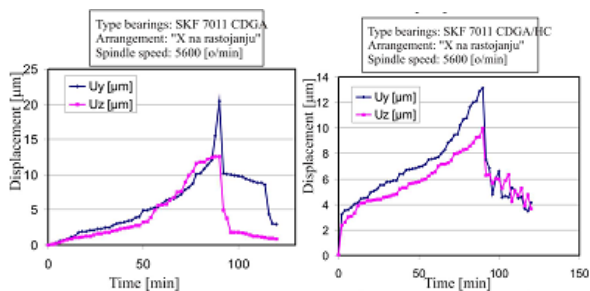


Fig. 1. Dependence of displacement the top spindle due to the thermal load over time [8]

Building on these results, the Laboratory for Machine Tools, Faculty of Engineering, in the analysis of thermal-elastic behavior of main spindle assembly with ball bearings with angular contact (conventional or hybrid bearing), the paper presents the analysis of

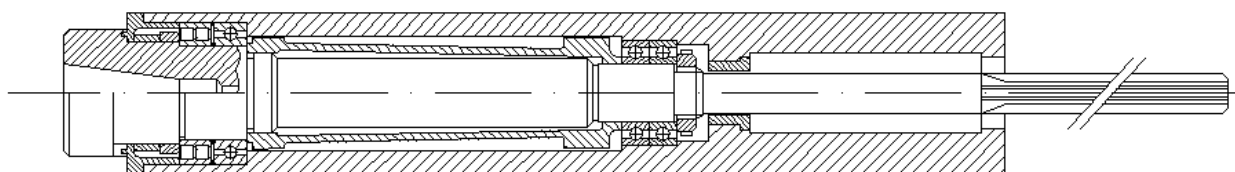


Fig. 2. A main spindle with double roller bearing in the front of suport

The analysis is applied to the finite element method, where the two-dimensional computer model (2D) (Fig. 3), make it the main spindle 1, the front bearing (two-row roller bearings and ball bearings with angular contact) 2, rear bearing 3, housing (quict) 4 and rings 5 and 6. Based on a surface model, is defined nets from the the 6174 final elements 20,337 nodes.

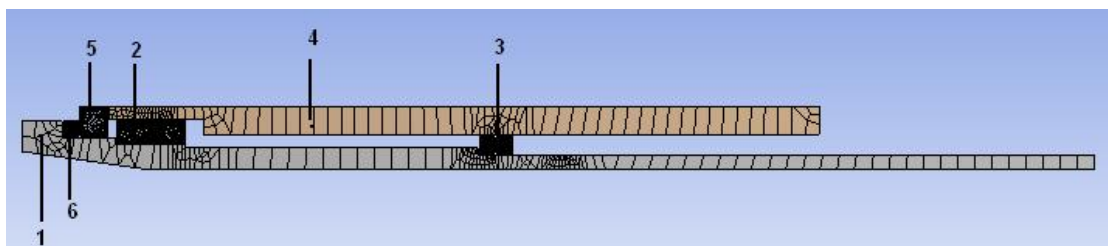


Fig. 3. Discretized model of main spindle assembly

In addition to the previous preprocessor is necessary to define the characteristics materijal of individual parts assembly _ and sources of heat, which in this case are the bearings. It should be in mind that the bearings are modeled as a single unit (without considering the heat transfer between the balls and rollers and rings) is required to define the temperature of the heat source. The values of the temperature on the outer ring ball and roller bearing (considered to be the same temperature and on inner ring - bearing temperature is uniform) were experimentally determined for the stationary temperature state of the considered assembly for the following spindle speed: $n_1=2800$ [rev/min], $n_2=3550$, $n_3=5600$, $n_4=6300$ [1],[3] are shown in Table 2.

thermal-elastic behavior of main spindle assembly with cylindrical double row roller bearing, using the finite element method.

2. THERMAL-ELASTIC MODEL OF MAIN SPINDLE ASSEMBLY

2.1 Thermal model and the results

The goal of the analysis of thermal-elastic behavior of main spindle assembly with cylindrical double roller bearing and ball bearing angular contact with the front support, the determination of the characteristic points of deformation under the influence heat load. Constructional solution analyzed main spindle assembly is shown in Figure 2.

Discretization is performed 2D finite element PLANE 85, while for defining contact pairs used finite elements TARGET 187 and CONTA 174 FOR a contact-rings and spindle or rings and housing. As a result of the previous Fig. 3 shows a discretized model of the considered assembly.

Spindle speed [rev/min]	Temperature ambient [°C]	Temperature outer ring roller bearing [°C]	Temperature outer ring ball bearing [°C]
2800	21,9	25,9	25,5
3550	20,8	26,2	25,6
5600	21,7	33,1	30,9
6300	22,3	37,1	34,0

Table 2 The experimentally determined temperature elements main spindle assembly in the stationary temperature state

As noted earlier, sources of heat in the considered main spindle assembly the only bearings, while the inner mechanisms of conduction of heat: convection due to rotation bearing, convection due to rotation spindle, conduction between the outer ring and housing and inner ring and main spindle [12]. To you performed computer analysis is necessary to define the values of

the coefficient convection and heat conduction.

Convection due to rotation bearing is realized heat transfer between the bearing and the surrounding air [12]. In table 3 are listed the values of the coefficient convection through the bearing for discussed speeds.

Spindle speed [rev/min]	Coefficient convection α [W/m ² K]
2800	160,8
3550	252,2
4500	400,1
5600	614,4
6300	775

Table 3. The values of the coefficient convection for the different number of rotations spindle [12]

Convection due to rotation main spindle defined according to the theory of computing of coefficient convection during currents the air around the flat plate. Starting from the constructional solution which main spindle assembly can be concluded that the transfer heat convection happening on outer surfaces and inner cone surface of the spindle nose (cone surface is considered as a cylindrical surface mean diameter) [2]. The values of coefficient convection on outer and inner cone surface of and the spindle nose are shown in table 4.

Spindle speed [rev/min]	Coeff. convection for outer cylindrical surface h [W/m ² K]	Coeff. convection for inner cone surface h [W/m ² K]
2800	29,18	21,44
3550	37,56	25,1
4500	40,3	32,65
5600	46,1	34,2
6300	55,5	36,1

Table 4. The values of the coefficients convection for different number rotation spindle [2]

Heat transfer between the outer ring bearing and housings and the inner ring and the main spindle depends on the gap between the ring and the housing, or the ring and spindle (for gap of 10 [μm]). The values of coefficients heat transfer between the ring and main spindle and ring and the housing (quiet) are shown in table 5.

Contact place	Coefficient convection λ [W/m ² K]
Inner ring bearing / main spindle	30,41
Outer ring bearing / housing (quiet)	49,95

Table 5. The coefficient convection values between the ring and housing and ring and spindle [12]

Based on the previously presented values of coefficient convection values and thermal transfer finite

element method defined computer models thermal behavior of main spindle assembly for different spindle speeds as follows: $n_1=2800$ [rev/min], $n_2=3550$, $n_3=5600$ i $n_4=6300$. On figure 4 shown a computer model of the thermal behavior of the main spindle assembly for $n_4=6300$.

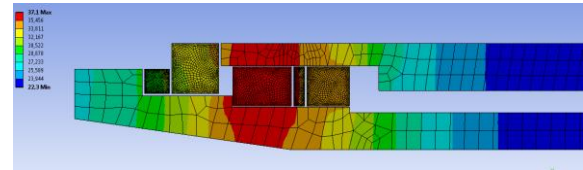


Fig. 4. Shows a computer model of the thermal behavior of the main spindle assembly $n_4=6300$

Computer modeling determined temperature values for the stationary temperature state of main spindle assembly in characteristic points of the main spindle nose (Fig. 5) (S1-point on outer surface of the main spindle nose; S2-point on the outer surface of the main spindle nose and ring 6, S3-point in the middle of the inner cone surface of the main spindle nose).

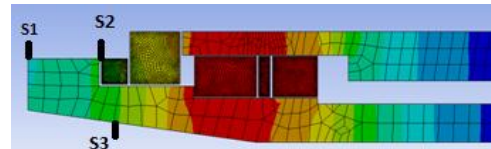


Fig. 5. The position of the characteristic points on the main spindle

Table 6 shows the temperature values in the stationary temperature state for characteristic points and different spindle speeds. The values temperature on the outer surface of the spindle have slightly lower than the temperature on the inner cone surface, which is explained with a larger convection due to rotation of spindle. Also, the temperature in point S₂ is slightly higher than the temperature in point S₁, because the point S₂ is closer to the heat source.

Spindle speed [rev/min]	Characteristic point S ₁ [°C]	Characteristic point S ₂ [°C]	Characteristic point S ₃ [°C]
2800	23,2	23,8	24,1
3550	22,6	23,4	23,7
5600	25,4	27,2	27,8
6300	27,1	29,3	30,1

Table 6. The temperature value in characteristic points main spindle nose

2.2 Elastic model and results

In the modeling of the elastic behavior was considered only the influence of heat load without the action of external forces. Heat load was defined based on the results of thermal analysis, and represents arrangement of temperature fields throughout the main spindle.

The boundary conditions, in this analysis, relating to constrain of movement in certain locations or nodes of the finite elements.

Because whole assembly main spindle assembly in the housing, the outer surface of the quill can not be spread in the vertical direction (y-axis), while the rear surface of the quill relies on the inner surface of the quill, which restricts her movement in the horizontal direction (x-axis).

Based on this the nodes that belong to the outer surface of the quill, take away the degrees of freedom U_y which allowed movement in the X direction of the nodes which belonging to the back surface of the pinole, take away the degrees of freedom U_x which was allowed to move in the Y direction. Main spindle assembly next-double row cylindrical bearing, bearing is with one ball bearing angular contact with the in the front the palm, and with two ball bearings with angular contact in rear support in the "O" arrangement. As single row ball bearings with angular contact doesnt allow move in the x direction, the nodes that belong to the bearings seized U_x degree of freedom, which was allowed to move only in the Y direction (Fig. 6). Between nodes finite element belonging to bearings and nodes that belonged quill and spindle defined stiff contact pairs.

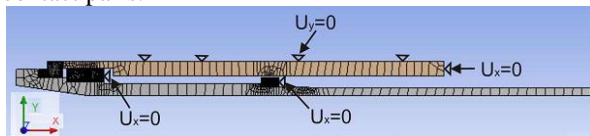


Fig. 6 Restrict of degrees of freedom of movement in the X and Y direction

Fig. 7 a. and 7 b. shown results computer modeling of elastic behavior of main spindle assembly under the effect of heat load, for speed $n_4 = 6300$ [rev/min] in the axial x (7.a.) and radial y (7b) direction.

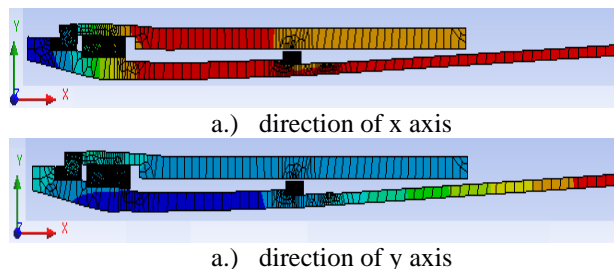


Fig. 7. Computer model of main spindle assembly after thermal load for spindle speed $n_4=6300$

The values displacement determined at the main spindle nose and the outer and inner rings of bearings. Characteristic points on the main spindle where determine displacement are shown on Fig. 8. Based on the results of displacements at points S_1 and S_2 can be made conclusion about the accuracy main spindle under the effect of thermal load, while based on displacements in points of S_3 , S_4 , S_5 and S_6 may consider changes in gap-fold into bearings, also as a result of heat loads.

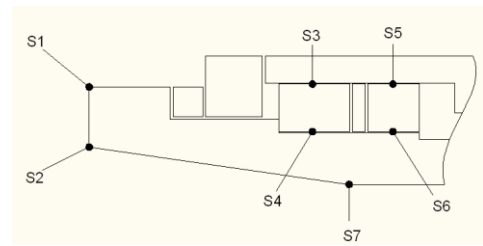


Fig. 8. Characteristic points on main spindle assembly in which defined displacement

Displacement value of the characteristic points in the x direction are shown in table 7 and the displacement value in the y direction are shown in table 8.

Spindle speed [rev/min]	Displacements of the characteristic points in the axial direction [μm]						
	S1	S2	S3	S4	S5	S6	S7
2800	-3,5	-3,5	-1,6	-1,6	-0,4	-0,4	-1,2
3550	-3,6	-3,6	-1,7	-1,7	-0,4	-0,4	-1,1
5600	-9,5	-9,8	-4,1	-4	-0,9	-1	-2,9
6300	-13	-14	-5,9	-5,9	-1,5	-1,7	-4,3

Table 7. Displacements of the characteristic points in the x direction

The largest axial displacements from the considered, have points of S_1 and S_2 and it directly affects the accuracy of the main spindle in the axial direction, particularly in larger numbers spindle speed (above 5000 rev/min). The main spindle nose elongates (moves to the left side). Axial displacements of outer and inner ring bearing are identical for one bearing, wherein greater in-double row cylindrical roller bearings than ball bearing with angular contact. Also axial movement of rings indicates that there isnt change of axial gap-fold in the bearings.

Spindle speed [rev/min]	Displacements of the characteristic points in the radial direction [μm]						
	S1	S2	S3	S4	S5	S6	S7
2800	0	0	0,3	-0,5	0,2	-0,5	-1,3
3550	-0,5	-0,6	0	-0,9	0	-0,8	-1,7
5600	0,2	-0,2	0,9	-1,3	0,5	-1,4	-3,6
6300	2,5	1,8	2,5	-5,3	1,6	-8,3	-3,7

Table 8. Displacements of the characteristic points in the y direction

Considering the displacement value of the characteristic points in the radial direction can be concluded that the displacements to the main spindle nose (S_1 , S_2) is small (for three at spindle speed less than $1 \mu\text{m}$, and at maximum spindle speed are below $3 \mu\text{m}$). This shows great accuracy main spindle in the radial direction under the influence of heat load. Observing the displacements bearing ring in the radial direction can be concluded larger displacement inner from outer rings, as well as different direction displacement. Previously shows that under the influence of thermal load leads to change of gap-fold in the radial direction, which affects the on static stiffness and dynamic behavior of the bearing and main spindle

assembly. Here you can see some larger displacements the rings ball bearing from double row cylindrical roller bearings.

Forasmuch function of the inner cone surface of the main spindle nose, analyzed the influence of thermal deformation on the accuracy of the same (tables 7 and 8). The calculation changes the angle of the cone surface can be concluded that it is negligibly small, and for maximum spindle speed is less than one angular second.

3. CONCLUSIONS

Summing up the results of research, it can be concluded that the paper is an attempt to make a testing thermal-elastic behavior of high speed main spindle bearing with cylindrical and ball bearings with angular contact. Based on the developed mathematical model can still in the design phase, with the maximum reliability prediction of thermal-elastic behavior of this circuit in exploitation. As noted in the paper, the importance of high speed main spindle in the structure of machine tools is very large and it is placed a series of recuest, and as the most important in the work of prominent limited temperature rise at the front of the bearing, and lower displacement on the spindle nose. Any research in this paper also show the possibility of the application of modern numerical method calculation for identify the thermal behavior of main spindle, wherein said method allows the determination of the most important thermal and elastic characteristics.

4. REFERENCES

- [1] Blanuša, V., Zeljković, M., Živković, A., Štrbac, B., Hadžistević, M.: Application of modern methods for measuring the temperature, Proceedings (in Serbian), CD rom, Infoteh-Jahorina, PRS-Manufacturing system, Page. 491-496, ISSN: 99938-624-2-8, 2012.
- [2] Blanuša, V., Živković, A., Zeljković, M.: Computer analysis of thermal behavior of the assembly spindle with double row roller bearings, Proceedings (in Serbian), CD rom, 38 JUPITER conference, 25 Symposium CAD/CAM, Page. 32-38, ISSN: 978-86-7083-757-7, 2012.
- [3] Blanuša, V.: Temperature measuring main spindle assembly, Exam paper (in Serbian), Faculty of Technical Sciences, Novi Sad, 2011.
- [4] Bossmanns, B., Jay, F.: A thermal model for high speed motorized spindles, International Journal of Machine Tools and Manufacture, ISSN: 0890-6955, Vol. 39, Pages 1345-1366, 1999.
- [5] Haitao, Z., Jianguo, Y., Jinhua, S.: Simulation of thermal behavior of a CNC machine tool spindle, International Journal of Machine Tools and Manufacture, ISSN: 0890-6955, Issue 6, Pages 1003-1010, 2006.
- [6] Jedrzejewski, J.: Effect of the thermal contact resistance on thermal behavior of the spindle radial bearings, International Journal of Machine Tools and Manufacture, ISSN: 08909-6955, Vol.28, No.4, Pages 409-416, 1988.
- [7] Zeljković, M., Živković, A., Borojev, Lj.: Thermal-elastic behaviour numerical analysis of the high speed main spindle assembly, International Conference „Heavy Machinery“, ISSN:978-86-82631-45-3, Pages E57-E62, 2008.
- [8] Živković, A.: Experimental and computer analysis of thermal-elastic behavior of complex high speed main spindle of machine tools, Master's thesis (in Serbian), Faculty of Technical Sciences, Novi Sad, 2007
- [9] Živković, A., Zeljković, M., Borojev, Lj.: Thermo-elastic model assembly high speed main spindle, Proceedings (in Serbian), CD rom, Infoteh-Jahorina, C- Information systems in manufacturing technologies, ISSN: 99938-624-2-8, Vol.6, Ref. C10, Pages 170-174, 2007.
- [10] Živković, A., Zeljković, M., Borojev, Lj.: Influence thermal load on preload bearing balls with angular contact, Proceedings (in Serbian), CD rom, 33 JUPITER conference, 20 Symposium CAD/CAM, ISSN: 978-86-7083-628-0, Pages 2.1-2.6, 2007.
- [11] Živković, A., Zeljković, M., Borojev, Lj.: Influence of thermal preloading bearings on stiffness main spindle assembly, Proceedings (in Serbian), CD rom, Conference on production engineering with foreign participants, ISSN: 978-86-7892-131-5, Pages 409-412, 2008.
- [12] Živković, A., Zeljković, M., Borojev, Lj.: Experimental testing of thermal-elastic behavior of the high speed main spindle assembly, Proceedings (in Serbian), CD rom, 34 JUPITER conference, 30 Symposium NU robot and FMS, ISSN: 978-86-7083-628-0, Pages 3.13-3.18, 2008

Authors: Prof. dr. Milan Zeljković, Mr. Ass. Aleksandar Živković, MSc. Vladimir Blanuša, University of Novi Sad, Faculty of Technical Sciences, Department for Production Engineering, Trg Dositeja Obradovica 6, 21000 Novi Sad, Serbia, Phone.: +381 21 485-2320.

E-mail: milanz@uns.ac.rs
acoz@uns.ac.rs
blanusa@uns.ac.rs

ACKNOWLEDGEMENT:

The paper is part of a research on project "Modern approaches to the development of special bearings in mechanical engineering and medical prosthetics," TR 35025, supported by the Ministry of Education and Science, Republic of Serbia.

11th INTERNATIONAL SCIENTIFIC CONFERENCE
MMA 2012 - ADVANCED PRODUCTION TECHNOLOGIES

PROCEEDINGS



Section E:
**MECHANICAL ENGINEERING AND
ENVIRONMENTAL PROTECTION**

Novi Sad, 20-21 September 2012

Arsovski, S., Lazić, M., Krivokapić, Z., Tadić, D., Grubor, S.

AN APPROACH TO DEFINE OPTIMAL TECHNOLOGY PORTFOLIO OF ELV RECYCLING

Abstract: End of live (*ELV*) recycling is related to different technologies. Level, amount of usage and distribution of technologies could significantly influence the effectiveness of *ELV* recycling. The subject of the paper is approach to define technological portfolio, using deterministic methods and methods in case of decision under uncertainty. In this paper is presented proposed methodology.

Key words: Technology portfolio, End - of - Life Vehicle (*ELV*), recycling.

1. INTRODUCTION

ELV recycling is contemporary and sustainable answer on many different and often opposite requests, as: (1) economic growth, (2) energy saving, (3) basic material spending etc. [1,2]. *ELV* recycling is organizing through recycling centers, distributed on different ways [3,4]. Depend on purpose in those centers are implemented different technologies, with different levels of automatization, flexibility, effectiveness, production rate etc. [5]. That means, in some cases adequate technological solution is not appropriate and sufficient for region (Serbia) as whole. It is reason for necessity of *ELV* technology portfolio planning.

General approach of technology planning has four phases:

- * *prioritize and quantity values,*
- * *create innovative portfolio alternatives,*
- * *determine and forecast relationship and*
- * *find the optimal technology portfolio.*

Each of phases is very complex. An example, value of an organization is often difficult to define and access for many reasons, dominantly related to different stakeholders and problems of reliable information. Identifying the innovative solutions is connected with creativity process and depends on owners and researchers.

Problem of *ELV* portfolio planning could resolve using two groups of methods, deterministic and

methods used for in deterministic situations. In this paper authors emphasize using of deterministic methods.

2. QUANTIFICATION OF VALUES AND RISK ATTITUDES

Each technology has different values, expressed by the characteristics or attributes of this technology that are significant and desirable for decision makers.

The characteristics have to be completely defined, measured, monitor and changed based on feedback from decision makers. For decision making is related degree of subjective preference [6].

A simultaneous rating approach is the simplest method based on subjective preference of various values by the decision maker. For *ELV* recycling these values are:

Profitability: The amount of expected present value of net profit achieved from development or application of desired technology portfolio in next 5 years.

Quality: Technology related quality characteristics, as waste rate, reliability, mean time to failure, flexibility through faster adaptation on changes, etc.

Productivity: The amount of present worth of added value divided with total costs.

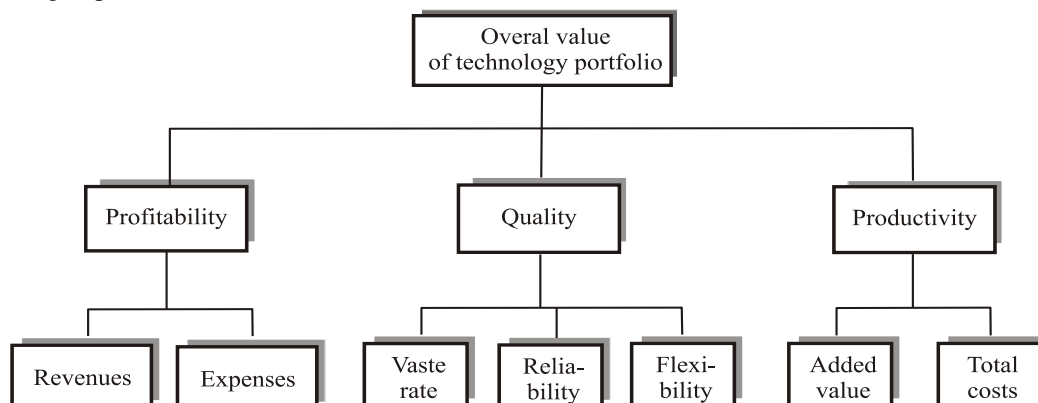


Fig. 1. The hierarchy of values for technology portfolio

Analytical Hierarchy Process (*AHP*), as second and very popular approach, starts with set up the hierarchy of values. In Fig. 1. is presented the hierarchy of values for *ELV* technology portfolio.

Next steps in *AHP* approach are:

- » set up a standard scale for pair-wise comparison,
- » develop an comparison matrix w for n values in a hierarchy,
- » estimate the average preferences or weights of the n value in a hierarchy,
- » check matrix consistency,
- » revise the pair-wise comparison for consistency and
- » distribute the relative preference of a value to values through a sub-hierarchy.

The third modern method is based on utility theory by *Neuman and Morgenson*. In area of *ELV* technology portfolio utility theory is related to money and risk attitude. The risk premium determines prevalent utility function (Fig. 2).

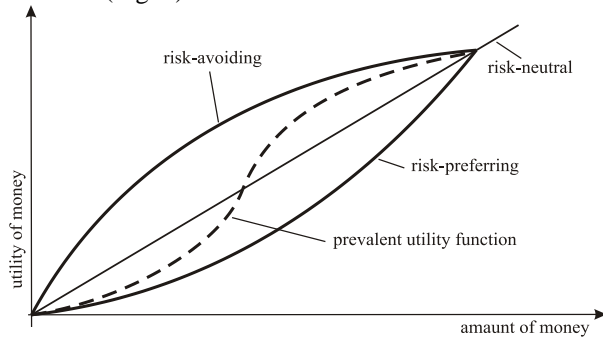


Fig. 2. Risk attitudes towards money

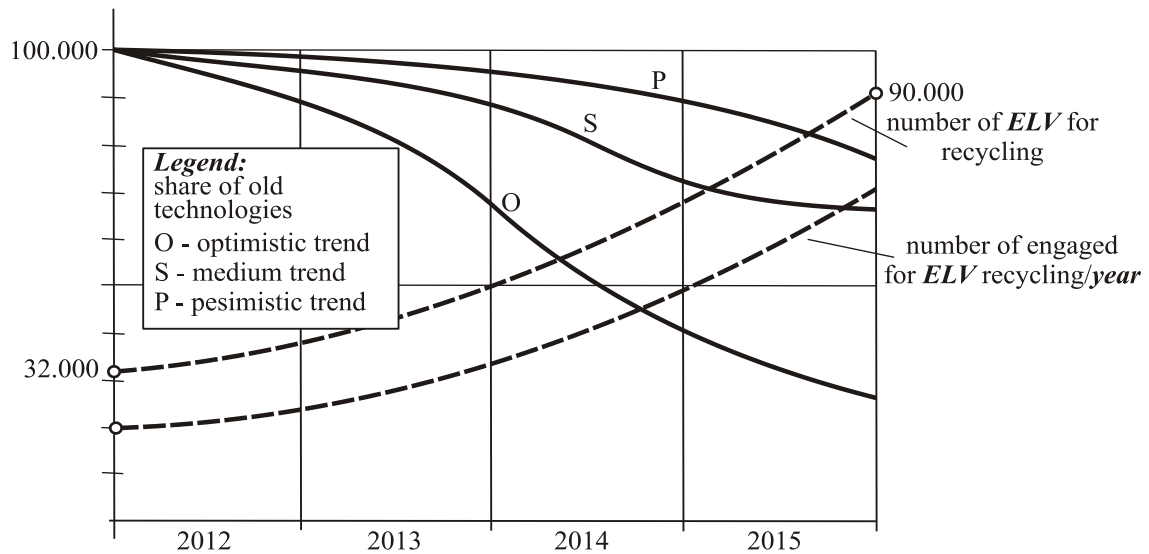


Fig. 3. Forecasting the ELV recycling technologies in Serbia

4. DETERMINATION AND FORECASTING OF ELV TECHNOLOGY USING QUALITATIVE APPROACH

For technology forecasting is used *Hierarchical Influence Tracing System* (Fig. 5).

In figure 6 is presented analysis using *AHP* in area of rubber recycling technologies.

In next phase is used *Decision-Focused Scenario Analysis* as iterative process (Fig. 7).

3. CREATING THE INNOVATIVE PORTFOLIO ALTERNATIVES

This phase is very creative and used many techniques and tools. The most widely are: brainstorming, lateral thinking and theory of inventive problem solving.

Brainstorming purpose of *ELV* technology portfolio planning is conveyed in relaxed atmosphere, with no criticism and encourage for creative solution. Through two sessions are formulated three innovative portfolio alternatives:

- » redistribution of existing technologies,
- » exchange of amount of existing technologies in *ELV* recycling centers, and
- » introduction the new recycling technologies for:
 - recycling of electrical and electronic waste,
 - displacing fluids and toxic material from *ELV*,
 - rubber recycling.

In Fig. 3. is presented forecasting of *ELV* recycling technologies in Serbia.

In Fig. 4. is presented risk analysis of recycling technologies in Serbia, based on expert assessment during second *Delphi* session.

Theory of Inventive Problem Solving (TRIZ) is based on 40 principles. For purpose of the paper is emphasized principle of technology evolution in combination with principle of related solution and principle of unrelated combination.

Using this approach is determined mayor scenarios and assessed scenario implications.

Finding the optimal technology portfolio is performed using *benefit-cost (B/C)* ratio method. In Table 1 is presented preliminary results of portfolio analysis.

From those aspects is estimated as favorable technology B.

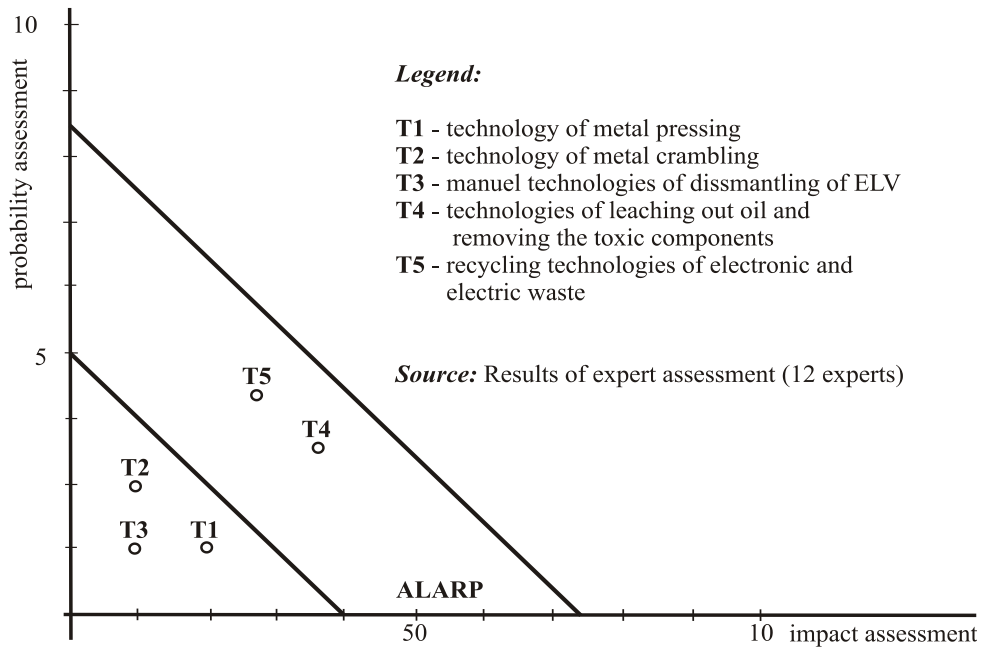


Fig. 4. Risk assessment of introduction of different recycling technologies

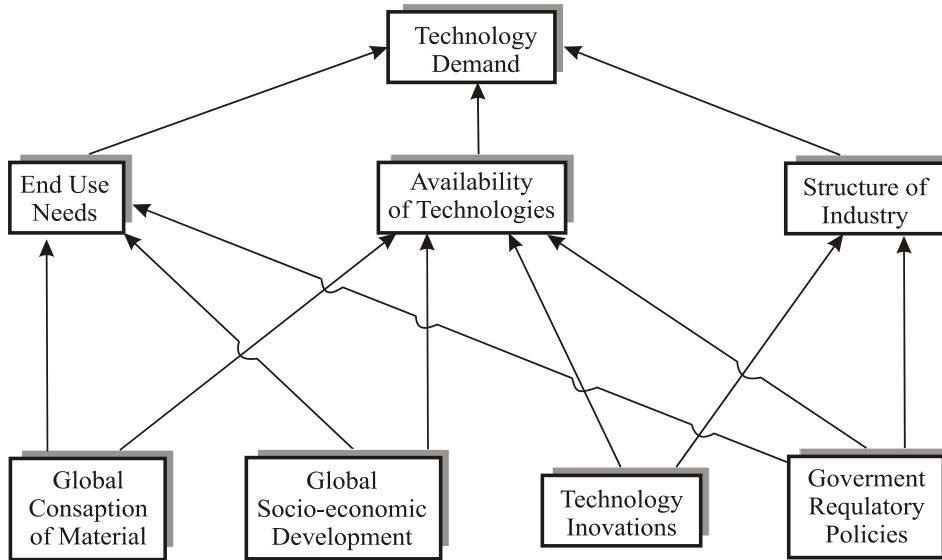
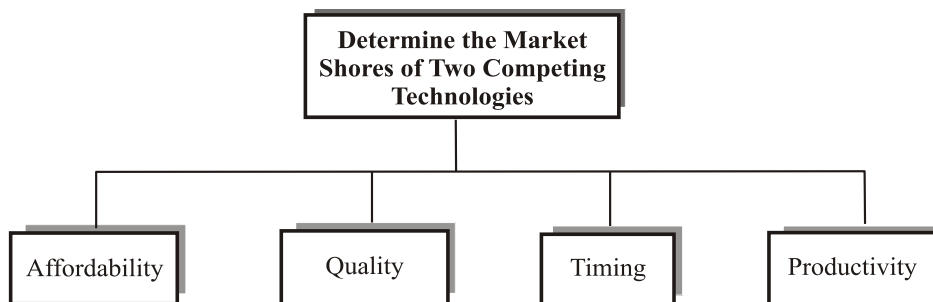


Fig. 5. Hierarchical Influence Tracing System



	Affordability	Quality	Timing	Productivity	Success Probability
Weight	0.25	0.3	0.1	0.35	
Technology A	0.3	0.4	0.7	0.5	0.440
Technology B	0.4	0.3	0.5	0.4	0.380

Fig. 6. Success probability of two rubber recycling technologies

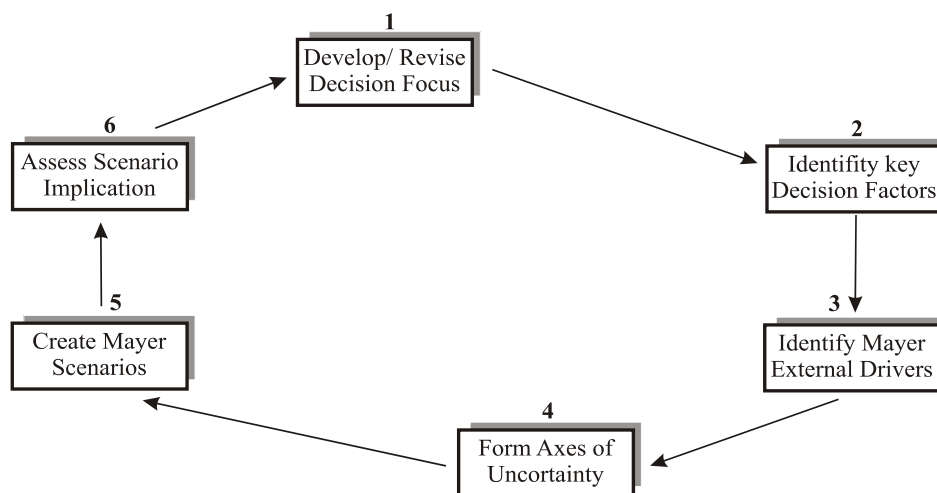


Fig. 7. Process of Scenario Development

Technology	Total benefit (€ million)	Total costs (€ million)	B/C
A	20	5	4.0
B	15	3	5.0
C	17	4	4.0
D	13	4	3.2
E	11	3	3.6

Table 1. B/C ratios of different rubber recycling technologies

5. CONCLUSION

From previous investigation can be concluded:

- portfolio of technology of ELV recycling is changing,
- quantification of values and risk are input for optimization of technology portfolio,
- using value and AHP approach is identified structure of values,
- using utility theory is determined prevalent utility function,
- according trend analysis of ELV technologies in Serbia are identified expanded potential for ELV recycling technologies,
- according expect assessment of risk are identified technologies related with medium risks,
- using benefit/cost method in present situation is choiced technology B for rubber recycling.

6. REFERENCES

- [1] Kanjevac Milovanović K., Arsovski S., Kokić Arsić A., Savović I., Stepanović B., *The impact of the CE marking on the competitiveness enterprises*, 5. International Quality Conference, Quality Festival 2011, pp. 17 - 26, ISBN: 978-86-86663-68-9
- [2] Arsovski S., Grubor S., Tonić N., Kokić Arsić A., Kanjevac Milovanović K., *Postupak ocenjivanja životnog ciklusa proizvoda*, Festival kvaliteta 2011 - 6. Nacionalna konferencija o kvalitetu života, pp.

B131-B136, ISBN: 978-86-86663-68-9.

- [3] Tadić D., Arsovski S., Stefanović M., *Designing of network for the dismantling centers of the End-of-Life vehicles by Fuzzy ABC method*, 5. International Quality Conference, Quality Festival 2011, pp. 201 - 206, ISBN: 978-86-86663-68-9
- [4] Aleksić A., Arsovski S., Tonić N., Grubor S., *Kapa-citet za oporavak centra za demontažu vozila na kraju životnog ciklusa*, Festival kvaliteta 2011 - 6. Nacionalna konferencija o kvalitetu života, pp. B131-B136, ISBN: 978-86-86663-68-9.
- [5] Pavlović M., Arsovski S., Arsovski Z., Mirović Z., Lazić M., *Design Methodology for Discrete Event Simulation Solutions in Manufacturing Environment*, *Strojarstvo*, br. 3, 2011.
- [6] Stefanović M., Tadić D., Đapan M., Mačužić I., *Software for Occupational Health and Safety Risk Analysis Based on Fuzzy Model*, *International Journal of Occupational Safety and Ergonomics*, 2010.

Authors: Prof. dr Slavko Arsovski, Prof. dr Miodrag Lazić, Prof. dr Danijela Tadić, Sonja Grubor, dipl. ing., University of Kragujevac, Faculty of Engineering, Center for Quality, Sestre Janjić 6, 34000 Kragujevac, Serbia, Phone.: +381 34 302-590, Fax: +381 34 302-591.

E-mail: cqm@kg.ac.rs

Prof. dr Zdravko Krivokapić, Univerzitet Crne Gore, Masinski fakultet u Podgorici,

E-mail: zdravkok@ac.me

ACKNOWLEDGMENTS

The research presented in this paper was supported by the Ministry of Science and Technological Development of the Republic of Serbia, Grant III-035033, and with Title: Sustainable Development of Technologies and Equipment for Recycling of Motor Vehicles.

Avdic, N., Goletic, S.

SELECTION CRITERIA FOR CLEAN WATER DECANTERS OF SBR WASTEWATER TREATMENT PLANTS

Abstract: Frequent dilemma for the selection of technologies and equipment for design and construction of wastewater treatment has led us to analyze one of the segments, that is indispensable in plants for wastewater treatment, decanters. The analysis of efficiency and operational characteristics of three different decanters that are now mostly used for pumping water from the reactor after biological processes of sedimentation provide information not only on the part of the equipment applied in Sequenced Batch Reactor, but also in choosing the number of cycles in them and thus the capacity of the plant.

Key words: wastewater, Sequenced Batch Reactor SBR, tube decanter, floating decanters, Wall-mounted decanter

1. INTRODUCTION

Environmental sustainability means for the water to produce clean drinking water and the protection of waters against harmful discharges. In the countries of former Yugoslavia, the issue of wastewater treatment plays a very important role in the future. Increasingly stringent requirements of EU environmental policies are followed.

For municipalities and industrial companies it means, to plan to build biological wastewater treatment plants. In the biological wastewater treatment plants, two key principles have prevailed. On the one hand, the classical continuous process, and on the other hand the so-called Sequenced Batch Reactor SBR or procedures. Both methods are assumed after a mechanical pre-biological treatment of wastewater bacteria. This use of various strains of bacteria in the wastewater that contained pollutants (carbon, nitrogen and phosphate) as building blocks for their metabolism, and transform the problematic substances to the aquatic environment primarily in water and carbon dioxide and store these substances in their cells.

The continuous process is based on the fact that the services required for the biological wastewater treatment stages "aeration / nitrification" (carbon removal and conversion of ammonium to nitrate), "denitrification" (conversion of nitrate to elemental nitrogen, which escapes as a gas) and "sedimentation" (separation of the bacterial mass held by the clear water) into separate pools. Each tank is provided for precise treatment level, whichever is the appropriate process rather than continuously. The cycle varies depending on the day incoming wastewater flows undocumented migrants by the respective treatment tanks so that the determination of pool size based on the maximum inflow or the amount expected to be at maximum wastewater constituents needs.

In contrast, SBR process will find the treatment steps "Ventilation / nitrification," instead of "denitrification" and "sedimentation", followed by the end of the clear water in a single treatment basin. The different treatment steps are consecutively performed in so-

called cycles. At the beginning of a cycle, for example, finds the "denitrification" takes place, then the "Ventilation / nitrification" and finally the "sedimentation" with subsequent expiry of the clear water. The incoming wastewater is controlled by the process system and pumped as needed in the individual treatment steps. For this purpose SBR plants do not generally require a storage tank before the SBR reaction tank. Further details on SBR process and the differences from the traditional activated sludge process can be found in the literature [1].

2. HIGH FLEXIBILITY OF THE SBR PROCESS

The SBR process has gained importance in the past 20 years, especially when highly variable wastewater flows, such as occur in tourist areas, or if after completion of the sewage connection rate of the population to the central sewage system is still low, and a stable inflow is expected until several years after commissioning the new plant.

Thanks to the buffer pool before the SBR reactor pool water can be targeted to the biological cleaning process are supplied, this is the classic continuous process not readily possible. This allows the SBR process, the process conditions for optimal degradation process influenced specifically, what is with all other biological treatment processes not possible. Numerous scientific studies show that SBR process special thanks to the flexibility of control have a higher rate of degradation in the reduction of nitrogen. Operational experience with SBR plants also show that even in very unfavorable conditions such as at low influent load and low water temperatures, the limits of the EU directives can be safely maintained.

In countries such as e.g. Bosnia, Serbia or Montenegro wastewater treatment plants with a high degree of flexibility is of great importance. In contrast to countries such as Germany there is not fully developed infrastructure with a high number of people who are connected to public sewer system. In projects where the population is connected to the sewerage system, are

often coupled existing sewage networks for cost reasons, old and new sewer lines, so that will be calculated at a high rate of groundwater flow through leaky ducts must. Furthermore, there will be also in the future, many residents who are not in the long run is connected to the public sewer system to a wastewater treatment and transport the waste water collecting fecal than by truck to the sewage plant will be. These conditions must when planning a new plant to be considered. Experience has shown that SBR wastewater treatment plants are suitable for these conditions better than the classical continuous process. Whether the SBR method or a continuous process is used, but must be checked in each individual case.

Core of each SBR wastewater treatment plant is the clear-water decanters, integrated in the respective control SBR. The clear water decanter targeted drainage basin of the SBR allows the end of a cleaning cycle. Performance, flexibility, and design of the selected plain water decanter, in addition to a best matched control prevail in order to harness the power of SBR wastewater treatment optimally.

3. THREE DIFFERENT TYPES OF PLAIN WATER DECANTERS

There are three main groups currently on the market to clear water decanters. Tube decanter, floating decanter, and wall mounted decanters (Figure 1).

Tube decanter in most SBR reactors worldwide, since it was developed early Decanter principle. This type of decanter is characterized by its robust and simple way. The Tube decanter is attached via a hinge at the lower discharge pipe, and can be winched up and down behind. In most applications and types is the run-off amount is constant and can not be adapted to changing requirements in the operation of a SBR system. This type of decanter is perfect for SBR solutions with low cleaning requirements.

Floating decanters are becoming more and in modern SBR plants. Even if the structure is designed more expensive than pipe decanters, the big advantage is the flexibility in operation. The unit floats on the current water table level, so that time-consuming maneuvers for insertion and removal as the tube decanter

eliminated and valuable response time is obtained. This can work in individual cases up to 90 minutes per cycle [2]. Depending on the technical design, the amount of water to be derived can be freely set. In order to increase the efficiency and safety of the clarified water discharge decanter, a turbidity probe will be installed on floating decanter. This probe detects the cut point between sludge and clear water. If the mud line at a sufficient distance away from the decanter, the process may begin earlier than the clear water trigger for statically defined control processes or in tube decanter. This process can be more valuable time to be saved. Figure 2 shows the potential savings time a floating decanter with and without turbidity probe compared to tube decanter.

Extremely low maintenance and user-friendly is the system of wall-mounted decanter, which is currently only a few manufacturers are [3]. This system has the same properties as the floating decanter, but with the advantage that the accessibility of the wall mount is ideal for operating personnel. The compact design has a side effect of a lower purchase price as a floating decanter or even tube decanter. Another big advantage is that the wall is mounted decanter for a failure of the measurement technique as an emergency overflow. The water level exceeds the specified maximum water level, the excess water flows over the weir acting like an assault decanter threshold in the course of the treatment plant. While floating decanter float with the rising water level and the drain pipe may be torn off, the sewage in SBR reactor when raised tube decanter unnoticed on the Beck crown of the SBR basin flow into the treatment plant site. The wall-mounted decanter this is excluded. Finally, it should be noted that some tube floating decanters and decanters the assembled pipe joints were exposed to high wear, which are bacterial mass over the cracks in the joint reaches the treatment plant discharge and have contaminated the waters. Since the wall-mounted decanter has had no joints, this danger is not given here.



Fig. 1. From left: Pipe decanter, decanter-floating, wall-mounted decanter

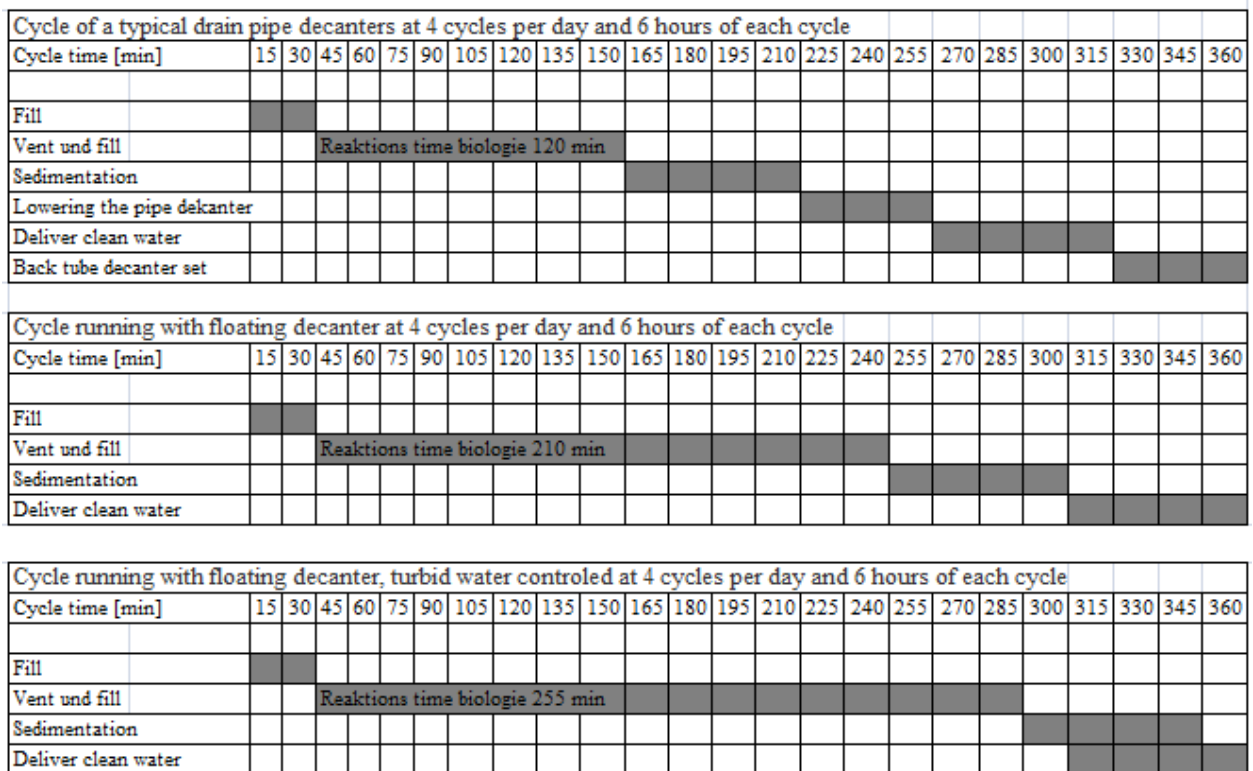


Fig. 2: Potential savings time a floating decanter with and without turbidity probe compared to tube decanter.

5. SUMMARY

SBR wastewater treatment plants are suitable in many cases, especially well for municipal and industrial wastewater projects in the countries of former Yugoslavia. With proper selection of the clear water decanter in combination with a flexible and modern management, the performance of a sequencing batch reactor, even under unfavorable conditions can be optimally used. Already in the planning of a SBR wastewater treatment plant, the choice of a suitable decanter and a modern, flexible control are considered. It is recommended to manufacturers that offer the entire SBR control and the related clean water decanters as a single system and have sufficient experience and references. Especially decanters and floating wall mounted decanter can only be used optimally when the overall control of SBR wastewater treatment plant contains all the controls of this machine and can implement them as commands. Hints for selection and testing of a suitable control SBR will be developed by the working group "SBR Dynamic Control" [4]. These should be respected by the operator of a SBR wastewater treatment plant on the purchase of a controller.

6. REFERENCES

- [1] Dr. Jürgen Wiese „Entwicklung von Strategien für einen integrierten Betrieb von SBR-Kläranlagen und Mischkanalisationen“, Dissertation an der Universität Kaiserslautern 2004
- [2] Angabe der HST Hydro-Systemtechnik GmbH, Deutschland (www.systemtechnik.net) zu einem Sanierungsprojekt in Deutschland
- [3] <http://www.systemtechnik.net/produkte/hydroklar-slide/>
- [4] <http://www.iswa.uni-stuttgart.de/>

Authors: **Dr.sc. Nurudin Avdić**, University of Sarajevo, Faculty of Sciences, Zmaja od Bosne 33, 71000 Sarajevo, Bosnia and Herzegovina, Phone.:+38733 279-862, E-mail: nurudina@bih.net.ba

Dr.sc. Šefket Goletić, University of Zenica, Faculty of Mechanical Engineering, Fakultetska 1, 72000 Zenica, Bosnia and Herzegovina, Phone.:+387 32 449-124 E-mail: goletic@mf.unze.ba

Badida, M., Bartko, L., Králiková, R., Sobotová, L.

RESEARCH OF SELECTED ACOUSTIC DESCRIPTORS OF THREE LAYER SANDWICH ABSORBERS

Abstract: In spite of existing European and national legislation aimed at noise abatement, public interest and concern about noise are high. The EU Directive 70/157/EEC [15] for setting and controlling environmental noise is aimed at creating less noisy and more pleasant environment for European residents within “Sustainable Development in Europe”. The authors are presenting a methodology for measuring selected acoustic descriptors (sound absorption coefficient and sound transmission loss) for acoustic materials, which are currently in process of development. Emphasis is put on sandwich structures of absorbers. Verification results of the proposed methodology are presented.

Key words: environmental noise, noise wall, sound absorption coefficient, sound transmission loss, absorber, sandwich absorber

1. INTRODUCTION

In the European Union, about 80 million persons are exposed to high noise levels, which are unacceptable or result in sleep disorders and other undesirable influences. There are approximately 170 million people living in the so-called “grey regions”, where noise is very annoying.

Noise protection measures for reducing the effect of noise caused by transportation (road, railway and air transport) can be passive and active. Active measures try to prevent the origination of noise, while passive measures are adopted only then, when noise arises. Passive noise protection measures can be divided into two groups, namely: measures preventing acoustic noise propagation (noise barriers and/or walls, noise protection embankments and the like) [6].

Attention is paid to the design process and materials used for construction of noise walls and to their properties. The authors have focussed their attention on the research of new acoustic materials made on the basis of recycled raw materials and applicable for the structures of sandwich absorbers (two-layer and multiple-layer absorbers).

The paper presents a proposed methodology for measuring selected acoustic descriptors (the sound absorption coefficient α and the sound transmission loss TL) [1].

2. PROPOSAL OF METHODOLOGY FOR MEASURING SELECTED ACOUSTIC DESCRIPTORS OF ACOUSTIC MATERIALS, WHICH ARE CURRENTLY IN PROCESS OF DEVELOPMENT

Out of several possible acoustic descriptors, the authors have focused their attention on the two following descriptors:

- sound absorption coefficient (α),
- transmission loss (TL).

For measuring the sound absorption coefficient (α) and the transmission loss (TL) there are two theoretically available methods, namely: the method of standing wave ratio and the method of transfer function. The authors have used in their work the method of transfer function. This method can be used for measuring the sound absorption coefficient, the reflection factor, the normal impedance and the normal admittance. Based on this method is the impedance tube (Fig. 1).



Fig. 1. The impedance tube

The proposed methodology of measurement includes the use of the impedance tube, two positions of positioning the microphones and the system of numerical frequency analysis for determining the sound absorption coefficient of sound absorbers for normal incidence of sound. It can also be applied for determining acoustic surface impedance or acoustic surface admittance for sound absorbing materials, due to the fact that the impedance ratios of sound absorbing materials are proportional to their physical properties, such as airflow resistance, porosity, elasticity and density.

This test method is similar to the test method specified in STN EN ISO 10534-1 [7] in terms of using an impedance tube with a sound source connected to

one of its ends and a test specimen mounted into the tube at its other end. However, the actual test method is different. In this test method the plane waves are generated in the tube by the sound source and the decomposition of the interference field is achieved by measuring acoustic pressures in two fixed positions of microphones mounted on the wall of the tube or by a microphone shifted in the tube and the subsequent calculation of the complex acoustic transfer function, by absorption at normal incidence and by impedance ratios of the acoustic material. This test method is designated to provide an alternative method of measurement, in general much faster than that included in STN EN ISO 10534-1[7].

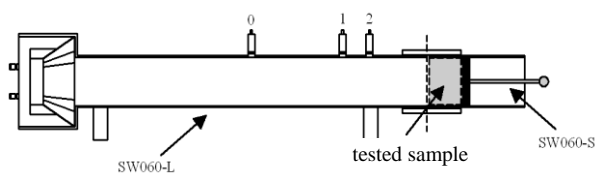
The proposal of methodology for measuring selected acoustic descriptors by using an impedance tube and by applying the method of transfer function is presented in [1].

3. VERIFICATION OF THE PROPOSED METHODOLOGY FOR MEASURING ACOUSTIC DESCRIPTORS FOR ACOUSTIC MATERIALS, WHICH ARE CURRENTLY IN PROCESS OF DEVELOPMENT

The proposed methodology of measurement was verified by measuring selected acoustic descriptors, namely: the sound absorption coefficient (α) and the transmission loss (TL) for the materials, which are currently in process of development.

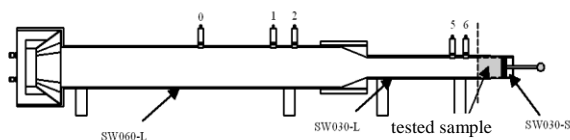
3.1 Instruments, software and other equipment

The system for measuring the sound absorption coefficient (α) (for the frequency bands of 100 Hz to 800 Hz and 400 Hz to 2500 Hz, respectively) is shown in Fig. 2. It is comprised of a tube with inner diameter of 60 mm – SW060-L and of a holder of the tested sample with inner diameter of 60 mm – SW060-S.



Legend: 0, 1, 2 – mounting sockets for microphones

Fig. 2. The system for measuring the sound absorption coefficient (100 Hz to 800 Hz and 400 Hz to 2500 Hz, respectively)



Legend: 0, 1, 2, 5, 6 – mounting sockets for microphones

Fig. 3. The system for measuring the sound absorption coefficient (800 Hz to 6300 Hz)

The system for measuring the sound absorption coefficient (α) (for the frequency bands of 800 Hz to

6300 Hz) is shown in Fig. 3. It is comprised of a tube with inner diameter of 60 mm – SW060-L, of a tube with inner diameter of 30 mm – SW030-L and of a holder of the tested sample with inner diameter of 30 mm – SW030-S.

The system for measuring the transmission loss (TL) (for the frequency bands of 100 Hz to 800 Hz and 400 Hz to 2500 Hz, respectively) is shown in Fig. 4. It is comprised of a tube with inner diameter of 60 mm – SW060-L and of an extension piece of the tube with inner diameter of 60 mm – SW060-E.

The system for measuring the transmission loss (TL) (for the frequency bands of 1600 Hz to 6300 Hz) is shown in Fig. 5. It is comprised of a tube with inner diameter of 60 mm – SW060-L, of a tube with inner diameter of 30 mm – SW030-L and of an extension piece of the tube with inner diameter of 30 mm – SW030-E.

3.2 Selection of materials for the experimental part

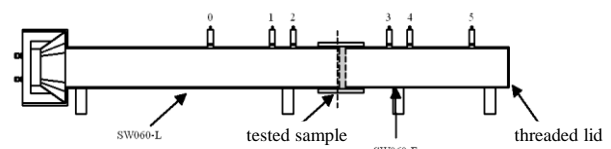
The selected acoustic descriptors (the sound absorption coefficient α , the transmission loss TL) were measured for the following acoustic materials, which are currently in process of development:

- Ekomolitan (Fig. 6)
- Recycled rubber (Fig. 7)

Measurement were also carried out, for comparison, for the material Nobasil (Fig. 8), which is a component part of various sandwich structures of noise walls (barriers).

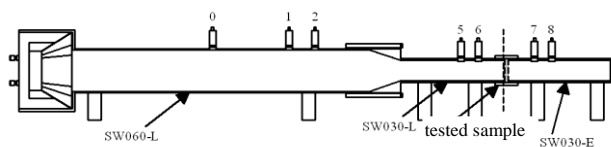
3.3 Preparation of test samples

The test samples of the three-layer sandwich absorbers were prepared in various combinations of materials, such as Ekomolitan, Nobasil and recycled rubber (Figs. 9. a 10.).



Legend: 0, 1, 2, 3, 4, 5 – mounting sockets for microphones

Fig. 4. The system for measuring the transmission loss TL (100 Hz to 800 Hz and 400 Hz to 2500 Hz, respectively)



Legend: 0, 1, 2, 5, 6, 7, 8 – mounting sockets for microphones

Fig. 5. The system for measuring the transmission loss TL (1600 Hz to 6300 Hz)



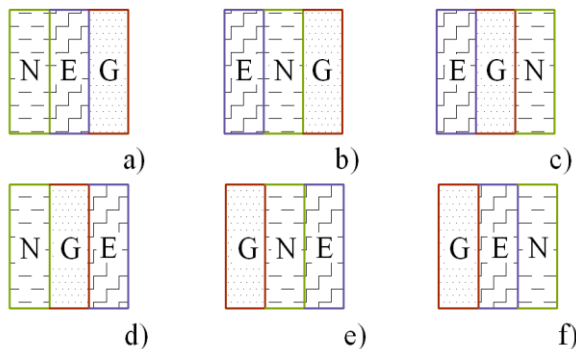
Fig. 6. Ekomolitan



Fig. 7. Recycled rubber



Fig. 8. Nobasil



Legend: N – Nobasil, G – recycled rubber, E – Ekomolitan

Fig. 9. Three layer sandwich samples

Dimensions of the test sample:

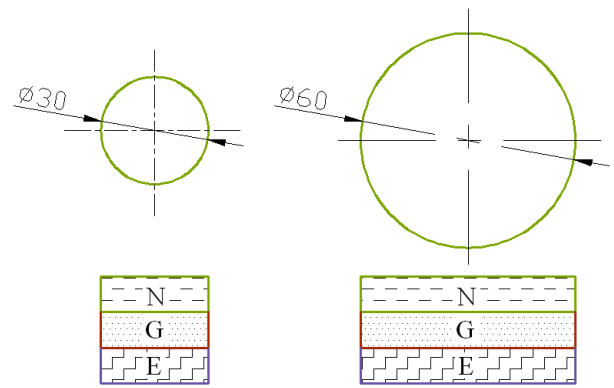


Fig. 10. Dimensions of three layer test sample

3.4 The measured values of the sound absorption coefficient and of the transmission loss

This part of the paper presents outputs from the measurement of the sound absorption coefficient carried out for a three-layer sandwich test sample composed of 2 cm thick Ekomolitan positioned closer to the sound source and of 2 cm thick Nobasil and of 2 cm thick recycled rubber positioned at the end (Fig. 11.), as well as outputs from the measurement of transmission loss for a three-layer sandwich having the same material composition (Fig. 12.) [1].

4. CONCLUSION – EVALUATION OF MEASURED VALUES

The sound absorption coefficient (α) is a dimensionless number varying from 0 to 1. The closer is the measured value to 1 or is equal to 1, the sample of the measured absorber, and thus the absorber itself, will have a better (higher) sound absorption.

We have also measured the transmission loss (TL). It is a value in dB, based on the ratio of the sound wave incident at the front side of the acoustically absorbing material to the sound waves transmitted from the rear side. TL represents the sound damping properties of the material, i.e. the higher that value is, the more efficient is the damping of the sound.

The authors have measured the coefficient of sound absorption (α) and the transmission loss (TL) for various combinations of three-layer sandwich absorbers composed of materials such as Ekomolitan, recycled rubber and Nobasil. Table 1. includes the measured values of descriptors.

The frequency spectrum of noise caused by transportation reaches its maximum in the frequency range of 500 Hz to 1500 Hz, and the most intensive noise is caused at the frequency of 1000 Hz.

Noise walls (barriers) are often constructed as noise panels with a supporting frame using sandwich absorbers. For the purpose of the thesis, samples representing a sandwich composed of materials such as recycled rubber, Nobasil and Ekomolitan were made. The arrangement of individual layers of the sandwich was different. Measurements have been carried out for three-layer sandwiches. (Fig. 13 and Fig. 14).

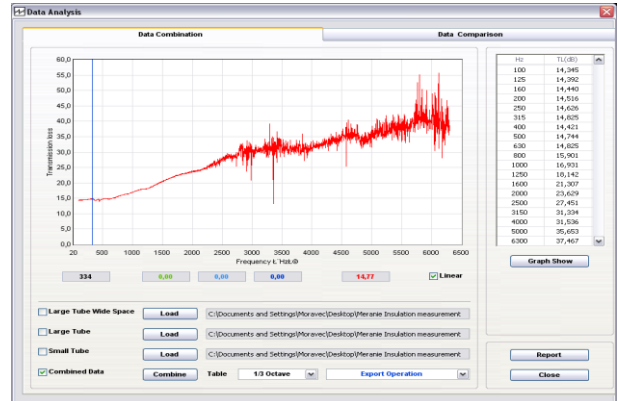
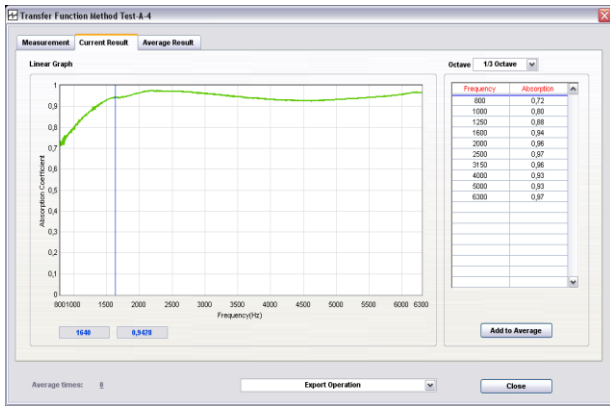
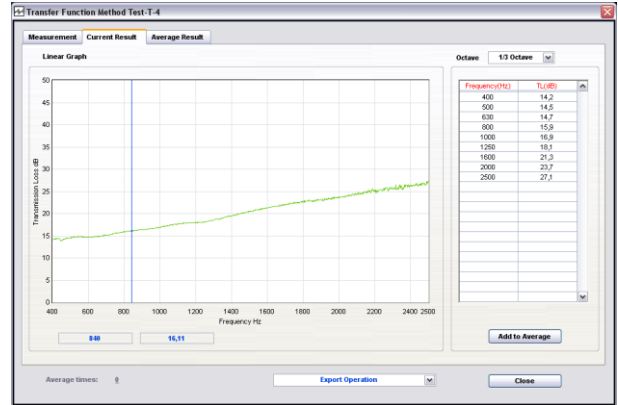
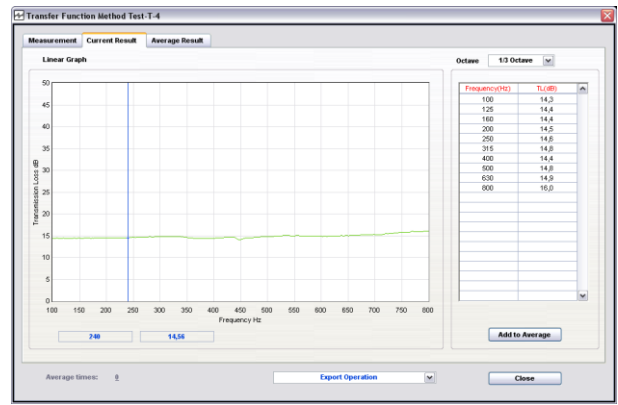
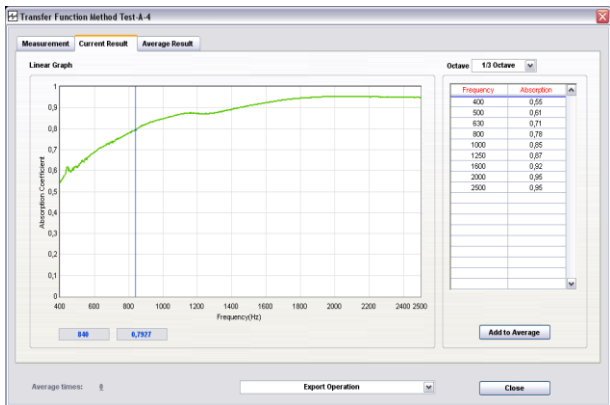


Fig. 11. Display of the sound absorption coefficient for a three-layer material, composed of 2 cm thick Ekomolitan positioned closer to the sound source and of 2 cm thick Nobasil and of 2 cm thick recycled rubber positioned at the end

Fig. 12. Display of the transmission loss for a three-layer material, composed of 2 cm thick Ekomolitan positioned closer to the sound source and of 2 cm thick Nobasil and of 2 cm thick recycled rubber positioned at the end

Frequency f [Hz]	Sound absorption coefficient α [-]						Transmission loss TL [dB]					
	Recycled rubber + Ekomolitan + Nobasil	Recycled rubber + Nobasil + Ekomolitan	Nobasil + Recycled rubber + Ekomolitan	Ekomolitan + Recycled rubber + Nobasil	Ekomolitan + Nobasil + Recycled rubber	Nobasil + Ekomolitan + Recycled rubber	Recycled rubber + Ekomolitan + Nobasil	Recycled rubber + Nobasil + Ekomolitan	Nobasil + Recycled rubber + Ekomolitan	Ekomolitan + Recycled rubber + Nobasil	Ekomolitan + Nobasil + Recycled rubber	Nobasil + Ekomolitan + Recycled rubber
500	0,786	0,622	0,469	0,716	0,624	0,505	15,845	14,816	15,324	15,086	14,744	15,375
630	0,715	0,673	0,495	0,741	0,704	0,551	17,060	14,991	15,450	15,642	14,825	16,075
800	0,609	0,649	0,479	0,693	0,777	0,567	19,336	16,151	16,526	16,893	15,901	17,932
1000	0,515	0,612	0,506	0,672	0,841	0,648	21,458	18,201	18,101	16,220	16,931	17,652
1250	0,445	0,549	0,625	0,689	0,872	0,628	21,515	16,690	15,048	17,916	18,142	21,949
1600	0,381	0,472	0,718	0,779	0,931	0,654	25,195	21,604	20,000	20,140	21,307	24,455

Table 1. The values of the materials with thickness of 6 cm

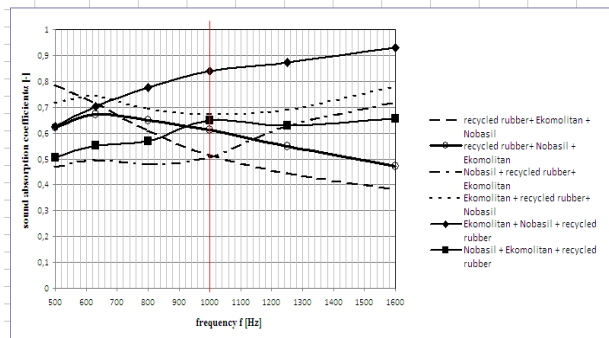


Fig. 13. Sound absorption coefficient of three-layer sandwiches (total thickness of the sandwiches: 6 cm)

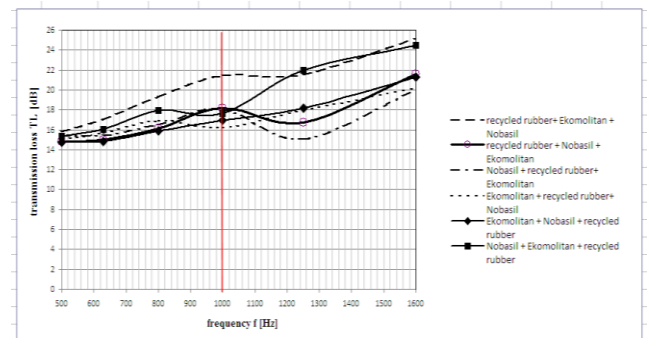


Fig. 14. Transmission loss of three-layer sandwiches (total thickness of the sandwiches: 6 cm)

It follows from the measured values of the sound absorption coefficient of the sandwich absorbers that the sequence of individual layers (of utilized materials) is of crucial importance. The sequence of the sandwich layers of the measured materials, starting from the noise source (for the frequency of 1000 Hz), is recommended as follows:

- Ekomolitan + Nobasil + recycled rubber.

It can be stated on the basis of the measured values of transmission loss of the sandwich absorbers (Fig. 14.) that the sequence of individual layers of materials utilized in the sandwich is also of crucial importance.

The sequence of the sandwich layers of the measured materials utilized for three-layer sandwiches, starting from the noise source, is recommended as follows:

- Recycled rubber + Ekomolitan + Nobasil.

ACKNOWLEDGEMENT

This paper has been prepared on the basis of the research project KEGA 049 TUKE 4/2012

6. REFERENCES

- [1] Badida, M., Lumnitzer, E., Bartko, L.: *Možnosti znižovania dopravného hluku*. Košice: Elfa, 2011. 303 s. ISBN 978-80-8086-181-0.
- [2] Badida, M., Lumnitzer, E., Fiľo, M., Biľová, M.: *Determination of the uncertainties of noise measurements*. In: Annals of the Oradea University: Faculty of management and technological engineering. Vol. 7, 2008. p. 64-72. ISSN 1583-0691.
- [3] Badida, M., Lumnitzer, E., Romanová, M.: *The application of recycled materials for products that provide noise reduction in living and working environment*. In: Acta Acoustica United with Acoustic. Vol. 92. Stuttgart: Hirzel Verlag, 2006. p. 108. ISSN 1610-1928.
- [4] Lumnitzer, E., Badida, M., Liptai, P.: *Využitie recyklantov z autovrakov pri návrhu protihlukových opatrení v lomoch*. In: TOP 2010: technika ochrany prostredia, 15-17.jún 2010, Častá – Papiernička, Bratislava. s. 251-256. ISBN 978-80-970438-0-3.

- [5] Matel, F., Ochocová, R., Badida, M., Lumnitzer, E.: *Kompaktné prvky z gumárenského recyklátu vyrobené technológiou mikrovlnného ohrevu*. Úrad Priemyselného Vlastníctva SR, Banská Bystrica, 2003.
- [6] Nebergová, K.: *Ekologické aspekty dopravy*. Praha: ČVUT, 2005. 163 s. ISBN 80-01-003131-4.
- [7] STN EN ISO 10534-1: 1996, *Akustika. Určovanie koeficienta zvukovej pohltivosti a akustickej impedancie v impedančných trubiciach*. Časť 1: Metóda použitia stojatej vlny.
- [8] STN EN ISO 10534-2: 1998, *Akustika. Určovanie koeficienta zvukovej pohltivosti a akustickej impedancie v impedančných trubiciach*. Časť 2: Metóda transformačnej funkcie.
- [9] STN ISO 10847: 2000, *Akustika. Stanovenie vložného útlmu vonkajších protihlukových bariér všetkých typov na mieste trvalého uloženia* (in situ).
- [10] STN EN 1793-1: 1997, *Zariadenia na zníženie hluku z cestnej dopravy. Skúšobné metódy určovania akustických vlastností*. Časť 1: Určenie zvukovej pohltivosti.
- [11] STN EN 1793-2: 1997, *Zariadenia na zníženie hluku z cestnej dopravy. Skúšobné metódy určovania akustických vlastností*. Časť 2: Určenie vzduchovej nepriezvučnosti.
- [12] STN EN 1793-3: 1997, *Zariadenia na zníženie hluku z cestnej dopravy. Skúšobné metódy určovania akustických vlastností*. Časť 3: Normalizované spektrum dopravného hluku.
- [13] Nariadenie vlády SR č. 115/2006 Z. z., o minimálnych zdravotných a bezpečnostných požiadavkách na ochranu zamestnancov pred rizikami súvisiacimi s expozíciou hluku.
- [14] Nariadenie vlády SR č. 339/2006 Z. z., ktorým sa ustanovujú podrobnosti o prípustných hodnotách hluku, infrazvuku a vibrácií a o požiadavkách na objektivizáciu hluku, infrazvuku a vibrácií.
- [15] Smernica Rady EÚ zo 6. februára 1970 o aproximácii právnych predpisov členských štátov o prípustnej hladine hluku a o výfukových systémoch motorových vozidiel. [online] [cit 2010-11-21]. Dostupné na internete: <http://eur-lex.europa.eu/LexUriServ/LexUriServ.do?uri=CELEX:31970L0157:sk:NOT>
- [16] Ministerstvo dopravy, pôšt a telekomunikácií SR. Použitie, kvalita a systém hodnotenia protihlukových stien. Účinnosť od: 01-12-2006. [online] [cit 2011-02-01]. Dostupné na internete: http://www.telecom.gov.sk/files/doprava/dopinfracesinfra/tech_predpisy/2006/tp_08_2006_.pdf
- [17] Bartko, L., Vargová, J.: *Zásady navrhovania a materiály vhodné pre konštrukciu protihlukových stien*. In: Ekológia a environmentalistika : zborník príspevkov doktorandov zo 7. Študentskej vedeckej konferencie : 24. mája 2010, Zvolen. Zvolen : TU, 2010. s. 21-27. ISBN 978-80-228-2111-7.
- [18] Bartko, L., Vargová, J.: *Analýza prístupov ku konštrukčnému a materiálóvemu riešeniu protihlukových stien*. In: Ochrana životného prostredia pred hlukom : zborník z odborného seminára: Hodnotenie kvality prostredia 2010 : zborník z konferencie : 1. ročník odborného seminára a konferencie s medzinárodnou účasťou : zborník príspevkov : 22.-23. september 2010, Košice. Košice : TU, SjF, 2010. s. 138-143. ISBN 978-80-553-0489-2.

Authors: Dr.h.c. prof. Ing. Miroslav Badida, PhD., Ing. Ladislav Bartko, PhD., doc. Ing. Ružena Králiková, PhD., doc. Ing. Lýdia Sobotová, PhD.
 Technical University of Košice,
 Faculty of Mechanical Engineering,
 Department of Environmentalistics,
 Park Komenského 5, 040 02 Košice,
 Slovakia
 Phone: +421 55 602-2716.
 E-mail: miroslav.badida@tuke.sk
ladislav.bartko@tuke.sk
ruzena.kralikova@tuke.sk
lydia.sobotova@tuke.sk

Dzoganova, Z., Badida, M.

IMPACT ASSESSMENT OF MECHANICAL PROPERTIES OF DEGRADED PET BOTTLES IN ENVIRONMENTAL DEGRADATION OF HIGHER TEMPERATURE

Abstract: Plastic bottles are one of the most common packing materials in market. Plastic bottles are mainly made from polyethylene terephthalate and called as PET bottles. PET has great abrasion resistance, chemical resistance, weather resistance, degradation and is dimensionally stable and therefore is widely used for production fibers and foils. For experiments, two types of plastic bottles were selected from which were made some samples and were taken into high temperature artificial environmental degradation. After the exposition time the samples were taken out from environment degradation. To find out how the mechanical properties of PET bottles were changed the tensile test where were defined certain parameters was made.

Key words: PET bottles, degradation, mechanical properties

1. INTRODUCTION

Nowadays plastics are one of the most used materials in industry. The knowledge of the positive plastics properties are the main reason of customers about their great interest. The main plastics characteristic is good qualities of versatile use and cost availability. There is the question, which is concerned by the behavior of these substances in the environment. By influence of time and external conditions during the life of polymers there is unintentional but irreversible change of their structure and properties. These changes are termed like aging, degradation, corrupting, corrosion or breach [1], [2].

Plastics degradation (aging) is defined like a file of physical and chemical process ongoing into plastics and leading gradually to irreversible changes of their properties. Plastic degradation is divided into natural and artificial degradation. Natural degradation is understood as slow going change of plastics properties by action of the light, air, carbon dioxide and the water. These changes limit second use of product and finally make it impossible. In the most cases a plastic aging is manifested by yellowing and fragility. The cause of deteriorating of plastics properties and truncating their life is physical, physical-chemical and chemical influence of environment and also the biological degradation of polymers. The degradation of plastic in the artificial conditions is called as artificial degradation [3], [4].

Degradation is usually limited by life of product. The life of material is possible to define as the time during which important properties are practically kept on the level which is enough for right product function. It depends on materials and conditions of product use. The self-degradation of polymers can take place in the cause of exposition of polymers surface to sunlight, temperature, cold, chemical compounds or microorganisms for example. The polymer surface can be broken by diffusion of external environment into polymer. This polymer can react with the environment. Because of these reactions products diffusion can

occurs at polymers surface or they can be released in the environment [5], [6], [7].

The thermal degradation is the special way of plastics degradation which is caused by thermal impact on selected polymer. The polymers are very sensitive to heat. The sensitivity is due to low strength of covalent bonds which create the polymer structure. The effect of increased temperature to the polymers can be seen in two ways. The first one is the softening of polymer or increasing the kinetic energy from received heat up to overcoming the attractive forces and after that the polymer behaves as a liquid. The second one is the structure change of polymer. Some polymers are broken down into low molecular products or into monomers without chemical change of structure – they depolymerize [5], [8], [9].

2. MATERIALS AND METHODS

In experiments the plastics bottles mainly made from PET material were used. For production of test samples two types of used plastics bottles with different thickness and color were chosen. First group obtains transparent bottles with thickness about 0,16 mm (marked like white PET) and second group obtains colored green PET bottles with thickness about 0,27 mm (marked like green PET). From PET bottles the test samples in size 200 x 20 mm in 5 pieces were made by shearing, in different environment and exposition, in hot environment and cold environment.

Natural environment – test samples were saved in laboratory before test in test conditions, by the temperature 20 ± 2 °C. Five test samples were exposed to environment with low temperature for winter environment simulation.

For simulation of environment in summer the test samples were exposed to the environment with higher temperature. The test samples were positioned in oven and exposed to temperature 50 ± 2 °C for 7, 14 and 21 days (168, 336 and 504 hours). This temperature was measured by contactless method using the type of pyrometer IRtec MicroRay HVAC – Fig. 1. After

above mentioned periods of days of exposition the static tensile test was made to test the materials.



Fig. 1 The pyrometer IRtec MicroRay HVAC

The main test to determine the mechanical properties – tensile test was chosen from spectrum of different tests. Experiments were proceeded under standard for finding tensile properties of plastics STN EN ISO 527-1 (64 0605). Tensile test was performed by tensile test machine TIRA – test 2300 – Fig. 2.



Fig. 2 The tensile test machine – TIRA test 2300



Fig. 3 The course of tensile test

Every test sample from natural environment and after selecting from degradation environment was caught in jaw of tensile machine and by speed of transom in 20 mm/min it was tested until breaking. It was on mind by catching then axis of test sample was the same as tensile direction. On Fig. 3 is shown the sample in jaw of tensile machine during tensile test.

After breaking of test sample, the machine evaluated strength characteristics (yield strength, tensile strength and relative extension) using program.

3. RESULTS FROM EXPERIMENTS

3.1 Natural environment

Measured and calculated values of tensile test – yield strength (σ_Y), tensile strength (σ_M) and relative extension (ϵ_M) – from natural environment are given on Fig. 4 to Fig. 6.

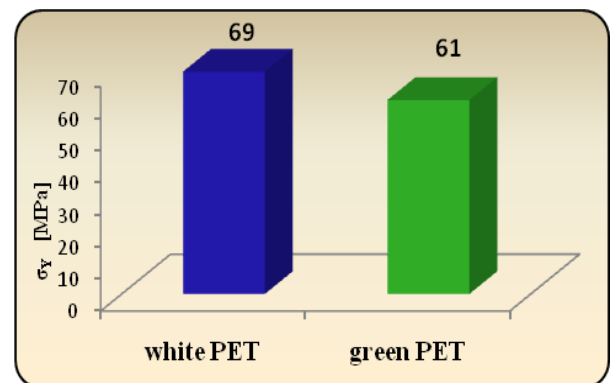


Fig. 4 The average values σ_Y of tested samples in natural environment

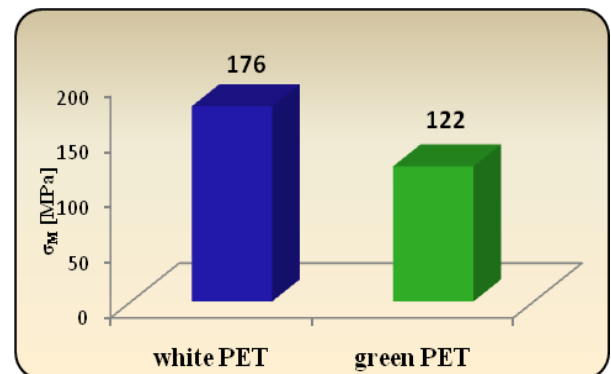


Fig. 5 The average values σ_M of tested samples in natural environment

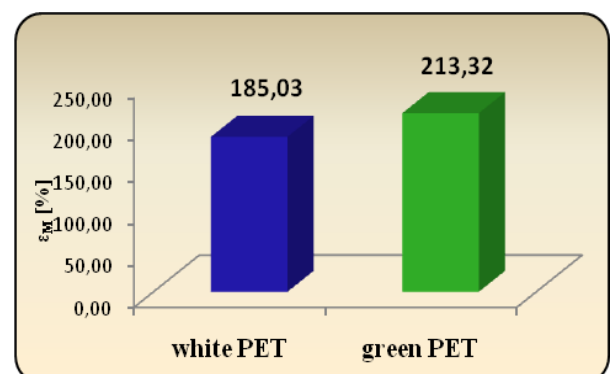


Fig. 6 The average values ϵ_M of tested samples in natural environment

The breach of tested sample from natural environment and the detail of breach after performed tensile test on this material are shown on Fig. 7 and Fig. 8.

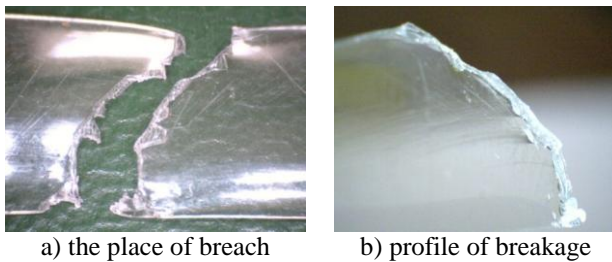


Fig. 7 The breach of tested sample white PET in natural environment

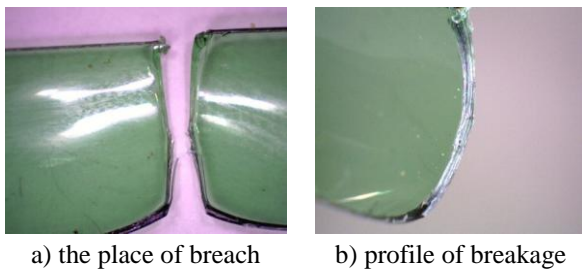


Fig. 8 The breach of tested sample green PET in natural environment

3.2 Discussion

After experimental test for determination of tensile properties of tested materials from natural environment next conclusions were drawn:

- The yield strength value of green PET material has slightly decreasing tendency against white PET material, about 10.30 %.
- The tensile strength value of green PET material is about 30.70 % lower than white PET material.
- The relative extension value of green PET material was about 13.30 % higher values than white PET material.

3.3 Environment of higher temperature

The measured and calculated values from tensile test – yield strength (σ_Y), tensile strength (σ_M) and relative extension (ϵ_M) – from environment of higher temperature are given on Fig. 9 to Fig. 11.

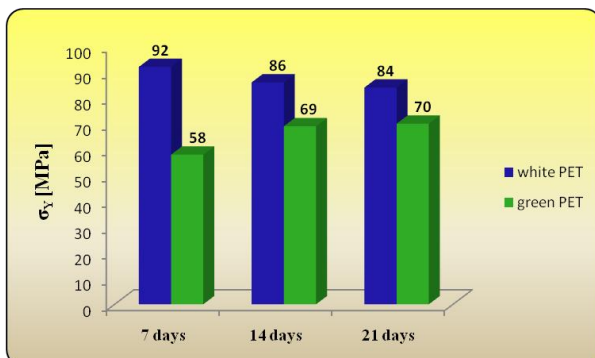


Fig. 9 The average values σ_Y of tested samples in environment of higher temperature

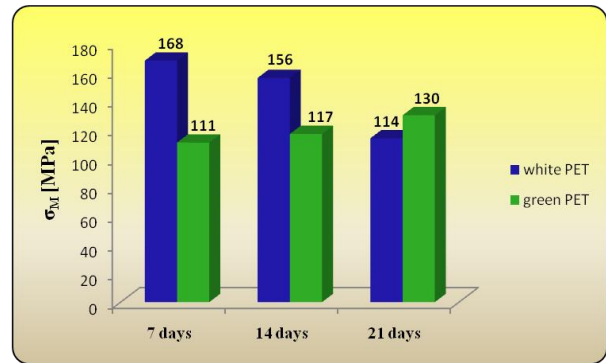


Fig. 10 The average values σ_M of tested samples in environment of higher temperature



Fig. 11 The average values ϵ_M of tested samples in environment of higher temperature

The breach of tested sample from environment with higher temperature and the detail of breach after done tensile test on this material are shown on Fig. 12 and Fig. 13.

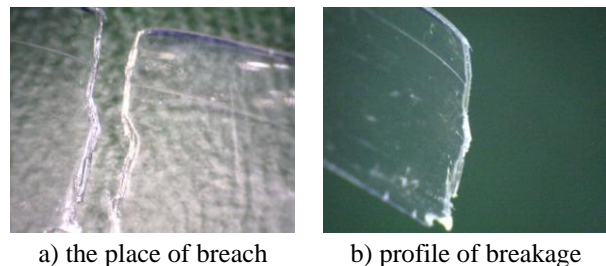


Fig. 12 The breach of tested sample white PET in environment of higher temperature

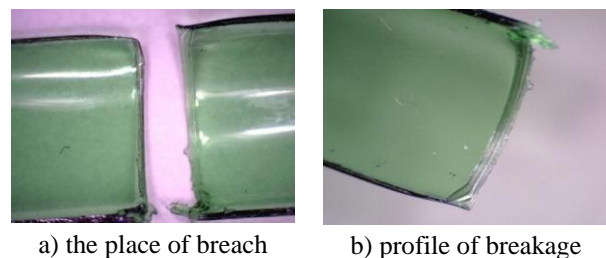


Fig. 13 The breach of tested sample green PET in environment of higher temperature

3.4 Discussion

After experimental test for determination of tensile properties of tested materials from environment with higher temperature next conclusions were drawn:

PET material – white:

- The yield strength value of exposed material to higher temperature was about 6.5 % lower after 14 days of exposition; and after 21 days of exposition was about 8.7 % lower in comparing with the measured value after 7 days of exposition.
- The tensile strength value of exposed material to higher temperature after 14 days of exposition was about 7.1 % lower; and after 21 days of exposition was about 32.1 % lower in comparing with the measured value after 7 days of exposition.
- The relative extension value of exposed material to higher temperature after 14 days of exposition was about 3.1 % lower; and after 21 days of exposition was about 32.4 % lower in comparing with the measured value after 7 days of exposition.

PET material – green:

- The yield strength value of exposed material to higher temperature was about 19 % higher after 14 days of exposition; and after 21 days of exposition was about 20,7 % higher in comparing with the measured value after 7 days of exposition.
- The tensile strength value of exposed material to higher temperature after 14 days of exposition was about 5,4 % higher; and after 21 days of exposition was about 17,1 % higher in comparing with the measured value after 7 days of exposition.
- The relative extension value of exposed material to higher temperature after 14 days of exposition was about 31,1 % higher; and after 21 days of exposition was about 46,7 % higher in comparing with the measured value after 7 days of exposition.

4. CONCLUSION

The tested samples of both PET material types show interesting mechanical properties. While white PET material exposed to higher temperature show decrease of the values of mechanical properties with increasing time of exposition, green PET material exposed to higher temperature show increase of the values of mechanical properties with increasing time of exposition.

As we know recycling is processing of used materials into new products to prevent waste generation of potentially useful materials. It saves raw materials and also energy needed to produce new products. Under this results we can state that these materials are possible to recycle again because they do not show negative deterioration of mechanical properties of tested materials.

5. ACKNOWLEDGEMENT

This paper has been prepared on the basis of the research project KEGA 049TUKE-4/2012.

6. REFERENCES

- [1] Mark, Herman F.: *Encyclopedia of polymer science and technology: Degradation to magnetic polymers*. Jacqueline I. Kroschwitz; Dean Gonzales. Canada: John Wiley and Sons, 2003. 735. A John Wiley and Sons, Inc., Publication; sv. 12
- [2] Kniewald, Dušan et al.: *Náuka o plastoch*. Košice : TU-SJF, 2007. 244 s. ISBN 978-80-8073-815-0.
- [3] Dulebová, Eudmila – Greškovič, František: *Vplyv plnív na vybrané vlastnosti plastov používaných v elektrotechnickom priemysle*. In: Transfer inovácií. roč.14, (2009), s. 172. Online: <<http://www.sjf.tuke.sk/transferinovacii/pages/archiv/transfer/14-2009/pdf/172-176.pdf>>
- [4] Kruliš, Z. et al.: *Termoplasty v praxi*. Verlag Dashofer. Praha. 2002
- [5] Ducháček, V.: *Polymery - výroba, vlastnosti, zpracování, použití*. 2. vyd. Vysoká škola chemicko-technologická v Praze, Praha 2006. ISBN 80-7080-617-6
- [6] Honzík, Roman: *Plasty se zkrácenou životností a způsoby jejich degradace*. [cit. 2011-03-06]. Online: <<http://biom.cz/cz/odborne-clanky/plasty-se-zkracenou-zivotnosti-a-zpusoby-jejich-degradace>>. ISSN: 1801-2655
- [7] Mechanical engineering: *Degradation of Polymers*. 2006, 2007-12-04 [cit. 2011-03-06]. Online : <<http://www.me.wpi.edu/People/Sisson/Polymers/>>
- [8] Stoklasa, Karel: *Makromolekulární chemie I*. [online]. 2005 [cit. 2011-03-02]. Online : <http://vitani-prvnacku.ic.cz/podkl/Skripta_MMCH_I.pdf>
- [9] *Encyclopedia of polymer science and technology/ Degradation to magnetic polymers*. Vol. 6, 3rd ed. Hoboken: Wiley-Interscience, 2003. s. 735. ISBN 0-471-28781-4 (v. 5-8)
- [10] Badida, M. – Bosák, M. a kol.: *Recyklácia a recyklačné technológie*. TU, Košice, 2007. 623 s. ISBN 978-80-8073-946-1.

Authors: Ing. Zdenka Dzoganova, Technical University of Kosice, Faculty of Mechanical Engineering, Department of Environmentalistics, Park Komenskeho 5, 042 00 Kosice, Slovakia, Phone.: +421 55 602-2927.
E-mail: zdenka.dzoganova@tuke.sk

Dr.h.c. prof. Ing. Miroslav Badida, PhD., Technical University of Kosice, Faculty of Mechanical Engineering, Department of Environmentalistics, Park Komenskeho 5, 042 00 Kosice, Slovakia, Phone.: +421 55 602-2927, Fax: +421 55 602-2716.
E-mail: miroslav.badida@tuke.sk

Fedorčáková, M. , Šebo, J.

THE RESULTS OF APPLICATION OF WASTEWATER BY NEW DEVELOPING ELECTROLYTIC FLOTATION METHODS

Abstract: Cyanobacteria are during the summer months in stagnant water fundamental threat to water workers, vacationers who use the polluted waters and fishermen. High production of cyanobacteria adversely affects water quality and threatening aquatic animals and plants living in the affected area. We are constantly looking to improve the methods, techniques and hydrological interventions to limit this phenomenon. Paper points to the utility and availability of new developing electrolytic flotation wastewater methods for a particular case study carried out in selected Slovak site.

Key words: Electro flotation, Cyanobacteria, Stagnant Water.

1. INTRODUCTION

The occurrence of cyanobacteria in excessive standing water is a global problem. As a result of proliferation of cyanobacteria the process of eutrophication occurs, which causes excessive nutrient enrichment of water. Overgrowths of cyanobacteria create a water bloom. This blue-green algae bloom in the water affects the chemical and physical properties of water and releases dangerous toxins. These toxic substances are hazardous to human health as well as for individual dwelling organisms in the environment. Water prevents flower water, fish culture, leisure and continuing use of stagnant water.

2. DISPOSAL METHOD OF CYANOBACTERIA

Nowadays many methods for the disposal of cyanobacteria are available. Methods and techniques of disposal and removal of water by the Flower [1] are based on mechanical, chemical, biological and electrolytic principle. Mechanical equipment used to remove sediments show low efficiency and their application is expensive [2]. The chemical disposal is undesirable due to amount of chemical concentrations, as this may cause a negative impact on other organisms and its use affects [3] only a limited amount of cyanobacteria. The shortcomings of these methods eliminates the electrolytic method of disarming, whose principle is electro flotation.

3. APPLICATION METHOD ELECTRO FLOTATION WATER DISPOSAL

Electro flotation method was used for the disposal of cyanobacteria in 14 pooled samples of water from the study sites. The principle of physical-chemical process is the separation of suspended solids in the sample of the observed surface water or directly in standing water and subsequent mechanical removal, more in [4].

3.1 Description of the monitored location

Analysis and microscopic evaluation of water samples containing water blooms of Slovak Kačato Lake was carried out, located on the outskirts of Roznava, surrounded by a wooded area of deciduous

trees. The right side consists of marshy shore. There is an agricultural area under oilseed rape, on the left side. Due to the use of chemical sprays and artificial fertilizers, water quality can be affected by increased nitrogen content. The size of the water body is 0.3 hectares and a depth is 4 m. A spring is springing near the pond inlet to the water body. Outflow from the pond inlet flows into the left-hand tributary of Slana River. The river Čremošná. Fauna is consisted mainly of carp, frogs, as well as wild ducks. The pond is used as a fishing ground Rožňava district.

4. PROCESS ELECTRO FLOTATION

To conduct the experiment based on electro flotation method, samples of the above mentioned locations were obtained. The sample is poured into a 6 l glass jar. In the containers were placed electrodes, 10 x 10 cm with a distance of 10 mm, necessary for the conduction of electro flotation. The electrodes were connected to the battery Progress 20, the voltage was set at 24 V, and the effective charging current was on average 10 to 15 A. Contaminated water was placed between the electrodes.

The effect of current implied a dissolving anode, which is formed due to coagulation agent, which gradually was mixed with contaminated water. Electro flotation was carried out within a period of 15 minutes. During the measurements to monitor the emergence of floating bubbles generated on the surface of samples and subsequent deposition on the surface fleet.

Accumulated fleet from surface samples was collected mechanically. After realization of electro flotation sample was taken and the water just after the application of electrolysis is also sampled fleet. Water without fleets showed the clarity with pinkish tinge



Fig.1. Illustrate process electro flotation

Battery	Description
Manufacturer	HELVI
Model	Progress 20
Voltage	230 V 50/60 Hz
Battery voltage	12 – 24 V
Dimensions	280x285x470 mm
Mass	12,2 kg

Table 1. Description of battery Progress 20

5. MICROSCOPIC ANALYSIS AND EVALUATION

The samples were subjected to microscopic analysis in the laboratory at the Technical University in Kosice, Department of Environmental Science. Microscopic analysis also looked at the content of suspended solids during the whole measurement.

The analysis showed a positive effect of electro flotation. After the removal of the mechanical sedimentary fleet near the water clear, pinkish color was seen. This phenomenon was caused due to rusty electrodes. However, no threat to water quality after flotation was observed. Water (Fig. 2) showed the occurrence of cyanobacteria, which created the fleet, and despite the effect of electro flotation method the micro life has survived without signs of damage.

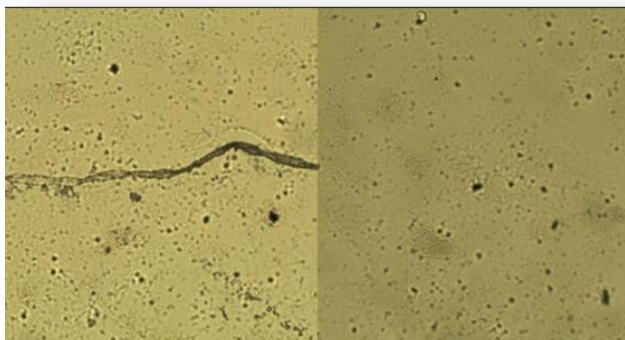


Fig. 2. Images of water samples by electro flotation, observed under the microscope

The method of electro flotation is constantly under development. It looks different proportions and design of electrolytic devices for the most efficient elimination of cyanobacteria, which while not harming other organisms.

The main advantages of using electro flotation methods include respect for the environment, harmless to other organisms, simplicity, and ease of access through the solution.

The disadvantage is power consumption needed for electrolysis, but use of solar cells could eliminate this. At this point it is not possible to comment on the life of the electrolytic device located on the surface of stagnant water, there are only estimates and carry out the experiments. Within the project "Implementation and modification of technology to reduce the occurrence of cyanobacteria in Stagnant Waters" ITMS: 26220220028, supported by the Research & Development Operational Programme funded by the ERDF, to verify the long-term operation of the plant on a large standing water.

6. SUMMARY

The problem of eutrophication is complex and specific conditions for individual lakes. Disposal of water blooms is one way to prevent damage to the environment and human health. The best available method of disposal of water flowers shows today use electro flotation wastewater in the presence of a combination of methods and other methods. The effect, which is achieved after only a few minutes of standing water in the sample taken from Lake Kačato was remarkable. Exposure to the electrodes on the sample water cyanobacteria were paralyzed and fleets in a thin layer on the surface. It can be said that electro flotation method is highly effective cleaning method of surface water by cyanobacteria, which requires the effective application of extensive polluted waters. The method of electro flotation is constantly under development.

7. REFERENCES

- [1] Komárek, J.: *Cyanoprokaryota*, Teil 1., Nachdruck, 1998, 548s., ISBN 978-3-8274-2111-1,
- [2] Holoda, E., Pistl, J.: *Všeobecná mikrobiológia a genetika mikroorganizmov*. Praktické cvičenia, Katedra mikrobiológie a imunológie UVL, Košice, 2001, 161s., ISBN 978-80-889-8562-4, (in Slovak),
- [3] Vysoká škola báňská – Technická univerzita Ostrava. *Ekologické aspekty. Metódy obnovy eutrofizovaných nádrží*. [online] [cit 2012-02-20]. Dostupné na internete: <http://hgf10.vsb.cz/546/Ekologicke%20aspekt%20y/cviceni/cviceni_lenticky/obnovy_eutro_nadrzi.htm>, (in Czech),
- [4] Fedorčáková, M., Šebo, J., Malega, P.: *Koncept implementácie technológie na znižovanie výskytu siníc*, 2010. In: *Trendy a inovatívne prístupy v podnikových procesoch* : 13: Košice, december 2010. - Košice : TU, S'JF, 2010. - ISBN 978-80-553-0570-7, (in Slovak),
- [5] Šebo, D., Fedorčáková, M.: *Vývoj technológie na znižovanie eutrofizácie stojatých vôd*, 2010. In: *TOP 2010 : Technika ochrany prostredia : zborník prednášok* : 15.-17. jún 2010, Častá - Papiernička. - Bratislava : STU, 2010 S. 365-368. - ISBN 978-80-970438-0-3, (in Slovak),
- [6] Nariadenie vlády SR č. 242/1993 Z. z., ktorým sa ustanovujú ukazovatele prípustného stupňa znečistenia vôd, (in Slovak),
- [7] Sinice – vodné cyanobaktérie. *Zneškodňovanie siníc*. [online] [cit 2012-01-11]. Dostupné na internete: <<http://sinice.webnode.sk/zneskodnovanie-sinic/>>, (in Slovak),
- [8] Slovenská agentúra životného prostredia. Odborná organizácia Ministerstva životného prostredia SR. *Metódy sanácie vôd ex situ*. [online] [cit 2012-02-25]. Dostupné na internete: <<http://charon.sazp.sk/Envirozataze/AtlasSanMetod/Jar/default.htm?url=WordDocuments%2Fflotcia.htm>>, (in Slovak),
- [9] Centre for ecological sciences. *Energy. Limnology*. [online] [cit 2012-02-20]. Dostupné na internete: <<http://ces.iisc.ernet.in/energy/monograph1/Limpage4.html>>.

Authors: Ing. Monika Fedorčáková, PhD., Ing. Juraj Šebo, PhD., Technical University of Kosice, Faculty of Engineering, Park Komenského 5, 040 01 Kosice, Slovakia
E-mail: monika.fedorcakova@tuke.sk;
juraj.sebo@tuke.sk;

Georgiadis, P.

DYNAMIC DECISION SUPPORT SYSTEM FOR PLANNING AND CONTROL IN CLOSED-LOOP RECYCLING NETWORKS

Abstract: Closed-loop recycling networks (CLRN) have been an area of increasing attention during the last decade in real-world and in academia. In Europe, the recycling industry was encouraged to reuse recycled waste materials as the basic raw material, under the objectives of European Union's Sixth Environment Action Programme 2002-2012. These economical and ecological trends, have promoted the necessity of integrating management issues into CLRN. Such an approach is presented in this paper which integrates strategic capacity and inventory management aspects into a system dynamics (SD) model of a single producer CLRN and provides a decision support system for planning and control.

Key words: Closed-loop recycling networks; System Dynamics; Dynamic decision support system

1. INTRODUCTION

Efforts for waste reduction have promoted the necessity of integrating forward and reverse supply chains into closed-loop networks [1, 2]. Closed-loop recycling networks (CLRN), in particular, are typical networks for material recovery. According to the latest data, in Europe the recycling industry within EU-27 countries exhibited a significant increase in the yearly volume trade of waste between 2002 and 2010: from 20.87 to 37.57 million tons for paper and board waste; from 2.97 to 4.2 for glass waste; and from 2.26 to 7.71 for plastic waste [3]. These trends have promoted the need for holistic modeling approaches which facilitate the integration of management issues into CLRN [4]. Fig.1 exhibits a very generic description of such a CLRN. Capacity planning and inventory management, both in the reverse channel and in the forward channel of *Recycling Loop 1*, are important strategic issues that restrict the flows of reusable materials and of original products. In particular, the producers face the challenging problem of adapting their capacity and the level of inventories in an effort to increase the total supply chain profit. Such decisions are quite simple in a steady-state situation. However, in an uncertain business environment, such as the reverse channel

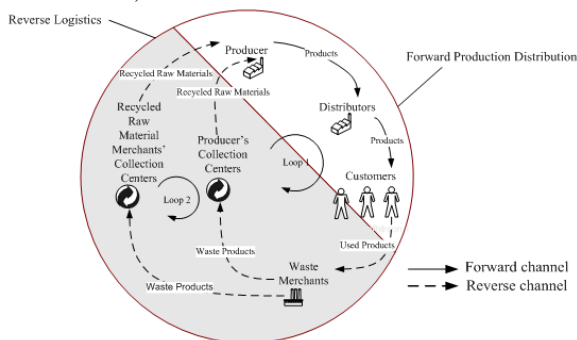


Fig. 1. Closed-loop structure of Recycling Networks

which is characterized by uncertainty in volumes, timing and quality of end-of-use product returns, the decision making process is important to be supported by a modelling approach, which has the ability to evaluate the

long-term profitability, taking into consideration the dynamics of stocks and flows that exist in the recycling loop [5]. Such an approach is presented in this paper. The approach is based on the Theory of System Dynamics (SD) and is presented by using data from a Greek paper producer with recycling activities at a regional level.

2. THE DYNAMIC MODEL

2.1. Generic stocks and flows diagram

Stocks and flows, along with feedback loops, are the two central concepts of SD theory. Stocks are the accumulations (e.g. inventories) of the inflows (e.g. production rate) and the outflows (e.g. shipments) of a system. The structure of a system in SD methodology is captured by linking the stock and flow structure with feedback mechanisms and is represented by stock and flow diagrams [6].

A SD CLRN model can be viewed as consisting of two interconnected networks. The first network is the material network which includes the stocks and flows of products, used products, waste products and recycled raw material exhibited in a stock and flow diagram. The second network is the information network which includes the flow of information (for example serviceable inventory level in end products) through the actors involved in the recycling loop (producer, distributors, customers, waste merchants and recycled raw material merchants). The two networks interact via a set of decision rules which control the material flows. The analytical presentation of the two interconnected networks and of control rules cannot be given within the limited paper's length. However, Fig. 2 depicts the generic stocks and flows diagram of *Recycling Loop 1* shown in Fig. 1. The system is bounded to a single producer who operates collection centers, indexed by $m=1, \dots, M$, located in $m=1, \dots, M$ regions. The producer produces different types of end products indexed by $q=1, \dots, Q$, which are produced by different categories of recycled (waste) materials indexed by $n=1, \dots, N$. The percentage of material input of quality n for producing 1 item of end-product q is given by c_{nq} . Stocks are

represented by rectangles, inflows are represented by pipes pointing into (adding to) the stock and outflows are represented by pipes pointing out of (subtracting from) the stock. The arrows (causal links) in stock and flow diagrams represent the relations among variables. The direction of the causal links displays the direction of the effect. Signs “+” or “-” at the upper end of the causal links exhibit the sign of the effect. When the sign is “+”, the variables change in the same direction; otherwise they change in the opposite one.

2.2 Control rules

The general form of the embedded control rules is indicatively presented in Figs.3 and 4 for the case of governing the *Production Rate* and the *Production Capacity* in the forward channel respectively. Fig. 3 represents the stock-flow structure along with the negative feedback mechanism which controls the *Serviceable Inventory*. The mechanism is based on the well-established stock management structure suggested by Sterman [6] and regulates *Production Rate*. The mathematical representation is given by the following equations (the reader must refer to Figs. for the notation).

$$SI_q^P(t) = SI_q^P(t=0) + \int_0^t [R_q^P(t) - S_q^D(t) - S_q^I(t)] dt \quad [tn] \quad (1)$$

$$R_q^P(t) = \min \left(O_q^P(t), \frac{I_1^P(t)}{dt}, \frac{I_N^P(t)}{dt} \right) \quad [tn/tu] \quad (2)$$

$$O_q^P(t) = \min E D_q(t) + AdjSI_q^P(t), C^P(t) * pca_q \quad [tn/tu] \quad (3)$$

Eq. (1) represents the stock equation for *Serviceable Inventory* (SI_q^P). By eq.(2), *Production Rate* (R_q^P) results from *Production Orders* (O_q^P), but constrained by the availability in *Inventory in Recycled Materials* (I_n^P) expressed in terms of q -type product units using the index c_{nq} . *Production Orders* (O_q^P) defined by (3), are based on a decision rule which combines the *Expected Demand* ($E(D_q)$) with an adjustment (*Serviceable Inventory*

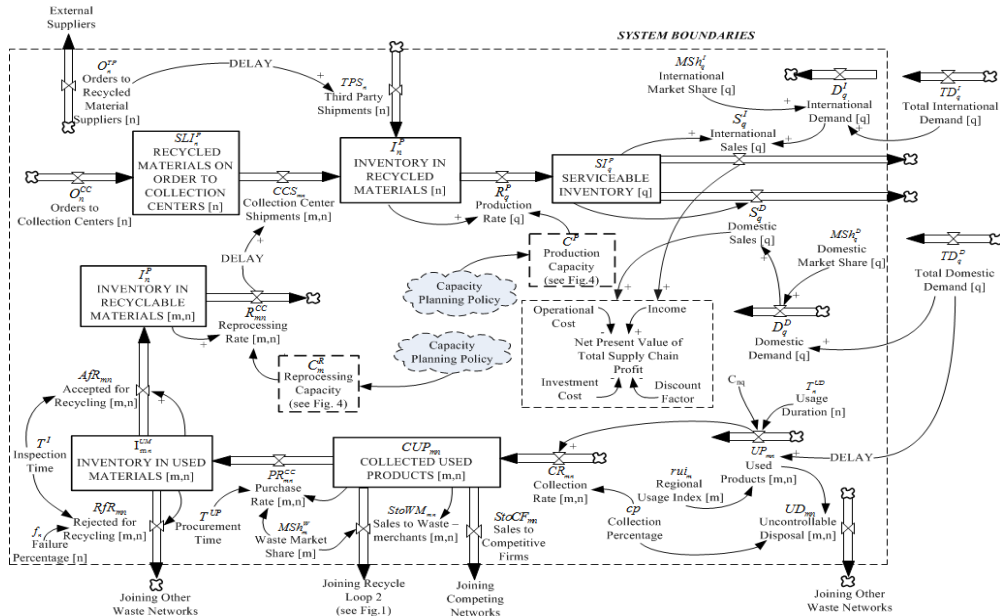


Fig. 2. Generic stocks and flows diagram of Recycling Loop 1. System boundaries reflect a single-producer CLRN.

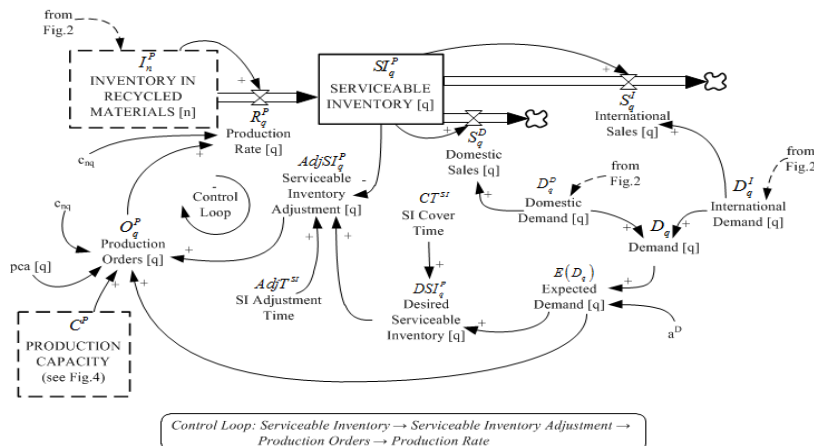


Fig. 3. Control rule for *Serviceable Inventory*; CT^{SI} and $AdjT^{SI}$ are control parameters.

Adjustment_q ($AdjSI_q^P$) that brings the Serviceable Inventory_q (SI_q^P) in line with its desired value (Desired Serviceable Inventory_q (DSI_q^P)):

$$AdjSI_q^P(t) = \frac{DSI_q^P(t) - SI_q^P(t)}{AdjT^{SI}} \quad [tn/tu] \quad (4)$$

$$DSI_q^P(t) = E(D_q(t)) * CT^{SI} \quad [tn/tu] \quad (5)$$

where, $AdjT^{SI}$ (*SI Adjustment Time*) represents how quickly the producer decides to close the gap between the desired and the actual inventory level and CT^{SI} (*SI Cover Time*) is the base stock expressed in time units.

Production Orders_q (O_q^P) are limited by the Production Capacity (C^P); based on historical data, the assignment of capacity in producing each q -type product is expressed in percentage (pca_q). Expected Demand_q ($E(D_q)$) in (3) is a forecasted value for firm's demand (sum of domestic and international demand), calculated from a first-order exponential smoothing of Demand_q (D_q) with parameter a^D , implying a smoothing coefficient of $1/a^D$:

$$E D_q(t) = E(D_q(t-dt)) + \frac{1}{a^D} [D_q(t) - E(D_q(t))] dt \quad [tn/tu] \quad (6)$$

In a similar way Figure 4 represents the rule for controlling the Production Capacity (the mathematical equations are not provided for brevity). The rule is based on the anchoring and adjustment heuristic approach [6] and its extensions [5]. Capacity (C) is reviewed periodically every P time units, after which a decision is made whether to invest on capacity or not and to what extent. Capacity expansion decisions, i.e. new additional investments on capacity, are determined by using a closed-loop controller. In particular, the model continuously evaluates the Discrepancy ($Disc$) between the desired (*Desired Capacity* (DC)) and the actual level of Capacity (C). This discrepancy reflects the system's error in actual capacity. *Desired Capacity* is the driving force for capacity planning. The source of input information to *Desired Capacity* is the forecasted values of Demand_q (D_q), for the case of capacity planning in the production line. For the case of collection centers, *Desired Capacity* is linked to the forecasted values of materials Accepted for Recycling_{mn} (AfR_{mn}) (see Fig.2). Based on the system's error the controller dictates Capacity Expansion Rate ($C_ExpRate$) as a pulse change in actual capacity, in strategic time periods of integer multiples of P . This input pulse reflects an expansion decision in capacity and consequently, determines the rate of change of capacity towards the desired value. Naturally, the capacity adjustment involves long delays for capacity acquisition (contracts with suppliers, transportation, installation, labor training) creating a supply line of capacity on order. The Capacity Adding Rate ($C_AddRate$) captures this delay (T) and is determined by delaying the values of Capacity Expansion Rate ($C_ExpRate$) using a third-order delay function with average delay time T . Finally, Capacity (C) is increased by capacity acquisition and is decreased by Capacity Discarding Rate ($C_DiscRate$). The latter is defined by the Average Lifetime ($AvgLife$) of capacity.

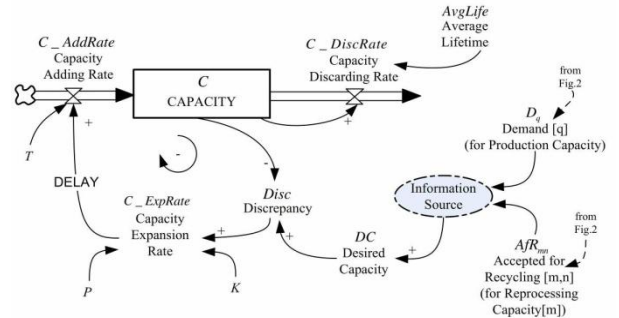


Fig. 4. Strategic capacity planning control mechanism; P and K are control parameters.

3. DYNAMIC DECISION SUPPORT SYSTEM

The presented SD model includes the following types of system parameters that may be tuned to reproduce the behavior of a specific recycling network:

- Physical parameters, which depend on product and operational characteristics;
- Operational parameters that describe inventory control policies; and
- Smoothing parameters used in forecasting through exponential smoothing.

The control parameters which fully describe the capacity planning policies are P^P , K^P (in production line) and P_m^R ,

K_m^R (in each m collection centre), while the control parameters for the management of serviceable inventories are $AdjSI_q^P$ and CT^{SI} . By assigning specific values to the system and control parameters, and by running the model using the simulation software PowerSim 2.5[®], we obtain the dynamics of stocks and flows during the planning horizon. Since the dynamic behavior may be used to evaluate the performance of a specific capacity planning policy, the SD model can be viewed as a strategic decision support system for the conduct of various "what-if" scenario analyses. This capability is discussed in the following section.

4. THE CASE OF PAPER RECYCLING: DYNAMIC ANALYSIS AND RESULTS

4.1 Case description

A Greek paper-mill located in southern Greece produces board paper (packaging paper from 100% recycled waste-paper). Board paper production line produces four types of products; $Q=4$, ($q=1$ [Testliner]; $q=2$ [Corrugating medium]; $q=3$ [Gray paper board]; $q=4$ [Duplex board]). The producer mainly satisfies domestic demand and exports to Turkey and Bulgaria. Backlog in customer orders is not permitted (i.e. unfilled orders are lost). Eight categories of waste-paper are used in the recycling operation; $N=8$, $n=1$ [Brown-A]; $n=2$ [Brown-B]; $n=3$ [Gray-paper]; $n=4$ [Mixed-paper]; $n=5$ [Newsprints]; $n=6$ [Kraft]; $n=7$ [White-paper 3A]; $n=8$ [White-paper 2A]. The producer operates three collection centers, located in three regions ($M=3$) of southern Greece. At each collection center, waste-paper is inspected, sorted to n categories and compressed. The compressed n categories of waste-paper are then transported to the paper-mill. The producer imports

compressed waste-paper from Bulgaria and Turkey, but at a higher cost, when its inventory in waste-paper is below the desired safety stock.

4.2 Strategic Capacity Planning

We use the SD model in conjunction with an optimum-seeking grid search procedure to determine the near-optimal values of control variables that describe the capacity planning policies. These values maximize the net present value (NPV) of total supply chain profit. The procedure revealed that the policy $P_B: [K^P=0.5, P^P=10 \text{ years}; K_m^R=1.5, P_m^R=1 \text{ year } \forall m]$ maximizes the NPV of total supply chain. The proposed capacity planning policy dictates the following:

i) Capacity planning in the production line (paper-mill): The capacity must be reviewed every $P^P=10$ years and at this point the magnitude of capacity expansion equals to the observed discrepancy between the desired and the actual level of capacity multiplied by $K^P=0.5$.

ii) Capacity planning in the collection centers: The capacity at each collection center must be reviewed every $P_m^R=1$ year and the magnitude of capacity expansion equals to the observed discrepancy between the desired and the actual level of capacity multiplied by $K_m^R=1.5$.

4.3 Dynamic Behaviour

The dynamics of capacity planning, under policy P_B , are shown in Fig.5 (compression capacity is shown for the largest collection center ($m=1$)). The dynamics of total supply chain profit under policy P_B is exhibited in Fig.6. Expansion of production capacity at 10th year, results in an increase in the paper-mill's production rate. The latter dictates more aggressive expansions in the capacity of collection centers (increase of compression rate). The system seeks new states in both capacities under the effect of time delays in capacity acquisitions. During the transient period, the increased needs in compressed waste paper at the paper-mill level are satisfied by increased orders placed to external importers. This is shown in Fig.6 through the dynamics of supplies from external suppliers. Increased orders, but at a higher procurement cost, affect negatively the rate of change of NPV until the system reaches its new state.

Figure 7 displays the dynamics of Serviceable Inventory under policy P_B for different values of control parameters *Serviceable Inventory Adjustment_q* ($AdjSI_q^P$) and serviceable inventory cover time CT^{SI} (*SI Cover Time*).

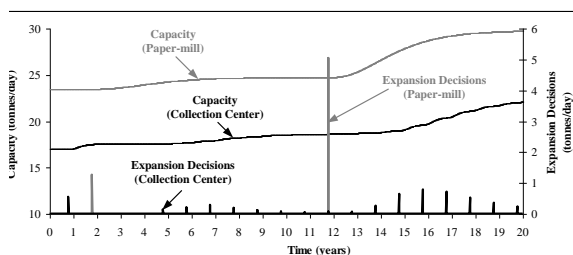


Fig. 5. Dynamics of capacity planning under best policy; $P_B: [K^P=0.5, P^P=10 \text{ years}; K_1^R=1.5, P_1^R=1 \text{ year}]$.

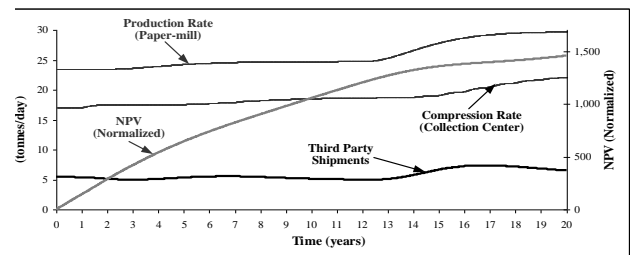
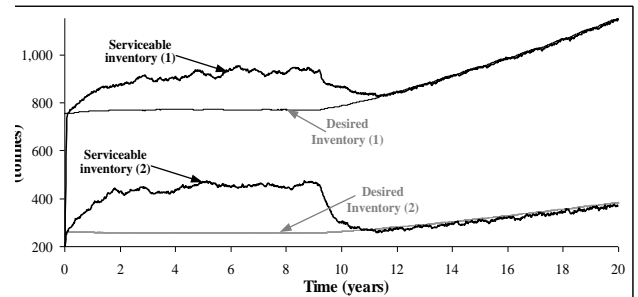


Fig. 6. Dynamic behavior of total supply chain profit under best policy; $P_B: [K^P=0.5, P^P=10 \text{ years}; K_1^R=1.5, P_1^R=1 \text{ year}]$.



- 1: [SI CoverTime=30days, Serviceable Inventory Adjustment=5 days]
- 2: SI CoverTime=10days, Serviceable Inventory Adjustment=10 days]

Fig. 7. Dynamics of Serviceable Inventory under $P_B: [K^P=0.5, P^P=10 \text{ years}; K_1^R=1.5, P_1^R=1 \text{ year}]$ and different $AdjSI_q^P$ CT^{SI} values.

5. REFERENCES

- [1] M. Fleischmann, *Quantitative Models for Reverse Logistics*, Springer, Germany, 2001.
- [2] M.A. Ilgin, S.M. Gupta, *Environmentally conscious manufacturing and product recovery (ECMPRO): A review of the state of the art*, Journal of Environmental Management, 91(3) (2010), p.p. 563-591.
- [3] Eurostat: Recycling data reporting, Available from: <http://epp.eurostat.ec.europa.eu/portal/page/portal/waste/data/wastemanagement/recycling>, Accessed June 2012.
- [4] P. Georgiadis, G. Tagaras, D. Vlachos, *Long-term Analysis of Closed-loop Supply Chains*, in: R. Dekker, M. Fleischmann, and L.N. Van Wassenhove (Eds.), *Reverse Logistics*, Springer-Verlag, 2004, pp. 313-331.
- [5] P. Georgiadis, D. Vlachos, G. Tagaras, *The impact of product lifecycle on capacity planning of closed-loop supply chains with remanufacturing*, Production Operations Management, 15(4) (2006), p.p. 514-527.
- [6] J.D. Sterman, *Business Dynamics: Systems Thinking and Modeling for a Complex World*, McGraw-Hill, New York, 2000.

Author: Assoc. Prof. Patroklos Georgiadis, Aristotle University of Thessaloniki, Department of Mechanical Engineering, Industrial Management Division, 54124 Thessaloniki, Greece, Phone.:+30 2310 996-046, Fax:+30 2310 996-018.

E-mail: geopat@auth.gr

Goletić, Š., Imamović, N.

IMPACT OF STEEL PRODUCTION TECHNOLOGY ON ENVIRONMENT

Abstract: *The technological process of steel production takes place in the converter steel plant by LD process. This process is a set of mechanical, gas-dynamic, heat, chemical, physical-chemical processes and phenomena. As the main product of this technological process is the liquid steel, this is further casting on continuous casting machine or on separate line in the ingots. Billets are further processed in rolling mills in the construction and reinforcement and ingots in the forge plant processed in forged products. As byproducts different types of solid waste, emissions of dust and gases into the air and industrial wastewaters are generated. By applying of measures for reduction of emissions and waste generation, significant reduction of environmental load is achieved and ensured recycling of industrial waste, industrial wastewater and thermal energy from emitted converter gases.*

In this paper, the dominant sources of emissions and waste production at the facility for the production of steel are presented, as well as taken measures to limit and control emissions and the effects achieved by implementation of these measures. Measures for restriction of emissions and environmental protection are defined by adjustments plan done in accordance with BAT recommendations of the European Union.

Keywords: *converter steel plant, process technology, the environment, emissions, converter gases*

1. INTRODUCTION

Steel production in Zenica has a 118-year tradition. Zenica steel mill is historically one of the largest steel manufacturers in Southern Europe. Steel is one of the most important materials used in the automotive industry, construction and other economic sectors. Global steel production has an upward trend due to increasing demand for this material even though it is recycled with a high percentage around 68% [1]. It is believed that the steel will be the main structural material in the future [2].

Steel production has a high impact on all elements of the environment due to emissions of dust and waste gases into the air, especially greenhouse gas emissions and discharges of wastewater and water environment pollution, waste generation and noise and more. In some parts of the world, these impacts are well managed, in many others are not. Thus, in Zenica the effects of steel production activities on the environment are expressed due to many years' of high emissions that are result of inadequate implementation of necessary measures for limiting and control an emission that is environment protection [2].

Steel plants today have many opportunities to comply production with stricter requirements for the preservation of environmental quality. In this way they can respond effectively to the challenges of stringent requirements for sustainable development. So many leaders in the steel industry, as in other sectors are beginning to adapt their procedures to reduce environmental emissions and negative impacts on the environment, and improve its business image. They have initiated voluntary projects for emissions reduction and environmental protection. Best available techniques and eco-design are effective means of achieving that goal. Zenica steel plant is on the track of the realization of this goal, which is defined in the plan

of adjustment. The implementation of projects defined in this plan have already achieved high results in the reduction of emissions of dust into the air and water, reduce waste generation and noise, etc. The goal is to harmonize this steel plant with European environmental standards and BAT by 2015, which is a very ambitious goal for inherited poor environmental practices and the lack of effective measures for environment protection [2].

2. PROCESS OF STEEL PRODUCTION

Production of steel in BOF steel plant in Zenica is done by Linz-Donawits procedure (LD process) in the two convertors of the total designed capacity of 1.1 million t / y steel of different assortment. The products range under the current conditions is low carbon steel, and production of high carbon steel is planned. Current production is significantly reduced due to the global economic crisis and lower demand for steel and it is about 650,000 t / y of steel.

Production of steel in the converter takes place by blowing of pure oxygen ($wO_2 = 99.99\%$) through liquid pig iron, which is causing burning of carbon and phosphorus. The process is discontinuous and takes place through the following technological stages:

- Charging (scrap metal, flux, liquid pig iron),
- oxidative refining by oxygen blowing (de-carbonization and removal of impurities),
- control of heat status after blowing (carbon, temperature),
- second oxygen blow, if necessary,
- tapping of steel and de-oxidation in the ladle, and then casting on continuous casting machines or in ingots,

- tapping of slag and converter lining control and preparation for the next heat.

Converter charge is normally consists of 80-85% liquid metal and 20-15% steel scrap, and non-metallic additives (lime, bauxite, iron ore) which are added to form the slag. The steel scrap and nonmetallic additives are first charged, and than liquid iron. Liquid iron is delivered from the blast furnace in the transport ladle capacity of 140t and stored in the mixer from where can be taken for charging of new heat in the converter. Upon completion of the charging, in converter is performed the oxidative refining of metals by oxygen blowing and heating of metal without the heat from the outside, on account of the physical heat of liquid pig iron and heat exothermic chemical reaction. Oxygen is blowing through the high pressure water cooled lance tube, that leading to strong mixing of the heat. During the process of blowing oxygen, in converter are occurred very strong reactions to the oxidation of impurities with generation of large amounts of gas. Gaseous CO and SO_x output from the heat, a hard volatile P₂O₅ SiO₂ in addition of CaO is separate in the form of slag. Ladle gases are composed predominantly of CO, with a high temperature (about 1200-1600°C) and carry a large amount of dust. Therefore, converter gas prior to discharge into the atmosphere must pass through the treatment, which an aim is to utilize physical and chemical heat of gas and dust removal.

The purpose of the oxygen converter process is oxidation of impurities from the metallic charge and heating of steel heat up to the tapping temperatures. The process of oxidation in the converter is achieved by:

- reducing the carbon content in the prescribed level (from ≈ 4% to <1%, often much lower),
- set of useful content (alloying) elements,
- removal of harmful impurities in the lower level through the slag or gas converter.

Upon completion of oxidation and achieving of requested quality parameters, heat is tapping from the converter. During tapping of heat into ladle the needed de-oxidation and alloying agents are added (secondary metallurgy). The resulting de-oxidation products mainly are in the slag but one part, in the form of non-metallic inclusions, still remain in the steel after solidification. Liquid steel after its produced is being transported for further processing.

From converter steel plants the large quantities of dust are generated during charging and tapping of liquid iron, scrap and non-metallic additives charging, oxygen blowing as well as steel and slag tapping. Technological steel production scheme in the converter, with an indication of the main sources of emissions into the environment, is shown in Fig. 1.

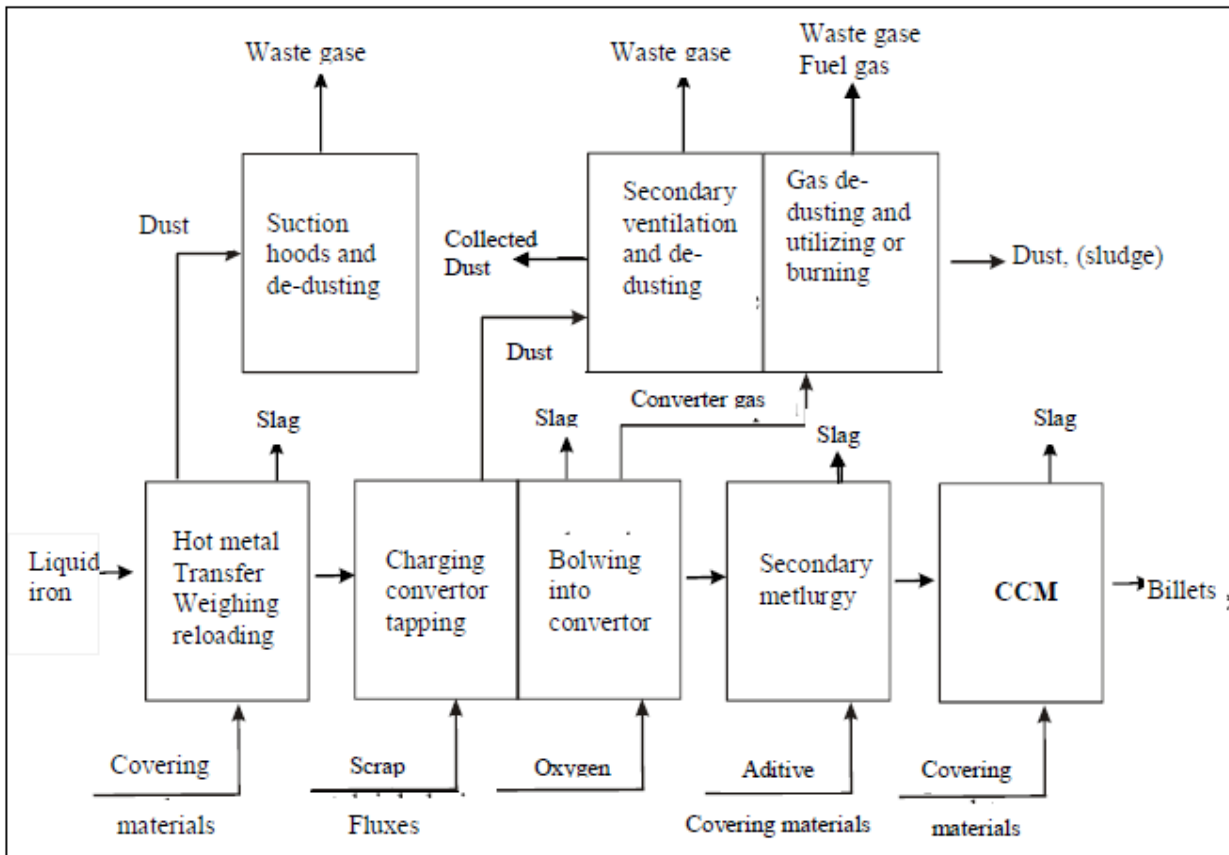


Fig. 1. Technological scheme of production of steel in the converter and the sources of emissions into the environment

3. EMISSION SOURCES AND ENVIRONMENTAL PROTECTION MEASURES

Steel plants present the great polluters of the environment and the burden all elements of the environment (air, water, soil, etc.). In particular it is considered that the steel plants are the major source of CO₂ emissions and thereby contribute to global climate change. The emission of pollutants occurs in all stages of technological and steelmaking operations. Places of emissions and waste generation are shown in simplified block diagram (Fig.1).

Air emissions are from numerous sources, as:

- convertor dust and converter gases,
- dust from mixers,
- dust from handling non-metallic additives and alloys,
- waste gases from addition heating of waste heat boilers ,
- flue gases from the ore drying furnace,
- flue gases from steam super heaters,
- flue gases from the filter sludge drying furnace (DHD),
- flue gases from the furnace for drying and preheating ladles and tundishes,
- uncontrolled emissions from the bays and the handling area [3].

BOF gases contain the most of CO (55-80%), and a large amount of dust (consisting of metal oxides, including oxides of heavy metals). Content of SO₂ and NO_x, PCDD/F and PAH is relatively low. Gas temperature at the converter exit reach up to 1600°C, and therefore gases have to pass through the waste heat boiler to produce technological steam that can be used for technology needs during steel production or in other technological processes in the Plant.

In order to minimize and control dust emissions in convertor gas, it is cleaned in wet technical cleaning system that is consist of a scrubber for rough dust, venture tube system and scrubber for fine dust. Gases that are cleaned of dust and cooled are extracting by exhauster and through the chimney release into the atmosphere. Collected dust with water are discharged from the dust cleaning system and transported into the system for wastewater treatment and then again using the same process. Sludge from the treatment system is dried in a rotary drying furnace that used blast furnace gas for heating. Flue gases and dust from the furnace passes through a wet de-dusting system before being release through the chimney into the atmosphere. Muddy water is returned to the settling basins. Dried converter dust is transported on sinter plant.

Dust emissions measurement after technical system for cleaning of converter gases is performed continuously and the average value is 39.5 mg/Nm³, which is lower than the limit value of 50 mg/Nm³. For de-dusting of mixer's gases in late 2011 the very efficient bag filter system was installed whose efficiency is 99.8%. Emission of dust behind this filter is 20 mg/Nm³ which is significantly lower than the limit value of 50 mg/Nm³.

In the process of steel production the large quantities of process water is used for cooling of technological equipment and wet de-dusting of gases. Process waters are in closed systems. Water for facilities cooling are in a clean closed system, and water for wet de-dusting the waste gases are in so called dirty closed system. Water in clean cycle (cooling the converter oxygen lance and mold cooling on continuous casting machine), after performing a function cooled and send back into the process. Dirty water cycle (wet purification of gases and the secondary cooling in continuous caster) after purification on DHD and DSD system are again returned to the process. Wastewater treatment system has such solution that allows the settling of suspended particles in the two radial thickeners, cooling fan coolers, separation of sludge in a rotary vacuum filters and pressuring of cooling water by centrifugal pumps. Deposition of suspended solids is increased by flocculants dosing, and stabilization of water and maintain the pH value is achieved by additional chemical treatment with hydrated lime.

The sewage is only discharged waste water from the filter furnace for drying ore and bauxite, part of the water for equipment cooling, and waste water during de-sludge of wastewater cleaning system. The waste waters are discharged in the Bosnia River thru sewage system. The quantity of wastewater is estimated to be about 45 m³ / t of steel [3,4].

The industrial wastewaters from BOF Steel plant comply to the request from Regulation regarding conditions for discharging of wastewaters into natural recipient or public sewage system (Gazette F B&H NO.4/12) as per all tested parameter beside concentration of suspend matters and pH that are higher from allowed limit values.

Water management plan request further reduction of water using, increase of amount of water in the close systems, reduction of emissions into water and more efficient cleaning of wastewaters that are discharged into sewage system and further in River Bosnia, to be able to comply with all given criteria for effluent quality.

Monitoring results of wastewater from April 2012 are given in Table 1.

The Steel Plant great quantity of solid waste, including:

- converter slag (110 kg/t steel),
- ladle slag (39,8 kg/t steel),
- slag from mixers,
- refractory waste (19 kg/t steel),
- converter dust (6 kg/t steel),
- dust from mixers,
- dust from handling non-metallic additives and alloys a,
- Scrap metal (various types of skulls, remains from the continuous casting, continuous casting of burn-out) - 42 kg/t steel and others. [3,4]

Related to the mentioned solid waste, steel production in BOF Steel plant present the closed system because all technological waste is processed in secondary raw materials and used ether in operational plant of the Plant or delivered to the other business

subjects as raw material for the production of cement, construction materials, artificial fertilizers, etc. There is very small amount of waste that ends on an industrial

dump yard. This shows that the principles of cleaner technology are applied in this Steel Plant, which is the ultimate goal of this company.

Parameters	Method of testing	Limit value	The test results
Flow (m ³ /dan)	ISO 748	-	7923
Temperature (°C)	BAS DIN 38404-4:2010	30	27,6
pH value	ISO 10523	6,5 – 9,0	9,4
Electrical conductivity (µS/cm)	ISO 7888	-	421
Washed rest of the 105 °C (mg/l)	BAS DIN 38409-1:2010	-	412
Volatile matter in 550 °C (mg/l)	BAS DIN 38409-1:2010	-	92
Total suspended solids	ISO 11923	35	282
Alkalinity (mg/l)	ISO 9963-1	-	106
COD-Cr (mgO ₂ /l)	ISO 6060	125	8
BOD5 (mgO ₂ /l)	ISO 5815-1/ISO 5815-2	25	3
Total N (mg/l)	-	15	1,4
NH ₄ -N (mg/l)	ISO 7150	10	0,3
NO ₃ -N (mg/l)	ISO 7890-3	10	0,3
NO ₂ -N (mg/l)	ISO 2918	-	<0,005
Total P	ISO 6878	2,0	0,10
Chloride (mg/l)	ISO 9297	250	21
Sulfate (mg/l)	ISO 10304	200	82,2
Toxicity Test with Daph.magna (%)	ISO 6341	50	85
Fe (mg/l)	ISO 6332	2,0	0,09
Mn (mg/l)	ISO 6333	1,0	0,009
Zn (mg/l)	ISO 8288	2,0	0,02
Total Cr	ISO 9174	0,5	0,001
Cu (mg/l)	ISO 8288	0,5	0,009
Ni (mg/l)	ISO 8288	0,5	0,001
Pb (mg/l)	ISO 6333	0,5	0,013
Cd (mg/l)	ISO 5961	0,1	0,001

Table 1. Monitoring results of BOF wastewater, April 2012

4. CONCLUSIONS

Steel production in Zenica was designed and largely operates on the principle of cleaner technologies that allow rational use of raw materials, energy and water, and limiting air and water emissions and waste production within the BAT recommendations and emission standards. Many projects for reduction of emissions and environmental protection are implemented, which achieved significant effects on reducing the environmental load. It is planned implementation of several strategic projects, which by the end of 2015 need to ensure the reduction of emissions below the given limit values, and the overall utilization of industrial waste, as well as thermal energy from converter gases for production of process steam.

5. REFERENCES

- [1] World Steel Association. Steel statistical yearbook 2008. Brussels: World Steel Udruga. See also: [http://www.worldsteel.org/pictures/publicationfiles/SSY2008\[1\].pdf](http://www.worldsteel.org/pictures/publicationfiles/SSY2008[1].pdf); 2009.
- [2] Gojić, M., Črnko, J., Kožuh, S.: *Production of Steels in 20th Century*, Kemija u industriji, 7/8; 317-328

- [3] Goletić, Š., et al.: *Plan aktivnosti sa mjerama i rokovima za postupno smanjenje emisija odnosno zagađenja i za usaglašavanje sa najboljom raspoloživom tehnikom za BOF Čeličanu*, Univerzitet u Zenici, 2007.

- [4] Goletić, Š.: *Zaštita okoliša kod pokretanja integralne proizvodnje u ArcelorMittal Zenica*. VII Naučno-stručni simpozijum sa međunarodnim učešćem "Metalni i nemetalni materijali" (proizvodnja-osobine-primjena), Ed. Fuad Begovac, Zenica, 7 (1): 639-644; 2008.

Authors: Dr.sc. Šefket Goletić, Mr.sc. Nusret Imamović, University of Zenica, Faculty of Mechanical Engineering, Fakultetska 1, 72000 Zenica, Bosnia and Herzegovina, Phone: +387 32 449-124
E-mail: goletic@mf.unze.ba; nimamovic@mf.unze.ba

Hroncová, E., Ladomerský, J.

MODEL FOR EVALUATION OF CO-COMBUSTION OF COMPOSTED SEWAGE SLUDGE

Abstract: Sewage sludge as a waste is problematic regarding its utilization. Because of high water content, sludge combustion is not very attractive. Improvement of energy balance can be achieved by production of compost for energetic utilization (CEU). The principle of energy balance improvement is in combined composting of sewage sludge with other compostable organic material. It appears to be economically advantageous to use CEU as a fuel in energy producing combustion devices instead of combustion in waste incineration plants. According to contemporary air protection legislation, CEU is classified as a waste when used as a fuel. We propose an objective model for evaluation of emissions from co-combustion of co-composted sewage sludge in the wood fired boiler or wood-coal co-combustion fired grate boiler, based on the real emission measurement. The results of emission measurements and waste analysis will clearly show if it would be possible, according to air protection legislation requirements, to burn co-composted sewage sludge in wood fired boilers, and what secondary measures (flue gas treatment) should be taken.

Key words: model, sewage sludge, compost, co-combustion, emissions

1. INTRODUCTION

Sewage sludge is one of the wastes which production is increasing. Landfill disposal of organic wastes, including sewage sludge, is not allowed or is being systematically reduced in developed countries. Application to the soil is problematic because of the risk of contamination, therefore often rejected by agriculture [1]. Main methods of sewage sludge utilization are co-combustion, co-incineration, or incineration [2]. The co-firing of pulverized coal with dried sewage sludge has demonstrated that the sewage may be milled and fired successfully as a pulverized fuel in the range 0-30, 50, 70, and 100% [3].

The interest in waste to energy utilization is very significant in developed countries [4]. Often discussed topic is the question, whether waste could be an alternative to fossil fuels, and waste energy potential is evaluated [5].

Thermogravimetric characteristics of coal and sewage sludge co-combustion are presented in paper [6]. Energy gain from sewage sludge combustion is low due to its high water and inorganic content. There is a suggested technology for improvement of energy balance of sewage sludge – production of so-called “energy-compost”, known as compost for energetic utilization (CEU). The principle of energy balance improvement is in combined composting of sewage sludge with other compostable organic material. Water content is significantly decreased in the composting process. It is relatively low-cost, which is its major advantage, compared to sewage sludge drying.

Compost for energetic utilization is a potential mixed solid fuel from biodegradable waste, produced by aerobic fermentation of selected types of waste from sewage treatment plants, agriculture, gardening, forestry, food production and processing, lumber industry, paper mills, leather and textile industry and other organic wastes. Compost for energetic utilization is dry, lumpy bulk material with granulometric

structure of mixed particles with size less than 50 mm, grey to dark colour, without any intense odour, heat of combustion 10 – 15 MJ.kg⁻¹ and ash content less than 20%. This product is stored in open storage facilities and its maximum water content is 40%. Required fuel quality should be achieved by the control of composted materials.

Wood combustion in boilers can have satisfactory emission results even when combusting industrial waste wood (e.g. from wood and wood fibre composite) in lower grade wood boilers, provided that combustion optimization is performed based on emission measurement [7, 8, 9]. Nowadays it is important to solve issues of emission control while there is an increasing intention to co-combust sewage sludge in wood fired boilers. Analysis of energy efficiency of sewage sludge combustion is well known, however influence of different processing techniques such as composting on the following combustion process is not always clear. Main attention is paid to trace elements content and emissions [10].

Primary interest is focused on co-combustion of sewage sludge with coal [11, 12]. Fluidized bed coal fired boilers are most commonly used for co-combustion of sewage sludge and other waste with coal [13]. It has been proved that all emission limits can be fulfilled except for the HCl, as long as the energy content of sewage sludge in fuel mix is below 25%. Also very little percentage of nitrogen is converted to nitrogen oxides [14].

We assume, that in case of CEU combustion, very good results could show its co-combustion with wood or other kind of combustible biomass, eventually combustion of CEU by itself in the biomass fired boilers. From the environmental point of view, we suggest a comparative analysis of environmental assets of wood combustion and bio-charcoal production [15]. The aim of this paper is to develop a model for evaluation of emissions from co-combustion of co-

composted sewage sludge in the wood fired boiler or wood-coal co-combustion fired grate boiler, based on the real emission measurement.

2. PLAN OF ANALYSIS AND EXPERIMENTS

Even though CEU is produced from biodegradable waste, according to air protection legislation it is not considered to be a fuel. Combustion of CEU should therefore be regarded as a combustion or co-combustion of waste and emissions from this combustion cannot be evaluated according to emission limits for biofuel combustion.

Main environmental problem associated with energy utilization of waste is air pollution. Second most important problem which requires environmentally acceptable solution is the residual solid waste from combustion (fly-ash, bottom ash, slag).

Only the practical experiences from co-combustion of very small fractions of sludge (ca 2 %) indicate no important problems [16]. Therefore, suitability of CEU for certain combustion device has to be confirmed in the technical aspects (optimal particle size, fuel conveyor routes, fuel dosage) as well as in the aspects of air protection during trial run for evaluation of new fuel suitability (optimization of fuel mixture composition, analysis of emissions according to waste combustion limits). The objective of the experimental plan of co-combustion of CEU is reduction of negative impact of emissions to the extent which is economically reasonably achievable. Consequent evaluation of compliance with emission regulation requirements and overall feasibility study for the co-combustion of CEU with nominal fuel – coal, wood or coal-wood mixture in the trial combustion device will be performed. Suitability of sewage sludge energy utilization in proposed way will be assessed according to combustion trial runs. In case of positive result, it will be possible to determine the extent of parameters needed to be monitored in the produced CEU from a large number of sludge's derived from different biological sewage treatment plants and the extent of emissions monitoring required.

2.1 Expected course of experiments

In the experimental device (combined pulverized coal fired boiler with grate for co-combustion of wood) pulverized brown coal will be used. The addition of CEU with wood chips will gradually increase, with the ratio of CEU ending at 100% (added alone without wood chips). This stage will take 1-2 weeks.

Energy efficiency will be determined in dependence with the increasing CEU overall mass ratio in the fuel. It will be increased from 5% to 20%, eventually 25%, 50% and 100%. The key to co-combustion are certainly technological requirements. In this stage, which will last approximately 2 weeks, technological limits to maximum ratio of CEU in the fuel will be determined. With this maximum ratio of CEU in the fuel, consequent tests for environmental acceptability of CEU and coal co-combustion will be performed.

Similarly, in the wood fired experimental device the addition of CEU will be gradually increased. This stage will be finished within 1 week.

2.2 Settings of combustion process operation

Although combustion device - boiler co-firing wood and brown coal will be combusting a new certified fuel, combustion conditions will be so strictly observed, as if a waste was co-combusted:

- Fuel composition with the regard on metals content will be regularly checked by rapid analysis method ED XRF and Hg content by rapid analysis using cold vapour inductively coupled plasma mass spectrometry. It is necessary to put special emphasis on Hg content control to assure the compliance with the limit value.
- Once every 2 weeks a sample of CEU will be collected from the storage facility. In case of exceeding limits of metals content, combustion will be interrupted, and a sample will be sent for analysis to the certified laboratory.
- 100 g of sample will be stored in deposit for preparation of mixed sample from the one year period, which will be sent so certified laboratory for analysis.
- Combustion of CEU will not be done during warm up process of the combustion device, until the temperature inside the combustion chamber reaches 850°C.
- Emission limits will be defined for co-combustion of 3 types of fuel, standard fuel has oxygen concentration reference value 6% and wood and CEU 11%. Co- combustion plant shall be designed, equipped, built and operated in such a way that the emission limit values determined according to or set out in Directive 2000/76/EC are not exceeded in the exhaust gas.
- Combustion of CEU will be terminated, if emission monitoring system would register any problems with CO or NO_x emissions, regardless the cause (even if it would not be related to co-combustion of CEU).
- Flue gas dispersion model will be elaborated, confirming the sufficient stack height for metals emission dispersion, proving it would not affect human health or environment.
- Emission measurements during combustion experiments will show the migration rate of metals from fuel to emissions and solid wastes such as bottom ash and slag. Several variants of co-combustion will be evaluated, solely wood, solely coal, coal and CEU, wood and CEU, coal wood and CEU.
- Emission measurements during combustion experiments will show the impact of co-combustion of CEU on CO, TOC (Total Organic Carbon), NO_x and SO₂ emissions.
- Emission measurements during combustion experiments will determine the maximum safe ratio of CEU in fuel from the emissions of CO, TOC, NO_x and SO₂ point of view.
- Samples of fly ash and slag will be collected during stabilized co-combustion with maximum safe ratio of CEU in fuel. Leaching tests will be performed with the 10% slag and 90% fly-ash mixture. Results will be compared with the same tests on slag and fly

ash from combustion of coal.

- At the final stage of combustion experiments, authorized emission measurement will be carried by certified laboratory during co-combustion of coal with CEU according to proposed combustion process settings. Measured emissions will be PM (particulate matter), CO, TOC, NO_x, SO₂, HCl, HF, heavy metals and dioxins.
- Samples of slag and fly-ash will be collected to be sent to leaching tests in certified laboratory.
- Technological procedure for sustainable co-combustion of coal with CEU or CEU with wood will be designed in defined conditions.
- Compliance with the limits for the heavy metals content in the one year mixed bulk sample of CEU will be a necessary condition for continuation of energy utilization of CEU for the next time period (year). This will assure that no excess heavy metals emissions would occur and no random high emissions episodes would happen.

3. CONCLUSION

In this paper we propose a model for evaluation of emissions from co-combustion of co-composted sewage sludge in the wood fired boiler or wood-coal co-combustion fired grate boiler, because these emissions cannot be assessed according to emission limits for biofuel combustion. Other combustible materials than regular fuels can be incinerated only under conditions set for waste incineration, or according to conditions set for waste and fuel co-combustion.

In general, according to current knowledge and experiences, it can be concluded that each individual case of waste combustion and alternative way of waste utilization should be assessed individually and it is not always possible to predict its environmental impact.

The results of emission measurements and waste analysis will clearly show if it would be possible, according to air protection legislation requirements, to burn co-composted sewage sludge in wood fired boilers, and what secondary measures (flue gas treatment) should be taken.

4. ACKNOWLEDGEMENTS

This work was supported by the Slovak Research and Development Agency under the contract No. APVV-0353-11.

5. REFERENCES

- [1] Antonious, G. F., Kochhar, T. S., Coolong, T.: *Yield, quality, and concentration of seven heavy metals in cabbage and broccoli grown in sewage sludge and chicken manure amended soil*, Journal of Environmental Science and Health, Part A: Toxic/Hazardous Substances and Environmental Engineering, Volume 47, Issue 13, p.p. 1955-1965, 2012.
- [2] Werther, J., Ogada, T.: *Sewage sludge combustion*, Progress in Energy and Combustion Science, Volume 25, pp. 55-116, 1999.
- [3] Morgan, D. J. and van de Kamp W. L.: *The co-firing of*

pulverised bituminous coals with straw, waste paper and municipal sewage sludge, The Journal of Combustion Science and Technology, Volume 121, p.p. 317-332, 1996.

- [4] Berenyi, E. B.: *The status of municipal waste combustion in the United States*, J. Hazard. Mater., Volume 47, No. 1-3, p.p. 1-17, 1996.
- [5] *Waste - an alternative to fossil fuels*, Eur. Power News, Vol. 22, No. 6, p. 25, 1997.
- [6] LIU Liang, et al: *Investigation on the co-combustion characteristics of coal and sewage sludge by thermogravimetric analysis*, Acta Scientiae Circumstantiae, 05/2006. http://en.cnki.com.cn/Article_en/CJFDTOTAL-HJXX200605021.htm.
- [7] Ladomerský, J.: *Emission analysis and minimization from the wood waste combustion*, Wood Research, Volume 45 (4), p.p. 33 – 44, 2000.
- [8] Ladomerský, J., Hroncová, E., Samešová, D.: *Investigation of appropriate conditions for wood wastes combustion on basis of emission*, Drewno, Volume 46, p.p. 90-98, 2003.
- [9] Ladomerský, J., Hroncová, E.: *Optimization of combustion conditions of particleboard waste from the point of emissions*, Air Protection Volume 2, p. 14 – 17, 2009.
- [10] Miller, B. B., Kandizoti, R., Dugwell, D. R.: *Trace Element Emissions from Co-combustion of Secondary Fuels with Coal: A Comparison of Bench-Scale Experimental Data with Predictions of a Thermodynamic Equilibrium Model*, Energy Fuels, Volume 16 (4), p.p. 956-963, 2002.
- [11] Leckner, B.: *Co-combustion - a summary of technology*, Thermal Science, Volume 11, Issue 4, 5-40, 2007.
- [12] Toraman, O., Y.: *Emission Characteristics of Co-combustion of Sewage Sludge with Olive Cake and Lignite Coal in a Circulating Fluidized Bed*, Journal of Environmental Science and Health, Part A: Toxic/Hazardous Substances and Environmental Engineering, Volume 39, Issue 4, p.p. 973-986, 2004.
- [13] Murakami, T. et al.: *Combustion characteristics of sewage sludge in an incineration plant for energy recovery*, Fuel Processing Technology, Volume 90, p.p. 778-783, 2009.
- [14] Leckner, B., et al: *Gaseous emissions from co-combustion of sewage sludge and coal/wood in a fluidized bed*, Fuel, Volume 83, Issues 4-5, p.p. 477-486, 2004.
- [15] Ladomerský, J., Hroncová, E., *Qualitative analysis of unusual procedures of carbon sequestration*, First World Scientific Conference - PETrA 2011, p. 6, Praha 2011.
- [16] Luts D., et al.: *Co-incineration of dried sewage sludge in coal-fired power plants: a case study*, Water Science and Technology, Volume 42, p.p. 259-268, 2000.

Authors: Ing. Emília Hroncová, PhD., Technical University in Zvolen, Faculty of Ecology and Environmental Sciences, Department of Environmental Engineering, T. G. Masaryka 24, 960 53 Zvolen, Slovakia, Phone: +421 5206 448, Fax: +421 5206 279.
E-mail: emilia.hroncova@tuzvo.sk

Prof. Mgr. Juraj Ladomerský, CSc., University of Central Europe in Skalica, Kráľovská 386/11, 909 01 Skalica, Slovakia, Phone: +421 34 664 7061, Fax: +421 34 664 7063.
E-mail: jladomersky@yahoo.co.uk

Hronec, O., Vilček, J., Adamišín, P., Andrejovský, P., Huttmanová, E.

USE OF PHRAGMITES AUSTRALIS (CAV.) TRIN AND ITS REPRODUCTION IN THE REVITALIZATION OF CONTAMINATED SOILS

Abstract: Significant resistance of *Phragmites australis* (Cav.) Trin against strongly alkalized soils was found by previous investigation, when it grows also on the grounds with pH 9.1 and produces very large biomass. Therefore we have verified the most suitable method of reproduction of this plant, both in generative and vegetative ways, including possibility of its growing on intoxicated grounds. We have found out that generative reproduction is technically more demanding and less successful, on the contrary, vegetative reproduction showed statistically significant results.

Key words: imission, alkalization, magnesium, fertilizing of soils, *Phragmites australis*

1. INTRODUCTION

Slovak republic is a country extremely rich in the natural crystal magnesite. Manufacture of the magnesite sinters by thermic disintegration and sintering operation belongs among dust technologies. Two factories process magnesite raw material in the middle of Slovakia in the region of the towns Jelsava and Lubenik namely:

SMZ Jelsava a.s., and Slovmag Lubenik a.s. Magnesium oxide, which alkalizes 12,000 ha of agricultural and 6,600 ha of forest soils, issues into the atmosphere during manufacturing process. The place of the interest is characterized by high oversaturation of the soils with magnesium where pH is 8-9 and higher. Neither practice nor science have known magnesitephilic plants still, which would be able to draw off macrobiotic element from the soil by accumulation of magnesium in above-ground parts. Magnesium immissions causes a lot of unfavorable effects to the soil, vegetation and animals. This manifests through the less productive and economic results. The sites, where in past the fall of solid reduction was higher than 20 g.m⁻² showed disintegration of original phytocoenose in 30 days and only several resistant kinds were left, which are of very low importance as to production, agriculture, forest growing and aesthetic point of view. The root system of these plants is very weak, reaching the depth only 30-40 mm and they cannot protect soils sufficiently against the erosion [1,2,3,4,5,6,7].

By calcinations of the magnesite in rotary and shaft furnaces solid and vapor waste products originate, which are ejected into the atmosphere and hence to the soil. They cause alkalization of the soil as well chemical and mineralogical changes are originated: pH value is changed (above 8), macronutrient ratio is changed, biologic value and quality of humus is reduced, the soil erosion is increased, reception of phosphorus and microelements in the soil is reduced, the seeds of the nonresistant kinds cannot germinate, therefore reduction of free grown plants occurs.

Long-term observation and investigation showed,

that in this contaminated area was *Phragmites australis* (Cav.) Trin appeared in last years, which is originally humid plant, but in this area it grows literally in dry sites, where ground water is in the depth of several meters. Striking vitality of *Phragmites australis* (Cav.) Trin was found, as mega-population in more sites, where the pH value reached pH = 9.1 and in such sites, where it does not occur and according to the published statements its presentation was not recorded in the past [5]. It is hopeful, dominant, resistant, anti-erosive and technically available kind providing alternative solution of sanitation and fertilization of alkalized soils. Productivity and physiological relationship supporting this fact is discussed in works [8,9,10,11,12,13,14].

Therefore we have established the aim to verify different methods of *Phragmites australis* (Cav.) Trin reproduction with possibility of its using for broadcast fertilization of excessively contaminated soils with the magnesite.

2. MATERIAL AND METHODS

Phragmites australis belongs to the family *Poaceae*, genus *Phragmites*. *Phragmites australis* occurs in two forms: S = terrestrial form. V = littoral form. Terrestrial ecoform occurs in the marginal parts of the pond, where is minimum fluctuation of ground water and respectable humus substratum. Littoral form is flooded by regular water with fluctuant water column from 20-90 mm. The substratum is sandy-loamy with low content of the organic sediments.

The cultivation and reproduction of *Phragmites australis* in the greenhouse and field conditions was realized in the greenhouse of the Secondary Training Centre of Agriculture in Stitnik and field experiment was realized in the site of the soil devastated by magnesium immission in Jelsava in the immission area of exhalation sources. These methods of reproduction have been verified.

2.1 Vegetative reproduction

Green cuttings reproduction

Green vegetative cuttings of *Phragmites australis* were removed from the individual sites during five different terms from 9th to 25th May 2002. The segments were cut by the scissors, only matured stolons were chosen, from which part in the length of 30-40 mm from the top was cut and immediately put into the prepared bucket full of water. Green stalks were removed in five terms: the 1st term: 9th May, the 2nd term: 1st May, 3rd term: 12th May, 4th term: 17th May, 5th term: 25th May.

Top green cutting reproduction

- in water solution
- in prepared composition in pot and seed box

The cuttings of *Phragmites australis* were processed on the day of their removal. The possibility of two methods of top green cutting reproduction was verified. The segments were cut from the top in length 300 mm, close (5 mm) under the node in slanting cut by budding knife. The segments cut in this way were dipped into the stimulator - STUMULAX - I and poked into the prepared box in 30 x 30 mm spacing. The box contained a composition of the soil (peat) mixed with sand in 1: 1. The bottle we full with ratio water from the pond and stimulator at the knife-point was added. The cuttings prepared in the same way as for the seed box were put into the bottle and covered with the plastic bag.

Middle green cutting with one node from the stalk reproduction

- in prepared composition in pot,
- in prepared composition in reproduction seed boxes.

This method of reproduction was from the middle green cutting of the *Phragmites australis*. Smaller segments were cut from the brought segments. The process was as follows: From the segment in the length of 300-400 mm was cut in lower part close under the node in slanting cut by budding knife and above the node in the height of 60-80 mm in straight cut. The component part of such cutting was a stalk and a part of the leaf. From one 300-400 mm cutting were removed 1-2 pieces of such segments, the top parts were not used as they were not matured enough. The stalk segments prepared by this method were dipped into the stimulator and poked into the prepared composition (sand and compost) in the pots with 180 mm in diameter and in the boxes 80 mm deep to the depth of 40 mm.

Root segment (rhizome) reproduction

Shallow grown roots of the *Phragmites australis* in the above mentioned sites under the surface of the soil were pulled from the soil by the above ground parts in the length of 0.5 to 1 m and were cut. These ones containing the top bud were cut with one node, the others were cut with two nodes. Root segments prepared by this method were planted into the prepared composition in the pots. The top cuttings were placed with vegetative top of the root 10 mm above the soil

surface and the middle root segments with two nodes were placed in horizontal position in the prepared pots in the depth of 50-60 mm above the root.

2.2 Generative reproduction

Seed reproduction of the *Phragmites australis*

Summitas was isolated in two terms: the 1st term 20th October 2001, the 2nd term 15th November 2002. The seeds from the summitas were stripped by the comb and together with the glumes were sown on 20th January 2002 in the boxes with the composition (compost soil, sand), covered with 10 mm layer of the soil and put into the greenhouse with temperature 20°C. Grown plants 30 mm high with 2-3 leaves were planted in the boxes in 4 x 20 mm spacing since April and when they reached the height about 100 mm and had 3-4 leaves they were replanted in the pots with 120 nun in diameter.

Preparation of the location (or the planting)

For the planting of the pre cultivated plants the area 250 m southern from SMZ Jelsava, near the Muráň river was chosen. The area with the acreage 10 x 20 m was demarcated and it was enclosed with the wooden fence. At the beginning of June the sad was removed from one half of the location. The samples of the soil were taken and the results are presented in the Tab 2. The pH value (pH/KCl) was 8.1. The content of the magnesium in the soil was 2988 mg.kg⁻¹.

Planting of the *Phragmites australis*

Phragmites australis was planted on 22nd June 2002, at the day temperature of 31 °C from 9:00 am to 1:00 pm. The method was as follows: The holes deep 150 mm were digged and about 2 liters of water was poured there. *Phragmites australis* with the root ball was digged and planted into the holes in 600 x 600 mm spacing.

The care after planting on the site

Young plants after planting (because of the high temperatures in July and August) were regularly watered. Weeding preparation Roundup was applied in September. The new overgrows of *Phragmites australis* obtained by root segment reproduction were established in 2003. The plants were evaluated during the vegetation (number of growths, internodes, leaves on the plants in 2002 - 2003). The measurements were done in regular intervals. The measurements were continued in 2004 and acquired values 2002-2004 were evaluated and they are shown in the tables.

The investigation of *Phragmites australis* was realized in 2002-2004. During each year several measurements were done, which is shown in the tables. The height of the plant, number of growths and number of leaves was measured. For the analysis itself, the results of two comparable seasons were used (interannual ± 6 days):

- the 1st summer measurement (22nd July 2002, 20th July 2003, 25th July 2004)
- the 2nd summer measurement (30th August 2002, 2nd Sept. 2003, 5th Sept. 2004)

The comparison and the measurement took place

in 64 localities, whilst the plants in the localities 1-32 were sown from the seeds and the plants in the localities 33-64 were from the root segments.

The sites (localities), from which seeds and vegetative parts were removed for the verification of the most suitable method of *Phragmites australis* reproduction occurs near the factories Slovmag Lubenik and SMZ Jelsava.

Statistical evaluation of the results

The following methods for statistical evaluation of the results were used: index analysis, correlation analysis and hypothesis testing.

The interannual changes of the method of reproduction (vegetative, generative) were investigated by the index analysis. The correlation analysis was used for finding out the dependability among the height of the plant, the number of the growths and the number of the leaves of the plant for all plants together and for individual methods of reproduction particularly as well. At the hypothesis testing we were concentrated on the testing of the equality of the average value above presented parameters of the plants (the height of the plant, the number of the growths and the number of leaves) obtained generatively and vegetatively.

3. RESULTS AND DISCUSSION

The occurrence of *Phragmites australis* under the dry conditions against its appearance in the wetlands with the still water was the impulse for the verification of *Phragmites australis* reproduction in these localities. Several methods of *Phragmites australis* reproduction were tested, namely vegetative and generative. The samples were taken from the described localities. The cultivation of the plants was realized on the contaminated soil in the distance of 250 m southern from the factory SMZ Jelsava. The soil samples showed pH 8.1 determined electrometric and the content of permissible nutrients 67 mg P.kg⁻¹ of the soil according to Egner, 62 mg K.kg⁻¹ of the soil according to Schaschabel and 2986 mg.kg⁻¹ of the soil by method AAS in leach according to Schaschabel. The seeds for the seeding were taken in September 2001 from the free grown plants. The seeding was realized under the greenhouse conditions in spring 2002. The results achieved at vegetative and generative reproduction were noticed in the tables.

In 2003 the growth and the development of the plants in the testing locality was observed under the field conditions from the seeds sown in 2002 as well as the growth and the development of the plants cultivated from the root segments (rhizoma) planted in 2002. The new overgrows in the test location were established from the root segments planted in 2003. During the vegetation the number of plants, the growths, the number of internodes and the number of the leaves on the highest plant was measured. Phenological investigation of the place of the interest continued. The original plant kind representation was confirmed.

In 2004 the measurement during vegetation period in the overgrow planted in 2002 continued. The results

of the measurements during 2002-2004 were statistically evaluated.

1 st summer measurement (22/07/2002, 20/07/2003, 25/07/2004)			
		2003/ 2002	2004/ 2003
from seed	height in mm	2.399	1.036
	leaves number	1.257	1.121
	growths number	1.927	1.148
vegetative	height in mm	2.195	1.051
	leaves number	1.105	1.107
	growths number	1.830	1.147
total	height in mm	2.288	1.043
	leaves number	1.179	1.114
	growths number	1.876	1.147
2 nd summer measurement (30/08/2002, 2/09/2003, 5/09/2004)			
		2003/ 2002	2004/ 2003
from seed	height in mm	2.442	1.093
	leaves number	1.573	1.062
	growths number	1.930	1.083
vegetative	height in mm	2.191	1.113
	leaves number	1.363	1.072
	growths number	1.958	1.095
total	height in mm	2.309	1.103
	leaves number	1.463	1.067
	growths number	1.944	1.032

Table 1. Interannual changes of the observed signs

The highest index accumulation was noticed in 2003, i.e. one year after seeding. At the first or the second comparative measurement in 2003 the plants grew in average about 128.8%, or about 130.9 % more than in 2002. The more significant accumulation of the total height in mm was at the plants from the seed (139.9%, or 144.2 %), than at the plants from the root segments (119.5 %, or 119.1 %). The change of the plant height in 2004 in comparison to 2003 was less significant - increasing of 4.3 %, or 10.3 %, whilst lower dynamic at the first summer measurement was noticed at the plants from the seed -3.6 % increasing in comparison to 5.1 % at the plants from the root segments, at the second summer measurement 11.3 % increasing of the plants from the root segments in comparison to 9.3% increasing of the plants from the seed.

The similar process - higher increasing in 2003, lower in 2004 was noticed at the observed parameter "leaves number". In 2003 the number of leaves increased in 17.9 % at the first measurement, or 46.3 % at the second one. In 2004 the increase of leaves number was 11.4 %, or 6.7 %. The higher increase of the leaves number was noticed at the plants from the seed (25.7 % and 57.3 % at the measurements in 2003 and 12.1 % and 6.2 % at the measurements in 2004) in comparison to the plants from the root segment (10.5 % and 36.3 % at the measurements in 2003 and 10.7 % and 7.2 % at the measurements in 2004).

Likewise the third observed parameter growths number - showed the similar change dynamic. In 2003

increased the growths number at the observed plants in 87.6 % or 94.4 %, in 2004 14.7 % or 3.2 %. At the first summer measurements the higher dynamic of the increasing number of growths at the plants from the seed (92.7 % in 2003 and 14.8 % in 2004) was noticed in comparison to the plants from the root segments (83 % and 14.7 % in 2004). At the second summer measurements was the dynamic of the increasing at the plants from the root segments (95.8 % in 2003 and 9.5% in 2004) and at the plants from the seed (93 % in 2003 and 8.3 % in 2004) similarly the same.

No significant dependence among the plant height in mm, leaves number and growths number was found out.

Hypothesis testing

The final part of the statistic evaluation of *Phragmites australis* cultivation was devoted to the hypothesis testing. The truthful of the assumption that the average values of the observed parameters the height of the plant in mm, the leaves number and the number of growths shows for both compared methods of reproduction the same values. The testing was done individually for both summer measurements for years 2002, 2003 and 2004. Enumeration of p-values was realized by using MS Excel software. The values are shown in Tab 2.

	height in mm	leaves number	growths number
Measurement 22/07/2002	0.061	0.27	0.53
Measurement 30/08/2002	0.062	0.01 ⁺	0.57
Measurement 20/07/2003	0.071	0.17	0.53
Measurement 02/09/2003	0,070	0.74	0.05 ⁺
Measurement 25/07/2004	0.030 ⁺	0.07	0.46
Measurement 05/09/2004	0.020 ⁺	0.98	0.02 ⁺

Table 2. Reached p-values at the individual measurements

On the basis of such performed analysis it can be stated that the significant differences at the average height of the plants reproduced generatively and vegetatively were found out. The plants reproduced vegetatively reached at each observed measurement higher accumulation in comparison to generative plants. This accumulation was not during the two first years statistically significant. Till in 2004 it can be affirmed with the probability higher than 95 %, that the average height of the plants reproduced from the root segments is significantly higher, than the plants reproduced from the seeds. The decreasing p-value in the Tab 2 persuades about the verity of such statement.

The method of reproduction has no influence to the leaves number according the performed analysis. The fining, that during vegetative period differences between the number of growths at the plants reproduced from the root segments in comparison to

the plants reproduced from the seeds are increased, was interesting. This assumption can be accepted at the second summer observation during last two years with the probability 95 %. Presented hypothesis for the measurement processed on 15/10/2004 (this measurement was not the subject of the comparative analysis) could be accepted with the probability 99 %.

Statistical results showed only low to medium dependence among the observed parameters (the height of the plant, the leaves number, the number of the growths). At the hypothesis testing we were concentrated on the test of the concord of average values above described parameters of the plants obtained generatively and vegetatively. During the third year of the observation statistically significant differences were found out concerning the average height of the plants and the number of growths received by generative and vegetative reproduction on the behalf of vegetative reproduction.

The result of verified methods of vegetative and generative reproduction is, that the most suitable method of reproduction in given area and under given conditions is the root segments reproduction. The biomass production is influenced by the climate conditions. Cultivating of *Phragmites australis* from the seeds showed, that during individual observed years was the germinative activity different but generally the seeds germinated slowly.

4. CONCLUSIONS

In consequence of the mining and processing of the magnesite ore, some areas of Slovakia have strongly damaged soil, when pH increased to 9 and more. The physical and chemical characteristics of the soil were changed, the erosion increased and phytocoenose decreased. A large number of the soils is impossible to use for agriculture. The fertilization requires huge resources. The future for the fertilization and prospective use of the soils is seen in the possible cultivation of *Phragmites australis* (Cav.) Trin, which was selected in given area. It is an invasive plant with the possible technical and agricultural use.

Thence during years 2002-2004 the most suitable method of the reproduction of this plant was investigated, i.e. generatively and vegetatively. On the basis of the statistical evaluation of the results arises, that the vegetative root segment reproduction is more suitable and can be recommended under these conditions.

5. ACKNOWLEDGEMENT

This work was supported by the Slovak Research and Development Agency under contract No. APVV 0131-11 and Scientific Grant Agency of the Ministry of Education of the Slovak Republic under contract No. VEGA 1/0070/12 and 1/0008/13.

6. REFERENCES

- [1] Hronec, O., Vilček, J., Tomáš J., Adamišín, P., Huttmanová, E.: *Environmental Components Quality in Problem Areas in Slovakia*, Mendelova univerzita, Brno, 2010.
- [2] Steinnes E., Sjøbakk T.E., Donisa C., Brännvall M.L.: *Quantification of Pollutant Lead in Forest Soils*. Soil Sci. Soc. Am. J., 69, 1399-1404, 2005.
- [3] Hovmand M.F., Kemp K., Kystol J., Johnsen I., Riis-Nielsen T., Pacyna J.M.: *Atmospheric heavy metal deposition accumulated in rural forest soils of southern Scandinavia*. Environmental pollution, 155, 537-541, 2008.
- [4] Kaleta, M.: *Vegetation circustanes in Jelsava area concentrated on the immission conditions*. Veda SAV, Bratislava, Quaestiones Geobiologicae 17, 131 pp., 1975.
- [5] Hronec, O., Hajduk, J.: *Significant resistance of Phragmites australis Cay. Trin. on the soils intoxicated with magnesium immissions*. Ecology 2, 117- 24, 1998.
- [6] Vilček, J.: *Bioenergy production of agricultural soil cover*. Ekológia, 22, No.2: 177-182, 2003.
- [7] Vilček, J., Hronec, O., Bedrna, Z.: *Environmental pedology*. VÚPOP, Bratislava, 2005.
- [8] Dykyjová, D.: *Kontaktdiogramme als Hilfsmethode Fur vergleichende Biometrie, Allometrie und Produktionsanalyse von Phragmites Okotypen*. Rev Rom. Biol. - Zoologie T 14, Bucarest, 107-119, 1969.
- [9] Květ, J.: *Mineral nutrients in shoots of red (Phragmites communis Trin.)* Polskie Arch. Hydriol. Warszawa, 20, 137-147, 1973.
- [10] Mason, C. F., Bryant, R. J.: *Production, nutrient content and decomposition of Phragmites communis Trin and Typha angustifolia L.*, Journ. Ecio., Oxford 63, 71-95., 1975.
- [11] Brisson, J., S. de Blois, Lavoie, C.: 2010. *Roadside as Invasion Pathway for Common Reed (Phragmites australis)*. Invasive Plant Science and Management, 3(4), 506-514, 2010.
- [12] Chambers, R., L. Meyerson., Saltonstall, K.: *Expansion of Phragmites australis into tidal wetlands of North America*. Aquatic Botany, 64(3), 261-273, 1999.
- [13] Mal, T., Narine, L.: *The Biology of Canadian Weeds. 129. Phragmites australis (Cav.) Trin. ex Steud.* Canadian Journal of Plant Science. 84(1). 365-396 , 2004.
- [14] Derr, J.: *Common Reed (Phragmites australis) Response to Postemergence Herbicides*. Invasive Plant Science and Management, 1(2), 153-157, 2008.

Autors: Prof. h.c., prof., Ing. Ondrej Hronec, DrSc. University of Central Europe in Skalica, Kráľovská 386/11, 909 01 Skalica, Slovakia, **prof. Ing. Jozef Vilček, PhD.**, Soil Science and Conservation Research Institute, Bratislava, Raymanova 1, 08001 Prešov, Slovakia, University of Presov in Presov, Slovakia, **doc. Ing. Peter Adamišín, PhD., Emilia Huttmanová, PhD.**, University of Presov in Presov, Ul. 17. novembra 15, 080 01 Presov, Slovakia, **Pavol Andrejovský, PhD.**, University of Economics Faculty of Business Economy, Kosice, Tajovského 13, 041 30, Košice, Slovakia.

E-mail: ondrej.hronec@unipo.sk
jozef.vialcek@unipo.sk
peter.adamisin@unipo.sk
emilia.huttmanova@unipo.sk
pavol.andrejovsky@euke.sk

Kheifetz, M., Pynkin, A., Pozilova, N., Prement, G., Klimenko, S.

DESIGN DECISIONS DURING MODELLING TRANSFER OF QUALITY PARAMETERS IN LIFE CYCLE OF MACHINE DETAILS

Abstract: *It is shown, that computer support of life cycle of products with use of CALS-technologies demands development of through mathematical models of inheritance of a complex of parameters of quality of products. At the automated designing intensive methods of processing of details of machines it is offered to use domination of properties of relations of technological decisions. On a basis synergetic the approach models of loss of serviceability of units of friction are considered.*

Key words: *quality parameters, life cycle, technological inheritance*

1. INTRODUCTION

When in mathematical modelling, engineering and technological design, manufacturing and running of complex technical systems, the portability of decisions is based on principles of transfer of properties in life cycle of products. Application of synergistic concept makes it possible to generate a mathematical model of technological and operational inheritance of quality indexes, which describes various modes of behavior when in manufacturing and applying of technical systems.

Definition and estimation of changes in technological and operational processes of quality indexes of machines with a glance their mutual influence are complicated with multiply connected character of interactions of forming properties of products. To develop a mathematical apparatus of transfer of quality indexes at technological and operational inheritance it is necessary to decrease dimension of description problem of property transformation [1] in a correct way.

Replacement of set of the objects, cooperating with a product, by one object the technological or operational environment at identity of results of such a replacement, favors the correct decrease of dimension of description problem of property transformation. Definition of manifold characteristics allows, if disposing of cooperation results with a product, to find out rational level quality indexes and to carry out the directed formation of the technological and operational environment. These manifolds should favorable development of useful properties and suppression of development of the properties, which lower quality of products, by means of use of technological and operational barriers [2].

As a result, the method of processing is understood as a set of energy and information processes directed on change of a form, sizes, quality of a surface and physical and chemical properties of a constructional material [1, 2].

2. ALGORITHM OF CHOICE OF TECHNOLOGICAL SOLUTIONS

For the purpose of formalization of conditions of the purposeful creation of new methods of treatment, each aggregate of homogeneous elements of the system is described as some set of technological solutions (TS). Such approach [2, 3] allows presenting any method of treatment as a cortege, each component of which is an element of the TS set.

Let us suppose that any two elements of the treatment method possess even only one common property. Then there is a link between the two on the community of properties. The gives an opportunity to organize the choice of TS according to the equivalence and preference [3]. The equivalence permits to choose heterogeneous solutions, which, according to the aggregate of their properties, must correspond to each other. The preference allows to choose solutions but out of the number of the homogeneous ones that possess the best values of the essential properties.

Such an approach makes it possible to formalize conditions of TS choice according to a certain level of the established selection criterion and enables to choose a solution according to several criteria corresponding to various TS properties.

Making TS in the systems of the automatized projecting is traditionally based on the analysis of the equivalence ($x \equiv y$) and the preference (non-strict $x \leq y$ or strict $x < y$) of the solutions, which are inserted in the knowledge base. This presupposes the use of properties [4]:

- reflexivity ($x \equiv x$, $x \leq x$ – true; $x < x$ – false);
- symmetry ($x \equiv y \Rightarrow y \equiv x$ true; $x \leq y$ and $y \leq x \Rightarrow x = y$ – anti-symmetrical; $x < y$ and $y < x \Rightarrow$ mutual exclusion – non-symmetrical);
- transitivity ($x \equiv y$ and $y \equiv z \Rightarrow x \equiv z$, $x \leq y$ and $y \leq z \Rightarrow x \leq z$, $x < y$ and $y < z \Rightarrow x < z$ – true).

In the result, using the property of transitivity, the most preferable of all the previous solutions is compared with a new offered or chosen out of the knowledge base on the basis of properties of quality indexes.

However, in the general case different non-equivalent TS are the most preferable for different quality parameters from the whole complex of properties. In this it is necessary to use the dominating TS ($x \ll y$), characterized by the following properties :

- anti-reflexivity ($x \ll x$ - false);
- non-symmetry ($x \ll y$ and $y \ll x \Rightarrow$ mutual exclusion);
- non-transitivity ($x \ll z$ does not go out of $x \ll y$).

To determine the parameter prevalence, when there is no transitivity or symmetry, it is rational to apply a synergetic concept that uses a mode of analog random quantity, which is such a parameter value, when the density of its distribution has a maximum [5].

Thus, in computer-aided design the acceptance of technological solutions on perfection of manufacturing systems are to be carried out on a basis of synergetic analysis of technological and operational processes and objects [6].

3. THERMODYNAMIC MODEL OF PROCESSES OF PROCESSING

According to the synergetic conception of the steady mode adjusted to the dominating unsteady mode and can be excluded. This leads to the abrupt reduction of the number of the controlled parameters - degrees of freedom. The remaining unsteady mode can be the parameters of sequence, which define TS [5].

The equations in the process of such reduction of parameters group up into several universal classes of the following type [5]:

$$\frac{\partial}{\partial \tau} \vec{U}^* = G \left(\vec{U}^*, \nabla \vec{U}^* \right) + D \nabla^2 \vec{U}^* + \vec{F}(\tau),$$

where \vec{U}^* - controlled parameter; τ - current time; G - nonlinear function of \vec{U}^* and probably of a gradient $\nabla \vec{U}^*$; D - a coefficient, describing diffusion when its value is valid, or describing distribution of waves, at imaginary value; \vec{F} - fluctuating forces caused by interaction with an environment and by the dissipation within the system.

The equations of such type are similar to the describing elements of phase transitions of the first and the second type, which are defined by the criteria of transfer.

According to the synergetic conception phase transitions take place in the result of self-organization [5], the process of which is described by three degrees of freedom, which correspond to the parameter of sequence (S), the field conjugated to it (C), and governing parameter (G) [6].

It is possible to use the only degree of the freedom-parameter of sequence - for describing only the quasi-static phase transformation. In the systems considerably moved away from the state of thermodynamic balance, each of the pointed degrees of freedom obtains its own value [5]. Therefore, besides the process of relaxation to the balanced state during the time - τ^p - with the participation of two degrees of freedom, an auto-oscillatory condition can be realized. If three degrees of freedom participate, transition to the chaotic state is

possible [6]. As a result, the overall state of the technologic system is characterized by several conditions:

1) relaxational - realized when the time of relaxation of the sequence parameter much surpasses the times of relaxation of other degrees of freedom

$$(\tau_S^p \gg \tau_G^p \text{ and } \tau_S^p \gg \tau_C^p);$$

2) remembering - defined by the 'frozen' disorder at the transition point from the disorderly state and is realized when the relaxation time of the sequence parameter turns out to be much less than other times

$$(\tau_S^p \ll \tau_G^p \text{ and } \tau_S^p \ll \tau_C^p);$$

3) auto-oscillation - requires commensurability of the typical times of changing in the sequence parameter and in the governing parameter, or in conjugated field ($\tau_S^p \geq \tau_G^p$ or $\tau_S^p \geq \tau_C^p$);

4) stochastic - characterized by a strange attractor and is possible through the commensurability of all the three degrees of freedom ($\tau_G^p \geq \tau_S^p \geq \tau_C^p$).

Thus, at modelling of technological and operational inheritance, the decrease of dimension of a description task of transfer of quality indexes up to three degrees of freedom of environment is possible during processing and wear process of a product. Modelling of transfer processes on a basis of synergetic approach allows to take into account stability of formation of quality indexes and to consider mechanisms of management of stability of technological and operational processes using feedback [1].

4. THE ANALYSIS OF PROCESSES OF WEAR PROCESS OF SURFACES

At the analysis wear process of machine details and their interfaces it is expedient to consider a vector [7]:

$$\varphi(X, t) = [\xi_{u_1}(X, t), \dots, \xi_{u_i}(X, t), \dots, \xi_{u_n}(X, t)],$$

where $\xi_{u_i}(X, t)$ - speed of wear process of detail i (interface) at the moment of time t while loading influence X on a unit of a machine.

Then it is accepted, that the wear process possesses a consequence, if the module and a direction of vector $\varphi(X, t)$ at the moment of time t depends not only on the module and a direction of a vector X at present time, but also on the module and a direction of a vector X at the moment of time $\tau < t$, and also on the size of deterioration U of rubbed surfaces for a period $[0, t]$ (here U - a n -dimensional vector: $U = (u_1, \dots, u_i, \dots, u_n)$; at which u_i - size of deterioration of detail i) [7]:

$$u_i(t) = \int_0^t \xi_{u_i}(\tau) d\tau.$$

It is typical for wear process without consequence that the module and the direction of vector $\varphi(X, t)$ at the moment of time t depend on the module and a direction of a vector X only at present.

Depending on time τ_p , when the loss of the serviceability, connected to background of operation of a product, is kept, there are two kinds of consequences: the first and second sort. The consequence of the first

sort is characterized by the changes during loss of serviceability of the products caused by background of loading influence X , remains during all service life of product τ_0 , i.e. $\tau_p \geq \tau_0$. If $\tau_p < \tau_0$, it is a process with «fading memory» or a consequence of the second sort.

Dependences of intensity of wear process of units of friction of machines on operation time t differ from each other with a kind of connections between managing parameter – loading influence X and the wear process connected to it by intensity J .

The choice of ordering parameter H in each concrete case depends on research problems (definition of durability, comparison of wear resistance, an estimation of dynamic properties of system in view of wear process of its elements, etc.). It is possible, that for the same detail, but for various parameters, process of loss of serviceability can have or not have consequence at constant intensity of wear process J of rubbed surfaces. It is caused by a kind of connection (linear or nonlinear) between the ordering parameter H on which the estimation of a resource of serviceability of a researched product and by saved up deterioration U [1].

Let's consider various connections between external influences and parameters of system f_H , and also between characteristics of process of loss of serviceability g_H .

4.1. Model of loss of serviceability process of frictional units without consequence

In a case when connected to ordering parameter H intensity of wear process J depends only on size of loading influence X :

$$\begin{cases} J(t) = f_H(X(t)); \\ H(t) = g_H(X(t), U(t), t). \end{cases}$$

If process of wear process is considered as continuous stochastic process it is possible to receive a condition of wear process without consequence. Under constant conditions of friction the increment of deterioration $U(\Delta t) = U(t + \Delta t) - U(t)$ does not depend on time (process with independent increments), hence, speed of wear process $\xi_u = dU/d\tau$ is stationary during time τ [7]. Therefore such a wear process is described by a mode with storing: $(\tau_S^p \ll \tau_G^p \text{ and } \tau_S^p \ll \tau_C^p)$.

However processes of loss of serviceability of details during the periods extra earnings and catastrophic destruction of superficial layers cannot be described with the help of the resulted equations as intensity of wear process J during these periods is not a constant, and depends on sizes of saved up deterioration U of rubbed surfaces.

4.2. Models of loss of serviceability processes of frictional units with the consequence of the first sort

In cases when intensity of wear process J depends both on size of loading influence X and on size of saved up deterioration U , by the considered moment of time t :

$$\begin{cases} J(t) = f_H(X(t), U(t), t); \\ H(t) = g_H(X(t), U(t), t). \end{cases}$$

And at the account of a feedback of loading influence X^* with deterioration U :

$$\begin{cases} J(t) = f_H(X^*(t), U(t), t); \\ H(t) = g_H(X^*(t), U(t), t); \\ X^*(t) = q_H(X(t), U(t), t). \end{cases}$$

Changes during time τ of intensity of wear process J of rubbed interfaces at constant loading influence on an input of technical system X can be caused by two groups of reasons [7]:

not taking into account a feedback of loading X with deterioration U , such as distinction of physic and mechanical properties of a material on depth of a superficial layer of the product, caused by manufacturing techniques; the ageing of lubricants resulting in their deterioration of frictional properties, to change of a thermal operating mode of interface, and in some cases and to change of kinds of wear process of rubbed surfaces; increase while in service concentration of abrasive particles, products of deterioration, etc.;

taking into account changes of dependence g_H loading influence X^* on a detail of unit of friction as a result of deterioration of interface U which are connected to increase in backlashes in rubbed interfaces; with transformation of macrogeometry of surfaces of friction at wear process; with change of contact rigidity of mobile joints, etc.

Considered processes of loss of serviceability with consequence of the first sort concern to processes with strong correlation which have certain connection between sizes of parameter about $H_i(\Delta t)$ and $H_{i+1}(\Delta t)$ even at rather big $\tau = t_{i+1} - t_i$.

Here $H_i(\Delta t) = H(t_i + \Delta t) - H(t_i)$;

$H_{i+1}(\Delta t) = H(t_{i+1} + \Delta t) - H(t_{i+1})$, $t_i < t_{i+1}$.

Thereof processes of loss of the serviceability, caused by the first and second groups of the reasons, are characterized auto-oscillatory $(\tau_S^p \geq \tau_G^p \text{ or } \tau_S^p \geq \tau_C^p)$ and stochastic $(\tau_G^p \geq \tau_S^p \geq \tau_C^p)$ by modes with two and three degrees of freedom of technical system.

4.3. The model of loss of serviceability process of frictional units with consequence of the second sort

Consequence of the second sort is shown at change of loading influence as special transitional in wear process of rubbed surfaces [7].

In a transition period $[t_0, t_1]$ intensity of wear process J differs from those values which it accepted at the previous level of loading influence X_{i-1} , and from the value corresponding to new level X_i :

$$J(t) = \begin{cases} f_H(X_i, X_{i-1}, \dots, X_{i-n}, t), & t_0 \leq t \leq t_1; \\ f_H(X_i, t), & t > t_1. \end{cases}$$

Occurrence of transition periods speaks the several reasons [7]: an operational heredity of the materials deformable during friction of superficial layers of details; change diagram specific pressure in a zone of contact of details at transition from one level of loading influence on another and connected to it «secondary

aging» rubbed surfaces; gradual restoration of conformity between size of loading influence and distribution of greasing and products of deterioration on rubbed surfaces.

Proceeding from representations about the nature of the phenomena of frictional units with consequence of the second sort it is possible to conclude, that wear processes in transition periods $[t_0, t_1]$ are characterized by strong correlation connection between increments of deterioration $U_i(\Delta t)$ and $U_{i+1}(\Delta t)$ [7].

In this connection they should be considered as relaxational ($\tau_S^p \gg \tau_G^p$ and $\tau_S^p \gg \tau_C^p$) with the characteristic period $[t_0, t_1]$.

Thus, downturn of dimension of a task of the description of transfer of properties of products in technological and operational processes is made by allocation of parameters of the order and definition of modes of a condition of system. After that on each of modes it is expedient to consider interrelations of the basic parameters of quality of a product with the determining parameter of the order and a condition of their steady formation.

4.4. Parameters of quality of surfaces of products

Parameters of quality of products of the mechanical engineering, being the basic, share on two categories [1]: what are characterized by the hereditary phenomena connected to properties of materials of products concern to the first; to the second - connected to geometrical parameters of their surfaces.

Parameters of both categories in multicoherent technological and operational environments mutually influence against each other. Geometrical parameters of products, such as their configurations and the sizes can influence the voltage distributed in a material of a basis and superficial layers. And, on the contrary, the voltage formed during technological operations and stages of operation, can lead eventually to changes of geometrical parameters of precision details. It testifies to mutual connection and conditionality of the phenomena accompanying technological and operational processes.

Inheritance of the basic parameters of quality is the most full is opened by consideration of sequence of processes with synergetic of positions of joint action of technology factors at mutual influence of parameters. Initial parameters of quality of details of the machine at various scale levels change while in service [1].

Exception is made with residual voltage and structure of the basic material which can be kept before full destruction of rubbed surfaces of details. In most cases already during the period extra earnings the roughness and structure of a superficial relief essentially varies, the sinuosity and structure of superficial layers of a detail change at the established wear process, and the geometrical form of a surface of friction remains within the limits of the admitted values accepted at manufacturing, practically up to the end of service of unit of friction if the estimation of its serviceability is made on parameters of accuracy.

5. CONCLUSION

As a result of the analysis of processes of wear process of surfaces and loss of serviceability of units of friction, studying of features of management by processes of processing the expediency of application synergetic the approach to technical systems is shown. On a basis synergetic the approach the mathematical model of technological and operational inheritance of parameters of quality in life cycle of products of the mechanical engineering, describing various modes of behaviour is generated by manufacture and application of technical systems. Mathematical modelling and algorithmization of decision-making, by definition of a kind of the equations have shown, that the system analysis at the automated designing methods of processing, besides equivalence and preference, should be based on domination of properties of relations of design decisions.

6. REFERENCES

- [1] Vasilyev, A., Dalskiy, A., Klimenko, S. and others: *Technological Basis of Machine Quality Control*, Mechanical Engineering, Moscow, 256 p. 2003.
- [2] Ryzhov, A., Averchenkov, V.: *Technological Process Optimization of Machine Working*, Navukovaia dumka, Kiyiv, 192 p. 1989.
- [3] Golodenko, B., Smolencev, V.: *Object-Orientated Forming Organization of New Methods of Combined Processing*, Mechanical Engineering Herald, № 4, pp. 25 – 28, 1994.
- [4] Korshunov, Y.: *Mathematical Basis of Cybernetics*, Energoatomizdat, Moscow, 496 p. 1987.
- [5] Haken, G.: *Synergetics*. Mir, Moscow, 404 p. 1980.
- [6] Olemskiy, A., Kopylyk, I.: *Theory of Spatio-temporal evolution of Nonequilibrium Thermodynamic System*, Physical Sciences Progress, V. 165, № 10, pp. 1105 – 1144, 1995.
- [7] Scorynin, Y.: *Accelerated Wearing Tests of Machine's Details and Equipment*, Science and Technology, Minsk, 159 p. 1972.

Authors: Prof. Dr. Kheifetz Mikhail, Presidium of the National Academy of Sciences of Belarus, Independence Avenue, 66, 220072, Minsk, Belarus
Phone: +375 17 284 18 22, Fax: +375 17 284 03 75.
E-mail: mlk-z@mail.ru

M.Sc. Pynkin Aleksander, M.Sc. Pozilova Natalja, M.Sc. Prement Gennadi, The State Scientific and Production Amalgamation "Center" of the National Academy of Sciences of Belarus, Sharangovich str., 19, 220018, Minsk, Belarus, Phone: + 375 17 259 06 90, Fax: +375 17 313 45 40.
E-mail: info@npo-center.com

Prof. Dr. Klimenko Sergej, Bakul Institute for Superhard Materials of the National Academy of Science of Ukraine, Phone/Fax: +380 44 430 85 00.
E-mail: atmu@ism.kiev.ua

Kovács, P.V., R., Beszédes, S., Ludányi, L., Hodúr, C., Szabó, G.

DEVELOPMENT OF A CONTINUOUS FLOW MICROWAVE TOROIDAL CAVITY RESONATOR

Abstract: Characteristics of the utilization of wastewaters sludge in anaerobic digestion (AD) process meet the requirements of “waste-to-energy” research and developments concept. One of the possible operations to enhance the biodegradability limited by macromolecules and other chemical components of produced sludge is the microwave irradiation. Research group of the Department of Process Engineering at the University of Szeged has investigated the applicability and the efficiency of microwave (MW) pretreatment for food industry sludge. Results of our experiments show that after MW pretreatment the solubility of organic matter increased which was manifested in higher volume of produced biogas and the enhanced methane ratio in it, moreover with the shortened adaptation period the rate of AD process was accelerated. Based our preliminary results and taking into consideration the data of process optimization development of a continuous flow modular MW unit equipped by toroidal cavity resonators for wastewater sludge conditioning has been proceeded. [1,2]

Key words: wastewaters sludge, toroidal cavity resonator, microwave (MW) pretreatment

1. INTRODUCTION

During the operation of toroid resonator energy is given to the treated material. As a result of energy transmission the temperature of the material rises and the dielectric properties change continuously. The effect of the microwave energy intake, variable power, impedance and dielectric relationships are formed in the microwave resonator. Some of these can be measured (e.g. power dissipation, reflected power), some of them can only be determined by calculation, knowledge of the other parameters [3].

This system contains a water-cooled, variable-power magnetron operating at 2450 MHz which is fed through a toroid transformer by a high voltage power supply. Material is transferred by a solenoid valve-controlled pneumatic cylinder in the continues-flow microwave treating system. Several modes can be selected by ball valves (e.g.: filling, draining, circulating, etc.).

Volumetric flow of the fluid is measured by a flow-meter and the electrical signal of it is received by a data collector. The microwave signal from the cavity resonator goes through the attached measuring head to the microwave power meter and the measured signal is converted to proportional signal DC. This signal DC, the electric signal of the flow-meter and the inlet and outlet temperature of the sludge are received by the measurement data collector and recorded on-line by software and displayed in the computer screen. The free measuring points of data collector could provide opportunities for the measurements of further parameters according to the treatment commitment (e.g. pH, conductivity, dissolved oxygen, turbidity, etc.).

2. MAGNETRON

Output power from the generator (magnetron) enters into the rectangular waveguides as form of traveling wave and it moves into the closed resonator area trough the excitation-gap formed on the cover. The fluid in the resonator – according to its dielectric properties- can change emerging power lines in the waveguide and the resonator and it takes up energy from the electromagnetic space. (Fig.1.)

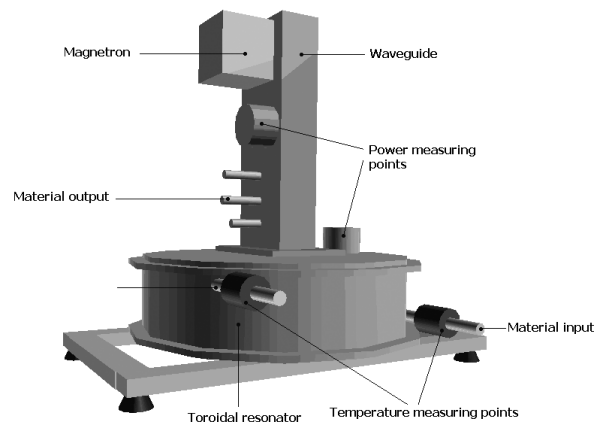


Fig. 1. Microwave treating system

High-voltage power supply feeding the magnetron consists of two transformers, one of them produces cathode heating voltage and heating current, the other produces the anode voltage which can be controlled by the primary circuit of an external auto-transformer. Magnetron is a specially designed high-frequency vacuum diode whose frequency is determined by the structure of the cavities in the anode block. Power of it is determined by the strength of the magnetic field of the permanent magnet around the anode block, the variable anode voltage, and the load-dependent anode current. Because of the high voltage transformer

primary voltage is ten times higher, and there is another voltage duplicate connection. As a consequence of these 4.6 kV DC voltage is provided for the anode of the magnetron.

Value of the magnetron power can be determined from known anode current, anode voltage and the magnetic flux density.

Magnetron anode block is divided by more even-numbered cavity resonator. Device is surrounded by a strong magnetic field installed by factory-set permanent magnets. Output coaxial waveguide joins to one of the cavities with a loop. Interaction required during the operation takes place in the interaction space between the anode and cathode. Cavities joins to this interaction space with these gaps (Fig.2.).

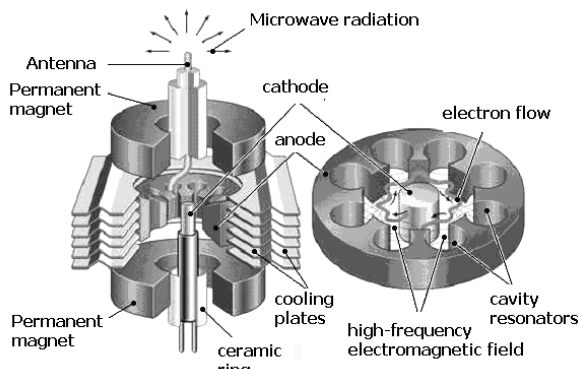


Fig. 2. Magnetron

Operating frequency of the magnetron is $2450\text{MHz} \pm 30\text{MHz}$. In absolute terms the frequency can be changing with $\pm 60\text{MHz}$ depending on the operating temperature. Frequency change is important because the size of the rectangular waveguides transferring magnetron energy determined by the wavelength belonging to the operating frequency. Magnetron power, as mentioned above, can be calculated based on available technical data, or by measuring different electrical parameters (anode voltage, anode current). Latter procedure can only be carried out by a special measurement method, very carefully, compliance with protection rules. Power measurement also can be performed as follows: Rectangular waveguide (and also the magnetron), is loaded by a calibrated certified closing charge with a calibrated and small reflection coefficient. There is a coupler gap at a particular place on the wider side of the waveguide generating elliptically polarized wave in the cylindrical cavity resonator. Attaching a detector to the measuring cavity, detector voltage proportional with the output power can be measured and knowing of detector-closing impedance output microwave power can be provided. (Fig.3.)

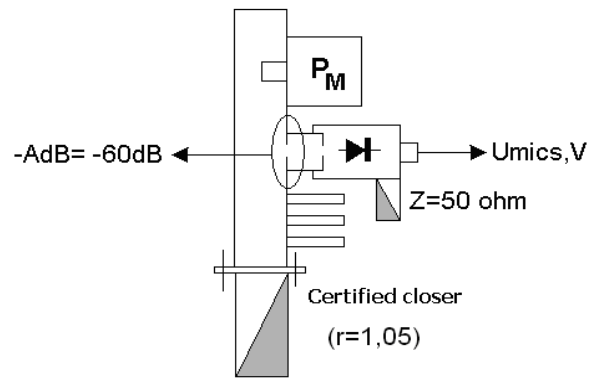


Fig. 3. Measurement configuration

Considering the attenuation of output circular holes ($-A_{DB} = -60\text{ dB}$), magnetron-power can be calculated at different primary voltages of the high voltage transformer (Fig.4.).

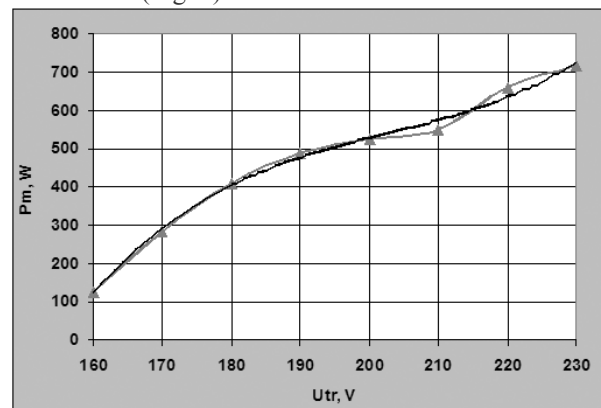


Fig. 4. Power of magnetron at different control voltages

Figure 4 shows that at $U_{tr} = 160\text{V}$ voltage-control excitation stops, but the corresponding microwave power as expected only a total of 120 watts.

3. TUNING RODS

Adequacy of the junction can be measured with measuring cavity and the junction itself between the magnetron and the load is made by using the tuning rods. (Fig.5.)

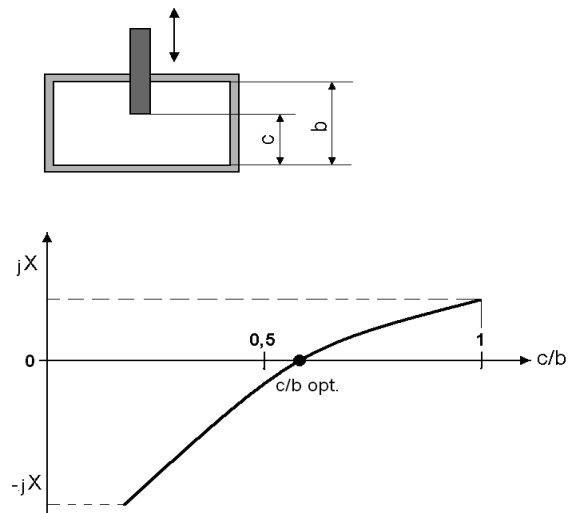


Fig. 5. Tuning rods

Tuning rod is located at the symmetry axis of the wider side of the waveguide and because its thread design it can penetrate different c-values to the space of electric power supply line E, where it can represent capacitive or inductive reactance in the impedance of waveguide depending on the value of the penetration. Optimal c/b relationship can be set when the two reactance compensate each other and only real ohmic impedance remains as a load. In this case, reflected signal measuring by the measure cavity will be minimal. Usually varying degrees of phase shift created by the reactance of the load, therefore one tuning rod is no longer possible to compensate so using three tuning rod is the solution. [4]

4. RESONANT SLOT

Electromagnetic energy of the magnetron spread over the measuring cavity and the tuning rods to a resonant slot. Getting through this slot the energy gets in the toroidal resonator. As geometry and dimensions of the waveguide and the toroidal resonator are completely different interface between the waveguide output and the resonator input represents different impedance values. So output impedance of the waveguide does not match the input impedance of the toroidal resonator. It causes reflection. Therefore sizing of the resonant slot is very important. Determination of the slot size based on the criterion that wave resistance of the waveguide corresponding to the gap size should be identical of the wave resistance of the main waveguide. Second criteria of resonance is that circumference of the slot should be equal to the value of the operating wavelength. Rounding the ends of the slot means that the gap electric fields more evenly distributed.

5. TOROIDAL CAVITY RESONATOR

The length of waveguide is calculated from the trailing Z impedance. If a Z_0 wave resistance waveguide is closed with Z (usually complex) impedance, different impedance can be measured at different "l" distance from the closure.

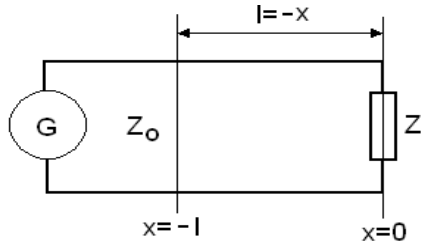


Fig. 6. Simplified illustration of microwave power supply line-section

It is known that at resonant frequency the impedance of series LC circuit is zero, and the admittance of it is infinite, the impedance of parallel LC circuit is infinite, and the admittance of it is zero. Therefore, the

$$l = \frac{n\lambda}{4} \quad (1)$$

scaled length (tuned) coaxial feeders, with a zero impedance, and infinite admittance can be replaced by series LC circuit.

The waveguides closed at these places are also cavity resonators as well. (Fig.2.)

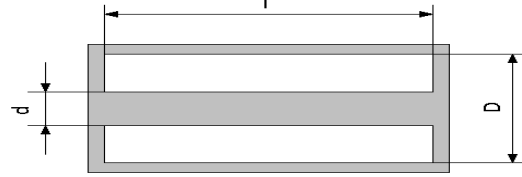


Fig. 7. Section of coaxial cavity resonator

The 'l' length of the resonator determines the resonant frequency according to the following relationship:

$$\omega_0 = \frac{\pi}{l\sqrt{\mu_a \epsilon_a}} = \frac{c\pi}{l\sqrt{\mu\epsilon}} \quad (2)$$

from this, if $\epsilon=1,0$ and $\mu=1,0$ (for air), then:

$$f_0 = \frac{\omega_0}{2\pi} = \frac{c}{2l} \quad (3)$$

The capacity per length unit in the coaxial resonator:

$$C = \frac{2\pi\epsilon}{\ln \frac{D}{d}} \quad (4)$$

the inductance per unit length:

$$L = \frac{\mu}{2\pi} \ln \frac{D}{d} \quad (5)$$

the impedance:

$$Z = \frac{1}{2\pi} \sqrt{\frac{\mu}{\epsilon}} \ln \frac{D}{d} \quad (6)$$

The coaxial resonators can be converted to toroidal-resonators, if "d" wide gap is formed on the inner conductor [5].

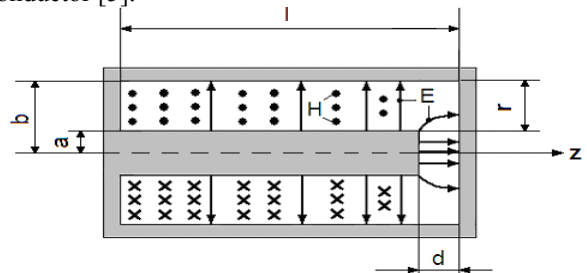


Fig. 8. Section of toroidal cavity resonator

The gap width "d" is considered a high-frequency capacity C, with the value of:

$$C = \epsilon_a \frac{S}{d} = \epsilon_a \frac{a^2 \pi}{d} \quad (7)$$

($S = a^2 \pi$ - surface of the condenser C)

The toroidal resonator is cylindrical symmetry, so the magnetic field lines H extend along concentric circles.

The inductivity L of the resonator is:

$$L = \frac{\Phi}{i} \quad (8)$$

(i – wall power)

Specifying the current density of the magnetic surface

$$\Phi = \int_S B dS = \mu_a \int_S H dS \quad (9)$$

$$\oint_L H dl = i \quad (10)$$

context can be used for the total current-density of the quasi-stationary field, and considering that the toroidal resonator-cylindrical wall is a high-frequency "r" radius inductance L, which is in parallel connection with the high-frequency capacitor C, we get

$$H = \frac{i}{2\pi r} \quad (11)$$

Applying the context:

$$L = \frac{\mu_a}{2\pi} \int_S \frac{dS}{r} = \frac{\mu_a}{2\pi} \int_0^l dz \int_a^b \frac{dr}{r} = \frac{\mu_a}{2\pi} l * \ln \frac{b}{a} \quad (12)$$

Applying the equations for L and C we can get the resonance frequency of the toroidal resonator and the value of the resonant wave length

$$\omega_0 = \frac{1}{\sqrt{LC}} = \frac{1}{a} \sqrt{\frac{2d}{\varepsilon_a \mu_a l * \ln \frac{b}{a}}} \quad (13)$$

and

$$\lambda_0 = \pi a \sqrt{\frac{2l}{d} \ln \frac{b}{a}} \quad (14)$$

On this basis the main dimensions of the microwave cavity toroidal-resonant sludge treatment plant we have developed are the following (Fig. 4.):

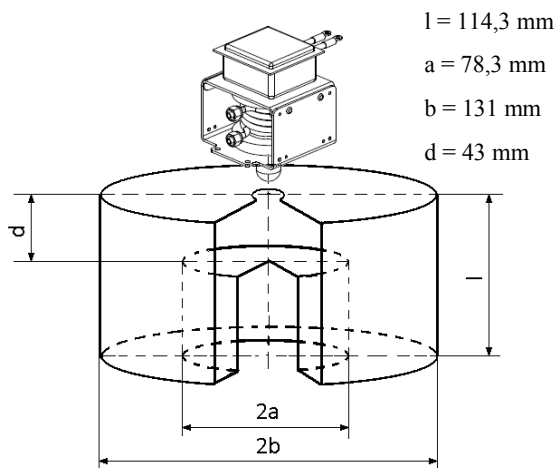


Fig. 9. Counted dimensions of the cavity resonator

Resonant wave length:

$$\begin{aligned} \lambda_0 &= \pi a \sqrt{\frac{2l}{d} \ln \frac{b}{a}} = \pi * 7,83cm \sqrt{\frac{2 * 11,43cm}{4,3cm} \ln \frac{13,1cm}{7,83cm}} \\ &= 40,69cm = 0,4069m \end{aligned}$$

Resonant frequency [6]:

$$f_0 = \frac{c}{\lambda_0} = \frac{3 * 10^8 m/s}{0,4059m} = 7,373 * 10^8 1/s$$

$$f_0 = 737,3MHz$$

6. REFERENCES

- [1] Beszédes, S., Kertész, Sz., László, Zs., Szabó, G., Hodúr, C. *Biogas production of ozone and/or microwave-pretreated canned maize production sludge*. Ozone Sci. & Eng. J. 31 (3), 257-261, 2009
- [2] Beszédes S., László Zs., Horváth H. Zs., Szabó G., Hodúr C.: *Comparison of the effects of microwave irradiation with different intensities on the biodegradability of sludge from the dairy- and meat-industry*. Bioresource Technology, 102, pp.: 814-822, 2011
- [3] J. Zhu, A.V. Kuznetsov, K.P. Sandeep (2007) „Mathematical modeling of continuous flow microwave heating of liquids”, International Journal of Thermal Sciences, Vol. 46, 328–341
- [4] L. Ludányi: *Study of Intermittent and Continuous-mode Microwave Drying*. Műszaki Kémiai Napok '01, Veszprém, ISBN 963 00 64677, p. 188-193. 2001
- [5] G. Szabó: *Gyorsfagyasztott baromfiipari termékek mikrohullámú felengedtetése üregrezonátoros kezelő térben*. HŰTŐIPAR 1: pp. 14-20, 1990
- [6] Singh, R.P.; Heldman. D.R: *Introduction to Food Engineering*. Academic Press London, 2001

Authors: Ass. Kovács Róbertné Veszelo vszki Petra, Assist. Prof. Dr Sándor Beszédes, Ass. Lajos Ludányi, Prof. Dr. Cecilia Hodúr, Prof. Dr. Gabor Szabo DSc. Rector Emeritus, University of Szeged, Faculty of Engineering, 6724 Szeged, Mars tér 7. Phone: +36 62 546 000, Fax: +36 62 546 003 E-mail: veszelov@mk.u-szeged.hu; beszedes@mk.u-szeged.hu; hodur@mk.u-szeged.hu; szabog@mk.u-szeged.hu

Križan, P., Matuš, M., Šooš, E.

DESIGN OF PRESSING CHAMBER OF BRIQUETTING MACHINE WITH HORIZONTAL PRESSING AXIS

Abstract: The goal of this contribution is to present the process of engineering design of briquetting machine pressing chamber. Presented construction of briquetting machine is not the new construction principle of briquetting machine. It's a design of experimental pressing stand. This equipment has one big advantage, provides the possibility to research the impact of structural and technological parameters changes. Authors in this contribution describing the lonely process of briquetting machine pressing chamber design. Described design comes from the basic input requirements and analysis of mathematical models related with process of biomass compacting and related with pressing conditions in briquetting chamber during biomass compacting. In this design are also included requirements resulting from designed experimental plan, that's mean requirements regarding research of impact of structural and technological parameters changes on final briquettes quality. Engineering design is also completed by stress analysis, thus by outputs of FEM analysis of designed pressing chamber construction.

Key words: biomass, briquette, briquetting machine, pressing chamber, compacting pressure, pressing temperature

1. INTRODUCTION

Biomass presents huge amounts of unutilized waste. Solid biofuels production is convenient way how to energetically recover the waste. Before the waste becomes biofuel it has to be modified. Very interesting possibility is to compact the modified waste into the solid high-grade biofuels. This can be performed by compacting technologies, e.g. briquetting or pelleting. The final products of briquetting and pelleting are briquettes and pellets with various shapes and sizes. The feature of these both technologies is pressing of material (waste) under high pressure and temperature without any binding material. It is very important to produce briquettes with Standards given quality. Briquettes quality is evaluated mainly by briquette density and bulk density. Other important briquettes quality indicators are mechanical durability, strength and hardness. During the pressing process there are many parameters which influencing the final briquettes quality.

2. PRINCIPLES OF BRIQUETTING MACHINE WITH HORIZONTAL PRESSING AXIS

In the case of biomass compacting for energy recovery are widely known briquetting and pelleting. At briquetting we know three basic principles [2, 4]. Difference is in used pressing tool and this influencing the final briquettes quality.

Pressing piston of hydraulic press – mostly is providing in closed pressing chamber, briquettes production is on the base of repeating hydraulic cycles - we can make one briquette per one hydraulic cycle.

Pressing piston of mechanical press – biomass is compacted into the briquettes sequentially in open pressing chamber with pressing cylindrical piston, briquettes are pressed in the pressing chamber and are extruded through the jaws which are creating needed

counter pressure.

Pressing screw of mechanical press – continuously production of briquettes in open pressing chamber with continuously rotating pressing screw, briquettes are pressed in the conical pressing chamber.

The main goal was to design the experimental pressing stand which allows continuous change of compacting pressure, pressing temperature, pressing speed and holding time. Besides these parameters we are planning to research the influence of structural parameters on final briquettes quality (shape and length of pressing chamber, conicalness of pressing chamber, friction coefficient, etc.). Also we would like to measure the acting axial pressure on the plug, radial pressure and counter pressure and therefore we need to fit the pressing stand with sensors and tensors. On the base of mentioned information we chose for pressing principle by pressing piston of hydraulic press.

3. DESIGN OF PRESSING CHAMBER PRINCIPLE

As was mentioned above mostly are using two basic principles at briquetting machines construction [2, 4]:

Closed pressing chamber system:

This system (Fig.1) is characterized that we can produce only one compact briquette per working cycle. Working cycle consist of chamber feeding, briquette pressing, stopper opening and briquette extruding. After the working cycle is briquette extruded from pressing chamber through open stopper and working cycle can be repeated. Counter pressure during pressing is created by stopper which is in this case closed.

Open pressing chamber system:

This system is assembled by 3 chambers (feeding, pressing and calibration), see Fig.2. After the feeding chamber is filled, can be material pressed through pressing chamber and through the calibration chamber. Counter pressure is created by friction forces from

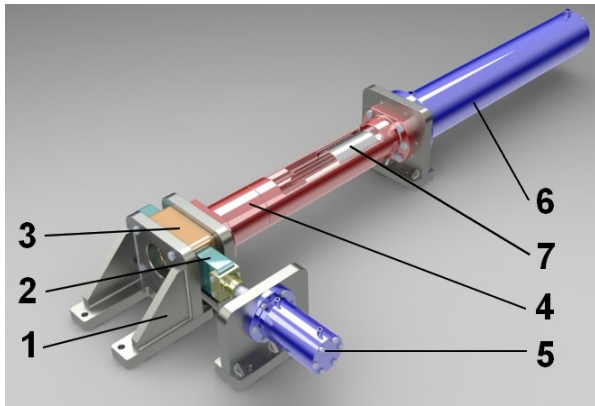


Fig. 1. Closed pressing chamber system (1– frame; 2 – stopper; 3 – stopper holder; 4 – pressing chamber; 5 – secondary hydraulic cylinder; 6 – main hydraulic cylinder; 7 – rod) [5]

pressed briquettes which are still in conical calibration chamber and also by the disc springs on the jaws (at the end of the system).

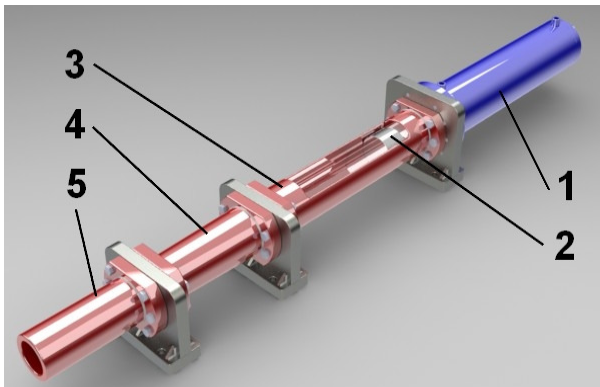


Fig. 2. Open pressing chamber system (1 – hydraulic cylinder; 2 – rod; 3 – feeding chamber; 4 – pressing chamber; 5 – calibration chamber) [5]

After analyzing of advantages and disadvantages of described systems we chose to use the open pressing chamber system.

Following Fig. 3 and Fig.4 shows the final design of experimental stand pressing chamber.

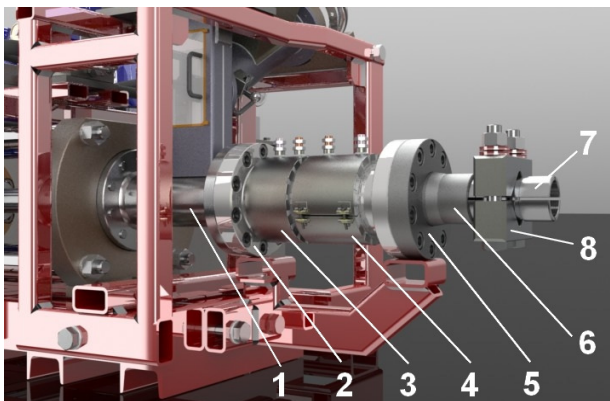


Fig. 3. Pressing chamber of experimental pressing stand (1 – pressing chamber; 2 – socket; 3 – heating equipment 1; 4 – heating equipment 2; 5 – flange; 6 – sleeve; 7 – collet; 8 – jaws) [5]

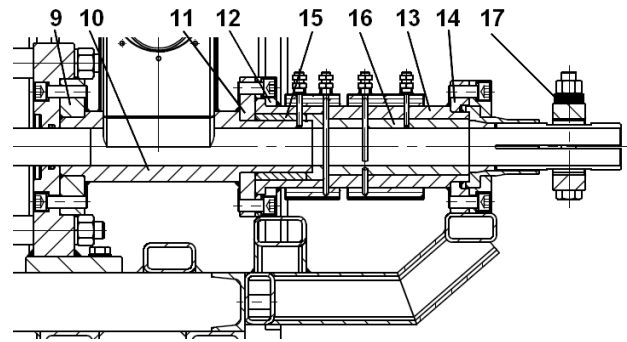


Fig. 4. Pressing chamber of experimental pressing chamber in sectional view (9 – flange 1; 10 – body of the pressing chamber; 11 – flange 2; 12 – flange 3; 13 – body of the socket; 14 – flange 4; 15 – tube spacers; 16 – calibration chamber; 17 – disc springs)

4. DESIGN OF PRESSING AND FEEDING CHAMBERS

Material pressing will be proceeding mainly in pressing chamber and at the beginning of the calibration chamber. In the rest part of calibration chamber the briquette dimensions will stabilize. Pressing part of equipment consist of pressing chamber, calibration chamber and collet with jaws. Therefore we used length of these parts at calculation of arising radial pressure and counter pressure.

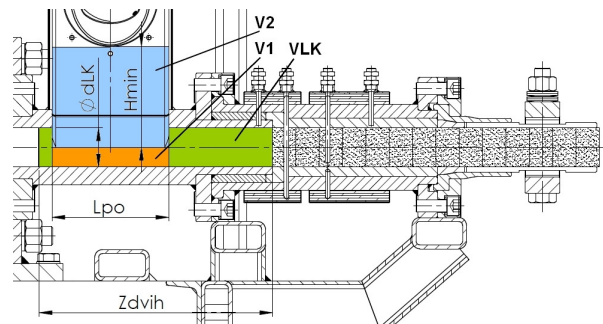


Fig. 5. Volumes determination for the calculation of minimal height [5]

Pressing chamber design was done on the base of final briquette dimensions. Very important is also to calculate the exact material dosing into the chamber, on the base of one briquette volume. We must take into the consideration the fact that at open pressing chamber besides pressing of one briquette, is needed to extrude from chamber also previous pressed plugs. We chose final briquette diameter $d_{LK} = 50$ mm and final briquette length $H = 30$ mm. We calculated briquette volume and after we also calculated input volume of material before pressing. It was determined on base of pressing ratio 1:10 (for wood sawdust). This calculated volume we can call as pressing chamber volume $V_{LK} [mm^3]$.

Now we were able to design the minimal height of feeding channel. Feeding channel is needed for the dosing of material for pressing. We can say that volume of pressing chamber is equal to volume of half cylinder V_1 and volume of rectangle V_2 of feeding channel (see Fig. 5).

5. CALCULATION OF PRESSURES ACTING AT PRESSING

At pressing in open pressing chamber is counter pressure p_G made up of static friction resistance between pressed material and walls of chambers (pressing and calibration). From this fact can be determined the size of counter pressure needed for pressing and also the static friction resistance of plug which was pressed before. After pressing is needed also some pressure for extrude the pressed plugs. For calculation of counter pressure p_G acting on pressed plug was used following equation (1) [1]. This equation was used also for radial pressure calculation.

$$p_G = p_K \cdot e^{\frac{4 \cdot \mu \cdot \lambda_H \cdot L_Z}{d_K}} \quad [MPa] \quad (1) \quad [1, 3]$$

where: p_K – piston axial pressure [MPa]
 μ – friction coefficient between pressing material and chambers walls [-]
 λ_H – ratio of main stresses [-]
 L_Z – length of pressed plug [mm]
 d_K – diameter of pressing chamber [mm]

Influence of pressing chamber length has impressive effect on final briquettes density and strength. If the pressing part will be very long, could arising the acting counter pressure. This high counter pressure will be created by length of pressed plug. Pressing piston couldn't extrude the pressed plug what can causes destruction of equipment. Vice versa if the pressing part will be very short, pressed briquette will haven't required strength and residual radial stress will tear it after the briquette left the calibration chamber.

$$\alpha = \frac{p_r}{p_K} \approx 0,15 - 0,20 \rightarrow \text{chosen} \dots 0,175 \quad (2) \quad [1, 3]$$

$$\alpha = \frac{p_r}{p_K} \Rightarrow p_r = \alpha \cdot p_K = 0,175 \cdot p_K$$

$$\lambda = \frac{\sigma_r}{\sigma_m} = \frac{p_r}{p_m} \in (0-1) \rightarrow \text{chosen} \dots 0,9 \quad (3) \quad [1]$$

$$\lambda = \frac{p_r}{p_m} = \frac{0,175 \cdot p_K}{p_m} \Rightarrow p_K = \frac{\lambda}{0,175} \cdot p_m$$

If we substitute the equations (2 and 3) into the equation (1) and after modifying we obtain the following equation (4), which can be used for calculation of acting axial pressure on pressed plug p_m .

$$p_m = \frac{p_G}{2,857} \cdot e^{\frac{4 \cdot \mu \cdot \lambda_H \cdot L_Z}{d_K}} \quad [MPa] \quad (4)$$

This pressure is needed for calculation of radial pressure p_r , on the base of equation (5).

$$p_r = \lambda \cdot p_m \quad [MPa] \quad (5) \quad [1]$$

This described process allowed us to calculate all required values of counter pressures, radial pressures and axial pressures acting on pressed plug, for the whole length of pressing chamber $L_Z = 420$ mm. On the

following Fig. 6 you can see pressing part with distribution of radial pressures and counter pressures acting on each plug. On the Fig. 7 is shown dependence of acting radial pressure on length of pressed plug. You can see that radial pressure is decreasing with increasing of length of pressed plug. Vice versa counter pressure is increasing with increasing of length of pressing chamber. This you can see on dependence of acting counter pressure on length of pressed plug (Fig.8). These pressures were calculated by above described process. We used these pressures at FEM analysis of pressing chamber.

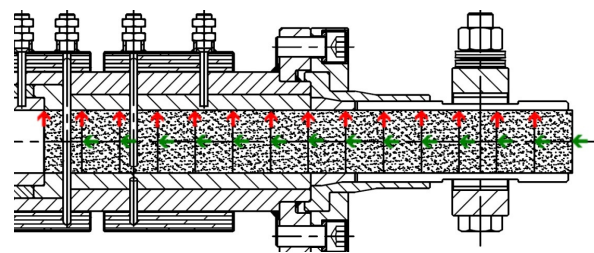


Fig. 6. Distribution of radial pressures (red colour) and counter-pressures (green colour) on the plugs in pressing chamber [2, 3, 4, 5]

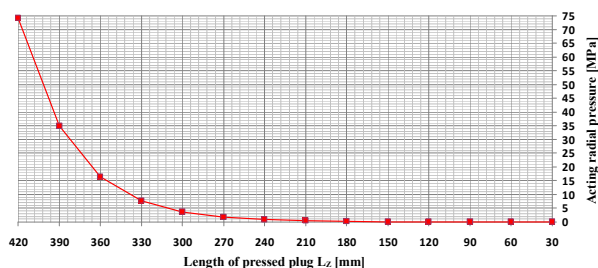


Fig.7 Dependence of acting radial pressure on length of pressed plug [2, 5]

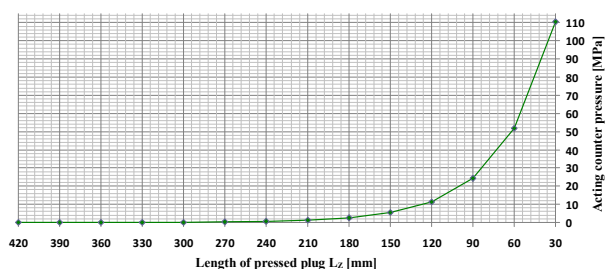


Fig. 8. Dependence of acting counter pressure on length of pressed plug [2, 4, 5]

6. FEM ANALYSIS OF PRESSING CHAMBER

At simulation we tried to get closer to real working conditions during pressing in pressing chamber. Working pressure in hydraulic circuit of pressing equipment is 30 MPa. With this pressure we can achieve compacting pressure in pressing chamber up to 235 MPa. Load acting in pressing chamber, calibration chamber and on collet comes from our calculations. During the pressing is radial component of pressing force bigger than friction component. Therefore we loaded the end of pressing chamber and the whole

calibration chamber with pressure which radial component is 75 MPa and friction component is 27 MPa. Collet is loaded during pressing with smaller pressure. According to our calculations we used for simulation in collet following values of radial component 1 MPa and friction component 0,35 MPa. On following Fig. 9, Fig. 10 and Fig. 11 you can see results of FEM analyses, it mean safety coefficient, tensions values and nodal points displacements values.

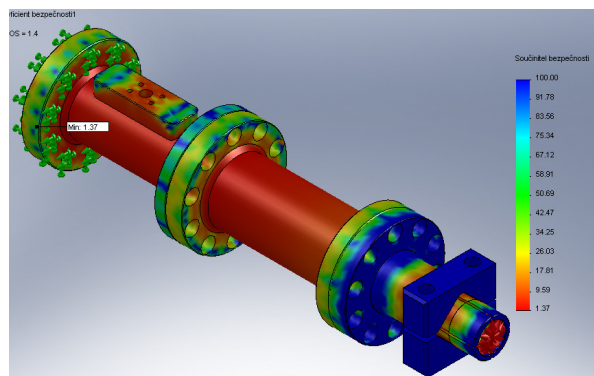


Fig. 9. Safety coefficient of pressing chamber [5]

Safety coefficient of pressing chamber is 1,37, is not so high but satisfies. The biggest tension was created in threaded holes of flange 1.

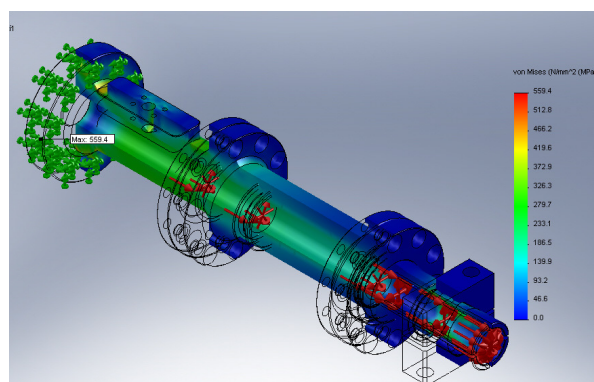


Fig. 10. Static nodal tensions in pressing chamber [5]

Pressures which are acting in pressing chamber cause internal forces. These internal forces cause deformations which reflected to nodal points displacements. On Fig. 11 you can see that the biggest displacements arising in collet.

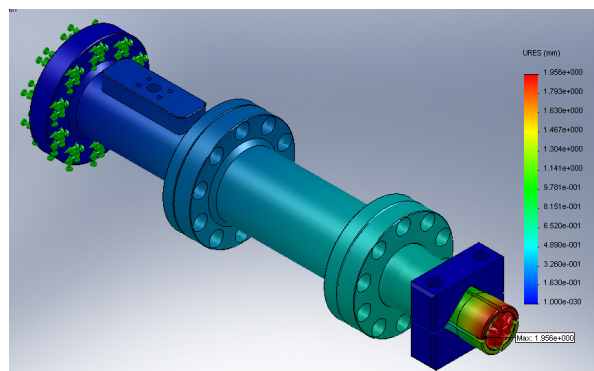


Fig. 11. Static displacements of nodal points in pressing Chamber [5]

7. CONCLUSION

This construction of experimental pressing (briquetting) equipment with horizontal pressing axis has more advantages. For example equipment will produce briquettes with dimensions as in real production, we will be able to measure acting pressures, deformations in dependence on input adjusted technological and structural parameters. This construction will allow us to find out influence of several technological and structural parameters change on final briquettes quality. We can make experiment with changing of pressing temperature, compacting pressure and allow us to make very simple changes of some parts of equipment (pressing chambers, pressing tool, cooling channel, etc.). And last but not least advantage is very low production costs for this experimental pressing stand. This equipment consists of parts which are very simple for producing in our conditions.

8. REFERENCES

- [1] Horrichs, W.: *Determining the dimensions of extrusion presses with a parallel-wall die channel for the compaction and conveying of bulk solids*, Aufbereitungs – Technik: Magazine, Duisburg, Germany, 1985, No.12.
- [2] Križan, P., *Process of wood waste pressing and conception of press construction*, Dissertation work, FME STU in Bratislava, Slovakia, July 2009, p.150, (in Slovak).
- [3] Storožev, M.V., Popov, J.A.: *Theory of metal shaping*, Alfa Bratislava, Slovakia, SNTL Praha, 1978, 63-560-78, p.488, (in Slovak).
- [4] Križan, P., Šooš, E.; Vukelić, Dj.: *Action of counter pressure on compacted briquettes in a pressing chamber*, Proceedings of the 10th International Scientific Conference, 9.-10.10.2009, Novi Sad, Serbia, Faculty of Technical Sciences, 2009, ISBN 978-86-7892-223-7, pp. 136-139
- [5] Tlachac, P.: *Design of laboratory compacting equipment with horizontal pressing axis*, Diploma work, Supervisor: P. Križan, FME STU in Bratislava, Slovakia, June 2012, p.145, (in Slovak)

ACKNOWLEDGMENT

This paper is an outcome of the project “Development of progressive biomass compacting technology and the production of prototype and high-productive tools”(ITMS Project code: 26240220017), on the basis of the Operational Programme Research and Development support funding by the European Regional Development Fund.

Authors: MSc. Peter Križan, PhD., MSc. Miloš Matúš, Prof. Ľubomír Šooš, PhD. Slovak University of Technology in Bratislava, Faculty of Mechanical Engineering, Nám. Slobody 17, 81231 Bratislava, Slovakia, Phone.: +421 2 572 96 537, Fax: +421 2 524 97 809.

E-mail: peter.krizan@stuba.sk;
milos.matus@stuba.sk;
lubomir.soos@stuba.sk



11th INTERNATIONAL SCIENTIFIC CONFERENCE NOVI SAD, SERBIA, SEPTEMBER 20-21, 2012

Maňko, M., Košíková, A.

ISO 50001 AS THE BASIS FOR IMPLEMENTING AN ENVIRONMENTAL MANAGEMENT SYSTEM

Abstract: *By the publishing of new standards for energy management system the international organization for standardization provided a new type of tool for defining the possibilities for company cost reduction as well as for indirect protection of natural resources. This tool can make significant contribution to the field of environmental protection in this period of global economic instability. The majority of organizations are looking for ways to reduce their expenses, and give priority to the economic aspect. The environment management system is determinant to provide the economic stabilization to the companies by applying the ISO 50001. This tool clearly demonstrates the company's cost-saving options which might be of interest to a unilaterally minded management and it has direct interest in global environmental protection. This article discusses the possibility of using the standard as the first steps towards the introduction of an environmental management in companies with a defensive approach to environmental protection.*

Keywords: *environmental management, environmental protection, ISO 50001*

1. INTRODUCTION

Despite the growing environmental awareness, in practice market environment, the main attention is still often focused on economic considerations. Despite the increasing pressure of legislative proceeding in favor of environmental protection, many organizations are confronted to their respect and interest in the organizations of such a systematic approach to managing its environmental aspects. This approach mainly depends on the environmental awareness of top managers. If the organization is not subject to direct pressure from their customers to implement an environmental management and if the top management is focused on achieving the best economic results, it is not possible to expect a proactive and systematic approach to managing environmental aspects and impacts of such an organization. Moreover, at the time of continuing economic instability in world markets and direct confrontation, small and large companies are concerned with the global economic crisis and in this case, economic stabilization is achieved through the reduction of fixed costs. Therefore, logically it is not possible to expect the implementation of environmental management by the company that is not forced to do so by their customers.

Implementation of environmental management system such as ISO 14001 is still seen by a lot of managers and top representatives of companies as something extra, which requires the input costs of ill-defined benefits or potential cost savings. This particularly works for organizations whose activities go few beyond, or even not achieve legislative defined emission or environmental limits. Although the introduction of environmental management system was able to improve their environmental behavior, it is not considered necessary and economically as an unnecessary investment. On the other hand, there is a standard that should rather supplement ISO 14001 as

its basis, and the ISO 50001 for system energy management. For the above mentioned reasons it is possible to assume that the standard ISO 50001 that defines requirements for the energy management system can precede the introduction of ISO 14001 and make the base for simplified implementation of environmental management according to ISO 14001. Question like why should this be so, or could it have already been so, were already mentioned in introduction. However, it is necessary to analyze the reality of this possibility and further discuss both standards and mainly analyze and compare their attractiveness and possibility of using them in a real market environment.

2. ISO 50001 STANDARD

2.1. Principle standards

The standard introduces principles guaranteeing the analysis of existing manufacturing processes, the reassessment of their use and the optimization of the use of production facilities and human resources. It deals with the management system and energy management in order to determine their optimal use and to achieve cost savings. It specifies the simple principle, the management of company define their goals and plans in the field of energy policy and these goals are gradually performed by the set of procedures and their effectiveness is measured and monitored by the organization to take effective precaution.

2.2 The contribution of standards for the organization

- It primarily delivers significant energy savings in the main production process and it saves money on expenses.
- It helps to optimize the utilization of production equipment to lower consumption.
- It helps to optimize the organization of work in order to save heat, air - conditioning and lighting.
- It allows to influence future consumption when planning future productin capacity.
- It confirms the importance of integration and optimization of quality management systems, energy management and environmental protection.

2.3 Advantage and disadvantage of standards:

+ Standard is an excellent tool for any organization because it constitutes a significant energy savings what is confirmed by several studies and practical applications even if only for a relatively short period.
- Due to the short history of ISO 50001 it is necessary to wait to detect any deficiencies.

3. ISO 14001 STANDARD

3.1. Principle standards

The standard defines a simple methodology, that management of the company define goals and plans in the field of environmental aspects and impacts of their activities (although only complete the legal limits). These plans and goals are gradually accomplished with appropriately configured procedures, which are monitored and measured in order to take effective steps for changes if needed. Standard imposes upon requirements for document management, human resources, infrastructure, implementing processes to communicate with the authorities and the public, and it is allowing the measurement of process performance through internal audits.

3.2. The contributions of organization are:

- An effective tool to manage effects of the organization's activities on the environment.
- Create a reputation of a prestigious company in the field of environmental protection.
- Reduce future costs resulting from the planning production of infrastructure especially in conjunction with the quality management system.
- Early recognition of problems and prevent any accidents, effective risk management.
- Providing more guarantees for the fulfillment of legislative requirements.
- Energy and material resources savings.

3.3 Advantages (+) and disadvantages (-) of standards

+ Standard is a good tool for helping to achieve the accomplishment of legal requirements in the field of environmental protection by reducing the risk of unexpected accidents. It is universal and applicable in all areas of human activites. Its structure is suitable for

integration with other standardized management systems.

- Certificate ISO 14001 is often underestimated by the authorities and also top leaders of organizations even if companies which are certificated present significantly lower risk with legal requirements and the emergence of unexpected events with negative impact on the environment.

4. STRUCTURE OF STANDARDS

As follows from the above brief summary and the descriptions of both standards it is not necessary to analyze and compare the structures of both standards in terms of the utilization of the structures of a system for the subsequent implementation of the second one. As every ISO standards for management systems these are also based on uniform PDCA cycle methodology. It facilitates the introduction of multiple systems using a single structure and therefore it supports the development of integrated management systems. The same philosophy is shared by ISO 50001, as it was assumed that this standard will be integrated into environmental management system ISO 14001 and it will create a superstructure that is more detailed and focused on energy issues. From a technical point of view it is possible to conclude that the using of established structures of energy management according to ISO 50001 it is sebsquent possible for subsequent simplified implementation of environmental management system according to ISO 14001. Whether and why this process of introducing an energy and environmental management should be relevant in practice, it is determinated by top representatives of the organizations themselves. They usually assess it in terms of attractiveness or standards for achieving its economic goals.

5. ACCTRACTIVENESS OF STANDARDS

When it comes to assessing the attractiveness of standards it is important to take into account in particular and within specific standards the awereness and attitude of the organization itself and its top managers. Top managers of companies are the people who define the strategy and development of a given company and therfore they take the decision concerning the introduction of management systems and their subsequent certification. Organizations that have not been forced to introduce an environmental management system and have not felt the need to systematically manage their environmental aspects and risks, will hardly look for motivation and the reasons for introduction of the ISO 14001 system even though their economical activities have achieved a significant success. Top managers of such organizations perceive environmental management system as surplus and their environmental awareness of the issue is purely financial. They do not see saving opportunities that a properly implemented and maintained environmental management system offers mainly with the possibility of reduction of material inputs and waste generation etc. The belief that a standard and system established

according to the standard will help them improve those factors is small and standard or potential certification is less attractive. Perhaps this is due to the relatively poor marketing and proven results. Despite of the great popularity of ISO 14001 as the second most widely certified management system in the world, the importance and benefits of the quite well-established standards is limited only for opportunity to better manage environmental risks and increase the company's image. For the unilaterally economically minded managers the ambition of economic stabilization of the firm that could exist on the market without ISO 14001 certification, the above mentioned arguments are not so attractive and their effort to reduce total fixed costs of the organization is not convincing. For so-minded managers is newly published standard for energy management system ISO 50001 more attractive. This standard presents clearly the main purpose of energy saving and its efficient and economic use. For this reason, it can be assumed to be a useful tool for a wide range of top managers. Partly for those who consider only economically it offers an opportunity and for those who see the benefits of savings in addition to the standards in the environmental sphere. There is a matter of time that ISO 50001 will be adopted and supported by the management and introduction of an energy management system. Of course, the motivation is saving company's costs. In the case that a system of energy management really shows savings energy costs in the company, it will have strong support in the leadership of the organization. Building and improving such a system will be a priority for top managers and therefore can be assumed that the overall structure and operation of system will be in the high level. Based on this strong and correctly maintained structure of the energy management system it is possible implement without significant cost even the environmental management system. The decision of top management of organization concerning the introduction of ISO 14001 after previous good experience with ISO 50001 is easier than in the case of a decision to introduce ISO 14001 with no previous experience with the successful ISO 50001. In addition, built structure of the energy management system brings benefits in the form of savings and it is useful for environmental management system and thereby saves many other costs that the company would have to spend in independent implementation of ISO 14001. In this case, any small requirement to the introduction ISO 14001 with

„stakeholders“ by top managers is more acceptable than if they were venturing into the implementation of ISO 14001 from the beginning and separately.

Based on the above it can be alleged that the road to implementing an environmental management system could be easier and more acceptable to the dismissive minded managers through successfully implemented energy management system according to ISO 50001.

6. CONCLUSION

Unilaterally economically minded managers are often negative for the introduction of standardized management systems such as ISO 14001. Their priority is saving costs and the introduction of environmental management system is perceived as additional costs. As shown in the article, that managers need the tool that offer a clear opportunity for cost savings. The energy management system according to ISO 50001 is such a tool. After the successful implementation and demonstration of the economic benefits of energy management, top managers are more willing to agree to the implementation of other tools. Throughout the structure already built within the system it is possible to introduce more systems e.g. EMS according to ISO 14001 with a much lower entry costs.

7. REFERENCES

- [1] EN ISO 50 001.
- [2] EN ISO 14 001.
- [3] International Organization for Standardization, Win the energy challenge with ISO 50001, 2011 ISBN 978-92-67-10552-9.
- [4] DIN EN 16001: Energy Management Systems in Practice - A Guide for Companies and Organizations, Federal Ministry for the Environment, Nature Conservation and Nuclear Safety, Berlin 2000.

Authors: Ing. Michal Maňko, PhD., Ing. Alžbeta Košíková, University of Central Europe in Skalica, Department of Ecology and Environmental Science, Kráľovská 386/11, 909 01 Skalica, Slovakia.
Phone: 00421 911 444 547
E-mail: michal.manko@inbox.com
kosikova@yahoo.com

Milanković, D., Milanović, B., Agarski, B., Crnobrnja, B., Ilić, M., Kosec, B., Budak, I.

LIFE CYCLE ASSESSMENT OF AN INTERMODAL STEEL BUILDING UNIT IN SERBIA

Abstract: *In order to minimize and eventually, in the future, eliminate the negative environmental impacts, such as emissions, waste, energy and excessive raw material consumption etc., of construction, and simultaneously move closer to sustainable development in the society, the life cycle assessment of buildings is essential. This paper provides an insight in environmental life cycle assessment (LCA) of a typical intermodal steel building unit (ISBU) in Serbia. The goal of this study was to determine the impact of ISBU lifetime on environment. For materials and methods in this work, a combination of input–output and process analysis was used in assessing the potential environmental impact associated with the system under study according to the ISO14040 methodology. The study covered the whole life cycle including material production, construction, occupation, maintenance, demolition, and disposal.*

Keywords: *Life Cycle Assessment – LCA, intermodal steel building unit, environmental impact, Serbia*

1. INTRODUCTION

The built environment is a major contributor to both social and economic development and represents a large portion of real capital in many countries; but it is also a primary source of environmental impacts. Furthermore, existing building stock requires continuous investments for repair and renovations. The notion that building structures that would last for centuries is the best environmental solution to our problems does not match with our existing building use trends and knowledge of the built environment. Buildings will be replaced with newer designs that are more suited towards the needs of future occupants. Energy is an essential input to every production, transport, and communication process and is thus a driver for the economic as well as social development of any nation. The building construction industry consumes 40% of the materials entering the global economy and generates 40–50% of the global output of greenhouse gases and the agents of acid rain [1,2]. The growing concern of environmental problems, such as global warming, which have been linked to the extended use of energy, has increased both the importance of all kinds of so-called “energy saving measures”, and the necessity for an increased efficiency in all forms of energy utilization [6,7]. As a consequence of the latest reports on climate change and the need for a reduction in CO₂ emissions, huge efforts must be made in the future to conserve high quality, or primary energy, resources [9]. While consuming large amounts of energy, building industry has also cause large burden on the environment due to the environmental emissions by the production of building materials and the running of building system [2]. Extraction or purification of materials from their natural ores is an activity that consumes energy, generates waste, and also contributes to environmental damage with negative impacts such as resource depletion, biological diversity losses, and other. On the

other hand they provide the necessary infrastructure for many productive activities such as industries, services, commerce, and utilities, and thus satisfy a very basic human need. However, due to this very basic nature of buildings, stakeholders in development sometimes do not consider the environmental impacts of building, especially in developing economies. Life cycle assessment (LCA) is a very helpful tool in this regard as it not only provides an account of materials and energy involved in a product or system but also measures the associated environmental impacts [10].

2. METHODOLOGY

As a significant tool of environmental management, life-cycle assessment has become an internationally recognized criterion. It is the basis for establishing environmental policy and is generally used to guide the clean production, development of green production, and the environmental harmonization design [8,10]. A life-cycle assessment (LCA) is a technique to assess environmental impacts associated with all the stages of a product's life from-cradle-to-grave (i.e., from raw material extraction through materials processing, manufacture, distribution, use, repair and maintenance, and disposal or recycling), as illustrated in Figure 1. LCAs can help avoid a narrow outlook on environmental concerns by [5]:

- Compiling an inventory of relevant energy and material inputs and environmental releases;
- Evaluating the potential impacts associated with identified inputs and releases;
- Interpreting the results to help make a more informed decision.

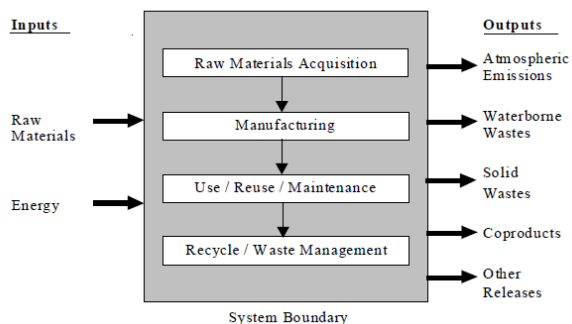


Figure 1. Life cycle stages

The LCA process is a systematic, phased approach and consists of four components: goal definition and scoping, inventory analysis, impact assessment, and interpretation [3,4]:

1. Goal Definition and Scoping
2. Life Cycle Inventory Analysis (LCI)
3. Life Cycle Impact Assessment (LCIA)
4. Interpretation

2.1 Goal and scope

The goal of this study is to estimate the environmental impacts of a typical intermodal steel building unit in Serbia. The system studied includes the part of a life cycle of the building, including manufacturing of building materials, construction, operation, and maintenance. For the demolition and disposal stage, due to lack of relevance data, landfilling is assumed. Transport for each life cycle stage was also included. Only the structure and envelope of the selected building are assessed. Special emphasis is put on energy consumption. The functional unit for this estimation was defined as 1 intermodal steel building unit for a period of 25 years which is used for office purpose (Figure 2a and 2b.).



Figure 2a. ISBU



Figure 2b. Intermodal steel building units in Novi Sad, Serbia for office purposes

2.2 Inventory

The second step of the LCA is inventory analysis. It contains the data collection and calculation procedures, and is of key importance since this data will be the basis for the study. Inventory is also tied to the scoping exercise since data collection and other issues may lead to refinement or redefinition of the system boundaries [3,4]. Data needed were gathered from EcoInvent Database v2.2 and other scientific publications such as journal articles, books etc.

Building parameters	Specifications
Dimensions	12.2 x 2.4 x 2.6
Service life	25 years
Floor area	~30m ²
Office volume	67.7 m ³
Structure	Steel
Envelope	Steel
Foundation	Reinforced concrete
Coverings	Gypsum, Plaster, Insulation
Floor finish	Linoleum
Windows	PVC

Table 1. Input data gathered for assessment of ISBU

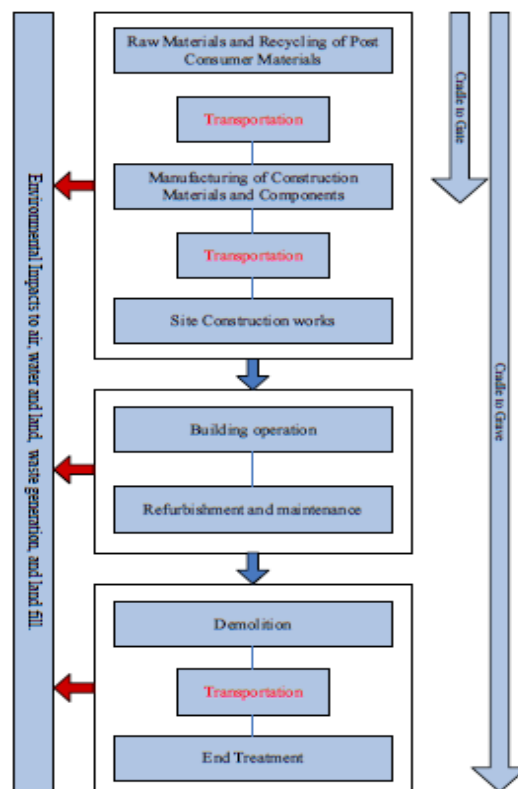


Figure 3. System boundaries

The LCA process has three major stages, building materials production phase, use phase, and the end-of-life phase. Each phase includes producing, transportation, distributing and so on. Fig. 3 (above) shows the model boundaries.

3. OBTAINED RESULTS

3.1 Impact Assessment

The assessment follows the LCI analysis first categorizes the impacts (resources consumption and

emissions) into a range of impact categories. The characterization step is then performed, which converts the quantities of various types of impacts under each category into equivalent quantities of a reference impact (e.g. methane into an equivalent amount of CO₂ under the global warming category), yielding one single impact indicator for each impact category. Each impact indicator retains the unit of measurement of the quantity.

In this case, the BEES method is employed. BEES is the acronym for Building for Environmental and Economic Sustainability, a software tool developed by the National Institute of Standards and Technology (NIST). BEES combines a partial life cycle assessment

and life cycle cost for building and construction materials into one tool. Results are presented in terms of life cycle assessment impacts, costs, or a combination of both. BEES strives to assist the architect, engineer, or purchaser to choose a product that balances environmental and economic performance, thus finding cost-effective solutions for protecting the environment. BEES uses the SETAC method of classification and characterization. Characterization results are illustrated on Fig. 4. Impact is represented via 12 impact categories according to BEES methodology. Fig. 5 presents the results of energy consumption compared during the production and installation stage and operation and use stage

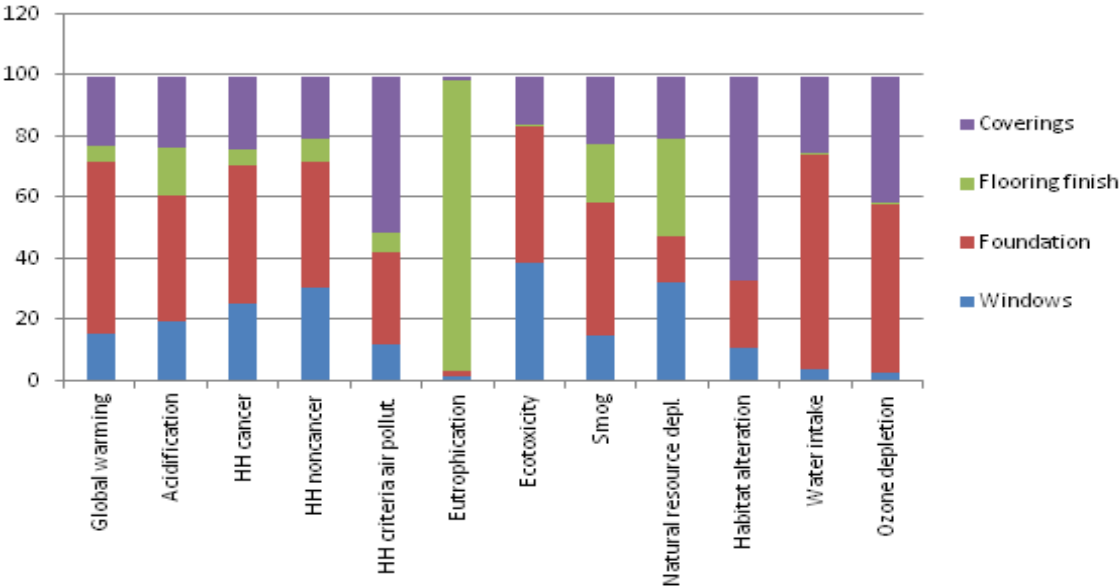


Figure 4. Characterization results of an ISBU production stage

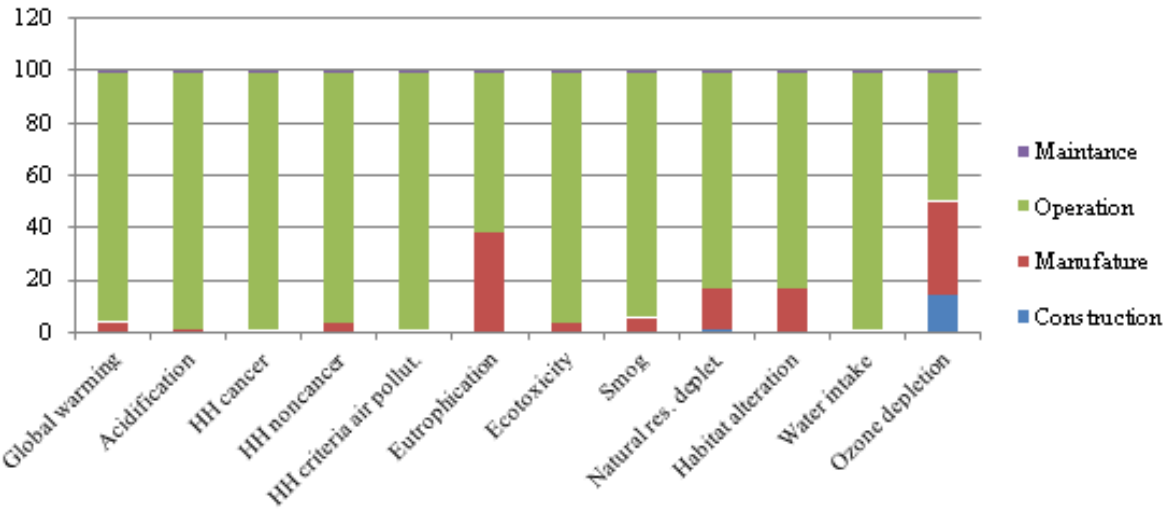


Figure 5. Characterization results of an ISBU regarding energy consumption

4. CONCLUSIONS

The general conclusion is that building with ISBU units from the aspect of evaluating the entire life cycle has its advantages. Based on the results obtained, ISBU that is analyzed indicates certain problem areas observed in

the product life cycle and that within the impact categories: Water intake, Ozone depletion and Global warming. The largest impact within the above mentioned categories results from processes of cement production that is used for the foundation on which the object is installed and also steel from which structure

and envelope is built. Processes observed in the use phase of the ISBU life cycle with its influence on the environment stands out from the rest, mainly because of the total electricity consumption in the assumed lifetime of 25 years. These problems can be successfully overcome if the existing structure is adapted to the rigorous requirements of a LEED (Leadership in Energy and Environmental Design) certification. A LEED-certified office is designed and constructed in accordance with the rigorous guidelines of the LEED for Offices green building certification program. LEED for Offices is a consensus-developed, third party-verified, voluntary rating system which promotes the design and construction of high-performance green offices. Main advantages of ISBU modules are:

- Strongest building construction on the planet
- Earthquake proof
- Fire proof
- Strong non-corrosion Corten steel
- Extreme security
- Recyclable - Green construction and modifications
- Saves trees
- Unibody construction
- Ideal for multiple floors and levels
- Fast construction
- Insulation: bonds easily with space-age Ceramic insulations
- Easily adapted to Prefab automation
- Easily adapted to custom homes/offices

Inter-modal Steel Building Units (ISBU) have become very popular and trendy for use as home, storage, prefab, and business construction purposes. Only recently has the world begun to realize their value in housing, office construction, storage and emergency shelters. The possibilities are virtually endless. One of the reasons for all the interest globally was the low cost of construction.

ACKNOWLEDGMENT

A part of result presented in this paper is obtained in the framework of the project “Continuous quality improvement of products and processes throughout the entire life cycle”, TR 114-451-1924/2011-02, supported by the Provincial Secretariat for Science and Technological Development of AP Vojvodina, Republic of Serbia.

5. REFERENCES

- [1] Cheng, EWL, Chiang, YH, Tang, BS: *Exploring the economic impact of construction pollution by disaggregating the construction sector of the input-output table*, Build Environ 4:1940–195, 2006
- [2] Adalberth, K.: *Energy use during the life cycle of buildings: a method*. Build Environ 32(4):317–320, 1997
- [3] Guinée, JB: *LCA - An Operational Guide to the ISO-Standards*, Kluwer Academic Publisher, Dordrecht, The Netherland 2002
- [4] Heijungs, R., Suh, S.: *The computational structure of life cycle assessment*. Kluwer Academic Publisher, Dordrecht, The Netherland, 2002
- [5] ISO 14040: *Environmental Management—Life Cycle Assessment—Principles and Framework*. International Organization for Standardization (ISO), Paris, 2006
- [6] Osman, A., Ries, R.: *Life cycle assessment of electrical and thermal energy systems for commercial buildings*. Int J Life Cycle Assess 12(5):308–316, 2007
- [7] Scheuer, C., Keoleian, G.A., Reppe, P.: *Life cycle energy and environmental performance of a new university building. Modeling challenges and design implications*. Energy Build 35:1049–1064, 2003
- [8] Anderson, J., Shiers, D.E., Sinclair, M.: *The green guide to specification: an environmental profiling system for building materials and components*, 3rd edn. Blackwell Science, Malden, MA, 2002
- [9] Borjesson, P., Gustavsson, L.: *Greenhouse gas balances in building construction: wood versus concrete from life-cycle and forest land-use perspectives*. Energy Policy 28(9):575–588, 2000
- [10] Kellenberger, D., Althaus, H-J: *Relevance of simplifications in LCA of building components*. Build Environ 44(4):818–825, 2009

Authors: MSc Darko Milanković, MSc Branislav Milanović, Assist. MSc Boris Agarski, MSc Branislava Crnobrnja, MSc Milana Ilić, Assist. Prof. Dr Igor Budak, University of Novi Sad, Faculty of Technical Sciences, Trg Dositeja Obradovica 6, 21000 Novi Sad, Serbia,

E-mail: dakamns@uns.ac.rs;

bane_m@uns.ac.rs;

agarski@uns.ac.rs;

brankacr@uns.ac.rs

milanai@uns.ac.rs;

budaki@uns.ac.rs;

Prof. Dr Borut Kosec, University of Ljubljana (Faculty of Natural Sciences and Engineering), Kongresni trg 12, 1000 Ljubljana, Slovenia,

E-mail: borut.kosec@omm.ntf.uni-lj.si

Muránsky, J.

DETERMINATION OF THE OPTIMAL PRODUCTION VOLUME RESPECTING THE ENVIRONMENTAL AND ECONOMIC CRITERIONS

Abstract: A mathematical method is applied to the solution of this problem. The individual factors of environmental and economic character are expressed by means of different equations having universal validity. The most important factor of the given ones is the so called natural capital, alias natural resources. They are derived from the environment. Each of summarized criterions is represented by its graphical form. An application to the automotive industry closes the paper.

Key words: optimal production volume, environmental and economic criterions, mathematical modeling, automotive industry

1. INTRODUCTION

Determination of the optimal production volume, applying mathematical methods and ecodesign principles is a significant step towards the identification of environmental and economic problems at source and hence leads towards a more sustainable society. Integration of environment aspects into the familiar product development process is important from both the environmental and economic perspective. Ecodesign projects, including exact methods, carried out all over the world have shown that besides helping to improve the environment, ecodesign and its mathematical tools also often offer business certain financial benefits. Exact access to the development of engineering products is one of the possibilities how to achieve the environmental and economic objectives. There are a lot of different analytical tools, by which this can be carried out. One of such tools, is described in this paper.

2. ENVIRONMENTAL AND ECONOMIC FACTORS AND THEIR EXPRESSION

Let us consider a production complex (for example, an engineering factory), situated in some locality, manufacturing x products during a time unit. The different harmful components are generated in that process too, having impact on the environment. The disposable quantity of the so-called natural capital is necessary to the activity of the considered production system. Natural capital is classifying to the non-renewable natural resources, and is derived from the environment. Minerals and fossil fuels are included in this category [2]. The structure of natural capital can be the as following:

- ores and their concentrates,
- raw material of energetic character (except of natural gas and crude oil,
- natural gas,
- crude oil.

Some sources and authors include selected metals and

their semi-finished products, selected plastics and their semi-finished products, consumption of electric energy per year, etc. [15], [18].

Let C_1 is a disposable quantity of natural capital during a year, for production of x products. If the value of x is increasing, of course, the value of C_1 will be decreasing. The following formulas can express this situation - $C_1/x \rightarrow 0$, and

$$K_1(x) = \frac{C_1}{x} \quad (1)$$

The factory must carry out activities for environment protection according to the valid legislature. Starting from the environment protection structure [5], [15], [16], these costs can be expressed as

$$\text{NOZP} = \text{EK} + \text{ENV} + \text{SOC}, \quad (2)$$

where NOZP-total costs for environmental protection, EK, ENV, SOC - main cost components of economic, environmental, and social character.

The economic part consists of these particular ones:

$$\text{EK} = \text{INV} + \text{PREV} + \text{SAN}, \quad (3)$$

where INV - capital expenditure in connection to the environment protection,
PREV - over-heads of the factory,
SAN - costs depending from the environment degradation (fines, fees, etc.).

The over-heads depend from the quantity of manufactured products x , so

$$\text{PREV} = V \cdot x, \quad (4)$$

where V - manufacturing costs per one unit of product

Environmental part of the total costs consists of two items:

$$\text{ENV} = \text{VONK} + \text{VNUT}, \quad (5)$$

where VONK and VNUT are environmental costs from the point of view of so called outside and inside environment, if

$$\text{VONK} = (\text{ODP} + \text{EMO} + \text{EMV}) \cdot x, \quad (6)$$

$$\text{and} \quad \text{VNUT} = \text{IM} \cdot x, \quad (7)$$

where ODP - quantity of solid wastes,
 EMO - quantity of emissions,
 EMV - quantity of liquid wastes,
 IM - quantity of imissions inside the factory.

All the presented items are incipient during the manufacturing of one product.

Particular result for the ENV is:

$$ENV = (ODP + EMO + EMV + IM) \cdot x \quad (8)$$

If the total costs for environment protection will be signified as $K_2(x)$, then after some derivations,

$$K_2(x) = C_2 \cdot x + INV + SAN, \quad (9)$$

where

$$C_2 = V + ODP + EMO + EMV + IM \quad (10)$$

The total costs for the manufacturing of x products in a factory, can be expressed as $K(x) = K_1(x) + K_2(x)$, and applying the substitutions, the following equation is obtained:

$$K(x) = \frac{C_1}{x} + C_2 \cdot x + INV + SAN. \quad (11)$$

The optimal number of products x is can be obtained after the differentiation of the equation (11) - i.e.

$$\frac{dK(x)}{dx} = -\frac{C_1}{x^2} + C_2 = 0 \quad (12)$$

and
$$x_{opt} = \sqrt{\frac{C_1}{C_2}}. \quad (13)$$

If $x = x_{opt}$ and $INV + SAN = C_3$, after substituting these expressions to the equation (11), the minimal value of the function $K(x)$ is determined as

$$K_{min} = \frac{C_1}{\sqrt{\frac{C_1}{C_2}}} + C_2 \sqrt{\frac{C_1}{C_2}} + C_3 \quad (14)$$

The graphical interpretation of these results is given in Fig.1.

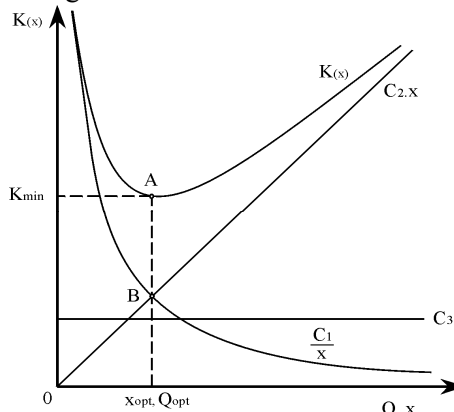


Fig.1 Graphical interpretation of the compromise solution between the economic and the environmental demands in the mechanical engineering industry

3. DISCUSSION

- The curve $K(x)$ sometime called as **the curve of the sustainable development** - has its minimum (point A), and represents, according to some approach, the compromise solution between the economic and the environmental demands on the micro-economic level.
- Consumption of the natural capital (habitually per annum) is gradually reduced by growing production, which is compensated with costs - to eliminate this consumption. Point B represents equality of both - costs and thus the **economic optimum of the environment quality - Q_{opt}** .
- The environment protection costs have their initiation part of the constant value, which consists of the capital expenditure part **INV** and constant payments **SAN**. It is presumed that **SAN = const**, to the $x = x_{opt}$ value. If $x > x_{opt}$, it will probably depend from the other concrete conditions.
- Perhaps, the presented method and approach can be applied to some parts in the LCC (Life Cycle Costing) analysis.

4. AN APPLICATION IN THE AUTOMOTIVE INDUSTRY

A European redoubtable car producer has provided some important input data to test the method described in this paper. These data are intentionally misrepresented (because of the firm secret). According to the provided data, the particular values of the function $K(x) = f(x)$ has been computed for a passenger car - vehicle weight ~ 1200 kg, and the following material structure [in %]: Ferrous 66, Aluminium and other light alloys 12, Plastics 12, Rubber 4, Glass 4, Zinc 1,5, Copper and its alloys 0,5. The computed data are illustrated in Tab.1.

x	y	C_1/x	$C_2 \cdot x$	$K(x)$
1	11	5,00	8,50	5,08
2	11	2,50	1,70	2,67
3	11	1,66	2,55	1,92
4	11	1,25	3,40	1,59
5	11	1,00	4,25	1,42
6	10	8,33	5,10	1,34
7	10	7,14	5,95	1,31
8	10	6,25	6,80	1,30
9	10	5,55	7,65	1,32
10	10	5,00	8,50	1,35
11	10	4,54	9,35	1,38
12	10	4,16	1,02	1,43
13	10	3,84	1,10	1,48
14	10	3,57	1,19	1,54
15	10	3,33	1,27	1,60
16	10	3,12	1,36	1,67

Table 1. The particular values of the function $K(x) =$

$f(x)$. The numbers in the right side of the columns are the exponents y . The particular values in the left side of the columns are multiplied by 10^y .

The graphical representation of the function $K(x)$, and its relevant parts, is illustrated in Fig.2.

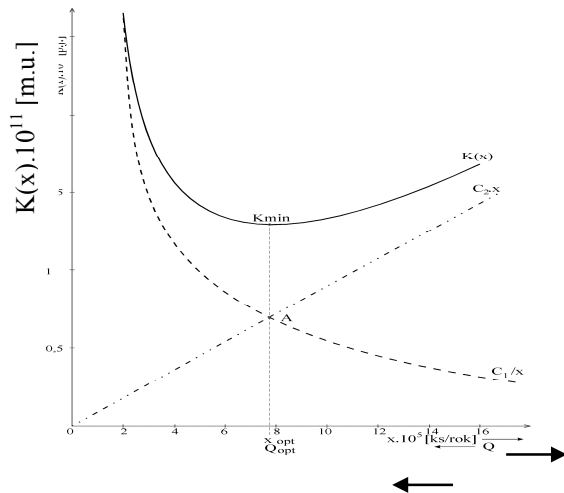


Fig. 2. The curve of the sust the presented applicat $x \cdot 10^5$ [pc/year] production) [5] Q
Abbreviations: **m.u.** - monetary units; **pc** - pieces.

The C_3 part is not illustrated in Fig.2, because of its irrelevant influence and constant value. Some comments to the Fig. 2:

- Value K_{min} of the curve $K(x)$ expresses a compromise between the economic and the environmental demands.
- The curve C_1/x is the curve of the natural capital consumption during the car production in the factory.
- x_{opt} is the optimal car production volume per year (about $7.8 \cdot 10^5$) for the given conditions.
- Q_{opt} is the optimum value of the environment quality for the given production process character.
- Point A represents the compromise solution.

5. CONCLUSION

There is the need for systematic approach to organize a factory in such a way that improving the environmental and economic performance of their products across product life cycles becomes an integrated part of operations and strategy. Determination of optimal production volume has operational and strategic purpose, too. The described method represents the way, how to determine it. An application in the automotive industry, this approach can bring not only environmental, but also economic benefits, as shown in the paper.

6. REFERENCES

- [1] Cenník Londýnskej burzy kovov z 22.07.2011 . Portál štatistickej ročenky SR 3794/2011
- [2] Gray, M.: Geodiversity : Valuing and Conserving Abiotic Nature. J.Wiley & Sons, Chichester, 2004, 220 p.
- [3] Koděra, R. : Aktuálne informácie o význame a zaujímavostiach a rozšírení rudných surovín. Available from: <http://www.geovzdelavanie.sk/seminar5/prezentacie/rudy.pdf>
- [4] Maury, X. : Plastic Omnium Auto Exterior: The first "Design for Recycling and Dismantling" Bumper, The ECODESIGN Program. In: GPEC Conf., Anger, 2009, 9 p.
- [5] Muránsky, J. :Ecodesign in mechanical engineering - methodology (in Slovak). SD(VLK), Košice,2004, 292 p., ISBN 80-8073-19-5
- [6] Muránsky, J. :Environmental compatibility of mechanical engineering products (in Slovak).SD (VLK), Košice,2008, 300 p., ISBN 978-80-969887-9-2
- [7] Muránsky, J. :Examples of ecodesign in mechanical engineering (in Slovak). SD(VLK), Košice, 2010, 235 p., ISBN 978-80-969887-9-3
- [8] Muránsky, J.:CoDe-09- A System for Environmental Assessment of Mechanical Engineering Products in their Conceptual Phase. In: Transactions of the Universities of Kosice, 2/2010, pp. 23 - 29, ISSN 1335-2334
- [9] Sutherland, J. : Environmentally Responsible Manufacturing Enterprises - A Key to Sustainable Development. Rep. of the Dep. of Mech. Engr. - Michigan Technological University, Michigan, 2008, p.16
- [10] Vodzinsky, V.: Surovinová politika pre oblasť nerastných surovín. Pracovný materiál, TU BERG, Košice, 2004, 16s.
- [11] Výnos úradu pre reguláciu sieťových odvetví z 28.07.2008 č.2/2008 - Ceny energií
- [12] Available from : http://www.sjf.tuke.sk/kpam/e-dokumenty/Zbornik_2009.pdf
- [13] Available from: <http://www.ekonomika.sme.sk/c/3194393/vo-.../>
- [14] Available from : web.tuke.sk/.../web_zva-2010.pdf
- [15] Available from : <http://www.portal.statistic.sk/showdoc.do?docid=3794>
- [16] Available from : <http://www.cecs.pdx.edu/~herm/capstone/mee9899/491stuff/mon7/>
- [17] Available from: <http://www.answers.google.com/answers/threadview?id=433981>
- [18] Available from : http://www.teeb.ecosyst/stud/eu-0810/an_2010

Author : Prof. Ing. Juraj Muránsky, PhD., CEU Prague, working place: Košice, Rožňavská 15, Slovakia. Phone: +421 944 160 860, E-mail: jurmur@netkosice.sk

Petelj, A., Hadžistević, M., Antić, A., Hodolić, J.

DETERMINATION OF ABSORPTION COEFFICIENT OF SAMPLE UNDER NON-LABORATORY CONDITIONS

Abstract: Due to small number of reverberation chambers in developing countries, there is a need for the determination of acoustic properties of materials in non-laboratory conditions. There is also a lack of "expensive" software for modeling the propagation of sound in rooms, which imposes need for alternative solutions. For these reasons, this paper examines the possibility of using the reverberation time formulations to predict the reverberation time and absorption coefficients of samples tested in ordinary rooms.

Key words: sound absorption coefficient, reverberation time formula, non-laboratory conditions

1. INTRODUCTION

The reverberation time formulations are designed for prediction of parameters in diffuse sound field. In the reverberation chamber method Sabine's formulation is used to determine the absorption coefficient of the sample. Reverberation chamber has approximately diffuse sound field but tested material sample makes sound field less diffuse if sample has a much higher value of absorption coefficient in comparison to absorption coefficients of chamber surfaces and if sample is of significantly lower surface area relative to the total surface area of the chamber, which is often the case. Despite the long practice of measuring in reverberation chambers, absorption coefficient can range up to 0.4 for the same sample in two different laboratories, which is a huge error [1]. One of the main characteristics of diffuse sound field is that reverberation time is the same regardless of the position of sound source and microphone. This phenomenon is observed in ordinary rooms with surfaces of similar values of absorption coefficients when the room is empty, i.e. without tested absorbent sample; therefore there are made measurements of reverberation time with and without absorbent sample. Measured values were used for comparison with calculated values using reverberation time formulations and for obtaining absorption coefficients in order to determine the deviations of the calculated absorption coefficients to the real one.

2. MEASUREMENTS SETUP

Measurements were performed in two rooms of irregular shape. One was a nuclear shelter room (hereinafter referred to as room 1) of area 32.60m² and the height 3.25m, and second one was storage room (hereinafter referred to as room 2) of surface 14.15m² and height 2.80m. Figure 1 shows floor plans of rooms.

Excitation of the room for reverberation time measurements were carried out by impulse sound, and the source was balloon whose circumference was around 80cm, which is considered adequate for this purpose [2]. Measurements were made by sound level

meter, which has option for automatic calculation of reverberation time.

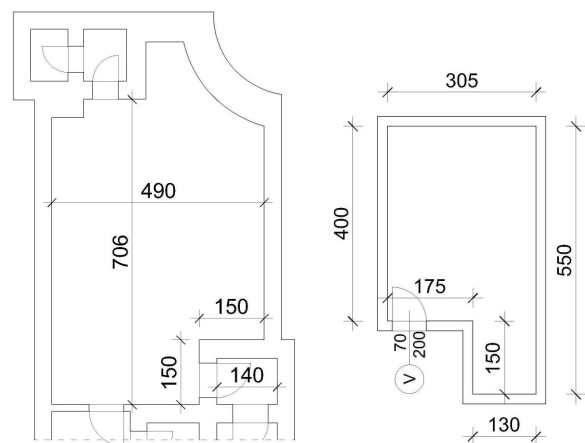


Fig. 1 Floor plans of rooms 1 and 2, respectively

Positions of microphones and sources were closer to the corner of a room or closer to the middle part of the room in both rooms. The minimum distance between microphone, source and reflective surfaces was 1m. The tested sample was glass wool, which was placed in several positions on the floor. Selected positions of the absorber were closer and further away from the sound source (distances between positions were 30cm), to determine the possible dependence of the reverberation time on the distance of absorber from the sound source. Different surfaces and thicknesses of samples were selected to determine how they affect the deviation of the calculated absorption coefficients from adopted ones from literature sources. In the room 1 measurements were performed with absorber samples of 10 cm layer thickness and of area 0.5, 1.0 and 1.5m², and in the room 2 measurements were performed with absorber samples of 5 and 10 cm thicknesses and 1.2m² area.

3. ADOPTED REVERBERATION TIME FORMULATIONS

Three formulas for reverberation time are chosen. The first one is Sabine's, which is still widely used and is part of the current standards regardless of the well-

known deficiencies. In the case of samples with high absorption it may give coefficient values greater than 1, which are not realistic. Formula used to less extent and recommended by some authors is the Millington's, which does not give values greater than 1 if Millington's coefficients are used. Dance and Shield [3] enabled easy transformation of Sabine's coefficients, which are available in various literatures, to Millington's coefficients, which are available to a much lesser extent, thus facilitating their implementation. The third formula used is Zhang's, for which the autor [4] claims that is the better version of Millington's formula. It also uses Millington's coefficients.

Sabine's, Millington's and Zhang's formulas are given below:

$$T_s = \frac{55.3V}{c \sum \alpha_i S_i} \quad (1)$$

$$T_m = \frac{55.3V}{-c \sum S_i \ln(1 - \alpha_i)} \quad (2)$$

$$T_z = \frac{55.3V}{-cS \sum \ln(1 - \alpha_i \frac{S_i}{S})} \quad (3)$$

where:

T_s - reverberation time according to Sabine

T_m - reverberation time according to Millington

T_z - reverberation time according to Zhang

V - volume of room

c - sound velocity

α_i - absorption coefficient of room element

S_i - surface area of room element

4. ADOPTED ABSORPTION COEFFICIENTS

Tables 1 and 2 show the materials of which rooms parts were made, adopted Sabine's coefficients for a given material, as well as the values when they are converted to Millington's coefficients via formula [1]:

$$\alpha_m = 0.071\alpha_s^3 - 0.416\alpha_s^2 + 0.99\alpha_s + 0.005 \quad (4)$$

Sample surface (m ²)	Sabine's α			Millington's α				
	Adopted	without side surfaces of sample	with side surfaces of sample	Adopted	without side surface of sample		with side surfaces of sample	
					Millington f.	Zhang f.	Millington f.	Zhang f.
0.5	0.85	2.90	1.81	0.59	0.74	1.60	0.57	1.00
1.0	0.85	1.97	1.41	0.59	0.70	1.32	0.58	0.94
1.5	0.85	1.62	1.21	0.59	0.67	0.60	0.57	0.45

Table 3. Adopted and calculated absorption coefficients of samples for room 1

Since the Millington's formula showed the best results, analysis of the octave bands were done using this formula. Since the available literature absorption coefficients are for the octave bands from 125Hz to 4kHz, these bands were analyzed. In most cases, large deviations of calculated absorption coefficients relative to the adopted ones were noticed. Only for the 125 and 500 Hz octave bands the calculated coefficients are

Material	Sabine's α	Millington's α
Door, steel	0.073333 ^[5]	0.075391
Floor, ceramic tiles	0.013333 ^[6]	0.018126
Walls and ceiling, concrete	0.018333 ^[1]	0.023011
Person	0.435417 ^[7]	0.363055
Glass wool (10cm)	0.85 ^[1]	0.589543

Table 1. Absorption coefficients for room 1

Material	Sabine's α	Millington's α
Walls, plastered concrete blocks	0.046667 ^[8]	0.05030126
Floor, concrete	0.0275 ^[1]	0.031911877
Door, wood	0.06666667 ^[1]	0.052836073
Ceiling, wood	0.03833333 ^[1]	0.045532914
Person	0.435417 ^[7]	0.363055052
Glass wool (10cm)	0.85 ^[1]	0.589542875
Glass wool (5cm)	0.668333 ^[1]	0.502030721

Table 2. Absorption coefficients for room 2

The selected coefficients are mean values of the coefficients for the individual octave bands from 125Hz to 4kHz, since the values for these octaves are available in the literature.

5. RESULTS AND ANALYSIS

5.1 Predictions of absorption coefficients

Calculated Millington's coefficients were significantly deviated from the adopted coefficients and in the way that decreasing sample surface results in increasing deviation. However when the side surfaces of the samples were included in calculations, the deviations were minor. When it comes to Sabine's formula, the deviations are reduced by including surfaces of edges in the calculations, but they were still non-negligible. Zhang' formula resulted in better results than Sabine's, but worse than Millington's. Table 3 shows the adopted and calculated absorption coefficients for the room 1.

similar to adopted ones. For the band whose center frequency is 250Hz obtained values were lower than adopted coefficients, while for the octave bands 1 kHz, 2kHz and 4kHz the calculated coefficients were higher. A general increase in the calculated absorption coefficients with increasing frequency is observed. The exception is the 250Hz band coefficient.

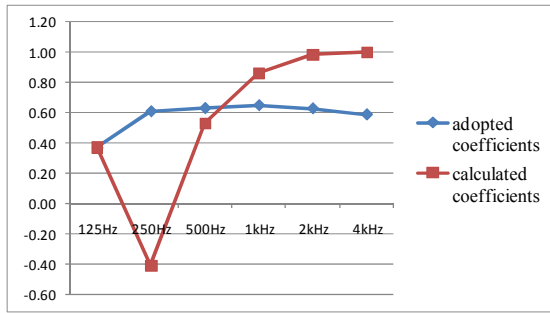


Fig. 2. Absorption coefficients of 0.5m² surface sample

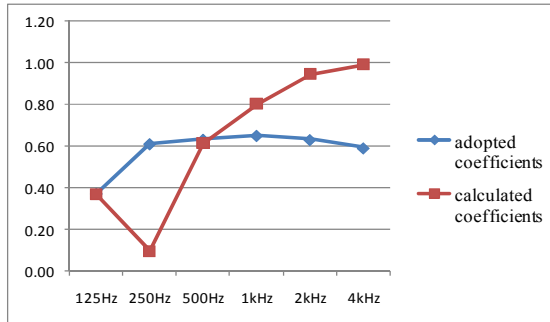


Fig. 3. Absorption coefficients of sample of surface 1m²

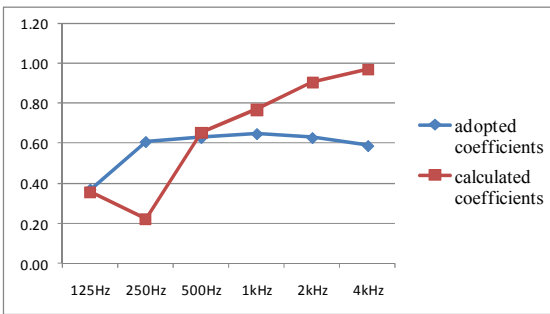


Fig. 4. Absorption coefficients of sample of surface 1.5m²

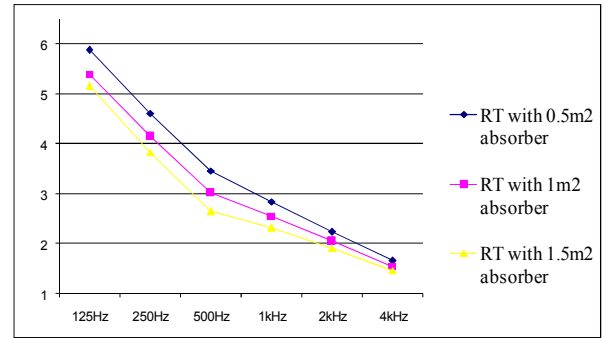


Fig. 5. Measured reverberation times with absorber samples

Figure 5 shows decrease of measured reverberation times for all three samples as central frequencies are higher and there is no significant deviation of reverberation time for 250Hz frequency band. Therefore measured reverberation time is not reason for extremely low calculated absorption coefficient for this band. Since sound velocity and room volume are constant, adopted values of absorption coefficients are cause for this deviation.

Results obtained for room 2 are similar to room 1. Small deviations of the calculated Millington's coefficients were obtained by including lateral surfaces of the samples in the calculation. For Sabine's coefficients, the deviation was reduced by including surfaces of edges in the calculation, but it was still significant. Zhang's formula gave similar results as Sabine's. Table 4 shows the adopted and calculated absorption coefficients for room 2.

The adopted absorption coefficients are larger than the calculated obtained by Millington's formula for 125 and 250 Hz octave bands for both sample thicknesses. Within other bands adopted absorption coefficients are smaller than calculated ones. A general increase in obtained coefficients with increase of central frequencies is observed in room 2 as well.

Sample thickness (cm)	Sabine's α			Millington's α				
	Adopted	without side surfaces of sample	with side surfaces of sample	Adopted	without side surface of sample		with side surfaces of sample	
					Millington f.	Zhang f.	Millington f.	Zhang f.
5	0.67	1.07	0.91	0.50	0.56	0.92	0.50	0.78
10	0.85	1.53	1.12	0.59	0.72	1.36	0.61	1.15

Table 4. Adopted and calculated absorption coefficients of samples for room 2

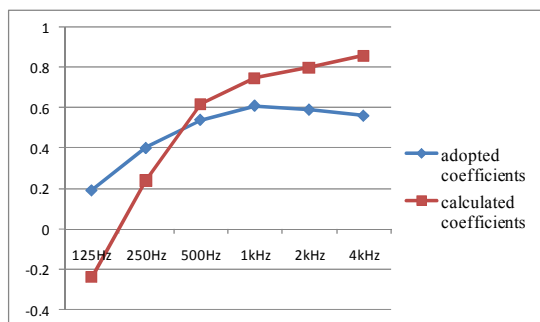


Fig. 6. Absorption coefficients of 5cm thickness sample

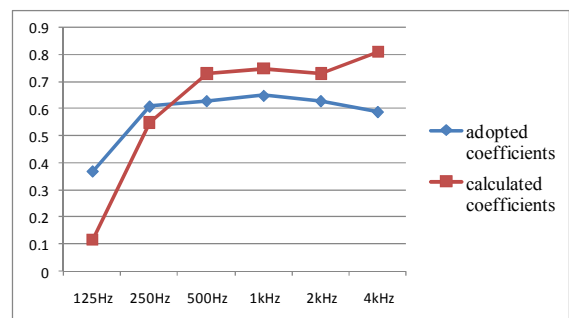


Fig. 7. Absorption coefficients of 10cm layer sample

5.2 Predictions of reverberation time

In the room 1 the mean value of the measured reverberation times of empty room was 4.00s. The maximum deviation of the measured reverberation time from the mean value was 0.05s. Reverberation time is also calculated by Sabine's, Millington's and Zhang's formulas. While Sabine's formula ($t = 4.88s$) showed significant deviation from the measured values, Millington's formula ($t = 3.99s$) resulted in a slight deviation. Reverberation time calculated by Zhang's formula (4.11s) resulted in some bigger deviation than Millington's, but much smaller than Sabine's formulation.

In the room 2 the mean value of the measured reverberation times of the empty room was 1.21s and there was no deviation of measured times from mean value. Sabine's formula resulted in reverberation time of 1.26s, and the deviation was not significant (0.05s). Obtained reverberation time by Millington's formula was 1.15s, and deviation was negligible as well (0.06s). The best prediction gave Zhang's formula with reverberation time 1.20s.

Analysis for individual octave bands are made only by Millington's formula from the reasons mentioned earlier in the paper. Prediction of reverberation time for individual octaves of empty rooms using the formula resulted in large deviations. The smallest deviation was for the 250Hz octave band, where the calculated reverberation time was 0.27s shorter than measured one. The maximum deviation was for the 4kHz octave band, where the calculated time was longer by nearly 2s than measured one.

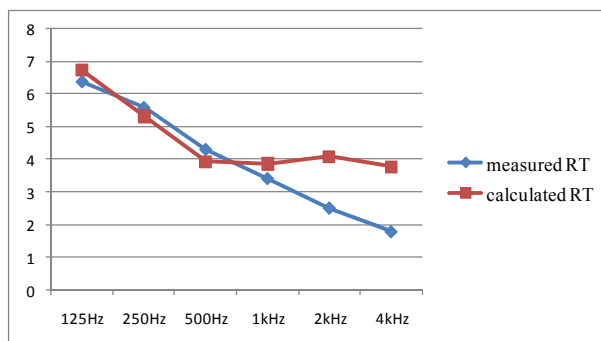


Fig. 8. Measured and calculated reverberation times in room 1 without absorber

Figure 8 show that higher the frequency shorter the measured reverberation times in empty room. This is not the case with calculated reverberation times due to similar values of adopted absorption coefficients for 500Hz to 4kHz frequency bands.

Regarding octaves in room 2 the observed deviations are large for reverberation time of empty room in most cases. The least is deviation of 500Hz band, (0.03s) and the biggest for 125Hz octave (0.66s).

5.3 The dependence of the reverberation time of the distance of sound absorber from the sound source

In room 1 measurement were performed with samples placed at different distances from the source.

Different correlations between reverberation time and distance are obtained. It was observed that as the sample is further from the sound source, the reverberation time is greater only for the sample of surface 1.5 m². Due to the lack of a clear dependence of reverberation time and absorption coefficient on the distance of sample from the sound source, it has not been further analyzed.

6. CONCLUSIONS

Sabine's and Zhang's formulas did not result in good approximations of reverberation time and absorption coefficients of samples in most cases. Application of Millington's formula in combination with Millington's coefficients taking into account the lateral surfaces of the samples has resulted in small deviations from measured values, but it is limited to determination of mean reverberation time and mean absorption coefficient of the sample for the frequency range that includes the octave bands from 125Hz to 4kHz, as application to single octave parameters did not give satisfactory results. Tests included samples of several thicknesses and sizes and rooms of certain dimensions and shapes, therefore additional measurements are required to establish the general applicability of the method.

7. REFERENCES

- [1] Cox, J., D'Antonio, P.: *Acoustic Absorbers and Diffusers*, Taylor & Francis, 2009.
- [2] Jambrosic, K., Horvat, M., Domitrovic, H.: *Reverberation time measuring methods*, Acoustics 08 Paris, 2008.
- [3] Dance, S. M., Shield, B. M.: *Modeling of sound fields in enclosed spaces with absorbent room surfaces*, Appl. Acoust. 58, 1–18, 1999.
- [4] Zhang, Y.: *A method to predict reverberation time in concert hall preliminary design stage*, Ph.D., Georgia Institute of Technology, 2005
- [5] http://www.maplesolution.com/sound_ab.php
- [6] Rossing, T. D.: *Springer Handbook of Acoustics*, Springer, 2007.
- [7] Jacobsen, F., Poulsen, T., Rindel, J. H., Gade, A. C., Ohlrich, M.: *Fundamentals of Acoustics and Noise Control*, Department of Electrical Engineering, Technical University of Denmark, 2009.
- [8] Beranek, L. L.: *Concert Halls and Opera Houses: Music, Acoustics, and Architecture*, Springer-Verlag New York Inc., 2004.

Authors: MSc Ana Petelj, Assoc. Prof. Dr Miodrag Hadžistević, Assis. Prof. Dr Aco Antić, Prof. Dr Janko Hodolić, University of Novi Sad, Faculty of Technical Sciences, Trg Dositeja Obradovica 6, 21000 Novi Sad, Serbia,

E-mail: petelja@uns.ac.rs;
miodrags@uns.ac.rs;
antica@uns.ac.rs;
hodolic@uns.ac.rs

Sabolová, J., Fedorčáková, M.

HYDRODYNAMIC MODELING OF FLOOD EVENTS IN SELECTED AREA

Abstract: For effective evaluation of flood protection and flood protection measures using of GIS devices and hydrodynamic modeling is successful. The hydrodynamic modeling can serve as basis for an assessment of flood-protection measures and suggestions how to reduce or even eliminate an extension of floods in the area. An area along the Olšava River is stricken by floods very often, like it was in May and June in 2010. Knowing of quality of input data for modeling is a key in assessment of accuracy and credibility of results.

Key words: GIS, Assessment, Modeling, Flood-protection, Hydrodynamic modeling.

1. INTRODUCTION

Monitoring and analysis of hydrological processes is becoming due to the increasing frequency of floods increasingly important. Their understanding and interdependence can help us model simulation in computer environment. GIS is a tool for processing large amounts of data and information obtained from measurements and observations, but they are highly dependent on their correct interpretation. The advantage of modeling is the ability to simulate not only the real situation in the study area, but also proposals for measures to prevent negative impacts of floods and assess their impact.

2. SITUATION IN SLOVAKIA

To harmonize the legislation of the Slovak Republic and the European Union has been transposed European Parliament and Council 2007/60/ES on the assessment and management of flood risks [1] in the legal system of the SR Act no. 7/2010 Z. z. on flood protection [2], which came into force on 1 February 2010.

In Slovakia, the use of software is based on hydrodynamic models developed abroad and there are especially MIKE and HEC-RAS. MIKE is created by an international consulting and research organization DHI, which operates in Slovakia. HEC-RAS is developed the U.S. Army Corps of Engineers (USACE) Hydrologic Engineering Center (HEC) in 1964. This product is constantly improved and is compatible with existing GIS tools. With the extension ArcGISu - HecGeoRas can prepare geometry data necessary for hydrodynamic modeling such as a digital terrain model, cross sections, flow lines, troughs, shores, etc. Its advantage is that it is free software (freeware). For this reason he was selected for hydrodynamic modeling of flood situation in the water flow Olšava.

3. COLLECTION AND PROCESSING OF DOCUMENTS

Slovak Water Management Enterprise, state enterprise, has created a work team, using surveying instruments recorded flood boundary and water level of

floods in the river Olšava. They obtained good basis for comparison of results of mathematical modeling of the actual state during floods and to calibrate the mathematical model of unsteady flow on the flow field of interest.

In modeling the flow of water is used the input data of different types and formats:

- maps,
- surveying terrain data,
- hydrological data,
- hydro data,
- calibration data. [3]

Based on the morphology of the terrain density measurement points were chosen to capture the changes in flow, the depth of the bottom of the bed, banks and other bed inequalities. Reconnaissance, which was examined at trough of water flow and its surroundings have been designated positions and ways of stabilizing control points. In the vicinity of the watercourse to a distance of approximately 100 m elevation points were targeted in the field. This focus trough profiles need to refine and better knowledge of the DTM during the relief. For hydrodynamic modeling a required knowledge of geometry on the flow structures such as bridges, culverts, and protective structures is needed. On the flow Olšava Bohdanovce in the village there is a bridge, whose geometric parameters had to be addressed. The focus points of the flow were used at Olšava universal surveying station LEICA TCR 802 ultra and Leica GPS 900 CS (two pieces of single-frequency apparatus with radio modem). It focuses and sets out detailed points using RTK (real time kinematic) method of connecting to the network state space SKPOS. The measurements of cross sections of flow Olšava in the month of May was in the bed of low water level, making it possible in some sections to pass the so-called trough waders.

The quality of spatial data in the DTM stream Olšava: The origin of spatial data - as input for the creation of DTM was used vectorized contour lines in scale 1: 5000 measured points and valley profiles. Positional accuracy (horizontal and vertical) -

positional and vertical accuracy of contours in scale 1: 500, according to 74/2001 Coll Decree 461/2009 [4], $|\Delta d| \leq 0,67[(dm + 12)/(dm + 20)]$, where dm is the length calculated from the coordinates and dm is the length of the connector determined from direct measurements. The accuracy of measured points and cross-valley profiles are used according to manufacturer's GPS device using the RTK method boundaries in position 2 cm and 4 cm in height. Attribute accuracy - the accuracy of the attributes have been compared and updated using aerial photographs, inspections and measurements in the field - as high-quality ratings. Completeness - all objects (in this case Bohdanovce Bridge) to modeling field focused on field measurements and mapping.

When creating a DTM to maintain logical consistency and accuracy schematics. Time information - measurements were made in March 2011, another inspection was in May 2011. Contours in Scale 1: 5000 are from 2007.

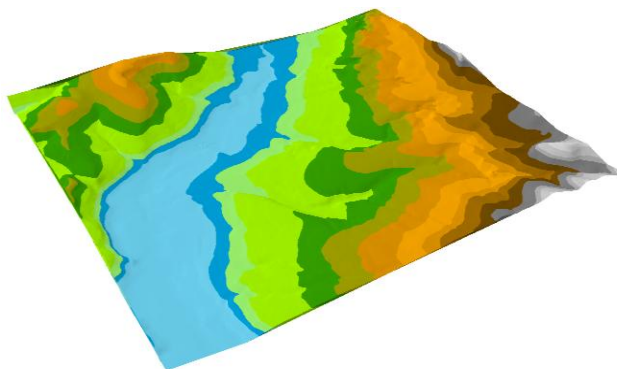


Fig. 1. Digital terrain model of the river Olšava

Main stages of hydrodynamic modeling are:

- 1) for - processing,
- 2) hydraulic calculation,
- 3) post - processing.

Pre-processing using HEC-GeoRasu GIS allows us to prepare the geometry of elements with attributes that are necessary for hydrological calculation in the program HEC-RAS. The role of pre - processing can be summarized as:

- preparation of 2D curves defining the flow axis, cross sections, stream banks and water flow directions,
- using tools for creating applications HecGeoRas 3D data based on DMT.

Specifically, the adjustment curves prepared in the previous step generate the trough geometry files for import into HEC-RAS. [5]



Fig. 2. The View layer - created using Processing HecGeoRas in ArcScene

4. POST-PROCESSING

When importing data output from the program HecRas requires an export definition file from HecRas, e.g. the surface area in a grid format TIN resolution size of grid cells. The level of detail and accuracy Grid layer is directly proportional to the value of grid resolution. In the processing of input data can be [5] relatively in conformity follows the drop-down menu on-Terror PostRas.

It is designed to map levels of the individual Q and polygons that represent the flood line. This can determine the area of flooding and water level in each grid cell.

Maps show the depths of our depth of water in each grid cell for each Q_{max} . They are generated at the entrance to the results of hydrodynamic modeling and GIS by calculating the difference between the amount of raster digital terrain model and the calculated levels of dimensions.

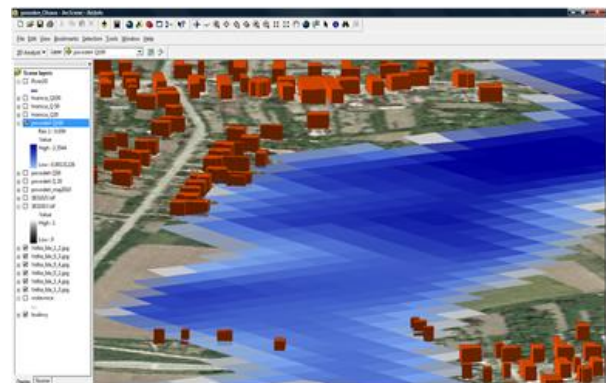


Fig. 3. View map grid depth Q100 levels in ArcScene

Extent of flood polygon is consistent with floods recorded in May 2010, but there are minor inaccuracies, maximum 20 m, which attributed to DTM inaccuracies. Also in the values of levels in the first two profiles that are in the hydraulic calculation, uncertainties arise due to lack of back-casting level curves, so these levels should be taken up more or less as a guide.

The applicability of data obtained from the modeling:

- assessment of flood threats and flood risk,
- proposals for flood control and anticipation of n-year stream flow, which is managed by the Slovak Water Management Enterprise, state enterprise,
- creation of water management plans under the Municipalities Act,
- to develop community development plans, as a basis for insurance carriers.

5. SUMMARY

Hydrodynamic model of the flood situation in the selected areas were acquired for flood flow lines Q20, Q50, Q100 and Q flow rate, which was during the floods in May 2010.

Since the 2010 flood hit the area with nearly a century wave flow, as during the initial aid of surveying instruments recorded in detail the incident that left a high damage to assets. The results of modeling for Q may 2010 were compared with actual flood will be helpful in the evaluation of flood activity in the design of flood prevention measures, but also in developing spatial plans of municipalities and water management plans.

6. REFERENCES

- [1] Directive Europe Parliament and Council Directive 2007/60/ES on the Assessment and Management of Flood risk,
- [2] Act. 7/2010 Z.z on Flood Protection,
- [3] Minarik et al.: *Flood potential in Slovakia. Methodology*, 2011, 68s., (in Slovak),
- [4] 74/2001 Coll Decree 461/2009, Instructions for cadastral renewal,
- [5] HAZLINGER, M.: 2007, *Comparison of modeling flood threats using Phoenix models and HEC-RAS model in the selected area*, (in Slovak).

Autors: **Ing. Jana Sabolová**, Faculty of Mining, Ecology, Process Control and Geotechnology - Institute of Geodesy, Cartography and Geographic Information Systems, Park Komenského19, 043 84 Kosice, Slovak also Water Management Enterprise, state enterprise, Mark Kosice

E-mail: jana.sabolova@svp.sk,

Ing. Monika Fedorčáková, PhD., Technical University of Kosice, Faculty of Engineering, Park Komenského 5, 040 01 Kosice,

E-mail: monika.fedorcakova@tuke.sk

Šebo, J., Fedorčáková, M.

**ECONOMIC OPTIMIZATION OF RECYCLING ORIENTED DISASSEMBLY OF
CONSUMER ELECTRONICS: THE CASE STUDY OF MOBILE PHONE**

Abstract: *The planning of disassembly of consumer products is a complex process. Different aspects such as product design, secondary material prices, possibilities of disassemble automation, labor costs and others play a role in selection of optimal disassembly strategy and sequence. In our article we present the case study of mobile phone disassembly sequence optimization based on hierarchical end-of-life decision model. By application of the model we identify which connection to dismantle and which leave intact, and which strategy of two (recycling or disposal) to apply for each component of mobile phone, to be economically optimal.*

Key words: *disassembly, recycling, mobile phone, optimization*

1. INTRODUCTION

Currently a number of environmental aspects influence the decisions in manufacturing industry. The concepts like Environmentally Conscious Manufacturing, Closed Loop Supply Chain and others have developed to cope with these aspects. Disassembly has an important role in these concepts. The determination of optimal disassembly sequence and end-of-life (EOL) options for product and its individual components are well-known problems in respective literature.

2. METHODOLOGY

Lee [1] define EOL option decision problem as to choose the EOL option that maximizes profit. Based on the hierarchical representation of the product, the optimal EOL option for each level is determined in his model. He finds the optimal EOL option by integrating two steps: maximize the economic value of EOL component options and minimize the disassembly cost, i.e. maximizes {Profit - Disassembly Cost}. In the model, because of remanufacturing strategy perspective, it is assumed that either the Remanufacturing (r) or Disposal (n) option should be selected for each subassembly or component. He uses following determination of the profits for each option [Gonzales and Adenso-Diaz (2005) in 1]:

Remanufacturing Profit $P_{r,i} = R_{r,i} - C_{r,i}$

$R_{r,i}$: the revenue obtained when the remanufacturing option is applied

$C_{r,i}$: the cost incurred when the remanufacturing option is applied

Disposal Profit $P_{n,i} = R_{n,i} - C_{n,i}$

$R_{n,i}$: the revenue obtained when the disposal option is applied

$C_{n,i}$: the cost incurred when the disposal option is applied.

For n components in the same layer, the EOL option decision model is formulated by integer programming, as shown in Equation (1) [1]:

$$z(x,y) = \sum_{i=1}^n \{P_{n,i}(1 - x_i) + P_{r,i}x_i\} - \sum_{i=1}^n \sum_{j=i+1}^n y_{ij}d_{ij}a \tag{1}$$

subject to $2y_{ij} \geq x_i + x_j$ for all $i = 1, 2, \dots, n$ and $j = 1, 2, \dots, n$

$x_i = 1$, if component i is remanufactured

0, if component i is disposed

$y_{ij} = 1$, if components i and j are disconnected

0, otherwise

d_{ij} = cost incurred if components i and j are disconnected.

The bottom-up approach is used to determine the EOL options for the entire product [1].

In the article we apply above described model to optimize disassembly of mobile phone (MP) Nokia 7250i. Unlike the original model, we do not consider remanufacturing but we think about recycling as a second alternative to disposal. When applying the model we start with composition of Bill of Material (BOM) and Connection diagram. Then, based on real data and calculations we arrange a table of profits/losses for the individual components and sub-assemblies for both alternatives. Based on the measured disassembly times and unit disassembly costs we compute disassembly costs for each connection identified by a connection diagram. Then we use formula (1) for finding the optimal EOL option. By using the formula we calculate the profits for all evaluated sub-assemblies (for each sub-assembly all EOL option combinations of individual components). Based on the calculation and diagrams we make the final table with economically optimal (maximum profit, respectively minimum loss) options for the treatment of individual components and sub-assemblies. Also, we identify the most appropriate disassembly sequence (i.e., which connections to maintain and which to disconnect).

3. MODEL CALCULATION

3.1 Graphical representation of the MP Nokia 7250i

As a basis for below calculations and final

identification of the optimal EOL option and disassembly sequence we first draw a BOM (Fig. 1) and connection diagram (Fig. 2).

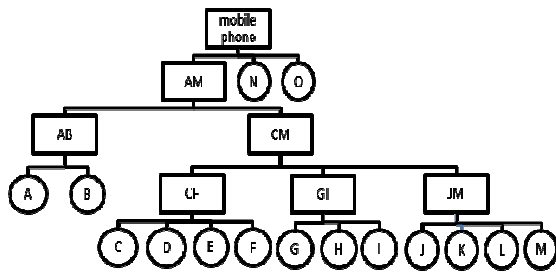


Fig. 1. BOM of MP Nokia 7250i

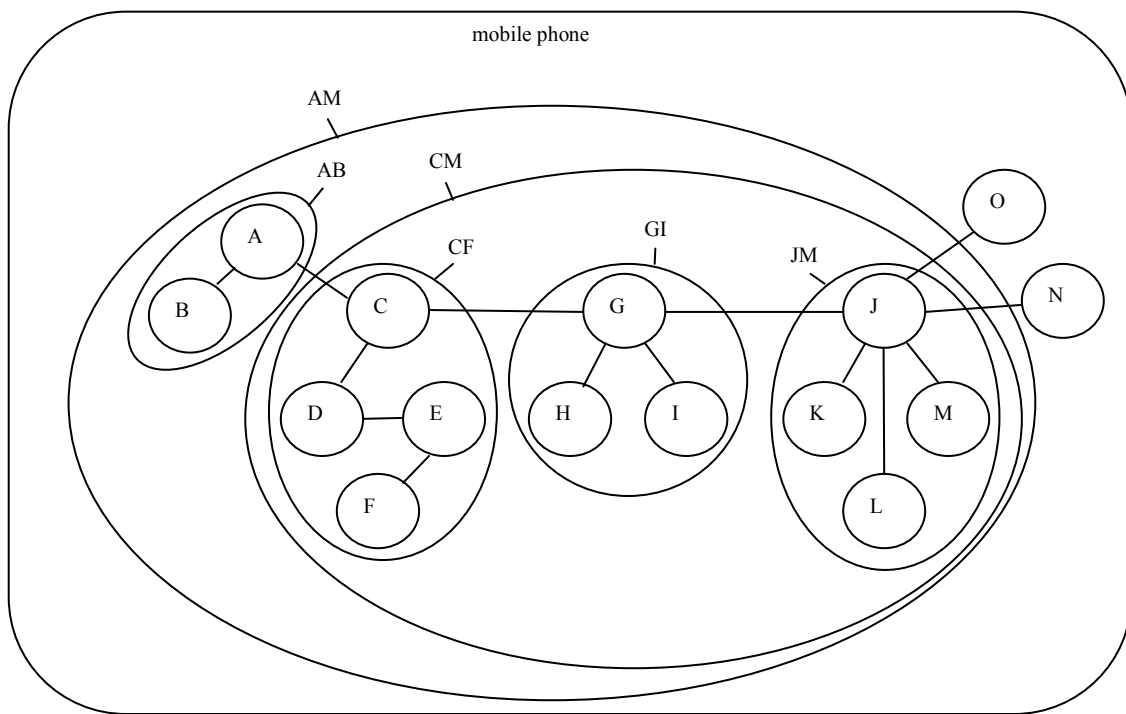


Fig. 2. Connection diagram of MP Nokia 7250i

3.2 Profits/losses from the disassembly of individual components and subassemblies of MP Nokia 7250 for recycling and disposal options

Summary of profits/losses (and the revenues and costs) for individual components for recycling and disposal options are listed in Table 1. Below is a detailed description of the calculation of the revenues and costs based on actual data, such as purchase prices of secondary materials, weight and material composition of components and subassemblies of examined mobile phone, transport costs etc. Due to the need to include distance in the calculation we assume that the hypothetical disassembly operation is located in the Technical University campus.

Determination of revenues and costs for the individual components for recycling alternative

Revenues in this alternative is the sale of discarded parts (or materials) as a secondary raw material. In calculating the revenues of individual components we use material composition and weight of each component [2] and the actual purchase prices for 1 kg of secondary raw materials [3,4].

As the costs for recycling alternative we consider transportation costs to buyer of secondary materials (in our considered case is 2 km from hypothetical disassembly operation) in the mass-transport container. The costs are 0.0003186 €/kg (or 0.00003186 eurocents /g) [5]. It is a very low number so these costs we consider to be zero. We assume also that the costs of recycling of batteries are covered by the recycling fee (Recycling fee for 1 kg of batteries marketed in Slovak Republic is equal to 1.49 €/kg (see e.g.[6])), so in our calculation we consider also them to be zero.

Determination of revenues and costs for the individual components for disposal alternative

In the disposal alternative of the disassembled components are revenues equal to zero, as the companies that dispose of waste collect a great variety of secondary raw materials free of charge. In our considered case the waste company Kosit (Kosice) take without charge these secondary raw materials: paper and cardboard, glass, plastics, metals, bulky waste (washing machines, refrigerators, sinks, cabinets, ...), green waste, textiles, electronic waste (TV, monitor ...), tires, a small building waste (to 1 m³), waste oils, paints and thinners.

Regarding costs for this alternative, we consider again only transport costs (calculated above), which are very low and therefore we consider them equal to zero.

Component/sub-assembly	Label	$R_{r,i}$	$C_{r,i}$	$P_{r,i} = R_{r,i} - C_{r,i}$	$R_{n,i}$	$C_{n,i}$	$P_{n,i} = R_{n,i} - C_{n,i}$
Frame of LCD	C	0,02508	0	0,02508	0	0	0
Display cover	E	0,03876	0	0,03876	0	0	0
Contact area of keyboard	D	2,77704	0	2,77704	0	0	0
Display	F	0	0	0	0	0	0
Keyboard	B	0	0	0	0	0	0
Front cover	A	0	0	0	0	0	0
Camera cover	I	0,0057	0	0,0057	0	0	0
Camera module	H	0,1218	0	0,1218	0	0	0
Mother board	G	16,3212	0	16,3212	0	0	0
Back cover	N	0	0	0	0	0	0
Internal plastic cover	J	0	0	0	0	0	0
GSM signal module	K	0	0	0	0	0	0
Power connector	L	0	0	0	0	0	0
Vibration engine	M	0,00931	0	0,00931	0	0	0
Battery	O	0	0	0	0	0	0
Sub-assembly	CF				0	0	0
	GI				0	0	0
	JM				0	0	0
	CM				0	0	0
	AB				0	0	0
	AM				0	0	0
Product	Mobile p.				0		

Table 1. Profits/losses from the disassembly of individual components and subassemblies of MP Nokia 7250 for recycling and disposal options

3.3 The cost of disassembly of the connections between components of MP Nokia 7250i

When calculating the cost of disassembly of each connection we assume, that the studied MP is manually disassembled with the normal tools (e.g. screwdriver). For manual disassembly is the dominant cost - total cost of labor. Other costs are negligible, hence in our calculations equal to zero. Total cost of labor we calculate from the average wage of employees in industry in Slovak republic in 2011 [7] and is equal to 1114,048 €. If the annual working time fund equals to 2000 hours (i.e. 7.2 million seconds), the resulting total labor cost of a working second is equal (rounded) to 0.1857eurocents/second. The final costs of the disassembly of connections, identified by a connection diagram, are shown in Table 2.

Connections	Disassembly time (sec)	Disassembly costs (eurocent)
JN	5	0,9285
JO	2	0,3714
AC	10	1,857
GJ	51	9,4707

CG	7	1,2999
CE	11	2,0427
EF	4	0,7428
CD	19	3,5283
AB	4	0,7428
GH	4	0,7428
GI	6	1,1142
JK	4	0,7428
JL	4	0,7428
JM	6	1,1142

Table 2. The cost of disassembly of the connections between components of MP Nokia 7250i [own measurements and calculations on the base of 8 and 2]

3.4 Disassembly optimization of MP Nokia 7250i

Based on the formula (1) we compute gradually profits/losses for each sub-assemblies and combinations of EOL alternatives (recycling or disposal) of parts of these sub-assemblies. For example for sub-assembly CF with 4 parts C, D, E, F we have created 16 combinations (Table 3). Combination

example: component C is disposed, component D is recycled, components E is recycled and component F is disposed - notation CnDrErFn. (Note: for each component A, B, C O in subsequent calculations index n represents a disposal alternative and index r recycling alternative). For each combination we calculate profit/loss and we identify the optimal combination for a given sub-assembly, which is that with highest profit (or lowest loss). Thus, for example in the case of sub-assembly CF is the most advantageous combination (the one that brings the highest profit from particular EOL options for individual components) CnDnEnFn (Table 3) so it means disposal of all four components respectively all subassembly CF.

The individual sub-assemblies were identified based on a hierarchical representation of the MP (Fig. 3). The hierarchical representation we draw based on information in above BOM (Fig. 1) and connection diagram (Fig. 2). The calculation of individual sub-assemblies proceeds bottom-up in the hierarchical representation of the MP. Most profitable combinations for individual sub-assemblies are presented in Table 4.

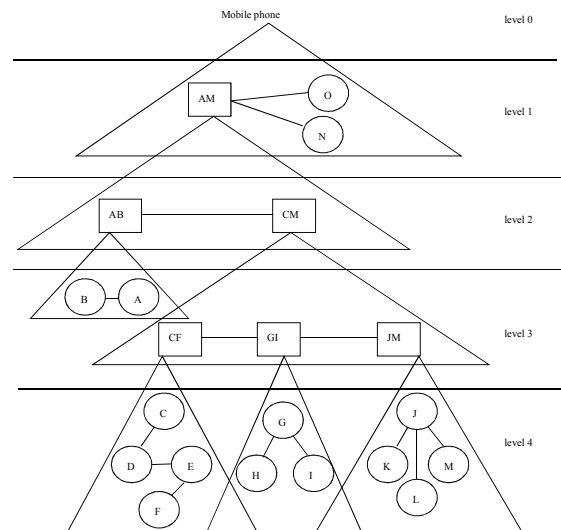


Fig. 3. The hierarchical representation of the MP Nokia 7250i

profit(CrDrErFr)	=(0,02508 + 2,77704 + 0,03876 + 0)-(3,5283 + 2,0427 + 0 + 0 + 0 + 0,7428)	= -3,47292
profit(CrDrErFn)	=(0,02508 + 2,77704 + 0,03876 + 0)-(3,5283 + 2,0427 + 0 + 0 + 0 + 0,7428)	= -3,47292
profit(CrDrEnFr)	=(0,02508 + 2,77704 + 0 + 0)-(3,5283 + 2,0427 + 0 + 0 + 0 + 0,7428)	= -3,51168
profit(CrDrEnFn)	=(0,02508 + 2,77704 + 0 + 0)-(3,5283 + 2,0427 + 0 + 0 + 0 + 0)	= -2,76888
profit(CrDnErFr)	=(0,02508 + 0 + 0,03876 + 0)-(3,5283 + 2,0427 + 0 + 0 + 0 + 0,7428)	= -6,24996
profit(CrDnErFn)	=(0,02508 + 0 + 0,03876 + 0)-(3,5283 + 2,0427 + 0 + 0 + 0 + 0,7428)	= -6,24996
profit(CrDnEnFr)	=(0,02508 + 0 + 0 + 0)-(3,5283 + 2,0427 + 0 + 0 + 0 + 0,7428)	= -6,28872
profit(CrDnEnFn)	=(0,02508 + 0 + 0 + 0)-(3,5283 + 2,0427 + 0 + 0 + 0 + 0)	= -5,54592
profit(CnDrErFr)	=(0 + 2,77704 + 0,03876 + 0)-(3,5283 + 2,0427 + 0 + 0 + 0 + 0,7428)	= -3,498
profit(CnDrErFn)	=(0 + 2,77704 + 0,03876 + 0)-(3,5283 + 2,0427 + 0 + 0 + 0 + 0,7428)	= -3,498
profit(CnDrEnFr)	=(0 + 2,77704 + 0 + 0)-(3,5283 + 0 + 0 + 0 + 0 + 0,7428)	= -1,49406
profit(CnDrEnFn)	=(0 + 2,77704 + 0 + 0)-(3,5283 + 0 + 0 + 0 + 0 + 0)	= -0,75126
profit(CnDnErFr)	=(0 + 0 + 0,03876 + 0)-(0 + 2,0427 + 0 + 0 + 0 + 0,7428)	= -2,74674
profit(CnDnErFn)	=(0 + 0 + 0,03876 + 0)-(0 + 2,0427 + 0 + 0 + 0 + 0,7428)	= -2,74674
profit(CnDnEnFr)	=(0 + 0 + 0 + 0)-(0 + 0 + 0 + 0 + 0 + 0,7428)	= -0,7428
profit(CnDnEnFn)	=(0 + 0 + 0 + 0)-(0 + 0 + 0 + 0 + 0 + 0)	= 0

Table 3. Profit (+)/loss (-) for various combinations of EOL options (recycling and disposal) of individual components that make up sub-assembly CF

profit(CnDnEnFn)	=(0 + 0 + 0 + 0)-(0 + 0 + 0 + 0 + 0 + 0)	= 0
profit(JnKnLnMn)	=(0 + 0 + 0 + 0)-(0 + 0 + 0 + 0 + 0 + 0)	= 0
profit(GrHrIr)	=(16,3212 + 0,1218 + 0,0057)-(0,7428 + 1,1142 + 0)	= 14,5917
profit(CFrGlrJMr)	=(0 + 14,5917 + 0)-(1,2999 + 0 + 9,4707)	= 3,8211
profit(AnBn)	=(0 + 0)-(0)	= 0
profit(ABrCmR)	=(0 + 3,8211)-(1,857)	= 1,9641
profit(AMrNrOr)	=(1,9641 + 0 + 0 + 0)-(0,9285 + 0,3714 + 0)	= 0,6642

Table 4. Most profitable (or least loss) combinations for all subassemblies

Table 5 represents the transformation of the previous calculations, summarized in Table 4 to the optimal (profit maximizing) EOL alternatives (recycling or disposal) for individual components and sub-assemblies of MP. Note: In the case of indifference of alternatives we state „Dispose/Recycle“

Component/sub-assembly	Label	Optimal alternative
Frame of LCD	C	Dispose

Display cover	E	Dispose
Contact area of keyboard	D	Dispose
Display	F	Dispose
Keyboard	B	Dispose
Front cover	A	Dispose
Camera cover	I	Recycle
Camera module	H	Recycle
Mother board	G	Recycle
Back cover	N	Dispose/Recycle

Internal plastic cover	J	Dispose
GSM signal module	K	Dispose
Power connector	L	Dispose
Vibration engine	M	Dispose
Battery	O	Dispose/Recycle
Sub-assembly	CF	Dispose/Recycle
	GI	Recycle
	JM	Dispose/Recycle
	CM	Recycle
	AB	Dispose/Recycle
	AM	Recycle
Product	Mobile phone	Recycle

Table 5. Optimal EOL alternatives (recycling or disposal) for individual components and sub-assemblies of MP Nokia 7250i

Based on calculations in previous tables and connection diagram we determine the optimal disassembly sequence (Table 6), so we define which connections to disconnect and which to maintain.

Connection	Disassembly operation
JN	disconnect
JO	disconnect
AC	disconnect
GJ	disconnect
CG	disconnect
CE	maintain
EF	maintain
CD	maintain
AB	maintain
GH	disconnect
GI	disconnect
JK	maintain
JL	maintain
JM	maintain

Table 5. Optimal disassembly sequence of MP Nokia 7250i

4. CONCLUSION

On the base of the application the model on the mobile phone case, we can conclude that this model is relatively easy calculable for this complexity level products. The output of the model in a form of EOL option and disassembly sequence seems to be reasonable and consistent with generally known and practiced sequences in the case of mobile phones, it means to dispose almost all parts of mobile phone excluding printed circuit board which is suitable for recycling. In the case of battery which is suitable for special recycling/disposal, the model gives indifferent

result „Dispose/Recycle“. In real case this would not be a complication because EOL option for battery is usually set by environmental legislation.

5. ACKNOWLEDGEMENT

This contribution is the result of the project implementation: Center for research of control of technical, environmental and human risks for permanent development of production and products in mechanical engineering (ITMS: 26220120060) supported by the Research & Development Operational Programme funded by the ERDF. This contribution has been supported by research grant VEGA 1/0102/11 (Methods and techniques of experimental modeling of production and nonproductive processes in enterprises).

6. REFERENCES

- [1] Lee H.B., Cho N.W., Hong Y.S.: A hierarchical end-of-life decision model for determining the economic levels of remanufacturing and disassembly under environmental regulations, *Journal of Cleaner production*, 18 (2010), p.1276-1283.
- [2] K. Dóry: Technicko-ekonomické hodnotenie demontáže mobilných telefónov, diploma work, Technical university of Košice, 2012
- [3] Plzeňský skart a.s (online). Plzeň : 2012 [cit. 2012-04-14]
http://www.plzenskyskart.cz/vykupni-cenik-maloobchodni#kategorieCeniku_397
- [4] P+K s.r.o. (online), <http://www.p-k.sk/?content=sluzby&subcontent=vykup-zelezneho-srotu-a-farebnych-kovov>
- [5] Kosit a.s. Košice, cenník služieb
- [6] SLOWMAS, http://www.slovmas.sk/pdf/cennik_2012.pdf
- [7] Statistical Office of Slovak Republic, www.statistics.sk
- [8] How to replace mobile phone LCD. Demonstration of how to replace mobile phone LCDs for Nokia 6110, 6110i, 7250, 7250i (online) www.youtube.com.

Authors: Ing. Juraj Šebo, PhD., Ing. Monika Fedorčáková, PhD., Technical University of Košice, Faculty of Mechanical Engineering, Department of Industrial Engineering and Management, Nemcovej 32, 04200 Košice, Slovak Republic, Phone.: +421 55 6023241

E-mail: juraj.sebo@tuke.sk;
monika.fedorcakova@tuke.sk;

Sekulić, M., Hadžistević, M., Kovač, P., Gostimirović, M., Jurković, Z.

CURRENT TRENDS IN SUSTAINABLE PRODUCT DESIGN

Abstract: Companies all over the world increasingly need to innovate their products and processes to: keep up with competitive pressure, increase productivity within the region or worldwide, defend or expand market share and to create the ability to attract foreign investments. Product innovation is becoming one of the key strategic options available to firms, supply chains and integrated industrial sectors in developing economies to compete better in today's global market. Growing global concerns about environmental problems such as climate change, pollution and biodiversity loss and about social problems related to poverty, health, working circumstances, safety and inequity, have fostered sustainability approaches for industry. Improved product design which applies sustainability criteria - Design for Sustainability (D4S) - is one of the most useful instruments available to enterprises and governments to deal with these concerns. D4S includes the more limited concept of Ecodesign or Design for the Environment. In this paper, current trends in sustainable product design have been reported.

Key words: sustainable product design

1. INTRODUCTION

In light of increasing pressures to adopt a more sustainable approach to product design and manufacture, the requirement to develop sustainable products is one of the key challenges facing industry in the 21st century. Sustainable product development initiatives (mainly through eco-design) have been evolving for some time to support companies develop more sustainable products. Sustainability is a frequently and carelessly used term across the world by researchers and corporations. According to the United Nation's Brundtland commission (WBCD, 1987), sustainable development was defined as "meeting the needs of the present without compromising the ability of future generations to meet their own needs"[1].

Sustainable products are those products providing environmental, social and economic benefits while protecting public health, welfare, and environment over their full commercial cycle, from the extraction of raw materials to final disposition according to the Sustainable Products Corporation in Washington DC [2].

Although the concept of sustainability has been in practice worldwide over centuries, the application towards consumer products has always been overshadowed by costs and extra efforts manufacturers have to encounter. But, with regulations implemented by federal and state governments, nationally and locally and by foreign countries, OEMs are beginning to understand the consequences of damage that could be caused by harmful chemical and hazardous materials which results from improper conduct of design, manufacture and disposal. Through responsible business practices and sustainable product offerings, business leaders can balance their short term and long term profitability, while considering the economic, environmental, and social impact of their activity, Figure 1.

Sustainable development is a significant aspect in

our society today and many scholars are now attempting to build models for sustainable development to include all aspects of environment, society and economy. There have been three main reasons that have accelerated this mind shift: regulation proliferation, resource scarcity and reputation management.

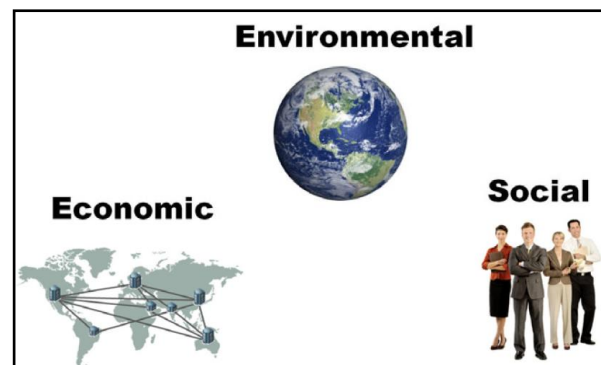


Fig. 1. Environmental, economic and social impact of products [3]

2. PRODUCTS AND SUSTAINABILITY

Sustainable product design, also known as Design for Sustainability or D4S, including the more limited concept of Ecodesign, is one globally recognised way companies work to improve efficiencies, product quality and market opportunities (local and export) while simultaneously improving environmental performance.

Three key elements of sustainability are planet, people and profit (3P), Figure 2. They are linked to the element of product innovation. Product innovation is directly linked to sustainability: both are oriented towards change and the future. Product innovation is concerned with creating new products and services that generate value only if they fit in this future. To be sustainable, product innovation must meet a number of

challenges linked to people, planet and profit: social expectations and an equitable distribution of value along the global value chain, and the innovation must work within the carrying capacity of the supporting ecosystems.

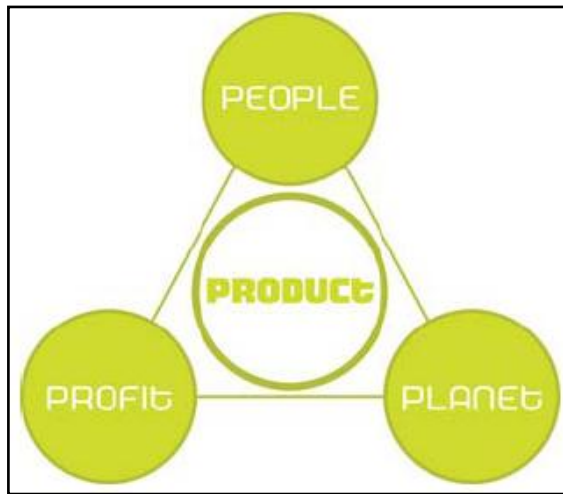


Fig. 2. Three key sustainability [4]

2.1 Product life cycles and sustainable design

Product sustainability is more than producing different kinds of products. It is about a different way of thinking about and making products. Company incorporate sustainability concerns into its design function, Figure 3.

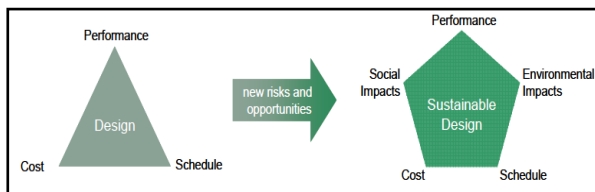


Fig.3. The shift to sustainable design [5]

During the conventional product life-cycle, materials move through a system comprised of the following stages: Extraction, Production, Distribution, Consumption and finally Disposal which is an “open loop” approach, Figure 4. It is a linear system and we live on a finite planet that can not support such a system indefinitely.

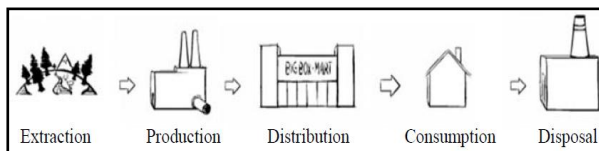


Fig.4. Conventional production [6]

A product life-cycle view is one that considers the sustainability of a product across all stages of production and consumption — from its origins to its end as a desirable service. The stage commonly treated as a point of origin is product *development*, where initial marketing and product planning take place. The start of physical activity is the *material production* phase, in which resources for making products are harvested.

The next stage, when needed, is *material processing*, which converts resources into feedstocks. The *product fabrication* phase then turns these input materials into finished goods. From there products enter *distribution* networks that support *customer transactions*, after which the *consumer use* phase begins. Products stay with the user until a consumer deems its service no longer useful and moves to get rid of it. At this point, *end-of-life* disposition determines whether a product is reused, recycled or dissipated. In a continuous, cradle-to-cradle cycle, end-of-life processes feed into another cycle of development. The result is a need to think about sustainability for each stage of activity and across the life cycle(s) of a product.

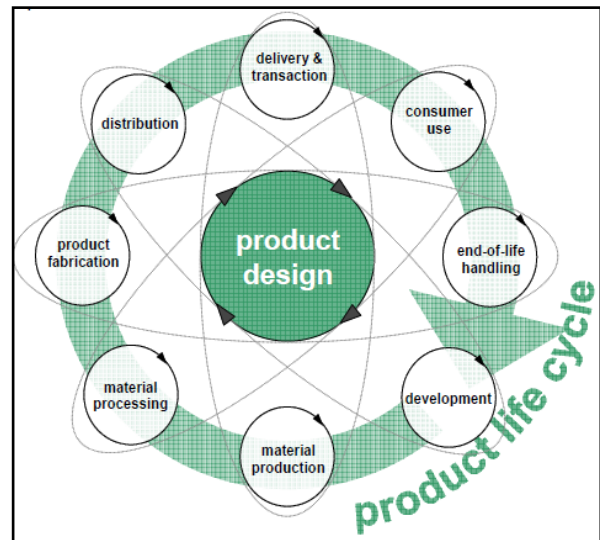


Fig.4. Product life cycle and sustainable design [5]

Sustainable design offers a variety of opportunities to prosper. Companies can gain access to markets, increase market share, reduce or avoid compliance costs, and more easily attract investor capital. There are also positive ripple effects related to product performance, cleaner production, customer satisfaction and brand loyalty, employee morale, and community relations.

3. THE DESIGNER'S FIELD GUIDE TO SUSTAINABILITY

In *The Philosophy of Sustainable Design*, Jason F. McLennan [8] said designers should "eliminate negative environmental impact completely through skillful, sensitive design." Practical application varies among design disciplines (product design, architecture, landscape design, urban planning, etc.), but they all share some common principles:

- Use non-toxic, sustainably produced, or recycled materials which have a lower environmental impact than traditional materials.
- Use manufacturing processes and produce products which are more energy efficient than traditional processes and end products.

- Build longer-lasting and better-functioning products which will have to be replaced less frequently, which reduces the impact of producing replacements.
- Design products for reuse and recycling. Make them easy to disassemble so that the parts can be reused to make new products.
- Consult sustainable design standards and guides,
- Consider product life cycle. Use life cycle analysis tools to help you design more sustainable products.
- Shift the consumption mode from personal ownership of products to provision of services which provide similar functions.
- Materials should come from nearby, sustainably managed renewable sources that can be composted when their usefulness is exhausted.

Industrial design firm Lunar from San Francisco has recently published a simple, clear, and inspiring Designer's Field Guide to Sustainability [7]. Lunar Design developed a visual roadmap for sustainable product development and the product life cycle. The Designer's Field Guide to Sustainability covers 15 issues in the design process, including suggestions on how to make products recyclable and safe for humans and the environment. Other tips touch on using less energy and materials when manufacturing products, making products both sustainable and appealing to consumers, and thinking about a product's life to determine what parts should be durable or disposable. The model is centered around four questions and strategies to guide the development process:

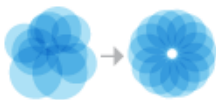
- **What is it trying to accomplish?**

01-Question the premise of the design.



✓ Consider other approaches to the problem at hand. Is the form factor that you had in mind really the best way of accomplishing the task? Is any form factor the best way of accomplishing the task? Maybe a service fits the mold better? Perhaps the answer lies within an existing product?

02-Make it less complex.



✓ Simple, elegant designs can reduce material, weight, and manufacturing processes. Simple designs usually also mean less material variety and can help make a product more recyclable.

03-Make it more useful.



✓ At first glance, this may seem to contradict point number 2, but there is a big difference between usefulness and complexity. Taking advantage of a natural or logical extra use for a product will not only make the product more desirable and

interesting, it will also help reduce the number of products headed for landfills. Multiuse products can reduce consumption and increase convenience

- **How is it brought to life?**

04-Reduce material variety.



✓ Designing as many aspects of the product as you can from the same material makes recycling the product at its end of life easier, more efficient, and more profitable.

05-Avoid toxic or harmful materials and chemicals.



✓ Materials like PVC, neoprene or polystyrene, and toxic chemicals and additives like bisphenol A and formaldehyde should be avoided when possible. Many of these materials have suitable non-toxic counterparts, like copolyesters or bioplastics, and additives can be eliminated by choosing materials wisely.

06-Reduce size and weight.



✓ Lightweight products can reduce carbon emissions and cost by making the shipping process more efficient. Weight can often be saved by focusing on choosing lightweight materials, simplifying designs, and eliminating unnecessary fasteners and components.

07-Optimize manufacturing processes.



✓ Determine which manufacturing processes make the most sense for your product. For lower volumes or less complex parts, consider vacuum forming instead of injection molding. For some complex metal geometries consider casting instead of machining.

08-Design packing in parallel with products.



✓ Simple, elegant designs can reduce material, weight, and manufacturing processes. Simple designs usually also mean less material variety and can help make a product more recyclable.

- **How is it used?**

09-Design for upgradeability.



✓ In the electronics industry, the technology in a product can become obsolete long before the design. Designing products that can be upgraded to keep up with rapidly changing technical performance can save materials and money.

10-Create durable and high quality designs.



✓ People want high quality products that will look and function beautifully long after the competing product has died, and they're willing to pay a little more for that type of design. Designed properly, products can transcend the "throw away" culture that dominates electronics today.

11-Design for life after death.



Most products don't last forever. Products designed to have secondary usages after their primary function has lapsed can add value to the product, and may fill a need that would be filled by another purchased product instead.

- *Where does it end up?*

12-Make it modular.



✓ Modular designs are not only more easily recycled at the end of their life but also more easily repaired, and therefore last longer. Modular designs can also be more efficiently manufactured and shipped, reducing energy consumption at the beginning of the product's life.

13-Use recycled, recyclable, renewable and biodegradable materials.



✓ This one's obvious, but should always be kept in mind. Design with recycled or easily recyclable plastics (HDPE, PP, PS, PVC), biodegradable plastics (PLA, PHB, polyamide, bio-derived polyethylene), paper, cardboard, wood, stainless steel, aluminum, etc.

14-Minimize fasteners.



✓ Minimizing fasteners can make large portions of the product more easily recyclable at the end of life since removing snap-on parts can be done completely and quickly without the use of tools. This also eliminates multiple fasteners from the product BOM and reduces the amount of assembly time necessary to get products out the door, which reduces cost on two fronts.

15-Don't use paint.



✓ Painting a material generally makes it harder to recycle at the product's end of life because the paint cannot be easily separated from the material. As a result, many painted products are either not recycled or are

irresponsibly melted down to burn off the paint, creating toxic fumes and lower quality recycled material. Design products to take advantage of the natural beauty of materials.

4. CONCLUSIONS

The principles of sustainable design are compatible with the principles of any good design philosophy. Design for sustainability places additional emphasis on reducing the environmental impact of a product during its manufacture, use and disposal, or reuse. It uses strategies such as avoiding use of toxic substances during production, minimizing materials used, minimizing energy or water required during use, and designing for repair, reuse or disassembly and recycling. Mechanical engineering and product designers have to work together to create the next generation of sustainability products.

5. REFERENCES

- [1] Brundtland, G. H.: *UN Brundtland commission reference*, Oxford University Press, Oxford, 1987.
- [2] Sustainable Products Corporation, <http://www.sustainableproducts.com>
- [3] Kumar, J., Graf, P.: *Future Centred Design: Designing for Sustainable Business*, Design, User Experience, and Usability (Editor Marcus A.), Springer-Verlag Berlin Heidelberg, 2011., pp. 449–457.
- [4] Crul, M.R.M., Diehl, J.C.: *Design for Sustainability - a practical approach for developing economies*, Delft University of Technology, Faculty of Industrial Design Engineering, The Netherlands, 2007.
- [5] http://www.bsr.org/reports/BSR_Sustainable_Design_Report_0508.pdf
- [6] Leonard, A.: *The Story of Stuff.*, 2005, from <http://www.storyofstuff.com/>
- [7] http://www.lunar.com/docs/the_designers_field_guide_to_sustainability_v1.pdf
- [8] McLennan, J.F.: *The Philosophy of Sustainable Design*, Ecotone LLC, Kansas City, 2004.

Authors: Assist. Prof. Dr. Milenko Sekulić, Assoc. Prof. Miodrag Hadžistević, Prof. Dr. Pavel Kovač, Prof. Dr. Marin Gostimirović, University of Novi Sad, Faculty of Technical Sciences, Department for Production Engineering, Trg Dositeja Obradovića 6, 21000 Novi Sad, Serbia, Phone.: +381 21 450-366, Fax: +381 21 454-495.

Assist. Prof. Zoran Jurković, University of Rijeka, Faculty of Engineering, Vukovarska 58, Rijeka, Croatia
E-mail: milenkos@uns.ac.rs
miodrags@uns.ac.rs
pkovac@uns.ac.rs
maring@uns.ac.rs
zjurkovic@riteh.hr

Simonovic, S.

BOTH LEANER AND CLEANER PRODUCTION BY PRODUCT DESIGN

Abstract: *Product design principles for lean manufacturing and cleaner production are exposed. Lean thinking doesn't have life cycle approach to waste and pollution by default, so lean and green thinking can be contradictory. Once the product eco friendliness is perceived by lean as something that adds value to the product, lean thinking automatically tends to shift toward pollution and waste prevention that is to the design for both lean and green.*

Key words: *Value Adding, Life Cycle, Green*

1. INTRODUCTION

It is impossible to effectively realize neither lean manufacturing nor cleaner production unless certain product design principles are applied. Also, without design stage product consideration it is impossible to thoroughly reconcile lean and green thinking. This work exposes product design principles for lean manufacturing and cleaner production and shows way how both lean and green can be reconciled in design phase. Following terminology is introduced:

'Substance' means any chemical element and its compounds, with the exception of radioactive substances and genetically modified organisms [1].

'Pollution' means the direct or indirect introduction, as a result of human activity, of substances, vibrations, heat or noise into the air, water or land which may be harmful to human health or the quality of the environment, result in damage to material property, or impair or interfere with amenities and other legitimate uses of the environment [1].

'Installation' means a stationary technical unit where one or more activities listed in Annex I are carried out, and any other directly associated activities which have a technical connection with the activities carried out on that site and which could have an effect on emissions and pollution [1].

'Emission' means the direct or indirect release of substances, vibrations, heat or noise from individual or diffuse sources in the installation into the air, water or land [1].

'Waste' means any substance or object which the holder discards or intends or is required to discard [2]

'Hazardous waste' means waste which displays one or more of the hazardous properties listed [2].

'Waste management' means the collection, transport, recovery and disposal of ecological waste, including the supervision of such operations and the after-care of disposal sites, and including actions taken as a dealer or broker [2]

'Collection' means the gathering of waste, including the preliminary sorting and preliminary storage of waste for the purposes of transport to a waste treatment facility [2].

'Prevention' means measures taken before a substance, material or product has become waste that

reduces:

(a) the quantity of waste, including through the re-use of products or the extension of the life span of products;

(b) the adverse impacts of the generated waste on the environment and human health; or

(c) the content of harmful substances in materials and products [2].

'Re-use' means any operation by which products or components that are not waste are used again for the same purpose for which they were conceived [2]

'Treatment' means recovery or disposal operations, including preparation prior to recovery or disposal [2].

'Recovery' means any operation the principal result of which is waste serving a useful purpose by replacing other materials which would otherwise have been used to fulfill a particular function, or waste being prepared to fulfill that function, in the plant or in the wider economy [2].

'Preparing for re-use' means checking, cleaning or repairing recovery operations, by which products or components of products that have become ecological waste are prepared so that they can be re-used without any other pre-processing [2].

'Recycling' means any recovery operation by which waste materials are reprocessed into products, materials or substances whether for the original or other purposes. It includes the reprocessing of organic material but does not include energy recovery and the reprocessing into materials that are to be used as fuels or for backfilling operations [2].

'Disposal' means any operation which is not recovery even where the operation has as a secondary consequence the reclamation of substances or energy [2].

'Reusability' means the potential for reuse of component parts diverted from an end-of-life vehicle; [3]

'Recyclability' means the potential for recycling of component parts or materials diverted from an end-of-life vehicle [3].

'Recoverability' means the potential for recovery of component parts or materials diverted from an end-of-life vehicle [3].

'Life cycle' means consecutive and interlinked stages of a product system, from raw material

acquisition or generation of natural resources to the final disposal [4].

'Life cycle assessment (LCA)' means compilation and evaluation of the inputs, outputs and the potential environmental impacts of a product system throughout its life cycle [5].

'Cleaner production' is a proactive approach which involves preventing the pollution of air, water and land, reducing waste at source, minimizing risks to the population and the environment, and minimizing the use of raw materials, including energy and water [6].

2. WASTE ACCORDING TO LEAN THINKING

In its most basic form, lean manufacturing is the systematic elimination of waste from all aspects of an organization's operations, where waste is viewed as any use or loss of resources that does not lead directly to creating the product or service a customer wants when they want it [7].

As a consequence following waste forms can be discerned by lean approach:

Overproduction waste means making what is unnecessary when it is unnecessary and in an unnecessary amount.

It is a mirror image of the Just-In-Time definition.

Inventory waste appears when anything—materials, parts, assembly parts—is retained for any length of time. This includes not only warehouse stock, but also items in the factory that are retained at or between processes

Conveyance Waste is created by conveying, transferring, picking up/setting down, piling up, and otherwise moving unnecessary items. Also created by problems concerning conveyance distances, conveyance flow and conveyance utilization rate.

Defect Production Waste is related to costs for inspection of defects in materials and processes, customer complaints, and repairs.

Process-Related Waste relates to unnecessary processes and operations traditionally accepted as "necessary".

Operation-Related Waste relates to unnecessary movement, movement that does not add value, movement that is too slow or too fast.

Idle Time Waste is waste of which the causes originate in waiting from materials, operations, conveyance, inspection, as well as idle time attendant to monitoring and operation procedures [8, 9].

3. PRINCIPLES OF DESIGN FOR LEAN MANUFACTURING

There are several design principles that favorably influence lean manufacturing:

a) Design for ease of machining means that product should, as far as possible, include off the shelf items, standard items or component that are possible to make with a minimum of experimental tooling. Product features such as part tolerances, surface finish requirements, etc., should be resolved with respect to the consequences of the unnecessary embellishment on the durability of production process and thereby on the

production costs. Designers, added by their team members, must be familiar enough with manufacturing alternatives, capabilities and limitations so that they do not unknowingly make choices that are unnecessary difficult, impossible, costly, and time consuming to manufacture [10, 12].

b) Design for ease of assembly is design principle according to which product should consist of minimal number of parts. Parts should be assembled by adding them from the top, and the product never has to be turned over. Parts should be designed to be self aligning, require no tools for assembly, are secured immediately upon insertion, and do not need to be oriented. Whether for automated or hands assembly, fasteners (screws, pulleys, cotter-pins, etc.), are to be avoided as much as possible. Subassemblies should be designed as modules having testable functions. In that way design, quality assurance and assembly should be integrated. There are also issues of access to fasteners and lubrication points, access to certain points of surfaces for sake of testing, location points for accurately holding components and subassemblies, standardization of subassemblies for multiple models, and reduction of number of times the parts and subassembly must be turned over during assembly [10,13].

c) Design for ease of automation relates to the product characteristics that will, for example, in the case of assembled components, help to simplify automatic part feeding, orienting and assembly operations. In the case of assembled components it is important to design products to be assembled from the top down and to avoid forcing machines to assemble from the side and particularly from the bottom. The ideal assembly procedure should be performed on one face of the part, with straight vertical motions and keeping the number of faces to be worked on to a minimum [15].

d) Modular design puts a limited number of functions in each product constituent. Interfaces and interaction between constituents are well defined and are generally fundamental to the primary function of the product. Interfaces should be robust, standardized and early defined so that detail design of modules can be developed within those interface parameters. System architecture for modular design ought to be thought out with great details at the outset of the project. It establishes a product platform that may become basis for entire family of products. Successive innovations may each be concentrated in one or another module, thereby facilitating continuous product innovations at low incremental development and manufacturing cost. Modularity makes it easier to change a product without having to redo much or the entire product. The product can be upgraded by replacing module or by adding to. Parts that wear out more quickly can be easily replaced. Modular design mediates the desires of customers for product variety with the desire of manufacturer and retailers for simplicity by incorporating variety into a limited numbers of modules. In these way designers reduces manufacturing cost and inventory. Risky technologies can be concentrated in one or few modules. Standard modules can be introduced that are not seen by customer providing similar benefits [10,

14].

e) Design for group technology enables flow oriented production system that is non-stock production. In this respect group technology is used to define families of products and components which can be manufactured in well-defined production cells. Each part is designed so that corresponds to in advance determined part family. In that way, group technology also reduces unnecessary variety and redundancies in product design. In Group technology, production items are grouped into families on the basis of such characteristic as part shapes, part finishes, materials, tolerances which all results in certain kind of succession of production operations that characterize particular production cell. Each part family is represented by master part. Products are designed so that their features can be matched to respective features of a master part that is to a product family [10, 17, and 18].

4. PRINCIPLES OF DESIGN FOR CLEANER PRODUCTION

The objective of design for cleaner production is to reduce the product's detrimental environmental impact while maintaining or improving its functionality. Two main product-related environmental objectives are:

- Conservation of resources, recycling and energy recovery
- Prevention of pollution, waste and other impacts

Following waste hierarchy as priority order should be applied:

- (a) prevention;
- (b) preparing for re-use;
- (c) recycling;
- (d) other recovery, e.g. energy recovery; and
- (e) disposal. [2]

Departing from this hierarchy can be applied where this is justified by life-cycle thinking on the overall impacts of the generation and management of waste [2].

A life cycle approach should be used to identify the relevant environmental aspects and impacts during the entire product life cycle, thus helping to define design approaches. Reliable information like that obtained by Life Cycle Assessment (LCA) method can be used [16].

Integration of environmental aspects as early as possible into the product design and development process offers the flexibility to make changes and improvements to products. In contrast, waiting until later stages of the process may preclude the use of desirable environmental options, because all the major technical decisions have already been made.

These new approaches may result in improved resource and process efficiencies, potential product differentiation, reduction in regulatory burden and potential liability, and costs savings. In addition, globalization of markets, shifts in sourcing, manufacturing and distributing all influence the supply chain, and therefore have an impact on the environment [4].

By considering the goals of the organization,

economic and social aspects, and the product type, the organization may decide upon a combination of design approaches to meet the strategic environmental objectives. Possible design approaches can be:

- a) Design for improvement of materials efficiency means checking if environmental impact can be reduced e.g. by minimal use of materials, use of low impact materials, use of renewable materials, and/or use of recovered materials;
- b) Design for improvement of energy efficiency means considering total energy use throughout the product's life cycle (including use phase), check if environmental impact can be reduced, e.g. reduction of energy use, use of low impact energy sources, use of energy from renewable sources;
- c) Design for sparing use of land is particularly to be considered when land-consuming infrastructure or materials are utilized in the product system;
- d) Design for cleaner production and use means considering using cleaner production techniques, avoiding use of hazardous consumables and auxiliary materials and using an overall systems perspective to avoid decisions based on a single environmental criterion;
- e) Design for durability strives to improve the product's longevity, reparability and maintainability; considers environmental improvements emerging from new technologies;
- f) Design for optimizing functionality means considering opportunities for multiple functions, modularity, automated control and optimization; comparing the environmental performance to that of products tailored for specific use;
- g) Design for reusability, recoverability and recyclability strive to ease disassembly, reduce material complexity, use of recyclable materials, subassemblies, components and materials in future products;
- h) Avoidance of potentially hazardous substances and materials in the product: checking for human health, safety, and environmental aspects, lower impact of materials and transportation.
- i) Design for disposability

These design approaches are instrumental to generate design options that can be checked against the feasibility and potential benefits for customers, the organization and stakeholders. [4]

5. LEAN AND GREEN COMPATIBILITY

There are some obvious environmental benefits associated with lean manufacturing:

Design for ease of machining reducing machining time consequently reduces energy consumption, pollution, use of auxiliary, often toxic fluids, mass of waste materials, and pollution.

Design for easy of assembly reduces time of assembly, consequently energy consumptions and means needed.

Design for group technology and modular design greatly reduces raw materials stocks, in-process material stocks, and finished goods materials stocks.

But lean philosophy doesn't see pollution as a

waste, so it is not automatically geared toward systematical elimination of pollution. Therefore it would be possible that, if straightforwardly applied, principles of product design for lean be detrimental to environmental friendliness of product. For example riveted instead of screwed joints are preferred for ease of assembly. So, the entire unit must be replaced when only a part of it needs repair. Many non-repairable, non-refillable products are now available. These include common items such as flashlights, ink pens, razors, and cameras. They are usually less expensive to produce than more durable alternatives. However, because they often have shorter lives they often must be replaced much more frequently than their counterparts. Consequently, they are often more expensive to use and usually create more solid waste over time.

Certainly, environmental friendliness of product can have its prize but from the lean point of view crucial question is does implementation of green features adds value to product and not only what is cost of green introduction. Once the product eco friendliness is perceived by lean as something that adds value to the product, all activities that contribute to the product eco friendliness would be favored by lean.

6. CONCLUSION

Lean manufacturing doesn't have life cycle approach to waste and pollution by default. Lean and green thinkings become completely compatible when product eco friendliness is perceived like something which adds value to product in sense of lean philosophy. Under the circumstance lean thinking automatically tends to shift toward pollution and waste prevention, that is to the design for both green and lean.

7. REFERENCES

- [1] European Parliament and Council: *Directive 2008/1/EC of 15 January 2008 concerning integrated pollution prevention and control*
- [2] European Parliament and Council: *Directive 2008/98/EC of 19 November 2008 on waste and repealing certain Directives*
- [3] European Parliament and Council: *Directive 2005/64/EC of 26 October 2005 on the type-approval of motor vehicles with regard to their reusability, recyclability and recoverability and amending Council Directive 70/156/EEC*
- [4] ISO/TR 14062:2002(E) *Environmental management — Integrating environmental aspects into product design and development*
- [5] ISO 14040:2006: *Environmental management — Life cycle assessment — Principles and framework*, International Organization for Standardization, Geneva.
- [6] Hillary, Ruth: *Environmental Management Systems and Cleaner Production*, John Wiley & Sons, Ltd. (UK) 1997
- [7] United States Environmental Protection Agency EPA: *Lean Manufacturing And The Environment-Research on Advanced Manufacturing Systems and the Recommendations for Leveraging Better Environmental Performance* 100-R-03-005 , October 2003
- [8] Hirano, Hiroyuki: *The Complete Guide to Just In Time Manufacturing 2nd ed*, Taylor & Francis Group, LLC, 2009
- [9] Carreira, Bill: *Lean manufacturing that works: powerful tools for dramatically reducing waste and maximizing profits*, American Management Association, 2004
- [10] Browne, J. et al: *Production Management Systems- An Integrated Perspective*, Addison Wesley, 1996
- [11] Shingo, Shigeo: *Modern Approaches to Manufacturing Improvement: The Shingo System*, Productivity Press, Portland, Oregon, 1990
- [12] Boothroyd, G., Dewhurst, P., Kknight, W.: *Product Design for Manufacturing*, Marcel Dekker, New York, 1994
- [13] Boothroyd, G., Dewhurst, P.: *Product Design for Assembly*, Boothroyd Dewhurst, Wakefield, 1989
- [14] Ashok, R. et al- *Total Quality Management*, John Wiley & Sons, 1996
- [15] Lascz, J.Z.: *«Product design for robotic and automatic assembly» in Robotic Assembly* , edited by K. Rathmill, IFS Publications Ltd., UK, 1985, 2000
- [16] ISO 14004:2004 *Environmental management system – General guidelines on principles, systems and support techniques*
- [17] Mitrofanov, S. P.: *Scientific Principles of Group Technology* , Mashinostroyenie, Moscow, 1970.
- [18] Burbidge, J. L: *The Introduction of Group Technology*, John Wiley & Sons, New York, 1975

Author: Svetomir Simonović, Ph. D., Professor,
 Technical College, Visoka tehnička škola, Bulevar
 Zorana Đinđića 152a, 11070 Novi Beograd,
 E-mail: svetomir@sezampro.rs

Tichá, M., Budak, I.

LCA APPLICATION IN EPD AND ECO-EFFICIENCY

Abstract: The paper presents the possible uses of the standards of ISO 14000, Environmental management, based on Life Cycle Assessment (LCA), in the environmental practices of industrial businesses. Two studies were chosen as examples to demonstrate these possibilities. The goal of the studies was to enhance the competitiveness of products using assessment and evaluation of environmental impacts associated with product systems. EPD Czech Cement and Eco-Efficiency Carlsbad Mattoni mineral water bottled in 1.5 l PET containers followed the basic approaches and possibilities outlined in ISO standards ISO 14025 and 14045.

Key words: LCA, EPD, Eco-Efficiency, cement, plastic bottles

1. INTRODUCTION

LCA (Life Cycle Assessment) is the most significant analytical information tool, which can help to assess the impact of a selected product; specifically the effect a product's production system has on the environment during its entire lifecycle. No other tool offers such a comprehensive view of the product, which can prevent the transfer of environmental impacts from one life cycle phase to another. The growing importance of LCA shows the development of the group of standards under ISO 14000, which increasingly use LCA as a basis for other applications.

The two included environmental assessments of products (cement and bottled water) show the possibilities of using standards based on LCA in the practice of industrial business. Cement was treated and certified according to ISO 14025 Type III Environmental Declarations (EPD) and bottled mineral water according to the draft standard ISO 14045 Eco-efficiency.

2. EPD CZECH CEMENT

ISO 14025 Type III Environmental Declaration (EPD) presents quantified environmental life cycle product information to enable comparisons between products fulfilling the same function. [7]

In the case of EPD, the scope and form of completing an LCA study follows the requirements of PCR (Product Category Rules), in this case, PCR 2010:09 Cement, version 0.1. Cement is a building block used for a variety of different purposes, which means that the treatment of cement, from the moment it leaves the factory gates, may vary significantly. LCA, in this instance, has therefore not been done from the "cradle to grave", but from the "cradle to gate". For the same reasons, a functional unit was replaced by a reference unit, i.e. 1 t of cement. Figure 1 graphically illustrates the LCA system boundaries for cement.

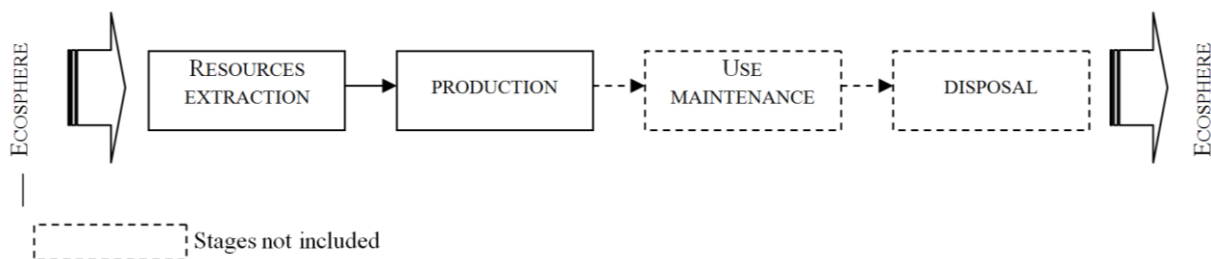


Figure 1. System boundaries of cement

PCR also regulates the internal structure of the system, which is defined as upstream, core and downstream processes. Upstream processes include the mining and processing of raw materials, including their transport to the plant. Core processes, in this particular case, are the processes within the cement factory. Downstream processes include the use and end of life stages. In the cement example, these downstream processes were not included.

LCA study results are based on site specific data for the

core processes and general data for the upstream processes, with the exception of mining limestone. The results calculated by the inventory analysis and impact categories were according to the PCR directions presented in the categories of resource consumption, hazardous and other wastes and the category of impact on global warming, ozone depletion, acidification, eutrophication and formation of photo-oxidants. The results of these categories are shown in simplified form in Tables 1, 2 and 3.

RESOURCES	Phases of a Life Cycle for a Product		Total	Unit
	Upstream processes	Core processes		
Raw Materials/Materials	1,19	1865,94	1867,12	kg
Energy	1346,62	4080,04	5429,06	MJ
Water	170	170	340	l

Table 1. Resource consumption per 1000 kg of cement

Impact Category	Equivalent Category	Phases of a Life Cycle for a Product		
		Upstream processes	Core processes	Total
for 1000 kg of cement produced in Czech Republic				
Global Warming	kg CO ₂ eq.	173,00	634,00	808,00
Ozone Depletion	kg CFC-11 eq.	0,000000002	0,000000124	0,000000126
Acidification	kg SO ₂ eq.	1,98	1,05	3,03
Photo-oxidant Creation	kg C ₂ H ₄ eq.	0,15	0,09	0,23
Eutrophication	kg PO ₄ ³⁻	0,07	0,02	0,09

Table 2. Impact Category per 1000 kg of cement

Waste production	Phases of a Life Cycle for a Product		
	Upstream processes	Core processes	Total
Hazardous waste, kg	0,0627	0,0025	0,0653
Other waste, kg	627,03	0,49	627,52

Table 3. Hazardous and other wastes produced per 1000 kg of cement

Based on the results of LCA studies, which were the basis for developing an application for certification, the Czech cement product was awarded a certificate, valid for 3 years.

3. ECO-EFFICIENCY OF CARLSBAD MINERAL WATER MATTONI

Eco-efficiency is a management tool that allows you to assess the environmental impact of the life cycle of a product together with the product's value. It puts into context the environmental behavior of a product system and the value of a product system.

The goal of the study of Mattoni mineral water bottled in 1.5 l PET containers was to provide an overview of the product system's impacts on the

environment and gather data for communicating environmental performance and improved environmental profile of the Carlsbad Mattoni mineral water company.

a. Environmental impacts of a life cycle

For the purpose of calculating the eco-efficiency of the product, two LCA studies were completed looking at the development range of the bottled mineral water Mattoni manufactured and distributed in 2011 - product B and for a comparative basis the same product produced in 2001 – product A, which was used as an indicator to calculate environmental stress.

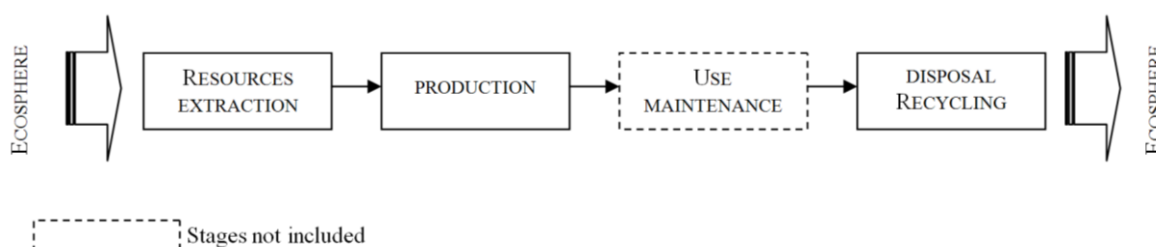


Figure 2. System Boundaries for Carlsbad mineral water Mattoni

Comparing the results of both studies, there was a reduction of environmental impacts in almost all parameters by product B produced in 2011. The LCA results for the product were used for

calculating the environmental load indicators, which were evaluated as the most serious in terms of impact on the environment. These were:
- The total energy consumption, indicator categories -

MJ (Graph 1)

- Results of impact on global warming, indicator categories - CO₂ eq.
- Results of acidification impact, indicator categories SO₂ eq.

The LCA results were calculated and integrated as a sum of three vectors: energy, global warming and acidification (Figure 3). The resulting vector illustrates the reduction of environmental impacts.

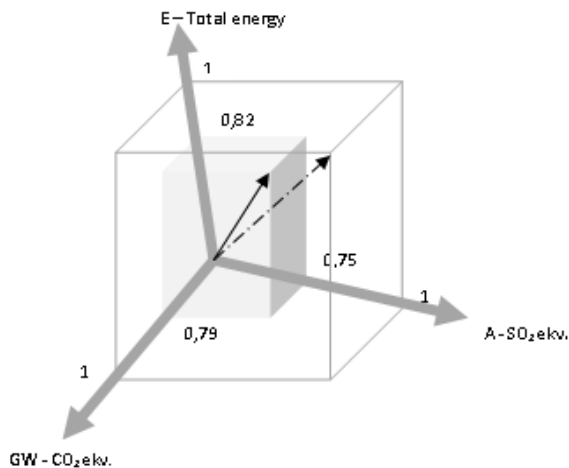


Figure 3. Schematic representation of integration of environmental stress

b. The value of a product system

To assess the value of a product system, the characteristics of the product were evaluated based on individual customer preferences. Quantification of the functional value of a product system was expressed by using the QFD (Quality Function Deployment), which allows for determining the importance of customer requirements and the weight of their relationship. Created weighting factors were used to calculate the weighted average of product characteristics obtained from surveys. The results led to the QFD matrix calculation of the indicators of a product system that was 0.9366 for Product A in 2001 and 1.4238 for Product B in 2011.

Eco-efficiency of the product system was calculated as the ratio between product value and environmental stresses of the product system. The following equation expresses the relationship:

$$\text{Eco - efficiency of product A} = \frac{0,9366}{1,7321} = 0,54$$

$$\text{Eco - efficiency of product B} = \frac{1,4238}{1,3615} = 1,05$$

The basis of the eco-efficiency product of the two systems was calculated by factor X as the ratio between the eco-efficiency of product B and the eco-efficiency of product A.

$$\text{Factor} = \frac{1,05}{0,54} = 1,93$$

The factor value shows that the measured product, bottled natural mineral water Mattoni, produced and distributed in 2010, and specifically its product system, has 1.93 times better results than the previous product

development series, which was delivered to the market in 2001.

The causes can be found not only in reducing the environmental load of product in 2010, but also in increasing the product value. A reduced bottle weight and an increased recovery of packaging material and packaging waste had an effect on reducing environmental impacts. The increase in product value was mainly due to the shape of packaging, packaging quality, weight, packaging and quality drinks.

4. CONCLUSIONS

The role of EPD and Eco-efficiency is helping to create a sustainable society. Each tool has its advantages and disadvantages.

EPD is primarily a brand of marketing that enables businesses to increase their market competitiveness. Its other advantages are the rules of PCRs), which allow you to process LCA / EPD in an exactly specified range, allowing for the easier comparison of products and its use with sub-EPD systems to build more complicated complexes, such as buildings. This environmental label but does not commit the producer to anything; it only merely states the status of the environmental stress of the products, which product and, specifically, which product system creates. Potential EPD will take full advantage of market saturation for certified products. When their number exceeds a certain threshold, the market will exhibit a preference for products with lower environmental impacts, reducing impacts on the environment throughout the production, supply and consumption cycle.

The goal of Eco-efficiency to promote the reduction of environmental burden connected with the life cycle of products with continuous customer satisfaction. This tool directly encourages businesses to think about product innovation in terms of reducing environmental burdens and increasing the product's useful properties. The method has a relatively large potential, but also a certain risk of abuse as it partially removes the requirement in the standards for assessing the eco-efficiency study by using a third party in the event that the results will be presented to the public.

The benefit, which is common to both tools, is the fact that, thanks to the LCA studies, required work in both cases, the sponsors obtained a comprehensive overview of the environmental impact connected to the product system. LCA provides a comprehensive overview of the inputs of raw materials, other materials and energy. These are items that a company has to buy. Environmental results are thus closely related to the business economy. The sponsor also receives an overview of emissions and wastes that are regulated by national rules. It is therefore in the interest of the company to not only know the extent of their portion of the life cycle of a product, but also in other phases of the range, which have environmental impacts and can involve the company.

ACKNOWLEDGMENT

A part of result presented in this paper is obtained in the framework of the multilateral cooperation "The platform for building the network of LCA centers and R&D institutes from Central and Southeastern Europe", TR 114-451-3774/2011-01, supported by the Provincial Secretariat for Science and Technological Development of AP Vojvodina, Republic of Serbia.

5. REFERENCES

- [1] Col.: *Eco-efficiency Indicator Handbook for Products*, Japan Environmental Management Association for Industry (JEMAI), 2004
- [2] Černík, B., Tichá, M.: *Hodnocení skládkování a spalování zbytkového komunálního odpadu metodou LCA*, zpráva Programu VaV MŽP ČR 720/2/00 "Intenzifikace sběru, dopravy a třídění komunálního odpadu", pp. 86, Praha, 2002.
- [3] Černík, B., Tichá, M.: *Hodnocení využití druhotných surovin z komunálního odpadu metodou LCA*, závěrečná zpráva Programu VaV MŽP ČR 720/2/00 "Intenzifikace sběru, dopravy a třídění komunálního odpadu", pp. 29, Praha, 2003.
- [4] Černík, B., Tichá, M.: *Life Cycle Assessment of environmental impacts of beverage packaging in the Czech Republic*, Programm VaV MŽP CR Project SP/II/2f1/16/07, Prague, pp. 436, 2009.
- [5] ČSN EN ISO 14040 Environmental management – Posuzování životního cyklu – Zásady a osnova, ČNI 2006
- [6] ČSN EN ISO 14044 Environmental management – Posuzování životního cyklu – Požadavky a směrnice, ČNI 2006
- [7] ČSN EN ISO 14025 Environmental management – Type III environmental declarations – Principles and procedures, ČNI 2006
- [8] Obroučka, K.: *Výzkum spalování odpadů, zpráva Programu VaV MŽP ČR 720/16/03 "Výzkum spalování odpadů"*, VŠB-TU Ostrava, pp. 672, 2005.
- [9] Tichá, M., Černík, B.: *Posouzení environmentálních dopadů přírodní minerální vody Mattoni*, Praha, pp. 34, 2011.
- [10] Tichá, M.: *Studie posouzení životního cyklu cementu*, VÚM Praha, pp. 65, 2011.
- [11] Weidema, B.P., Wesnaes, M. S.: *Data quality management for life cycle inventories – an example of using data quality indicators*, Journal of Cleaner Production, Vol. 4, no 3-4, pp. 167, 1996.

Authors: Ing. Marie Tichá, The University of J. E. Purkyně in Ústí nad Labem, Faculty of the Environment, Kralova vysina 3132/7, 400 96 Usti nad Labem, Czech Republic,
E-mail: marie.ticha@iol.cz

Assist. Prof. Dr Igor Budak, University of Novi Sad, Faculty of Technical Sciences, Institute for Production Engineering, Trg Dositeja Obradovica 6, 21000 Novi Sad, Serbia,
E-mail: budaki@uns.ac.rs

Vasiliev, A., Borodavko, V., Kroutko, V., Kheifetz, M., Gaiko, V.

FORMATION OF QUALITY PARAMETERS IN LIFE CYCLE OF MACHINE DETAILS ON THE BASIS OF TECHNOLOGICAL INHERITANCE

Abstract: From positions of technological inheritance of operational parameters actions on quality management of products of mechanical engineering are offered. The mathematical model of inheritance of quality indexes in life cycle of the product, describing various modes of behavior is developed by manufacture and application of technical systems. Use of mathematical model at computer designing gives ample opportunities for reduction of expenses at manufacturing and operation of constructive - complex products of mechanical engineering.

Key words: quality parameters, life cycle, technological inheritance

1. INTRODUCTION

The use of a principle of superposition is a distinctive feature of existing approaches in definition and forecasting of quality indexes of machine-building production. According to this principle, each of technology contributors operates irrespective of others, and the result of joint action is defined as their partial sum represented in this or that form [1, 2].

Technological systems are multiply connected, objects of manufacture are characterized by nonlinearity, irreversibility and non-equilibrium. However application of a principle of superposition reduces the multiply connected interactions which are carried out in technological systems, to one-coherent, ignoring mutual influence of technology contributors [3]. Growth of requirements to quality of manufacturing of machine elements make the methods of definition and forecasting the qualities based on a principle of superposition, practically useless as the effect of mutual influence of factors is commensurable with the results of their direct influence. Process of property change of products should be considered as a set of cooperating processes, changes and preservations of properties [4, 5].

Plurality of product properties, each of which is characterized by corresponding set of quality indexes, is also display of multicoupling of technology factors in the process of formation of product quality. Product properties are interdependently formed in the process of manufacturing. However in work practice of mechanical engineering this fact is insufficiently taken into account. Such isolated consideration of process of formation of the allocated quality indexes can lead to serious mistakes at designing and realization of technological processes [1, 2]. The technical difficulties connected to the description of multiply connected interactions, at formation of set of quality indexes at product manufacturing can be got over on the basis of application of modern information technologies and methodology of acceptance of technological solutions [4, 5].

2. THE CONCEPTUAL APPROACH

The mathematical device of methodology is based on substantive provisions [3]: quality of a detail is formed during all its technological background and the set of quality indexes is a result of backgrounds; each technological or connected to it influence lead to changes of all quality indexes of material blank; change of any quality index results in change of all other quality indexes of material blank.

Characteristics of technological mediums and laws of their change have permitted to generate the primary goal of the directed formation quality indexes of a product: at knowing initial and final properties of a manufacture subject to define the optimal technological medium from the point of view of property transformation. The major feature of the approach is formation for each technological repartition of through process of manufacturing of a product of the optimum technological medium providing the most rational distribution of levels of quality indexes on repartitions and giving to process of formation of product quality a necessary orientation. While changing medium or its characteristics, it is possible to operate forming product properties.

2.1. Model of multiply connected interactions of a medium

Necessary adjusting influences on structure change, structure and conditions of interaction of technological medium elements and of the element with a manufacture subject can be determined on the basis of comparison of characteristics of medium of a technological process and desirable processes. On the basis of the conceptual approach it is offered to define the following factors [3]: operative change quality index i while using technological method $j - (m_i)_j$; changes of quality index i of the product connected to conditions of realization of technological method $j - (u_i)_j$; changes of quality index i in interaction with medium of an operation level, realizing a technological method $j - (S_i)_j$.

Operatively forming component $(K_i)_{on_j}$ values of

parameter K_i is:

$$(K_i)_{j}^{on} = (m_i)_j (K_i)_{j-1} + (u_i)_j (K_i)_{j-1},$$

where $(K_i)_j$ – a set of levels of product quality indexes after performance of operation of its manufacturing in view of laws of a technological heredity; $(K_i)_{j-1}$ – a set of levels of the quality indexes describing a product condition after performance of the previous operation.

If the method is not realized $(m_i)_j = 1$, $(u_i)_j = 0$, otherwise $0 < (m_i)_j \leq 1$. Change of a sign and value of a quality index occurs as a result of cumulative change of factors $(m_i)_j$ and $(u_i)_j$. For each technological method the regular conditions of realization determining values $(m_i)_j$ are found. The factor $(m_i)_j$ takes into account regular conditions of realization of a method (in particular, the regular economically justified conditions of processing), and $(u_i)_j$ – distinguished from regular, and also other conditions in addition describing the medium (basing and fastening of preparation, elastic characteristics of elements of technological system, etc.).

Analytical definition of factors $(m_i)_j$, $(u_i)_j$, $(S_i)_j$ is impossible, therefore they are defined by statistical processing of an experimental material.

For a concrete method with an index of realization r composed $(u_i)_j (K_i)_{j-1}$ it is allocated in a regular component (C) :

$$[(K_i)_{j}^{on}]_r = (m_i)_j [(K_i)_{j-1}^{on}]_r + C.$$

2.2 Techniques of definition of factors of transfer

At definition of values of factors of operative change of quality indexes $(m_i)_j$ techniques of the maximal crossing of set of entrance and target values of quality indexes, and also averaging of borders of ranges (Fig. 1) are used.

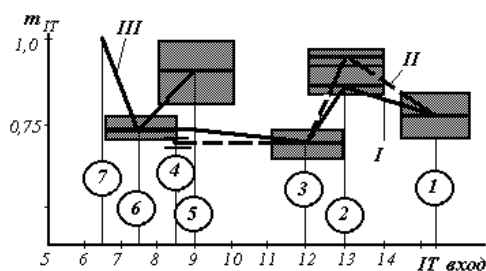


Fig.1. Comparison of factors of operative change of accuracy of the size (m_{IT}) for methods of processing of external cylindrical surfaces: 1, 2, 3, 4 – accordingly точение draft, полустистовое, fair, thin; 5, 6, 7 – accordingly grinding preliminary, final, thin; I, III – a technique of the maximal crossing of sets; II – a technique of averaging of borders

At known $(m_i)_j$ values $(u_i)_j$ are defined according to

$$[(u_i)_j]_r = [(K_i)_{j}^{on}]_r / [(K_i)_{j-1}^{on}]_r - (m_i)_j.$$

At knowing $(m_i)_j$, $(u_i)_j$

$$(S_i)_j = \frac{(K_i)_j^{on}}{(K_i)_{j-1}^{on}}$$

Tables of the average values of factors of operative change of properties $(m_i)_j$ for the basic technological methods of processing of external and internal cylindrical surfaces, and also planes are used.

It is established, that the optimum error of definition of factors of operative change of quality indexes of processable material blanks for methods of abrasive machining on the average is in 3 times higher, than for edge cutting machining, that testifies to the greater sensitivity of corresponding technological mediums to condition change of realization and a condition of objects forming them.

Average value of a relative error of definition of size m_{IT} factor of operative change of accuracy of the sizes for group of methods of detail sharpening and grindings from constructional carbonaceous steels has made 2,5 %, and roughnesses m_{Ra} – 11,0 %. Dependences of characteristics of technological medium of an operation level on a condition of objects forming them are adequately represented with the help of linear regression models or are piecewise -linear approximated at the relative error which are not exceeding 10 %

It is established, that preservation and mutual influence of properties are especially shown while flat-topped diamond-abrasive machining, polishing and super finishing when the removed allowance is within the limits of initial height of rough edges asperity.

2.3. Definition of factors of preservation and interference

Multicoupling of technological mediums, distinction of the physical processes accompanying interaction of mediums with a subject of work, is a principal cause of absence of the uniform methodical approach to definition of elements of factors of preservation and mutual influence of formed properties k_{ij} matrixes $[k_{ij}]$. Factors are defined at realization of through technological process of product manufacturing at continuous research of quality condition of a subject of manufacture.

Primary value k_{ij} for an initial phase of process:

$$k_{ij} \approx \frac{(K_i)_1 - S_{ij}(K_i)_0}{(K_i)_0},$$

where $(K_i)_1$ – value of parameter K_i after operation performance; $(K_i)_0$ – value of parameter K_i prior to the beginning of operation performance; S_{ij} – factor of change of a quality index at interaction of a subject of manufacture with the technological medium of an operation level.

In contrast to m_i , u_i , factors k_{ij} have physical dimension.

The offered device of the description of transformation of quality indexes in view of their interaction and mutual influence in multiply connected technological mediums is adequate to real processes of

property formation of mechanical engineering products and can be used for forecasting technological decisions. Application of the offered approach allows from 2 up to 5 times to reduce a relative error of preliminary definition of level of quality index in comparison with the value received on the basis of known laws of mechanical engineering technology [3].

3. CALCULATING AND ANALYTICAL METHOD

Consideration of mutual influence of technology factors at interaction of technological mediums with a subject of manufacture allows to bring in corresponding specifications to a settlement - analytical method of definition of a total error of machining. Preparations of an error arising at processing are interconnected and influence against each other and a total error of processing. Making errors are formed as a result of interaction of preparation with the technological medium of a level of operation, and with the technological medium of a level of process.

3.1. Definition of an error of processing

In result the mathematical device of definition of values of components and a total error of processing is developed. For the first it is fair that

$$\begin{bmatrix} \Delta Y \\ \varepsilon \\ \Delta H \\ \Delta u \\ \Delta T \end{bmatrix}_j = \begin{bmatrix} 1 & a_{\Delta Y, \varepsilon} & a_{\Delta Y, \Delta H} & a_{\Delta Y, \Delta u} & a_{\Delta Y, \Delta T} \\ a_{\varepsilon, \Delta Y} & 1 & a_{\varepsilon, \Delta H} & a_{\varepsilon, \Delta u} & a_{\varepsilon, \Delta T} \\ a_{\Delta H, \Delta Y} & a_{\Delta H, \varepsilon} & 1 & a_{\Delta H, \Delta u} & a_{\Delta H, \Delta T} \\ a_{\Delta u, \Delta Y} & a_{\Delta u, \varepsilon} & a_{\Delta u, \Delta H} & 1 & a_{\Delta u, \Delta T} \\ a_{\Delta T, \Delta Y} & a_{\Delta T, \varepsilon} & a_{\Delta T, \Delta H} & a_{\Delta T, \Delta u} & 1 \end{bmatrix} \begin{bmatrix} \Delta Y \\ \varepsilon \\ \Delta H \\ \Delta u \\ \Delta T \end{bmatrix}_{\partial j}$$

where $(\Delta Y, \varepsilon, \Delta H, \Delta u, \Delta T)_j^T$ – a vector - column of values of making errors (an error caused by elastic deformations; an error of installation; an error of adjustment; an error caused by dimensional deterioration; an error caused by thermal deformations), determined in view of mutual influence; a - factors of transformation of the errors, taking into account mutual influence of errors; $(\Delta Y, \varepsilon, \Delta H, \Delta u, \Delta T)_{\partial j}^T$ – a vector - column of the determined values, the making errors determined on the basis of a traditional settlement - analytical method.

The square of final value of total error Δ is defined in the form

$$\Delta^2 = [\lambda_i P_i]^T [P_i],$$

where λ_i – the factors determining the form of a curve of distribution of the making error P_i ; T – symbol of transposing.

The account of multiconnectivity of technological mediums at definition of a total error of processing allows more than in 2 times to raise accuracy of existing methods of calculation.

3.2. Model of formation of quality indexes

The developed device of the description of transformation of properties of products allows distributing in the desirable image levels of properties of a product on stages of technological process of its manufacturing. For any part of through technological process of manufacturing of a product and for any of properties of the last on the basis of the developed technique can be determined and the desirable level of values of corresponding quality indexes is if necessary optimized.

So, for example, after end of procuring repartition the achieved levels of quasi-stable K_c^3 and changing K_v^3 quality indexes are defined as following:

$$\begin{cases} K_c^3 = S_c^3 \cdot K^M + k_c^{3,M} K^M; \\ K_v^3 = S_v^3 \cdot K^M + k_v^{3,M} K^M, \end{cases}$$

where S_c^3, S_v^3 – factors of property change of a subject of manufacture as a result of its interaction with the technological medium of a level of procuring repartition; K^M – levels of quality indexes of an initial material; $k_c^{3,M}, k_v^{3,M}$ – factors of preservation and mutual influence of properties of the initial material, shown at a procuring stage of through process of manufacturing of a product.

Similar parities can be determined for repartitions of manufacturing of details and assembly of a product. These parities can be considered as model of formation of properties of a product in through technological process of his manufacturing. Practically for any stage N of group of operations parities of a kind can be received:

$$K_N = H_N \cdot K^M,$$

where K_N – value of the quality index generated after stage N ; H_N – factor of transformation of properties of a product in relation to initial (K^M).

Introduction of set of criteria of optimization it is possible to proceed to the decision of problems of optimization of values of quality indexes for each stage (operation) of technological process. As not all quality indexes are equivalent from a position of technological maintenance of their values expediently to define desirable levels not for everything, and only for hard-to-achieve quality indexes, considering thus "by default", that other indexes will be provided. Use of "passport" of a subject of the manufacture including, for example, for a detail the data about most hard-to-achieve levels of quality indexes and the general number of its surfaces, allows to lower dimension of technological problems solved in a correct way.

4. TECHNOLOGICAL ALGORITHM

Distribution of levels of properties in a combination to definition of quantitative characteristics of possible property transformation allows changing essentially existing approaches to construction of technological processes [6].

For successful performance of the set of functions the technological medium should be provided with necessary reserves. A reserve of the technological medium sets of its characteristics and values form the last which are not used at performance by the medium of set functions and conditions of their realization. The estimation of medium on each of its parameters can be carried out on the basis of the offered quantitative characteristics. The medium of any level should possess necessarily a reserve on parameters (opportunities) which size should correspond optimum to set of carried out functions and a range of possible changes of conditions of their realization. The choice of technological mediums and any of the technological objects possessing rational reserves, can effectively be carried out on the basis of the suggested device of an estimation of quality of corresponding technological decisions. Formation of a reserve of medium can be carried out on each of its separately taken parameters and should take into account both stochastic character of the last, and their interaction.

In view of influence of all cycle of manufacturing of a detail on its operational properties the algorithm according to which on required operational properties values of parameters of a condition of a superficial layer of a ready detail are recommended is developed and the technological process of its manufacturing providing the specified parameters is formed, modes of cutting, the characteristic of the tool and the equipment, mark lubricant-cooling agent (the lubricant-cooling technological medium), providing necessary parameters of a condition of a superficial layer of preparation and a semifinished item at each stage of processing are appointed.

The technological algorithm includes the following stages:

- Proceeding from operational properties and conditions of operation of elementary surfaces of detail requirements to condition of a surface of a detail are established;
- On the basis of mathematical models or in a database on a required condition of a superficial layer modes of processing, the tool, the equipment, lubricant-cooling agent, necessary for realization of final processing the set of details are defined;
- On parameters of a condition of a superficial layer mode of processing, the tool, the equipment, and lubricant-cooling agent, necessary for realization of the previous operation (transition) of processing are defined.

Designing of technological processes of product manufacturing in view of mutual influence of formed quality indexes is ineffective outside of his automation on the basis of modern computer facilities. Designing of individual routing technological processes (RTP) of detail manufacturing is desirable for carrying out in a mode of the automated synthesis at the minimal dialogue of the user with system [7, 8].

Strategy of the sanction of a problem of automated synthesis of RTP in view of laws of change, preservation and mutual influence of formed quality indexes, provides: performance of synthesis of RTP in the automated mode on a basis general technological

principles and reception of the basic characteristics of a route; forecasting change of quality indexes in view of laws of property transformation on the basis of structure generated by RTP; performance of necessary updating RTP in case a desirable level of values of quality indexes does not achieve.

5. REFERENCES

- [1] Kolesnickov, K., Balandin, G., Dalskiy, A. and others: *Technological Basis of Machine Quality Control*, Mechanical Engineering, Moscow, 256 p. 1990.
- [2] Kuznetsov, N., Tzeitlin, V., Volkov, V.: *Technological Methods of Machine's Details Reliability Growth*, Mechanical Engineering, Moscow, 304 p. 1993.
- [3] Vasilyev, A., Dalskiy, A., Klimenko, S. and others: *Technological Basis of Machine Quality Control*, Mechanical Engineering, Moscow, 256 p. 2003.
- [4] Yaschericyn, P., Averchenkov, V., Kheifetz, M., Koukhata, S.: *Analysis of Property Relations of Technological Solutions at Designing of Combined Methods of Materials Processing*, Report of National Academy of Sciences of Belarus, V. 45, № 4, pp. 106 – 109, 2001.
- [5] Vityaz, P., Kozhuro, L., Filonov, I., Kheifetz, M. *Property Control of Technological Medium at Electrophysical Processing*, Heavy Engineering Construction, № 7, pp. 18 – 23, 2004.
- [6] Kheifetz, M., Chemisov, B. and others: *Intelligent Production: State and Future Prospects*, PSU, Novopolotsk, 268 p. 2002.
- [7] Ryzhov, A., Averchenkov, V.: *Technological Process Optimization of Machine Working*, Navukovaia dumka, Kiyiv, 192 p. 1989.
- [8] Rakovich, A.: *Automatization of Technological Processes and Equipment Aids Designing*, ITC of National Academy of Sciences of Belarus, Minsk, 276 p. 1997.

Authors: Prof. Dr. Vasiliev Alexander, Bauman Moscow State Technical University, 2nd Baumanskaya str, 5, 105005, Moscow, Russia, Phone.: +7 499 267 30 08, Fax: +7 499 263 65 08.
E-mail: vas@bmstu.ru

M.Sc. Borodavko Vladimir, M.Sc. Kroutko Viacheslav, The State Scientific and Production Amalgamation "Center" of the National Academy of Sciences of Belarus, Sharangovich str., 19, 220018, Minsk, Belarus, Phone: + 375 17 259 06 90, Fax: +375 17 313 45 40.
E-mail: info@npo-center.com

Prof. Dr. Kheifetz Mikhail, Dr. Gaiko Viktor, Presidium of the National Academy of Sciences of Belarus, Independence Avenue, 66, 220072, Minsk, Belarus Phone: + 375 17 284 18 22, Fax: +375 17 284 03 75.
E-mail: mlk-z@mail.ru, gayko@presidium.bas-net.by



11th INTERNATIONAL SCIENTIFIC CONFERENCE NOVI SAD, SERBIA, SEPTEMBER 20-21, 2012

Vlčej, J., Milanović, B., Milanković, D., Hodolič, J.

IMPLEMENTATION OPTIONS OF LCA METHOD IN PRACTICE IN SLOVAK REPUBLIC

Abstract: *The LCA method is considered a universal method that is useful within any organization, regardless of its nature and scope of business, in terms of objective assessment of the product lifecycle. Implementation of the method requires processing of formalized procedures using exact methods, allowing identification of environmental consequences and impacts of products and activities on environmental components. It turns out that it is a suitable instrument of innovation and modification of voluntary instruments for realization of European environmental policy as eco-labeling, eco-design, environmental behaviour, etc. In addition it provides significant results when analyzing the impacts of products, processes and activities of the inputs and outputs on the components of the environment.*

Key words: *Life Cycle Assessment, implementation options, practical application, Slovak Republic*

1. INTRODUCTION

Life cycle assessment (LCA) method is the most important and widely-used analytical-informational tool, which makes it easier to identify and assess the impact of the selected product on the environment during its entire lifecycle, from raw material acquisition to its production, through production of the necessary materials, its use and safe disposal after expiring. The basis of the LCA method is the establishment of all the energy and material flows which connect the monitored system with its surroundings. By determining the quantity and quality of inputs and outputs we can determine the changes which cause the substance withdrawal from the environment (inputs from the aspect of monitored system) and substances brought into the environment (from the aspect of the monitored system they are outputs). Specifically we talk about systematic, by standards established ISO 14040 procedures. The LCA provides a systematic framework for identification, analysis and consequent reduction of negative environmental impacts in relation to different phases of product life cycle. It is an important tool in creating new products or production systems, as well as changing and improving existing ones. Through the LCA it is possible to obtain the necessary information for decision-making in the field of strategy, within the current company management.

2. THE CURRENT STATE OF RESEARCH AND APPLICATION OF LCA IN SLOVAKIA AND COMPARISON WITH THE COUNTRIES OF WESTERN EUROPE

LCA methodology is well established in industrialized and the environmentally conscious countries, as one of the common environmental management tools, and serves for protection of

environment and for effective socio-economic acceptability of production. At present, in Central Europe, the LCA method does not have a sufficient scientific, educational and knowledge background to be effectively used in favour of development and protection of environment and to streamline production costs, which by default belongs to key strategic objectives.

In terms of the level of implementation of LCA methods in the Slovak Republic, there have been proposed a number of projects but still there has not been the development of specific LCA methods into practice. Principles of LCA method, which are based on the approach of „life cycle thinking“, were mentioned in the Slovak Republic within the waste management program until 2005, but there is no mention of this approach in the new program from 2010. Even the LCA method is one of the most dynamic tools for voluntary environmental management systems and supports the principles of environmental management systems for compliance with sustainable development, it is currently not among the priorities in the development of waste management in the Slovak Republic. At present in Slovak Republic, within science establishment, there is an acute absence of information about LCA. The most serious issue is an absence of quality data on inputs into the production process, and also the quality of data on outputs (emissions, waste) is quite low. Therefore, there has been created several research projects at universities in Kosice, Zvolen, Bratislava, and the current UCE in Skalica regarding options for LCA method implementation.

The actual limitations are also seen through missing legislative regulation that could motivate or encourage companies to address the issue of implementation of LCA method of product in the corporate sector. This is directly linked to the absence of interest of the

company's management to make use of LCA method. Deeper and higher quality improvement of legislative issues of LCA method could be achieved through increasing competition between companies in Slovak Republic, where each individual company would be able to develop and sell products with the lowest environmental impacts otherwise they could lose their reputation and position on the market. Through this example the degree of difference of LCA method implementation in Slovak Republic and other Central European countries compared with the developed countries of Western Europe can be seen. One of the reasons for explanation and further investigation of this issue is the difference in consumer culture among the citizens of compared countries. In developed countries it is common that a customer selects a product which doesn't have the lowest price but he is willing to pay a higher price just to choose products that have lower environmental impact. In less developed countries, such as Slovak Republic, for the majority of customers, as the main criteria for choosing a product, would not be the product with the lowest environmental impacts. This is also influenced by the lower life standard of citizens and consumer culture in Slovak Republic compared to more developed countries of Western Europe. Introducing LCA method in business and product policy companies and its more precise integration and implementation in the national education program and industrial sectors in Slovak Republic, as well as the associated awareness increase on sustainable development, production and environmental protection seems as an initial solution for the observed issues.

3. ADVANTAGES AND DISADVANTAGES OF THE LCA METHOD APPLICATION

LCA method is now considered one of the most promising tools assisting in introducing the principles of sustainable development into practice. This is the reliable source of information that is important for scientific and technological development. At the level of government, local government and NGOs, there is often used a comparison between several products in terms of negative environmental impacts and the LCA method allows this. Comparison can be used, for example, for the basis of the determination of organic labelling of cheap products in order to substantiate the extent of environmental taxes and to influence the energy, raw material and the waste policy.

LCA results and conclusions do not always offer the perfect solution. It allows including all relevant circumstances, which the responsible person must take into account. Given the complexity of the waste treatment issue, it cannot be prescribed which method is going to be used. All decisions arising from the information gathered from LCA, must take into account specific local conditions, including economic and social circumstances.¹

Often criticized elements of LCA are a subjective choice that can cause many problems. This applies for example, to the status of system boundaries, data source selection, allocation rules, transport scenarios and often relating to waste management and forecasting consumer behaviour. Many of these elements are usually based on rough estimates and they do not have much to do with the real world. For example, supply system may change very fast, and use of the product also has a number of options that may be significantly different from instructions that are recommended in the behaviour of the product. Many product systems are changing (for example changing the supply chain) and require frequent updating of LCA studies. Some details may show seasonal differences, which means that some product may be superior to others for a certain period, and vice versa.²

LCA results also show a geographic dependence. Regarding this, for example, it is not possible that the results of LCA developed in Europe to be applied in the some part of e.g. Canada, without taking into account some relevant local features (such as the electricity in Canada is largely produced from hydropower, while in Europe is a mix of resources including brown coal, nuclear energy, etc.).³

Further, involvement of the environmental impact from transport means that each transport process is a burden on the environment. All sewage and sanitation intervention is associated with a quantifiable amount of transport activity having specific impacts on the environment. Excluding the impact of the transport it crates the underestimate state of their impact on the environment. As an example, a transfer of products or their components could be used. It seems as the connection between environment and economy is supporting the consumption of locally produced products and this is not only economical, but also friendly to environment.

Analysis of the LCA method is a difficult process as well as time consuming. The search activity across a large number of data from different areas requires enormous effort. Even after meeting these requirements it is always questionable whether the data actually reflect the status and properties of a system under scope. Without teamwork and application of rationalization tools for example, modern computing resources, these individual actions are hardly feasible in acceptable intentions and required level.⁴

LCA method provides wide spectral, and does not bring only benefits, but also certain dissension in some specific cases. Professionals working in this field are making an effort to streamline the LCA method and adapt it to certain terms and conditions. Many private companies and government organizations are involved in creating database and application with development software. The most popular software tools for assessment include GaBi LCA (Germany), SimaPro

¹ McDougall F., Draeger K., Integrovaný systém nakládání s odpady a využitie LCA

² Tichá M., Možnosti a obmedzení metody LCA, Odpadové fórum 2009

³ Tichá M., Možnosti a obmedzení metody LCA, Odpadové fórum 2009

⁴ Kočí V., Příručka základních informací o posuzování životního cyklu, ETC consulting, Praha 2010

(Netherlands), Umberto (Germany), Boustead Model (UK), etc.⁵

The very nature of LCA lies in its ambivalence. LCA works with data concerning the use of resources, the amount of solid waste and pollutant emissions generated, because it is possible to predict the general effects on the environment (for example, the problem of global warming caused by carbon dioxide release during the entire life cycle). LCA method is not able to contain the specific environmental problems. Its use cannot be estimated through the specific consequences on the environment. Through LCA it can be obtained the necessary information for decision-making strategies. Information that LCA method provides can help professionals not only in eco-design, but in corporate marketing also and for the selection of a new product and eco-labelling, as well as for institutions in government sector. LCA studies provide not only information about products and services, but also about internal processes.⁶

4. LCA METHOD - AREAS OF APPLICATION

4.1 Internal improvement of production systems

A significant number of LCA studies were prepared for internal use in industrial enterprises. Also, in the future, this area can be considered as one of the priority. LCA can identify opportunities to improve internal production processes within individual companies or corporations. Using LCA, the individual production processes with the highest share in environmental impact can be identified, that can help management to identify processes with greatest consumption of energy and fuel and the possibility of savings. LCA is an essential analytical tool for achieving industrial ecology within companies. For internal business purposes, a very useful extension of LCA is the economical field, or LCC (Life Cycle Costing).

4.2 Tool for communicating with the public

Outcomes of LCA are relatively well presentable to the public. Wide range of industrial companies (Volkswagen, Nokia, Shell, Motorola, etc.) use LCA to create quality relationships with the public. During the past years many LCA studies has been performed and dedicated to the quality of communicating with the public. The fact that it originates from 90th years, public communication was the main impetus for faster development of LCA through creating of robust framework anchored in a series of standards - ISO 14040. In developed countries, companies provide LCA studies of their products for industry partners and the general public as a matter of course. The increasing public interest in environmentally friendly products puts a pressure on manufacturers to perform LCA studies on their products, and also to demand the same

from their subcontractors. Intermediate producers and subcontractors can also use the LCA method in promoting their products. Due to these facts, it is necessary to evaluate the product life cycle in terms of the perception of marketing, where the life-cycle of the product have 4 basic stages - start-up, growth, peak, and decline, in which are necessary to monitor the quality of the product starting in the early days and to the period when the product enters the decline phase.⁷

4.3 LCA method - the elimination of harmful substances

If the goal is to completely reduce negative burden on the environment, there must be an interest in the environmental impacts associated with the operation technology regarding the removal of harmful substances that are present in the environment (such as pollutants from contaminated soil or environmental impacts associated with the technologies which remove harmful substances from the environmental media that man released, such as waste water, solid waste, waste gases, etc.). Localities contaminated with toxic substances, as well as waste water and gases are not only undesirable legacy from the past, but also it has to take into count their creation in the future. Technological processes that serve for removing pollutants must not be in conflict with the strategy of sustainable development. Energy and fuel difficulty associated with the technology for removal of harmful substances may constitute a significant criterion for the choice of that technological process and logistics operations and their operation arrangement. Appropriate analytical tool, to identify transactions with major environmental impacts and operations, which could reduce these impacts, is the LCA method.⁸

LCA method can be applied to compare the importance of various environmental emission flows, which is very useful in the field of sewage, remediation and decontamination technologies with no difference whether it is cleaning fluid, air, water or solid materials. Any such technology is designed to reduce unwanted substances (generally toxic) in the contaminated locality or medium. The purpose of these technologies is to decrease the environmental burden on the environment. Expression of the environmental burden of contamination due to decrease of concentration or amount of contaminants in the effluent or waste medium is not sufficient, because it shows that the process of removing pollutant requires energy consumption, fuel, materials and chemicals and express its own burden to the environment. This burden, however, is usually not seen as a factor affecting the efficiency and usefulness of sewage remediation technologies or interventions.⁹

⁵ Rajničová, L. : Analýza možností využitia LCA v rozhodovacom procese v odpadovom hospodárstve. Novus Scienta 2007, Herľany: 2007. s. 489 – 497.

⁶ Rajničová, L. : Analýza možností využitia LCA v rozhodovacom procese v odpadovom hospodárstve. Novus Scienta 2007, Herľany: 2007. s. 489 – 497.

⁷ Kočí V., Příručka základních informací o posuzování životního cyklu, ETC consulting, Praha 2010

⁸ Kočí V., Příručka základních informací o posuzování životního cyklu, ETC consulting, Praha 2010

⁹ Kočí V., Příručka základních informací o posuzování životního cyklu, ETC consulting, Praha 2010

5. ESTIMATING LIFE-CYCLE COSTS

Life cycle assessment of the product also requires the determination of the cost of the product life cycle. One of the tools to manage the product cost is - Life Cycle Costing (LCC). LCC estimates product costs, which emerge over the life cycle. It represents a broader view of the cost of the product, which in addition to costs arisen in connection with the manufacture and sale includes the costs incurred in the pre-production stage (the cost of research and development, construction costs and technological preparation of production), costs associated with the disposal of the effects of production and other costs that are not included in the normal operational calculations. It also allows the calculation of the life cycle into account price changes and changes in the cost of products throughout the product lifecycle. The reason for the development of this approach was shortening product life cycle and development costs associated with the preparation of a new product, and its withdrawal from the factory, respectively. The assessment of profitability at present do not takes these aspects into count enough and compares prices and costs from the sale and production of the product, but it is necessary to take into account the costs incurred in the pre-production stage and post-production stage. LCC studies should be prepared before the start of the manufacturing process and also throughout the life cycle including the end of life. Strategic management is crucial, and LCC studies prepared especially before the start of the production process along with the calculation of the target cost. In the pre-production phase, it is possible to make substantial measures regarding the future development of costs and benefits or possibly decide whether the product will be included in the production program.¹⁰

6. CONCLUSION

The LCA method has a great future, and therefore it is rightly considered as one of the most important tools for achieving sustainable development and a major tool of a new formed integrated product policy. For this purpose it evolves further, especially in other impact categories and sets the parameters necessary for calculations of negative impacts. Application procedures are specified, united and improved. Problems of collecting and processing vast amounts of data are solved. It can be assumed that with the development of the LCA method the database and the software will be specified and will become cheaper, so the overall efficiency of the method application will rapidly increase. Probably in the near future the average results for some materials will be available for free.

The importance of evaluation of product life cycle from the perspective of the manufacturing process, but also in terms of marketing management, for firms brings positive benefits. Environmental pollution is a current

issue and everlasting discussed about how to effectively produce products that would greatly exempt the environment.

ACKNOWLEDGMENT

A part of result presented in this paper is obtained in the framework of the multilateral cooperation "The platform for building the network of LCA centres and R&D institutes from Central and Southeastern Europe", TR 114-451-3774/2011-01, supported by the Provincial Secretariat for Science and Technological Development of AP Vojvodina, Republic of Serbia.

7. REFERENCES

- [1] Teplická, K., Hodnotenie kvality výrobku prostredníctvom hodnotenia jeho životného cyklu, Košice
- [2] Serafinová K., Možnosti aplikácie metódy LCA pre energetické procesy využívajúce odpadnú biomasu, Ostrava
- [3] Kočí V., Čistení odpadních vod, sanace kontaminovaných púd z pohledu metody LCA
- [4] Tichá M., Černík B., Posouzení systémů zberu a recyklace obalových odpadů metodou LCA, acta environmentalia universitatis comenianae, Bratislava: Bratislava 2011
- [5] Tichá M., Možnosti a obmedzení metódy LCA, Odpadové fórum 2009
- [6] McDougall F., Draeger K., Integrovaný systém nakládání s odpady a využitie LCA
- [7] Weinzettel J., Kudláček I., Štúdia LCA s využitím programu SimaPro
- [8] Kočí V. Posudzovanie životného cyklu – LCA, - 1. vyd. – Chrudim : Vodní zdroje ekomonitor, 2009. – 264 s. ISBN 978-80-86832-42-5
- [9] Kočí V., Příručka základních informací o posuzování životního cyklu, ETC consulting, Praha 2010
- [10] Rajničová, L. : Analýza možností využitia LCA v rozhodovacom procese v odpadovom hospodárstve. Novus Scienta 2007, Herľany: 2007. s. 489 – 497.

Authors: Mgr. Jozef Vlčej, Dr.h.c. prof. Ing. Janko Hodolič, Dr.Sc University of Central Europe in Skalica, Department of Ecology and Environmental Science, Kráľovská 386/11, 909 01 Skalica, Slovakia. Phone: 00421 911 444 547
E-mail: j.vlcej@sevs.sk j.hodolic@sevs.sk

MSc Branislav Milanović, MSc Darko Milanković, University of Novi Sad, Faculty of Technical Sciences, Institute for Production Engineering, Trg Dositeja Obradovica 6, 21000 Novi Sad, Serbia, Phone.: +381 21 450-366, Fax: +381 21 454-495.
E-mail: bane_m@uns.ac.rs; dakam@uns.ac.rs

¹⁰ Teplická, K., Hodnotenie kvality výrobku prostredníctvom hodnotenia jeho životného cyklu, Košice



11th INTERNATIONAL SCIENTIFIC CONFERENCE NOVI SAD, SERBIA, SEPTEMBER 20-21, 2012

Vojinović Miloradov, M., Šenk, N., Okuka, M., Turk Sekulić, M., Radonić, J.

POLYPARAMETER MODEL FOR DEFINING PARTITIONING PROCESSES OF SEMIVOLATILE ORGANIC COMPOUNDS

Abstract: *In order to define gas/particle partitioning of semivolatile organic compounds, seven EPA polychlorinated biphenyls (PCBs) and sixteen EPA polycyclic aromatic hydrocarbons (PAHs) were chosen, and twenty air samples have been collected at six urban, industrial and highly contaminated locations in Vojvodina. Gas/particle partitioning values of PCBs and PAHs gas molecules, that were gained experimentally, have been compared with polyparameter-linear free energy relationship (PP-LFER) model estimated values. Significant deviation has been noticed during comparative analysis of estimated polyparameter model values for complete set of seven PCBs congeners. Higher agreement of experimental and estimated values was for polycyclic aromatic hydrocarbons, especially for molecules with four rings. These results are in good correlation with literature data where polyparameter model has been used for predicting gas/particle partitioning of studied group of organic molecules.*

Key words: *semi-volatile organic compounds, polyparameter model, gas/particle partitioning*

1. INTRODUCTION

Air pollution and toxic substances in ambient air are a risk to human population and environment, and one of the global problems of environmental contamination. As a result of conflict situations in Western Balkans (from 1991-1999), total or partial destruction of industrial and military targets, in biotic and abiotic environmental matrix a large amount of pollutants was emitted, including semivolatile organic compounds (SVOCs), primarily polychlorinated biphenyls (PCBs) and polycyclic aromatic hydrocarbons (PAHs), dioxins and other organochlorine compounds. Based on UNEP/UNHCS report, at the territory of Republic of Serbia, there have been identified four ecologically critical locations – hot spots – Novi Sad, Pančevo, Kragujevac and Bor [1]. European Union recognized contamination problems of Western Balkans and in the frame of Fifth framework programme accepted APOPSBAL project, that determined the consequences, environmental status and exposition level of human population at the territory of Former Yugoslav Republics [2].

PCBs and PAHs are semi-volatile organic compounds (SVOCs) distributed in the environment with moderate vapor pressure, low solubility and low reactivity. Gaseous molecules in the atmosphere are found free or sorbed to suspended solid phase. PCBs are easily sorbed to suspended solids (aerosols) and associated to organic components of soil and suspended organic matter in aquatic ecosystems and sediment. PCBs are detected in all environmental mediums: water, soil, sediment, air, and living organisms (eg. frog livers). Even though anthropogenic sources of these compounds are reduced to maximum in the last decades, due to ubiquity of PCBs in abiotic and biotic material, atmospheric transport and

cyclic movement, they are still a major pressure to public health and human exposition.

Despite the low vapor pressure (0.03-0.00013 Pa at 20°C, EPA congeners), PCBs evaporate from the soil, and the presence, distribution and transport through the atmosphere are the main mechanism of PCBs gas molecules movement [3]. Three decades after restriction, atmospheric levels of PCBs show state of stationary status. This indicates that PCBs are still emitted in the atmosphere with primary (evaporation from old or damaged equipment with PCBs) or secondary emission sources (contaminated soil, water).

Polycyclic aromatic hydrocarbons are a combination of two or more condensed aromatic rings, and physical and chemical properties of individual compounds differ. Their main property is their semi-volatility or volatility, which makes them mobile through the environment. In the atmosphere, PAHs gas molecules are free in gaseous phase or sorbed to solid particles. Naphthalene, acenaphthene, anthracene, fluorene and phenanthrene are present primarily in gaseous phase. PAHs that have four rings (fluoranthene, pyrene, benz(a)anthracene and pyrene) are present in both gaseous and solid phase, and PAHs with five or more rings (benz(a)pyrene, benzo(ghi)perylene) are sorbed to solid particles [4]. Half life in the atmosphere of particles with diameter in the range of 0.1-0.3µm, and to which PAHs are sorbed onto, is several days.

PCBs and PAHs are detected in all environmental mediums, in regions far away from emission sources (eg. oceans and polar regions), where they were never produced or used [5,6]. Atmospheric transport is the dominant mechanism of dispersion and distribution of PCBs and PAHs gas molecules to thousand kilometers away from emission sources [5-7]. After emission to the

environment, PCBs and PAHs do not subject to degradation processes, but instead, they start dynamic equilibrium cyclic processes and distribution between environmental mediums. PCBs and PAHs have low solubility in water, and high solubility in lipids, resulting in bioaccumulation in adipose tissue and biomagnificate through food chain [8,9]. Even at low concentrations, PCBs and PAHs have toxic effect to human population and wildlife, with catalytic action in carcinogenesis, immune dysfunction, neurological diseases, reproductive and endocrine disorders.

Research that provided a broader framework from which the results presented in this paper were gained [10,11], is conceived with the aim of determining the scope, structure and specific quality characteristics, which directly or indirectly define partitioning and transport of PCBs and PAHs through the environmental mediums in Western Balkan territory.

In the research presented in the paper, compatibility of experimentally gained data and values calculated using polyparameter model, for partitioning of PCBs and PAHs in the presence of atypical primary emission sources were analyzed.

2. DISTRIBUTION MODELLING OF GAS MOLECULES IN THE ATMOSPHERE

Gas/particle partitioning assessment of PCBs and PAHs gas molecules has been analyzed in many theoretical studies and models [12,13]. Distribution of gas molecules is usually represented with gas/particle partitioning coefficient, K_p ($\text{m}^3 \text{air} \mu\text{g}^{-1} \text{aerosol}$), equation (1):

$$K_p = \frac{C_p}{C_{GTSP}} = \frac{\varphi}{TSP - \varphi TSP} \quad (1)$$

where C_p and C_G are concentration of analyte in particulate and gaseous phase ($\text{mol m}^{-3} \text{air}$), respectively, and TSP is concentration of total suspended atmospheric solids ($\mu\text{g aerosol m}^{-3} \text{air}$). Fraction of individual compounds sorbed onto particulate phase of the sample in total detected amount φ (0-1), are calculated with the equation (2):

$$\varphi = \frac{C_p}{C_p + C_G} = \frac{K_p TSP}{1 + K_p TSP} \quad (2)$$

The content of atmospheric solids, aerosols, has the dominant effect to sorption processes, which is highly important for transport and behaviour of SVOCs in the atmosphere. Atmospheric particles are structured of different phases, and can be group to adsorbing phase (mineral dust, elemental carbon), and absorbing phase (water soluble organic matter – WSOM, water insoluble organic matter – WIOM and water phase). Nonhomogeneity and mixing of different phases can lead to slowing of sorption processes, if one phase disables distribution of analytes to the other phase, or accelerating of sorption, when two phases form a new one, with different content and properties for sorption processes.

2.1. Polyparameter model

Distribution modelling of semivolatile apolar, polar and ionizable organic compounds to WIOM of atmospheric particles with absorption models can be described with PP-LFER model [14].

Gas/particle partitioning of a given compound in the atmosphere for absorption process can be characterized by five molecular descriptors. In the following PP-LFERs these descriptors are shown in equation (3):

$$\log K_{isorbent/air} = sS_i + aA_i + bB_i + lL_i + vV_i + c \quad (3)$$

where S_i , A_i , B_i , L_i and V_i are the compound-specific Abraham descriptors for the polarizability/dipolarizability, electron acceptor (H-bond donor) capability, electron donor (H-bond acceptor) capability, logarithm of the hexadecane/air partitioning coefficient, and McGowan volume, respectively [15]. Abraham descriptors have specific values for individual compounds (sorbate) and measured in laboratory conditions. For a number of different polar, apolar and ionizable organic compounds, these descriptors have been measured and published.

Corresponding to the Abraham descriptors are the sorbent (i.e., particle)-specific descriptors s , a , b , l , and v , along with the fitting constant, c . Sorbent-specific descriptors can be calculated by performing a multiple-linear regression using experimental $\log K_p$ values as the dependent variables and Abraham descriptors as the independent variables [14].

Based on the research results [14, 15], for apolar, polar and ionizable organic compounds, it is recommended to use sorbent-descriptors that showed typical sorption properties, Berlin W and Duebendorf F.

PP-LFER model based on Abraham descriptors shows a valuable degree of accuracy, and at the same time it is applicable for a numerous different polar, apolar and ionizable organic compounds. However, the usage of PP-LFER model is difficult for compounds that do not have Abraham descriptors calculated yet (PCDDs/Fs, PBDEs etc.).

3. MATERIAL AND METHOD

A total number of 20 air samples was obtained from six urban and industrial monitoring stations in two cities of Vojvodina region, Serbia – Novi Sad and Pančevo. In Novi Sad, locations were chosen based on the distance from emissions of PCBs and PAHs. With this criteria three locations were selected – Oil refinery Novi Sad (location N1), Sangaj (location N2) and City center (location N3). With similar criteria, three locations in Pančevo were chosen – Oil refinery Pančevo (location P1), Chemical industry (location P2) and City hall (location P3).

Conventional high volume sampling method was applied, with quartz filters for collecting the atmospheric particles and polyurethane foam filters (PUF) for retaining the free gas molecules of PCBs and PAHs. The samples were analyzed using GC-ECD (HP 5890) supplied with a

Quadrex fused silica column 5% Ph for PCBs, while 16 US EPA polycyclic aromatic hydrocarbons were determined in samples using a GC-MS instrument (HP 6890 - HP 5972) supplied with a J&W Scientific fused silica column DB-5MS. All analytical procedures were done in the laboratories of the Research Centre for Environmental Chemistry and Ecotoxicology (RECETOX), Masaryk University, Brno, CR, coordinated by dr. Jana Klanova and dr. Ivan Holoubek.

4. RESULTS AND DISCUSSION

In figure 1. only four experimentally gained values of gas/particle partitioning coefficient for polychlorinated biphenyls, at locations in Vojvodina, are in domain of model assessed log K_p values, which represents 9.5% of total number of experimentally gained values, i.e. 16% if only relevant data are observed. Three of four values that

are in domain of mathematical assessment of the model, are for congener PCB 52, that is frequently detected, and just one for congener PCB 153. Values on x-axes are results of low experimental K_p values, and are not relevant for analysis of the results.

Deviation of experimental and modelled values is the highest for PAHs that are dominantly in gaseous phase (naphthalene, acenaphthylene, acenaphthene, fluorene, phenanthrene and anthracene, fig. 2). Best compatibility between experimentally gained and modelled log K_p values is for PAHs that are present in both gaseous and particulate phase (fluoranthene, pyrene, benz(a)anthracene and chrysene). As a result of some PAHs not being present in gaseous phase, logK_p values are marked as zero, and it does not represent a relevant data, and also was not considered in the analysis.

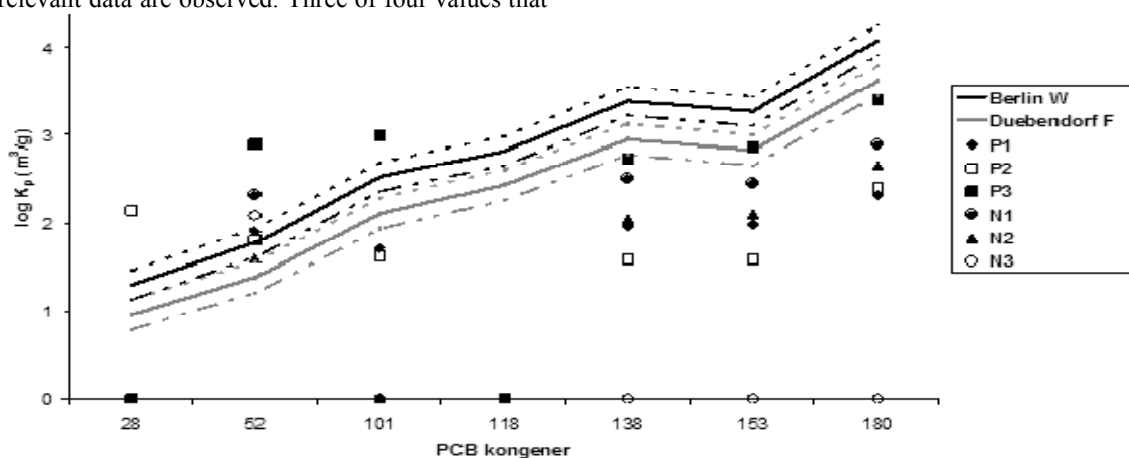


Fig. 1 Experimentally gained and PP-LFER model estimated log K_p values at 15 °C and 50% relative humidity using PP-LFER for the Berlin W and Duebendorf F samples at localities in Novi Sad and Pančevo for polychlorinated biphenyls.

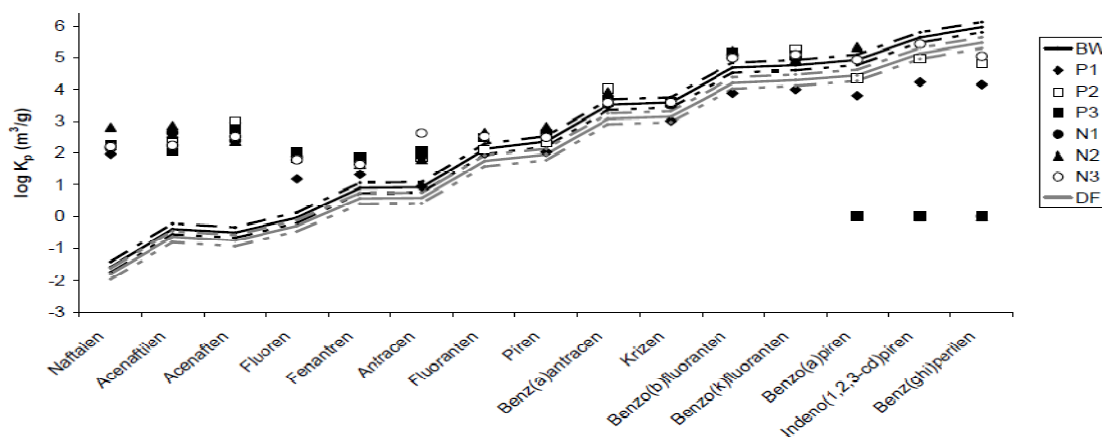


Fig. 2 Experimentally gained and PP-LFER model estimated log K_p values at 15 °C and 50% relative humidity using PP-LFER for the Berlin W and Duebendorf F samples at localities in Novi Sad and Pančevo for polycyclic aromatic hydrocarbons

5. INSTEAD OF CONCLUSION

In the paper, experimentally gained gas/particle partitioning coefficients of polychlorinated biphenyls and polycyclic aromatic hydrocarbons in heterogenous multicomponent system in 20 ambient air samples has

been shown. Samples were collected at the territory of Vojvodina in urban, industrial and residential areas of cities Novi Sad and Pančevo. Experimentally gained data were compared to mathematically modelled values, using polyparameter model.

Based on the conclusions from comparison of experimentally gained and modelled values, polyparameter model is not recommended for modelling of PCBs congeners' behaviour in specific ambient conditions in Novi Sad and Pančevo. Positive match of experimentally gained and PP-LFER modelled values was gained in only 9.5% of ambient air samples, i.e. in 16% if only relevant data are observed. Parallel analysis of adsorption, absorption and polyparameter model gas/particle partitioning of PCBs congeners shows that the best Junge-Pankow simulation of realistic conditions is the best for representing ecostatus of Western Balkan. For polycyclic aromatic hydrocarbons, assessment of Kp values with PP-LFER model is gained for PAHs with four rings, compounds that are found in both gaseous and particulate phase – fluoranthene (C₁₆H₁₀), pyrene (C₁₆H₁₀), benz(a)anthracene (C₁₈H₁₂) and chrysene (C₁₈H₁₂). Experimentally gained values are in domain of allowed deviation and are matching modelled values up to 62.5%. Gained results are in consistency with literature evaluations of polyparameter model. For other EPA PAHs, deviation is higher, only 20 data are in domain of allowed deviation, which is 21% from total number of experimentally gained values, and 24% if only relevant data are observed. Based on the results, polyparameter model is not recommended for polycyclic aromatic hydrocarbons primarily present in gaseous phase.

ACKNOWLEDGEMENT

This research was supported by FP5 EU (ICFP501A2PR02 – APOPSBAL) and Ministry of Education and Science, Republic of Serbia (III46009).

6. REFERENCES

- [1] UNEP (1999), The Kosovo conflict – consequences for the environment and human settlements. <http://www.grid.unep.ch/btf/final/finalreport.pdf>
- [2] APOPSBAL, Assessment of the selected POPs in the atmosphere and water ecosystems from the waste generated by warfare in the area of former Yugoslavia, Final report, 2005.
- [3] M. Turk Sekulić, Rasprostiranje, depozicija i raspodela polihlorovanih bifenila u heterogenom multikomponentnom sistemu, Doktorska disertacija, Fakultet tehničkih nauka, Univerzitet u Novom Sadu, Novi Sad, Srbija, 2009.
- [4] J. Radonić, Atmosferski transport i modelovanje raspodele između čvrste i gasovite faze policikličnih aromatičnih ugljovodonika, Doktorska disertacija, Fakultet tehničkih nauka, Univerzitet u Novom Sadu, Novi Sad, Srbija, 2009.
- [5] I. Iwata, S. Tanabe, N. Sakai, R. Tatsukawa, Distribution of persistent organochlorines in the oceanic air and surface seawater and the role of ocean on their global transport and fate, Environ. Sci. Technol. 27 (1993) 1080–1098.
- [6] D.E. Schulz-Bull, G. Petrick, R. Bruhn, J.C. Duinker, Chlorobiphenyls (PCB) and PAHs in water masses of the northern North Atlantic, Mar. Chem. 61 (1998) 101–114.
- [7] C.J. Halsall, A. J. Sweetman, L.A. Barrie, K.C. Jones, Modelling the behaviour of PAHs during atmospheric transport from the UK to the Arctic, Atmos. Environ. 35 (2001) 255–267.
- [8] J. Skei, P. Larsson, R. Rosenberg, P. Jonsson, M. Olsson, D. Broman, Eutrophication and contaminants in aquatic ecosystems, Ambio 29 (2000) 184–194.
- [9] J.E. Baker, Critical pathways of Bioaccumulation in aquatic food webs, State of the art workshop: Bioaccumulation of organic compounds and mercury in aquatic food webs, Ispra, Italia., JRC. 2002.
- [10] M. Turk, J. Jaksic, M. Vojinovic Miloradov, J. Klanova, Determination of POPs in Gaseous Phase by Active and Passive Sampling Methods, Environ. Chem. Lett. J. 5 (2007) 109–113.
- [11] J. Radonić, M. Turk Sekulić, M. Vojinovic Miloradov, P. Čupr, J. Klánová, Gas-particle partitioning of persistent organic pollutants in the Western Balkan countries which suffered recent PCB spills, Environ. Sci. Pollut. Res. 16(1) (2009) 65–72.
- [12] J.F. Pankow, T.F. Bidleman, Interdependence of the slopes and intercepts from log-log correlations of measured gas-particle partitioning and vapor pressure-1. Theory and analysis of available data, Atmos. Environ. 26A (1992) 1071–1080.
- [13] W.E. Cotham, T. Bidleman, Polycyclic aromatic hydrocarbons and polychlorinated biphenyls in air at an urban and a rural site near lake Michigan, Environ. Sci. Technol. 29 (1995) 2782–2789.
- [14] H.P.H. Arp, R.P. Schwarzenbach, K.U. Goss, Ambient Gas/Particle Partitioning. 2. The Influence of Particle Source and Temperature on Sorption to Dry Terrestrial Aerosols, Environ. Sci. Technol. 42 (2008b) 5951–5957.
- [15] H.P.H. Arp, R.P. Schwarzenbach, K.U. Goss, Ambient Gas/Particle Partitioning. 1. Sorption Mechanisms of Apolar, Polar, and Ionizable Organic Compounds, Environ. Sci. Technol. 42 (2008) 5541–5547.

Authors: Prof. emeritus Dr. Mirjana Vojinović Miloradov, M.Sc. Nevena Šenk, M.Sc. Marija Okuka, Assist. Prof. Dr. Maja Turk Sekulić, Assist. Prof. Dr. Jelena Radonić, University of Novi Sad, Faculty of Technical Sciences, Department of Environmental Engineering and Occupational Safety and Health, Trg Dositeja Obradovića 6, 21000 Novi Sad, Serbia, Phone: +381 21 485 2405, Fax: +381 21 6350 696
E-mail: miloradov@uns.ac.rs,
nevenasenk@uns.ac.rs,
marijaokuka@uns.ac.rs,
majaturk@uns.ac.rs,
jelenaradonic@uns.ac.rs

11th INTERNATIONAL SCIENTIFIC CONFERENCE
MMA 2012 - ADVANCED PRODUCTION TECHNOLOGIES

PROCEEDINGS



Section F:
OTHER PRODUCTION ENGINEERING
TECHNOLOGIES

Novi Sad, 20-21 September 2012

Alexandrov, S., Lyamina, E., Manabe, K.

A THEORETICAL STUDY ON SURFACE ROUGHING IN PURE BENDING OF VISCOPLASTIC SHEETS

Abstract: An analysis of plane-strain bending at large strains for a rigid viscoplastic incompressible material model is performed. The Mises-type yield criterion is adopted. The yield stress depends on the equivalent strain rate (the quadratic invariant of the strain rate tensor). The solution is combined with an empirical equation for surface roughness evolution.

Key words: Pure bending, large strains, viscoplasticity, surface roughing

1. INTRODUCTION

Pure plane-strain bending at large strains is one of the classical problems in plasticity theory. A unified method to analyze this process for isotropic incompressible materials has been proposed in [1]. The method has been extended to a class of anisotropic materials in [2]. The process of bending can also provide some data for the empirical model for surface roughness evolution proposed in [3].

2. KINEMATICS

The approach proposed in [1] is based on the mapping between Eulerian Cartesian coordinates (x, y) and Lagrangian coordinates (ζ, η) in the form

$$\begin{aligned} \frac{x}{H} &= \sqrt{\frac{\zeta}{a} + \frac{s}{a^2}} \cos(2a\eta) - \frac{\sqrt{s}}{a} \text{ and} \\ \frac{y}{H} &= \sqrt{\frac{\zeta}{a} + \frac{s}{a^2}} \sin(2a\eta) \end{aligned} \quad (1)$$

where H is the initial thickness of the sheet, s is an arbitrary function of a , a is a function of the time, t , and $a = 0$ at $t = 0$. At the initial instant, $a = 0$,

$$s = 1/4. \quad (2)$$

Substituting Eq. 2 into Eq. 1 and applying l'Hospital's rule gives $x = \zeta H$ and $y = \eta H$ at the initial instant when the shape of the specimen is the rectangle defined by the equations $x = -H$, $x = 0$ and $y = \pm L$. The initial shape and the Cartesian coordinate system are shown in Fig. 1. It is possible to assume, with no loss of generality, that the origin of this coordinate system is located at the intersection of the axis of symmetry and surface AB throughout the process of deformation. An intermediate shape is also shown in Fig. 1. It is obvious that $\zeta = 0$ for AB and $\zeta = -1$ for CD throughout the process of deformation. According to Eq. 1, any intermediate shape is determined by two circular arcs, AB and CD , and two straight lines, AD and CB . These circular arcs coincide with coordinate curves of the plane polar coordinate system $r\theta$ defined by the following transformation equations

$$\frac{r}{H} = \sqrt{\frac{\zeta}{a} + \frac{s}{a^2}} \text{ and } \theta = 2a\eta. \quad (3)$$

Geometric parameters of the shape at any instant are given by (Fig. 1)

$$\begin{aligned} \frac{R_{AB}}{H} &= \frac{\sqrt{s}}{a}, \quad \frac{R_{CD}}{H} = \sqrt{\frac{s}{a^2} - \frac{1}{a}}, \\ \frac{h}{H} &= \frac{\sqrt{s} - \sqrt{s-a}}{a} \end{aligned} \quad (4)$$

where R_{AB} is the radius of surface AB , R_{CD} is the radius of surface CD , and h is the current thickness of the sheet. It is possible to verify by inspection that the Lagrangian coordinates coincide with trajectories of the principal strain rates and that the mapping given by Eq.1 satisfies the equation of incompressibility at any instant. It will be shown in the next section that the assumption that the Lagrangian coordinates coincide with the trajectories of the stress tensor allows one to solve the stress equations.

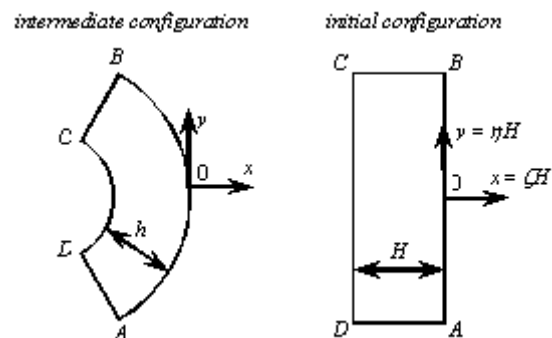


Fig. 1. Coordinate systems, initial shape and intermediate shape in pure bending.

In the case under consideration these two conditions (coincidence of the trajectories for the principal stresses and principal strain rates and the equation of incompressibility) are equivalent to the associated flow rule of the classical rate formulation of plasticity theory.

The strain rate components can be found from Eq. 1 and, then, the position of the neutral line is determined

by

$$\zeta = \zeta_n = -ds/da, \quad (5)$$

the equivalent strain rate by

$$\dot{\xi}_{eq} = \frac{|\zeta + ds/da| da}{\sqrt{3}(\zeta a + s)} dt \quad (6)$$

and the equivalent strain by

$$\varepsilon_{eq} = \frac{1}{\sqrt{3}} \ln[4(\zeta a + s)], \quad (7)$$

$$\varepsilon_{eq} = \frac{1}{\sqrt{3}} \ln \left\{ \frac{\zeta a + s}{4[\zeta a_c(\zeta) + s_c(\zeta)]^2} \right\},$$

$$\varepsilon_{eq} = -\frac{1}{\sqrt{3}} \ln[4(\zeta a + s)]$$

in regions 1, 2 and 3, respectively. In region 1, $0 \geq \zeta \geq -1/2$, the principal strain rate $\dot{\xi}_{\zeta\zeta} < 0$ (and $\dot{\xi}_{\eta\eta} > 0$) during the entire process. In region 3, $-1 \leq \zeta \leq \zeta_n^f$, the principal strain rate $\dot{\xi}_{\zeta\zeta} > 0$ (and $\dot{\xi}_{\eta\eta} < 0$) during the entire process. A property of all curves $\zeta = const$ in region 2, $\zeta_n^f \leq \zeta \leq -1/2$, is that each of these curves coincides with the neutral line at one time instant. Consider any ζ -curve of this class and denote a_c the value of a at which the curve coincides with the neutral line. Then, $\dot{\xi}_{\zeta\zeta} < 0$ ($\dot{\xi}_{\eta\eta} > 0$) at $a < a_c$ and $\dot{\xi}_{\zeta\zeta} > 0$ ($\dot{\xi}_{\eta\eta} < 0$) at $a > a_c$ for this curve. Obviously, the time instant at which the sign is changed depends on the curve such that $a_c = a_c(\zeta)$. The corresponding value of s will be denoted by $s_c(\zeta)$ where $s_c(\zeta) = s[a_c(\zeta)]$. These values of $a_c(\zeta)$ and $s_c(\zeta)$ are involved in Eq. 7. Also, ζ_n^f is the ζ -coordinate of the neutral surface at the end of the process. If $s(a)$ were known, Eq. 5 would determine $a_c(\zeta)$ and, therefore, $s_c(\zeta)$. Thus, $s(a)$ is the only unknown function in the analysis of kinematics and this function should be found from the analysis of stress.

3. STRESS ANALYSIS

The only non-trivial equilibrium equation in the plane polar coordinate system (r, θ) in terms of the radial and circumferential stresses has the form

$$\frac{\partial \sigma_r}{\partial r} + \frac{\sigma_r - \sigma_\theta}{r} = 0. \quad (8)$$

It is obvious that $\sigma_r \equiv \sigma_{\zeta\zeta}$ and $\sigma_\theta \equiv \sigma_{\eta\eta}$. The plane-strain yield condition in the case under consideration is

$$\sigma_r - \sigma_\theta = \pm \frac{2}{\sqrt{3}} \sigma_0 \Phi(\xi_{eq}) \quad (9)$$

where the upper sign corresponds to the region $-1 \leq \zeta \leq \zeta_n$ and the lower sign to the region $\zeta_n \leq \zeta \leq 0$. Also, the function $\Phi(\xi_{eq})$ satisfies the condition $\Phi(0) = 1$, σ_0 is the yield stress in tension at

$\xi_{eq} = 0$. Using Eq. 3 it is possible to replace r and differentiation with respect to r with ζ and differentiation with respect to ζ in Eq. 8. Then, using Eq. 9,

$$\frac{\partial \sigma_r}{\partial \zeta} = \mp \frac{a \sigma_0 \Phi(\xi_{eq})}{\sqrt{3}(\zeta a + s)}. \quad (10)$$

The function $\Phi(\xi_{eq})$ should be prescribed and ξ_{eq} can be excluded by means of Eq. 6. The boundary conditions on the radial stress are

$$\sigma_r = 0 \quad (11)$$

for $\zeta = -1$ and $\zeta = 0$. Since there are the two boundary conditions for the differential equation of first order, the function $s(a)$ and, consequently, the neutral line position (see Eq. 5) should be found from the solution to Eq. 10 simultaneously with constant of integration. Also, the radial stress must be continuous across the boundary of the aforementioned regions 1, 2, and 3. Once the solution for stress components has been found, the bending moment per unit length is determined by integration [1]

$$M = \frac{H^2}{2a} \int_{-1}^0 \sigma_{\theta\theta} d\zeta. \quad (12)$$

At the initial instant, the polar coordinate system (r, θ) transforms to the Cartesian coordinate system (x, y) . In order to facilitate numerical solution of Eq. 10 for the initial stage of the process, the second derivative d^2s/da^2 at the initial instant can be found analytically.

4. SOLUTION FOR THE INITIAL STAGE OF THE PROCESS

Since the distribution of the damage parameter is uniform at the initial instant, $\zeta_n = -1/2$ at $a = 0$. Then, it follows from Eq. 5 that

$$ds/da = 1/2 \quad (13)$$

at $a = 0$. Moreover, at the initial instant

$$\sigma_r = 0 \quad \text{everywhere,}$$

$$\sigma_\theta = \frac{2}{\sqrt{3}} \sigma_0 \Phi_0(\zeta)$$

$$\text{in the range } -1 \leq \zeta < -1/2, \quad (14)$$

$$\sigma_\theta = -\frac{2}{\sqrt{3}} \sigma_0 \Phi_0(\zeta)$$

$$\text{in the range } -1/2 < \zeta \leq 0.$$

The function $\Phi_0(\zeta)$ determines the through-thickness distribution of the function $\Phi(\xi_{eq})$ at the initial instant. Thus, it follows from Eqs. 2, 6 and 13 that

$$\Phi_0(\zeta) = \Phi \left(\left| \zeta + \frac{1}{2} \right| \frac{4}{\sqrt{3}} \frac{da}{dt} \right). \quad (15)$$

It is seen from this equation that the function $\Phi_0(\zeta)$ is symmetric relative to the neutral line. Therefore, it follows from Eq. 14 that $\int_{-1}^0 \sigma_\theta d\zeta = 0$, as it should be in

pure bending. The solution of Eq. 10 in the range $-1 \leq \zeta \leq \zeta_n$ satisfying Eq. (11) at $\zeta = -1$ can be written in the form

$$\sigma_r = -\frac{a\sigma_0}{\sqrt{3}} \int_{-1}^{\zeta} \frac{\Phi(\xi_{eq})}{(za+s)} dz \quad (16)$$

where z is a dummy variable of integration. Then, the radial stress acting at $\zeta = \zeta_n$ is

$$\sigma_{32} = -\frac{a\sigma_0}{\sqrt{3}} \int_{-1}^{\zeta_n} \frac{\Phi(\xi_{eq})}{(za+s)} dz. \quad (17)$$

The solution of Eq. 10 in the range $\zeta_n \leq \zeta \leq -1/2$ satisfying the boundary condition $\sigma_r = \sigma_{32}$ at $\zeta = \zeta_n$ can be written in the form

$$\sigma_r = \sigma_{32} + \frac{a\sigma_0}{\sqrt{3}} \int_{\zeta_n}^{\zeta} \frac{\Phi(\xi_{eq})}{(za+s)} dz. \quad (18)$$

Then, the radial stress acting at $\zeta = -1/2$ is

$$\sigma_{21} = \sigma_{32} + \frac{a\sigma_0}{\sqrt{3}} \int_{\zeta_n}^{-1/2} \frac{\Phi(\xi_{eq})}{(za+s)} dz. \quad (19)$$

Finally, the solution of Eq. 10 in the range $-1/2 \leq \zeta \leq 0$ satisfying the boundary condition $\sigma_r = \sigma_{21}$ at $\zeta = -1/2$ can be written in the form

$$\sigma_r = \sigma_{21} + \frac{a\sigma_0}{\sqrt{3}} \int_{-1/2}^{\zeta} \frac{\Phi(\xi_{eq})}{(za+s)} dz. \quad (20)$$

Substituting the boundary condition (11) at $\zeta = 0$ into Eq. 20 gives

$$\sigma_{21} + \frac{a\sigma_0}{\sqrt{3}} \int_{-1/2}^0 \frac{\Phi(\xi_{eq})}{(za+s)} dz = 0. \quad (21)$$

Using Eqs. 5 and 19 it is possible to transform Eq. 21 to $I_1 + I_2 - I_3 = 0$, (22)
where

$$\begin{aligned} I_1 &= \int_{-ds/da}^{-1/2} \frac{\Phi(\xi_{eq})}{(za+s)} dz, \\ I_2 &= \int_{-1/2}^0 \frac{\Phi(\xi_{eq})}{(za+s)} dz, \\ I_3 &= \int_{-1}^{-ds/da} \frac{\Phi(\xi_{eq})}{(za+s)} dz \end{aligned} \quad (23)$$

Differentiating each of these integrals with respect to a and, then, putting $a = 0$ and taking into account Eqs. 2 and 13 give

$$\begin{aligned} \left. \frac{\partial I_1}{\partial a} \right|_{a=0} &= 4 \left. \frac{d^2 s}{da^2} \right|_{a=0}, \\ \left. \frac{\partial I_2}{\partial a} \right|_{a=0} &= 4 \int_{-1/2}^0 \left(\frac{d\Phi}{d\xi_{eq}} \frac{\partial \xi_{eq}}{\partial a} \right) dz - \\ &\quad - 16 \int_{-1/2}^0 \Phi_0 \left(z + \frac{1}{2} \right) dz, \\ \left. \frac{\partial I_3}{\partial a} \right|_{a=0} &= -4 \Phi_0 \left. \frac{d^2 s}{da^2} \right|_{a=0} - \\ &\quad - 4(1 - D_0) \int_{-1/2}^{-1} \left(\frac{d\Phi}{d\xi_{eq}} \frac{\partial \xi_{eq}}{\partial a} \right) dz + \\ &\quad + 16 \int_{-1/2}^{-1} \Phi_0 \left(z + \frac{1}{2} \right) dz. \end{aligned} \quad (24)$$

Since $\Phi(\xi_{eq})$ is a prescribed function of ξ_{eq} , the derivative $d\Phi/d\xi_{eq}$ at $a = 0$ can be found as a function of ζ by means of Eqs. 2, 6 and 13. The derivative $\partial \xi_{eq}/\partial a$ at $a = 0$ can be evaluated using Eq. 6. It is convenient to introduce the new variable γ by the equation $\gamma = \zeta + 1/2$. Then,

$$\left. \frac{\partial \xi_{eq}}{\partial a} \right|_{a=0} = \mp E_0(\gamma), \quad (25)$$

$$E_0(\gamma) = \frac{4}{\sqrt{3}} \left[\left. \frac{d^2 s}{da^2} \right|_{a=0} - 16\gamma^2 \right] \frac{da}{dt}$$

It is also convenient to introduce the following notation

$$\Omega(\gamma) = E_0(\gamma) \left(\frac{d\Phi}{d\xi_{eq}} \right) \Big|_{a=0}. \quad (26)$$

Differentiating Eq. 22 with respect to a , using Eqs. 24 and Eq. 26, and replacing ζ with γ yield

$$\begin{aligned} 2 \left. \frac{d^2 s}{da^2} \right|_{a=0} + \int_0^{1/2} \Omega(\gamma) d\gamma - \int_0^{-1/2} \Omega(\gamma) d\gamma - \\ - \left[\int_0^{-1/2} \Phi_0 \frac{\partial D}{\partial a} \Big|_{a=0} d\gamma \right] - \\ - 4 \left[\int_0^{-1/2} \gamma \Phi_0 d\gamma + \int_0^{1/2} \gamma \Phi_0 d\gamma \right] = 0 \end{aligned} \quad (27)$$

It is seen from Eq. 25 that $E_0(\gamma)$ is an even function of γ . It follows from Eq. 6 that ξ_{eq} at $a = 0$ is also an even function of γ . Therefore, $d\Phi/d\xi_{eq}$ being a function of ξ_{eq} is also an even function of γ at $a = 0$. Finally, the definition for the function $\Omega(\gamma)$ given in Eq. 26 shows that it is an even function of γ . Then,

$$\begin{aligned} \int_0^{1/2} \Omega(\gamma) d\gamma - \int_0^{-1/2} \Omega(\gamma) d\gamma = \\ = \int_0^{1/2} \Omega(\gamma) d\gamma + \int_{-1/2}^0 \Omega(\gamma) d\gamma = 2 \left[\Sigma_1 \left(\frac{1}{2} \right) - \Sigma_1(0) \right] \end{aligned} \quad (28)$$

where $\Sigma_1(\gamma)$ is the anti-derivative of $\Omega(\gamma)$.

Analogously, it is seen from Eq. 15 that the function $\Phi_0(\zeta)$ involved in Eq. 27 can be replaced with an even function of γ , say $\Phi_1(\gamma)$. Then, the anti-derivative of the function $\gamma\Phi_1(\gamma)$ is an even function of γ , say $\Sigma_2(\gamma)$. Therefore, $\Sigma_2(1/2) = \Sigma_2(-1/2)$ and

$$\begin{aligned} & \int_0^{-1/2} \gamma\Phi_0 d\gamma + \int_0^{1/2} \gamma\Phi_0 d\gamma = \\ & = \Sigma_2\left(-\frac{1}{2}\right) - 2\Sigma_2(0) + \Sigma_2\left(\frac{1}{2}\right) = . \\ & = 2\left[\Sigma_2\left(\frac{1}{2}\right) - \Sigma_2(0)\right] \end{aligned} \quad (29)$$

Substituting Eqs. 28 and 29 into Eq. 27 leads to

$$\left.\frac{d^2s}{da^2}\right|_{a=0} = 4\left[\Sigma_2\left(\frac{1}{2}\right) - \Sigma_2(0)\right] - \Sigma_1\left(\frac{1}{2}\right) + \Sigma_1(0). \quad (30)$$

The right hand side of Eq. 30 can be evaluated and, then, using Eqs. 2 and 13 the function $s(a)$ at the initial stage of the process can be approximated by

$$s(a) = \frac{1}{4} + \frac{a}{2} + \frac{1}{2}\left(\left.\frac{d^2s}{da^2}\right|_{a=0}\right)a^2. \quad (31)$$

5. SURFACE ROUGHNESS EVOLUTION

Having the solution for $s(a)$ it is possible to find the equivalent strain from Eq. 7 and the radial strain from Eq. 1. These two strains are involved in the empirical surface roughness evolution proposed in [3]. Thus the evolution of surface roughness in pure bending can be predicted and comparison with experimental data can be made.

6. CONCLUSIONS

The general solution proposed describes the process of pure bending of incompressible, rigid viscoplastic material at large strains. The dependence of the yield stress on the equivalent strain rate is quite arbitrary. Using the solution found and the empirical equation proposed in [3] the evolution of surface roughness can be predicted. Then, experimental data can be used to approximate the function involved in this empirical equation.

7. REFERENCES

- [1] Alexandrov S., Kim J.-H., Chung K. and Kang T.-J.: *An alternative approach to analysis of plane-strain pure bending at large strains*, Journal of Strain Analysis for Engineering Design, V.41, pp. 397-410, 2006.
- [2] Alexandrov S. and Hwang Y.-M. *The bending moment and springback in pure bending of anisotropic sheets*, International Journal of Solids and Structures, V.46, pp.4361-4368, 2009.
- [3] Alexandrov S., Manabe K. and Furushima T. *A new empirical relation for free surface roughening*, Transactions of. ASME Journal of Manufacturing Science and Engineering. V.133, Paper 014503, 2011

Authors: Prof. Dr Sergei Alexandrov, Dr Elena Lyamina, A.Yu. Ishlinsky Institute for Problems in Mechanics, Russian Academy of Sciences, Moscow, Russia,
E-mail: sergei_alexandrov@yahoo.com

Prof. Dr Ken-ichi Manabe, Tokyo Metropolitan University, Mechanical Engineering Department, Tokyo 192-0397, Japan

ACKNOWLEDGEMENT

The research described in this paper was supported by RFBR and JSPS (grant RFBR-12-08-92103).

Božičković, Z., Dobraš, D., Božičković, R.

ELIMINATION OF PERMANENT DEFORMATIONS IN THE LONGITUDINAL WELDING PROCESS OF CONICAL PIPES WITH ONE SEAM

Abstract: The solving of this problem was directed at finding the optimal shape of the elastic line of pipe deformation before the welding process in order to obtain minimal elastic-plastic deformations after welding. For the experimental research of the longitudinal welding, it is taken a pipe of 6 m length, top diameter of 92 mm, bottom diameter of 168 mm and pipe thickness of 3 mm. The quality of material is S235 JR. Thermo-mechanical analysis of pipes welding without pre-deformation has been performed by numerical process simulation using the licensed software ANSYS. The presented results show that low values of aberration of numerically calculated and measured deflection values show a high reliability of numerical model in welding process simulation.

Key words: welding, elastic-plastic deformation, numerical simulation

1. INTRODUCTION

Recently, structural elements with variable cross-section are increasingly used for steel bearing structures, either obtained by hot or cold forming, and with the aim to achieve optimal stress utilisation and less weight. There is an increasing need for developing pipes by cold forming on hydraulic presses in order to produce products faster for the market with different wall thicknesses, different material quality and variable (conical) section along the length of pipe. During the welding of steel structure, a moving heat source creates a permanent deformation of structural element and residual stresses. The permanent deformation and residual stresses are closely related to each other and are not identical for similar types of structures and materials of all kinds. The elimination of permanent deformations and reduction of residual stresses can be performed before, during and after welding. This paper examines the impact of elastic pipe pre-deformation during welding on elastic pipe deformations after welding.

2. PROBLEM DESCRIPTION

The welding of conical shape steel pipes in its final stage, i.e. the welding stage, has a problem of maintaining tolerances on dimensions and forms. The most common related problems in welding are elastic-plastic deformations and residual stresses. Therefore, the research is focused on finding the influential factors on stress and deformation states during welding.

The problem referred to welding of conical pipes with one longitudinal seam consists of the followings:

- The pipe with a variable cross-section needs to be hold stuck with three supports in elastic deformation state for the whole time duration of welding. The middle support is not on the same level with two end supports, which provides the pipe pre-deformation during welding.
- The problem is finding a position for the middle support with regard to two end supports that will

ensure an optimal shape of elastic deformation line during welding in order to obtain minimal residual stresses and welding deformations.

- The stuck and elastically deformed pipe obtains elastic-plastic deformations during welding (the curve of elastic deformation line is increased) on the side of weld and in the direction of concentrated force action and thus complicates the problem of defining equipment and tools that provide a counter deflection during the process.

The above mentioned and identified problems show that their solving is focused on finding the optimal shape of elastic deformation line of variable cross-section pipe with one longitudinal weld before welding process in order to obtain minimal elastic-plastic deformations as well as factor values of stress concentration.

3. EXPERIMENT

The experimental work was carried out in the production system of "DALEKOVOD" TKS Dobož on real samples, i.e. on products for commercial use. For the experimental research of longitudinal welding, it is taken a pipe of 6 m length, top diameter of 92 mm, bottom diameter of 168 mm and pipe thickness of 3 mm. The multipoint measuring amplifier UGR-100 manufactured by HBM has been used for power supply and conditioning of measurement points. Corresponding connector cables and connector boxes, as well as a personal computer, have been used for data collection and data processing from individual measurement points of inductive sensors. Deflections have been registered by using inductive motion sensors. The research on elastic-plastic deformations during the welding of polygonal conical pipes has been carried out on octagonal cross-section pipes of S 235 JR quality prescribed by standard EN 10025. The welding is performed with additional material – CARBOFIL wire of diameter 1.2 mm and quality prescribed by EN 10204-2.2 standard. The geometric pipe shape is obtained in a process of free bending on hydraulic

presses [2]. The welding groove is shaped, i.e. formed, without prior preparation with a root gap of 1 mm, using the free bending procedure and it presents the prepared area for pipe seam creation.

3.1 Position determination of pipe supports and inductive motion sensors

In order to perform a longitudinal welding, the pipe is placed in a position that will give a minimum of deformation and residual stresses after welding using optimal welding parameters. During the pipe preparation for longitudinal welding and the process of welding and unloading, the deflections are identified using inductive sensors W50 and W100, whose position layout on a pipe is shown by scheme, Fig. 1. Here, the bottom edge of the pipe refers to the generating pipe which is located on the opposite side of pipe seam.

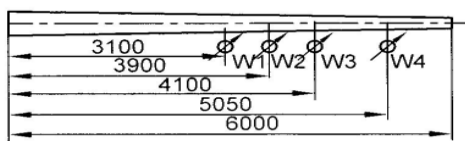


Fig. 1. The position scheme of inductive motion sensors

The pipe is placed in a position as shown in Figure 2. The supports A and B are movable and allow for slight motion in the horizontal direction. The support "C" is unmovable. The main function of support C is to bring a pipe from the horizontal position in the position for welding and thereby ensure an elastic deformation that is maintained during the welding process. The position scheme of supports is shown in Fig. 2 and presents a static indefinite beam.

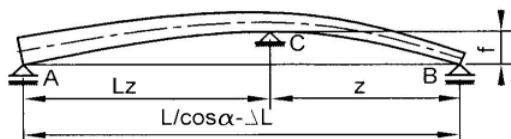


Fig. 2. The position scheme of pipes for welding

The elastic line of pre-deformation is:

$$y'' = \frac{-M_z}{W_z} = \frac{-F_A \cdot z}{W_z} \quad (1)$$

$$y'' = \frac{-F_A \cdot L^3 \cdot [L \cdot R - (R-r) \cdot z] \cdot z}{0,638 \{ [R \cdot L - (R-r) \cdot z]^4 - [(R-\delta) \cdot L - (R-r) \cdot z]^4 \}} \quad (2)$$

where:

D – bottom pipe diameter (bottom base),

d – upper pipe diameter (upper base),

R – pipe radius in the bottom base,

R_z – pipe radius in the intersection z,

r – pipe radius in the upper base,

L – pipe length,

z – pipe length in the intersection z,

δ – pipe thickness.

Data needed for the calculation of pre-deformation force and resistance of supports are:

- the maximum allowable stress at the yield point
R_{eH} = 239,9 [MPa],

- the moment of resistance of the bottom pipe base
W_d = 55,296 cm³,
- the moment of resistance of the upper pipe base
W_g = 15,894 cm³,
- the force position for pre-deformation has been taken as 28% of pipe length from the upper base.

The welding has been performed with the welding parameters shown in Table 1.

Current intensity, [A]	150
Voltage, [V]	17
Wire speed [m/min]	3
Welding speed, v _z , [mm/min]	500
Gas flow, l/min	12
Power U·I, [W]	2550
Heat input, (U·I·η)/v _z , [J/mm]	5.35

Table 1. Welding parameters

The change of deformation state during welding is monitored via inductive motion sensors (W1, W2, W3, W4), Fig. 3.



Fig. 3. Longitudinal conical pipe welding

The measured deflections on the pipe during the experiment are shown in Table 1.

Time h: min: sec	Deflect ion W1 mm	Deflecti on W2 mm	Deflect ion, W3 mm	Deflection W4 mm
Preparation for welding – pre-deformations				
0:00:00	-0.003	-0.009	-0.01	-0.008
0:00:09	1.087	1.987	2.19	1.724
0:00:15	2.131	4.051	4.565	3.493
0:00:21	3.765	7.102	7.909	6.086
0:00:30	5.599	10.439	11.573	8.93
0:00:38	7.516	14.013	15.528	12.018
0:00:45	10.183	18.95	20.973	16.296
0:00:52	13.31	24.701	27.32	21.259
0:00:59	15.393	28.515	31.503	24.505
0:01:07	17.522	32.378	35.756	27.756
0:01:16	19.251	35.547	39.263	30.441
0:01:23	21.31	39.322	43.434	33.691
0:01:30	22.748	37.12	46.373	35.822
0:01:38	24.045	39.394	49.031	37.176
0:01:45	25.569	42.231	52.157	38.013
0:01:53	27.265	45.375	55.65	38.516
0:02:04	29.102	48.745	59.416	38.604
0:02:26	31.024	52.227	63.259	38.151
0:05:45	34.651	59.537	70.872	35.966

0:07:12	34.728	54.836	58.824	38.594
Welding				
0:12:57	34.881	55.092	59.322	38.604
0:17:16	34.885	55.099	59.444	38.624
0:17:16	34.838	55.156	59.93	38.635
0:18:43	34.747	55.249	60.777	38.497
0:20:09	34.637	55.365	61.798	38.032
0:21:36	34.498	55.509	63.082	37.52
0:21:36	34.345	55.662	64.332	37.663
0:23:02	34.138	55.889	64.627	38.351
0:28:00	33.871	56.025	61.97	38.625
Unloading and cooling				
0:51:50	0	-12.799	-15.364	15.047

Tables 2. The measured deflections on the pipe during the experiment

The change of pipe deflection as a function of time at the welding stage in places of inductive motion sensors is shown in Fig. 4.

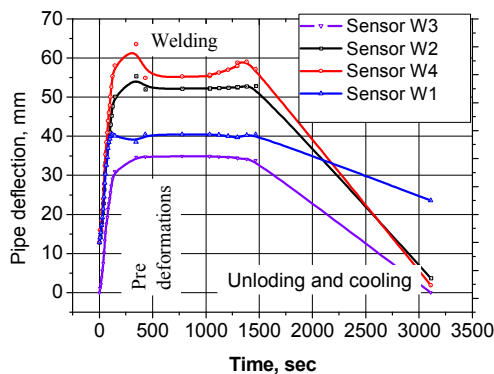


Fig. 4. The change of pipe deflection as a function of time at measurement points

It is noted that the pipe deflections at measurement points of signal sensors W2 and W3 are slightly higher than signal sensors W1 and W4.

The deflection of the pipe axis is presented by the equation:

$$W_z = 0,6923 + 21,06 \cdot L_z^2 + 0,7086 \cdot L_z^3 \quad (3)$$

The residual plastic deformations after unloading and cooling of the pipe of length $L=6000$ mm (Figure 6) are presented by regression analysis equation:

$$\varepsilon = 0,0023366 \cdot L_z + 1,72 \quad (4)$$

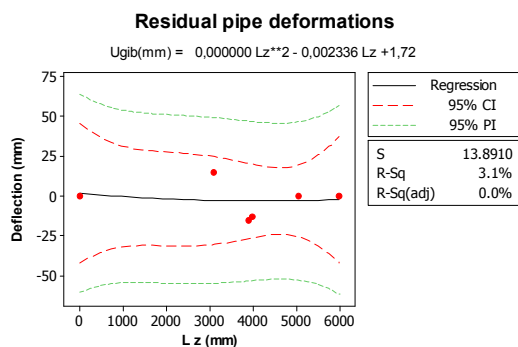


Fig. 5. The residual plastic deformations

According to EN 40-2 standard, "Dimensions and tolerances for lighting columns", the examined pipe has a deflection within tolerable limits.

4. NUMERICAL SIMULATION

Here, the problem referred to numerical welding process simulation with reference to the pipe deformations during and after welding has been analysed. The attention is directed towards establishing a numerical approach for pipe welding process modelling, where welding is performed along one pipe edge as shown in Figure 6. The first step of numerical simulation using the method of finite elements is a convergence study of results in order to find the adequate network density. Fig. 6. illustrates the formed seam shape for welding. The angle of groove is 45° .

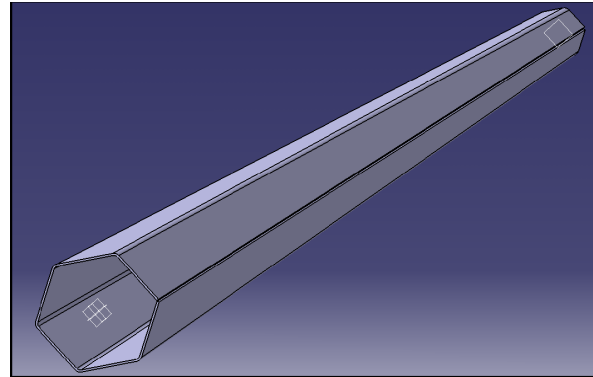


Fig. 6. The formed pipe geometry with the edge along which welding is performed

According to the convergence function shape of deformation and stress, the network of finite elements begins to make stable results if the number of finite elements in the model is 12060. The number increase of elements over 12060 does not ensure an extremely better result. Due to high temperatures and stress gradients near the weld, a very sophisticated network of finite elements is used for modelling of the weld itself. For the purpose, shell type finite elements have been used for pipe modelling. Because of the fact that the software package ANSYS has been used for these studies, therefore, finite elements of SHELL 57 and SHELL 63 type have been used. In order to improve the accuracy of finite shell elements, the finite elements with eight degrees of freedom per node [3] based on high order shear theory have been developed. For the simulation of welding using the method of finite elements, the following data are taken:

- the number of nodes in the model of finite elements: 12261 nodes,
- the number of finite elements : 12060
- current intensity: 150 A,
- voltage: 21 V,
- the degree of procedure utilisation: 0.85,
- welding speed $v_z=500$ mm/min,
- process efficiency degree $\eta=0,85$,
- supports,
- degree of movement freedom.

4.1 Thermo-mechanical characteristics of essential and additional materials

For numerical welding analysis it is necessary, as accurately as possible, to know thermo-mechanical characteristics of essential and additional materials at increased temperatures. These characteristics are exclusively obtained by experimental tests, and only very rarely can be found in literature in its original form. In numerical simulation, thermo-mechanical characteristics have been taken from literature, and as the most similar to the characteristics of essential and additional materials considered in the experiment. The quality of materials A36 and 309L by ASTM are with similar characteristics as the essential material S 235 JR, and additional material Carbofil 1. Mechanical and chemical characteristics are prescribed by EN 10025-2 standard for essential material and EN10204-2.2 for additional material [1].

4.2 Displacements of nodes on the bottom pipe edge

In order to compare them with experimental results, vertical displacements (W_y) of the bottom pipe edge determined by FEM (ANSYS) are therefore presented. Displacements are given in the nodes that are located on the bottom pipe edge, where inductive motion sensors are placed in the experiment. FEM analysis was performed for pipes after welding process without a pre-deflection of pipes.

The obtained data clearly show that the maximum displacement value is $W_y=37.365$ mm and that it is located at node 7485 which coordinate is $L_z = 3.800$ mm (measured from the bottom pipe edge). These results of displacements in vertical level by application of FEM analysis is graphically illustrated in Figure 7.

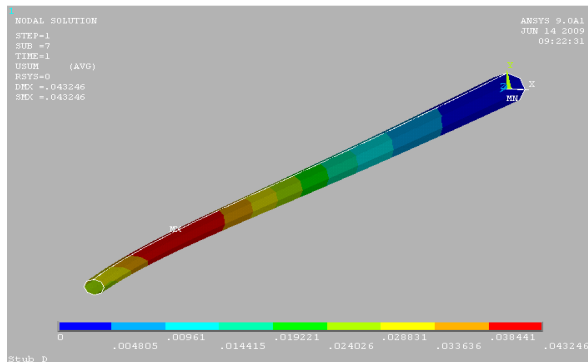


Fig. 7. Total pipe displacements

Fig. 7 presents a displacement simulation of bottom pipe edge.

Displacement of pipe axis diagrammatically presents the displacement of the bottom pipe edge, Fig. 8.

The diagram presents a displacement of the pipe axis after welding process of one seam pipe. Based on this diagram, it is possible to design tools for pre-deformation before welding. In practice, the pipe deflection increases to 10 percent.

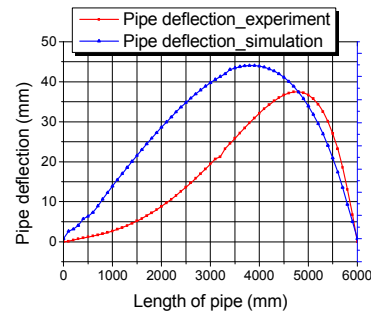


Fig. 8. Displacement of the pipe axis in the vertical direction

5. FINAL REMARKS

The research results show the problem complexity of deformation state in the selection of technology for the welding of conical one-seam pipes. In order to verify the numerical simulation of welding process using the method of finite elements, comparisons with experimental results are performed.

Based on presented results it is concluded that low aberration values of numerically calculated and measured values show a high availability and reliability of numerical modes in the simulation process. Therefore, the FEM analysis can use residual displacements at the bottom edge of the pipe as a measure of pipe preload before welding process in order to eliminate residual displacements after welding or reduce to tolerable levels.

6. REFERENCES

- [1] Božičković, Z. *Elastic-plastic strains of polygonal tubes with variable cross-section during longitudinal welding*, PhD thesis, The Faculty of Mechanical Engineering, Banja Luka 2010, pp. 90-97
- [2] Božičković, Z. *Optimization of discontinuous formation of polygonal tubes on CNC-hydraulic tandem press*, Master's thesis, The Faculty of Mechanical Engineering, Banja Luka 1996, pp. 30-40
- [3] Maksimović S., Ružić, D., Maksimović K. *An improved 4-node shell finite element used in postbuckling and failure analysis*, LUXFEM - 1st International Conference on Finite Element for Process, Luxemburg, Luxemburg City, 13-14, 2003.

Authors: PhD Zdravko Božičković, assistant professor, University of East Sarajevo – Faculty of Mechanical Engineering Sarajevo, Vuka Karadžića 30, BH, RS, Phone: + 387 (0)57 340 847, Fax: + 387 (0) 57 340 847.

E-mail: zdravko.bozickovic@gmail.com

PhD Dragoslav Dobraš, assistant professor,

PhD Ranko Božičković, Associate Professor, University of Banja Luka - Faculty of Mechanical Engineering Banja Luka, Vojvode Stepe Stepanovića 75, BH, RS, Phone: + 387 (0)51 462 400, Fax: + 387 (0)51 465 085.

E-mail: dragoslav.dobras@unibl.rs, rankob@teol.net

Brkljač, N., Simić, R., Kovač, P., Brkljač, B.

FEM IN FUNCTION OF PNS - APPLIED IN DERIVING APPROXIMATE FORMULA FOR CALCULATION OF THEORETICAL SCF IN BUTT WELD JOINTS

Abstract: In this paper are presented approximate formulas intended for calculation of theoretical stress concentration factor (SCF) of butt weld joints with V and X seam, in both cases under the action of tension forces. Presented formulas are defined as functions of geometric parameters of the joint, and derived by planned numerical simulation (PNS) procedure through statistical processing of SCF values determined by stress analysis of joints computational models utilizing finite elements method (FEM).

Key words: stress concentration factor (SCF); planned numerical simulation (PNS); butt weld joint.

1. INTRODUCTION

Experience acquired from practice and confirmed through number of experimental investigations suggests that during the usage of structural parts in the most cases there appear fatigue cracks which as the rule of thumb begin at the points with prominent **stress concentration**¹. On that basis it was concluded that fatigue strength of structural part depends significantly of the effect of its stress concentrator. Essential assumption for creation of reliable structures is strict estimation of stress state in the region of stress concentration, which is caused by the variable geometry of mechanical part, considering that the action of stress concentration has crucial influence on the reduction of permanent endurance limit.

In the general case stress concentration is described by: theoretical² stress concentration factor K_t , relative stress gradient χ and effective³ stress concentration factor K_f , (Ger. „Kerbwirkungszahl“).

Factor K_t defined as theoretical stress concentration factor is based on conventional

¹ Term *stress concentration* is understood as rapid local stress change in mechanically stressed body, at the place of existence of stress concentrator, which in its nature can be result of design, technology or exploitation, as well as result of characteristic effect of structural load.

² For this factor in literature is also used term: geometric stress concentration factor (Ger. *Formzahl; Formziffer*) – since it characterizes stress change in dependence from geometric factor. Index *t* points out that given stress concentration factor refers to theoretical.

³ Peterson calls this factor: („*fatigue notch factor*“, [1]) or „*fatigue stress concentration factor*“, [2], or „*effective stress concentration factor in fatigue*“, [3], and denotes it with K_f (where letter in subscript comes from word *fatigue*); same terms are also used by Heywood, [4]. In literature in Russian language this factor is called: „*эффективный коэффициент концентрации напряжений*“, [5], [6], [7], same term is also used in our domestic literature, [8]. Thorough names classification for all terms that are used in connection with stress concentration and fatigue resistance can be found in [9], where name: „*effective stress concentration factor*“ is used for defining ratio between *static strength* of part without notch and part with notch, and is denoted by symbol K_e . In the same reference factor K_f is called „*fatigue notch factor for normal stress*“...

assumptions of theory of elasticity, in which it is regarded that material is elastic, homogeneous and isotropic. Theoretical stress concentration factor K_t is determined as the ratio of maximal and nominal⁴ stress in the region of stress concentration of mechanical part, i.e. $K_{t\sigma} = \sigma_{\max} / \sigma_{nom}$, for normal stresses and $K_{t\tau} = \tau_{\max} / \tau_{nom}$, for shear stresses.

2. STRESS CONCENTRATION IN WELD JOINTS

Weld joints, as a rule, possess more or less significant stress concentrators. Creation of weld joint produces local changes in dimensions of cross section, which leads to the stress concentration in loaded components. Precise location and size of stress concentration in weld joints depends on joint design and on direction of load action. Weld toe is usually the primary place of fatigue failure, Fig. 1, for joints which have good penetration at the weld root.

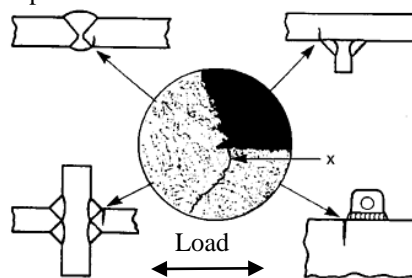


Fig. 1. Fatigue cracks initiated by defects characteristic for toes of seam welds, taken from [10].

In circumstances when penetration at the root is weak or root opening is significant, or in load carrying fillet welds which have insufficient weld thickness, root surface can become the region of the largest stress concentration. Fatigue cracks in these situations begin at the weld root and in the general case propagate

⁴ Nominal stress is equal to the average stress in „*net cross section*“ of the part with stress concentrator, and is determined by using elementary formulas of strength of materials without taking into account stress concentration.

through the weld.

When carrying out weld joints it aims above all toward providing full penetration welds and obtaining seam with appropriate mechanical properties without welding defects (cracks, porosity, fissures, etc.). Less attention is usually devoted to the external seam shape. At the same time, strength of the weld joint is to a large extent determined by the external seam shape and seam dimensions. Prominent strength reduction is particularly observed in joints which have weld face carried out with rapid transition to the base metal, which results in significant stress concentration.

Parameters of the geometry/shape of weld joints, which have influence on fatigue, i.e. dimensions of elements in joint and seam dimensions, are defined by project documentation. Deviations from the project geometric specifications can arise from production process (axial and angular misalignment – shifts, lack of penetration, or reduction of plate thickness caused by weld sag) and should be taken into account when geometric data necessary for stress analysis at notch location in weld joints are defined.

However, all geometric data of weld joints, necessary for stress analysis at the location of notch, are not contained within project documentation. Some of these data, which depend on the production process and on the achieved welding quality, are: radius and angle of the weld toe, penetration depth at the weld root, weld surface profile, width and height of weld face in butt joints and angle between tangent on weld face and metal surface. Special geometric parameters characterize errors in welding such as weld undercut, sag, burn-through and others. In contrast to parameters that characterize project, parameters that characterize welding process have a large degree of scattering and should be taken into account statistically. In the stress analysis at the notch location average values can be used, although it is usual to introduce assumption of the most unfavourable case when stress concentration factor at the notch is considered, i.e. zero weld toe radius value and large weld toe angles.

Today it is well known that notches have harmful influence on fatigue strength, which is directly related with stress concentration. Thus, e.g. in monograph [7], dedicated to fatigue of weld joints, considering factors of influence on fatigue strength that are caused by welding, Труфяков emphasizes that in welded parts and specimens fatigue cracks mostly begin along the line joining seam with the base metal, therefore exactly at the place with prominent stress concentration. Furthermore, he indicates that their propagation is related to the influence of normal stresses and concludes that determination of stress concentration in pointed out places is of the utmost importance, considering that stress concentration shows essentially the largest influence on fatigue strength of specimens, machine and structure parts.

2.1 Approximate formulas for calculation of SCF, at notch locations in weld joints

Theoretical stress concentration factors at notch locations in weld joints in the beginning were determined through analysis of models of cross section

of weld joints, by using the method of conformal mapping [12], [13] and experimentally by using polarization optical methods. Although the accuracy of the results obtained with these methods is to the certain degree questionable, their value in the development of theory and practical application is indisputable. These methods, broadly used in the period from thirties until seventies years of the twentieth century, were suppressed by numerical methods: FEM and BEM (boundary elements method).

Through development of finite and boundary element methods, based on the use of computers, approximate formulas for calculation of stress concentration factors for the most diverse shapes of weld joints were derived on the basis of parametric studies. Regarding this topic numerous researchers around the world were engaged during the last few decades, [14], [15], [16], [17], [18], [19], [20], [21], [22], et al.

Besides the above mentioned papers in the last few years extensive researches have been carried out in the world and there have been derived approximate formulas for determination of stress concentration factors in different types of tubular joints, like e.g.: [23], [24], et al.

2.2 Approximate formulas for calculation of SCF along weld toe, in butt joints with V and X seam

Approximate formulas, that will be presented in this paper, for calculation of theoretical SCF K_t in butt joints with V and X seam, in both cases under the action of tension forces, are derived by the authors of this paper. Idealized shape of seams in butt joints, which are used in computational models, with defined geometric parameters is shown on drawing in Fig. 2.

Formulas are derived through PNS procedure of planned numerical simulation („planned factorial experiment“), by statistical processing of factor values K_t determined in stress analysis of used computational models utilizing finite elements method (FEM).

In order to cover more efficiently broader experimental space of parameters, for PNS was chosen so called central compositional experiment plan, described in [11], where besides points that are in corners of parametric hypercube and points in its centre, which repeat, there also exist points on planned distance outside the hypercube.

In Fig. 3 is shown computational model of weld butt joint with X-seam used for stress analysis that is performed using FEM. For discretization were used planar elements with 8 nodes and quadratic Lagrange interpolation of displacements field between nodes. Since the model is symmetric, by geometry and by loading, computation was performed using only half of the model (V-seam), that is quarter of the model (X-seam). In order to compute stress more accurately on radius of transition and in the zone of weld toe discretization in these places was performed by elements of smaller dimensions (Detail D₁). Number of elements on radius of transition, between weld toe and weld face, was varied in order to achieve optimal number of elements, until the level when further

increase in number of elements on radius in comparison to adopted number has no significant influence on computational value of maximal stress any more. Uniform tension stress state along the plate thickness in the zone of load action was achieved with choice of length L (Fig. 3a) sufficiently far from the weld toe, $L > 3t$.

Formulas for calculation of theoretical stress concentration factor K_t in butt joint with V- and X-seam (Fig. 2a and Fig. 2b) are defined as functions of geometric parameters of the joint:

- for joint with V - seam:

$$K_t = C \cdot t^{p_1} \cdot \rho^{p_2} \cdot h^{p_3} \cdot \theta^{p_4}, \quad (1)$$

for geometric parameters in the range:

$$t = 6 \text{ to } 10 \text{ mm}; h = 1 \text{ to } 3 \text{ mm}; \\ \rho = 0.20 \text{ to } 1 \text{ mm and } \theta = 120^\circ \text{ to } 165^\circ.$$

- for joint with X - seam:

$$K_t = 1 + C \cdot t^{p_1} \cdot \left(\frac{t}{\rho}\right)^{p_2} \cdot h^{p_3} \cdot \theta^{p_4}, \quad (2)$$

for geometric parameters in the range:

$$t = 10 \text{ to } 30 \text{ mm}; h = 1 \text{ to } 9 \text{ mm}; \\ t/\rho = 4.0 \text{ to } 100.0 \text{ and } \theta = 95^\circ \text{ to } 175^\circ, \text{ where:}$$

t = plate thickness in mm; h = weld face height in mm; ρ = radius of roundness in mm and θ = weld face angle in degrees, formed between plate surface and tangent on weld face in the intersection point of radii ρ and R .

Constants and exponents in formulas are given in Table 1.

For illustration, in Table 2 are shown comparative values of theoretical stress concentration factor K_t , for examples of idealized butt joint produced with V- and X-seam (Fig. 2), determined by approximate formulas: eq. (1) and eq. (2), and by finite elements method.

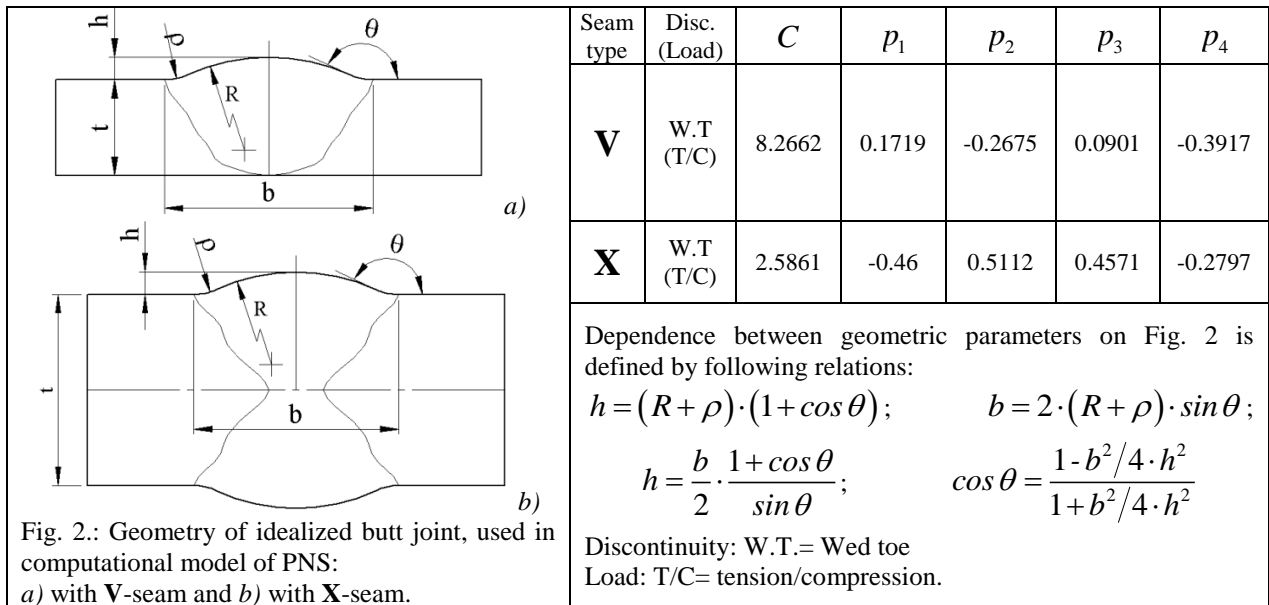


Table 1: Constants and exponents in formulas (1) and (2)

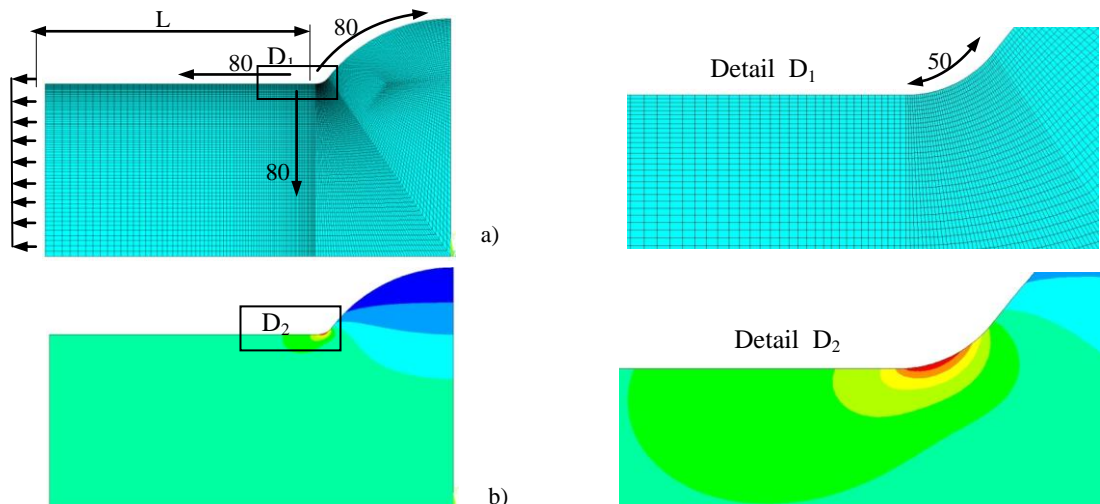


Fig. 3. Computational model of idealized butt weld joint with X-seam for stress analysis utilizing FEM, used in PNS procedure: a) finite elements mesh and b) image of stress state.

Seam shape	Geometric parameters of butt weld joint, with shape acc. to Fig. 2.					Theoretical stress conc. factor K_t		
	t [mm]	b [mm]	h [mm]	ρ [mm]	θ [°]	Determined by FEM	Determined by formulas	
V	8	15	2.5	0.5	143.13	2.17	2.21	eq. (1)
	8	15	2.5	1.0	143.13	1.81	1.84	
X	25	25	4.7	0.5	138.79	3.24	3.22	eq. (2)
	25	25	4.7	1.0	138.79	2.65	2.56	

Table 2.: Example of comparative SCF values, determined by FEM and by approximate formulas eq. (1) and (2).

3. CONCLUSION

PNS procedure (Planned Numerical Simulation) has proved as very effective and acceptable in deriving formulas for calculation of theoretical stress concentration factor, using computer software based on finite elements method. By applying described procedure it is possible to determine parametric formulas with high degree of accuracy, eq. (1) and (2), especially when it is used for deriving formulas with narrower range of parameter values.

Application of parametric formulas for calculation of theoretical SCF in engineering practice is acceptable, under assumption that strict care is taken about scope of their validity.

Approximate formulas, derived on the basis of results of parametric studies, using finite and boundary elements methods, more clearly show influential parameters of studied problems. Therefore they are very applicable for dimensioning and optimization tasks, aimed at increasing endurance limit.

4. REFERENCES

- Peterson, R. E.: *Relation between stress analysis and fatigue of metals*, Proc SESA, 11(2), p.p. 199–206, 1950.
- Peterson, R. E.: *Stress concentration phenomena in fatigue of metals*, Trans. ASME, 55, p.p. 157-71, 1933.
- Peterson, E. R., Wahl, M. A.: *Two and Three Dimensional Cases of Stress Concentration, and Comparison with Fatigue Tests*, Trans. ASME, 57, p.p. A15 – A22, 1936.
- Heywood, B. R.: *Designing against Fatigue*, Chapman and Hall, London, 1962.
- Серенсен, С. В., Когаев, В. П., Шнейдерович, Р. М.: *Несущая способность и расчет деталей машин на прочность*, 3-е, перераб. и доп., „Машиностроение“, Москва, 1975.
- Когаев, В. П., Махутов, Н. А., Гусеков, А. П.: *Расчеты деталей машин и конструкций на прочность и долговечность*, Машиностроение, Москва, 1985.
- Труфяков, И. В.: *Усталость сварных соединений*, „Наукова Думка“, Киев, 1973.
- Babin, N., Brkljač, N., Šostakov, R.: *Metalne konstrukcije*, FTN, Novi Sad, 2006.
- Pilkey, W. D., Pilkey, F. D.: *Peterson's Stress Concentration Factors*, Third Edition, John Wiley & Sons, Hoboken, New Jersey, 2008.
- Maddox, J. S.: *Fatigue strength of welded structures*, Woodhead Publishing, Cambridge, 1991.
- Kovač, P.: *Modelovanje procesa obrade. Faktorni planovi eksperimenta*. FTN, Novi Sad, 2006.
- Кархин, А. В., Копельман, А. Л.: *Концентрация напряжений в сварных соединениях*, Сварочное производство, 2, p.p. 6-7, 1976.
- Турмов, Г. П.: *Определение коэффициента концентрации напряжений в сварных соединениях*, Автоматическая сварка, 10, p.p. 14-16, 1976.
- Rainer, G.: *Errechnen von Spannungen in Schweißverbindungen mit der Methode der Finiten Elemente*, FKM - Forschungsheft No 74, Frankfurt/M, 1979.
- Rainer, G.: *Parameterstudien mit finiten Elementen, Berechnung der Bauteilfestigkeit von Schweißverbindungen unter äußeren Beanspruchungen*, Konstruktion, 37(2), p.p. 45–52, 1985.
- Yung, J. Y., Lawrence, F. V.: *Analytical and graphical aids for the fatigue design of weldments*, Fatigue Fract. Engng Mater. Struct, 8(3), p.p. 223–241, 1985.
- Lehrke, H. P.: *Berechnung von formzahlen für schweißverbindungen*, Konstruktion, 51(1/2), p.p. 47–52, 1999.
- Anthes, R. J., Köttgen, V. B., Seeger, T.: *Einfluß der Nahtgeometrie auf die Dauerfestigkeit von Stumpf und Doppel T Stößen*, Schweißen und Schneiden, 46(9), p.p. 433–436, 1994.
- Radaj D., Sonsino C. M., Fricke W.: *Fatigue assessment of welded joints by local approaches*, 2nd ed, Woodhead Publishing Ltd, Cambridge, 2006.
- Iida, K., Uemura, T.: *Stress concentration factor formulas widely used in Japan*, Fatigue Fract Engng Mater Struct, 19 (6), p.p. 779–786, 1995.
- Radaj, D., Helmers, K.: *Bewertung von Schweißverbindungen hinsichtlich Schwingfestigkeit nach dem Kerbspannungskonzept*, Konstruktion, 49, p.p. 41–27, 1997.
- Brennan, P. F., Peleties, P., Hellier, K. A.: *Predicting weld toe stress concentration factors for T and skewed T-joint plate connections*, International Journal of Fatigue, 22, p.p. 573–584, 2000.
- Van Wingerde, A. M., Packer, J. A., Wardenier, J.: *Simplified SCF formulae and graphs for CHS and RHS K and KK connections*, J. Construct Steel Res., 57, p.p. 221–252, 2001.
- Chang, E., Dover, W. D.: *Parametric equations to predict stress distributions along the intersection of tubular X and DT-joints*, Int. Journal of Fatigue, 21, p.p. 619–635, 1999.

Authors:

Mag. scient. Nikola Brkljač, Ph.D. Pavel Kovač, M.Sc. Branko Brkljač, University of Novi Sad, Faculty of Technical Sciences, Trg Dositeja Obradovica 6, 21000 Novi Sad, Serbia,
E-mail: brkljac@uns.ac.rs, pkovac@uns.ac.rs
M.Sc. Radoslav Simić, NIS-GAZPROMNEFT, Narodnog fronta 12, 21000 Novi Sad, Serbia
E-mail: radoslav.simic@nis.eu

ACKNOWLEDGEMENT

Results of this paper were supported by Project TR – 35036 Ministry of Education and Science (Serbia): Application of information technologies in ports of Serbia - from machine monitoring to connected computer network system with EU environment.

Brüning, H., Vollertsen, F.

SELF-ALIGNING CAPABILITY OF LASER BASED FREE FORM HEADING PROCESS

Abstract: *In micro range, the balance between gravitational forces and forces related to the surface of a body are oppositional compared to macro range. By downsizing geometry of a body, forces related to the surface decrease slower than gravitational forces and at a certain stage, the surface tension exceeds gravitational force. A benefit of this behavior is applied by the laser melting process where the face surface area of a rod is molten by laser beam energy. The resulting sphere sticks to the rod and can be formed after cooling in a secondary process step. In this article the robustness of the laser melting process is investigated.*

Key words: *Laser melting, laser based free form heading, size effect, micro perform, microforming*

1. INTRODUCTION

Compared to some decades ago, both, capabilities and main characteristics of products have gone through a huge change. Nowadays, newly invented products have to have an increased functionality by the same size or at least the same amount of functions by a decrease in outer geometries. These boundary conditions, which base on the expectations of customers, are flanked by a steady pressure on the market because of prices. The result is that products are subject to function compaction. This can be seen in many fields of technology, such as automotive electronics and telecommunication.

As soon as an existence for a great market is most probable, the individual cost per product unit decreases with increasing batch size. Thus, especially in parts which belong to micro range but are placed in macro products, mass production is aspired. An economic production always suffers under inefficiencies, such as time inefficiencies but also inefficiencies in utilization of material resources. Fabrication of metallic components in high quantities under boundary conditions as above can be carried out by cold forming. Due to the fact that function compaction inevitably leads to miniaturization of work pieces, processes which are established in macro range have to be transferred into micro range. Parts belong to micro range, if the length of maximum 1mm is not exceeded in more than one dimension [1]. Unfortunately, knowledge gained in macro range is not, or only with restriction, applicable in micro range [2].

This effect is obvious by looking at the conventional multi stage upsetting process, which is part of many mass production chains. Material needed for each step is provided and the initial length l_0 of the work piece is reduced progressively. Depending on the basic material and the sample diameter d_0 , a certain length l_0 , called upset length of the workpiece can be compressed in one step. The quotient of upset length l_0 and sample diameter d_0 is called upset ratio s . The upsetting process is limited in two dimensions: the upset ratio s is the limit against buckling and the maximum natural

strain ϕ as a limit of formability of basic material [3]. In macro range, a maximum upset ratio $s=2.3$ can be achieved while in micro range this value is reduced to $s=1.6$ for the same work piece material [4] so that the conventional upsetting process becomes more and more inefficient with increasing miniaturization as stated by Vollertsen [5]. Work hardening materials represent an exposed roll in this context, as the conventional upsetting process has to be interrupted several times for heat treatment operations further decreasing process efficiency by means of time and overall costs due to handling and needed process energy. One approach to avoid these problems is the laser based free form heading process which has been demonstrated in [6] taking advantage of the above mentioned scaling effect. Preforms generated in this process can finally be upset in open dies [7], closed dies, or calibrated by rotary swaging [8].

Previous investigations show, that the microstructure of preforms generated by laser melting is dendritic [9]. Nevertheless, a good formability is achieved even though the dendritic microstructure does not generally allow high strain ratios. Upsetting of preforms in closed dies necessitates an exact defined volume of the work piece so that defects, such as incomplete die filling [10], after massive forming operation can be eliminated. In case of conventional upsetting of rotationally symmetrical work pieces, a variation of initial diameter causes a deviation in final work piece volume if the upset length is kept constant. In this paper, this effect is investigated for the above mentioned laser free form heading process.

2. METHOD

2.1. Experimental set-up

The laser based free form heading process takes advantage of the shape-balance effect [11], which means that in micro range surface tension exceeds gravitational force. The laser beam energy is focused on the bottom surface of a rod and causes the end of the rod to melt. Within certain limits, the molten part of the rod sticks to the rod and automatically adopts a

spherical shape due to surface tension. As soon as the weight of the spherical, molten part exceeds surface tension at the intersectional area between molten and solid rod material, the molten part releases. The process of generating material preforms by laser melting enables upset ratios $s \geq 500$ for rod diameter $d_0 = 0.2\text{mm}$. The maximum achievable upset ratio increases with decreasing rod diameter which is great advantage compared to conventional upsetting process.

The experiments are carried out using rods of austenitic chromium nickel steel 1.4301 (X5CrNi18-10) as wrought material with initial diameters d_0 ranged from 0.3mm to 0.5mm. The longitudinal axis of the rod is placed coaxially to the laser beam. The focus layer of the laser beam is adjusted on the bottom surface of the rod so that irradiation takes place in a right angle. As soon as the molten material forms a spherical geometry, the diameter of the sphere necessarily exceeds the initial rod diameter which causes the lower end of the sphere to move upwards out of focus layer. This phenomenon is called defocussing effect [6] and decreases the total efficiency of laser based free form heading process unless feeding of rod is applied [12]. Due to the fact that the used material for specimen is susceptible for oxidation at high temperatures, Argon is used as shielding gas. The specimens are brought to the aspired length by a bite cutting process and the top and bottom surface are finally fine grinded. Fig. 1 shows a schematic view of both, the conventional upsetting process (Fig. 1a) and the laser based free form upsetting process (Fig. 1b). F_p demonstrates the required punch force while the associated arrow shows its direction.

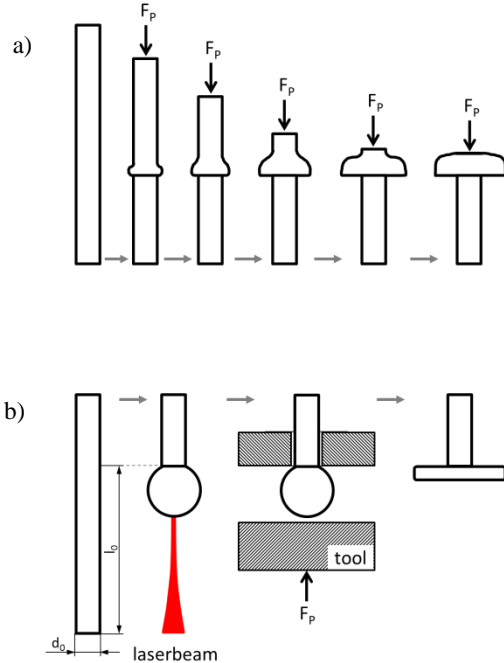


Figure 1.(a) Conventional and (b) laser based free form heading

It is clearly visible, that the process chain of laser based free form heading is shorter. Table 1 represents the

corresponding laser parameters.

Laser type	Fiber laser, cw
Wavelength	1085nm
Focal distance	100mm
Beam radius	0.02mm
Divergence angle	40mrad
Max. power	300W

Table 1. Specifications of the used laser system

2.2. Energy balance

The required energy E_S to melt a certain amount of material being the basis for the volume V_S of the sphere generated by a laser based free form heading process can be estimated by an adiabatic model [6]:

$$E_S = V_S \rho [c_p (T_M - T_0) + H_M] + b = P_L t_L \alpha \quad (1)$$

with ρ as density of basic material, c_p as specific heat capacity, T_M and T_0 as melting and initial temperature, H_M as latent heat, b representing offset term such as spatter formation, P_L as laser power, t_L as irradiation time and α as material specific absorption coefficient.

This model fits well with experimental results, but at least for larger material accumulations the model overestimates the accumulated volume. This behavior is among others based on the defocusing effect as well as on heat conduction within the rod and heat radiation against ambient atmosphere. The longer the accumulation process takes place, the greater is the part of energy dissipated through the rod by heat conduction. In order to achieve comparable results despite these effects while applying the above mentioned model for different rod diameters, the effect of irradiation time has to be taken into account. The law of similarities demands the following relations [13] based on (1):

$$E = m_l^3 m_T \quad (2)$$

with m_l as length scale and m_T as temperature scale. Comparable results exist, if the relative quantity of heat dissipation is the same for all scaled experiments. This means:

$$m_T = 1 \quad (3)$$

Similarity in heat radiation can be described as follows:

$$m_t = m_l / m_T^3 \quad (4)$$

Herein, m_t is the time scale. Respecting similarity in heat conduction gives the scaling rule for irradiation time:

$$m_t = m_l^2 \quad (5)$$

The scaling rule for laser power P_L is the result of inserting (5) and (4) in (2)

$$m_p = m_l^{\frac{2}{3}} \quad (6)$$

3. EXPERIMENT

The influence of both, a small variation of rod diameter d_f of about $\pm 1\%$ as well as variations of about $\pm 25\%$ of rod diameter d_f on the resulting volume of the spherical material accumulations are investigated.

Small variations in diameter of the rods are realized by rotary swaging. Rods with initial diameter d_i of 1.0mm - 2.0mm are reduced to $d_f \sim 0.5\text{mm}$. The initial and the final rod diameter are listed in table 2. It can be

seen that the absolute value of natural strain $|\varphi_r|$ varies between 0 and 2.77 according to the initial rod diameter d_i .

d_i [mm]	$\varphi_r = \ln(d_f^2/d_i^2)$	d_f [mm]
2.0	-2.77	0.501
1.5	-2.22	0.494
1.0	-1.37	0.503
0.495	0	0.495

Table 2. Initial and final rod diameter

For all final rod diameters d_f three different pulse energies E_L with constant power $P_L=64W$ but varying irradiation times $t_{p1}=500ms$, $t_{p2}=1500ms$ and $t_{p3}=4000ms$ have been applied thus resulting in different final sphere diameters d_s of the material accumulation. Due to the fact that the differences in final rod diameters are very small, neither the laser beam power P_L nor the irradiation time t_p have been scaled according to the law of similarities.

In addition to small variations of rod diameters, also huge variations have been applied. Starting from rods with $d_0=0.3mm$ and ending at $d_0=0.5mm$ with increments $\Delta d_0=0.1mm$. Rods were irradiated with different pulse energy E_L but this time, laser power P_L and irradiation time t_p were scaled according to the law of similarities, see paragraph 2.2 so that a relationship between pulse energy E_L and volume V_S of the sphere can be determined.

4. RESULTS

4.1. Influence of small variations of rod diameter

The volume V_S of the resulting spheres is shown in Fig. 2 for small variations in rod diameter exemplarily for a laser beam energy $E_L=256J$.

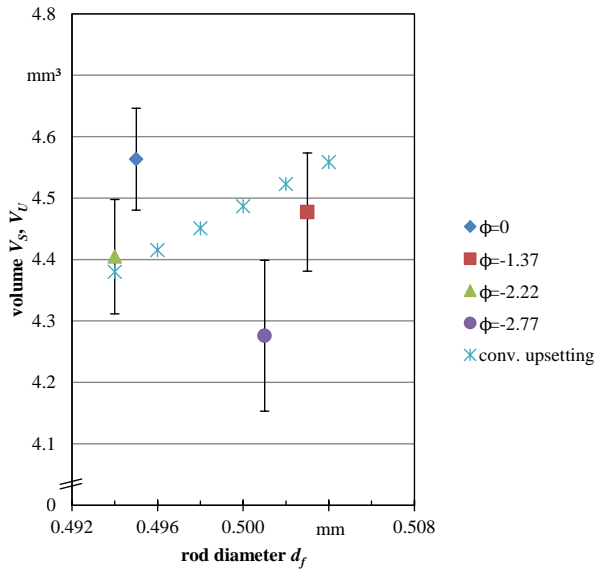
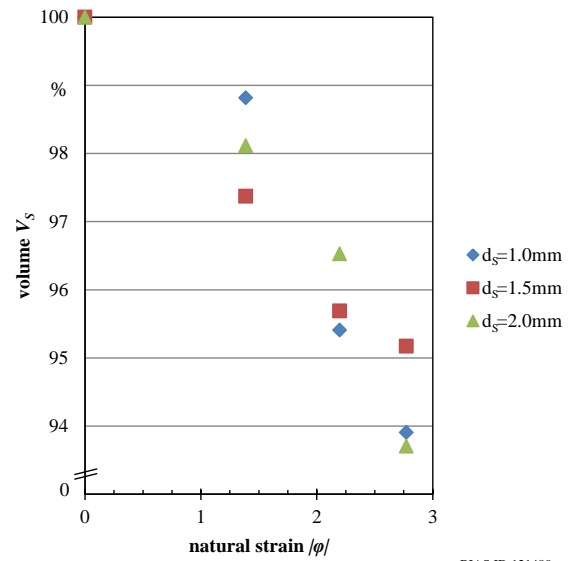


Figure 2. Volume V_S and V_U in dependence of rod diameter d_f for $E_L=256J$

Additionally, the theoretical volume V_U of a specimen with constant upsetting length l_0 generated by a fictitious conventional upsetting process is also displayed. It can be seen that the volume V_U of the specimen by conventional upsetting increases quadratic with increasing rod diameter. This behavior is expected because V_U can be determined by:

$$V_U = \frac{\pi}{4} d_f^2 l_0 \sim d_f^2 \quad (7)$$

The expected behavior that volume V_S is independent of rod diameter is not proved by these results. Due to the fact, that also for smaller pulse energies E_L the same characteristic collocation of function values is visible, the volume V_S of sphere is plotted in dependence of natural strain φ_r caused by rotary swaging. This relation



BIAS ID 121480

Figure 3. Volume V_S in dependence of natural strain $|\varphi|$ of rod induced by rotary swaging

is plotted in Fig. 3 for different sphere diameters d_s . It is obvious that there is a correlation between the volume of the spheres and natural strain of rods induced by the initial rotary swaging process. The larger the absolute value of natural strain $|\varphi_r|$, the smaller is the resulting material accumulation by constant pulse energy E_L . This behavior might be based on the fact that strain induced martensite comes into being by rotary swaging process. The martensitic microstructure, whose grain size is smaller than the initial austenitic grain size, might have a lower absorption coefficient α with the consequence, that less pulse energy E_L can be used to melt the rod and form the material accumulation.

4.2. Influence of strong variations of rod diameter

A stronger variation of rod diameter is carried out by using rods with diameter d_{rod} of 0.3mm, 0.4mm and 0.5mm. The pulse energy E_L is ranged between 1.28J - 160J. Both, laser power P_L and irradiation time have been scaled for each rod diameter as shown in

paragraph 2.2. The resulting sphere volumes V_S in dependence of pulse energy E_L are shown in Fig. 4.

An almost linear correlation between pulse energy E_L and volume V_S of the sphere independent of rod diameter d_{rod} is detected as predicted by formula (1) for pulse energies $E_L \leq 160\text{J}$. Particularly interesting are those energy regimes where volumes V_S of different rod diameters d_{rod} overlap. For example, this is the case for $30\text{J} < E_L < 40\text{J}$ and $50 < E_L < 100\text{J}$. In other words: the resulting volume V_S is within certain limitations independent of rod diameter d_{rod} by given pulse energy E_L . Transferring this knowledge into possibly practical application of laser free form heading, another unique advantage compared to conventional multi stage upsetting process is obvious: the laser free form heading process is within certain limitations self-aligning. This means, that variations of rod diameters are balanced by the process and thus not negatively effecting the outcome. In contrast, the results of conventional upsetting processes are directly dependent on the accuracy of the initial rod diameter. As soon as this value is not exact, the resulting part does also not have the right volume by given upsetting length l_0 causing defects such as incomplete form filling.

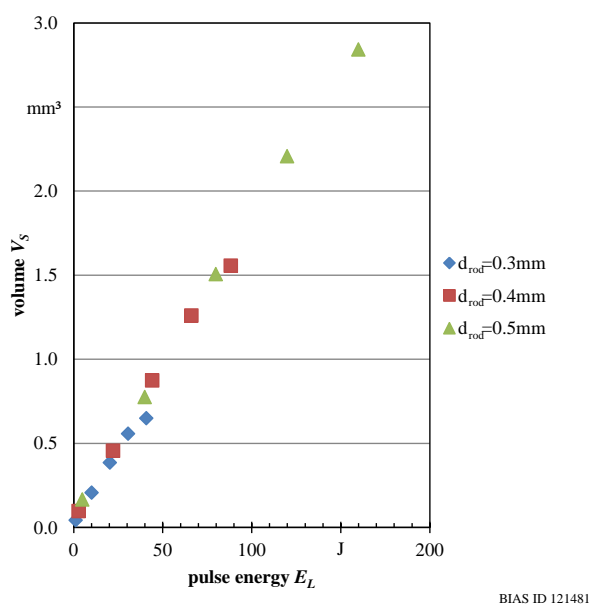


Figure 4. Volume V_S in dependence of pulse energy E_L for rod diameters $d_{rod}=0.3\text{-}0.5\text{mm}$

5. SUMMARY

The self-aligning capability of the laser based free form heading process is investigated. Within the experiments which have been carried out, small variations of rod diameter of $\pm 1\%$ as well as huge variations of rod diameter of $\pm 25\%$ have been evaluated. A relation between natural strain ϕ_r of rods and the absorption coefficient α of laser beam energy E_L is detected which is assumed to be based on the lower absorption coefficient α of martensite compared to austenite. The investigations on self-aligning capability of laser free form heading process come to the conclusion, that a variation of rod diameter within certain limits does not affect the resulting sphere volume V_S . This makes the

presented process more than a good alternative in micro range for conventional upsetting. The quality of goods manufactured by a conventional upsetting process is directly dependent of the geometric accuracy of initial wrought material. For example a slight variation in initial diameter of axially symmetric parts is amplified by the power of two regarding the final volume of the part. Thus laser based free form heading recommends itself as a trend-setting process for upsetting in micro range.

ACKNOWLEDGEMENT

The authors gratefully acknowledge the financial support by Deutsche Forschungsgesellschaft (DFG, German Research Foundation) for Subprojekt A3 "Stoffanhäufen" within the SFB 747 (Collaborative Research Centre) "Mikrokaltumformen – Prozesse, Charakterisierung, Optimierung".

6. REFERENCES

- [1] Masuzawa, T. (2000) State of the Art of Micromachining. Keynote Paper. Annals of the CIRP 49:473-488.
- [2] Geiger, M., Kleiner, M., Eckstein, R., Tiesler, N., Engel, U. (2001) Microforming. Annals of the CIRP 50:445-462.
- [3] Lange, K., Umformtechnik, Band 2: Massivumformung (1988) Springer-Verlag, Berlin.
- [4] Meßner, A., Kaltmassivumformung metallischer Kleinstteile: Werkstoffverhalten, Wirkflächenreibung, Prozessauslegung (1998). Meisenbach Verlag, Bamberg.
- [5] Vollertsen, F. (2008) Categories of size effects. Prod. Eng.-Res. Dev. 2, p. 377-388.
- [6] Vollertsen, F., Walther, R. (2008) Energy balance in laser-based free form heading. Annals of the CIRP 57:291-294.
- [7] Brüning, H., Vollertsen, F. (2012) Formability of micro material preforms generated by laser melting. 37th Matador Conference (in press).
- [8] Kuhfuß, B., Piwek, V., Mouri, E., Vergleich charakteristischer Einflussgrößen beim Mikro- und Makrorundkneten. In: 4. Kolloquium Mikroproduktion p. 219-228 (2009). BIAS Verlag, Bremen.
- [9] Stephen, A., Vollertsen, F. (2010) Upset ratios in laser-based free form heading. Physics Procedia 5:227-232.
- [10] Ilschner, B., Singer, R.F., Werkstoffwissenschaften und Fertigungstechnik (2001) Springer-Verlag, Berlin.
- [11] Vollertsen, F. (2011) Size Effects in Micro Forming 14th International Conference on Sheet Metal (Sheet Metal 2011) eds.: J. R. Dufloy, R. Clarke, M. Merklein, F. Micari, B. Shirvani, K. Kellens. Trans Tech Publications Zürich-Durten 3-12.
- [12] Stephen, A., Brüning, H., Vollertsen, F. (2011) Fokuslagensteuerung beim laserbasierten Stoffanhäufen. In: Kolloquium Mikroproduktion und Abschlusskolloquium SFB 499. KIT Scientific Publishing, Karlsruhe.
- [13] Sakkietibutra, J., Vollertsen, F. Größeneffekte beim Stauchmechanismus am Beispiel geometrisch skaliertes Brückenaktuatoren. In: Größeneinflüsse bei Fertigungsprozessen p. 97-116 (2009). BIAS Verlag, Bremen.

Authors: Prof. Dr.-Ing. Frank Vollertsen, Dipl.-Ing. Heiko Brüning, Bremer Institut für angewandte Strahltechnik GmbH, Klagenfurterstr. 2, 28359 Bremen. Tel.: +49-421-21858129 Fax.: +49-421-21858063. E-mail: vollertsen@bias.de bruening@bias.de

Deželak, M., Stepišnik, A., Pahole, I., Ficko, M.

METHODS FOR SPRINGBACK PREDICTION AND COMPENSATION

Abstract: *New demands in the automotive industry have led to an increase in the use of Advanced High-Strength materials. However, higher values of strength usually lead to reduced formability and increased sensitivity of springback. Today, springback is one of the most important factors that influence the quality of sheet metal forming products. We separate the following types of springback considering the geometry of the product and the forming regime: angular change, sidewall curl and twist. During the forming process, sheet metal undergoes a complicated deformation history, which is why the accurate prediction and consequently the compensation of the springback can be very difficult. In this paper the procedure for springback prediction and compensation of car body parts is presented.*

Key words: *sheet metal forming, deep drawing, springback, FEM*

1. INTRODUCTION

The springback phenomenon is the result of the stress state in the material following the forming process and means a change of shape in the sheet metal forming product after the removal of the forming forces. Steel sheets with high strength and aluminium alloys are more sensitive to the springback effect due to the greater degree of elastic deformation than conventional mild steels. There are three general types of springback considering the geometry of the product and the forming regime: angular change, sidewall curl and twist (Fig. 1) [1]. During the deep drawing process, sheet metals show a combination of angular changes and sidewall curls which usually occur in the walls of the products, while the effect of torsion springback deviation (twist) is visible in the entire area of the product with changeable cross-sections.

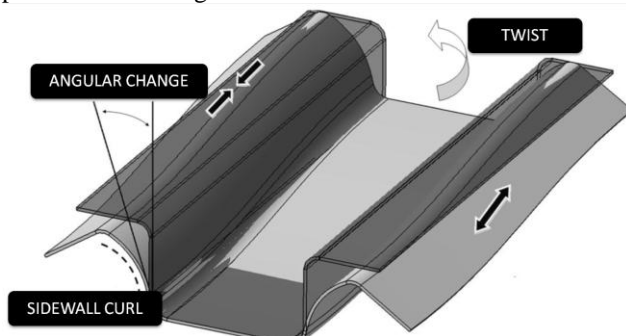


Fig. 1 General types of springback

Angular change follows the sheet metal bending in plain strain, when a sheet metal strip is bent over a punch radius. The stress gradient in the thickness direction causes the residual bending moment after tool withdrawal. This bending moment is the reason for the geometrical errors in the shape of the part angle deviation compared to the punch angle after the bending operation. The key to eliminate the angular change is to eliminate or minimize this residual bending moment.

Sidewall curl occurs when the sheet metal is drawn over the die radius or through the drawbead. Sheet

metal undergoes a bending and unbending process and both cause uneven stress distribution through the thickness direction. Sidewall curl is seen as a drawing part wall curvature deviation compared to the geometry of the forming tools.

Torsional springback or twist is defined as two-cross sections rotating differently along their axis caused by torsion moments [1]. They occur because of the unbalanced elastic residual stresses in the flanges and walls of the sheet metal part. The geometrical parameters of the sheet metal part have the biggest influence on the twist springback. Maximizing the torsional stiffness of the part by adding geometrical stiffeners (ribs) or by redesigning to avoid long, thin sections is a common strategy for twist springback minimization.

2. METHODS FOR SPRINGBACK PREDICTION

2.1 Finite Element Method – FEM

Finite element method (FEM) simulations are nowadays the most important tool for springback behaviour prediction of sheet metal parts in the process design step [2]. Presented below are several examples of FEM springback simulations compared to measured experimental values. In all cases special software for sheet metal processes (PamStamp) simulation was used.

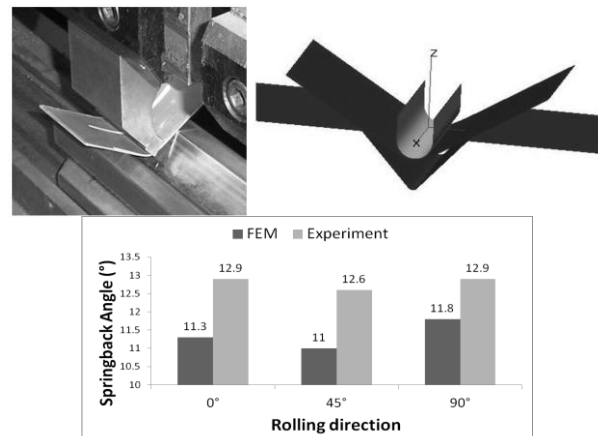


Fig. 2. Springback after the pure bending test

Springback after bending (angular change) is the simplest case of geometrical deviation after the forming punch removal. For pure bending of dual phase sheet metal strips (thickness 1.2mm, tensile strength 780MPa) we can see the comparison between the FEM simulation and the experimental data (Fig. 2). The effects were analysed of the sheet metal rolling direction on springback after bending with a 5mm punch radius. Although we can see some deviation between the simulation and the experiment results, the tendency of springback according to the rolling direction is comparable.

The next case of springback is presented in an experiment called the draw/bend test. This is a simplified method of the deep drawing process, where the sheet metal is pulled over the radius. After the experiment progression, springback occurred. It is the result of flexible angular changes and sidewall curl. Their sum is expressed in $\Delta\theta$ angle. Details of the experiment and the results were summarized by source [3]. Fig. 3 demonstrates the comparison of the experimental springback results and the results of FEM simulations for the HSLA material.

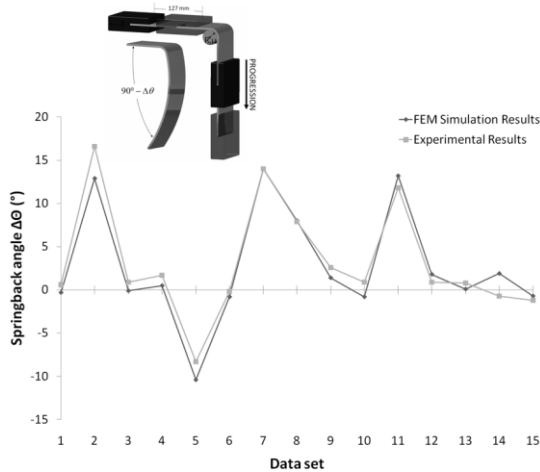


Fig. 3 Draw/bend test

The next example [4] presents the prediction of springback of an industrial case (Fig. 4), as calculated using numerical simulations and compared to experimental measurements. Comparison of the simulation and the experimental results show some deviation. The main reason could be in using a relatively simple material-model (Hill 48), which is good enough for forming simulations, but has some disadvantages in springback modelling. This yield criterion is today widely used and for this reason, the accuracy of the springback simulations is still limited. In spite of the deviation, the springback tendency is clearly seen and this data are very useful in forming process design.

It is necessary to know and understand the influence of numerical parameters on the simulation results for the successful application of the finite element method to predict springback. Plenty of numerical parameters in each simulation step (tool closing, forming, springback) can have a significant impact on final springback prediction results. Careless determination of the numerical parameters can cause additional errors in the FEM approach.

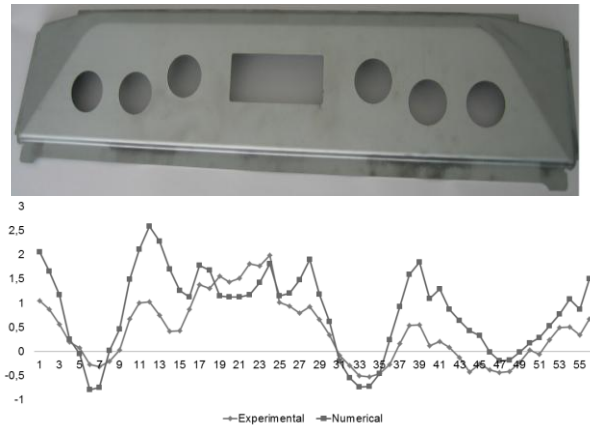


Fig. 4 Springback results (experimental and numerical) after deep drawing the industrial part

Springback is calculated with the FEM software based on implicit or explicit algorithms. One of the most important parameters when using explicit algorithms is defining the velocity of the forming tools. It is usually overestimated, because this reduces the CPU time of the whole forming simulation. We checked the influence of the prescribed die velocity for a simple forming case of a U- drawing part and found some connections (Fig. 5 right). The starting velocity was defined as a growing function up to 5m/s and multiplied by the reduction factor k . The effect of the latter was analysed. When $k = 1$ (the highest velocity) simulations show less springback compared to values of 0.5 and 0.1.

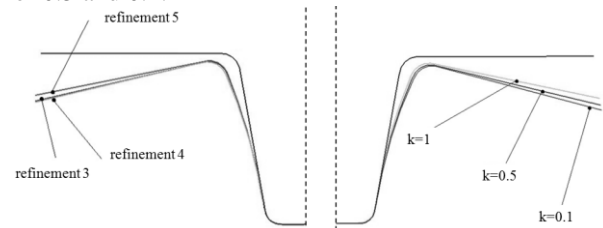


Fig. 5 The effect of the blank mesh refinement and die velocity on springback.

The blank mesh refinement during the forming process is also a very important numerical parameter. The adaptive meshing automatically refines the mesh in the blank areas where it is important relating to the die or punch geometry.

According to the same size of the mesh elements on the start of simulation we can see (although in our case it is not so clear) the effect of the different meshing parameters on the FEM springback prediction. The more fine mesh is used the more the springback appears (Fig. 5 left).

The preliminary condition of a successful springback prediction is therefore a more precisely prepared numerical simulation. This means better tool mesh quality, advanced contact definition, lower forming velocities, sufficient number of integration points through the thickness ...[5].

In view of the above-presented comparisons between the FEM and the experimental springback results we can see some degree of unreliability in the FEM springback predictions. We think that the reasons lie in

the sheet metal forming process being too simplified when it is modelled. In other words: it is hard to make a representative model of such a complicated process. Besides complexity, a problem of the robustness of the sheet metal parts' production can play an important role in the geometrical deviations and for this reason a stochastic analyses of springback should be integrated into the design chain.

2.2 Artificial Intelligence Methods

Sometimes artificial intelligence methods are used for improving springback prediction, mostly for academic examples. They can be used as optimization algorithms or as an evaluation method. Combining the FEM methods and artificial intelligence can improve our springback prediction to better reflect the measured data [6].

In the following case for improving the FEM springback results a Weka workbench was used [7]. The Weka workbench is a collection of ML algorithms and data preprocessing tools. It includes methods for all the standard data mining problems: regression, classification, clustering, association rule mining, and attribute selection. We used classification methods under the function category, because the "new knowledge" can be written down as a mathematical equation in a reasonably natural way. In our case, the ML system based on experiments and the simulation draw/bend test, and six different algorithms were used: *Linear Regression*, *Isotonic Regression*, *Least Medium Square*, *SMO*, *Gaussian Processes* and *Multilayer Perceptron* [7].

The attributes (inputs) for each case of sheet metal material were radius, normalized holding force or back force, the coefficient of friction, sheet thickness, yield stress, factor of normal anisotropy, elastic module and the result of the FEM simulation. The regression variable as a measured angle value in the experiment we assume to be absolutely correct.

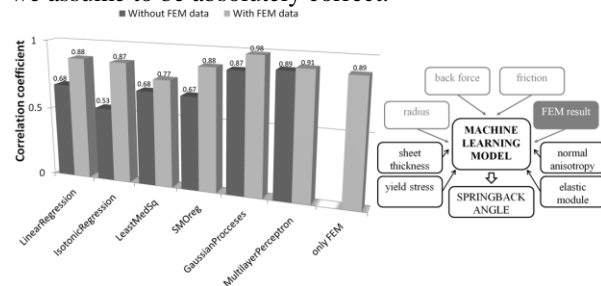


Fig. 6. Finite Element Method Combined with Machine Learning for Springback Prediction

If we take a look at the results (Fig. 6) of the correlation coefficients we can see that the last three tested methods (SMO, Gaussian Processes and Multilayer Perceptron) are more suitable for springback prediction. One of the reasons is definitely in the nonlinearity of the complex springback phenomenon and these methods are able to model these kinds of phenomena. However, in combination with the FEM it raises the correlation coefficient to a higher level compared to the solely FEM method.

3. METHODS FOR SPRINGBACK COMPENSATION

We realize that it is impossible to completely overcome springback but it can be limited and monitored by setting the optimal forming parameters to reach a higher level of sheet metal plastic deformation. The invention of the *Displacement Adjustment (DA)* method [8] was an important progression in the area of springback compensation.

In papers [9, 10] there are presented two on DA based methods: *Smooth displacement adjustment (SCA)* and *Surface Controlled Overbending (SCO)*. Their main purpose is the DA method application on complicated sheet metal parts from the automotive industry. All the stated methods are a significant progression in springback compensation although there are lots of applicability limitations at the moment. The main limitation is due to too few reliable FEM springback results because of not using advanced material models for sheet metal modelling in industry. There is a cost-benefit conflict in material modelling. Models that are appropriate for forming simulations usually lack the final part geometry prediction after the tool elements withdrawal.

A few software packages for sheet metal forming simulation contain modules for automatic springback compensation. These kinds of tools are very useful, but their drawback is currently the problem of mesh robustness when the compensation of an auto body part is done. Excessive local solving of the geometrical deviation (wrinkles) can cause a corruption to the die and punch shape. However, in the near future, the software for automatic springback compensation will reach a satisfactory level for industrial applications.

3.1 Guide Curve Method

In the last link of the sheet metal forming design chain, when optimal technological parameters for springback minimization are found (blank holder force, drawing radii, drawbeads construction...) the springback compensation can only be completed with geometrical changes to the die shape. This can be conducted with the *Guide Curve Method (GCM)* based on the DA philosophy (Fig. 7). This relatively simple method showed positive efficiency according to the invested work and costs and the final result.

Because of the GCM implementation, the simulation and validation time of the complete forming process is extended but in this way physical tryouts are started with an initial geometrical correction which usually reduces the number of tool shape adaptations. The GCM is applicable not only in forming the planning process but also when tryouts on real tools are performed and corrections are implemented.

The groundwork of the GCM is the FEM springback simulation result. The exported mesh in the stl file is inserted into a 3D environment tool (Catia V5) and the deviation analysis between the FEM result and the reference CAD geometry is done. The reference curves (guide curves) of both the FEM result and the CAD

reference are created and they are elements for drawing the tool surface reconstruction. New iterations start the FEM simulation with the adapted die shapes. If the geometry of the part after springback is suitable within the tolerance allowance this is the end of the springback compensation in the planning phase and the physical tool is then manufactured. A single iteration (surface adaptations) is made inside a 3D environment tool and for this reason the surfaces keep their quality. A similar compensation process is also executed in the physical tryouts and tool corrections phase, with the exception that for the springback evaluation in spite of the FEM results, real measurements are used.

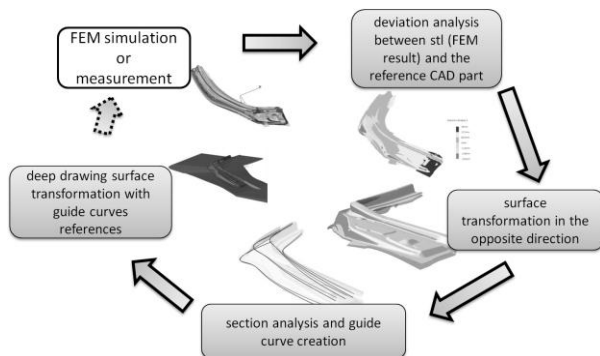


Fig. 7 Guide Curve Method

3.2 Springback Compensation of an A-pillar

The special shape of the A-pillar (Fig. 8) causes twisting of the part after the forming operation. For the actual auto body part the GCM based on FEM simulations was used. Although physical tool corrections were needed, their number was reduced by a half. Measurements based on the GCM enabled quicker, more precise and controllable adaptations of the forming tools.

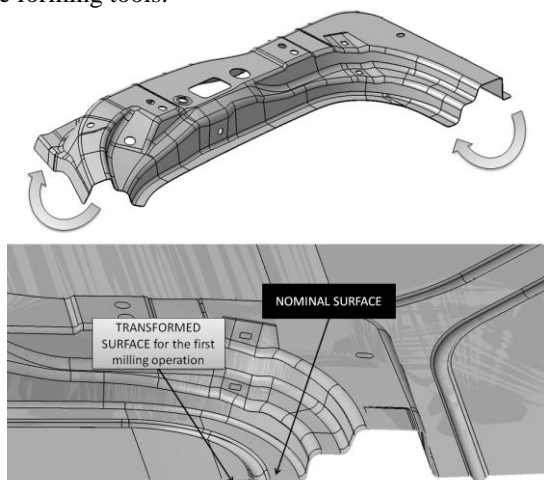


Fig. 8 The twisting tendency of the A-pillar after forming, and the springback compensation in the first forming operation

4. CONCLUSION

This paper presents a few approaches for springback prediction and compensation. The conclusions obtained in this study were as follows.

1) In spite of the limited reliability of the FEM springback results this method is very useful. Even if

there are problems with accuracy, the springback tendency (direction of a part area deformation) is well predicted.

2) There is a cost-benefit conflict in sheet metal material modelling. With advanced (costly) material models better springback prediction is possible.

3) Combination of the FEM and the Artificial Intelligence Methods allows a more accurate springback prediction.

4) Performing geometrical springback compensation in the first tryout significantly reduces the time for physical tool modification.

5) In the springback prediction and compensation process it will be soon necessary to take into account the stochastic nature of the sheet metal material.

ACKNOWLEDGEMENTS

“Operation part financed by European Union, European Social Fund”

5. REFERENCES

- [1] WorldAutoSteel. Advanced High Strength Steel Application Guidelines. (2009).
- [2] Meinders T, Burchitz I, Bonte M, Lingbeek R. Numerical product design: Springback prediction, compensation and optimization. *International Journal of Machine Tools and Manufacture* (2008), vol. 48, no. 5, pp. 499-514.
- [3] Carden WD, Geng LM, Matlock DK, Wagoner RH. Measurement of springback. *International Journal of Mechanical Sciences* (2002), vol. 44, no. 1, pp. 79-101.
- [4] Volk M, Deželak M, Nardin B, Stepišnik S. Prediction of the Spring-back Calculated with Numerical Simulations for the Household Industry. (2011), pp. 1078-1085.
- [5] Xu W. Sensitive factors in springback simulation for sheet metal forming. *Journal of Materials Processing Technology* (2004), vol. 151, no. 1-3, pp. 217-222.
- [6] Marwala T. *Finite-element-model Updating Using Computational Intelligence Techniques*: Springer-Verlag London, 2010.
- [7] Witten IH, Frank E. *Data Mining, Practical Machine Learning Tools and Techniques, Second Edition*: Elsevier, 2005.
- [8] Gan W, Wagoner RH. Die design method for sheet springback. *International Journal of Mechanical Sciences* (2004), vol. 46, no. 7, pp. 1097-1113.
- [9] Lingbeek R, Huétink J, Ohnimus S, Petzoldt M, Weiher J. The development of a finite elements based springback compensation tool for sheet metal products. *Journal of Materials Processing Technology* (2005), vol. 169, no. 1, pp. 115-125.
- [10] Lingbeek RA, Gan W, Wagoner RH, Meinders T, Weiher J. Theoretical verification of the displacement adjustment and springforward algorithms for springback compensation. *International Journal of Material Forming* (2008), vol. 1, no. 3, pp. 159-168.

Authors: Mihael Deželak¹, MSc. Andrej Stepišnik¹, D.Eng. Ivo Pahole², doc. dr. Mirko Ficko²,

¹Emo -Orodjarna d.o.o., Slovenia

²University of Maribor, Faculty of mechanical engineering, Slovenia

E-mail¹: mihael.dezelak@emo-rodjarna.si

Ivanisevic, A., Milutinovic, M., Skakun, P., Movrin, D., Kacmarcik, I., Plancak, M., Vilotic, D., Alexandrov, S.

EXPERIMENTAL DETERMINATION OF FORMING LIMIT DIAGRAM FOR BRASS

Abstract: Forming limit diagram (FLD) expresses possibility of material to be deformed in different stress-state condition determined by triaxiality stress ratio. This diagram allows design and optimization number of phases at cold bulk forming process.

In this paper results of experimental determination of FLD for brass CW603N are presented. The aim of investigation was to determine forming limit diagram for this material using simple types of specimens (cylindrical, tapered, flanged and Rastegajev specimen) in upsetting process. Dies applied in this experiment were flat plates. Strain path and history of triaxiality stress ratio are determined experimentally for different types of specimens. FLD for the brass CW603N represents relationship between limit strain and average value of triaxiality stress ratio.

Key words: Upsetting, brass, forming limit diagram, strain path, triaxiality stress ratio

1. INTRODUCTION

Formability is the capability of the material to be plastically deformed without cracking or some other damaging form. Formability is not a unique material property it is affected by both process and material variables.

In bulk metal forming theoretical and empirical formability criteria are used.

Empirical criterions are based on experimental investigation of real forming processes and they are presented as Forming Limit Diagram (FLD) in two variants. First variant is strain based and it shows interrelation between components of strains of free surface at the moment of the crack appearance. Application of this FLD-type is shown in the papers [1, 2, 3].

Second variant of empirical formability criterion is stress based criterion. This criterion defines relationship between limit strain and stress indicator in the critical zone of the specimen.

Material formability (M_f) depends on kind of material (H), its micro structure (S), process temperature (T), strain rate ($\dot{\varphi}$), stress state (T_σ) and other factors [4]:

$$M_f = F(H, S, T, \dot{\varphi}, T_\sigma \dots) \quad (1)$$

Quantitative measure of limit formability is effective strain, (φ_ϵ^l), i.e. strain in the moment of material structure damage or strain localization. For the given material, with defined initial microstructure and in cold forming conditions by quasi static deformation, material formability is a function only on stress state:

$$\varphi_\epsilon^l = F(T_\sigma) = F(\beta) \quad (2)$$

where is:

T_σ – stress tensor

β – triaxiality stress ratio at the critical point of specimen, i.e. at the point of structure damage. Stress ratio is defined as:

$$\beta = \frac{\sigma_x + \sigma_y + \sigma_z}{\sigma_e} = \frac{\sigma_1 + \sigma_2 + \sigma_3}{\sigma_e} \quad (3)$$

where are:

$\sigma_x, \sigma_y, \sigma_z$ – normal stress components in orthogonal directions (x, y, z)

$\sigma_1, \sigma_2, \sigma_3$ – components of principal normal stress

σ_e – effective stress.

Graphical interpretation of the relationship (2) is the forming limit diagram – FLD (Fig. 1). Forming limit diagram shows that in bulk metal forming processes in which compressive stresses prevail ($\beta < 0$) higher values of limit strains can be achieved than in the processes in which tensile stresses are predominant ($\beta > 0$).

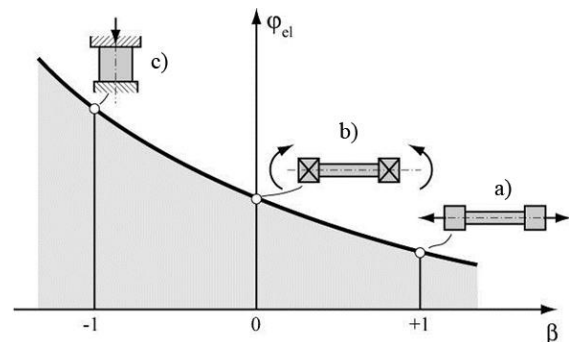


Fig. 1. Forming limit diagram: a) uni-axial tension test, b) torsion test, c) uni-axial compression test

Forming limit diagram is determined experimentally, by employing basic deformation models [4]:

- uni-axial tensile test, $\beta = +1$
- torsion test, $\beta = 0$
- uni-axial compression test, $\beta = -1$.

Limit strain at $\beta = +1$ experimentally is performed by tension test in stage of uniform deformation. Criterion of uniform deformation as a limit value by $\beta = +1$, is based upon the fact that in the tension test uni-axial stress state exists only in the phase of homogeneous deformation, i.e. till the moment of maximum load. In localized deformation three-axial tensile stress state occurs ($\beta > +1$), which accelerates voids initiation in the micro structure of the material, their growth, voids linking and finally, crack of the specimen [5].

Instead of uni-axial compression experiment, cylinder upsetting by flat dies in real friction conditions often is used.

For more detailed construction of FLD application of more sophisticated methods is needed.

In the case of non-monotonous processes [9] stress indicator (β) changes during deformation and its average value is inserted in the FLD diagram. Average value of stress indicator is defined as:

$$\beta_{av} = \frac{1}{\varphi_e'} \int_0^{\varphi_e'} \beta(\varphi_e) d\varphi_e \quad (4)$$

where is:

$\beta(\varphi_e)$ – history of stress ratio which indicates change of stress-state as a function of effective strain.

By determination of stress indicator (β), for the case that material damage occurs at free surface of the specimen, two methodologies, based upon deformation theory i.e. flow theory, are applied.

In the paper [9] determination of stress components at free surface of cylinder (equatorial surface) was conducted by employing deformation theory, i.e. by using following relations:

a) Stress- strain relationship:

$$\frac{d\varphi_\theta}{\sigma_\theta - \sigma_m} = \frac{d\varphi_z}{\sigma_z - \sigma_m} \quad (5)$$

b) Hydrostatic stress:

$$\sigma_m = \frac{\sigma_r + \sigma_\theta + \sigma_z}{3} = \frac{\sigma_\theta + \sigma_z}{3} \quad (6)$$

c) Misses yield criterion:

$$\sigma_\theta^2 + \sigma_z^2 - \sigma_\theta \cdot \sigma_z = \sigma_e^2 \quad (7)$$

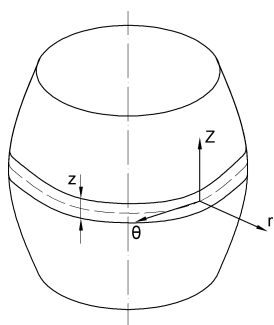


Fig. 2. Cylindrical specimen after deformation

By combining of above equations stress components σ_z , σ_θ and stress indicator β at the free surface at the cylinder can be obtained:

$$\sigma_z = \pm \sigma_e \left[1 - \frac{1+2\alpha}{2+\alpha} + \left(\frac{1+2\alpha}{2+\alpha} \right)^2 \right]^{-1/2} \quad (8)$$

$$\sigma_\theta = \sigma_z \cdot \left(\frac{1+2\alpha}{2+\alpha} \right) \quad (9)$$

$$\beta = \frac{\sigma_x + \sigma_y + \sigma_z}{\sigma_e} = - \frac{1 + \frac{1+2\alpha}{2+\alpha}}{\sqrt{1 - \frac{1+2\alpha}{2+\alpha} + \left(\frac{1+2\alpha}{2+\alpha} \right)^2}} \quad (10)$$

where are:

σ_r , σ_θ , σ_z – stress components in the directions of corresponding axis (r ; θ , z), whereas at free surface $\sigma_r = 0$;

σ_m – hydrostatic stress; σ_e – effective stress.

In the equations (8,9,10) “ α ” is strain ratio defined as:

$$\alpha = \frac{d\varphi_\theta}{d\varphi_z} \quad (11)$$

Prior to that, strain path is defined as:

$$\varphi_\theta = f(\varphi_z) = A\varphi_z + B\varphi_z^2 \quad (12)$$

A and B – coefficient of regressive curve.

In the paper [8], average value of stress indicator was determined by flow theory:

$$\beta_{av} = \frac{2}{\varphi_e'} (\varphi_1' + \varphi_2') \quad (13)$$

where:

φ_1' and φ_2' – components of main strains in fracture zone

φ_e' – effective strain in the moment of specimen fracture:

$$\varphi_e' = \frac{2}{\sqrt{3}} \int_0^{\varphi_e'} \sqrt{(A + 2B\varphi_z)^2 + A + 2B\varphi_z + 1} d\varphi_z \quad (14)$$

In the present paper, results of formability of brass CW603N obtained by upsetting different types of billets with flat plates are presented. Objective of the current investigation is determination of FLD diagram for brass by simple upsetting tests.

2. EXPERIMENTAL DETERMINATION OF FLD



Fig. 3. Sack&Kiesselbach hydraulic press

Upsetting of CW603N billets was conducted in Laboratory for Technology of Plasticity, on Sack&Kiesselbach hydraulic press with 6.3MN rated force by flat plates, Fig. 3.

For FLD determination four types of billets (RT, BC, TP, CC) were used. For lubrication mineral oil was applied. In Table 1 initial dimensions of billets are presented.

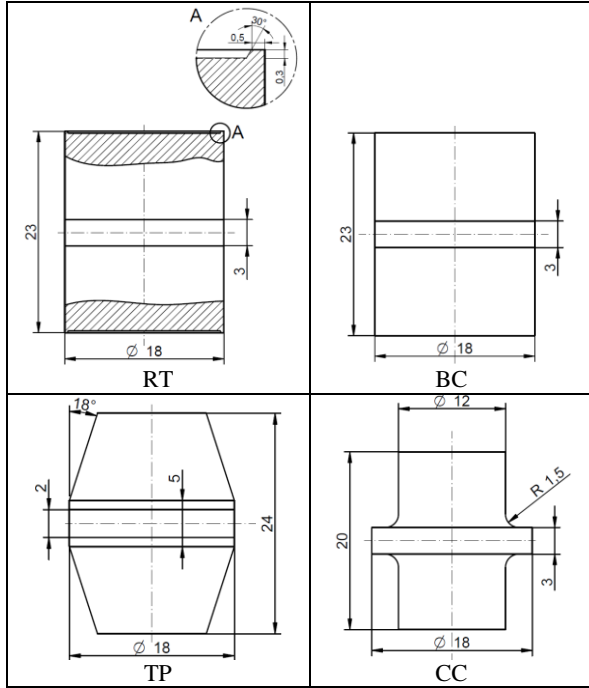


Table 1. Types of billets with initial dimensions used in experiment

Each billet had marked zone Z around equatorial plane which was used for local strain determination. For billets RT, BC and CC zone Z=3mm and for TP zone Z=2mm. After every deformation phase, local strains were calculated based on height of marked zone Z and diameter in equatorial plane D:

$$\varphi_z = \ln \frac{Z}{Z_0}, \varphi_\theta = \ln \frac{D}{D_0}, \varphi_r = -(\varphi_\theta + \varphi_z) \quad (15)$$

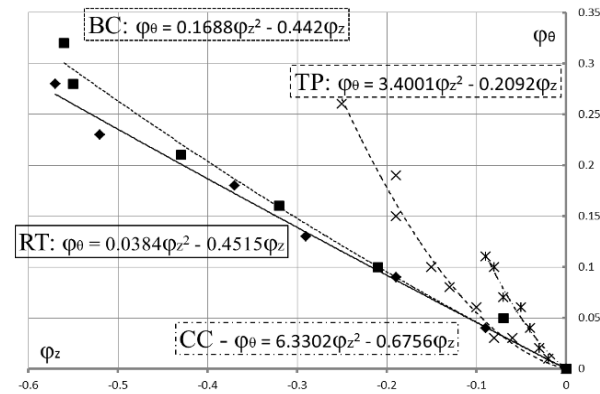


Fig. 4. Strain path for different types of specimens

In Fig. 4 strain path diagram for four types of billets is presented.

Relationship between deformations in two

orthogonal directions is approximated by expression (12). Fig. 5 presents specimens before and after deformation.

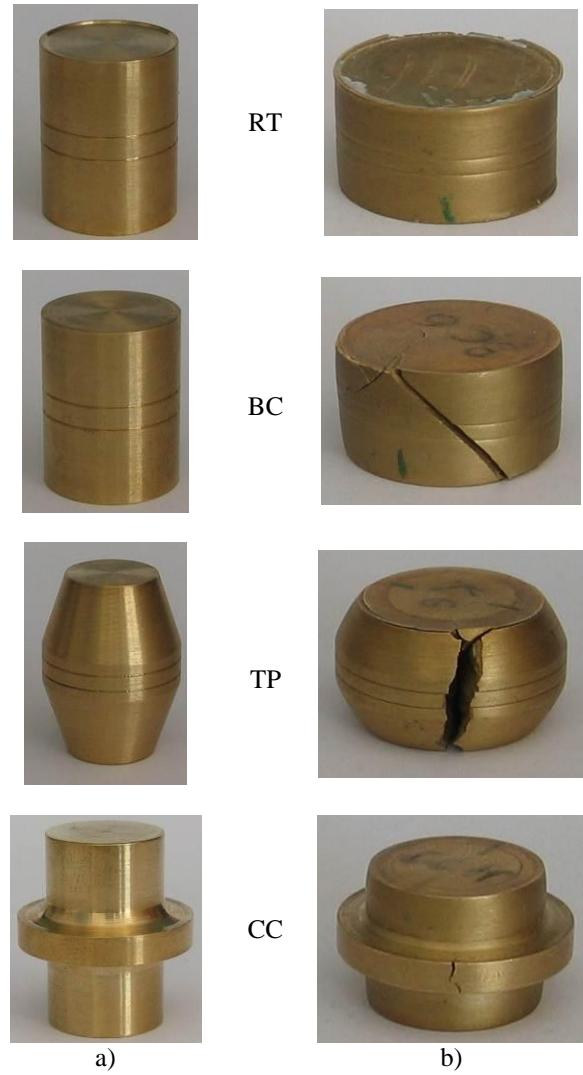


Fig. 5. Specimens before (a) and after (b) deformation

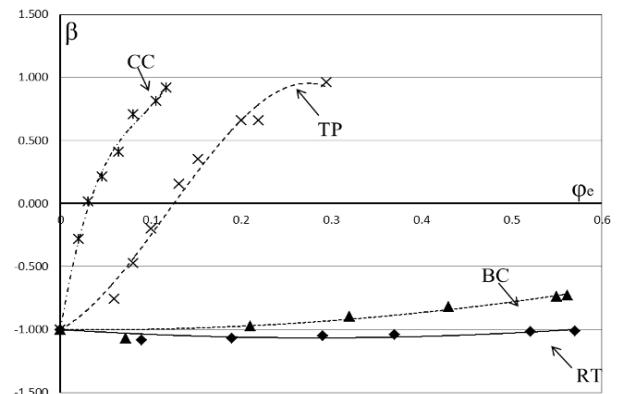


Fig. 6. History of stress ratio all types of billets

Based on this data, change of stress ratio during upsetting process of each particular specimen series is obtained (diagram, Fig. 6). Average value of stress index (β_{av}) was calculated by expression (4). Obtained data, together with the values of effective limit strains, were superimposed into forming limit diagram, Fig. 7.

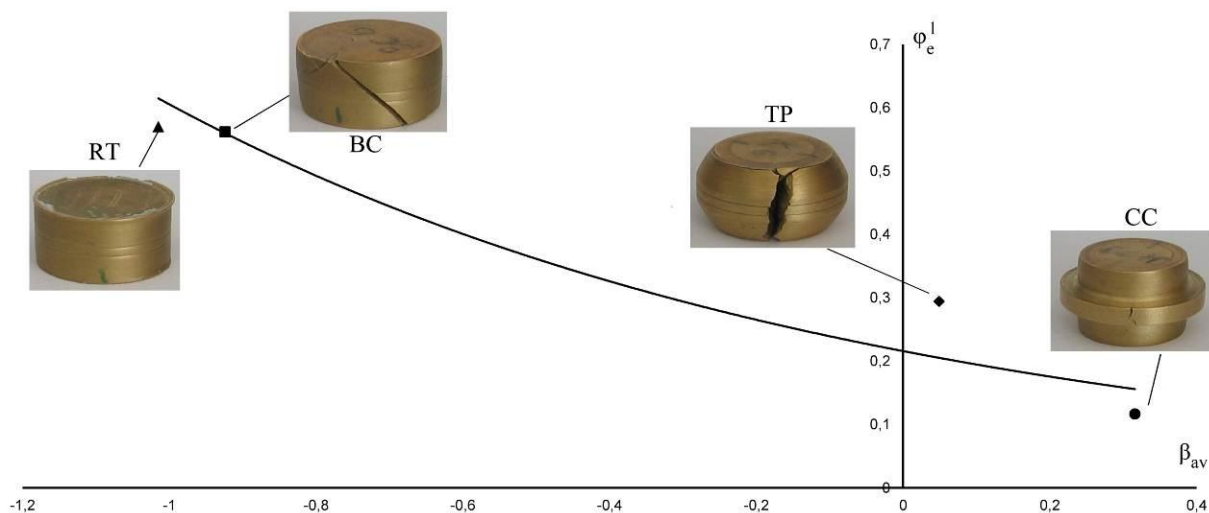


Fig. 7. FLD for CW603N

3. CONCLUSION

General method for FLD determination is based on application of three basic tests (upsetting of cylinder, torsion and uniaxial tension test).

In this paper procedure of FLD determination for brass using different upsetting tests is presented. Stress state in critical zone was varied by applying different billet geometries.

Strain path diagram shows that there is a difference in forming conditions between used types of upsetting tests (figure 5). This difference is more obvious in the diagram which represents history of triaxiality stress ratio (figure 6).

Finally, FLD of brass shows that the best forming conditions exist in Rastegajev upsetting test and upsetting of straight cylinder. The worst conditions occur in collar cylinder test. Upsetting of tapered specimen test is positioned near to the torsion test ($\beta \approx 0$).

For more detailed determination of FLD it is necessary to introduced new upsetting tests which would cover interval of stress indicators of $\beta_{av} = -0.8 \div 0$.

4. REFERENCES

- [1] Gänser P.: *Free-surface ductility in bulk forming processes*, International Journal of Plasticity, p.p. 755-772, 2001.
- [2] Ragab A.R.: *Fracture limit curve in upset forging of cylinders*, Materials Science and Engineering, p.p.114-119, 2002.
- [3] Landre J.: *On the utilization of ductile fracture criteria in cold forging*, Finite Elements in Analysis and Design, p.p. 1785-186, 2003.
- [4] Vujović, V., Shabaik A.: *Workability Criteria for Ductile Fracture*, Trans. ASME J. Engng Mater. Technol, p.p. 245-249, 1986.
- [5] Sidjanin L.: *Three stages in Ductile Fracture Process in Comercial Carbon Steel*, 8th Congress On Material Testing, p.p.41-49, Budapest, 1982.

- [6] Bandstra J. P., Koss D. A.: *Modeling the ductile fracture process of void coalescence by void-sheet formation*, Materials Science and Engineering, p.p.490-495, 2001.
- [7] Vilotić D., Plančak M., Čupković Đ., Alexandrov S., Alexandrov N.: *Free Surface Fracture in Three Upsetting Tests*, Experimental Mechanics, p.p. 115-120, 2006.
- [8] Alexandrov S., Vilotić D.: *Theoretical Experimental Analysis of Fracture Initiation at the Free Surface in Upsetting by Conical Dies*, Steel Research International 2, p.p. 375-381, 2008.
- [9] Vilotić D., Alexandrov S., Plančak M., Movrin D., Ivanisević A., Vilotić M.: *Material Formability at Upsetting by V-shape Dies*, Steel Research International, Special Edition, p.p. 923-928, 2011.

Authors: M.Sc. Aljosa Ivanisevic, Mr Mladimir Milutinovic, Mr Plavka Skakun, M.Sc. Dejan Movrin, M.Sc Igor Kacmarcik, Prof. Dr Miroslav Plančak, Prof. Dr Dragisa Vilotić, University of Novi Sad, Faculty of Technical Sciences, Institute for Production Engineering, Trg Dositeja Obradovica 6, 21000 Novi Sad, Serbia, Phone.: +381 21 485 2513, E-mail: aljosa@uns.ac.rs

Prof. Dr Sergei Alexandrov A.Yu. Ishlinsky Institute for Problems in Mechanics, Russian Academy of Sciences, Moscow, Russia

ACKNOWLEDGEMENT

Results of investigation presented in this paper are part of the research realized in the framework of the project TR 035020, financed by the Ministry of Science and Technological Development of the Republic of Serbia and also supported by RFBR-12-08-97024 grant. Authors are grateful for financial support.

Jovanic, D., Jovanovic, M.

ECONOMIC EFFICIENCY OF WELDING SIMULATOR USE FOR WELDING PERSONNEL TRAINING

Abstract: Economic benefit of introduction of CS Wave welding simulator in training of welding personnel is presented in the paper. The Technical College of Applied Sciences in Zrenjanin has acquired the simulator within the project "Welders' Training and Certification in Banat" financed by the Regional Socio-Economic Development Programme 2-RSEDP2 of the European Union. The total costs of welders' training by using Manual metal arc welding (111): parent material costs, filler material costs, electricity costs, costs of device and costs of trainer, are compared to the saving resulted from optimal use of simulator in training which is 20% in relation to the total number of classes envisaged in the document IAB-089r4-10- minimum requirements for the education, training, examination and qualification of international welder [1].

Key words: Welding simulator, Virtual welding, Economic Efficiency

1. INTRODUCTION

The role of simulator in welders' training is primarily important in a professional approach to training from the very beginning. It enables rise in productivity and quality of welded joints. The cost saving in base material, filler material and electricity assure cheaper, safer and more environmentally-friendly training. Welding simulator also contributes to changing the image of welding environment which is usually seen as dirty and dangerous while the welding job as a hard one. The use of Virtual Reality helps attract younger people, which is important for assuring a younger generation of welders since, for example, the average age of welders is 55 in the USA [2].

2. MANUAL METAL ARC (MMA) WELDING COST

The most important costs of MMA welding process with covered electrode when welding device is used are the following: base material costs, electrode costs, electricity costs trainer costs and welding device costs [3,4].

2.1 Base Material Cost

Base material (steel plates and tubes) consumption is 15-20 kg per day per welder on average. The price being 1 EUR/kg, the base material costs are:

$$T_{BM} = 15-20 \text{ EUR per day}$$

2.2 Electrodes Cost

Electrode costs may be calculated according to the following formula:

$$T_{\text{electrodes}} = C_{\text{electrode/wire}} \cdot k'_t \left[\frac{\text{EUR}}{\text{kg}_{\text{dep}}} \right] \quad (1)$$

where :

$$C_{\text{electrodes}} \left[\frac{\text{EUR}}{\text{kg}_{\text{electrodes}}} \right] - \text{electrode unit price}$$

$$k'_t \left[\frac{\text{kg}_{\text{electrodes}}}{\text{kg}_{\text{deposite}}} \right] - \text{coefficient of electrode melting}$$

Filler material – electrodes consumption is 3-5 kg per training day with the price being 2 EUR/kg, the electrode costs are :

$$T_{\text{electrodes}} = 6-10 \text{ EUR per day}$$

2.3 Electricity costs

Electricity costs may be calculated according to the formula:

$$T_{\text{Elect.}} = \left[\frac{U \cdot I \cdot ED}{1000 \cdot \eta_s} + N_0 (1 - ED) \right] \cdot \frac{C_{\text{1electr.}}}{k_t \cdot ED} \left[\frac{\text{EUR}}{\text{kg}_{\text{dep}}} \right] \quad (2)$$

where:

U (V)- electric arc voltage

I (A)- welding power supply

η_s - welding device degree of efficiency

ED- intermittency, electric arc lighting-up time

N_0 (kW) - power used by the device in downtime when the arc is not lit up

$$k_t \left[\frac{\text{kg}_{\text{depozita}}}{h} \right] - \text{electrode melting coefficient}$$

$$C_{\text{1el.energ.}} \left[\frac{\text{EUR}}{\text{kWh}} \right] - \text{Electricity unit price}$$

For ED intermittency of 50%, the electricity being 160A and voltage $U = 20 + 0.04 \cdot I$ (V) = 26V

$$T_{\text{Electricity costs.}} = 1,45 \text{ EURkg/depozita}$$

For metal mass in electrode and 0.67 electrode mass ratio of ϕ 4mm electrode the result is:

$$T_{\text{Electricity costs.}} = 3-4 \text{ EUR per day}$$

2.4 Workers salaries costs

Workers salaries costs may be calculated according to the following formula:

$$T_{\text{salaries}} = \frac{T_{\text{netsalaries}} \cdot \text{dop.}}{k_i \cdot \varepsilon} \left[\frac{\text{€}}{\text{kg}_{\text{depozita}}} \right] \quad (3)$$

$T_{\text{salaries}} = 25$ EUR per day (net salaries)

where;

$T_{\text{net salaries}}$ - net salary of workers and

dop.- contributions

These costs occur when simulator is used as well

2.5 Welding device costs

$$T_{\text{aparata}} = \frac{C_N(\text{amort.} + \text{osig.} + \text{odrz.} + \text{kamate})}{\text{br. satiradagod.}} \cdot \frac{1}{k_i \cdot ED} \quad (4)$$

where:

Br. satiradagod. – Number of working hours per year

C_N (€)-purchase price of welding device

amort.- annual rate of depreciation

osig. - annual insurance premium and

odrz. - annual amount for maintenance

These costs are much higher when simulator is used than when a welding device is used since it is much more expensive.

2.6 Total costs of welding

$$T = \sum_{i=1}^n T_i \left[\frac{\text{EUR}}{\text{day}} \right] \quad (5)$$

In the following part the daily costs per welder are taken to be 30 EUR per day, i.e. these are taken to be the value of base and filler material saved when welding simulator is used.

3. ECONOMIC EFFICIENCY OF WELDING SIMULATOR

Welders' training time for particular welding processes and joint types according to the **IAB-089-2003/EWF-452-467-480-481** is shown in Table 1.

Type of weld	Total number of theory classes and practicals MMA (111)
FW	A+S (+P) –theory module 20+5 (+8) E1+E2- practicals module 90+50
BPW	A+ B+S (+P) –theory module 20+18+5 (+8) E1+E2+E3+E4- practicals module 90+50+75+75=290
BTW	A+B+C+S (+P) –theory module 20+18+7+5 (+8) E1+E2+E3+E4+E5+E6- practicals module 90+50+75+75+75+75= 440

Table 1. Welders' training time for particular welding procedures and joint types

Where:

FW- fillet weld

BPW- Butt Plate Weld

BTW- Butt Tube Weld

P module (For Stainless steel or aluminum)

The Table 2 shows cost saving in welding simulator use in welders' training by individual modules of MMA process in case it is used 20% or 30% of time of the total training time. Cost saving in filler and base material with welding simulator use are 30 EUR per day.

	Total number of theory classes and practicals MMA (111)	Cost saving per welder (EUR/day)	
		20%	30%
FW	E1+E2- practicals 90+50=140 (14 days)	84	126
BPW	E1+E2+E3+E4 90+50+75+75=290 (29 days)	174	261

Table 2. Cost saving in welding simulator use in welders' training by individual modules of MMA procedure

Cost saving in welding simulator use may be in IWE, IWT, IWS and IWP training. The IWE, IWT and IWS training time according to the IAB-252-07- Minimum Requirements for the Education, Examination and Qualification) is shown in Table 3:

Practical Training	hours
Oxyacetylene welding and cutting	6
MMA	10
MIG/MAG	14
TIG	10

Table 3. IWE, IWT and IWS practical training time

4. CONCLUSION

Welding simulator assures significant cost saving in welders' training. The rate of cost saving depends on length of training i.e. modules which are tested. The total cost saving per training of one welder is 84 - 126 EUR for FW (Fillet welder), 174 - 261 EUR and for BPW (Butt Plate Welder). Additional cost savings are made if one welding simulator is used for several welders. Thus, for training for four to five welders, which is an optimal number in a group for training, the cost saving may be up to 1000 Euros per course.

5. REFERENCES

- [1] European Welding Federation, www.ewf.be
- [2] American Welding Society, www.aws.org/
- [3] www.fssb.hr- Mechanical Engineering faculty, Slavonski Brod, Croatia
- [4] Jovanić D, Milić R , Herold A,: *Određivanje troškova elektrolučnih postupaka zavarivanja*, Processing 2004, jun 2004, Beograd, Srbija i Crna

Authors: **Mr Dušan Jovanić, dipl.maš.ing.**, Technical College of Applied Sciences in Zrenjanin, Dj. Stratimirovica 23, Zrenjanin, Serbia, **Mr Miloš Jovanić, dipl.maš.ing.**, Welding Institute of Slovenia, Ptujška 19, Ljubljana, Slovenia

E-mail: jovanickosta@gmail.com
milos.jovanovic@i-var.si

Jovanovic, V., Langraudi, N., Tomovic, M. M.

BOND GRAPH THEORY AND ITS USE FOR HYDRAULIC SYSTEM MODELING

Abstract: In this paper, bond theory will be presented and its application related to vehicle dynamics. Since vehicle and its subsystems such as suspension are in essence multidisciplinary problems, finding the right mathematical model to describe them might be a challenge for conventional mathematical methods which are usually used separately for dynamics and hydraulics. The nod graph methodology which can describe the energy of the system as a whole and use generalized equations to relate different forms of energy can be used for more accurate mathematical system that would be used for controller development. Control hardware that is used for manipulating of hydraulic system will be presented with a bond graph and its associated dynamic model.

Key words: Bond graph, Vehicle control, Hydraulic suspension system

1. INTRODUCTION

Recent advances in microcomputers led to expansion of embedded systems and shift from electro-mechanical systems to mechatronics. Specifically, automotive applications of computer based control is today increasingly focused on variety of areas such as fuel injection control, drive-by-wire throttle control, cruise control, electronically controlled discrete and continuously variable transmissions (CVT), steering and suspension control, anti-spin control, and anti-lock braking [1].

These types of engineering systems are becoming increasingly complex and multidisciplinary. They are designed and built from components which are developed in different engineering disciplines [2]. Therefore, multidisciplinary mathematical modeling techniques are required to accurately describe such systems. These methods need to support multidisciplinary nature of development of complex products and their computational analysis [2]. One of those is the bond graph theory.

Physical systems can be described through transformations of variables that are in essence power conserving [3]. In addition, devices such as electrical transformers, gears, levers, and linkages may be represented as power-conserving transformations. Processes in engineering systems might be defined as rigid and solid body mechanics, fluid mechanics, electricity and magnetism, semiconductor physics, thermodynamics, etc [4]. If an engineering system is working based on an interaction of more than one physical domain, their interaction has to be considered and such system is based on a multi-domain physical processes.

2. BOND GRAPH THEORY

The bond graph technique is used for modeling of dynamical multiport systems of a multidisciplinary nature [5]. It was created by Professor Henry Paynter at Mechanical Engineering department at Massachusetts Institute of Technology [4]. Bond graphs have been used

for analysis of distributed parameter systems for many years [6]. It is an umbrella for various methods under this name, ranging from mathematical models and bond graph techniques, to computer programs that use this method, but also related to applications to different fields.

This theory was developed for the purpose of dealing with complex problems with which the conventional mathematical approaches were more time consuming [4]. The basis of the theory is that energy and power are the fundamental variables describing system behavior. These variables are the ones that allow all physical interactions and transactions [5]. The concurrent exhibition of physical and mathematical data makes bond graph an appropriate technique to support engineers during system design and analysis, throughout modeling, simulation, selection of instrumentation and actuator architecture, controller synthesis and supervision [7]. Bond graphing allows better visual representation of an engineering system comprised of separate components as a unified whole [8]. The components are grouped under a small number of generalized elements that might be from very different disciplines. In addition, it provides a visual representation of a system from which derivation of the governing equations is algorithmic [8]. Bond graphs can contribute to a more productive working environment and to better fundamental understanding of the key physical attributes needed for optimal function deployment [1].

The bond graph is composed of the "bonds" that have connections between them which represent physical processes. They link together ports (single-port, double-port or multi-port elements). Examples of single port components are resistors (energy dissipating device), capacitors and inductors (energy storage devices). Double port devices include transformer and gyrator. Three port components might be in a flow junction, parallel junction, and common effort junction.

2.1 Models of Variable Structure

Engineering systems are typically represented with mathematical modeling approaches. The mathematical

model has to accurately present the real system. However, some approximation is necessary due to the complex nature of mathematical modeling. [4].

It is important to develop a model that would have the least possible complexity but still include those portions of the power train system dynamics that are relevant for a particular control design that usually includes torques, forces, frequencies and speeds [1]. Well-designed closed loop system will reduce usual discrepancies of 10-20 % through feedback operations. These discrepancies are especially important to be considered since the real time use will account for all field operating conditions such as road friction and roughness, system reliability, changes related to aging of equipment etc. Essentially, during mathematical modeling many of these parameters will not be considered due to desired level of simplicity of a mathematical model. Real time simulation is an essential requirement in simulations for vehicle dynamics application since the driver expects an immediate response[9].

In addition, bond graph models describe lumped finite dimensional approximations of the actual set of concerned partial differential equations, e.g. for heat transfer problems [6]. Some variables are important for its control and analysis while others are of lesser importance. Therefore, any kind of modeling will start from analyzing the system and defining which are the ones that should be considered and which are the ones that should not be included in the mathematical model [4].

2.2 Power Variables

The first assumption of the bond graph theory is that the total energy is considered as shared system function in both formalisms. That amount of energy is equal to the corresponding expressions (energy transformations) of the energy stored in the system. Hence, the equivalence among the key variables in both formalisms is first established[7]. For that purpose, it is important to identify the key variables. One of the features of modeling and analysis of dynamic physical systems are the power-conserving transformations [3]. They can present relations between two sets of variables – the complementary power variables, as mathematical abstractions, or as transformations as idealized devices such as electrical transformers, gears, levers or linkages [3]. They can also be linear or nonlinear in their nature. All these similitudes give us a model that is using the same “tools” or main elements in many scientific areas enabling to model multi-disciplinary systems.

2.3 Bond Graphs

Bond graph theory uses the effort-flow analogy to describe physical processes graphically in the form of elementary components (bond graph elements) with one or two ports that represent places where interactions with other processes take place [4].

3. BOND GRAPH APPLICATION TO A HYDRAULIC SUSPENSION SYSTEM

Pneumatic and hydraulic braking and suspension systems are one of the typical modeling problem areas in the field of vehicle dynamics [10]. Usually hydraulic systems are described as a network or as a block diagram [11]. If represented as a network, components are shown as interconnected in order to provide graphical understanding of the real, physical structure. It is common that analogy with electrical Kirchhoff's current law is used to understand the flow rates. Alternately, hydraulic systems might be represented by using standard symbols for hydraulic circuits. In addition, bond graphs can also be used for modeling multi energy domain systems and hydraulic systems[11]. Nowadays, various vehicle stability control systems such as ABS brakes, traction control, and yaw rate control are commercially available[12].

3.1 Presentation of Hydraulic suspension

Suspension is a system of springs, shock absorbers and linkages that connect a vehicle to its wheels and allow relative motion between the two. Hydraulic suspension is another form of suspension setup for modern vehicles which uses four independent dampers filled with hydraulic fluid, controlled by the main control unit inside the vehicle. To develop appropriate control system for it, even though every vehicle subsystem is getting more complex, a thorough in-depth analysis should be designed to exclude everything that is either not strictly essential or would eventually produce more data than needed. Three basic analogies that are appearing in a hydraulic suspension system are between mechanical, hydraulic and electrical areas (Fig. 3). The physical process in engineering system is presented with two variables, the effort and the flow (they are power variables since their product is power) [4].

These variables for a hydraulic suspension system are:

$$\text{Electricity: } U = R * I \quad (2)$$

$$\text{Mechanics: } F = [m*s] * V \quad (3)$$

$$C = [J*s] * w \quad (4)$$

$$\text{Hydraulics: } P = s * Q \quad (5)$$

Where is:

- U – Voltage [V]
- R – Resistance [Ω]
- I – Electrical current [A]
- F – Force [N]
- m – mass [kg]
- s – Laplace variable
- V – Speed [km/h²]
- P – Pressure [N/m²]
- S – Cross-sectional area [m²]
- Q – Volumetric flow rate [m³/s]

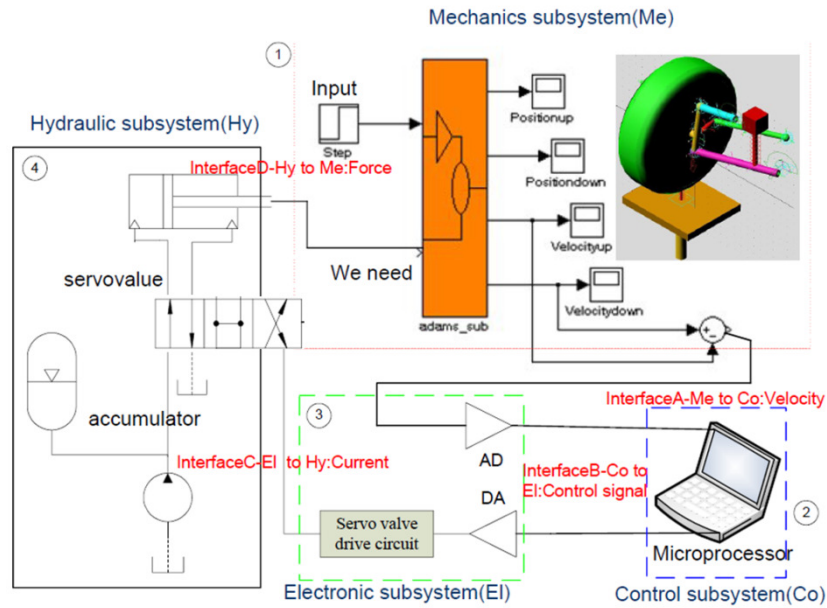


Fig. 1. Collaborative simulation of active suspension – Piston out [13]

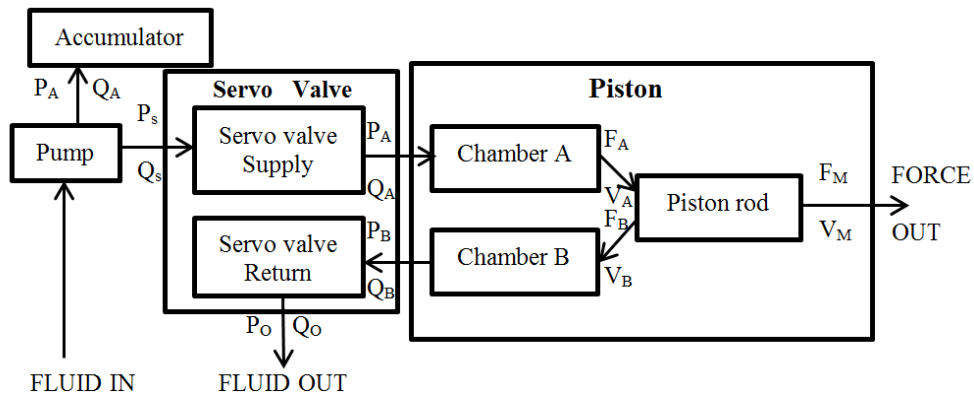


Fig. 2. Block diagram of a hydraulic system model (piston is going out)

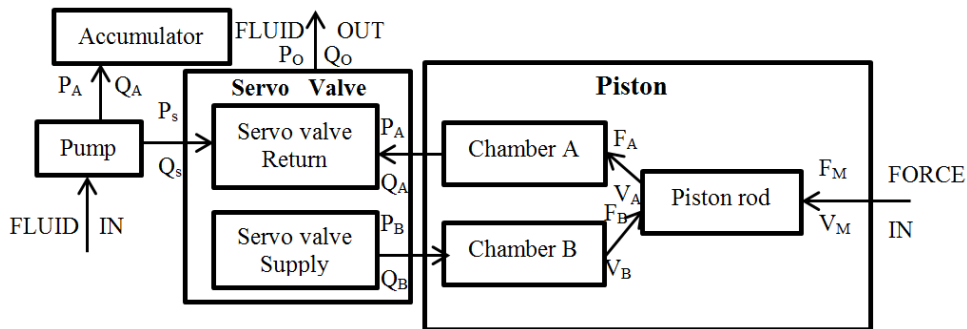


Fig. 3. Block diagram of a hydraulic system model (piston is going in)

Hydraulic subsystem, given in the Fig. 1 is analyzed from the standpoint of preparing for bond graph modeling technique. The system consists of pump, accumulator, servo valve 4/3 that is either closed or when open at its servo valve supply for the hydraulic cylinder Chamber A – position 1. Position 2 is neutral, all lines are closed. Position 3 is for the piston to go back in, in which the servo valves direct fluid supply to Camber B. The process diagram for the piston is going out is given in Fig. 2 and for the situation when piston is going back in is given in the Fig. 3.

Bond graph model for double acting hydraulic cylinder is given in the Fig. 4 [14]. A double-acting piston has two flow outlets (symbolized by the 2 ports at the right hand side), and as such, has two TF elements (transformers) in the bond graph model. The cross-sections of the piston are not equal, due to the presence of the piston rod. An additional C element (storage) is needed to model fluid compressibility in the other chamber. An additional R element (resistive) is used to model internal leakage across the cylinder chambers [14].

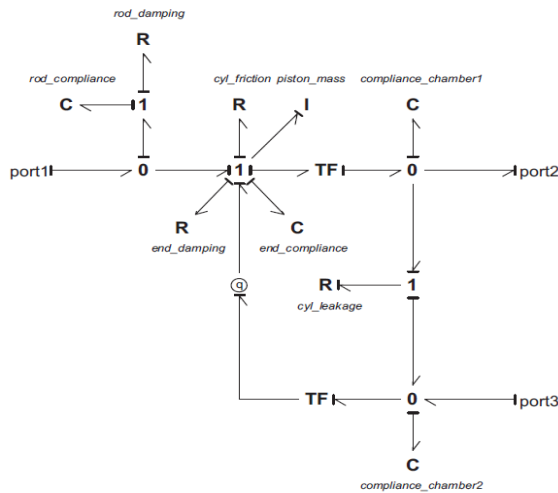


Fig.4. Bond graph - double-acting hydraulic piston [14]

According to Margolis et al. [12], the suspension unit, its schematic and bond graph for each wheel in the car is given in Fig. 5. Realistic kinematics is simplified to the model given in this Fig. The mass m_u , represents the tire and wheel and other mass that moves vertically with the wheel. The suspension components are spring, k_s , damper, b_s , and a force generator, $F_{c_{ij}}$.

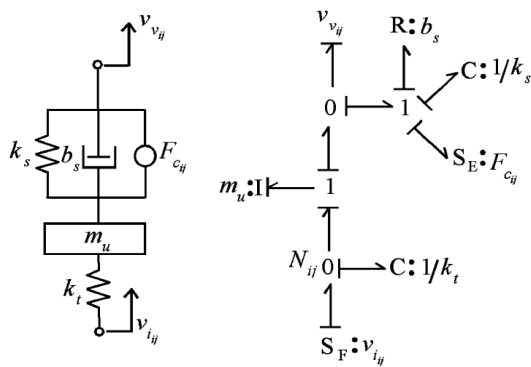


Fig. 5. Schematic/bond graph - suspension unit [12]

The spring and damper may well be nonlinear by inserting the appropriate constitutive law while solving the equations of motion for the entire system. However, for the intended use of the graph theory, the simple linear spring and damper is acceptable.

4. CONCLUSION

Real time simulation is an essential requirement in simulations for vehicle dynamics application since the driver expects an immediate response [9]. For that purpose, methods that would enable real time control of automotive systems have to be multidisciplinary in nature. Bond graph theory, although not so new, has recently gained attention in a scientific community due to its multidisciplinary nature, especially for the application in a mathematical modeling of mechatronics systems. In this paper, an overview of bond graph theory application on one active suspension system has been given.

5. REFERENCES

- [1] Hrovat, D. and W.E. Tobler, *Bond graph modeling of automotive power trains*. Journal of the Franklin Institute, 1991. 328(5-6): p. 623-662.
- [2] Borutzky, W., *Bond Graph Methodology: Development and Analysis of Multidisciplinary Dynamic System Models*. 1 ed 2010: Springer.
- [3] Karnopp, D., *Power-conserving transformations: physical interpretations and applications using bond graphs*. Journal of the Franklin Institute, 1969. 288(3): p. 175-201.
- [4] Damic, V. and J. Montgomery, *Mechatronics by bond graphs: an object-oriented approach to modelling and simulation 2003*, Berlin; New York: Springer.
- [5] Filippo, J.M.-D., et al., *A survey of bond graphs: Theory, applications and programs*. Journal of the Franklin Institute, 1991. 328(5-6): p. 565-606.
- [6] Baaiu, A., et al., *Port-based modelling of mass transport phenomena*. Mathematical & Computer Modelling of Dynamical Systems, 2009. 15(3): p. 233-254.
- [7] Donaire, A. and S. Junco, *Derivation of Input-State-Output Port-Hamiltonian Systems from bond graphs*. Simulation Modelling Practice and Theory, 2009. 17(1): p. 137-151.
- [8] Das, S., *Mechatronic modeling and simulation using bond graphs 2009*, Boca Raton: CRC Press.
- [9] Romero, G., et al., *Efficient simulation of mechanism kinematics using bond graphs*. Simulation Modelling Practice and Theory, 2009. 17(1): p. 293-308.
- [10] Pacejka, H.B., *Modelling complex vehicle systems using bond graphs*. Journal of the Franklin Institute, 1985. 319(1-2): p. 67-81.
- [11] Borutzky, W., B. Barnard, and J.U. Thoma, *Describing bond graph models of hydraulic components in Modelica*. Mathematics and Computers in Simulation, 2000. 53(4-6): p. 381-387.
- [12] Margolis, D. and T. Shim, *A bond graph model incorporating sensors, actuators, and vehicle dynamics for developing controllers for vehicle safety*. Journal of the Franklin Institute, 2001. 338(1): p. 21-34.
- [13] Wang, H., S. Wang, and M.M. Tomovic, *Active suspension integrated design and simulation based on Collaborative Optimization*. Journal of Automobile Engineering, 2012. manuscript.
- [14] Kurniawan, A., E. Pedersen, and T. Moan, *Bond graph modelling of a wave energy conversion system with hydraulic power take-off*. Renewable Energy, 2012. 38(1): p. 234-244.

Authors: **Dr. Vukica Jovanovic**, Mechanical Engineering Technology, Old Dominion University, 1 Old Dominion University, Norfolk, VA 23529, U.S.A., Phone: +1 757 683-3769; **Nicolas Langroudi**, Institut Français de Mécanique Avancée (IFMA), Campus de Clermont-Ferrand les Cézeaux - BP265, 63175 AUBIERE Cedex, France; **Dr. Mileta M. Tomovic**, Mechanical Engineering Technology, Old Dominion University, 1 Old Dominion University, Norfolk, VA 23529, U.S.A., Phone: +1 757 683-3775
E-mail: v2jovano@odu.edu
nlangroudi@gmail.com
mtomovic@odu.edu

Karpe, B., Kosec, B., Gojić, M., Anžel, I., Kitak, S., Bizjak, M.

MATHEMATICAL MODELING OF THE MELT COOLING RATE IN THE MELT-SPINNING PROCESS

Abstract: Rapid solidification of metallic melts is important for the development of the advance metallic materials, because enables the production of new alloys with superior properties according to conventionally treated alloys. In practice it turned out, that single roll melt spinning process has one of the highest melt cooling rates among all continuous casting processes. But, because very short solidification time and movement of the melt and substrate, melt cooling rate is very difficult to measure with confidence. Primary goal of our work was to determine the limits of cooling rate over the ribbon thickness and to outline, which property or typical feature of the process has the greatest influence on cooling rate of the melt. On the basis of developed mathematical model, a computer program was made and used for melt cooling rate calculation in the melt-spinning process. Our calculations show that distance from the contact surface in relation to the thermal properties of the melt, chilling wheel material and contact resistance between metal melt and chilling wheel have the greatest influence on melt/ribbon cooling rate. In the case of continuous casting, significant long term surface temperature increase may take place, if the wheel is not internally cooled. Comparison between cooling rates calculated at various thermal resistance assumptions of particular constituents is outlined. New method for determining contact resistance through variable heat transfer coefficient is introduced which takes into account physical properties of the casting material, process parameters and contact time/length between metal melt/ribbon and substrate and enables cooling rate prediction before the experiment execution.

Key words: Rapid solidification, Metallic materials, Melt-spinning, Cooling rate, Mathematical modeling

1. INTRODUCTION

Rapid solidification (RS) of metallic melts is important for the development of the advance metallic materials, because enables the production of new alloys with superior properties according to conventionally treated alloys [1]. What is the speed of solidification, which divides between classical procedures of casting and rapid solidification, is not exactly specified. Differences in interpretation refer to the development of final microstructure, but the characteristic of all rapid solidification techniques is a final non-equilibrium state of the microstructure [2], which can be seen as: refined grains, extended solubility in metal matrix, quantitative and qualitative change of microstructural constituents, reduced micro segregation, etc.

In general, rapid solidification of melts could be achieved by two approaches:

- with high undercooling of the melt prior solidification, by reduction or even elimination of heterogeneous nucleation sites in so called containerless processes (atomization, droplet emulsion technique, drop tube technique, magnetic levitation, etc.)
- with rapid cooling to bypass heterogeneous nucleation kinetically (melt-spinning, splat quenching, remelting of surface layer, etc.) [3].

Single roll melt spinning (Fig. 1) is one of the most commonly used processes for rapid solidification. Its major advantage is the possibility of continuous production of rapidly solidified material in the form of

thin ribbons or foils, even on large industrial scale [4]. In this technique, a thin stream of melt is directed onto a circumferential surface of a rotating wheel, where so called melt puddle forms (Fig. 2).



Fig. 1. Melt-spinner - Faculty of Natural Science and Engineering, University of Ljubljana

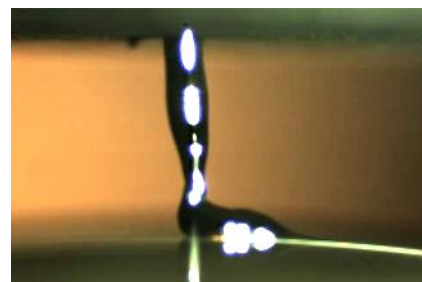


Fig. 2. Close-up speed camera snap shot of the melt puddle (tin casting) on the circumferential surface of the chill wheel, free jet melt-spinning

Ribbon is then dragged out from the puddle by relative motion of the wheel. Microstructure of the ribbon can be completely crystalline, amorphous or combined and depends upon the contact resistance between the melt and substrate, latent heat of crystallization of casting material, heat transfer in the melt and the wheel, and nucleation and crystal growth characteristics of the particular casting material [5].

2. HEAT TRANSFER CALCULATION

For calculation of temperature distribution inside the melt puddle and chill wheel, we used explicit finite difference method (FDM) with cylindrical coordinate system. Thermal properties of the melt and wheel

$$\frac{1}{r} \cdot (\lambda \cdot \frac{\partial T}{\partial r}) + \frac{\partial}{\partial r} \cdot (\lambda \cdot \frac{\partial T}{\partial r}) + \frac{1}{r^2} \cdot \frac{\partial}{\partial \varphi} \cdot (\lambda \cdot \frac{\partial T}{\partial \varphi}) + q''' = \rho \cdot c \cdot \frac{\partial T}{\partial t} \quad (1)$$

And for chill wheel, where no latent heat is released:

$$\frac{1}{r} \cdot (\lambda \cdot \frac{\partial T}{\partial r}) + \frac{\partial}{\partial r} \cdot (\lambda \cdot \frac{\partial T}{\partial r}) + \frac{1}{r^2} \cdot \frac{\partial}{\partial \varphi} \cdot (\lambda \cdot \frac{\partial T}{\partial \varphi}) = \rho \cdot c \cdot \frac{\partial T}{\partial t} \quad (2)$$

Where r , φ represent spatial coordinates in cylindrical coordinate system [m; rad], T temperature [K], ρ density [kgm^{-3}], λ thermal conductivity [$\text{Wm}^{-1}\text{K}^{-1}$], c specific heat of the melt or chill wheel material [$\text{Jkg}^{-1}\text{K}^{-1}$], and q''' volumetric heat generation rate [Wm^{-3}].

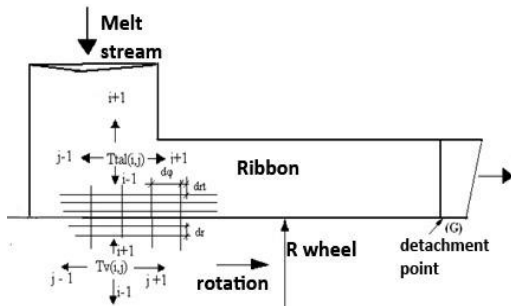


Fig. 3. Idealized geometry of the melt puddle used in mathematical model

Ribbon thickness is assumed to be proportional to circumferential velocity of the chill wheel ($uw-1$) and the pressure in the crucible ($p0.5$), as predicted by continuity and Bernoulli equations. Temperature of the melt in the puddle direct under the impinging jet stays equal to casting temperature, because strong turbulences in that region. To ascertain the influence of the casting material thermal properties, chill wheel material, inner and external cooling of the chilling wheel, and contact resistance on cooling rate of the ribbon, comparison between calculated cooling rates at various assumptions was made: ideal isothermal wheel versus copper wheel, influence of various contact resistance, and influence of solidified ribbon thickness.

3. RESULTS AND DISCUSSION

Fig. 4. represents calculated cooling curves of contact and free surface of cast ribbons in the case of an assumption of ideal isothermal cooling wheel and Fig. 5. calculated cooling curves as a function of the

material ($\lambda(T)$, $c(T)$) are temperature dependent and calculated for each iteration step with linear interpolation from tabulated values of particular casting material. Density in solidification interval of the casting material is changing linearly, whereas density of the wheel material is approximated as constant. Because melt puddle is thin compare to its width and length we made an assumption of two-dimensional (2D) transient heat transfer. A schematic diagram of the idealized melt puddle geometry used in mathematical model is shown in Fig. 2. Assuming 2D transient heat transfer with variable thermal properties and internal heat generation (latent heat of crystallization), general partial differential equation for the melt is reduced to:

distance from the contact surface.

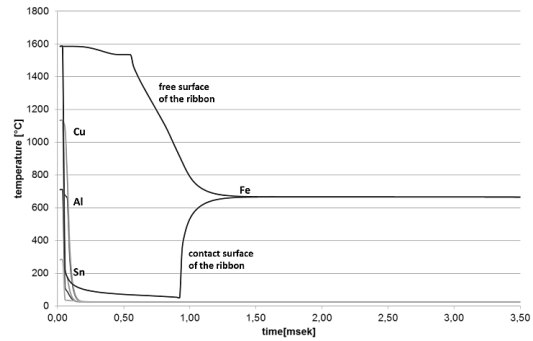


Fig. 4. Calculated cooling curves of free and contact surface of ribbons under assumption of ideal isothermal wheel

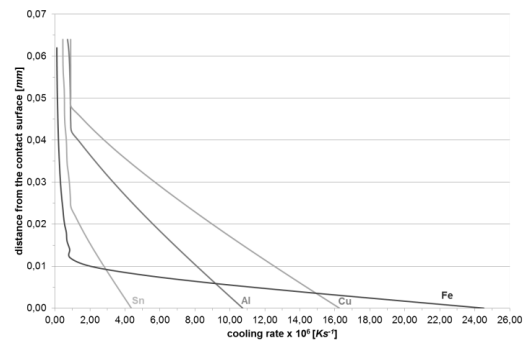


Fig. 5. Cooling rate as a function of a distance from the contact surface (Ideal isothermal wheel, ideal contact)

Calculations under assumption of ideal isothermal wheel indicate that 60 μm thick ribbon would cool down to chill wheel temperature in an instant of time for most of the cast materials. The only exception is iron, as an example of material with high volumetric latent heat of crystallization, high melting point and relatively low thermal conductivity, where cooling rate of the 60 μm thick ribbon free surface is much lower ($\approx 10^5$) than cooling rate of the contact surface

($\approx 2.5 \cdot 10^7$). Since in this calculation only takes into account the physical properties of the melt, we can conclude, that thermal properties of the melt itself, have significant influence on cooling rate across the transverse cross-section of the cast ribbon. Higher is the volumetric heat of crystallization of casting material ($\Delta H_{Fe} > \Delta H_{Cu} > \Delta H_{Al} > \Delta H_{Sn}$), steeper will be melt cooling rate decrease, as a function of a distance from contact surface. When a layer of melt of a certain thickness solidifies, represent the only heat resistor and therefore the cooling rate in the remaining melt depends mainly on the thermal conductivity ($\lambda_{Cu} > \lambda_{Al} > \lambda_{Sn} > \lambda_{Fe}$) of this solidified layer.

The next stage in calculations of heat transfer from the melt is to take into account real wheel material (copper) with finite thermal diffusivity (Fig. 6). If we compare the calculation results to the results under assumption of ideal isothermal wheel, for all materials significantly longer solidification time, lower melt cooling rate over entire transverse cross section of a ribbon (Fig. 7), and higher final temperature of the ribbon after detachment from the circumferential surface of the wheel is observed, although ribbon is only 60 μm thick.

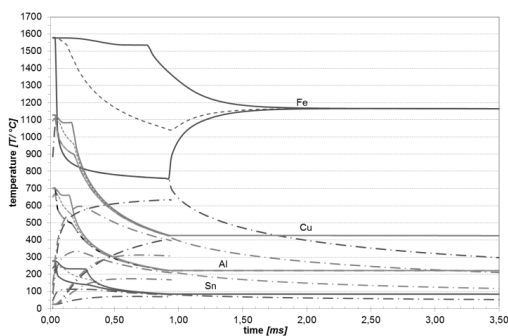


Fig. 6. Calculated cooling curves of contact and free ribbon surface cast on copper wheel. Hatched curves represent heating rate of copper wheel surface and 0.1 or 0.3 mm beneath the surface (thickness of cast ribbons 60 μm , contact time 0 – 923 ms, ideal contact)

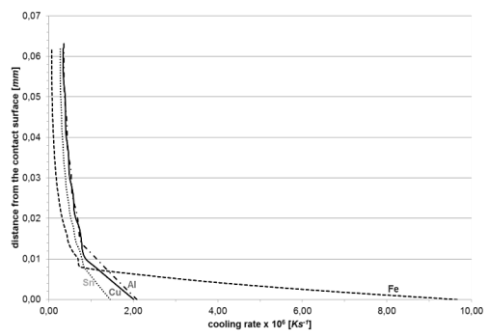


Fig. 7. Cooling rate as a function of a distance from the contact surface (copper wheel, ideal contact)

Decreased cooling rate of the melt and increased wheel surface temperature results from a fact that a high heat transfer takes place over short period of time. In spite of the high thermal diffusivity of copper, energy has no time to diffuse much into the wheel, and the surface of the wheel will heat up significantly.

Consequently, because smaller temperature difference between the melt and the surface of the wheel, heat transfer rate and thus cooling rate of the remaining melt will also be reduced. Assumption of ideal isothermal wheel is not physically realistic, because real materials can't absorb so much energy without heating up significantly.

Among thermal properties of the melt, volumetric heat of crystallization have major influence on melt cooling rate across the transverse cross-section of the cast ribbon. Fig. 8 represent contact and free surface cooling curves of Al ribbon in dependence of the amount of the released crystallization heat. If we assume 50 % lower crystallization heat, solidification time for free surface of 60 μm thick ribbon will decrease for 30 %, and when amorphous solidification is presumed, 50 % shorter is the time of solidification.

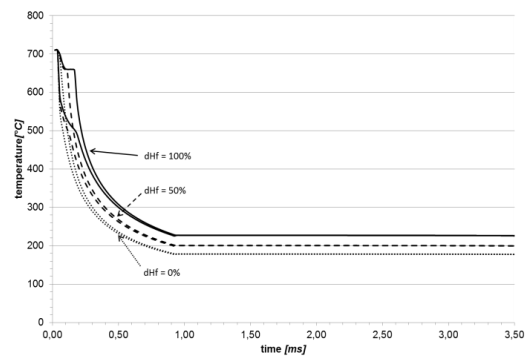


Fig. 8. Hypothetical calculated cooling curves of free and contact surface of Al ribbon as a function of different assumptions of latent heat of crystallization (ribbon thickness 60 μm , contact time 0.923 msec, ideal contact)

In situations where a detailed description of thermal physics is very complicated, such as in melt-spinning process, combined modes of heat exchange are usually taken in to account with the overall heat transfer coefficient (α), which includes conduction and radiation of heat, as well as any convective effects. Ideal contact between the melt and wheel surface is not physically realistic, because there are no metallic atomic bonds between atoms of the melt and atoms of the surface of the wheel. By applying different values of heat transfer coefficient into calculations of heat transfer between melt and copper wheel surface, influence of contact resistance on cooling rate (Fig. 9) could be estimated. In comparison to ideal contact (Fig. 6,7), cooling rate of the ribbon and cooling rate as a function of a distance from the contact surface (Fig. 9) are relatively much lower when some contact resistance is considered, although the contact resistance value is very low ($10^{-6} \text{ (m}^2 \cdot \text{K) / W}$). Value for constant contact resistance for aluminum was obtained with subsequent microstructure analyses and reported by other authors [6]. Integral method calculation of the heat transfer coefficient gives the most logical results for entire duration of the contact. Calculated solidification time is practically the same to those obtained by overall (constant) heat transfer coefficient, but final temperature of the ribbon at the detachment point is

much greater, especially for longer contact time. Constant contact resistance approximation ($10^{-6}(\text{m}^2\cdot\text{K})/\text{W}$) for longer contact time predicts even lower ribbon temperature than ideal contact calculation, which is physically unlikely. The local heat transfer coefficient $\alpha(x)$ is calculated with the integral method for liquid metals flow over flat plate [7]. The equation for local heat transfer coefficient $\alpha(x)$ calculation, included in the numerical scheme is:

$$\alpha(x) = \frac{3 \cdot \lambda}{2 \cdot \sqrt{8}} \cdot \sqrt{\frac{u_w}{a \cdot x}} \quad (3)$$

Where u_w represent circumferential velocity of the wheel [ms^{-1}], λ thermal conductivity of the casting material [$\text{Wm}^{-1}\text{K}^{-1}$], a temperature diffusivity of the casting material [m^2s^{-1}], and x distance from the initial contact point to the actual calculation point [m].

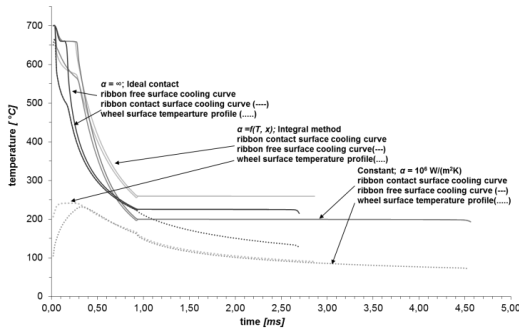


Fig. 9. Cooling curves of free and contact surface of Al ribbon and contact surface of the copper wheel as a function of different contact resistance (ribbon thickness $60 \mu\text{m}$, contact time 0.923 msec)

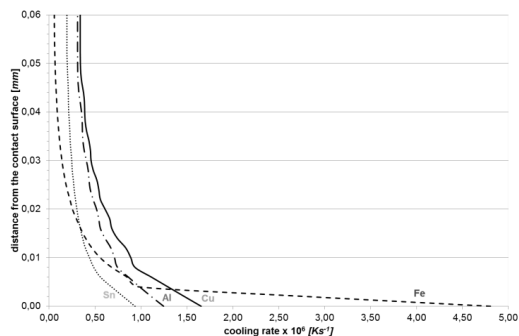


Fig. 10. Cooling rate as a function of a distance from the contact surface for different cast materials ($\alpha(x)$ = integral method)

Fig. 11 shows calculated temperature profiles in steel or copper wheel, when aluminum melt is cast. As we can see, surface temperature will increase significantly, especially for a wheel of low thermal diffusivity. Because limited thermal diffusion in the wheel, the energy can penetrate only a short distance in the wheel, which results in a higher temperature at the wheel surface. The magnitude of temperature increase depends on the wheel material. For steel wheel, which has much lower thermal diffusivity than copper, an increase of surface temperature is over $400 \text{ }^\circ\text{C}$, and heat penetration depth about 0.5 mm . On contrary, copper

wheel surface temperature increase is about $200 \text{ }^\circ\text{C}$ and penetration depth twice as much.

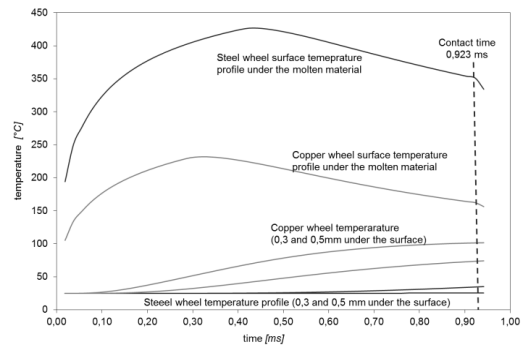


Fig. 11. Wheel temperature increase as a function of contact time and wheel material (Al casting)

Irrespective of contact resistance approximation, when aluminum melt is cast, the wheel surface temperature after reaching its maximum decrease, although it is in contact with hotter ribbon. This seems unlikely, but if we consider the wheel as a whole, its enthalpy is constantly rising, since temperature more than 0.3mm under the surface is increasing the entire contact time. Namely, conduction heat transfer rate in the wheel is faster than the heat transfer rate across ribbon/wheel interface and through solidified ribbon.

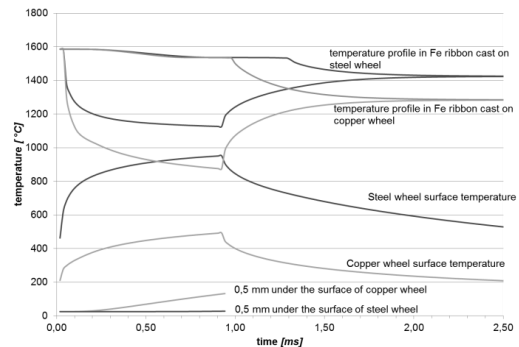


Fig. 12. Cooling curves for Fe ribbon and temperature profile in the wheel as a function of chill wheel material (ribbon thickness $60 \mu\text{m}$, contact time 0.923 msec , $\alpha = \text{const. } 10^6 \text{ W/m}^2\text{K}$)

When materials with higher melting point are cast, surface temperature will increase much higher (Fig. 12). Obviously, such a large deviation in calculation of cooling and solidification rate of the melt. Importance of wheel material selection is evident. Pure deoxidized copper has the highest thermal diffusivity between all commercially useful materials and therefore is the best choice for the wheel material. In the case of the need for increased strength, oxide dispersive strengthened (ODS) copper alloys are best solution. When thicker ribbons are cast or materials with lower thermal conductivity, thermal resistance in already solidified region of the ribbon becomes the limiting factor of the heat transfer. High cooling and solidifying rates, through entire cross section of the ribbon can be achieved only when very thin ($< 30 \mu\text{m}$) ribbons are cast (Fig. 13, 14).

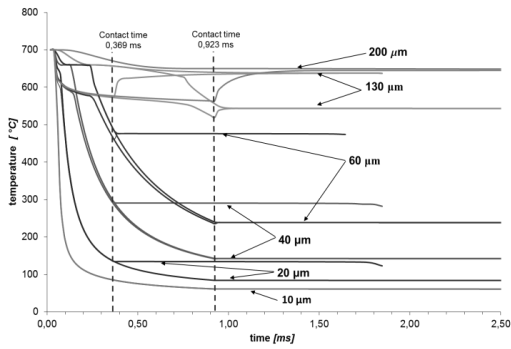


Fig. 13. Cooling curves of aluminum ribbon as a function of its thickness ($\alpha(x)$ = integral method)

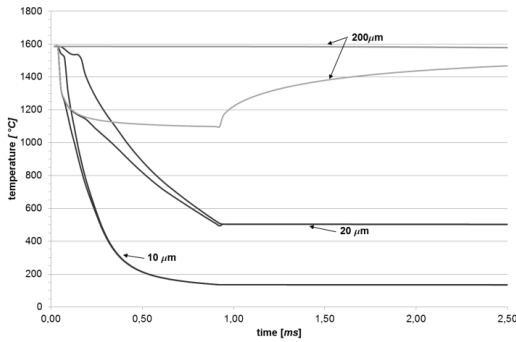


Fig. 14. Cooling curve of iron ribbon as a function of its thickness ($\alpha(x)$ = integral method)

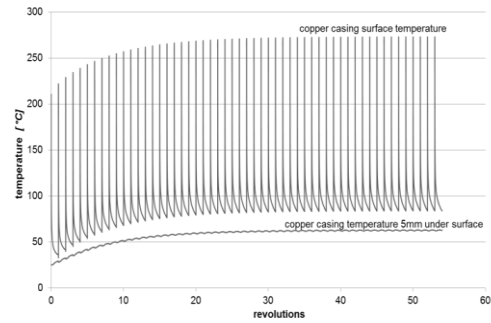
During continuous casting process, significant “long term” surface temperature increase may take place, if the wheel is not externally or internally cooled. In calculations discussed above, we have assumed that the wheel surface is at room temperature at the beginning of the contact.

For first ten to hundred revolutions surface temperature increase may indeed not be significant, but when continuous casting is performed, especially when materials with high melting point are cast, surface temperature of the wheel can increase in such an extent, that formation of the ribbon will be disturbed, because of decreased cooling and solidifying rate in the melt puddle.

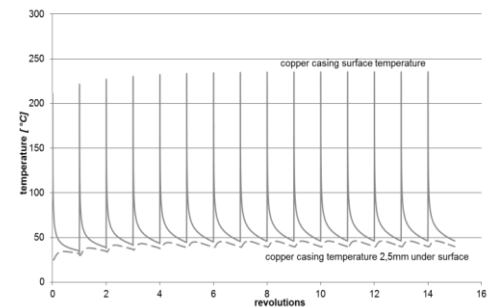
Fig. 15 shows calculated temperature profiles in inner water cooled wheel ($R_w = 0.2$ m) with different casing thickness. From the outside, wheel is convectively cooled with surrounding atmosphere, and from the inside with water stream. For simplicity of the mathematical model, convective heat transfer coefficients are taken as constants ($\alpha_{water} = 5000$ W/(m²·K) and $\alpha_{air} = 50$ W/(m²·K)) and represent average values, calculated from forced convection correlation equations. No radiation from the crucible is taking into account. To ascertain influence of external cooling, we also make an assumption of exaggerated value for convective heat transfer coefficient ($\alpha_{air} = 1000$ W/(m²·K)).

Each saw tooth spike corresponds to the temperature of the wheel surface being underneath the puddle. As we can see, internally water cooled wheel will reach the periodic steady state after few revolutions. Conducting of heat into the wheel and cooling of the inner casing surface with water stream is

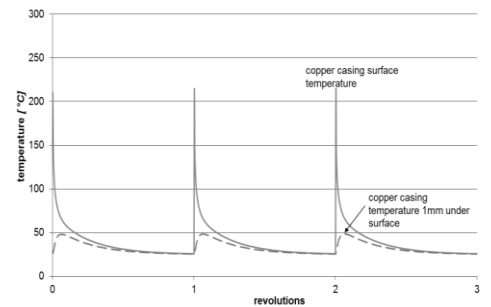
much faster than external convective cooling with surrounding atmosphere. If we reduce wheel casing thickness up to 2 mm, internal water cooling will be more effective, and wheel surface temperature that melt will effectively “feel” at the beginning of the next pass of the wheel under the puddle, will be practically the same as at the first revolution (Fig. 7c), even if high melting temperature materials are cast.



a) 10 mm thick casing



b) 5 mm thick casing



c) 2 mm thick casing

Fig. 15. Surface temperature of the internally water cooled wheel as a function of copper casing thickness a) 10 mm b) 5 mm c) 2 mm (aluminum casting, wheel radius 0.2 m)

But if we reduce wheel casing even further, beneath the heat penetration depth under the melt puddle, convective heat resistance on the inner side (wheel – water interface) becomes significant (Fig. 16). Even if we assume heat transfer coefficient value on inner side of a casing as high as 100000 W/(m²·K), which can be reached only with high pressure impingement water jets [8], heat removal from the melt will still be slower as in the case of full or internally water cooled wheel with 10 mm thick casing (Fig. 15a). Reducing the thickness of the wheel casing is

unsuitable, from rapid solidification and from steadiness point of view.

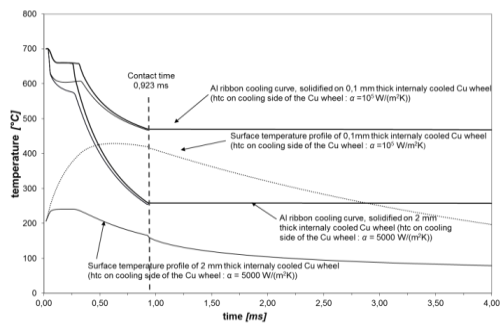


Fig. 16. Temperature profile in aluminium ribbon and surface temperature of the internally water cooled wheel as a function of copper casing thickness (0.1 and 2 mm thick casing)

In the case of external cooling with gas, “long term” surface temperature increase is practically the same as in the case without external cooling, although we assume exaggerated value [7,8] ($\alpha_{\text{air}} = 1000 \text{ W}/(\text{m}^2\cdot\text{K})$) for convective heat transfer coefficient. Namely, duration of one revolution of the wheel is so short that external gas convective cooling would have significant influence on the wheel surface temperature.

4. CONCLUSIONS

In our numerical model (FDM), new method for determining contact resistance through variable heat transfer coefficient is introduced which takes into account physical properties of the casting material, process parameters and contact time/length between metallic melt or metallic ribbon and substrate respectively, and enables cooling and solidifying rate prediction before the experiment execution.

Comparison of the results, acquired at different assumptions of heat transfer resistances shows, that heat contact resistance between the melt and the chill wheel, and finite thermal diffusivity of the wheel material have grate influence on cooling rate of the ribbon an must not be neglected in heat transfer calculations. The fact that the wheel surface temperature is increasing significantly under the melt puddle, selection of the wheel material is not trivial. Because copper has the highest thermal diffusivity between all commercially useful materials, we propose deoxidized copper for a wheel material, and in the case of the need for increased strength, oxide dispersive strengthened (ODS) copper alloys.

For continuous casting, internally cooled wheel is preferable, but only in the case, when wheel casing thickness is correctly selected. When too thick casing is applied, water cooling will not have adequate influence on wheel surface temperature increase. When the casing of the wheel is too thin, thermal resistance on the cooling side becomes the limiting factor, which reduces the heat transfer from the melt and consequently its cooling and solidifying rate.

ACKNOWLEDGEMENT

The authors want to thank professor Ladislav Kosec (University of Ljubljana) for mentorship at study of rapid solidification and development of advanced shape memory materials, professor Albert C. Kneissl (University of Leoben) for scientific cooperation at synthesis and characterization of rapidly solidified alloys, and professor Mirko Soković (University of Ljubljana) for technical informations and discussions.

5. REFERENCES

- [1] Libermann, H.H.: *Rapidly solidified alloys*, Marcel Dekker, London, 1993.
- [2] Lojen, G., Anžel, I., Kneissl, A.C., Unterweger, E., Kosec, B., Bizjak, M.: *Microstructure of rapidly solidified Cu-Al-Ni shape memory alloy ribbons*, Journal of Materials Processing Technology, p.p. 220-229, 2005.
- [3] Herlach, D., Galenko, P., Holland, A., Moritz, D.: *Metastable solids from undercooled melts*, Pergamon Materials Series, London, 2006.
- [4] Karpe, B., Kosec, B., Kolenko, T., Bizjak, M.: *Heat transfer analyses of continuous casting by free jet meltspinning device*, Metallurgy, 50 (2011) 1, p.p. 13-16, 2011.
- [5] Collins, L.E.: *Overview of rapid solidification technology*, Canadian Metallurgy Quarterly, 25 (1986) 2, p.p. 59-71, 1986.
- [6] Wang, G.X., Matthys, E.F.: *Modeling of rapid solidification by melt spinning: effect of heat transfer in the cooling substrate*, Material Science and Engineering, A136 (1991), p.p. 85-97, 1991.
- [7] Karpe, B., Kosec, B., Bizjak, M.: *Modeling of heat transfer in the cooling wheel in the melt-spinning process*, Journal of Achievements in Materials and Manuf. Engineering, 46 (2011) 1, p.p. 88-94, 2011.
- [8] Ciofalo, M., Piazza, I. Di, Brucatto, V.: *Investigation of the cooling of hot walls by liquid water sprays*, International Journal of Heat and Mass Transfer, 42 (1999), p.p. 1157-1175, 1999.

Authors: Dr. Blaž Karpe, Prof. Dr. Borut Kosec, M.Sc. Sonja Kitak, Ass. Prof. Dr. Milan Bizjak, University of Ljubljana, Faculty of Natural Sciences and Engineering, Aškerčeva 12, 1000 Ljubljana, Slovenia, Phone: +386 1 20 00 410, Fax: +386 1 47 04 560.

E-mail: blaz.karpe@omm.ntf.uni-lj.si
borut.kosec@omm.ntf.uni-lj.si
sonja.kitak@guestarnes.si
milan.bizjak@omm.ntf.uni-lj.si

Prof. Dr. Mirko Gojić, University of Zagreb, Faculty of Metallurgy, Aleja narodnih heroja 3, 44103 Sisak, Croatia, Phone: +385 43 533 379, Fax: +385 43 533 380.

E-mail: gojic@simet.hr

Prof. Dr. Ivan Anžel, University of Maribor, Faculty Mechanical Engineering, Smetanova 17, 2000 Maribor, Slovenia, Phone: +386 2 220 78 65, Fax: +386 2 220 79 29.

E-mail: ivan.anzel@uni-mb.si

Kraišnik, M., Vilotić, D., Šidanin, L., Petrović, Ž.

INITIAL MICROSTRUCTURE STATE IMPACT TO STEEL C45E FORMABILITY

Abstract: Material formability is ability of permanent change in shape and dimensions of specimen without occurrence of cracks or other forms of damage to the structure itself. This ability is numerically valorized by size of effective limit strain and it depends on the type of material, initial structure and forming conditions.

In this paper we analyzed initial microstructure state impact to steel C45E (Č 1531) formability in various forming processes (upsetting, torsion and tension). Research of steel C45E was conducted on specimens in normalized state and after that we performed comparison to results showing formability of the same material with soft annealed initial structure

Key words: Material formability, Initial microstructure, Forming limit diagram, Cold upsetting

1. INTRODUCTION

Optimal design of plastic forming technological processes is mainly based on research directed to behavior of certain material in different forming conditions from the aspect of achieving maximum strain values. This approach provides establishment of rational production concept for metal components in complex geometrical shapes and with excellent mechanical characteristics.

Key item in the area of forming and use of metals through which relationship between material behavior within forming system, process parameters and external conditions during plastic forming is established is formability. Essentially, formability is very complex material attribute which is directed to estimation of ability to permanently change shape under certain forming conditions without occurrence of cracks, deformation localization or any other unwanted form of surface damage or damage to the inner specimen structure. We can use any physical quantity as forming limit indicator, as long as it represents quantitative level of damage to the material structure under certain forming conditions [2].

However, it is generally accepted that in bulk forming processes numerical indicator of metal formability is effective strain value (φ_e^l) in the critical forming zone at the moment cracks or localized deformation occur.

Formability of certain material depends on large number of factors which can generally be divided into two groups: material factors and factors of forming conditions [1-3]. Implicit form of this function is represented with equation (1):

$$F_M \equiv \varphi_e^l = f(H_M, S_M, T_O, \varphi, T_\sigma \dots) \quad (1)$$

If we limit consideration of equation (1) to a specific material with precise chemical structure (H_M), with previously defined initial state structure (S_M), under cold forming conditions ($T_O = \text{const}$), under conventional forming conditions ($\varphi = \text{const}$), we can state that under those circumstances state of stress

represented by stress tensor (T_σ) presents pronounced and dominant impact to material formability:

$$F_M = f(T_\sigma) = f(\beta) \quad (2)$$

Where:

β - is state of stress indicator in the specimen critical zone.

Graphical interpretation of equation (2) is forming limit diagram. In order to define it we use three basic forming models (uni-axial tension- $\beta = +1$, torsion- $\beta = 0$ and uni-axial upsetting- $\beta = -1$) [3], Fig. 1.

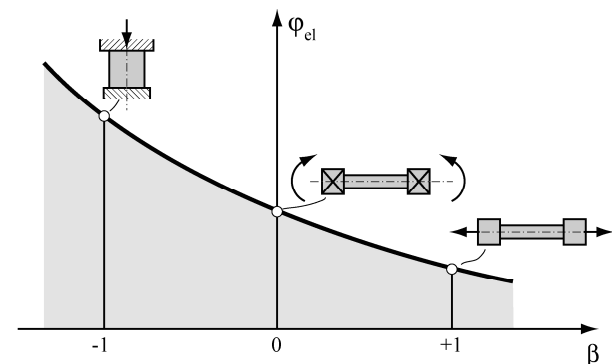


Fig. 1. Forming limit diagram - Basic models [1, 3]

In this paper we presented steel C45E formability results for basic forming models in which we further on integrated data obtained by upsetting of tapered specimen by flat plate. Experimental research is conducted on specimens in normalized state. After that we performed comparison of strain limits for basic models whose initial microstructure is equivalent to soft annealed state, based on the results presented in this paper [1].

Aim of research presented in this paper is establishing forming limit abilities of steel C45E under normalized conditions and under soft annealing conditions of initial microstructure.

2. STRESS-STRAIN RELATIONSHIP DURING FREE UPSETTING PROCESS

The first step in research of formability in certain process of plastic forming is experimental and numerical identification of the place where critical damage to the material structure occurs. In the free upsetting processes cracks are characteristic to the free surfaces on the specimen which occur as a consequence of pressure on contact surfaces of tool and work-piece. Actually, tension components of stress lead to nucleation, growth and coalescence of cracks at the free surface and they are often called secondary stress because they do not occur as a consequence of immediate action of executive machine part. Considering the fact that radial stress component is not generated on the free surfaces of the specimen during plastic forming processes nor there are any friction mechanisms present due to inability to have direct contact with the tool, identification of stress-strain state in the critical damage area on the specimen became easier.

Starting with relation which connects stress-strain components in the area of plastic flow (3), pattern through which hydrostatic stress is defined (4) and using Von Misses yield criterion (5):

$$\frac{d\varphi_\theta}{\sigma_\theta - \sigma_m} = \frac{d\varphi_z}{\sigma_z - \sigma_m} \quad (3)$$

$$\sigma_m = \frac{\sigma_r + \sigma_\theta + \sigma_z}{3} = \frac{\sigma_\theta + \sigma_z}{3} \quad (4)$$

$$\sigma_\theta^2 + \sigma_z^2 - \sigma_\theta \cdot \sigma_z = \sigma_e^2 \quad (5)$$

Vujović and Shabaik [3] defined equations for defining stress components σ_z and σ_θ in the place where crack occurred:

$$\sigma_z = \pm \sigma_e \cdot \left[1 - \left(\frac{1+2\alpha}{2+\alpha} \right) + \left(\frac{1+2\alpha}{2+\alpha} \right)^2 \right]^{\frac{1}{2}} \quad (6)$$

$$\sigma_\theta = \sigma_z \cdot \left(\frac{1+2\alpha}{2+\alpha} \right) \quad (7)$$

Based on previous equations, indicator of state of stress β can be defined as follows:

$$\beta = \frac{\sigma_r + \sigma_\theta + \sigma_z}{\sigma_e} = \frac{1 + \frac{1+2\alpha}{2+\alpha}}{\sqrt{1 - \frac{1+2\alpha}{2+\alpha} + \left(\frac{1+2\alpha}{2+\alpha} \right)^2}} \quad (8)$$

Where:

σ_r , σ_θ and σ_z – are components of main stresses in the direction of r , θ and z axis,

σ_m – is hydrostatic stress,

σ_e – is effective stress.

Coefficient α represents deformation accrual rate and it is defined with the following pattern (9):

$$\alpha = \frac{d\varphi_\theta}{d\varphi_z} \quad (9)$$

In order to apply previous equation it is necessary to determine “strain path“ $\varphi_\theta = f(\varphi_z)$. In this paper dependence in question is approximated with second

degree polynomial:

$$\varphi_\theta = f(\varphi_z) = A\varphi_z + B\varphi_z^2 \quad (10)$$

Where:

A and B are coefficients of approximated function.

Principal strain components φ_z , φ_θ and φ_r in the critical zone of the specimen are determined according to the height of the marked area Z (Fig. 2) and specimen size in equatorial plane, using incompressibility condition:

$$\varphi_z = \ln \frac{Z_i}{Z_0}, \quad \varphi_\theta = \ln \frac{D_i}{D_0}, \quad \varphi_r = -(\varphi_z + \varphi_\theta) \quad (11)$$

Where:

Z_0 and D_0 – are initial values of marked area height and specimen size,

Z_i and D_i – are values of marked area height and specimen radius after i upsetting phases.

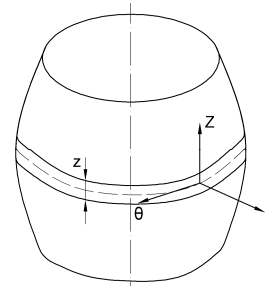


Fig. 2. Cylindrical specimen after deformation [1]

Effective strain at the lace cracks occurred is determined according to the following pattern (12):

$$\varphi_e = \frac{\sqrt{2}}{3} \sqrt{(\varphi_z - \varphi_\theta)^2 + (\varphi_\theta - \varphi_r)^2 + (\varphi_r - \varphi_z)^2} \quad (12)$$

In formability tests which are based on non-monotonous plastic forming processes it is necessary to identify change in state of stress indicators β during forming and during defining forming limit diagram it is necessary to use average value β_{av} , which is determined as follows [1, 4]:

$$\beta_{av} = \frac{1}{\varphi_e^I} \int_0^{\varphi_e^I} \beta(\varphi_e) d\varphi_e \quad (13)$$

Here:

$\beta(\varphi_e)$ – is forming process history which is state of stress indicator of change serving as function of effective strain at the place the crack occurred.

In order to determine average value of state of stress indicator β_{av} we observe that if the critical material damage occurs at the free surface of the specimen, we can also use methodology based on flow theory [4, 5]. In this case average value of β -factors is determined according to strain limits:

$$\beta_{av} = \frac{2}{\varphi_e^I} (\varphi_1^I + \varphi_2^I) \quad (14)$$

Where:

φ_1 and φ_2 – are components of principal logarithm strains in the zone cracks occurred,

φ_e^I – effective strain at the moment specimen is destroyed.

Effective limit strain is determined by numeric integration of the following equation (15):

$$\varphi_e^l = \frac{2}{\sqrt{3}} \int_0^{\varphi_z^l} [1 + A + 2B\varphi_z + (A + 2B\varphi_z)^2]^{\frac{1}{2}} d\varphi_z \quad (15)$$

3. EXPERIMENTAL RESEARCH

Experimental research was conducted in two phases. In the first phase we used basic forming models and defined FLD for C45E steel. Second phase was directed towards research of limit formability of normalized tapered samples while upsetting by flat plates.

3.1 Normalized material microstructure

Upsetting process of cylindrical specimens by flat plates was realized incrementally until cracks occurred at the free surface. For the research purposes we used 3 samples with initial dimensions $\varnothing 20 \times 25$ mm (Fig. 3a).

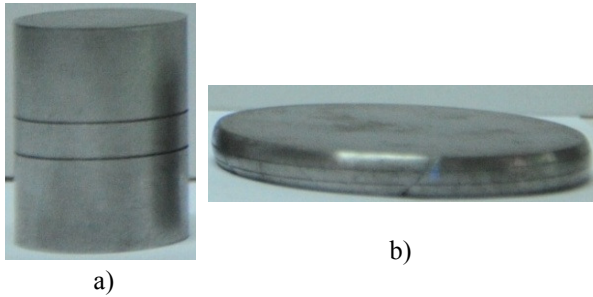


Fig. 3. Upsetting of cylinder by flat plates
a) initial specimen, b) specimen after forming

Strain components in the critical zone are determined according to identification of marked area change in height ($Z_0=4$ mm) and initial specimen radius D_0 in different phases of upsetting (pattern 11). By regressive analysis we determined dependence of principal strains $\varphi_\theta = f(\varphi_z)$ at the place cracks occurred in the form of second degree polynomial, respecting binding condition that in the beginning of upsetting $\varphi_\theta = \varphi_z = 0$:

$$\varphi_\theta = -0.3718\varphi_z + 0.4574\varphi_z^2 \quad (16)$$

Graphical interpretation of the previous equation with individual experimental points (φ_θ , φ_z) is presented on Fig. 4.

Using approximative function (16) and pattern (8), we determined state of stress value indicators for individual phases of upsetting, or in other words forming history in the form of second degree polynomial (Fig. 5):

$$\beta = 0.1803\varphi_e^2 + 1.2234\varphi_e - 1 \quad (17)$$

Finally, based on pattern (13) we calculated average value of β -factors for the cylindrical specimens upsetting process performed with flat plates for specimens with normalized initial structure – $\beta_{av} = -0.2963$. Effective strain limit, determined according to the pattern (12) is $\varphi_e^l = 1.0434$.

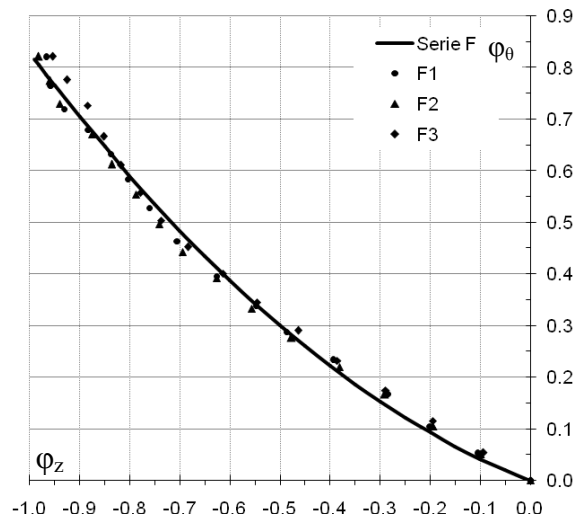


Fig. 4. "Strain path" - upsetting of cylinder by flat plates

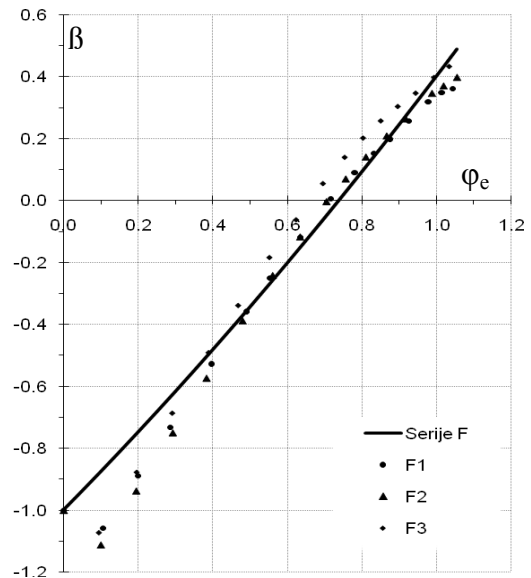


Fig. 5. "Forming history" - upsetting of cylinder by flat plates

Uni-axial tension and torsion tests were realized in conditions of monotonous forming. After processing experimental data we obtain following information:

- uni-axial tension $\beta = +1$ $\varphi_e^l = 0.0780$
- torsion $\beta = 0$ $\varphi_e^l = 0.6212$

On Fig. 6 are photographs of test pieces formed in the processes of uni-axial tension and torsion.

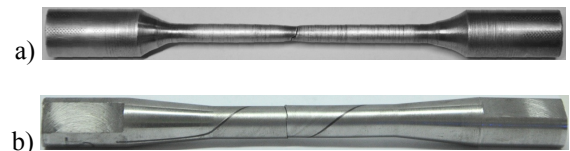


Fig. 6. Specimens after deformation:
a) uni-axial tension, b) torsion

In order to fully characterize formability of normalized steel C45E we created a model for upsetting of tapered specimens by flat plates. Initial shape and dimensions of the new model (Fig. 7a) are

defined in order to establish dominant impact of tension components of stress to the development of damage to the structure and occurrence of the crack. In this manner it was allowed that values β_{av} and φ_e^1 are significantly different for the processes of upsetting cylindrical and tapered specimens which contributes better defining of FLD. From the mechanical aspect, geometrical shape of new forming model is similar to the one we get while upsetting cylindrical specimen with very high values of contact friction coefficient. These findings initialized hypothesis that tapered specimens behave like cylindrical specimens whose barrel – like shape is artificially created.

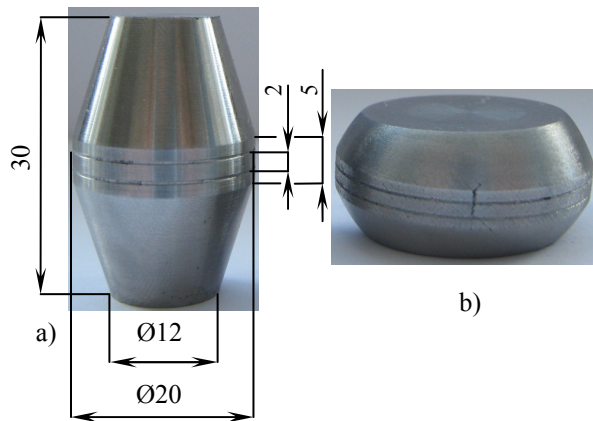


Fig. 7. Upsetting of tapered specimen
a) initial specimen, b) specimen after forming

Methodological and conceptual approach in realization and evaluation of data obtained in experimental research of formability in upsetting of tapered specimen by flat plates is identical to ones applied to cylinder upsetting process.

Graphical image of “strain path” $\varphi_\theta = -0.3360\varphi_z + 2.5986\varphi_z^2$ and “forming history” $\beta = -9.4133\varphi_e^2 + 8.8553\varphi_e - 1$ are provided on Fig. 8 and 9.

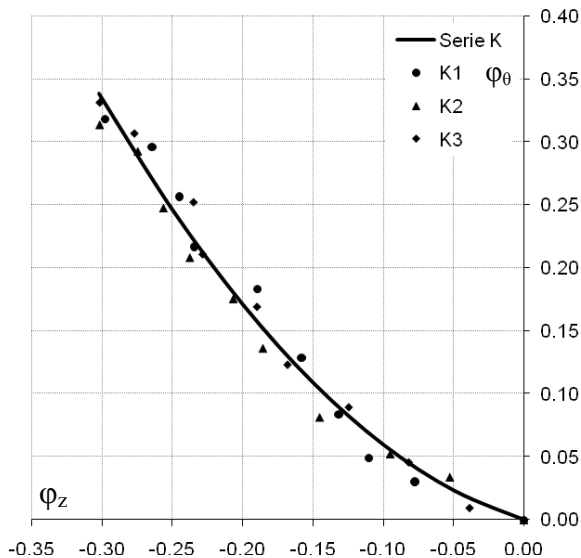


Fig. 8. “Strain path” – Upsetting of tapered specimens by flat plates

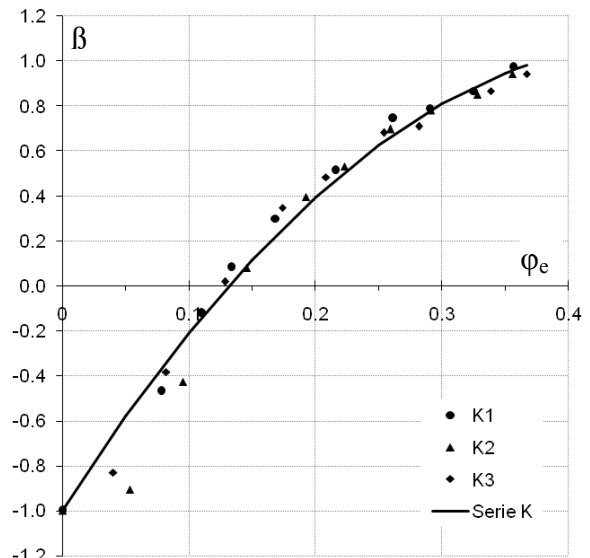


Fig. 9. “Forming history” - Upsetting of tapered specimens by flat plates

Average values β_{av} and strain limits φ_e^1 for individual specimens K1-3 and K series are provided in Table 1.

Specimen mark	β_{av}	φ_e^1
K1	0.2041	0.3565
K2	0.1445	0.3556
K3	0.2073	0.3668
Serie K	0.1862	0.3595

Table 1. β_{av} and φ_e^1 – Upsetting of tapered specimens by flat plates

3.2 Soft annealed material microstructure [1]

For the purpose of analysis of different states of microstructure to steel C45E formability we used experimental research results obtained by Vilotić and associates [1]. Their study refers to analysis of forming limits for shaping short (CS) and high cylindrical (CH) or high prismatic specimens (PH) in upsetting process with V-shape dies (Fig. 10). Initial microstructure of all specimens corresponds to soft annealed state.

In this case values of β -factors and strain limits of basic models are:

Forming model	$\beta_{(av)}$	φ_e^1
Uni-axial tension	+1	0.15
Torsion	0	0.73
Upsetting of cylinder by flat plates	-0.40	1.12

Table 2. β_{av} i φ_e^1 – Basic forming models -soft annealed microstructure [1]

Experimental research results for forming models in Fig. 10 are provided in Table 3.

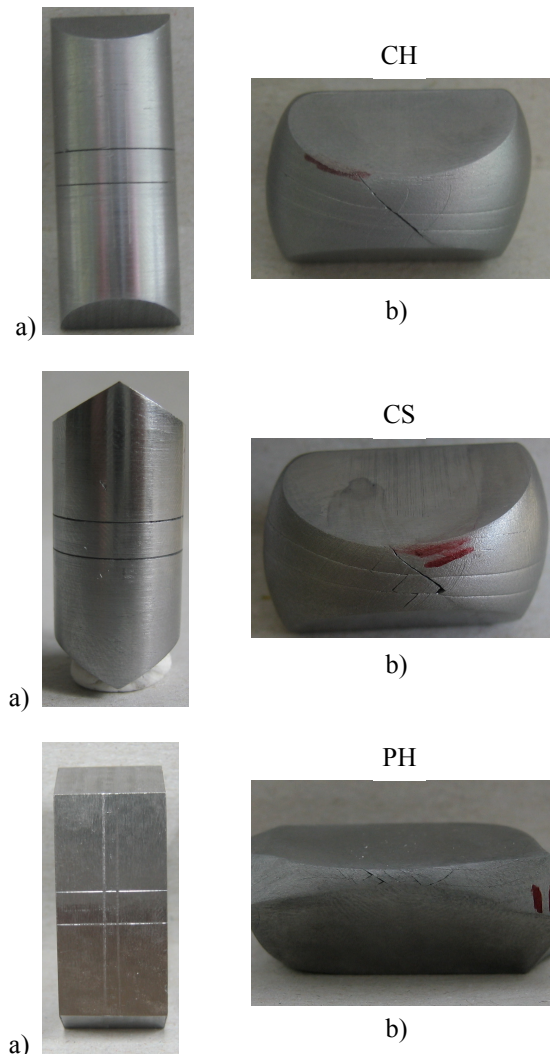


Fig. 10. Specimens of steel C45E: a) before, b) after upsetting by V-shape dies [1]

Specimen mark	β_{av}	φ_e^I
Serie CH	-0.166	0.833
Serie CS	0.062	0.965
Serie PH	-0.253	1.025

Table 3. β_{av} i φ_e^I – Cylindrical and prismatic specimens upsetting-soft annealed microstructure [1]

3.3 Initial microstructure state impact to formability - basic forming models

Microstructure state impact to formability, especially in case of two-phase ferrite-pearlite steels depends on size, shape and interaction of crystal grains of basic matrix (ferrite), shape, size and arrangement of carbides and finally content and arrangement of inclusions [6]. However, the greatest impact to formability has content and shape of carbon carbides.

Due to complex formability function character, and for the purpose of identification of initial microstructure state impact, it is necessary to use models which form in identical forming conditions

while conducting experimental research. Such approach provides elimination of impact of other factors (equation 1) to strain limit size. For the above mentioned reasons we analyzed initial microstructure state impact to formability based on results obtained by application of basic forming models. On Figure 11 are graphical images of effective strain limits for normalized and soft annealed structure.

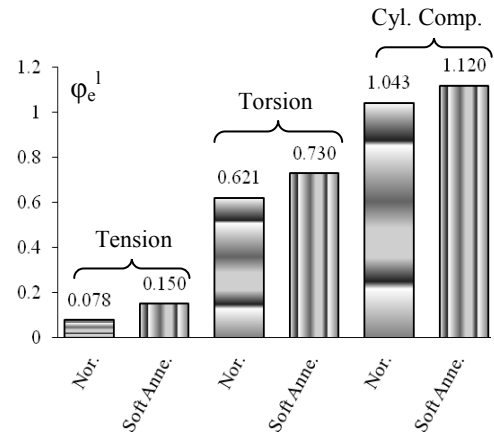


Fig. 11. Strain limits for different initial microstructure states - basic models

Comparing numerical values we notice that greater strain limits are achieved for all models with initial soft annealed structure. However, the increase rate is not constant. The greatest difference was noticed in process of uni-axial tension, and the least in cylinder upsetting. These observations are in direct connection with generated state of stress to pearlite grains forming ability.

Namely, in normalized structure cementite in pearlite occurs in shape of elongated slices of different orientation in relation to load impact direction. Due to very low forming ability caused by hardness and brittleness, breaking of cementite is made easier in the forming process. Structure damage starts at lower forming levels, it intensifies in following phases and conditions early occurrence of cracks at the outer specimen surface.

On the other hand, with soft annealed structure cementite is present in shape of spherical particles equally arranged in ferrite basis. Specimen forming under these circumstances is better from formability aspect, which is experimentally verified through strain limits.

3.4 Forming limit diagram of steel C45E

According to presented experimental and numerical data we defined FLD for steel C45E. In Figure 12 we can see comparative analysis of forming limit curves for normalized and soft annealed initial structure. Research results for individual specimens are presented through average values of series for tested forming models.

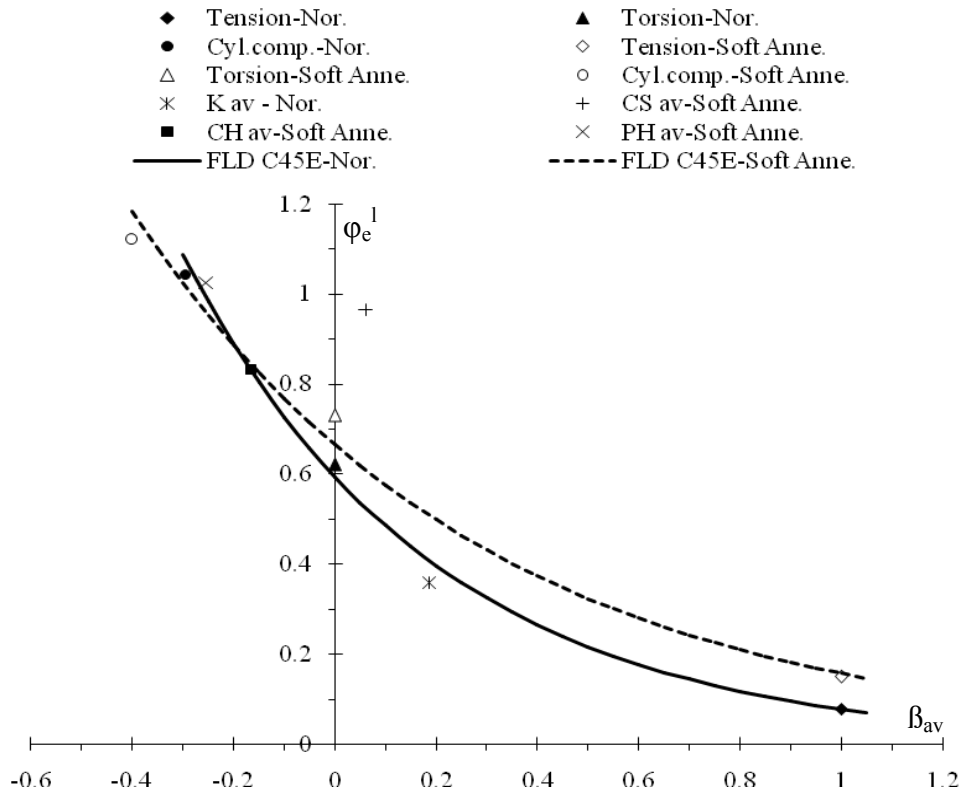


Fig. 12. FLD of steel C45E – Comparative analysis for normalized and soft annealed initial structure Ohio, 2003.

4. CONCLUSION

Research in the area of initial microstructure state impact to strain limits size is very significant because it provides the opportunity to make adequate choice in thermal treatment for steel and thus achieve optimal shape and arrangement of carbide particles in metal basis which directly influences increase in formability.

Comparing FLD for normalized and soft annealed structure we notice significant differences in achieved strain limits for basic forming models. Numerically presented, material formability of normalized specimens for basic models (uni-axial tension, torsion and cylinder upsetting by flat plates) for 48%, 14.93% and 6.88% respectively lesser in comparison with models with soft annealed structure.

Based on the research results presented we can state that soft annealed structure compared to normalized structure allows greater material formability especially under conditions of tension stress components domination.

5. REFERENCES

- [1] Vilotić, D., Alexandrov, S., Plančak, M., Movrin, D., Ivanišević A., Vilotić, M.: *Material Formability at Upsetting by V-Shape Dies*, Steel research international, p.p. 923-928, Special Edition 10th International Conference on Technology of Plasticity - ICTP, Aachen, Germany, 25th – 30th September 2011.
- [2] Dieter, G., Kuhn, H., Semiatin, L.: *Handbook of Workability and Process Design*, ASM International, ISBN: 0-87170-778-8, Material Park

- [3] Vujović, V., Shabaik A.: *Workability Criteria for Ductile Fracture*. Trans., ASME J. Engng. Mater. Technol., Vol. 108, p.p. 245-249., 1986.
- [4] Vilotić D., Plančak M., Čupković Đ., Alexandrov S., Alexandrova N.: *Free Surface Fracture in Three Upsetting Tests*, Experimental Mechanics Vol.46: p.p. 115–120, 2006.
- [5] Alexandrov, S.: *Fracture prediction in steady ideal plastic flows*, Acta Mechanica Vol.163, p.p. 127–138, 2003.
- [6] Vujović, V.: *Formability*, Faculty of Technical Sciences, Department of Production Engineering, Novi Sad, 1992. (in Serbian)
- [7] Gouveia, B.P.P.A., Rodrigues, J.M.C., Martins, P.A.F.: *Ductile fracture in metalworking: experimental and theoretical research*, Journal of Materials Processing Technology, Vol. 101: p.p. 52–63, 2000.

Authors: Ass. Mr Milija Krašnik, Doc. Dr Žarko Petrović University of East Sarajevo, Faculty of Mechanical Engineering, Vuka Karadžića 30, 71123 East Sarajevo, BiH, Phone.:+387 57 340847, **Prof. Dr Dragiša Vilotić, Prof. emeritus Dr Leosava Šidanin**, University of Novi Sad, Faculty of Technical Sciences, Department for Production Engineering, Trg Dositeja Obradovića 6, 21000 Novi Sad, Serbia, Phone.: +381 21 4852349, E-mail: milijakrašnik@yahoo.com, vilotic@uns.ac.rs, lepas@uns.ac.rs, zpetrovic@bata.gov.ba

Kuzman, K., Kacmarcik, I., Pepelnjak, T., Placak, M., Vilotic, D.

EXPERIMENTAL CONSOLIDATION OF ALUMINIUM CHIPS BY COLD COMPRESSION

Abstract: Solid state recycling of metal chips and scrap presents a relatively novel eco-friendly solution in which high deformations and hydrostatic pressures are induced to the chips in order to achieve proper material bonding. This paper deals with consolidation of aluminium chips obtained by milling process. All chips were cut from the same AlMgSi1 ingot in total of 4 different milling regimes. Afterwards, chips were cold compressed in closed die, by punch and die with 32mm diameter. The influences of type of chips as well as compression load values on final billets' densities were investigated. Additionally, this research elaborates possibilities for further enhancement of mechanical properties of obtained billets.

Key words: Aluminium chips recycling, chips compression, solid state recycling, severe plastic deformation

1. INTRODUCTION

Aluminium and its alloys are widely used in modern industry due to their good mechanical properties and low relative density. Main areas of application of Al-alloys are in transportation, packaging and civil industries. Another important advantage of these alloys is their great recyclability, i.e. they can be recycled unlimited number of times without degradation of mechanical properties. It is said that recycling of aluminium saves approximately 95% of the energy used to produce the same amount of material from a raw ore [1]. Nevertheless, even more energy savings is possible when Al-alloys are solid state recycled. In solid state recycling, scrap from Al-alloys obtained in industry, undergo large pressures and are compacted into solid billet at room or elevated temperatures. In this process no material remelting takes place and therefore, low amount of energy is consumed, which also leads to lower green house emissions.

Research regarding solid state recycling started in the 1990s. Authors Gronostajski et al. in [2] granulated different aluminium chips obtained in industry. Granulated particles were cold compressed and hot extruded. Microstructure of the obtained workpieces was examined and it was concluded that low porosity and relatively good density was obtained. Latter work of Gronostajski et al. in [3] included composition of different Al-FeCr composites by solid state recycling. Once again, Al-chips were first granulated, than mixed with FeCr particles and afterwards cold compressed and hot extruded. Mechanical properties and microstructure of obtained billets were compared. Results showed that better mechanical properties were obtained by smaller initial particles. Fogagnolo et al. in [4] avoided granulation of chips and performed direct cold compression by 650 MPa followed by hot pressing (500°C) and extrusion. Influence of particles size and compression pressures of billets' final densities was investigated by Samuel in [5]. Xia and Wu in [6] consolidated aluminium pure particles by back pressure

ECAP process. ECAP die was preheated at 100°C and particles were wrapped in the foil. In [7] Tekkaya et al. consolidated three different aluminium chips into solids by cold compression and hot extrusion. Third type of the chips was mixed with SiC particles. This research showed that yield strengths of compacted billets were only slightly lower than casted material of the same alloy.

The main issue in consolidation of aluminium chips is breakage of aluminium oxide (Alumina – Al₂O₃). This very thin layer (≈ 4nm) forms almost instantly when aluminum is exposed to oxygen. Therefore, formation of this thin layer is inevitable in industrial circumstances. In order to achieve proper bonding, high deformations are essential to assure good alumina breakage and its distribution throughout the whole material volume.

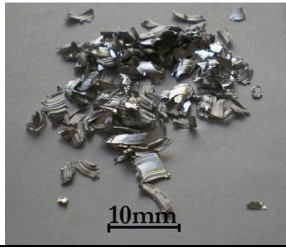
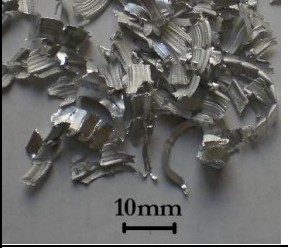
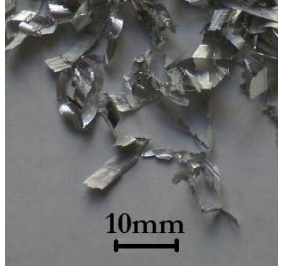

2. PRODUCTION OF CHIPS

Chips were produced from ingot ϕ 110 mm of AlMgSi1 alloy (Fig. 1). This alloy belongs to aluminium 6xxx wrought series, which is widely used in industrial applications. AlMgSi1 contains following alloying elements:

0.7-1.3% Si, 0.4-1.0% Mn and 0.6-1.2% Mg.

The task of this research was to evaluate the influence of chips' type on final relative density of cold-compressed billets. All chips were cut on conventional milling machine at Laboratory for Cutting at Mechanical Faculty Ljubljana, with different cutting parameters. Cutting tool feed rate of 35 mm/min and rotation velocity of 160 revolutions per second was kept constant, while depth and width of the cut was varied. Four different types of chips (A, B, C and D) were obtained, all with different geometries and shapes (Table 1). Chips A were the smallest, with square shape. B-types were slightly larger than A, but also square shape. Both types C and D exhibited longer rectangular geometry, with type D being the longest [8].

Table 1. Types of obtained chips and ingot during cutting process

Type A	Type B
	
Type C	Type D
	

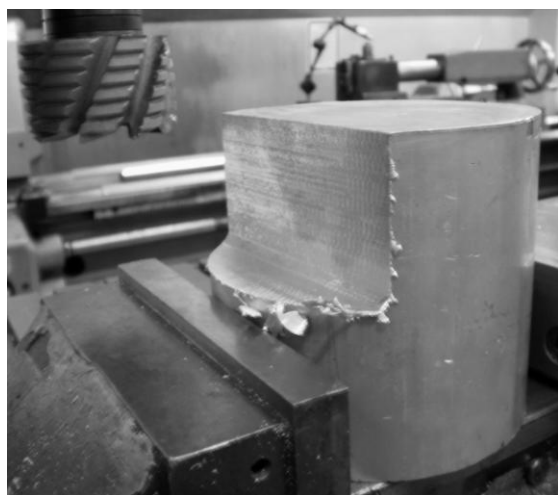


Fig. 1. Cutting of the AlMgSi1 ingot on a milling machine

3. EXPERIMENTAL PROCEDURE

Experimental investigation was carried out on a 2.5 MN hydraulic press. Aluminium chips were compacted in die 32x50mm and by punch 32mm. Due to relative low filling density of the chips, several precompacting operations were needed. Total of 5 – 7 precompacting were performed, depending on the type of the chips. Punch, counter punch and die used in experiment are presented in Fig. 2.

In order to evaluate the influence of compression pressure on billets' final densities, three different maximal loads after precompacting were employed. At first chips were compacted by 245 kN load and latter by 98 kN and 8.8 kN loads. Billets compressed with highest loads (245 kN) exhibited highest relative densities (95÷98%). Relative density is a ration between measured density of billet and theoretical density of aluminium. When forces of 98 kN and 8.8 kN were employed, billets exhibited significantly lower relative densities ($\approx 80\%$ and $\approx 65\%$, retrospectively).

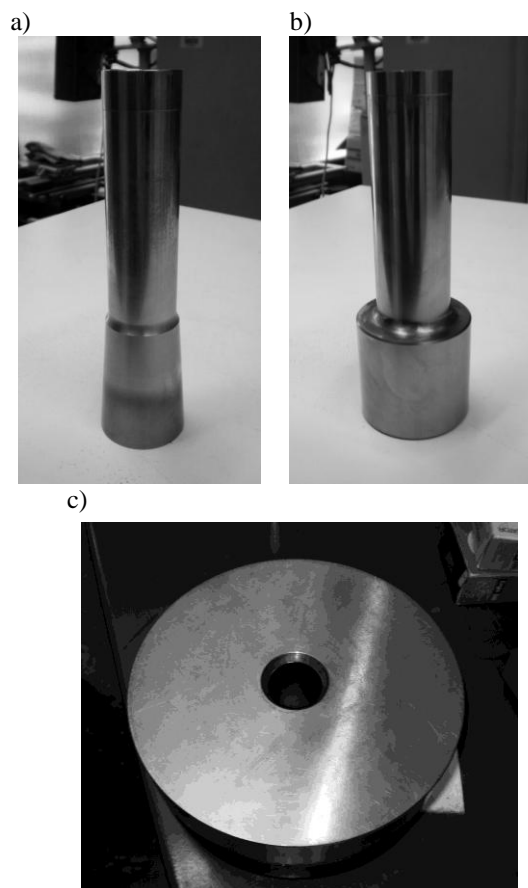


Fig. 2. Photographs of the punch (a), counter punch (b) and die (c) for chips compression

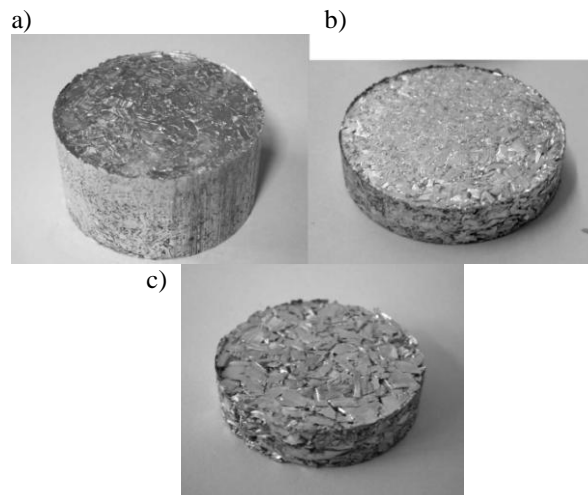


Fig. 3. Billets compressed with: a) 8.8 kN, b) 98 kN, c) 245 kN maximal load

Influence of chips type on relative density of final billet was also investigated, when compression was performed by maximal 245 kN load. As expected, billets obtained from smallest A- and B-type chips showed highest relative density ($\approx 98\%$), while billets from C- and D-type chips exhibited $\approx 95\%$ relative density (Fig. 4).

In order to evaluate compactness of compressed chips, free upsetting was performed on press Amsler in Laboratory for Forming Technologies at Mechanical Faculty in Ljubljana.

typical shape	cutting regime [w x h]	typical shape	cutting regime [w x h]
A	5 x 5 mm	C	10 x 5 mm
B	8 x 7 mm	D	15 x 5 mm

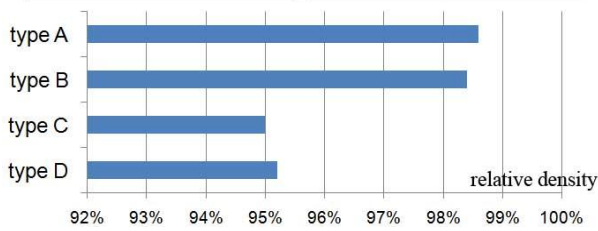


Fig. 4. Influence of type of chips on final billets' densities

Teflon tapes were put on both contact sides between billet and tools to reduce friction. Fig. 5. provides load-stroke curve for free upsetting process.

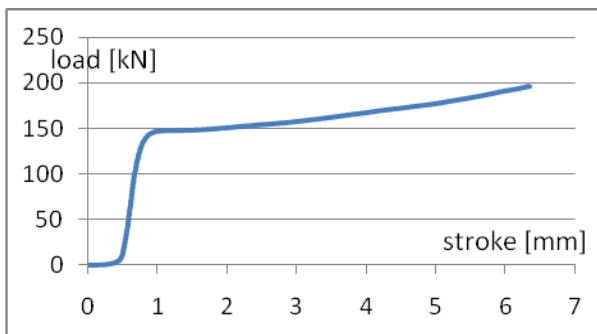


Fig. 5. Load-stroke diagram for free upsetting of cold compressed billets

While upsetting, disintegration of surface layer occurred (Fig. 6.) due to low homogenization of material in previous compacting process.



Fig. 6. Compacted billet after free upsetting

4. POSSIBILITIES FOR FURTHER ENHANCEMENT OF MECHANICAL PROPERTIES OF THE BILLETS

Although compressed billets possess high relative density and compactness, the quality of the bond between the chips remains an issue. This issue was especially perceived during free upsetting experiment, when outer surface started to disintegrate. Particularly large shear deformations would contribute to better

material bonding. Along large shear deformations, high hydrostatic pressures are a necessity as well, especially for ensuring that workpiece remains compact during processing. There are several solutions for improvement of mechanical characteristics of materials such as forward extrusion or severe plastic deformation.

In previous work authors used forward extrusion for achieving better material bonding as in this process billets undergo large shear deformations. Billets were in most cases preheated at temperature above recrystallization. Even better material bonding can be achieved by severe plastic deformation (SPD), mainly due to the fact that in these processes little or no change of material shape takes place. High hydrostatic pressures prevent material deterioration and therefore enable extremely high shear deformations to be induced. The most applied SPD techniques are equal channel angular pressing, twist extrusion and high pressure torsion [9].

In equal channel angular pressing (ECAP), billet is extruded through an L-shaped die (Fig. 7a). There are many variants of this process, such as back pressure ECAP (Fig. 7b), ECAP processes with different L-angle values, double turn ECAP or ECAP with forward extrusion. Due to different contact interface on the upper and lower side of the billet in ECAP, a slightly tilted shape occurs (Fig. 7a). This phenomenon can be avoided if counter punch (Fig. 7b) is used. Counter punch also increases hydrostatic pressure and force F_{bp} must be set lower than main ECAP force F . The main advantage of ECAP is the possibility to induce very high homogenous deformation practically unlimited number of times and ability to produce relatively large billets [10], [11], [12].

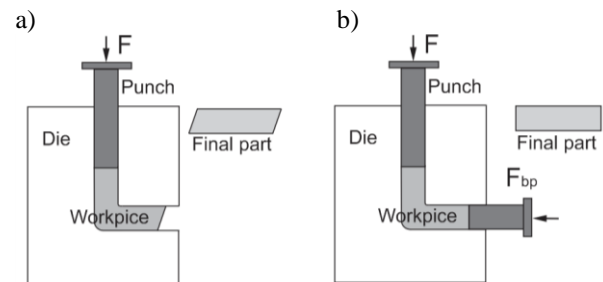


Fig. 7. Comparison between classical ECAP and Back pressure ECAP (BP-ECAP)

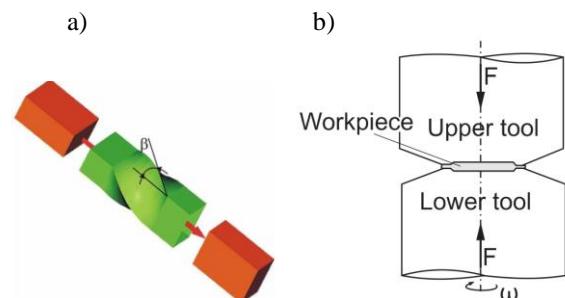


Fig. 8. Severe plastic deformation techniques: a) Twist extrusion, b) High pressure torsion [13]

Twist extrusion (TE) consists of specific tooling through which material is rotated by a certain angle (e.g. 90 °C) and in that way, initial and final material shape remains constant (Fig. 8a). As is ECAP, there are several variations of TE, such as: back pressure TE, hydrostatic TE, high velocity TE...

High pressure torsion (HTP) represents a SPD technique in which a disc-like specimen is fixed between upper and lower rotating tools (Fig. 8b). Due to friction phenomenon and disability of the material to change shape, extremely high shear deformations and hydrostatic pressures occur. The main characteristics of this process are simple tooling design and inhomogeneous deformation. Major setback is that only thin cylindrical billets can be processed.

5. CONCLUSION REMARKS

Recycling aluminium chips by solid state recycling is more energy efficient than conventional recycling. In this process, aluminium chips are compressed by high pressures which induce their bonding. This paper investigates the influence of chips shape and size on final relative densities of obtained billets. Total of 4 different chips types were employed. The influence of compression load is examined as well. Results showed that smaller and simpler chips prove to be better input materials for cold compression. Billets from larger and more complex chips exhibited lower relative densities. As expected, higher compression loads result in better material bonding and higher density of the billets.

After cold compression, an open issue remains on the quality of the bonding between the chips, despite high relative densities. This was practically verified by free upsetting. Although billets showed good compactness, the outer surface started to deteriorate due to weak material bonding. The load – stroke diagram for free upsetting of compressed billets is given as well. One of the solutions might be in employing severe plastic deformation techniques to the obtained billets, which is planned in future research.

6. REFERENCES

- [1] International Aluminium Institute – Global Aluminium Recycling: A cornerstone of sustainable development.
- [2] Gronostajski J.Z., Kaczmar J.W., Marciniak H., Matuszak A.: *Production of composites from Al and AlMg2 alloy chips*, Journal of Materials Processing Technology 77, p.p. 37–41, 1998.
- [3] Gronostajski J.Z., Marciniak H., Matuszak A., Samuel M.: *Aluminium-ferro-chromium composites*, Journal of Materials Processing Technology 119, p.p. 251-256, 2001.
- [4] Fogagnolo J.B., Ruiz-Navas E.M., Simón M.A., Martínez M.A.: *Recycling of aluminium alloy and aluminium matrix composite chips by pressing and hot extrusion*, Journal of Materials Processing Technology 143–144, p.p. 792–795, 2003.
- [5] Samuel M.: *A new technique for recycling aluminium scrap*, Journal of Materials Processing Technology 135, p.p. 117-214, 2003.

- [6] Xia K., Wu X.: *Back pressure equal channel angular consolidation of pure Al particles*, Scripta Materialia 53, p.p. 1225–1229, 2005.
- [7] Tekkaya A.E., Schikorraa M., Beckera D., Biermann D., Hammer N., Pantke K.: *Hot profile extrusion of AA-6060 aluminum chips*, Journal of materials processing technology 209, p.p. 3343–3350, 2009.
- [8] Kuzman K., Kacmarcik I, Pepelnjak T., Plancak M.: *Solid state recycling by Cold compression of Al-alloy Chips*, Journal for Technology of Plasticity Vol 37/1, accepted paper.
- [9] Azushima A., Kopp R., Korhonen A., Yang D.Y., Micari F., Lahoti G.D., Groche P., Yanagimoto J., Tsuji N., Rosochowski A., Yanagida A., *Severe plastic deformation (SPD) processes for metals*, CIRP Annals - Manufacturing Technology 57, p.p. 716-735, 2008.
- [10] Rosochowski A., Olejnik L., *Numerical and physical modelling of plastic deformation in 2-turn equal channel angular extrusion*, Journal of Materials Processing Technology 125-126, p.p. 309-316, 2002.
- [11] Iwahashi Y., Horita Z., Nemoto M. and Langdon T.: *The process of grain refinement in equal channel angular pressing*, Acta mater. 46/9, p.p. 3317-3331, 1998.
- [12] Valiev R.Z., Islamgaliev R.K., Alexandrov I.V.: *Bulk nanostructured materials from severe plastic deformation*, Progress in Materials Science 45, p.p. 103-189, 2000.
- [13] Beygelzimer Y.: *A new severe plastic deformation technique: Twist Extrusion*, Donetsk Institute of Physics and Technology, presentation.

Authors: **K. Kuzman, T. Pepelnjak**, University of Ljubljana, Faculty of Mechanical Engineering, Askerceva 6, 1000 Ljubljana, Slovenia.

I. Kacmarcik, M. Plancak, D. Vilotic, University of Novi Sad, Faculty of Technical Sciences, Institute for Production Engineering, Trg Dositeja Obradovica 6, 21000 Novi Sad, Serbia, Phone.: +381 21 485 2513, E-mail: igorkac@uns.ac.rs

ACKNOWLEDGEMENT

Results of investigation presented in this paper are part of the research realized in the framework of the project “Research and development of modeling methods and approaches in manufacturing of dental recoveries with the application of modern technologies and computer aided systems”–TR 035020, financed by the Ministry of Science and Technological Development of the Republic of Serbia, as well as a part of the investigation within the project EUREKA E!5005 financed also by Serbian Ministry of Science and Technological Development. Authors are very grateful for the financial support.

Nedić, B., Jovanović, D., Marušić, V.

SOME SCRATCH TEST RESEARCH RESULTS Zn COATINGS

Abstract: Most studies of Zn coatings focuses on the characterization of coatings and their links to the basic material, while very little is known about the effects of substrate on the characteristics of the coating. Surface finish has a great influence on determination of the physical and mechanical properties and structure of the surface layer. This paper presents the preliminary results scratch testing of Zn coating. The research was performed with samples of different hardness, different previous grinding and different thickness Zn coatings.

Key words: Zn coating, galvanic coating, scratch test, adhesion testing

1. INTRODUCTION

Creating metal coatings on the surface of another metal has a dual role, corrosion protection and changing characteristics of the metal surface, such as hardness, electrical conductivity, and decoration and so on. But when the metal coatings are damaged, they can not simply be fixed, that makes them different from the organic coating.

The effect of processing procedure and conditions of pre-treatment and preparation of surfaces to which coatings are applied, technological heritage, is very little explored. Surface layers of machined surfaces obtained by different treatment processes and regimes may have a different structure, which only in the period of exploitation may be experienced. Therefore, it can be said that the characteristics of surface layers are formed as a result of different processing conditions in the technological chain of production of the finished part. The basic parameters that are inherited through the process of technological development can be divided into two groups. On the one hand there are parameters related to properties of materials: their compositions, structure, stress state, etc., while on the other hand are parameters related to macro and micro geometry of the surface (geometrical parameters). This indicates the complexity of the problem and the need for further studies [9].

Neat treatment and surface finish has a great influence on determining the physical - mechanical properties and structure of the surface layer. In this paper is investigation of the influence of the previous surface treatment and coating thickness on the characteristic scratch testing Zn coating.

2. ELECTRO DEPOSITED Zn COATINGS

Electro deposited galvanic coatings and metals are crystalline in nature. In the crystallization process - there are three independent processes:

- 1) formation of seeds (centers) or crystal nuclei,
- 2) crystal growth rate,
- 3) increase the speed of crystals on account of their merger.

These processes run in parallel. The creation and quality of metal coatings are influenced by many factors: The concentration of ions significantly affects the quality of the coating, the composition of the electrolyte affect the properties and appearance of the coatings. Current density has a large impact on the formation rate of crystal nuclei, mixing is performed to maintain constant concentration of metal ions; the temperature plays a significant role in the speed of chemical reactions. Metals are polycrystalline particles, so the characteristics of the coating are affected by the structure of the substrate [6].

Zinc coatings are used for corrosion protection of machinery parts, steel plates, wire, etc., located in different climate conditions, in closed environments with moderate humidity, at the polluted gases areas, flue gases area and in atmosphere containing sulfur vapor. These coatings are used to protect pipes, tanks and other parts, which are in contact with water at temperatures up to 70°C. Color of Zn coating is usually light gray, become dark during time, and therefore does not provide a decorative look. Zinc also protects the iron from corrosion when the coating is porous or damaged, because it forms a couple in which the iron is cathodically protected [3, 4].

Life of the protective effect of the coating depends on its thickness. For metal objects, which are used in relatively dry air in closed rooms, sufficient thickness of zinc coating of 10-15 µm. For items that are outside the room, in the air that is polluted by industrial gases, the thickness increases to 20 - 25 µm, and for articles intended for use in industrial environments, in terms of enhanced effects of moisture, sea water or water vapor, the thickness of zinc coating moving to 50 µm. Coating is more resistant if the zinc cleaner [1, 2, 3].

The hardness of metal Zn coatings is 45 to 120 HB.

3. EXPERIMENTAL INVESTIGATION

For the purpose of testing the samples were made 15 x 6.3 x 10 mm (Figure 1). On samples from the front side were embedded serial numbers of the sample, and through lateral surfaces were drilled openings designed to mounting each sample individually for coating.

Samples are made of spring steel 67SiCr5 (Č4230). After the sample design, milling, heat treatment was done by improving the different hardness (Table 1).

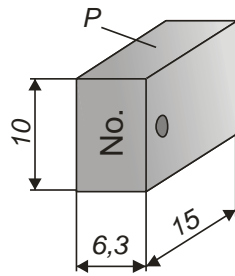


Fig. 1. Sample

Production samples were carried out with several ways: RG - Roughly grinding, FG - Final grinding, RP - Roughly polishing and FP - final polishing. In this way they obtained different characteristics of the surface layer and the surface topography of various samples. Application of metal coatings was performed at the facility for electroplating factory "Zastava Arms", Kragujevac in production conditions, with different times in order to obtain different thicknesses of Zn coating.

Zinc coating was carried out as follows:

- I. alkaline degreasing without cyanides with industrial detergent,
- II. rinse with water,
- III. pickling in diluted hydrochloric acid in a 1:1 ratio,
- IV. rinse with water,
- V. electro-chemical coating of zinc,
 - temperature coating-room,
 - strength of current $I = 3 \text{ A/dm}^2$,
 - time 8 - 35 min,
- VI. enlightening in 2% HNO_3 for a period of 50 seconds,
- VII. rinse with water,
- VIII. blowing.

Table 1 shows the data on the tested samples: marking of grinding, the hardness after heat treatment and obtained layer of Zn.

Sample number	Type production	Hardness samples, HRC	Thickness Zn coatings μm	Ra * μm
4	RG	33	20,0	0,819
15	RG	45	23,9	0,70
35	RG	38	19,5	0,73
118	RG	19	23,9	0,844
8	FG	48	26,2	0,523
31	FG	49	18,80	0,612
26	FG	40	20	0,81
45	FG	39	28,9	0,719
49	FG	29	27,43	0,71
12	RP	35	36,57	0,6
23	FP	26	28,96	0,45

Table 1 Hardness and thickness of Zn samples

* After applying Zn coatings

Coating thickness measurement was performed in a laboratory galvanizing area of factory "Zastava Arms" in Kragujevac. Samples with coatings of Zn in which the thickness were up to $16 \mu\text{m}$ were not further analyzed.

4. EQUATIONS

After production the samples, before applying the coatings, were measured hardness and surface topography parameters and the longitudinal and transverse direction. Measurements were taken at the surface of the sample P (Fig. 1).

Applying Zn coatings leads to a deterioration of surface quality and roughness increases significantly. Class roughness of Zn coating can deteriorate for one, even for the two classes.

Tests adhesive properties of coatings were carried out to help Scratch Tester ST-99, Fig. 2. The analysis of measurement results in terms of traces of wear and tear of constant increase in normal load (200 N/min) and constant sliding velocity (40 mm/min) obtained data on adhesive resistance or strength adhesive link between the coating and base material. By monitoring changes in force and the coefficient of friction with the change of the load for the duration of contact, it is possible to determine the "critical value of force F_{NCi} " at which the change in their values [5, 6].

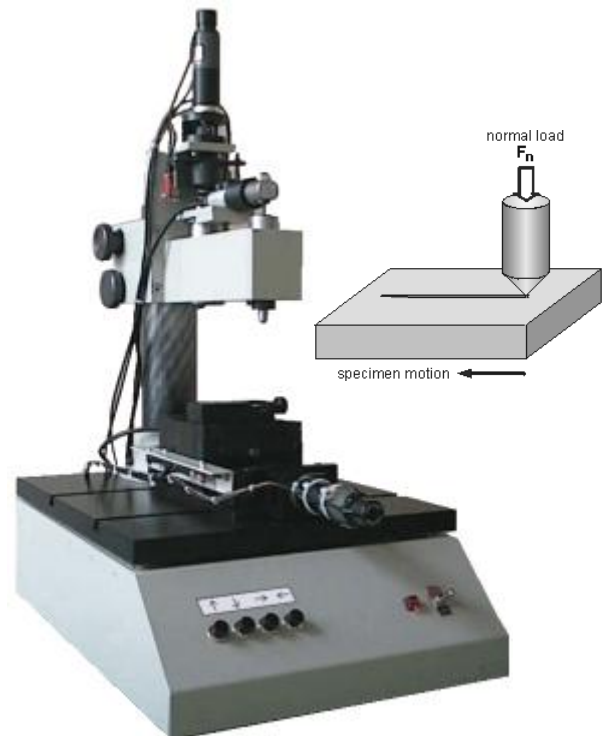


Fig. 2. Scratch tester ST-99

In Fig. 3. is presented Scratch test diagram for sample 12 obtained by rough polishing. Characteristic areas with local minimal and maximal values, where there is significant change of friction coefficient can be noticed in the diagram. Position of these areas is accurately determined and photos of surface of Scratch test marks are taken. In Figures 4a-f are presented appearances of the surfaces where surface layers with Zn coating were deformed.

In Fig. 4a can be noticed first contact of the needle of Scratch test device and surface. Zn is taken away from prominence spots or embedded in sample surface.

Fig. 4b corresponds with b position in diagram in Fig. 3, where friction coefficient significantly increases. In Fig. 4b are areas with significant removal of Zn coating and scratch on one large prominence.

Fig. 4c corresponds with c position in diagram in Fig. 3, with local minimum of friction coefficient. In Fig. 3 can be noticed that this value of friction coefficient corresponds with lower damage of Zn coating. Same can be said for d position in Fig. 3, where Local minimums and maximums can be seen, corresponding with less or more damaged Zn coating and base material of the sample. Left and right of these areas are light spots, Fig. 4c and 4d, obtained by total removal of Zn coating.

In Fig. 4e, with position that corresponds with local maximum in diagram in Fig. 3 there is significant scratch of the base material, not just Zn coating.

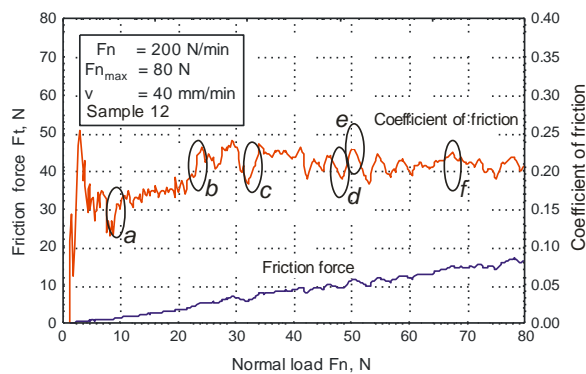
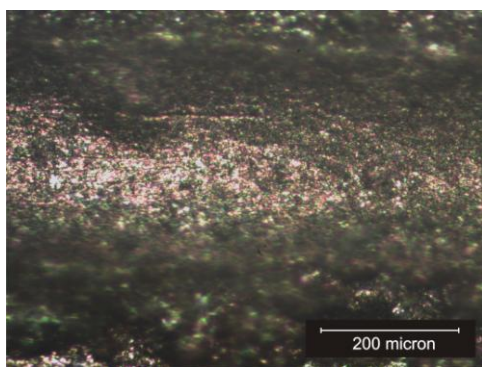
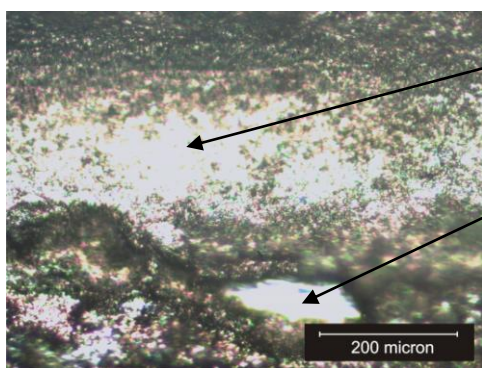


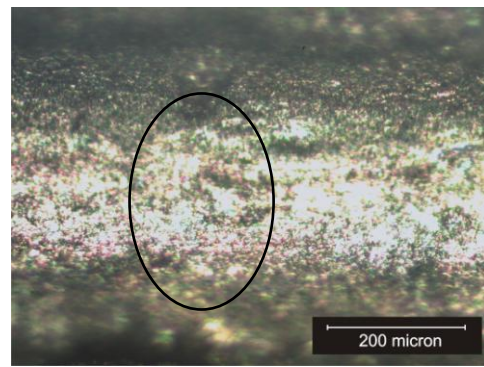
Fig 3. Coefficient of friction and friction forces for sample 12



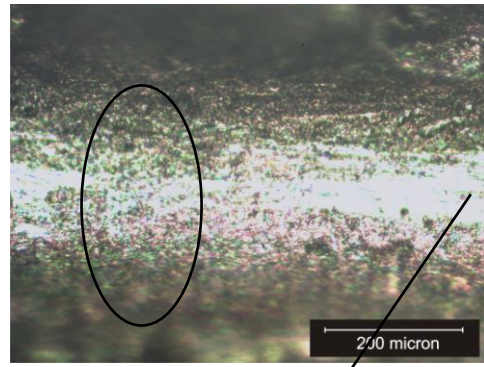
Locate a



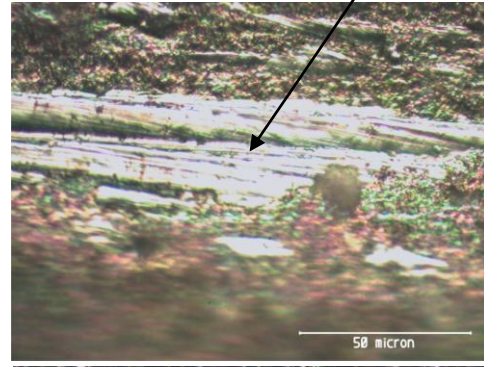
Locate b



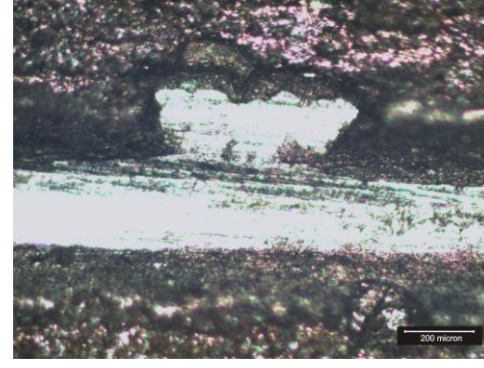
Locate c



Locate d



Locate e



Locate f

Fig. 4. Appearance of Scratch test marks

Fig. 4f shows that with higher values of normal load F_n Zn coating is removed (light surface of the mark) and that local maximum corresponds with contact of the needle of Scratch test device.

In Fig. 5 is presented profile of surface of Scratch test mark just before the end, and it can be clearly seen that Zn coating was extruded. This extrusion is more significant for thicker coatings.

Investigations of influence of Zn coating thickness on friction coefficient with samples obtained with fine grinding show that with increase of coating thickness friction coefficient also increases (Fig. 6).

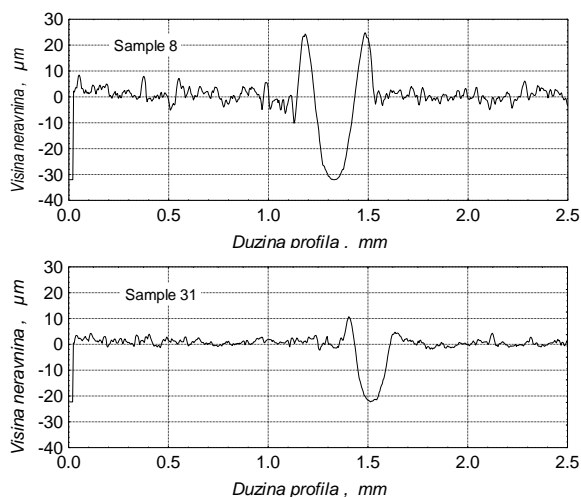


Fig. 5. Extrusion of sample material with different thicknesses of Zn coatings

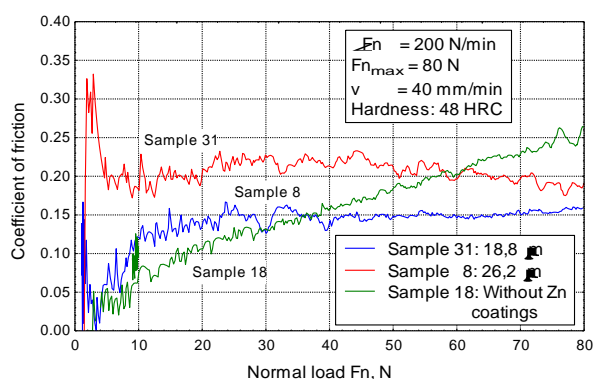


Fig. 6. Change of friction coefficient with different thicknesses of Zn coating

In Fig. 6 is also presented the diagram of friction coefficient, obtained with Scratch test of sample without Zn coating.

Performing the scratch test on the Zn coating causes additional problems. Firstly, it was not possible to reveal the iron substrate directly under a reflected light optical microscope due to the absence of colour contrast. An etch ant (20 g CrO₃ and 1 g Na₂S₀₄ per 100 ml H₂O; 1 - 2 s etch) had to be used subsequent to scratch testing to discriminate between the Zn coating and the Fe substrate. The max load was set to a sufficiently high value of 80 N.

Secondly, the ductile character of the Zn coatings implies that the stylus simply ploughs through and perforates the Zn coating at a certain normal load, into the iron the substrate. The load at perforation of the coating was assumed to be critical load.

5. FINAL REMARKS

Realised investigation showed that Scratch test cannot successfully be used for investigations of adhesion characteristics of conventional electro deposited Zn coatings. With this method force needed to separate Zn coating from the base cannot be determined. Zn coatings have low hardness, therefore during investigations are removed or embedded in surface wrinkles.

These investigations can be used for investigation of influence of base hardness, topography and coating thickness on way and intensity of removal of Zn coating from investigated surface.

6. REFERENCES

- [1] Đorđević, S., Maksimović, M., Pavlović, M. G., Popov, K. I., *Galvanotehnika*, Tehnička knjiga, Beograd, 1998.
- [2] Proskurkin, E. V., Popovič, V. A., Moroz, A. T., *Cinkovanje*, "Metalurgija", Moskva, 1988.
- [3] Creutz, H. G., Martin, S., *Present Technology and Future trends*, Plating and surface finishing, pp. 681-686, 1975.
- [4] Volker Kunz, *ZINTEK-TECHSEAL-TRI-COAT* Catalogue, Trebur 2001.
- [5] Ivković B., Nedić B., Ješić D., *Scratch test - merenje abrazione otpornosti materijala i kvaliteta prevlaka*, DEMI 2001, Banja Luka, 2001.
- [6] Nedić, B., Jovanović, D., Lakić Globočki, G., *Influence Of Previous Machining On Characteristics Of Galvanic Coatings*, Serbiantrib - 12th International Conference on Tribology, Kragujevac, 2011.
- [7] SRPS C.T7.111:1991, SRPS C.T7.117:1991
- [8] ISO 4539
- [9] Adhesion testing of coated surfaces, Programme of Scientific Support to Standardisation, Stage II, Final report, OSTC, Prime Minister's Services Scientific, Technical and Curtura, Affairs, 2009. http://www.belspo.be/belspo/home/publ/pub_ostc/NO/rNOB018_en.pdf, 20.03.2012.
- [10] N. Amir, M. Bin Sudin and F. Ahmad, *Adhesion Properties of Metallic Coatings on Mild Steel Substrates*, ICPER 2008 (International Conference), Selangor, 27-28 March 2008.
- [11] N. Amir, *A Study on the Adhesion Properties of Metallic Coatings*, Project Dissertation for the Bachelor of Engineering, Universiti Teknologi Petronas, Tronoh, Perak, 2004.
- [12] M. Ye, J.L. Delplancke, G. Berton, L. Segers and R. Winand, "Characterization and Adhesion Strength, Study of Zn Coatings Electrodeposited on Steel Substrates", *Surf. Coat. Technol.*, 105, 1998.

Authors: Prof. dr Bogdan Nedić, Fakultet inženjerskih nauka, Kragujevac, Srbija,

E-mail: nedic@kg.ac.rs

Mr Desimir Jovanović, Zastava oružje AD, Kragujevac, Srbija,

E-mail: zo.tehnologija@open.telekom.rs

Prof. dr Vlatko Marušić, Strojarski fakultet, Slavonski Brod, Hrvatska, E-mail: vlatko.marusic@sfsb.hr

ACKNOWLEDGEMENT

This paper is part of project TR35034 The research of modern non-conventional technologies application in manufacturing companies with the aim of increase efficiency of use, product quality, reduce of costs and save energy and materials, funded by the Ministry of Education and Science of Republic of Serbia.

Neugebauer, R., Voelkner, W., Mauermann, R., Israel, M.

CLINCHING IN STEEL AND RAILWAY CONSTRUCTION, SHIPBUILDING AND COMMERCIAL VEHICLES

Abstract: Clinching as an alternative joining technology to welding or bolting today is restricted up to circa 4mm single sheet thickness. There is no industrial experience in clinching higher sheet thickness up to 10mm. However, the branches of industry working with thick sheet metal (utility and rail vehicle engineering, shipbuilding and general structural steel engineering) represent a major potential for using this highly efficient and economic joining technology. Thus the need arises to predict the process conditions and joint quality as well by experimental and numerical analysis. This paper demonstrates investigations in both fields to understand the impact of relevant parameters and restrictions of thick sheet clinching.

Key words: joining, clinching, fatigue, distortion, accessibility

1. INTRODUCTION

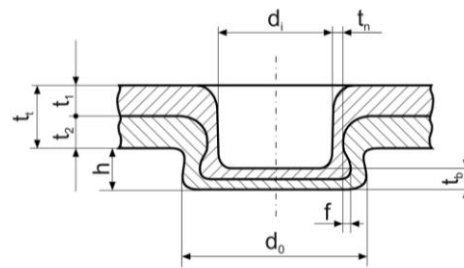
Welding as the main joining technology to connect thick sheets offers unrivalled flexibility but there are disadvantages such as processing time, fatigue weakness, thermal distortion and corrosion. Contrary clinching is not that flexible because of the necessary two side access and the restrictions in joining direction – the upper sheet should have higher strength and should be thicker than the bottom sheet. On the other hand a clinching process is very fast and accurate and the joints have a very good fatigue-potency. Due to the low variable cost using clinching this joining technology is highly efficient, especially for mass production.

Clinching is found in thin sheet applications in the range of 0.5 to 4mm single sheet thickness $t_{1,2}$ (Fig. 1), often used in the automotive industry or white goods. As already pointed out, in mass production, e.g. washer drum, the breakeven point is achieved at the fastest in comparison with other joining technologies. System suppliers like Eckold, Tox, BTM deliver the common C-frames and tools (punch, die; Fig. 2) on the basis of experience. The clinching process is dependent on knowledge – in engineering and in production process. Thick sheet clinching today is not in mass production. It is discussed recently [1,2] and is the focus of the article.

2. CLINCHING PROCESS

2.1 Principle and process parameters

The principle terms and geometry parameters of a clinched joint are shown in Fig. 1 whereas Fig. 2 shows the clinching process in three steps. There are descriptions of applications [3,4,5] and standard procedures [6,7]. Special clinching variants [8,9,10] and hybrid technologies [11,12] are described. The complexity of the clinching procedure is defined by a number of significant variables (Table 1).



- $t_{1,2}$ thickness (total, blank 1, blank 2)
- t_b bottom thickness
- t_n neck thickness
- f undercut
- h height of joint
- d_i inner point diameter
- d_o outer point diameter

Fig. 1. Principle geometry of a crosscut

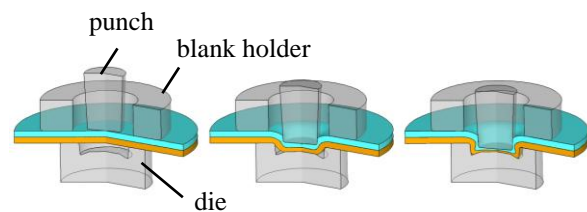


Fig. 2. Clinching process

tool parameters	process parameters	material parameters
<u>punch</u> : diameter, radii, angles	<u>blank holder</u> : force, spring stiffness	thickness, flow curve, pretension
<u>die</u> : diameter, depth, radii, angles	<u>machine</u> : force, stiffness, velocity	(for both: upper and lower sheet)

Table 1. Principle geometry of a crosscut

To understand the whole process detailed material flow and hardening has to be considered (Fig. 3). Before offsetting there is needed a force for fixing the sheets on the die that is applied by the blank holder. Plastifying the material in the “offsetting” step involves

a substantial increase in force. The increasing material upsetting between the punch and bottom of the die causes the material to flow radial and therefore to form the undercut between the two pieces of sheet metal to be connected. The maximum force is reached at the point of the maximum punch stroke.

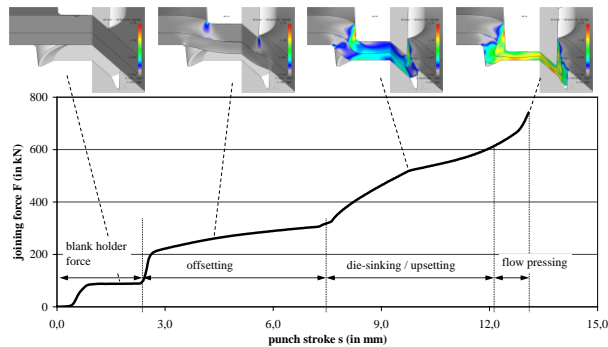


Fig. 3. Steps in the clinching process and correlation to the stroke-force-curve; S380 / S235 6+4mm; d_o : 30 mm; strain with color bar from 0 to 2

2.2 Predictability

Due to the large number of variables in the clinching process (Table 1) analytical methods to describe the process are limited. [13,14] use a volume based approach to define suitable tool geometries. First research in adapting existing analytical approaches for calculating the force and the stresses in the tool were done by [15]. To predict force and tool geometry as well as the final joint geometry, especially neck thickness and undercut, FE-analysis is an instrument often used [16,17,18,19,20,21,22,23,24]; also predicting process details including mathematical methods [25,26,27] or process design methods [28].

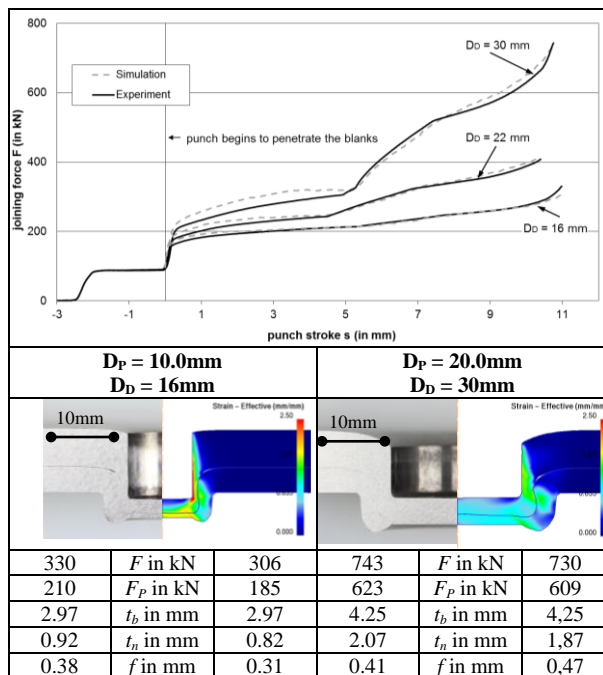


Fig. 4. Verification of simulation and experiment; S380MC – 6mm in S380MC – 4mm; die diameters $D_D = 16/30\text{mm}$; punch diameters $D_p = 10/20\text{mm}$

As a basis for numerical simulation one main parameter is the flow curve of the sheet material. Regarding the very strong deformation in the clinching process experimental data for very high values of strain are needed. This data is carried out in compression tests using round blanks. In Fig. 4 is shown the verification of simulation and experiment for the material combination S380MC (6.0mm) in S380MC (4.0mm). As to be seen, there is a quiet good correlation between the force-stroke-curves in experiment and simulation and between the geometrical data as well. The proved predictability of FE-analysis is the basis for further numerical investigations on the thick sheet clinching.

In Fig. 5 cross correlations between parameters on the basis of FE-analysis are shown for the small clinch joint with a die diameter of 16mm. The diagram illustrates the complexity of the clinching process and the effect of changed parameter values on the joint quality. In the considered room of variation the raising punch diameter leads to an increasing undercut. In contrast the effect of the die depth on the undercut is strongly nonlinear in this area and the minimum value of undercut for each punch diameter depends on the die depth. Such correlations can easy be studied in numerical analysis whereas the expenses are very high in order to describe these relationships experimentally.

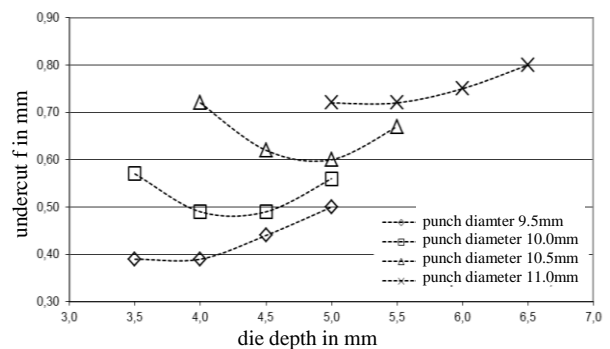


Fig. 5. Die depth and punch diameter versus undercut

3. PROPERTIES OF CLINCHING CONNECTIONS

3.1 Joint geometry

As already pointed out in chapter 2.2 the geometrical parameters of clinched connections can be identified in experimental studies and numerical analysis as well. The neck thickness t_n and the undercut f are the most important parameters regarding the joint strength whereas the bottom thickness t_b is very important for non destructive quality control. Based on a joint with known neck thickness, undercut and bottom thickness it is possible to draw conclusions from the bottom thickness to the other two parameters.

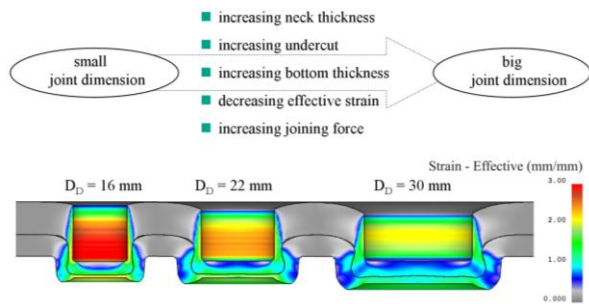


Fig. 6. Tendencies for joint dimension vs. joint geometry and force

As shown in Fig. 6 the correlations between the tool parameters and the joint geometry are sometimes difficult to describe and seldom linear. Supplemental the geometry is affected by a lot of other parameters, shown in Table 1. To get information about the dimension amount of the influence on the clinch joint geometry of all these parameters sensitivity studies have to be done.

3.2 Static and fatigue strength

Laying-up structures is only possible with known strength values of the connections. The demand on the joints geometry is varying depending on the appearing load: shear tension, pullout or peeling load. For shear loaded joints the focus is in tendency to maximize the neck thickness. In contrast for peel loaded joints the undercut should be as large as possible.

Fig. 7 shows the force-stroke-curve for the three point (die) dimensions of 16mm, 22mm and 30mm of the material combination S380 (6mm) in S235 (4mm). The increasing point dimension has an impact on the joint strength and also on the required energy to destroy the joint.

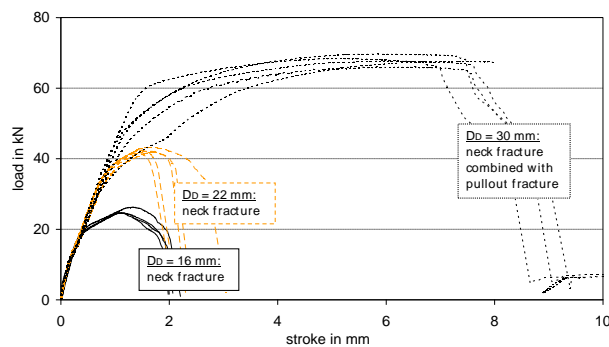


Fig. 7. Joint strength, typical curves for quasi-static testing, S380 (6mm) in S235 (4mm); Die diameters 16/22/30mm

An example for fatigue level is shown as showcase in Fig. 8 for the same material combination and the middle die dimension of 22 mm. HCF (high cycle fatigue) is on a high level compared to the quasi-static strength, about 62%. This is similar to the known level of thin sheet clinching. As to be seen in Fig. 8, the failure mode can change according to the load level. In the pictured case it changes from neck fracture for high load levels to a fracture in the sheets in / near the joint

using lower load levels. Hitherto investigations show, that the failure mode has a significant influence on the fatigue strength.

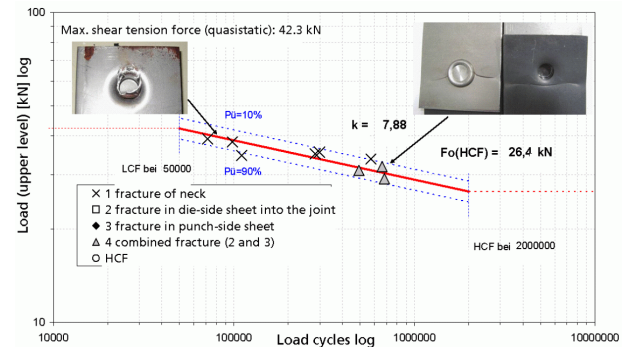


Fig. 8. Joint strength, typical fatigue curve, S380 / S235 6+4mm

Summing up the results of joint geometry and joint strength following conclusions have to be pointed out: Input parameters must be adjusted according to requirements. If small flanges or joining forces are required, small spot diameters will be selected. If high strength is required, big tool diameters will be used.

3.3 Distortion

Local radial flow inside a clinch spot is not constant over the thickness of both plates. Local strain vectors inside the spot are caused by radial and bending load to the structure. Global elastic deformation of the structure is the consequence. Blank holder force variation can minimize the bending portion of the load. To quantify the global distortion, which is induced by this local deformation, a 3.0m x 1.0m framework structure was assembled by clinching. This framework and the measured distortion of the structure are shown in Fig. 9 and 10.

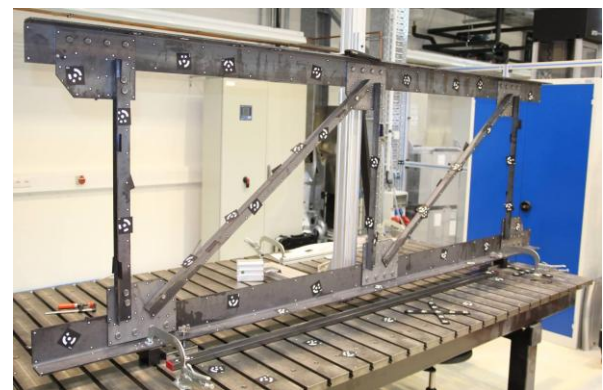


Fig. 9. Framework structure; S355MC; thickness combinations: 6mm + 6mm and 6mm + 4mm; clinching with a die diameter of 22mm

To quantify the distortion the framework was optical measured with the GOM TRITOP system. Fig. 10 shows the vector plot of distortion in y-direction comparing the framework before clinching and after clinching. The overall distortion in this direction is 5.57mm, whereas the distortion in the other two directions is nearly zero. Considering the very low

stiffness in the y-direction and the length of the assembly of 3.0m this distortion is very low.

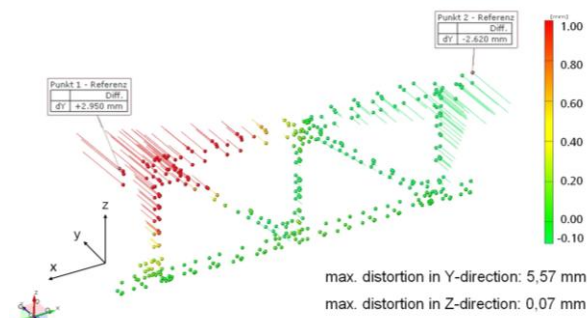


Fig. 10. Measured distortion in Y of the steel frame
x: 3.0m; z: 1.0m

4. LIMITS

4.1 Joining equipment / accessibility

Standard equipment in thin sheets are C-frames with 50kN. For clinching thick sheets frames up to 1000kN are required (compare with the needed forces in Fig. 4). Next to the task (material thickness and strength) the outer point diameter d_0 is much above all important for C-frame-force. With force and throat depth the dimension of the frame is determined and so accessibility (Fig. 11). Alternatively a single or multi spot joining operation using a conventional press or press brake is conceivable. The necessary access on both sides with a C-frame is one of the strongest limits.

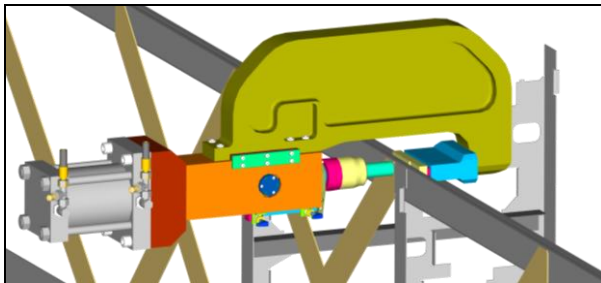


Fig. 11. Testing accessibility of a C-Frame on a clinched construction (source: Eckold GmbH)

4.2 Material restrictions

The preferred joining directions for clinching, thin sheet as well as thick sheet, are "thick to thin" and "hard to soft". If thickness or strength of the plates are on same level or inverted ratios the joint strength will be degrade. One further application limit regarding the material is elongation at material fracture. When using brittle or high strength material a fracture of the neck or die side cracks may occur during the clinching process. In this case a process layout focussing low tensile stress and low deformation level in the sheets is required – best to design with numerical simulation.

5. CONCLUSION

Clinching of thick sheet with single thickness from 4mm to 10mm is possible with a performance comparable to the state-of-the-art clinched joints in thin sheet. The good numerical forecast is the basis for

further numerical investigation on size effects, functional relations and sensitivity studies on the clinching process. However, general statements for tool and process design are not deliverable yet because of the complex correlations between the parameters and the clinching result and because of the changing boundary conditions for each case of application.

Main advantages are the process safety and a better ratio in price vs. strength (€ / kN) compared to welding or bolting, especially when going to mass production. The high fatigue level and the low structure distortion are further benefits of clinching in thick sheet applications. The main disadvantages are the limited accessibility with C-frames and a restriction to overlap joints with restricted thickness a limited ratio of the joined material.

6. REFERENCES

- [1] Israel, M., Jesche, F., Mauermann, R., Trojer, A.: *Dickblechclinchen - Innovatives Fügeverfahren für den Stahlbau*, Der Stahlbau, 79 (7), p.p. 510-514, 2010.
- [2] Mauermann, R., Israel, M.: *Umformfügen für Schienenfahrzeugstrukturen*, Rad-Schiene 11. Internationale Schienenfahrzeugtagung, Dresden 23. - 25. Februar 2011.
- [3] Mucha, J., Kaščák, L., Spišák, E.: *Joining the carbody sheets using clinching process with various thickness and mechanical property arrangements*; Archives of Civil and Mechanical Engineering, 11 (1), p.p. 135-148, 2011.
- [4] Israel, M., Trojer, A.: *Dickblechclinchen einer Fachwerkstruktur. Clinching of thick sheets in a framework structure*, Joining in Automotive Engineering 2009, Automotive Circle International-Konferenz Fügen im Automobilbau, Bad Nauheim, 2009.
- [5] Varis, J.: *Economics of clinched joint compared to riveted joint and example of applying calculations to a volume product*, Journal of Materials Processing Technology, 172 (1), p.p. 130-138, 2009.
- [6] DVS/EFB: *Clinchen - Überblick. Merkblatt DVS/EFB 3420*, DVS-Verlag, Düsseldorf, 2002.
- [7] Mauermann, R.: *Entwicklung und Optimierung von Aluminium-Fügeverfahren auf Basis der FE-Analyse*, Schweißtechnische Lehr- und Versuchsanstalt -SLV-, Duisburg: Fügen von Aluminiumprofilen und -blechen 2012, Duisburg, 07./08. März 2012.
- [8] Borsellino, C., Di Bella, G., Ruissi, V.F.: *Study of new joining technique: Flat clinching*, Key Engineering Materials, 344, p.p. 685-692, 2007.
- [9] Neugebauer, R., Dietrich, S., Kraus, C.: *Dieless clinching and dieless rivet-clinching of magnesium*, 12th International Conference on Sheet Metal, p.p. 693-698, Palermo, Trans Tech Publications, Stafa-Zürich, 2007.

- [10] Neugebauer, R., Dietrich, S., Kraus, C., Mauermann, R.: *Mechanical joining of magnesium alloys with a heated anvil as counter tool*. Kainer, K.U., Deutsche Gesellschaft für Materialkunde e.V. -DGM-, Magnesium. 8th International Conference on Magnesium Alloys and their Applications 2009, Weimar, 26-29 October 2009.
- [11] Balawender, T., Sadowski, T., Kneć, M.: *Technological problems and experimental investigation of hybrid: Clinched - Adhesively bonded joint*, Archives of Metallurgy and Materials, 56 (2), p.p. 439-446, 2011.
- [12] Mauermann, R., Grützner, R., Neugebauer, R.: *Combination of hydroforming and joining*, Steel research international, 76 (12), p.p. 939-944, 2005.
- [13] Varis, J., Lepistö, J.: *A simple testing-based procedure and simulation of the clinching process using finite element analysis for establishing clinching parameters*, Thin-Walled Structures, 41, p.p. 691-709, 2003.
- [14] Lee, C.-J., Kim, J.-Y., Lee, S.-K, Ko, D.-C., Kim, B.-M: *Design of mechanical clinching tools for joining of aluminum alloy sheets*, Materials and Design, 31, p.p. 1854-1861, 2010.
- [15] Israel, M.: *The Suitability of Analytical and Numerical Methods for Developing Clinching Processes with Thick Sheet Metal*, 2. WGP-Jahreskongress, Berlin, 27.-28.06.2012 (in print: Springer-Verlag, 2012).
- [16] Coppieters, S., Lava, P, Sol, H., Van Bael, A., Van Houtte, P., Debruyne, D.: *Determination of the flow stress and contact friction of sheet metal in a multi-layered upsetting test*, Journal of Materials Processing Technology, 210, p.p. 1290-1296, 2010.
- [17] Fricke, H., Israel, M.: *Simulation von Hybridfügeprozessen. Unterschiedliche Werkstoffe prozesssicher verbinden*, Adhäsion, 55 (7/8), p.p. 24-29, 2011.
- [18] He, X.: *Recent development in finite element analysis of clinched joints*, International Journal of Advanced Manufacturing Technology, 48 (5-8), p.p. 607-612, 2010.
- [19] Jayasekara, V., Min, K.H., Noh, J.H., Kim, M.T., Seo, J.M., Lee, H.Y., Hwang, B.B.: *Rigid-plastic and elastic-plastic finite element analysis on the clinching joint process of thin metal sheets*, Metals and Materials International, 16 (2) , p.p. 339-347, 2010.
- [20] Lebaal, N., Oudjene, M., Roth, S.: *The optimal design of sheet metal forming processes: Application to the clinching of thin sheets*, International Journal of Computer Applications in Technology, 43 (2), p.p. 110-116,2012.
- [21] Paula, A., Aguilar, M.T.P., Pertence, A.E.M., Cetlin, P.R.: *Finite element simulations of the clinch joining of metallic sheets*, Journal of Materials Processing Technology, 182, p.p. 352-357, 2007.
- [22] Saberi, S., Enzinger, N., Vallant, R., Cerjak, H., Hinterdorfer, J., Rauch, R.: *Influence of plastic anisotropy on the mechanical behavior of clinched joint of different coated thin steel sheets*, International Journal of Material Forming, 1, p.p. 273-276, 2008.
- [23] Shi, B., Wang, Y., Liu, S., Tian, H.: *Design method of the parameters of tools for clinching technology*, Advanced Materials Research, 455-456 , p.p. 1491-1496, 2012.
- [24] Zhou, Y., Lan, F., Chen, J.: *Influence of tooling geometric parameters on clinching joint properties for steel-aluminum hybrid car-body structures*; Proceedings - 2010 3rd IEEE International Conference on Computer Science and Information Technology, ICCSIT 2010 5 , art. no. 5564063, p.p. 441-445, 2010.
- [25] Long, J.-Q., Lan, F.-C., Chen, J.-Q.: *Neural network-based mechanical property prediction in the mechanical clinching joints*, Jisuanji Jicheng Zhizao Xitong/Computer Integrated Manufacturing Systems, 15 (8) , p.p. 1614-1620, 2009.
- [26] Oudjene, M., Ben-Ayed, L.: *On the parametrical study of clinch joining of metallic sheets using the Taguchi method*, Engineering Structures, 30 (6), p.p. 1782-1788, 2008.
- [27] Oudjene, M., Ben-Ayed, L., Delamézière, A., Batoz, J.-L.: *Shape optimization of clinching tools using the response surface methodology with Moving Least-Square approximation*, Journal of Materials Processing Technology, 209, p.p. 289-296, 2009.
- [28] Neugebauer, R., Rössinger, M., Wahl, M., Schulz, F., Eckert, A., Schützle, W.: *Predicting dimensional accuracy of mechanical joined car body assemblies*. 14th International Conference Sheet Metal SheMet 2011, Leuven, Trans Tech Publications: Clausthal-Zellerfeld, 2011.

Authors: Prof. Reimund Neugebauer, Prof. Wolfgang Voelkner, Dr. Reinhard Mauermann, Markus Israel Dipl.-Ing, Fraunhofer Institute of machine tools and forming technology, 09126 Chemnitz, Reichenhainer Straße 88, Germany, Phone: 0049 371 5397 0
 E-mail: reimund.neugebauer@iwu.fraunhofer.de
 wolfgang.voelkner@iwu.fraunhofer.de
 reinhard.mauermann@iwu.fraunhofer.de
 markus.israel@iwu.fraunhofer.de

Novak-Marcincin, J., Novakova-Marcincinova, L.

PRODUCTION OF PARTS REALIZED BY FDM RAPID PROTOTYPING TECHNOLOGY AND THEIR TESTING

Abstract: Paper presents knowledge about types of test in area of materials properties of selected methods of rapid prototyping technologies. In today used rapid prototyping technologies for production of models and final parts materials in initial state as solid, liquid or powder material structure are used. In solid state various forms such as pellets, wire or laminates. Basic range materials include paper, nylon, wax, resins, metals and ceramics are used. In Fused Deposition Modelling (FDM) rapid prototyping technology as basic materials ABS, polyamide, polycarbonate, polyethylene and polypropylene are mainly used. For advanced FDM applications are used special materials as silicon nitrate, PZT, aluminium oxide, hydroxyapatite and stainless steel.

Key words: rapid prototyping, fused deposition modelling, rapid prototyping materials, materials testing

1. INTRODUCTION

Rapid Prototyping (RP) involves creating a realistic model of a product's user interface to get prospective customers involved early in the design of the product. Using rapid prototyping, you model the look and feel of the user interface without investing the time and labour required to write actual code. Then you show the prototype to prospective customers, revise the prototype to address their comments, and keep repeating these two steps. Your goal is to produce a complete, agreed-upon design of the product's user interface before writing a single line of actual code. When walkthroughs and usability tests show you that customers are delighted with your prototype user interface, then programmers can model it when they code the actual product [1].

Rapid prototyping can be defined as a group of techniques used to quickly fabricate a scale model of a physical part or assembly using three-dimensional computer aided design (CAD) data. Construction of the part or assembly is usually done using 3D printing technology. The first techniques for rapid prototyping became available in the late 1980s and were used to produce models and prototype parts. Today, they are used for a much wider range of applications and are even used to manufacture production-quality parts in relatively small numbers. Some sculptors use the technology to produce exhibitions.

There are a multitude of experimental RP methods either in development or used by small groups of individuals. This paper will focused on RP techniques that are currently commercially available, including Stereolithography (SLA), Laminated Object Manufacturing (LOM), Selective Laser Melting (SLM) and Fused Deposition Modelling (FDM) techniques.

2. BASIC RAPID PROTOTYPING METHODS

Stereolithography (SLA), also known as optical fabrication, photo-solidification, solid free-form fabrication and solid imaging, is an additive

manufacturing 3D printing technology used for producing models, prototypes and production parts. The term Stereolithography was coined in 1986 by Charles W. Hull who patented it as a method and apparatus for making solid objects by successively printing thin layers of the ultraviolet curable material one on top of the other. Hull's patent described a concentrated beam of ultraviolet light focused onto the surface of a vat filled with liquid photopolymer. The light beam draws the object onto the surface of the liquid layer by layer, and using polymerization or cross-linking to create a solid, a complex process which requires automation. In 1986, Hull founded the first company to generalize and commercialize this procedure 3D Systems Inc. which is currently based in Rock Hill Sc. [1].

The Laminated Object Manufacturing (LOM) technique is used to produce low cost polymeric products (from polyvinyl chloride) that have to meet certain mechanical properties, especially if they are used to perform functional tests. The workers of Faculty of Mechanical Engineering and Naval Architecture of University of Zagreb (Croatia) realised testing the influence of the position of products in the machine working area on the mechanical properties of the product [2].

The test specimens made by LOM procedure was made of PVC film. The test bodies in LOM procedure was made on the machine SD 300 Pro, produced by Solido. SD 300 Pro is a machine which can produce transparent prototypes of PVC film, has small dimensions, and is practical for use in offices. Tests were carried out on specimens made using various orientations in the working area (Fig. 1):

- Lxy - test specimen laid in xy plane with height in z direction 4 mm,
- Pxy - test specimen raised in xy plane with height in z direction 10 mm,
- Pz - test specimen raised in z-axis with height 75 mm and 80 mm depending on whether the specimen is for tension or bending tests.

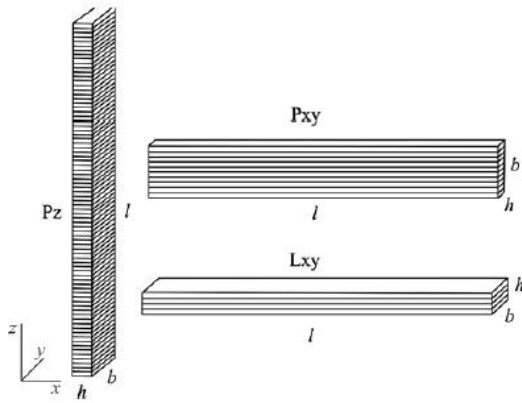


Fig. 1. Orientation of layers in test specimen produced by LOM [2]

LOM procedure provides low surface roughness parameters in all three orientations. However, the lowest are in Lxy orientation which is only logical since the final layer is pure PVC film, independent of the construction (lamination) method. In test specimens Pxy and Pz, R_a is 95 times greater ($R_a = 3 \mu\text{m}$) than in Lxy orientation. The specimens of Lxy orientation have the highest strain, even up to an average of $\varepsilon_p = 207\%$, whereas the test specimens of Pz orientation have only $\varepsilon_p = 24\%$, which is 8.5 times lower value. However, it is interesting to note that the highest strength is not the feature of the test specimens of Lxy orientation, but the test specimens of Pxy orientation. Orientation affects also the fracture surface and in test specimens Pxy the surface is toothed, i.e. delamination of layers has occurred, whereas in Lxy and Pz the surface is flat. Such fracture in Pxy orientation occurs because the stresses are applied along each layer, and in Pz orientation the fracture occurs perpendicularly to the applied test force, and this is at the same time the layer lamination. The tests carried out at LOM test specimen lead to the conclusion that Pxy orientation features optimal properties. Possibly, in case of minimal roughness requirement and higher yield stress, Lxy orientation should be selected. The price and the manufacturing speed also depend on the orientation and chamber filling, so that the orientations in z-axis direction should be avoided as much as possible [2].

Selective Laser Melting (SLM) is the digitally driven process if direct from sliced 3D CAD data in layer thicknesses ranging from 20 to 100 μm products are realized. The process then builds the part by distributing an even layer of metallic powder using a recoater, then fusing each layer in turn under a tightly controlled inert atmosphere. Once complete, the part is removed from the powder bed and undergoes heat treatment and finishing. For the SML components were realized on the TU of Cluj-Napoca (Romania) tests with application of different SML machine parameters. SLM is a complex thermo-physical process which depends on a lot of: material, laser, scan and environmental parameters. For two selected materials, a parameter study has been performed to optimize the process regarding part density, since porosity has a harmful effect on the mechanical properties of the part. Four main process parameters were selected for experiment: laser power, layer thickness, scan speed

and hatching space. These factors determine the energy supplied by the laser beam to a volumetric unit of powder material, defined as energy density, an experimental quantity which has large influence on part density. After choosing the types of supports used for parts to be processed the next step is to see what material file is assigned for the future manufacturing component. Were two types of material used for manufacturing in the test, one is Ti6Al7Nb and the other is stainless steel 316L. For the first material the optimal laser power could range from 50 to 200 W and the optimal power for stainless steel 316L is above 160 W. If the power applied on the powder bed is less than 100 W the components are not so strongly melted. The best power chosen to be applied to the next components, samples or final components is 160 W, the best parameters between the good melting, process stability and final components with good results. One of the machine parameters who can be changed is the speed of scanning witch has the following calculating relationship applied on selective laser melting machine SLM 250 Realizer. The scanning speed was tested on samples to see if the standard scan speed of 400 mm/s is the best speed to melt the stainless steel powder or could be another one. To see that, different scanning speeds were attributed to the samples. The samples with higher scanning speed were not fully melted. The big value of scanning speed parameters is not optimal one because the powder layer is not strongly and fully melted [3].

Stratasys Fused Deposition Modelling (FDM) is a typical RP process that can fabricate prototypes from ABS plastic. Researchers of Gyeongsang National University Jinju (Korea) and University of California, Berkeley (USA) realized selected tests the properties of parts fabricated by the FDM [4]. Using a Design of Experiment (DOE) approach, the process parameters of FDM, such as raster orientation, air gap, bead width, colour, and model temperature were examined. The FDM machine possesses a second nozzle that extrudes support material and builds support for any structure that has an overhang angle of less than 45° from horizontal as a default. If the angle is less than 45° , more than one-half of one bead is overhanging the contour below it, and therefore is likely to fall. Experiments were performed in which the effect of several process parameters on the mechanical behaviour of FDM parts was examined.

Fig. 2 shows magnified views of the fractured surfaces of the specimens. The Axial ($[0^\circ]_{12}$) specimens showed tensile failure of individual fibers resulting in the highest tensile strength among the FDM specimens. This strength was lower than that of the injection moulded ABS partially because the gaps between fibers reduced the effective cross sectional area. The transverse ($[90^\circ]_{12}$) specimens resulted in the lowest tensile strength because the tensile loads were taken only by the bonding between fibers, and not the fibers themselves. The cross specimen ($[0^\circ/90^\circ]_6$) consisted of a layer of fibers oriented in the 0° direction, followed by a layer in the 90° direction. The resulting failure load for this pattern, as might be expected, fell between the $[0^\circ]_{12}$ and $[90^\circ]_{12}$ specimens. The Criss-cross

$([45^\circ/-45^\circ]_6)$ specimen showed shear failure along the 45° line in the macroscopic view but the microscopic view revealed the repeated failures of individual fibers by shearing and tension [4].

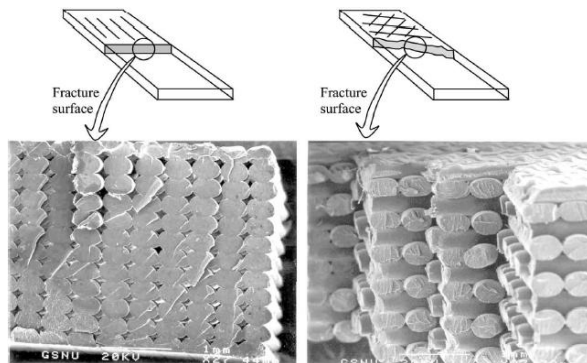


Fig. 2. Fracture surfaces of $[0^\circ]_{12}$ and $[45^\circ/-45^\circ]_6$ specimen [4]

3. DESIGN AND PRODUCTION OF THE PART BY FDM METHOD

In rapid prototyping techniques you create the realistic model of a product's user interface and you provide the look and feel of the user interface to get prospective customers involved early in the design of the product. Prototype is then shown to these customers and revised to address their comments. Final goal is to produce a complete, agreed-upon design of the product's user interface before writing a single line of actual code. After the tests that shows you that customers are delighted with your prototype user interface, programmers can model it when they code the actual product.

To prototype successfully, first select an appropriate rapid prototyping tool. There are hundreds of rapid prototyping tools available. They range from simple graphics packages that allow you to draw screens to complex systems that allow you to create animation. Each tool is better for some functions than for others. There is no perfect rapid prototyping tool. Identify your prototyping needs, then find the tool that most closely meets those needs. You can learn about different prototyping tools by consulting computer magazines, technical reports, and books that describe prototyping tools. Although several rapid prototyping techniques exist, all employ the same basic five-step process. The steps are [5]:

1. Creation of CAD models of the product parts.
2. Conversion of CAD models into STL formats.
3. Using of STL files in Rapid Prototyping devices.
4. Production of the parts by one layer atop another.
5. Cleaning of parts and assembly of the product.

Model of selected part was created and subsequently modified in CAD/CAM/CAE system CATIA V5 R19. Transfer of models between CATIA and another CA systems was implemented using the exchange format IGES where they were treated. On Fig. 3 is example of CAD model of parts in CATIA.

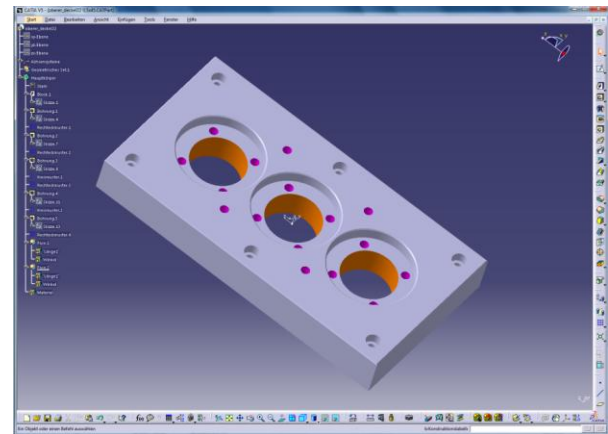


Fig. 3. Model of the part in CATIA system

On the Department of Manufacturing Technologies there is FDM UPrint 3D printer from Dimension available (Fig. 4). It is a small 3D printer with 635 x 660 x 787 mm dimensions suitable for office environment which uses the printing principle of Fused Deposition Modeling. Maximum dimensions of printed prototype are 203 x 152 x 152 mm. This printer prints only one layer of constant thickness 0.254 mm which is as the accuracy of the print in the Z axis very acceptable. This printer used as building material thermoplastic ABCplus Ivory which comes in standardized packages as fiber with a diameter of 1.6 mm rolled onto a reel. Each spool contains 500 cubic centimeters of material. The support material used is resin Soluble SR-P400 which comes in the same package as a building material. After printing the prototype it is necessary to clean the prototype of the auxiliary material [6].



Fig. 4. 3D FDM printer UPrint from Dimension

For this Fused Deposition Modelling printer can be used Catalyst program which serves to complete printing settings such as disposition of components on working desktop or set-saving modes where savings can be achieved by building and supporting material to 40% depending on the shape and parts at the expense of strength of the prototype. Catalyst is application for communication with 3D printers. In a first step are generated STL data in the CAD system that can be loaded to the Catalyst program for layered rendering of the model (Fig. 5).

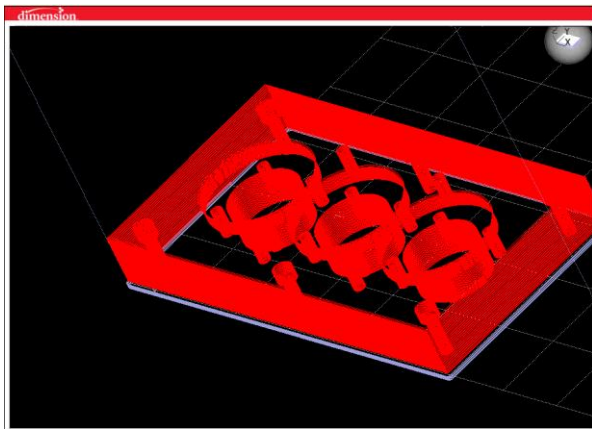


Fig. 5. Layered model of the part in Catalyst software

After starting of print cycle the system warms up printing jet and whole work area for working temperature. This lasts about 15 minutes, during which the nozzle and purifying device are calibrated. Followed by the print itself, the nozzle is moving over X - Y pad and working in the Z axis. After printing it is necessary to separate the support material from the building one. In the semi-simple components the support material can be separated without any problems, as because of reducing temperature it is particularly fragile. On Fig. 6 is view of workplace of 3D FDM printer UPrint with printed part [7].

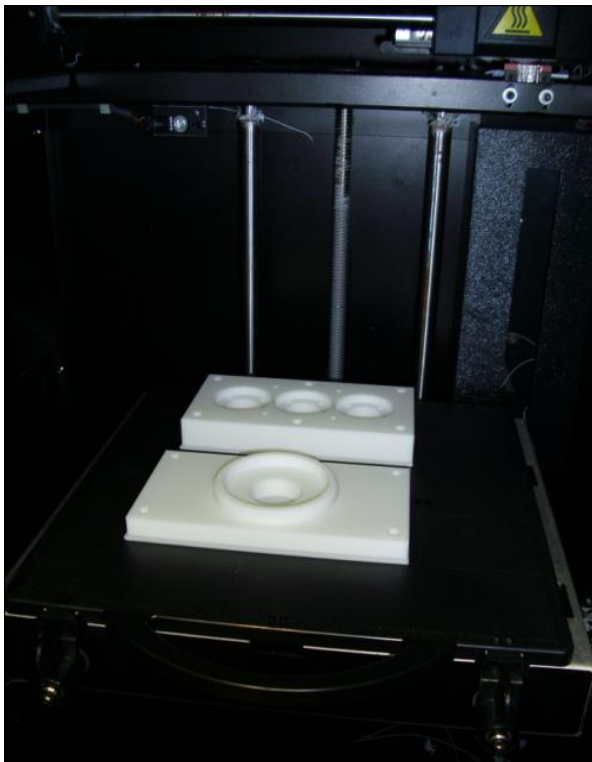


Fig. 6. Printed prototype of 3D part by FDM method

4. CONCLUSION

Printing method Fused Deposition Modeling is one of the cheapest methods on market, whether it is the price of equipment or material used. Speed of devices that are used for this method and accuracy of the print is surprising but it also has some weaknesses that may

not suit all users. Among the biggest weakness there is fixed thickness of the layer that can not be changed using this printer. Great layer thickness causes uncertainty in the Z axis and also affects the surface, which can be in some types of prototypes quite important, especially when it comes to functional area components.

5. ACKNOWLEDGMENTS

The Ministry of Education, Science, Research and Sport of SR supported this work, contract VEGA No. 1/0032/12, KEGA No. 002TUKE-4/2012 and ITMS project 26220220125.



6. REFERENCES

- [1] Plancak, M.: *Rapid Prototyping & Rapid Tooling*. FTN Publishing, Novi Sad, 2009.
- [2] Pilipovic, A., Raos, P., Sercer, M.: Experimental testing of quality of polymer parts produced by Laminated Object Manufacturing - LOM. *Technical Gazette*, Vol. 18, No. 2, 2011.
- [3] Pacurar, R., Balci, N., Prem F.: Research on how to improve the accuracy of the SLM metallic parts. In: *Proceedings of the 14th International Conference on Material Forming Esaform*, Queens Univ. Belfast, 2011, p. 1385-1390.
- [4] Ahn, S. H., Montero, M., Odell, D., Roundy, S., Wright, P. K.: Anisotropic material properties of fused deposition modeling ABS. *Rapid Prototyping*, Vol. 8, No. 4, 2002, p. 248-257.
- [5] Marcincinova, L. N., Barna, J., Fecova, V., Janak, M., Marcincin, J. N.: Intelligent design of experimental gearbox with rapid prototyping technology support. In: *15th IEEE International Conference on Intelligent Engineering Systems*, Poprad, 2011, p. 77-80.
- [6] Marcincinova, L. N., Fecova, V., Marcincin, J. N., Janak, M., Barna, J.: Effective utilization of Rapid Prototyping technology. *Materials Science Forum*, Vol. 713, 2012, p. 61-66.
- [7] Marcincin, J. N., Barna, J., Marcincinova, L. N., Fecova, V.: Analyses and Solutions on Technical and Economical Aspects of Rapid Prototyping Technology. *Technical Gazette*, Vol. 18, No. 4, 2011, p. 657-661.

Authors: Prof. Ing. Jozef Novak-Marcincin, PhD., Ing. Ludmila Novakova-Marcincinova, Technical University of Kosice, Faculty of Manufacturing Technologies, Department of Manufacturing Technologies, Bayerova 1, 08001 Presov, Slovakia, Phone.: +421 51 7723012, Fax: +421 51 7733453.
E-mail: jozef.marcincin@tuke.sk
ludmila.marcincinova@tuke.sk

Plancak, M., Stefanovic, M., Pecelj, Dj., Mihajlovic, G., Vilotic, D., Ivanisevic, A.

INFLUENCE OF PROCESS PARAMETERS ON LOAD REQUIREMENT IN ORBITAL FORGING OPERATIONS

Abstract: One of the relatively new bulk metal forming process, which in some cases offers significant advantages when compared to other alternative technologies, is orbital forging. It's application is specially advantageous when flat parts with large diameter to height ratio have to be manufactured. However, this process is very time consuming and thus not applicable for mass production.

The main characteristic of orbital forging is swinging movement of the upper die around vertical axis. This results in forging load being applied only on a small portion of the total contact area between the die and the workpiece. As a consequence of such die – workpiece constellation, forming load in orbital forging is significantly lower than in conventional operations.

Current paper presents investigation related to the load requirement as a function of main process parameters, such as billet dimensions, inclination angle, and logarithmic deformation. In the investigation numerical and analytical methods were applied.

Key words: Orbital forging, forming load, process parameters

1. INTRODUCTION

Forging is a metal forming operation which enables manufacturing of workpieces of different shapes, sizes and materials in very effective way. It is one of the oldest metal forming operations known, dating back to 5000 B.C. [1]. It can be performed at room temperature or at elevated temperatures (cold, warm and hot forging).

Beside “classical” hot close – die forging with flash, which is most elaborated and most applied variant of forging, there exist some other advanced types of forging technology.

In close – die forging without flash workpiece is completely surrounded by the dies, there is no excess material. This forging operation requires equal volume of starting billet and the finishing die. If this conditions is not fulfilled, not complete die filling or die damage are likely to occur [2], [3].

Isothermal forging is characterized by the die heating to the same temperature as the hot billet before forging operation. In this way the low flow stress of billet material is kept during forming operation and high quality forgings can be manufactured with lower load. Process is industrially applied for production of high quality workpieces made of expensive materials [3].

Warm forging uses advantages of the both hot and cold forging. In case of steel, forging temperature is between 450° - 900°, depending on steel type and required workpiece properties. Because of lower temperature then in hot forging higher accuracy of forgings can be achieved and due to higher temperature than in cold forging lower force is required [3].

In high precision forging process made components are ready to be assembled, without any subsequent machining operation. In order to achieve this, a number

of pre – conditions have to be fulfilled: high quality die cavity, no draft angle (or very small one), narrower tolerances, accurate control of temperature development during forging etc. [4].

Incremental forging is characterized by only partial contact between the die and workpiece. Whole forging operation is completed in a several numbers of increments. Typical example of incremental forging is orbital or rotary forging.

2. ORBITAL (ROTARY) FORGING

In order to reduce forming load and to increase workability of applied materials a number of incremental processes have been developed and successfully implemented in industrial practice.

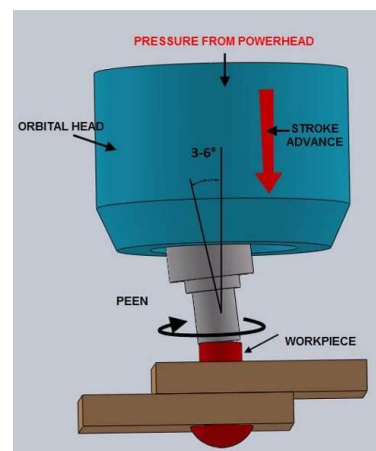


Fig. 1. Kinematics of orbital forging

Typical example is orbital (rotary) forging. In this forging variant billet is placed at the fixed lower die and is subjected to the action of upper die which moves

towards the billet. In the same time upper die swings around an axis which is slightly tilted with respect to the axis of the lower die (Fig. 1). In this way forging load is applied to only a portion of the total workpiece area. Consequently, load is only a portion of that in conventional forging.

It should be noted that in further development of this process different sub – types of upper and lower die movement have been realized, as it is shown in the Table1.

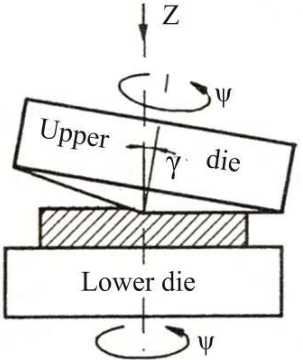
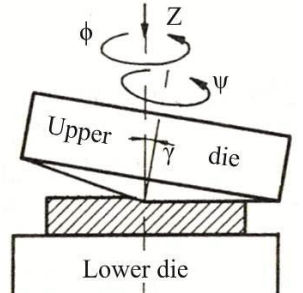
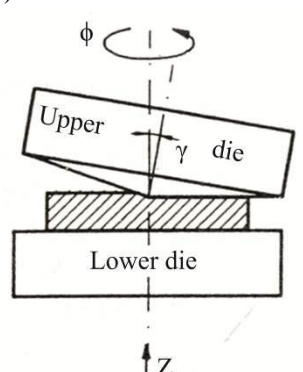
<p>a)</p> 	<p>Upper die - rotation ψ - translational z</p> <p>Lower die - rotational ψ</p> <p>Workpiece - rotational with lower die ψ</p>
<p>b)</p> 	<p>Upper die - rotational ψ - orbital (rocking) ϕ - translational z</p> <p>Lower die - stationed</p> <p>Workpiece - stationed</p>
<p>c)</p> 	<p>Upper die - orbital (rocking) ϕ</p> <p>Lower die - translational z</p> <p>Workpiece - stationed</p>

Table 1 – Types of upper and lower die movement

Because of lower forging load which occurs in orbital forging, friction and wear of the dies are also considerably lower. This results in higher quality and accuracy of the forged components. Also, formability of the billet material is increased which means that materials with lower formability potential can be also successfully forged by orbital forging.

Basically, any ferrous and non - ferrous material can be orbital forged, in cold or warm conditions (650° - 800° for steel).

Great variety of workpiece geometries can be manufactured by orbital forging but due to the nature of

this processes flat products with high diameter to thickness ratio are most easily and most successfully orbital forged (Fig. 2).



Fig. 2. Parts obtained by orbital forging



Fig. 3. Ejected gear after orbital forging

In Fig. 3 typical orbitally forged component (gear) is shown after being ejected from the die.

Main disadvantages of this process are relatively long cycle time (10 – 15 sec. in average, depending on workpiece geometry) and complicated design of the forging machine, which is caused by large lateral (tangential) forces which occur during the forging process [5, 6].

Orbital forging has been subject of numerous investigations. Analysis of technical areas where successful orbital forging can be implemented is given in [5]. Machine design for concept product forms is suggested. Compaction of powder by orbital forging is elaborated in [6]. Influence of main process parameter on final compact density is revealed. FE prediction and experimental data are in good agreement. In [7] main economical features of orbital forging are analyzed. Comparison of classical and orbital forging of cross joint component shows that orbital forging load is significantly lower that the load in “classical” forging.

Current paper elaborates a process of orbital forging of steel cylindrical billet. Influence of different relevant parameters on forging load has been investigated by numerical analysis.

3. NUMERICAL ANALYSIS OF ORBITAL FORGING OF CYLINDRICAL BILLETS

Simulation of rotary forging of steel C45E billets

was conducted by Finite Element method program package SimufactForming v10. This FE software has specific module that enables orbital movement simulation of the tool. Material C45E used in simulation is defined through flow curve:

$$\sigma = 289,671 + 668,779\varphi^{0,3184} \quad (1)$$

which is obtained in Rastegajev test [8]

3.1 Influence of initial billet

In Fig. 4 influence of initial billet geometry on load obtained by numerical analysis is given in load time diagram. Three different initial billet geometries with the same volume are orbitally forged to the final height of 10mm and final diameter of 52mm. Coefficient of friction was $\mu=0.12$ and inclination angle of the upper die axis was $\gamma=1.25^\circ$.

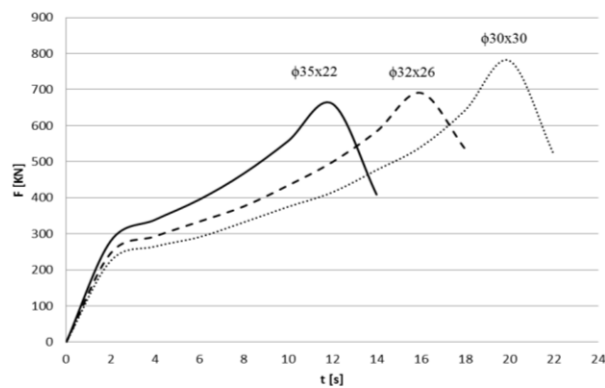


Fig. 4. Load – time diagram for three different billet geometry

Figure 5 shows load – stroke relationship.

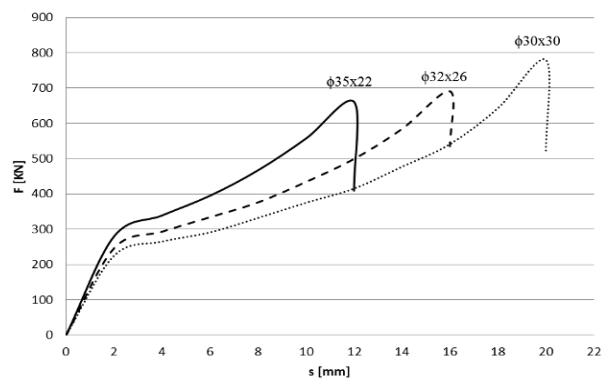


Fig. 5. Load – stroke diagram for three different billet geometry

Diagrams in Fig. 4 and Fig. 5 clearly indicate that billets with lower “ D_0/H_0 ” ratio require higher load in orbital forging.

3.2 Influence of inclination angle

Impact of inclination angle of upper die on forging load has been determined by analyzing the initial billet with the geometry $\phi 30 \times 30$ which was then forged to the final height of 10mm. Configuration at the beginning and at the end of the numerical analysis is shown in figure 6. Billet was divided on 3926 elements (Fig. 6) type Tetraheder (157), mesher was slMes

Terta. Dies are set as rigid bodies.

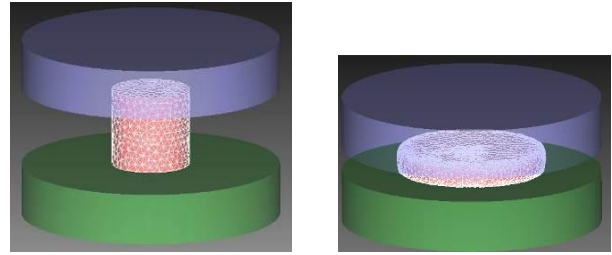


Fig. 6. Beginning and end of the process of rotary forging

Upper die performed rotary movement with 250 rotations/min. Lower die moved vertically with the velocity of 1mm/s.

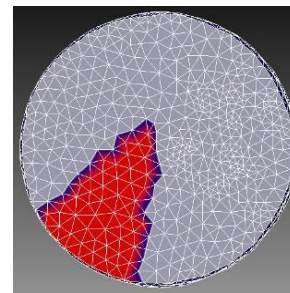


Fig. 7. Contact surface on billet in the end of forming process

Three different inclination angles are analyzed ($\gamma=1.25^\circ$, $\gamma=2^\circ$, $\gamma=3^\circ$). In Fig. 7 contact surface of the die and billet at the end of the process for rotary forging with inclination angle of $\gamma=1.25^\circ$ is presented. Contact surface between upper die and billet is approximately one eighth of the billet cross section area.

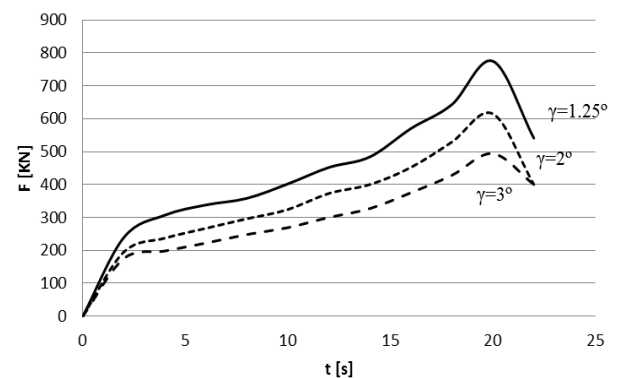


Fig. 8. Load–time diagram

Influence of inclination angle on forming load, obtained by FE – numerical analysis, is given in Fig. 8. As it can be seen, load – time curve exhibits relatively gradual increase till the final stage of the process when steep rise can be observed. After reaching maximal value, load decreases. This is so called calibration phase of the process when no vertical movement of the lower die takes place as it is illustrated in load – stroke and load – deformation diagram (Fig. 9).

The highest values of the forging load occur in the case when inclination angle is $\gamma=1.25^\circ$. In this case maximal load reaches 780 kN. Minimal load (500 kN)

takes place in case when $\gamma=3^\circ$.

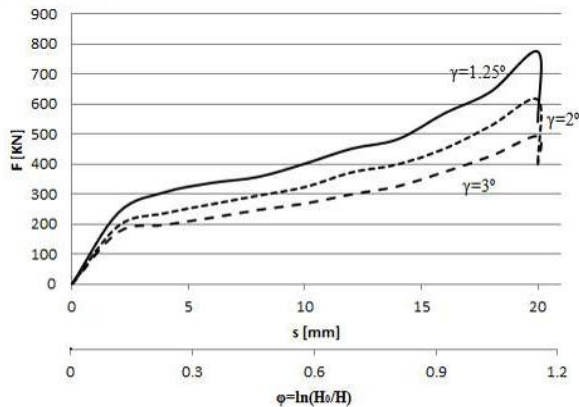


Fig. 9. Load–stroke and load–deformation ϕ diagram

In Fig. 10. load for orbital forging is compared with load needed for “classical” forging, obtained numerically and analytically by the expression (2).

$$F = \sigma A \left(1 + \frac{\mu D}{3 H}\right) \quad (2)$$

As it can be seen, load which occurs in orbital forging is significantly lower (in all three cases of inclination angle) than load occurring in “classical” forging.

Difference between analytical and numerical solution for classical forging ($\gamma=0^\circ$) is negligible.

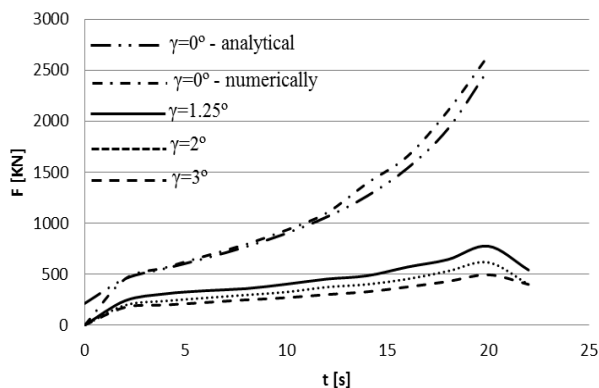


Fig. 10. Load – time diagram, $\mu=0.12$

4. CONCLUDING REMARKS

Orbital forging is a typical incremental metal forming operation which enables manufacturing of great variety of components, especially those with large diameter to height ratio. In this paper influence of some of the relevant process parameters on the forging load is elaborated by numerical analysis (FE).

It has been concluded that both, billet geometry and inclination angle have significant influence on forging load. The greater inclination angle “ γ ” the smaller maximal forging load and vice versa.

In case when “ γ ” is 3° , maximal load is 500 kN whereas by $\gamma=1.25^\circ$ this load is 780 kN. However, lower load at greater inclination angle does not mean that, in every practical greater “ γ ” should be chosen. Greater “ γ ” implies higher lateral loading of the die and

press which is one of the main drawback of orbital forging. Therefore, in every specific case optimal angle has to be set up.

In further work on current subject experimental investigation are planned which would verify numerical and analytical results.

5. REFERENCES

- [1] Kalapokian S.: *Manufacturing Processes for Engineering Materials*, Persons Prentice Hall, 2008.
- [2] Lange K.: *Handbook of Metal Forming*, Society of Manufacturing Engineering, 1994.
- [3] Altan T., Ngaile G., Shen G.: *Cold and hot forging, Fundamentals and application*, ASM International, USA, February 2005.
- [4] Milutinovic M., Vilotic D., Movrin D.: *Precision forging – tool concepts and process design*, Journal for Technology of Plasticity, 33, p.p. 73 – 89, 2008.
- [5] Standring P.M.: *Rotary forging – new challenges in a globalized market*, School of Mechanical, Materials, Manufacturing Engineering & Management, University of Nottingham, UK, p.p. 305 – 311, 2002.
- [6] Sabadus D., Frunza D., Canta T.: *High – density compaction of powder by using rotary forging technology*, Plastic Deformation of Metals Dpt., Technical University of Cluj-Napoca Romania, p.p.381 – 386, 2002.
- [7] Plancak M., Vilotic D., Stefanovic M., Movrin D., Kacmarcik I.: *Orbital forging – a plausible alternative for bulk metal forming*, International Research/Expert Conference, Dubai, UAE, 2012
- [8] Ivanisevic A., Vilotic D., Plancak M., Kacmarcik I., Movrin D., Milutinovic M., Skakun P.: *Contact stress and forming load in upsetting of prismatic billets by V-shape dies*, Journal for Technology of Plasticity, 2012, Accepted paper.

Authors: Prof. Dr Miroslav Plancak, Prof. Dr Dragisa Vilotic, M.Sc. Aljosa Ivanisevic University of Novi Sad, Faculty of Technical Sciences, Trg Dositeja Obradovica 6, 21000 Novi Sad, Serbia, Phone.: +381 21 485 2337, E-mail: plancak@uns.ac.rs

Prof. Dr Milentije Stefanovic University of Kragujevac, Faculty of Engineering, Kragujevac, Serbia

Dipl. Ing. Djordje Pecelj, Dipl. Ing. Goran Mihajlovic Zastava Kovacnica a.d. Kragujevac, Serbia

ACKNOWLEDGEMENT

Results of investigation presented in this paper are part of the research realized in the framework of the project EUREKA E!5005 financed by Serbian Ministry of Science and Technological Development. Authors are very grateful for the financial support.

Radić, N., Jeremić, D.,

**INVESTIGATION THE INFLUENCE OF ELASTIC MEDIA ON THE BUCKLING
NANOPLATE APPLYING NONLOCAL ELASTICITY THEORY**

Abstract: *The work has, through the application of the nonlocal theory of elasticity, examined the influence of the stiffness of the elastic media on the critical force of buckling of the single layer nanoplates. The observed nanoplates are simply supported and the critical force is produced through the application of Navier's method. The results are obtained for different values of the nonlocal parameter, different lengths and different values of the Winkler's coefficient of stiffness.*

Keywords: *Nanoplates, Buckling, Nonlocal elasticity, Elastic medium*

1. INTRODUCTION

Since the discovery of nanotubes, nanostructure elements attract great attention from scientists, because of their extraordinary mechanical, chemical and electrical features in comparison with conventional structure materials. In the last few years nanostructure elements nanobeams, nanomembranes and nanoplates are very often used as components in nanoelectromechanical devices. Because of its extraordinary mechanical and electrical features these nanoelements have perspective of diversified application in nanotechnology industry, including storage and energy conversion, sensors of deformation, mass and pressure, solar cells. In the following years it is expected their ever – increasing application in space crafts, biomedicine, bioelectronics, high – speed microelectronics, etc. Basic shortcoming of nanoplates or graphene sheets application can be found in their still difficult production. Having regards that majority of the potential application of nanoplates depends its mechanical behavior, mechanical analysis of nanoplates is of primary interest in the following period. Nanolevel experimental researches are very difficult, and molecular dynamics simulations are very expensive. Because of that, theoretical analysis of nanostructures has been given prominence and the application of nanotechnology has been based on that. There are three theoretical approaches in the analysis of mechanical behavior of nanostructures. Those are atomistic, hybrid atomistic – continuous and third continuous based on continuum mechanics. The first two, atomistic and hybrid atomistic – continuous are difficult for calculations and cannot be applied to larger nanostructures. Because of that, continuum mechanics are more applied in the analysis of flexing, stability and vibrations of nanostructures. It has been confirmed that the results acquired through nanostructure analysis with application of continuum mechanics is in good concordance with atomistic and hybrid approach. Continuous modeling of nanostructures has in previous years attracted significant attention from the scientists. However, it is necessary to upgrade the classical continuum mechanics for calculating small length effect, which occurs on nanolevel. The results from

experimental and atomistic simulation indicate significant influence of length effect on mechanical features of nanostructure when its dimensions are sufficiently small. Ignoring the small length effect and atomistic forces of mechanical analysis of nanostructures can lead to significant errors in solutions, and thus to wrong design of nanodevice. When the length of nanoplate or nanobeam is sufficiently reduced, the influence of inter – atomic and inter – molecular forces cannot be neglected and has a significant influence on both static and dynamic behavior. Classical continuum mechanics with its equations cannot take into consideration the influence from the length effect on mechanical behavior of nanostructure. In order to overcome this shortcoming, Eringen [1] has developed nonlocal theory of continuum which can be integrated into equations of classical continuum mechanics, by which precise anticipation of mechanical behavior of nanostructure can be determined. Eringen's nonlocal theory is based on presumption that pressure force in every material point depends on the deformity field of every point of continuous body. Interatomic forces and size of atom are directly inserted into constitutive equations, as well as parameters of the features of materials. By recognizing the importance of the nonlocal theory of elasticity in the analysis of structures of small length in the last few years, a large number of research papers has been published in which the static and dynamic and analysis of stability of nanobeams, nanorod, circular nanoplate, nanorings and nanotubes. However, in comparison with one – dimensional nanostructures (nanobeams and nanosticks), very small number of papers is dealing with the analysis of mechanical behavior of nonlocal nanoplates (graphene sheets). Nanoplates such as graphene will certainly have a significant role in making projects for future generations of nanoelectric devices. Single-layer sheets of graphene consist of string of carbon atoms which are, through covalent bonds, connected into a grid. When pressure is applied to plane, it has tendency towards buckling. Understanding the behavior of nanoplates when it comes to buckling is significant from the aspect of their correct dimensioning. For proper handling of graphene sheets in nanoelectromechanical devices, analysis of stability

under the effect of pressure must be conducted. Although buckling of nanoplate is the important part in proper designing of nanodevices from this problematic, a very small number of research papers were published. The problems of nanoplates buckling were considered in [2],[3],[4], [5],[6]. In the majority of works the elastic medium upon which single layer nanoplates rests, is modeled as a base of Winkler type base which is approximated with a serie of narrowly located and mutually independent elastic springs. Influence of the elastic medium on the behavior of nanoplate is taken in consideration in regards toward the stiffness of the springs. More realistic and accurate way of modeling the elastic medium can be achieved if the influence of the base on nanoplate is represented via two parameters. This type of modeling the base is called the Pasternak model type for modeling elastic medium. The first parameter in the Pasternak model represents normal pressure, while the second parameter takes into consideration the influence of shear stress between the elastic medium and nanoplates. The Pasternak models more physically realistic, taking into consideration the influence of elastic medium on the behavior of nanostructure and for that purpose it is applied in this work.

2. MATHEMATICAL FORMULATION

According to Eringen, nonlocal constitutive behavior of Hookean solid is described in the following constitutive differential equation:

$$1 - \mu \nabla^2 \sigma_{ij}^{NL} = \sigma_{ij}^L \quad (1)$$

Where σ_{ij}^{NL} is a nonlocal tensor of stress, σ_{ij}^L is a local tensor of stress, ∇^2 is Laplacian, $\mu = e_0 a^2$ is nonlocal parameter which represents small length effects, a is an internal characteristic of length and $e_0 a$ the constant. The choice of the length coefficient $e_0 a$, which has dimensions of length is the most important step upon which depends the validity of nonlocal model. This coefficient is determined based on adequate dispersion curve which is created based on the atomistic model. Based on conservative assessment, length coefficient has value of $e_0 a < 2 \text{ nm}$ for carbon nanotubes. Hooke's law which provides connection between the stress and deformation for orthotropic material, in nonlocal form has the following form:

$$1 - \mu \nabla^2 \begin{pmatrix} \sigma_{xx}^{NL} \\ \sigma_{yy}^{NL} \\ \sigma_{xy}^{NL} \end{pmatrix} = \begin{bmatrix} E_{11} & E_{12} & 0 \\ E_{12} & E_{22} & 0 \\ 0 & 0 & G_{12} \end{bmatrix} \begin{pmatrix} \varepsilon_{xx} \\ \varepsilon_{yy} \\ 2\varepsilon_{xy} \end{pmatrix} \quad (2)$$

from which,

$$\begin{aligned} E_{11} &= E_1 / (1 - \nu_{12} \nu_{21}), \quad E_{12} = \nu_{12} E_2 / (1 - \nu_{12} \nu_{21}) \\ E_{22} &= E_2 / (1 - \nu_{12} \nu_{21}) \end{aligned} \quad (3a-c)$$

According to which σ_{xx}^{NL} , σ_{yy}^{NL} , σ_{xy}^{NL} normal and sheer nonlocal stress, ε_{xx} , ε_{yy} i ε_{xy} are normal and sheer deformation. E_1 i E_2 are Young's modul in directions

1 and 2. G_{12} is a sheer module and ν_{12} I ν_{21} are Poisson's coefficients.

We will observe nanoplate of length L_x in x direction and length L_y , as it is represented on the Fig. 1.

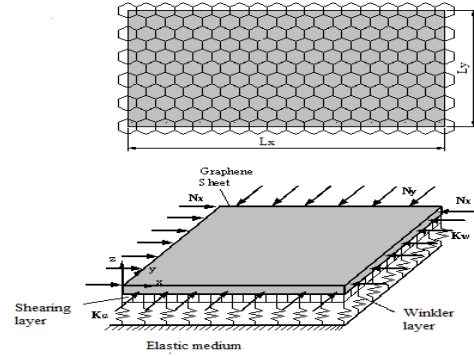


Fig. 1. Single layered nanoplate embedded on the elastic medium

The displacements of an arbitrary point of the nanoplate in relation to displacements of middle surface is derived from the following expression:

$$\begin{aligned} u_x &= u(x, y, t) - z \frac{\partial w}{\partial x} & u_y &= v(x, y, t) - z \frac{\partial w}{\partial y} \\ u_z &= w(x, y, t) \end{aligned} \quad (4a-c)$$

Deformations are given in the following expressions

$$\begin{aligned} \varepsilon_{xx} &= \frac{\partial u}{\partial x} - z \frac{\partial^2 w}{\partial x^2} & \varepsilon_{yy} &= \frac{\partial v}{\partial y} - z \frac{\partial^2 w}{\partial y^2} \\ \varepsilon_{xy} &= \frac{1}{2} \left(\frac{\partial u}{\partial y} + \frac{\partial v}{\partial x} + 2z \frac{\partial^2 w}{\partial y \partial x} \right) \end{aligned} \quad (5a-c)$$

By using the principle of virtual displacements the following differential equilibrium equations are provided:

$$\begin{aligned} \frac{\partial^2 M_{xx}}{\partial x^2} + 2 \frac{\partial^2 M_{xy}}{\partial x \partial y} + \frac{\partial^2 M_{yy}}{\partial y^2} + N_{xx} \frac{\partial^2 w}{\partial x^2} + N_{yy} \frac{\partial^2 w}{\partial y^2} \\ + 2N_{xy} \frac{\partial^2 w}{\partial x \partial y} + k_w w - k_G \left(\frac{\partial^2 w}{\partial x^2} + \frac{\partial^2 w}{\partial y^2} \right) = 0 \end{aligned} \quad (6)$$

where k_w and k_G are Winkler's stiffness coefficients and sheer layer of elastic media. N_{xx} , N_{yy} and N_{xy} are the resulting forces which take effect in the surface of the plane, while M_{xx} , M_{yy} and M_{xy} are the resulting moment of bending and they can be obtained from the following expressions:

$$N_{xx}, N_{yy}, N_{xy}, M_{xx}, M_{yy}, M_{xy} = \int_{-\frac{h}{2}}^{\frac{h}{2}} \sigma_{xx}, \sigma_{yy}, \sigma_{xy}, \sigma_{xx} z, \sigma_{yy} z, \sigma_{xy} z \, dz$$

By using the equations (5a-c), (2) and (7) a link can be established between the resulting moments and the displacement.

$$\begin{aligned} M_{xx} - \mu \nabla^2 M_{xx} &= -D_{11} \frac{\partial^2 w}{\partial x^2} - D_{12} \frac{\partial^2 w}{\partial y^2} \\ M_{yy} - \mu \nabla^2 M_{yy} &= -D_{22} \frac{\partial^2 w}{\partial y^2} - D_{12} \frac{\partial^2 w}{\partial x^2} \end{aligned}$$

$$M_{,xy} - \mu \nabla^2 M_{,xy} = -2D_{66} \frac{\partial^2 w}{\partial x \partial y} \quad (8a-c)$$

Where D_{11} , D_{22} , D_{66} and D_{12} express bending stiffness of the nanoplate and are defined in the following expressions:

$$\begin{aligned} D_{11} &= \frac{E_1 h^3}{12(1-\nu_{12}\nu_{21})} & D_{22} &= \frac{E_2 h^3}{12(1-\nu_{12}\nu_{21})} \\ D_{12} &= \frac{\nu_{12} E_2 h^3}{12(1-\nu_{12}\nu_{21})} & D_{66} &= \frac{G_{12} h^3}{12} \end{aligned} \quad (9)$$

Finally, by using equations (6) and (8a-c) we receive the main differential equation of equilibrium

$$\begin{aligned} D_{11} \frac{\partial^4 w}{\partial x^4} + 2(D_{12} + 2D_{66}) \frac{\partial^4 w}{\partial x^2 \partial y^2} + D_{22} \frac{\partial^4 w}{\partial y^4} + N_{xx} \frac{\partial^2 w}{\partial x^2} \\ + N_{yy} \frac{\partial^2 w}{\partial y^2} + k_w w - k_G \left(\frac{\partial^2 w}{\partial x^2} + \frac{\partial^2 w}{\partial y^2} \right) - \mu \nabla^2 \\ \times \left[N_{xx} \frac{\partial^2 w}{\partial x^2} + N_{yy} \frac{\partial^2 w}{\partial y^2} + k_w w - k_G \left(\frac{\partial^2 w}{\partial x^2} + \frac{\partial^2 w}{\partial y^2} \right) \right] = 0 \end{aligned} \quad (10)$$

3. THE SOLUTION

In this work we will observe the nanoplate which is placed on the simple supported on all four sides. That means that the values of the vertical displacement and the moments of bending on those edges is equal to zero. It can be mathematically formulated in the following way:

$$w = 0, \quad -D_{11} \frac{\partial^2 w}{\partial x^2} - D_{12} \frac{\partial^2 w}{\partial y^2} = 0, \quad x = 0, L_x$$

$$w = 0, \quad -D_{12} \frac{\partial^2 w}{\partial x^2} - D_{22} \frac{\partial^2 w}{\partial y^2} = 0, \quad x = 0, L_y \quad (11)$$

The equation (10) with counturing conditions (11) can be solved with Navier's method ancpiting the solution in the following form:

$$w = \sum_{m=1}^{\infty} \sum_{n=1}^{\infty} W_{mn} \sin\left(\frac{m\pi}{L_x} x\right) \sin\left(\frac{n\pi}{L_y} y\right) \quad (12)$$

where m and n are numbers of halfe wave.

If equation (12) is inserted into equation (10) we will receive the values of nondimensional critical buckling load

$$\frac{\alpha^4 + D_1 R^2 \alpha^2 \beta^2 + D_2 R^4 \beta^4 + \left[1 + \left(\frac{\mu}{L_x^2}\right) \alpha^2 + R^2 \beta^2\right] [K_W + K_G \alpha^2 + R^2 \beta^2]}{\left(\frac{\mu}{L_x^2}\right) [\alpha^4 + k + 1 R^2 \alpha^2 \beta^2 + k R^4 \beta^4] + \alpha^2 + k R^2 \beta^2} \quad (13)$$

where is :

$$\frac{N_{cr}}{D_{11}} = \frac{N_{cr} L_x^2}{D_{11}}, \quad R = \frac{L_x}{L_y}, \quad k = \frac{N_{yy}}{N_{xx}}, \quad \alpha = m\pi, \quad \beta = n\pi$$

$$K_W = \frac{k_w L_x^4}{D_{11}}, \quad K_G = \frac{k_G L_x^2}{D_{11}}, \quad D_1 = \frac{2(D_{12} + 2D_{66})}{D_{11}}$$

$$D_2 = \frac{D_{22}}{D_{11}}$$

4. NUMERICAL RESULTS AND DISCUSSION

In this work we examined the orthotropic nanoplate with the following mechanical features:

$E_1=1765\text{GPa}$, $E_2=1588\text{GPa}$, $\nu_{12}=0.3$, $\nu_{21}=0.27$ i $h=0.34\text{nm}$

where h is the thickness of nanoplate

For better interpretation of the behavior of nanoplates, new measurement unit is introduced which we call load ratio and it is marked with LR

$$LR = \frac{NCRN}{NCRL}$$

$NCRN$ is the critical force of buckling in accordance to nonlocal theory, and $NCRL$ is the critical force of buckling in accordance to local theory.

Based on the analytical solution (13) the following figure display the results fom the research

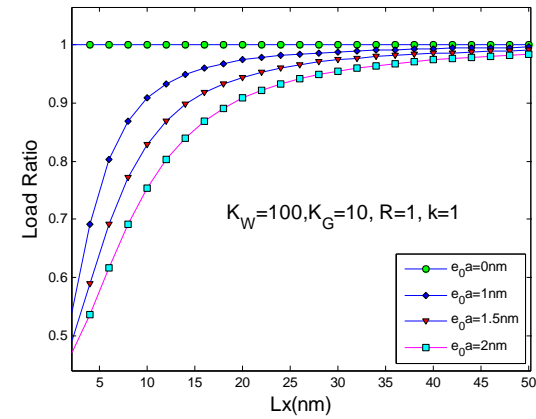


Fig.2. Change in the load ratio with length for different values of the nonlocal parameter

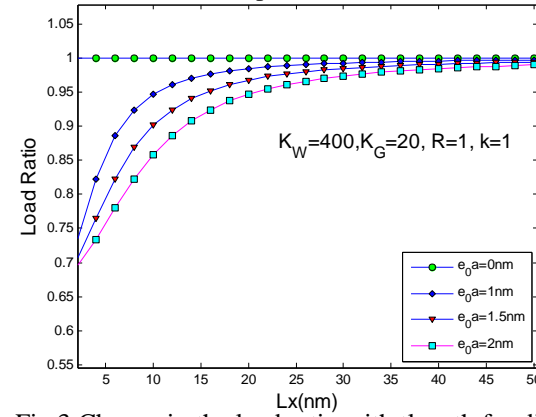


Fig.3 Change in the load ratio with length for different values of the nonlocal parameter

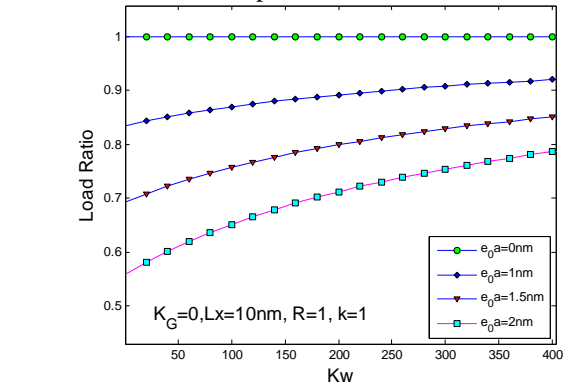


Fig.4. Change in the load ratio with Winkler's

coefficient of stiffness for different values of the nonlocal parameter

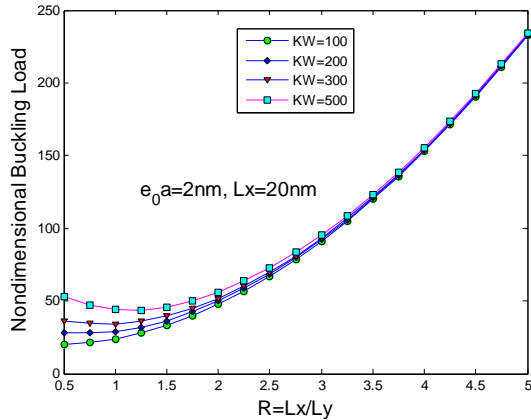


Fig.5. Change in Nondimensional Buckling Load with aspect ratio for different values Winkler's coefficient according to the local theory

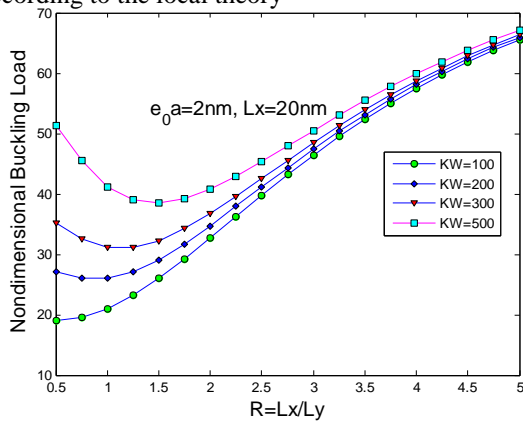


Fig.6. Change in Nondimensional Buckling Load with aspect ratio for different values Winkler's coefficient according to the nonlocal theory

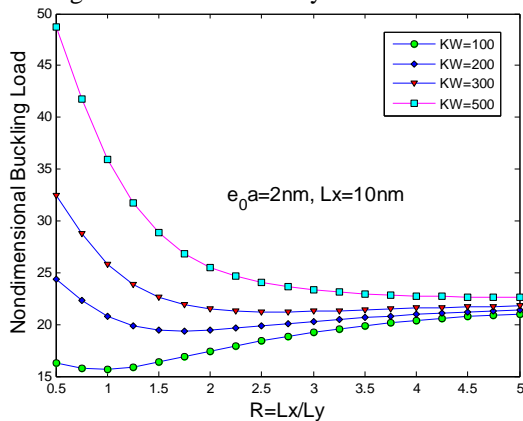


Fig.7. Change in Nondimensional Buckling Load with aspect ratio for different values Winkler's coefficient according to the non local theory

Based on Fig. 1. and Fig.2. it can be deduced that in the process of using small lengths of nanoplates we have a big deviation in the value of critical force when we apply nonlocal theory. The deviation is reduced with the increase of the length of nanoplate, and with the length 45 nm the deviation is very small. With the increase in value of the Winkler's coefficient of stiffness, the relation between the load ratio between the local and nonlocal theory is decreasing, which can be clearly seen on the Fig.3, and the value of the length

according to which the load ratio is equal to one is also decreased. With the increasing of value of the nonlocal parameter the load ratio is reducing and the most unfavorable case is when that values is 2 nm. With the increase in values of the nonlocal parameter, small length effect is also increased to the value of the critical force of buckling. Difference in the application of nonlocal and local theory can be clearly seen on the Fig.1,2 and 3. With the increase of the R value, the length L_y is decreasing and then the small length effect comes to prominence. That can be clearly seen if we compare the results presented on Fig.6. and Fig.7. when the length is reduced from 20 nm to 10 nm. Winkler's coefficient of stiffness also significantly influences the plates behavior. On Fig. 7. we can see values of $K_w=500$. With the increase of values in R the value of the critical force stops to increase and the trend continues with the further increase in the values of K_w .

4. CONCLUSION

Small length effect related to nanoplates, conjugated with the stiffness of elastic media and the value of critical force in accordance with nonlocal theory, depends on the values of Winkler's coefficient and the length of nanoplate. With the change of length under the same values of stiffness results in significant change in the values of critical force.

5. REFERENCES

- [1] Eringen,C.: *Nonlocal Continuum Field Theories*, Springer-Verlag, New York, 2002.
- [2] Pradhan,S.C.,Murmu,T.: *Buckling of biaxially compressed orthotropic plates at small scales*, Mech. Res.Commun,36, 933-938, 2009.
- [3] Pradhan,S.C.,Murmu,T: *Small scale effect on the buckling of single-layered graphene sheet under biaxial compression via nonlocal continuum mechanics*, Comput. Mater. Sci. 47, 268-274, 2009.
- [4] Pradhan,S.C.,Murmu,T.: *Small scale effect on the buckling analysis of single-layered graphene sheet embedded in elastic medium based on nonlocal plate theory*, Physica E, 42, 1293-1301,2010
- [5] Aksencer,T.,Aydogdu,M.: *Levy type solution method for vibration and buckling of nanoplates using nonlocal elasticity theory*, Physica E,43, 954-959,2011
- [6] Pradhan,S.C.,Phadikar,J.K.: *Nonlocal theory for buckling of nanoplates*, Int. Journal of Struct. Stab. and Dynamics,3,411-429,2011
- [7] Murmu,T.,Adhikari,S.: *Nonlocal vibration of bonded double-nanoplate systems*, Composites Part B, 42,1901-1911,2011.

Authors: Doc. dr Nebojša Radić, Dejan Jeremić, graduate mechanical engineer, University of East Sarajevo, Faculty of mechanical engineering, Vuka Karadžića 30, 71420 Lukavica, BiH-Republic of Srpska, Phone.: +387 57 340-847, Fax: +387 340-847. E-mail: nesor67@yahoo.com, dejan.jeremic@yahoo.com

Rajnovic, D., Sidjanin, L.

THE DUCTILE TO BRITTLE TRANSITION TEMPERATURE OF UNALLOYED ADI MATERIAL

Abstract: In material selection, especially in low temperature conditions, one of very important factors it is a ductile to brittle transition temperature, i.e. the temperature when material becomes too brittle to use. In this paper transition temperature determined by impact energy in temperature interval from -196 to $+100^{\circ}\text{C}$ of unalloyed austempered ductile iron with different microstructures have been studied. It was found that transition temperature is influenced by amount of retained austenite, as well as ausferrite morphology. The lowest transition temperature was obtained for ADI material austempered at 350°C for 1 hour, which possesses the most favorable combination of retained austenite volume fraction accompanied with fine acicular appearance of ausferrite. If amount of retained austenite is lower (in case of austempering at 300°C for 1 hour) or morphology is too coarse (after austempering at 400°C for 1 hour) than ductile to brittle transition temperature shifts to higher temperatures.

Key words: ADI material, transition temperature, microstructure, fracture mode

1. INTRODUCTION

In recent years, there has been great interest in the processing and developing of austempered ductile irons (ADI). The ADI materials possess a unique microstructure of ausferrite, produced by the heat treatment (austempering) of ductile irons. The ausferrite is a mixture of ausferritic ferrite and carbon enriched retained austenite [1, 2]. Due to this unique microstructure, the ADI materials have remarkable combination of high strength, ductility and toughness together with good wear, fatigue resistance and machinability [3]. Consequently, ADI materials are used increasingly in many wear resistant and tough engineering components in different sectors including automotive, trucks, construction, earthmoving, agricultural, railway and military [3].

During the austempering, the ADI undergoes a two stage transformation process [1-3]. In the first stage, the austenite (γ) transforms into mixture of ausferritic ferrite (α) and carbon enriched retained austenite (γ_{HC}), a product named - ausferrite. If the casting is held at the austempering temperature too long, then the carbon enriched retained austenite (γ_{HC}) further decomposes into ferrite (α) and carbides [1]. The occurrence of carbides in the microstructure makes the material brittle and therefore, that reaction should be avoided. Hence, the optimum mechanical properties of ADI material can be achieved upon completion of the first reaction, but before the second reaction starts, i.e. inside processing window.

The austempered ductile iron (ADI) materials are widely used for large parts of machinery that work in all weather conditions. In view of that, it is of a great importance to know the behavior of ADI at low temperatures [4, 5]. One very important criterion for materials selection, especially in low temperature applications, is the ductile to brittle transition temperature.

For that reason, in this paper ductile to brittle transition temperature of unalloyed austempered ductile iron have been studied.

2. EXPERIMENTAL PROCEDURE

The unalloyed ductile iron has been examined in as-cast and austempered condition. The chemical composition (in mas. %) of as-cast material was: 3.53% C, 2.53% Si, 0.347% Mn, 0.045% Cu, 0.069% Ni, 0.055% Cr, 0.031% Mg, 0.018% P and 0.042% S.

The ductile iron has been produced in commercial foundry and cast into the standard 25.4 mm (1 inch) Y-block sand molds. The samples for mechanical testing were machined from the lower parts of Y blocks in order to avoid any segregation or porosity. After machining, the samples have been heat treated to produce an ADI material. The samples were austenitized at 900°C for 2 hours in protective atmosphere of argon and then rapidly quench in salt bath at an austempering temperature of 300, 350 or 400°C . The austempering time was 1 hours in all cases. Austempering temperature and time were chosen upon literature and previous experiments [1, 4] in order to achieve different microstructure morphologies with different content of retained austenite.

To define transition temperature curves, Charpy impact test was performed in interval from -196 to $+100^{\circ}\text{C}$. The impact energy was measured on unnotched Charpy specimens ($10 \times 10 \times 55$ mm) using a instrumented Charpy impact machine „RPSW/A“, Schenck-Treble with a maximum energy capacity of 300 J. The testing procedure was according to EN 10045. At least three specimens for each temperature were tested. In case of testing at -196 , -100 , -60 and -40 the specimens were cooled in a bath containing mixture of ethyl alcohol and liquid nitrogen for 10 minutes. For tests at -20 , 0 and $+100$ an environmental chamber was used to cold or heat the specimens for 30 minutes. After the specimens have

reached the required temperature, they were quickly fractured within 5 seconds time interval. According to standard EN 10045 the 5 seconds time interval is acceptable for the duration of the test and no significant temperature loss can be expected [5].

Besides the determination of impact energies at different temperatures, other mechanical properties, namely, tensile properties (EN 10002) and Vickers hardness (ISO 6507) have been determined at room temperature.

Conventional metallographic preparation technique (mechanical grinding and polishing followed by etching with nital) was applied prior to light microscopy (LM) examinations of samples cut from Charpy specimens. For microstructural characterization, a “Leitz-Orthoplan” metallographic microscope was used. The volume fraction of retained austenite in

ADI material was determined by x-ray diffraction technique using “Siemens D-500” diffractometer with nickel filtered Cu K α radiation.

3. RESULTS AND DISCUSSIONS

3.1 Microstructure

The light micrographs of the ductile iron microstructure (polished and etched surface) are given in Fig. 1. The spheroidisation of graphite in all specimens was more than 90%, with average graphite volume fraction of 10.9%, nodule size of 25 to 30 μm and nodule count of 150 to 200 per mm^2 , Fig. 1a. The as-cast microstructure of ductile iron was mainly ferritic with up to 10% of pearlite, Fig. 1b.

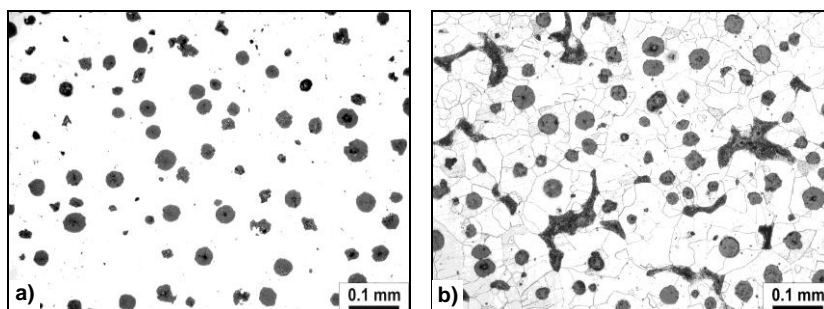


Fig. 1. Microstructure of as-cast ductile iron material: a) polished; b) etched

The influence of austempering temperature on microstructure morphology of unalloyed ADI material is shown in Fig. 2. The microstructure of all samples is fully ausferritic consisting of mixture of ausferritic ferrite and carbon enriched retained austenite. However, increasing the transformation temperature from 300 to 400°C changes the ausferritic morphology, from needle-like (Fig. 2a) to more plate-like (Fig. 2c). At lower temperatures, undercooling is larger leading to a slow diffusion rate of carbon [6]. Consequently,

nucleation of ausferritic ferrite plates is favorable, while their growth is delayed. In these conditions, the resultant microstructure is consisted of fine but dense ausferritic ferrite plates of acicular morphology [6, 7]. At higher austempering temperatures the carbon diffusion rate is higher and faster, promoting growth of ausferritic ferrite plates, which will be larger and coarse in nature [7]. These microstructure differences at lower and higher austempering temperatures are clearly visible in Fig. 2a to 2c.

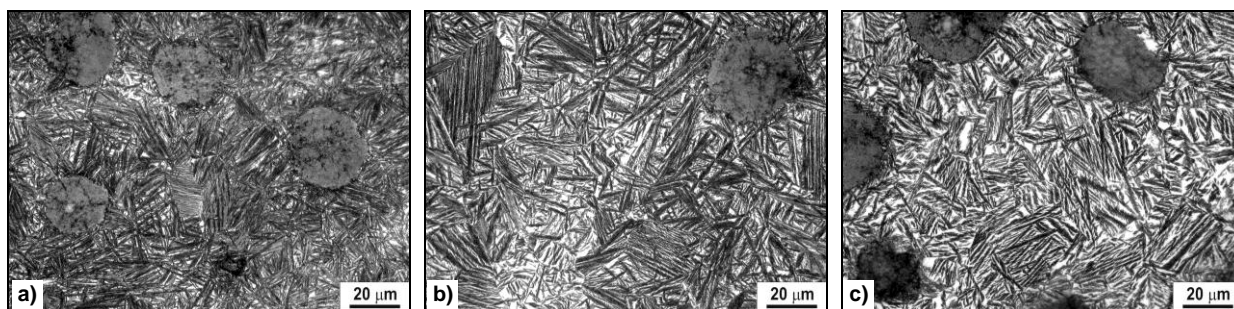


Fig. 2. Microstructure of unalloyed ADI material austempered for 1 hour at: a) 300°C; b) 350°C; c) 400°C

The volume fraction of retained austenite (V_γ) for ADI material is given in Table 1. With the increase of austempering temperature, the value of retained austenite increases, also. At higher austempering temperature the diffusion of carbon is increased, growth of ausferritic ferrite plates is more favorable than nucleation and the resulting microstructure is coarse and more plate-like [7]. In these conditions, the higher volume of austenite can be enriched with carbon

and stabilized, resulting in overall increase of retained austenite volume fraction (V_γ).

Austempering temperature/time	300°C/1h	350°C/1h	400°C/1h
Volume of retained austenite, V_γ (%)	16%	24.9%	31.4%

Table 1. Volume fraction of retained austenite, V_γ (%)

3.2 Mechanical properties

The mechanical properties of materials used, tested at room temperature are given in Table 2. It can be seen that the mechanical properties of ADIs after austempering are significantly increased. This is

contributed to change of microstructure from ferritic/pearlitic of as-cast ductile irons to ausferritic in ADI materials. The increase of ductility at higher austempering temperatures is correlated to increase of retained volume fraction [2, 3, 8].

Material	Proof strength, $R_{p0.2}$ [MPa]	Tensile strength, R_m [MPa]	Elongation, A_5 [%]	Impact energy, KO [J]	Hardness HV30
As-cast	326	473	22.2	118.69	164
ADI-300°C/1h	1395	1513	3.8	64.64	460
ADI-350°C/1h	1071	1221	8.2	108.34	355
ADI-400°C/1h	759	1032	13.1	139.80	296

Table 2. Mechanical properties at room temperature

3.3 Transition temperature

The results of the Charpy impact testing in temperature interval from -196 to $+100^\circ\text{C}$ are given graphically in Fig. 3. It can be seen, from Fig. 3, that for each set of impact energy data there are three characteristic regions: the region of high values - upper shelf, the region of low values - lower shelf and the transition region.

That systematic variation of impact energy was fitted independently using Burr type function proposed by Todinov [9] and appropriate procedure published in literature [10]. The equation is:

$$E = E_L + (E_U - E_L)\{1 - \exp[-k(T - T_0)^m]\} \quad (1)$$

where: E - impact energy for given temperature T , E_L - lower shelf energy, E_U - upper shelf energy, k and m - parameters determining the scale and the shape of the curve and T_0 - location parameter determining the displacement of the curve along the temperature axis.

The calculated parameters of the transition curves and the values for transition temperature - $T_{0.5}$, defined as temperature at which impact energy is average of upper and lower shelf values ($E_{0.5}$), are given in Table 3. The transition temperature ($T_{0.5}$) is used commonly, in order to describe material behavior at low temperatures and it is at the same time an engineering data for materials selection.

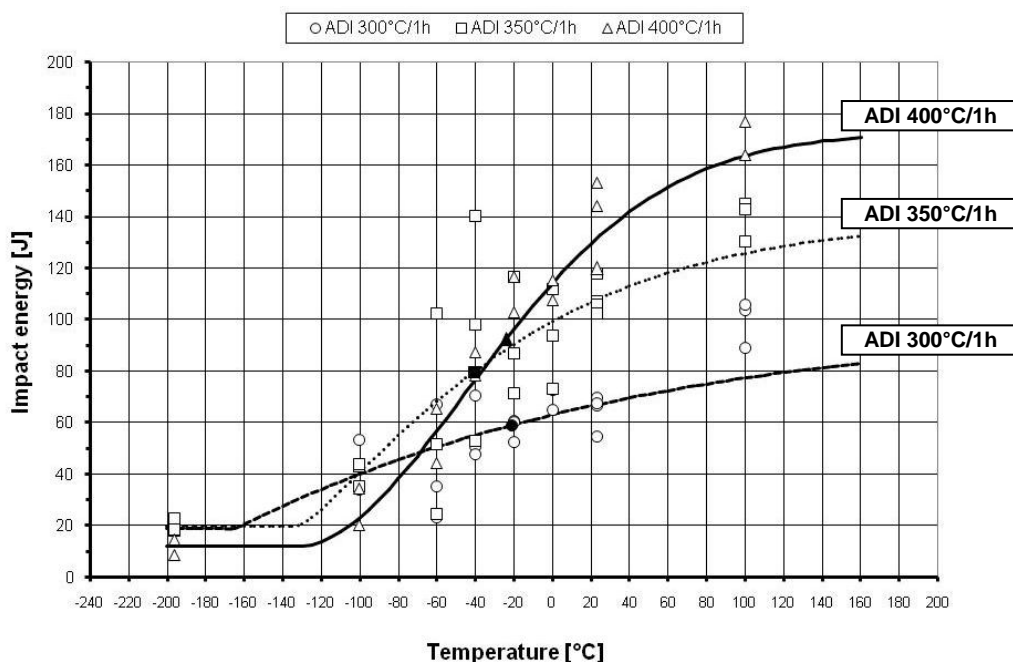


Fig. 3. The impact energies and transition temperature curves (● - $T_{0.5}$ for ADI 300°C/1h; ■ - $T_{0.5}$ for ADI 350°C/1h; ▲ - $T_{0.5}$ for ADI 400°C/1h)

Material	Lower shelf, E_L [J]	Upper shelf, E_U [J]	T_0 [°C]	k	m	Transition	
						Energy, $E_{0.5}$ [J]	Temp., $T_{0.5}$ [°C]
ADI-300°C/1h	18.87	99.43	-165.28	4.1337×10^{-3}	1.0300	59.15	-20.84
ADI-350°C/1h	19.90	139.37	-131.70	2.8035×10^{-3}	1.2221	79.64	-40.86
ADI-400°C/1h	11.99	172.65	-131.26	1.2207×10^{-4}	1.8497	92.32	-24.20

Table 3. The parameters of the transition curve equation and transition temperature $T_{0.5}$

It is well known that materials with bcc crystal structure (like ferrite) are sensitive to low temperatures, i.e. they become suddenly brittle. On the other hand, materials with fcc crystal structure (austenite) are more stable, exhibiting only a slight change in fracture mode. Hence, the presence of retained austenite in volume fraction of 16, 24.9 and 31.4% for ADI austempered at 300°C/1h, 350°C/1h and 400°C/1h, respectively, significantly influence the behavior of ADI material at low temperatures delaying appearance of brittle fracture. The lowest transition temperature of $T_{0.5}=-40.86^{\circ}\text{C}$ was determined for ADI material austempered at 350°C for 1 hour, which possesses the most favorable combination of retained austenite volume fraction accompanied with fine acicular appearance of ausferrite. If amount of retained austenite is lower (in case of austempering at 300°C for 1 hour) or morphology is too coarse (after austempering at 400°C for 1 hour) than ductile to brittle transition temperature shifts to higher temperatures of $T_{0.5}=-24.20^{\circ}\text{C}$ and $T_{0.5}=-20.84^{\circ}\text{C}$, respectively. Therefore, the transition temperature is not only determinate by amount of retained austenite but also with its refinement, i.e. with appearance of fine acicular ferrite with austenite present as film in-between the ferrite sheaves [11]. Furthermore, from Fig. 3 it might be observed that ADI material austempered at 400°C for 1h possesses highest impact energies until -32.63°C . At temperatures lower than -32.63°C the ADI austempered at 350°C for 1h have the highest impact energies, while from -101.41 to -196°C the ADI 300°C/1h exhibits highest values. It appears, that at very low temperatures the microstructure refinement (fine acicular ausferrite) has the most important influence on ductility, while at higher temperatures the amount of retained austenite is dominant factor which give high ductility.

4. CONCLUSIONS

The results obtained show that ductile to brittle transition temperature of unalloyed ADI material depends both on amount of retained austenite and microstructure morphology.

At higher temperatures, impact energies are primary influenced by amount of retained austenite, while at low temperatures the fine acicular appearance of ausferrite yields higher energies.

The lowest transition temperature of $T_{0.5}=-40.86^{\circ}\text{C}$ was determined for ADI 350°C/1h, whereas temperatures of $T_{0.5}=-24.20^{\circ}\text{C}$ and $T_{0.5}=-20.84^{\circ}\text{C}$ have been determined for ADI 300°C/1h and ADI 400°C/1h, respectively.

5. ACKNOWLEDGMENT

The Ministry of Education and Science of the Republic of Serbia supported the present work through the Technology Development Project TR34015.

6. REFERENCES

- [1] Sidjanin, L., Smallman, R. E.: *Metallography of bainitic transformation in austempered ductile iron*, Materials Science and Technology, 8/12, p.p. 1095-1103, 1992.
- [2] Elliott, R.: *The role of research in promoting austempered ductile iron*, Heat Treatment of Metals, 24/3, p.p. 55-59, 1997.
- [3] Harding, R. A.: *The production, properties and automotive applications of austempered ductile iron*, Kovove Materialy-Metallic Materials, 45/1, p.p. 1-16, 2007.
- [4] Rajnovic, D., Eric, O., Sidjanin, L.: *Transition temperature and fracture mode of as-cast and austempered ductile iron*, Journal of Microscopy, 232/3, p.p. 605-610, 2008.
- [5] Ratto, P. J. J., Ansaldi, A. F., Fierro, V. E., Aguera, F. R., Villar, H. N. A., Sikora, J. A.: *Low temperature impact tests in austempered ductile iron and other spheroidal graphite cast iron structures*, Isij International, 41/4, p.p. 372-380, 2001.
- [6] Yang, H. H., Putatunda, S. K.: *Influence of a novel two-step austempering process on the strain-hardening behavior of austempered ductile cast iron (ADI)*, Materials Science and Engineering A-Structural Materials Properties Microstructure and Processing, 382/1-2, p.p. 265-279, 2004.
- [7] Chang, C. H., Shih, T. S.: *Ausferrite Transformation in Austempered Alloyed Ductile Irons*, Transactions of the Japan Foundrymen's Society, 13, p.p. 56-63, 1994.
- [8] Rajnovic, D., Eric, O., Sidjanin, L.: *The standard processing window of alloyed ADI materials*, Kovove Materialy, 50/3, p.p. 1-10, 2012.
- [9] Todinov, M. T.: *Fitting impact fracture toughness data in the transition region*, Materials Science and Engineering A-Structural Materials Properties Microstructure and Processing, 265/1-2, p.p. 1-6, 1999.
- [10] Novovic, M., Effect of microstructure and prestaining on ductile to brittle transition in carbon- manganese weld metals, PhD thesis, The University of Birmingham, Birmingham, UK, 2001.
- [11] Aranzabal, J., Gutierrez, I., Rodriguez-Ibabe, J. M., Urcola, J. J.: *Influence of the amount and morphology of retained austenite on the mechanical properties of an austempered ductile iron*, Metallurgical and Materials Transactions A (Physical Metallurgy and Materials Science), 28A/5, p.p. 1143-1156, 1997.

Authors: M.Sc. Dragan Rajnovic,

Prof. Dr. Leposava Sidjanin,

University of Novi Sad, Faculty of Technical Sciences,
Department for Production Engineering,

Trg Dositeja Obradovica 6, 21000 Novi Sad, Serbia,

Phone.: +381 21 485-2338, Fax: +381 21 454-495.

E-mail: draganr@uns.ac.rs, lepas@uns.ac.rs

Skakun, P., Plančak, M., Vilotić, D., Lužanin, O., Milutinović, M., Movrin, D.

MANUFACTURING OF GEAR-LIKE COMPONENTS BY METAL FORMING – POSSIBILITIES AND LIMITATIONS

Abstract: In the last several decades, improvement and development of metal forming methods to enable production of gears and gear-like components has been taking place. Application of these methods has many advantages among which are material and energy savings, quality improvement, and high productivity.

There are a number of metal forming methods which can be applied in production of gears and gear-like components. In this paper, some of the most frequently used metal forming methods are presented: forging, orbital forging, extrusion, rolling, GROB technique and fine blanking.

Also, some results of investigation of radial extrusion of gear like elements which are obtained in Metal forming laboratory at the Faculty of technical sciences in Novi Sad are described and analyzed.

Key words: metal forming, gear production

1. INTRODUCTION

There is a permanent demand in industry for metal components which transmit load and torque in different machines, devices and other equipment. For rotational transmission in most cases various gear and gear-like components are used for that purpose.

Although gears are predominantly produced by metal cutting technologies, manufacturing of such elements can be also performed by metal forming operation. This alternative offers a number of advantages when compared with machining operation: better material utilization, shorter production time, higher fatigue strength of produced gears, longer life-time of gears etc. However, manufacturing of gears and gear-like components by metal forming is limited by a number of factors: geometry (gear module, diameter), materials, high die and machine cost. Therefore, an optimal variant for gear production has to be adopted and applied for every specific case.

In the first part of this paper a short review of the possibilities for gear manufacturing by metal forming operations is given, while the second part presents some details of own investigation of gear cold extrusion.

2. DIFFERENT POSSIBILITIES OF GEARS PRODUCTION BY METAL FORMING METHODS

There are many different metal forming methods which are used in production of gears and gear-like components. Most common are forging, orbital forging, extrusion, rolling, GROB technique and fine blanking. Main characteristics of these methods are clarified further on.

2.1 Forging

Forging is applied in gear production both as a cold and hot operation.

In the 1950's the lack of gear cutting equipment in Germany induced the development of hot forging process to produce gears with finished formed teeth. This process was characterized by high degree of process control and the use of dies made by electro-discharge machining process which was quite new at that time [1]. After hot forging, the surface of the part does not have satisfactory quality. For this reason application of hot forging is connected with necessity of additional machining,

In Fig.1., the forming steps applied in hot forging of bevel gear are shown. Of the six required stages - from blank preparation to finished gear – the two belong to forging (second and third part in Fig.1.). The figure shows that once the forging is finished, there is a remaining flash present on the back face of the part, which has to be removed by machining. However, flashless gears can be produced by a tool with a completely enclosed cavity.



Fig. 1. Forming steps for forging bevel gears [1]

Better accuracy is achieved by cold forging, but in this case the values of required deformation force are much higher and also the underfilling of dies is likely to occur. For that reason, the value of deformation force is the limiting factor for application of cold forging process in gear production.

2.2 Orbital forging

Rotary or orbital forging is a relatively new forming technology (considerable expansion was made in 1960's). It is an incremental bulk metal forming process where upper die is inclined relative to the axis of the lower die. During relative rotation of the upper die, the contact area between the upper die and workpiece progresses through the workpiece, gradually deforming

it [2,3]. The principle of this process is presented in Fig. 2. Different shapes of workpieces require different movement of the dies. Compared with conventional forging, rotary forging has some advantages [4]: load and power are reduced due to small contact area between die and workpiece, it is possible to achieve higher deformation, wear of die is smaller and better surface quality and higher precision are obtained. Often those parts are near net shapes, which means that those parts are very close to their final shapes and dimensions. In this way finished workpieces can be manufactured with minimum machining.

Rotary forging is especially convenient for production of parts with high diameter-to-thickness ratio, such as spur bevel gears.

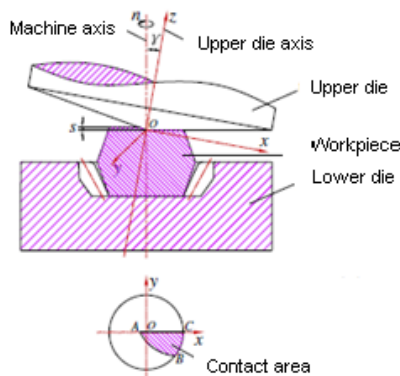


Fig. 2. Principle of orbital forging of bevel gear [4]

2.3 Extrusion

Extrusion as well as forging has wide application in gear-like components manufacturing. Extrusion process has been used in production of starter motor pinions and splined shafts for many years [1]. Initially, the forward extrusion was used, but today backward and radial extrusions are also applied. Compared to forging, the advantages of extrusion are lower risk of defect formation such as incomplete formation of tooth or die failure in near-net shape forming [5]. In Fig. 3. parts produced by cold extrusion are presented.



Fig. 3. Cold extruded splines and gears [1]

2.4 Rolling

Among the forming techniques for teeth shaping, rolling has found widespread application. There are different rolling techniques, among which the most common are rolling with flat and rolling with round tools.

The basic principle of cold rolling with flat tools involves two rolling rods with geared profile which move in opposite directions to form the rolling blank.

The rolling blank is centered and is able to rotate freely. The upper and lower rods have translatory and synchronous motion relative to one another [6]. The more the tool teeth penetrate into rolling blank, the more the process progresses. Rolling tools are divided into three zones (Fig. 4.): initial rolling phase, penetration phase and calibrating phase.

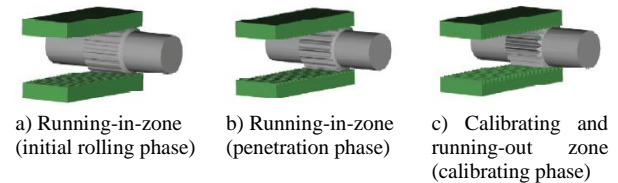


Fig. 4. Flat rolling technique – rolling zones [6]

The forming of gear-like components using the round rolling technique can be performed with two (Fig.5.) or three round tools. The advantage of this process compared to rolling with flat tools is that in this process the length of part is not limited.

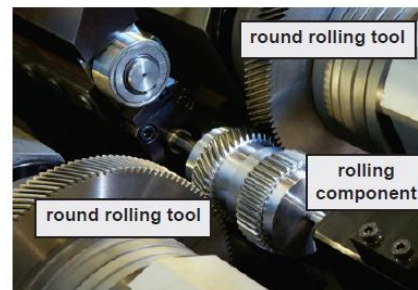


Fig.5. Round rolling technique with two rolling tools [6]

2.5 GROB technique

This technique was developed in early 60's by Ernst Grob. He developed technique and machines for cold forming of splines in a solid material (Fig. 6.) [7]. Basic principal of GROB spline shaft production is that entire cylindrical length to be formed is divided in numerous forming steps. This lowers the necessary deformation force compared to processes which apply total deformation power.

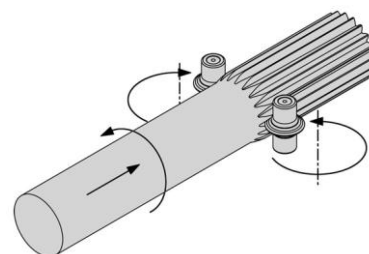


Fig. 6. GROB technique - rolling of solid material [7]

Over the years, beside this basic technique, some new were developed. They were applied to sheet metal forming (Fig. 7.), tubular metal forming (Fig. 8.), to cold reduction of solid and tubular materials etc.

There are many advantages of this process: forming cycle is short, tool life is long, surface quality is high, it is applicable to different materials, with the possibility of forming long workpieces, etc.



Fig. 7. GROB technique - cold formed sheet metal components [7]



Fig. 8. GROB technique - cold formed tubular metal components [7]

2.6 Fine blanking

Conventional blanking is a shearing process in which a punch and die are used to separate part from the sheet metal. Because of the stress state in the shear zone, in conventional blanking some parts of sheared surface have lower quality and such parts have to be remachined. This process was improved by involving additional part of tooling, ring indenter, which creates hydro-static stress that improves material ductility which slows down the fracture, Fig.9. [8]. Parts produced by this technique have smoother edge with minimal burrs. High quality of sheared surface is obtained by this process and any additional operations are not necessary. Because of additional equipment tooling costs are higher compared to blanking, which makes fine blanking more convenient for high volume production.

In Fig. 10. and Fig. 11. some examples of gear-like components manufactured by fine blanking are presented.

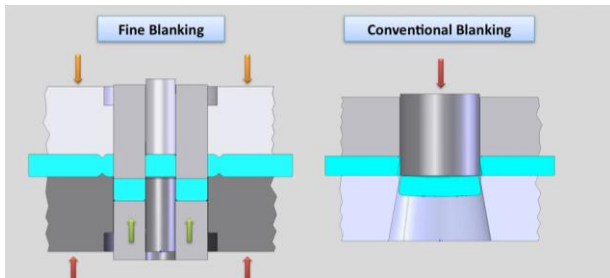


Fig. 9. Comparison of fine blanking and conventional blanking [9]



Fig. 10. Parts of automatic and dual-clutch transmission manufactured by fine blanking [10]



Fig. 11. Sprockets manufactured by fine blanking [11]

3. COLD EXTRUSION OF GEAR-LIKE COMPONENTS

Experimental, theoretical and numerical investigations of manufacturing of different types of gear-like components have been conducted in Metal forming laboratory at the Faculty of technical sciences in Novi Sad [12,13]. The gear-like component with straight parallel flanks, presented in Fig. 12. is one of the manufactured profiles. Material of the billet was Al 99,5.

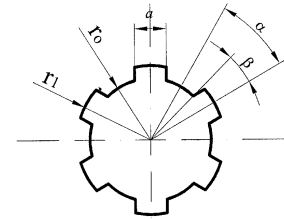


Fig. 12. Gear like component with straight parallel flank

Theoretical solution for deformation force was based upon Upper Bound theory, while simulations were performed using DEFORM 3D, Ver.10.2 software. In Fig.13. comparative diagrams of theoretical, experimental and numerical results are presented.

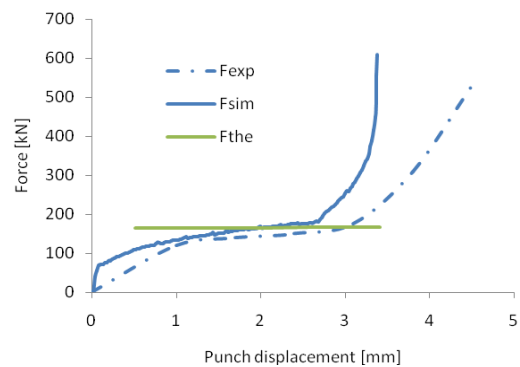


Fig. 13. Comparative load-stroke diagrams for theoretical, experimental and numerical solution

The comparative diagrams show that there is a relatively good agreement between numerically and experimentally obtained results, except in the final, corner filling phase when certain difference can be observed. In this phase numerically predicted load is slightly higher than experimental. Also, for the same load experimental stroke is somewhat longer than numerical. This could be attributed to elastic deformation of the die, and the press as well as extrusion of the flash through the clearance between the punch and the die.

As it can be seen from the diagram theoretical solution does not describe final stage of the process in appropriate way. One way to improve theoretical solution is to improve interpretation of velocity fields within the different zones of component body. High pressures and loads which occur in extrusion of gears and gear-like components can be reduced by applying so called flow relief hole and flow relieve axis principles [14].

4. DISCUSSION AND CONCLUDING REMARKS

Application of metal forming operations in gear and gear like elements manufacturing is expanding. Different operations are applied for production of different product shapes and different quality of the part can be achieved. Metal forming methods can be used from production of gear blanks as a starting part for machining, to gear components which needs subsequent treatment up to production of net shape and near net shape parts, where subsequent machining is either unnecessary or minimized.

Forging has been applied for a long period of time for production of gear blanks, but gradually beside forging many metal forming operations were developed or adjusted for production of such type of elements.

Among the advantages of application of metal forming operations in production of gears and gear-like elements are the reduction of manufacturing costs (material, energy, time savings), improved mechanical properties and dimensional accuracy, and good surface finish.

However, there are still some weaknesses which have to be overcome, such as the insufficient corner filling or excessive forming force.

In the Metal forming laboratory at the Faculty of technical sciences, the process of extrusion of gear like-elements has been investigated. Theoretical, experimental and numerical analysis showed a relatively good agreement between experimental and numerical solutions. However, the theoretical solution needs improvement. It is necessary to take into consideration the final stage of the process – corner filling. Further investigation will include the concept of divided flow into theoretical solution, with the primary aim to improve it. In the process of metal forming of complex shapes, the total force at the end of the process is very large. The divided flow leads to total force reduction which should help better filling of the die.

ACKNOWLEDGEMENT

This paper is a part of the investigation within the project EUREKA E!5005. Authors are grateful for financial support.

5. REFERENCES

- [1] Dean, T.A.: *The net-shape forming of gears*, Materials and Design, Vol 21, pp 271-278, 2000.
- [2] ASM Handbook Committee (1978) *ASM Handbook Volume 14 Forming and Forging*, American society for metals, pp 384-392
- [3] Deng, X., Hua, L., Han, X., Y., Song: *Numerical and experimental investigation of cold rotary forging of a 20CrMnTi alloy spur bevel gear*, Materials & Design, Volume 32, Issue 3, 2011, pp 1376-1389
- [4] Canta, T.; Frunza, D., Sabadus, D. & Tintelecan, C. (1998). *Some aspects of energy distribution in rotary forming processes*. Journal of Materials Processing Technology, Vol. 80-81, (August 1998) pp. 195-198 ISSN 0924-0136
- [5] Song, J.H., Im, Y.T., *The applicability of process design system for forward extrusion of spur gears*, Journal of Materials processing technology, 184, 2007, pp 411-419
- [6] Neugebauer, R., Putz, M., Hellfritsch, U., *Improved process design and quality for gear manufacturing with flat and round rolling*, Annals of the CIRP, Vol. 56, No 1, 2007, pp 307-312
- [7] www.ernst-grob.ch
- [8] Kwak, T.S., Kim, Y.J., Seo, M.K., Bae, W.B., *The effect of V ring-indenter on the sheared surface in the fine blanking process of pawl*, Journal of materials processing technology, Vol 143-144, 2003, pp 656-661
- [9] www.wildautomotive.com
- [10] www.feintool.com
- [11] www.siamsprockets.com
- [12] Plancak, M., Vilotic, D., Skakun, P., *A study of radial gear extrusion*, International journal of forming processes, Vol 6, No 1, 2003., pp 71-86
- [13] Plancak, M., Skunca M., Math, M., *Analysis, FEM simulation and experimental verification of gear cold extrusion*, Journal for technology of plasticity, Vol 29, No 1-2, pp 11-24
- [14] Ohga, K., Kondo, K., *Investigation on cold die forging of a gear utilizing divided flow*, Bulletin of the JSME, Vol 28, No 244, 1985, pp 2442-2450

Authors: Mr Plavka Skakun, Prof. dr Miroslav Plančak, Prof. Dr Dragiša Vilotić, Doc. dr Ognjan Lužanin, Mr Mladomir Milutinović, M.Sc. Dejan Movrin . University of Novi Sad, Faculty of Technical Sciences, Department for Production Engineering, Trg Dositeja Obradovica 6, 21000 Novi Sad, Serbia, Phone.: +381 21 485-2334, Fax: +381 21 454-495.
E-mail: plavkas@uns.ac.rs
plancak@uns.ac.rs
vilotic@uns.ac.rs
luzanin@uns.ac.rs
mladomil@uns.ac.rs
movrin@uns.ac.rs

Topčić, A., Lovrić, S., Cerjaković, E.

COMPARATIVE ANALYSIS OF RE/RP VERSUS CONVENTIONAL APPROACHES OF TOOL DESIGNING IN SAND CASTING

Abstract: Business conditions at the global market are forcing manufacturing companies to adapt their products to the market demands, with default quality, lower development and production costs, and a significantly shortening of delivery time of products to the market. To meet these demands and maintain, i.e., to enhance competitiveness, manufacturing companies are forced to find new ways and approaches to implementation of set tasks. The development of a number of new manufacturing technologies and approaches based on Information Technologies (IT) achievements enable to the companies to enhance or completely replace with the new approaches their existing conventional (traditional) processes, in order to improve their own market competitiveness and the competitiveness of its products. In this paper is presented a comparative analysis of the application of Reverse Engineering (RE) and Rapid Prototyping (RP) in designing of sand casting tools compared to the conventional approach to designing of sand casting tools in case when there is no documentation for part which should be produce.

Key words: Rapid Prototyping (RP), Reverse Engineering (RE), Conventional Approaches, Tool Designing, Sand Casting

1. INTRODUCTION

Regardless of the permanent progress and development in the areas of production technologies and systems, many production companies, because of objective or subjective reasons still in their everyday practice relying on traditional proven approaches in the organization of production and on the application of technologies. This approach today results in a reduction of the competitive capabilities of the company which is expressed through: a gradual increasing of production costs per unit of output (products), stagnation or lag in product quality, and the most obvious manifestation is extension of time necessary to launch the product on the market (time-to-market). On the other hand, approaches that are based on the implementation of new knowledge/technologies into everyday practice provide a good base, not only to maintain, but also for improvement of the competitive capabilities of companies.

In recent years the need for shorter period of development/redesign of products, reducing of associated costs with the default quality forcing manufacturing companies to make additional efforts to find new ways to made development/redesign of the products more effective. As consequence of significant breakthroughs in different areas of information and production technologies the ways of designing of new or redesigning of existing products have greatly changed in comparison to the traditional approach. Advances in a wide range of Computer Aided (CA) tools, technologies and approaches are greatly enhance and automate the process of developing (designing/redesigning) of products, significantly shorten the development cycle and enable optimization of future product still in the early stages of development, thus enabling a completely new vision of the production process wholly [1]. As upgrade of

Computer Aided Design/Manufacturing/Engineering (CAD/CAM/CAE) technologies, a set of production technologies that bridges the gap between designing and manufacturing phases of products through direct manufacturing of parts based on three-dimensional (3D) CAD volume model has developed. These groups of technologies are known as Rapid Prototyping (RP) technologies [2]. In essence, Rapid Prototyping is the general name for several related technologies that produce physical objects directly from CAD files or other digital data by successive deposits and merging of layers of building material thereby forming a solid object - a product. Additional step forward in the field of integrated product development, especially when it comes to complex geometric shapes of functional products, or when there is a need to copy a certain part for which there is no adequate technical documentation by applying of Reverse Engineering (RE) has achieved. The term Reverse Engineering involves the approach to generation of three-dimensional solid CAD models based on existing physical forms of products using devices and software packages for three-dimensional digitization (Fig. 1).

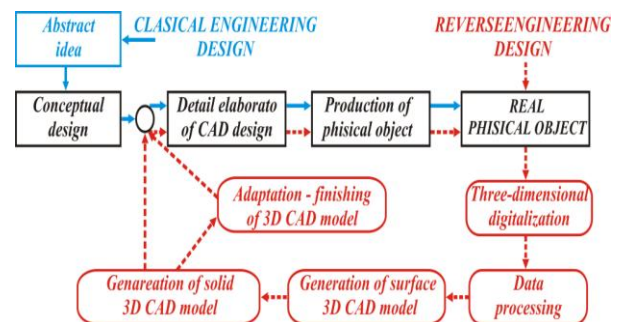


Fig. 1. Comparatives for the "classical" engineering approach and RE approach in the development (designing/redesigning) of products [4]

2. TOOL DESIGN FOR SAND CASTING

2.1 Task description

The technological process of sand casting is an area that has significant potential to utilize the advantages offered by the implementation of 3D digitizing methods, RE and RP processes especially in development and designing of individual segments of tools or entire tools. This approach has particular weight in the production of casting tools for complex geometric parts on the basis of samples for which there is no technical documentation [5]. In this case a comparative analysis of traditional versus RE/RP approach to designing and manufacturing of sand casting tools for production of cross members of scraper conveyor designed for transportation of coal from a broad mining excavation pit outside the pit to the landfill in coal mine Mramor has done, Figure 2.

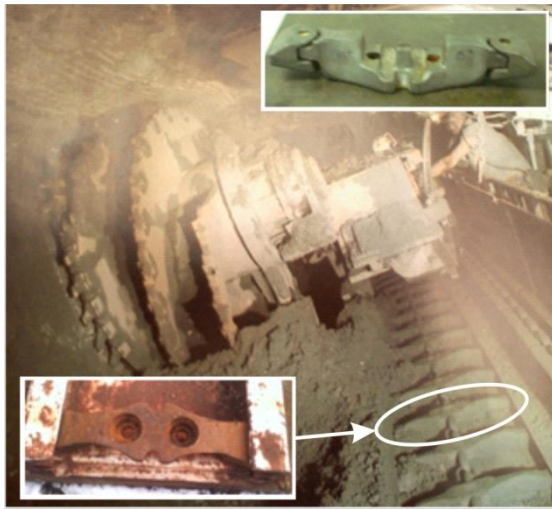


Fig. 2. Assembly of scraper conveyor

Production of cross members of scraper conveyor in Foundry Ltd. Tuzla is characterized by individual/low-rate initial production for the well-known customer with a clearly underlined short delivery time and frequent functional changes of form. In particular, because of new exploitation conditions on broad mining excavation pit in a coal mine (no need to transportation of coal by the circular segments) purchaser requires a redesign of the existing form of cross members of scraper conveyor through the elimination of its lateral moving segments, (Fig. 3).



Fig. 3. Redesigned shape of cross members of scraper conveyor according to requirements of the customer

2.2 Conventional approach

The conventional approach to designing and

manufacturing of segments of the sand casting tools in the Foundry Ltd. Tuzla, in the case when technical documentation for the parts does not exist, in the following steps occurs: receiving of samples that needs to be produced, measurement of samples by available measurement tools, creation of technical documentation for the submitted sample including a possible redesigning, preparing of technical documentation for the production of models and the core (the receiving of technical documentations, enlargement of basics drawings up to 2÷3% because of contraction of casting, designing and dimensioning of pouring system, feeders, gas vent, calculation of casting part mass, etc.), production of models and core in pattern shop (either manual or machine production in the wood – function of geometric characteristics of parts, Fig. 4), delivering of wooden models and core for preparation in production facility i.e. molding in a quartz sand, sand drying by CO₂ gas, sand compaction using a vibrator, rotating of sand casting box, extracting of models and obtaining of the mold cavity.

Upon completion of molding operations, finished mold has placed in a molding box, has poured by liquid metal, and depending on the characteristics of casted parts (volume, mass, shape, material) cooling of casted part for certain period of time has done. The molding box with a casted part goes to the separation (vibrating grid, sandblasting) of casted part and quartz sand after cooling. Thoroughly cleaned casted part goes on further processing i.e. cutting of feeder and intake system, grinding, polishing, possibly welding, etc, followed by heat treatment (normalization, relaxation of materials, etc), quality control, and placement in the warehouse of finished products or direct delivery to the customer.



Fig. 4. Wooden models of cross members and core of scraper conveyor

2.3 RE/RP approach

Unlike the conventional approach for production of sand casting tools described in the previous section, RE/RP approach to production of sand casting tools is based on the application of modern IT technologies through the implementation of three-dimensional digitization, reverse engineering, rapid prototyping and CAD inspection of produced/casted part against the starting part - sample. For the purpose of 3D

digitization of the redesigned form of cross members of scraper conveyor, as well as, of the finished casted part an optical scanner ZScanner™ 700 (Producer Z Corp, USA) was used. For the production of sand casting tools 3D printer z310 +, material zp130, binder zb58 (producer Z Corp, USA) with appropriate processing and post-processing parameters (thermal treatment, wax infiltration, infiltration by cyanoacrylate) was used. For data processing and CAD inspection, except for system software that comes with the above mentioned equipment, software package ProENGINEER Wildfire was used.

After 3D digitization of the redesigned cross members of scraper conveyor (Fig. 5a), the "raw" cloud of points (Fig. 5b) has generated and post-processed (elimination of "noise", reducing the amount of data, identifying key points of the data set, presentation of the geometry with well-defined points of the surface, fitting of curve lines through a set of points, bonding of surfaces, filling the gaps, etc.). In this way, through the reconstruction process (converting of cloud of points in the polygonal mesh model) the generation of 3D CAD solid model of redesigned cross members of scraper conveyor has accomplished (Fig. 5c). Ultimately collected and processed data are ready for transfer to any CAD/CAM software package aimed to the further: improvements, transformations, analysis, generation of tool path for individual CAM processes, etc.

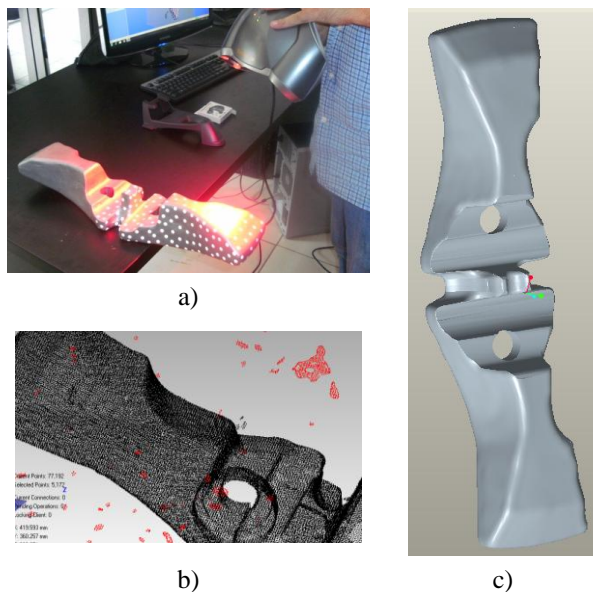


Fig. 5. Representation of 3D digitalisation by optical scanner (a), obtained "raw" clouds of points (b), resulting solid model of the redesigned form of cross member of scraper conveyor (c)

After creation of 3D CAD solid model of redesigned cross member of scraper conveyor designing of model and the core of mold for sand casting was carried out. In the case of model supporting panel for sand imprint and the subsequent integration of the core (Fig. 6a, right), slideway for assembly of core and mold has designed, chamfering of plates by 2 degrees in order to facilitate the extraction of models from the mold has done, and all holes on the model are

closed and will be subsequently processed after casting of the part. Similarly in a way that covers the lower part of the model with respect to all the requirements prescribed by casting technology the core of mold has designed (Fig. 6a - left). Designed parts of sand casting tool are made by three-dimensional printing (3DP) process (Fig. 6b) and as such were used in forming of molds for sand casting. In order to save building material for the 3DP process some of mold elements (e.g. handles for carrying core, intake system and the top plate with feeders) has made from wood [3].

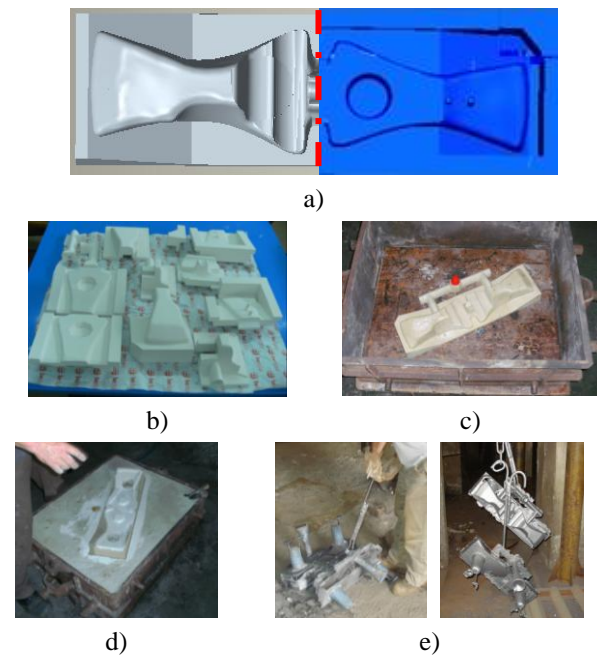


Fig. 6. Model and core of mold for sand casting (a), produced 3DP parts of tools for casting (b), forming of mold for sand casting (c), (d), casted part of cross member of scraper conveyor (e)

After forming of tool for sand casting in accordance with the requirements of the technological process of sand casting production (Fig. 6c and 6d) and post-processing raw part has produced - casted part ready for the following processing (Fig. 7a and 7b). After the casting and complete finalization of cross member of scraper conveyor in order to determine the accuracy of the produced part three-dimensional digitization - scanning (Fig. 7c) and CAD inspection (Fig. 7d) of obtained cast has done.

3. COMPARATIVE ANALYSIS

After production of redesigned cross member of scraper conveyor in both presented ways a comparative analysis of these approaches has done. Analysis was performed by three criteria: production costs, production time and qualitative characteristics of produced parts. From the standpoint of costs and production time only activities that affect the designing and production of model, core of mold and other core elements by conventional and RE/RP approach are observed. After production of above mentioned sand casting tool elements all following technological

operation in both approaches are identical with the same cost and time realization.

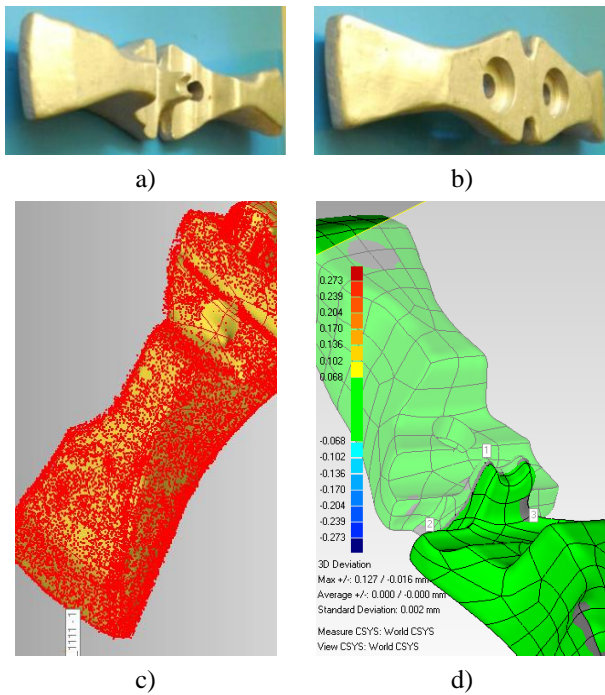


Fig. 7. Casted and postprocessed cross member of scraper conveyor (a) (b), overlapped CAD model and scanned clouds of points (c), results of CAD inspection (d)

Considering that as a starting point for the production of cast of cross member of scraper conveyor used his pattern, and that a measuring of pattern has made by conventional means in first case, and in by 3D digitalization-scanning in second case, the results of qualitative analysis in terms of dimensional and geometric accuracy is assumed to be identical. Results of comparative analysis are presented at figure 8.

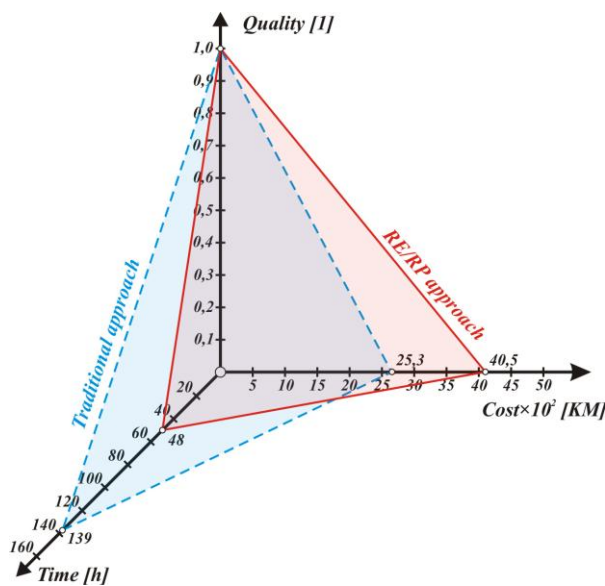


Fig. 8. Comparative analysis of the relationship between: time, cost and quality of tool for sand casting produced by traditional and RE/RP approach [3]

4. CONCLUSION

Application of RE/RP approach as shown in the specific example for production of sand casting tool has its validity on several grounds especially in the case of production of geometrically complex products for which from some reason technical documentation does not exist. The justification of this approach significantly increases with increasing levels of complexity of geometric forms that form the product, and because of it their exact definition is almost impossible without the usage of 3D digitalization devices and RE. On the other hand, the production of certain segments of the mold or whole mold by usage of RP system provides a rapid transformation of the 3D CAD model into a physical part with satisfactory accuracy, which, depending on the characteristics of building materials may be directly or indirectly used in the manufacture of sand casting tools. Application of RE/RP approach in production of segments or the entire mold for sand casting for products with complex geometric shape and for which there is no technical documentation significant shortening of a required time for designing and manufacturing of tools occurs, evidently increasing of qualitative characteristics related to geometric accuracy of the finished product, and to some extent incensement of its development and production cost.

5. REFERENCES

- [1] Topčić, A., Tufekčić, Dž., Cerjaković, E.: *Razvoj proizvodnja*, University of Tuzla, Tuzla, 2011.
- [2] Zaimović-Uzunović, N., Lemeš, S., Čurić, D., Topčić, A.: *Rapid Prototyping for sling design optimization*, Advances in Production Engineering & Management, Vol. 6: Num. 4, 238-310. ,271-281, December 2011.
- [3] Lovrić, S.: *Analysis of the bottlenecks in integrated product development (master thesis)*, University of Tuzla - Faculty of Mechanical Engineering Tuzla, Tuzla, September 2010
- [4] Topčić, A., Cerjaković, E., Babović Z., Trakić, E.: *Implementation of systems for Reverse Engineering in product development*, 1st International conference VALLIS AUREA 2008, p.p. 969-973, Požega (Croatia), DAAAM International Vienna, Požega, September 2008
- [5] Topčić, A., Tufekčić Dž., Fajić A., Cerjaković E.: *Implementation of Three Dimensional – 3DP printing process in casting*, 5th international symposium “Konstruisanje, oblikovanje i dizajn, KOD 2008”, Faculty of Technical Science Novi Sad (Serbia), April 2008

Authors: Prof.Dr. Alan Topčić, M.Sc. Sladjan Lovrić, M.sc. Edin Cerjaković, University of Tuzla, Faculty of Mechanical Engineering Tuzla, Univerzitetska 4, 75000 Tuzla, Bosnia and Herzegovina, Phone: +387 35 320 944, Fax: +387 35 320 921.

E-mail: alan.topcic@untz.ba
sladjan.lovric@untz.ba
edin.cerjakovic@untz.ba

Vilotić, M., Kakaš, D., Terek, P., Kovačević, L., Kukuruzović, D., Miletić, A.

SEVERE PLASTIC DEFORMATION BY COMPRESSION

Abstract: *This paper covers the problematic of creating ultra-fine grained metals by severe plastic deformation methods. Unlike surface treatment technologies which create thin layers of nanomaterials, severe plastic deformation methods can create nanosized grains almost within whole volume by introducing high values of effective strain. In this paper, compression by V-shape dies has been presented as method for creating ultra-fine grained metals. Friction coefficient between the V-shape dies and sample has been varied in order to find its influence on effective strain values at the center of specimens.*

Key words: *severe plastic deformation, compression by V-shape dies, ultra-fine grain, effective strain, numerical simulation*

1. INTRODUCTION

In recent years, a number of methods for refining the structure of metals by severe plastic deformation (SPD) have been developed. Some of those methods permit grain refinement to a nanometric level. Numerous investigations show that the metals having such a structure are characterized by a number of specific properties including significantly higher yield point than that produced by conventional deformation methods (rolling, drawing) [1].

The most important concern is to combine manufacturing process with metal fabrication. The self-assembly, non-traditional lithography, templated growth and biomimetics are some of the potential technologies [2]. In such processes, nanoparticles, delivered in the form of nanotubes, nanopowders, quantum-dots, and biomaterials are staked into final product in a designed way. The most challenging problem is the cost of making many of the raw components for functional nanomaterials. The cost of producing these materials often exceeds \$700/g and makes potential products economically infeasible. The time required for performing any engineering work at nano scale is also considerable for methods based on the material synthesis.

Another major challenge is the lack of chemical, morphological, or mechanical stability in many nanomaterials. These often lead to spatial distortions, suboptimal thermal behavior, reduced mechanical response and poor electrical properties, which lower the overall system performance. An alternative approach is to employ bulk nanomaterials and traditional shaping methods while constructing systems and devices at the micro and nano scales. However, conventional metallurgy cannot supply metals featuring grains substantially smaller than characteristic dimensions of the engineering micro-components. This and the encouraging economic forecasts for nanometals cause great interest in the development of new fabrication techniques, with mass production scale-up capabilities and low-cost [3].

The technologies claiming bulk capability include

electrodeposition and crystallization of initially amorphous metals. However, the two main competing technologies are compaction and sintering of nanopowders and severe plastic deformation of bulk metals. The latter process avoids the presence of impurities or porosity typical of powder metallurgy. It involves generation of a very large plastic strain in coarse-grain bulk metals using one of the newly developed metal forming processes [4, 5].

It is worth emphasizing that all metallic materials respond to severe straining in basically the same way. Technically, nanostructure can be achieved locally by a number of processes like cold rolling [6] or friction wear. However, these processes are difficult to control in terms of grain refinement in the whole deformed part and there is no room for the manipulation of grain structure efficiently [7].

2. GRAIN REFINEMENT

A simultaneous accumulation of localized dislocations and increase in the lattice misorientation are responsible for crystal subdivision and subsequently developed submicroscopic grains. However, some researches reveal that, particularly in pure metals, there exists a limit below which reducing the grain size further results in shifting in the deformation mechanism into a different yet unknown mechanism of plastic flow [3].

Under an applied stress, existing dislocations and dislocations generated by Frank-Read Sources will move through a crystalline lattice until encountering a grain boundary, where the large atomic mismatch between different grains creates a repulsive stress field to oppose continued dislocation motion. As more dislocations propagate to this boundary, dislocation 'pile up' occurs as a cluster of dislocations are unable to move past the boundary. As dislocations generate repulsive stress fields, each successive dislocation will apply a repulsive force to the dislocation incident with the grain boundary. These repulsive forces act as a driving force to reduce the energetic barrier for diffusion across the boundary, such that additional pile

up causes dislocation diffusion across the grain boundary, allowing further deformation in the material. Decreasing grain size decreases the amount of possible pile up at the boundary, increasing the amount of applied stress necessary to move a dislocation across a grain boundary. Higher the applied stress to move the dislocation the higher the yield strength (Fig. 1).

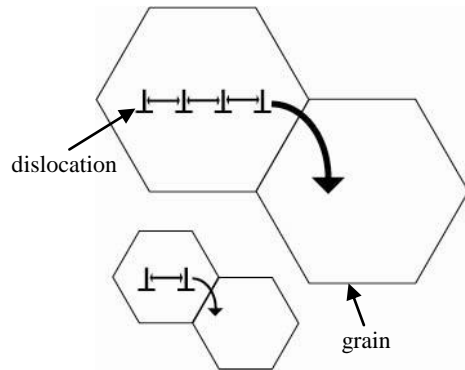


Fig. 1. Grain size and dislocation pileup [8]

Thus, there is then an inverse relationship between grain size and yield strength, as demonstrated by the Hall–Petch equation (Fig. 2) [9].

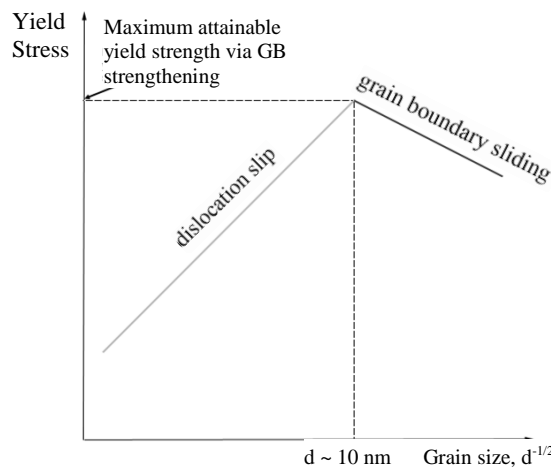


Fig. 2. Graphical illustration of the theoretical limit for grain boundary strengthening [10]

Obviously, there is a limit to this mode of strengthening, as infinitely strong materials do not exist. Grain sizes can range from about 100 μm (large grains) to 1 μm (small grains). Lower than this, the size of dislocations begins to approach the size of the grains. At a grain size of about 10 nm, [11] only one or two dislocations can fit inside of a grain (Fig. 1). This scheme prohibits dislocation pile-up and instead results in grain boundary diffusion. The lattice resolves the applied stress by grain boundary sliding, resulting in a decrease in the material's yield strength (Fig. 2). Alloys are more responsive to intensive straining than pure metals, which results in finer grains [12].

Valiev [13] formulated three requirements to obtain materials with submicron grain size: the fine grained material must have predominantly high angle boundaries, the structure must be uniform over the sample volume and the large plastic strains may not

have generated internal damage or cracks. Traditional deformation methods like rolling and wire drawing cannot meet these requirements. Therefore special deformation methods have been developed.

3. SPD METHODS

Ultra-fine grained material was accomplished in a controllable way, was due to an equal channel angular extrusion (ECAE) process introduced by Segal in the 1970s [7]. ECAE, also known as ECAP, gave an impetus to the development of the whole range of similar processes which led to establishing a new discipline of metal forming – SPD methods.

A billet of the test material is pressed through a die consisting of two channels with identical cross sections, intersecting at an angle ϕ , usually $60^\circ < \phi < 135^\circ$ and often $\phi = 90^\circ$ (Fig. 3). Some dies have a rounded corner with angle ψ , others have $\psi = 0$. The deformation occurs by simple shear parallel to the intersecting plane of the channels [14].

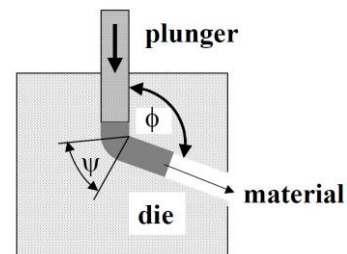


Fig. 3. Schematic illustration of a ECAP SPD method [14]

In spite of the actual popularity of the technique, some drawbacks of ECAP must be recognized. ECAP is a discontinuous process with limitations in up-scaling potential. Moreover, the volume fraction of useful material (with uniform microstructure and without cracks) can be rather low because only the portion of the billet that has passed through the shear zone, will receive the desired deformation and grain refinement. Barber et. al. figured out that for a sample with square cross section and an aspect ratio of 6, after 8 ECAP passes route A, only ~30% of the material is fully worked as intended. For route B, the efficiency is ~45% and for route C it is ~83% [15].

Other significant continuous SPD methods which increase the efficiency of ECAP are developed. They combine the concept of ECAP with classical rolling and include asymmetric rolling, continuous repetitive corrugation and straightening and conshearing process (Fig. 4).

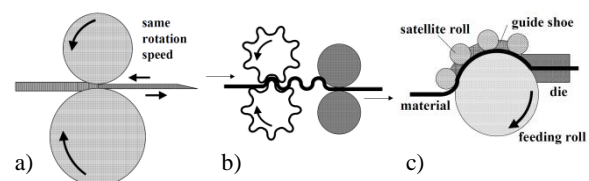


Fig. 4. Continuous SPD methods a) asymmetric rolling, b) continuous repetitive corrugation and straightening, c) conshearing process [14]

Another significant SPD technique is high-pressure torsion (HPT). Small discs (typically 10-20 mm diameter and 0.2-1 mm thick) are strained in torsion under an applied pressure of several GPa (Fig. 5). Although in a classical torsion test it is generally assumed that the center of the sample is not deformed, numerous investigations show that after several rotations the HPT-samples are uniform over the diameter [13], which shows that the real deformation in HPT is more complex than one can assume from the simple analytical expressions used in a classical torsion test. The main advantage of HPT is that extreme grain refinement (up to 100 nm) can be obtained [14].

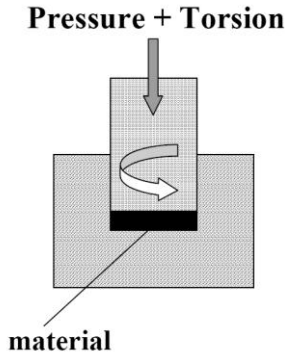


Fig. 5. Schematic illustration of a high-pressure torsion SPD method [14]

Based on aforementioned SPD methods, new upsetting SPD method has been proposed.

4. SPD BY V-SHAPE DIE COMPRESSION

Discontinuous SPD method for upsetting square shaped billet by V-shaped dies has been presented on Fig. 6 while V-shape die and billet geometry is presented on Fig. 7.

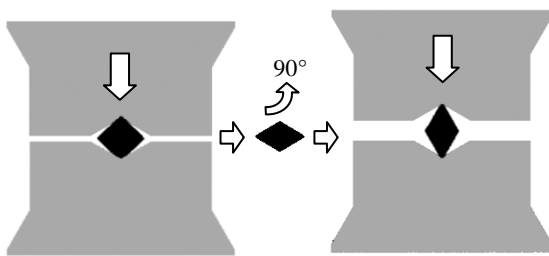


Fig. 6. V-shape die compression SPD method

V-shape die compression is multi-stage process in which, after single compression stage is completed, sample is removed from the dies and rotated for 90° in counter-clockwise direction and returned in the dies. Compression by V-shape die is completed when crack occurs inside of sample or when stroke in single compression stage becomes too low.

Compression by V-shape dies has been simulated by Simufact.Forming V10.0.1 software where friction coefficient value has been varied in order to find its influence on effective strain at the end of multi-stage compression. Since friction between the dies and the sample influences sample elongation during

compression, friction was one of the most important variables considered for simulation.

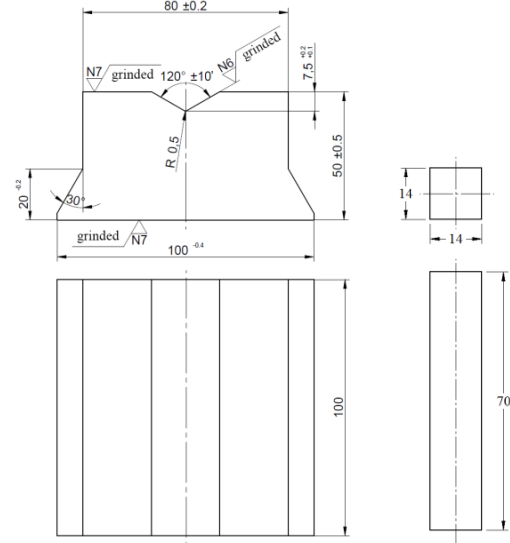


Fig. 7. V-shape die and billet geometry

Dies were made of X210Cr12 cold work tool steel (Č.4150) while billet was made of Ck15 unalloyed carbon steel (Č.1221). Hardness of the dies was 58+2 HRC and there was no lubrication medium used between dies and samples.

5. RESULTS AND DISCUSSION

Table 1 displays the influence of friction coefficient between dies and sample on effective strain at the center of the specimen at the end of compression process and maximum number of stages performed per process. It can be seen from the table that higher friction coefficient value causes higher value of effective strain at the end of compression process and more compression stages. Also, effective strain distribution with higher friction coefficient values is more uneven that in the case of $\mu = 0.12$.

$\mu = 0.12$	$\mu = 0.3$	$\mu = 0.4$
max number of stages = 5	max number of stages = 7	max number of stages = 8
$\epsilon_{ef} = 1.67$	$\epsilon_{ef} = 3.69$	$\epsilon_{ef} = 4.12$

Table 1. Friction coefficient influence on effective strain and the number of total compression stages

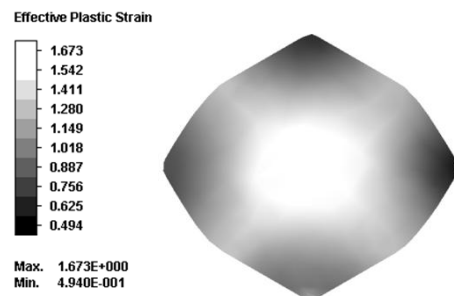


Fig. 8. Effective strain distribution after 5th stage compression by V-shape dies for $\mu=0.12$

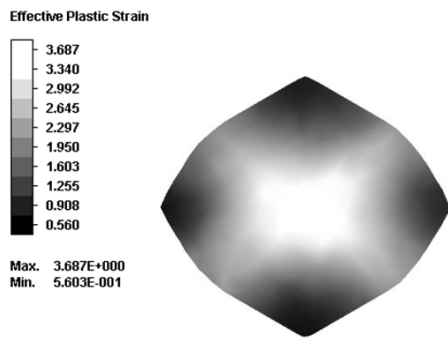


Fig. 9. Effective strain distribution after 7th stage compression by V-shape dies for $\mu=0.3$

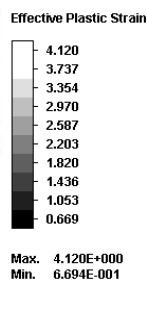


Fig. 10. Effective strain distribution after 8th stage compression by V-shape dies for $\mu=0.4$

Figures 8 to 10 displays effective strain distribution in samples with different friction coefficient values between V-shape dies and samples. As expected, sample with highest friction coefficient values includes highest effective strain. By increasing the friction coefficient, material flow in longitudinal direction is reduced allowing greater number of stages to be used for compression thus increasing total effective strain within sample.

6. CONCLUSION

It can be concluded that V-shape dies can be successfully used for creating fine-grained metals since effective strain can reach 4.12 values. Further research would include measurement of grain size, hardness and values of effective strain from experiment.

7. ACKNOWLEDGMENTS

This paper is a part of research included into the project "Project TESLA: science with accelerators and accelerator technologies", financed by Serbian Ministry of Science and Technological Development. The authors are grateful for the financial support.

8. REFERENCES

- [1] Kurzydłowski, K. J.: *Microstructural refinement and properties of metals processed by severe plastic deformation*, Bulletin of The Polish Academy of Sciences, 52, p.p. 301-311, 2004.
- [2] Wolf, E.L.: *Nanophysics and Nanotechnology*, Wiley-VCH Verlag, Weinheim, 2004.

- [3] Olejnik, L., Rosochowski, A.: *Methods of fabricating metals for nano-technology*, Bulletin of the Polish Academy of Sciences, Technical Sciences, 53, p.p. 413-423, 2005.
- [4] Segal, V.M., Reznikov, V.I., Drobyshevskiy, A.E., Kopylov, V.I.: *Plastic working of metals by simple shear*, Russ. Metall, 1, p.p. 99-105, 1981.
- [5] Segal, V.M., Reznikov, V.I., Kopylov, V.I., Pavlik, D.A., Malyshev, V.F.: *Process of structure formation during plastic straining*, Scientific and Technical Publishing, Minsk, 1994.
- [6] Chen, W., Ferguson, D., Ferguson, H.: *Severe plastic techniques*, Acta Metallurgica Sinica, 13, p.p. 242-253, 2000.
- [7] Segal, V.M.: *Materials processing by simple shear*, Mat. Sci. Eng., A197, p.p. 157-164, 1995.
- [8] Dislocation pileup, 10. July 2012, http://en.wikipedia.org/wiki/Grain_boundary_strengthening.
- [9] Callister, W.D.: *Fundamentals of Materials Science and Engineering, 2nd ed.*, Wiley & Sons, 2004.
- [10] Hall-Petch effect strengthening limit, 10. July 2012, <http://core.materials.ac.uk/search/detail.php?id=3248>.
- [11] Schuh, C., Nieh, T.G.: *Hardness and Abrasion Resistance of Nanocrystalline Nickel Alloys Near the Hall-Petch Breakdown Regime*, Mat. Res. Soc. Symp. Proc, p.p. 27-32, Boston, 2003.
- [12] Hasegawa, H., Komura, S., Utsunomiya, A., Horita, Z., Furukawa, M., Nemoto, M., Langdon, T. G.: *Thermal stability of ultrafine-grained aluminum in the presence of Mg and Zr additions*, Mat. Sci. Eng., A265, p.p. 188-196, 1999.
- [13] Valiev, R.Z., Islamgaliev, R.K., Alexandrov, I.V.: *Bulk nanostructured materials from severe plastic deformation*, Progr. Mat. Sci., 45, p.p. 103-189, 2000.
- [14] Verlinden, B.: *Severe plastic deformation of metals*, 2nd International Conference on Deformation Processing and Structure of Materials, p.p. 3-18, Association of Metallurgical Engineers of Serbia, Faculty of Technology and Metallurgy and Institute of Nuclear Sciences Vinca, Belgrade, 2005.
- [15] Barber, R.E., Dudo, T., Yasskin, P.B., Hartwig, T.: *Product Yield of ECAE Processed Material*, Ultrafine Grained Materials III, p.p. 667-672, 2004.

Authors: Marko Vilotić, mag. sci., Prof. Dr. Damir Kakas, M.Sc. Pal Terek, M.Sc. Lazar Kovacević, M.Sc. Dragan Kukuruzović, M.Sc. Aleksandar Miletić, University of Novi Sad, Faculty of Technical Sciences, Institute for Production Engineering, Trg Dositeja Obradovića 6, 21000 Novi Sad, Serbia, Phone.: +381 69 383-382-2, Fax: +381 21 454-495.

E-mail: markovil@uns.ac.rs
 kakasdam@uns.ac.rs
 terekpal@gmail.com
 lazarkov@uns.ac.rs
 ing.kukuruzovic@gmail.com
 miletic@uns.ac.rs

11th INTERNATIONAL SCIENTIFIC CONFERENCE
MMA 2012 - ADVANCED PRODUCTION TECHNOLOGIES

PROCEEDINGS



Section G:
BIO-MEDICAL ENGINEERING - CAx

Novi Sad, 20-21 September 2012

Matin, I., Markovic, D., Puskar, T., Hadzistevic, M., Hodolic, J., Vukelic, Dj., Potran, M.

RECONSTRUCTION OF THE DENTAL CAD MODEL

Abstract: This paper describes flow chart of the simulation model modelling. The main objective of the work is to prepare correct facet/solid model for numerical simulation. Inlet facet model create using RE techniques. This 3D digitizing geometrically complicated model was created into My VGL software package. The proposed faced model has some unclear geometry, uncorrected facets, and errors. This model requires analysis, and subsequently corrections and reconstruction using software package Pro/E. This paper also describes advanced modeling tools and methods for CAD model reconstruction using Pro/E module such as Pro/SURFACE ISDX, Pro/Part, Pro/Assembly and IDD.

Keywords: dental cast; analyze; solid; surface reconstruction;

1. INTRODUCTION

Investment casting (IC), or “lost-wax” casting, is a precision casting process whereby wax patterns are converted into solid metal parts following a multi-step process. IC enables economical production of near net shaped metal parts containing complex free-form geometries and features from a variety of metals, including difficult-to-machine or non-machinable alloys. To produce precision components, the near net shape of castings can reduce machining time and cost to bring components into specifications. Despite its popularity, traditional IC suffers from high tooling investments for producing wax patterns. As such, IC is prohibitively expensive for low-volume production typical in prototyping, pre-series, customized or specialized component productions. Investment casting (IC) has benefited numerous industries as an economical means for mass producing quality near net shape metal parts with high geometric complexity and acceptable tolerances. The economic benefits of IC are limited to mass production. The high costs and long lead-time associated with the development of hard tooling for wax pattern molding renders IC uneconomical for low-volume production. Traditional IC consists of the block mold and the more common ceramic shell processes. The process chain for the ceramic shell process (Fig. 1) consists of the tooling, shell fabrication and casting stages.

CAD Design of Mold	Mold Production	Wax Pattern Injection • Formation of Cluster Arrangement	Ceramic Shell Production	Pattern Removal • Autoclaving	Pre-Heating/Firing	Casting	Knockout • Finishing • Inspection
--------------------	-----------------	---	--------------------------	----------------------------------	--------------------	---------	---

Fig. 1. Conventional investment casting [1]

Upon cooling, the mold is stripped to extract the patterns. Individual patterns are attached onto a wax sprue system to form a cluster in the shell fabrication stage. The cluster is repeatedly dip coated in investment slurry containing graded suspensions of refractory particles and followed by stucco application to build shell thickness and strength. When dried, the wax pattern is melted out via autoclaving to reveal the

cavities (impressions) of the ceramic shell. The shell is fired to build strength and remove residual volatiles. In the casting stage, molten metal is poured into the heated shells to form the castings, which are extracted after cooling by cracking the shell during the knockout process. Individual castings are separated, cleansed and subjected to finishing processes. IC using BEGO machine is suboptimal compare with advanced Rapid Investment Casting (RIC). Few RP&T techniques for RIC are indicated in Fig.2.

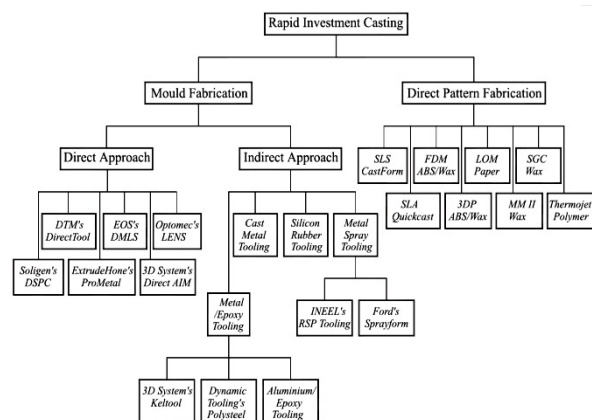


Fig. 2. Advanced techniques for RIC [1]

As RP techniques rely on CAD data for input, the accuracy of digital models created by the mold maker can directly affect the outcome of the fabrication process. To create accurate patterns and tooling, a high level of proficiency in shrinkage compensation factors, post-machining allowances and foundry laboratory requirements are pre-requisites to consider during the modelling process. Besides human factors, the CAD system used can sometimes be the limiting factor in the production of accurate digital representations of the required design and the conversion of native CAD data from My VGL and Pro/E to data fully acceptable by RP or MAGMASOFT systems (i.e., STL format). In STL format, the surfaces of modelled geometries are approximated by arrays of triangles whose sizes are determined by the user. The setting of the chord length

is often a compromise between the file size or the required amounts of computing resources necessary and the final accuracy of the converted data. Besides this, STL files are prone to problems related to missing or reversed surfaces. [1,2,3]. Much research has been conducted to address issues related to STL file repair and data interfacing. Alternative data formats to replace STL such as CLI and SLC, which circumvent the tessellation process by directly slicing a CAD model to improve data accuracy have also been worked on. In this paper, 3D model reconstruction on of metal-ceramic crown part that has undergone the run-in time is studied, using RE modeling techniques. In the stage of surface data acquisition, since the dental crown has very complicated and irregular contour, a non-contact mode is preferred. In point cloud data pre-processing, salient outliers are manually removed; Gaussian filter is used for noise suppression; curvature-based sampling is adopted for data reduction. In the model reconstruction stage, the surface reconstruction which is based on enclosed triangular Bezier surface patches is used for it can deal with arbitrary shape contours. Then, hole patching, smoothing and reduction are added for refinement of the surface creation. The objective goal of this paper are super-feature reconstruction of the inlet facet scanning model, and creating simulation model, which are consists of correct solid features of dental cast with model of gate subsystem.

2. SPECIFICATION OF SCANNING MODEL

A complete surface model of a typical 3D object is then constructed from the integration of its multiple partial views. Since the method is effective in the registration of range images, it is attractive for many applications where surface models of 3D objects must be constructed. This study is concerned with the problem of range image registration for the purpose of building facet model of three-dimensional object [4]. Facet model was exported from My VGL to into Pro/E for further unclear feature reconstruction. My VGL is used in a variety of application areas such as industrial CT, medical research, life sciences, and many others. Project files (and folders) i.e., VGL files contain basic information on the project including references to the object files and supplementary files belonging to the project. The data range mapping determines the range of gray values used for scanning object, i.e. it specifies the maximum number of different gray values available for dental cast. The size of the data range is always smaller than or equal to the numbers of gray values in the data type [4,5]. The 3D window shows the result image of the rendering process see Fig.3. User specifies rendering parameters for voxel data sets with the Volume Rendering tool and rendering parameters for polygonal models with the Polygon Rendering tool. The coordinate system tripod in the lower left corner of the 3D window indicates the orientation of the currently chosen datum coordinate system as indicated in Fig.1. Software provides basic features for scanning object as well as for saving images or image stacks. Thus the software allows user to handle the two basic file types: object files, and project files (and folders).

Object files contain voxel data representing dental real object, basically the output of the CT-scanner (after scanning and low reconstruction) or some other device, or contain other data representing your real object, such as polygons. Scanner settings and additional information might be included in the data files or in separate files. Fig.3. presents few X-sections and shaded representation view of the scanning facet model generated in My VGL.

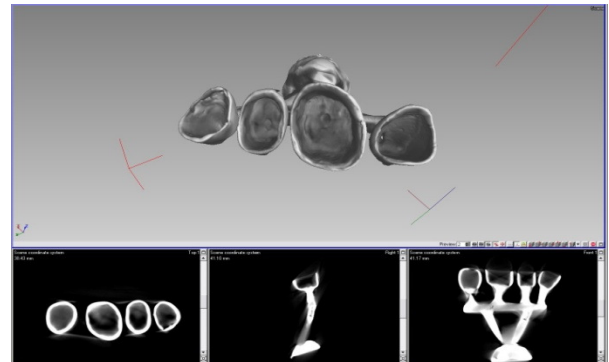


Fig. 3. Few sections of the scanning model

A complete flow chart of simulation model design is shown in Fig. 4.

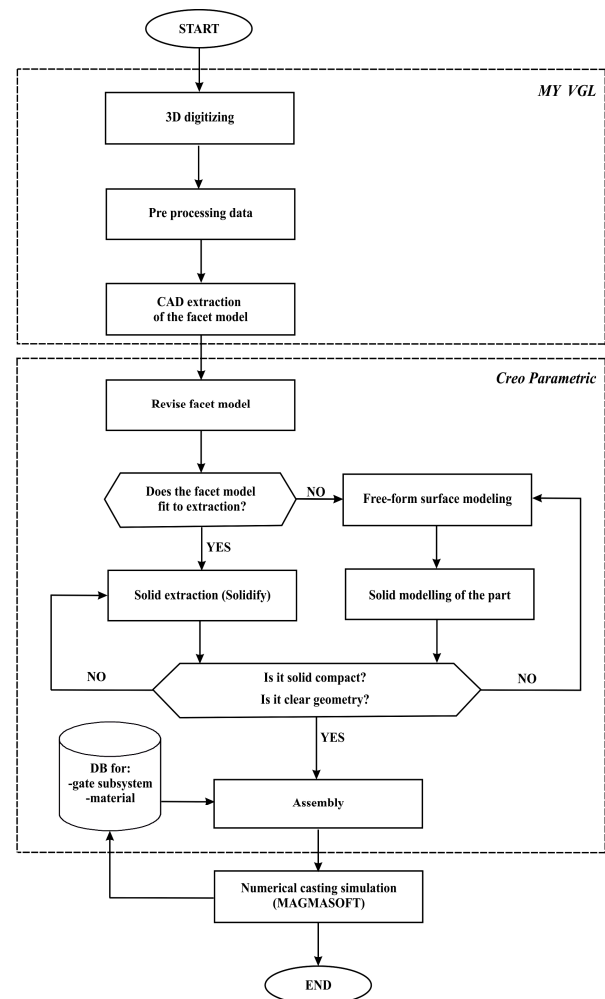


Fig. 4. Flow chart of the simulation model modeling

Simulation model consists of dental model and model of gate subsystem. The flow chart of simulation model modelling can be divided into two operation box. The first one presents 3D scanning and facet model creation into My VGL software package. Second operation box presents revise facet/solid model and assembly creation into software package Creo Parametric as total solution.

3. REVISE OF THE MODEL USING PRO/E

3.1. Super-feature design

Free-form surfacing features are called super-features, because they can contains limitless number of curves and surfaces [6]. The freeform surfacing user interface ISDX offers the best of both worlds—it is a self-contained, intuitive modeling environment and also a Pro/E feature. Freeform surfacing features are flexible; they have their own internal parent/child relationships, and can also have relationships with other Pro/E features. Free-form surfacing (ISDX) is a design environment within Pro/E that allows user to create free-form curves and surfaces quickly and easily, and to combine multiple elements into super-features. We tries to accomplish all of the following tasks with Freeform surfacing advanced tools such as:

- Create curves and surfaces at the part level.
- Create simple features or multiple-element super-features.
- Create a Curve on Surface (COS), a special curve type that lies on a surface.
- Create surfaces from boundaries that do not have to be trimmed to corners.
- Reconstruction individual geometric entities or a combination of entities in the feature.
- Create internal parent/child relationships for Freeform Surfacing features.
- Create parent/child relationships between Freeform Surfacing features and model features and integration CAD/CAE feature as UDF.

We used inner and outer quilts for creating and manipulating of non solid surfaces. Quilts represent a “patchwork” of connected nonsolid surfaces. A quilt consists of a single surface or a collection surfaces. A quilt contains information describing the geometry of all surfaces that compose a quilt and information on how quilt surfaces are “stitched” (joined or intersected). Quilts are generated as set of blend boundary surfaces. All quilts must be joined to one surface (OQ). After that our research team generated inner join quilt using same operation (IQ). We used OQ for thin solid design (TS). After that we intersect and trim rest of solid part TS with IQ. After creation joined surface using merge join option our research team analyzed Pro/E functions in free form surfacing such as curvature, radius, tangent options for surface, reflection, draft check, dihedral angle, radius, shaded curvature, etc. If analyses pass, then surface have G1 characteristics.

3.2. Cleaning the facet geometry and shrink wrap model extraction

A facet model of a metal-ceramic crown parts without gate subsystem after using the clean command with the

free-form option is indicated in Fig. 6. Facet model of with gate subsystem after using clean command with the mechanical option is indicated in Fig. 7.

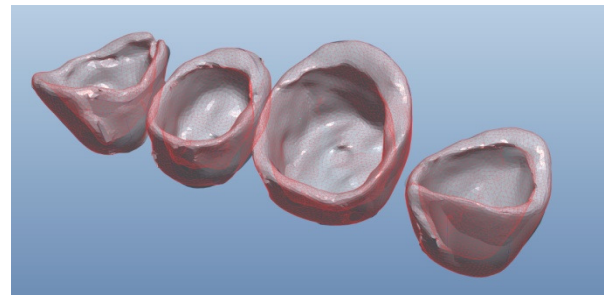


Fig. 6. Facet dental model without gate subsystem

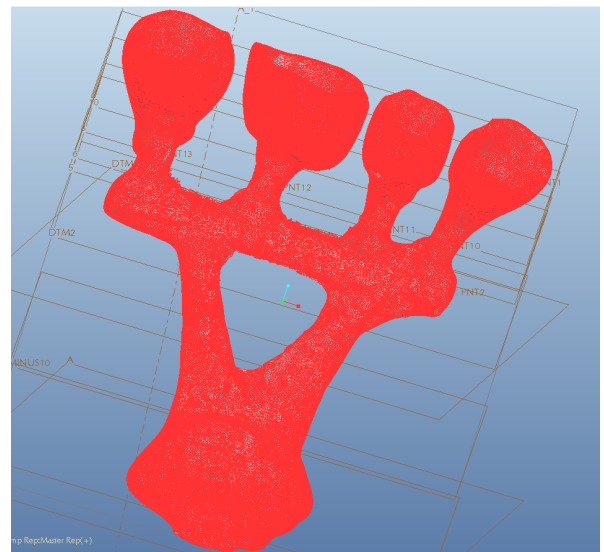


Fig. 7. Model with gate subsystem after using clean command with the mechanical option

After cleaning the facet geometry, user extract shrink-wrap model. We try to adjust the quality level of solidify the shrink-wrap model using the create shrink-wrap advanced tools. The higher the quality means the more detailed the shrink wrap. However, processing time increases as well. The recommended method for creating a shrink wrap model is to specify a low quality setting, preview the results, and gradually increase the quality level as necessary. All geometry imported and created inside the Style feature becomes part of the Style feature. Objects internal to the Style feature, such as individual surfaces, curves, and so on do not have parent-child dependencies outside the Style feature or between each other. This enables that to freely manipulate surfaces without being concerned with references and parent-child relationships between Style feature objects and the rest of the model. Quality is inversely proportional to the size of the triangles used to create the faceted model. At a lower setting, the system creates fewer, larger triangles more quickly, producing a roughly accurate representation of the object's shape. At a higher setting, the system creates many smaller triangles, producing a more detailed, more accurate representation of the model.

3.3. Checking the geometry and verifying the feature

All imported and exported geometry must be verified into Import Data Doctor (IDD). IDD was used for control import options from MY VGL file, providing user with immediate access to most commonly used import settings including use template, enable ATB, and import as facet model. IDD extends the troubleshooter dialog box with a series of new error, warning, and geometry checks unique to the IDD environment. IDD Match Tool is a repair mode tool that replaces poor quality n-sided imported surfaces with good quality n-sided surfaces or patches. Multiple enhancements to IDD modes, selection, filters, and features help streamline, simplify, and shorten the data repair process of the Geometry and Topology Structure (GTS).

3.4. Data Base of the gate subsystem

Data base (DB) consists of few CAD models of the gate subsystem. Model contains different GPS [20]. Various geometrical product specifications are:

- Average diameter of the runners ($\varnothing 4\text{mm}$, $\varnothing 5\text{mm}$, $\varnothing 6\text{mm}$).
- Central angle between sprue and vertical runner datum plane (12° , 15° , 20°).
- Investment materials (remanium 2000+ (CoCrMoW) acc. to DIN EN ISO 9693 / DIN EN ISO 22674, Trivest, Castorit super C, BEGO's Wirobond C (CoCrMoW), Heranium Partial Denture Alloys (CoCr) acc. to EN ISO 22674 etc).

4. CONCLUSION

At last, the errors of the whole reconstruction process are evaluated. The results indicate that complete RE work has good performance, which can improve quality of a dental restoration and contribute to the success of prosthetic therapy. The objective of this research was to develop a correct simulation model of dental crown (solid and facet) with good performance using Pro/E. The described working process modelling are feature-based, parametric, based on solid and facet models and object-oriented. The resulting models can be directly imported into CAD or CAE systems without loss of the semantics and topological information inherent in feature-based representations. In addition, the feature-based approach facilitates methods capable of producing highly accurate models, even when the original data has substantial errors. The IDD improves quality design, reduces noise and errors, and provides geometric and technological information necessary for numerical simulation. Future research will be directed towards three main goals. The first is to generate product using RP relatively RIC. Another line of research is the numerical simulation using MAGMASOFT. And another line of research is selection of casting parameters, materials and model of gate subsystem from DB, using fuzzy logic and soft computing.

5. REFERENCES

- [1] Cheah, C.M., Chua, C.K., Lee, C.W., Feng, C., Totong, K.: Rapid prototyping and tooling techniques: A review of applications for rapid investment casting, *International Journal of Advanced Manufacturing Technology* 25: pp. 308–320., 2005, DOI 10.1007/s00170-003-1840-6.
- [2] ----: Application software for visualization and documentation of industrial Computer tomography/voxel data Reference Manual 2.0., Volume Graphics GMBH, Heidelberg, Germany, 2009.
- [3] Zhang, L., Wang, H., Xu, H.: Application of the reverse engineering to 3D reconstruction on a denture, 2nd International Conference on Mechatronics and Intelligent Materials, *Advanced Material Research*, Vol. 490-495, pp. 2032-2036, 2012.
- [4] Jevremovic, D.P., Puskar, T.M., Budak, I., Vukelic, DJ., Kojic, V., Eggbeer, D., Williams, R.J.: An RE/RM approach to the design and Manufacture of removable partial dentures with a biocompatibility analysis of the F75 Co-Cr SLM alloy, *Materiali in Tehnologije* 46 (2), pp. 123-129, 2012.
- [5] ----: Heraeus Kulzer GmbH catalogue, Hanau, Germany, www.heraeus-dental.com, accessed 2011.
- [6] ----: Dentaaurum catalogue, www.dentaaurum.com, accessed 2012.
- [7] Application of an integrated CAD/CAE/CAM system for die casting dies, *Journal of Materials Processing Technology* 139, pp.465-468., 2003.

Authors: Mr. Ivan Matin, Prof. dr Miodrag Hadžistević, Prof. dr Janko Hodolić, Doc. dr Đorđe Vukelić, University of Novi Sad, Faculty of Technical Sciences, Department for Production Engineering, Trg Dositeja Obradovica 6, 21000 Novi Sad, Serbia, Phone.: +381 21 450-366, Fax: +381 21 454-495.

E-mail: matini@uns.ac.rs
miodrags@uns.ac.rs
hodolic@uns.ac.rs
vukelic@uns.ac.rs

Prof. dr Dubravka Marković, Dr Michal Potran, Doc.dr Tatjana Puškar, Medical faculty Novi Sad, Department of dentistry, Hajduk Veljkova 12, 21000 Novi Sad, Serbia, Phone.: +381 21 661-33-62, Fax: +381 21 526-120.

E-mail: dubravkamarkovic@yahoo.com
tatjanapuskar@yahoo.com
michalpotran@gmail.com

ACKNOWLEDGMENTS

Results of the investigation presented in this paper are a part of the research realized in the framework of the project "Research and Development of Modeling Methods and Approaches in the Manufacturing of Dental Recoveries with the Application of Modern Technologies and Computer Aided Systems"– TR-035020, financed by the Ministry of Education and Science of the Republic of Serbia.

Petrović, S., Matić, A., Devedžić, G., Ristić, B., Čuković, S.

DIFFERENCES IN TIBIAL ROTATION AND TRANSLATION IN ACL DEFICIENT AND HEALTHY KNEES

Abstract: Anterior cruciate ligament (ACL) reconstructive surgery is used for achieving stability of the knee and normal gait pattern. Anterior – posterior translation and internal – external rotation are defined as the leading pathological parameters of the ACL deficiency. Nineteen adult men were examined in this study. Patients were walking along defined pathway at their own speed. Pathological parameters were defined based on kinematic data obtained by recording with six infrared cameras. Maximal values of the AP translation and IE rotation in early stance phase were recorded during preoperational measurement. Significant value decrease of the AP translation and IE rotation were recorded after reconstructive ACL surgery.

Key words: anterior cruciate ligament, gait cycle, knee kinematic, reconstruction

1. INTRODUCTION

Anterior cruciate ligament (ACL) injuries are very common. Therefore, each year many people undergo ACL reconstructive surgery. Ligaments reconstruction is commonly based on using patellar tendon graft or a hamstring graft in order to resume knee stability and pain relief, and possibility of the recovery to athletic activities [1, 2].

Normal function of the knee lies in complex relationship of the movement and stability. Anterior cruciate ligaments of the knee are of the essential importance for providing passive restraint anterior – posterior knee movement. Primary function of the ACL is to prevent occurrence of the tibial translation along anterior – posterior (AP) direction, and to keep internal – external (IE) rotation in the appropriate limits [2, 3].

Purpose of this study is to present more precise and objective method for determining ACL deficient knees, and for judging the successfulness of the reconstructive surgery.

2. METHODS AND MATERIALS

2.1 Patients

Nineteen adult men with ACL deficient knees have voluntarily agreed to participate in experiment of the gait analysis. Mean height of the patients is 183.33 ± 2.24 cm, mean weight is 86 ± 3.48 kg, and mean value of the patients' age is 29.89 ± 1.73 .

Test analysis and surgery were performed at Clinical Centre Kragujevac, (Clinic for Orthopedics and Traumatology).

2.2 Instrumentation and protocol

3D kinematic data were recorded using OptiTrack (Natural Point, Inc., Oregon, www.naturalpoint.com) system with six infrared cameras (V100:R2) resolution 640x480 and software ARENA (Natural Point, Inc., Oregon, www.naturalpoint.com). On the patient's lower extremity four fluorescent markers, each 10mm in diameter, were set (Fig. 1):

- at region of the great trochanter (RGT),
- at lateral epicondyle of the femur (LEF),
- at tuberosity of the tibia (TT), and
- at the centre of the ankle joint (CAJ) .

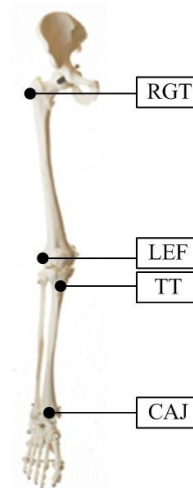


Fig. 1. Clinical positions of the leg landmarks

Patients walked 5.00m long pathway along which cameras were placed.

By protocol, patients had task to walk at their own speed. This task was performed four times. Preoperational measuring was performed the day before surgery and post operational measuring 15 days after the surgery.

2.3 Kinematic data

Movement curves were recorded in regions of the fluorescent markers' positions for the ACL deficient and healthy knees.

Patients gait were presented with a three-dimensional curves, which were exported from ARENA software in standard VICON .c3d format, and were further processed in Catia V5 (Dassault Systemes, France, www.3ds.com) and MatLab (The MathWorks,

Inc., USA, www.mathworks.com).

In order to define pathological gait parameters, phases of the gait cycle were assigned on the basis of centre ankle joint curve in sagittal plane (Fig. 2) [4].

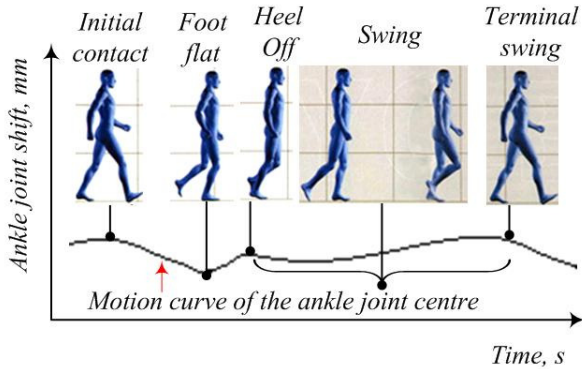


Fig. 2. Phases of the gait cycle

Gait cycle begins when one foot contacts the ground, and ends when that foot contacts the ground again. Initial contact between foot and the ground labels beginning of the ankle joint center curve descend to local minimum. Local minimum labels foot flat phase of the gait cycle. Continuous curve increase, marking heel-off and transition in swing phase. In this phase, movement curve is conditionally horizontal. Curve decrease to next local minimum labels end of the swing phase and transition in terminal swing phase which define end of the gait cycle [4].

Classification of the movement curves were performed in two groups, one group with deficient ACL knees, and another group with healthy ACL knees.

Values which define tibial shift relative to the femur are given in function of time, e.g. defined in the percentage of the gait cycle relative to time.

2.4 Data analysis

Femoral coordinate system can be considered for referent coordinate system that does not change its orientation because tibial translation and rotation (AP translation and IE rotation) relative to the femur occurs in the deficient ACL knees [4, 5, 6, 7].

If we consider tibia as rigid body, its movement can be identified with movement of the marker placed at the tuberosity of the tibia. In one moment (point TT_1), coordinate system of the tibia occupies certain position relative to the femur. In that case, it is possible to define tangent line on the movement curve t_1 and corresponding normal line n_1 at the point TT_1 . In next moment (point TT_2), coordinate system of the tibia capture another position relative to the femoral coordinate system where it is possible to determine tangent line on the movement curve t_2 and corresponding normal line n_2 at the point TT_2 .

Tangent and normal lines on the movement curve of the tibia will match respectively with x – axis and y – axis at any time [4]:

$$x_{ii} \perp y_{ii} \quad i \quad t_i \perp n_i \Rightarrow x_{ii} \parallel t_i \quad i \quad y_{ii} \parallel n_i \quad (1).$$

Determination of the IE rotation angle is based on definition of the movement curve tangent line coefficient and on definition of the angle between tangent line and AP axis of the femoral coordinate system (Fig. 3) [4, 7]:

$$t = f'(x_i) = \frac{dy_i}{dx_i} \quad (2).$$

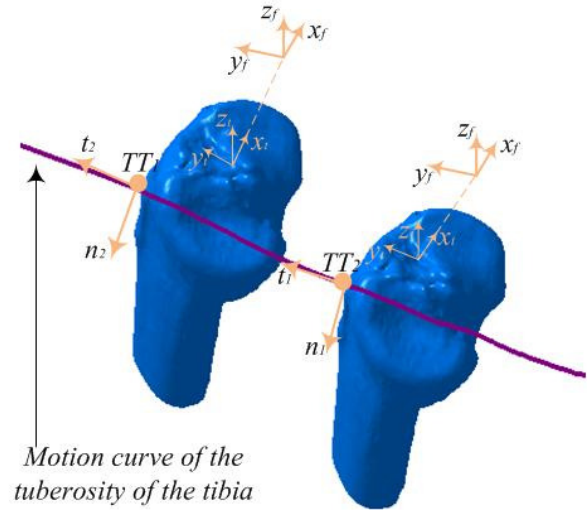


Fig. 3. Tibial translation along AP direction and IE rotation

LEGEND:

TT_1 - tuberosity of the tibia in one moment, TT_2 - tuberosity of the tibia in one moment, x_f - mediolateral axis of the femur, y_f - anteriorposterior axis of the femur, z_f - superior - inferior axis of the femur, x_t - mediolateral axis of the tibia, y_t - anteriorposterior axis of the tibia, z_t - superior - inferior axis of the tibia, t_1, t_2 - tangent line of the curve at the point TT_1 , e.g. TT_2 , and n_1, n_2 - normal line of the curve at the point TT_1 , e.g. TT_2

Value of the distance between points TT_1 and TT_2 along all directions and planes indicates possibility of the ACL deficient knees. Since displacement along inferior – superior and medial – lateral directions is negligible, determination of the tibial translation along AP direction (Fig. 3) is conducted by successive calculating the affine coordinates along AP direction [4]:

$$d_{TTAP} = (TT)_{i+1} - (TT)_i \quad (3),$$

where is

$(TT)_i$ - tuberosity of the tibia in i - th moment, and $(TT)_{i+1}$ - tuberosity of the tibia in i+1 - th moment.

3. RESULTS

In order to obtain curves of the AP translation and IE rotation eight order Fourier approximation is applied.

The horizontal axis shows percentage distribution of the gait cycle and the vertical axis shows difference of the tibial translation changing in milimeters, e.g. difference of the IE angle rotation changing.

Diagrams at the Figure 4 show that these pathological parameters have the big influence on the knee stability. Measurements before operation, at the initial contact between foot and the ground which correspond to 20% of the horizontal axis, points to the high amplitudes of the AP translation, e.g. IE rotation. Before, surgery, mean value of the AP translation is 6.619 ± 1.447 mm, and for IE rotation is $6.169 \pm 0.711^\circ$ [7].

Curves on diagrams which show patients' walk pattern after surgery has lower amplitudes, and intensity of the AP translation and IE rotation changes is decreased. Mean value along AP direction is 3.0901 ± 0.551 mm, and IE rotation is $2.382 \pm 0.477^\circ$ [4].

Student t – test was used for purpose of the statistical significance of the experimental results. It can be seen that the character of the change in preoperational and post operational period is not random, but is created under the influence of the systematic or experimental factors for possible error $P < 0.1$ and for certainty of the $P > 99\%$.

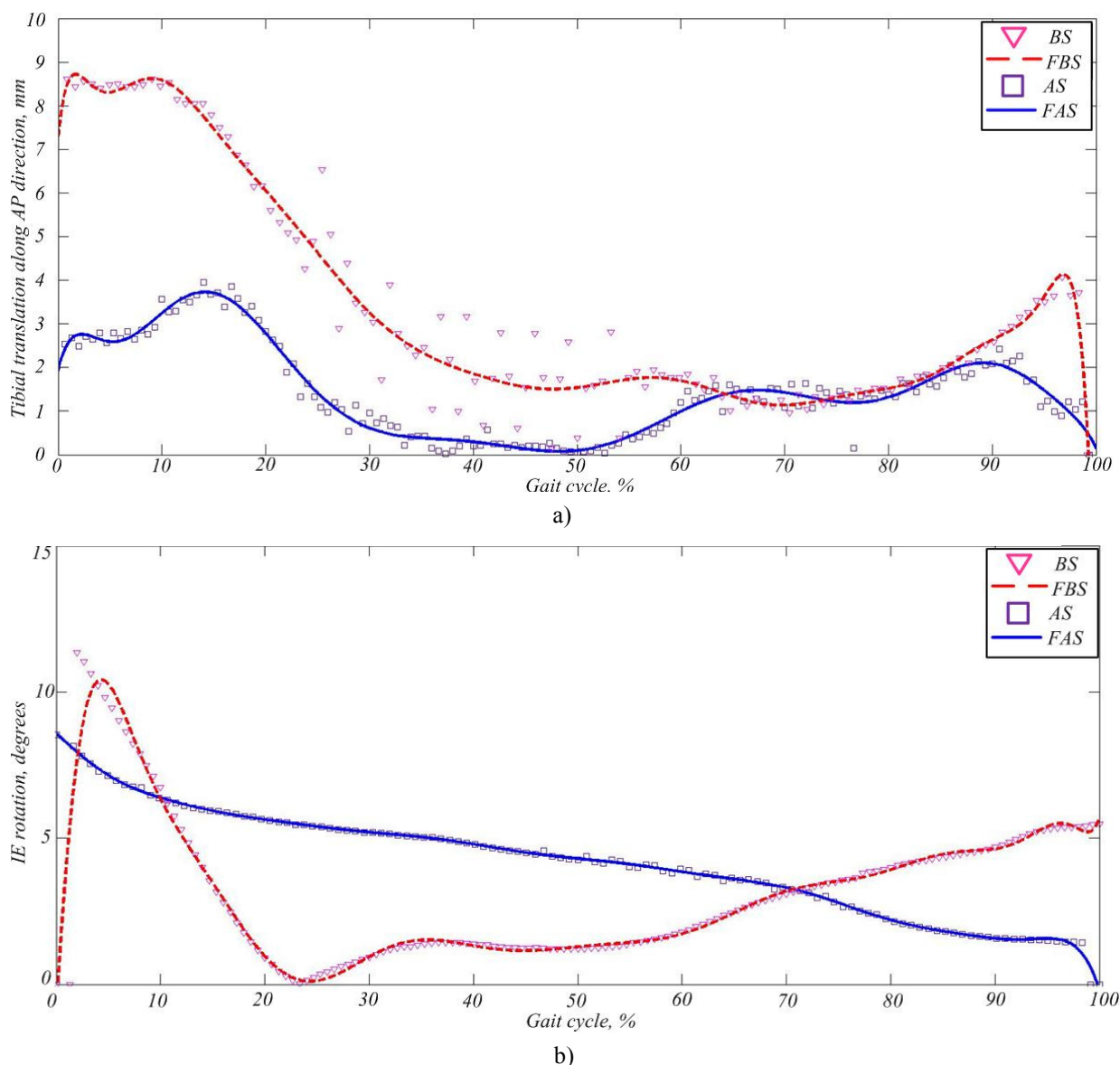


Fig.4. Values of the pathological parameters during gait cycle for: a) AP translation, and b) IE rotation

LEGEND:

BS - Changes of the tibial AP translation (or changes of the IE angle) before surgery, *FBS* – Fitted curve of the tibial AP translation (or changes of the IE angle) before surgery, *AS* - Changes of the tibial AP translation (or changes of the IE angle) after surgery, and *FAS* - Fitted curve of the changes tibial AP translation (or changes of the IE angle) after surgery after surgery.

4. DISCUSSION AND CONCLUSIONS

Knowing knee kinematics is of the great importance for getting relevant knee function information which can be used for improvement treatment of the knee pathology [6]. In this study inovative gait analysis technique is applied.

Stable knee joint implies small values of the AP translation and IE rotation. In order to achieve fuctional role of the ACL, gait cycle specific phases which have influence on pathological kinematic of the ACL deficient knee joint have to be determined.

Numerous reserchers have noticed tibial translation along AP direction and higher values of the IE rotation using in vitro and in vivo experiments [8, 9]. Results of this study shown in Figure 4, concides with results [3, 6]. Maximal values of the AP translation and IE rotation occur in early stance phase when heel strikes [5]. After ligament reconstruction surgery, these values decreased.

Andriacchi et al. and M. Kozanek et al. have shown that there is conection between AP translation and flexion – extension of the knee movement. At initial contact between foot and the ground, anterior position of the tibia relative to the femur is related with extensor mechanisam pulling on the tibia [2,6]. During foot flat phase tibia sliding posteriorly as the knee flexion. This is in agreement with Bergamini et al. which were shown ACL decrease during knee flexion [9]. Our results show (Fig.4) maximal values of the AP translation when knee is in extension, e.g. heel strikes.

Bull et al. in study show that there is significant reduction of the pathological IE rotation across the whole range of the knee motion measured after ACL reconstruction surgery [10]. This correspond with results shown in Figure 6b, where maximal values of the IE rotation at the begginig of the gait cycle occurs, and after reconstruction surgery decrease [11].

Using the same clinical position of the leg landmarks, limitations of this study are minimized which are related to the measurement errors and data noise coming from skin and soft tissue motion.

ACKNOWLEDGNMENTS

This work has been partly supported by Ministry of Education and Science of Serbia, Grants No. III-41007 and project supported by Faculty of Medicine Kragujevac, Grant JP 20/10.

5. REFERENCES

- [1] Dauty M., Menu P., Dubois C.: *Effect of running retraining after knee anterior cruciate ligament reconstruction*, Annals of Physical and rehabilitation Medecine, 53, p.p 150 – 161, 2010.
- [2] Beasley L.S., Weiland D.E., Vidal A. F., Chhabra A., Herzka A.S., Feng M.T., West R.V.: *Anterior Cruciate Ligament Reconstruction: A Literature Review of the Anatomy, Biomechanics, Surgical Considerations, and Clinical Outcomes*, Operative Techniques in Orthopaedics, 15, p.p. 5 – 19, 2005.

- [3] Scanlan S.F., Chaudhari A.M.W., Dyrby C.O., Andriacchi T.P.: *Differences in tibial rotation during walking in ACL reconstructed and healthy contralateral knees*, Journal of Biomechanics, 42, p.p. 1817 – 1822, 2010.
- [4] Matić A., Ristić B., Devedžić G., Filipović N., Petrović S., Mijailović N., Čuković S.: *Gait analysis in the patients with chronic anterior cruciate ligament injury*, Serbian Journal of Experimental and Clinical Research, 13, p.p. 49 - 54, 2012.
- [5] Yeow C.H., Gan W.L., Lee P.V.S., Goh J.C.H.: *Effect of an anterior - sloped brace joint on anterior tibial translation and axial tibial rotation: A motion analysis study*, Clinical Biomechanics, 25, p.p. 1025 - 1030, 2010.
- [6] Kozanek M., Hosseini A., Liu F., Van de Velde S.K., Gill T.J., Rubash H.E.: *Tibiofemoral kinematics and condylar motion during the stance phase of gait*, Journal of Biomechanics, 42, p.p. 1877 - 1884, 2009.
- [7] Shelburne K., Pandy M.G., Torry M.R.: *Comparasion of shear forces and ligament loading in the healthy and ACL - deficient knee during gait*, Journal of Biomechanics, 37, p. p. 313 -319, 2004.
- [8] Koh A.S.B., Nagai T., Motojima S., Sell T.C., Lephart S.M.: *Concepts and Measurement of In Vivo Tibiofemoral Kinematics*, Operative Techniques in Orthopedics, 15, p.p. 43-48, 2005.
- [9] Bergamini E., Pillet H., Hausselle J., Thoreux P., Guerard S., Camomilla V., Cappozzo A., Skalli W.: *Tibio-femoral joint constraints for bone pose estimation during movement using multi-body optimization*, Gait & Posture, 33, p.p. 706 - 711, 2011.
- [10] Bull A.M.J., Ernshaw P.H., Smith A., Katchburian, Hassan A.N.A, Amis A.A.: *Intraoperative measurement of knee kinematics in reconstruction of the anterior cruciate ligament*, The journal of bone & joint surgery, 84-B, p.p 1075 - 1081, 2002.
- [11] Wang H., Fleischli J. E., Zheng N.N.: *Effect of lower limb dominance on knee joint kinematics after anterior cruciate ligament reconstruction*, Clinical Biomechanics, 27, p.p. 170 - 175, 2012.

Authors: Prof. Dr. Goran Devedžić, Suzana Petrović, dipl.ing., Saša Čuković, dipl.ing., University of Kragujevac, Faculty of Engineering, Department for Production Engineering, Sestre Janjić 6, 34000 Kragujevac, Serbia, Phone.: +381 34 -, Fax: E-mail: devedzic@kg.ac.rs
suzana.petrovic@mfgk.rs
cukovic@kg.ac.rs

Prof. Dr Branko Ristić, Dr Aleksandar Matić, University of Kragujevac, Faculty of Medicine, Svetozara Markovića 69, 34000 Kragujevac, Serbia, Phone.: +381 34 306 - 800, Fax: E-mail: branko.ristic@gmail.com
aleksandarmatic@gmail.com

Puskar, T., Jevremovic, D., Eggbeer, D., Lapcevic, A., Trifkovic, B., Vukelic, D., Williams, R.J.

DETERMINATION OF CORROSION CHARACTERISTICS OF DENTAL ALLOY BY INDUCTIVELY COUPLED PLASMA MASS SPECTROMETRY

Abstract: Corrosion resistance is one of the characteristics that dental alloy should possess as it should be placed in the oral cavity. Adverse tissue reactions of the gingiva and the periodontium close to dental cast alloys may be caused by the effects of released metal elements. Corrosion effect of dental Co-Cr-Mo alloy was investigated by ICP MS according to the EN ISO 10271 and EN ISO 22674. Co- Cr dental alloy Remanium GM 800+ (Dentaurum Ispringen, Germany was tested in artificial saliva for 7 days at 37°C. The released metals were detected by Nexion 300X ICP MS (Perkin Elmer, USA). The results showed that the metal release was very low for Co, Cr and Mo, far below the permitted levels. ICP-MS can be considered as very reliable method for such a research.

Key words: dental alloy, corrosion resistance, ICP MS

1. INTRODUCTION

Alloys are in use for many years in dentistry as a material for fabrication of dental devices. Demands for mechanical properties as well as for the stability of dental alloys in oral environment are very high. Dental alloys should withstand high cyclic loads up to 800N per occlusal unit, high humidity, temperature changes from 0°C to 70°C, and acidity variations from pH 2 to pH 11 [1,2,3]. Corrosion resistance is one of the characteristics that dental alloy should possess as it should be placed in the oral cavity. The release of metallic ions from the alloy into saliva should be as low as possible, because they could diffuse in mucosae tissue or they could be ingested, transported and accumulated in distant parts of the organism [4,5]. Many studies have reported toxic and carcinogenic effects induced when humans and animals are exposed to certain metals [4,5,6,7]. Adverse tissue reactions of the gingiva and the periodontium close to dental cast alloys may be caused by the effects of released metal elements. Tissue reactions depend upon the amounts of elements available which are a function of corrosion rates [8]. All previously mentioned indicate that the investigation of potential release of metals from dental alloys in oral environment is necessary step in testing new products before they are allowed to be introduced in clinical practice and in controlling products that are in use for many years.

The insight that we have on stability of the alloy and the safety for use are strongly dependent on the tools available which allow us to perform our investigation. The detection and analysis of the released metals at the trace level poses a number of challenges to the analyst [9]. In previous investigations besides atomic absorption spectrophotometry (AAS) nuclear corrosion monitoring (NCM), electron microscopy (ESCA), microphotography and SEM were used [5,10,11,12]. All of the mentioned methods have their limitations, for example AAS has limited linearity and therefore is recommended for low-level analytes.

ICP MS offers the capability of specification with

multi-element detection, of isotope measurements to improve precision and accuracy excellent sensitivity and detection limits and wide dynamic range [13]. ICP-MS is suitable for analyzes that are requiring the lowest detection limits and the greatest level of productivity.

Favourable characteristics of ICP-MS can be summarized in a few points:

- Instrument detection limits are at or below the single part per trillion (ppt) level for much of the periodic table;
- Analytical working range is nine orders of magnitude;
- Productivity is unsurpassed by any other technique and
- Isotopic analysis can be achieved readily [14].

The principal of ICP MS function is that samples are introduced into argon plasma as aerosol droplets. The plasma dries the aerosol, dissociates the molecules and then removes an electron from the components, thereby forming singly-charged ions, which are directed into a mass filtering device known as the mass spectrometer [15]. Most commercial ICP-MS systems employ a quadrupole mass spectrometer which rapidly scans the mass range. Upon exiting the mass spectrometer, ions strike the first dynode of an electron multiplier, which serves as a detector [15]. The impact of the ions releases a cascade of electrons, which are amplified until they become a measurable pulse. The software compares the intensities of the measured pulses to those from standards, which make up the calibration curve, to determine the concentration of the element [15]. For each element measured, it is typically necessary to measure just one isotope, since the ratio of the isotopes, or natural abundance, is fixed in nature [15]. ICP-MS can be used to measure the individual isotopes of each element; this capability brings value to investigations interested in one specific isotope of an element or in the ratio between two isotopes of an element.

2. MATERIALS AND METHOD

Corrosion effect of dental Co-Cr-Mo alloy was investigated by ICP MS according to the EN ISO 10271 and EN ISO 22674 [16,17]. A rectangular plate sample of 34mm x 13mm x 1.5mm of dental Co-Cr-Mo alloy was made according to the standard technological procedure that was common in today dental laboratory using lost wax technique. Non precious Co-Cr alloy Remanium GM 800 + (Dentaurum Ispringen, Germany) was used. The composition of the alloy is given in Table 1. First, wax model was made. It was invested in Rema dynamic investment and vacuum casted in Nautilus CC system (Bego, Germany). After casting the sample was divested, blasted and polished. The sample was fixed with nylon thread and immersed in glass container with artificial saliva with pH=6.8 [18]. It was held for 7 days (+/- 0.1) at 37°C. After that the sample of artificial saliva was taken and was analyzed in Nexion 300X ICP-MS (Perkin Elmer, USA) (Fig. 1).

Chemical composition (in mass %)	Co	Cr	Mo	Si
	63.3	30	5	1
Others less than 1%: Mn, N, C				

Table 1. Chemical Composition of Remanium GM800+ (Dentaurum Ispringen, Germany) dental alloy according to the manufacturer



Fig. 1. Nexion 300X ICP-MS

An ICP-MS consists of the following components (Fig. 2):

- Sample introduction system – composed of a nebulizer and spray chamber and provides the means of getting samples into the instrument;

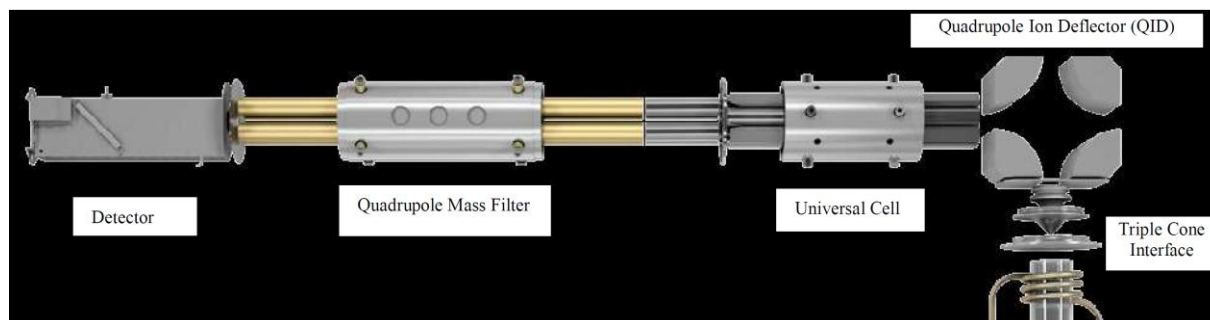


Fig. 2. The ion optic path of the PerkinElmer NexION ICP-MS

- ICP torch and RF coil – generates the argon plasma, which serves as the ion source of the ICP-MS;
- Interface – links the atmospheric pressure ICP ion source to the high vacuum mass spectrometer;
- Vacuum system – provides high vacuum for ion optics, quadrupole, and detector;
- Collision/reaction cell – precedes the mass spectrometer and is used to remove interferences that can degrade the detection limits achieved;
- Ion optics – guides the desired ions into the quadrupole while assuring that neutral species and photons are discarded from the ion beam;
- Mass spectrometer – acts as a mass filter to sort ions by their mass-to-charge ratio (m/z);
- Detector – counts individual ions exiting the quadrupole and
- Data handling and system controller – controls all aspects of instrument control and data handling to obtain final concentration results.

3. RESULTS

The corrosion characteristics of Co-Cr alloy was investigated by analysis of element release in artificial saliva. After the investigating period of 7 days the results of the released metals from the Co-Cr dental alloy were far under the permitted level.

According to ISO 22674 the quantity of released metal from the alloy should not exceed 200µg/cm² in 7 days period [17]. The results of the investigation are shown in Table 2.

4. DISCUSSION

The investigation of corrosion characteristics of dental alloy can be done by analysing the release of metal ions in electrolytic solution. Today, there are three widely accepted analytical methods for analyze of metal release: atomic absorption, atomic emission and mass spectrometry. The most common techniques in use today are:

- Flame Atomic Absorption Spectroscopy;
- Graphite Furnace Atomic Absorption Spectroscopy (GFAA);
- Inductively Coupled Plasma Optical Emission Spectroscopy (ICP-OES) and
- Inductively Coupled Plasma Mass Spectrometry (ICP-MS) [15].

	Mo	Co	Cr
Mean value of the released element ($\mu\text{g/l}$)	70.52	35.27	0.74
Volume of the artificial saliva	0.05	0.05	0.05
Dilution	1	1	1
Mean value (μg)	3.53	1.76	0.04
The surface area of the sample (mm^2)	990.09	990.09	990.09
The result of element release ($\mu\text{g/cm}^2$)	0.356	0.178	0.004

Table 2. The results of the investigation

Performing atomic absorption spectroscopy requires a primary light source, an atom source, a monochromator to isolate the specific wavelength of light to be measured, a detector to measure the light accurately, electronics to process the data signal and a data display or reporting system to show the results. Whatever the system, the atom source used must produce free analyte atoms from the sample [15]. The source of energy for free atom production is heat, most commonly in the form of an air/acetylene or nitrous-oxide/acetylene flame. The sample is introduced as an aerosol into the flame by the sample-introduction system consisting of a nebulizer and spray chamber. The burner head is aligned so that the light beam passes through the flame, where the light is absorbed. The major limitation of Flame AA is that the burner-nebulizer system is a relatively inefficient sampling device. Only a small fraction of the sample reaches the flame, and the atomized sample passes quickly through the light path. An improved sampling device would atomize the entire sample and retain the atomized sample in the light path for an extended period of time, enhancing the sensitivity of the technique [14,15]. This leads us to the next technique – electrothermal vaporization using a graphite furnace. With Graphite Furnace Atomic Absorption (GFAA), the sample is introduced directly into a graphite tube, which is then heated in a programmed series of steps to remove the solvent and major matrix components and to atomize the remaining sample [19]. Graphite Furnace analysis times are longer than those for flame sampling, and fewer elements can be determined using GFAA. However, the enhanced sensitivity of GFAA, and its ability to analyze very small samples, significantly expands the capabilities of atomic absorption.

ICP is argon plasma maintained by the interaction of an RF field and ionized argon gas [15]. The plasma can reach temperatures as high as 10 000 K, allowing the complete atomization of the elements in a sample and minimizing potential chemical interferences. Inductively Coupled Plasma Optical Emission Spectroscopy (ICP-OES) is the measurement of the light emitted by the elements in a sample introduced into an ICP source. The measured emission intensities are then compared to the intensities of standards of known concentration to obtain the elemental concentrations in the unknown sample [15]. Sequential-type systems can select any wavelength and focus it on a single detector. However, this is done one element at a time, which can lead to longer analysis times.

With Inductively Coupled Plasma Mass

Spectrometry (ICP-MS), the argon ICP generates singly charged ions from the elemental species within a sample that are directed into a mass spectrometer and separated according to their mass-to-charge ratio. Ions of the selected mass-to-charge ratio are then directed to a detector that determines the number of ions present [15]. ICP-MS combines the multi-element capabilities of ICP techniques with exceptional detection limits equivalent to or below those of GFAA. It is also one of the few analytical techniques that allows the quantification of elemental isotopic concentrations and ratios, as well as precise speciation capabilities when used in conjunction with HPLC or GC interfaces [14]. This feature enables the analytical chemist to determine the exact form of a species present – not just the total concentration. However, due to the fact that the sample components are actually introduced into the instrument, there are some limitations as to how much sample matrix can be introduced into the ICP-MS.

In addition, there are also increased maintenance requirements as compared to ICP-OES systems. Inductively coupled plasma-mass spectrometry (ICP-MS) is the method of choice for analyzing metal release from dental alloy in investigated medium because of its multi-element capability, low detection limit (ppt) and wide dynamic range (10⁹ orders of magnitude).

5. CONCLUSION

Although Co-Cr dental alloys are used for fabrication of dental devices for many years the research of their stability in oral environment are current. A growing amount of results provide evidence that toxic and carcinogenic metals are capable of interacting with nuclear proteins and DNA causing oxidative deterioration of biological macromolecules [4, 20]. Detailed studies in the past two decades have shown that metals like iron, copper, cadmium, chromium, mercury, nickel, vanadium possess the ability to produce reactive radicals, resulting in DNA damage, lipid peroxidation, depletion of protein (4). Current analytical methods for analysing metals at trace levels give researchers new opportunities for detection and quantification of metals with possible new perspective on their interaction with biomolecules.

According to presented results investigated Co-Cr dental alloy Remanium GM 800 + (Dentaurum Ispringen, Germany) has good corrosion characteristics and stability in oral environment. ICP-MS can be considered as very reliable method for such a research.

ACKNOWLEDGEMENT

Results presented in this paper are obtained in the framework of the project "Research and development of modelling methods and approaches in manufacturing of dental recoveries with the application of modern technologies and computer aided systems" – TR 035020, financed by the Ministry of Education, Science and Technological Development of the Republic of Serbia.

7. REFERENCES

- [1] Rosenstiel, S., Land, M., Fujimoto, J.: *Contemporary fixed prosthodontics*, Mosby, St Louis, 2006.
- [2] Aframian, D.J., Davidowitz, T., Benoliel, R.: *The distribution of oral mucosal pH values in healthy saliva secretors*, Oral Diseases, 12, p.p. 420–423, 2006.
- [3] Lavrenko, V.A., Shvets, V.A., Boshitskaya, N.V., Makarenko, G.N.: *Comparative study of the chemical resistance of titanium nitride and stainless steel in media of the oral cavity*. Powder Metallurgy and Metal Ceramics, 40(11-12), p.p. 630-636, 2001.
- [4] Valko, M., Morris, H., Cronin, M.T.D.: *Metals, Toxicity and Oxidative Stress*. Current Medicinal Chemistry, 12, p.p. 1161-1208, 2005.
- [5] Wataha, J.C., Craig, R.G., Hanks, C.T.: *The Release of Elements of Dental Casting Alloys into Cell-culture Medium*. Journal of Dental Research, 70, p.p. 1014-1018, 1991.
- [6] Lee, J.C., Son, Y.O., Pratheeshkumar, P., Shi, X.: *Oxidative stress and metal carcinogenesis*. Free Radical Biology and Medicine, 53, p.p.742–757, 2012.
- [7] Yang, M.: *A current global view of environmental and occupational cancers*. Journal of Environmental Science and Health. Part C: Environmental Carcinogenesis and Ecotoxicology Reviews, 29, p.p. 223–249, 2011.
- [8] Schmalz, G., Langer, H., Schweikl, H.: *Cytotoxicity of Dental Alloy Extracts and Corresponding Metal Salt Solutions*. Journal of Dental Research, 77, pp. 1772-1778, 1998.
- [9] Lobinski, R.: *Characterizing speciation of trace elements in the chemistry of life*. Fresenius' Journal of Analytical Chemistry, 369, pp. 113-114, 2001.
- [10] Bergman, M, Ginstrup, O.: *Dissolution Rate of Cadmium from Dental Gold Solder Alloys*, Acta Odontologica Scandinavica, 33, pp.199-210, 1975.
- [11] Brune, D.: *Mechanism and Kinetics of Metal Release from Dental Alloys*. International Endodontic Journal, 21, pp.135-142, 1988.
- [12] Johansson, B.I., Lemons, J.E., Hao, S.Q.: *Corrosion of Dental Copper, Nickel, and Gold Alloys in Artificial Saliva and Saline Solutions*. Dental Materials, 5, pp. 324-328, 1989.
- [13] Montes-Bayona, M., DeNicolab, K., Carusob, J.A.: *Liquid chromatography-inductively coupled plasma mass Spectrometry*. Journal of Chromatography A, 1000, pp. 457-476, 2003.
- [14] Niessen, W.M.A.: *Current Practice of Gas Chromatography-Mass Spectrometry*. CRC Press Taylor and Francis group 2001.
- [15] Thomas, R.: *Practical Guide to ICP-MS: A Tutorial for Beginners*, Second Edition. Scientific Writing Solutions, Gaithersburg, Maryland, USA, CRC press Taylor and Francis group 2008.
- [16] EN ISO 10271:2001. *Dental metallic materials. Corrosion test methods*.
- [17] EN ISO 22674:2006. *Dentistry-Metallic materials for fixed and removable restorations and appliances*.
- [18] Aframian, D.J., Davidowitz, T.R., Benoliel, R.: *The distribution of oral mucosal pH values in healthy saliva Secretors*. Oral Diseases, 12, pp. 420-423, 2006.
- [19] Pramanik, B.N., Ganguly, A.K., Michael, L.: Gross, M.L.: *Applied Electrospray Mass Spectrometry: Practical Spectroscopy Series Volume 32*, CRC Press Taylor and Francis group 2002.
- [20] Haeri, M., Wollert, T., Langford, G.M., Gilbert, J.L.: *Electrochemical control of cell death by reduction-induced intrinsic apoptosis and oxidation-induced necrosis on CoCrMo alloy in vitro*. Biomaterials, 33, pp. 6295-6304, 2012.

Authors: Doc. dr Tatjana M. Puskar, Clinic for Prosthodontics, Medical Faculty - Department of dentistry, University of Novi Sad, Hajduk Veljkova 3, 21000 Novi Sad, Serbia. E-mail: tpuskar@uns.ac.rs.

Prof. Robert J. Williams, Dominic Eggbeer, Centre for Dental Technology and the National Centre for Product Design and Development Research, Cardiff Metropolitan University, Cardiff, United Kingdom.

Prof. dr Danimir P. Jevremovic, Ana Lapcevic, Clinic for Prosthodontics, School of Dentistry, Zrenjaninski put 179, 13000 Pančevo, University Business Academy in Novi Sad, Serbia. E-mail: dr.danimir@sbb.rs, analapcevic82@gmail.com.

Mr Branka Trifkovic, University of Belgrade, School for Dentistry, Clinic for Prosthodontics, Rankeova 4, 11000 Belgrade, Serbia. E-mail: brankatr@yahoo.com.

Doc. dr. Djordje Vukelic, University of Novi Sad, Faculty of Technical Sciences, Institute for Production Engineering, Trg Dositeja Obradovica 6, 21000 Novi Sad, Serbia, Phone.: +381 21 485-23-26, Fax: +381 21 454-495, E-mail: vukelic@uns.ac.rs.

Radulović, J., Mijailović, N., Trajanović, M., Filipović, N., Radulović, N.

ESTIMATION OF EXPOSURE DOSE OF HUMAN HEAD DURING CT SCANNING PROCEDURE USING MONTE CARLO SIMULATION

Abstract: In this study we present method for determination of exposure dose on human head during computer tomography (CT) scanning procedure. Method is based on scan data obtained by CT. The gray level of image is converted to attenuation coefficient distribution in the head model. The exposure dose is calculated using this model data by Monte Carlo method simulation. This method is based on quantification of interaction between X-ray photon and head tissue. Obtained simulation results can be helpful to improve design, safety and quality of CT system for head imaging.

Key words: Monte Carlo, Computer Tomography, Exposure Dose

1. INTRODUCTION

Recent studies in radiology suggest that computed tomography (CT) scans comprise only (3-11) % of all radiological exams, yet contribute to (35-45) % of the total radiation dose to the patient population [1,2].

Further research into the complex relationship between radiation exposure, image quality, and diagnostic accuracy should be encouraged, in order to establish the minimum radiation dose necessary to provide adequate diagnostic information [3].

According to this information protection of patients during scanning procedure is main requirement during imaging procedure and design of CT devices. The one way to minimize radiation dose is to better understand mechanisms of dose absorption and factor like construction of X-ray device, type of filter being used and characteristic of patient tissue. Dose reduction can be achieved using appropriate filterers [4,5] suitable reconstruction algorithms [6,7] or special mode of X-ray source operation [7].

In this study we try to calculate dose of CT scanner by Monte Carlo Simulation using multi slice image data.

The final goal is to develop tool for exposure dose calculation with the aim of enhancing quality of CT devices.

2. COMPUTER TOMOGRAPHY

2.1 Basic relation

Computer tomography (CT) is a non-destructive method for characterizing 3D objects by using X-ray radiation. This method is based on the differences in attenuation coefficient of X-ray beams for various materials and tissues. The final result is a grey level CT image where corresponding grey level is proportional to attenuation coefficient.

CT medical imaging includes exposure of the object of radiation at one side and detecting attenuated radiation at the other side of the object and this procedure is repeated from more than one direction. The next step is image reconstruction from the projection by using a number of techniques. All of these techniques are based

on solving systems of integral equations which are formed as a result of total attenuation of the radiation beam from the source to the detector. Monochromatic X-ray reduction for homogenous materials is given by the relation

$$I = I_0 e^{-\mu d}, \quad (1)$$

where I_0 is intensity of initial radiation, I is final intensity radiation after path length d in tissue with linear attenuation coefficient μ . If there are multiple materials, the equation becomes:

$$I = I_0 e^{-\sum \mu_i d_i}. \quad (2)$$

Linear attenuation coefficient is very sensitive to energy variation of initial X-photon; that is to say the equations 1 and 2 are valid only for monochromatic beam.

If a polychromatic X-ray source is used, taking into account the fact that the attenuation coefficient is a strong function of X-ray energy, the complete solution would require solving the equation over the range of the X-ray energy (E) spectrum utilized:

$$I = \int I_0(E) e^{-\mu(E)d} dE. \quad (3)$$

This equation largely complicates the reconstruction process and obtaining final results. For this reason the equation (1) is more applicable with a note that μ represents effective attenuation coefficient with spectral characteristics included.

2.2 CT number

CT numbers are also known as the Hounsfield units which are proportional to mean linear attenuation coefficient and they are formed at the end of reconstruction process.

The corresponding CT number is given by

$$CT = K \frac{\mu_t - \mu_w}{\mu_w}. \quad (4)$$

Where μ_t , μ_w are linear attenuation coefficients of X-ray in tissue and water respectively and K is scale factor. The K is chosen to satisfy -1000 value of CT

number for air and 1000 for some kind of cortical bone tissue. According to representation a Hounsfield unit in binary number system it is very useful take 1024 value for K . Then CT number ranges from -1024 to 1023 and 11-bit is used for representation. For 12-bit representation CT number takes values from -1024 to +3071.

3. MONTE CARLO METHOD

The Monte Carlo method is stochastic procedure for simulation of a finite number particle transport by using random number generation. In every iteration suitable random numbers determine direction and space angle of particle trajectory, energy of particle and type of their interaction with transported medium (tissue). The appropriate variables are obtained as a mean value of finite numbers of iteration. The accuracy of the estimated values is proportional to the number of iterations. Monte Carlo is stochastic method because the variable being sought can be obtained only in finite volume but not in one point unlike deterministic method.

If we consider motion of a particle, we should suppose a one point source with coordinates (0,0,0) as shown in Fig. 1.

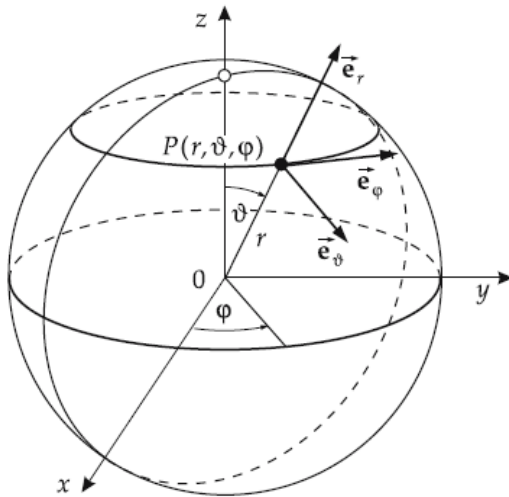


Fig. 1. Cylindrical coordinate for particle source

Random direction of particle motion is defined by equations

$$\begin{aligned} \theta &= \arccos(1 - 2\xi_1) \\ \varphi &= 2\pi\xi_2 \end{aligned} \quad (5)$$

where θ is polar angle, φ is azimuth angle and ξ_1, ξ_2 are random generated numbers with uniform density distribution in the interval (0-1).

Unit vector direction of particle motion is expressed by

$$\begin{aligned} \vec{\Omega} &= \sin(\theta) \cdot \cos(\varphi) \cdot \vec{e}_x + \\ &\sin(\theta) \cdot \sin(\varphi) \cdot \vec{e}_y + \cos(\theta) \cdot \vec{e}_z \end{aligned} \quad (6)$$

Let's assume now that the particle is passing through a much more homogenous region as shown on Fig. 2.

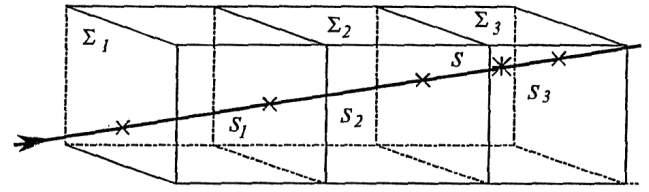


Fig. 2. Particle in non-homogenous media

The regions are characterized by macroscopic cross sections for absorption $\Sigma_1, \Sigma_2, \Sigma_3$, which are actually linear attenuation coefficients.

Tracking starts by generating a new random number ξ_3 and calculating the equation

$$t = -\ln(1 - \xi_3). \quad (7)$$

If we find

$$\begin{aligned} S_1 s_1 &< t \\ S_1 s_1 + S_2 s_2 &< t \\ S_1 s_1 + S_2 s_2 + S_3 s_3 &> t \end{aligned} \quad (8)$$

the interaction takes place in the region 3 after it travelled the distance s in the region 3,

$$s = \frac{t - \Sigma_1 s_1 + \Sigma_2 s_2}{\Sigma_3}. \quad (9)$$

By analogy with this way we can find place of interaction and distance having been crossed for any region.

If the particle meets the requirement for interaction we will have increment of a total received dose of radiation for the amount of photon energy, otherwise there is no absorption and photon comes to detector without loss of energy.

4. MATERIAL AND METHODS

The first step in this study was to determine spectrum of X-ray source. We used low dose 3DCT scanner [8], X-ray tube Model XRS-125-7K-P for X-ray production with 4 mm aluminium filter and obtained spectrum as shown in Fig. 3.

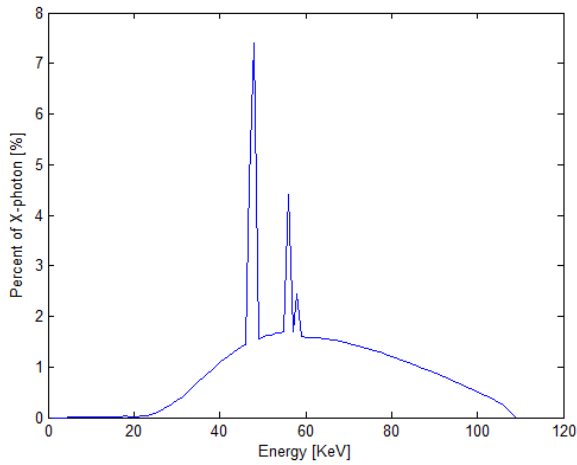


Fig. 3. Spectral distribution energy of X-photon

Calculation of the spectrum was performed by SpekCalc [1] a software for X-photon spectrum estimation. Mean energy of X-photon of this spectrum is given by relation

$$\bar{E} = \frac{\int_E f(E) \times E dE}{\int_E f(E) dE} \quad (10)$$

where E is X-photon energy and $f(E)$ represents a probability density function.

The mean energy is $\bar{E} = 73.72$ KeV. The next step is geometry determination of the problem and for this we used CT image as shown in Fig. 4.

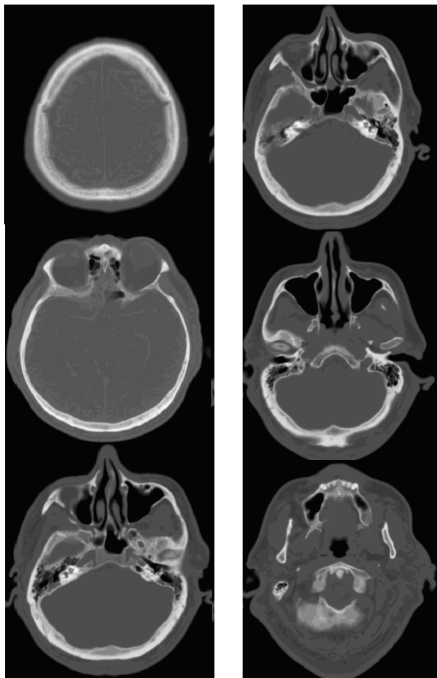


Fig. 4. Multi slice CT image

CT images are segmented and surface is produced for human head.

Model data consists of surface points shown in Fig. 5.

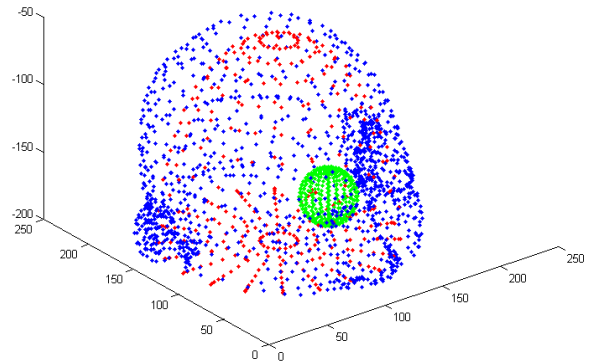


Fig. 5. Head model divided into three regions

The attenuation coefficient for water at effective energy \bar{E} has value $m_w = 0.1965 \text{ cm}^{-1}$. By substituting that in the equation (4) we can get a macroscopic cross section for any domain in the model. CT numbers for the structures having been considered are given respectively:

- CT=929 (Bone tissue external sphere) 170.5 mm diameter
- CT=-780 (Air shell internal) 27 mm diameter
- CT=85 (Internal sphere soft Tissue),

and they are obtained by an averaging on the domain. During imaging procedure X-ray source rotates around head of patient, the procedure is finished when the source has closed a full circle. In our case we need to apply discretization by dividing full circle into ten segments. Each of these segments represents one direction source-detector between which there is object. For every direction we apply procedure described in section 3. The total amount of absorption energy is 8 % of initial radiation what corresponds to a received dose of 112 μS .

5. FINAL REMARKS

In this study we have briefly presented basic relation and technique of CT imaging method. Critical point of application of this diagnostic method is exposure dose of X-photon radiation.

The main goal of our research is estimation of the absorbed radiation dose using Monte Carlo simulation of X-photon transport in head tissue of the patient. For simulation we have created geometrical model from CT images. The model is divided into a number of regions with realistic dimensions and attenuation coefficients obtained from spectra data and grayscale level of images being used.

The final dose is around 112 μS and this result is comparable with value from 35 to 72 μS which was predicted for this scanner, according to 2007 ICRP [10].

The difference between the predicted and calculated

doses is the result of the approximations which were included in the calculation. Material characteristics of each voxel were not taken into account; instead, mean value in certain domain was attributed to every point of that domain. Also, the energy of X-photons was taken as the mean value and attenuation coefficients were calculated based on the unique energy value. In reality, the photons are polychromatic and this coefficient should be calculated for each energy value separately. Finally, the accurate initial radiation value can be obtained by measuring, but in this case, the estimation was done on the bases of scanner characteristics.

There are several goals of future research: to improve accuracy by using a more realistic geometrical model with a lot of sub-domains in model or even voxel representation of model, to do calculation which would include the attenuation coefficient dependence on energy to a higher degree and to compare the calculated values with the radiation dose values having been measured for the scanner being considered.

6. ACKNOWLEDGMENT

This paper is part of project III41017 Virtual human osteoarticular system and its application in preclinical and clinical practice, funded by the Ministry of Education and Science of Republic of Serbia (<http://vihos.masfak.ni.ac.rs>).

7. REFERENCES

- [1] Imhof H, Schibany N, Ba-Ssalamah A, Czerny C, Hojreh A, Kainberger F, et al. *Spiral CT and radiation dose*, European Journal of Radiology 47 (2003) 29-37
- [2] Takayuki Yamada, Shuichi Ono, Masahiro Tsuboi, Haruo Saito, Akihiro Sato, Toshio Matsuhashi, Tadashi Ishibashi, Shoki Takahashi, *Low-dose CT of the thorax in cancer follow-up*, European Journal of Radiology 51 (2004) 169-174
- [3] Mayo JR, Aldrich J, Muller NL. *Radiation exposure at chest CT: a statement of the Fleischner society*. Radiology 2003;228:15-21.
- [4] Nan-Ku Laia, Ying-Lan Liao, Tuo-Rong Chen, Yu-Sheng Tyana, Hui-Yu Tsai, *Real-time estimation of dose reduction for pediatric CT using bismuth shielding*, Radiation Measurements 46 (2011) 2039e2043
- [5] D.J. McLaughlin, R.B. Mooney, *Dose reduction to radiosensitive tissues in CT. Do commercially available shields meet the users' needs?* Clinical Radiology (2004) 59, 446-450
- [6] Seung Hyun Lee, Myung-Joon Kim, Choon-Sik Yoon, Mi-Jung Lee, *Radiation dose reduction with the adaptive statistical iterative reconstruction (ASIR) technique for chest CT in children: An intra-individual comparison*, European Journal of Radiology 81 (2012) e938-e943
- [7] Ting-Yim Lee, Rethy K. Chhem, *Impact of new technologies on dose reduction in CT*. European Journal of Radiology, European Journal of Radiology 76 (2010) 28-35
- [8] www.medicaproducts.com
- [9] G Poludniowski, G Landry, F DeBlois, P M Evans, F Verhaegen, *SpekCalc: a program to calculate photon spectra from tungsten anode X-ray tubes*, 2009 Phys. Med. Biol. 54 N433
- [10] Valentin J. *International Commission on Radiation Protection, Managing patient dose in multi-detector computed tomography (MDCT)*: ICRP publication 102. Ann ICRP 2007.

Authors: PhD, Full Professor. Jasna Radulovic, University of Kragujevac, Faculty of Engineering, Sestre Janjic 6, 34000 Kragujevac, Serbia, Phone.: +381 34 335 990, Fax: +381 34 333 192.

PhD student, Nikola Mijailovic, University of Kragujevac, Faculty of Engineering, Sestre Janjic 6, 34000 Kragujevac, Serbia, Phone.: +381 34 335 990, Fax: +381 34 333 192

PhD, Full Professor. Miroslav Trajanovic, University of Nis, Faculty of Mechanical Engineering, Aleksandra Medvedeva 14, 18000 Nis, Serbia, Phone.: +381 18 500 662, Fax: +381 18 588 244.

PhD, Full Professor. Nenad Filipovic, University of Kragujevac, Faculty of Engineering, Sestre Janjic 6, 34000 Kragujevac, Serbia, Phone.: +381 34 335 990, Fax: +381 34 333 192

MSc student, Nikola Radulovic, University of Kragujevac, Faculty of Medical Science, Svetozara Markovica 69, 34000 Kragujevac, Serbia, Phone: +381 34 306 800, Fax: +381 34 306 800

E-mail: jasna@kg.ac.rs

nmijalovic@kg.ac.rs

miroslav.trajanovic@masfak.ni.ac.rs

fica@kg.ac.rs

nidzoni85@gmail.com

Raspudic, V.

KINEMATIC ANALYSIS OF LOWER EXTREMITIES IN CAD ENVIRONMENT

Abstract: The current CAD computer technologies can be used to perform three-dimensional biomechanical analysis of human locomotion to provide insight into the way of achieving motion in normal and pathological conditions, as well as a diagnostic tool for diagnosing and correcting pathologies and providing a way to optimize the specific activity of locomotor system. Within this research, special attention is focused on the development of new interactive methods in simulating the movement of virtual models within CAD computer technologies, based on real data captured by the Elite measurement system.

Key words: biomechanics, computer simulation, kinematic analysis

1. INTRODUCTION

CAD has been traditionally used to assist in engineering design and modeling for representation, analysis and manufacturing. Recent advances in computing technologies have helped in the advancement of CAD in biomedical engineering in applications ranging from clinical medicine, customized medical implant design to tissue engineering [1]. Current CAD systems that are being used in applications for traditional mechanical design and analysis still provide simple simulation and analysis tools for the biomechanical analysis of the human body. For example, CATIA from Dessault Systems, provides tools such as HBR (Human Builder), HME (Human Measurement Editor), HPA (Human Posture Analysis) and HAA (Human Activity Analysis). Their functions and capabilities are primarily intended for the ergonomic or static analysis, and not for dynamic analysis [2].

The possibilities of computer simulation of moving structures give more information than any other visual means, such as drawings, photographs and video projections, because it is possible to emphasize certain phases and key structural units for the analysis of motion. The aim of this research is to develop new interactive methods in computer simulations for analyzing various forms of human body locomotion within CAD computer technologies and to provide the possibility of integration of biomechanical kinematic and dynamic data with conventional motion analysis of mechanical components.

Special attention is focused on the study of locomotion when climbing stairs, as an activity that requires large amount of metabolic energy, and thus represents difficulty in performing daily activities for people with disorders of the musculoskeletal system, particularly for people with lower limb amputation. The developed approach of analyzing biomechanical data in computer environment that is regularly used to modeling, motion and strength analysis of prosthesis and implants will benefit in a better design of these devices.

2. METHODS

2.1 Experimental measurement

ELITE measurement system (Bioengineering Technology & Systems) allows recording of spatial coordinates of markers set on specific anatomic points on the human body and signal processing of recorded data in real time [3]. The system may include more cameras, constructed so that they are particularly sensitive to infrared (IR) part of spectrum. Number of cameras that are used depends on the size of the visual field and type of motion that is recorded. For the analysis of 2D problems, where it is necessary to analyse movement in the sagittal plane, only one camera may be sufficient, while for the analysis of spatial problems multiple cameras are needed [Fig.1]. Flashes that are mounted on cameras emit infrared rays that are rejected on the reflective surface of the markers set on the body of the examined subjects. The sensitivity of the camera only allows detection of light from the markers, while ignoring other sources (skin, cloth ...). ELITE system uses passive markers, which allows absolute freedom of movement of subjects. Number of markers is not limited, and their diameter ranges from 1 mm to 1 cm.

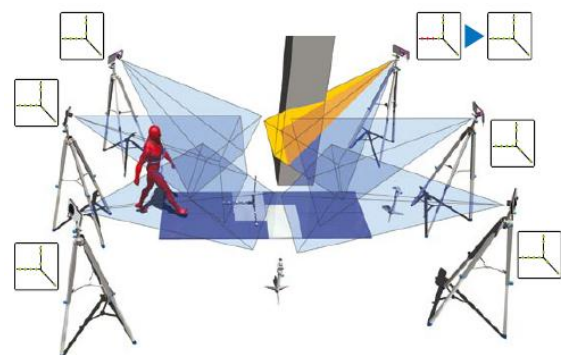


Fig. 1. Sheme of a measurement system [3]

The gait analysis equipment used for this experimental measurement consisted of Elite system

with two CCD cameras and stairs that consisted of two steps with the standard slope of 17 cm in height and 29 cm in depth. Measuring took place in a pre-calibrated working volume of 2.2 m length, 1.8 m height and 1.5 m wide, with a recording frequency of 50 Hz.

The first step was mounted with the Kistler force platform for measuring of three component ground reaction forces.

Ten subjects ranging in age from 21 to 39, with no apparent abnormalities of the locomotor system, were studied. The climbing was performed with the speed that the subjects considered as their normal speed of climbing. Special attention was given to naturalness in walking and a constant walking velocity. Subjects were walking barefoot. The five reflective markers have been attached to palpable landmarks of lower extremities, and their position is defined according to the procedure described in (Perry, 1992) and (Cappozzo et al., 1995) [4,5].

The markers of 1 cm in diameter have been used, and they were placed on the following characteristic landmarks:

- marker 1: hip (upper front edge of the great trochanter);
- marker 2: knee (top of the fibula);
- marker 3: ankle (3 mm and 8 mm below the top front of the lateral malleolus);
- marker 4: heel;
- marker 5: the root of the little finger (top of the fifth metatarsal).

In order to correctly interpret the recorded data, it is necessary to classify markers. Markers are numbered and assigned to the appropriate anatomic position on the subject, which forms a 2D model for each camera as a set of points connected by lines. On the basis of this information the stereophotogrametric reconstruction of 3D coordinates of markers can be done.

A number of experiments has been repeated for each of the subjects. For further analysis only successfully saved files have been used, where it was possible to reconstruct the cycle of climbing and where the full contact between foot and the platform has been achieved.

2.2 Biomechanical simulation

In biomechanical tests, due to extreme complexity of the structure of human body, structural diagram of the human skeleton is usually displayed as a mechanism comprised of members, which are connected in a series of kinematic chains. The kinematic model of lower extremities developed in this research consists of 15 members (5 joints and 10 links) [Fig. 2].

The mobility of the system is realized through three rotational degrees of freedom between the individual joints and links (spherical joints), and through one translational and one rotational degree of freedom between the proximal and distal links in the direction of their longitudinal axis (cylindrical joints) [Fig. 3].

These kinematic models have enabled a computer simulation that accurately mimics the captured data with spatial coordinates of markers, and the three-

dimensional computer reconstruction of their trajectories and their projections in the sagittal, frontal and transverse plane.

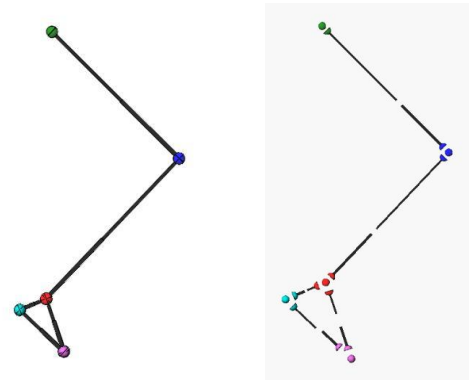


Fig. 2. Kinematic model in assembled and exploded state

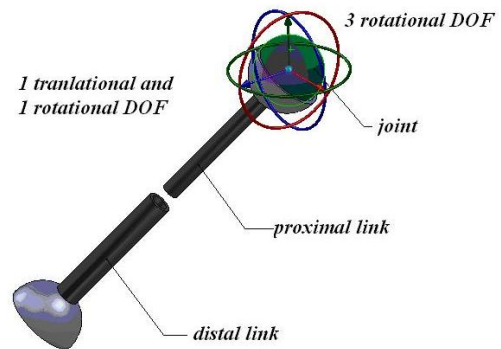


Fig. 3. Display of degrees of freedom (DOF) between links (proximal and distal) and spherical joints

3. RESULTS OF SIMULATION

Figures 4 and 5 represent an example of the processed results to x and y coordinates of markers of the hip, knee and ankle joints.

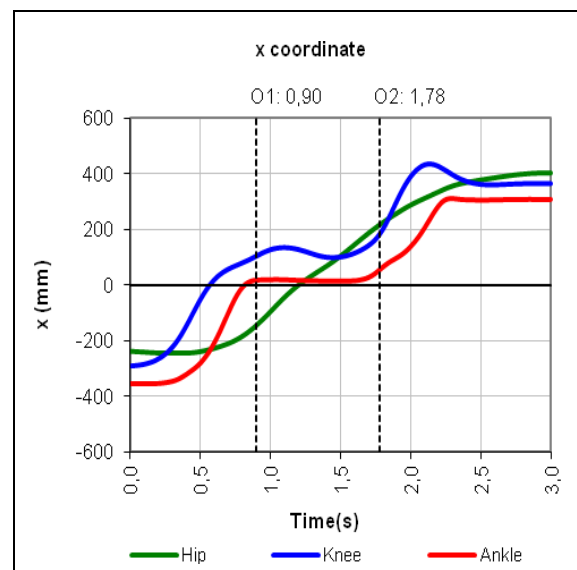


Fig. 4. An example of x coordinates of measured data

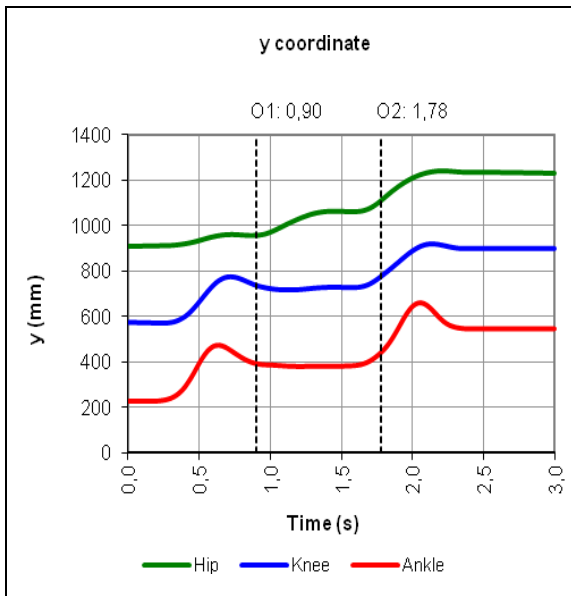


Fig. 5. An example of y coordinates of measured data

Based on the recorded data from the force platform, the moments of the beginning and end of the stance period have been defined. The tag O1 marks the beginning of foot contact with the surface (force platform), and the tag O2 marks the end of foot contact.

Using the developed kinematic model of lower extremity, a 3D computer reconstruction of spatial trajectories has been done for every recorded measurement [Fig. 6].

The joints trajectories represent an important biomechanical characteristic, because they are directly related to the energy consumption. Spatial motion is performed in a way that requires a minimum of energy consumption, so that every movement that causes a change of the trajectories above normal maximal limits causes energy dissipation.

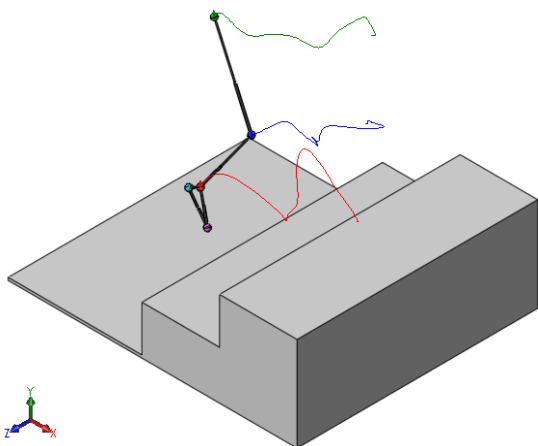


Fig. 6. Computer reconstruction of spatial trajectories

The dependences of translation velocities and accelerations of the hip, knee and ankle joint during the climbing have also been determined.

In order to develop statistical models that are used as a comparative basis, the average multiple samples have been introduced. From individual patterns, a typical pattern for every subject has been determined.

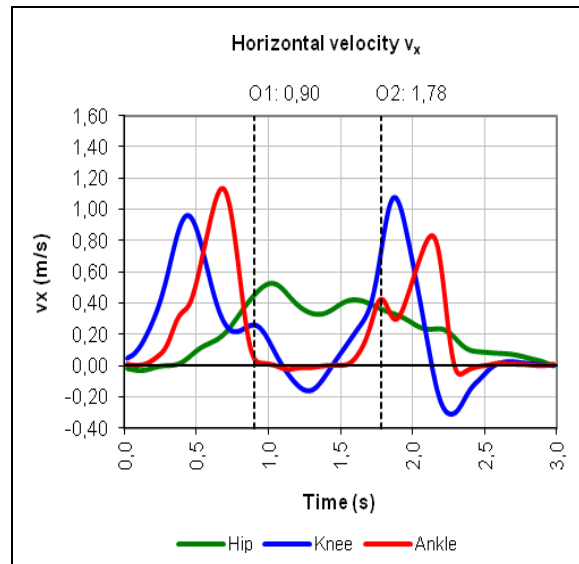


Fig. 7. Horizontal component of velocity

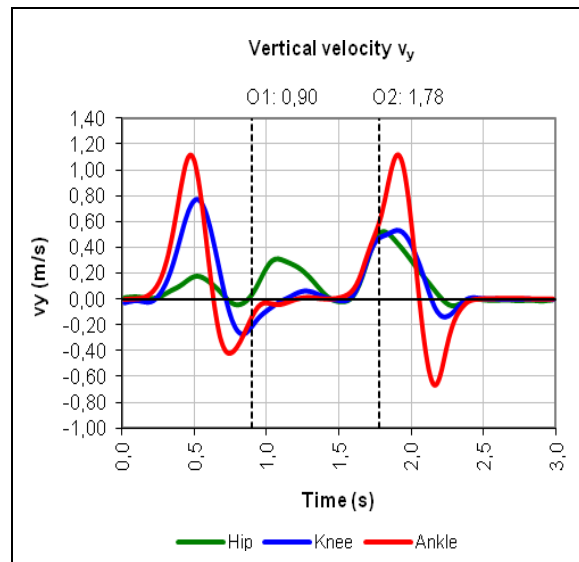


Fig. 8. Vertical component of velocity

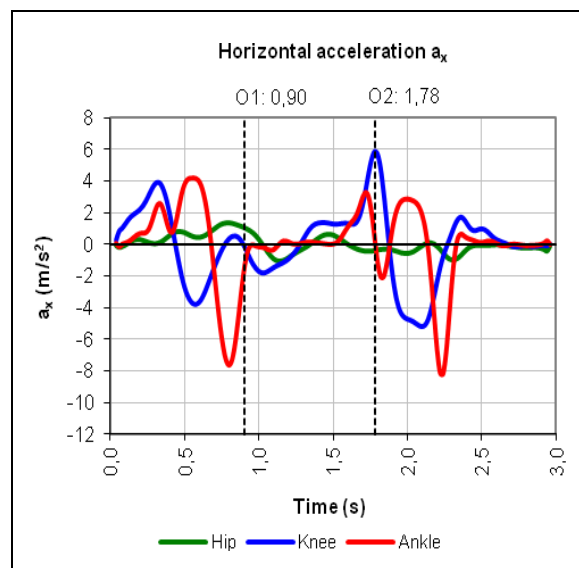


Fig. 9. Horizontal component of acceleration

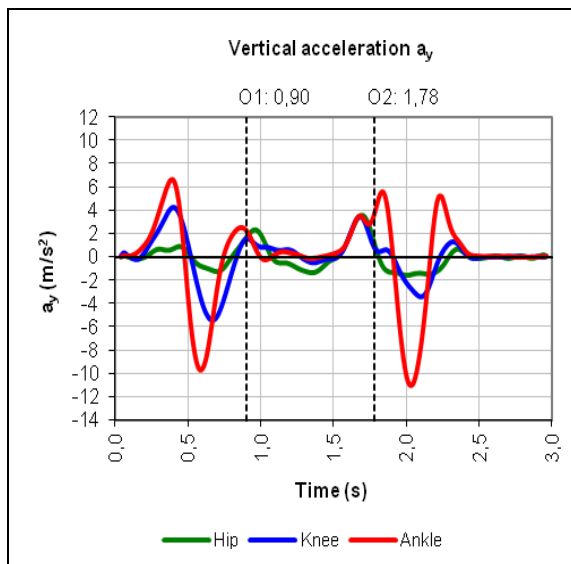


Fig. 10. Vertical component of acceleration

The typical patterns for one of the examined subjects are shown on Figures 7 - 10. These data can also be simultaneously tracked in their vector representation on the kinematic model during the motion simulation, which is represented in Figure 11 for the sagittal plane.

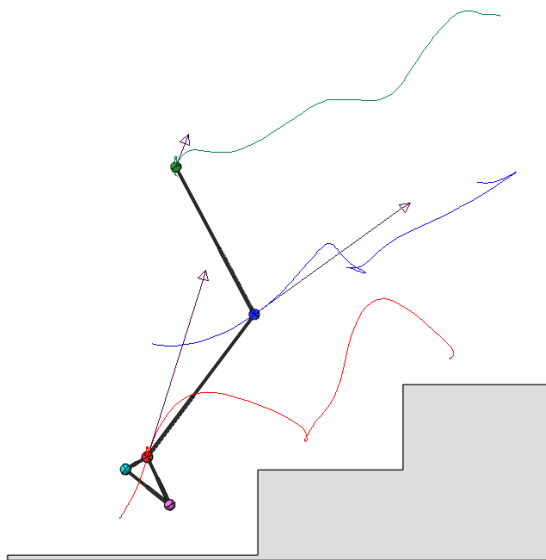


Fig. 11. Joint trajectories with velocity vectors representation in sagittal plane

4. CONCLUSION

The development of methodology for 3D computer simulation that will truly emulate the real human body motion of a recorded magnetic or optical monitoring within the CAD system provides a detailed biomechanical analysis of kinematics and dynamics in various aspects of locomotion.

In this study the biomechanical kinematic analysis during stair climbing has been analysed. An automatised method for determination of spatial orientation of lower limb segments has been established. 3D coordinates of the marked points

recorded by the ELITE measuring system and Kistler force plate were the input data for the computer simulation, which calculates and reconstructs the spatial orientation and trajectories of joints of the developed CAD kinematic models. Time dependences of velocity and acceleration vectors have been determined.

The methodology of combining data captured by the magnetic tracking system with the current CAD/CAE computer technologies developed in this research can be used for three-dimensional biomechanical analysis of different forms of locomotor movements and as a diagnostic tool for identifying gait disorders and finding optimal parameters for their removal. It also can find application in improving the structure and control concepts for lower limb prosthetic devices [6], in order to achieve a reciprocal way of climbing stairs.

5. REFERENCES

- [1] Sun W. et al.: *Bio-CAD modeling and its applications in computer-aided tissue engineering*, J Computer-Aided Design, No. 37, pp. 1097-1114, 2005.
- [2] Lee K.: *CAD System for Human-Centered Design*, Computer-Aided Design & Applications, Vol.3, No.5, pp.615-628, 2006.
- [3] *ELITE System Manual*, BTS, Milano, 1994.
- [4] Perry J.: *Motion Marker Systems*, In: *Gait Analysis, Normal and Pathological Function*, SLACK Incorporated, ISBN: 1-55642-192-3, USA, 1992.
- [5] Cappozzo A. et al.: *Position and orientation of bones during movement: anatomical frame definition and determination*. *Clinical Biomechanics*, Vol. 10, No. 4, pp. 171-178, ISSN: 0268-0033, 1995.
- [6] Vucina A., Hudec M., Raspudic V.: *Kinematics and Forces in the Above-Knee Prosthesis during the Stair Climbing*. *Int.j.simul.model.*, pp. 17-26, ISSN: 1726-4529, 2005.

Author: Doc.dr.sc. Vesna Raspudic, University of Mostar, Faculty of Mechanical Engineering and Computing, Matice hrvatske bb, 88000 Mostar, Bosnia and Herzegovina, Phone.: +387 36 337-028, Fax: +387 36 337-012.

E-mail: vesna.raspudic@sve-mo.ba

Tabaković, S., Zeljković, M., Živković, A., Grujić, J.

DEVELOPMENT OF THE ENDOPROSTHESIS OF THE FEMUR ACCORDING TO THE CHARACTERISTICS OF A SPECIFIC PATIENT

Abstract: Arthroplasty of the hip joint is one of the most widely implemented endoprothetical aids in humans. Each year, around 800,000 operations such this, are done in the world. The main factors influencing the success of the surgery are the operative procedure, the degree of adaptation elements of prosthesis to the patients, and its mechanical properties. Due to the large number of influencing factors, the best results are achieved by the development of prostheses tailored to the patient. The custom-made development of the endoprosthesis body includes four group activities as follows: data acquisition from diagnostic images and the reconstruction of the morphology of the affected elements of the skeletal system, definition of a computer model for a hip endoprosthesis, verification using the appropriate computer analysis and production by applying the NC technology. This paper describes the specific activities present in the development of hip endoprosthesis specifying their advantages and limitations. The presented results are the part of the research on development of the custom made endoprostheses at the Faculty of technical sciences.

Key words: custom-made endoprsthesis, hip joint, CAD, CAE

1. INTRODUCTION

The intensity of life activities and illnesses occurring as a consequence have a significant impact on the elements of the locomotion system. In everyday physical activities, every person makes approximately 10,000 steps per day [1], and as the consequence, the elements of the hip and knee joints suffer the most, since they are exposed to the most intensive workloads. Due to the problems in these elements of the locomotion system, there are about 800,000 total hip replacement surgeries performed yearly worldwide [2].

According to the form and manner in functioning, the hip is a spherical joint establishing the connection between the pelvis and the femur. This joint consists of several elements, as presented in Fig. 1.

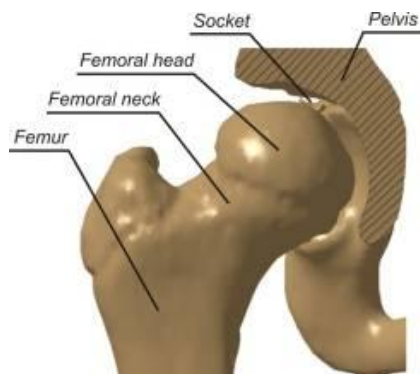


Fig. 1. Elements of the hip

Operative treatment of replacing the natural with the artificial hip joint is generally composed of several phases: separation of the natural femoral head and the neck from the femur bone (Fig. 2a); installation of the acetabular component presenting the artificial seat of the hip joint (Fig. 2b); installation of the endoprosthesis body into the medullary channel of the femur bone with

the elements replacing the natural neck (Fig. 2c); setting of the artificial head to the neck of the prosthesis body (Fig. 2d); and, connection of elements of the artificial hip joint into a unity (Fig. 2e) [2].

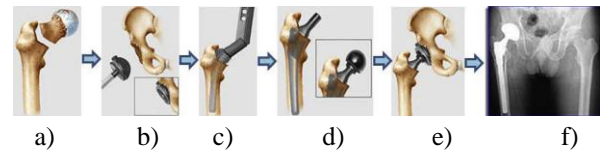


Fig. 2. Phases of the operative treatment of replacing the natural with the artificial hip joint [3]

The success of the operative treatment of replacing the natural hip joint with the artificial one is measured by the time period necessary for the recovery of the patient and the exploitation life of the prosthesis. The main factors influencing the success of the surgery are the operative procedure, the degree of adaptation of prosthesis elements to the patient, and its mechanical properties.

From the aspect of the development of the endoprosthesis, the most significant element of the artificial hip joint is the femoral stem. It provides the connection between the hip joint and the femur, and it overtakes the largest workload during the physical activities. In developing the endoprosthesis body, it is important to bear in mind that the femur is the mechanically most loaded bone in the human locomotion system.

The success of the installation of the hip joint endoprosthesis, as well as the exploitation life in the organism, depend on many factors, from which the most important one is the proper selection of the shape and the size of the endoprosthesis body. The most common method for the development of the endoprosthesis is the "methodology of the typization". Beginning with the stated methodology, the most

common method is the systematization of endoprosthesis according to the type (primary, revision...), the dimensions (usually up to 10 per type), and the mode of fixing into the femur (cement, cementless). The selection of prosthesis for a particular patient, from the offered set of prosthesis, is based on the following: the complexity of the disease, patient's age and femur dimensions.

In the recent year, the research in the area of biomedical engineering has been directed towards the development and manufacture of prosthesis according to the morphological characteristics of a patient (so-called custom-made endoprosthesis). This type of endoprosthesis, apart from femur dimensions and shape, maximally considers the type and the extent of the disease [4], as well as some other parameters. The objectives in the development of the hip joint endoprosthesis tailored for a specific patient are the maximum design speed providing minimal invasiveness in the operative treatment, short recovery period and long exploitation life of the implant. This can be achieved by using the computer technologies that enable the design, analysis and simulation of the product behaviour in all developmental stages. The custom-made development of the endoprosthesis body includes three group of activities [5] as follows:

- Data acquisition from diagnostic images and the reconstruction of the morphology of the affected elements of the skeletal system;
- Definition of a computer model for a hip endoprosthesis;
- Verification using the appropriate computer analysis;

The paper describes the activities in the development of the hip joint endoprosthesis tailored for a specific patient, as well as the tendency to develop each of these based on the contemporary research in the area.

2. DATA ACQUISITION AND FEMUR MORPHOLOGY RECONSTRUCTION

Determining the properties of the diseases in the elements of the human locomotion system largely depends on the sharpness and the quality of images used in diagnostics. Furthermore, for the development of endoprosthetic implant the significant role is attributed to the recording method, recording angle and device calibration. Hence, in the past years, there has been an intensive development of the methods based on the spatial images of the diseased limb (mainly by applying tomographic recording methods) [6], which generate digital copies of the desired cross-section of the subject. In medicine, and hence in the orthopaedics as well, the most commonly used are the computerized tomography (CT) and magnetic resonance imaging (MRI). Both methods allow the generation of a series of images showing the cross section of the diseased tissue (Fig. 3).

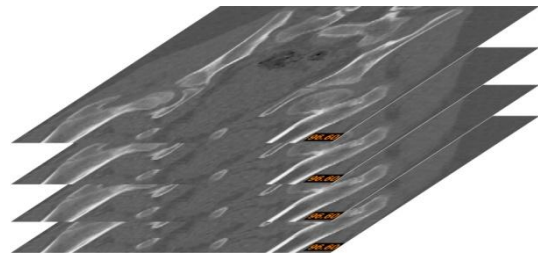


Fig. 3. CT image of the pelvis region

The application of the tomographic imaging in diagnostics enables the determination of the type and the extent of the disease, as well as the measuring of characteristic sizes of the diseased limbs [6]. This enables the possibility to define the geometric parameters of the femur [3]. In addition, the application of tomographic methods provides prerequisites for the formation of spatial computer models of the diseased limb in order to design the endoprosthesis, and in later phases, to simulate its behaviour in the exploitation conditions, as well as to simulate the surgical procedure. Modelling of the diseased femur, among others, is performed by applying specialized software systems for the reconstruction of tomographic images. This procedure consists of three following activities:

- Preparation activities;
- Manual or automated segmentation of the bone and tissue mass;
- Definition of output data in the form of a database containing the coordinates of the cloud of points or the creation of a volumetric model by introducing volume elements (voxels) between segmented image planes.

First, the preparation activity includes the processing of diagnostic images most commonly in the form of a series of image planes with the cross section of the recording object. It implies the correction of contrasts in order to segment the bone mass more easily, as well as the input into the software system for the reconstruction of the bone system morphology.

Tissue segmentation includes the identification of the image area belonging to relevant organs. This is one of the most significant steps in the reconstruction process based on the series of images, and the accuracy of the generated model highly depends on it [2]. Fig. 4. presents the diagnostic image and the segmentation of the femur bone tissue.

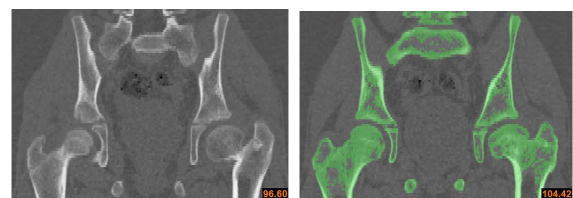


Fig. 4. Example of the hip segmentation on a diagnostic image

Further process in the organ reconstruction (in this case, femur and its medullary channel) includes the generation of the characteristic points which describe

the formation of a spatial femur model. A simpler form in the femur description is the cloud of characteristic points (Fig. 5) which is suitable for further processing [7] and the reconstruction of the areas in the CAD software systems (CATIA, PTC Creo, and the like).



Fig. 5. Cloud of points describing the femur

The model of the affected skeleton segment can also be obtained by replacing the elementary unit (pixel) images with spatial elements (voxels), realized in the specialized software system for the reconstruction of the tomographic images (ScanIP, Mimics, etc.). As a result, the volumetric model of the reconstructed femur is obtained (Fig. 6).



Fig. 6. Computer model of the femur

Both described procedures allow the generation of a computer model suitable both for defining the necessary parameters and for computer verification of the designed endoprosthesis body.

The reconstruction of the femur geometry implies the reconstruction of the outer and the internal geometry of the femur, i.e. medullary channel. Spatial model of the internal geometry of the femur, obtained by the reconstruction of the points of clouds, is presented in Fig. 7.



Fig. 7. Computer model of the medullary channel

3. DESIGN OF THE ENDOPROSTHESIS

Design of the endoprosthesis body tailored for a specific patient, from the application of tomographic image methods of the patient, is based on defining the following: characteristic cross sections of the endoprosthesis based on the adequate cross sections of the femur (Fig. 8a) and the properties of the medullary channel in it. The subsequent design phases for the endoprosthesis imply the formation of the geometric surface around the defined cross sections and hence the formation of the endoprosthesis body (Fig. 8b).

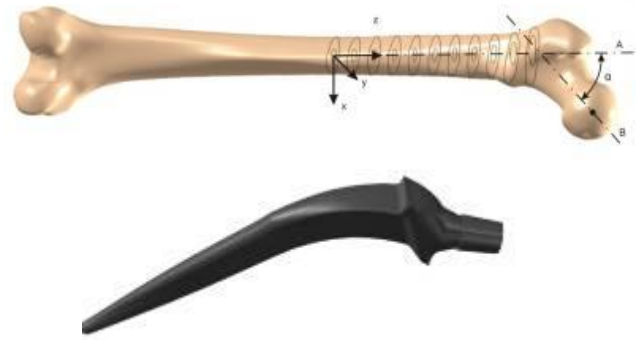


Fig. 8. Computer model of the femur (a) and the endoprosthesis body (b)

In order to minimize the period for designing the endoprosthesis body, there are two methods utilized for implementing the influential parameters (geometric, exploitation and operative) into the geometric form creating the computer model of the endoprosthesis body. Both methods, apart from including the existing ones, also allow for the introduction of new influential factors. These two methods are as follows:

- Method of parameter modelling, and
- Method for model definition by applying general mathematical laws (general mathematical models).

Parameter modelling is the most suitable method for creating computer models for a group of products with the similar geometry. In the case of the endoprosthesis body, it implies the typization of elements of its geometry, separate individual definitions of each element, and the definition of constraints. Geometry of the endoprosthesis body consists of a series of surface or volumetric shapes that determine the lower (distal), middle (medial) and upper (proximal) segment of the endoprosthesis. The method of parameter modelling, most common, apart from the generalized geometry defined by general sizes, also includes the application of a database containing the values of these sizes (Fig. 9).

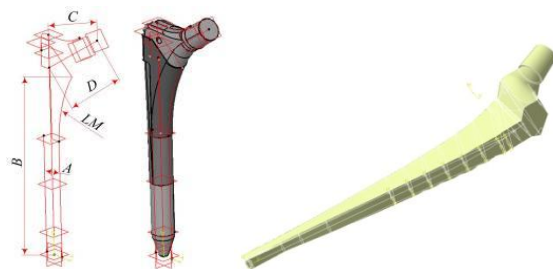


Fig. 9. Appearance of the parameter model [8,9]

The parameter modelling method is suitable for application in designing the body of the hip endoprosthesis when the Rtg method is used for diagnosing the disease. The application of the Rtg method can be used to define the limited number of geometric parameters of the femur. The advantage of this method is in the relatively simple automation of the geometric parameter input, since it is a plane imaging.

Drawbacks of this method include complexity and “rigid” structure of the model. That structure disables the introduction of new geometric parameters into the design process.

Second method, in which the geometry of the endoprosthesis body is described by applying spatial generated models, is based on the application of mathematical laws made from polynom expressions. This method is suitable to describe parts of complex geometric forms [10]. This general mathematical method for describing the endoprosthesis body, due to its generalized form, has several advantages in relation to parameter modelling. They primarily include the significantly more flexible procedure for describing the geometry that can be utilized for more types of endoprosthesis, and the final model form which contains the decreased number of geometric elements. The most commonly used are polynom and rational Bezier curves¹ and similar functions. Fig. 10. shows a segment of the general model of an endoprosthesis body for a hip joint developed by applying the rational Bezier function.

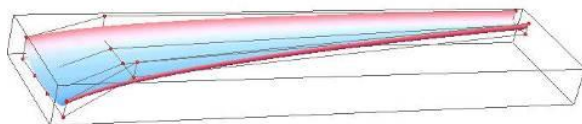


Fig. 10. Segment of a general model of an endoprosthesis body

4. VERIFICATION OF THE SOLUTION

The final phase in the development of the endoprosthesis according to the characteristics of a specific patient is the computer verification of the behaviour in exploitation conditions. Apart from defining the set of exploitation values, this is also an introduction into the optimization of the shape and the dimensions of the endoprosthesis.

Verification of the solution includes the evaluation of the endoprosthesis behaviour using the computer simulation in exploitation conditions by applying software systems for the computer model analysis with the finite element method [Heller, Weinans]. Considering the properties of tension and the conditions to which the endoprosthesis can be exposed under the transfer of the force from the leg to the pelvis and vice versa, it can be observed that the endoprosthesis and the artificial joint are exposed to constant workloads (static ones in standing and dynamic ones in motion). Behaviour analyses in static and dynamic conditions are used to evaluate the developed solutions, as well as to optimize geometric parameters of the endoprosthesis from the aspect of static, kinematic and dynamic properties. Regardless the software system that performs the verification of the endoprosthesis body and the type of analysis, the procedure itself includes the following: discretization of the developed model (Fig. 11), definitions of

workload, environmental conditions and constraints, and the calculations of forces and deviations in individual model nodes.

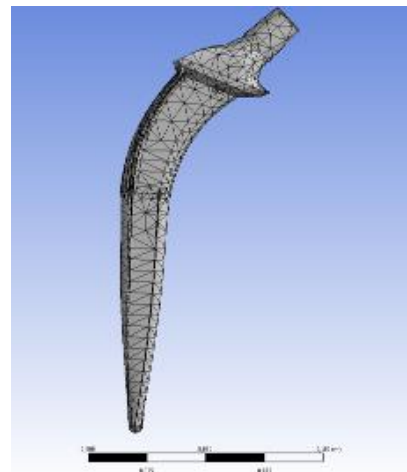


Fig. 11. Discretized model of the endoprosthesis body of the hip joint

The success in the simulation of the endoprosthesis behaviour depends on defining the forces and constraints which can be obtained by biomechanical analyses of the human locomotion system [11]. In doing so, the distal part of the prosthesis provides the positioning in medullary channel of the femur. In orthopaedic practice, the prosthesis body is placed in the femur so that the resultant force is acting at an angle of $\alpha=20^\circ$ to the vertical plane (Fig. 12a). However, the structure of the pelvis and the operative procedure as such (Fig. 12b) can, as a consequence, also have another angle of the action of the resultant force. In order to determine the relation between the angle of the force and the behaviour and the exploitation of the endoprosthesis body in the exploitation conditions, the analyses have been performed for diverse values of this angle. Fig. 12c. shows the force angle on the discretized model of the endoprosthesis.

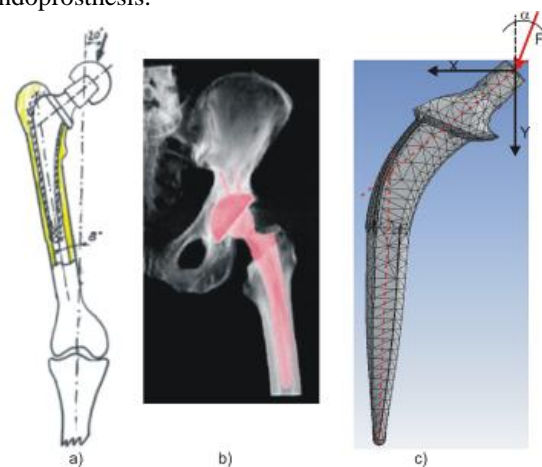


Fig. 12. Load on the endoprosthesis body of the femur: a) load angle; b) X-ray image of the implanted endoprosthesis; c) force angle on the discretized model in static analysis

¹ Bezier curves were developed by Pierre Bezier for the demands of the automobile factory Renaults at the beginning of 1960s [10].

4.1 Static analysis

For the analysis on the behaviour of the endoprosthesis body, in static conditions, apart from the load angle and the force intensity (4,000N), incarcerations should also be defined. Most commonly, they are defined as the fixation of a third of the height of the distal part. Fig. 13. shows graphic results, and Table 1 shows maximal values of the Van-Misses stresses depending on the load angle.

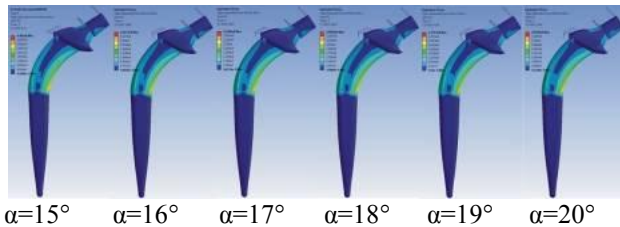


Fig. 13. Graphic presentation of the equivalent Van-Misses stresses

Load angle [α°]	Maximal equivalent Von-Misses stress σ_{ekv} [MPa]
15	449.5
16	431.7
17	413.8
18	395.8
19	377.7
20	359.4

Table 1. Maximal equivalent Van-Misses stresses

4.2 Analyses on the exploitation life of the endoprosthesis body

On the other hand, the main objective of implementing the endoprosthesis is the return of the function of the diseased organ for a longer period of time. Therefore, the development of the endoprosthesis for a specific patient must also include the analysis on the exploitation life in the organism. Based on the biomechanical researches, it has been concluded that the twenty-year-long life span of the endoprosthesis implies $N=2 \cdot 10^8$ cycles [12]. Table 2 presents the life span of the endoprosthesis and the minimal safety factor obtained for the model of total endoprosthesis for the hip joint tailored for a specific patient (in Fig. 14. it is presented within the reconstructed model of the femur).

[α°]	Min. safety factor	Life of failure $\times 10^8$ cycles
15	1.08	0.9
16	1.18	1.3
17	1.34	1.5
18	1.67	1.7
19	1.98	1.9
20	2.01	2.3

Table 2. Minimal safety factor and life of failure shown in cycles for different load angles



Fig. 14. Connection of endoprosthesis and femur

5. FINAL CONSIDERATIONS

Based on the analyses of papers in the field of designing endoprosthetic implants, acquisition of diagnostic images and biomechanics of the locomotion system, it can be concluded that the future of the endoprosthetics, among others, implies the development of endoprosthetic implants tailored for a specific patient. The reasons include a significantly longer exploitation life of the endoprosthesis designed for a specific patient, shorter post-operative recovery, less invasiveness of the operative procedure, etc.

Further research in the field of medical prosthetics follows the direction of lowering the costs of implants by shortening and partially automating the development of an endoprosthesis. Furthermore, new research is being performed in the direction of including a greater number of geometric and exploitation parameters used for defining the shape and the dimensions of an implant.

The procedure for developing an endoprosthesis body described in this paper contains a combination of three group activities (bone reconstruction based on tomographic images, endoprosthesis design and verification using the FEM methods) which are being developed independently. Hence, the directions of future researches can be observed through their individual development.

Geometric reconstruction of the femur (and other elements of the skeletal system), as well as the definitions of their geometric properties, present a series of standardized activities which can almost entirely be automated by applying adequate software technologies (as well as additional libraries of classes, such as VTK library) [13].

Defining the computer based model of the endoprosthesis based on the general mathematical models and the integration of methods for defining the characteristic parameters (position of individual anatomic surfaces on the femur) can also be automated to a larger degree. Hence, the designer is left with only the key decisions related to the character of the disease and the implementation procedure of the endoprosthesis.

Software systems for computer verification enable

the automation of the shape and mass optimization for the endoprosthesis by correcting the adequate parameters on a geometric model of the endoprosthesis prior to its production.

Further improvement and automation of individual designing phases can greatly shorten the time for the development and the production of an endoprosthesis tailored for a specific patient, which would be a justification for the high price for this type of implant.

6. REFERENCES

- [1] Callaghan, J., Rosenberg, A., Rubash, H.: *The adult hip*, Lippincott Williams & Wilkins, ISBN: 0-7817-5092-X, (2007)
- [2] Pawlikowski, M., Skalski, K., Haraburda, M.: *Process of hip joint prosthesis design including bone remodeling phenomenon*, Computers and Structures, Vol.: 81, Pages: 887–893, (2003)
- [3] Jun, Y., Kuiwoon, Ch.: *Design of patient-specific hip implants based on the 3D geometry of the human femur*, Advances in Engineering Software, ISSN: 0965-9978, Volume 41, Issue 4, Pages 537-547, (2010)
- [4] Grujic, J.: *Computer based modeling and experimental testing of hip prostheses*, (in Serbian), MSc thesis, Faculty of Technical Sciences, Novi Sad (2008)
- [5] Jun, Y: *Morphological analysis of the human knee joint for creating custom-made implant models*, Int J Adv Manuf Technol Vol. 52, Pages:841–853, DOI 10.1007/s00170-010-2785-1, (2011)
- [6] Miller, T.: *Imaging of hip arthroplasty*, European Journal of Radiology, ISSN: 0720-048X, DOI: 10.1016/j.ejrad.2011.03.103 (2011)
- [7] Wei, X., Fang, X., Zhang, Q., Zhou, D.: *3D Point Pattern Matching Based on Spatial Geometric Flexibility*, Computer Science and Information Systems, Volume 7, Issue 1, *Advances in Computer Animation and Digital Entertainment*, UDC 004.93, DOI: 10.2298/CSIS1001231W (2010)
- [8] Devedžić, G., Petrović, S., Ćuković, S., Ristić, B., Jovanović, Z., Ćirović, Z.: *Towards Digital Template For Artificial Hip Implants Selection*, 34th International Conference On Production Engineering, Niš, Serbia, pp.: 347-351, ISBN:978-86-6055-019-6 (2011)
- [9] Tabaković S., Živković A., Grujić J., Zeljković M.: *Using CAD/CAE software systems in the design process of modular, revision total hip endoprosthesis*, Academic Journal of Manufacturing Engineering – AJME, Editura Politehnica, Vol. 9, No. 2/2011, pp. 97-102, ISBN 1583-7904 (2011)
- [10] Farouki, R.: *The Bernstein polynomial basis: A centennial retrospective*, Computer Aided Geometric Design Vol. 29 pp.: 379–419, (2012)
- [11] Fraldi, M., Esposito, L., Perrella, G., Cutolo, A., Cowin, S.: *Topological optimization in hip prosthesis design*, Biomech Model Mechanobiol, ISSN: 1617-7959, Volume 9, Issue 4, Pages 389-402 (2010)
- [12] Tabaković S., Živković A., Grujić J., Zeljković M.: *Design process of modular, revision total hip endoprosthesis*, International Conference on Manufacturing Science and Education – MSE, University of Sibiu, pp. 395-398, ISBN 1843-2522, (2011)
- [13] Milojević, Z., Navalusić, S., Milankov, M., Obradović, R., Harhaji, V., Desnica, E.: *System for Femoral Tunnel Position Determination Based on X-ray*, HealthMED, ISSN 1840-2991, Vol. 5, No. 4, Pages 894-900, (2011)

Authors: Assist. Prof. Dr. Slobodan Tabaković, Prof. Dr. Milan Zeljković, MSc. Aleksandar Živković
 University of Novi Sad, Faculty of Technical Sciences,
 Department for Production Engineering, Trg Dositeja
 Obradovica 6, 21000 Novi Sad, Serbia, Phone.: +381
 21 485-2320.
 E-mail: tabak@uns.ac.rs
milanz@uns.ac.rs
acoz@uns.ac.rs

MSc. Jovan Grujić, Grujić & Grujić, Novi Sad, Serbia

ACKNOWLEDGMENTS

The work is part of a research project on "Modern approaches to the development of special bearings in mechanical engineering and medical prosthetics," TR 35025, supported by the Ministry of Education and Science, Republic of Serbia.

Trajanović, M., Tufegdžić, M., Arsić, S., Veselinović, M., Vitković, N.

REVERSE ENGINEERING OF THE HUMAN FIBULA

Abstract: Making personalized implants, scaffolds and fixators require the existence of high-quality 3D geometric models of the bones. This paper describes the process of reverse engineering of the human fibula, which is based on its anatomical landmarks and morphological properties. As an input into the process, the data obtained by computer tomography were converted into a polygonal model and stored in STL format. In the process of remodeling in CAD software package, referential anatomical landmarks of the upper and lower extremity of fibula and its mechanical axis were defined. By creating and merging sets of curves, surface models of the fibular extremities and body were formed. By their further merging, 3D surface model of the fibula was obtained. This model can be used in Computer Assisted Orthopedics (Surgery) as well as for creating a generic parametric model of the fibula.

Key words: reverse engineering, fibula, anatomical landmarks, 3D model

1. INTRODUCTION

In modern preclinical and clinical practice there are many situations when we need a good 3D geometric models of the bones. Computer Assisted Orthopedics is increasingly part of everyday orthopedic practice. Systems for planning and simulation of orthopedic treatment help orthopedists not only to completely plan the operation, but also to test different operative procedures, simulate implant placement or fixation, or to simulate the stress state of the fixator after its application. These systems work with geometric model(s) of the patient's bone(s). In addition, development of personalized (customized) implants or scaffold also requires presence of good models of the bones. Geometric models of bones can be created using data obtained by computed tomography or other scanning technology. Polygonal 3D models obtained by the processing of these data, relatively well approximate the shape and dimensions of the bones. These models are usually written in a simple STL format, which contains only details of the geometrical position of the vertex, the lists of the vertices that make individual triangles, and triangles perpendiculars.

However, the polygonal model has certain disadvantages. First of all, it is an approximate model since the continuous surface is represented by flat triangles. In addition, this model does not allow to create a link between the anatomical elements of the bone and geometric elements of the model, that is important when some knowledge of the bone had to be presented.

Stojkovic *et al.* in [1] presented a method of making 3D surface model of the femur, which is based on reference anatomical landmarks. In the paper of Veselinovic *et al.* [2], a similar method was used for the modeling of the tibia.

The paper presents a methodology to generate 3D surface model of the fibula, which includes: data acquisition, identification and selection of the anatomical-morphological landmarks needed to build

model¹, formatting of polygonal model when it is being done and the healing and smoothing of bone, separation of the main parts of fibula (proximal and distal epiphysis and the body) based on anatomical landmarks which morphologically define the fibula, creating sets of B-splines and creating a surface model.

2. ANATOMICAL LANDMARKS

Anatomical landmarks or anatomical reference parameters are a readily recognizable anatomic structure used as a point of reference in establishing the location of another structure or in determining certain measurements. Most of these anatomical landmarks, are palpable and recognizable by their geometry [3,4]. They have broad application in orthopedic surgery and are mainly used for the quantification of morphological parameters (eg distances, angles) and to define the coordinate systems of the joints. Anatomical landmarks can be applied at all stages of treatment of patients: diagnosis, preoperative planning, surgery and post-operative monitoring. The precise localization of anatomical landmarks on the bones in 3D CAD software packages is of the great importance for biomechanical studies, design and positioning of implants, intra-operative navigation, biomechanical studies of the joints, evaluation of deformity, resection of the tumor and production of models.

3. ANATOMICAL CHARACTERISTICS OF FIBULA

The fibula is a paired long bone placed on the lateral side of the leg connected above and below with tibia. The main parts of fibula are two extremities, proximal and distal and the body between them Fig. 1. [5]

The upper extremity (epiphysis proximalis) is composed of the head with the styloid apex and a flattened articular surface, directed upward for

¹ For a given bone is done only once.

articulation with a corresponding surface on the lateral condyle of the tibia.

The body or shaft (*corpus fibulae*) presents 3 borders, anterior, posterior and interosseus and 3 surfaces, lateral, medial and posterior, between them.

The lower extremity (*epiphysis distalis*) is lateral malleolus with smooth triangular articular surface which articulates with a corresponding malleolar surface on the lateral side of the talus, malleolar fossa and a malleolar groove.

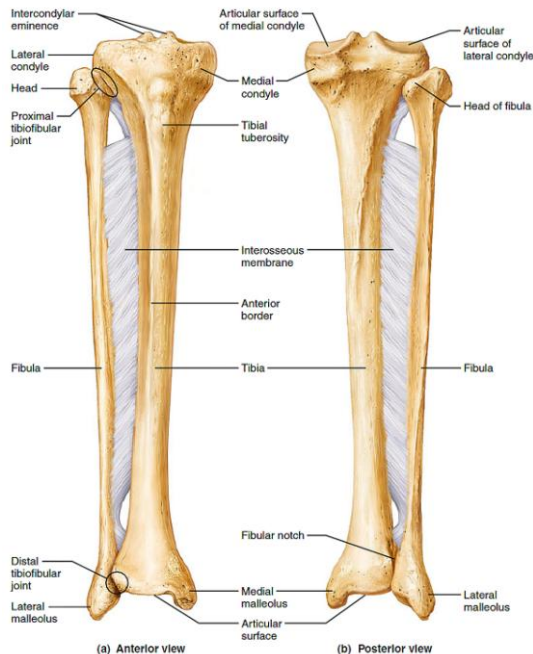


Fig. 1. The right tibia and fibula [6]

4. DATA ACQUISITION

In order to obtain the input data, i.e. cloud of points, for making the model CT (Computer Tomography - CT), MRI (Magnetic Resonance Imaging - MRI), optical microscopy, micro-CT, ultrasound, mammography and X-rays can be used [7,8].

In our study a CT scan of the fibula is used, separated from the CT slices, and performed in resolution of 0.5 mm. After segmentation and visualization, data is converted into a polygonal model, written in STL (STereoLitography) format, which is the basic structure for CAD modeling.

5. REVERSE MODELING OF THE 3D SURFACE MODEL OF FIBULA

Import of STL data into CAD system results in the generation of one or more cloud of points. In the next phases of remodeling, the geometric characteristics of higher order (curves and surfaces) are being designed, the specific Referential Geometric Entities (RGEs) that describe the anatomical landmarks are defined and 3D surface model of the fibula is created, according to the methodology previously described in [1,2], in the following order:

1. Formatting of polygonal model;

2. Determination of Referential Geometric Entities on the extremities;
3. Defining the mechanical axis of the bone;
4. Determination the Referential Geometric Entities and axis of the body of the fibula;
5. Creating curves on the upper and lower extremity of the fibula in a pre-defined planes;
6. Generation of 3D surface model of the fibula.

5.1 Formatting of polygonal model

Methodology of editing cloud of points and polygonal model creation, i.e. the development of the initial 3D model was conducted through: importing cloud of points (in stl format), cleaning and alignment, creating, cleaning and smoothing of polygonal model.

5.2 Determination of reference anatomical landmarks on the extremities of the fibula from the initial 3D model

After anatomy description of the bone, the procedures to identify and define anatomical landmarks (reference characteristics) are carried out. These characteristics are defined for a given bone only once, and are important for creating the anatomical axis and the anatomical planes. They should be chosen to approximate the bone in a separated segment in the best possible way.

At the upper extremity (*epiphysis proximalis* s. *extremitas proximalis*) the following elements are pointed out:

- **ACF** (*apex capitis fibulae*) - apex of the fibular head as the most prominent point, which can be palpated under the skin (shown at Fig. 2.);
- **FACF** (*facies articularis capitis fibulae*) - surface for articulation with the lateral condyle of tibia, shown at Fig. 2. Center of this surface is used to define the mechanical axis of the fibula.

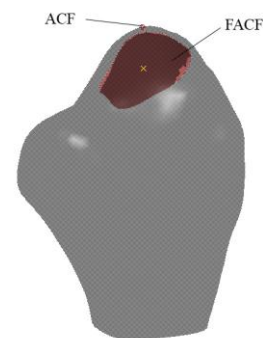


Fig. 2. Anatomic landmarks on the upper extremity of the fibula

At the lower extremity the following elements are defined:

- **FAML** (*facies articularis malleoli lateralis*) - surface for articulation with the talus faced medially. Center of this surface in our research is used to define the mechanical axis of the fibula. FAML can be approximated by a triangle whose apex is directed downward (Fig. 3.);
- **FOML** (*fossa malleoli lateralis*) - pitfall of the lateral malleolus, which is approximated with a part of

the sphere;

- **SML** (sulcus malleoli lateralis) - longitudinal groove as a passageway for the tendons of peroneal muscles;

- **AML** (apex malleoli lateralis) - top of the lateral malleolus, as the most distal point on the lateral malleolus.

FAML, **FOML**, **SML** i **AML** are presented at Fig. 3.

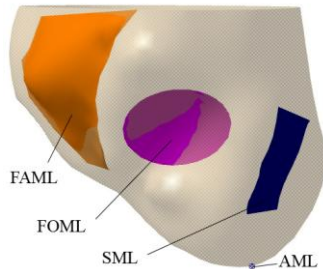


Fig. 3. Anatomic landmarks on the lower extremity of the fibula

5.3 Defining the mechanical axis of the fibula

The mechanical axis defines vertical orientation of the fibula in our approach to its reverse modeling. It is obtained by connecting the centers of the articular surfaces at the upper (FACF) and the lower extremity (FAML) of fibula. **A-P** (anterior-posterior) plane is defined by mechanical axis and ACF.

5.4 Determining the axis of the body of the fibula

In our research, 30 cross-sections perpendicular to A-P plane were created on the fibular body, thus obtaining 30 contour curves, with sets of points through which the interpolation B-splines are pulled. By processing of contour curves in the planes of intersection, we obtain interpolation set of curves from which a surface model of the body of the fibula is created (NURBS - Non-Uniform Rational Basis Spline model). Using method of GCM (Gravity Center Method) further described in [9], 3D spatial curve is obtained which represents the axis of the body of the fibula, shown in Fig. 4. This axis approximates the propagation of the fibular body volume.

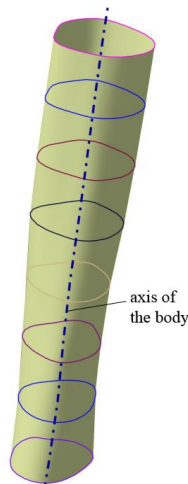


Fig. 4. The axis of the body of the fibula

The axis of the fibular body and mechanical axis of the fibula, including the axis which connects the proximal (ACF) and distal point (AML), which will be used as a rotation axis to create 3D surface model of the distal extremity, are shown at Fig. 5.

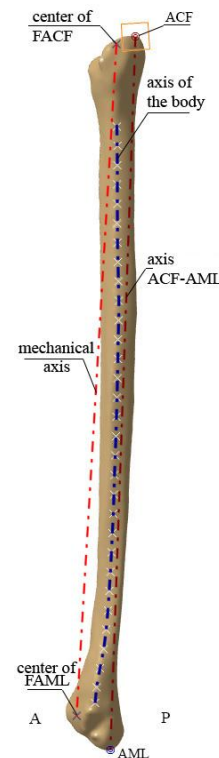


Fig. 5. Axis of the fibula

5.5 Creating curves on the upper and lower extremity of the fibula in a pre-defined planes

In the intersections of polygonal model of the upper extremity of the fibula with the plane that passes through the mechanical axis of the bone and AML, and planes at certain angles to this plane (10° , 20° , 30° , 45° , 60° , 75° , 90° , ...), where the axis of rotation is the mechanical axis, a set of curves is obtained. These curves were used for creating of surface model of a given extremity of the fibula (Fig. 6.). The common point of obtained curves is in the center of the articular surface on the head of the fibula (**FACF**). The loft function is used for creating a surface model of the upper extremity.



Fig. 6. The curves on the upper extremity of the fibula

To generate the curves on the lower extremity of the fibula, as reference plane we take the plane which passes through mechanical axis and AML, as long as the axis of rotation for set of predefined planes is used

the axis which connects (ACF) on the upper extremity with the lowest point on the lateral malleolus (AML) at the lower extremity of the fibula. The obtained set of curves has a unique common point corresponding to the lowest point of the lateral malleolus (AML) (Fig. 7). To create a surface model of lower extremity with the afore mentioned set of curves loft function was used.

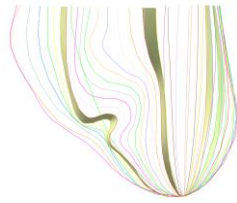


Fig. 7. The curves on the lower extremity of the fibula

5.6 Generation of 3D surface models of the fibula

By merging surface model of the body of the fibula with surface models of its upper and distal extremity (with merging distance of 0.001mm), a 3D surface model of the fibula is built. Anterior and posterior view of this model is shown at Fig. 8.

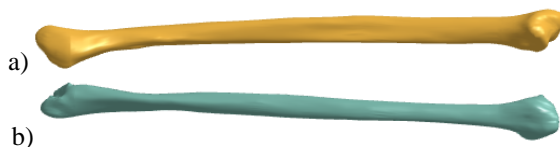


Fig. 8. 3D surface model: a) anterior view; b) posterior view

6. CONCLUSION

The method of reverse engineering can be applied in procedure of defining of anatomical landmarks and creating 3D surface models of the fibula from data obtained from CT. However, the manual modeling process requires considerable time and effort. Improvements can be made in the part of generating of the intersection planes with upper and lower extremity of the fibula in terms of optimization of angles of rotation relative to the selected reference plane and the axis of rotation, in order to provide more accurate approximation of the initial 3D model. For the automatic identification of anatomical landmarks some of existing algorithms should be applied.

The results obtained in this study can be considered as preliminary, but they present the basis for future studies of geometric shape (model) and anatomical characteristics of the fibula, as well as for the formation of a generic parametric model using CAD software package. The obtained model can be used for prototyping of same missing pathologically altered bony parts (after tumor resection) and also for the virtual planning of some other procedures in reconstructive bone microsurgery.

7. ACKNOWLEDGMENT

This paper is part of project III41017 Virtual human osteoarticular system and its application in preclinical

and clinical practice, funded by the Ministry of Education and Science of Republic of Serbia, for the period of 2011-2014.

8. REFERENCES

- [1] Stojkovic, M., Trajanovic, M., Vitkovic, N., Milovanovic, J., *Referential Geometrical Entities for Reverse Modeling of Geometry of Femur*, icit2.vip2009.pdf
- [2] Veselinovic, M., Stevanovic, D., Trajanovic, M., Manic, M., Arsic, S., Trifunovic, M., Misic, D., *Method for Creating 3D Surface Model of the Human Tibia*, 34th International Conference on Production Engineering, Niš, Serbia, 2011
- [3] Starly, B., Fang, Z., Sun, W., Shokoufanadeh, A., and Regli, W., *Three-Dimensional Reconstruction for Medical-CAD Modeling*, Computer-Aided Design & Applications, Vol. 2, Nos. 1-4, p.p. 431-438, 2005
- [4] S.Van Cauter, M. De Beule, A. Van haver, P. Verdonk Verheghe, B., *Automated extraction of the femoral anatomical axis for determining the intramedullary rod parameters in total knee arthroplasty*, International Journal for Numerical methods in biomedical engineering, 28:158-169, Published online 14 November 2011 in Wiley Online Library (wileyonlinelibrary.com).
- [5] Williams P. L., *Gray's anatomy*, thirty eight edition, New York, 1995
- [6] Marieb N. E., Wilhelm B. P., Mallatt J., *Human Anatomy*, Sixth Edition Media Update, 2010 Pearson education, Inc., San Francisco, Copyright © 2012
- [7] Subburaj, K., Ravi, B., Agarwal, M., *Automated identification of anatomic landmarks on 3D bone models reconstructed from CT scan images*, Computer medical imaging and graphics 33, p.p. 359-368, 2009
- [8] Chelule, K.L., Dr. Coole, T., Cheshire, D.G., *Fabrication of Medical Models from Scan Data via Rapid Prototyping Techniques*, http://www.deskartes.com/news/fabrication_of_medical_models_fr.htm, Copyright 1996-2008 DeskArtes Oy.
- [9] Vitković, N., Milovanović, J., Trajanović, M., Korunović, N., Stojković, M., Manić, M., *Methods for creating geometrical model of femur anatomical axis*, 34th International Conference on Production Engineering, Niš, Serbia, 2011.

Authors: Prof. Dr. Miroslav Trajanović, M.Sc. Milica Tufegdžić, Prof. Dr. Stojanka Arsić*, M.Sc. Marko Veselinović, M.Sc. Nikola Vitković, University of Nis, Faculty of Mechanical Engineering, Aleksandra Medvedeva 14, 18000 Nis, Serbia, *University of Nis, Faculty of Medicine, Blvd. Dr Zorana Djindjica 81, 18000 Nis, Serbia.
E-mail: miroslav.trajanovic@masfak.ni.ac.rs
miltufegdzc@gmail.com
stojanka@medfak.ni.ac.rs
marko.veselinovic@masfak.ni.ac.rs
vitko@masfak.ni.ac.rs

Uzelac, M., Vilimonović, M.

BASIC PRINCIPLES OF THE USE OF CONE BEAM CT DEVICE IN RADIOLOGY OF A PATIENT'S CRANIOFACIAL REGION

Abstract: Cone Beam CT represents the greatest technical innovation in everyday dental practice in the past decade. Reliable and functional 3D radiological views make it easier and widen the span of clinical indications in everyday use. The possibility of integration and interaction with the state-of-the-art technical devices is opening new perspectives for oral implantology, reconstructive maxillofacial surgery, and research projects.

Keywords: Cone Beam CT, Computed Tomography, 3D, Radiology

1. INTRODUCTION

Cone Beam computed tomography (CBCT) was first introduced thirteen years ago as a new concept of diagnostic radiology. A few years ago, with the increasing availability of the devices that make this kind of diagnostic possible, with the upgrade of the devices technical characteristics and accompanying software support, this technique became the golden standard among the diagnostic methods of the craniofacial region in dentistry as well as in otorhinolaryngology. The concept development is based on the construction of simpler, i.e. cheaper, devices that can generate 3D dataset delivering the lower amount of X-ray radiation to the patient, followed by the increasing availability of the technology. Compared to the „classical“ computed tomography techniques that use multiple or extended X-ray exposure of the patient, the technical concept of the CBCT device during one circular cone beam X-ray exposure provides a radiological dataset. Using the specific mathematical algorithms the radiological dataset is processed and the 3D view of the region of interest is reconstructed. The full capacity of this technology is reached in oral surgery where the main field of work are the changes in the high contract tissues, like mandibular bones and teeth, together with high spatial precision of the reconstructed 3D view.

Even though this technology has been present on our market for the last three years, the number of the general dental population, as well as the population specialising in some kind of surgery in the facial region, familiar with this technique, is surprisingly low. Considering that this diagnostic concept uses X-rays, it is necessary to have guidelines that define indications and use according to the technical possibilities of the concept. Developed countries (Germany, France, UK...) have already recognised this need and have developed national guidelines on CBCT use. However, the large number of health systems does not have the capacities for the development of such guidelines. The purpose of this work is to present the consolidated guidelines for the CBCT use in dentistry, developed under the European SEDENTEXCT project/panel, with the special focus on the sections that are closely related

to oral surgery. The main idea of the Panel was to review all available professional and scientific literature in order to develop evidence based guidelines and good clinical practice guidelines. The conclusions reached during the Panel were merged together and formulated in March 2011.

Even though the technical characteristics of the technology are not the purpose of this work, it is necessary to define the basic characteristics of the radiological dataset generated with the CBCT technology.

2. BASIC PRINCIPLES OF 3D CONE BEAM IMAGING

What is *Cone Beam* Imaging? It is a diagnostic procedure of acquisition of craniofacial region radiological images, obtained from the projection images on the X-Ray unit and their visualisation on the workstation – PC. The process of obtaining the rendered view of the acquired radiological images is done using computed tomography (CT) i.e. primary reconstruction of executed projections – raw images, using specialised mathematical algorithms and its visualisation on the workstations – PC (secondary acquisition).

2.1 Acquisition of radiological images

By measuring the total X-ray attenuation coefficient in all directions in the plane, i.e. finding the attenuation coefficient at each point, we can calculate the structure of an object (Fig. 1).

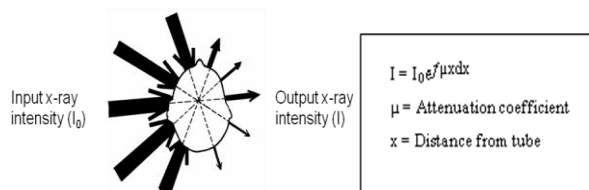


Fig. 1. Principle of computed tomography

There are several technological solutions, i.e. radiological devices, for the needs of acquisition of radiological images using computed tomography: *Fan Beam CT* (traditional medical method, linear detector); *Multirow –Detector CT* (320 parallel lines max); *Cone Beam CT* (new method for craniofacial region *CMOS Flat Panel* or *Image Intensifier* detector).

In *Cone Beam CT* system the constitutive unit of the image is so-called isotropic cube-shaped voxel (hence the name *Cone Beam*; it comes from the input cube-shaped X-ray that falls on the detector). The size of the field of view that can be visualised, i.e. the size of the region that can be scanned in one scanning procedure, depends on the size of the detector (active surface for the acquisition of the input X-ray beam).

As we have already mentioned, there are two types of detectors. In actual use, *CMOS Flat Panel* detector turned up to be a better solution (highest resolution images, no geometric distortion, shorter data acquisition process, etc.).

2.2 Image Reconstruction

The aim of the CT reconstruction is to find the correct distribution of the attenuation values of 2D cross-sections (each 3D image is made of 200-300 two dimensional cross-sections, i.e. the detector primary acquisition is a two dimensional cross-section of the pulsed input X-ray beam), knowing the attenuation sums in all directions. The principle of tomographic calculation is volume (entire area of input radiation) separation into constitutive units – voxels and definition of attenuation value in each voxel.

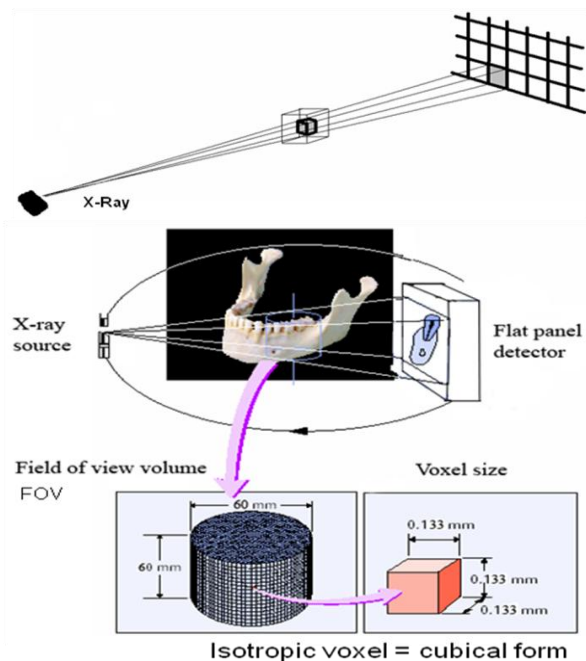


Fig. 2. CT image reconstruction

2.3 Image Visualisation

Image visualisation on a workstation is done by the multiplanar reconstruction, i.e. multiplanar view. The main views of a radiological image are the following: sagittal, coronal, axial and custom angulation. The corresponding imaging software also provides a 3D

rendered view of the scanned region.

The region of interest (ROI) shown on the software can be the entire exposed region of a patient or just one part of ROI.

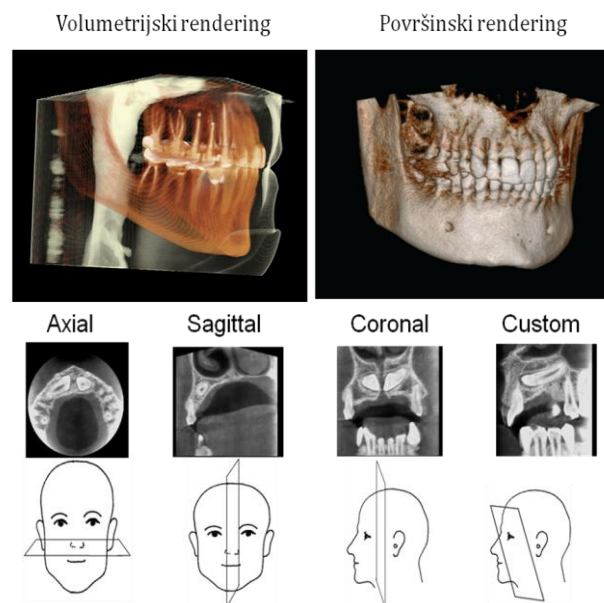


Fig. 3. CT image visualization

3. CBCT IMAGING GENERAL GUIDELINES

When using CBCT, the necessary radiation delivered to a patient is optimised, according to the ALARA principle (as low as reasonable achievable) where the patient receives the lowest dose possible to get the correct diagnostic radiology.

The document is established under SEDENTEXCT project and it represents a systematic review of currently available professional and scientific literature that deals with the use of CBCT technology in dental and maxillofacial radiology. It takes into account the analysis of doses and risks, basic principles of radiology, justification and referral criteria, device characteristics that affect the radiation optimisation, establishment and verification of radiological technique standards, safety measures for the clinical staff performing diagnostic procedures, economic assessment of the use of the technology, establishment of the educational level needed for conducting radiological procedures. The special conclusions of the Panel were formulated as general and special recommendations for the use of CBCT devices. Considering the volume of the entire document, we will only present one part of the guidelines that are necessary for the correct diagnostic radiology in the field of oral surgery.

The authors point out that the guidelines should be re-examined in five years time and that new guidelines should be established on a scientific level, taking into account the development of the technology and its scientific verification.

The first group of selected general rules can be generally related to all radiology techniques, but is especially important when it comes to the use of the techniques that generate 3D dataset, CBCT and MSCT:

- CBCT examinations must not be performed without previous clinical examination of the patient and anamnestic data collection.
- CBCT examinations must always undergo a justification process in order to determine if the potential diagnostic benefit outweighs the risk of X-ray exposure.
- CBCT examinations should potentially bring new information in order to improve patient's management.
- CBCT examinations should not be performed in a routine manner or as a screening test, i.e. without estimating the patient benefit-risk ratio.
- CBCT examinations should only be used in cases when the diagnostic question can't be answered by conventional techniques (that expose patients to the lower doses of radiation).

The other group of selected general rules relates to the formulation of diagnostic requests according to the CBCT device technical characteristics, i.e. the dataset generated by its use:

- When performing the CBCT examinations, the analysis and the diagnostic report of the entire 3D dataset is necessary.
- When an evaluation of a soft tissue is required, the use of MR or MSCT is recommended.
- CBCT devices should offer a possibility to choose the size of 3D dataset and examinations must use the smallest size that is compatible with the clinical situation in order to minimise the radiation exposure of the patient.
- CBCT devices should offer a possibility to choose the resolution of 3D dataset and examinations must use the smallest resolution and the lowest dose that can provide adequate diagnostics.
- Analysis of CBCT 3D dataset of the teeth, their supporting structures, the mandible and maxilla, up to the floor of the nose including the maxillary sinus cavities should be performed by dento-maxillo-facial radiologist or, when it is not possible, a trained dental practitioner from the adequate field of dentistry.

The second group of the general rules is especially important because it brings out the importance of the analysis of the entire radiographic region, use of all computer tools in order to improve the radiological analysis, possibility to choose the image and the resolution size, impossibility to diagnose qualitative changes in soft tissues, need for change of perspective when it comes to 3D imaging versus classical radiography (extracting the layers of interest), as well as the importance of continuous education regarding new technologies. Unjustified expansion of the examined field or augmentation of resolution during radiography, conducting CBCT diagnostics with the aim of monitoring the soft tissue changes, doubles or triples the effective doses received by a patient without the improvement of the diagnostic results.

The third group of the general rules relates to the establishment of the quality system in CBCT

radiography, quality control, but basically it represents the job of the competent institutions that are specifically dealing with this field of radiology.

3.1 Special Guidelines

The special guidelines were established on the basis of the researches conducted against specific clinical tasks or set of tasks and they define the justification of the diagnostic choice, the guidelines for resolution and field size selection.

4. DISCUSSION

The Panel conclusions provide important and necessary information in formulation of the diagnostic algorithms in dentistry. However, beside the basic radiological capacities of the technique, the special advantages are acquired through software solutions that allow full use of the 3D dataset. Even though they don't promote any manufacturer, the Panel conclusions provide guidelines in choosing adequate characteristics and concepts depending on diagnostic needs.

It is also important to point out some of the useful software solutions, as unlimited choice of tomographic cross-sections, the possibility of graphic marking of the neural pathway and 3D reconstruction. Definitely, the most useful is the possibility of graphic marking of the neural pathway that is realised by choosing the finest layer provided by the radiographic technique and marking the pathway in the orthogonal projection when the „ceiling" and the „floor" of the neural pathway can be identified with absolute certainty. Computer synthesis of the marked dataset provides reliable localisation of the pathways either in 2D projection or in 3D reconstructed dataset. The possibility of sensitivity modification of the 3D reconstructed dataset in the region where high X-ray contrast structures are being analysed, allows the possibility of acquiring spatial orientation of all anatomic details of interest.

The education for the use of most conventional radiological techniques is qualitatively covered through undergraduate studies or different kinds of graduate programs. The main characteristics of this diagnostic concept are only to become the part of our general or continuous education program. In our country, at the moment, we have only informal workshops available where one can get acquainted only with the necessary information. We hope that our university centres will soon be able to offer the same possibilities.

5. REFERENCES

- [1] Al-Ekrish AA, Ekram M. *A comparative study of the accuracy and reliability of multidetector computed tomography and cone beam computed tomography in the assessment of dental implant site dimensions.* Dentomaxillofac Radiol. 2011 Feb;40(2):67-75.
- [2] Algerban A, Jacobs R, Fieuws S, Willems G. *Comparison of two cone beam computed tomographic systems versus panoramic imaging for localization of impacted maxillary canines and detection of root resorption.* Eur J Orthod. 2011 Feb;33(1):93-102.

- [3] Alqerban A, Jacobs R, Lambrechts P, Loozen G, Willems G. *Root resorption of the maxillary lateral incisor caused by impacted canine: a literature review*. Ciin Oral Investig. 2009 Sep;13(3):247-55. Epub 2009 Mar 11. Review.
- [4] Alqerban A, Jacobs R, Souza PC, Willems G. *In-vitro comparison of 2 cone-beam computed tomography systems and panoramic imaging for detecting simulated canine impaction-induced external root resorption in maxillary lateral incisors*. Am J Orthod Dentofacial Orthop. 2009 Dec;136(6):764.e1-11; discussion 764-5.
- [5] Arisan V, Karabuda ZC, Ozdemir T. *Accuracy of two stereolithographic guide systems for computer-aided implant placement: a computed tomography-based clinical comparative study*. J Periodontol. 2010 Jan;81(1):43-51.
- [6] Botticelli S, Verna C, Cattaneo PM, Heidmann J, Mel-sen B. *Two- versus three-dimensional imaging in subjects with unerupted maxillary canines*. Eur J Orthod. 2011 Aug;33(4):344-9. Epub 2010 Dec 3.
- [7] Cotton TP, Geisler TM, Holden DT, Schwartz SA, Schindler WG. *Endodontic applications of cone-beam volumetric tomography*. J Endod. 2007; 33: 1121-1132
- [8] Haiter-Neto F, Wenzel A, Gotfredsen E. *Diagnostic accuracy of cone beam computed tomography scans compared with intraoral image modalities for detection of caries lesions*. Dentomaxillofac Radiol. 2008 Jan;37(1):18-22.
- [9] Haney E, Gansky SA, Lee JS, Johnson E, Maki K, Miller AJ. *Comparative analysis of traditional radiographs and cone-beam computed tomography volumetric images in diagnosis and treatment planning of maxillary impacted canines*. Am J Orthod Dentofacial Orthop 2010; 137:590-597
- [10] Hassan B, Metska ME, Ozok AR, van der Stelt P, We-sse-link PR. *Comparison of five cone beam computed tomography systems for the detection of vertical root fractures*. J Endod. 2010 Jan;36(1):126-9.
- [11] Hassan B, Metska ME, Ozok AR, van der Stelt P, We-sse-link PR. *Detection of vertical root fractures in endodontically treated teeth by a cone beam computed tomography scan*. J Endod. 2009 May;35(5):719-22.
- [12] Hohlweg-Majert B, Pautke C, Deppe H, Metzger MC, Wagner K, Schulze D. *Qualitative and Quantitative Evaluation of Bony Structures Based on DICOM Data-set*. J Oral Maxillofac Surg. 2011 Jun 22.
- [13] Honda K, Björnland T. *Image-guided puncture technique for the superior temporomandibular joint space: value of cone beam computed tomography (CBCT)*. Oral Surg Oral Med Oral Pathol Oral Radiol Endod. 2006 Sep;102(3):281-6.
- [14] Honda K, Larheim TA, Maruhashi K, Matsumoto K, Iwai K. *Osseous abnormalities of the mandibular condyle: diagnostic reliability of cone beam computed tomography compared with helical computed tomography based on an autopsy material*. Dentomaxillofac Radiol. 2006 May;35(3):152-7.
- [15] Honda K, Matumoto K, Kashima M, Takano Y, Kawas-hima S, Arai Y. *Single air contrast arthrography for temporomandibular joint disorder using limited cone beam computed tomography for dental use*. Dentomaxillofac Radiol. 2004 Jul;33(4):271-3.
- [16] Honey OB, Scarfe WC, Hilgers MJ, Klueber K, Silveira AM, Haskell BS, Farman AG. *Accuracy of cone-beam computed tomography imaging of the temporomandibular joint: comparisons with panoramic radiology and linear tomography*. Am J Orthod Dentofacial Orthop. 2007 Oct;132(4):429-38.
- [17] Katheria BC, Kau CH, Tate R, Chen JW, English J, Bo-uquot J. *Effectiveness of impacted supernumerary tooth diagnosis from traditional radiography versus cone beam computed tomography*. Pediatr Dent. 2010; 32: 304-309
- [18] Loubele M, Guerrero ME, Jacobs R, Suetens P, van Steenberghe D. *A comparison of jaw dimensional and quality assessments of bone characteristics with cone-beam CT, spiral tomography, and multi-slice spiral CT*. Int J Oral Maxillofac Implants. 2007 May-Jun;22(3):446-54.
- [19] Melo SL, Bortoluzzi EA, Abreu M Jr, Correa LR, Correa M. *Diagnostic ability of a cone-beam computed tomography scan to assess longitudinal root fractures in prosthetically treated teeth*. J Endod. 2010 Nov;36(11):1879-82.
- [20] Naitoh M, Nakahara K, Suenaga Y, Gotoh K, Kondo S, Ariji E. *Comparison between cone-beam and multislice computed tomography depicting mandibular neurovascular canal structures*. Oral Surg Oral Med Oral Pathol Oral Radiol Endod. 2010 Jan;109(1):e25-31.
- [21] Nakata K, Nalyoh M, Izumi M, Inamoto K, Ariji E, Na-kamura H. *Effectiveness of dental computed tomography in diagnostic imaging of periradicular lesion of each root of multirooted tooth: a case report*. J Endod 2006; 32: 583-587
- [22] Young SM, Lee JT, Hodges RJ, Chang TL, Elashoff DA, White SC. *A comparative study of high-resolution cone beam computed tomography and charge-coupled device sensors for detecting caries*. Dentomaxillofac Radiol. 2009 Oct;38(7):445-51.
- [23] A.C. Miracle and S.K. Mukherji, *Conebeam CT of the Head and Neck, Part 1: Physical Principles*, AJNR Am. J. Neuroradiol., Jun 2009; 30: 1088 - 1095

Authors: Milan Uzelac, dr.med., Milan Vilimonovic,
 Tim Co., Jovana Rajića 5c, 11000 Beograd, Serbia,
 Phone: +381112836786, Fax: +381112833342
 E-mail: milan@timco.rs

Vilotić, M., Lainović, T., Kakaš, D., Blažić, L., Marković, D., Ivanišević, A.

ROUGHNESS ANALYSIS OF DENTAL RESIN-BASED NANOCOMPOSITES

Abstract: The most widely used biomaterials for tooth reconstruction are the resin-based composites. These restorative materials consist of organic resin phase, inorganic filler particles and silane- the filler-resin interface. Contemporary composites are filled with nanoparticles, which are expected to improve materials properties. The aim of this study was to determine surface roughness of polished dental resin-based composites using atomic force microscopy analysis. Comparison of surface roughness parameters in the two directions was done (along and perpendicular to grinding tracks) among three different dental resin-based composites, each representative for its material group (nanofilled, microfilled, and microhybrid composites).

Key words: surface roughness, AFM, grinding tracks, resin-based nanocomposites, dental finishing and polishing procedure

1. INTRODUCTION

The task of the modern restorative dentistry is to repair the damaged tooth structure, and to rehabilitate the patients' oral health, as well as the function and natural esthetics of the teeth. After adequate cavity preparation and pre-treatment, damaged tooth structure needs to be reconstructed with chosen artificial restorative material [1].

Resin-based composites (RBCs) are the most commonly used biomaterials in contemporary dental practice [2]. RBCs are tooth-colored, highly aesthetic restorative materials, which consist of three different phases: organic resin matrix, inorganic filler particles and silane- the filler-resin interface [3]. The main resins of the organic phase are: bisglycidyl dimethacrylate (Bis GMA) or urethane dimethacrylate (UDMA), and some other resins added for the viscosity correction, such as triethylene glycol dimethacrylate (TEGDMA) [1]. These are photo-polymerizable monomers that convert to the cross-linked polymers upon exposure to visible light, which activates photo-initiators incorporated in the single-paste material. Inorganic filler particles consist of silica in the form of quartz, or silicates of various types [1]. Fillers in composites have multiple roles: to reduce polymerization shrinkage, the coefficient of thermal expansion and water sorption and solubility; to mechanically reinforce the material; to improve optical and aesthetic characteristics of the material; to enable better initial polishing and polish retention, and to reduce wear during the masticatory forces [4, 5, 6, 7, 8, 9]. Formulation of filler particles, have been passed from macro-, micro-, down to the nano-particles [10] (fig. 1). Microhybrid composites, so-called universal restorative composites, are composed of filler particles of different sizes (15-20 μm and 0,01-0,05 μm) and have good mechanical properties for use in the lateral occlusal region, but relatively poor aesthetic qualities, to be used in the esthetic zone [11]. Microfilled composites have been developed in order to obtain high-quality aesthetic materials that meet the needs of restorative dentistry in

the esthetic zone. Microfilled composites have average particle size in range of 0,01-0,05 μm .

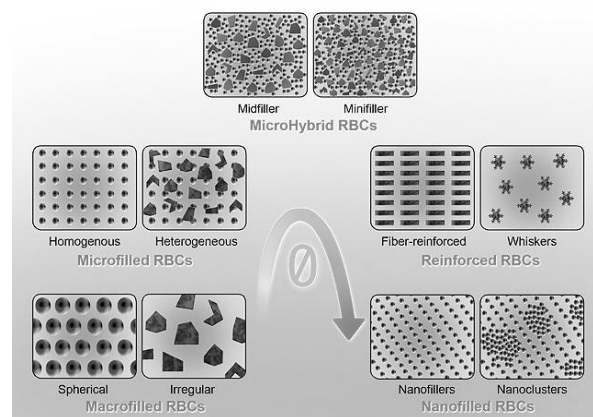


Fig. 1. Diagrammatic summarization of development of filler particles in resin-based composites (RBCs) [12]

Due to the relative poor mechanical strength, these materials are indicated for use in low-stress oral regions [11]. Trying to create a material that meets both of these properties, the mechanical resistance and the aesthetic and polishing qualities, nanofillers have been developed [8].

Finishing and polishing procedures are necessary clinical steps to establish a proper reconstruction of dental crowns and to restore anatomical and morphological form of the tooth [13].

The aim of this study was to determine surface roughness of polished contemporary dental RBCs using atomic force microscopy analysis.

2. MATERIALS AND METHODS

Three representative dental resin-based composites were tested in the study: nanofilled (Filtek Ultimate Translucent), microfilled (GC Gradia Direct Anterior) and microhybrid (Filtek Z250). Detailed information about materials used in the study is shown in the tables

1, 2 and 3.

One specimen of each material was made by using cylindrical plastic molds (4 mm diameter x 2 mm depth). Plastic molds were placed on the glass microscope slide, filled with material and covered with a polyester strip and a glass slide, taking care to obtain a flat surface without any defects and entrapped air. Material was then polymerized for 40 sec. with a SmartLite® IQTM 2 LED unit (Dentsply Caulk). After removing glass plate and polyester strip from the top of the samples, they were polished with multi-step polishing system- Super Snap (Shofu, Inc. Kyoto, Japan).

Name: Filtek Ultimate Translucent
Manufacturer: 3M ESPE, St. Paul, MN, USA
Classification: Nanofilled
Lot no: N225533
Shade: Clear shade
Matrix: Bis-GMA, UDMA, Bis-EMA, TEGMA and PEGDMA
Fillers: non- agglomerated/non-aggregated 20 nm silica filler, non- agglomerated/non-aggregated 4-11 nm zirconia filler, and aggregated zirconia/silica cluster filler (average cluster particle size – 0,6-20 µm)
Filler loading: 72,5 wt%, 55,6 vol%

Table 1. Details of Filtek Ultimate Translucent tested in the study

Name: GC Gradia Direct Anterior
Manufacturer: GC Dental Products Corporation, Tokyo, Japan
Classification: Microfilled (Micro-fine hybrid)
Lot no: 1106011
Shade: A2
Matrix: UDMA, dimethacrylate co-monomers, -II-
Fillers: Silica, 850 nm (0,85 µm) and prepolymerized filler
Filler loading: 73wt% 64-65 vol% (silica- 38 wt%, 22 vol%; prepolymerized filler- 35 wt%, 42 vol%)

Table 2. Details of GC Gradia Direct Anterior tested in the study

Name: Filtek Z250
Manufacturer: 3M ESPE, St. Paul, MN, USA
Classification: Microhybrid
Lot no: N367949
Shade: A2
Matrix: Bis-GMA, UDMA, Bis-EMA, TEGMA
Fillers: Zirconia, silica 10 – 3500 nm (0,01-3,5 µm)
Filler loading: 75-85 wt%, 60 vol%

Table 3. Details of Filtek Z250 tested in the study

During the polishing procedure, each abrasive disk was used only once for each material, in the dry condition, for 1 minute, using handpiece rotating 10000 revolutions per minute (recommended speed by manufacturer). Four different abrasive disks were used during polishing procedure: black (coarse), violet (medium), green (fine) and red (extra-fine). One single operator did all of the polishing treatments, trying to simulate clinical finishing and polishing procedure. Two mutually perpendicular grinding directions were used during polishing procedure (Fig. 2).

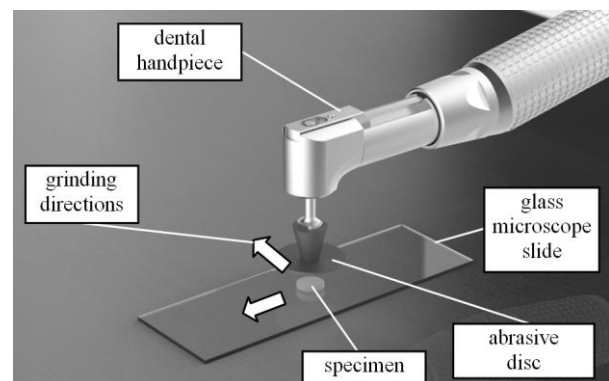


Fig. 2. Grinding setup and grinding directions

Immediately after the polishing treatment, topography of each specimen was examined by Veeco di CP-II Atomic Force Microscope. Specimen's surface has been scanned at points which lie at half distance between specimen's center and perimeter in contact mode with CONT20A-CP tips. 1 Hz scan rate and 256 × 256 resolution were used to obtain topography on a 90 µm × 90 µm scanning area. Before the scanning, specimen's surface has been blown through with cold air by hairdryer. Cleaning specimen's surface with alcohol created damaged surface.

Once AFM images were obtained, surface roughness analysis was carried out on each AFM image, beginning by identifying the grinding tracks. After that, three analyzing lines along and three analyzing lines perpendicular to the grinding tracks were set on each AFM image, so that the roughness parameters in each line can be calculated. The purpose of setting the analyzing lines in this way was to compare roughness parameters in line and perpendicular to grinding tracks and to discover the influence that abrasive discs had on each material.

Measured topography data were processed by Image Processing and Data Analysis v2.1.15 software. Following parameters were compared among specimens: average roughness (R_a) and maximum peak-to-valley distance (R_{p-v}).

3. RESULTS AND DISCUSSION

Figures 3, 4 and 5 displays AFM images obtained from the surface of each specimen, while tables 4, 5 and 6 contain values of (R_a) and (R_{p-v}) roughness parameters from each analyzing line. Fig. 6 displays comparison of roughness parameters between all specimens, along and perpendicular to grinding tracks.

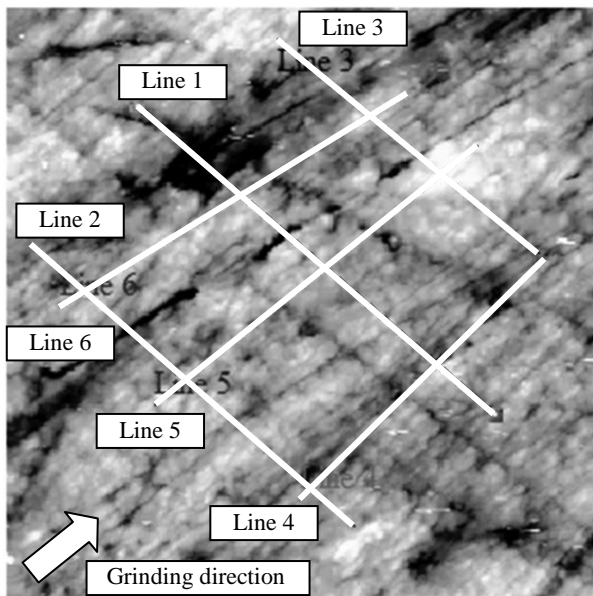


Fig. 3. AFM image and analyzing lines for Filtek Ultimate Translucent (nanofilled)

Measuring location	R_a [nm]	R_{p-v} [nm]
Line 1	57.91	380.9
Line 2	32.04	239.0
Line 3	36.64	193.4
Line 4	26.16	214.7
Line 5	29.82	193.3
Line 6	29.28	165.6

Table 4. R_a and R_{p-v} parameters on analyzing lines for Filtek Ultimate Translucent

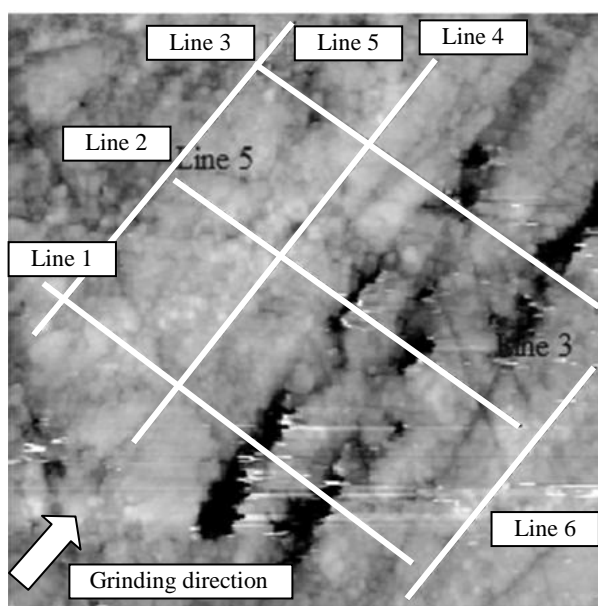


Fig. 4. AFM image and analyzing lines for GC Gradia Direct Anterior (microfilled)

Measuring location	R_a [nm]	R_{p-v} [nm]
Line 1	87.62	786.5
Line 2	94.66	745.4
Line 3	85.68	774.7
Line 4	37.24	194.1
Line 5	48.92	333.3
Line 6	49.16	401.7

Table 5. R_a and R_{p-v} parameters on analyzing lines for GC Gradia Direct Anterior

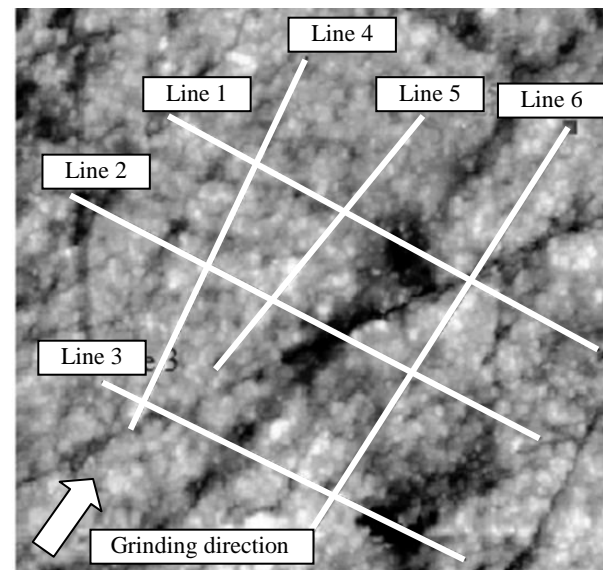


Fig. 5. AFM image and analyzing lines for Filtek Z250 - (microhybrid)

Measuring location	R_a [nm]	R_{p-v} [nm]
Line 1	43.27	375.8
Line 2	37.52	351.4
Line 3	37.81	284.5
Line 4	21.25	154.2
Line 5	31.82	174.7
Line 6	29.44	162.9

Table 6. R_a and R_{p-v} parameters on analyzing lines for Filtek Z250

Based on the values of surface roughness parameters it can be concluded that Filtek Ultimate Translucent had the lowest values of (R_a) and (R_{p-v}) compared to GC Gradia Direct Anterior and Filtek Z250 (Fig. 6), which confirms the existence of advanced material features due to the nanoparticles filler composition. Also, when comparing same roughness parameters along and perpendicular to grinding tracks, Filtek Ultimate Translucent showed the best behavior in terms of surface uniformity after grinding by abrasive discs - there were the smallest

differences in terms of roughness values in the both analyzing directions. In all cases, measuring roughness along grinding tracks showed lower values than perpendicular to grinding tracks.

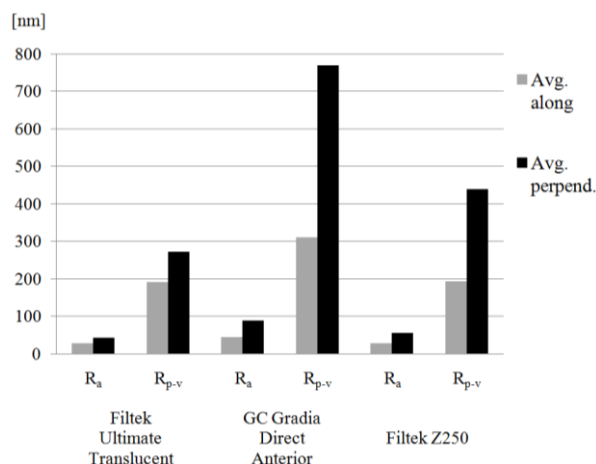


Fig. 6. Comparison of roughness parameters among dental resin-based nanocomposites along and perpendicular to grinding tracks

4. CONCLUSION

Based on obtained values of surface roughness parameters it can be concluded that Filtek Ultimate Translucent had the lowest surface roughness among the three tested groups of resin-based composites and the highest surface uniformity after dental finishing and polishing procedure. Smoother material surface prevents bacterial biofilm retention which is the main cause of dental and periodontal pathology. Any improvement of the material properties is allowing better therapeutic possibilities.

5. ACKNOWLEDGMENTS

This paper is a part of research included into the project "Project TESLA: science with accelerators and accelerator technologies", financed by Serbian Ministry of Science and Technological Development. The authors are grateful for the financial support (Vilotić, Kakaš).

This paper represents a part of the research realized in the framework of the project "Research and development of modeling methods and approaches in manufacturing of dental recoveries with the application of modern technologies and computer aided systems" – TR 035020, financed by the Ministry of Science and Technological Development of the Republic of Serbia (Lainović, Blažić, Marković, Ivanišević).

The authors would like to thank 3M (East) AG company branch in Serbia, and Mikodental, Šabac-general dealers of Shofu, Japan for Serbia, for the material support.

6. REFERENCES

[1] Nicholson, J.W., Czarnecka, B.: *The clinical repair of teeth using direct filling materials: engineering considerations*, Proceeding of the institution of mechanical engineers, part H: Journal

of engineering in medicine, 220, p.p. 635-645, 2006.

- [2] Sadowsky, S.J.: *An overview of treatment considerations for esthetic restorations: a review of the literature*, Journal of prosthetic dentistry, 96, p.p. 433-442, 2006.
- [3] Cramer, N.B., Stansbury, J.W., Bowman, C.N.: *Recent advances and developments in composite dental restorative materials*, Journal of Dental Research, 90(4), p.p. 402-416, 2011.
- [4] Chen, M.H.: *Update of dental nanocomposites*, Jour. of dental research; 89(6), p.p. 549-560, 2010.
- [5] Khaled, S.M.Z., Miron, R.J., Hamilton, D.W., Charpentier, P.A., Rizkalla, A.S.: *Reinforcement of resin based cement with titania nanotubes*, Dental Materials, 26, p.p. 169-178, 2010.
- [6] Curtis, A.R., Palin, W.M., Fleming, G.J.P., Shortall, A.C.C., Marquis, P.M.: *The mechanical properties of nanofilled resin-based composites: The impact of dry and wet cycling pre-loading on bi-axial flexure strength*, Dental Materials, 25, p.p. 188-197, 2009.
- [7] Yu, B., Lim, H., Lee, Y.: *Influence of nano- and micro-filler proportions on the optical property stability of experimental dental resin composites*, Materials and Design, 31, p.p. 4719-4724, 2010.
- [8] Mitra, S.B., Wu, D., Holmes, B.N.: *An application of nanotechnology in advanced dental materials*, JADA, 134, p.p. 1382-1390, 2003.
- [9] Heintze, S.D., Zellweger, G., Zappini, G.: *The relationship between physical parameters and wear of dental composites*, Wear, 263, p.p. 1138-1146, 2007.
- [10] Ferracane, J.: *Resin composite - state of art*, Dental Materials, 27, p.p. 29-38, 2011.
- [11] Sideridou, I.D., Karabela, M.M., Vouvoudi, E.Ch.: *Physical properties of current dental nanohybrid and nanofill light-cured resin composites*, Dental Materials, 27, p.p. 598-607, 2011.
- [12] Malhotra, N., Mala, K., Acharya, S.: *Resin-based composite as a direct esthetic restorative material*, Compendium of Continuing Education in Dentistry, 32, p.p. 14-23, 2011.
- [13] Morgan, M.: *Finishing and polishing of direct posterior restoration*, Practical Procedures and Aesthetic Dentistry, 16, p.p. 211-217, 2004.

Authors: Marko Vilotić, mag. sci., Prof. Dr. Damir Kakaš, M.Sc. Aljoša Ivanišević, University of Novi Sad, Faculty of Technical Sciences, Institute for Production Engineering, Trg Dositeja Obradovića 6, 21000 Novi Sad, Serbia, Phone: +381 21 450366, Fax: +381 21 454495. Dr Tijana Lainović¹, Prof. dr. Larisa Blažić^{1,2}, Prof. dr. Dubravka Marković^{1,2}, ¹University of Novi Sad, Faculty of Medicine, School of Dentistry, Hajduk Veljkova 3, 21000 Novi Sad, Serbia, Phone: +381 21 6615706, ²Clinic of Dentistry of Vojvodina, Hajduk Veljkova 12, 21000 Novi Sad, Serbia, Phone: +381 21 6612222; Fax: +381 21 526120. Email: markovil@uns.ac.rs, tijana.lainovic@gmail.com, kakasdam@uns.ac.rs, larisa.blazic@gmail.com, dubravkamarokovic@yahoo.com, aljosa@uns.ac.rs

Vitković, N., Veselinović, M., Mišić, D., Manić, M., Trajanović, M., Mitković, M.

GEOMETRICAL MODELS OF HUMAN BONES AND IMPLANTS, AND THEIR USAGE IN APPLICATION FOR PREOPERATIVE PLANNING IN ORTHOPEDICS

Abstract: Geometrically accurate and anatomically correct three-dimensional geometric model(s) of human bones (or bone sections) and implants are essential for successful preoperative planning in orthopedic surgery. Such models are often used in various software systems for the preparation and control of surgical interventions. In this paper, the process of models' creation and their usage in application for the preoperative planning in orthopedics are presented. Models are created by using reverse engineering techniques, CAD (CATIA) and 3D Content creation software (Blender). The application is web oriented, and developed with use of modern web technologies like HTML5 and WebGL. In relation to commercial and free software systems currently in use, this application has several advantages such as: implementation of adaptive geometrical models, the ability to work across multiple platforms, ease of installation and use, etc.

Key words: geometrical models, bones, application, web, preoperative planning

1. INTRODUCTION

In orthopedic surgery, but also in all other sub-branches of surgery, where there is need for preoperative planning or creation of customized implants (fixators), there is a specific requirement to know the exact geometrical model of the human bone. Therefore, it is very important to create geometry of the bone rapidly and accurately. Having such models, it is possible to build customized bone implants (fixators) using rapid prototyping technologies, or performing preoperative planning procedures in adequate applications.

The classification and analysis of 3D modeling methods for the creation of human bones geometrical models are presented in [1]. This paper describes the study and the development of a script for a commercial software package (3ds Max) able to reconfigure the template model (deformable by Free Form Deformation method - FFD) of a femur starting from two orthogonal images representing the specific patient's anatomy. Although this study provides an outstanding contribution to the research field, there are some drawbacks. First one is the semi-automatic image segmentation (X-ray images) which is always problematic due to previously known problems with the X-ray images (superposition, inaccurate patient positioning, artifacts, etc.). The parametric model presented in this paper is not limited to the input data from only one source, because parameter values can be acquired from any available medical imaging devices: CT, X-ray, MRI, ultrasound, etc. The second drawback is creation of the script for the application in only one software (3ds Max). The points model created by this method can be used in any 3D graphic application which works with cloud of points model(s).

The 3D reconstruction process which is based on anatomical properties is presented in [2]. The purpose of this study is to create a 3D model of human femur by using multiple X-ray images and anatomical properties

of the femur. For 3D reconstruction, firstly, the 2D shape and specific parameters of the bone are measured from X-ray images. Then, the corresponding CT model is modified as it follows: the axial scaling, shearing transformation and radial scaling. Findings presented in [1,2] are the basis for the development of method presented in this paper.

In [3], the authors are trying to create composite bone model with possible bone part adaptation and replacement from generic database of bone models. This is a useful approach when 3D scanning methods are available, but for 2D scanning methods more precise and patient-adapted models are required. In [4], the authors suggest application of standard bone fracture models database and its implementation in application for planning orthopedic operations. In [4] good example of preoperative procedures and techniques is presented.

2. THE GEOMETRIC MODELS CREATION PROCESS

The developed method contains three preparatory processes which must be performed in order to generate a valid geometrical model (surface, solid, parametric model) of the specific human bone, as presented in Fig. 1. The applied method for creating the human bone geometrical model is based on anatomical properties (anatomical model) and human bone morphology.

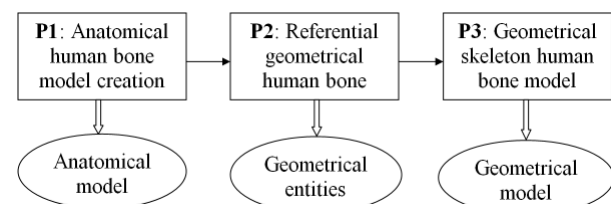


Fig.1 Preparatory processes for geometrical models creation

Anatomical bone model is, in its essence, a semantic (descriptive) model in which anatomical definitions are taken from medical sciences, and it defines terms referring to certain areas on geometrical bone model. In other words, the anatomical model can be described as a set of anatomical landmarks which are defined on each bone and well known in medicine.

In connection with that, the first step is semantic defining of anatomical areas on human bone, i.e. creation of anatomical bone model, as well as informing about basic bone morphology (P1).

After creating the anatomical model, creating of the basic model geometry is introduced. Initial preparatory processes are thoroughly presented in [5] and [6], demonstrating application of the following operations: Computer Tomography (CT) scanning part of the human body or dry samples (in this case femur); Preprocessing of raw data (scans) and its transformation into STL format; Importing the scanned model in STL format into CAD application (for example CATIA) and its further preprocessing; Cleaning the cloud of points; Tessellation and Healing the tessellated model. At the end of the preparatory processing processes, polygonal geometrical bone model is created.

The upper stated processes are so called preparatory processes for a very important procedure of referential geometry defining - RGEs (planes, lines, axis, points, and so) [6] which is defined on polygonal human bone model in accordance with its anatomical and morphological features. After defining RGEs (P2), follows the examination of polygonal bone model in order to create geometrical entities which will serve as base for creating the geometric model(s). Geometrical entities are mainly spline curves (B-spline) and are defined to follow bone geometry and topology the best way possible and all in accordance with anatomical bone model (P3). Spline curves defined on femur condyles are presented in Fig. 2.

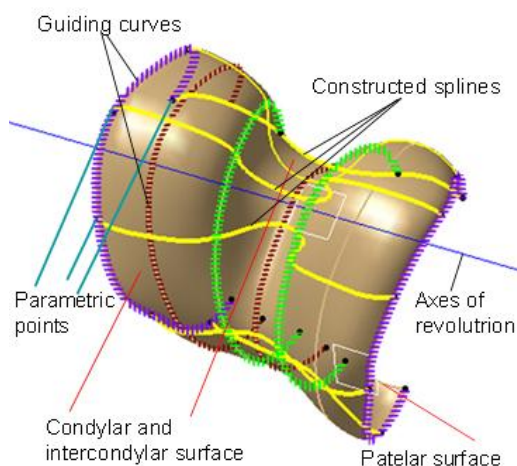


Fig. 2. Femur condyles surface model with defined spline curves and parametric points

These entities serve as the basis for the creation of adequate geometrical models. They can be used for the creation of:

- Geometrical points for the parametric bone model [6]

- Polygonal, Surface and Volume models [5,7]
- Finite Element Models [8],
- Geometrical models of human bones missing parts (due to bone illness or bone fractures).
- etc.

The parametric and polygonal models are used in web application, created by authors, for the preoperative planning in orthopedics. To provide further information, a brief description of the process of creating polygonal and parametric models of human bones will be presented.

The parametric model consists of a set of points whose coordinates are defined by parametric functions. This model can be regarded as a mathematically defined cloud of points model. Points are created at specific anatomical positions on spline curves defined in the P3 process (Fig. 2), as shown in [6].

Parametric functions are created for each point individually and they provide the dependency of points coordinates on pre-defined parameters. The parameters are, in most cases, morphometric measurements, and they are defined for each bone (femur, tibia, fibula) separately. Their values can be acquired from various medical images (CT, X-ray) by the use of classical (ruler) or computer software measuring techniques. An example of parameters defined on the femur polygonal model is shown in the Fig. 3.

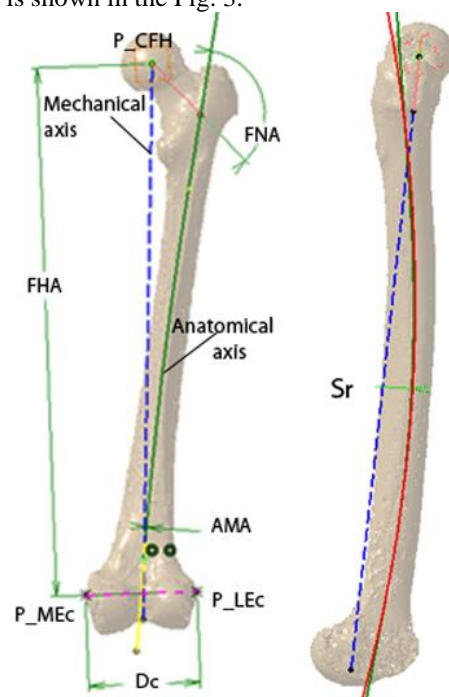


Fig. 3. Bone parameters defined on Femur polygonal model

Parameters are:

- FNA – Femoral Neck Angle
- FHA – Distance between P_CFH and line connecting P_MEc and P_LEc
- DC – Distance between P_MEc and P_LEc
- AMA – Angle between Anatomical and Mechanical Axis in Anterior Posterior view
- Sr – Shaft radius in Lateral-Medial view
- Femoral Head Radius - FHR

The polygonal model can be obtained in two general ways, and they are:

- by using the techniques presented in [5], which are based on the transformation of CT (DICOM) model into the polygonal model
- by using a parametric points model as input data to form a polygonal model by creating correctly connected triangles.

3. THE PROCESS OF CREATING MEDICAL FIXATOR SOLID MODEL

This paper describes a method for creating a geometric model of the tibia internal fixator by Mitkovic. Based on the fact that the bones are not shaped as typical geometrical forms, and that two identical bones do not exist in reality, there is a requirement to define optimal geometry of the fixator, which can be applied on more than just one tibia. The fixator by Mitkovic consists of two parts: distal and proximal, whose geometrical models are made separately and then connected in one whole model. The first step in creating a geometrical fixator model is to create the fixator's outer contour projection, perpendicular to tibia shaft tangential plane, on the tibia surface, Fig 4. Fixator's contour geometry was created on the basis of existing (real) fixator geometry and topology by Mitkovic.

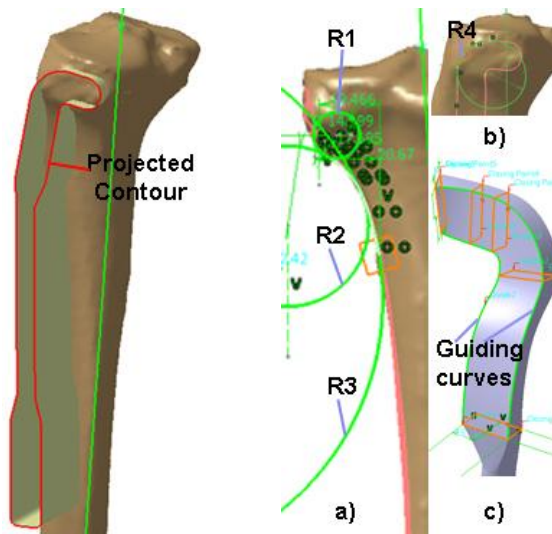


Fig. 4. Fixator contour projection Fig. 5. a,b) Constructed circles, c) Fixator volume model

A projection curve is used to create the proximal and distal curve guidelines and limitations for the design of optimal fixator geometrical model. The process of creating proximal part guiding curves consists of two individual steps: creating the outer (lateral) and inner (medial) circles with adequate radius values on the tibia model surface. The proximal part of guiding curves is created by cutting and connecting the created circles, Fig 5a,b. The fixator proximal part volume model is created by dragging the rectangle profile along the contour curves, Fig. 5c. The fixator distal part volume model is formed by extrusion of adequate profiles to

the merging point with the proximal model. The complete fixator solid model for the specific bone (patient) is created by merging proximal and distal part models.

In order to obtain optimal values of guiding curves radiuses (and thus fixing the model so it can be applied to a number of different patients) measurements on ten different tibia (patients age 20 to 55, male and female) were performed and mean values were obtained and presented in Table 1. Values given in Table 1 were used to create a guiding curve with mean radiuses values, which is used to create fixator volume model with optimal geometry.

Tibia	Radius R_1	Radius R_2	Radius R_3	Radius R_4
Mean Value	15.5969	26.1637	83.0417	17.9543

Table 1. Specific guiding curves radiuses mean values for ten different tibia bones

4. THE APPLICATION OF THE MODELS

Polygonal bone and fixator models are used in a web application for the preoperative planning in orthopedics. The application is based on the use of WebGL and HTML5 technologies, implemented through THREE3D open source engine. The application allows the transformation of basic models (rotation, translation, scaling), and pairing bone and fixator models in the appropriate assembly, Fig. 8.

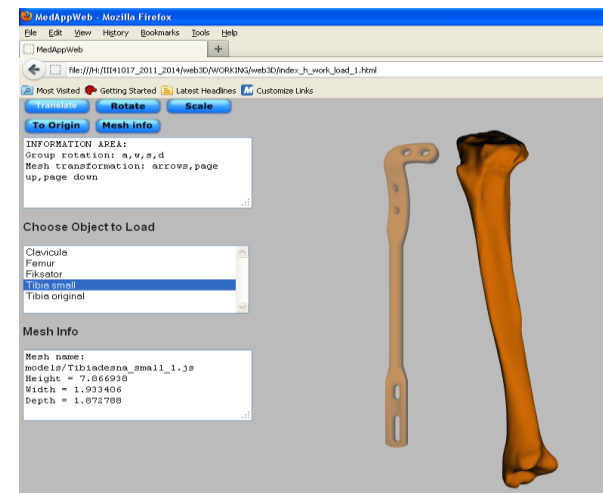


Fig. 8. Web application for the preoperative planning in orthopedics

In order to successfully apply the models in the application, it is necessary to previously perform the transformation processes, ie., to create the appropriate format of the model. Possible file formats are: .js in the form of JSON (JavaScript Object Notation), .3ds (3D Studio) .obj (Object), etc. In the current phase of development, JSON notation is used in applications (an example of entries for tibia model are presented in (1)). JSON data format allows data entry on: vertices, triangles, lights, normals, etc.. which completely defines the corresponding 3D model, and the scene

where the object model exists. JSON models are created on the basis of polygonal (STL) models in Blender software.

```
{ "vertices" : 71251,
  "faces" : 142498,
  "normals" : 71251,},
"materials": [ { }],
"vertices"=[-0.157411,1.041358,0.140951,...]
"normals"=[0.861171,0.032258,-0.507248,...]
```

5. CONCLUSION

Methods for creating human bone and fixators geometrical models are presented in this paper. Considering anatomical and morphological properties of the human bone, presented method(s) enables creation of more realistic, geometrically accurate and anatomically correct models as presented in [6,9,10]. The resulting model(s) of human bone(s) and fixators can be used for various purposes: preoperative planning in orthopedics (presented in this paper), learning processes, implant manufacturing, FEM analysis, etc.

In addition to the process of creating geometric models, their use in a web application for the preoperative planning in orthopedics is presented. The application enables basic geometric transformations of bone and implant models, such as : translation, rotation, scaling, zooming, etc., as well as the option to receive data on models (basic measurements, triangle quantity, and such), and to measure adequate distances on models, both individually and as part.

Further work in the research includes improving the method of creating a geometric model for the construction of better quality models in terms of accurate geometry and morphology, as well as creating models of a large number of implants (fixators) and bones (library of models). Regarding the application for preoperative planning, further focus is directed towards the improvement of the algorithm for managing the parametric model. Adequate algorithm will allow creation of patient bone geometrical models, solely on the basis of a number of predefined parameters whose values can be read (measured) from the input medical images.

ACKNOWLEDGEMENT

The paper is part of the project III41017 - Virtual Human Osteoarticular System and its Application in Preclinical and Clinical Practice, sponsored by Republic of Serbia for the period of 2011-2014.

6. REFERENCES

- [1] Filippi, S., Motyl, B., Bandera, C.: *Analysis of existing methods for 3D modelling of femurs starting from two orthogonal images and development of a script for a commercial software package*, Computer methods and programs in biomedicine, 89, p.p. 76-82, 2008
- [2] Kyu Lee, M., Hyuk Lee, S., Kim, A., Youn, I., Soo Lee, T., Hur, N., Choi, K.: *The Study of Femoral*

3D Reconstruction Process Based on Anatomical Parameters Using a Numerical Method , Journal of Biomechanical Science and Engineering, 3, p.p. 443-451,2008

- [3] Matthews, F., Messmer, P., Raikov, V., Wanner, G., Jacob, A., Regazzoni, P., Egli, A.: *Patient-specific three-dimensional composite bone models for teaching and operation planning*, Journal of Digital Imaging, 22, p.p. 473-482, 2009
- [4] Sourina, O., Sourina, A., Howe, T.: *Virtual Orthopedic Surgery Training on Personal Computer*, International Journal of Information Technology, 6, p.p. 16-29, 2000
- [5] Stojkovic, M., Trajanovic, M., Vitkovic, N., Milovanovic, J., Arsic, S., Manic, M.: *Referential Geometrical Entities for Reverse Modeling of Geometry of Femur*, Proceedings of VIP IMAGE 2009, p.p. 189-194, Taylor & Francis Group, Porto, Portugal, 2009
- [6] Vitković, N., Trajanović, M., Milovanović, J., Korunović, N., Arsić, S., Ilić, D.: *The geometrical models of the human femur and its usage in application for preoperative planning in orthopedics*, ICIST 2011, Kopaonik, Serbia, 2011
- [7] Veselinovic, M., Vitkovic, N., Stevanovic, D., Trajanovic, M., Arsic, S., Milovanovic, J., Stojkovic, M.: *Study on creating human tibia geometrical models*, Proceedings of the 3rd International Conference on E-Health and Bioengineering - EHB, p.p. 195-198, Iași, Romania, 2011
- [8] Trajanović, M., Korunović, N., Milovanović, J., Vitković, N., Mitković, M.: *Application of computer models of mitković selfdynamizable internal fixator in rehabilitation of femur traumas*, FACTA UNIVERSITATIS Series: Mechanical Engineering, 8, p.p. 27 - 38, 2010
- [9] Vitković, N., Milovanović, J., Trajanović, M., Korunović, N., Stojković, M., Manić, M.: *Different Approaches for the Creation of Femur Anatomical Axis and Femur Shaft Geometrical Models*, Proceedings of ICPE 2011, ICPE 2011, Niš, Serbia, p.p. 351-354, 2011
- [10] Stojkovic, M., Milovanovic, J., Vitkovic, N., Trajanovic, M., Arsic, S., Mitkovic, M.: *Analysis of femoral trochanters morphology based on geometrical model*, Journal of Scientific and Industrial Research, 71, p.p. 210-216, 2012

Authors: M.Sc. Nikola Vitković, M.Sc. Marko Veselinović, Dr Dragan Mišić docent, Prof. Dr. Miodrag Manić, Prof. Dr. Miroslav Trajanović, University of Niš, Faculty of Mechanical Engineering in Niš, LIPS, Aleksandra Medvedeva 14, 18000 Niš, Serbia, Phone.: +381 18 500-669, **Prof. Dr. Milorad Mitković**, University of Niš, Faculty of Medicine

E-mail: vitko@masfak.ni.ac.rs

marko.veselinovic@masfak.ni.ac.rs

draganm@masfak.ni.ac.rs

miLOSS@masfak.ni.ac.rs

miodrag.manic@masfak.ni.ac.rs

miroslav.trajanovic@masfak.ni.ac.rs

mitkovic@gmail.com

Williams, R.J., Eggbeer, D., Lapcevic, A., Trifkovic, B., Puskar, T., Budak, I., Jevremovic, D.

RE-CAD/CAM APPROACH IN DESIGN AND MANUFACTURING OF DENTAL CERAMIC CROWNS IN COMBINATION WITH MANUAL INDIVIDUALIZATION

Abstract: CAD/CAM technology in dentistry offers high-end ceramic restorations, known for its quality, preciseness, swiftness and repeatability. However, some features are still human-dependent. A young female patient required smile enhancement, since suffering from colour change on three devitalized frontal teeth. After fiber post placement, teeth were prepared for metal-free restoration. Consequently, abutments were scanned using extraoral scanner (Sirona, InEos Blue; Beinsheim, Germany). CAD software (version 3.8) has been used to create three crown copings, with cut-back in the incisal region. After finalization of the virtual modeling, data file has been transferred to a milling unit (Sirona, MCXL, Beinsheim, Germany) that produced crown copings out of a ceramic block (IPS e.max CAD, Ivoclar Vivadent, Schaan, Liechtestein). Crowns were tried for the fit and occlusion in the so-called blue stage, after which final strength and shape has been achieved by thermal treatment in the ceramic furnace. Individualization has been done manually, creating special effect in the cut-back region. Crowns were cemented adhesively. CAD/CAM offers modern and relevant way of producing ceramic restorations, however, special effects still require manual adjustments.

Key words: CAD/CAM, dentistry, extraoral scanner, computer aided inspection

1. INTRODUCTION

Striving towards its primary goal – *primum non nocere* („above all, do not harm“ eng.), the area of dental prosthetics has introduced numerous novel technologies and methods that allow the manufacture of precision, custom-made, optimal dental replacements. During the past decade, efforts have been concentrated towards an advancement of the modelling and manufacture of dental replacements by introducing advanced computer aided (CA) systems, new materials and machining technologies, as opposed to the traditional way of manual manufacture, which is prone to numerous subjective errors. Amongst modern CA systems that have found broad application in this area, the most widely used are 3D digitization systems, computer aided design (CAD) with reverse engineering (RE) and computer aided manufacturing (CAM). The development and implementation of such technologies and systems have paved the way towards a significant advancement in conventional modelling, manufacture and the inspection of dental replacements [1-5].

RE-CAD/CAM approach has been introduced in dentistry as a precise, efficient, accurate and error-free tool to produce high-quality dental restorations [1,2]. Practically, it can produce ceramic crowns in matter of hours, enabling reconstruction during single visit [3]. With the use of CAD/CAM, however, limited aesthetic results can be achieved, since individualization is still human-dependent.

CAD/CAM consists of three major parts [4,5]:

- 1) 3D digitization,
- 2) RE-CAD and
- 3) CAM.

Current problem with CAM unit is related to the milling process. It utilizes ceramic blocks, which are namely made out of a single material type. Further development enabled different translucency within a block, where enamel and dentin characteristics are

reproduced [6]. These variations are possible within leucite blocks only. Since natural teeth exhibit variations in colour and translucency, they are hard to reproduce with uniform blocks.

2. CASE REPORT ON APPLICATION OF RE-CAD/CAM APPROACH IN DESIGN AND MANUFACTURING OF CERAMIC CROWNS

A young female patient, 35-year's old, came into the practice requiring aesthetic enhancement of her anterior teeth. With clinical inspection, it has been concluded that left central, as well as right lateral incisors are devitalized and therefore significantly darker comparing to natural teeth. Right central incisor had a pre-existing metal-free restoration, with an active metal post reinforcement. The appointment was set in two weeks, and three metal-free crowns were planned. Interestingly, exactly on the treatment day, existing crown with the post broke. After removal of the metal post remainings, it became obvious that only dowel metal core can be inserted, due to a very insufficient dentin layer. In order to mask metal background, layers of opaquer were baked prior to cementation. Two other teeth were reconstructed with fibre posts. As a result, however, an uneven background became apparent (Fig. 1).



Fig. 1. Situation prior to impression taking

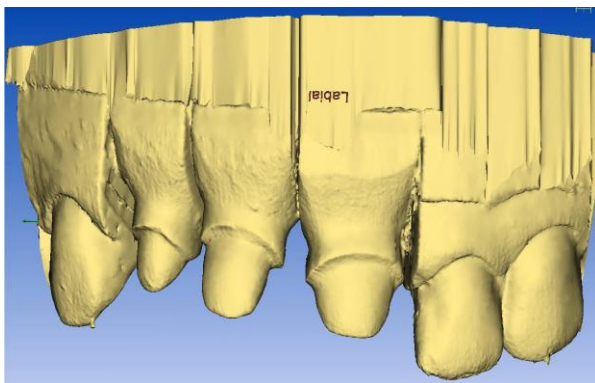
2.1 3D digitization

After impression taking, a dental cast model was made. For this purposes, a special, scanable gypsum was used (Fujirock EP OptiXscan, GC, Japan). Model was scanned with Cerec In Eos Blue (Sirona, Beinsheim, Germany) 3D digitization system (Fig. 2a). The scanner uses structured light (stripe projection) and has a narrow triangulation angle for deep cavities [7,8].

Blue light indicates a model part that is currently being scanned [10]. The model appears as a virtual model in CAD CEREC version 3.8 (Fig. 2b).



a) Cerec In Eos Blue 3D digitization system with the detail during the scanning process



b) The result of 3D digitization in CAD CEREC
Fig. 2. The 3D digitization system with the digitization result

2.2 RE-CAD design of dental crowns

First step in creation of virtual crowns is determination of preparation line and insertion axis (Fig. 3). Operator can choose among several possibilities, that are implicated in various morphological bases (such as young, adult, old, Asian, etc.). Consequently, proposal of the crown is created by the software (Fig. 4) [9].

Further modifications of the crowns can be done using manual tools. Once finished, crown is fixed by the software and treated as a natural tooth. Then, a contra lateral incisor is created. Initially, there is an overlap between two crowns, that can be corrected using several crown equators (Fig. 5) [11,12]. Small modifications of the crown shape can be done using manual tools such as adding, removing, smoothing etc. (Fig. 6).

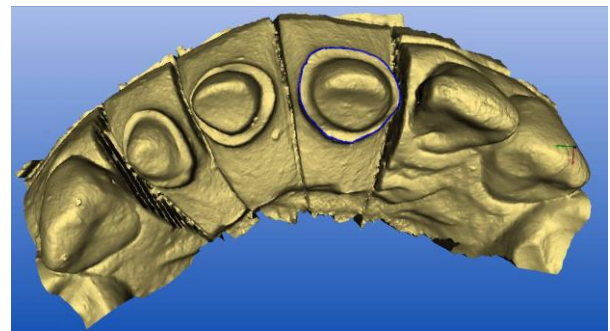


Fig. 3. Determination of the preparation line

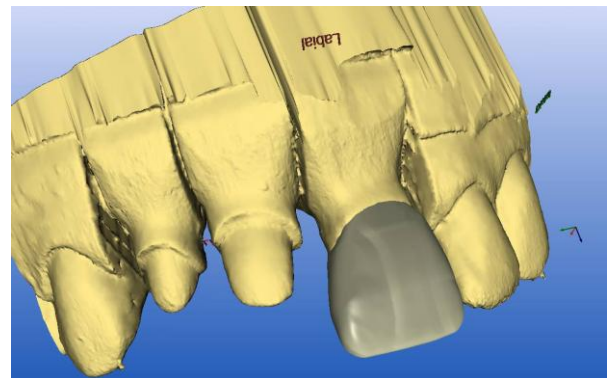


Fig. 4. CAD model of the left central incisor

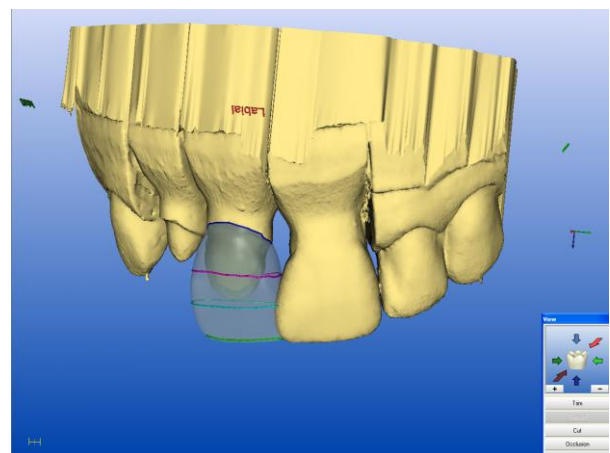


Fig. 5. Processing of the right central incisor in the CAD module

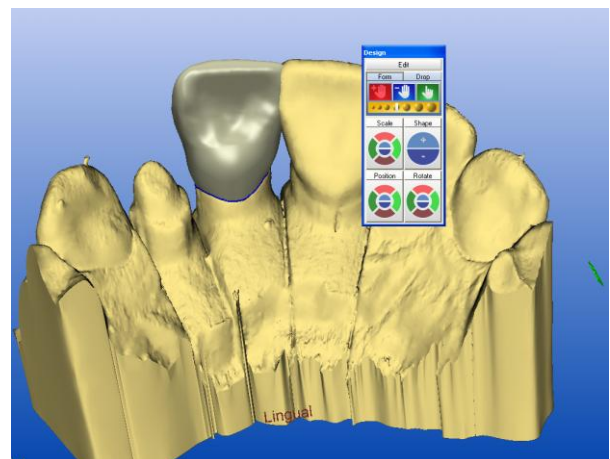


Fig. 6. Manual modification of the size and shape with specific toolbar

Major challenge is creation of cervical isthmus, that appears a consequence of uneven gingival margins. If not paid attention to, it can create disrupted optical image of central incisors, normally know to be the most symmetric teeth in the jaws.

2.3 CAM of dental ceramic crowns

When finished in the CAD, modeled crowns are proceeded to CAM module (Sirona MCXL). This is a new version of the milling machine, with accuracy of 25 μm and 60% faster comparing to the previous version. Lithium-disilicate blocks were used (IPS e.max CAD; Ivoclar Vivadent AG; Schaan, Liechtenstein), exhibiting 350 MPa flexural strength (Fig. 7).

To achieve optimal translucency, LT (low translucency) block was the choice. This block enables some level of light penetration, enabling life like appearance but still covering background colour to some intent.

CAM unit mills in a so-called blue block stage, where both hardness and strength of the material are not fully achieved (meta-silicate stage). Since blue blocks do not support stock milling (milling of multiple units out of a block), three C14 blocks were used. After milling and initial trial, blocks were crystalized in a ceramic furnace (Programat P300, Ivoclar Vivadent AG; Schaan, Liechtenstein).

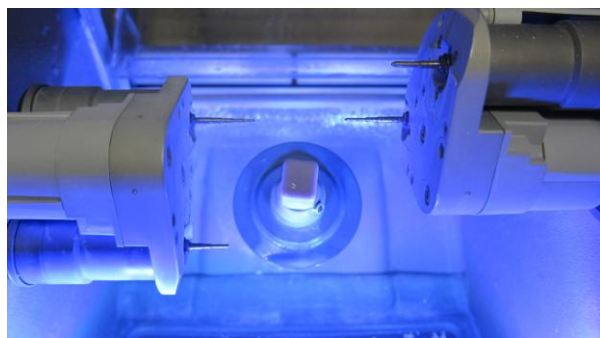


Fig. 7. Cerec CAM unit with blue lithium-disilicate block

2.4 Manual individualization of dental ceramic crowns

Milling, however, is the final stage in current possibilities of the CAD/CAM systems, in regards of individualization. Any further characteristics have to be done manually.

Individualization can be done using two basic techniques:

1. layering and
2. staining.

Layering creates in depth, profound esthetic appearance. It, however, requires significant technical skills.

Staining is used as a toll to modify optical impression by superficial colouring of the restoration. In this case, both techniques were used. Fig. 8 presents the application of layering technique with ceramic powders, while the application of staining technique with ceramic stains is shown on Fig. 9.



Fig. 8. Application of the layering technique with ceramic powders

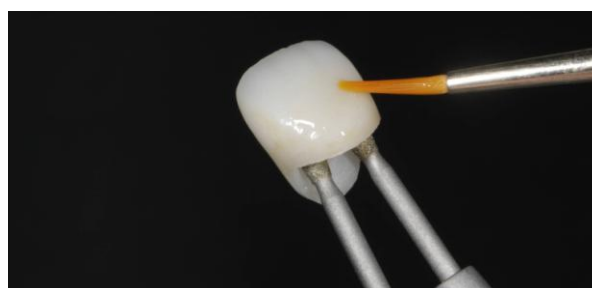


Fig. 9. Application of staining technique with ceramic stains

The other issue that cannot be solved with CAD/CAM systems only is background colour coverage. LT ingots still transmit light in a sufficient manner, that enable background colour influence if thickness of the restoration is not more than 1 mm. To predict this unwanted effect, background colour is simulated in the lab by the special die composite (Fig. 10). Therefore, the determination of the final esthetic result is still human-dependent. Finished restorations are shown in Fig. 11.



Fig. 10. Final colour modifications on a special composite die



Fig. 11. Final restoration

3. CONCLUSION

CAD/CAM in dentistry is a unique approach, that improves classic treatment procedure. Through 3D digitization, it transfers real teeth into digital information, that can be processed into virtual objects within the specialized RE-CAD software. With the support of data bases with predefined teeth shapes, the software creates restoration automatically. However, manual control is enabled as well. CAM is a highly-sophisticated manufacturing procedure, with high accuracy and time saving.

Within this paper, an case report that comprises all three stages of dental CAD/CAM approach – 3D digitization, RE-CAD modelling and CAM manufacture – has been presented. However, esthetic factors, such as individualization, colour features, effect of the background and final appearance are still human dependent. That is why the special attention in this paper is focused on this stage that includes activities for further automation.

ACKNOWLEDGEMENT

A part of result presented in this paper is obtained in the framework of the project “*Research and development of modelling methods and approaches in manufacturing of dental recoveries with the application of modern technologies and computer aided systems*” – TR 035020, financed by the Ministry of Education, Science and Technological Development of the Republic of Serbia.

4. REFERENCES

- [1] Mörmann, W.H.: *The evolution of the CEREC system*, The Journal of the American Dental Association, 137, p.p.7S-13S, 2006.
- [2] Trifković, B.: *Preciznost optičkih metoda skeniranja u stomatološkim CAD/CAM tehnologijama*, Magistarska teza, Stomatološki fakultet, Univerzitet u Beogradu, 2009.
- [3] Peumans, M., Van Meerbeek, B., Lambrechts, P., Vanherle, G.: *Porcelain veneers: a review of the literature*, Journal of Dentistry, 28, p.p. 163-77, 2000.
- [4] Duret, F.: *CAD/CAM in dentistry: Present and future application*, Quintessence International, 27, p.p. 433-436, 1996.
- [5] Takahsi, M., Yasuhiro, H., Jun, K., Siochi, K., Yukimichi, T.: *A review of dental CAD-CAM: current status and future perspectives from 20 years of experience*, Dental Materials, 28(1), p.p. 44-56, 2009.
- [6] Land, M.F., Hopp, C.D.: *Survival rates of allceramic systems differ by clinical indication and fabrication method*. Journal of Evidence-Based Dental Practice, 10, p.p. 37-38, 2010.
- [7] Wiedhahn, K., Kerschbaum, T., Fasbinder, D.F.: *Clinical long-term results with 617 Cerec veneers: a nine-year report*, International Journal of Computerized Dentistry, 8, p.p. 233-246, 2005.
- [8] Huang, L.C.: *Anterior rehabilitation using Cerec 3 veneer software - a case report*, International Journal of Computerized Dentistry, 7, p.p. 263-267, 2004.
- [9] Jevremovic, D.P., Puskar, T.M., Budak, I., Vukelic, Dj., Kojic, V., Eggbeer, D., Williams, R.J.: *An Re/Rm Approach to the Design and Manufacture of Removable Partial Dentures with a Biocompatibility Analysis of the F75 Co-Cr SLM Alloy*, Materiali in tehnologije, 46(2), p.p.123-129, 2012.
- [10] Mehl, A., Endler, A., Mörmann, W., Attin, Th.: *Accuracy testing of a New Intraoral 3D Camera*, International Journal of Computerized Dentistry, 12, p.p. 11-28, 2009.
- [11] Huang, L.C.: *Anterior rehabilitation using Cerec 3 veneer software - a case report*. International Journal of Computerized Dentistry, 7, p.p. 263-267, 2004.
- [12] Schneider, O.: *Cerec veneers - practical procedure and case presentation*, International Journal of Computerized Dentistry, 6, p.p. 283-292, 2003.

Authors: Robert J. Williams, Dominic Eggbeer, Centre for Dental Technology and the National Centre for Product Design and Development Research, Cardiff Metropolitan University, Cardiff, United Kingdom.

Prof. dr Danimir P. Jevremović, Ana Lapčević, Clinic for Prosthodontics, School of Dentistry, Žarka Zrenjanina 179, 13000 Pančevo, University Business Academy in Novi Sad, Serbia. E-mail: dr.danimir@sbb.rs.

Mr Branka Trifković, University of Belgrade, School for Dentistry, Clinic for Prosthodontics, Rankeova 4, 11000 Belgrade, Serbia. E-mail: brankatr@yahoo.com;

Doc. dr Tatjana M. Puškar, Clinic for Prosthodontics, Medical Faculty – Department of dentistry, University of Novi Sad, Hajduk Veljkova 3, 21000 Novi Sad, Serbia. E-mail: tpuskar@uns.ac.rs

Doc. dr Igor Budak, University of Novi Sad, Faculty of Technical Sciences, Department for Production Engineering, Trg Dositeja Obradovica 6, 21000 Novi Sad, Serbia, Phone.: +381 21 485-2255, Fax: +381 21 454-495. E-mail: budaki@uns.ac.rs.

11th INTERNATIONAL SCIENTIFIC CONFERENCE
MMA 2012 - ADVANCED PRODUCTION TECHNOLOGIES

PROCEEDINGS



AUTHOR INDEX

Novi Sad, 20-21 September 2012

Author Index

A

Adamišin, P.....	347
Agarski, B.	369
Alexandrov, S.	415, 435
Andrejkovič, M.	207, 211
Andrejovský, P.....	347
Antić, A.....	93, 377
Anžel, I.....	447
Arsić, S.....	527
Arsovski, S.....	315
Assenova, E.....	97
Avdic, N.....	319

B

Babić, B.....	285, 301
Badida, M.....	323, 329
Baralić, J.	1
Barna, J.	277
Bartko, L.	323
Beju, L.D.....	101, 255
Beniak, J.	5
Benkó, P.....	105, 163
Beno, J.	17
Beño, M.	45
Berić, J.	137
Beszédes, S.	357
Bilic, B.....	9
Bizjak, M.....	41, 447
Blagojević, D.	141
Blanuša, V.....	309
Blažič, L.	535
Bob, M.	69
Bojanić, M.....	215
Borodavko, V.....	403
Borojević, S.....	57, 109
Bosák, M.....	211
Bouzakis, E.	115
Bouzakis, K.-D.....	115, 193, 247
Božičković, R.....	419
Božičković, Z.....	419
Brkljač, B.	423
Brkljač, N.....	423
Brüning, H.....	427
Budak, I.....	369, 399, 543

C

Cerjaković E.....	297, 493
Cichosz, P.....	145, 187
Crnobrnja, B.....	369
Cus, F.	29, 171, 203

Č

Čiča, Đ.....	57, 227
Čok, V.	305

Ć

Ćojbašić, Ž.	61
Ćuković, S.....	505

D

Danilov, I.....	281
Delić, M.....	167
Devedžić, G.....	505
Deželak, M.	431
Dimic, Z.	259
Djapic, M.....	65, 79, 273
Dobraš, D.	419
Dolinšek, S.	21
Dučić, N.	61
Dudić, S.....	183
Duhovnik, J.	305
Dzoganova, Z.....	329

E

Eggbeer, D.....	509, 543
Epler, I.....	65
Erić, M.....	219

F

Fedorčáková, M.....	333, 381, 385
Ficko, M.	431
Filipović, N.	513
Fuerstner, I.	223

G

Gaiko, V.	403
Gajić, V.	133
Georgiadis, P.	335
Gerardis, S.	115
Globočki – Lakić, G.	57, 227
Gogolak, L.	223
Gojić, M.	41, 447
Goletić, Š.	319, 339
Gostimirović, M.	13, 17, 37, 391
Grubor, S.	315
Grujić, J.	521
Gyenge, C.	69

H

Hadžistević, M.	153, 167, 197, 377, 391, 501
Hajduová, Z.	207, 211
Herić, M.	297
Hodolić, J.	153, 377, 407, 501
Hodúr, C.	357
Homar, D.	21
Hroncová, E.	343
Hronec, O.	347
Huttmanová, E.	347

I

Ilić, M.	369
Imamović, N.	339
Irgolic, T.	171
Israel, M.	467
Ivanisevic, A.	435, 477, 535

J

Jahn, M.	231
Jakovljevic, Z.	121
Janković, P.	25
Jeremić, D.	481
Jevremovic, D.	509, 543
Jovanic, D.	439
Jovanovic, M.	439
Jovanovic, V.	235, 443
Jovanović, D.	463
Jovičić, G.	243, 293
Jovišević, V.	109
Jurković, Z.	391

K

Kacmarcik, I.	435, 459
Kakaš, D.	137, 141, 497, 535
Kamberović, B.	167
Kandeva, M.	97
Kandikjan, T.	263
Karakašić, M.	305
Karpe, B.	447
Kheifetz, M.	353, 403
Kitak, S.	447
Klančnik, G.	41

Klimenko, S.	53, 353
Kljajin, M.	305
Kokotovic, B.	259
Koldžin, D.	125
Kopač, J.	21, 29, 37
Korunović, N.	289
Košarac, A.	239
Kosec, B.	41, 369, 447
Kosec, L.	41
Košiková, A.	365
Kováč, M.	45
Kovač, P.	13, 17, 37, 391, 423
Kovačević, L.	137, 141, 497
Kovács, P.V.	357
Kraišnik, M.	453
Králíková, R.	323
Kramar, D.	37
Kravchenko, M.P.	129
Krecu, D.	133
Krivokapić, Z.	315
Križan, P.	87, 361
Kroutko, V.	403
Kukuruzović, D.	137, 141, 497
Kuzinovski, M.	145, 187
Kuzman, K.	459

L

Ladomerský, J.	343
Lainović, T.	535
Langraudi, N.	443
Lapcevic, A.	509, 543
Lazarević, I.	301
Lazić, M.	315
Legutko, S.	133
Lenčeš, I.	197
Lovrić, S.	493
Ludányi, L.	357
Lukić, D.	243, 293
Lukic, Lj.	65, 79, 273
Lukić, N.	281
Luttmann, A.	231
Lužanin, O.	489
Lyamina, E.	415

M

Majernik, M.	211
Manabe, K.	415
Manić, M.	539
Maňko, M.	365
Mankova, I.	17
Mansour, G.	247
Markovic, D.	501, 535
Marušić, V.	463
Matić, A.	505
Matin, I.	501
Matuš, M.	87, 361
Mauermann, R.	467
Medić, V.	125
Melnic, A.L.	129
Mihajlovic, G.	477
Mijailović, N.	513

Miković, V.	281
Milanković, D.	369, 407
Milanović, B.	369, 407
Milenković, I.	183
Miletić, A.	137, 141, 497
Miletić, O.	251
Milin, D.	149
Miljanić D.	219
Miljković, Z.	285, 301
Milojević, Z.	215, 255
Milošević, M.	243, 293
Milovanović, J.	289
Milutinović, A.	227
Milutinovic, D.	73, 259
Milutinovic, Mi.	73, 259
Milutinovic, Mi.	435, 489
Mircheski, I.	263
Mišić, D.	539
Mišković, A.	49
Mitić, M.	301
Mitković, M.	539
Mitrović, A.	33
Mitsi, S.	247
Mladenovic, G.	269
Morača, S.	149
Movrin, D.	435, 489
Muránsky, J.	373

N

Nagode, A.	41
Navalušić, S.	101, 255
Nedić, B.	1, 463
Nemedi, I.	153, 223
Neugebauer, R.	467
Nikolic, B.	179
Nikolic, N.	79, 273
Nochvay, V.M.	129
Novak-Marcincin, J.	277, 473
Novakova-Marcincinova, L.	473

O

Okuka, M.	411
----------------	-----

P

Pacurar, A.	69
Pahole, I.	431
Palenčar, R.	197
Pecelj, Dj.	477
Pecenica, N.	79
Penfold, N.	157
Pepelnjak, T.	459
Peták, T.	105, 163
Petelj, A.	377
Peterka, J.	45
Petrović, M.	285
Petrović, P.B.	281
Petrović, S.	505
Petrović, Ž.	453
Plančak, M.	435, 459, 477, 489
Polonsky, L.G.	129

Popovic, M.	269
Popp, I.O.	83
Potran, M.	501
Pozilova, N.	353
Prement, G.	353
Pucovsky, V.	13, 17
Puskar, T.	501, 509, 543
Puzović, R.	53
Pynkin, A.	353

R

Radić, N.	481
Radlovački, V.	167
Radonić, J.	411
Radonjić, S.	33, 61
Radovanović, M.	25
Radulović, J.	513
Radulović, N.	513
Rafa, A.	69
Rajnović, D.	485
Raspudic, V.	517
Reibenschuh, M.	171
Ristić, B.	505
Rodić, D.	13, 17

S

Sabolová, J.,	381
Sagris, D.	247
Savić, B.	175
Savković, B.	13
Schmidt, A.	231
Schwartzová, H.	207
Sekulić, M.	17, 37, 153, 391
Sekulic, S.	179
Simić, R.	423
Simonovic, S.	395
Skakun, P.	435, 489
Skordaris, G.	115
Slavkovic, N.	73, 259
Slavković, R.	61, 175
Sobotová, L.	323
Sovilj, B.	133
Sovilj-Nikić, I.	33, 133
Sredanović, B.	57, 227
Stefanović, M.	219, 477
Stevanović, D.	289
Stoic, A.	29
Stojković, M.	289
Szabó, G.	357

Š

Stepišnik, A.	431
Šarić, T.	93
Šebo, J.	333, 385
Šenk, N.	411
Šešlija, D.	183
Šidanin, L.	453, 485
Škorić, B.	137, 141
Šogorović, D.	49
Šooš, L.	13, 83, 361

T

Tabaković, S.	215, 521
Tadić, B.	219
Tadić, D.	315
Tanović, Lj.	53
Terek, P.	137, 141, 497
Tichá, M.	399
Todić, M.	251
Todić, V.	153, 243, 293
Tomov, M.	145, 187
Tomovic, M.M.	443
Topčić, A.	297, 493
Torok, J.	277
Trajanović, M.	289, 513, 527, 539
Trifkovic, B.	509, 543
Trifunović, M.	289
Trlin, G.	9
Tsiafis, Ch.	247
Tsiafis, I.	193
Tsolis, G.	193
Tufegdžić, M.	527
Turk Sekulić, M.	411

U

Urosevic, V.	175
Uzelac, M.	531

V

Varga, Gy.	133
Vasiliev, A.	403
Veg, E.	175
Veselinović, M.	527, 539
Vičević, M.	255
Vilček, J.	347
Vilimonović, M.	531
Vilotić, D.	435, 453, 459, 477, 489
Vilotić, M.	137, 141, 497, 535
Višekruna, V.	49
Vitković, N.	527, 539
Vlajković, H.	175
Vlčej, J.	407
Voelkner, W.	467
Vojinović Miloradov, M.	411
Vojkovic, V.	9
Vollertsen, F.	427
Vranjevac, I.	273
Vrba, I.	197
Vukelić, Dj.	501, 509
Vukman, J.	243, 293
Vuković, N.	301
Vulanović, S.	167

W

Wang, H.	235
Williams, R.J.	509, 543

X

Xanthopoulou, M.	193
Xenos, Th.	193

Z

Zabkar, B.	29
Zadnik, Ž.	305
Zeljковиć, M.	57, 101, 215, 239, 243, 255, 309, 521
Zivanovic, S.	259
Zorc, B.	41
Zuperl, U.	171, 203
Zvončan, M.	45

Ž

Živković, A.	93, 309, 521
-------------------	--------------

11th INTERNATIONAL SCIENTIFIC CONFERENCE
MMA 2012 - ADVANCED PRODUCTION TECHNOLOGIES

PROCEEDINGS



INFORMATION ABOUT DONATORS

Novi Sad, 20-21 September 2012

MINISTARSTVO PROSVETE, NAUKE I TEHNOLOŠKOG RAZVOJA



Nemanjina 22-26
11000 Beograd

www.mps.gov.rs

REPUBLIKA SRBIJA
AP Vojvodine

SEKRETERIJAT ZA NAUKU I
TEHNOLOŠKI RAZVOJ
AP VOJVODINE



Bulevar Mihajla Pupina 16
21108 Novi Sad

Tel: (021) 487 4641

(021) 487 4550

Fax: (021) 456 044

E-mail: secretary@apv-nauka.ns.ac.rs

<http://apv-nauka.ns.ac.rs/vece/index.jsp>

Univerzitet u Novom Sadu
Fakultet tehničkih nauka
Vladimira Perića-Valtera 2
21000 Novi Sad
Srbija

ФАКУЛТЕТ ТЕХНИЧКИХ НАУКА



FTN marketing služba:

Tel: (021) 485 20 61

Fax: (021) 458 133

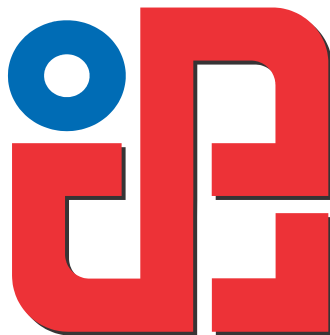
E-mail: agak@uns.ac.rs

www.ftn.uns.ac.rs

POTRAŽITE INFORMATOR!

Univerzitet u Novom Sadu
Fakultet tehničkih nauka
Vladimira Perića-Valtera 2
21000 Novi Sad
Srbija

DEPARTMAN ZA PROIZVODNO MAŠINSTVO



sekreterijat departmana:
Tel: (021) 450-366, 485-23-20
Fax: (021) 454-495
E-mail: ipm@uns.ac.rs
www.ftn.uns.ac.rs
www.dpm.ftn.uns.ac.rs

POTRAŽITE INFORMATOR!



majevica

HOLDING A.D.

Dobrodošli

Hvala Vam što ste nas posetili. Proizvodimo: mašine alatke, odlivke, stabilne rezervoare, cisterne i poljoprivredne mašine.

- ▼ Majevica Holding a.d.
- ▼ Mašine Alatke a.d.
- ▼ Livnica a.d.
- ▼ Pumpe i cisterne a.d.
- ▼ Poljooprema a.d.
- ▼ O nama
- ▼ Kontaktirajte nas



Mašine alatke a.d.



Livnica a.d.



Pumpe i cisterne a.d.



Poljooprema a.d.

Kontakt:

Majevica Holding a.d.
21400 Bačka Palanka
Žarka Zrenjanina 123
SRBIJA

Telefon: +381 (0) 21 751 388
Fax: +381 (0) 21 60 40 175
E-mail: info@majevica.co.rs
poljoprod@majevica.co.rs
picprod@majevica.co.rs

Majevica Holding a.d.
21400 Bačka Palanka
Žarka Zrenjanina 123
SRBIJA
www.majevica.co.rs



Kompanija **OSA računarski inženjering d.o.o.** je osnovana 1989. godine kao jedno od prvih 100 privatnih preduzeća u bivšoj Jugoslaviji. Glavna delatnost OSE, od njenog osnivanja, bio je inženjering, razvoj softverskih rešenja i implementaciju profesionalnih grafičkih sistema za projektovanje i izradu tehničke dokumentacije. Više od dve decenije iskustva u IT oblasti obezbedilo je OSI dobru poziciju kako na lokalnom tako i na tržištu Adriatik regije u sva tri proizvodna programa:

- Jedini smo distributer **Autodesk** softvera (softvera za 2D i 3D projektovanje u svim inženjerskim oblastima) na teritoriji cele Adriatik regije. Usled proširenja distributivne mreže, sa Srbije na sve zemlje bivše Jugoslavije uključujući i Albaniju, 2011. godine osnovane su dve ćerke firme **OSA Softver** u Hrvatskoj i **OSA Sistemi** u Sloveniji.
- OSA je ovlašćeni distributer vodećih svetskih kompanija u proizvodnji mašina za štampu i skeniranje **Océ i Canon**, kao i sistema za kovertiranje proizvođača **Kern**.
- OSA razvija sopstveno softversko rešenje za upravljanje dokumentima i poslovnim procesima **Unidocs**. Sistem se već više od 10 godina komercijalno prodaje putem partnerske mreže na teritoriji Srbije, Crne Gore, Bosne I Hercegovine, Slovenije, Makedonije, Bugarske, Rumunije, Kazakstana, Turkmenistana, Tadžikistana i Kirgistan. Unidocs je namenjen rešavanju problematike upravljanja, arhiviranja i skladištenja elektronske dokumentacije bez obzira na tip i veličinu organizacije u kojoj se implementira, što ga čini konkurentnim kako na domaćem tako i na inostranom tržištu.

Pored nas prodaju vezanu za sve proizvode, korisničku podršku, obuku kadrova, servisiranje i snabdevanje potrošnim materijalom pruža mreža autorizovanih partnera a ukoliko želite da postanete jedan od njih kontaktirajte nas putem mail-a na kontakt@osa.rs ili pronađite više informacija na našem web sajtu www.osa.rs.

UniDocs

Autodesk

Authorised Value Added Distributor





HITARD

ENGINEERING

oil & gas engineers

An Engineering and Design Office for
The Process Industry



What we do

Complete project services

- Thermal / process design
- Bid calculations
- Setting plans
- Mechanical design calculation
- Fabrication drawings
- Pipe Stress Engineering

...for equipment such as

- Shell and tube heat exchangers
- Helixchangers
- Rodbaffle exchangers
- EMBaffles exchangers
- Vessels
- Columns

- Reactors
- Condensers
- Filters and strainers
- Air coolers
- Separators
- Skids & Modules
- Storage Tanks
- Piping

We use



State of the art computer programs for thermal, bid and mechanical design calculations

- PVElite
- CodeCalc
- Microprotol
- NozzlePro
- Compress
- HTRI
- CAESAR II

.... according to the latest codes and standards

- ASME
- Eurocodes
- AD-2000
- BS codes
- RTOD / Stoomwezen
- TEMA Standards
- API Standards

..and the latest CAD tools for fabrication drawings and 3D modeling

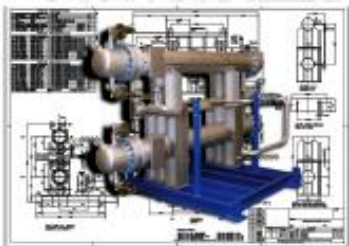
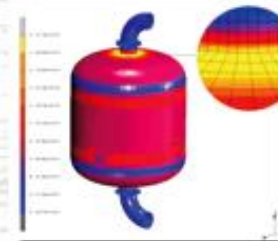
- AutoCAD
- AutoCAD Mechanical
- SolidWorks
- Pro/Engineer
- CADWorks
- OneSpace Designer Drafting

Finite element analysis

Hitard uses FEA when local stresses need to be calculated in complex structures or equipment with cyclic loading (pressure, temperature) cases.

For FEA we use:

- Pro/MECHANICA
- Ansys
- Nozzle/PRO
- MSC. Softwares



Hitard Engineering Netherlands
Karel Doormanstraat 75
3012 GD Rotterdam
P.O. Box 1700, 3000 BS Rotterdam
The Netherlands
Phone: +31(0)10 4330 331
Fax: +31(0)10 4330 336
E-mail: info@hitard.nl
www.hitard.nl

Hitard Engineering Serbia
Jevrejska 4
1st floor
21000 Novi Sad
Serbia
Phone: +381(0)21 472 79 27
Fax: +381(0)21 427 515
E-mail: info@hitard.com
www.hitard.com

cevi, rešetke, ventili, creva, usisne korpe...

Cevi za ventilaciju i klimatizaciju



TEXOFLEX - ZR



TEXOFLEX - ZTG



ALUTEX - A12



IZOTEX - A12



TEXOFLEX - AL

Ventilacione plastične rešetke

Ø100, 110, 120, 150 mm



Usisno izduvni ventili

Ø 100, 125 i 150 mm



Cevi za odprašivanje



TEXOFLEX - PP

Usisno potisne cevi za prehrambenu industriju



TEXOFLEX - NT

za navodnjavanje



TEXOFLEX - UP

Usisne korpe



Ø 52 i Ø75 mm

Creva za zalivanje



TEXOFLEX - DC

Providna creva



TEXOFLEX - GL

Cevi za dimnjake - INOX



TEXOFLEX - RF

delovi za dimnjak od Ø90 do Ø200 mm



Cevi za zaštitu elektro kablova i uvodnice



TEXOFLEX-SA



TEXOFLEX-EF



NOVI KNEŽEVAC

www.labinprogres.hr

TPS d.o.o. preduzeće je ćerka Tvornice poljoprivrednih strojeva **Labinprogres-TPS d.o.o.**, priznatog proizvođača poljoprivredne mehanizacije.

Proizvodni program preduzeća čine:

- traktori,
- motokultivatori,
- motokopačice,
- motokosačice,
- prikolice,
- razni priključci.



TPS d.o.o. / Nemanjina 102 / 23330 Novi Kneževac / Srbija / Tel.: + 381 230 81 203 / Fax : + 381 230 83 333 / e-mail: info.tps@cimos.eu



MILE DRAGIĆ
PRODUCTION

A. Makedonska 11, 23000 Zrenjanin, Srbija
T./F. 023 530 457, 023 534 986, 023 562 271
E. mdragic@armyequipment.com
W. www.armyequipment.com



WWW.ARMYEQUIPMENT.COM

PROIZVODNJA MILE DRAGIĆ

Kompanija „Proizvodnja Mile Dragić“ (MDP) osnovana je 1985. godine, i danas je priznata u međunarodnim okvirima kao lider u proizvodnji pancira, balističkih i interventnih šlemova, balističkih ploča, interventne opreme i druge zaštitne opreme. Svi MDP proizvodi izrađuju se od visokokvalitetnih materijala, sa težnjom da se postigne balans između bezbednosti, udobnosti, težine i cene. Ukoliko to kupac zahteva, možemo pojačati određene karakteristike naših proizvoda.

Proizvodna oprema najnovije generacije, sistem obezbeđenja kvaliteta i korišćenje visokokvalitetnih materijala osiguravaju proizvodnju prema najvišim međunarodnim standardima.



PREDUZEĆE ZA PROIZVODNJU GASNE I ENERGETSKE OPREME, INŽENJERING I TRGOVINU

22320 INDIJA Kralja Petra I b.b.

+ 381 (0) 22 561-630, 555-132

office@gasteh.com

www.gasteh.com

VOĐEĆI U TEHNOLOGIJI ZA PRIMENU PRIRODNOG I TEČNOG NAFTNOG GASA I PROIZVODNJU GASNE OPREME U SRBIJI



Postrojenja i instalacije za:

Prirodni gas (PG) Natural gas (NG)



- glavne memo-regulacione stanice
- memo-regulacione stanice za industrijske potrošače i široku potrošnju
- regulacione stanice

Komprimovani prirodni gas (KPG) Compressed natural gas (CNG)

- memo-regulacione stanice za CNG



Tečni naftni gas (TNG) Liquefied petroleum gas (LPG)

- postrojenja propan-butan gasa (TNG-a) za industriju i autopunionice
- skladišta propan-butan gasa

Mešani gas (MG) Synthetic natural gas (SNG)

- mešačke stanice TNG-vazduh



Gasna oprema (TNG, PG, MG i CNG)

- regulatori pritiska direktnog dejstva i sa pilotom
- sigurnosno ispusni i prestrujni ventili
- zaporni i regulacioni ventili za gas
- nepovratne klapne i ventili
- razvodne glave
- izolacione prirubnice i komadi
- procesna oprema za gas (filteri, zagrejači i odorizatori gasa, isparivači TNG-a)
- merna i kontrolna oprema
- industrijski gorionici i peći

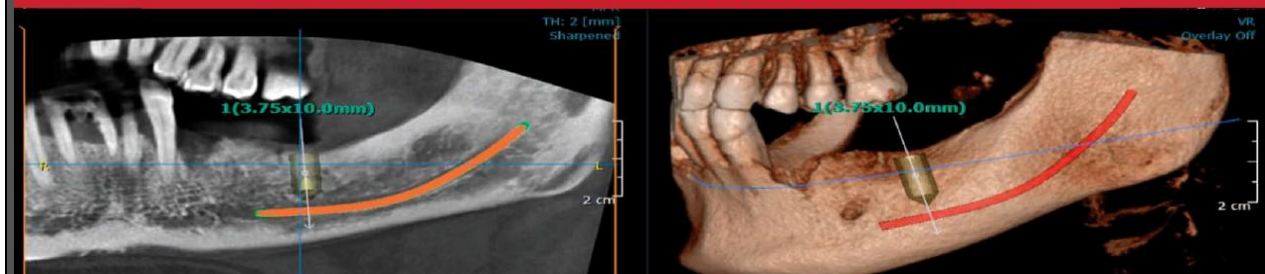


SCANORA 3D i CRANEX 3D, CBCT 3D RENDGEN SISTEMI PODIŽU RENDGEN DIJAGNOSTIKU, IMPLANT PLANIRANJE I VOĐENJE HIRURŠKIH PROCEDURA NA DO SADA NEDOSTIŽAN NIVO.

TIM CO BEOGRAD, EKSKLUZIVNI ZASTUPNIK SOREDEX-a za SRBIJU, CRNU GORU I BIH



3D CONE BEAM CT RENDGEN DIJAGNOSTIKA



Cone Beam CT uređaji predstavljaju najveću tehničku inovaciju u oblasti radiografije kraniofacijalne regije pacijenta, u poslednjih deset godina.

Pouzdati i funkcionalni trodimenzionalni radiološki prikazi olakšavaju i šire spektar kliničkih indikacija u svakodnevnom radu. Mogućnost integracije i interakcije sa najsavremenijim tehničkim uređajima otvara nove vidike oralnoj implantologiji, rekonstruktivnoj maksilofacijalnoj hirurgiji, naučno istraživačkim projektima ORL kao i u svakodnevnoj stomatološkoj praksi.

U prethodnje dve godine, organizovanjem interaktivnih radionica i kontinuiranih edukacija sa preko 150 polaznika, preduzeće Tim Co Beograd je uspelo da našoj stručnoj javnosti ne samo približi već i da edukuje veliki broj doktora za korišćenje 3D CBCT radiološkog sistema. U okviru tih nastojanja sa ponosom organizujemo radionicu na 11. Internacionalnoj Naučnoj Konferenciji MMA 2012 na Fakultetu Tehničkih Nauka u Novom Sadu, u okviru sekcije za biomedicinski inženjering.

Polaznici radionice imaju mogućnost za ad na Cone Beam radnim stanicama sa instaliranim softverom nDemand 3D, jedinom softverom za rad sa CBCT podacima prevedenim na Srpski jezik.

www.timco.rs
www.soredex.com

FKL[®] O

FABRIKA KOTRLJAJUĆIH LEŽAJA I KARDANA

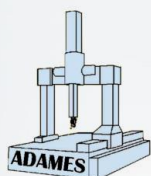
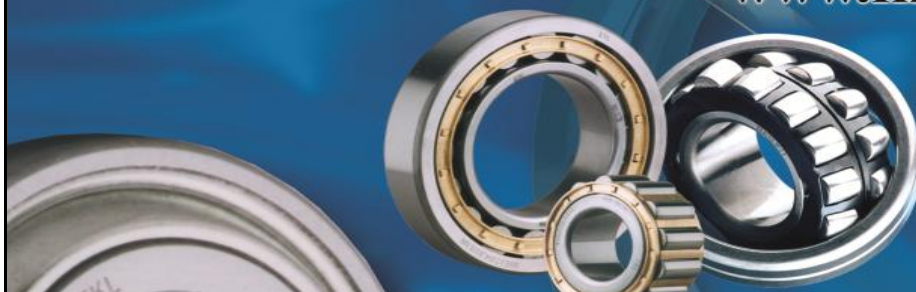
Dugogodišnja saradnja sa
Institutom za proizvodno mašinstvo
na primeni CNC mašina i razvoju novih proizvoda

Industrijska zona bb
21235 Temerin

Tel: +381 21 68 41 100

Fax: +381 21 842 650

www.fkl-serbia.com



TROKORDINATNI MERNI UREĐAJI

ADAMES

SRBIJA - 24430 ADA, ARANJ JANOŠA 50.

TEL: +381 (0)64 30 40 810 • E-MAIL: ADAMES@OPEN.TELEKOM.RS

